Jinlei Li
Robert Ming-Der Chow
Nalini Vadivelu
Alan David Kaye
Editors

Ultrasound Fundamentals

An Evidence-Based Guide for Medical Practitioners

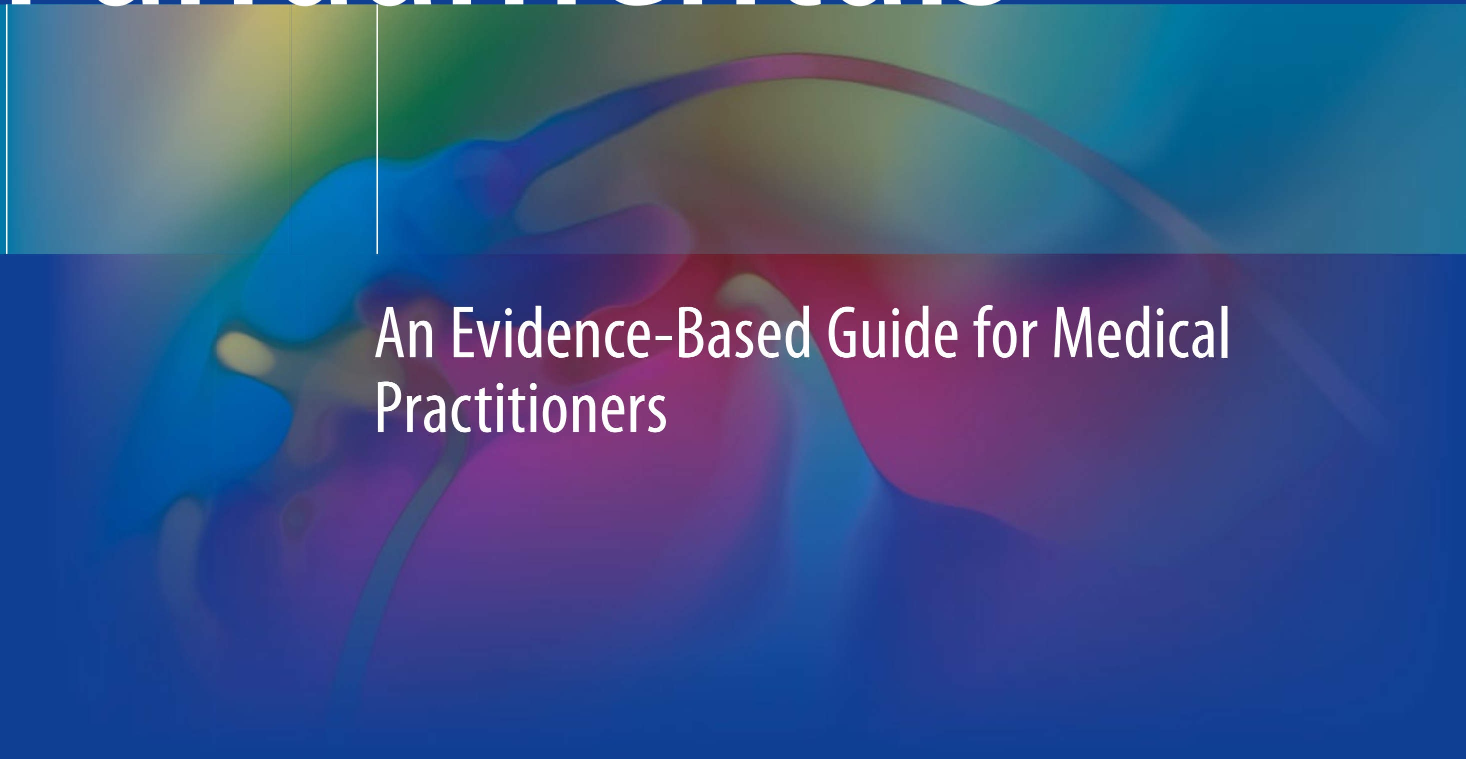

Springer

Ultrasound Fundamentals

Jinlei Li • Robert Ming-Der Chow
Nalini Vadivelu • Alan David Kaye
Editors

Ultrasound Fundamentals

An Evidence-Based Guide for Medical Practitioners

Springer

Editors
Jinlei Li
Department of Anesthesiology
Yale University School of Medicine
New Haven
CT
USA

Nalini Vadivelu
Department of Anesthesiology
Yale University
New Haven
CT
USA

Robert Ming-Der Chow
Department of Anesthesiology
Yale University School of Medicine
New Haven
CT
USA

Alan David Kaye
Department of Anesthesiology and Pharmacology
Toxicology and Neurosciences
LSU Health Shreveport
Shreveport
LA
USA

Department of Anesthesiology
Department of Pharmacology
Louisiana State University School of Medicine
Louisiana State University Health Sciences
Center
New Orleans
LA
USA

ISBN 978-3-030-46838-5 ISBN 978-3-030-46839-2 (eBook)
https://doi.org/10.1007/978-3-030-46839-2

© Springer Nature Switzerland AG 2021
This work is subject to copyright. All rights are reserved by the Publisher, whether the whole or part of the material is concerned, specifically the rights of translation, reprinting, reuse of illustrations, recitation, broadcasting, reproduction on microfilms or in any other physical way, and transmission or information storage and retrieval, electronic adaptation, computer software, or by similar or dissimilar methodology now known or hereafter developed.
The use of general descriptive names, registered names, trademarks, service marks, etc. in this publication does not imply, even in the absence of a specific statement, that such names are exempt from the relevant protective laws and regulations and therefore free for general use.
The publisher, the authors, and the editors are safe to assume that the advice and information in this book are believed to be true and accurate at the date of publication. Neither the publisher nor the authors or the editors give a warranty, expressed or implied, with respect to the material contained herein or for any errors or omissions that may have been made. The publisher remains neutral with regard to jurisdictional claims in published maps and institutional affiliations.

This Springer imprint is published by the registered company Springer Nature Switzerland AG
The registered company address is: Gewerbestrasse 11, 6330 Cham, Switzerland

Dr. Jinlei Li, M.D., Ph.D., F.A.S.A: I want to thank my mother Shuzhen Zang, M.D., father Lin Li, husband Yong, and children Claire and Alex for their unconditional love and continuous support.

Robert Ming-Der Chow, M.D.: I want to thank my parents Nina and KC Chow as well as my sister Sonya and brother-in-law Marc for their unwavering support in all that I do. I also wish to thank my uncle Curtis Hsu and aunt Ann Hsu for believing in me since I was a child. Lastly, I wish to thank Robert Jason Yong, M.D., M.B.A., Andrew Vaclavik, M.D., and Milan Stojanovic, M.D., for their invaluable teaching and mentorship.

Dr. Nalini Vadivelu, M.D.: I wish to thank my husband Thangamuthu Kodumudi and our sons Dr. Gopal Kodumudi and Vijay Kodumudi for their unwavering support. I wish to thank my brother Dr. Amarender Vadivelu for his unconditional care. I wish to thank my mentors, colleagues, residents, and students from all over the world who constantly inspire me to reach greater heights.

Dr. Alan David Kaye, M.D., Ph.D.: I want to thank my mother Florence and wife Dr. Kim Kaye, M.D., for their unwavering support and love. I wish to thank Dr. Matthew, Eng, M.D., for his excellent teaching of ultrasound to our department and myself. Finally, I wish to thank Dr. Charles Fox, M.D., for his amazing support and friendship over the past 30 years, since we met the first day of intern orientation back in 1989.

Foreword

Ultrasound has radically changed the way we practice medicine. This modality gives us diagnostic possibilities in so many situations. It is also used to provide insight into pathological conditions. Ultrasound use, in combination with diagnostic procedures, makes them easier and safer as well as improves patient satisfaction. The benefits of its use are too numerous to name.

During my 35-year career in obstetrics and maternal fetal medicine, I have seen the vast benefit of this modality. For my patients, it provides a window into the womb to view their unborn child, but its benefits do not stop there. Ultrasound is used to diagnose, treat, and care for the unborn child. It truly has allowed us to treat a new patient category, the fetus.

The book *Ultrasound Fundamentals: An Evidence-Based Guide to Medical Practitioners* encompasses many of the uses of ultrasound in modern medicine. This extensive evaluation tackles the basic physics of ultrasound, progressing its active use in practices across the spectrum of medicine. The editors have assembled a wide range of authorities that reflect upon their vast experiences using this modality. This text touches on almost all specialties and provides state-of-the-art techniques that should afford our patients better outcomes.

Ultrasound has truly revolutionized medicine. It has become an inexpensive, highly accurate, and portable imaging modality that we can take to the patient in the clinic, operating room, critical care areas, hospital floor, or in our radiology suites. This imaging modality has truly changed medicine, and I believe the reader will find this textbook very helpful. More importantly, our patients will benefit from the presentations.

David F. Lewis, MD, MBA
Chairman, Obstetrics & Gynecology, Dean, School of Medicine
LSU Health Science Center – Shreveport, Shreveport
LA, USA

Preface

As a physician, I am certainly not the only one who can appreciate the increasingly important role that ultrasound plays in education and patient care. Some consider ultrasound to be the new stethoscope, which is certainly not an overstatement in my mind. As a matter of fact, I personally feel ultrasound techniques supply us with a third eye to look deep into the human anatomy, physiology, and pathology, from top to bottom. Training to effectively use this third eye should start in medical school, which is one of the reasons why I wanted to create an introductory ultrasound book for medical students, the future of medicine. In addition, there are many healthcare workers, including practicing physicians, physician assistants, nurses, advanced nurse practitioners, and physical therapists, who need to use ultrasound at work, but did not have adequate training in the past. Therefore, a visual tool that would allow healthcare workers to learn on the job effectively and efficiently is desirable. These considerations are the motivation behind this book, along with the hopes of empowering learners and practitioners with the ability to visualize the body from head to toe via ultrasound. Unique and pragmatic, *Ultrasound Fundamentals* is a back to basics manual on normal and pathologic sonoanatomy of the head and neck, upper and lower extremities, chest, abdomen, and other major organ systems.

In this book, every chapter has been written by expert physicians who actively practice in a variety medical fields while using ultrasound. This concise and evidence-based ultrasound text includes key topics ranging from the head and neck to the upper and lower extremities, covering all the clinically relevant sonoanatomy. In addition, this 33-chapter book emphasizes the practical use of ultrasound for the diagnosis and treatment of a multitude of conditions in various specialty areas such as airway management, cardiovascular disease assessment, pulmonary status evaluation, orthopedics, gynecology, and pediatrics. The optimal techniques and the step-by-step interpretation of normal and pathologic sonoanatomy are discussed in detail. This text can be used as a starting point for the study of ultrasound-guided diagnosis and treatment, a refresher manual for sonoanatomy on major organ systems, or a last-minute guide before a bedside procedure. There is a great breadth of material that is covered in a comprehensive manner, making it a great resource for board review and exam preparation for various medical, surgical, and allied specialties.

Jinlei Li, M.D., Ph.D., F.A.S.A.
Associate Professor
Program Director, Regional Anesthesia and Acute Pain Medicine Fellowship
Department of Anesthesiology, Yale University School of Medicine
Director of Regional Anesthesia Service, Yale New Haven Health
New Haven, CT, USA

Contents

Part I Ultrasound Basics

Ultrasound Physics & Overview . . . 3
Atin Saha and Mahan Mathur

Ultrasound Probe Selection, Knobology and Optimization of Image Quality . . . 17
Marcelle Blessing

Basic Ultrasound Needling Techniques . . . 25
Benjamin Portal, Karina Gritsenko, and Melinda Aquino

Practical US Guided Vascular Access . . . 29
Sean P. Clifford and Jiapeng Huang

Part II Head and Neck Ultrasound

Ultrasound for Head Assessment: Diagnosis and Treatment . . . 47
Alan David Kaye, Matthew Brian Novitch, and Jennifer Kaiser

Ultrasound-Guided Neck Assessment . . . 55
Andrew Brunk, Erik Helander, and Alan David Kaye

The Utility of Ultrasound in Airway Management . . . 61
Amit Prabhakar, Babar Fiza, Natalie Ferrero, and Vanessa Moll

Ultrasound Technique for Common Head and Neck Blocks . . . 65
Avijit Sharma, Praba Boominathan, and Robert Ming-Der Chow

Part III Upper and Lower Extremity Ultrasound

The Techniques and Merit of Ultrasound in Orthopaedics . . . 79
Cristina Terhoeve, Robert Zura, John Reach, and Andrew King

Shoulder Joint Sonoanatomy and Ultrasound-Guided Shoulder Joint Injection . . . 87
Allan Zhang and George C. Chang Chien

Elbow Joint Sonoanatomy and Ultrasound-Guided Elbow Joint Injection . . . 99
Allan Zhang and George C. Chang Chien

Wrist Joint Sonoanatomy and Ultrasound-Guided Wrist Joint Injection . . . 109
Jason Kajbaf and George C. Chang Chien

Ultrasound Guided Brachial Plexus Block . . . 121
Jinlei Li, Avijit Sharma, Ellesse Credaroli, Nalini Vadivelu, and Henry Liu

Hip Joint Sonoanatomy and Ultrasound-Guided Hip Joint Injection . . . 129
Jason Kajbaf and George C. Chang Chien

Knee Joint Sonoanatomy and Ultrasound-Guided Knee Joint Injection 135
Jason Kajbaf and George C. Chang Chien

Ankle Sonoanatomy and US Guided Joint Blocks. 143
Soo Yeon Kim, Chaiyaporn Kulsakdinun, and Jung H. Kim

Ultrasound Guided Nerve Blocks for Lower Extremity 149
Christopher M. Harmon, Kelly S. Davidson, Erik Helander, Matthew R. Eng, and Alan David Kaye

Part IV Chest and Abdomen Ultrasound

The Role of Ultrasound in the Management of Cardiac Patients 163
Alan David Kaye, Cody M. Koress, O. Morgan Hall, Mitchell C. Fuller, Matthew Brian Novitch, Jinlei Li, and Henry Liu

Ultrasound for Chest: Heart and TTE 171
Paula Trigo Blanco

Ultrasound for Chest: Lung and Pleural Examination and Diagnosis 185
You Shang, Xiaojing Zou, and Hong Wang

Ultrasound-Guided Nerve Blocks for Chest. 193
Kaitlin Crane, Ibrahim N. Ibrahim, Elliott Thompson, Monica W. Harbell, Elyse M. Cornett, and Alan David Kaye

Ultrasound Guided Nerve Blocks for Abdomen. 205
Shilpa Patil, Anusha Kallurkar, Yury Rapoport, Pankaj Thakur, Andrew P. Bourgeois, Elyse M. Cornett, Matthew R. Eng, and Alan David Kaye

Part V Ultrasound in Specialty Care

The Role of Ultrasound in the Critical Care Setting 221
Alan David Kaye, Cody M. Koress, Amir O. Elhassan, Caroline Galliano, Nicholas S. Moore, Christina J. Pollock, Matthew Brian Novitch, Krish D. Sekar, and Amit Prabhakar

Clinical Utilization of Ultrasound in Vascular Disease 227
Matthew Brian Novitch, Anna J. Sudbury, Mitchell C. Fuller, Jennifer J. Dennison, Cody M. Koress, Amit Prabhakar, Vanessa Moll, Elyse M. Cornett, and Alan David Kaye

Pediatric Ultrasound. 239
Allan Brook, Einat Blumfield, and Andrew Brook

Fundamentals of Gynecologic Ultrasound 251
Barry Hallner, Nia Thompson, and Lisa Peacock

Ultrasound for Spine and Nerve Blocks 271
Chiedozie C. Uwandu, Emily Bouley, Timothy Montet, Mark R. Jones, and Alan David Kaye

Use of Ultrasound in Urology. 285
Hemangini Thakkar, Patil Bhushan, Jamil S. Syed, and Sujata Patwardhan

Ultrasound Guided Interventions 307
Junaid Raja, Igor Latich, and Mahan Mathur

Ultrasound Application in Dermatologic Conditions 317
Chang Ye Wang, Kavita Darji, Felipe Aluja Jaramillo, Ximena Wortsman, and A. Mary Guo

Part VI Emergency Ultrasound

Fundamentals of Point of Care Ultrasound Applications in Perioperative Settings 337
Sonya Bohaczuk and Yan Lai

Ultrasound for Abdomen and FAST: Evaluation and Diagnosis 351
Christopher L. Moore, Jacob Avila, and John W. Combs

Practicality of Ultrasound in Emergency Medicine 365
Jason Arthur, Scott Bomann, and Christopher L. Moore

Index 373

Contributors

Melinda Aquino, MD Montefiore Medical Center, Bronx, NY, USA

Jason Arthur, MD/MPH University of Arkansas for Medical Sciences, Department of Emergency Medicine, Little Rock, AR, USA

Jacob Avila, MD, RDMS University of Kentucky, Emergency Medicine, Lexington, KY, USA

Patil Bhushan Department of Urology, KEM Hospital, Mumbai, India

Paula Trigo Blanco, MD Southern New Hampshire Medical Center, Anesthesiology, Nashua, NH, USA

Marcelle Blessing, MD Yale University School of Medicine, Department of Anesthesiology, New Haven, CT, USA

Einat Blumfield, MD Children's Hospital of Montefiore, Albert Einstein College of Medicine, Radiology, Bronx, NY, USA

Sonya Bohaczuk, MD Mount Sinai West and St. Luke's Hospitals, Department of Anesthesiology, Perioperative, and Pain Medicine, Icahn School of Medicine at Mount Sinai Medical Center, New York, NY, USA

Scott Bomann, MD, MPH, DO, FACEP, FACEM Wellington Regional Hospital, Department of Emergency Medicine, Wellington, New Zealand

Praba Boominathan, MD Department of Anesthesiology, Yale University School of Medicine, New Haven, CT, USA

Emily Bouley, MD Harvard Medical School, Beth Israel Deaconess Medical Center, Department of Anesthesia, Critical Care, and Pain Medicine, Boston, MA, USA

Andrew P. Bourgeois, MD Department of Anesthesiology, LSU Health Sciences Center, New Orleans, LA, USA

Andrew Brook, BA Albert Einstein College of Medicine class of 2024, Bronx, NY, USA

Allan Brook, MD, FACR, FSIR Montefiore Medical Center, Radiology, Bronx, NY, USA

Andrew Brunk, MD Department of Anesthesiology, LSUHSC, New Orleans, LA, USA

George C. Chang Chien, DO GCC Institute, Newport Beach, CA, USA

Ventura County Medical Center, Ventura, CA, USA

Robert Ming-Der Chow, MD Department of Anesthesiology, Yale University School of Medicine, New Haven, CT, USA

Sean P. Clifford, MD Department of Anesthesiology & Perioperative Medicine, University of Louisville, Louisville, KY, USA

John W. Combs, MD Jackson Memorial Hospital, Emergency Medicine, Miami, FL, USA

Elyse M. Cornett, PhD Department of Anesthesiology, LSU Health Shreveport, Shreveport, LA, USA

Kaitlin Crane Department of Anesthesiology, LSU Health Shreveport, Shreveport, LA, USA

Ellesse Credaroli, MD Department of Anesthesiology, Yale University, New Haven, CT, USA

Kavita Darji, MD Department of Dermatology, Saint Louis University School of Medicine, St. Louis, MO, USA

Kelly S. Davidson, MD Department of Anesthesiology, LSU-HSC, New Orleans, LA, USA

Jennifer J. Dennison, BS Medical College of Wisconsin, Wauwatosa, WI, USA

Amir O. Elhassan, MD Ohio State University Health Sciences Center, Department of Anesthesiology, Columbus, OH, USA

Matthew R. Eng, MD Department of Anesthesiology, LSU Health Sciences Center, New Orleans, LA, USA

LSU-HSC New Orleans, Anesthesiology, New Orleans, New Orleans, LA, USA

Natalie Ferrero Emory University Hospital Midtown, Department of Anesthesiology, Division of Critical Care, Atlanta, GA, USA

Babar Fiza, MD Emory University Hospital Midtown, Department of Anesthesiology, Division of Critical Care, Atlanta, GA, USA

Mitchell C. Fuller, BS Medical College of Wisconsin, Wauwatosa, WI, USA

Caroline Galliano, BS Louisiana State University Health Sciences Center, Department of Anesthesiology, New Orleans, LA, USA

Karina Gritsenko, MD Montefiore Medical Center, Bronx, NY, USA

A. Mary Guo, MD Department of Dermatology, Saint Louis University School of Medicine, St. Louis, MO, USA

O. Morgan Hall, BS Department of Anesthesiology, LSU School of Medicine, New Orleans, LA, USA

Barry Hallner, MD Female Pelvic Medicine and Reconstructive Surgery, Louisiana State University Health, New Orleans, LA, USA

Monica W. Harbell, MD Department of Anesthesiology and Perioperative Medicine, Mayo Clinic Arizona, Phoenix, AZ, USA

Christopher M. Harmon, MD Department of Anesthesiology, Thomas Jefferson University Hospital, Sidney Kimmel Medical College, Philadelphia, PA, USA

Erik Helander, MBBS Department of Anesthesiology, University of Florida-Gainesville, Gainesville, FL, USA

Jiapeng Huang, MD, PhD, FASA, FASE Department of Anesthesiology & Perioperative Medicine, University of Louisville, Louisville, KY, USA

Ibrahim N. Ibrahim Department of Anesthesiology, LSU Health Shreveport, Shreveport, LA, USA

Felipe Aluja Jaramillo, MD Department of Radiology, Fundación Universitaria Sanitas, Country Scan, Bogotá, Colombia

Mark R. Jones, MD Harvard Medical School, Beth Israel Deaconess Medical Center, Department of Anesthesia, Critical Care, and Pain Medicine, Boston, MA, USA

Jennifer Kaiser Medical College of Wisconsin, Milwaukee, WI, USA

Jason Kajbaf, DO University of California, Los Angeles, Department of PM&R, Los Angeles, CA, USA

Anusha Kallurkar, MD Department of Anesthesiology, LSU Health Shreveport, Shreveport, LA, USA

Alan David Kaye, MD, PhD Departments of Anesthesiology and Pharmacology, Toxicology, and Neurosciences, Lousiana State University Health Sciences Center, Shreveport, LA, USA

Department of Anesthesiology, Department of Pharmacology Louisiana State University School of Medicine, Louisiana State University Health Sciences Center, New Orleans, LA, USA

Soo Yeon Kim, MD Department of Physical Medicine and Rehabilitation, Montefiore Medical Center, Bronx, NY, USA

Jung H. Kim, MD Department of Anesthesiology, Perioperative, and Pain Medicine, Icahn School of Medicine at Mt. Sinai St. Luke's and Mt. Sinai West Hospitals, New York, NY, USA

Andrew King, MD Department of Orthopaedic Surgery, Louisiana State University Health Sciences Center, New Orleans, LA, USA

Cody M. Koress, BS, MD Department of Anesthesiology, LSU School of Medicine, Louisiana State University Health Sciences Center, New Orleans, LA, USA

Chaiyaporn Kulsakdinun, MD Department of Orthopedics, Montefiore Medical Center, Bronx, NY, USA

Yan Lai, MD, MPH, FASA Mount Sinai West and St. Luke's Hospitals, Department of Anesthesiology, Perioperative, and Pain Medicine, Icahn School of Medicine at Mount Sinai Medical Center, New York, NY, USA

Igor Latich Department of Radiology and Biomedical Imaging, Yale School of Medicine, New Haven, CT, USA

Jinlei Li, MD, PhD Department of Anesthesiology, Yale University School of Medicine, New Haven, CT, USA

Henry Liu, MD Department of Anesthesiology & Perioperative Medicine, Hahnemann University Hospital Drexel University College of Medicine, Philadelphia, PA, USA

Department of Anesthesiology & Perioperative Medicine, Penn State Milton S. Hershey Medical Center, Hershey, PA, USA

Mahan Mathur, MD Department of Radiology and Biomedical Imaging, Yale School of Medicine, New Haven, CT, USA

Vanessa Moll, MD, PhD, DESA Emory University School of Medicine, Department of Anesthesiology, Division of Critical Care Medicine, Atlanta, GA, USA

Timothy Montet Lousiana State University Health Science Center, Department of Anesthesiology, New Orleans, LA, USA

Nicholas S. Moore, BA Harvard Medical School, Boston, MA, USA

Christopher L. Moore, MD Yale School of Medicine, Department of Emergency Medicine, New Haven, CT, USA

Matthew Brian Novitch, MD University of Washington School of Medicine, Department of Anesthesiology, Seattle, WA, USA

Shilpa Patil, MD Department of Anesthesiology, LSU Health Shreveport, Shreveport, LA, USA

Sujata Patwardhan, MS (Surg), Mch Urology Department of Urology, KEM Hospital, Mumbai, India

Lisa Peacock, MD Louisiana State University Health, Department of Obstetrics and Gynecology, New Orleans, LA, USA

Christina J. Pollock, MD University of Arizona School of Medicine, Department of Anesthesiology, Tucson, AZ, USA

Benjamin Portal, MD Montefiore Medical Center, Bronx, NY, USA

Amit Prabhakar, MD, MS Emory University School of Medicine, Department of Anesthesiology, Division of Critical Care, Atlanta, GA, USA

Junaid Raja Department of Radiology and Biomedical Imaging, Yale School of Medicine, New Haven, CT, USA

Yury Rapoport, MD Department of Anesthesiology, LSU Health Shreveport, Shreveport, LA, USA

John Reach, MD Department of Orthopaedic Surgery, Yale School of Medicine, New Haven, CT, USA

Atin Saha, MD, MS Department of Radiology and Biomedical Imaging, Yale School of Medicine, New Haven, CT, USA

Krish D. Sekar, MD Louisiana State University Health Sciences Center, Department of Anesthesiology, New Orleans, LA, USA

You Shang, MD Institute of Anesthesiology and Critical Care Medicine, Union Hospital, Tongji Medical College, Huazhong University of Science and Technology, Wuhan, China

Avijit Sharma, MD Department of Anesthesiology, Yale University School of Medicine, New Haven, CT, USA

Anna J. Sudbury, BS Medical College of Wisconsin, Wauwatosa, WI, USA

Jamil S. Syed, BS Department of Urology, Yale University School of Medicine, New Haven, CT, USA

Cristina Terhoeve, DNB, DMRD, DMRE Department of Orthopaedic Surgery, Louisiana State University Health Sciences Center, New Orleans, LA, USA

Hemangini Thakkar, MD Department of Urology, KEM Hospital, Mumbai, India

Pankaj Thakur, MD Department of Anesthesiology, LSU Health Shreveport, Shreveport, LA, USA

Elliott Thompson, BS Department of Anesthesiology, LSU Health Shreveport, Shreveport, LA, USA

Nia Thompson, MD, MPH Female Pelvic Medicine and Reconstructive Surgery, Louisiana State University Health, New Orleans, LA, USA

Chiedozie C. Uwandu, MD Harvard Medical School, Beth Israel Deaconess Medical Center, Department of Anesthesia, Critical Care, and Pain Medicine, Boston, MA, USA

Nalini Vadivelu, MD Department of Anesthesiology, Yale University, New Haven, CT, USA

Hong Wang, MD, PhD, FASE, FASA Department of Anesthesiology, West Virginia University, Morgantown, WV, USA

Chang Ye Wang, MD Department of Dermatology, Saint Louis University School of Medicine, St. Louis, MO, USA

Ximena Wortsman, MD Department of Dermatology, University of Chile and Pontifical Catholic University of Chile, Santiago, Chile

Allan Zhang, DO Department of Radiology, University of Connecticut Health Center, Farmington, CT, USA

Xiaojing Zou, MD Institute of Anesthesiology and Critical Care Medicine, Union Hospital, Tongji Medical College, Huazhong University of Science and Technology, Wuhan, China

Robert Zura, MD Department of Orthopaedic Surgery, Louisiana State University Health Sciences Center, New Orleans, LA, USA

Part I

Ultrasound Basics

Ultrasound Physics & Overview

Atin Saha and Mahan Mathur

1 Introduction

This chapter will elucidate the basic physics principles upon which ultrasound imaging is based. In addition, ultrasound transducer instrumentation will be reviewed and common ultrasound artifacts will be discussed. Basic knowledge of how a system produces and acquires ultrasound waves will enhance understanding of the perceived anatomy. A comprehensive grasp of ultrasound physics is vital for both the proper interpretation and acquisition of ultrasound images.

2 What Is Ultrasound?

To understand ultrasound, we must first understand sound. A sound wave is generated by the propagation of "vibrational energy" through a medium (gas, liquid or solid); in other words, molecules striking other molecules [1]. If measured from a single location, the molecular movements are detected as pressure waves alternating between rarefaction (decreased pressure in a medium) and compression (increased pressure in a medium) with each repetition of a pressure wave referred to as a cycle [1, 2]. Basic sound wave properties are described by its wavelength and frequency. Ultrasound is named as such to reflect the fact that sound waves utilized in this form of imaging have frequencies above the range of human hearing (that is, greater than 20 kHz) [3].

2.1 Wavelength & Frequency

Wavelength (λ) can be defined as the distance between two similar points on a wave occurring in a cycle (for example the distance between two peaks or troughs) (Fig. 1). Imagine you are standing in a stationary position and observing a wave propagate, a peak followed by a trough; the time it takes for the complete cycle to pass is defined as the wave's period and is expressed in seconds per cycle. It is often easier to work with the inverse of the period, which is also known as a wave's frequency, represented as cycles/second. Ultrasound transducers (devices that generate and acquire ultrasound waves) are categorized by the frequency of sound they utilize. The speed of sound (velocity) in a medium is defined by the wavelength multiplied by its frequency.

2.2 Strength of a Wave

There are three parameters that describe the strength of a wave: amplitude, power and intensity. Amplitude is the size of the wave and is defined graphically as the difference between the average and maximum values of the wave (Fig. 1). Power is the energy generated per unit time (Joules/second) and is expressed in Watts. As a sonographer, the output power may be altered to generate brighter images. This occurs by increasing the voltage to the piezoelectric crystals of the transducer, resulting in increased force of vibration which subsequently leads to stronger soundwaves transmitted to the body [1]. Intensity represents the concentration of energy in a cross-section of a sound beam and is mathematically defined as the power divided by the cross-sectional area of the sound wave.

3 Ultrasound Image Generation

It is important to highlight that ultrasound does not strictly depict tissue structures, but rather the interfaces between tissues of differing acoustic impedances. This concept helps one to understand fundamentally how ultrasound images are generated.

An ultrasound pulse is emitted from the transducer, and the echoes returning to the transducer from differing depths within the body are processed to generate a two-dimen-

---

A. Saha (✉) · M. Mathur
Department of Radiology and Biomedical Imaging,
Yale School of Medicine, New Haven, CT, USA
e-mail: atin.saha@yale.edu

© Springer Nature Switzerland AG 2021
J. Li et al. (eds.), *Ultrasound Fundamentals*, https://doi.org/10.1007/978-3-030-46839-2_1

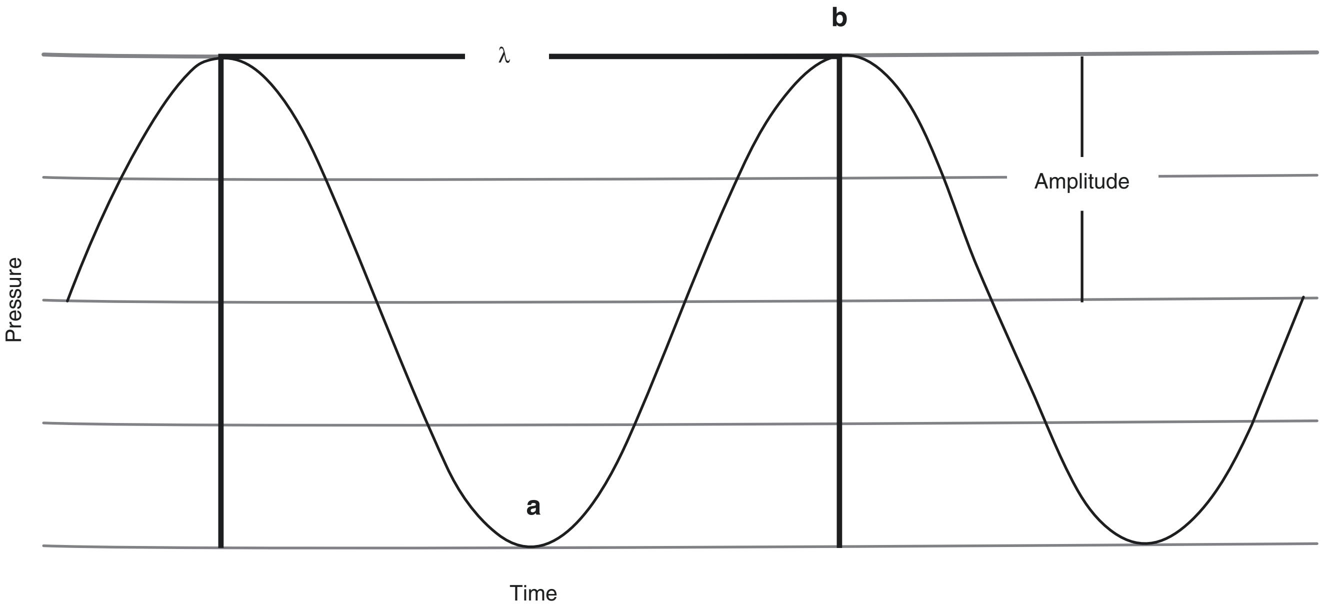

Fig. 1 Sound waves consist of varying pressures through a medium. The distance between similar pressure points on a curve is classified as a wavelength (λ) and the distance between the average and maximum values of a wave is defined as the amplitude. A region of decreased pressure in a medium is defined as rarefaction (**a**) while a region of increased pressure is defined as compression (**b**)

sional image. The time delay between the emission of an ultrasound pulse and the return of the reflected sound wave is known as the round-trip time [5]. Reflection of the sound wave occurs due to differing sound propagation properties at the boundaries of differing media. For example, this can be seen at the interface between the renal cortex and its surrounding fat [6, 7].

The following is an analogous example that illustrates this concept: imagine you had a basketball and decided to bounce it off of three different types of backboards - glass, concrete and steel. Think of the basketball as a sound wave. If you were to use the same force and transmit the basketball ("sound wave") towards the different backboards you would expect the ball to be reflected differently off the backboards towards you given differing intrinsic properties of the glass, concrete and steel.

3.1 Intrinsic Features Influencing Ultrasound Studies

Before discussing the concept of image generation, it is important to define acoustic impedance (*Z*). Acoustic impedance is the frequency-dependent resistance that an ultrasound beam encounters as it passes through a tissue [8, 9].

$Z = \rho \bullet c$, where Z = acoustic impedance, ρ = density of the medium, c = speed of sound in the medium.

Tissues within the body have differing densities (ρ) and thus different impedances. At tissue interfaces, an incident ultrasound beam is partially reflected and partially refracted. When a wave passes through the medium changing the direction of travel, it is described as a refracted wave (Fig. 2) [9].

The difference in acoustic impedance between two tissues forming an interface determines the amount of reflection and refraction of an incident beam. The reflection gradient (R) describes this mathematically for incident angles perpendicular to a tissue interface [9].

$R = \left(\frac{Z1 - Z2}{Z1 + Z2} \right)^2$, where $Z1$ and $Z2$ are the acoustic impedances of respective tissues at an interface.

The greater the difference between the acoustic impedances, the greater the amount of energy from an incident ultrasound wave is reflected back. As discussed previously, acoustic impedance is a function of the density of the medium. Therefore, the greater the difference in densities of the tissue interface, the bigger the reflection and smaller the refraction component of an incident ultrasound wave.

Inserting acoustic impedances into this formula, one can begin to understand the appearance of ultrasound images at different interfaces. For example, at the interface of renal tissue ($Z1 = 1.65 \times 10^6$) and muscle ($Z2 = 1.68 \times 10^6$) [10], $R = 0.0014$. This means that the kidney-muscle interface reflects approximately 0.1% of the incident energy.

On the other hand, at the interface of renal tissue ($Z1 = 1.65 \times 10^6$) and air ($Z2 = 0.0004 \times 10^6$) [10], $R = 0.999$, which means that the kidney-air interface reflects approximately 99.9% of the incident energy, allowing approximately 0.1% of the energy to travel into the tissues. This explains why air and soft-tissue interfaces obscure evaluation of

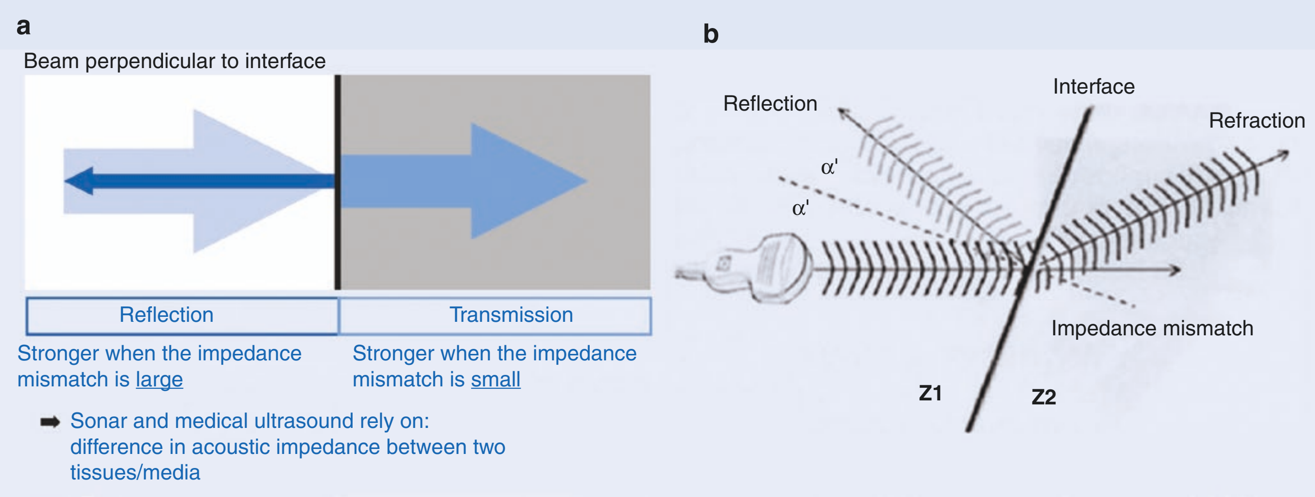
a
Beam perpendicular to interface
Reflection
Transmission
Stronger when the impedance mismatch is large
Stronger when the impedance mismatch is small
➡ Sonar and medical ultrasound rely on: difference in acoustic impedance between two tissues/media
b
Reflection
Interface
Refraction
α'
α'
Impedance mismatch
Z1
Z2

Fig. 2 (**a**) Generation of an ultrasound image: reflection versus transmission. (**b**) Interaction of ultrasound with interfaces in the body according to the laws of wave optics. (Diagram and adapted caption courtesy of Schäberle et.al 2018 Springer)

deeper structures and why lungs and air-filled bowel loops are sub-optimally examined via ultrasound.

It is rare to find smooth interfaces between tissues in the body and often, the interfaces will be rough. A sound wave hitting a rough surface will scatter in multiple directions in the form of a spherical wave instead of along a single path [11]. Therefore, in the clinical setting, ultrasound images are generated from a mixture of reflected and scattered sound waves. When an ultrasound beam is perpendicular to a structure it appears clearly delineated and bright, as the information utilized to generate the image is primarily derived from reflected sound waves [9]. If the ultrasound beam interacts with the target tissue in a tangential manner, then only diffusely reflected echoes are available for image generation, and the image will appear less clearly delineated and less bright (even though the acoustic impedances may be the same in the above-mentioned examples).

As a sound beam travels through the human body, the beam undergoes attenuation (loses energy) through a process called scatter. The loss of energy of an ultrasound beam occurs through the conversion to heat [12]. A higher transmitted frequency leads to increased attenuation and limits the depth penetration of an ultrasound beam [13]. The increased attenuation can be compensated to a degree by adjusting the time-gain compensation parameter [14]. Time-gain compensation allows for the increase in gain as time passes which results in equally echogenic tissues appearing similar regardless of tissue depth.

Interference is an important concept to understand as it can affect the ultrasound image. As discussed previously, a sound wave has a compression phase and a rarefaction phase. When multiple sounds waves are superimposed, they can be out-of-phase thus canceling each other out, (destructive interference) or can be in-phase (constructive interference). The spatial distribution of both destructive and constructive interferences is responsible for the visual appearance of an ultrasound image. The way that sound waves interfere with each other can alter the amplitude and subsequently the image brightness [15].

3.2 Ultrasound Modes

There are three basic ultrasound modes that enable clinicians to extract desired information from the target organs of interest.

Amplitude-Mode: This mode has limited applications. As an example, this can be utilized to measure the corneal thickness in ophthalmology. A line through the target is scanned, after which amplitudes of the ultrasound wave echoes are returned to the transducer, and are subsequently converted and displayed as a function of round-trip time. This one-dimensional information can be utilized to infer depth of a structure [16, 17].

Brightness-Mode: This mode is utilized to detect static structures and appreciate anatomy. Amplitudes from a returning ultrasound wave are displayed as points with differing brightness. The brightness of a point represents the strength of the return wave. Once all the echoes from the subsequent transmitted pulses have returned, a complete 2D Brightness-mode image is displayed [16–18].

Motion-Mode: This mode is utilized to image rapidly moving structures such as cardiac valves or vessel walls. Unlike the brightness mode, the motion mode utilizes repeated emission of an ultrasound beam in a stationary location to gain information from moving structures at different time points. Information is displayed along a time axis which describes the motion of the structure at varying time points [16, 17].

4 Resolution

The minimum distance between two structures that still allows for discernibility as separate structures is known as the image resolution. This applies to all imaging modalities including computed tomography and magnetic resonance imaging. In ultrasound, image resolution is specifically defined as the spatial discrimination between two structures that have differing acoustic impedance [9].

Axial resolution is the ability to separate two closely spaced echoes that lie in a plane parallel to the direction of the sound wave [14, 17]. In other words, helping to discriminate between structures that lie anterior/posterior to each other. The shorter the wavelength (and therefore, the higher the frequency) of the excitation pulse, the better the axial resolution. However, as discussed previously, the higher the frequency, the more the wave is attenuated. Thus, high frequency limits the maximum depth from which the echoes can be reflected. The best achievable axial resolution is 0.5λ [20].

Lateral resolution is the ability to separate two closely spaced echoes that are in the perpendicular plane to the direction of the incident wave. The smaller the width of the ultrasound beam, the better the lateral resolution of the image.

5 Ultrasound Transducer

Piezoelectric crystals within most modern ultrasound transducers are the most important components for ultrasonography. These crystals function sequentially: first, to generate ultrasound waves by altering the crystal length when subjected to an electrical current and second, to receive ultrasound waves and convert changes in deformation of the crystal to electrical current which allows for formation of an image. Quartz, lithium niobate and tourmaline are a few materials that possess piezoelectric properties [21].

An ultrasound transducer contains multiple individual piezoelectric elements that allow it to produce an image by shifting the functional elements in a systematic manner. As an example, take a transducer with 9 elements. To generate the first scan line, elements 1–4 may be activated to produce the first incident wave. For the second scan line, a one element shift is made, resulting in activation of elements 2–5. For the third scan line, another one element shift is made, resulting activation in elements 3–6. This continues in a similar fashion, until a total of 6 scan lines are produced. The number of scan lines can also be altered by adjusting the number of elements being activated to generate a scan line [9, 14].

5.1 Types of Transducers

There are four main types of transducers utilized to image the body: curvilinear, phased array, linear array and endocavitary. Having a good understanding of the advantages and limitations of each transducer will assist in obtaining the best image possible.

Curvilinear transducers (Fig. 3) are ideal for abdominal imaging. They have excellent tissue penetration which allows for imaging of deeper structures. Typical frequency range is from 2–5 MHz [4].

Phased array transducers (Fig. 4) are best utilized to image through small regions, particularly in more difficult areas, such as between ribs. They are commonly used in cardiac imaging. A pie-shaped field of view is created utilizing electronic beam steering. Typical frequency range is from 2–7 MHz [4].

Linear array transducers (Fig. 5) are best for imaging superficial structures such as muscles, nerves, vasculature or soft tissues. They produce a rectangular image. Typical frequency range is from 5–10 MHz [4].

Endocavitary transducers (Fig. 6) are placed inside a body cavity and are primarily used for obstetric, gynecologic or otolaryngology applications. They produce wide angle images up to 180 degrees. Typical frequency range is from 8–13 MHz [4].

5.2 Transducer Position

All transducers have a position indicator which corresponds to the marker on the image screen. This allows the sonographer to identify the image orientation being displayed on the screen (Fig. 7).

Standard ultrasound imaging planes include the transverse (also known as axial), sagittal and coronal planes. In the transverse plane, the transducer marker is pointed to the patient's right (Fig. 8) In the sagittal plane (imaging anterior

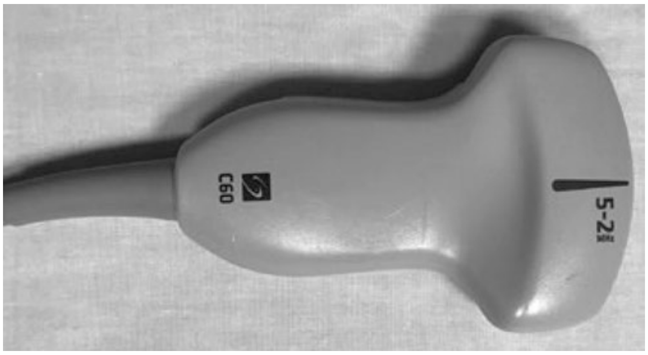

Fig. 3 Curvilinear Transducer. (Diagram and adapted caption courtesy of Creditt et al. 2017 Springer)

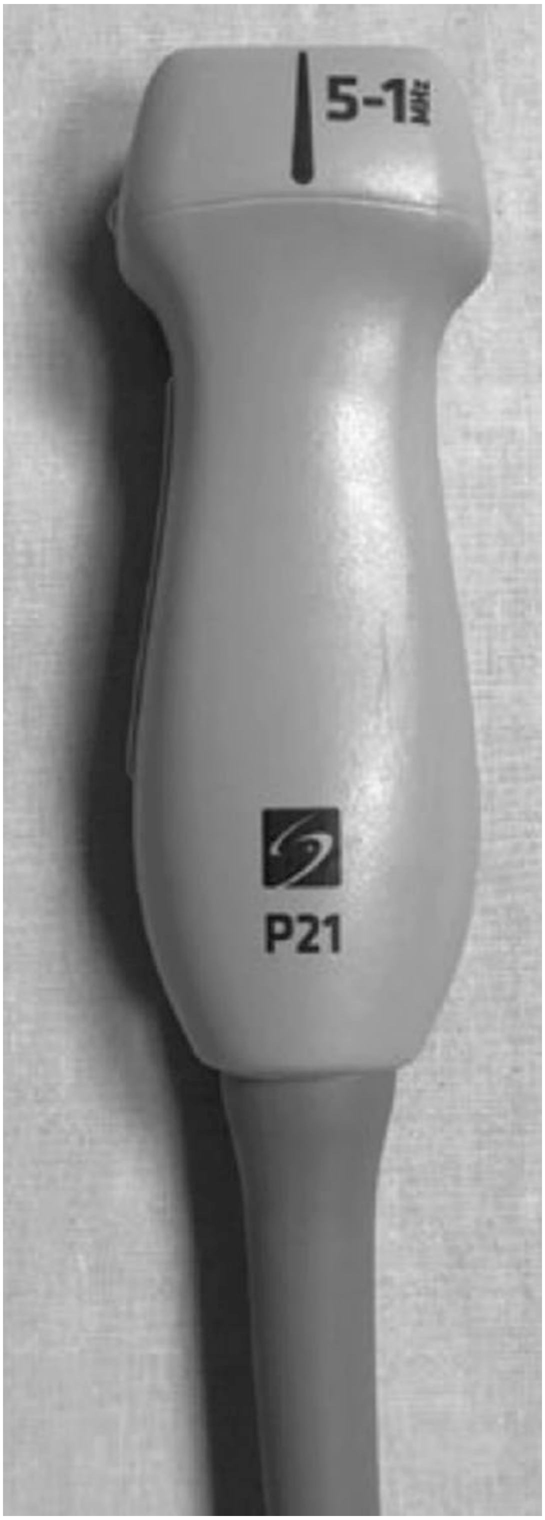

Fig. 4 Phased Array Transducer. (Diagram and adapted caption courtesy of Creditt et al. 2017 Springer)

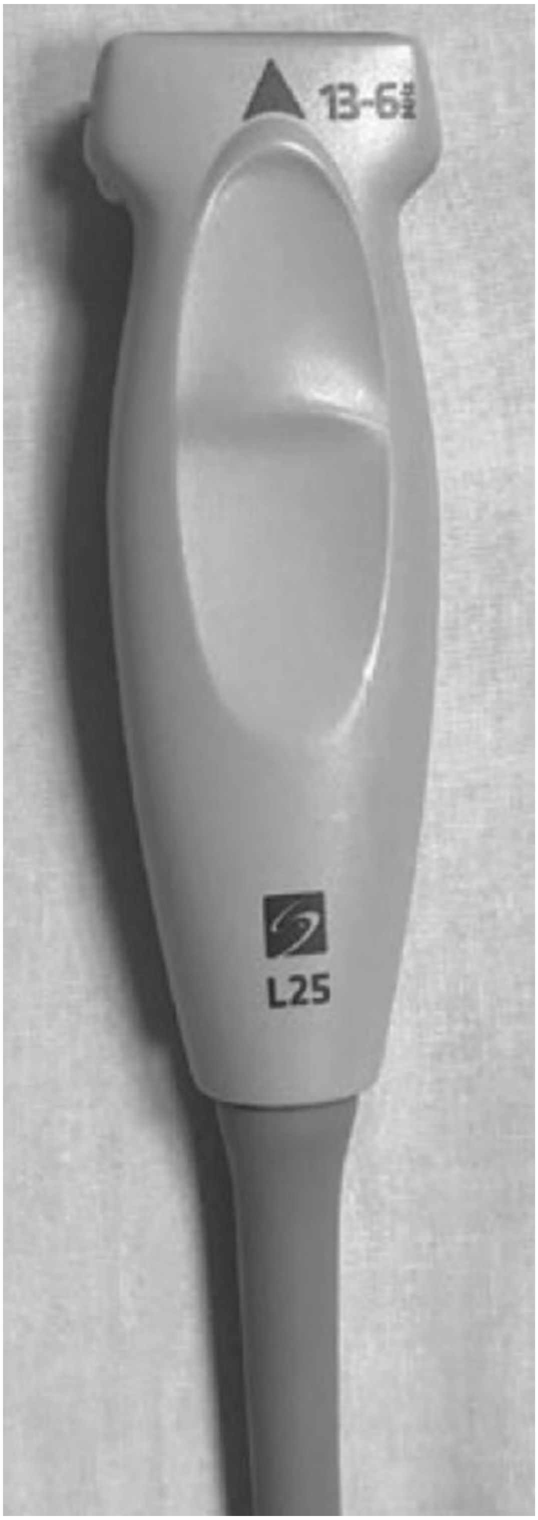

Fig. 5 Linear Array Transducer (Diagram and adapted caption courtesy of Creditt et al. 2017 Springer)

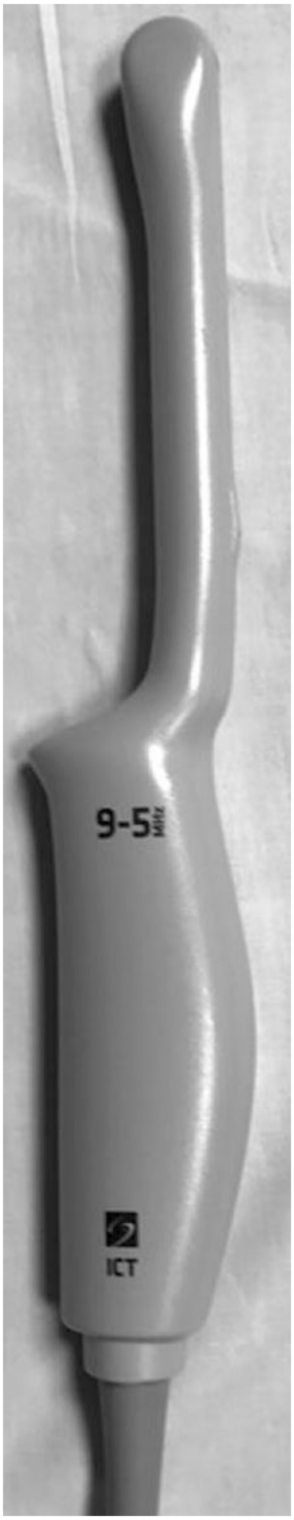

Fig. 6 Endocavitary transducer (Diagram and adapted caption courtesy of Creditt et al. 2017 Springer)

to posterior), the marker should be pointed towards the patient's head or cephalad (Fig. 9). In the coronal plane (transducer lateral to the patient's body) the marker should point towards the patient's head by convention (Fig. 10).

6 Doppler Sonography

Doppler sonography provides crucial information about the flow of blood within the body, including both direction and velocity. The Doppler effect was first described by Austrian physicist Christian Doppler in the 1840s [19]. It states that a sound wave that is reflected from a moving object undergoes a change or shift in frequency. More specifically, if an object is moving towards the transducer the incident wave will have a lower frequency than the reflected sound wave and vice-versa for objects moving away from the transducer. In medical imaging, this effect can be harnessed to calculate blood velocity, utilizing sound waves that are reflected by the traveling red blood cells (Fig. 11). The blood flow velocity is calculated as a function of incident angle, emitted and received frequencies based on the following equation:

$$V = \left(F_r - F_0\right) \cdot \left(\frac{c}{\cos\alpha \cdot 2F_0}\right),$$ where V is the blood flow velocity, F_r is received frequency, F_0 is the transmitted frequency, c is the speed of sound in the soft tissue, α is the angle between the transmitted beam and the direction of blood flow [9].

As velocity is a function of the cosine of the incident angle, special attention is required to ensure the Doppler angle is at or below 60 degrees. Even minor deviations greater than 60 degrees will lead to inaccurate velocity calculations given the properties of a cosine curve.

6.1 Pulsed Wave Doppler

Pulsed wave doppler is utilized to further characterize and quantify changes in flow over time. Similar to gray-scale brightness-mode image generation, pulsed wave Doppler systems operate by transmitting a short pulse, switching off for a time interval, and then switching back on. Reflected waves arriving during the switched off time period are not evaluated. By controlling the Doppler gate or "listening time" we can interrogate a vessel of a particular depth. The Doppler gate is defined by the time interval that the system is actively "listening" to the returning echoes [22].

Imagine you are a rubber ball that is so elastic that it always bounces back to exactly where it was thrown from. Now see yourself as "the ball" cocked in a sling shot on a racquetball court which is then subsequently launched.

Before you are launched, two things are known: one is that you will be traveling at a constant velocity through sound, while the second is that the distance between the launch and the racquetball court wall is fixed. The time it will take from you to come back or in physics terms the "round-trip time" can be calculated. This can be obtained by dividing

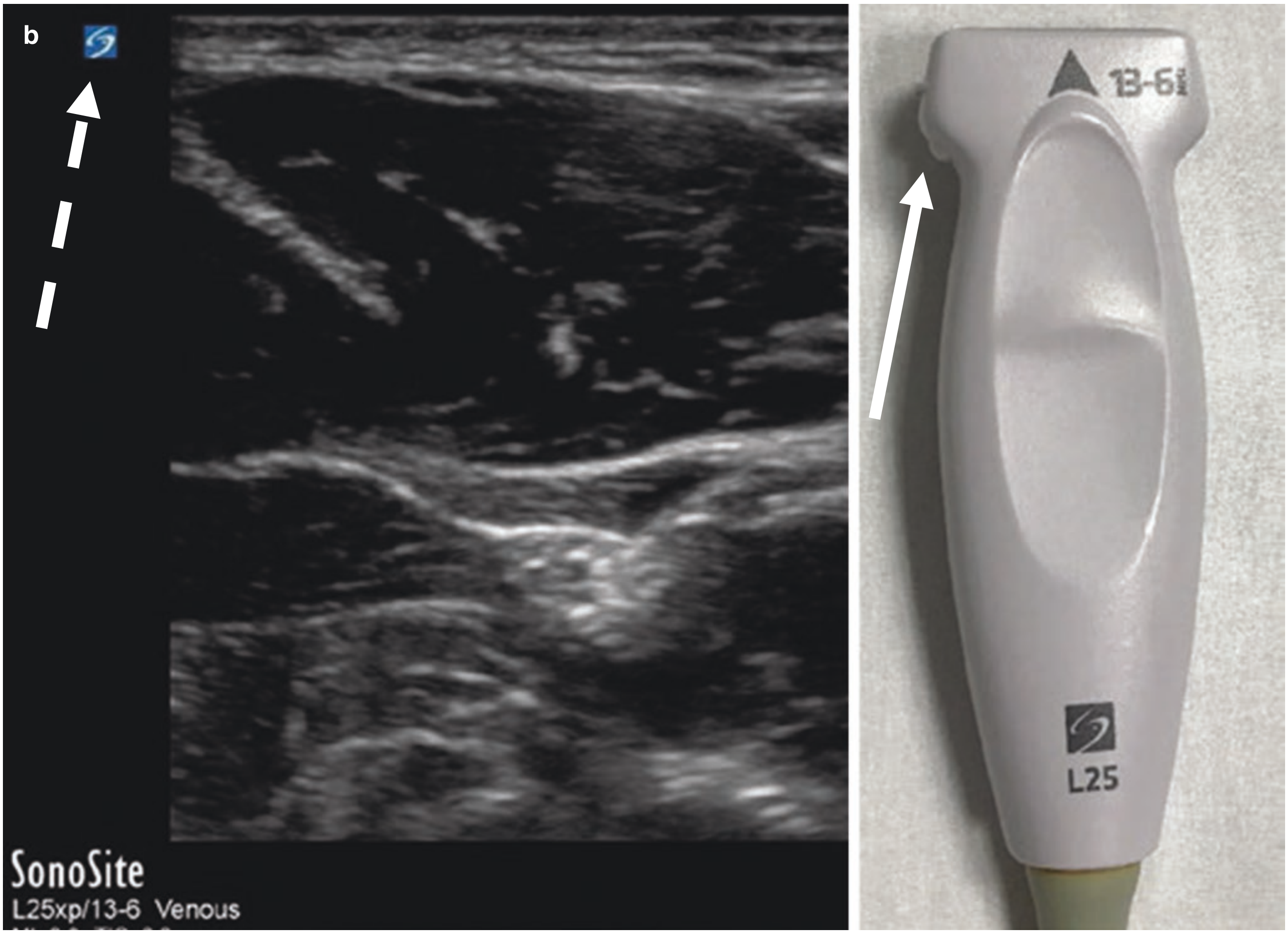

Fig. 7 The small bump (arrow) on the left side of the transducer corresponds to the blue box on the left side of the image screen (dashed arrow). (Diagram and adapted caption courtesy of Creditt et al. 2017 Springer)

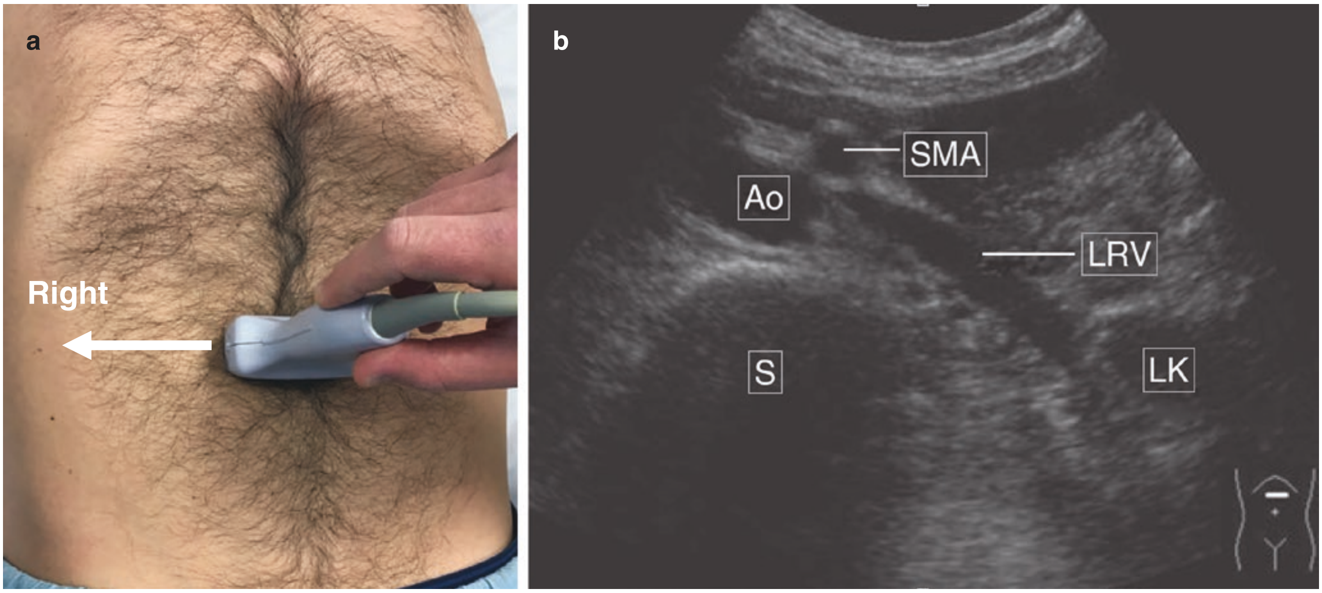

Fig. 8 Transverse plane: (**a**) The transducer marker is directed towards the patient's right side (**b**) Corresponding ultrasound image: *Ao* Aorta, *SMA* superior mesenteric artery, *LRV* left renal vein, *S* Spine, *LK* left kidney. (Diagram and adapted caption courtesy of Creditt et al. 2017 and Xu et al. 2018 Springer)

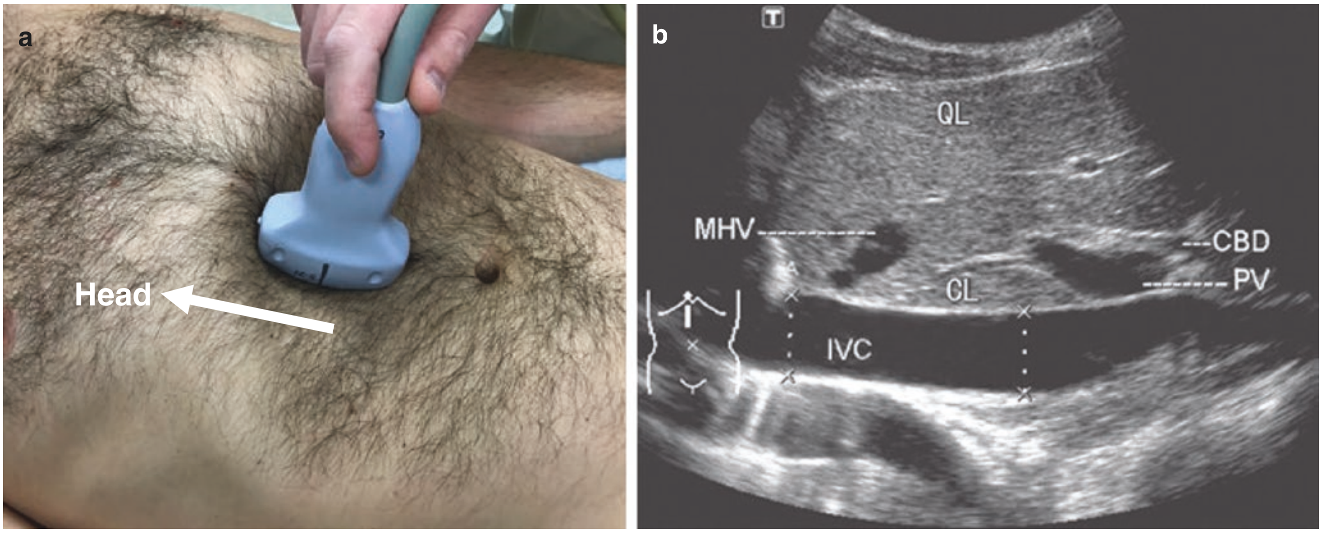

Fig. 9 Sagittal plane: (**a**) The transducer marker is directed towards the patient's head with the transducer positioned at the midline of the abdomen (**b**) Corresponding ultrasound image: *MHV* middle hepatic vein, *QL* quadrate hepatic lobe, *CL* caudate hepatic lobe, *CBD* common bile duct, *PV* portal vein, *IVC* inferior vena cava. (Diagram and adapted caption courtesy of Creditt et al. 2017 and Zang 2018 Springer)

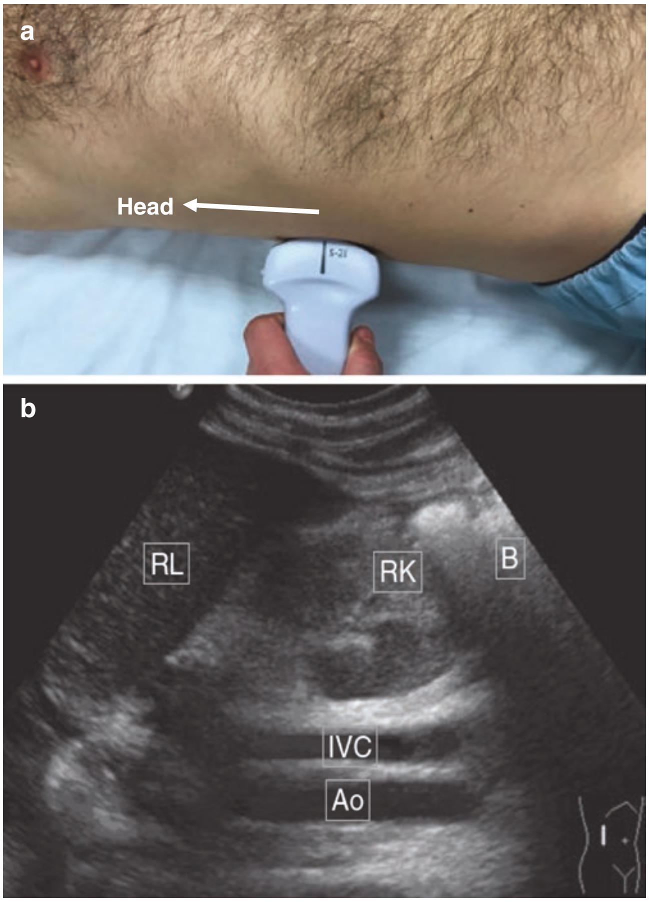

Fig. 10 Coronal plane: (**a**) The transducer marker is directed towards the patient's head with the transducer positioned on the lateral side of the abdomen. (**b**) Corresponding ultrasound image: *RL* right hepatic lobe, *RK* right kidney, *B* Bowel, *IVC* inferior vena cava, *Ao* abdominal aorta (Diagram and adapted caption courtesy of Creditt et al. 2017 and Xu et al. 2018 Springer)

the distance between the wall and launch site by the velocity of the rubber ball traveling in air.

This concept allows the sonographer to selectively listen to certain vascular structures by "turning on" the transducer during the time interval we expect the signal from a vessel to be coming back while ignoring the other signals. To "turn on" the transducer we can create what is called a time-filter. This process allows for selectively interrogating a particular vessel at a certain depth. The combination of 2D-real time gray scale imaging and pulsed Doppler sonography is called Duplex Doppler Sonography. This is the standard technique utilized to evaluate for deep venous thrombosis.

6.2 Color Doppler

Color Doppler ultrasound displays flow data in color for a defined area, superimposed on a 2D gray scale image. As discussed, in standard duplex ultrasound, a sample volume is outlined in the real time gray scale image for which Doppler shift frequencies are obtained by interpreting separate scan lines. In regards to color Doppler, simultaneously measuring flow velocities at different vessel sites requires multiple sample volumes to be placed along adjacent beam paths. However, this data cannot be interpreted by Fourier transform due to time constraints and the copious amount of data acquired. Instead, a technique called autocorrelation is utilized. This technique compares two consecutive reflected beams from the sampled sites for a given color scan line to identify phase shifts in order to estimate mean Doppler shift frequency [23].

The mean frequency shift is utilized to determine the color shade. Low frequency shifts are assigned a darker color

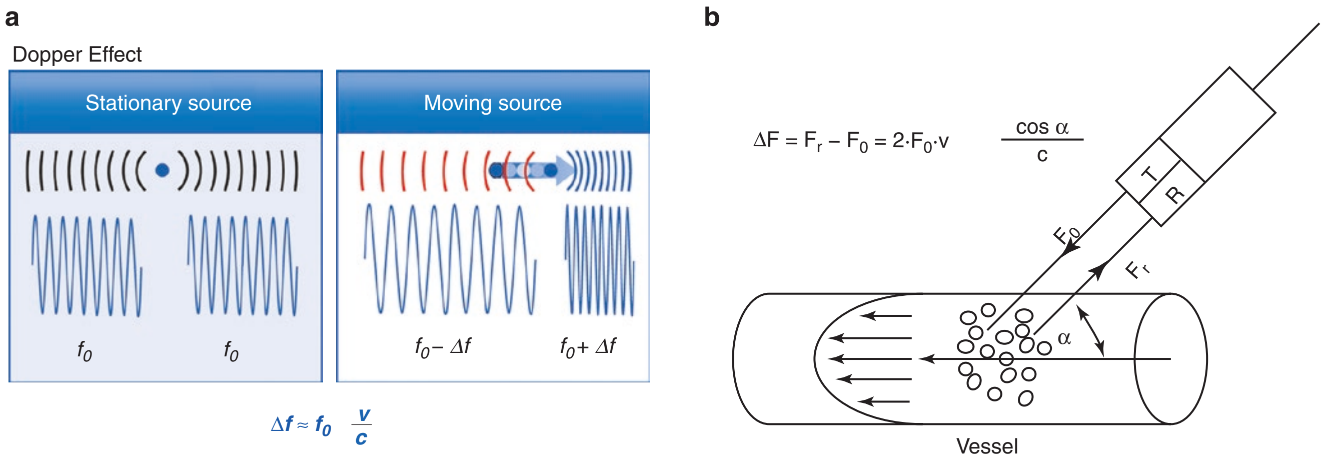

Fig. 11 Doppler effect. (**a**) Dependence of the Doppler shift (change in frequency between source and receiver) on the velocity of the moving source and its direction of motion relative to the reflector. (**b**) Diagram of Doppler interrogation of a vessel with laminar blood flow. The arrows in the vessel are vectors representing different flow velocities. Blood flow is fastest in the center and decreases toward the wall. The drawing illustrates the effect of the angle of incidence on the Doppler measurement. In the equation for calculating the Doppler shift, the cosine of this angle is utilized. The Doppler shift increases with the acuity of the angle (cosine of 90° = 0) (*T* transmitter, *R* receiver, F_0, emitted frequency, F_r reflected frequency). (Diagram and adapted caption courtesy of Schäberle et.al 2018 Springer)

while high-frequency shifts are assigned a lighter color. In addition, based on the phase shift away or towards the transducer, a blue or red color is assigned respectively (Fig. 12).

6.3 Power Doppler

Unlike color Doppler which utilizes frequency shifts to determine blood flow, power Doppler utilizes the amplitude of the Doppler signal. Differing hues of a single color reflecting the total energy of the received wave are utilized to represent blood flow. Power Doppler does not provide information regarding directionality of blood flow, however it is superior in detecting slow flow and is largely independent of the Doppler angle [24].

7 Artifacts

The generation of ultrasound images is based on several assumptions. These assumptions include that the only source of sound wave generation is the ultrasound transducer, that sound waves travel in a linear fashion and at a constant velocity, that attenuation is uniform within a scan plane, and that each reflector in the body will produce a single echo. Any deviation from these assumptions results in artifacts, which can provide important diagnostic information on tissue composition. Artifacts can often be distinguished by physically shifting the transducer. Actual tissue structures will remain visible, while artifacts will change position or may even disappear.

7.1 Shadowing

Shadowing is a common artifact utilized to characterize structures (Fig. 13). It occurs when sound waves are predominantly reflected off the tissue interface and/or absorbed. As discussed in the previous sections, shadowing occurs behind air secondary to increased reflection at air-tissue interfaces. An incident sound wave will be predominantly reflected, although some will interact with interfaces in front of the air, producing secondary reflections that travel back to the air surface. This results in secondary reflections which are received by the transducer manifesting as low-level echoes behind an air interface. This accounts for the “dirty shadowing” appearance which is often a sign that a structure contains air [25].

Shadowing also occurs secondary to increased absorption by osseous structures and calcifications [26], as can be seen with gallstones (Fig. 13). This limits the energy available for the generation of secondary reflections, with associated shadows appearing more anechoic posterior to the calcified/ossified structures. This creates a “clean shadowing” appearance.

7.2 Posterior Enhancement

Posterior acoustic enhancement is helpful in identifying cystic structures that contain fluid. Sound waves are much less attenuated by fluid-filled structures than by solids and therefore possess greater strength after passing through a fluid structure. As a result, structures deep to fluid-filled struc-

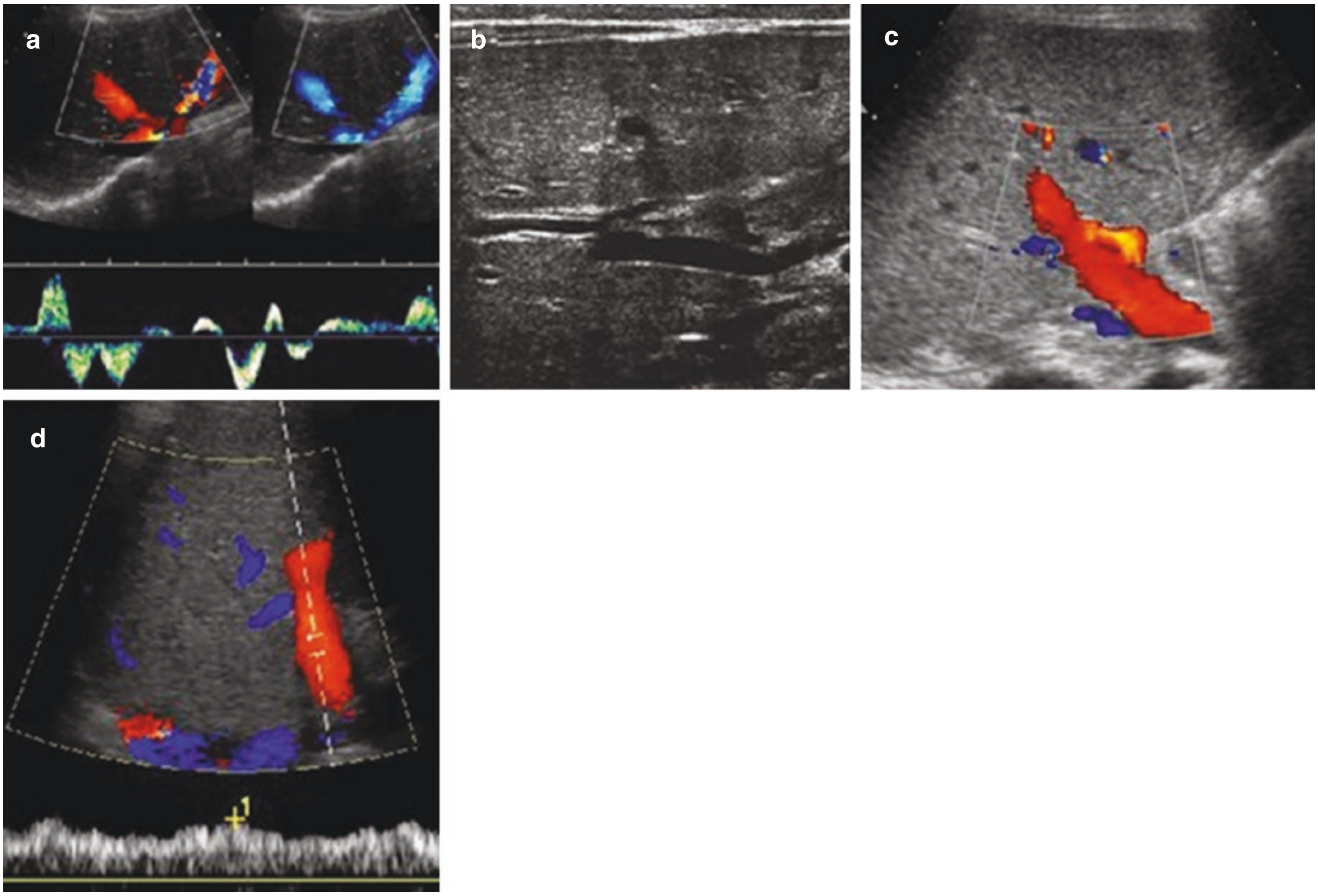

Fig. 12 Liver vessels: (**a**) Hepatic veins, bidirectional undulating flow demonstrated by color doppler signal (either red or blue signals, indicating two flow directions during the respiratory cycle) with cardiac and respiratory modulation also demonstrated by spectral flow analysis. (**b**) Main portal vein entering liver on gray-scale imaging (**c**) Main portal vein flow on color Doppler (red color signals) (**d**) Duplex-Doppler flow profile confirms appropriate directionality of portal flow, where +1 indicates maximum velocity. (Diagram and adapted caption courtesy of Riccabona 2014 Springer)

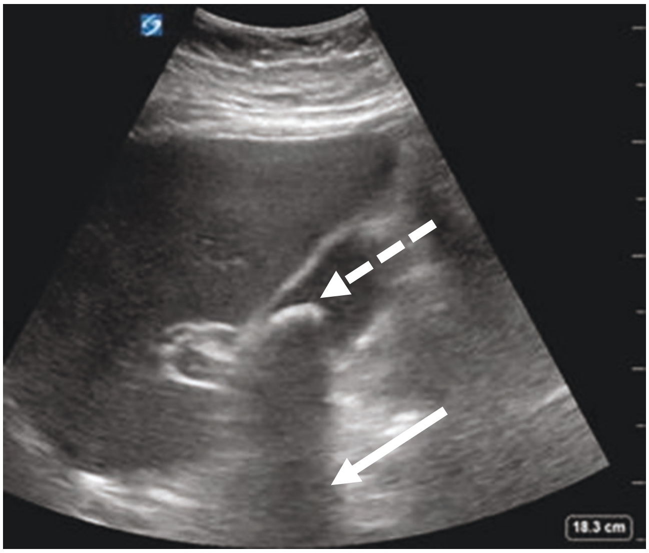

Fig. 13 Gallstone shadowing: Posterior acoustic shadowing (arrow) helps properly identify gallstones (dashed arrow) within the gallbladder and can help distinguish stones from other structures such as polyps. (Diagram and adapted caption courtesy of Vitto et.al 2018 Springer)

tures, such as a cyst, will produce stronger reflections and appear brighter (also known as increased through transmission) (Fig. 14) [25, 26].

7.3 Mirror Images

If we think about a mirror, it is a highly reflective surface that is smooth. Air is the best acoustic mirror in the human body as it is a highly reflective surface for sound waves (see Sect. 3.1). Thus, the interfaces between air and soft tissue are prone to producing mirror images. The base of the right lung can often serve as a mirror on abdominal ultrasounds, duplicating the liver, diaphragm or other right upper quadrant structures (Fig. 15). The trachea also provides a smooth air-soft tissue interface, acting as a mirror for neck structures [25, 27].

7.4 Reverberation

Reverberation artifact (Fig. 16) occurs when there is a strong reflective surface in the near field. A highly reflective surface

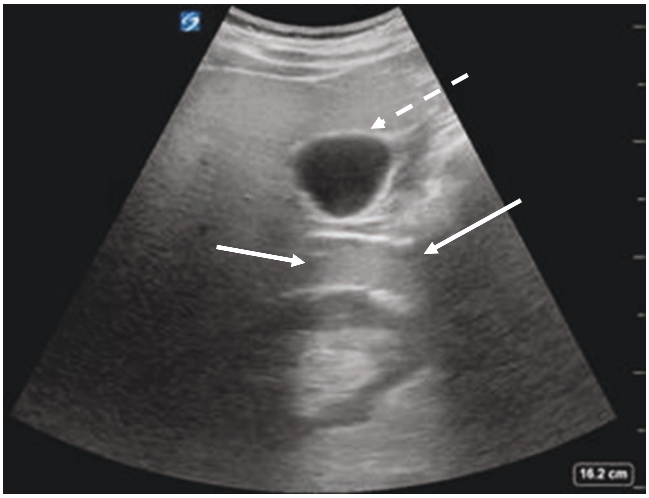

Fig. 14 Gallbladder with posterior acoustic shadowing: As sound passes through fluid-filled structures, such as the gallbladder (dashed arrow), acoustic energy is increased resulting in posterior acoustic enhancement in which the structures posterior to the structure appear brighter (solid white arrows). (Diagram and adapted caption courtesy of Vitto et.al 2018 Springer)

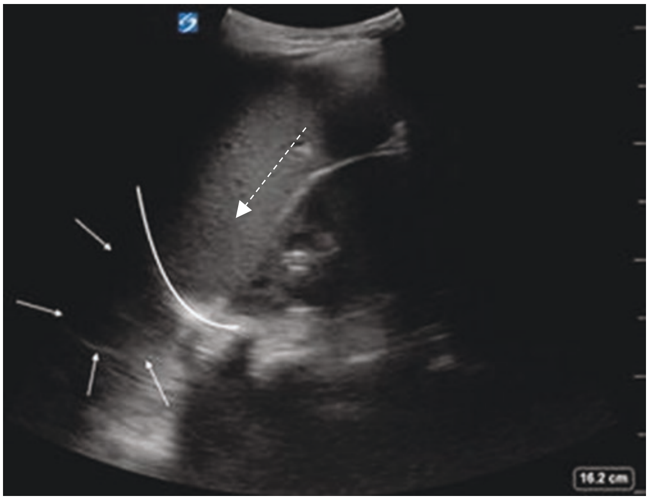

Fig. 15 Liver with mirror artifact: In the image above, there appears to be two livers, one above (dashed arrow) and one below (white arrows) the diaphragm (white line). (Diagram courtesy of Vitto et.al 2018 Springer)

may produce a reflective sound wave that is strong enough to be reflected off the transducer itself and back into the body, which can then interact with the near-field reflective surface multiple more times, creating a ping-pong like effect [25]. As a result, the subsequent echoes produced are interpreted as arising deep to the original reflective surface in the near field. This can produce bright bands or low-level echoes, best appreciated at the superficial aspect of the cystic structures [27]. This can often be mitigated by repositioning the transducer.

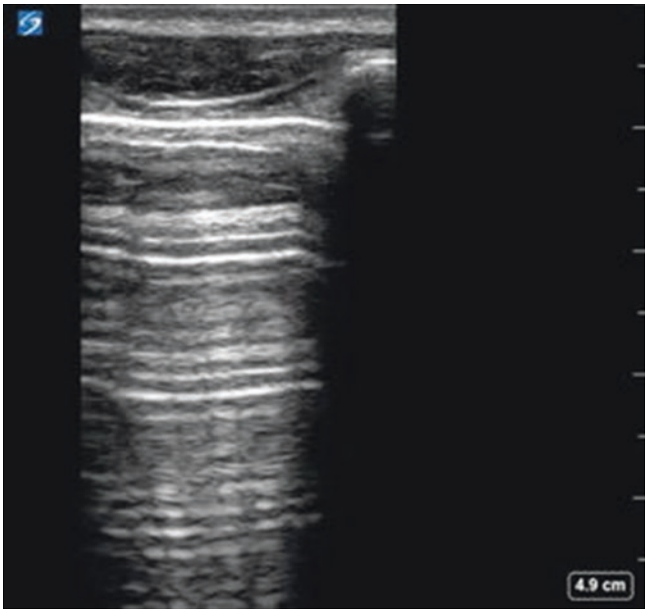

Fig. 16 Imaging of lung tissue with reverberation artifact: When sound bounces between two greatly reflective structures, it will reverberate over and over, creating a line of sound down the image screen known as reverberation artifact. It is seen here with the pleural line of the lungs. (Diagram and adapted caption courtesy of Vitto et.al 2018 Springer)

7.5 Ring Down

When a sound wave interacts with air bubbles that have trapped fluid between them, the fluid can be excited, causing the fluid to resonate or ring like a tuning fork. This causes a continuous sound wave to be generated and transmitted back to the transducer along with the original echo. The sound generated is interpreted as having originated from reflector surfaces deep to the air surface, thus a series of bright echoes are produced deep to the air [25, 26]. Ring down artifacts can be seen in the setting of air-filled bowel or when imaging metal.

7.6 Comet Tail

A comet tail artifact is similar to a ring-down artifact with small, bright, linear artifacts seen deep to highly reflective targets [27]. This is an artifact that helps to identify cholesterol crystal deposition within the gallbladder wall (Fig. 17).

7.7 Side Lobe

The majority of sound waves transmitted into the body are concentrated in the center and are called the main lobe. There are weaker sound beams on either side of the

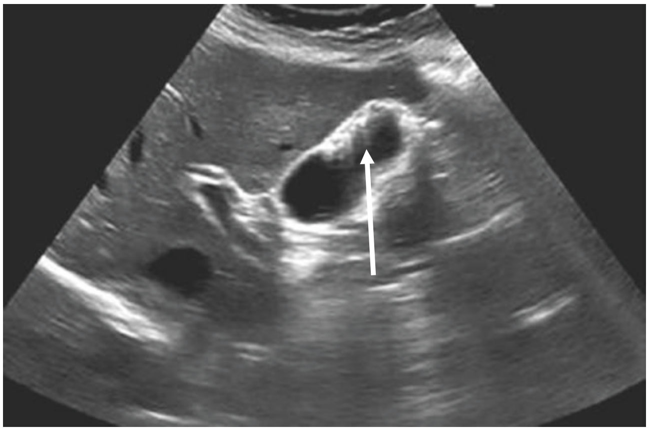

Fig. 17 Echogenic intramural foci with comet-tail artifacts (arrow) indicative of cholesterol crystals within Rokitansky-Aschoff sinuses and diagnostic of adenomyomatosis of the gallbladder. (Diagram and adapted caption courtesy of Nicolau et.al 2012 Springer)

center beam called side-lobes. These side-lobe beams come into play only when there is a strong-reflective surface from which reflections are generated. These obliquely deflected side-lobe echoes are processed as if they were originating as echoes from the main beam and are misrepresented in the generated ultrasound image [25–27].

7.8 Anisotropy

Anisotropy describes the property of being directionally dependent. In the field of ultrasound imaging, this manifests as alterations in displayed echogenicity when imaging tissues based on different angles. For example, when imaging tendons (which have unidirectionally oriented fibers), a scan which is performed perpendicular to the long axis of the tendon will produce a strong reflection and a brighter image. On the other hand, incident sound waves generated from angling the transducer and deviating from 90 degrees to the longitudinal plane of the tendon fibers will result in weaker reflections [25].

7.9 Transducer Piezoelectric Crystal Failure

Quality control is an essential aspect of ultrasound imaging. Dysfunction of the piezoelectric crystals will lead to an ultrasound image that contains dark bands that can appear to be radiating from the transducer. These dark bands will maintain their position even when the transducer is moved [25].

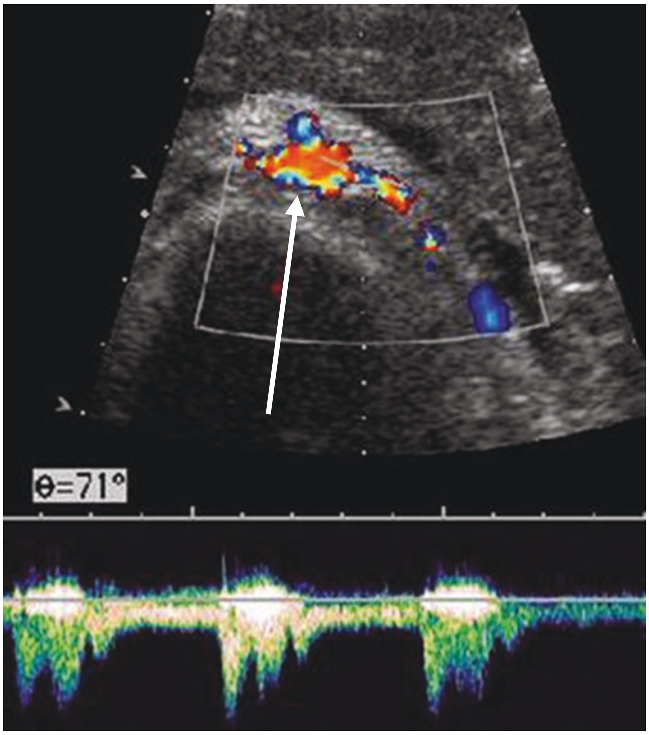

Fig. 18 Elevated flow velocity with turbulent atypical flow at the site of left renal artery stenosis, also seen as aliasing (arrow) of color doppler signals and narrow vessel diameter. (Diagram and adapted caption courtesy of Riccabona et.al 2014 Springer)

8 Aliasing

In the field of ultrasound imaging, the minimum sampling rate for the analog ultrasound echo is at least twice that of the Doppler frequency shift [25, 28]. Sampling below this rate will lead to aliasing, with the highest frequency components misrepresented in the digitized output. This manifests as a wraparound of high-frequency signals from the extremes of the color scale [28] (Fig. 18). Aliasing can be distinguished from a true change in flow direction, as the former will result in changes between lighter color shades. In severe aliasing, multiple wraparounds can be seen. This can serve as a surrogate marker for a region of high velocity flow.

Aliasing can be reduced by increasing the pulse repetition frequency. However, the maximum pulse repetition frequency is limited by vessel depth, as a finite wait time is required to receive an echo before generating a second pulse [25]. The other option would be to reduce the observed frequency shift, thus allowing the system to utilize a lower sampling rate. Given that the observed frequency shift is a function of cosine, increasing the Doppler angle closer to 90 degrees can decrease the observed frequency shift.

8.1 Tissue Vibration

In regions of turbulent flow within a vessel, pressure variabilities in the lumen of the vessel produce vibrations within the vessel wall and adjacent peri-vascular soft tissues. These vibrations may result in the production of a Doppler frequency shift which will be displayed as a mixture of colors reflecting the variable vibration directions [25, 29]. Tissue vibration artifact can be seen with pseudoaneurysms, aneurysms, and arteriovenous fistulas as well as other conditions which promote turbulent flow.

8.2 Twinkle

Twinkle artifact manifests on color Doppler imaging, and arises due to signal aliasing extending deep from the surface of a strongly reflective tissue interface [25, 29] (Fig. 19). Twinkle artifact can often be used to detect nephrolithiasis, particularly in cases where the gray scale imaging findings may be equivocal.

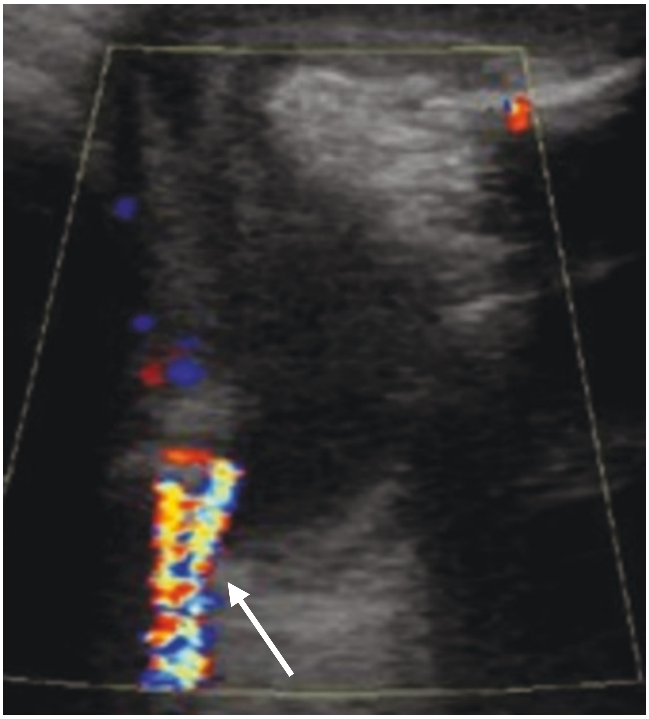

Fig. 19 Twinkling artifact (arrow) caused by an urethral stone. (Diagram and adapted caption courtesy of Riccabona et.al 2014 Springer)

9 Conclusion

Ultrasound utilizes soundwaves with frequencies above the range of human hearing to image the human body. The piezoelectric crystal within the ultrasound transducer serves as both the generator of inciting sound waves and the receiver for reflected sound waves. These reflected waves are then processed and displayed as images. A key concept to remember is that ultrasound does not strictly depict tissue structures but rather the interfaces between tissues of differing acoustic impedances. Gray scale images provide structural information while Doppler imaging helps further characterize vasculature. These techniques are commonly utilized together in clinical practice. Lastly, ultrasound can act differently at differing tissue interfaces, resulting in several types of artifacts. These artifacts, at times, can provide valuable information regarding the underlying pathology.

References

1. Coltrera MD. Ultrasound physics in a nutshell. Otolaryngol Clin N Am. 2010;43(6):1149–59.
2. Thorsen AJ, Lakin GE. Basic physics of ultrasonography. In: Seminars in colon and rectal surgery, vol. 4: Elsevier; 2010. p. 186–90.
3. Wells PN. Physics and bioeffects. In: Diagnostic ultrasound. 2nd ed: CRC Press; 2008. p. 14–31.
4. Creditt A, Tozer J, Vitto M, Joyce M, Taylor L. Clinical ultrasound: a pocket manual: Springer; 2017. p. 1–18.
5. Boote EJ. AAPM/RSNA physics tutorial for residents: topics in US: Doppler US techniques: concepts of blood flow detection and flow dynamics. Radiographics. 2003;23(5):1315–27.
6. Ziskin MC. Fundamental physics of ultrasound and its propagation in tissue. Radiographics. 1993;13(3):705–9.
7. Aldrich JE. Basic physics of ultrasound imaging. Crit Care Med. 2007;35(5):S131–7.
8. Abu-Zidan FM, Hefny AF, Corr P. Clinical ultrasound physics. J Emerg Trauma Shock. 2011;4(4):501.
9. Schäberle W. Ultrasonography in vascular diagnosis: a therapy-oriented textbook and atlas: Springer; 2018. p. 3–49.
10. Chan V, Perlas A. Basics of ultrasound imaging. In: Atlas of ultrasound-guided procedures in interventional pain management: Springer; 2011. p. 13–9.
11. Shung KK, Sigelmann RA, Reid JM. Scattering of ultrasound by blood. IEEE Trans Biomed Eng. 1976;6:460–7.
12. Pinton G, Aubry JF, Bossy E, Muller M, Pernot M, Tanter M. Attenuation, scattering, and absorption of ultrasound in the skull bone. Med Phys. 2012;39(1):299–307.
13. Jirık R, Taxt T, Jan J. Ultrasound attenuation imaging. J Electr Eng. 2004;55(7-8):180–7.
14. Hangiandreou NJ. AAPM/RSNA physics tutorial for residents: topics in US: B-mode US: basic concepts and new technology. Radiographics. 2003;23(4):1019–33.

15. Burckhardt CB. Speckle in ultrasound B-mode scans. IEEE Trans Sonics Ultrason. 1978;25(1):1–6.
16. Case TD. Ultrasound physics and instrumentation. Surg Clin N Am. 1998;78(2):197–217.
17. Shriki J. Ultrasound physics. Crit Care Clin. 2014;30(1):1–24.
18. Martin K. Introduction to B-mode imaging. Diagn Ultrasoun Phys Equip. 2010:1–22.
19. White D. Johann Christian Doppler and his effect—a brief history. Ultrasound Med Biol. 1982;8(6):583–91.
20. Lieu D. Ultrasound physics and instrumentation for pathologists. Arch Pathol Lab Med. 2010;134(10):1541–56.
21. Gautschi G. Piezoelectric sensors. In: Piezoelectric Sensorics: Springer; 2002. p. 73–91.
22. Nelson T, Pretorius D. The Doppler signal: where does it come from and what does it mean? Am J Roentgenol. 1988;151(3):439–47.
23. Loupas T, Powers J, Gill RW. An axial velocity estimator for ultrasound blood flow imaging, based on a full evaluation of the Doppler equation by means of a two-dimensional autocorrelation approach. IEEE Trans Ultrason Ferroelectr Freq Control. 1995;42(4):672–88.
24. Bude RO, Rubin JM. Power Doppler sonography. Radiology. 1996;200(1):21–3.
25. Hertzberg BS, Middleton WD. Ultrasound: the requisites. Elsevier Health Sci. 2015:3–39.
26. Kirberger RM. Imaging artifacts in diagnostic ultrasound—a review. Vet Radiol Ultrasound. 1995;36(4):297–306.
27. Scanlan KA. Sonographic artifacts and their origins. AJR Am J Roentgenol. 1991;156(6):1267–72.
28. Mitchell DG. Color Doppler imaging: principles, limitations, and artifacts. Radiology. 1990;177(1):1–10.
29. Hindi A, Peterson C, Barr RG. Artifacts in diagnostic ultrasound. Rep Med Imaging. 2013;6:29–48.

Ultrasound Probe Selection, Knobology and Optimization of Image Quality

Marcelle Blessing

1 Introduction

Ultrasound has become an invaluable tool for various medical specialties as the clinical applications continue to broaden. Comprehensive ultrasound evaluations have always been available for subspecialties such as gynecology or cardiology. As small, laptop-sized ultrasound machines have become commonplace in many clinical settings, a broad range of clinicians can now incorporate ultrasound into their daily practice. New portable, pocket-sized hand held ultrasound devices will likely make bedside point-of-care ultrasound even more common. A thorough understanding of ultrasound equipment is needed for success in using it for imaging and procedural guidance. If the wrong probe is chosen for a specific purpose, the technical difficulty is increased while also potentially compromising procedural safety. Without image optimization, key anatomy may not be visualized. Fortunately, appropriate probe selection is not difficult. In addition, optimization of the target and needle visualization require only a few easily mastered maneuvers and adjustments. For many tasks, there are multiple probe types that would be appropriate. This chapter will review the basic equipment, machine settings, image optimization techniques and nomenclature needed for bedside ultrasound.

2 Probe Selection

The frequency of sound waves used for ultrasound in medicine range from 1–20 MHz. As ultrasound frequencies vary based on probe selection, different ultrasound probes are utilized to optimize different fields of view. Each probe is programmable for a range of frequencies within the aforementioned limits. This range of frequencies is referred to as bandwidth. Probes are described by the frequencies they use and by the size and shape of their face (“footprint”) (Fig. 1).

Piezoelectric crystals in the ultrasound probe send and receive sound waves to create images. The arrangement of these piezoelectric crystals in the transducer determine the shape of the image the probe will obtain.

Linear probes use high frequency (6–15 MHz) ultrasound beams to visualize shallow structures with high axial and lateral resolution. The piezoelectric crystals are arranged in a straight line within a flat transducer. Ultrasound beams emerge perpendicular to the line of transducer elements and parallel to each other, creating a rectangular shaped image with a linear surface. Clear images of superficial structures are created at the expense of visualizing deeper structures because of the probe’s high resolution and poor penetration. Attenuation occurs as high frequency sound waves attempt to penetrate deeper structures. As such, their role is limited to visualizing structures to a depth of 4 cm (Fig. 2).

Lower frequency (1–5 MHz) curvilinear probes permit imaging of deeper structures, while providing a wider depth of field with less resolution. This occurs due to the fact that the crystals are arranged in a curve, resulting in a fan-shaped ultrasound beam. The field of view is wider than the footprint of the probe, creating a sector or “pie-shaped” image. Images produced always have a curved surface. Curvilinear probes are ideal for deeper peripheral nerve blocks, central neuraxial blocks and intra-abdominal exams (Fig. 3). They are particularly helpful for obese patients. Curved probes with a smaller footprint are useful for performing deeper nerve blocks in small areas, such as with infraclavicular nerve blocks.

Phased array probes are ideally suited for echocardiography. Like curvilinear probes, their lower frequencies (typically 2–8 MHz) penetrate deeper structures, providing a large depth of field; however, their small, flat footprint makes them ideal for situations such as visualizing between ribs. A small number of piezoelectric crystals arranged closely together generate a sectorial view, allowing sound waves to be delivered from a single point while fanning outward.

M. Blessing (✉)
Yale University School of Medicine, Department of Anesthesiology, New Haven, CT, USA
e-mail: marcelle.blessing@yale.edu

© Springer Nature Switzerland AG 2021

J. Li et al. (eds.), *Ultrasound Fundamentals*, https://doi.org/10.1007/978-3-030-46839-2_2

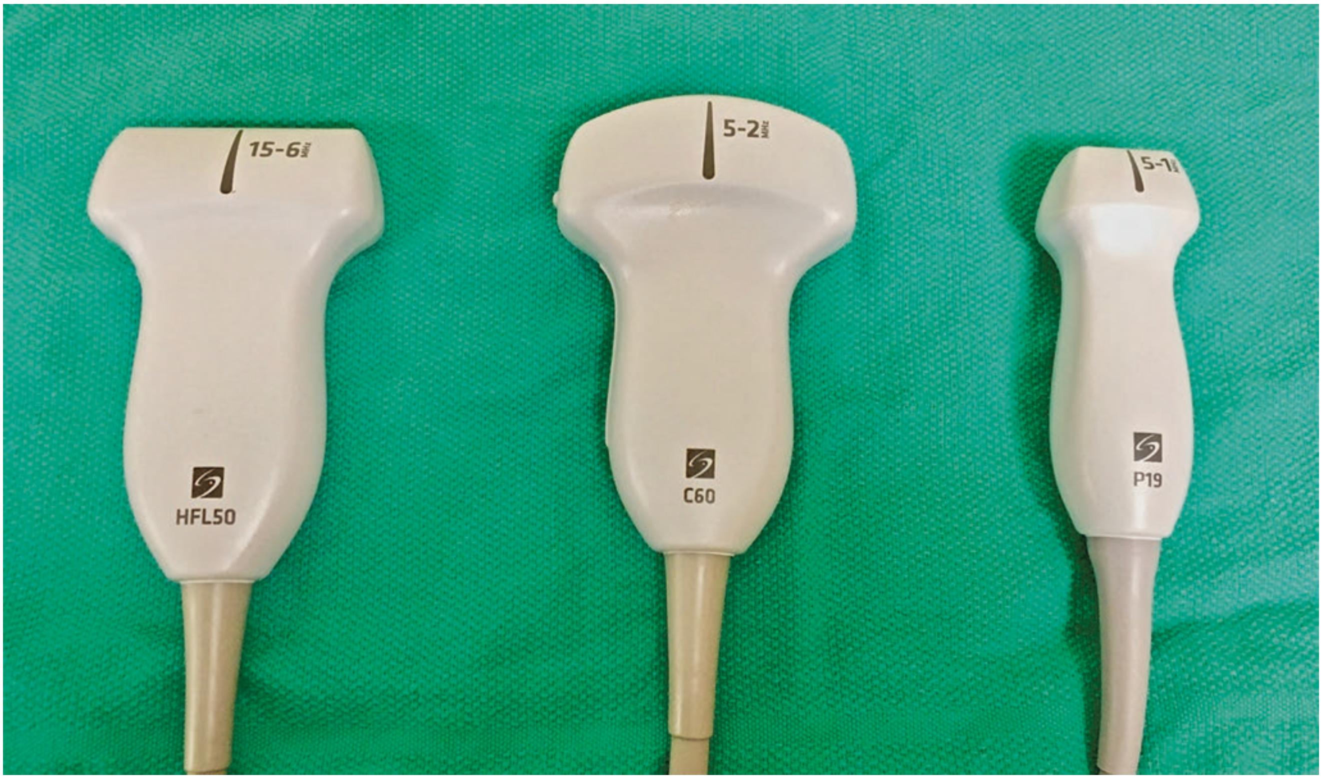

Fig. 1 Examples of common ultrasound probes (left to right): linear probe, curvilinear probe, phased array probe

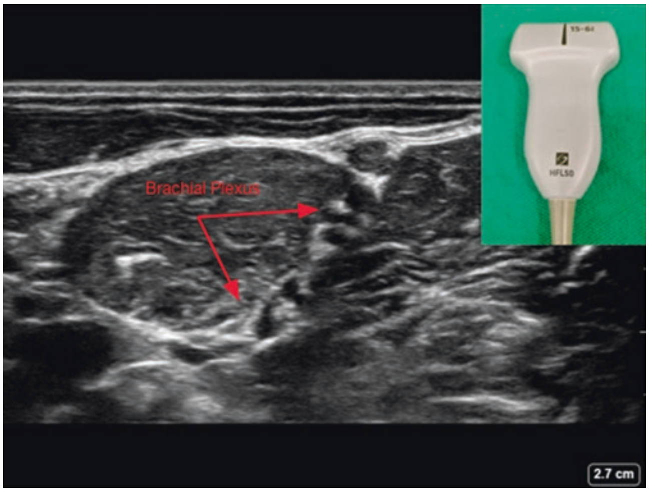

Fig. 2 A linear ultrasound probe and subsequent image obtained of the brachial plexus within the interscalene groove. Note the shallow depth (2.7 cm) and high resolution of superficial structures

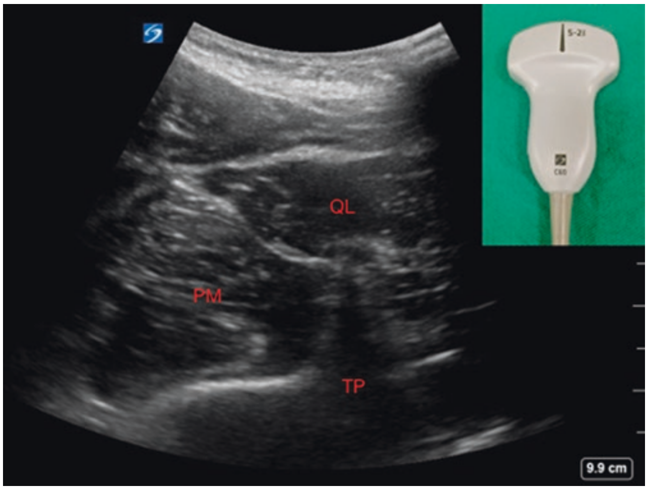

Fig. 3 A curvilinear ultrasound probe and the image obtained of the quadratus lumborum muscle. Note the decrease in resolution of superficial structures compared to Fig. 2, and greater depth of image. *QL* quadratus lumborum, *TP* transverse process, *PM* psoas major

Several other types of specialized probes exist to serve specific subspecialties. Transesophageal probes, endovaginal probes and endorectal probes are examples of specialized endocavitary probes. Endobronchial ultrasound is performed using small ultrasound probes attached to flexible fiberoptic devices. Intravascular ultrasound (IVUS) makes use of miniature ultrasound probes attached to intravascular catheters to assess blood flow within vessels (Table 1).

Table 1 Applications of different probe types by specialty

Ultrasound Use	Recommended Probe
Anesthesiology: Nerve Blockade	Linear probe (superficial peripheral nerve blocks) Small footprint linear probe (pediatric blocks) Curvilinear probe (deep blocks, obese patients, neuraxial blocks)
Breast	Linear probe
Cardiology	Phased-array probe (transthoracic echo) TEE probe
Colorectal	Endocavitary probe (transanal/transrectal exam)
Dermatology	Linear probe
ER – eFAST exam	Curvilinear probe
Gastrointestinal	Curvilinear probe
Gynecological/Obstetrics	Endocavitary probe (transvaginal exam) Curvilinear probe (transabdominal exam)
Musculocutaneous	Linear probe (most common) Curvilinear (deeper structures, obese patients)
Neonatology	Phased-array probe (cranial exam) Linear probe (abdominal exam)
Ophthalmology	Small footprint linear probe
Otolaryngology	Linear probe
Vascular	Linear probe (neck and extremity vessels) Curvilinear probe (aorta and IVC) Intravascular probe (IVUS)

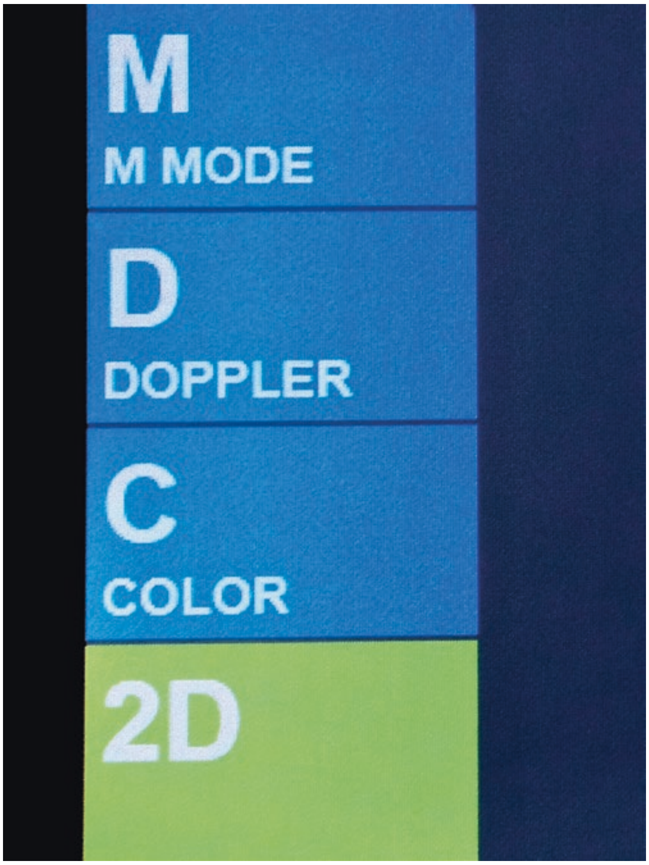

Fig. 4 Mode selection on a bedside ultrasound touchscreen

3 Knobology

Most ultrasound machines have presets that optimize scanning for specific tissue types. If the correct preset is chosen, often less adjustment of parameters will be needed to optimize image quality. The following parameters are commonly adjusted during ultrasound image acquisition:

Frequency: Once probe selection occurs, the range of frequencies has already been selected. For a given probe, the operator can choose a frequency in the upper, middle or lower range of a probe's bandwidth.

Mode: Most modern ultrasound machines utilize brightness or B-mode, also referred to as 2D mode, for both diagnostic visualization and real time procedural guidance. M-mode or motion mode is also available on most machines. M-mode displays B-mode images over time, and is especially useful in echocardiography. It can be combined with Doppler mode, which is used for assessing flow in the arteries and veins (Fig. 4).

Gain: Adjusting the brightness (or gain) is a crucial feature of modern ultrasound machines. Increasing the gain will make the image whiter. Many machines have an autogain setting that automatically sets the gain for the user. Gain can also be fine-tuned manually for either the whole image or within the near or far fields. Gain should be minimized to only what is needed to highlight the target structures. Excessive gain will cause increased noise in the background, making target structures harder to distinguish (Fig. 5). Time gain compensation (TGC) refers to the increased gain at greater depths. TGC attempts to offset the attenuation that occurs when imaging deeper structures, in order to keep the gain uniform across a field of depth.

Depth: The user can set the depth manually within the range that a probe penetrates. Depth should be minimized to only what is needed to visualize target structures. By decreasing depth, the superficial structures will be magnified and the resolution increases. Also, scanning at greater depths decreases the frame rate, thereby decreasing image quality. If ultrasound is used for procedural guidance, depth should be sufficient to visualize critical structures that could be damaged.

Focus: Adjusting the focus optimizes lateral resolution at a specific depth, by producing a narrow beam at the focal zone. Focus occurs for a target at a specific depth, not for the entire image.

Doppler: The Doppler principle is applied to color flow Doppler, power Doppler and pulse wave Doppler to assess blood flow. In color Doppler, blood flow is displayed in a window overlaying a B mode image. Red represents flow towards the transducer and blue represents flow away from

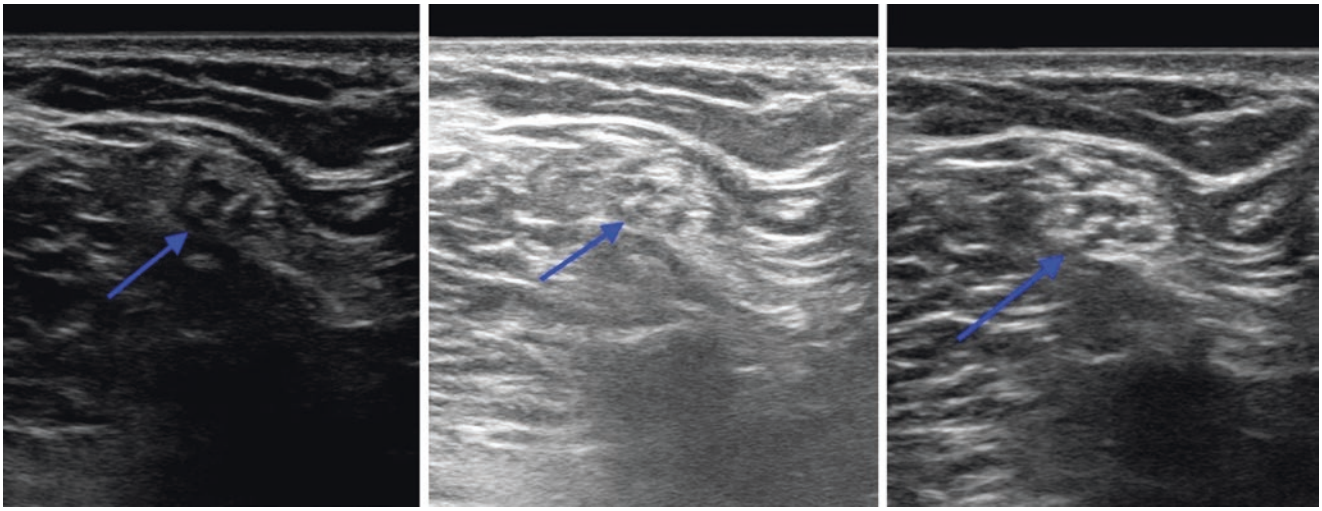

Fig. 5 An ultrasound image series of the tibial nerve with (from left to right): too little, too much, and appropriate gain. Note how appropriate gain settings enhance the contrast of the borders surrounding the nerve

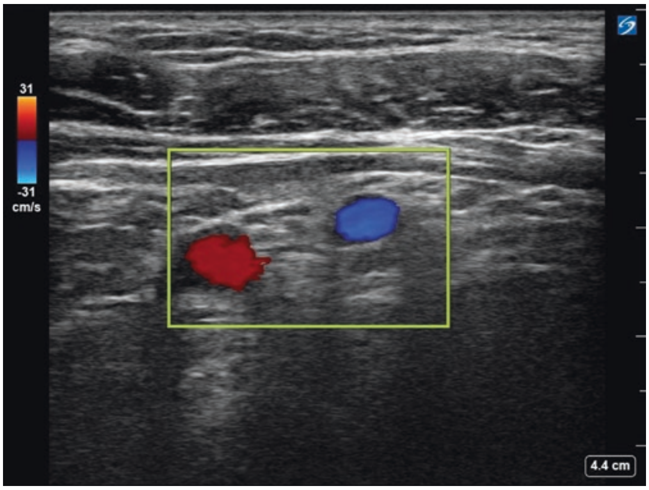

Fig. 6 A color flow Doppler ultrasound image of the brachial artery (left) and brachial vein (right) in the antecubital fossa

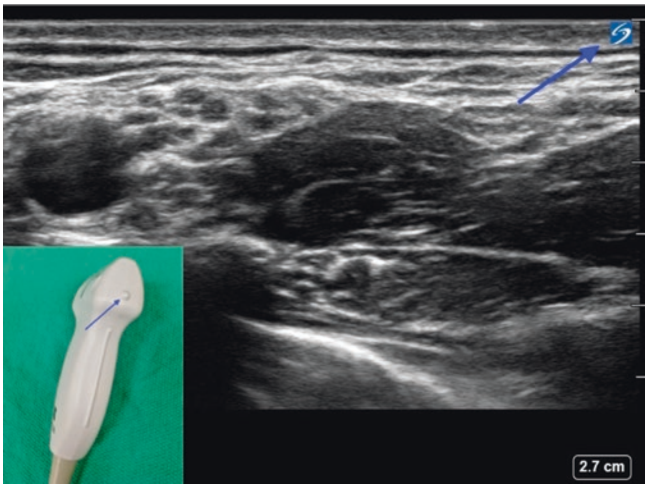

Fig. 7 A linear probe with orientation marker (blue arrow), and corresponding orientation marker on ultrasound screen (logo)

the transducer (Fig. 6). Power Doppler is also superimposed on a B mode image, and can identify small amounts of blood flow, making it a more sensitive exam. Power Doppler mode measures the strength of the Doppler signal, but does not indicate the direction of flow. Pulsed Wave Doppler provides graphical information about the velocity of blood flow within a vessel or heart chamber at a specific point.

4 Scanning Terminology

Ultrasound scanning must begin with correct probe orientation. Rotation of the probe 180 degrees may occur if this step is overlooked. All ultrasound probes have an orientation marker to assist with rapid orientation. Conventions of probe orientation with respect to the body vary in different disciplines; regardless, it is critical that the user is correctly oriented (Fig. 7).

Ultrasound scanning planes are described using the basic anatomic planes: transverse, sagittal and less commonly coronal. These planes are perpendicular to one another. Oblique angles can be utilized within these planes to acquire an off-axis image.

Transverse (or axial) View: This plane divides the body into superior (cranial) and inferior (caudal) parts.

Sagittal (longitudinal) View: This plane divides the body into right and left (Fig. 8).

Coronal View: This plane divides the body into dorsal and ventral sections.

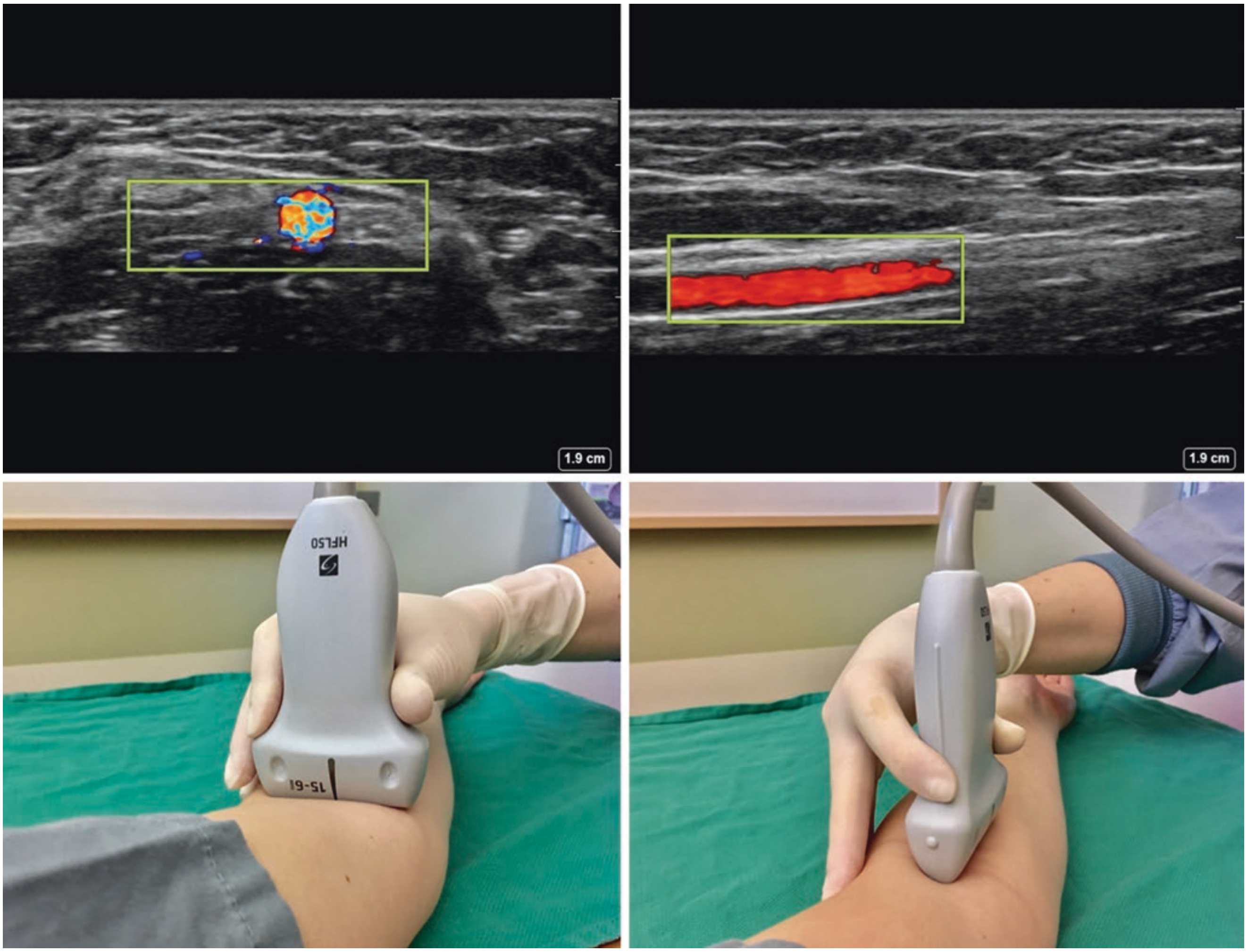

Fig. 8 Left: A short axis view of the brachial artery with the probe held in a transverse position scanning in antecubital fossa. Right: A long axis view of the brachial artery with the probe held in a sagittal position scanning antecubital fossa

5 Probe Manipulation

PART (Pressure, Alignment, Rotation, Tilt) describes the basic probe maneuvers needed for optimizing ultrasound images [1].

By increasing the pressure applied to the probe, tissue under the probe is compressed and the echogenicity of structures under the probe may be enhanced (Fig. 9). Pressure may be applied evenly or sometimes more to one side of the probe than the other, which can enhance needle visualization by tilting the ultrasound beams towards a needle path. Excessive pressure may cause patient discomfort and will likely compress veins. Compressing veins may be useful when performing procedures, so long as their location is noted. Alignment (or sliding) centers an anatomical target on the screen and can be used to follow a target both proximally and distally to assess the course of its anatomy. Rotation clockwise or counter-clockwise brings the probe from a transverse to a longitudinal view. Rotation may help to remove obstacles obscuring a target or to identify an optimal needle path for a procedure. Fine rotation is often needed to identify the full length of a needle when performing procedures with ultrasound. Tilting can optimize the image quality by bringing the ultrasound beam into perpendicular alignment with a given structure. For some anatomical structures, altering the tilt of the probe may dramatically enhance their visualization (Fig. 10). Tilting is also useful for following the needle tip during procedures.

6 Structure Visualization and Needle Orientation

Axis and plane are two concepts that need to be understood in order to perform ultrasound guided procedures. In terms of axis, targets such as nerves and blood vessels are typically described as in short-axis (transverse) versus long-axis (longitudinal) view.

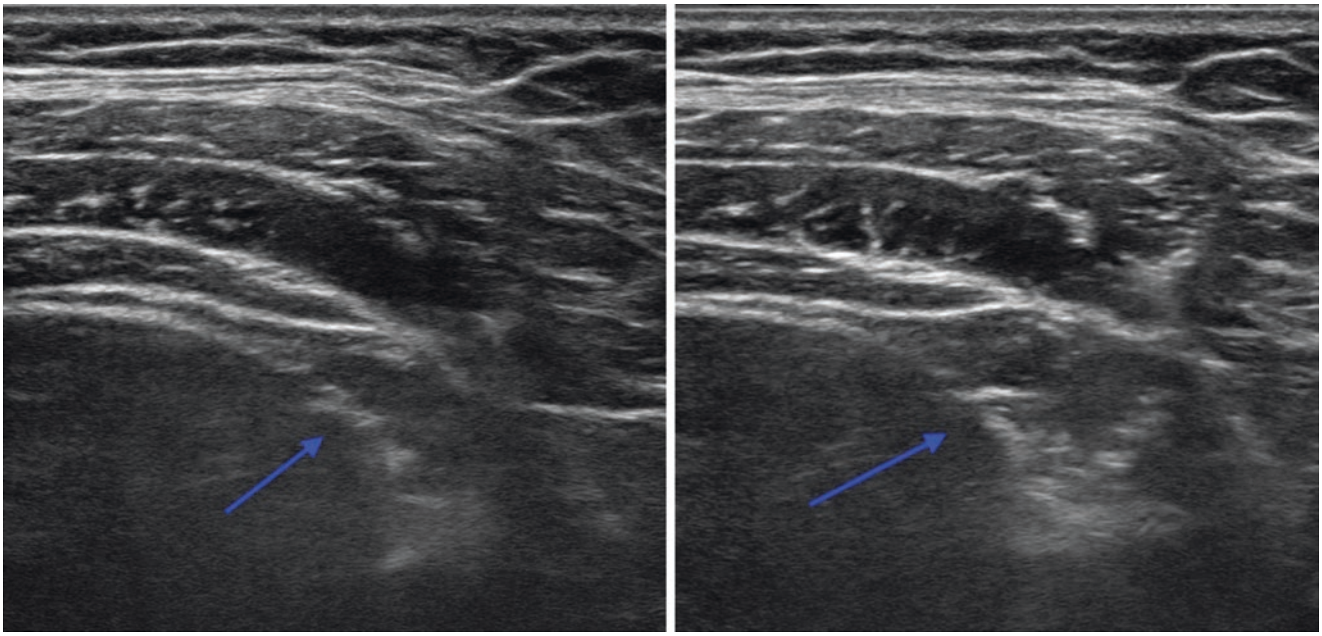

Fig. 9 An ultrasound image of the quadratus lumborum muscle. On the left, the muscle is poorly defined. On the right, more pressure was applied with the ultrasound, enhancing the echogenicity and making the contours of the muscle more visible

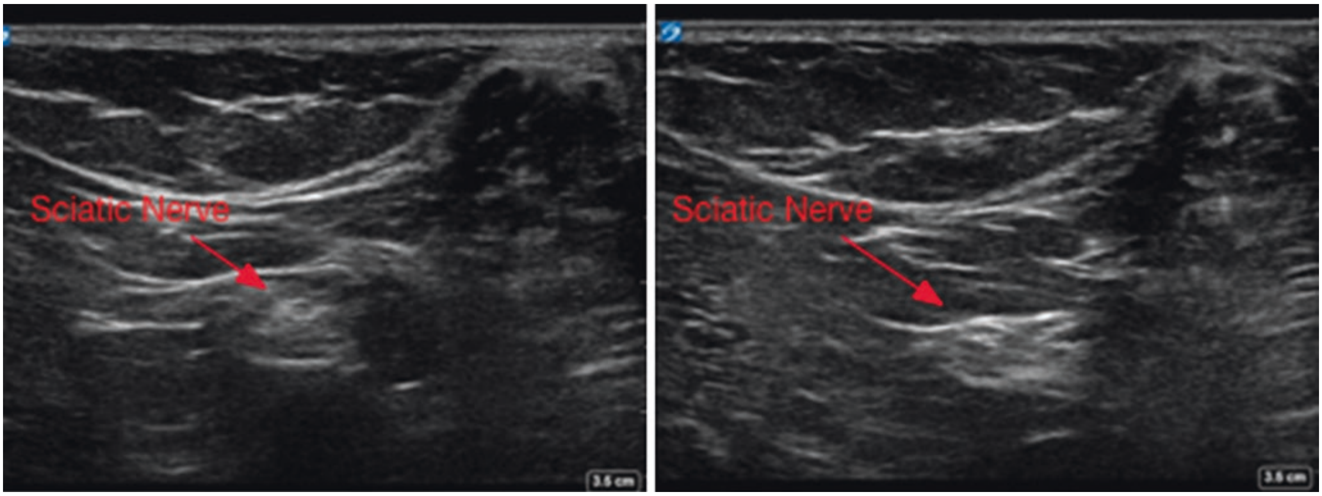

Fig. 10 The effect of tilting ultrasound probe. Image on the left shows the sciatic nerve in the popliteal fossa with cephalad tilt of the probe. On the right, the probe is tilted caudally, greatly enhancing visualization of the sciatic nerve

With respect to planes, two needle insertion techniques are commonly used with ultrasound-guided procedures: in-plane (needle advanced in the plane of the ultrasound probe) and out-of-plane (needle advanced perpendicular to the ultrasound probe) (Fig. 11). Both techniques are acceptable; however, in-plane needling has the advantage of showing the entire course of a needle. To visualize the entire course of a needle successfully, proper alignment and rotation of the probe are necessary. Oftentimes, small adjustments are needed because of the narrow width of the ultrasound beam. Although the needle trajectory may be shorter with out-of-plane approaches, the needle tip identification with out-of-plane needling may be difficult and misidentification of the needle tip is common. This is due to the fact that only the part of the needle that is advancing under the probe is visualized. Tilting and sliding the probe, while the needle is advanced out-of-plane, can enable needle tip visualization.

Axis and plane are then combined to describe the approach to an ultrasound-guided procedure. For example, ultrasound-guided central line placement is frequently performed with a short-axis out-of-plane needle insertion approach, while

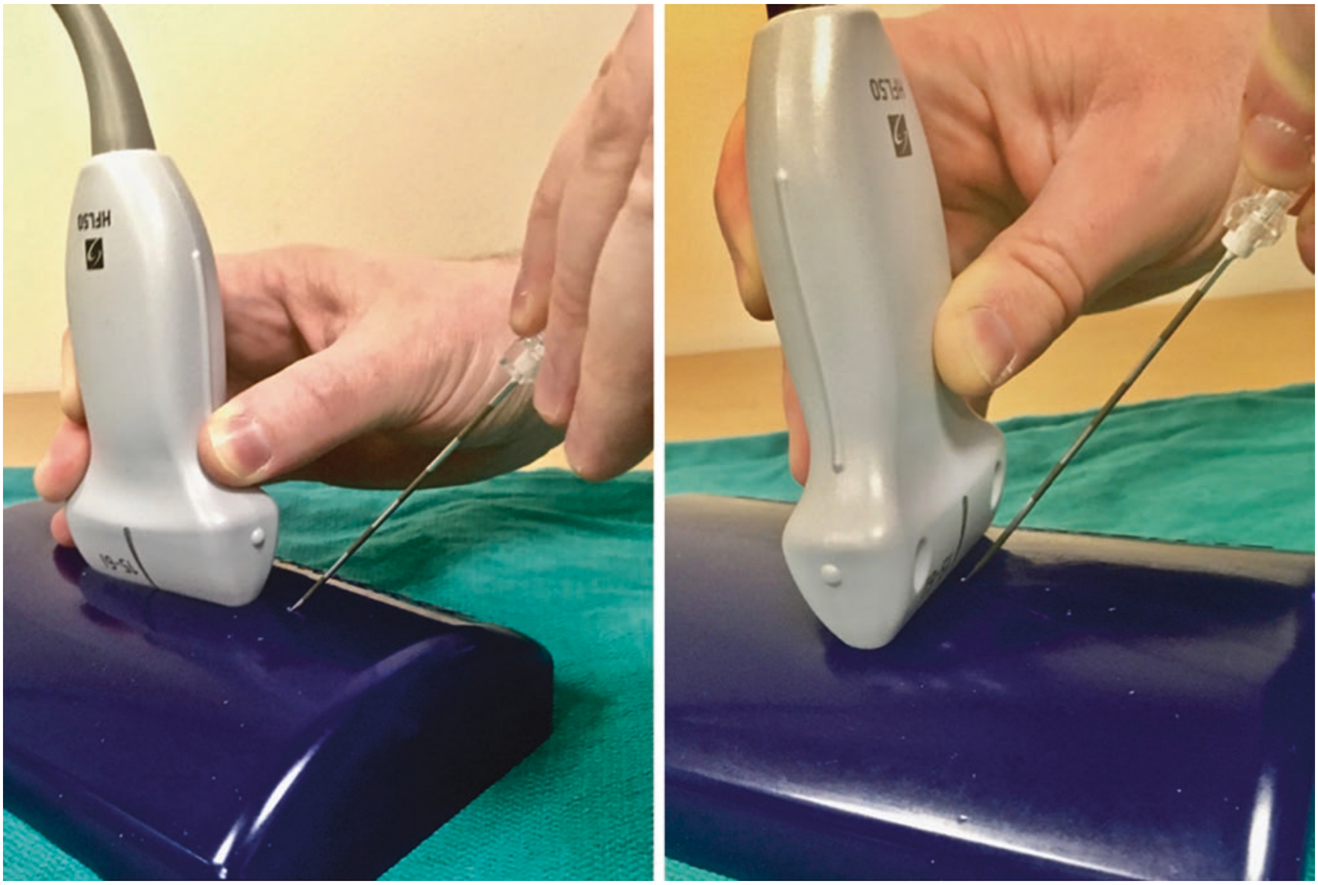

Fig. 11 Left: An in-plane needle approach. Note that the needle is advanced in plane of ultrasound beam. Right: An out-of-plane needle approach. Note needle is advanced perpendicular to the ultrasound probe

peripheral nerve blockade is often performed with a short-axis in-plane needle insertion approach.

7 Needle Visualization

Needle visualization is enhanced by using larger needles, shallow needle insertion angles and echogenic needles. When guiding a needle, it is crucial to identify the needle tip. If the needle shaft is misidentified as the needle tip, because the probe is not in-plane with the needle, the needle tip may be further than appreciated and could damage critical structures. Many specialized needles are available for ultrasound-guided procedures. Needles marketed as echogenic typically have etching on the needle to increase the reflection of ultrasound beams back to the transducer. They may also include specific echogenic indicators at the tip. Needles with enhanced echogenicity are popular for ultrasound-guided nerve blockade and make needle visualization easier [2]. Even with echogenic tips however, needles may be difficult to visualize when inserted at steep angles. Thus, several ultrasound manufacturers have added proprietary software tools for enhancing needle visualization at steep angles (Fig. 12). Using a curvilinear probe will also make needles at steeper angles more visible. In addition, commercial needle guides are also available to hold needles in plane with an ultrasound probe to facilitate visualization.

8 Summary

As new applications of ultrasound become more prevalent, knowledge of its function is increasingly expected to provide optimal medical care. A basic understanding of ultrasound equipment and nomenclature is critical to serve as a foundation for ultrasound guided procedures. This foundation, along with the diagnostic and interventional applications covered in subsequent chapters, will enable the use of bedside ultrasound in a variety of clinical settings.

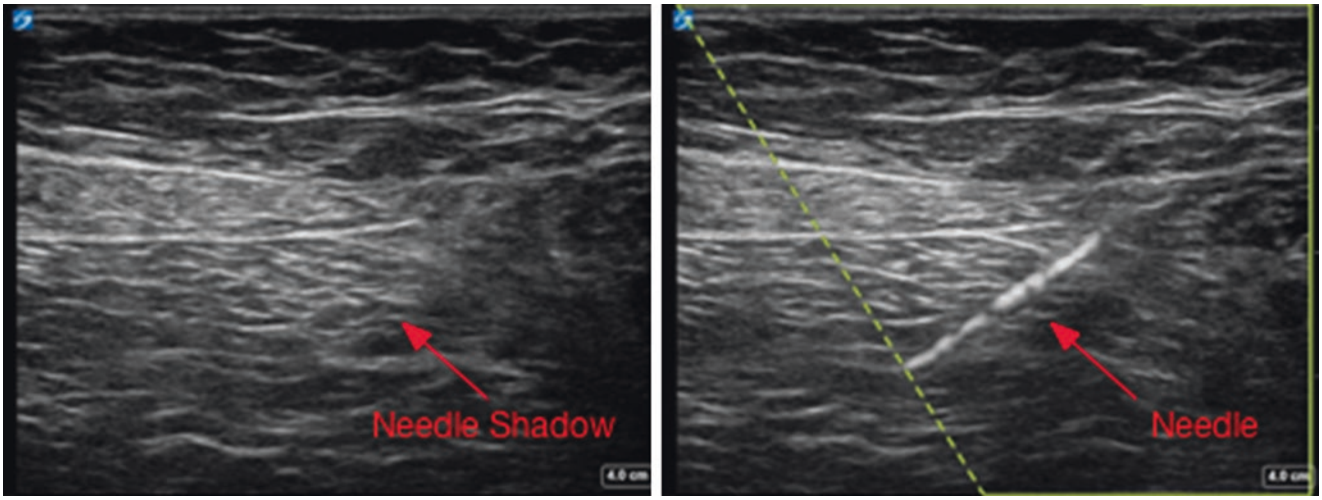

Fig. 12 An obturator nerve block with steep insertion of needle. On the left, only a subtle needle shadow is visible. On the right, in the area where needle visualization is enhanced using Sonosite's Advanced Needle Visualization, needle visibility is greatly enhanced

References

1. Ihnatsenka B, Boezaart AP. Ultrasound: basic understanding and learning the language. Int J Shoulder Surg. 2010;4(3):55–62.
2. Hocking G, Christopher HM. Optimizing the safety and practice of ultrasound-cuided regional anesthesia: the role of echogenic technology. Curr Opin Anaesthesiol. 2012;25(5):603–9.

Basic Ultrasound Needling Techniques

Benjamin Portal, Karina Gritsenko, and Melinda Aquino

1 Introduction

Ultrasound guidance offers several advantages when compared to blind techniques. These include a greater likelihood of success, fewer complications, and less time spent on a procedure. The art of optimizing an image produced by ultrasound is an essential skill for successful performance of an ultrasound-guided nerve block. Having a solid foundation and understanding of basic needling techniques will increase the success rate of the practitioner’s procedure.

2 In-Plane Vs out-of-Plane Approach

There are two basic approaches that are used to advance the needle to get to your target location; the in-plane and the out of plane approach.

During an in-plane approach, the needle is placed in line with the ultrasound transducer and parallel to the beam, which allows the needle shaft and tip to be constantly visualized throughout the procedure (Figs. 1 and 2). Thus, the needle trajectory can be followed in real time. It is important to insert the needle at the center (or seam) of the ultrasound transducer. If the needle is not inserted in the middle, it is likely to be partially imaged or not at all. If the needle tip is out of view, one should not continue to advance the needle, as unseen adjacent structures can be damaged or one could overshoot the target. Instead, one should rotate or angulate the transducer probe to bring the needle tip back into view. Applying pressure with the transducer may also enhance imaging of the needle shaft. With the in-plane technique, the operator can oscillate the needle or inject fluid to find the tip of the needle via tissue displacement.

The out-of-plane technique is used when a wide field of view is needed and direct observation of the needle is not. In this technique, the needle is placed perpendicular to the transducer (Figs. 3 and 4). It is important to determine which side of the probe is medial vs lateral of the patient. The needle shaft and tip are visualized as a hyperechoic dot on ultrasound. However, visualization of the actual tip of the needle and shaft is difficult and unreliable. The needle tip may be difficult to locate accurately without the use of echogenic tip needles. Once the needle is penetrated through the skin, one method to find the needle is to slide the transducer toward the needle, and bounce the needle in the skin to differentiate the orb of the needle from the surrounding tissues. Once the needle is in view, the operator advances the needle with one hand while simultaneously advancing the transducer with the other hand at the same rate to keep the needle in view until the appropriate vessel or nerve is reached.

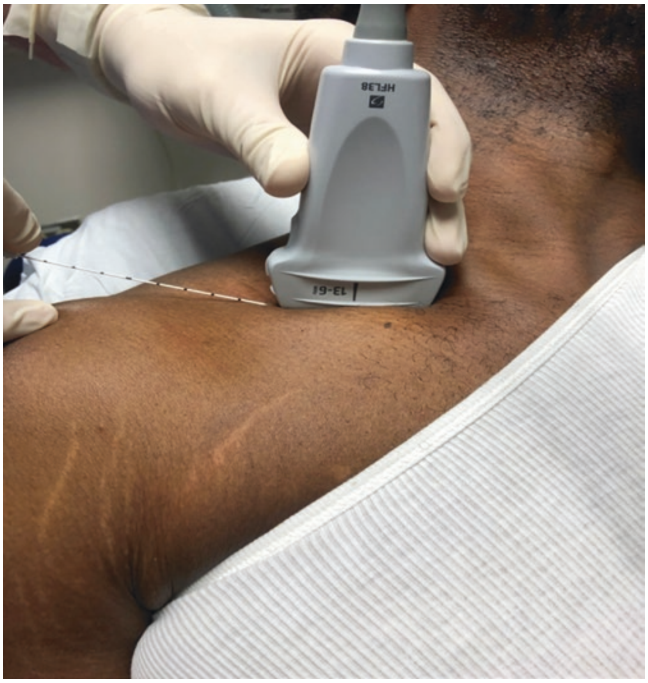

Fig. 1 In – Plane Technique

B. Portal · K. Gritsenko (✉) · M. Aquino
Montefiore Medical Center, Bronx, NY, USA
e-mail: KGRITSEN@montefiore.org

© Springer Nature Switzerland AG 2021
J. Li et al. (eds.), *Ultrasound Fundamentals*, https://doi.org/10.1007/978-3-030-46839-2_3

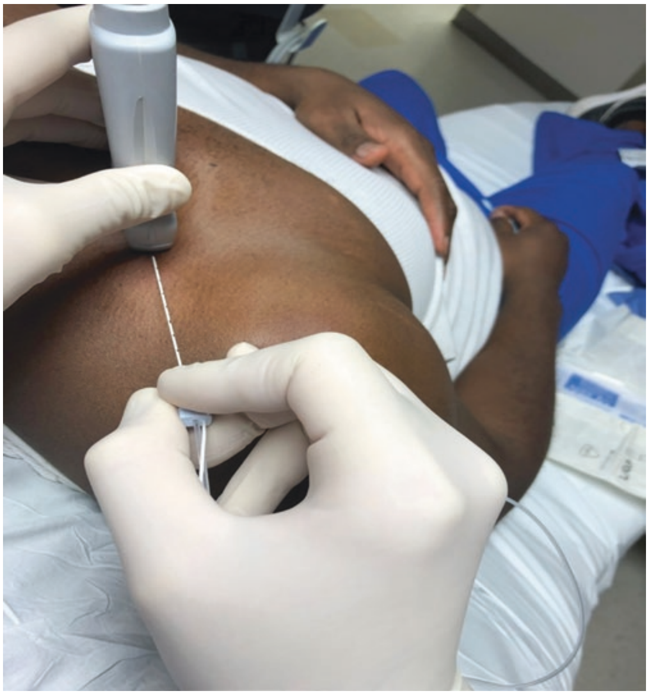

Fig. 2 In- Plane Technique

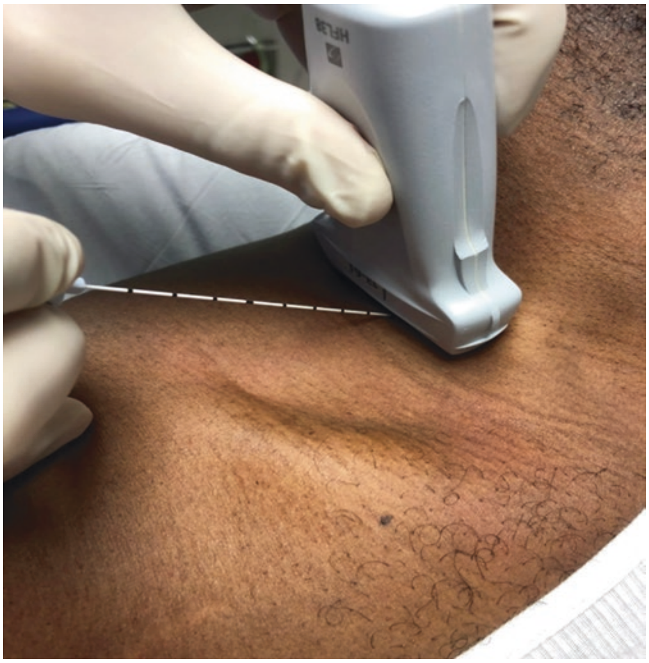

Fig. 3 Out of plane technique

3 Proper Needle Handling Techniques

Proper needle handling skills are required for accurate and smooth needle insertion during ultrasound guided nerve blocks. If the operator is not ambidextrous, many people prefer to use the dominant hand to handle the needle and inject local anesthetic, while using the non-dominant hand to manipulate the ultrasound probe. It is imperative that the non-dominant hand holds the probe as still as possible in order to get a still image and to limit any motion which may take the needle out of view. Resting the non-dominant hand on the patient is a technique that is often utilized to minimize movement (Fig. 5). When the needle is introduced, the bevel is pointed upwards largely due to convention.

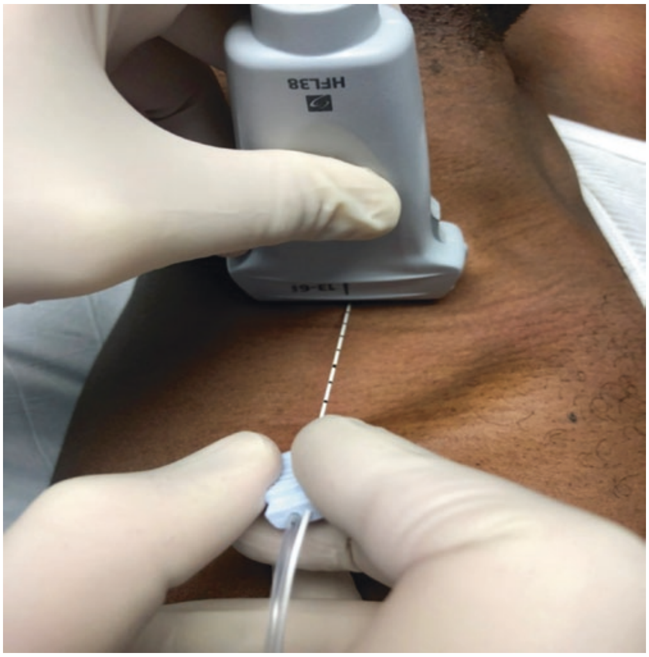

Fig. 4 Out of plane technique

Advancing the needle using a short ‘in-and-out’ or ‘side-to-side’ motion causes deflection of the adjacent soft tissues and makes the trajectory of the needle more discernible within the otherwise stationary field [1].

The angle at which the needle shaft and US beam intersect (needle-beam angle) greatly affects needle visibility. The smooth metallic surface of a standard needle is a specular reflector of US waves, hence a greater number of echoes will return to the transducer as the needle-beam angle approaches 90° [2].

As a result, in- plane needle tip and shaft visibility is better at larger needle-beam angles; the optimal angle appears to be 55°. Needles placed perpendicular to the beam are easier to visualize than needles placed parallel or at a less acute angle to the beam.

Interestingly, out of plane needle tip visibility is better at smaller needle-beam angles (30°); however, the reason for this is not clear [3].

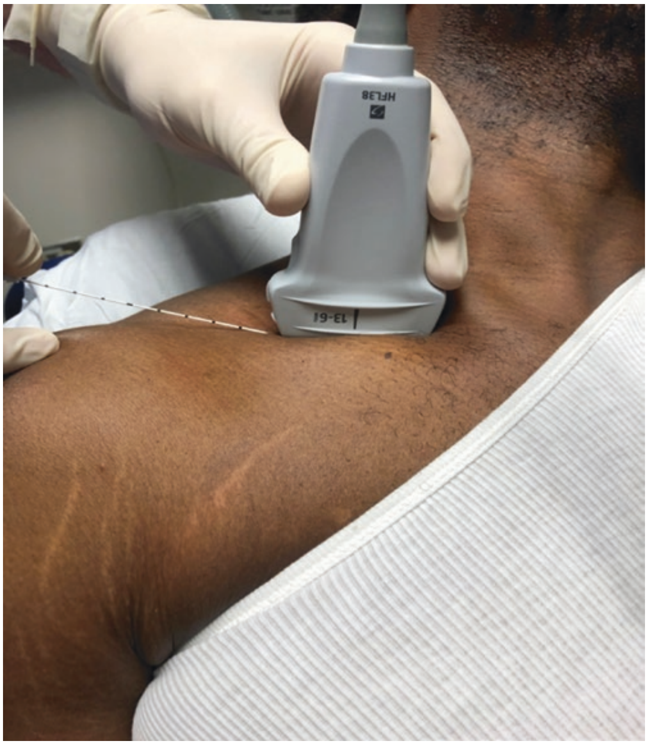

Fig. 5 Proper Needle Handling

4 Needle Selection

Large bore needles are more easily seen and easier to direct under ultrasound. As such, they are often preferred for deep blocks. However, this comes at the expense of increased tissue trauma and patient discomfort. Small bore needles are more difficult to visualize, but may produce fewer artifacts. Thus, they are preferred for more superficial blocks [4].

The use of a long bevel (14° angle) versus a short bevel (45° angle) needle can be a contributor to peripheral nerve injury. Selander et al. demonstrated in a rabbit sciatic nerve model that although the overall frequency of nerve injury was lower with short beveled needles, the severity of the injury was greater. Cadaveric studies suggest that an intrafascicular injection is rare and difficult to accomplish with blunt-tipped block needles, even with an intraneural injection [5].

The short bevel non-cutting needles provide greater resistance, and therefore, enhance the feedback of the needle traversing different tissues. The long bevel cutting needles that are commonly available in the operating room do not provide as much tactile information while traversing different tissues [6].

Insulated needles may be used during ultrasound guided nerve blocks if nerve stimulation is desired. Furthermore, insulated needles are generally short bevel needles that are less sharp than the hypodermic needles. They are therefore less likely to produce paresthesia upon nerve contact than sharper hypodermic needles.

Echogenic needles are available, but are not specifically designed for nerve blocks at the present time. Needles with echogenic tips may greatly enhance visualization, especially when the needle is inserted using the out of plane approach. Echogenic needle designs can include a polymer coating that traps microbubbles or a dimpled distal shaft. The superior needle tip and shaft visibility of echogenic needles has been demonstrated in both the laboratory and clinical settings, and it is especially significant at small needle-beam angles [7–9].

There appears to be little difference in visibility between needles primed with either water or air. Inserting a guidewire will significantly increase needle shaft visibility. However, this effect is lost if very tightly-fitting guidewires are used, as there is no longer an acoustic interface between the shaft and guidewire. For the same reason, stylet and hollow needles have similar visibility. However, if a stylet is used, pumping the stylet up and down several times within the shaft may transiently increase needle echogenicity [10]. The effect of this "pump maneuver" is attributed to the formation of microbubbles about the needle tip and shaft [11].

5 Body Ergonomics

In order to have a successful block, proper body ergonomics are essential to handle the transducer and needle, while viewing the screen at the same time. Positioning helps to avoid operator fatigue and body injury, and also allows for a time-efficient performance of the procedure. All necessary equipment should be within hands reach of the operator to eliminate any interference with the scanning procedure. In addition, the lights in the room should be adjusted in order to view the ultrasound machine, needles and procedural site adequately. The operator should orient and position the ultrasound machine to the side of the patient that allows for a direct line of vision while manipulating the needle and probe. The patient should also be leveled to the proper height relative to the operator. The operator should also learn how to hold the transducer properly. The hand should be placed close to the transducer contact as opposed to high up on the transducer. In addition, it is important to have both the arm and hand comfortably supported on the patient (Fig. 6).

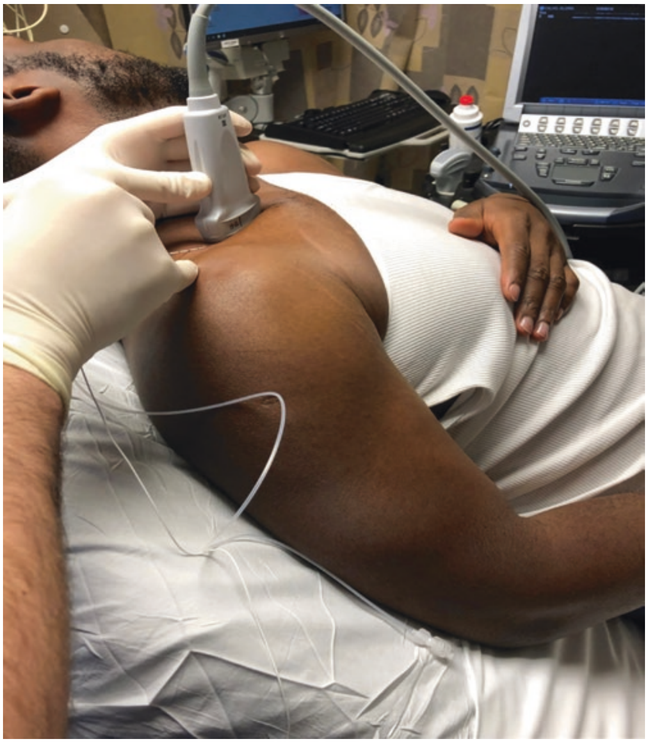

Fig. 6 Proper body ergonomics

6 Conclusion

Understanding the basics of needling techniques and the different positions with which one can get a complete and accurate picture, is the first step of mastering ultrasound guided diagnostic and regional techniques. It takes repetition, practice and patience for the novice to gain control of the ultrasound probe while finding the needle in the correct anatomical position. This chapter highlights the different needles, approaches, and proper body positions needed for a safe and effective approach to using ultrasound guidance for delivery of anesthesia or medication.

References

1. Chapman GA, Johnson D, Bodenham AR. Visualisation of needle position using ultrasonography. Anaesthesia. 2006;26:64–7.
2. Sites BD, Brull R, Chan VW, Spence BC, Gallagher J, Beach ML, Sites VR, Hartman GS. Artifacts and pitfall errors associated with ultrasound-guided regional anesthesia. Part I: understanding the basic principles of ultrasound physics and machine operations. Reg Anesth Pain Med. 2007;32:412–8.
3. Schafhalter-Zoppoth I, McCulloch CE, Gray AT. Ultrasound visibility of needles used for regional nerve block: an in vitro study. Reg Anesth Pain Med. 2004;29:480–8.
4. Chin KJ, Perlas A, Chan V, Brull R. Needle visualization in ultrasound-guided regional anesthesia: challenges and solutions. Reg Anesth Pain. 2002;14:169–75.
5. Liu SS, Ya Deau JT, Shaw PM, Wilfred S, Shetty T, Gordon M. Incidence of unintentional intraneural injection and postoperative neurological complications with ultrasound-guided interscalene and supraclavicular nerve blocks. Anaesthesia. 2011;66:168–74.
6. Shariat AN, Horan PM, Gratenstein K, McCally C, Frulla AP. Equipment for peripheral nerve blocks. Last accessed 29 Apr 2015.
7. Bergin D, Pappas JN, Hwang JJ, Sheafor DH, Paulson EK. Echogenic polymer coating: does it improve needle visualization in sonographically guided biopsy? AJR Am J Roentgenol. 2002;178:1188–90.
8. Jandzinski DI, Carson N, Davis D, Rubens DJ, Voci SL, Gottlieb RH. Treated needles: do they facilitate sonographically guided biopsies? J Ultrasound Med. 2003;22:1233–7.
9. Gottlieb RH, Robinette WB, Rubens DJ, Hartley DF, Fultz PJ, Violante MR. Coating agent permits improved visualization of biopsy needles during sonography. AJR Am J Roentgenol. 1998;171:1301–2.
10. Bisceglia M, Matalon TA, Silver B. The pump maneuver: an atraumatic adjunct to enhance US needle tip localization. Radiology. 1990;176:867–8.
11. Schafhalter-Zoppoth I, McCulloch CE, Gray AT. Ultrasound visibility of needles used for regional nerve block: an in vitro study. Reg Anesth Pain Med. 2004;29:480–8.

Practical US Guided Vascular Access

Sean P. Clifford and Jiapeng Huang

1 Introduction

The ability to obtain vascular access is a required skill for nearly all medical and surgical specialties. Cannulation of veins and arteries is critical for the administration of fluids and medications; it also a necessity for the purpose of monitoring patient hemodynamics. The traditional landmark technique for obtaining vascular access is purely based on the presumed location of vessels, and blind insertion of a needle until blood is returned [1]. Confirmation of successful cannulation relies on crude measures such as blood pulsation, color of the aspirated blood, and pressure measurements with a fluid column or transducer. Landmark techniques for vascular cannulation have a 60–95% success rate with complication rates as high as 5% to 19% [2]. Complications may include inadvertent arterial puncture, hematoma, pneumothorax, hemothorax, arterial-venous fistula, venous air embolism, nerve injury, thoracic duct injury, intraluminal dissection, intrathecal placement [3], and puncture of the aorta.

Ultrasound (US) technology has made significant contributions to the safety, efficiency, and quality of vascular access in both pre-procedure screening and real-time procedural guidance. The use of US imaging before or during vascular cannulation greatly improves first-pass success rate and reduces complications. This is of particular importance in central venous catheterization, where arterial puncture followed by placement of a large-bore cannula into the carotid artery poses a significant risk, including catastrophic events such as stroke and even death. The American Society of Echocardiography (ASE) and the Society of Cardiovascular Anesthesiologists (SCA) published their comprehensive guidelines for performing US guided vascular cannulation in 2011 and strongly recommended real time US guidance during IJV cannulation whenever possible with category A, level 1 evidence [1]. Both the Agency for Healthcare Research and Quality and the National Institute for Health and Care Excellence have also advocated US guidance for central venous access. Recent studies further demonstrate that US guidance may increase the safety of non-IJV, peripheral venous, and arterial access [4, 5]. In addition, US imaging is helpful to diagnose catheter malposition and procedure related complications, such as thrombosis, hemothorax, and pneumothorax [6]. This chapter aims to provide a comprehensive, yet practical approach for US guided vascular access.

2 Principles of US Guidance for Vascular Access

Choosing the appropriate probe is the first step in achieving successful vascular access. The instrument of choice is a high frequency probe (≥7mHZ) with a smaller footprint, especially in pediatric patients. High frequency probes provide better resolution for superficial structures like arteries and veins. The disadvantage of high frequency probes is poor penetration, which is usually not a major issue during superficial vascular access. Challenges with this probe may be noted in obese patients as well as in the access of deeper vessels, such as the femoral arteries and veins, as the probe's lack of penetrance may not provide an optimized view. Commonly used linear array probes include the GE 9 L, Phillips L12–4mHZ, and Sonosite 13–6mHZ probes (Fig. 1).

Maintaining adherence to strict aseptic techniques is critical when using an US probe. A medium-sized clear dressing or a sterile probe cover should be placed over the US probe before imaging and guidance. Caution should be exercised to avoid any air bubbles between the dressing and the probe, since air causes significant acoustic shadowing and interference with the imaging of tissue structures. A generous amount of sterile ultrasonic gel should be placed inside the probe cover and the probe surface should be in full contact with the gel. It is helpful to place a rubber band at the concave

---

S. P. Clifford · J. Huang (✉)
Department of Anesthesiology & Perioperative Medicine,
University of Louisville, Louisville, KY, USA
e-mail: jiapeng.huang@louisville.edu

© Springer Nature Switzerland AG 2021

J. Li et al. (eds.), *Ultrasound Fundamentals*, https://doi.org/10.1007/978-3-030-46839-2_4

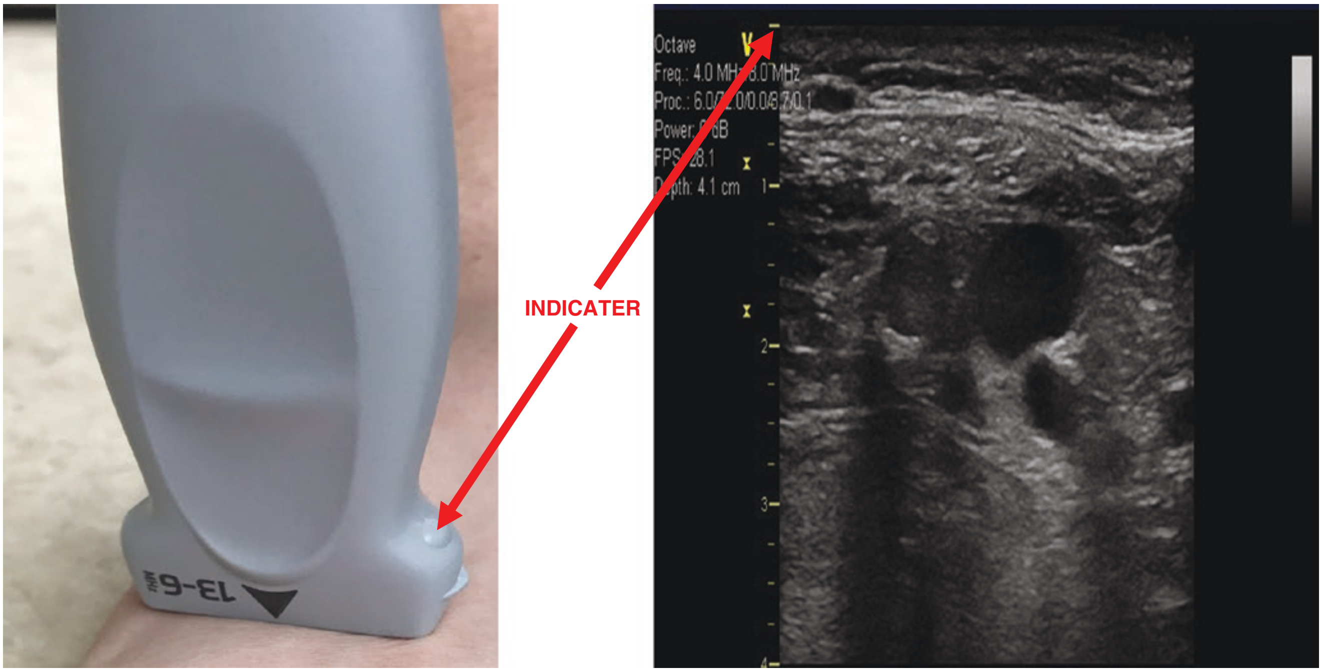

Fig. 1 Ultrasound probe orientation

part of the US probe to create a tight seal so that the probe surface is immersed in the gel; the gel serves as an excellent conductor for the US beam. The image should be clear, high quality, and free from any artifact. Other aspects of sterile technique, such as use of antiseptic prepping solution and appropriate attire are key. This includes the use of masks, sterile gloves, and gowns to reduce venous and arterial catheter related infections.

It is critical to ensure correct orientation of the probe indicator so that screen display and intended anatomical target are consistent. The structures on the side of the orientation indicator may be displayed either at the left or the right side of the screen display depending on the manufacturer and setting. It is essential to have awareness of this orientation before needle puncture and cannulation in order to avoid misidentifying key anatomic structures that could lead to potentially catastrophic complications. The operator should apply modest pressure on one side of the transducer to reveal the probe and screen display orientation. Following sterile gel application, the operator shall place the probe on the patient and maneuver the instrument while observing the screen to determine the appropriate anatomy and display orientation. Most proceduralists orient the probe so that the needle will be inserted from the right side of screen and advance toward the left side (Fig. 2). Operators should adopt a consistent orientation method to avoid confusion and medical errors.

There are two methods of using US for vascular access: real-time guidance versus static imaging. In real time guidance, the needle is simultaneously observed on the image display and directed toward the target vessel, avoiding surrounding structures. Static imaging uses the US beam to identify the site of needle entry point on the skin overlying the vessel [1]. Real-time techniques are the preferred method and have been shown to yield better results when compared with techniques that use US for landmark identification followed by traditional non–US-guided insertion [7]. When identifying potential cannulation sites in the neck, a pre-procedure screening prior to aseptic preparation should be performed on both sides to evaluate the anatomy, vessel size and patency, and needle pathway. This scanning should be performed cephalad to caudal and lateral to medial in a systematic fashion in order to select the best cannulation site (bigger vessel, lack of thrombosis, increased distance from the artery, etc.). This pre-planning can prevent the breakdown of the sterile field after the drape has been secured, if the practitioner finds out that the prepped site is not ideal for cannulation secondary

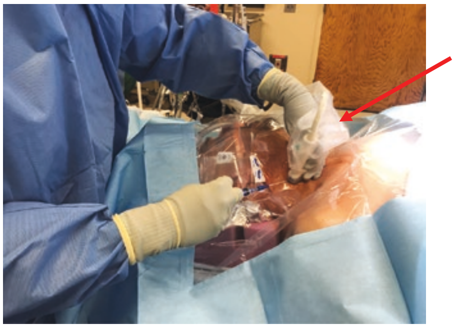

Sterile Probe Cover
Gels Inside

Fig. 2 Sterile techniques for ultrasound guided vascular access

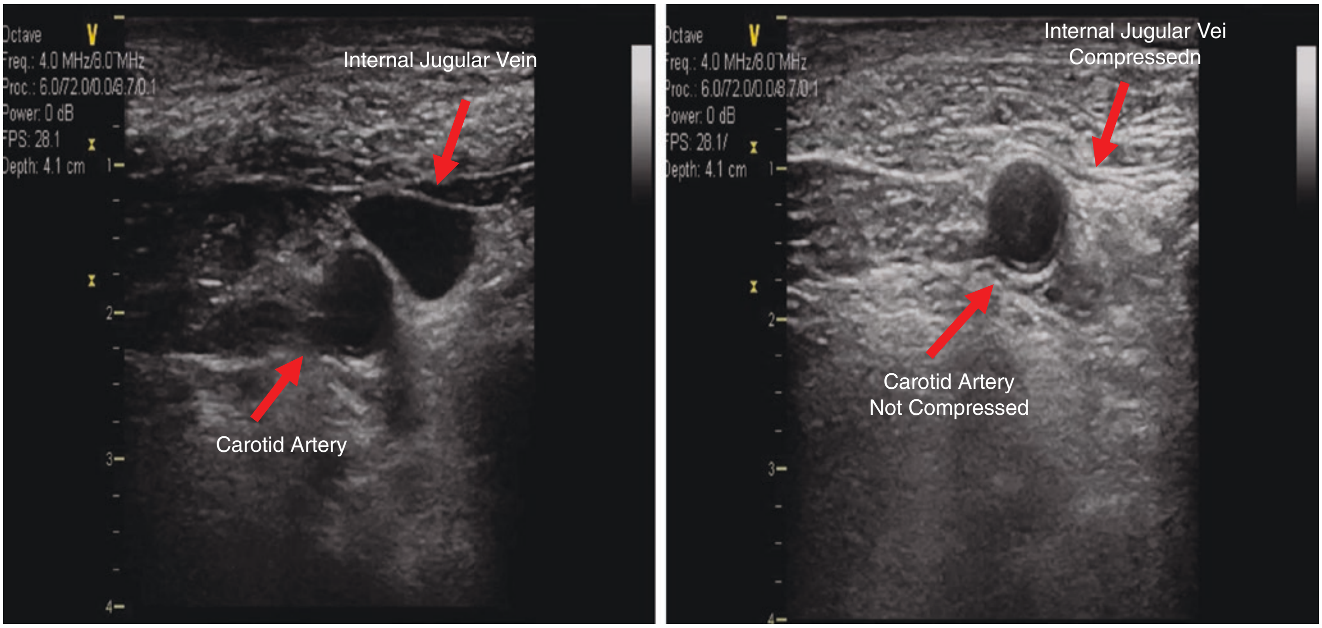

Fig. 3 Veins can be easily compressed with an ultrasound probe

to conditions such as a thrombosed vein, vein directly over the artery, large valve inside the vein, etc.

The practitioner should hold the US probe with the non-dominant hand while the catheter/needle assembly is held with the dominant hand to allow for fine adjustments to the spatial relationship between the US probe (image plane) and catheter direction. The seemingly simple task of cannulation actually requires delicate hand-eye coordination to complete. For beginners, it is recommended to move either the probe or the needle one at a time to obtain an optimized image of the needle and target structures. Once the needle is inserted past the subcutaneous tissue, the probe is manipulated to follow the trajectory of the needle with a focus on the needle tip. The practitioners' attention should be focused on the images on the screen, not fixed on the actual needle itself. The hand on the needle should apply gentle aspiration at all times until blood is returned. Once direct vision of the needle entering the vessel and desired blood return is achieved, the US probe should be placed on the sterile field while the non-dominant hand moves to stabilize the needle. Subsequently, the angiocatheter or guidewire is advanced into the vessel with the dominant hand. US is then utilized to verify that the wire is in the desired vessel lumen.

3 Vessel Identification

Misidentification of a vessel with US is a common cause of unintentional arterial cannulation. Understanding the relative anatomic positions of the artery and vein is essential [1]. Use of 2-dimensional US, color Doppler, and spectral Doppler imaging should each be considered to help identify the appropriate vessel to cannulate. Veins are thin-walled, compressible, and have respiration-related changes in diameter. In contrast, arteries are thicker-walled, not readily compressible by external pressure applied with an US probe, and are pulsatile during normal cardiac physiologic conditions (Fig. 3). To facilitate the separation between arteries and veins, patients should be placed in a head down position to increase the diameter of jugular and subclavian veins if tolerated. This maneuver is also helpful to reduce risks of air embolism due to the increased venous pressure. Note that pulsatility alone cannot be used to identify an artery during clinical conditions such as cardiopulmonary bypass, nonpulsatile ventricular circulatory assistance, and cardiac arrest. Color flow Doppler will show pulsatile blood flow in an artery predominantly during systole; blood flow is uniform in color and present during both systole and diastole in a vein (Fig. 4). It is important to consider that the color RED only indicates that flow is directed toward the probe, and the color BLUE indicates that flow is moving away from the probe. Color alone cannot be used to differentiate artery from the vein and will change depending on imaging angles. A pulse-wave Doppler within the vessel lumen displays a characteristic systolic, higher velocity flow inside an artery, while the flow in the vein is at a lower speed with biphasic systolic and diastolic components (Fig. 4).

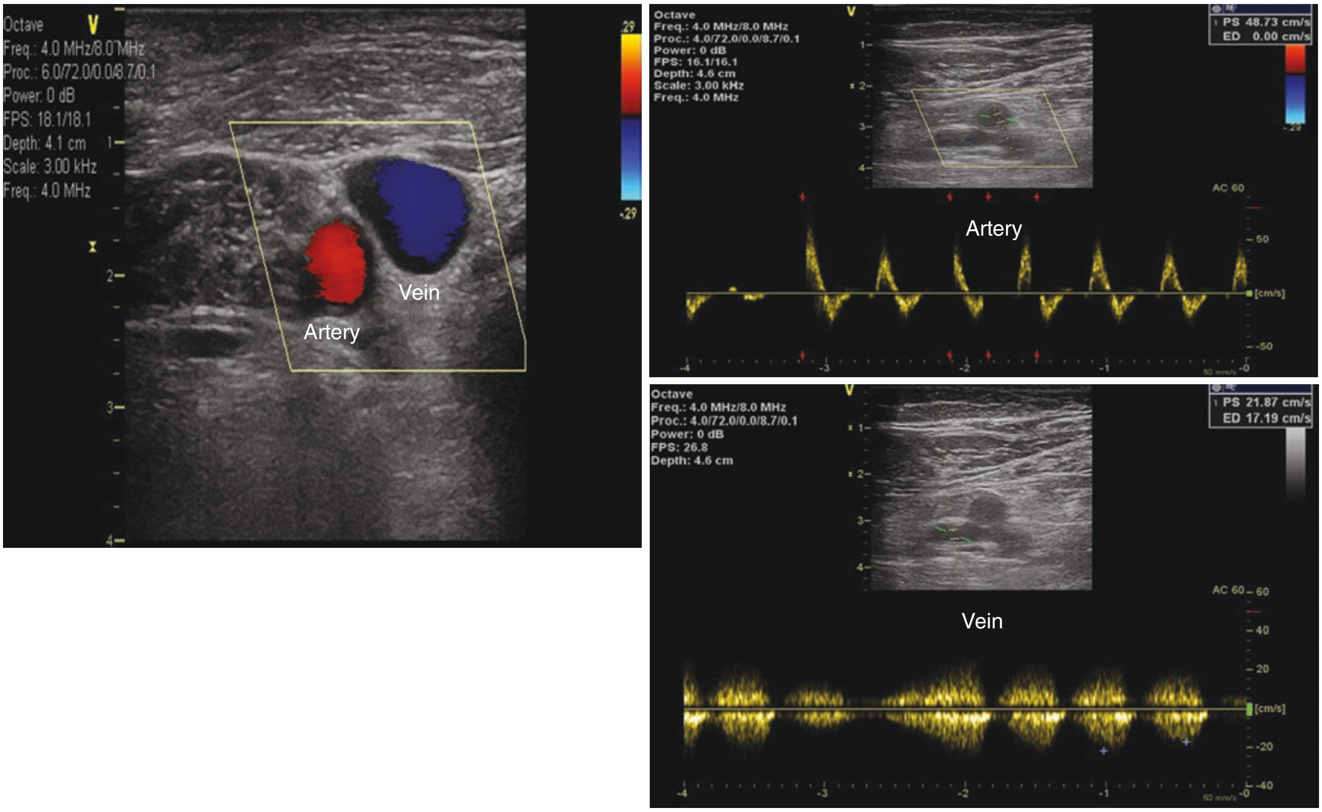

Fig. 4 Color Doppler and Spectral Doppler used to differentiate veins from arteries.

4 Vessel Abnormality Diagnosis

There are many pitfalls that can prevent successful cannulation or cause serious patient harm. Anatomic abnormalities such as thrombosis, atherosclerosis, dissection, valve impedance, or artificial grafts must be diagnosed before the procedure to prevent complications. Once these diagnoses are made, the decision to abort the planned cannulation, switch to a different site, or adopt a different access approach should be considered carefully. Purposeful or inadvertent entry into an artery with significant atherosclerosis, thrombosis, or dissection could cause stroke, myocardial infarction, acute renal injury, or bowel ischemia. Accessing a vein with thrombosis induces pulmonary embolism predictably, with the potential to strain the right heart. If the is a right to left intracardiac shunt that allows the dislodged clot to enter the cerebral circulation, a stroke may ensue.

Acute thrombi appear homogenous and anechoic or hypoechoic (black in appearance) on imaging. The vein walls where there are chronic thrombi are thickened with organized, hyperechoic and heterogeneous material attached. The veins are dilated and cannot be fully compressed (Fig. 5). The amount of pressure applied should be adequate to deform the adjacent artery to avoid false positive diagnosis. The clot may be seen attached to the wall or floating in the vessel lumen. A free-floating thrombus is always acute in nature. On color Doppler imaging, a filling defect of the lumen becomes evident and complete lack of color indicates complete occlusion [8].

An IJV valve is present in 80–100% of cases and it functions to prevent retrograde flow from the right atrium to the brain. It is usually located in the distal portion of the IJV. A large venous valve could potentially cause difficult central venous catheter placement, and if multiple or forceful attempts to overcome resistance are performed, the possibility of damage exists [9]. Caution with the guidewire and central line apparatus should be exercised when cannulating veins with valves (Fig. 6).

The carotid artery should be screened for abnormalities before attempting central venous line placement in the neck due to the potentially disastrous consequences of inadvertent arterial puncture or cannulation. Atherosclerotic plaques and calcification appear as irregular luminal narrowing and color Doppler may demonstrate aliasing with high flow velocities (Fig. 7a). Lack of color flow may exist when there is near complete or complete vessel occlusion. Carotid dissection can be diagnosed with a characteristic dissection flap or mural thrombosis that appears as a thickened hypoechoic wall (Fig. 7b). Synthetic vascular grafts are seen on US as tubular structures of uniform diameter with color completely filling the lumen during Color Doppler imaging. The wall is identified as echogenic, parallel lines or a series

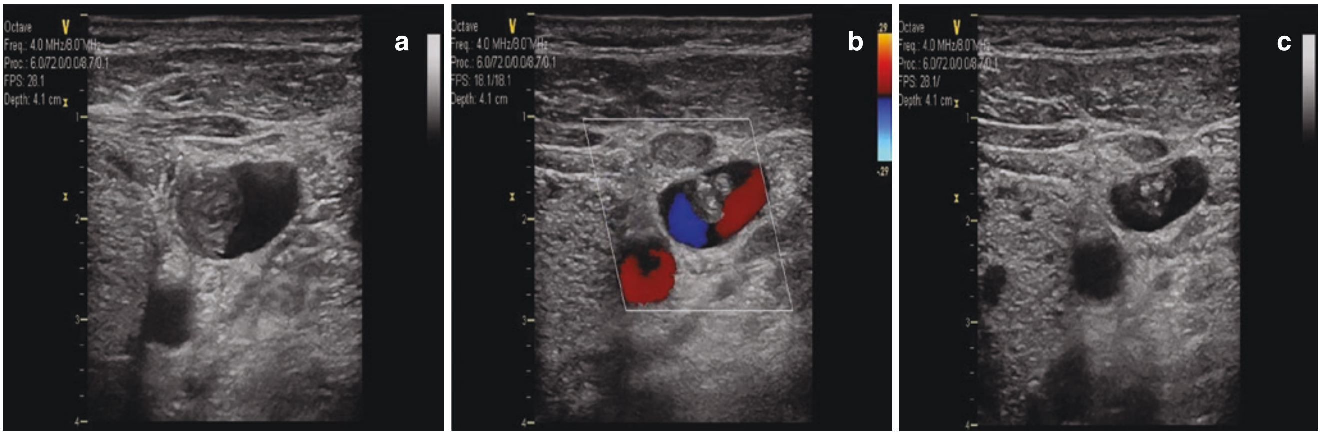

Fig. 5 A thrombosed internal jugular vein in 2D (**a**), Color Doppler (**b**), and with Compression (**c**)

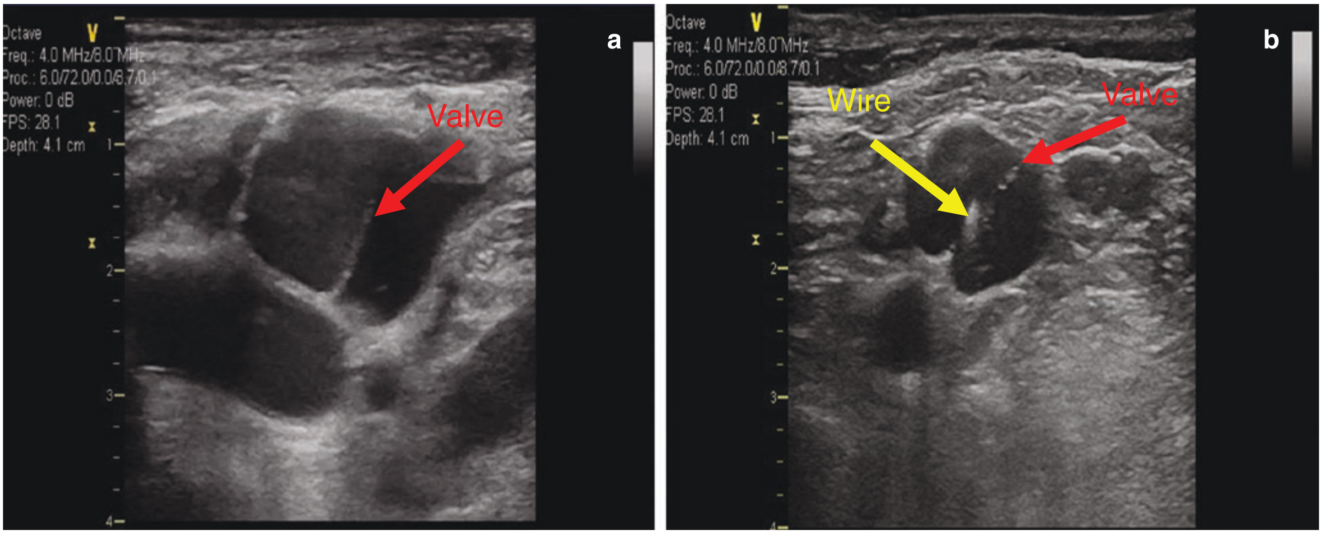
a
Valve
b
Wire
Valve

Fig. 6 An internal jugular vein valve in a distal (**a**) and a proximal (**b**) location. A guidewire is also imaged in (**b**)

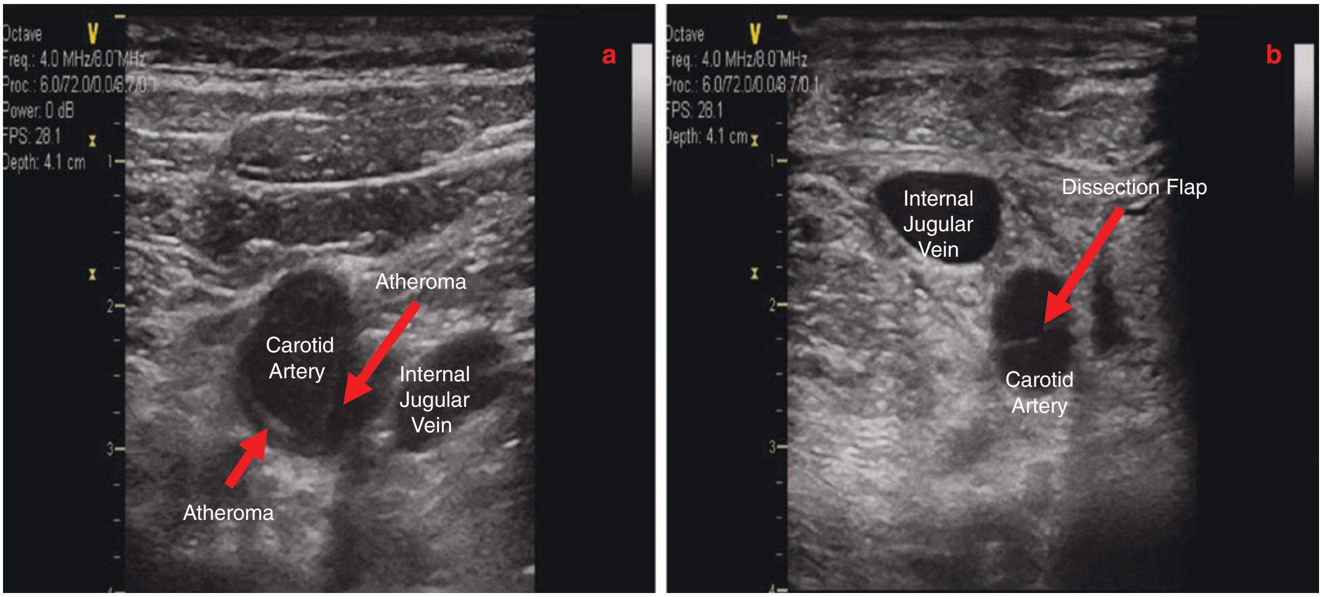
a
Atheroma
Carotid Artery
Internal Jugular Vein
Atheroma
b
Internal Jugular Vein
Dissection Flap
Carotid Artery

Fig. 7 Abnormalities of the carotid artery. (**a**): Atheroma of a carotid artery (**b**). Dissection of a carotid artery

of lines and dots. Some reports suggest that percutaneous access of vascular grafts may be safe; however, manual compression for hemostasis may be required for most patients. Other access routes are preferred whenever possible, as puncture site complications including hematoma, pseudoaneurysm, infection, lower extremity ischemia, and graft rupture are frequent [10].

5 US Guidance Approaches

Three main US techniques for vascular cannulation have been described. The target vessel can be visualized and accessed in the short axis, long axis, or oblique axis. The short axis technique uses an out-of-plane needle access approach, while both long axis and oblique techniques adopt an in-plane approach.

1. The Short Axis Out-of-Plane Approach (Fig. 8a): With the needle in the dominant hand and the US probe in the nondominant hand, the vessel is identified as described previously in a short axis view. The needle shaft and tip should be recognized from the characteristic echogenic appearance (hyperechoic or white) with ring-down reverberation artifact. The advantages of this technique are its ease of use and intuitiveness for novice operators. Disadvantages include the inability to view the full length of the needle and the potential for misinterpretation of the needle shaft as the needle tip. The tip may enter into undesirable structures outside the 2-dimensional imaging plane (such as the carotid artery during internal jugular vein cannulation) if this error is made. Three methods of needle insertion and visualization may be used.
   - A. The needle is inserted at an almost 90-degree angle to the skin and immediately adjacent to the US probe. The needle is advanced slowly in the plane of US beam. Tissue tenting from the needle pressure or direct visualization of the needle itself is closely observed until blood flashback is obtained. When the needle tip has penetrated the wall of the vessel, the tenting will resolve and the vessel will appear to reopen. The needle tip should be observed inside the lumen of target vessel.
   - B. The needle is inserted at a 45 to 60-degree angle to the skin with the entry point at the same distance from the probe as the depth of the vessel. The US probe is kept immobile and the needle is advanced along the 45-degree path until blood flashback is obtained. The needle will not be visualized until it enters the US plane. Following vessel tenting, the needle tip shall be observed to enter the lumen of target vessel.
   - C. The needle is inserted at a 45 to 60-degree angle to the skin and the entry point is adjacent to the US probe. As the needle advances, the US probe fans along the direction of needle progression. The goal is to follow the tip of the needle (bevel line) until it enters the lumen of the vessel and backflash is obtained. This requires a higher level of dexterity than the previously described techniques.
2. The Long Axis In-Plane Approach (Fig. 8b). The transducer is placed in a longitudinal plane with the probe marker fac-

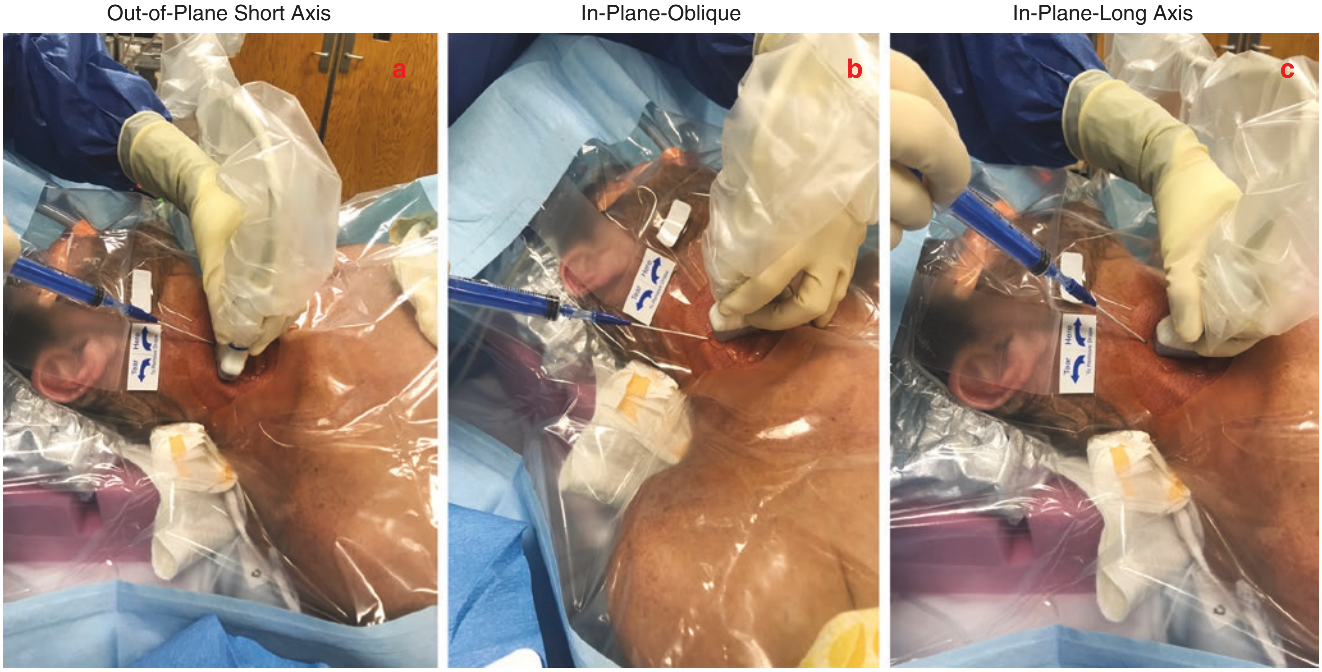

Fig. 8 Three techniques for ultrasound guided vascular access

ing cephalad to view the target vessel clearly. The needle is inserted just underneath the probe indicator. The needle should be visible as a bright, linear, hyperechoic structure advancing toward the target vessel. Careful maintenance of the long axis image of both the needle and vessel is critical as this allows visualization of the needle pathway and needle tip throughout the procedure. The disadvantage of this approach is the inability to view adjacent vessels or other important anatomic structures; slight deviation of the needle direction may cause unintended injury.

3. The Oblique In-Plane Approach (Fig. 8c): The short axis view of the target vessel is obtained, and the probe is then turned 30–45 degrees clockwise to obtain a lateral cephalad to medial caudad view of both artery and vein. The needle is inserted directly at the cephalad end of the probe and advanced in plane toward the target vessel. Blood is aspirated as the needle tip is visualized entering the lumen of the vessel. The advantage of this technique is the ability to view both artery and vein at the same time; the true needle tip can be followed as it enters the target vessel [11].

6 US Guided Internal Jugular Vein Cannulation

6.1 Pre-Procedure Checklist

It is advised to check and correct the coagulation status before central line placement. Inadvertent arterial puncture is a common mechanical complication of central line placement and may lead to hemothorax, hematoma, carotid artery dissection and stroke. US guidance reduces arterial puncture by 90% compared to landmark approach and complications are virtually eliminated [12]. Several studies demonstrate no major complications in patients with bleeding diathesis using US guided central venous access, [13–14] suggesting that routine correction of coagulopathy might not be necessary. However, if coagulopathy is present, the internal jugular vein is an optimal choice due to its superficial position and compressibility. Experienced proceduralists should perform the procedure with an in-plane techniques to avoid arterial puncture in this scenario.

6.2 US Screening

Each side of the neck should be scanned systematically before the decision is made on the location of IJV cannulation. The scanning should be performed in the cephalad to caudal and medial to lateral directions. Critical structures should be identified and abnormalities diagnosed. The trachea is a hypoechoic structure underneath the hyperechoic tracheal rings, which creates a comet tail artifact inside the airway. A normal thyroid gland can be visualized as a homogenous structure demarcated by clear anatomic borders. The gland is surrounded by a layer of deep fascia which anchors the gland to the trachea and larynx (Fig. 9).

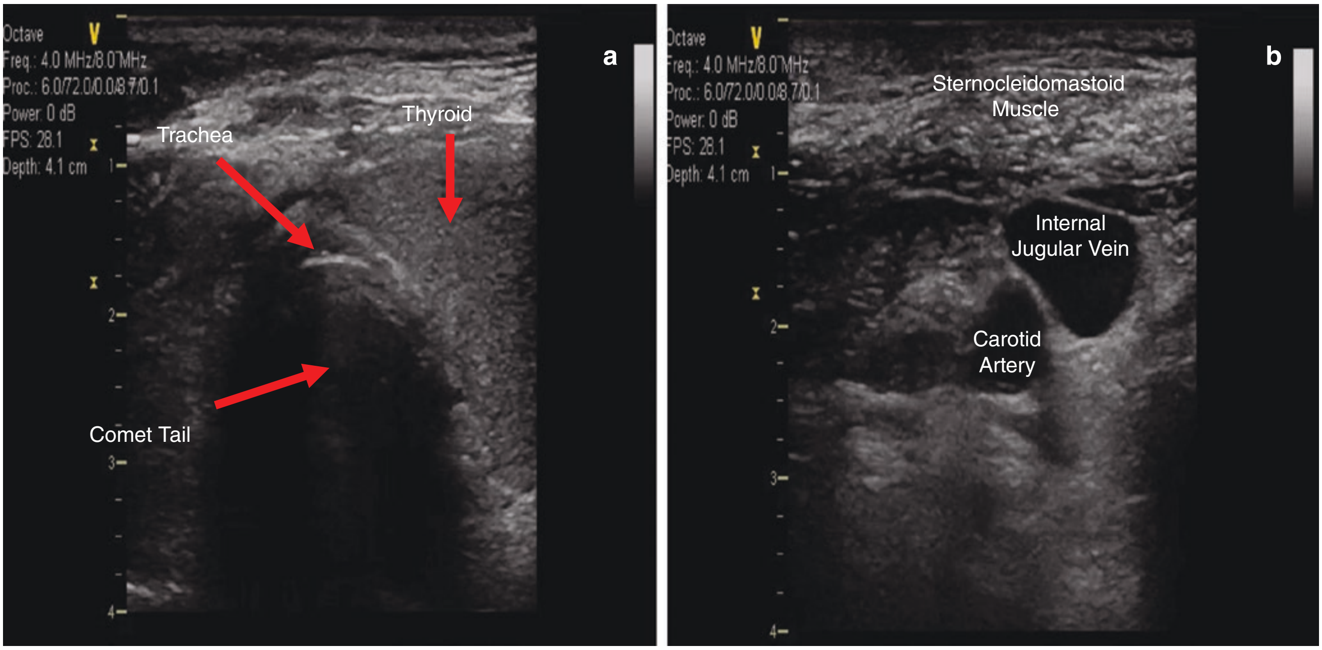

Fig. 9 Ultrasound screening of the neck from medial to lateral. In the medial position, trachea and thyroid are identified. In the lateral position, sternocleidomastoid muscle, carotid artery and internal jugular vein are identified

The relationship between the carotid artery and internal jugular vein varies significantly among patients and can be altered with head rotation and extension. In 49.8% of patients, the IJV lies lateral to the carotid artery. However, 22.5% of patients have the IJV positioned right above the carotid artery, and in 4.5% of patients, the IJV is actually medial to the carotid artery [1]. Preplanning of needle path with US is essential to avoid inadvertent carotid puncture.

Any abnormalities of the carotid artery (atheroma, dissection, or thrombus) and IJV (thrombus, valve, or foreign bodies) should be diagnosed, and that vessel should be avoided for puncture. We recommend scanning the entire neck down to the clavicle and subclavian vein to potentially identify a proximal thrombus, which would present a contraindication for cannulation.

6.3 Step-by-Step US Guided IJV Cannulation (Fig. 10)

1. The patient should be placed in Trendelenburg (head-down) position to increase the size of the IJV and reduce the incidence of air embolism.
2. Perform pre-procedure ultrasonic screening to determine which side should be cannulated.
3. Perform hand hygiene and use maximal sterile barrier precautions (i.e. mask, cap, gown, sterile gloves, and sterile full-body drape).
4. Perform skin antisepsis with >0.5% chlorhexidine with alcohol.
5. The US machine should be placed in a clear line of sight, so that the operator can visualize both the area of skin insertion and US screen without significant neck movement.
6. A sterile US probe cover should be applied over the high frequency US cable and probe, which should be immersed in sterile gel to improve image quality. It is critical to eliminate any air bubbles between the plastic cover and the probe to avoid acoustic shadowing and interference with the imaging of tissue structures.
7. Apply a generous amount of gel to the sterile neck area. Hold the US probe with the nondominant hand and scan the neck from medial to lateral and cephalad to caudad to identify abnormalities of the airway, thyroid gland, carotid artery and internal jugular vein. Make sure to scan all the way down to the clavicle and fan toward the

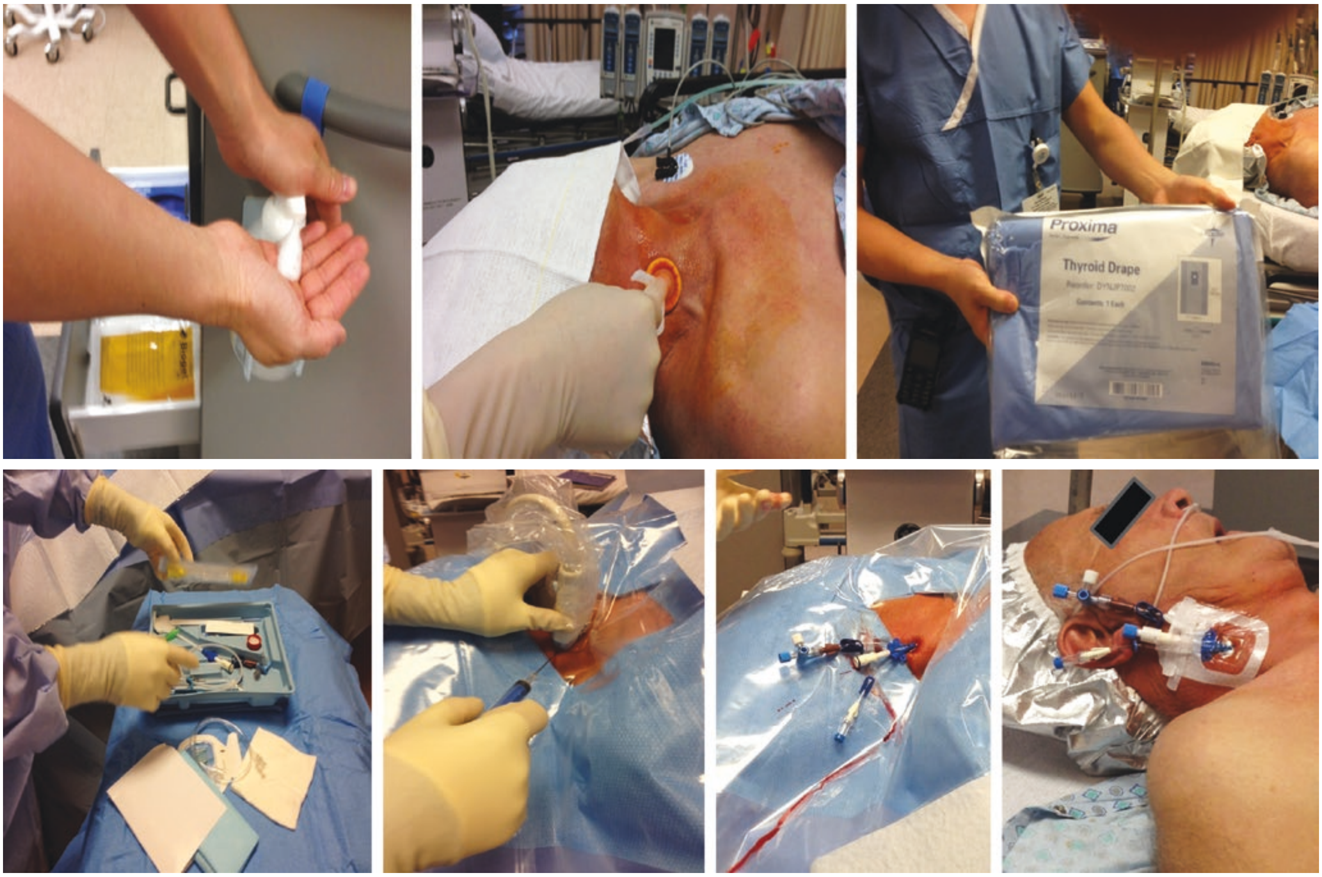

Fig. 10 Internal jugular venous cannulation

feet to rule out venous thrombosis in the proximal IJV and superior vena cava.

8. Position the probe indicator so that the image on the screen is aligned with the anatomic orientation.
9. Differentiate the IJV from carotid artery using 2-dimensional, color Doppler and spectral Doppler as described previously. Pay special attention to the relative relationship between the IJV and carotid artery (Fig. 11).
10. Turn the patient's head or flex/extend the head under real time US guidance so that the distance from the IJV to the carotid artery is maximized to avoid inadvertent arterial puncture.
11. Keep the IJV in the center of the US display and use the midline of the transducer as a visual guide. Very gentle pressure should be applied to avoid venous compression that would make vascular access more difficult.
12. Insert the needle into the skin at a 45 to 60-degree angle (unless using the 90-degree short axis approach) while maintaining constant negative pressure in the syringe. The needle should be introduced with a bevel up orientation to improve needle tip visualization and facilitate guidewire insertion.
13. As the needle advances deeper into the neck, the needle shaft and tip will produce an echogenic artifact with ring down reverberation (Fig. 12). Depending on whether this is an in-plane or out-of-plane approach, the needle tip is continuously visualized with the US probe. Slight fanning, tilting, or rocking of the probe may be required to maintain an optimized view. When the needle contacts the venous wall, tenting will be produced that will eventually resolve once the needle penetrates the vessel wall (Fig. 12). The negative pressure applied to the syringe will now ease and a backflash of venous blood will be observed in the syringe.
14. The syringe is removed from the needle, and the guidewire is passed through the needle into the IJV. Transverse and longitudinal views should be obtained to note appropriate guidewire location inside the IJV and not other critical structures such as the carotid artery. The authors recommend scanning as close to the superior vena cava as possible to ensure the guidewire does not go down the arms or in cephalad direction (Fig. 13). The ASE and the SCA recommend that real-time US be used for confirmation of successful vessel cannulation. It is vitally important for the guidewire to be visualized in the target vessel and that the adjacent structures be examined to confirm the absence of the guidewire. Because there may be ambiguity of the guidewire tip with short axis US imaging alone, manometry with a fluid-filled catheter through a flexible catheter in the vessel is recommended when long axis imaging is not used for confirmation of venous catheter placement. When available, transesophageal echocardiographic or fluoroscopic imaging of the guidewire in the superior vena cava or

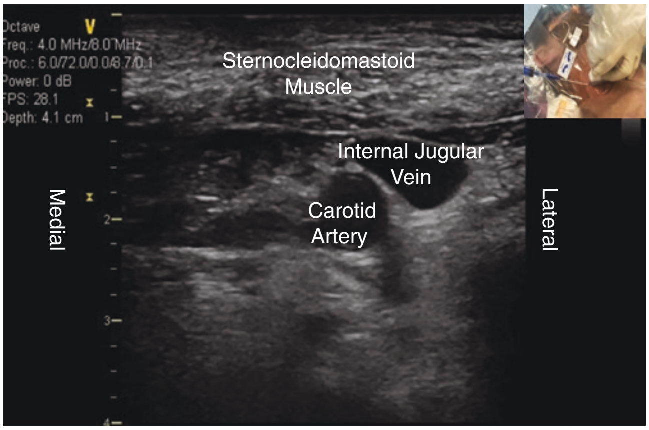

Fig. 11 Oblique In-Plane Approach Internal Jugular Vein Sonoanatomy

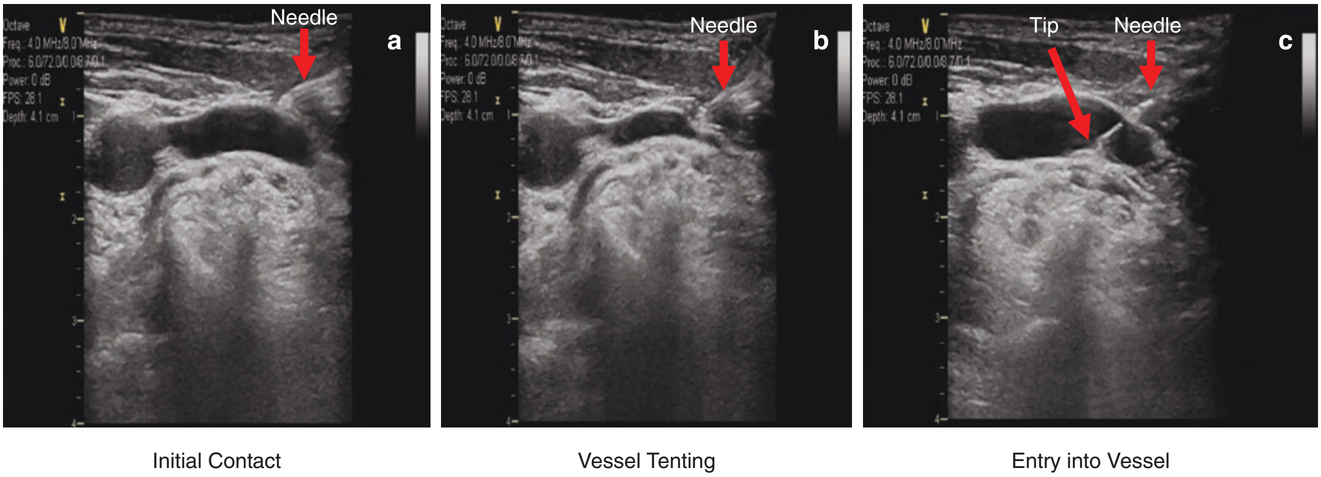

Initial Contact Vessel Tenting Entry into Vessel

Fig. 12 Incremental imaging of needle advancement into the internal jugular vein

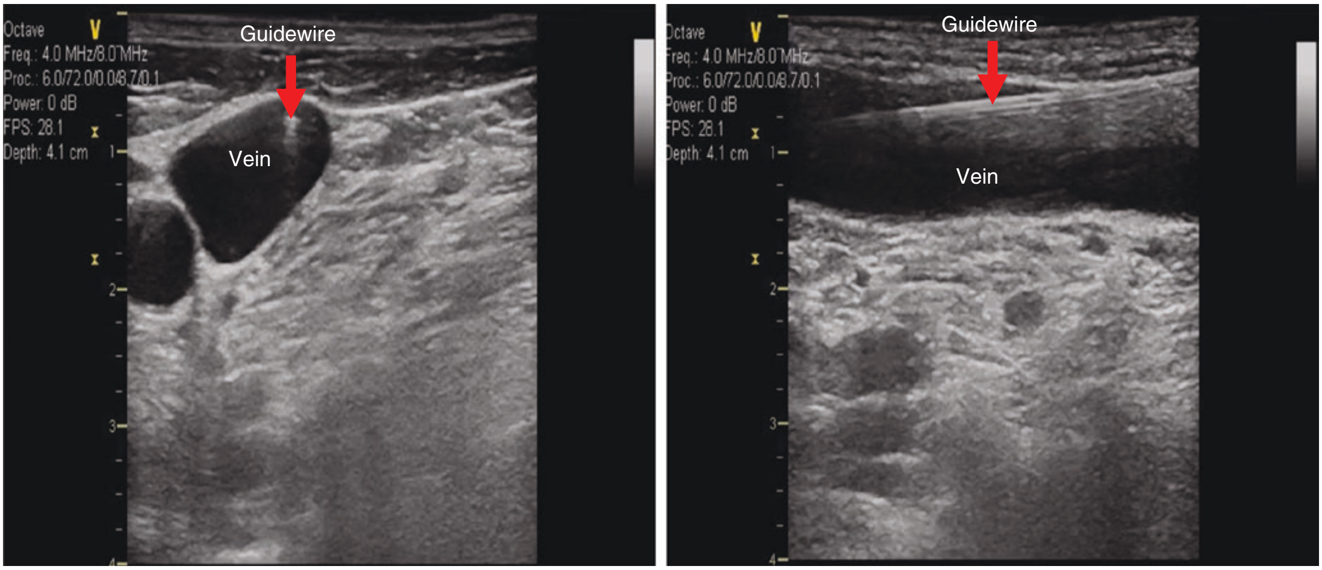

Guidewire in Short Axis View Guidewire Long Axis View

Fig. 13 A guidewire within the internal jugular vein, in both short and long axis views

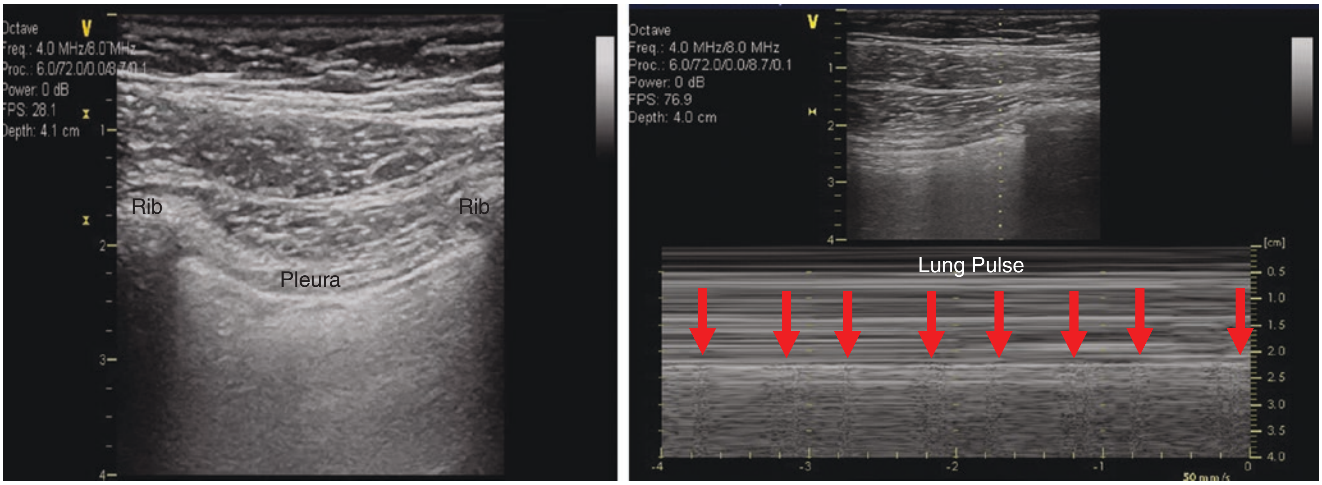

Lung Ultrasound M Mode Lung Ultrasound-Sea Shore Sign

Fig. 14 Normal lung ultrasound with typical sliding, lung pulse and sea shore sign

inferior vena cava provides definitive confirmation of placement into the central venous system [1].

15. Dilate the central line tract with a dilator and insert the preassembled central line apparatus. Secure the central line with dressing. After this is completed, ensure that the wire is removed.
16. Perform lung US to rule out pneumothorax and hemothorax. Using the same high frequency probe, both the anterior and posterior bilateral lung fields should be scanned systematically. The probe indicator should be pointed to the head and perpendicular to the pleura. The pleural line between the ribs (highly reflective and white appearance with acoustic shadowing below) can be easily identified with characteristic sliding with breathing and pulsation with heart contraction (Fig. 14). Absence of sliding, lung pulse, and identification of a lung point (the junction between normal lung sliding and absence of lung sliding) shall raise high suspicion for pneumothorax. Fluid accumulation (black on US) in the posterior lung field should raise serious concerns for hemothorax due to vessel injury [15].
17. The guidewire and other catherization instruments should be counted when the procedure is finished to prevent accidental guidewire retention inside the body. Guidewire retention is a rare complication of central venous catheter placement, and has been related to

operator fatigue, inexperience, inattention, and inadequate supervision of trainees. Recurring scenarios in cases involving guidewire loss include the worsening of patients' clinical condition during catheter placement as well as complex procedures necessitating more than one guidewire insertion. Intraoperative guidewire loss occurs at an estimated rate of 1:3291 procedures [19].

7 US Guided Subclavian Vein Cannulation

To cannulate the subclavian vein, both supraclavicular and infraclavicular approaches can be utilized. US scanning of the subclavian vein is limited by the clavicle as US cannot penetrate bone. In general, a smaller footprint probe is preferred due to the small space between the clavicle and ribs; however, a large high frequency probe can still be used [16]. The ASE and the SCA state that high-risk patients may benefit from US screening of the subclavian vein before attempted cannulation to identify vessel location and patency as well as to specifically identify a thrombus before attempted cannulation [1].

Three approaches are recommended for real-time US guidance of subclavian vein cannulation including: supraclavicular in-plane, infraclavicular in-plane, and infraclavicular out-of-plane techniques (Fig. 15).

1. The patient should be placed in Trendelenburg (head-down) position to increase the size of IJV and reduce the incidence of air embolism.
2. Perform pre-procedure ultrasonic screening to decide which side should be cannulated.
3. Perform hand hygiene and use maximal sterile barrier precautions (i.e. mask, cap, gown, sterile gloves, and sterile full-body drape).
4. Perform skin antisepsis with >0.5% chlorhexidine with alcohol.
5. The US machine should be placed in a clear line of sight for the operator so that the operator can visualize the area of skin insertion and US screen without significant neck movement.
6. A sterile US probe cover should be applied over the high frequency probe, which should be immersed in sterile gel to improve image quality. It is critical to eliminate air bubbles between the plastic cover and the probe to avoid acoustic shadowing because US can't transmit through air.
7. Apply a generous amount of gel to the sterile area. Hold the US probe with the nondominant hand and scan the subclavian vessels from either the supraclavicular or infraclavicular position.
8. Position the probe indicator so that the image on the screen is aligned with the anatomic orientation.
9. Differentiate the subclavian vein from subclavian artery using 2-dimensional, color Doppler and spectral Doppler as described previously. It is important to distinguish between pulsatility of the vein due to respiratory variation and pulsatility of the artery. Confirmation of the venous circulation can be facilitated by the injection of agitated saline or "echo contrast" into a vein of the ipsilateral arm (if available) with subsequent imaging of the microbubbles in the vein [1] (Fig. 16). Pleura is identified as a bright line inferior to the subclavian vessels, and it should never be entered to avoid the risk of pneumothorax.

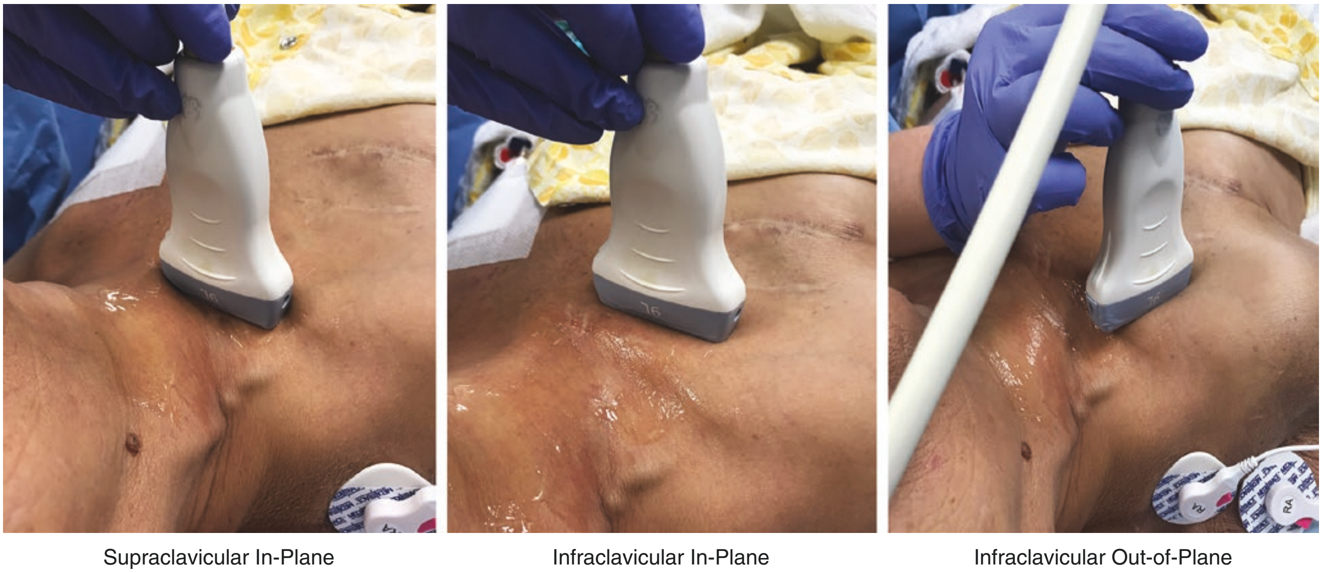
Supraclavicular In-Plane
Infraclavicular In-Plane
Infraclavicular Out-of-Plane

Fig. 15 Ultrasound guided subclavian vein cannulation techniques

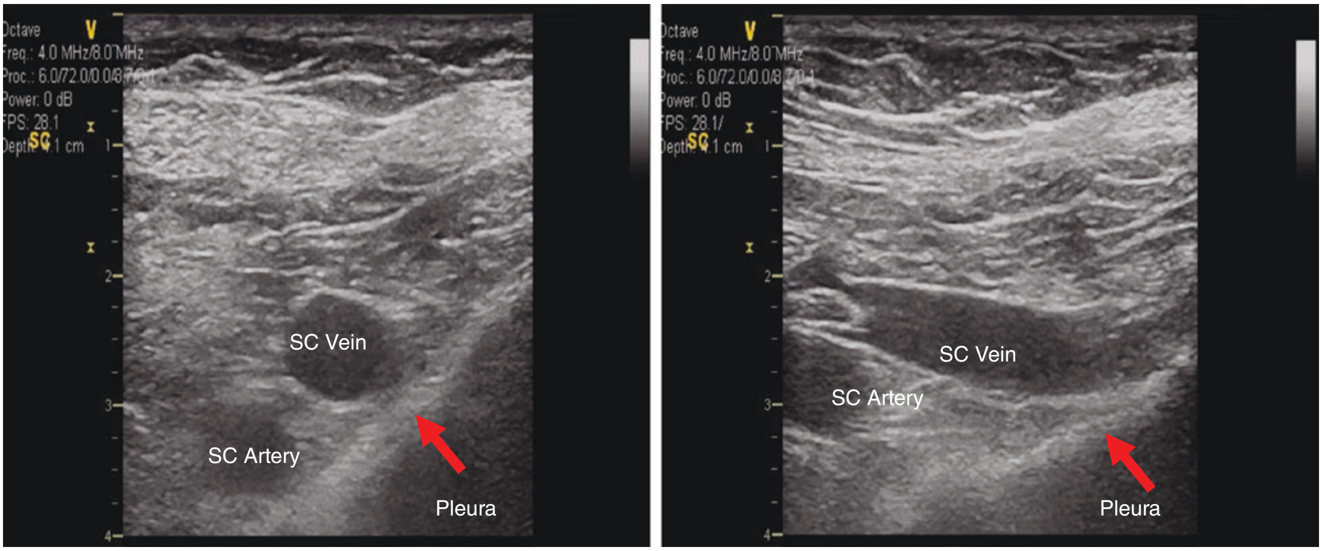

Subclavian Short Axis View

Subclavian Long Axis View

Fig. 16 The subclavian vein in short and long axis views. (*SC* subclavian)

10. Insert the needle into the skin at a 45 to 60-degree angle while maintaining constant negative pressure in the syringe. The needle should be introduced with a bevel down orientation to facilitate guidewire insertion into the superior vena cava.
11. As the needle advances deeper toward the subclavian vein, the needle tip is followed by either not moving the probe for in-plane technique or by fanning the probe for out-of-plane technique until the target vessel is entered.
12. The syringe is removed from the needle and guidewire passed through the needle into the subclavian vein. Using the approach described above, appropriate placement of the guidewire is confirmed.
13. Dilate the central line tract with a dilator, and insert the preassembled central line apparatus. Secure with the apparatus with and appropriate dressing.
14. Lung US is used to rule out pneumothorax and hemothorax as described above. The incidence of pneumothorax is higher with subclavian cannulation compared to internal jugular cannulation.
15. The location of the guidewire should be noted when the procedure is finished to prevent accidental guidewire retention inside the body.

8 US Guided Femoral Vein Cannulation

Femoral vein access has several advantages in critically ill patients due to avoidance of complications such as pneumothorax, hemothorax, and interruption of cardiopulmonary resuscitation during cardiac arrest. However, femoral vein access presents risks of bleeding, vascular injury, and significant infectious complications. US-guided femoral vein cannulation reduces the incidence of complications due to the lower rate of inadvertent vessel puncture [17].

Both in-plane and out-of-plane approaches have been utilized for femoral vein cannulation. The common femoral artery, femoral vein and femoral nerve lie within the femoral triangle in the inguinal-femoral region (Fig. 17). Because the femoral nerve and artery usually lie lateral to femoral vein, an in-plane technique might cause injury to the artery and nerve during the advancement of the needle. An out-of-plane approach is therefore the preferred technique. Following the same steps as described for neck vein cannulation, the needle tip should be visualized as it enters the femoral vein and the guidewire position should be confirmed.

9 US Guided Artery Cannulation

Arterial access is important for hemodynamic management in the critically ill patient. Common sites of arterial cannulation include the radial, brachial, femoral, axillary, and dorsalis pedis arteries. The major advantages of radial artery cannulation are that the hand has a dual blood supply and the artery is generally superficial with a non-tortuous pathway. US guidance for arterial cannulation improves success and reduces time to cannulation in comparison to the palpation method [18]. US guidance is particularly useful for patients with large body habitus, altered anatomy, low perfusion, nonpulsatile blood flow (such as in left ventricular assist device patients), and previously unsuccessful cannulation.

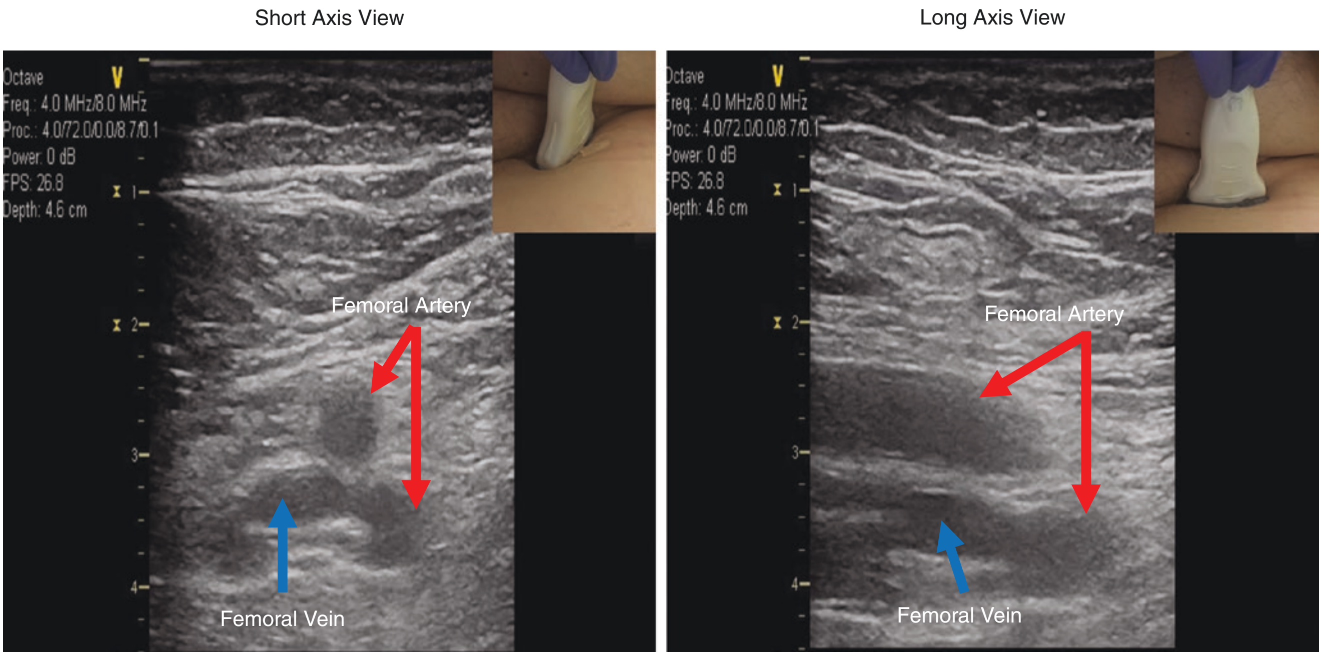
Short Axis View
Long Axis View
Octave
Freq.: 4.0 MHz/8.0 MHz
Proc.: 4.0/72.0/0.0/8.7/0.1
Power: 0 dB
FPS: 26.8
Depth: 4.6 cm
Femoral Artery
Femoral Vein
Femoral Artery
Femoral Vein

Fig. 17 The femoral vein in short and long axis views

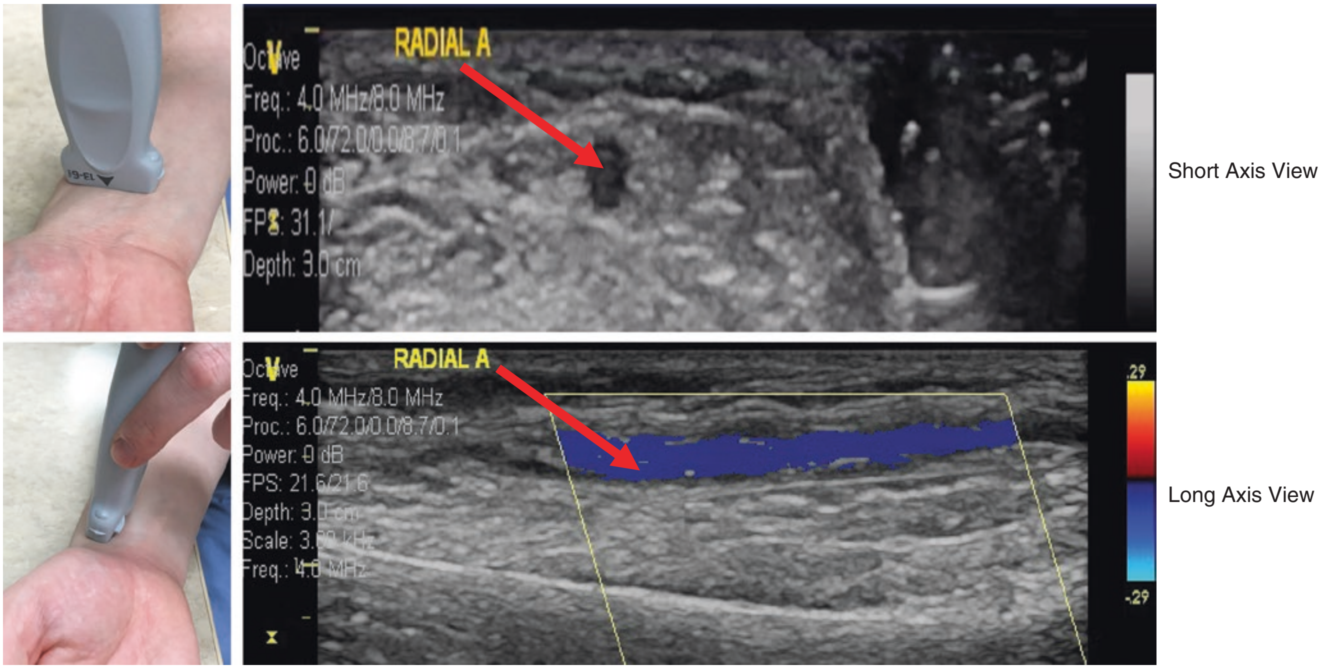
RADIAL A
Octave
Freq.: 4.0 MHz/8.0 MHz
Proc.: 6.0/72.0/0.0/8.7/0.1
Power: 0 dB
FPS: 31.1
Depth: 3.0 cm
Short Axis View
RADIAL A
Octave
Freq.: 4.0 MHz/8.0 MHz
Proc.: 6.0/72.0/0.0/8.7/0.1
Power: 0 dB
FPS: 21.6/21.6
Depth: 3.0 cm
Scale: 3.00 kHz
Freq.: 4.0 MHz
.29
-.29
Long Axis View

Fig. 18 The radial artery in short and long axis views

On US, the artery can be distinguished from the vein by the following features: lack of complete compressibilty, predominantly systolic blood flow, and higher velocity. Both in-plane and out-of-plane techniques can be used to cannulate the artery over the needle or over a guidewire (Fig. 18). The use of a probe covers and other sterile techniques should be observed for arterial cannulation as it is for central venous cannulation.

10 US Guided Peripheral Venous Cannulation

US-guided peripheral vein cannulation is a rescue technique usually performed after failed attempts with the palpation technique or in patients with known difficult access [12]. Large veins of the arm, such as the cephalic, basilic and bra-

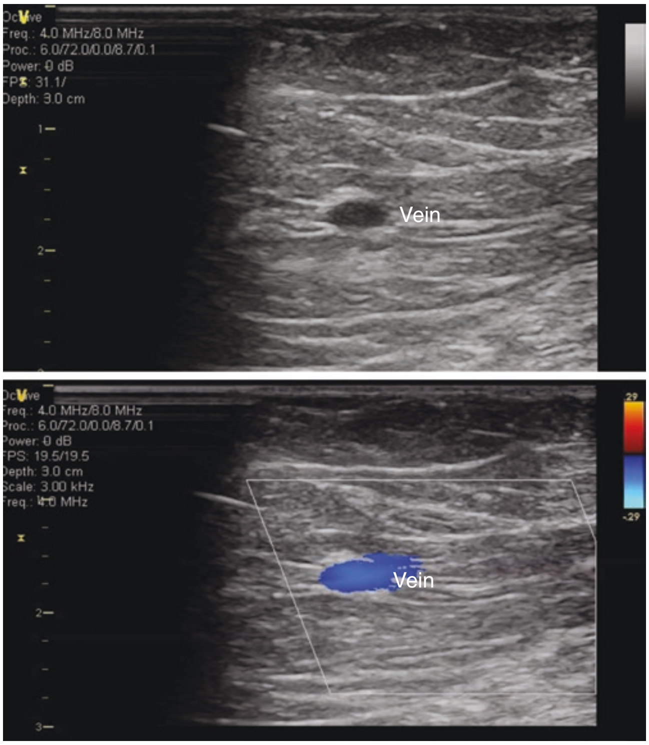

Fig. 19 ultrasound of the peripheral basilic vein with and without color Doppler

chial veins are the easiest to cannulate and therefore preferred options. US reduces the cannulation time and number of attempts [12].

Peripheral veins can be cannulated with both long and short axis approaches (Fig. 19). Because the peripheral veins are easily compressed and venous valves are frequently present, the.

use of the Seldinger technique can improve the success rate. This entails advancement of a guidewire through the needle after successful US guided puncture with subsequent catheter placement over the guidewire.

11 Troubleshooting for Guidewire Advancement

Even if the needle is successfully inserted into the target vessel, it is not guaranteed that the guidewire will advance smoothly. If the guidewire is not in proper place, it is very dangerous to insert and force the catheter apparatus. There are many scenarios that can inhibit the ability of the guidewire to advance smoothly, and each of the following situations should be managed accordingly based on US imaging and other diagnostic information.

1. The tip of the needle is partially inserted into the vessel. The guidewire goes outside of the vessel wall during advancement (Fig. 20a).

Diagnosis: Wire is not observed inside the vessel lumen.

Management: Advance the needle so that the tip is completely inside the lumen and re-advance the guidewire. If the vessel is very small, further head-down position or a Valsalva maneuver might be helpful in enlarging the vessel to accommodate the full needle tip.

2. The bevel is positioned incorrectly and not in the direction of blood flow. The guidewire goes the opposite direction of the blood flow (Fig. 20b).

Diagnosis: The bevel of the needle is directed to the opposite path of blood flow on US.

Management: Turn the bevel to align with the blood flow direction under real-time US guidance.

3. Valves inside the vein preventing guidewire advancement (Fig. 6).

Diagnosis: The venous valve can be easily diagnosed with US, and the wire might be caught on the valve.

Management: Manipulate the wire past the valve under real-time US guidance. Using 3D or bi-plane views might be helpful. If difficulty is still encountered, the procedure should be aborted and an alternative site attempted.

4. The proximal vessel (close to the heart) is stenotic either from internal atheroma and thrombosis or from external compression by a hematoma or other structures (Fig. 20c, d).

Diagnosis: Longitudinal view of the target vessel will reveal the small diameter of proximal vessel and identify the causes of narrowing.

Management: Gently manipulate the guidewire to pass the stenotic region under real time US guidance.

5. The guidewire enters into a branch vessel, not the proximal target vessel. This is especially true for IJV cannulation when the wire is crossed through the innominate vein onto the left side(Fig. 20e).

Diagnosis: Longitudinal view of the target vessel and branch vessel shall identify the wire inside the branch vessel.

Management: Withdraw the guidewire and change the direction of advancement under real-time US guidance.

6. Congenital anomalies. In patients with left persistent superior vena cava, the left neck vein is drained directly into the coronary sinus and the guidewire will be difficult to advance. Sometimes, the left side neck veins are connected to the left atrium, a bridge vein, or to the pulmonary veins causing great resistance to guidewires. For the right superior vena cava, there are anomalies such as lack of direct connection to the right atrium, total absence of right superior vena cava, and connection to the left atrium.

Diagnosis: It is challenging to diagnose these conditions with high frequency probes alone, due to inadequate penetration and inability to view deeper structures.

Management: In these situations, the procedure should be abandoned and alternative sites attempted.

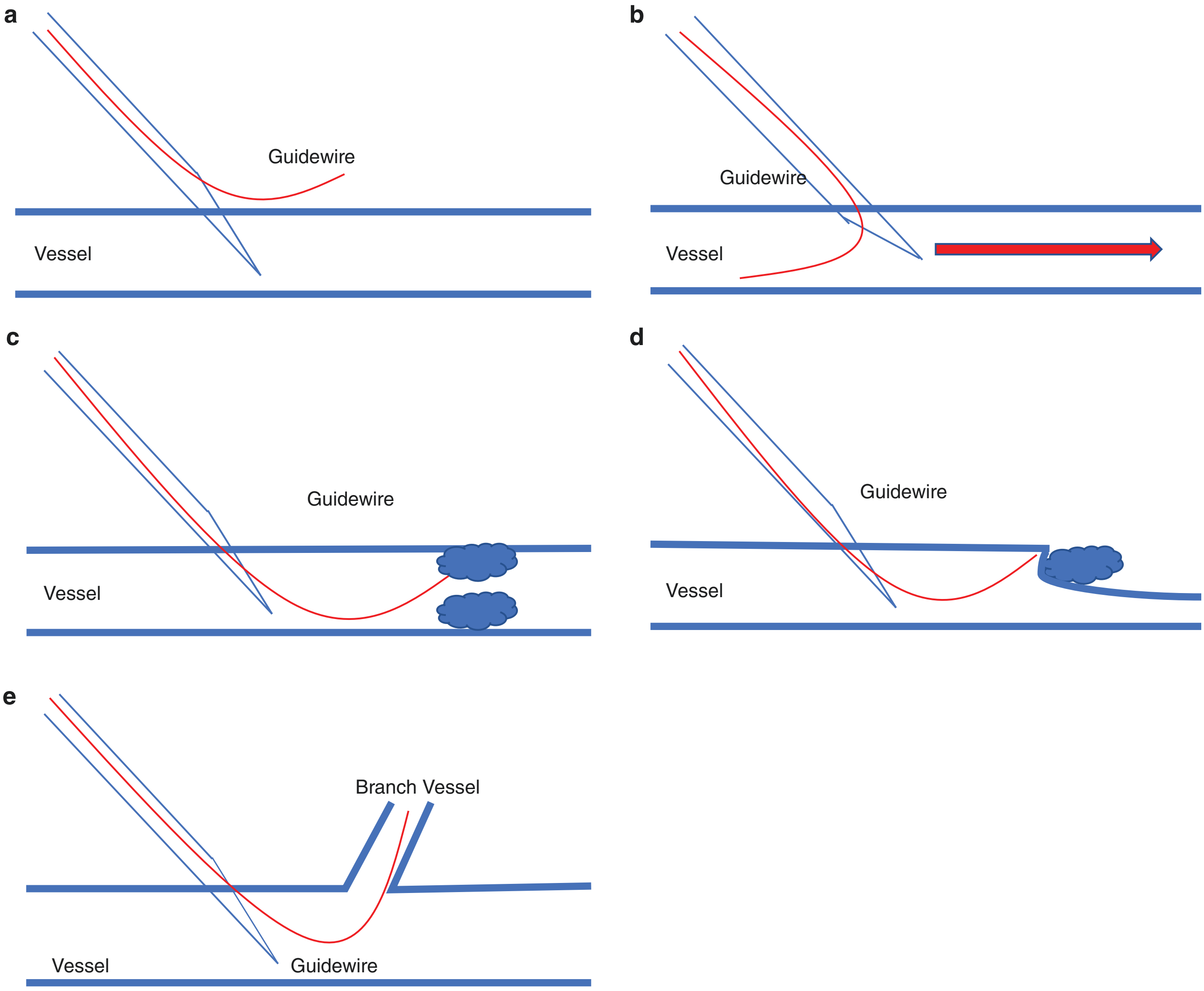

Fig. 20 Troubleshooting guidewire advancement

12 Conclusions

US technology has revolutionized vascular access and improved the safety and efficiency of this common medical procedure. For internal jugular vein cannulation, real-time US guidance should be used whenever possible to improve cannulation success and reduce complications. For other vessels, US guidance should be used as a rescue solution or at least as a screening tool. Proper training is necessary to understand the US anatomy, identify the optimal entry site and needle angle, and the limitations of the US-guided technique.

References

1. Troianos CA, Hartman GS, Glas KE, Skubas NJ, Eberhardt RT, Walker JD, Reeves ST. Councils on intraoperative echocardiography and vascular US of the American Society of Echocardiography. Guidelines for performing US guided vascular cannulation: recommendations of the American Society of Echocardiography and the Society of Cardiovascular Anesthesiologists. J Am Soc Echocardiogr. 2011;24(12):1291–318. https://doi.org/10.1016/j.echo.2011.09.021.
2. McGee DC, Gould MK. Preventing complications of central venous catheterization. N Engl J Med. 2003;348:1123–33.
3. Schepers M, Vercauteren M, De Bock D, Rodrigus I, Vanderplanken D, Camerlinck M. Case report: inadvertent intra-

thecal placement of a pulmonary artery catheter introducer. Anesth Analg. 2013;117(1):119–22. https://doi.org/10.1213/ANE.0b013e318269cd55.

4. Fragou M, Gravvanis A, Dimitriou V, et al. Real-time US-guided subclavian vein cannulation versus the landmark method in critical care patients: a prospective randomized study. Crit Care Med. 2011;39:1607–12.
5. Gu WJ, Tie HT, Liu JC, et al. Efficacy of US-guided radial artery catheterization: a systematic review and meta-analysis of randomized controlled trials. Crit Care. 2014;18:R93.
6. Vezzani A, Manca T, Vercelli A, et al. Ultrasonography as a guide during vascular access procedures and in the diagnosis of complications. J US. 2013;16:161–70.
7. Weiner MM, Geldard P, Mittnacht AJ. US-guided vascular access: a comprehensive review. J Cardiothorac Vasc Anesth. 2013;27(2):345–60. https://doi.org/10.1053/j.jvca.2012.07.007.
8. Garcia R, Labropoulos N. Duplex US for the diagnosis of acute and chronic venous diseases. Surg Clin North Am. 2018;98(2):201–18. https://doi.org/10.1016/j.suc.2017.11.007.
9. Fukazawa K, Aguina L, Pretto EA Jr. Internal jugular valve and central catheter placement. Anesthesiology. 2010;112(4):979. https://doi.org/10.1097/ALN.0b013e3181d436de.
10. Matsuo K, Atsushi Fujita A, Tanaka J, et al. Direct puncture of a surgically-exposed femoral artery graft for simultaneous stenting of coronary, carotid and innominate artery Stenoses. J Neuroendovascul Therapy. 2017;11:409–15.
11. DiLisio R, Mittnacht AJC. The “medial-oblique” approach to US-guided central venous cannulation—maximize the view, minimize the risk. J Cardiothorac Vasc Anesth. 2012;26:982–4.
12. Reusz G, Csomos A. The role of US guidance for vascular access. Curr Opin Anaesthesiol. 2015;28(6):710–6. https://doi.org/10.1097/ACO.0000000000000245.
13. Vigna PD, Monfardini L, Bonomo G, et al. Coagulation disorders in patients with cancer: nontunneled central venous catheter placement with US guidance – a single-institution retrospective analysis. Radiology. 2009;253:249–52.
14. Tercan F, Ozkan U, Oguzkurt L. US-guided placement of central vein catheters in patients with disorders of hemostasis. Eur J Radiol. 2008;65:253–6.
15. Brown SM, Blaivas M, Hirshberg EL, et al. Comprehensive critical care US. ISBN:978-1-620750-322. Soc Crit Care Med.
16. Weiner MM, Geldard P, Mittnacht AJC. US-guided vascular access: a comprehensive review. J Cardiothorac Vasc Anesth. 2013;27:345–60.
17. Iwashima S, Ishikawa T, Ohzeki T. US-guided versus landmark-guided femoral vein access in pediatric cardiac catheterization. Pediatr Cardiol. 2008;29:339–42.
18. Shiver S, Blaivas M, Lyon M. A prospective comparison of US guided and blindly placed radial arterial catheters. Acad Emerg Med. 2006;13:1257–79.
19. Vannucci A, Jeffcoat A, Ifune C, et al. Retained guidewires after intraoperative placement of central venous catheters. Anesth Analg. 2013;117:102–8.

Part II

Head and Neck Ultrasound

Ultrasound for Head Assessment: Diagnosis and Treatment

Alan David Kaye, Matthew Brian Novitch,
and Jennifer Kaiser

1 Introduction

Ultrasound imaging of the head can be a useful screening and confirmation tool for a wide range of pathology in fetal, infant, and adult life. It is commonly performed on infants due to incomplete formation of the structures of the skull and wide fontanelles, creating a window and making visualization of the cranium more feasible. Transcranial Doppler ultrasound evaluates blood flow in the major arteries of the brain. Common uses of ultrasound imaging of the head include evaluation for hydrocephalus, screening for intraventricular hemorrhage and periventricular leukomalacia, evaluation for congenital abnormalities, assessing risk of stroke, and localization of infections or tumors among others. Limitations of ultrasound include sensitivity to motion, such as an active or crying child, or larger patients with a resulting necessary increased depth of visualization. This chapter will discuss ultrasound of the head, its applications, methodology of performance for each application, and its contraindications and complications.

2 Basic Anatomy Markers in Intracranial Ultrasound

Cranial ultrasound can be performed a various number of ways, however Lowe and Bailey proposed a step-wise technique that can be followed by any provider [1].

1. Begin with gray scale imaging performed with a linear-array transducer via the anterior fontanelle in the coronal and sagittal planes.
2. Six to eight coronal images are obtained beginning at the frontal lobes just anterior to the frontal horns and extending to the occipital lobes posterior to the lateral ventricle trigones.
3. The transducer is rotated 90 degrees, and five images are obtained, including a midline sagittal view of the corpus callosum and cerebellar vermis in addition to the bilateral parasagittal images beginning in the midline and progressing laterally through the peripheral cortex.
4. Four color Doppler images may be obtained for screening vascular structures. This is done via color Doppler image of the Circle of Willis via the anterior or temporal fontanelle, used ot localize the middle or internal cerebral artery. Peak systolic velocity, end-diastolic velocity, and resistive index are measured.
5. Venous systems are evaluated for patency, also via a color Doppler image of the sagittal sinus and vein of the Galen in the sagittal plane.
6. Power Doppler imaging can search for areas of hyper- or hypo-vascularity as it may occur with various forms of vascular occlusion, ischemia, or infarction.
7. Lastly, screening images via other supplemental fontanelles and high-resolution linear images are needed. Visualization of the cerebellar hemispheres is optimized by improving detection of posterior fossa hemorrhages. Adjunct color Doppler images via the posterior fontanelle or foramen magnum can be used to screen for patency of transverse sinuses. Switching from a curved- to a linear-array transducer via the anterior fontanelle allows detailed interrogation of the convexity subarachnoid space and superficial cortex as well as deeper brain structures.

A. D. Kaye
Departments of Anesthesiology and Pharmacology, Toxicology, and Neurosciences, Lousiana State University Health Sciences Center, Shreveport, LA, USA

Department of Anesthesiology, Department of Pharmacology Louisiana State University School of Medicine, Louisiana State University Health Sciences Center, New Orleans, LA, USA
e-mail: akaye@lsuhsc.edu

M. B. Novitch (✉)
University of Washington School of Medicine, Department of Anesthesiology, Seattle, WA, USA
e-mail: mnovitch@mcw.edu

J. Kaiser
Medical College of Wisconsin, Milwaukee, WI, USA
e-mail: jkaiser@mcw.edu

© Springer Nature Switzerland AG 2021
J. Li et al. (eds.), *Ultrasound Fundamentals*, https://doi.org/10.1007/978-3-030-46839-2_5

Examples of neonatal ultrasound via images for Figs. 1, 2, 3, 4, 5, and 6 are adapted from Ultrasoundpaedia [2].

2.1 Transabdominal and Transperineal Ultrasound

Labor and its progress is one of the main uses of ultrasound of the head. Head position can be assess via transabdominal ultrasound relative to the occiput position transformed to a 12-hour clock face, and fetal head station can be defined as head-perineum distance by transperineal ultrasound. Fetal head position evaluation via ultrasound has been shown to be feasible and more accurate than cervical exam and vaginal examination in determining progression of labor [3]. In addition, fetal head ultrasound in the labor and delivery setting can help predict obstetric anal sphincter injuries (OASIS). Fetal head circumference percentile is associated with OASIS directly, as the larger the percentile the greater the risk [4]. Severe perineal lac-

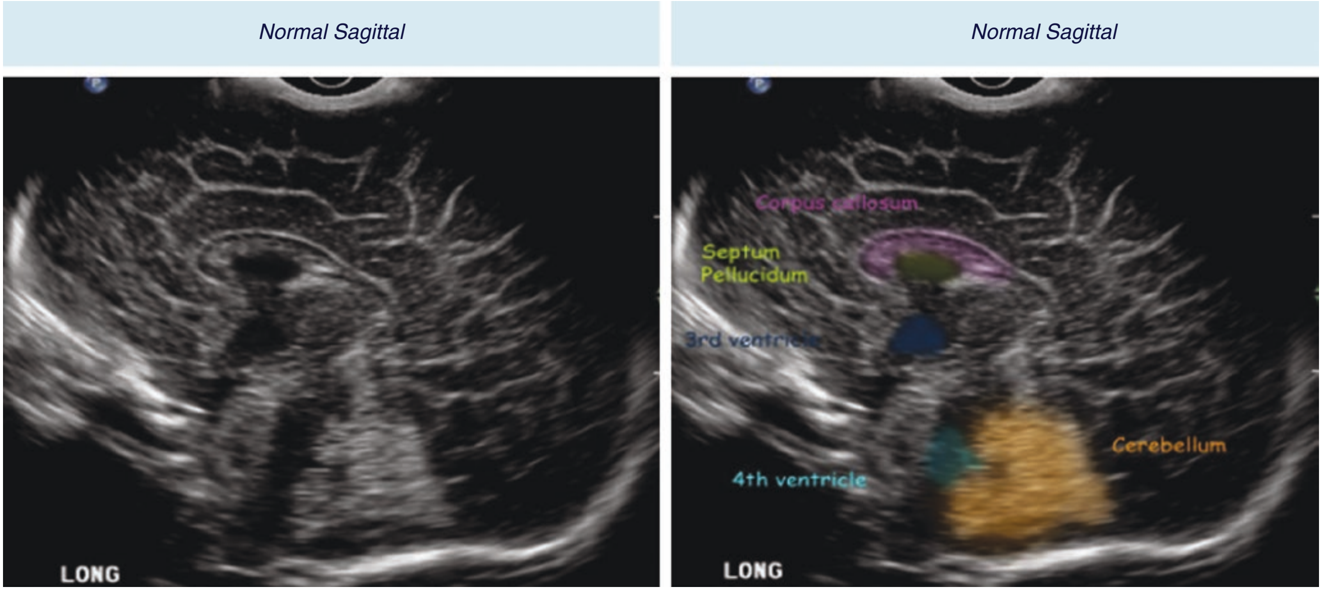
Normal Sagittal

Normal Sagittal

Fig. 1 Normal Sagittal view of the cranium via the anterior fontanelle. Labeled important markers of the sagittal view of the cranium via the anterior fontanelle

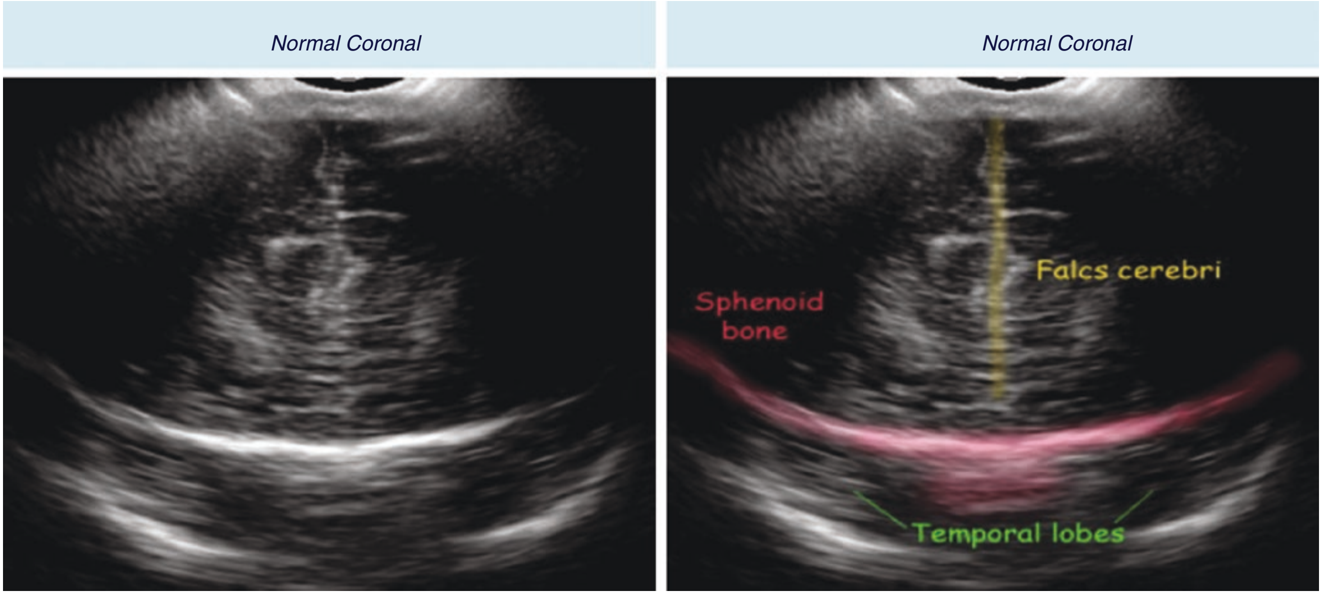
Normal Coronal

Normal Coronal

Fig. 2 Normal Coronal view of the cranium via the anterior fontanelle. Labeled important markers of the coronal view of the cranium via the anterior fontanelle

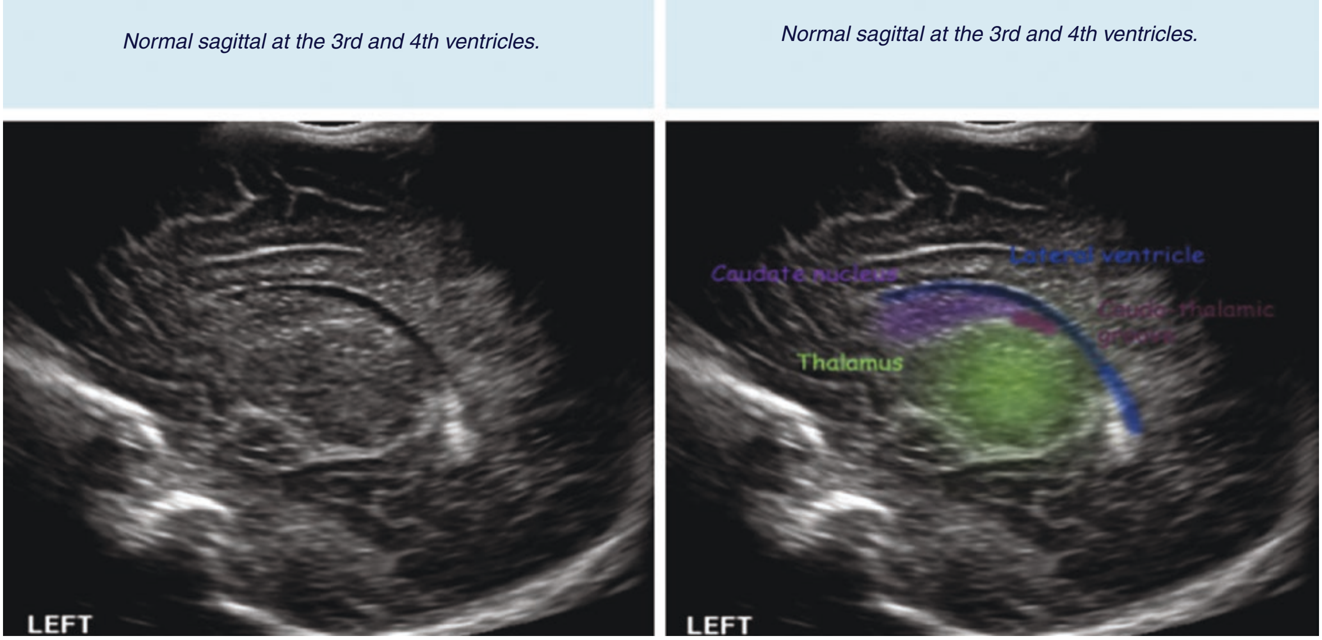
Normal sagittal at the 3rd and 4th ventricles.

Normal sagittal at the 3rd and 4th ventricles.

LEFT
Caudate nucleus
Lateral ventricle
Caudo-thalamic groove
Thalamus
LEFT

Fig. 3 Normal sagittal view of the cranium via the anterior fontanelle at the third and fourth ventricles. Labeled important markers of the sagittal view of the cranium via the anterior fontanelle at the third and fourth ventricles

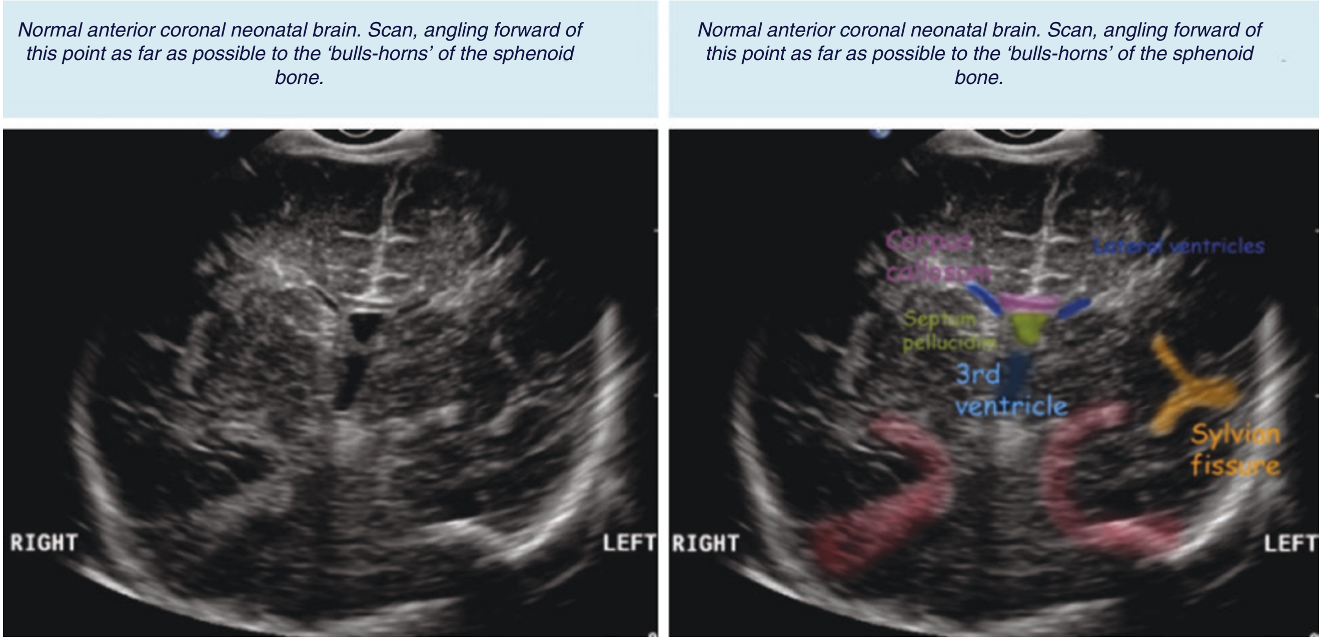
Normal anterior coronal neonatal brain. Scan, angling forward of this point as far as possible to the 'bulls-horns' of the sphenoid bone.

Normal anterior coronal neonatal brain. Scan, angling forward of this point as far as possible to the 'bulls-horns' of the sphenoid bone.

RIGHT
LEFT
Corpus callosum
Lateral ventricles
Septum pellucidum
3rd ventricle
Sylvian fissure
RIGHT
LEFT

Fig. 4 Normal anterior coronal neonatal brain. Scan done via angling forward of this point as far as possible to the bulls-horn of the sphenoid bone. Labeled important markers

erations impact short and long term health outcomes such as dyspareunia, fecal and urinary incontinence, and perineal pain. Use of this technique can help clinicians predict and better manage the outcomes of this common complication.

2.2 Cerebrovascular Function

Transcranial Doppler ultrasound (TCD) is an exceptional tool to evaluate cerebrovascular function. TCD assesses blood velocities within the cerebral vessels, cerebral auto-

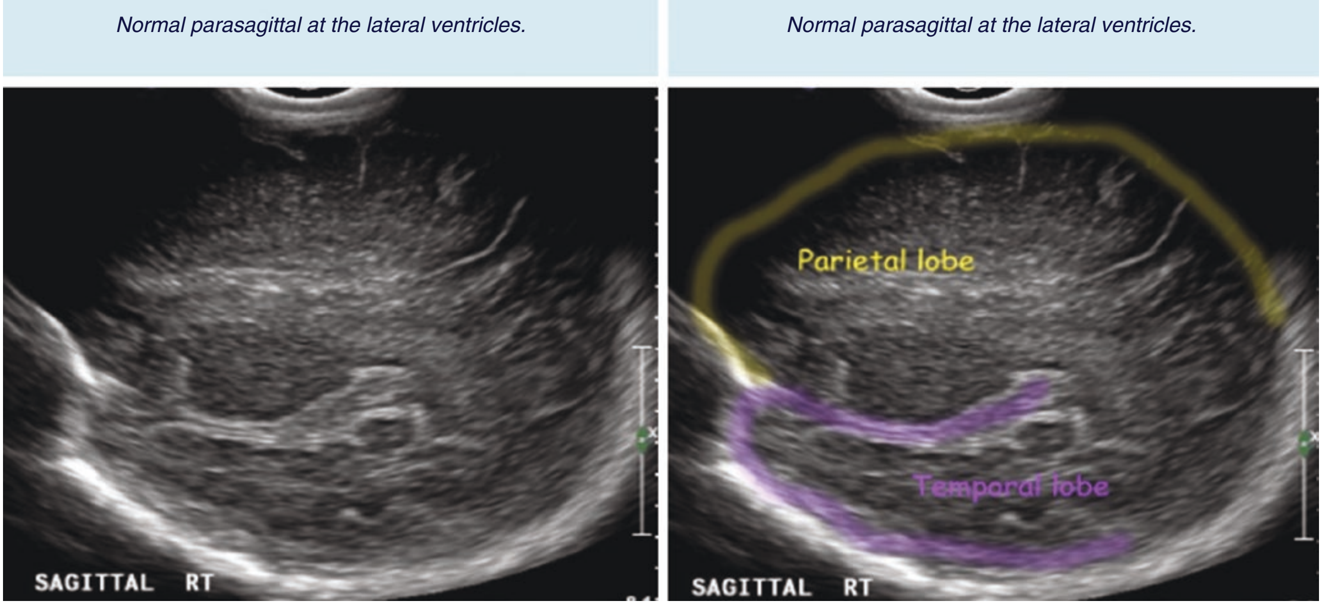

Normal parasagittal at the lateral ventricles.

Normal parasagittal at the lateral ventricles.

Fig. 5 Normal parasagittal view at the lateral ventricles. Labeled markers

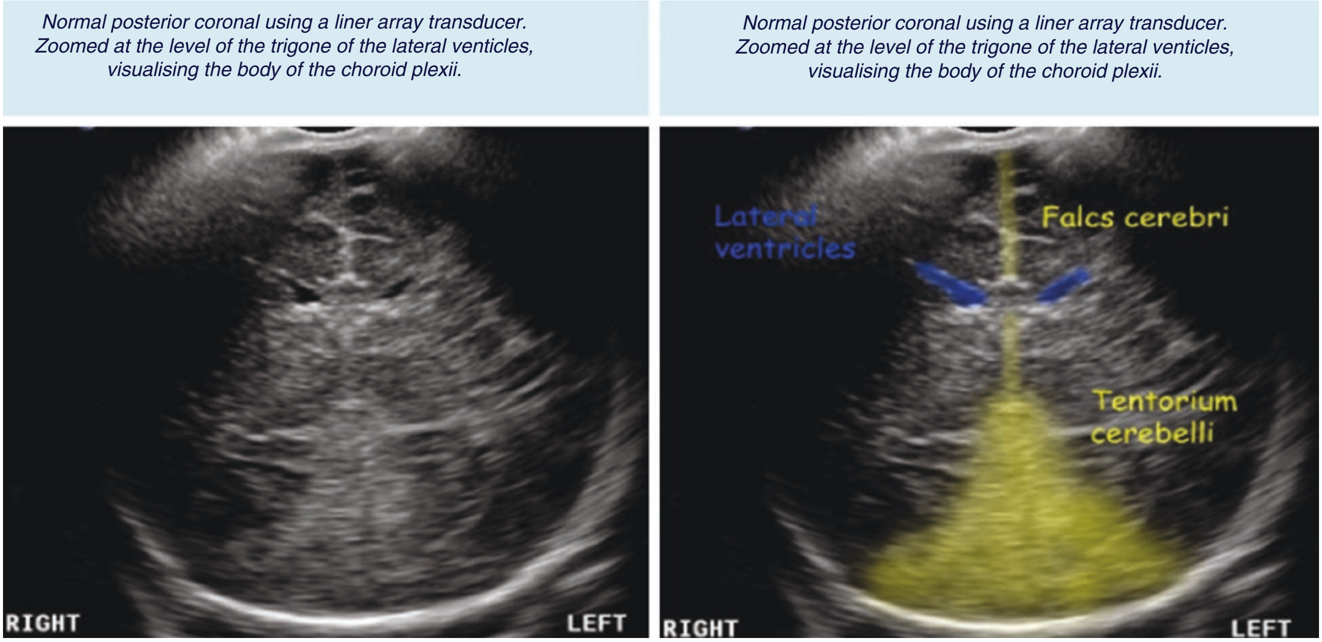

Normal posterior coronal using a liner array transducer. Zoomed at the level of the trigone of the lateral venticles, visualising the body of the choroid plexii.

Normal posterior coronal using a liner array transducer. Zoomed at the level of the trigone of the lateral venticles, visualising the body of the choroid plexii.

Fig. 6 Normal posterior coronal view using a linear array transducer, zoomed into the level of the trigone of the lateral ventricles to visualize the body of the choroid plexii. Labeled markers

regulation, cerebrovascular reactivity to CO(2), and neurovascular coupling, in both physiological states and in pathological conditions such as stroke and head trauma [5]. Accurate TCD relies upon the examiner's technical skill and anatomical knowledge. Three approaches are generally used: The transtemporal approach, the transocular approach to the carotid siphon, and the suboccipital or foramen magnum approach to the basilar artery and the intracranial segments of the vertebral arteries (Table 1). As the cerebral vascular is dynamic and vessel lumen size may change relative to pCO(2) levels, neurometabolic status, blood flow rates, and oxygen saturation of the blood, the examiner should keep in mind the clinical picture of the patient when assessing their cerebrovascular function via TCD

2.3 Transcranial Ultrasonography of the Brain Parynchema

Transcranial Ultrasonography (TCS) displays the brain parenchyma and intracranial ventricular system through the skull. Application if this technique is useful for many disease states specific to the cell bodies of the brain, in particular Parkinson's Disease, damage from ischemic injury, lenticular nucleus hyperechogenicity, and confirming postoperative position of deep brain stimulation electrodes. Intracerebral Hemorrhage appears homogenous, sharply demarcated and hyperechogenic in the acute phase. TCS specifically can be used for monitoring growth of the fluid collection, midline shift, and decrease in echogenic intensity as time passes (Fig. 7a, b).

TCS has been suggested to be beneficial for the early and differential diagnosis of Parkinson's Disease (PD). Substantia Nigra (SN) hyperechogenicity is found in about 90% of PD patients at cross section and is independent from PD duration and severity. In addition, this finding is present in about 9% of adults without a diagnosis of PD, and ongoing research is occurring to determine whether or not this is a valuable screening tool for the later development of PD in healthy patients with this finding. The combined finding of motor asymmetry, hyposmia and SN hyperechogenicity as a cost-effective method of confirming PD, with a specificity of nearly 100% if all three findings are present as evidenced by a 2012 study of over 600 patients [6]. Normal and abnormal findings are shown in Fig. 8.

Table 1 Commonly Used Planes of Approach for Transcranial Ultrasound

Foramen Magnum Approach	The foramen magnum is a passage of the central nervous system through the skull which connects the brain and the spinal cord. An occipital condyle is on either side of the foramen magnum.
Transtemporal approach	The transtemporal window is located above the zygomatic ridge between the lateral canthus of the eye and auricular pinna.
Transorbital approach	Passing through the eye socket.

2.4 TCS for Post-Operative Localization of Brain Implants

Deep Brain Stimulation (DBS) final lead placement is on average 2 mm away from the initial selected target site secondary to caudal brain shift after the cranium is opened and closed. Sufficient imaging techniques post-operatively is therefore necessary, and TCS is a valuable tool for confirmation of DBS electrode location. Gross DBS lead location is easily detected with TCS and can be seen in Fig. 9 a–d.

2.5 Novel Screening for Zika Virus

The Zika virus epidemic that occurred from January first 2016 to November 2016 caused global distress with a resulting race to learn a great deal about this travel-associated disease. Zika virus is a novel teratogenic agent associated with cerebral anomalies. Assessment of antenatal diagnosis and prognosis in fetuses was initially extremely difficult, however ultrasound imaging of the head in the first trimester or early second trimester was shown to be beneficial in early detection of cerebral abnormalities by those at the Pluridisciplinary Center for Prenatal Diagnosis of Martinique. Fourteen pregnant women with confirmed

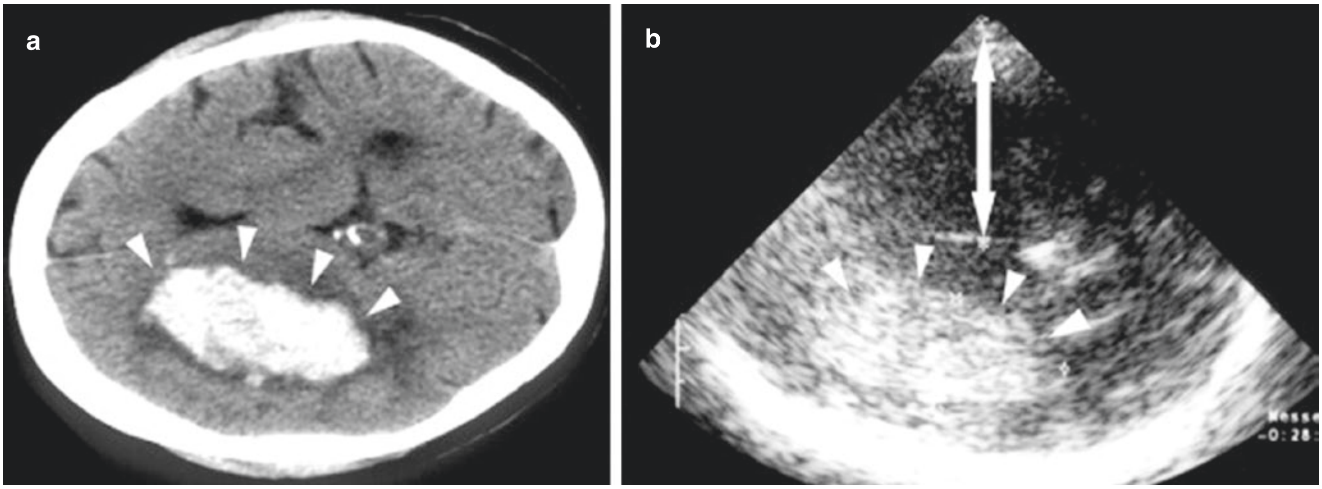

Fig. 7 (**a**, **b**): (**a**): CT image corresponding to the TCS image shown in (**b**) of a large intracerebral hematoma. (**b**): Corresponding TCS image showing acute increased echogenic hematoma. (Image from Walter [7])

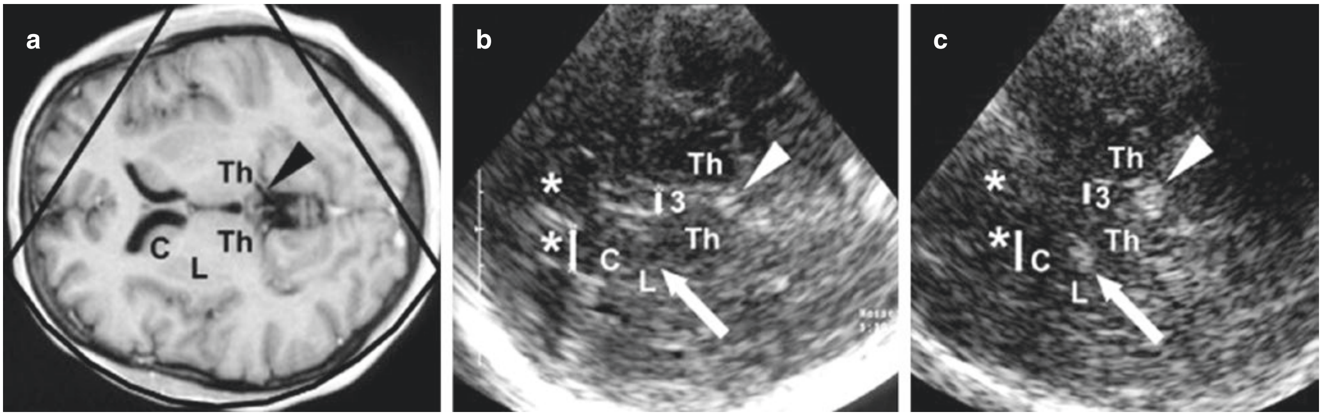
a
Th
Th
C
L
b
*
Th
3
*
Th
C
L
c
*
Th
3
*
Th
C
L

Fig. 8 Increased echogenicity of the lenticular nucleus can be seen in (**c**), relative to the normal findings in (**b**) and the corresponding MRI in (**a**). (Image from Walter [7])

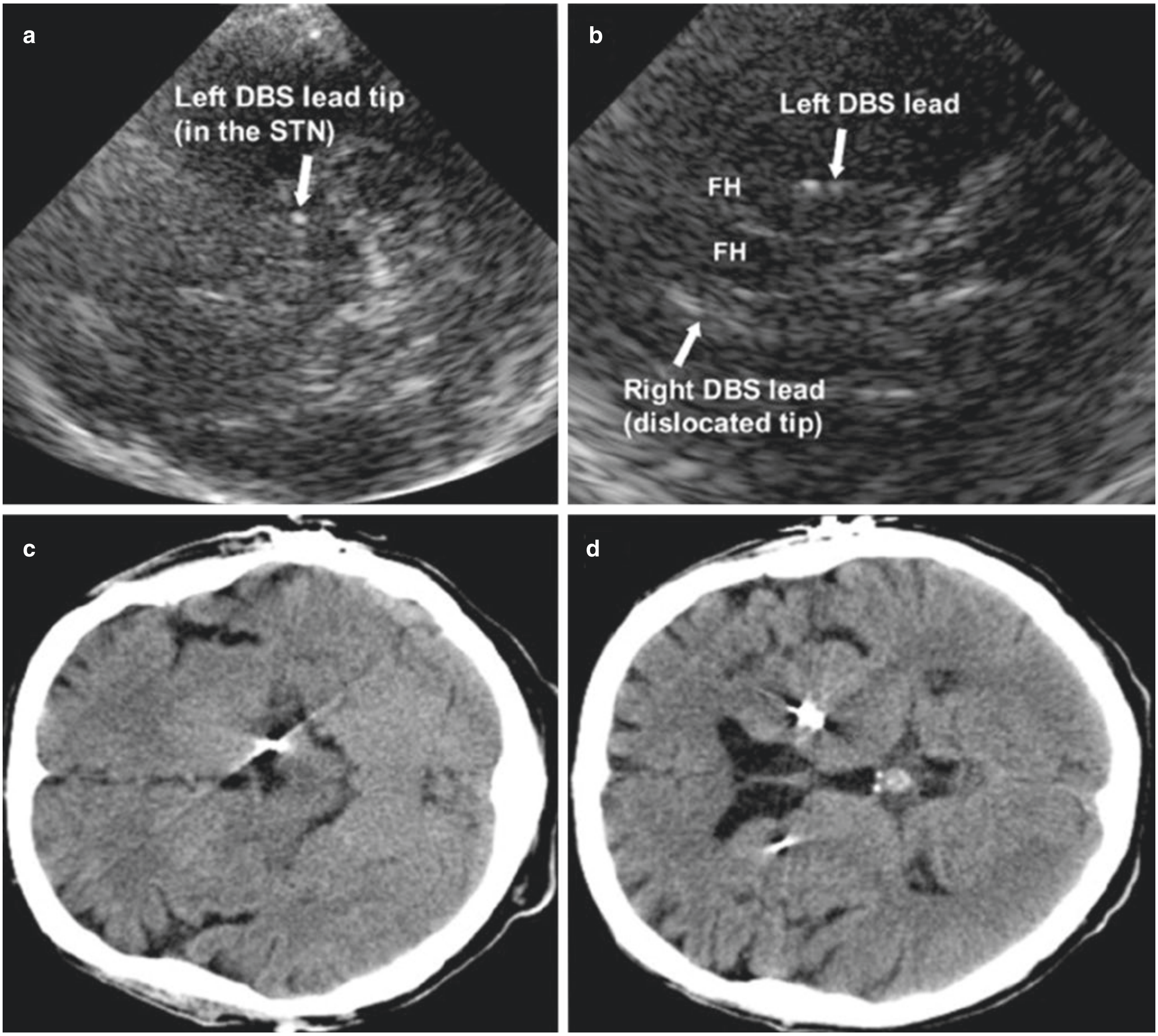
a
Left DBS lead tip (in the STN)
b
Left DBS lead
FH
FH
Right DBS lead (dislocated tip)
c
d

Fig. 9 (**a**–**d**): Postoperatie transcranial sonography of a patient with DBS and unilateral lead placement secondary to right sided lead dislocation. (**a**): TCS image showing left sided DBS lead tip in the subthalamic nucleus while the right-sided DBS electrode is not displaced due to dislocation. (**b**): TCS image showing more cranial parts of the left sided DBS lead and the tip of the dislocated right sided lead. (**c**): CT scan corresponding to (**a**). (**d**): CT scan corresponding to (**b**). (Image from Walter [7])

Zika virus infection had fetal head transabdominal ultrasound at several points between 16 and 28 weeks of gestation. It was found that while only 33% of fetuses had an abnormal ultrasound at 16–20 weeks of gestation, 90% had abnormalities between 20 and 24 weeks of gestation, with all developing abnormalities by 24–28 weeks of gestation. Major anomalies identified were ventriculomegaly (12 fetuses, 86%), cortical atrophy (11, 79%), calcifications (ten, 71%; particularly located at the corticosubcortical junction), and anomalies of the corpus callosum (ten, 71%). Prenatal assessment of head circumference measurement by imaging was not an effective screening tool for congenital Zika virus infection, with microcephaly only identified in nine (64%) fetuses. Thus, ultrasound monitoring was considered to be a good screening strategy to monitor Zika virus-exposed pregnancies, focusing at 22–26 weeks of gestation for confirmation of Zika-associated fetal abnormalities. In addition, identification of ventriculomegaly, cortical atrophy, calcifications, and anomalies of the corpus callosum should prompt laboratory screening for Zika virus in the mother [8].

3 Conclusion

Ultrasonography of the head has a wide variety of applications in a diverse set of patient populations. Its ability to monitor for vascular and parenchymal based changes make it a robust and dynamic imaging technique that can be adapted to almost any situation – whether it be traumatic or a routine outpatient screening procedure. With no radiation exposure, no to minimal discomfort during the procedure, and safety regarding infection and complication, ultrasonography of the head continues to be a leading option for visualization of the cranial structures.

References

1. Lowe LH, Bailey Z. State-of-the-art cranial sonography: part 1, modern techniques and image interpretation. Am J Roentgenol. 2011;196(5):1028–33. https://doi.org/10.2214/AJR.10.6160.
2. Ultrasoundpaedia. Normal Neonatal Head Ultrasound. 1. https://www.ultrasoundpaedia.com/normal-neonatal-head/. Published 2018. Accessed 6 Sep 2018.
3. Usman S, Wilkinson M, Barton H, Lees CC. The feasibility and accuracy of ultrasound assessment in the labor room. J Matern Neonatal Med. 2018:1–10. https://doi.org/10.1080/14767058.2018.1465553.
4. Ortega MV, Kim Y, Masiero J, Hebert K, Leung K, Leftwich H. Can fetal head circumference assessment on ultrasound help predict 3rd and 4th degree perineal lacerations? [40M]. Obstet Gynecol. 2018;131:151S. https://doi.org/10.1097/01.AOG.0000533096.49746.66.
5. Willie CK, Colino FL, Bailey DM, et al. Utility of transcranial Doppler ultrasound for the integrative assessment of cerebrovascular function. J Neurosci Methods. 2011;196(2):221–37. https://doi.org/10.1016/j.jneumeth.2011.01.011.
6. Busse K, Heilmann R, Kleinschmidt S, et al. Value of combined midbrain sonography, olfactory and motor function assessment in the differential diagnosis of early Parkinson's disease. J Neurol Neurosurg Psychiatry. 2012;83(4):441–7. https://doi.org/10.1136/jnnp-2011-301719.
7. Walter U. Transcranial sonography of the cerebral parenchyma: update on clinically relevant applications. Pers Med. 2012;1(1–12):334–43. https://doi.org/10.1016/J.PERMED.2012.02.014.
8. Schaub B, Gueneret M, Jolivet E, et al. Ultrasound imaging for identification of cerebral damage in congenital Zika virus syndrome: a case series. Lancet Child Adolesc Heal. 2017;1(1):45–55. https://doi.org/10.1016/S2352-4642(17)30001-9.

Ultrasound-Guided Neck Assessment

Andrew Brunk, Erik Helander, and Alan David Kaye

1 Introduction

Complications resulting from difficult intubations are not uncommon, and can result in significant morbidity and mortality. Information garnered from ultrasound (US) of the neck can provide valuable diagnostic information and aid in the preoperative assessment of the airway. Unlike CT scans or MRIs, ultrasound can provide real-time and dynamic information regarding the airway during the respiratory cycle. However, due to the high acoustic impedance of air, and because airway structures are filled with air, posterior structures of the airway cannot be adequately visualized [1, 2]. There are many important structures in the neck that can be evaluated using US. This chapter will focus strictly on the thyroid gland and the airway structures within the neck. Portions of the airway that can yield information, which can have clinical implications, include (but are not limited to): hyoid bone, vocal cords, cricoid cartilage, cricothyroid membrane and the trachea.

2 Hyoid Bone

2.1 Anatomy

The hyoid bone is a horseshoe-shaped, sesamoid bone located in the anterior neck. It has a central body, a pair of greater horns, and a pair of lesser horns. It sits at the base of the tongue, and with the neck in neutral position the mandible is found anteriorly, epiglottis and pharynx posteriorly and larynx inferiorly. Ten muscles on each side of the neck attach to the hyoid bone, and connect the bone to the mandible, tongue, thyroid cartilage, skull, manubrium and even scapula [3].

2.2 Sonoanatomy

For the purpose of ultrasound evaluation, the hyoid bone separates the upper airway into the suprahyoid and infrahyoid regions. When the probe is placed submentally in the sagittal plane the hyoid bone marks the posterior limit of the frame, and the floor of the mouth and the tongue can be evaluated [4]. The infrahyoid region includes the visceral, perivertebral, carotid, retropharyngeal, and anterior and posterior cervical spaces [5]. Ultrasound of the hyoid bone itself reveals a bright, hyperechoic structure, and can be done in either the transverse or sagittal plane. Transverse view shows a distinctive inverted horseshoe-shaped structure with acoustic shadowing (Fig. 1), and sagittal view shows a thin curve with posterior shadowing.

2.3 Pathology

The hyoid bone is in part responsible for maintaining upper airway patency. Obstructive sleep apnea (OSA), as its name suggests is characterized by apneic periods secondary to airway obstruction. More inferior and posterior position of the

---

A. Brunk
Department of Anesthesiology, LSUHSC, New Orleans, LA, USA
e-mail: abrunk@lsuhsc.edu

E. Helander
Department of Anesthesiology, University of Florida-Gainesville, Gainesville, FL, USA
e-mail: EHelander@anest.ufl.edu

A. D. Kaye (✉)
Departments of Anesthesiology and Pharmacology, Toxicology, and Neurosciences, Lousiana State University Health Sciences Center, Shreveport, LA, USA

Department of Anesthesiology, Department of Pharmacology Louisiana State University School of Medicine, Louisiana State University Health Sciences Center, New Orleans, LA, USA
e-mail: akaye@lsuhsc.edu

© Springer Nature Switzerland AG 2021

J. Li et al. (eds.), *Ultrasound Fundamentals*, https://doi.org/10.1007/978-3-030-46839-2_6

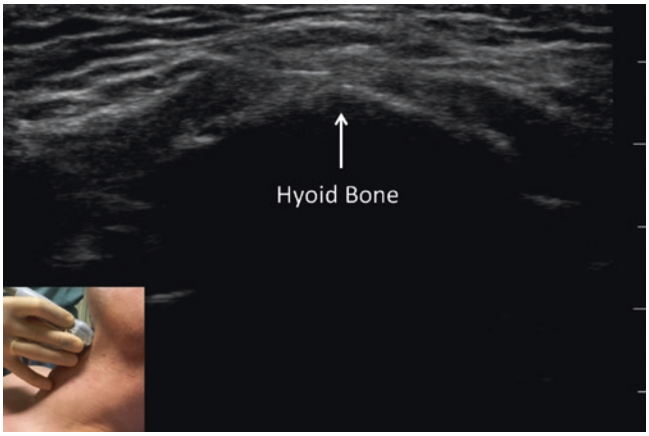

Fig. 1 Hyoid bone in transverse view

hyoid bone has been implicated in OSA, as has restricted hyoid bone movement [3].

3 Larynx

3.1 Anatomy

The larynx is an anterior midline structure that bridges the pharynx superiorly to the trachea below. It descends from its more superior position with time to reach its more inferior adult position [6]. It is located at the third to sixth cervical level, suspended from the hyoid bone above it. Nine cartilaginous structures compose the skeleton; the thyroid cartilage is the primary anterior structure and the cricoid cartilage the principal posterior cartilage [6]. The larynx houses numerous muscles including the intrinsic muscles essential to phonation, and the extrinsic muscles responsible for elevation and depression of the larynx as a whole. The recurrent laryngeal nerves and superior laryngeal nerves supply motor and sensory innervation to the larynx [7].

3.2 Sonoanatomy

A linear, high-frequency-transducer ultrasound image offers higher resolution images of the larynx than does CT or MRI due to the organ's superficial location [4]. Between the hyoid bone and the thyroid cartilage, the thyrohyoid membrane offers a window into the larynx in which the epiglottis can be visualized in both the transverse and parasagittal planes [8]. The thyroid cartilage itself offers another window into the larynx, and provides the best image of the vocal cords [8, 9].

3.3 Pathology

Laryngeal pathology includes a broad spectrum of conditions that affect patients of all ages. Laryngomalacia, characterized by supraglottic airway collapse with inspiration, is the most common cause of stridor in the neonate [10]. Allergic and immunologic responses may also affect the larynx, and angioedema with laryngeal involvement can be life threatening [11]. Malignancy can affect any area of the larynx, and both the tumor itself and radiation treatment can profoundly affect airway management.

4 Vocal Cords

4.1 Anatomy

The true vocal cords, also known as the vocal folds, are medial projections from the walls of the larynx. Their location with respect to the cervical vertebrae parallels that of the larynx, descending from higher cervical levels during childhood to approximately the C6 level in adulthood, though there is some variation [12]. The vocal cords approximate anteriorly at the anterior commissure, and have separate posterior attachments at the arytenoid cartilages bilaterally. Their movement is facilitated by the intrinsic laryngeal muscles, which are innervated by the recurrent laryngeal nerve (with the exception of the cricothyroid muscle) [13].

4.2 Sonoanatomy

As mentioned above, the vocal cords can be seen with ultrasound through the thyroid cartilage. The transverse plane is the preferred view [9]. In patients with calcified cartilage, the vocal cords can be viewed by combining the view from superior to the thyroid notch and the view through the cricothyroid membrane. The true vocal cords appear as two triangular hypoechoic structures with the hyperechoic vocal ligaments bordering them medially (Fig. 2). Located just superiorly, the false vocal cords are more hyperechoic than the true vocal cords [4]. To further distinguish between true and false vocal cords, the former will oscillate toward the midline whereas the latter is relatively immobile with phonation [6].

4.3 Pathology

Vocal cords paralysis can arise from injury to the recurrent laryngeal nerves or vagus nerves prior to the branch point.

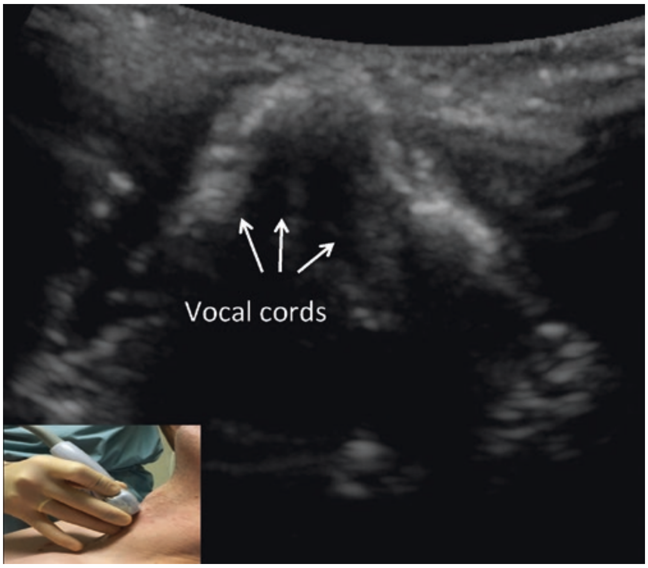

Fig. 2 Transverse view of vocal cords

Intracranial vagal involvement can be expected to cause multiple cranial nerve deficits whereas more distal lesions can show isolated vocal cord dysfunction. The most common cause of vocal cord paralysis is iatrogenic injury from mediastinal and neck surgery [13]. Malignancy can also cause paralysis secondary to nerve compression or injury, and direct damage to the vocal cords is a possible result of endotracheal intubation.

5 Cricoid Cartilage and Cricothyroid Membrane

5.1 Anatomy

The cricoid cartilage is a signet-ring-shaped structure with a thinner anterior band and a thicker posterior lamina [14]. The cricoid cartilage is located inferior to the thyroid cartilage, and the cricothyroid membrane connects the two.

5.2 Sonoanatomy

At the superior end of the trachea the cricoid cartilage can be identified as a hypoechoic, structure that is thicker than the tracheal rings below [4]. With the probe in a transverse orientation, the cricoid cartilage can be viewed as an arch-like structure while in a parasagittal view the cricoid cartilage appears more round [2]. The cricothyroid membrane appears as a hyperechoic structure bridging the hypoechoic thyroid and cricoid cartilages (Figs. 3 and 4), and can also provide a view of the vocal cords [15].

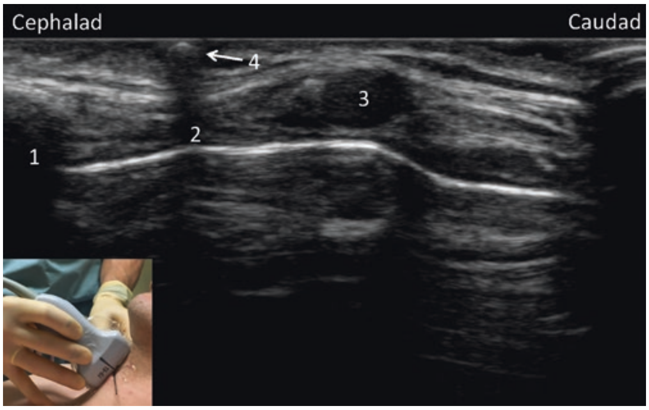

Fig. 3 Cricothyroid membrane in midsagial view with Touhy needle marking spot of cricothyroid membrane. 1:Thyroid carlage; 2: Cricothyroid membrane; 3: Cricoid carlage; 4: Touhy needle

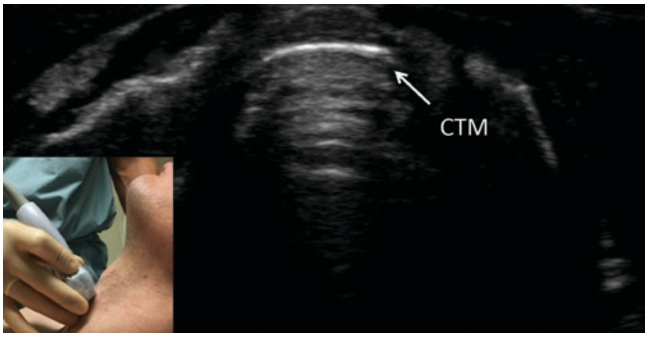

Fig. 4 Cricothyroid membrane in transverse view appearing as hyperechoic line. (*CTM* Cricothyroid membrane)

5.3 Pathology

Cricoid cartilage injury is rare, but when it does occur it is most often secondary to blunt force trauma. High velocity motor vehicle accidents and hanging injuries are the most common causes [16]. The cricothyroid membrane is of critical importance in airway emergencies, as cricothyroidotomy offers airway access when ventilation is inadequate and intubation is unsuccessful.

6 Thyroid

6.1 Anatomy

The thyroid gland has left and right lobes connected by an isthmus. The organ is situated anterior to the proximal trachea at the level of C4/5 and the second or third tracheal ring [17]. Each lobe is about 5 cm long and 2 cm in width and depth [18]. In adults the mass of the thyroid gland is approximately 25 grams on average [19].

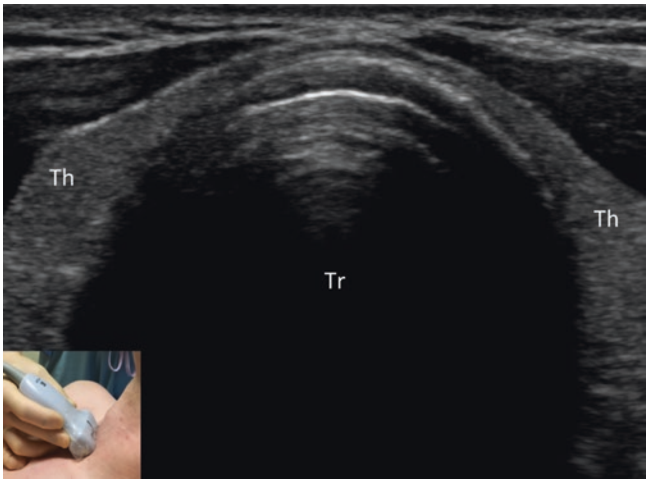

Fig. 5 Thyroid gland in with probe in transverse orientation. (*Tr* Trachea, *Th* Thyroid)

6.2 Sonoanatomy

Ultrasound is the first-line modality for imaging the thyroid [19]. The thyroid gland can be viewed at the level of the suprasternal notch anterolateral to the trachea (Fig. 5). In healthy patients has a homogenous appearance more hyperechoic than the adjacent strap muscles [8].

6.3 Pathology

A variety of pathologies have been reported in the thyroid gland. Thyroid cancer is the most common endocrine malignancy in the United States, and its incidence is increasing [19]. In addition to malignancies, hypothyroidism and hyperthyroidism are common disorders causing physiologic effects and altered response to some medical therapies. Large nodules, malignancies and goiter can cause physical effects including airway compression.

7 Trachea

7.1 Anatomy

The trachea is a tube-shaped structure of the lower respiratory tract. Whereas the cricoid cartilage at the superior end is a complete ring, the remainder of the trachea is composed of incomplete rings forming the anterior and lateral boundaries. Fibroconnective tissue links the 16-22 cartilagenous incomplete rings. The trachealis muscle and annular ligaments form the posterior border. The trachea terminates inferiorly at the carina where it bifurcates into the right and left main stem bronchi [20].

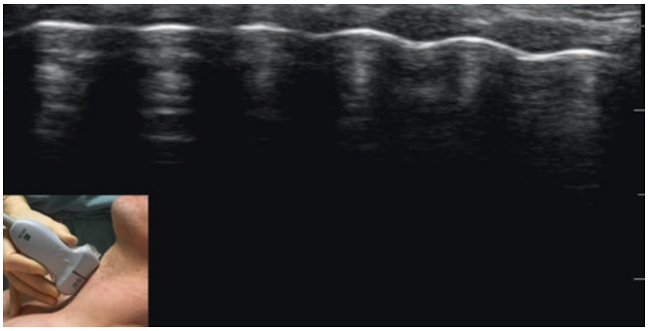

Fig. 6 Trachea in sagittal view. This is recognized as “beads on a string”

7.2 Sonoanatomy

The tracheal rings appear as inverted-U-shaped hypoechoic structures on transverse view at the level of the suprasternal notch. Parasagittal view reveals a “string of beads” appearance (Fig. 6) [2]. The cricoid cartilage represents the superior limit of the trachea, and with head extension six tracheal rings can often be imaged below it [4].

7.3 Pathology

Numerous conditions can affect the trachea. Diffuse tracheal wall thickening has been attributed to sarcoidosis, granulomatosis with polyangiitis and amyloidosis. Malignancies can affect the trachea, most commonly invading from adjacent structures. Squamous cell carcinoma is the malignancy most commonly leading to tracheal narrowing. Mediastinal masses that do not invade the trachea are also capable of causing narrowing due to external compression. Other causes of tracheal narrowing include postinfectious changes due to mycobacterium tuberculosis or Klebsiella rhinoscleromatis, and post-intubation tracheal stenosis [20].

8 Clinical Applications

Clinical applications for US of the neck include screening for pathology and evaluation of masses. Tumors or abscesses may be visible as well as signs of epiglottitis [8]. US has also been shown to aid in predicting difficult airways. In obese patients, those having more pretracheal soft tissue and a larger neck circumference tended to be a more challenging laryngoscopy [21]. Also, the inability to visualize the hyoid bone can be a predictor for difficult intubation [22]. Blocking of the superior laryngeal can be accomplished under US guidance in preparation for awake intubations [23, 24]. US can also be used as a tool for the confirmation of endotracheal tube (ETT) placement. The ETT can be seen as two hyperechoic lines within the trachea. Using a convex probe to image through the suprasternal notch, has shown to have a 98.9% sensitivity and a 94.1% specificity for diagnosing esophageal intubation. Using US to confirm ETT placement can also be especially helpful in cardiac arrest or states of airflow obstruction [9, 25]. The use of US to predict ETT tube size has also been shown to be more precise than age-based and height-based formulas [26]. If the cuff of a laryngeal mask airway (LMA) is filled with saline, US can be used to evaluate if there is any malposition or if the device is seated properly. In one study of pediatric patients, US had a sensitivity of 93% and specificity of 82% for detecting malposition of the LMA [27].

Arguably one of the most important skills for US use of the airway is the proper identification of the cricothyroid membrane. Using surface landmarks and palpation, proper identification of the cricothyroid membrane by anesthetists occurred only 30% of the time [28]. Pre-scanning and marking of this area before attempts at intubation can be life saving in the case of a "cannot intubate, cannot ventilate" situation.

References

1. Votruba J, Zemanová P, Lambert L, Vesela MM. The role of airway and endobronchial ultrasound in perioperative medicine. Biomed Res Int. 2015;2015. https://doi.org/10.1155/2015/754626.
2. Parmar SB, Mehta HK, Shah NK, Parikh SN, Solanki KG. Ultrasound: a novel tool for airway imaging. J Emerg Trauma Shock. 2014;7:155. https://doi.org/10.4103/0974-2700.136849.
3. Auvenshine RC, Pettit NJ. The hyoid bone: an overview. CRANIO® 2018:1–9. https://doi.org/10.1080/08869634.2018.1487501.
4. Kristensen MS. Ultrasonography in the management of the airway. Acta Anaesthesiol Scand. 2011;55:1155–73. https://doi.org/10.1111/j.1399-6576.2011.02518.x.
5. Gervasio A, Mujahed I, Biasio A, Alessi S. Ultrasound anatomy of the neck: the infrahyoid region. J Ultrasound. 2010;13:85–9. https://doi.org/10.1016/j.jus.2010.09.006.
6. Allen E, Murcek BW. Anatomy. Larynx Recurrent Laryngeal Nerve. StatPearls: Head and Neck; 2018.
7. Jacobsen B. Ashurst J V. Anatomy: Head and Neck, Thyrohyoid Membrane. StatPearls Publishing; 2018.
8. Kundra P, Ramesh A, Mishra SK, Ramesh A. Ultrasound of the airway. Indian J Anaesth. 2011;55:456. https://doi.org/10.4103/0019-5049.89868.
9. Osman A, Sum KM. Role of upper airway ultrasound in airway management. J Intensive Care. 2016;4:1–7. https://doi.org/10.1186/s40560-016-0174-z.
10. Bedwell J, Zalzal G. Laryngomalacia. Semin Pediatr Surg. 2016;25:119–22.https://doi.org/10.1053/j.sempedsurg.2016.02.004.
11. Depetri F, Tedeschi A, Cugno M. Angioedema and emergency medicine: from pathophysiology to diagnosis and treatment. Eur J Intern Med. 2018; https://doi.org/10.1016/j.ejim.2018.09.004.
12. Prakash M, Johnny JC. Whats special in a child's larynx? J Pharm Bioallied Sci. 2015;7:S55–8. https://doi.org/10.4103/0975-7406.155797.
13. Dankbaar JW, Pameijer FA. Vocal cord paralysis: anatomy, imaging and pathology. Insights Imaging. 2014;5:743–51. https://doi.org/10.1007/s13244-014-0364-y.
14. Silverman PM, Korobkin M. High-resolution computed tomography of the normal larynx. AJR Am J Roentgenol. 1983;140:875–9. https://doi.org/10.2214/ajr.140.5.875.
15. Singh M, Chin KJ, Chan VWS, Wong DT, Prasad GA, Yu E. Use of sonography for airway assessment: an observational study. J Ultrasound Med. 2010;29:79–85.
16. Heath KJ, Palmer M, Fletcher SJ. Fracture of the cricoid cartilage after Sellick's manoeuvre. Br J Anaesth. 1996;76:877–8. https://doi.org/10.1093/BJA/76.6.877.
17. Furlow PW, Mathisen DJ. Surgical anatomy of the trachea. Ann Cardiothorac Surg. 2018;7:255–60. https://doi.org/10.3978/16463.
18. Choi SH, Kim E-K, Kim SJ, Kwak JY. Thyroid ultrasonography: pitfalls and techniques. Korean J Radiol. 2014;15:267–76. https://doi.org/10.3348/kjr.2014.15.2.267.
19. Li Q, Lin X, Shao Y, Xiang F, Samir AE. Imaging and screening of thyroid cancer. Radiol Clin North Am. 2017;55(6):1261–71.
20. Lawrence DA, Branson B, Oliva I, Rubinowitz A. The wonderful world of the windpipe: a review of central airway anatomy and pathology. Can Assoc Radiol J. 2015;66:30–43. https://doi.org/10.1016/J.CARJ.2014.08.003.
21. Ezri T, Gewürtz G, Sessler DI, Medalion B, Szmuk P, Hagberg C, et al. Prediction of difficult laryngoscopy in obese patients by ultrasound quantification of anterior neck soft tissue. Anaesthesia. 2003; https://doi.org/10.1046/j.1365-2044.2003.03412.x.
22. Prasad A, Yu E, Wong DT, Karkhanis R, Gullane P, Chan VWS. Comparison of sonography and computed tomography as imaging tools for assessment of airway structures. J Ultrasound Med. 2011; https://doi.org/10.7863/jum.2011.30.7.965.
23. Krause M, Khatibi B, Sztain JF, Rahman P, Shapiro AB, Sandhu NS. Ultrasound-guided airway blocks using a curvilinear probe. J Clin Anesth. 2016; https://doi.org/10.1016/j.jclinane.2016.04.058.
24. Iida T, Suzuki A, Kunisawa T, Iwasaki H. Ultrasound-guided superior laryngeal nerve block and translaryngeal block for awake tracheal intubation in a patient with laryngeal abscess. J Anesth. 2013; https://doi.org/10.1007/s00540-012-1492-5.
25. Chou EH, Dickman E, Tsou PY, Tessaro M, Tsai YM, Ma MHM, et al. Ultrasonography for confirmation of endotracheal tube placement: a systematic review and meta-analysis. Resuscitation. 2015; https://doi.org/10.1016/j.resuscitation.2015.02.013.
26. Shibasaki M, Nakajima Y, Ishii S, Shimizu F, Shime N, Sessler DI. Prediction of pediatric endotracheal tube size by ultrasonography. Anesthesiology. 2010; https://doi.org/10.1097/ALN.0b013e3181ef6757.
27. Kim J, Kim JY, Kim WO, Kil HK. An ultrasound evaluation of laryngeal mask airway position in pediatric patients: an observational study. Anesth Analg. 2015; https://doi.org/10.1213/ANE.0000000000000551.
28. Elliott DSJ, Baker PA, Scott MR, Birch CW, Thompson JMD. Accuracy of surface landmark identification for cannula cricothyroidotomy. Anaesthesia. 2010; https://doi.org/10.1111/j.1365-2044.2010.06425.x.

The Utility of Ultrasound in Airway Management

Amit Prabhakar, Babar Fiza, Natalie Ferrero,
and Vanessa Moll

1 Introduction

Ultrasound utilization has become a mainstay in modern medical practice for a variety of diagnostic tests and procedures. Increased availability and usage can be attributed to decreased cost, increased clinician awareness, portability, safety, and ease of use. In recent years, the use of ultrasound for airway assessment and management has grown considerably, yielding promising results. While accurate anatomical assessment of the airway using ultrasound is dependent on operator skill, numerous studies have shown that clinician ability to reliably obtain accurate images requires minimal training and is easily reproducible [1]. This chapter will review relevant airway anatomy and the utility of ultrasound use for airway assessment and management.

2 Review of Basic Anatomy

All clinicians who are responsible for airway assessment and management need to have an understanding of basic airway anatomy. Generally, the airway can be divided into upper and lower sections. The upper airway consists of the mucous membrane lined pharynx and larynx. The pharynx is subdivided into the nasopharynx, oropharynx, and hypopharynx. The nasopharynx includes the posterior nasal cavity and is divided from the oropharynx via the palate and skull base. The oropharynx consists of the region between the palate and hyoid bone and connects the nasopharynx and hypopharynx. The hypopharynx is the area below the hyoid bone and connects the oropharynx to the cartilaginous larynx. The larynx contains the components necessary for speech, including the epiglottis and vocal cords. The lower airway consists of the trachea and lungs. The tubular shape of the trachea is supported by C-shaped hyaline cartilage, which allows for esophageal motility during swallowing. A detailed discussion of lung anatomy is beyond the scope of this chapter.

For the purpose of ultrasound assessment, the airway can be divided anatomically into suprahyoid and infrahyoid regions [2]. Suprahyoid anatomical structures include the mylohyoid, geniohyoid, tongue, and hyoid bone. Pertinent infrahyoid structures include the epiglottis, thyrohyoid membrane, pre-epiglottic space, thyroid cartilage, and tracheal cartilage. Curved low frequency transducers can be used to visualize deeper submandibular and supraglottic structures, while linear high frequency transducers are best suited to visualize superficial structures [2–7]. Ultrasound images of both the suprahyoid and infrahyoid structures have been found to correlate well with computed tomography [8]. The clinical relevance of the assessment of these aforementioned structures will be discussed below.

3 Predicting Difficult Airway Management

Throughout the years, numerous physical exam findings have been established for clinicians to help predict potential difficult airway management. These conventional markers include, but are not limited to patient height, weight, BMI, race, Mallampati score, thyromental distance, cervical spine range of motion, jaw mobility, and dentition [4]. While these assessments have been widely adopted internationally, they can have varying degrees of sensitivity and specificity, leaving clinicians vulnerable to the dreaded cannot intubate can-

---

A. Prabhakar (✉)
Emory University School of Medicine, Department of Anesthesiology, Division of Critical Care, Atlanta, GA, USA
e-mail: amit.prabhakar@emory.edu

B. Fiza · N. Ferrero
Emory University Hospital Midtown, Department of Anesthesiology, Division of Critical Care, Atlanta, GA, USA
e-mail: babar.fiza@emory.edu; natalie.anne.ferrero@emory.edu

V. Moll
Emory University School of Medicine,
Department of Anesthesiology, Division of Critical Care Medicine,
Atlanta, GA, USA
e-mail: vanessa.moll@emory.edu

© Springer Nature Switzerland AG 2021
J. Li et al. (eds.), *Ultrasound Fundamentals*, https://doi.org/10.1007/978-3-030-46839-2_7

not ventilate situation. Several studies have found that preoperative airway assessment with ultrasound has increased both the sensitivity and specificity relative to these conventional assessments.

The inability to visualize the hyoid bone using sublingual ultrasound has been found to have high sensitivity and specificity to predict difficult intubation with a positive likelihood ratio of 21.6 [5]. Another study found that morbidly obese patients with a shorter hyomental distance ratio, or the distance between the hyoid bone and mandibular mentum in the neutral to the hyperextended neck position, is a sensitive predictor for difficult airway management [9]. A hyomental distance ratio of 1.0–1.05 was found to be associated with difficult airway management when compared to patients with a hyomental distance ratio of 1.12–1.16 [9].

Increased pre-tracheal tissue at the level of the vocal cords has been shown to be predictive for difficult airway management in obese patients of middle eastern descent [10]. However, it is worth noting that these findings were not duplicated when applied to western patient populations [11]. Small pilot studies have also shown that an anterior neck thickness greater than 2.8 cm at the level of the hyoid bone and the thyrohyoid membrane are accurate predictors of difficult intubation, but larger studies are needed prior to validation for routine screening [12].

Ultrasound has also been found to be sensitive and specific for the detection of subglottic stenosis. Several studies have found that ultrasound evaluation of the narrowest diameter of the cricoid lumen, or the transverse diameter, correlate well with findings from magnetic resonance imaging [13, 14]. Detection of subglottic stenosis allows for practitioners to preemptively chose the right endotracheal tube size, minimizing the potential for complications like hypoxia or airway trauma due to repetitive manipulation [13, 15]. Ultrasound evaluation of the subglottic transverse diameter has been found to be superior to both age based and height based formulas to estimate the correct endotracheal tube size [15, 16].

4 Regional Anesthesia

Ensuring adequate anesthesia of the airway via regional techniques is an essential component for successful awake intubation in patients with a known or suspected difficult airway. Ultrasound utilization can help facilitate regional techniques when normal anatomical landmarks are difficult to assess, due to morbid obesity or a history of previous surgery involving the airway or neck. The superior laryngeal nerve provides sensation to the epiglottis and to the airway mucosa to the level of the vocal cords. This nerve can be visualized in the space between the hyoid bone and thyroid cartilage when looking transversely at the level of the hyoid bone [17]. Visualization of anatomical landmarks and needle placement under ultrasound guidance can help to ensure adequate analgesia and maximize first pass success.

5 Confirmation of Airway Placement

Capnography and auscultation of the lungs are the most commonly used methods to confirm appropriate airway placement in the normal healthy patient. However, these conventional methods may not be as accurate or reliable in situations such as cardiovascular collapse, emergent difficult airway management with potential esophageal intubation, or severe refractory bronchoconstriction. Successful intubation can be confirmed quickly and easily via transtracheal ultrasound by the “double tract” or “double lumen” signs characterized by two hyperechoic lines [18, 19]. Multiple studies have shown that transtracheal ultrasound is a rapid and reliable method to confirm proper airway placement and correlates well when compared to end tidal capnography [18, 19].

6 Utilization in Emergency Situations

Preparation is a critical component for the successful management of emergent difficult airway scenarios. A cricothyrotomy is lifesaving technique to secure a definitive airway in unstable patients who are unable to be intubated or ventilated by conventional methods. The procedure involves cannulating the cricothyroid membrane by either a needle or percutaneous approach. The cricothyroid membrane is most often identified by locating the space below the thyroid prominence and above the cricoid cartilage. Often times, these anatomical landmarks can be difficult to recognize due to patient body habitus or pathology affecting the area, such as a thyroid mass. The use of ultrasound has been proven to be a quick and effective adjunct to identify these difficult to ascertain anatomical landmarks. With only minimal training, clinicians have been found to be able to identify the cricothyroid membrane using ultrasound in less than 25 seconds [20]. A subsequent study done on cadavers found that clinicians were able to identify the cricothyroid membrane in less than 4 seconds and complete the procedure with a high success rate in less than 30 seconds [21].

After successful cricothyrotomy, a formal tracheostomy is generally performed within 24 hours to establish a more definitive and secure airway. Ultrasound for percutaneous tracheostomy can help to avoid anterior neck structures and minimize the risk for posterior tracheal injury [22–25]. A randomized controlled trial from 2016 found that an ultrasound guided approach has similar efficacy to a bronchoscopy guided tracheostomy [26].

7 Conclusion

This chapter has described how ultrasound utilization has shown promise as an easy, useful, and reliable adjunct to both airway assessment and management. While larger studies need to be done for further validation, it is imperative for clinicians responsible for airway management and assessment to be familiar with the most up to date literature regarding the many potential indications for ultrasound use.

References

1. Gottlieb M, Bailitz JM, Christian E, et al. Accuracy of a novel ultrasound technique for confirmation of endotracheal intubation by expert and novice emergency physicians. West J Emerg Med. 2014;15(70):834–9; Bajracharya GR, Truong AT, Truong DT, Cata JP. Ultrasound-assisted evaluation of the airway in clinical anesthesia practice: past, present, and future. Inter J Anesth Pain Med. 2015;1:1–10.
2. Adhikari S, Zeger W, Schmier C, Crum T, Craven A, et al. Pilot study to determine the utility of point-of-care ultrasound in the assessment of difficult laryngoscopy. Acad Emerg Med. 2011;18:754–8.
3. Singh M, Chin KJ, Chan VW, Wong DT, Prasad GA, et al. Use of sonography for airway assessment: an observational study. J Ultrasound Med. 2010;29:79–85.
4. Hui CM, Tsui BC. Sublingual ultrasound as an assessment method for predicting difficult intubation: a pilot study. Anaesthesia. 2014;69(4):314–9.
5. Wojtczak JA. Submandibular sonography assessment of hyomental distances and ratio, tongue size, and floor of the mouth musculature using portable sonography. J Ultrasound Med. 2012;31(4):523–8.
6. Ezri T, Gewürtz G, Sessler DI, Medalion B, Szmuk P, et al. Prediction of difficult laryngoscopy in obese patients by ultrasound quantification of anterior neck soft tissue. Anaesthesia. 2003;58:1111–4.
7. Prasad A, Yu E, Wong DT, Karkhanis R, et al. Comparison of sonography and computed tomography as imaging tools for assessment of airway structures. J Ultrasound Med. 2011;30:965–72.
8. Kheterpal S, Healy D, Aziz MF, Shanks AM, Freundlich RE, et al. Incidence, predictors, and outcome of difficult mask ventilation combined with difficult laryngoscopy: a report from the multicenter perioperative outcomes group. Anesthesiology. 2013;119:1360–9.
9. Ezri T, Gewurtz G, Sessler DI, Medalion B, Szmuk P, Hagberg C, Susmallian S. Prediction of difficult laryngoscopy in obese patients by ultrasound quantification of anterior neck soft tissue. Anaesthesia. 2003;58(11):1111–4.
10. Komatsu R, Sengupta P, Wadhwa A, Akca O, Sessler DI, Ezri T, Lenhardt R. Ultrasound quantification of anterior soft tissue thickness fails to predict difficult laryngoscopy in obese patients. Anaesth Intensive Care. 2007;35(1):32–7.
11. Pinto J, Cordeiro L, Pereira C, Gama R, Fernandes HL, Assunção J. Predicting difficult laryngoscopy using ultrasound measurement of distance from skin to epiglottis. J Crit Care. 2016;33:26–31.
12. Kundra P, Sandeep KM, Ramesh A. Ultrasound of the airway. Indian J Anaesth. 2011;55:456–62.
13. Lakhal K, Delplace X, Cottier JP, Tranquart F, Sauvagnac X, Mercier C, et al. The feasibility of ultrasound to assess subglottic diameter. Anaesth Analg. 2007;104:611–4.
14. Shibasaki M, Nakajima Y, Ishii S, Shimizu F, Shime N, Sessler DI. Prediction of pediatric endotracheal tube size by ultrasonography. Anesthesiology. 2010;113:819–24.
15. Kim EJ, Kim SY, Kim WO, Kim H, Kil HK. Ultrasound measurement of subglottic diameter and an empirical formula for proper endotracheal tube fitting in children. Acta Anaesthesiol Scand. 2013;57(9):1124–30.
16. Green JS, Tsui BC. Applications of ultrasonography in ENT: airway assessment and nerve blockade. Anesthesiol Clin. 2010;28:541–53.
17. Adi O, Chuan TW, Rishya M. A feasibility study on bedside upper airway ultrasonography compared to waveform capnography for verifying endotracheal tube location after intubation. Crit Ultrasound J. 2013;5(1):7.
18. Lakhal K, Delplace X, Cottier JP, Tranquart F, Sauvagnac X, Mercier C, Fusciardi J, Laffon M. The feasibility of ultrasound to assess subglottic diameter. Anesth Analg. 2007;104(3):611–4.
19. Nicholls SE, Sweeney TW, Ferre RM, Strout TD. Bedside sonography by emergency physicians for the rapid identification of landmarks relevant to cricothyrotomy. Am J Emerg Med. 2008;26(8):852–6.
20. Curtis K, Ahern M, Dawson M, Mallin M. Ultrasound-guided, Bougie-assisted cricothyroidotomy: a description of a novel technique in cadaveric models. Acad Emerg Med. 2012;19(7):876–9.
21. Rajajee V, Fletcher JJ, Rochlen LR, Jacobs TL. Real-time ultrasound-guided percutaneous dilatational tracheostomy: a feasibility study. Crit Care. 2011;15(1):R67.
22. Hatfield A, Bodenham A. Portable ultrasonic scanning of the anterior neck before percutaneous dilatational tracheostomy. Anaesthesia. 1999;54(7):660–3.
23. Kollig E, Heydenreich U, Roetman B, Hopf F, Muhr G. Ultrasound and bronchoscopic controlled percutaneous tracheostomy on trauma ICU. Injury. 2000;31(9):663–8.
24. Rajajee V, Williamson CA, West BT. Impact of real-time ultrasound guidance on complications of percutaneous dilatational tracheostomy: a propensity score analysis. Crit Care. 2015;19:198.
25. Gobatto AL, Besen BA, Tierno PF, Mendes PV, Cadamuro F, Joelsons D, Melro L, Carmona MJ, Santori G, Pelosi P, et al. Ultrasound-guided percutaneous dilational tracheostomy versus bronchoscopy-guided percutaneous dilational tracheostomy in critically ill patients (TRACHUS): a randomized noninferiority controlled trial. Intensive Care Med. 2016;42(3):342–51.
26. Muslu B, Sert H, Kaya A, et al. Use of sonography for rapid identification of esophageal and tracheal intubation in adult patients. J Ultrasound Med. 2011;30:671–6.

Ultrasound Technique for Common Head and Neck Blocks

Avijit Sharma, Praba Boominathan, and Robert Ming-Der Chow

1 Introduction

Local anesthetics have been used to perform regional blocks for head and neck surgeries for over 150 years. From its roots in using topical cocaine as the sole anesthetic in eye surgery, regional anesthesia has progressed immensely as an adjunct to general anesthesia, and has flourished in its role in opioid sparing multimodal analgesia. The various head and neck blocks that can be performed are used in plastic surgery, otolaryngology, dermatology, and neurosurgery [1]. Many of the blocks are sensory in nature, limiting some of the potential side effects related to motor blockade. The use of ultrasound further facilitates the ease with which these blocks can be formed while minimizing adverse effects. To perform these blocks safely, it is important to understand the salient regional anatomy. Sensory innervation for the face can be divided by the branches of the trigeminal nerve (cranial nerve V): the ophthalmic division V1, the maxillary division V2, and the mandibular division V3 [1]. These extend laterally to the mid ear, at which point the cervical plexus C2-C4 provides sensory innervation to the posterior head and neck [2]. Moving caudally, the ventral rami of the C5-T1 nerve roots provide motor and sensory innervation to the arm through the brachial plexus.

2 Trigeminal Nerve Block

2.1 Anatomy

The trigeminal nerve, or cranial nerve five is the largest cranial nerve and is responsible for facial sensation. The afferent fibers from the three main trigeminal branches converge onto the Gasserian ganglion which is found in Meckel's cave, an invagination of the dura mater located in the posterior cranial fossa [3–5]. To reach Meckel's cave, V1 and V2 fibers travel through the lateral wall of the cavernous sinus posteriorly where they meet V3 [5]. The trigeminal nerve branches V2 and V3 can be blocked at the pterygopalatine fossa before forming terminal nerve branches.

2.2 Sonoanatomy and Clinical Application

To perform a trigeminal block, patients are placed in the lateral decubitus position or supine position, with the side to be blocked facing up. A cleaning solution is applied to the area, and a sterilely covered high-frequency ultrasound probe is placed longitudinally below the zygomatic bone. The lateral pteryogoid muscle, lateral pterygoid plate, and maxillary bone are then identified (Fig. 1) [3]. Using Doppler, the nearby maxillary artery should be located. After anesthetizing the skin, a 22G needle is inserted in-plane with the probe in a lateral to medial direction aiming anteriorly toward the pterygopalatine fossa. To avoid the acoustic shadow of the coronoid process, the patient's mouth is slightly opened with the probe directed superiorly [3]. After negative aspiration, 4–5 mL of local anesthetic is injected deep to the lateral pterygoid muscle and plate. Dexamethasone or triamcinolone can be used as an adjunct to potentiate the effect of local anesthetics [3].

3 Supraorbital Nerve Block

3.1 Anatomy

The ophthalmic nerve (V1) exits the skull through the superior orbital foramen to provide sensory innervation to the forehead, eyebrows, upper eyelids, and nose [1]. The supraorbital nerve, a terminal branch of V1 innervates the forehead and can be blocked for frontal craniotomies, ventriculoperitoneal shunt placement, Ommaya reservoir placement, upper eyelid surgery, and dermatologic procedures [1].

A. Sharma · P. Boominathan · R. Ming-Der Chow (✉)
Department of Anesthesiology, Yale University School of Medicine, New Haven, CT, USA
e-mail: Avijit.sharma@yale.edu; praba.boominathan@yale.edu; Robert.chow@yale.edu

© Springer Nature Switzerland AG 2021

J. Li et al. (eds.), *Ultrasound Fundamentals*, https://doi.org/10.1007/978-3-030-46839-2_8

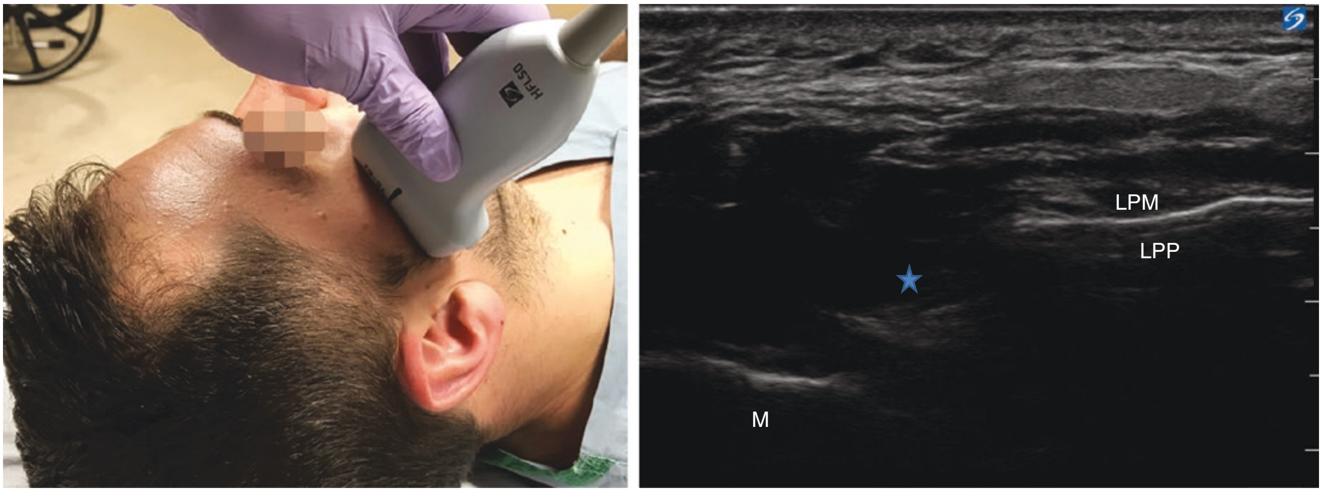

Fig. 1 Trigeminal Nerve Block: *LPM* lateral pterygoid muscle, *LPP* lateral pterygoid plate, *M* maxilla, *Blue Star* target

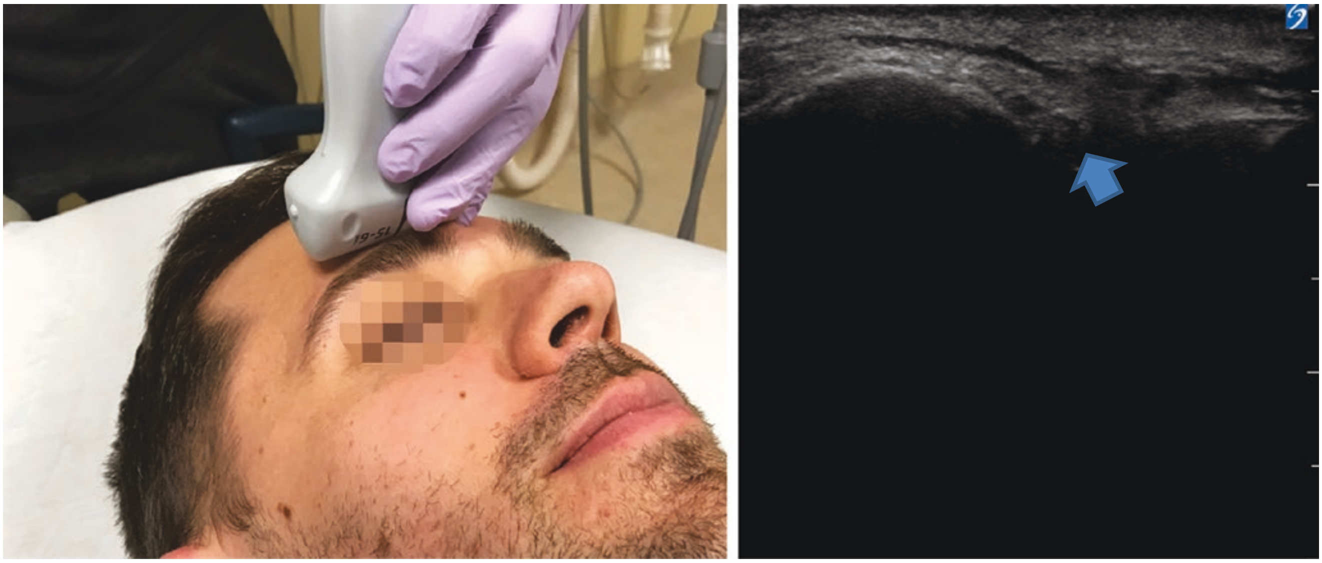

Fig. 2 Supraorbital Nerve Block: the blue arrow identifies the foramen or "bone gap"

3.2 Sonoanatomy and Clinical Application

For all superficial nerve blocks of the face, the patient is placed supine, with the head in a midline position. The supraorbital foramen is located on the superior part of the orbital rim and is in line with the pupil [1]. The skin overlying the target is cleansed with an antiseptic solution. A high frequency linear ultrasound probe with sterile covering is placed transversely above the orbital rim. The foramen is identified as a "bone gap" or break in the hyperechoic line which represents the orbital rim (Fig. 2). The Doppler function can be used to help identify nearby vessels to reduce the risk of intravascular injection. Due to the superficial nature of this block, a 25 gauge needle can be used in an in-plane approach, with the needle pointing in a lateral to medial orientation to reach the target. At this point, 1-2 mL of local anesthetic is injected after negative aspiration. This is followed by massage of the area to facilitate local anesthetic spread as well as to reduce hematoma formation [1].

4 Infraorbital Nerve Block

4.1 Anatomy

The maxillary nerve (V2) exits the skull via the foramen rotundum, passes through the pterygopalatine fossa and reaches the floor of the orbit via the infraorbital foramen. This nerve innervates the lower eyelids, lateral portion of the nose, roof of the mouth, upper lip, and maxillary sinus [1].

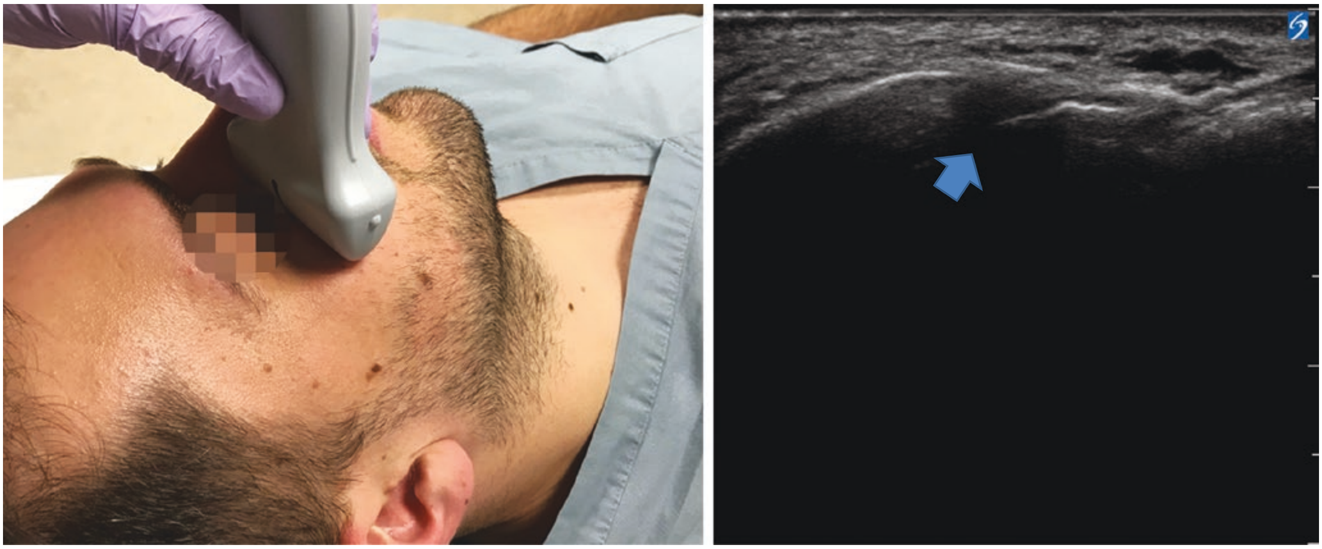

Fig. 3 Infraorbital Nerve Block: the blue arrow identifies the foramen or “bone gap”

The maxillary nerve can be blocked as it emerges from the skull at the foramen rotundum or more distally as the infraorbital nerve at the infraorbital foramen. Indications for this block include cleft lip repair, surgeries involving the lower eyelid or upper lip, sinus surgery, transsphenoidal hypophysectomy, rhinoplasty, and septal repair.

4.2 Sonoanatomy and Clinical Application

The patient is placed supine, with the head in a midline position. The infraorbital foramen can be visualized by placing the ultrasound probe in transverse orientation. The skin overlying the target is cleansed with an antiseptic solution. A high frequency linear ultrasound probe with sterile covering is placed transversely below the infraorbital ridge. The foramen is usually found in line with the pupil as well as the supraorbital foramen (Fig. 3). Small translational movements medially can help locate the “bone gap.” Once the foramen is located, a 25 gauge needle can be advanced to the target using a lateral to medial in-plane approach. After negative aspiration, 1–2 mL of local anesthetic can be injected around the nerve while avoiding an intraforaminal or intravascular injection.

5 Mental Nerve Block

5.1 Anatomy

The mandibular nerve (V3) is a mixed sensory and motor nerve that exits the cranium through the foramen ovale and provides sensation to the ear, anterior two-thirds of the tongue, temporal region of the skull, and the mandible [1]. The mandibular nerve provides motor innervation for the muscles of mastication [1]. A terminal branch of the mandibular nerve, the mental nerve gives sensory innervation to the chin, lower lip and anterior teeth. A mental nerve block can be performed for laceration repair and other procedures of the lower lip, skin, or teeth.

5.2 Sonoanatomy and Clinical Application

The patient is placed supine, with the head in a midline position. The skin overlying the target is cleansed with an antiseptic solution. A high frequency linear ultrasound probe with sterile covering is placed transversely between the upper and lower borders of the mandible (Fig. 4). Oftentimes, the second premolar on the target side is used as a reference for placing the center of the probe. This foramen also lies in line with the pupil. Once the “bone gap” is identified, a 25 gauge needle can be inserted in-plane via a lateral to medial approach. After negative aspiration, 1–2 mL of local anesthetic can be injected around the “bone gap.”

6 Greater Occipital Nerve Block

6.1 Anatomy

The greater occipital nerve arises from the second cervical nerve root running between the obliquus capitis inferior and semispinalis capitis [1, 6]. It then pierces semispinalis capitis and trapezius aponeurosis to become a subcutaneous structure [6]. Here, the greater occipital nerve is found medial to

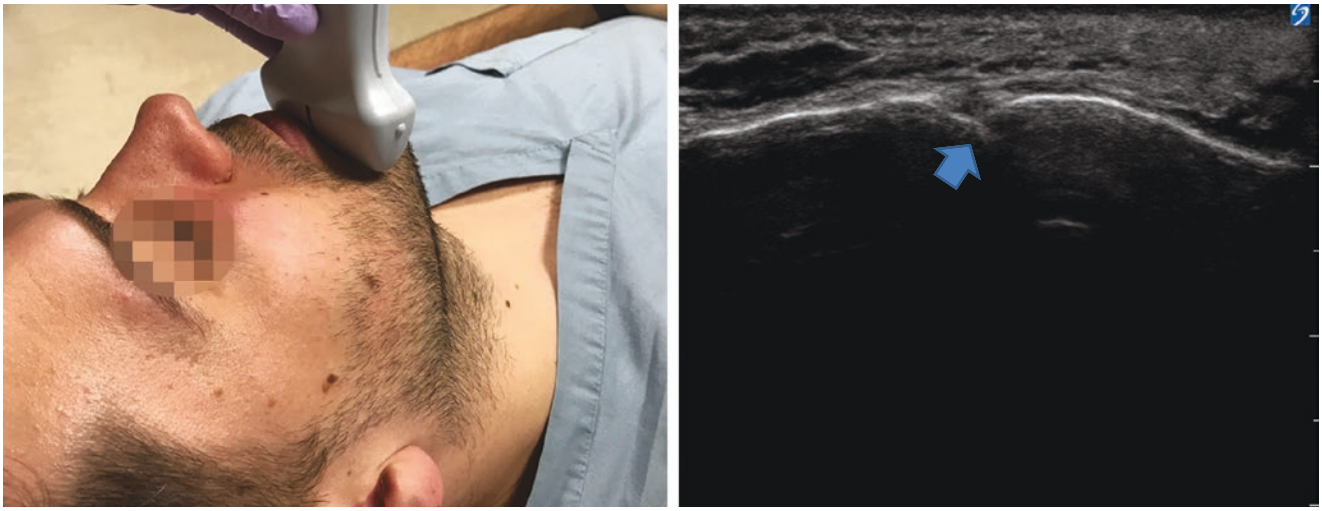

Fig. 4 Mental Nerve Block: the blue arrow identifies the foramen or "bone gap"

the occipital artery [6]. The greater occipital nerve provides sensation to the posterior scalp from the occipital protuberance to the vertex [6]. Blockade of this nerve is useful for pain relief after neurosurgical procedures such as posterior craniotomies and insertions of ventriculoperitoneal shunts [1]. These blocks can also be used to diagnose and treat various headaches including migraine, cervicogenic, and tension type headaches [6].

Distally, the greater occipital nerve block can be easily performed with palpation of landmarks [6–8]. The patient is placed in either the sitting or prone position. The nerve is located two thirds of the way on a line drawn from the mastoid to the occipital protuberance and lies medial to the occipital artery [6–8]. A 25 gauge needle is directed toward the occiput. After negative aspiration, 1–3 mL of local anesthetic is injected. Numbness over the top of the head is a sign of successful occipital nerve blockade.

6.2 Sonoanatomy and Clinical Application

Using ultrasound, this block can be performed using a classical distal technique or a newer proximal approach. With the distal greater occipital nerve block, a linear ultrasound probe is placed in a transverse plane at the level of the superior nuchal line. The center of the probe is would be placed lateral to the occipital protuberance. Proximally, the greater occipital nerve can be blocked at the level of the C2 vertebra an approach described by Greher et al. [9] Once the C2 vertebra is identified, the probe is moved laterally to locate the obliquus capitis inferior muscle [9]. The greater occipital nerve lies superficial to this muscle crossing lateral to medial [6, 9]. The needle is inserted out-of-plane to the probe and local anesthetic is injected around the nerve. This block has also been performed with injection targeted at the medial head of the semispinalis capitis which has been shown to produce superior injectate spread [6]. To perform this block, the patient is placed in a seated position. The probe is placed in a horizontal orientation on the target side, lateral to the nuchal ligament at the C1 level. This allows separation of the medial and lateral heads of the semispinalis capitis (Fig. 5). With an in-plane technique, a 25 gauge needle is inserted midline and advanced laterally until the tip is within the medial head. After negative aspiration, 1– mL of local anesthetic can be injected. Complications with this block are rare because of the superficial location of the nerve. However, it is important to note that the vertebral artery is lateral and deep to the greater occipital nerve.

7 Lesser Occipital Nerve Block

7.1 Anatomy

The lesser occipital nerve forms from the cervical plexus and is mainly composed of C2 fibers. After piercing deep fascia at Erb's point, the nerve travels subcutaneously towards the retroauricular area posterior to the sternocleidomastoid muscle [10]. This occurs on average 4.5 cm from the mastoid prominence along the posterior border of the sternocleidomastoid [11]. Occasionally, the lesser occipital nerve will pierce the sternocleidomastoid as it ascends to the cranium [12]. It innervates the lateral part of the scalp posterior to the ear [10]. Blockade of this nerve can result in pain relief caused by occipital neuralgia.

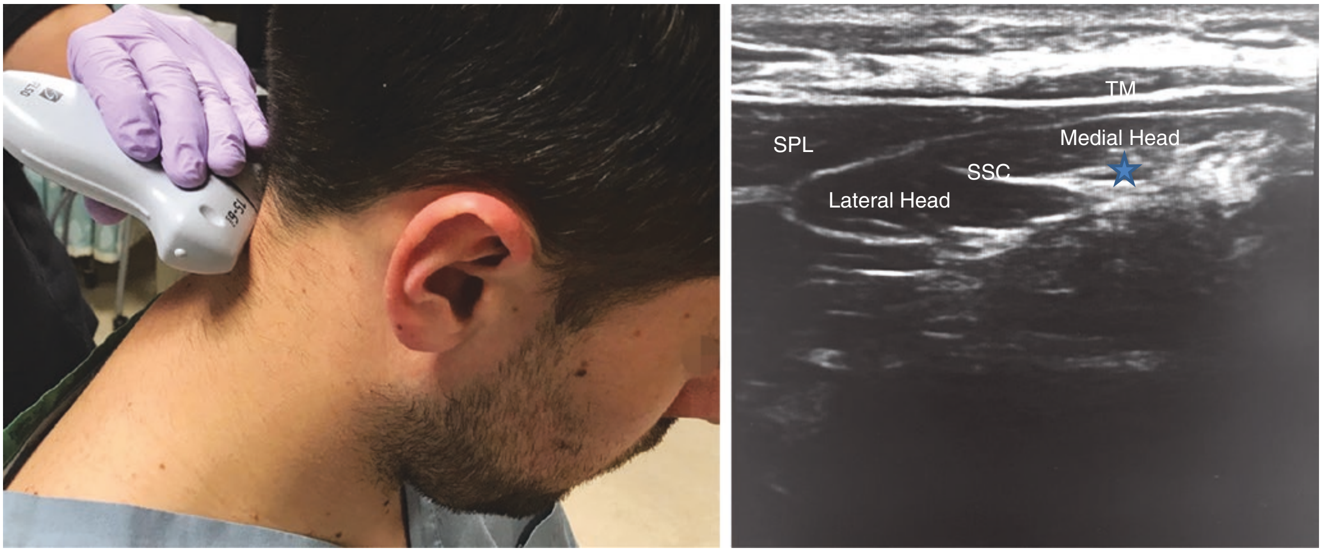

Fig. 5 Greater Occipital Nerve Block: *TM* Trapezius Muscle, *SPL* Splenius Muscle, *SSC* Semispinalis Capitis, *Blue Star* Target Site

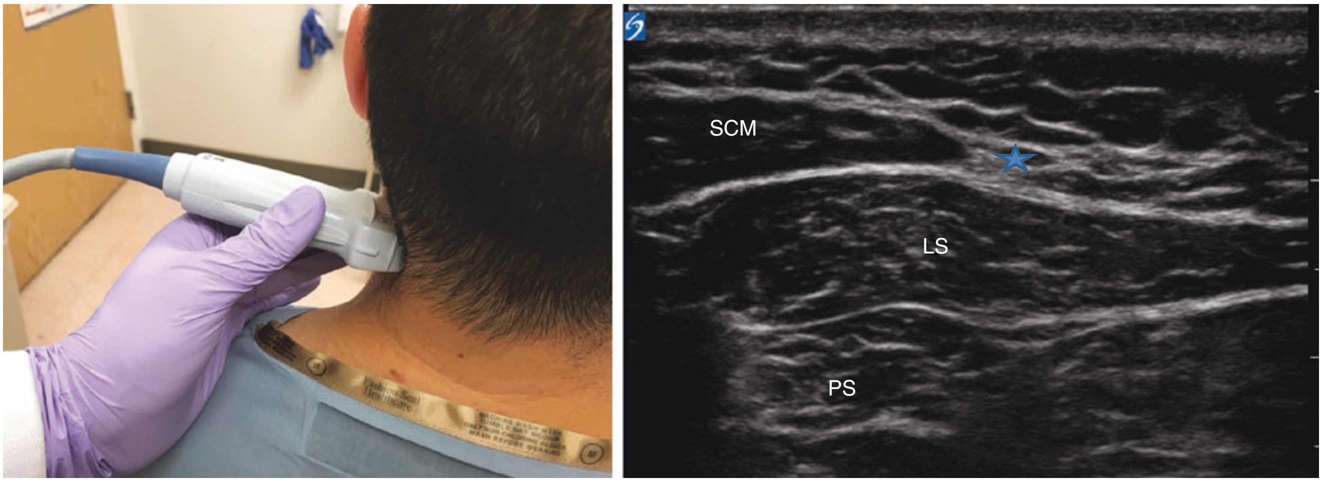

Fig. 6 Lesser Occipital Nerve Block: *SCM* Sternocleidomastoid Muscle, *LS* Levator Scapulae Muscle, *PS* Posterior Scalene Muscle, *Blue Star* Target Site

7.2 Sonoanatomy and Clinical Application

The block is performed with ease using ultrasound. The patient is placed in either the prone position or sitting with the neck flexed. The nerve is located one third of the way on a line drawn from the mastoid to the occipital protuberance and is lateral to the occipital artery [6–8]. A linear ultrasound probe is placed at the posterior border of the sternocleidomastoid muscle in the transverse orientation just below the mastoid process (Fig. 6). Moving in the cranial caudal plane, a nervous structure is identified that emerges beneath the sternocleidomastoid muscle [13]. With an in-plane technique, a 25 gauge needle is inserted midline and advanced until the tip is near the nerve. After negative aspiration, 1–3 mL of local anesthetic can be injected. Complications with this block are rare because of the superficial location of the nerve.

8 Cervical Plexus Block

8.1 Anatomy

The superficial cervical plexus provides sensory innervation to the neck, ear, angle of the mandible, shoulder, and clavicle. The anterior border of the superficial cervical plexus is the sternocleidomastoid, and the posterior border of the plexus is the prevertebral fascia. Two muscles flank the plexus: the longus capitis anteromedially, and the middle scalene muscle posterolaterally. The plexus is formed by the ventral rami of the spinal nerves C2, C3, and C4. These nerve roots join together and emerge from behind the posterior border of the sternocleidomastoid as the following terminal branches, listed from cranial to caudal: lesser occipital (C2, C3), greater auricular (C2, C3), transverse cervical (C2, C3) and supraclavicular (C3, C4) nerves. These superficial nerves travel a relatively long distance from the paravertebral space to supply innervation to the skin and subcutaneous tissues of the neck, as well as the posterior portion of the head and shoulders [14].

Spread of the local anesthetic is highly dependent on its location relative to the fascia, as some cervical fascial layers can contribute significantly to diffusion of local anesthetic. Cervical fascial layers fall into two broad categories: superficial and deep. The superficial fascial layer is typically referred to as the subcutaneous tissue, to avoid confusion with the superficial layer of the deep cervical fascia. In the category of deep cervical fascia there are three layers, listed from superficial to deep: (1) the superficial investing fascia, also known as the submandibular, sternocleidomastoid-trapezius, or masticator fascia, (2) the middle fascia, known as the strap muscle fascia or visceral fascia, and (3) the deep layer, known as the perivertebral or prevertebral fascia [14]. Another notable layer of fascia that appears sonographically distinct is the carotid sheath, which contains not only the common/internal carotid arteries and internal jugular vein, but also the deep cervical lymph nodes and the vagus nerve. Care should be taken to avoid damage to this sheath and its contents during cervical plexus blockade. Of note, the ansa cervicalis arises in the vicinity of the cervical plexus. The ansa cervicalis is a nerve loop with fibers from the C1-C4 nerve roots, which supplies motor innervation to the strap muscles of the neck, including the sternocleidomastoid. The anterior rami of C3 and C4 form a loop and join together with fibers from C5 to form the phrenic nerve. Deep cervical plexus blockade was noted to cause abnormalities in diaphragmatic motion in a majority of patients according to one study [15]. A true superficial cervical plexus block is not associated with phrenic nerve palsy. However, in the absence of significant pulmonary impairment or preexisting diaphragmatic pathology, the effect of diaphragmatic weakness from phrenic nerve palsy is masked by the increased utilization of the sternocleidomastoid as a muscle of respiration [14]. Incidental blockade of cranial nerves or nerve fibers of the cervical sympathetic chain may result in the development of Horner's syndrome, facial palsy, hoarseness, cough, or dysphagia. However, the vast majority of these adverse effects resolve on the first post-operative day [16].

The superficial blockade of the cervical plexus involves depositing local anesthetic more superficial to the investing fascia, in the layer of subcutaneous tissue. Ultrasound guidance can be used to identify individual nerves and perform selective blockade, depending on the site of surgery. This superficial block obviates many of the complications seen with deeper cervical plexus blockade, so long as the needle tip is maintained in the subcutaneous tissue. An intermediate depth block may also be performed in which local anesthetic is deposited into the middle investing fascia but superficial to the deep prevertebral fascia. Lastly, a true deep cervical plexus block involves injection of local anesthetic deep to the prevertebral fascia [17].Although deep cervical plexus blocks with ultrasound guidance are not well described in the literature, these blocks can be performed using landmark or nerve stimulator techniques [18].

8.2 Sonoanatomy and Clinical Application

The superficial cervical plexus block is performed with the patient supine or in the semi-sitting position, with the head turned slightly away from the side to be blocked. The neck and upper chest should be exposed such that the entire length of the sternocleidomastoid is visible. The posterior border of sternocleidomastoid may be palpated more easily by asking the patient to lift their head slightly off the bed.

The skin is cleansed with an antiseptic solution. A high frequency linear ultrasound probe with sterile covering is placed overlying the sternocleidomastoid at its midpoint, which roughly translates to the level of the cricoid cartilage. Once the sternocleidomastoid has been identified, the probe is moved laterally until the lateral edge of the sternocleidomastoid is in the middle of the screen. The brachial plexus can be identified between the anterior and middle scalene muscles here (Fig. 7). The cervical plexus appears as a group of small, honeycomb-like hypoechoic nodules immediately superficial to the prevertebral fascia overlying the interscalene groove. Note that the cervical plexus may not be easily visible in many individuals.

Once the plexus has been identified, the skin is anesthetized with subcutaneous infiltration of a small amount of local anesthetic. The block needle is passed through the skin, platysma muscle, and the investing fascia, with the needle tip abutting the cervical plexus. Both in-plane (medial and lateral) and out-of-plane approaches may be used in this block due to its superficial location. After negative aspiration, 1–2 mL should be injected to ensure adequate location relative to the plexus. A total of 5–15 mL local anesthetic should be injected thereafter, bathing the plexus and causing the prevertebral fascia and the sternocleidomastoid to peel away from one another. If the cervical plexus is not readily visible,

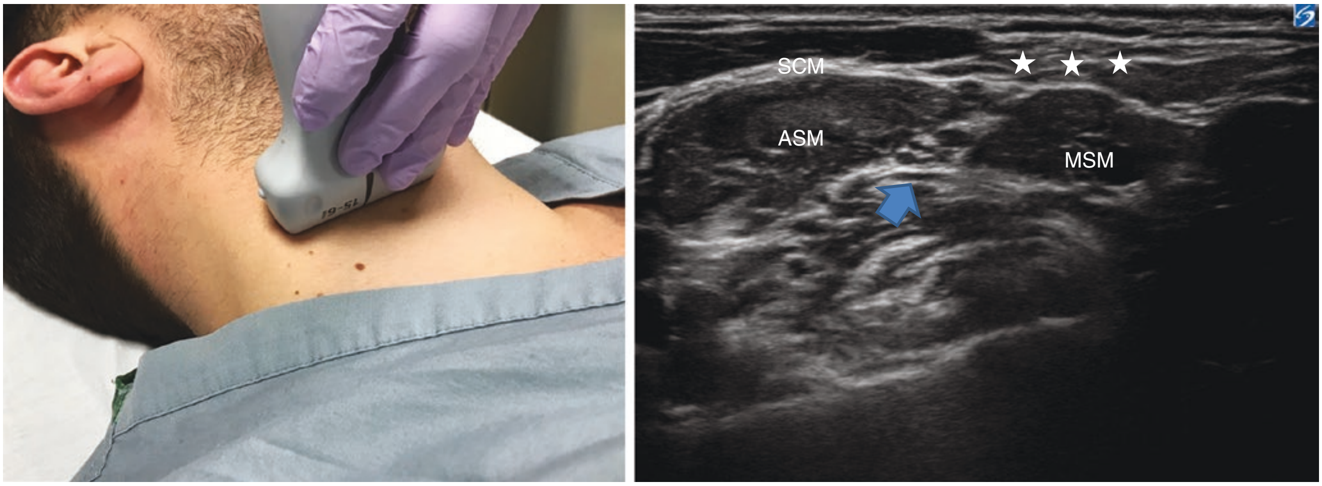

Fig. 7 Superficial Cervical Plexus Block: *SCM* sternocleidomastoid muscle, *ASM* anterior scalene muscle, *MSM* middle scalene muscle, *White Stars* designates target site for injection of superficial cervical plexus block, *Blue Arrow* designates the brachial plexus

aim to deposit 10 mL local anesthetic deep to the sternocleidomastoid, which produces a reliable block in most cases.

Because most of the nerves comprising the superficial cervical plexus are sensory, it is not necessary to use high concentrations of local anesthetic. Reasonable choices of local anesthetic include ropivacaine 0.25–0.5%, bupivacaine 0.25%, and lidocaine 1% [19, 20].

9 Brachial Plexus Blocks

Ultrasound-guided plexus blocks are a safe and effective alternative or addition to general anesthesia for surgeries involving the upper extremities. The use of ultrasound guidance to perform these peripheral nerve blocks has been shown to be at least equally safe to previously described landmark and nerve stimulator methods [21]. These blocks are particularly useful in high risk patient populations such as those with suspected or known difficult airways, the morbidly obese, the elderly, chronic pain patients with refractory post-operative pain, and patients with severe cardiac or pulmonary comorbidities to whom general anesthesia would pose a major risk, or those who have frank contraindications to general anesthesia. Furthermore, the use of peripheral nerve blocks in simple surgeries performed in the ambulatory setting can be highly advantageous with regard to decreased length of stay in the Post Anesthesia Recovery Unit (PACU), earlier resumption of diet, and improved analgesia, allowing for greater mobility of the operative extremity. For more complex surgeries, the use of peripheral nerve block catheters can be utilized to allow patients to reap the same benefits described above [22]. In this section we will discuss two commonly used ultrasound-guided blocks: interscalene and supraclavicular nerve blocks.

9.1 General Brachial Plexus Anatomy

The brachial plexus is comprised of the anterior rami from C5, C6, C7. C8 and T1. The spinal nerve roots of the brachial plexus fuse and separate through their course to form the trunks, divisions, cords, and branches. The five roots give rise to three trunks as they emerge between the anterior and middle scalene muscles: superior, middle, and inferior. As the plexus continues its course under the clavicle, each trunk gives off an anterior and posterior component, forming six divisions. The six divisions combine to form three cords: lateral, median, and posterior. These cords finally branch to form the five terminal nerve branches: the musculocutaneous, axillary, radial, median, and ulnar nerves [23].

10 Interscalene Nerve Block

10.1 Anatomy

The interscalene nerve block provides anesthesia and analgesia for open and arthroscopic surgeries involving the shoulder, proximal humerus, and lateral two-thirds of the clavicle [22]. Sparing of the ulnar nerve is common, as local anesthetic spread at this level often does not reach C8 or T1. The prevertebral fascia, superficial cervical plexus and sternocleidomastoid muscle are seen superficial to the brachial plexus [24]. In an interscalene nerve block, the brachial plexus is targeted at the level of the nerve roots or trunks.

A myriad of complications may be observed with an interscalene block, however, ultrasound guidance may reduce these adverse events. A misguided needle may result in violation of the pleura and subsequent pneumothorax.

Epidural and intrathecal blockade is also possible given the proximity of the target to the neuraxis. Ipsilateral blockade of the phrenic nerve is observed in nearly all interscalene blocks due to proximal spread of the local anesthetic. Therefore, patient selection is critical, as those with contralateral hemidiaphragmatic paralysis may suffer severe respiratory sequelae. Similarly, care must be taken in performing interscalene block in patients with pulmonary comorbidities, as phrenic nerve blockade may exacerbate existing dyspnea. Sympathetic fiber blockade may result from posterior tracking of local anesthetic, which may precipitate an ipsilateral Horner's syndrome. Local anesthetic systemic toxicity is a significant concern in interscalene blocks due to the proximity of the target to the vertebral artery; direct injection into the vertebral artery may precipitate seizures, particularly if the maximum allowed dose is exceeded [25].

10.2 Sonoanatomy and Clinical Application

The patient is positioned in the supine, sitting or semi-sitting position. A blanket may be positioned under the patient's head in lieu of a pillow to facilitate the proceduralist's access to the site. The patient's head is turned to the contralateral side.

The skin is disinfected, and a sterilely covered high frequency linear ultrasound probe is placed over the neck at the level of the cricoid cartilage, in the transverse plane. The carotid artery is identified, and the probe is moved posterolaterally to identify the anterior and middle scalene muscles, and the brachial plexus which lies between them (Fig. 8). Alternatively, the brachial plexus is first identified in the supraclavicular view (discussed in next section), and the probe is moved cranially until the interscalene view is identified. The plexus at the interscalene level appears as three stacked hypoechoic circles, known colloquially as the "stop light". It is recommended that color Doppler is applied to reduce the risk of vascular injury or injection. The skin overlying the needle insertion site is anesthetized with local anesthetic, and a block needle is inserted in a lateral-to-medial direction. The needle should be aimed between the nerve roots rather than directly at them to minimize the risk of neural injury. As the prevertebral fascia is traversed by the block needle, a tactile "pop" sensation is often felt. Contiguous spread of the local anesthetic around the nerve roots also indicates correct needle position. Careful aspiration should be performed to rule out intravascular placement prior to injecting local anesthetic around the plexus. It is recommended to repeat aspiration with every 5 mL injected to confirm that the needle has not migrated intravascularly or caused vascular trauma. A volume of 10–30 mL of local anesthetic may be used, with careful consideration of maximum allowable dose based on the patient's weight [26]. Appropriate spread of the local anesthetic in the brachial plexus can be monitored by scanning up and down the target site and observing local anesthetic spread cranially and caudally to the injection site.

11 Supraclavicular Brachial Plexus Block

11.1 Anatomy

The supraclavicular nerve block is performed at the level of the divisions. Recall these divisions are formed by the splitting of the superior, middle, and inferior trunks into anterior and posterior components. The supraclavicular nerve block has been often referred to the as the "spinal of the arm",

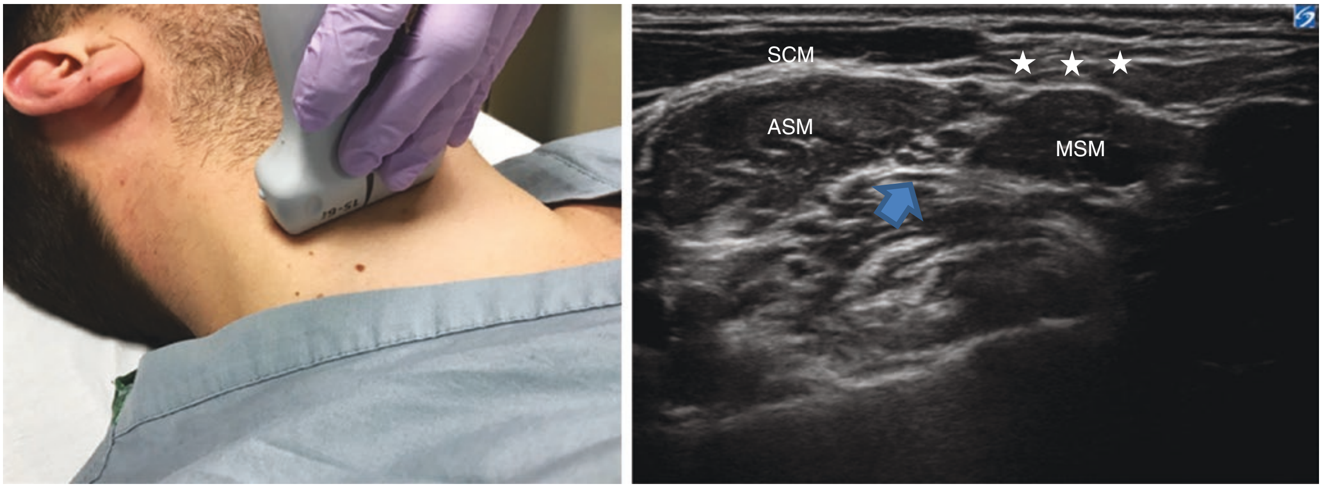

Fig. 8 Interscalene Nerve Block: *SCM* sternocleidomastoid muscle, *ASM* anterior scalene muscle, *MSM* middle scalene muscle, *White Star* designates target site for injection of superficial cervical plexus block, *Blue Arrow* designates the brachial plexus

providing a dense sensory and motor blockade with rapid and efficient onset from the mid-humerus to distal hand [25].

Similar to the interscalene block, complications related to the supraclavicular block have also been reduced with the widespread usage of ultrasound. The block is performed superior to the clavicle, with the first rib and underlying parietal pleura inferior to the plexus. Prior to ultrasound guidance, significant concerns regarding pneumothorax due to needle misplacement existed, however, the usage of ultrasound significantly reduces this risk. Apart from this, performance of the supraclavicular nerve block involves identification of the subclavian artery, which crosses over the first rib between the insertion sites of the anterior and middle scalene muscles. The proximity to the subclavian artery predictably highlights the risk of intravascular injection. As with the interscalene nerve block, the supraclavicular block also carries a risk of ipsilateral phrenic nerve palsy and Horner's syndrome [27].

11.2 Sonoanatomy and Clinical Application

The patient is positioned similarly to the position described for interscalene block: in the supine, semi-sitting, or sitting position with the head turned to the contralateral side. A sterile cleaning solution is applied to the area, and a sterilely covered high-frequency ultrasound probe is placed above the clavicle in the supraclavicular fossa. A short-axis view of the subclavian artery medially, first rib and pleura inferiorly, and the divisions of the plexus are identified (Fig. 9) [22].

On ultrasound imaging, the brachial plexus at the supraclavicular level appears as a cluster of hypoechoic structures lateral and posterior to the subclavian artery, colloquially referred to as "a bunch of grapes". The skin lateral to the ultrasound probe is anesthetized for an in-plane technique. The block needle is advanced to the angle formed by the first rib and subclavian artery, taking care to avoid the pulsating vasculature and shimmering pleura. After negative aspiration for blood, local anesthetic can be deposited in this "corner pocket", which typically corresponds to the ulnar constituents of the brachial plexus. Injection into this corner pocket also allows for lifting of the brachial plexus superiorly; this facilitates further injection of local anesthetic and reduces risk of pleural injury. The needle is withdrawn slightly to the subcutaneous tissue, then advanced into the plane immediately above the plexus. Hydro-dissection of the brachial plexus may be performed, avoiding direct needle puncture of neural structures [22]. A volume of 15–30 mL local anesthetic may be used, again with careful consideration of the maximum safe dose of local anesthetic based on weight to avoid toxicity.

12 Stellate Ganglion Block

Stellate ganglion blocks are frequently used for the treatment of sympathetically-mediated chronic pain syndromes, post-herpetic neuralgia, orofacial pain, atypical chest pain, chronic post-surgical pain, and peripheral vascular disease [28]. Fluoroscopy was utilized in the past to perform these blocks, however, the advent of an ultrasound-guided technique allows for visualization of salient structures surrounding the stellate ganglion including the vertebral arteries, thyroid gland, longus colli muscle, nerve roots, and esophagus [29].

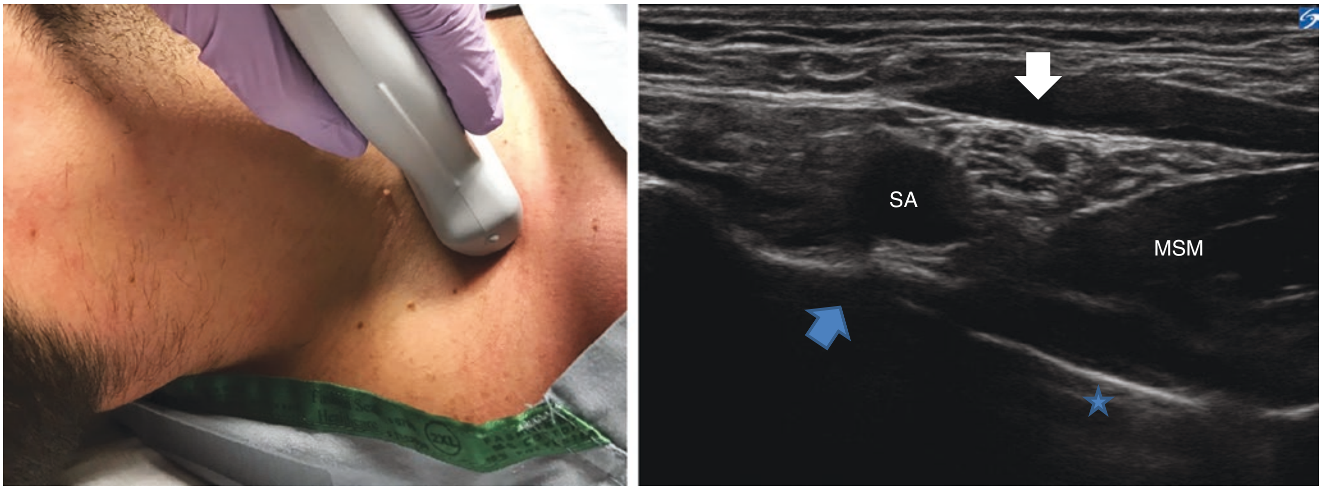

Fig. 9 Supraclavicular Nerve Block: MSM = Middle Scalene Muscle, White Arrow = Brachial Plexus, SA = Subclavian Artery, Blue Arrow = Designates first rib, Blue Star = Pleura

12.1 Anatomy

A thorough understanding of the cervical and thoracic sympathetic structures is crucial in performing a stellate ganglion block. The cervical sympathetic trunk is comprised of four ganglia: superior, middle, intermediate, and inferior cervical ganglia, and in about 80% of the population, the inferior cervical ganglion is fused with the first thoracic ganglion, forming the stellate ganglion [30]. If the inferior cervical ganglion and first thoracic ganglion are not fused, the stellate ganglion refers to the inferior cervical ganglion adjacent to the anterior C7 tubercle [28]. The stellate ganglion is bounded medially by the longus colli muscle, recurrent laryngeal nerve, trachea and esophagus; laterally by the scalene muscles, anteriorly by the first section of the subclavian artery and at the origin of the vertebral artery, and anteriorly by the apex of the lung [29]. The classical anatomic structure in its proximity is Chassaignac's tubercle at the level of C6, and at C7 it lies more medially in proximity to the anterolateral aspect of the vertebral body [29]. Fluoroscopy was historically used to achieve a stellate ganglion block, however, the advent of ultrasound facilitates avoidance of injuring critical vascular structures such as the vertebral artery, organs such as the thyroid and esophagus, and neural tissues; thus ultrasound-guided stellate ganglion blocks may be considered a safer technique for practitioners experienced with ultrasound [30].

Signs of a successful block will include Horner's syndrome, anhidrosis, nasal congestion, vasodilation, and increase in temperature [29]. One common complication associated with stellate ganglion block is dysphonia due to blockade of the ipsilateral recurrent laryngeal nerve. For this reason, bilateral stellate ganglion block is not advised to prevent loss of pharyngeal reflexes and respiratory sequelae. Extension of the block to the brachial plexus may cause somatic blockade; if this occurs the patient should be instructed to care for the upper extremity to avoid inadvertent injury. Intravascular injection due to close proximity to carotid, subclavian, and vertebral vessels may occur and underscores the importance of confirming negative aspiration prior to injecting local anesthetic. Epidural and intrathecal injection may also result.

12.2 Sonoanatomy and Clinical Application

In preparation for a stellate ganglion block, the patient is positioned supine with the neck slightly extended and head rotated to the contralateral side. After application of a sterile disinfecting solution, a sterilely covered high frequency linear ultrasound transducer is applied in the transverse axis at the level of the cricoid cartilage. The probe should then be moved to identify landmark structures: thyroid, carotid artery, and jugular vein, as well as the transverse process of C6, which may be differentiated from adjacent levels by its prominent anterior tubercle. The longus colli muscle may be identified superior to the transverse process of C6 on the ultrasound image (Fig. 10). The skin overlying the block needle insertion site is anesthetized, and the needle puncture site should be in a location that is in-plane with the transducer. The needle should be directed in a lateral-to-medial direction until it passes through the deep cervical fascia overlying the longus colli muscle. A small amount of local anes-

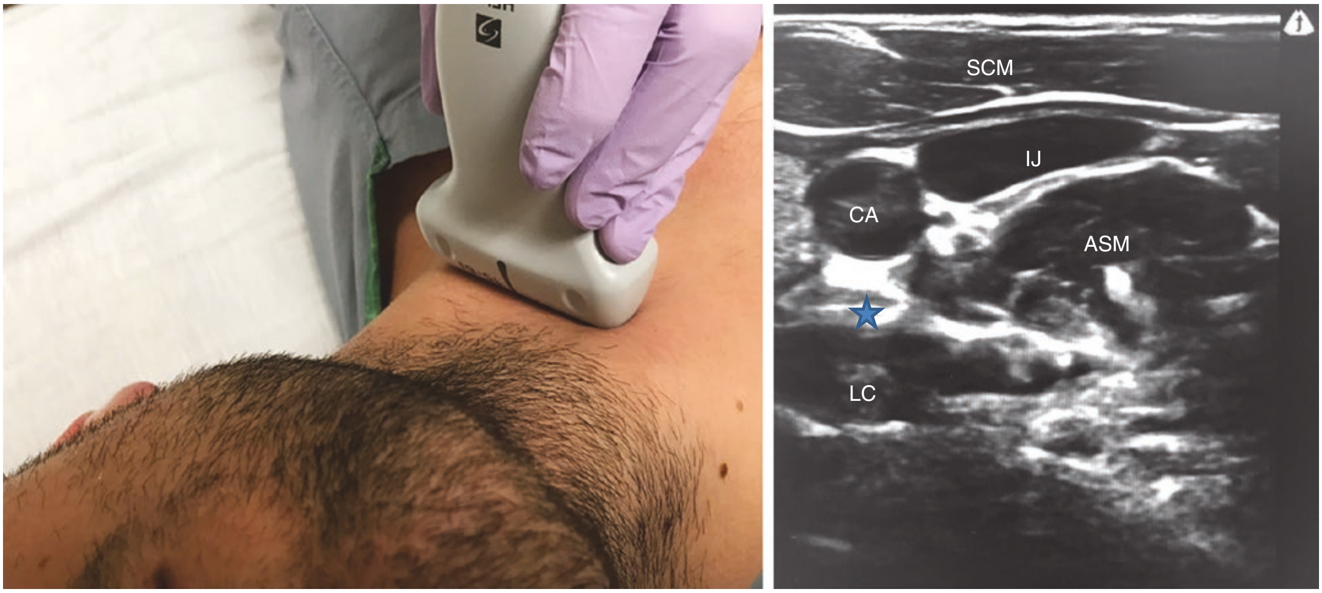

Fig. 10 Stellate Ganglion Block: *SCM* sternocleidomastoid muscle, *CA* Carotid Artery, *IJ* Internal Jugular Vein, *ASM* Anterior Scalene Muscle, *LC* Longus Colli Muscle, *Blue Star* Target Site

thetic (up to 5 mL) may be injected here, watching for separation of the carotid artery and the longus colli muscle.

References

1. Suresh S, Voronov P. Head and neck blocks in infants, children, and adolescents. Paediatr Anaesth. 2012;22(1):81–7.
2. Herlich A. Focused local anesthesia and analgesia for head and neck surgery. Int Anesthesiol Clin. 2012;50(1):13–25.
3. Nader A, Kendall MC, De Oliveria GS, et al. Ultrasound-guided trigeminal nerve block via the pterygopalatine fossa: an effective treatment for trigeminal neuralgia and atypical facial pain. Pain Physician. 2013;16(5):E537–45.
4. Zheng JP, Song M, Zhan XX, Li CZ, Zong XY, Zhang YZ. Endoscopic approach to the trigeminal nerve: an anatomic study. J Craniomaxillofac Surg. 2014;42(5):674–82.
5. Bathla G, Hegde AN. The trigeminal nerve: an illustrated review of its imaging anatomy and pathology. Clin Radiol. 2013;68(2):203–13.
6. Kariya K, Usui Y, Higashi N, et al. Anatomical basis for simultaneous block of greater and third occipital nerves, with an ultrasound-guided technique. J Anesth. 2018;32(4):483–92.
7. Arai T, Ishikawa K, Saito T, Hashimoto Y, Asai T, Okuda Y. Distance from the external occipital protuberance to the occipital artery for occipital nerve block. J Anesth. 2013;27(5):801–2.
8. Okuda Y, Ishikawa K, Usui Y, Nagao M, Ikeda T, Kitajima T. Use of an ultrasound doppler flowmeter for occipital nerve block. Reg Anesth Pain Med. 2002;27:444–5.
9. Greher M, Moriggl B, Curatolo M, Kirchmair L, Eichenberger U. Sonographic visualization and ultrasound-guided blockade of the greater occipital nerve: a comparison of two selective techniques confirmed by anatomical dissection. Br J Anaesth. 2010;104(5):637–42.
10. Juskys R, Sustickas G. Effectiveness of treatment of occipital neuralgia using the nerve block technique: a prospective analysis of 44 patients. Acta Med Litu. 2018;25(2):53–60.
11. Khavanin N, Carl HM, Yang R, Dorafshar AH. Surgical "safe zone": rapid anatomical identification of the lesser occipital nerve. J Reconstr Microsurg. 2019;35(5):341–5.
12. Tubbs RS, Fries FN, Kulwin C, Mortazavi MM, Loukas M, Cohen-Gadol AA. Modified skin incision for avoiding the lesser occipital nerve and occipital artery during retrosigmoid craniotomy: potential applications for enhancing operative working distance and angles while minimizing the risk of postoperative neuralgias and intraoperative hemorrhage. J Clin Neurosci. 2016;32:83–7.
13. Platzgummer H, Moritz T, Gruber GM, et al. The lesser occipital nerve visualized by high-resolution sonography--normal and initial suspect findings. Cephalalgia. 2015;35(9):816–24.
14. Kim JS, Ko JS, Bang S, Kim H, Lee SY. Cervical plexus block. Korean J Anesthesiol. 2018;71(4):274–88.
15. Castresana MR, Masters RD, Castresana EJ, Stefansson S, Shaker IJ, Newman WH. Incidence and clinical significance of hemidiaphragmatic paresis in patients undergoing carotid endarterectomy during cervical plexus block anesthesia. J Neurosurg Anesthesiol. 1994;6(1):21–3.
16. Martusevicius R, Swiatek F, Joergensen LG, Nielsen HB. Ultrasound-guided locoregional anaesthesia for carotid endarterectomy: a prospective observational study. Eur J Vasc Endovasc Surg. 2012;44(1):27–30.
17. Elmaddawy AEA, Mazy AE. Ultrasound-guided bilateral superficial cervical plexus block for thyroid surgery: the effect of dexmedetomidine addition to bupivacaine-epinephrine. Saudi J Anaesth. 2018;12(3):412–8.
18. Singh SK. The cervical plexus: anatomy and ultrasound guided blocks. Anaesth Pain Intens Care. 2015;19(3).
19. Sait Kavakli A, Kavrut Ozturk N, Umut Ayoglu R, et al. Comparison of combined (deep and superficial) and intermediate cervical plexus block by use of ultrasound guidance for carotid endarterectomy. J Cardiothorac Vasc Anesth. 2016;30(2):317–22.
20. Koshy RC, Thankamony H. Superficial cervical plexus block for urgent tracheostomy. Indian J Anaesth. 2019;63(1):65–6.
21. Soeding P, Eizenberg N. Review article: anatomical considerations for ultrasound guidance for regional anesthesia of the neck and upper limb. Can J Anaesth. 2009;56(7):518–33.
22. Raju PKB, Coventry DM. Ultrasound-guided brachial plexus blocks. Continuing Education in Anaesthesia, Critical Care & Pain. 2013;14(4):185–91.
23. Demondion X, Herbinet P, Boutry N, Fontaine C, Francke JP, Cotten A. Sonographic mapping of the normal brachial plexus. AJNR Am J Neuroradiol. 2003;24(7):1303–9.
24. Gervasio A, Mujahed I, Biasio A, Alessi S. Ultrasound anatomy of the neck: the infrahyoid region. J Ultrasound. 2010;13(3):85–9.
25. Zisquit J, Nedeff N. Interscalene Block. In: StatPearls [internet]: StatPearls Publishing; 2018.
26. Hussain N, Goldar G, Ragina N, Banfield L, Laffey JG, Abdallah FW. Suprascapular and Interscalene nerve block for shoulder surgery: a systematic review and meta-analysis. Anesthesiology. 2017;127(6):998–1013.
27. Guo CW, Ma JX, Ma XL, et al. Supraclavicular block versus interscalene brachial plexus block for shoulder surgery: a meta-analysis of clinical control trials. Int J Surg. 2017;45:85–91.
28. Piraccini E, Chang K-V. Stellate ganglion blocks. In: StatPearls [internet]: StatPearls Publishing; 2018.
29. Serna-Gutiérrez J. Ultrasound-guided stellate ganglion block. Revista Colombiana de Anestesiología. 2015;43(4):278–82.
30. Narouze S, Vydyanathan A, Patel N. Ultrasound-guided stellate ganglion block successfully prevented esophageal puncture. Pain Physician. 2007;10(6):747–52.

Part III

Upper and Lower Extremity Ultrasound

The Techniques and Merit of Ultrasound in Orthopaedics

Cristina Terhoeve, Robert Zura, John Reach,
and Andrew King

1 Introduction

Over the past decade, the utilization of musculoskeletal ultrasound imaging for both diagnostic and therapeutic purposes has been steadily rising in the field of orthopaedics. This increase is driven by technological advances which have made ultrasound more affordable and practical in the clinic setting. Ultrasound is frequently used in the evaluation of tendon, muscle, and ligament injuries as well as soft tissue masses. The advantages, disadvantages, and technological considerations of musculoskeletal sonography will be discussed in this chapter followed by a review of the most common pathologies for which ultrasound is used in Orthopaedic Surgery.

2 Advantages

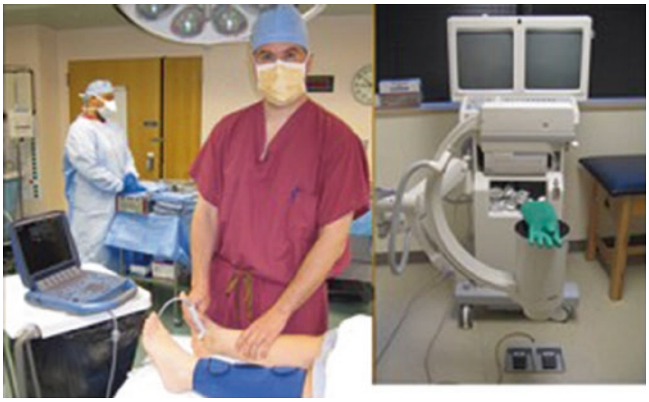

Fig. 1 A hand-held musculoskeletal ultrasound in use. Note the small size of the US machine on the left compared to a mini C-arm on the right. Various transducers are available to acquire specific imaging. Many Ultrasound systems are quite portable and may be taken by the surgeon from the floor to the clinic or operating room

Ultrasound is advantageous compared to other imaging modalities (Fig. 1) in that it is low cost, widely available, and there is no radiation exposure. The average reimbursement for an MRI is approximately $2000 whereas the reimbursement for a diagnostic musculoskeletal ultrasound is $150 [1]. A study published in 2008 looking at government published data sets found that the substitution of musculoskeletal ultrasound for MRI, when appropriate, would lead to estimated cost savings of $6.9 billion dollars from the period of 2006–2020 [2].

It allows for a dynamic evaluation of the musculoskeletal system and is particularly useful for the evaluation of soft tissue structures such as ligaments and tendons. Unlike MRI, metal hardware does not distort the sonographic image. As a result, ultrasound is very useful in the evaluation of soft tissue structures adjacent to orthopaedic hardware [3]. Doppler techniques allow for detection of soft tissue hyperemia and neovascularity. Ultrasound can be used as an extension of the physical exam, allowing patients to ‘see’ their own pathology; this leads to a better understanding of their disease process and a more constructive discussion of treatment options. It is time-saving for both the patient and physician in that the ultrasound can be performed at the initial specialist consultation visit; in contrast, a second trip must be made back to the office after a CT or MRI has been performed to review the imaging results and formulate a treatment plan. In pediatrics, ultrasound is often used in very young patients due to the high ratio of cartilage to bone in a child’s skeleton [4]. Lastly, it can be used to ensure accuracy of placement of diagnostic and/or therapeutic injections.

C. Terhoeve · R. Zura · A. King
Department of Orthopaedic Surgery, Louisiana State University Health Sciences Center, New Orleans, LA, USA

J. Reach (✉)
Department of Orthopaedic Surgery, Yale School of Medicine, New Haven, CT, USA
e-mail: john.reach@yale.edu

© Springer Nature Switzerland AG 2021
J. Li et al. (eds.), *Ultrasound Fundamentals*, https://doi.org/10.1007/978-3-030-46839-2_9

3 Disadvantages

While musculoskeletal ultrasound is widely used in Europe and Canada, acceptance in the United States has been slow. There is a steep learning curve, and reliability of the ultrasound study is dependent on a well-trained operator. To provide consistent results, physicians using musculoskeletal sonography should receive proper training. The American Medical Society for Sports Medicine (AMSSM) developed a curriculum for sports medical fellowships in 2010. This curriculum allows for specific training in the core competencies of sports sonography in order to include ultrasound proficiency in the toolbox of orthopaedic sports medicine physicians [5, 6]. Intrinsic limitations to sonography include reduced resolution at tissue depths greater than 3 cm (often an issue with obese patients), the "keyhole" nature of images which results in difficulty with orientation and understanding of visualized pathology; and the inability to see through bone, gas, or metal [3].

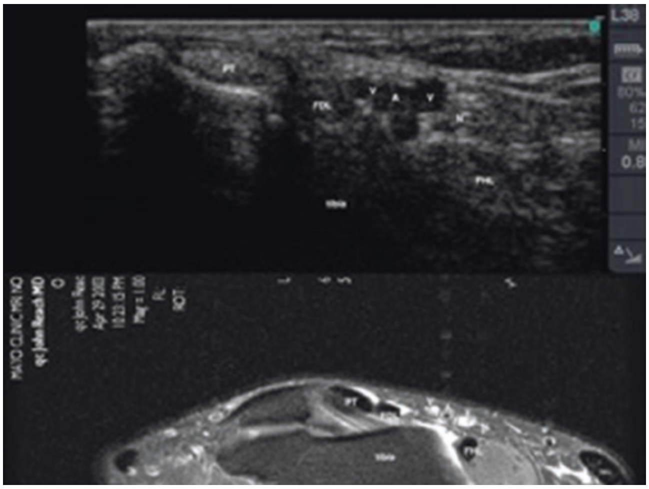

Fig. 2 Short axis US image of medial ankle structures compared to an MRI of the same area. Tendons become darker and brighter depending on their angulation with respect to transducer orientation, a property known as anisotropy. (TP Tibialis posterior, FDL flexor digitorum longus, FHL flexor hallucis longus, A posterior tibial artery, V Veins, N Tibial Nerve, T Tibia)

4 Technical Considerations

Ultrasound images are created by the placement of a probe directly on the skin which directs sound waves into the tissues immediately beneath it. It is the interaction of these sound waves at soft tissue interfaces which determines the appearance of the structure on the ultrasound image. There are several types of probes available to the technician/physician, each with different contact surfaces or footprints. Utilization of the proper type of probe for the pathology being evaluated allows one to maximize visualization of the structure(s) in question. A 17-5 MHz linear array probe is used for general musculoskeletal examinations; it is particularly useful for evaluating linear internal structures such as tendons, ligaments, and muscles. A 15-7 MHz hockey stick probe is used for detailed evaluation of superficial structures less than 6 cm deep to skin. A 5-2 MHz curved sector array is used for evaluation of deep structures up to 30 cm deep to skin.

In order to evaluate sonographic images, it is necessary to possess a detailed understanding of the appearances of both normal and pathologic structures (Fig. 2). Normal tendons appear as linear hyperechoic fibrillar structures. In tendinosis, there is loss of this normal fibrillar pattern and replacement with hypoechoic areas. There will be a focal area of discontinuity of the tendon fibers in the case of a frank tendon tear (Fig. 3). Ligaments appear as thin hyperechoic structures; they become thickened and hypoechoic or discontinuous when torn (Fig. 4). Muscle is hypoechoic with linear areas of increased echogenicity from the perimysium surrounding muscle fascicles. Subcutaneous fat is hypoechoic with small echogenic septations. Articular cartilage is anechoic. Fibrocartilaginous structures such as the glenoid and acetabular labra along with the meniscus appear as hyperechoic. Bone is densely hyperechoic. Step-offs and cortical irregularities may represent occult fractures (Fig. 5). Nerves have honey comb echogenicity and may be dependent on adjacent structures [7].

5 Soft Tissue Masses and Fluid Collections

Ultrasound is frequently used in the evaluation of soft tissue masses. It allows the physician to differentiate between solid and fluid filled masses, often eliminating the need for MRI. Solid lesions such as hemangiomas, lipomas, and giant cell tumors demonstrate internal vascularity on Doppler imaging. Cystic lesions are anechoic and ovular with a thin, well defined wall. The three criteria which confirm the diagnosis of a simple fluid collection on ultrasound are a well-defined posterior wall, anechoic, and increased through transmission of sound waves [8]. Lesions may be seen extending into the joint in the case of ganglia and popliteal cysts (Fig. 6). In patients with idiopathic dorsal wrist pain, ultrasound can diagnose an occult dorsal ganglion cyst with a sensitivity of 93%; this is equivalent to or better than diagnosis via MRI [9].

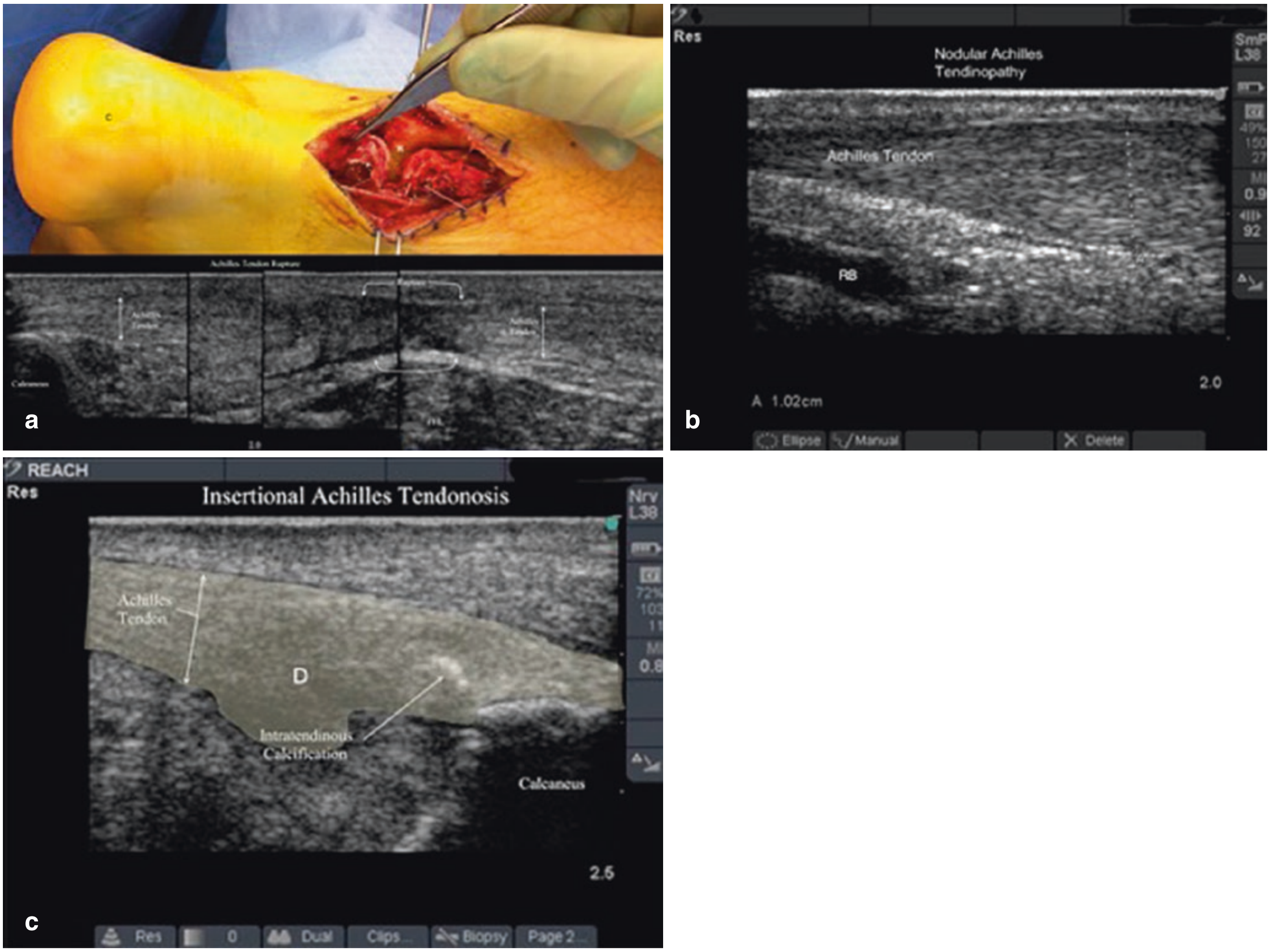
a
Achilles Tendon Rupture
Achilles Tendon
Rupture
Achilles Tendon
Calcaneus
FHL
b
Res
Nodular Achilles Tendinopathy
Achilles Tendon
RB
2.0
A 1.02cm
Ellipse
Manual
Delete
c
REACH
Res
Insertional Achilles Tendonosis
Nrv L38
Achilles Tendon
D
Intratendinous Calcification
Calcaneus
2.5
Res
0
Dual
Clips...
Biopsy
Page 2

Fig. 3 Achilles Tendon pathology as seen on ultrasound. (**a**) Achilles tendon rupture; (**b**) Nodular Achilles Tendinopathy; (**c**) Insertional Achilles Tendinopathy with hyperechoic calcifications and hypoechoic lakes of tendinopathy. (R Achilles Rupture, RB Retrocalcaneal Bursitis, C Calcaneus, FHL Flexor Hallucis Longus, D Tendinopathy)

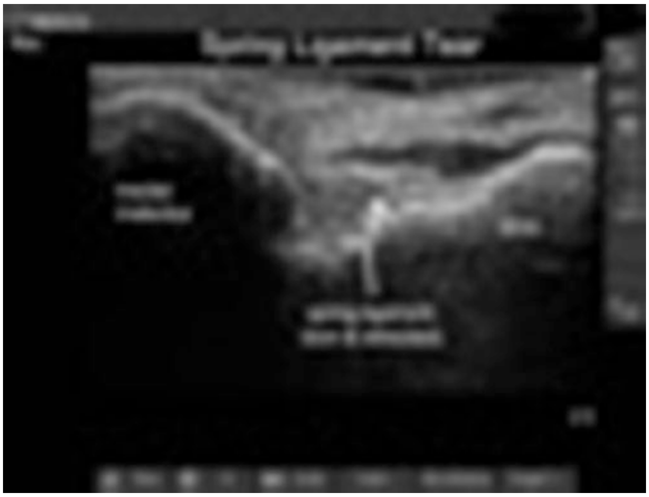
Spring Ligament Tear

Fig. 4 Spring (Deltoid) Ligament tear. (SL Spring Ligament, T Talus, PT Posterior Tibialis Tendon)

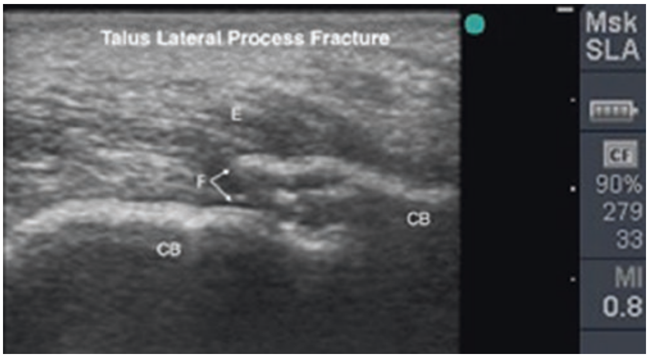
Talus Lateral Process Fracture
E
F
CB
CB
Msk SLA
CF
90%
279
33
MI
0.8

Fig. 5 Ultrasound Palpation Test: In cases of plain-film negative focal foot and ankle pain, the maximal point of tenderness is marked on the skin and localized on ultrasound imaging. Under direct visualization, the underlying anatomic structures are then palpated, manipulated and stressed dynamically by the transducer and the free examiner hand. In this case, the Ultrasound Palpation Test revealed a fracture of the lateral process of the talus in mountain biker with negative X-rays. Note the cortical discontinuity. (CB Cortical Bone; E Edema, F Fracture Step-Off)

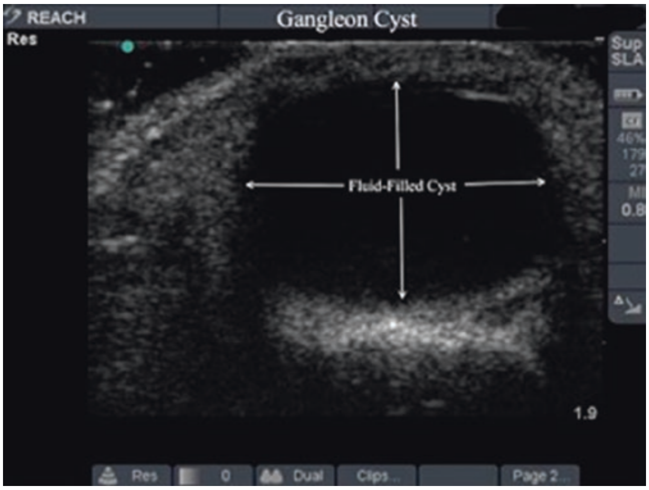

Fig. 6 Ganglion Cyst. Note the homogeneous hypoechoic mass. On color Doppler imaging there is no vascular ingrowth. An ultrasound-guided aspiration may be performed in at the same visit. Intraoperatively, the surgeon may trace the ganglion's stalk down to the underlying pathology, decreasing incisional and explorative co-morbidity. (G Ganglion Cyst)

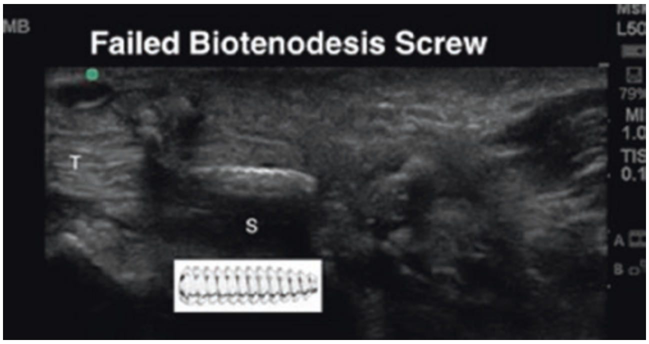

Fig. 7 Most modern suture anchors are radiolucent (plastic polyetheretherketone [PEEK] or bio-absorbable composite poly-L-lactic acid [PLLA]). Ultrasound clearly shows the failed PEEK screw in the soft-tissue just distal to the failed tendon repair. This was not apparent on plan film X-rays which were read as normal in this patient. (S screw; T failed tendon transfer)

6 Foreign Bodies

Ultrasound is used for foreign body localization in order to assist with extrication. Foreign bodies appear as hyperechoic foci with accompanying acoustic shadowing on sonography (Fig. 7). There may be a surrounding hypoechoic halo in the presence of edema, abscess, or granulation tissue [10, 11]. The presence of acoustic shadowing differentiates foreign bodies from scar tissue, gas bubbles, and normal intermuscular fascia [12]. Sonography has a sensitivity of 94–95% for the detection of foreign bodies including metal, glass, and wood [13–15]. Unlike metal and glass, wood is radiolucent in radiographs because its attenuation is similar to that of soft tissues. A missed foreign body can be asymptomatic or can lead to complications such as pain, infection/abscess, tendon rupture, vascular events, or neurological deficits [16–22].

7 Nerve Entrapment

Compression of peripheral nerves is most commonly diagnosed by clinical exam and electrodiagnostic testing. Ultrasound has been suggested by some authors as a less invasive means of diagnosing nerve compression than electrodiagnostic testing, particularly with carpal tunnel and cubital tunnel syndrome [23]. This is performed by measuring the cross-sectional area of the nerve being evaluated at the site of most compression. A recent meta-analysis showed comparable sensitivity and specificity of ultrasound and electrodiagnostic testing in the diagnosis of carpal tunnel syndrome [24].

8 Rotator Cuff Tears and Other Shoulder Pathology

On sonographic examination, a healthy rotator cuff is uniform in thickness with homogenous echogenicity. It is 4–6 mm anteriorly and somewhat thinner posteriorly. Tendinopathy is characterized as a thickened and heterogenous tendon. Subacromial bursitis is characterized as a band of decreased signal superficial to the cuff [25]. A partial thickness tear is a defined as a hypoechoic discontinuity in either the bursal or articular side of the rotator cuff tendon or as a mixed hyperechoic and hypoechoic region within the tendon. With a full thickness tear, there is either non-visualization of the cuff or focal discontinuity in the homogenous echogenicity of the cuff [26].

At this point, MRI is currently the standard of care in the United States for diagnosing rotator cuff tears. That being said, multiple studies have found MRI and ultrasound to have a comparable sensitivity and specificity of approximately 95% in the diagnosis of both full thickness and partial thickness rotator cuff tears [26–31]. Other shoulder pathology such as bicep tendonitis, calcific tendonitis, and subacromial bursitis can also be diagnosed effectively with ultrasound [32]. Ultrasound offers the potential for significant cost and time savings in that the imaging procedure and subsequent treatment plan can be discussed at the initial patient visit. In contrast to MRI, ultrasound also allows for a dynamic functional examination of the shoulder.

9 Peroneal Tendon Instability

Peroneus longus and peroneus brevis muscles are dynamic stabilizers of the ankle joint. Patients with peroneal tendon subluxation and dislocation present with pain, tenderness posterior to the lateral malleolus, and voluntary subluxation of the tendons with a subjective "snapping" sound. Dynamic ultrasound is the diagnostic exam of choice because it allows for visualization of peroneal tendon subluxation with ankle movement. Peroneal tendon tears can be diagnosed using sonography with a sensitivity of 100%, specificity of 85%, and accuracy of 90% [33] (Fig. 8). MRI is useful if considering surgical intervention to assess for the presence of synovitis, tendinosis, a low-lying peroneus brevis muscle belly, and a peroneus quartus [34].

10 Pediatric Developmental Dysplasia of the Hip (DDH)

In the first 6 months of life, ultrasound is the imaging exam of choice in the evaluation of the pediatric hip. Unlike radiography, sonography allows for examination of the cartilaginous femoral head and surrounding soft tissue structures such as the labrum. Diagnosis of developmental dysplasia with sonography has a sensitivity of 88% and specificity of 96%. Use of ultrasound to evaluate infants with risk factors for hip dysplasia or those with an equivocal physical exam has significantly decreased the rate of emergence of late DDH cases [35]. The risk factors necessitating sonographic screening are a positive family history, breech birth position, and conditions which result from intrauterine crowding such as neonatal clubfoot and torticollis. Screening is performed at 4–6 weeks of age. A sonographic exam performed at <4 weeks of age results in a high rate of false positive results due to physiologic immaturity of the hips [3].

There are two commonly used techniques to evaluate for hip dysplasia: the static Graf method which assesses morphology and the dynamic Harcke method which assesses femoral head stability. With the Graf method, coronal plane imaging is performed with the infant in the supine or lateral decubitus position. The alpha angle is created by lines along the bony acetabulum and the ilium. Normal is greater than 60°. The beta angle is created by lines along the labrum and ilium. Normal is less than 55° [36]. For the dynamic Harcke method, the hip is subjected to stress maneuvers in order to assess femoral head stability [37]. The Barlow maneuver dislocates a dislocatable hip with adduction and depression of the flexed femur. The Ortolani maneuver reduced a dislocated hip with elevation and abduction of the flexed femur. Based on ultrasound and physical exam findings, an infant's hip can be classified as normal, immature, mildly dysplastic, or severely dysplastic with femoral head displacement.

11 Injections

Numerous studies have demonstrated that the use of ultrasound to guide injections significantly increases accuracy, particularly with small joints (Fig. 9). Injections done without image guidance miss their target 14–71% of the time; the use of ultrasound decreases this failure rate to approximately 5% [38–46]. At this point in time, it is unknown whether this increased accuracy correlates with clinical efficacy. Injected corticosteroids diffuse through tissue planes, evident through

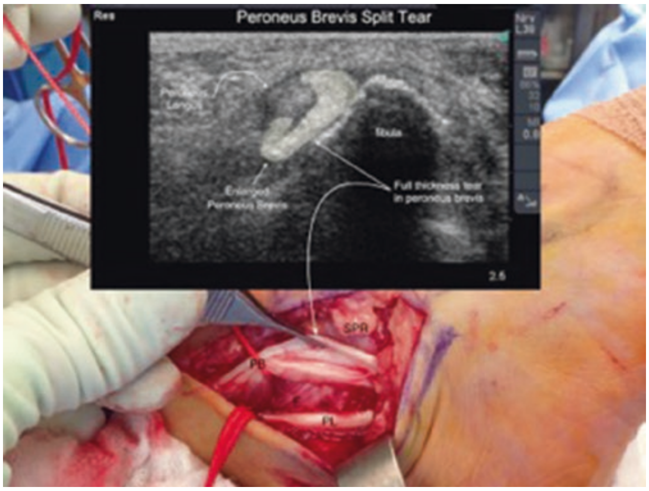
Peroneus Brevis Split Tear
Peroneus Longus
fibula
Enlarged Peroneus Brevis
Full thickness tear in peroneus brevis
SPR
PB
PL

Fig. 8 Peroneus brevis tendon split tear. On dynamic imaging the peroneus longus tendon sandwiches the brevis between itself and the fibula: a back and forth sawing motion cuts the brevis in-line with its collagen bundles much like a Gigli saw. (F Fibula, PL Peroneus Longus Tendon, PB Peroneus Brevis Tendon, SPR Superficial Peroneal Retinaculum)

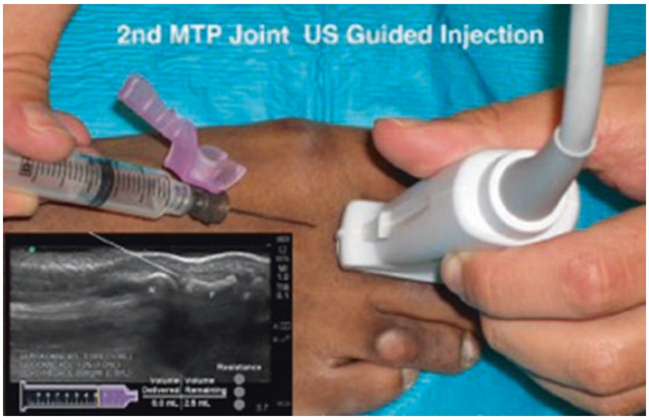

Fig. 9 Small, intermediate and large joints are difficult to accurately inject using only anatomic landmarks. Ultrasound-guided injections have been shown to be safe and accurate. Contrast is not required as the joint can been seen to expand on dynamic imaging. (M Metatarsal; P Proximal Phalanx)

common complications such as subcutaneous fat atrophy and depigmentation [1]. As such, it is unlikely that corticosteroid injections require pinpoint accuracy. In contrast, the use of sonographic guidance for injection of hyaluronic acid derivatives and platelet rich plasma could improve efficacy. More research is needed to determine if the use of ultrasound to guide injections improves clinical outcomes.

Key Points

- Ultrasound is highly operator dependent, but in experienced hands it is excellent for evaluation of musculoskeletal pathology.
- Ultrasound allows physicians to differentiate between solid and fluid filled soft tissue masses, often eliminating the need for MRI.
- Ultrasound is very useful for localizing foreign bodies, particularly wood as it is radiolucent, and can assist with extrication.
- Ultrasound has been suggested as a less invasive means of diagnosing peripheral nerve compression than electrodiagnostic testing.
- While MRI is currently the standard of care in the United States for diagnosing rotator cuff tears, MRI and sonography have comparable sensitivity and specificity in the hands of an experienced physician.
- Ultrasound is the diagnostic exam of choice for peroneal tendon instability as it allows visualization of subluxation and dislocation.
- Ultrasound screening for developmental dysplasia of the hip is performed at 4–6 weeks of age in infants with risk factors or those with an equivocal physical exam.
- Use of ultrasound guidance for injections improves accuracy but more research is needed to determine if this correlates with increased clinical efficacy

References

1. Harmon KG, O'Connor FG. Musculoskeletal ultrasound: taking sports medicine to the next level. Br J Sports Med. 2010;44(16):1135–6.
2. Parker L, Nazarian LN, Carrino JA, et al. Musculoskeletal imaging: Medicare use, costs, and potential for cost substitution. J Am Coll Radiol. 2008;5(3):182–8.
3. Linklater JM, Read JW, Hayter CL. Chapter 3 – imaging of the foot and ankle. In: Coughlin MJ, Saltzman CL, Anderson RB, editors. Mann's surgery of the foot and ankle. 9th ed. Philadelphia: Saunders; 2014. p. 61–120.
4. Khanna G, El-Khoury GY, Menda Y. Chapter 3 – imaging. In: Weinstein SL, Flynn JM, editors. Lovell and winter's pediatric orthopaedics. 7th ed. Philadelphia: Lippincott Williams & Wilkins; 2014. p. 62–7.
5. Finnoff J, Lavallee ME, Smith J. Musculoskeletal ultrasound education for sports medicine fellows: a suggested/potential curriculum by the American Society of Sports Medicine. Br J Sports Med. 2010;44(16):1144–8.
6. Finnoff J, Berkoff D, Brennan F, et al. American Medical Society for Sports Medicine recommended sports ultrasound curriculum for sports medicine fellowships. Br J Sports Med. 2015;25(1):23–9.
7. Spouge A. Chapter 10 – imaging overview. In: Miller MD, Thompson SR, editors. DeLee & Drez's orthopaedic sports medicine. 4th ed. Philadelphia: Saunders; 2015. p. 110–37.
8. Starr HM, Sedgley MD, Murphy MS. Ultrasound in hand surgery. J Hand Surg Am. 2014;39(12):2522–4.
9. Osterwalder JJ, Widrig R, Stober R, et al. Diagnostic validity of ultrasound in patients with persistent wrist pain and suspected occult ganglion. J Hand Surg Am. 1997;22(6):1034–40.
10. Peterson JJ, Bancroft LW, Kransdorf MJ. Wooden foreign bodies: imaging appearance. AJR Am J Roentgenol. 2002;178(3):557–62.
11. Little CM, Parker MG, Callowich MC, Sartori JC. The ultrasonic detection of soft tissue foreign bodies. Investig Radiol. 1986;21(3):275–7.
12. Crawford R, Matheson AB. Clinical value of ultrasonography in the detection and removal of radiolucent foreign bodies. Injury. 1989;20(6):341–3.
13. Bray PW, Mahoney JL, Campbell JP. Sensitivity and specificity of ultrasound in the diagnosis of foreign bodies in the hand. J Hand Surg Am. 1995;20(4):661–6.
14. Ober CP, Jones JC, Larson MM, et al. Comparison of ultrasound, computed tomography, and magnetic resonance imaging in detection of acute wooden foreign bodies in the canine manus. Vet Radiol Ultrasound. 2008;49(5):411–8.
15. Tantray MD, Rather A, Manaan Q, et al. Role of ultrasound in detection of radiolucent foreign bodies in extremities. Strategies Trauma Limb Reconstr. 2018;13(2):81–5.
16. Fakoor M. Prolonged retention of an intramedullary wooden foreign body. Pak J Med Sci. 2006;22(1):78–9.
17. Choudhari KA, Muthu T, Tan MH. Progressive ulnar neuropathy caused by delayed migration of a foreign body. Br J Neurosurg. 2001;15(3):263–5.
18. Yang SS, Bear BJ, Wieland AJ. Rupture of the flexor pollicis longus tendon after 30 years due to migration of a retained foreign body. J Hand Surg Br. 1995;20(6):803–5.
19. Jablon M, Rabin SI. Late flexor pollicis longus tendon rupture due to retained glass fragments. J Hand Surg Am. 1988;13(5):713–6.
20. Rainer C, Schoeller T, Wechselberger G, et al. Median nerve injury caused by missed foreign body case report. Scand J Plast Reconstr Surg Hand Surg. 2000;34(4):401–3.
21. Wendt JR, Ackley SM. Vascular complications of a foreign body in the hand of an asymptomatic patient. Ann Plast Surg. 1995;34(1):92–4.
22. Meurer WJ. Radial artery pseudoaneurysm caused by occult retained glass from a hand laceration. Pediatr Emerg Care. 2009;25(4):255–7.
23. Wiesler ER, Chloros GD, Cartwright MS, et al. Ultrasound in the diagnosis of ulnar neuropathy at the cubital tunnel. J Hand Surg Am. 2006;31(7):1088–93.
24. Fowler JR, Gaughan JP, Ilyas AM. The sensitivity and specificity of ultrasound for the diagnosis of carpal tunnel syndrome: a meta-analysis. Clin Orthop Relat Res. 2011;469(4):1089–94.
25. Lindell K, Sanders TG. Chapter 44 – glenohumeral joint imaging. In: Miller MD, Thompson SR, editors. DeLee & Drez's orthopaedic sports medicine. 4th ed. Philadelphia: Saunders; 2015. p. 452–87.
26. Ziegler DW. The use of in-office, orthopaedist-performed ultrasound of the shoulder to evaluate and manage rotator cuff disorders. J Shoulder Elb Surg. 2004;13(3):291–7.

27. Teefey SA, Rubin DA, Middleton WD, et al. Detection and quantification of rotator cuff tears. J Bone Joint Surg Am. 2004;86(4):708–16.
28. Al-Shawi A, Badge R, Bunker T. The detection of full thickness rotator cuff tears using ultrasound. J Bone Joint Surg Br. 2008;90(7):889–92.
29. van Holsbeeck MT, Kolowich PA, Eyler WR, et al. US depiction of partial-thickness tear of the rotator cuff. Radiology. 1995;197(2):443–6.
30. Iannotti JP, Ciccone J, Bus DD, et al. Accuracy of office-based ultrasonography of the shoulder for the diagnosis of rotator cuff tears. J Bone Joint Surg Am. 2005;87(6):1305–11.
31. de Jesus JO, Parker L, Frangos AJ, et al. Accuracy of MRI, MR arthrography, and ultrasound in the diagnosis of rotator cuff tears: a meta-analysis. Am J Roentgenol. 2009;192(6):1701–7.
32. Ottenheijm RP, Jansen MJ, Staal JB, et al. Accuracy of diagnostic ultrasound in patients with suspected subacromial disorders: a systematic review and meta-analysis. Arch Phys Med Rehabil. 2010;91(10):1616–25.
33. Grant TH, Kelikian AS, Jereb SE, et al. Ultrasound diagnosis of peroneal tendon tears a surgical correlation. J Bone Joint Surg Am. 2005;87(8):1788–94.
34. Kadakia AR. Chapter 111 – imaging of the foot and ankle. In: Miller MD, Thompson SR, editors. DeLee & Drez's orthopaedic sports medicine. 4th ed. Philadelphia: Saunders; 2015. p. 1331–42.
35. Rosendahl K, Markestad T, Lie RT. Ultrasound screening for developmental dysplasia of the hip in the neonate: the effect on treatment rate and prevalence of late cases. Pediatrics. 1994;94(1):45–52.
36. Graf R. The diagnosis of congenital hip-joint dislocation by the ultrasonic Combound treatment. Arch Orthop Trauma Surg. 1980;97(2):117–33.
37. Harcke HT. Screening newborns for developmental dysplasia of the hip: the role of sonography. Am J Roentgenol. 1994;162(2):395–7.
38. Esenyel C, Demirhan M, Esenyel M, et al. Comparison of four different intra-articular injection sites in the knee: a cadaver study. Knee Surg Sports Traumatol Arthrosc. 2007;15(5):573–7.
39. Eustace JA, Brophy DP, Gibney RP, et al. Comparison of the accuracy of steroid placement with clinical outcome in patients with shoulder symptoms. Ann Rheum Dis. 1997;56(1):59–63.
40. Heidari N, Pichler W, Grechenig S, et al. Does the anteromedial or anterolateral approach alter the rate of joint puncture in injection of the ankle? A cadaver study. J Bone Joint Surg Br. 2010;92(1):176–8.
41. Henkus HE, Cobben LP, Coerkamp EG, et al. The accuracy of subacromial injections: a prospective randomized magnetic resonance imaging study. Arthroscopy. 2006;22(3):277–82.
42. Im SH, Lee SC, Park YB, et al. Feasibility of sonography for intra-articular injections in the knee through a medial patellar portal. J Ultrasound Med. 2009;28(11):1465–70.
43. Rutten MJ, Collins JM, Maresch BJ, et al. Glenohumeral joint injection: a comparative study of ultrasound and fluoroscopically guided techniques before MR arthrography. Eur Radiol. 2009;19(3):722–30.
44. Rutten MJ, Maresch BJ, Jager GJ, et al. Injection of the subacromial-subdeltoid bursa: blind or ultrasound-guided? Acta Orthop. 2007;78(2):254–7.
45. Smith J, Hurdle MF, Weingarten TN. Accuracy of sonographically guided intra-articular injections in the native adult hip. J Ultrasound Med. 2009;28(3):329–35.
46. Gilliland CA, Salazar LD, Borchers JR. Ultrasound versus anatomic guidance for intra-articular and periarticular injection: a systematic review. Phys Sportsmed. 2011;39(3):121–31.

Shoulder Joint Sonoanatomy and Ultrasound-Guided Shoulder Joint Injection

Allan Zhang and George C. Chang Chien

1 Introduction

Ultrasonography (US) is an excellent imaging modality for the evaluation of shoulder joint and rotator cuff diseases. When used appropriately, US can offer diagnostic accuracies approaching 100% for full thickness rotator cuff tears and 91% for partial thickness tears [1, 2]. US can also accurately identify tendon dislocations as well as shoulder bursitis. The initial step to developing a comprehensive knowledge in US shoulder examination is to have a detailed understanding of the anatomy. Then, the US examination of the shoulder can be approached in a systematic and methodical manner in order to provide a thorough and yet efficient examination.

2 Anatomy

The shoulder joint is a complex articulation among the glenoid, proximal humeral head and distal clavicle (Fig. 1). Multiple tendinous and ligamentous attachments function together to allow for the dynamic mobility of the shoulder. The rotator cuff muscles serve to stabilize the shoulder as well as support motion for shoulder abduction and internal and external rotation. The rotator cuff is composed of four muscles attached as tendons onto the proximal humerus: the supraspinatus, infraspinatus, teres minor, and subscapularis (Fig. 2). The supraspinatus muscle originates in the suprascapular fossa and inserts predominately onto the superior facet of the greater tuberosity. A portion of the supraspinatus inserts onto the middle facet and overlaps with the infraspinatus insertion. The infraspinatus is located within the infrascapular fossa, below the scapular spine, and inserts onto the middle facet of the greater tuberosity. The teres minor is located just below the infraspinatus and inserts onto the inferior facet of the greater tuberosity posteriorly. Lastly, the subscapularis originates within the subscapular fossa, anterior to the scapula, and is the only rotator cuff muscle to insert on the lesser tuberosity. Understanding the facet anatomy and bony landmarks can facilitate correctly identifying individual rotator cuff tendon insertions on US examination (Fig. 3).

Careful evaluation of the long head of the bicep tendon should also be part of the US examination of the shoulder and is typically the first landmark identified when evaluating the shoulder. The long head of the bicep tendon originates from the supraglenoid tubercle and courses within the bicipital groove, a bony landmark between the greater and lesser tuberosities. It joins with the short head of the bicep in the middle upper arm to form a single muscle mass which have an unified tendon that inserts onto the radial tuberosity. Its function is to flex and supinate the forearm. Variant anatomy of the long head of the bicep tendon can rarely be seen as posterior attachment on the supraglenoid tubercle [18]. The long head of the bicep tendon is secured within the bicipital groove by the overlying transverse humeral ligament. As it courses superiorly, it arches through the rotator cuff interval where it is stabilized by the superior glenohumeral and coracohumeral ligaments. Any deficiency within these ligaments can result in subluxation/dislocation of the long head bicep tendon.

A. Zhang (✉)
Department of Radiology, University of Connecticut Health Center, Farmington, CT, USA
e-mail: azhang@uchc.edu

G. C. Chang Chien
GCC Institute, Newport Beach, CA, USA

Ventura County Medical Center, Ventura, CA, USA

© Springer Nature Switzerland AG 2021

J. Li et al. (eds.), *Ultrasound Fundamentals*, https://doi.org/10.1007/978-3-030-46839-2_10

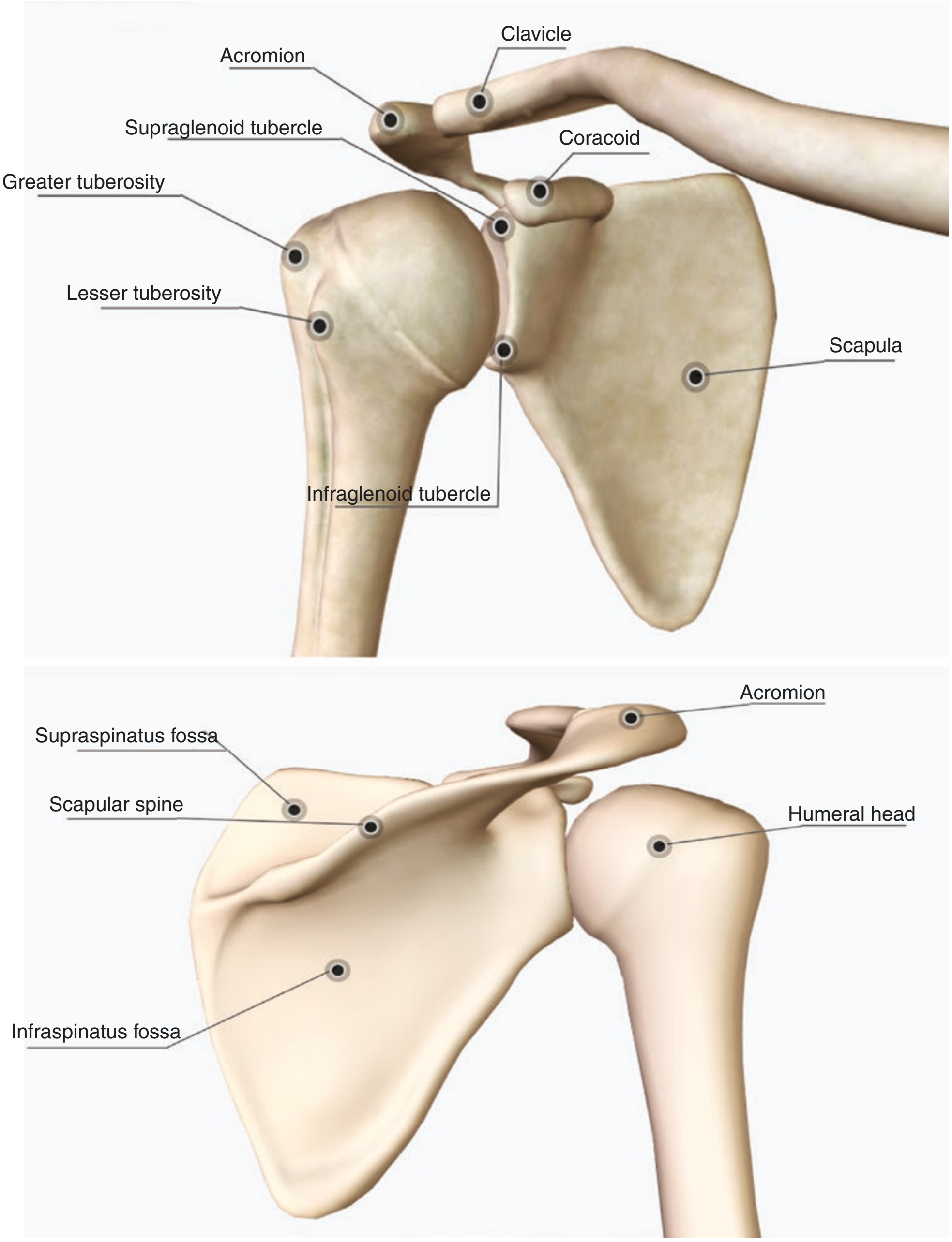
Acromion
Clavicle
Supraglenoid tubercle
Coracoid
Greater tuberosity
Lesser tuberosity
Scapula
Infraglenoid tubercle
Acromion
Supraspinatus fossa
Scapular spine
Humeral head
Infraspinatus fossa

Fig. 1 3-D renderings of the anterior (top) and posterior (bottom) bony anatomy of the shoulder

Complete US examination of the shoulder must also include the interrogation of the acromialclavicular joint. The acromioclavicular joint, formed by the acromion and clavicle is a synovial joint susceptible to degenerative arthritic changes. Another anatomical structure worth mentioning is the subacromial subdeltoid (SASD) bursa, a fluid-filled, saclike structure lined by synovial membrane. It is the largest bursa in the body and functions as a lubricant to reduce the friction between the supraspinatus and the acromion [10]. SASD bursitis can be a painful presentation of shoulder pain and is reliably diagnosed on ultrasound.

3 Patient Positioning and Sonographic Anatomy

Successful US evaluation of the shoulder is heavily reliant on positioning. Optimal positioning not only increases the diagnostic accuracy of the examination by way of minimizing US specific artifacts, it also improves patient comfort and overall experience. As with any anatomical structure evaluated with US, it should be done in both the long and short axis. The stepwise fashion of US evaluation of the shoulder is a method advocated in this chapter. It allows for a systematic and consistent approach to minimize errors.

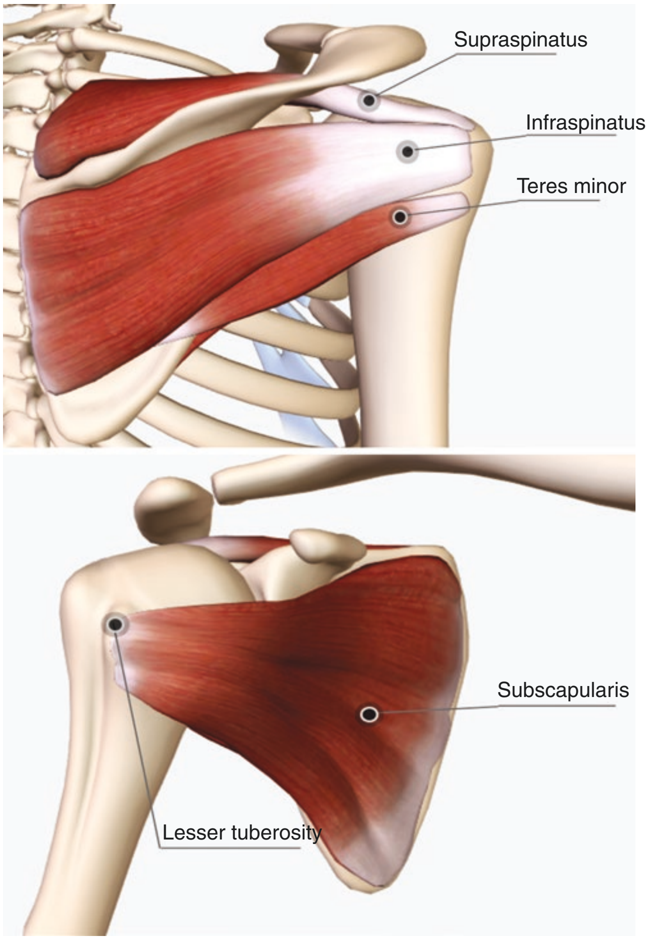

Fig. 2 3-D renderings demonstrating rotator cuff muscles

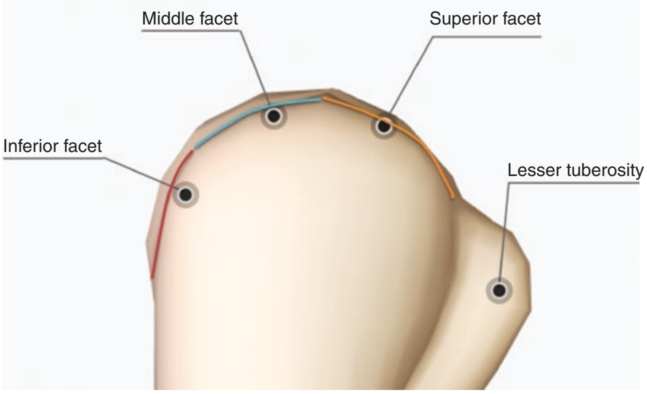

Fig. 3 Greater tuberosity facet anatomy

3.1 Long Head Bicep Tendon

The patient is initially asked to place the hand supinated over the thigh. The US transducer is then placed in the axial plane over the anterior shoulder (Fig. 4a). The bicipital groove is situated between the characteristic echogenic bony contours of the greater and lesser tuberosities (Fig. 4b). The long head of the bicep tendon will appear in short axis as hyperechoic and fibrillar (Fig. 4b). Angling of transducer will sometimes produce areas of hypoechoic shadows within the tendon secondary to anisotropy. It is important to not mistake this as partial tears or other pathology. The long head of the bicep tendon is followed both proximally and distally to evaluate for any abnormalities such tendonosis, tenosynovitis, or tendon tear. At this point, the transducer is turned 90 degrees to evaluate the long head of the bicep tendon in its long axis (Fig. 4b). Again, anisotropy can be produced depending on the obliqueness of the transducer.

3.2 Subscapularis

The patient is again asked to place the hand supinated over the thigh. Using the same technique for evaluating the long head of the bicep tendon, the transducer is again placed in axial orientation over the anterior shoulder. Moving medially, the subscapularis muscle will be visualized in its long axis coursing anterior toward the lesser tuberosity (Fig. 5). If anisotropy is encountered, ask the patient to externally rotate the shoulder [20]. The subscapularis tendon is then pulled laterally and its fibers will be oriented perpendicular to the sound beam [19]. Carefully inspect the subscapularis tendon by moving the transducer up and down to fully interrogate its entirety. The transducer is then rotated 90 degrees to visualize the subscapularis tendon in its short axis. It is important not to mistake the normal appearance of tendinous bundles of the subscapularis muscle as it the muscle interdigitates near the insertion on the lesser tuberosity as tears in the tendon.

3.3 Supraspinatus

The supraspinatus is the most commonly injured rotator cuff muscle and tendon [21]. To evaluate the supraspinatus, the patient is asked to place the dorsal aspect of the ipsilateral hand behind his back (Fig. 6a). This provocative maneuver, called the Crass position, hyperextends and internally rotates the arm, bringing the distal supraspinatus muscle and tendon into profile [6]. In this position, the greater tuberosity is located anteriorly on the patient. Simply place the transducer in the sagittal plane over the greater tuberosity and the long axis view of the supraspinatus tendon will be visualized (Fig. 6c). Rotating the transducer 90 degrees will now demonstrate the supraspinatus tendon in short axis (Fig. 6b). The Crass position was the first position introduced for the evaluation of the supraspinatus. However, this position of hyperextending and internally rotating the arm, may cause significant pain, especially in patients already with diseased tendons. The modified Crass position, where the patient's

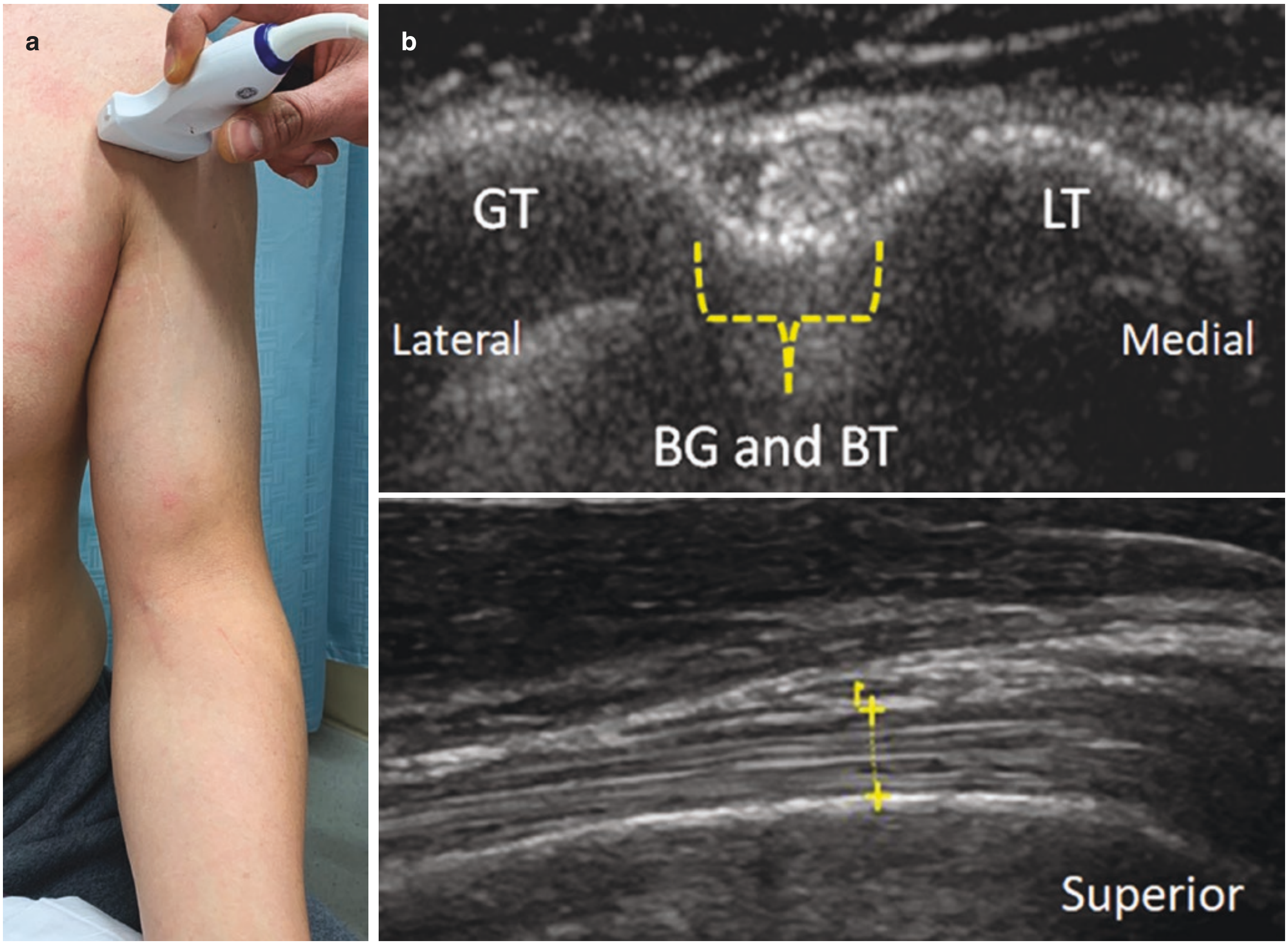

Fig. 4 (**a**) Patient positioning for evaluation of long head of the bicep tendon. (**b**) Long axis (top) and short axis (bottom) views of the long head of the bicep tendon. GT greater tuberosity, LT lesser tuberosity, BG bicipital groove, BT bicep tendon

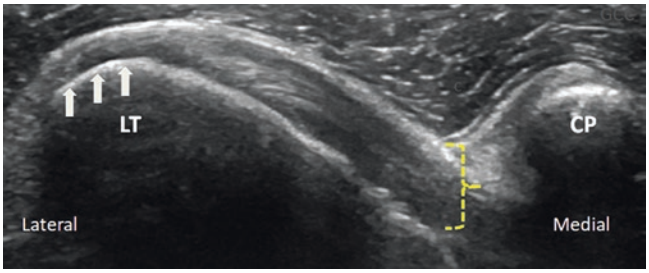

Fig. 5 Long axis view of the subscapularis muscle and tendon. CP coracoid process. Dashed bracket demonstrate the anterior and posterior margins of the subscapularis muscle. LT lesser tubercle of the humeral head. White arrows = These point to the subscapularis insertion on the LT, a common area of pathology

ipsilateral hand is placed on the closest hip or buttock region has been introduced (Fig. 7) [19, 20]. In this position, the greater tuberosity is located more laterally than the Crass position, as the degree of internal rotation is less [19, 20]. Placing the transducer obliquely in approximately 45 degrees inferior and lateral to the acromioclavicular joint will demonstrate the supraspinatus tendon in long axis attaching to the superior facet of the greater tuberosity. Sweep the full length of the supraspinatus tendon to ensure complete evaluation. Once this has been completed, rotate the transducer 90 degrees to examine the supraspinatus tendon in short axis.

3.4 Infraspinatus and Teres Minor

To visualize the infraspinatus tendon, the patient's arm is returned to the neutral position with the hand supinated. The transducer is placed over the posterior shoulder, in a slight oblique orientation, paralleling the scapular spine (Fig. 8). This position will demonstrate long axis view of the infraspinatus tendon (Fig. 9a-d). Other helpful technique includes having the patient reach for the contralateral shoulder with his ipsilateral hand [19, 20]. This will expose the distal infraspinatus tendon as it is moved away from underneath the acromion. The teres minor muscle and tendon is closed situated with the infraspinatus. Moving the

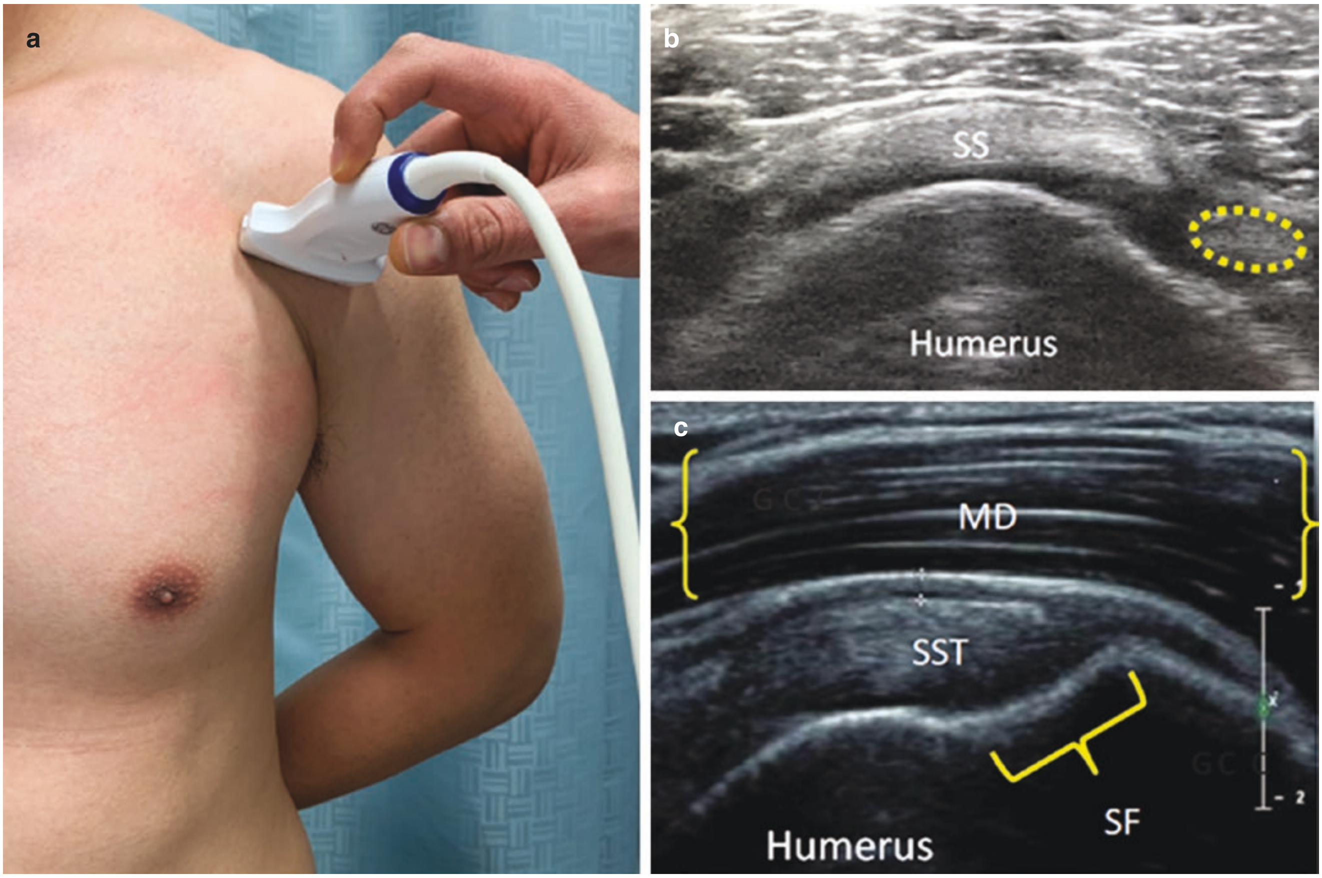

Fig. 6 (**a**) Crass position for evaluation of the supraspinatus in short axis. (**b**) Short axis view. SS supraspinatus, yellow dash bicep tendon, (**c**) Long axis view. SST supraspinatus tendon, SF superior facet, MD medial deltoid muscle

transducer slightly inferior to the infraspinatus, the teres minor muscle and tendon will appear as a thin, more superficial structure attaching to the inferior facet along the posterior aspect of the greater tuberosity. After examining the entirety of the infraspinatus and teres minor tendons in long axis, rotate the probe 90 degrees to evaluate them in the short axis.

3.5 Acromioclavicular (AC) Joint and Subacromial Subdeltoid Bursa

To locate the acromioclavicular joint, the patient's arm is placed in the neutral position with palm facing up. Palpate the clavicle and move laterally toward the acromion. Place the transducer in the coronal plane over the acromioclavicular joint (Fig. 10a-b). The acromioclavicular joint is then evaluated for narrowing, widening, offset, and bony irregularities. The subacromial subdeltoid (SASD) bursa is a potential space located inferior to the acromion, bounded laterally by the supraspinatus, and lies deep to the deltoid muscle (Fig. 11) [9]. On US, SASD bursa appears as a thin homogenous hypoechoic layer of synovial fluid overlying the supraspinatus tendon (Fig. 12) [14].

4 Commonly Encountered Pathologies of the Shoulder

Generally speaking, all muscular tendons of the shoulder are susceptible to tendinosis, tendinitis, and tenosynovitis. Tendinosis is chronic degeneration of the tendon fibers secondary to overuse; tendinitis is inflammation of the tendon [3]. Lastly, tenosynovitis is inflammation of the tendon sheath, a synovial membrane surrounding the tendon. While these terms are similar, they should not be confused with one another, as the pathophysiology among the three can be distinctly different. Importantly, tendinitis has been found to be quite uncommon and overly diagnosed, as tendon pathology, aka tendinopathy, have been found to be mostly a non-inflammatory disease process.

In addition, tendons can suffer from either partial or full thickness tears. Rotator cuff tears can further be categorized

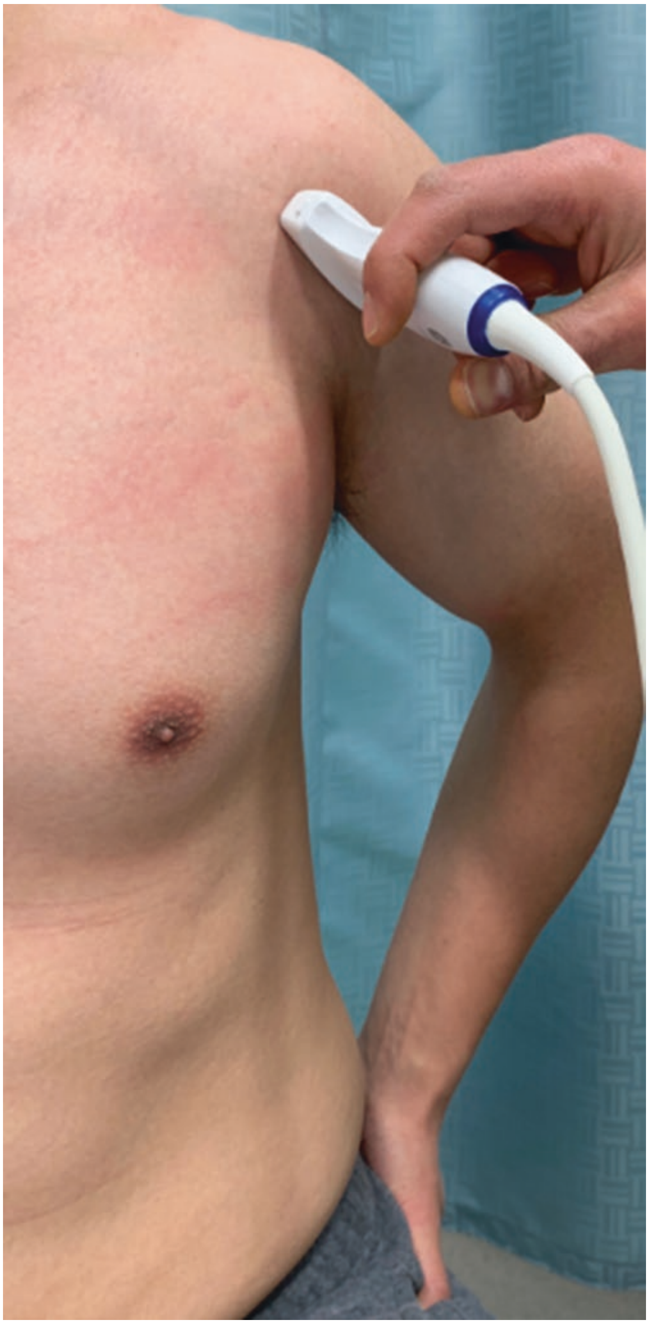

Fig. 7 Modified Crass position for evaluation of the supraspinatus

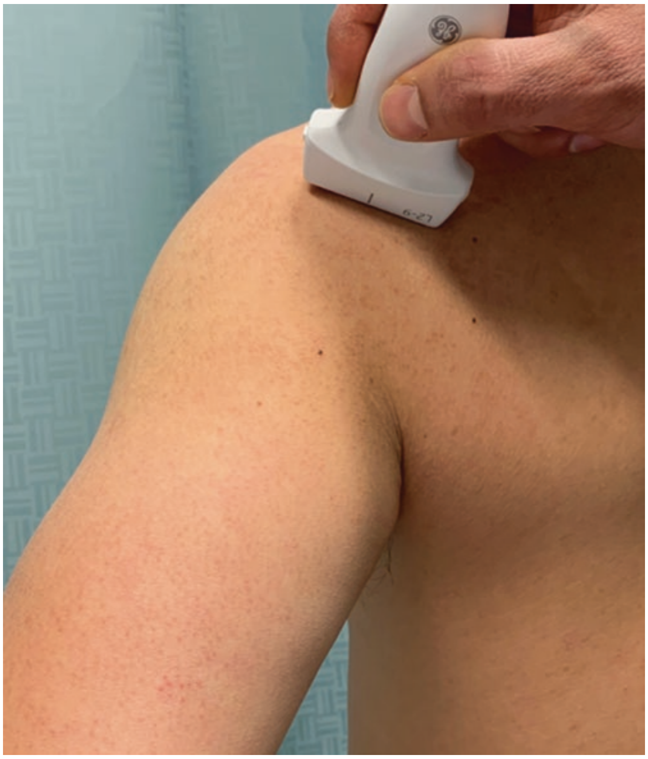

Fig. 8 Patient positioning for the evaluation of infraspinatus and teres minor

as articular sided, bursal sided, or intrasubstance tears. In certain cases, tendon tears can be associated with avulsed bony fragments at the insertion site. These bony fragments appear as linear echogenicities with posterior acoustic shadowing on US.

Long head bicep tendon subluxation/dislocation The extraarticular portion of the long head of the bicep tendon is secured within the bicipital groove by the transverse humeral ligament. As it moves more proximally and becomes intraarticular, the long head of the bicep tendon is stabilized by the coracohumeral and superior glenohumeral ligaments within the rotator interval. Any tears or deficiencies within these stabilizing ligaments can cause medial subluxation or dislocation of the long head of the bicep tendon. On US, this presents as absence of the expected hyperechoic tendon within the bicipital groove (Fig. 13a, b). Provocative maneuvers such as external rotation of the shoulder may induce subtle tendon subluxation/dislocation.

Rotator cuff tear The supraspinatus tendon is the most commonly injured rotator cuff tendon [21]. Full thickness tears of the supraspinatus tendon extending from the articular to bursal side will demonstrate an anechoic/hypoechoic area where normally the tendon appears hyperechoic (Fig. 14). It is important to evaluate the supraspinatus tendon in both the long and short axis, as one view may not demonstrate the tear as well as the other view. Partial tears can be articular sided, bursal sided, or intrasubstance. On US, these are characterized by focal anechoic areas disrupting the supraspinatus tendon without complete breakthrough (Fig. 15). Intrasubstance tears are tears within the tendon substance without contact with the articular or bursal side. They will appear as anechoic or hypoechoic areas

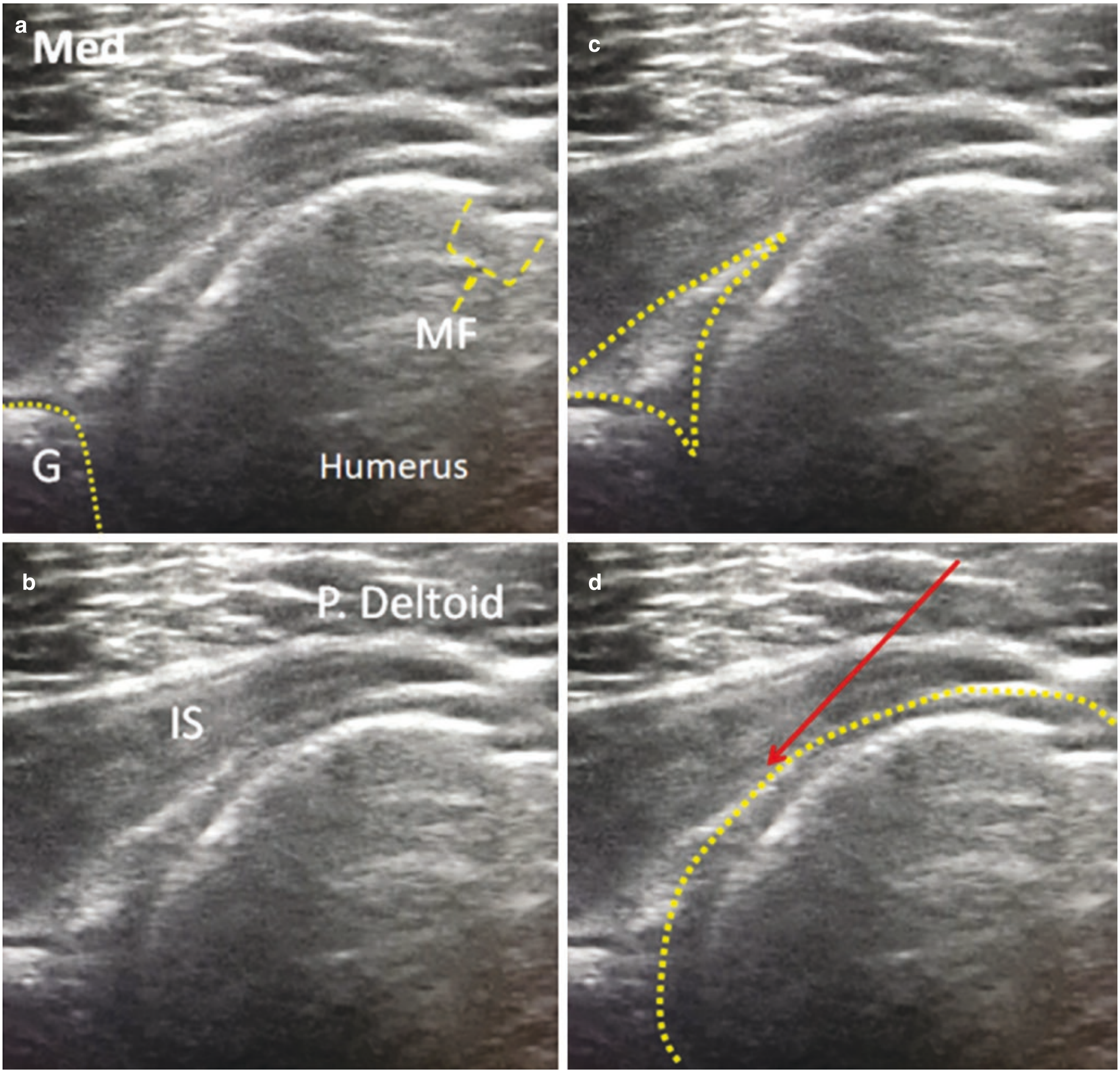

Fig. 9 (**a**) Osteology of the posterior shoulder under ultrasound. The glenoid (G), the humerus, and the middle facet (MF) where the infraspinatus inserts are highlighted. (**b**) The muscles of the posterior shoulder under ultrasound. The Posterior deltoid (P. Deltoid), and the Infraspinatus (IS). (**c**) The posterior labrum is outlined. (**d**) The articular cartilage on the surface of the humeral head is outlined. The arrow depicts one method of performing a glenohumeral joint injection under ultrasound guidance. The goal is to place the needle tip on top of the cartilage, near the intersection between the labrum and the cartilage

within the tendon. Isolated tears of the subscapularis tendon are infrequent [4, 5]. More commonly, subscapularis tendon tears are associated with accompanying supraspinatus injury. Similar to tears of the other rotator cuff muscle and tendons, tears of the infraspinatus and teres minor can be full or partial thickness. These tears will demonstrate similar imaging findings as that of supraspinatus tendons tears.

Calcific tendinosis Calcific tendinosis is pathologic deposition of calcium hydroxyapatite crystals within tendons [11, 15]. The most commonly affect rotator cuff tendon is the supraspinatus. The exact etiology of the hydroxyapatite deposition remains unclear. Metabolic and endocrine related theories have been proposed [15] and it is believed that they are a part of the healing cascade. On US, this appears as calcification of the distal supraspinatus tendon insertion (Fig. 16).

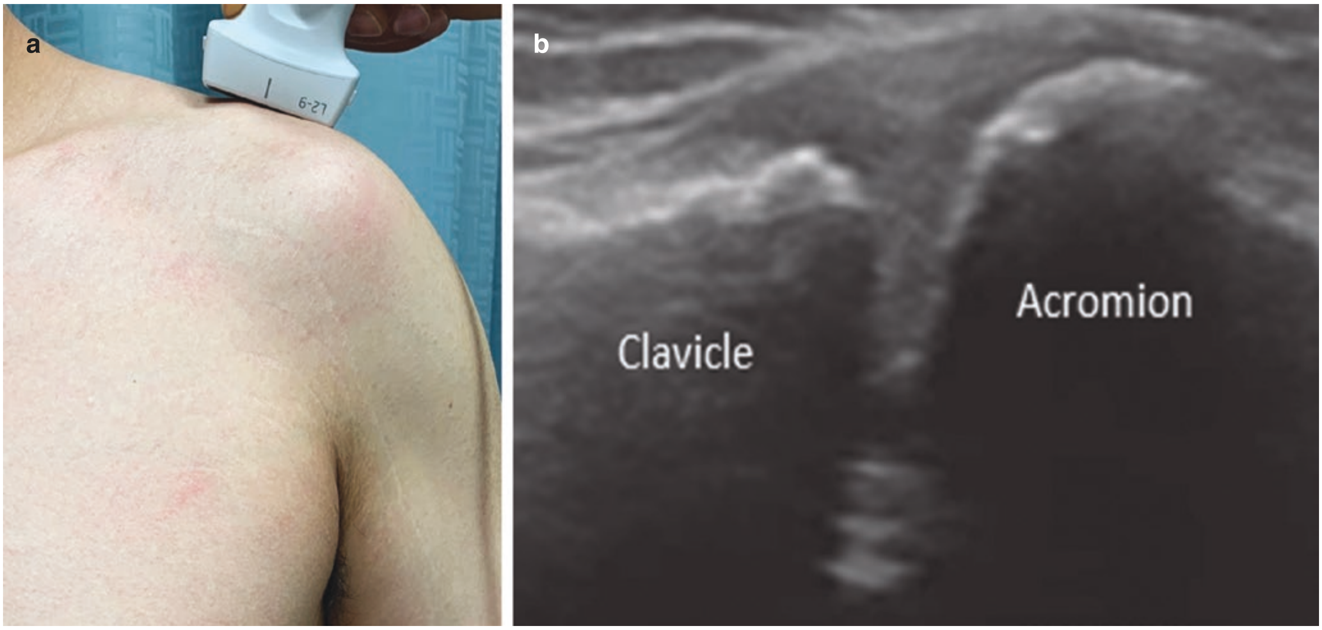
a
L2-9
b
Clavicle
Acromion

Fig. 10 (**a**) Patient positioning for evaluation of AC joint. (**b**) Sonographic appearance of the AC joint in coronal plane

Fig. 11 Anatomy surrounding the SASD bursa

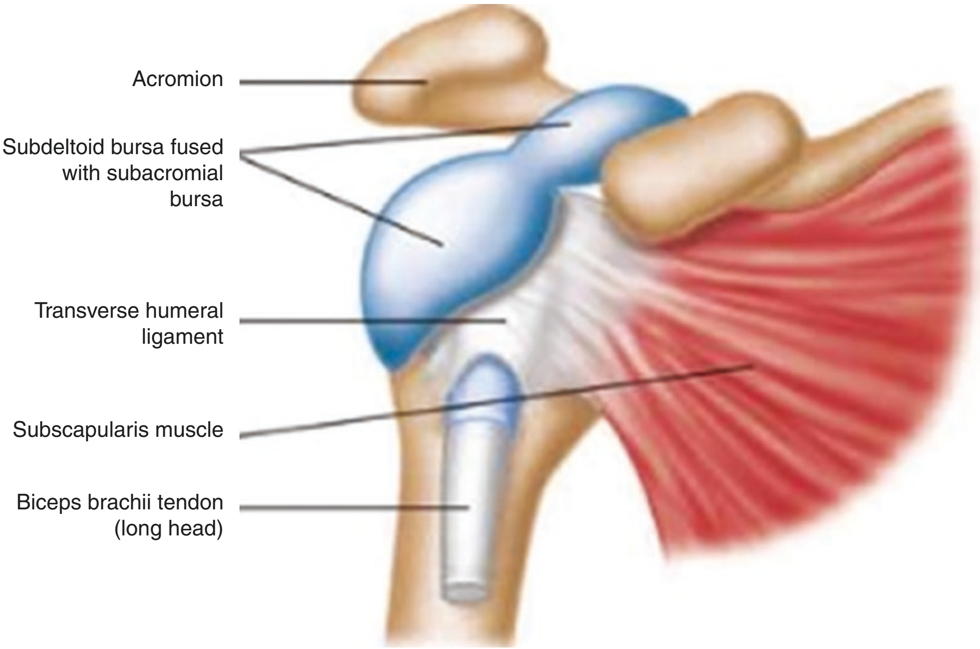
Acromion
Subdeltoid bursa fused with subacromial bursa
Transverse humeral ligament
Subscapularis muscle
Biceps brachii tendon (long head)

Acromioclavicular and glenohumeral joint osteoarthritis The normal AC joint measures approximately 3–5 mm and has smooth and well corticated margins [7]. The most commonly encountered pathology of the AC joint is degenerative arthritis. On US, this appears as a combination of joint space narrowing, marginal osteophytes, and subchondrol cystic changes. Similar imaging findings are seen in glenohumeral joint osteoarthritis.

Acromioclavicular joint injury Traumatic injury to the AC joint is stratified into grades based on severity and imaging appearances. Low grade AC joint injury may be normal on imaging or appear as subtle widening of the AC joint. As AC injury severity increases, cross sectional imaging such MRI may be required to evaluate subtle ligamentous injuries and/or osseous marrow edema.

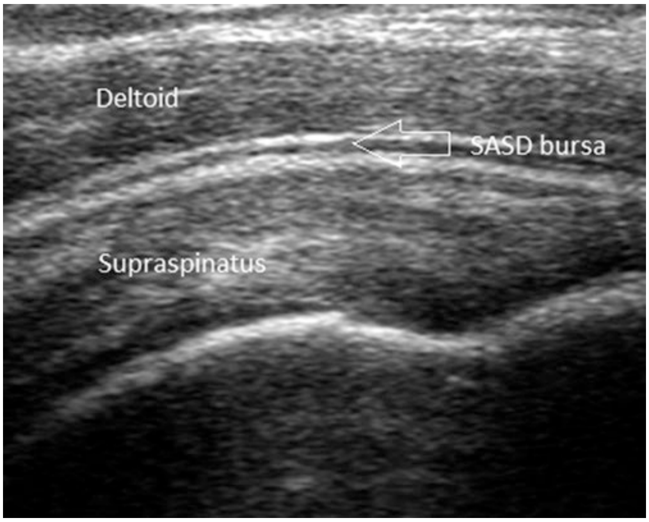

Fig. 12 Long axis view of the shoulder. SASD subacromial subdeltoid bursa

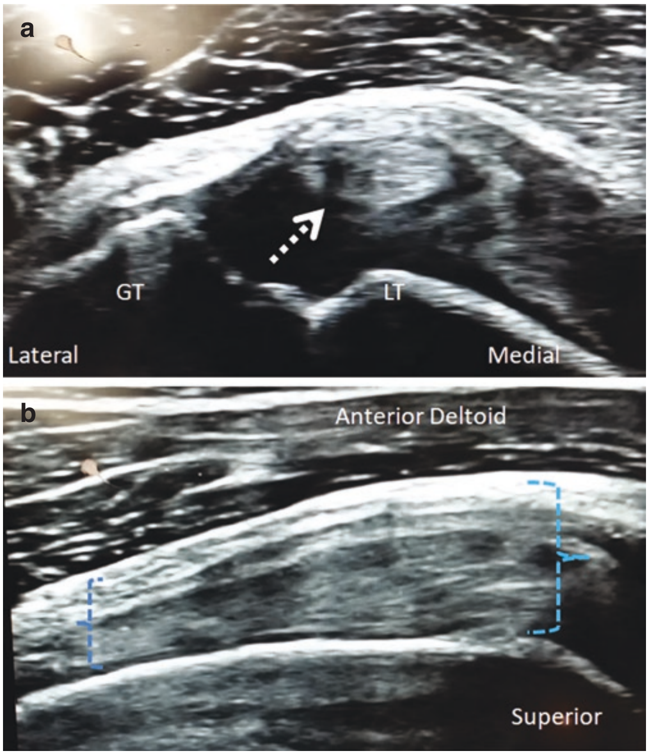

Fig. 13 (**a**) Short-axis view of the biceps which has subluxed out of the groove, and moved medial, shearing the subscapularis tendon. Dashed arrow demonstrates the subluxation. (**b**) Long-axis view of the biceps tendon. Dashed line demarcates the anterior and posterior margins of the BT. The BT has lost its striated pattern and is heterogeneous with multiple hypoechoic voids

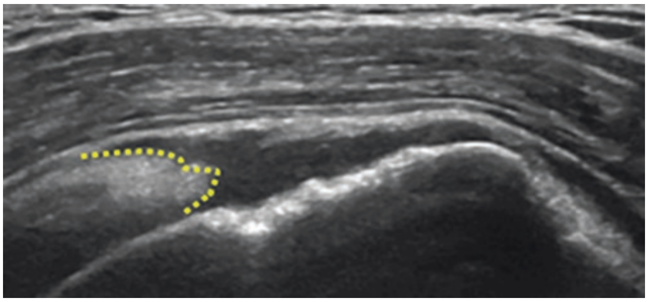

Fig. 14 Long axis view of the supraspinatus demonstrating full thickness rupture of the tendon with retraction of the muscle. Yellow dotted line depicts the edge of the retracted tendon

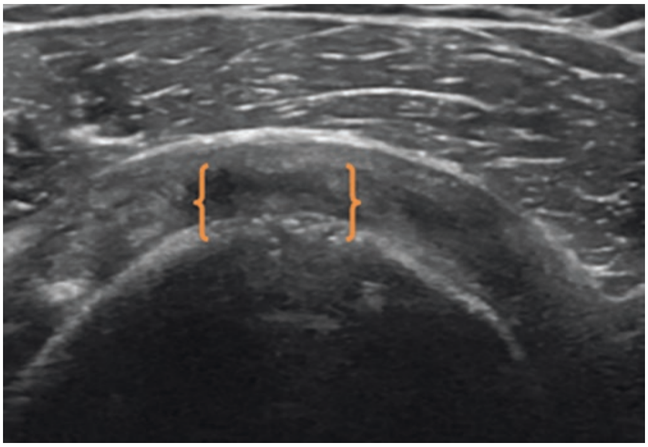

Fig. 15 Short axis view of the supraspinatus tendon demonstrating partial thickness articular sided tear (yellow brackets)

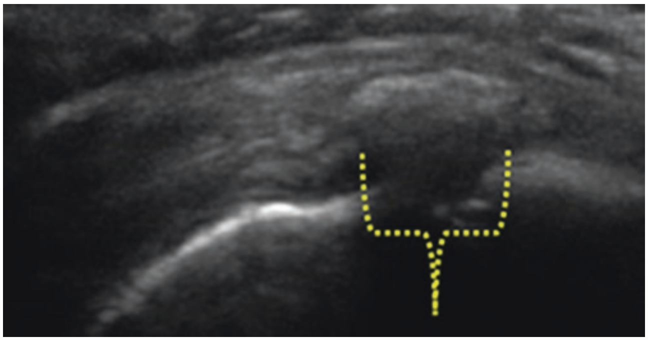

Fig. 16 Long axis view demonstrating curvilinear calcification deposition in the supraspinatus tendon

Subacromial impingement Subacromial impingement is the most common form of shoulder impingement and results in pathology arising from the subacromial space [8]. It represents a spectrum of rotator cuff disease ranging from subacromial bursitis to rotator cuff tendinopathy to full-thickness rotator cuff tears [8]. Subacromial impingement may be secondary to intrinsic and extrinsic etiologies and most commonly affects the supraspinatus muscle and tendon. Certain morphology of the acromion may also predispose patients to early impingement symptoms. Most often, however, chronic

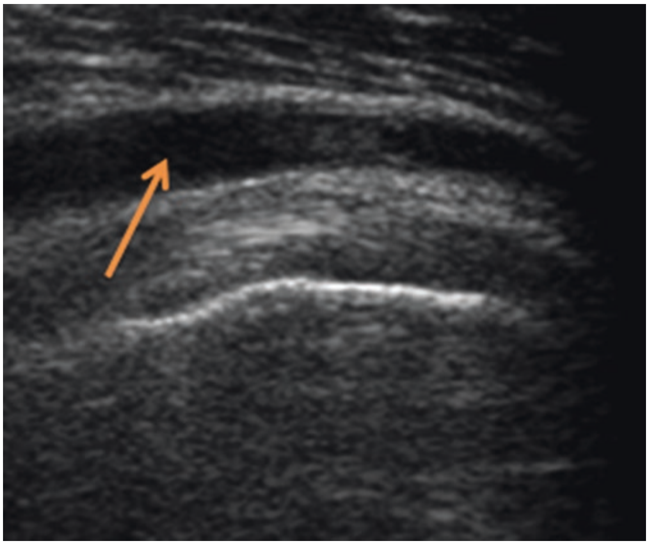

Fig. 17 Short axis view demonstrating heterogeneous fluid distention of the SASD bursa (yellow arrow)

degenerative osteoarthritis produce marginal osteophytes extending off the inferolateral aspect of the acromion. This results in narrowing of the subacromial space and mass effect on the supraspinatus tendon traversing underneath the acromion. On US, this can be evaluated dynamically. Starting in the same position for evaluating the AC joint, the transducer is moved laterally until the lateral edge of the acromion is visualized. The patient's arm is then passively abducted under real time evaluation. During abduction, the supraspinatus tendon and overlying subacromial-subdeltoid bursa should slide smoothly under the acromion. Interdisposition of the supraspinatus tendon and/or trapping of bursal fluid at the lateral acromion edge are indicative subacromial impingement [8].

Subacromial subdeltoid bursitis SASD bursitis is inflammation of the bursa and may be secondary to impingement, rotator cuff tears, infection, or inflammation. On US, characteristic finding is fluid distending the SASD bursa and hyperemia. This fluid may be homogenously anechoic or heterogeneously hypoechoic suggesting the presence of inflammatory debris (Fig. 17).

5 Interventional Techniques

Tendon fenestration The act of perforating a ligament or tendon is termed, fenestration. Ultrasound-guided fenestration occurs once the targeted area is identified via ultrasound and the needle is inserted into the tissue. The needle is then passed into the target, withdrawn, redirected, and passed into the targeted tissue [12]. There is no exact precedence for when to terminate the procedure [12–15]. When calcific tendinosis is identified, the fenestration process can be utilized to disrupt the calcium deposit and facilitate reabsorption of the calcium [15, 16]. Caution should be utilized not to create a larger defect, or worsen the injury. Depending on the degree of pre-existing injury, needle gauge should be carefully selected. Typically used needle gauge for calcific tendinosis fenestration is 18G–22G, while fenestration of the interstitial tendon tissue may range between 20–25G.

AC joint injection AC joint injection can be utilized to treat mild instability or osteoarthritis of the AC joint. Using the technique described in the above section, localize the AC joint under ultrasound guidance. Then using a 25G 1.5in needle, approach the AC joint from lateral to medial, In-Plane technique, or Out-of-Plane from posterior to anterior. 2–3 ml of injectate such as local anesthetic and corticosteroids, platelet rich plasma, or other solutions can be injected.

Glenohumeral joint injection The glenohumeral joint is a synovial joint, and as such, is susceptible to arthritic changes. The glenohumeral joint can be accessed both the anterior and posterior approach. The posterior approach offers several benefits over the anterior approach and will be discussed here. For the posterior approach, the patient is placed on his side, with the affected shoulder up. The transducer is aligned to the long axis of the infraspinatus tendon just inferior to the scapular spine. Several important bony land marks are identified (Fig. 9d). Ideal needle tip should be positioned between the free margin of the posterior glenoid labrum and articular cartilage of the humeral head [17]. Once this has been identified, a 22G or 25G 3.5in spinal need can be used to inject 3-5 ml of injectate consisting of local anesthetic and steroid into the glenohumeral joint.

Subacromial subdeltoid bursa injection Locate the SASD bursa by positioning the patient into the Crass or modified Crass position. The SASD will be a thin sliver of fluid deep to the deltoid muscle and superficial to the supraspinatus tendon. The needle target will be the bursa. A 25G 1.5-inch needle or 22G 3.5-inch spinal needle is inserted in-plane. A 3–5 ml of injectate of local anesthetic and corticosteroids, platelet rich plasma, or other solutions can be injected for therapeutic relief.

6 Conclusion

US can be a useful tool for diagnosis and guiding treatment in many shoulder pathologies. Having a fundamental understanding of the shoulder anatomy and its sonographic appearances will aid the clinician in both evaluating and treating patients.

References

1. Teefey SA, Hasan SA, Middleton WD, Patel M, Wright RW, Yamaguchi K. Ultrasonography of the rotator cuff: a comparison of ultrasonographic and arthroscopic findings in one hundred consecutive cases. J Bone Joint Surg Am. 2000;82(4):498–504.
2. Vlychou M, Dailiana Z, Fotiadou A, Papanagiotou M, Fezoulidis IV, Malizos K. Symptomatic partial rotator cuff tears: diagnostic performance of ultrasound and magnetic resonance imaging with surgical correlation. Acta Radiol. 2009;50(1):101–5.
3. Bass E. Tendinopathy: why the difference between tendinitis and tendinosis matters. Int J Ther Massage Bodywork. 2012;5(1):14–7.
4. Farin P, Jaroma H. Sonographic detection of tears of the anterior portion of the rotator cuff (subscapularis tendon tears). J Ultrasound Med. 1996;15(3):221–5.
5. Morag Y, Jamadar DA, Miller B, et al. The subscapularis: anatomy, injury, and imaging. Skelet Radiol. 2011;40(3):255–69.
6. Crass JR, Craig EV, Feinberg SB. The hyperextended internal rotation view in rotator cuff ultrasonography. J Clin Ultrasound. 1987;15(6):416–20.
7. Alasaarela E, Tervonen O, Takalo R, et al. Ultrasound evaluation of the acromioclavicular joint. J Rheumatol. 1997;24(10):1959–63.
8. Umer M, Qadir I, Azam M. Subacromial impingement syndrome. Orthop Rev (Pavia). 2012;4(2):e18.
9. Hirji Z, Hunjun J, Choudur H. Imaging of the bursae. J Clin Imaging Sci. 2011;1(1):22. https://doi.org/10.4103/2156-7514.80374.
10. van Holsbeeck M, Strouse PJ. Sonography of the shoulder:patient positioning and anatomy: evaluation of the subacromial-subdeltoid bursa. AJR Am J Roentgenol. 1993;160(3):561–4.
11. Siegal DS, Wu JS, Newman JS, Cura JL, Hochman MG. Calcific tendinitis: a pictorial review. Can Assoc Radiol J. 2009;60(5):263–72. https://doi.org/10.1016/j.carj.2009.06.008.
12. Wilson JJ, Lee KS, Chamberlain C, et al. Intratendinous injections of platelet-rich plasma: feasibility and effect on tendon morphology and mechanics. J Exp Orthop. 2015;2:5.
13. Jacobson JA, Yablon CM, Henning PT, Kazmers IS, Urquhart A, Hallstrom B, Bedi A, Parameswaran A. Greater trochanteric pain syndrome: percutaneous tendon fenestration versus platelet-rich plasma injection for treatment of gluteal tendinosis. J Ultrasound Med. 2016;35(11):2413–20.
14. Jacobson JA, Rubin J, Yablon CM, Kim SM, Kalume-Brigido M, Parameswaran A. Ultrasound-guided fenestration of tendons about the hip and pelvis: clinical outcomes. J Ultrasound Med. 2015;34(11):2029–35.
15. Klontzas ME, Vassalou EE, Karantanas AH. Calcific tendinopathy of the shoulder with intraosseous extension: outcomes of ultrasound-guided percutaneous irrigation. Skelet Radiol. 2017;46(2):201–8.
16. Jo H, Kim G, Baek S, Park HW. Calcific tendinopathy of the gluteus medius mimicking lumbar radicular pain successfully treated with barbotage: a case report. Ann Rehabil Med. 2016;40(2):368–72.
17. Zwar RB, Read JW, Noakes JB. Sonographically guided glenohumeral joint injection. Am J Roentgenol. 2004;183(1):48–50. https://doi.org/10.2214/ajr.183.1.1830048.
18. Buck FM, et al. Long biceps tendon: normal position, shape, and orientation in its groove in neutral position and external and internal rotation. Radiology. 2011;261(3):872–81. https://doi.org/10.1148/radiol.11110914.
19. Jacobson JA. Fundamentals of musculoskeletal ultrasound. Philadelphia: Elsevier; 2018.
20. Jacobson JA. Shoulder US: anatomy, technique, and scanning pitfalls. Radiology. 2011;260(1):6–16. https://doi.org/10.1148/radiol.11101082.
21. Morag Y, Jacobson JA, Miller B, et al. MR imaging of rotator cuff injury: what the clinician needs to know. Radiographics. 2006;26(4):1045–65.

Elbow Joint Sonoanatomy and Ultrasound-Guided Elbow Joint Injection

Allan Zhang and George C. Chang Chien

1 Introduction

The elbow accounts for approximately 20–25% of all upper extremity sports related injuries [1]. These injuries are generally divided into three categories: acute injuries, acute on chronic injuries (acute injuries made vulnerable to overuse), and chronic injuries (multiple repetition overuse injuries). Clinical examination and radiography are essential for the initial evaluation of the elbow. Cross sectional imaging such as CT and MRI are useful for detailed evaluation of the soft tissues, articular cartilage, and bony marrow injuries. More recently, US has emerged as an important diagnostic tool for the assessment of elbow injuries. It offers the clinician several distinct advantages over its cross sectional counterparts including dynamic real time examination, direct patient feedback, and ability to guide therapeutic interventions. If used skillfully, US can be a powerful diagnostic alternative or helpful adjunct to CT and MRI. In this chapter, discussion will first include the normal anatomy of the elbow and its sonographic appearance. US technique and positioning as well as several commonly encountered disease pathologies will be reviewed. Lastly, several fundamental US guided therapeutic interventions of the elbow will be presented.

2 Anatomy and US Technique

The elbow is a complex joint formed by the proximal radius, proximal ulna, and distal humerus and their three articulations: radiocapitellar, ulnotrochlear, and proximal radioulnar joints (Fig. 1).The medial elbow is stabilized by the ulnar collateral ligament (UCL), comprising of anterior, posterior, and transverse bands. The anterior band is the primary restraint against valgus force [2]. It extends from the medial epicondyle of the humerus to the sublime tubercle of the ulna (Fig. 2). Laterally, the elbow is stabilized against varus stress by the lateral collateral ligament complex (Fig. 3) [2]. It is composed of the radial collateral ligament, the lateral ulnar collateral ligament (LUCL), and the annular ligament (Fig. 3) [3]. The LUCL provides the primary varus restraint and arises from the lateral epicondyle of the humerus to the supinator crest of the ulna. The annular ligament surrounds the radial head and neck and inserts itself into the radial notch [3, 4]. The radial collateral ligament also originates from the lateral epicondyle and joins with the annular ligament to attach on the radial neck [3, 4].

Anteriorly within the elbow, the brachialis muscle and tendon inserts on the coronoid process of the ulna (Fig. 4). The bicep brachii overlies the brachialis muscle and inserts onto the radial tuberosity (Fig. 4). The short head of the bicep brachii is more superficial and inserts distally in comparison with the long head [3, 4]. Posteriorly, the triceps brachii muscle inserts onto the olecranon process of the ulna (Fig. 4). The anconeus is a sliver of muscle situated between the lateral epicondyle and posterior olecranon. Medially, the common flexor tendon, consisting of the flexor carpi radialis, palmaris longus, flexor carpi ulnaris, and flexor digitorum superficialis, arises from the medial epicondyle of the distal humerus. Laterally, the common extensor tendon, consisting of extensor carpi radialis brevis, extensor digitorum communis, extensor digiti minimi, and extensor carpi ulnaris, originates on the lateral epicondyle of the distal humerus.

Several nerves course through the elbow joint and should be noted carefully on US exam. The ulnar nerve courses posterior to the medial epicondyle, within the cubital tunnel (Fig. 5). The cubital tunnel is bounded medially by the medial epicondyle, laterally by the olecranon process, superiorly by the cubital tunnel retinaculum (a fibrous band of

---

A. Zhang (✉)
Department of Radiology, University of Connecticut Health Center, Farmington, CT, USA
e-mail: azhang@uchc.edu

G. C. Chang Chien
GCC Institute, Newport Beach, CA, USA

Ventura County Medical Center, Ventura, CA, USA

© Springer Nature Switzerland AG 2021
J. Li et al. (eds.), *Ultrasound Fundamentals*, https://doi.org/10.1007/978-3-030-46839-2_11

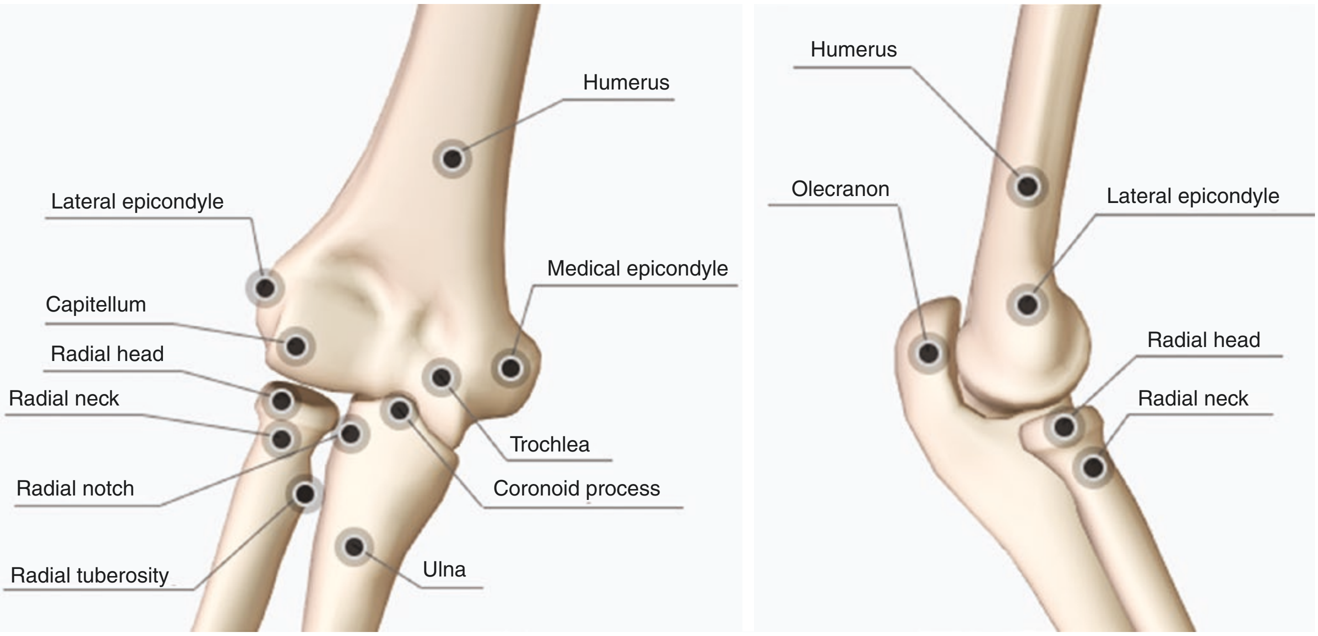
Humerus
Lateral epicondyle
Medical epicondyle
Capitellum
Radial head
Radial neck
Trochlea
Radial notch
Coronoid process
Radial tuberosity
Ulna
Humerus
Olecranon
Lateral epicondyle
Radial head
Radial neck

Fig. 1 3-D renderings of the anterior (left) and lateral (right) bony elbow anatomy

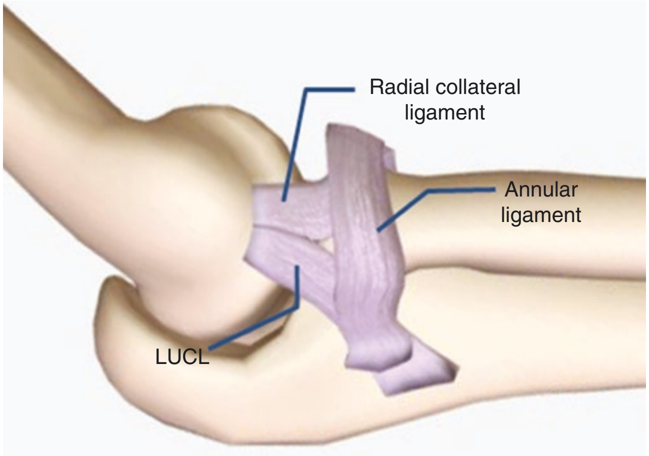
Radial collateral ligament
Annular ligament
LUCL

Fig. 3 3-D rendering of the stabilizing ligaments of the lateral elbow LUCL lateral ulnar collateral ligament

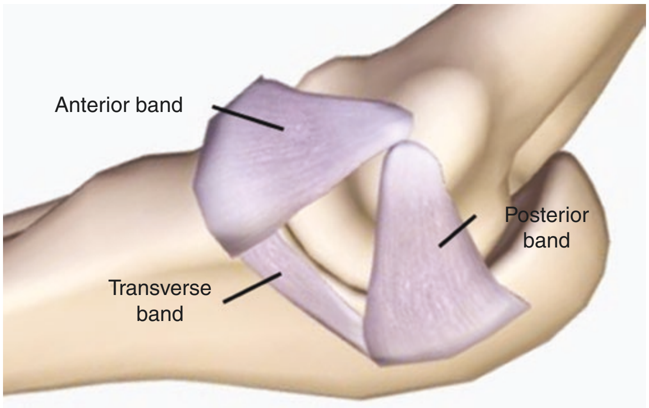
Anterior band
Posterior band
Transverse band

Fig. 2 3-D rendering of the three bands of the ulnar collateral ligament within the medial elbow

tissue), and inferiorly by the elbow joint capsule [5–7]. The median nerve enters the antecubital fossa, a triangular space in the anterior elbow joint, and courses medial to brachial artery and biceps brachii tendon (Fig. 5). The radial nerve initially courses posteriorly within the radial groove of the arm. It then folds around the lateral epicondyle and courses anteriorly to enter the antecubital fossa (Fig. 5). These nerves are all susceptible to compression syndromes and can give rise to elbow related pain [8].

In addition, a number of bursas has been identified around the elbow joint. Bursa is a fluid-filled, saclike structure lined by synovial membrane which forms in clefts between mobile structures in the musculoskeletal system. Bursas reduce friction between mobile structures such as muscles, tendons, bone, and skin. The term bursitis implies inflammation and is associated with tenderness over the bursa. The olecranon bursa is the most superficial of the elbow bursas, and swelling of this bursa is both common and easily observed [9].

Now that a fundamental understanding of the structural anatomy of the elbow has been obtained, the US appearances and techniques can then be discussed. A practical approach to US examination of the elbow is to divide it into four compartments: anterior, lateral, medial, and posterior. In each compartment, several important structures must be evaluated (Fig. 6). Generally speaking, a flat US transducer with frequency of 12–18 MHz is optimal for evaluating superficial

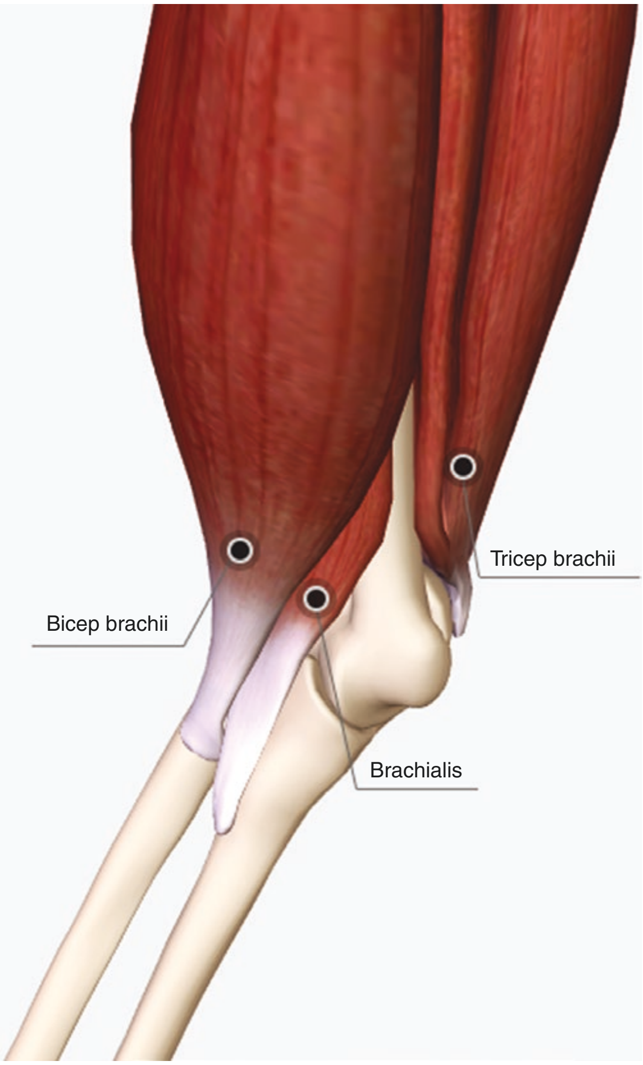

Fig. 4 Oblique view demonstrating muscular attachments at the elbow

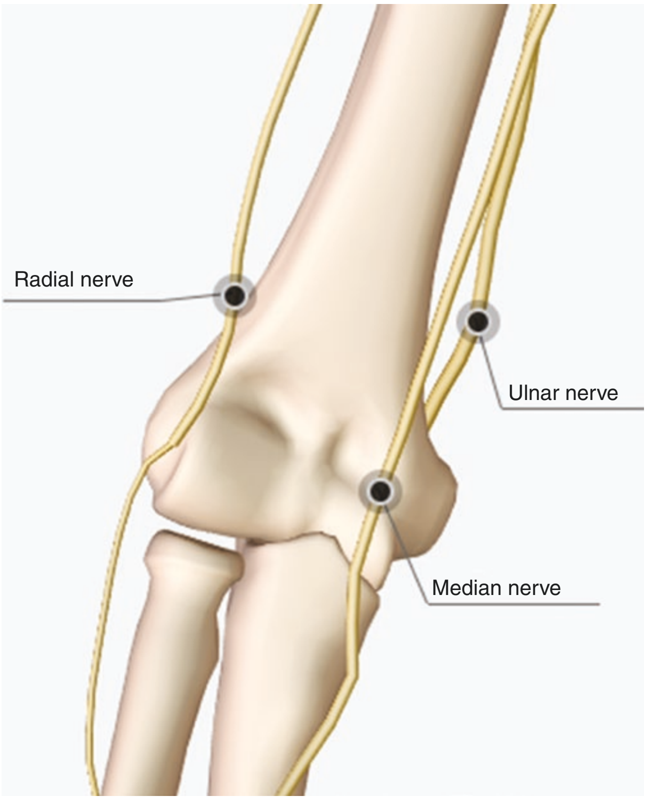

Fig. 5 Anterior view of the elbow joint following the courses of the radial, ulnar, and median nerves

musculoskeletal structures of the elbow [10]. Transducer frequency may be reduced in patients with large body mass in order to increase depth penetration.

2.1 Anterior Elbow

The important structures to be evaluated in the anterior compartment are the distal bicep muscle and tendon, the brachialis muscle and tendon, and the median nerve. The patient is positioned with the arm fully extended and supinated (Fig. 7a). This can be accomplished with the patient lying on his back or sitting. The examination should include both axial and sagittal planes extending at least 5 cm proximal and 5 cm distal to the joint [11]. To begin, the transducer is placed in axial plane over the distal humerus. Several important anatomical landmarks are demonstrated (Fig. 7b). The characteristic convex margins of the capitellum and the concave margin of the trochlea are noted. The capitellum articulates with the radius, while the trochlea articulates with the trochlear notch of the ulna. The articular surfaces are covered with hyaline cartilage which is hypoechoic on US (Fig. 7b). The hypoechoic muscle immediately anterior to the distal humerus is the brachialis. Superficial to the brachialis is the distal bicep brachii. The brachial artery is medial to the bicep brachii and can be reliably indentified by its pulsatile morphology. Slightly medial to the brachial artery is the median nerve. Scan the elbow joint both proximally and distally and be mindful as to not mistake anisotropy for pathology. The transducer is then rotated 90 degrees to evaluate the anterior structures in long axis (Fig. 7c).

2.2 Medial Elbow

The key structures evaluated in the medial compartment are the common flexor tendon origin, anterior band of the ulnar collateral ligament (UCL), and the ulnar nerve. The common flexor tendon originates from the medial epicondyle and together with the UCL, supports the elbow in valgus stress. To begin the exam, the patient is positioned with the forearm placed in forceful external rotation with the elbow extended or slightly flexed (Fig. 8a). The trans-

CHECKLIST FOR ELBOW US EVALUATION

Anterior Elbow	Distal bicep muscle and tendon Brachialis muscle and tendon Median nerve
Medial Elbow	Common flexor tendon origin Medial collateral ligament, anterior band Ulnar nerve
Lateral Elbow	Common extensor tendon origin Lateral collateral ligament complex Radial collateral ligament Radial nerve
Posterior Elbow	Triceps muscle and tendon Olecranon bursa

Fig. 6 Checklist for US elbow in each compartment

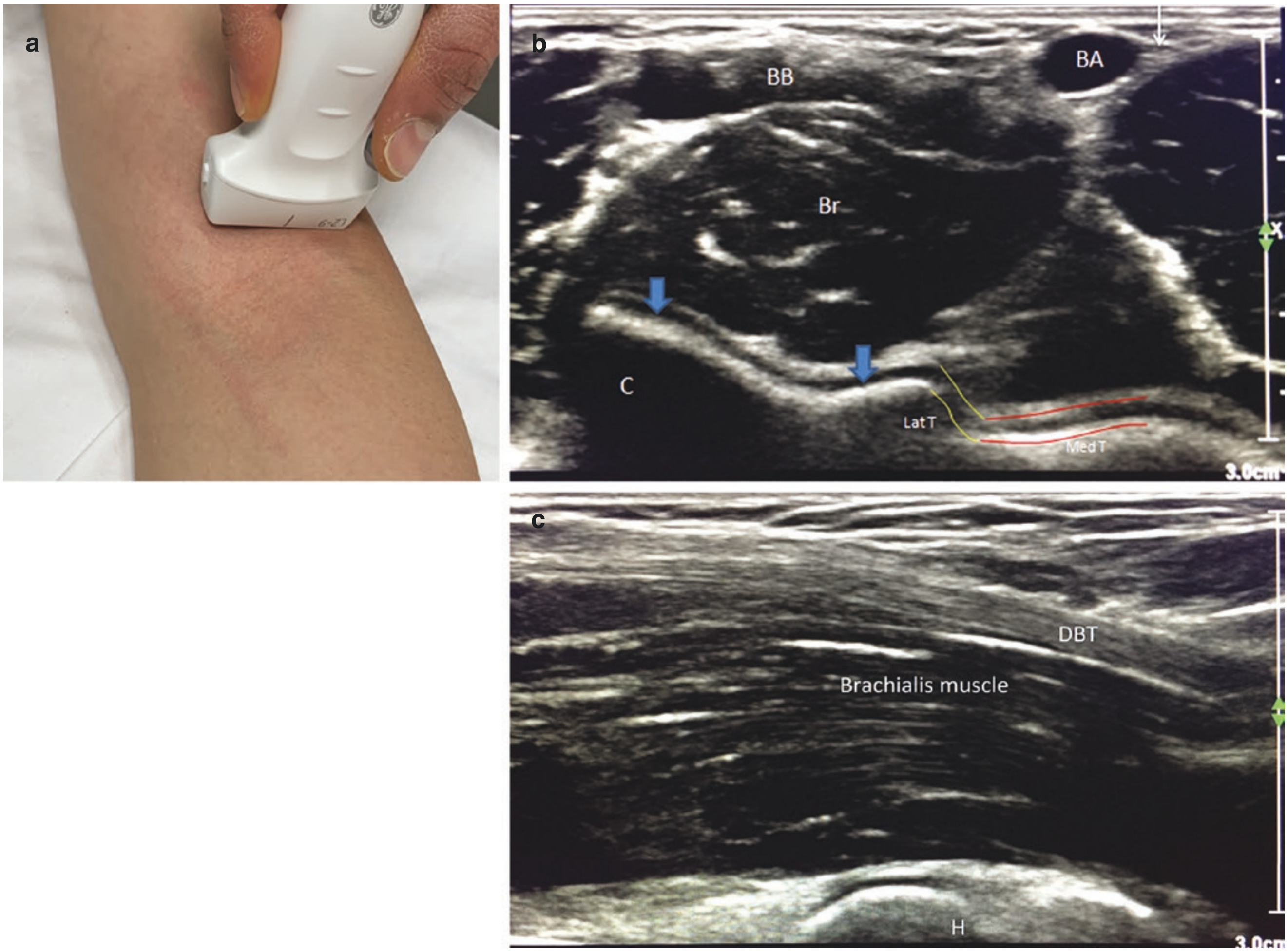

Fig. 7 (**a**) Transducer positioning for the anterior elbow in short axis. (**b**) Corresponding US appearance in short axis. BR brachialis muscle, BB bicep brachii, BA brachial artery, C capitellum, Lat T lateral trochlea(outlined in yellow), Med T medial trochlea(outlined in red), solid blue arrow = articular cartilage, arrow = median nerve. (**c**) Sagittal long axis image of the anterior elbow. DBT distal bicep tendon, H humerus

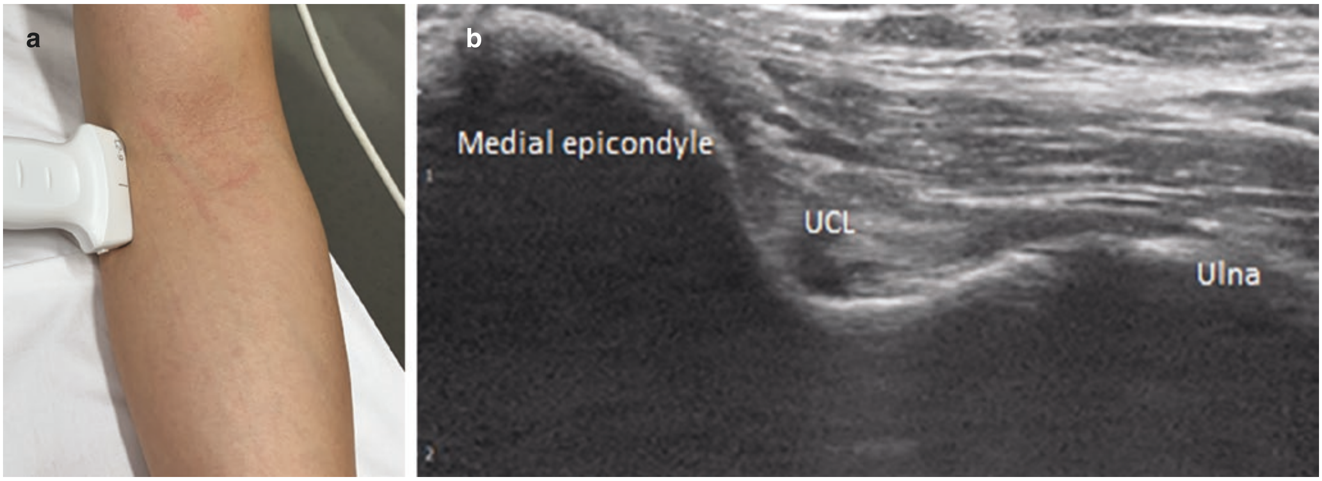

Fig. 8 (**a**) Arm positioning for medial evaluation of the elbow. (**b**) Corresponding long axis view of the medial elbow. CFM common flexor muscle, CFT common flexor tendon, UCL ulnar collateral ligament

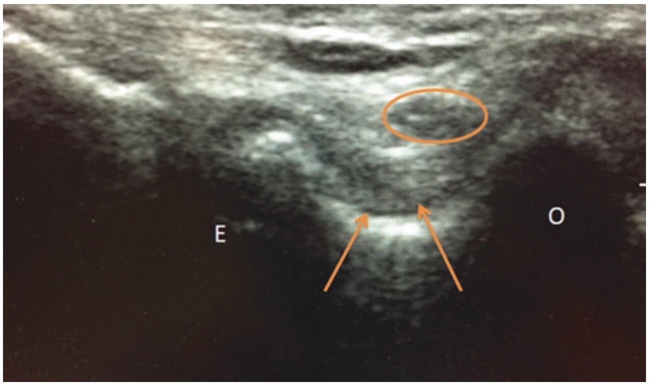

Fig. 9 Short axis view of the cubital tunnel. Yellow circle = ulnar nerve, arrow = posterior bundle of the UCL, E medial epicondyle, O olecranon

ducer is then placed in long axis with paralleling the forearm over the medial epicondyle of the humerus. Several key anatomic structures are identified in this view (Fig. 8b). The common flexor tendon should be viewed just anterior to the medial epicondyle with its characteristic fibrillar pattern. The anterior band of the UCL is seen attached from the medial epicondyle to the sublime tubercle of the ulna. These structures are then evaluated in short axis by rotating the transducer 90 degrees. Dynamic US may be performed to test ligamentous laxity of the UCL by applying a valgus stress with the elbow in slight flexion [12, 13].

Evaluation of the cubital tunnel should then follow. This is performed by turning the elbow outward so the olecranon process and the medial epicondyle can be palpated [14]. Placing the transducer in short axis between the medial epicondyle and olecranon process should yield the following image (Fig. 9). Notice the speckled pattern of the ulnar nerve.

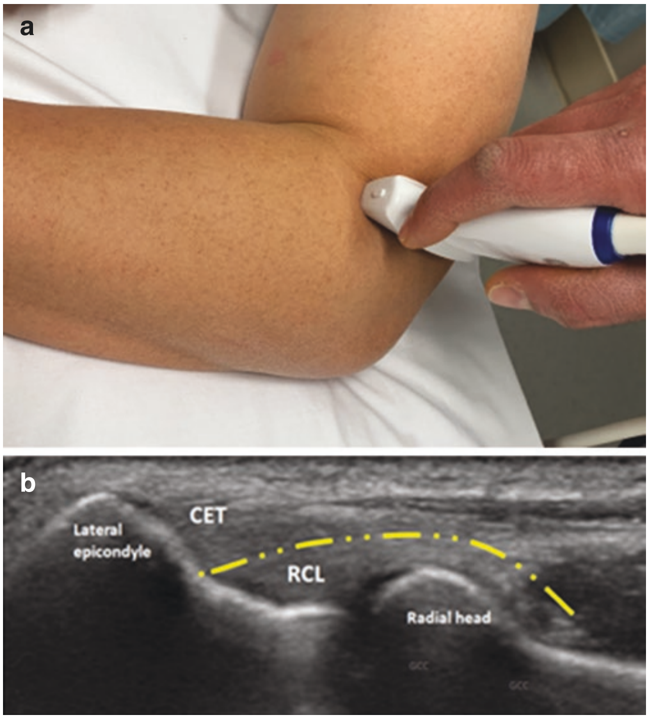

Fig. 10 (**a**) Arm positioning for evaluation of lateral elbow. (**b**) Corresponding US image. CET common extensor tendon, RCL radial collateral ligament

2.3 Lateral Elbow

The anatomical structures of interest in the lateral elbow are common extensor tendon origin, the lateral collateral ligament complex, and the radial nerve (Fig. 3). The exam is performed by placing the arm in internal rotation and flexion (Fig. 10a) [14, 15]. The transducer is placed on the lateral elbow in long axis orientation paralleling the forearm. Several important bony landmarks are identified including

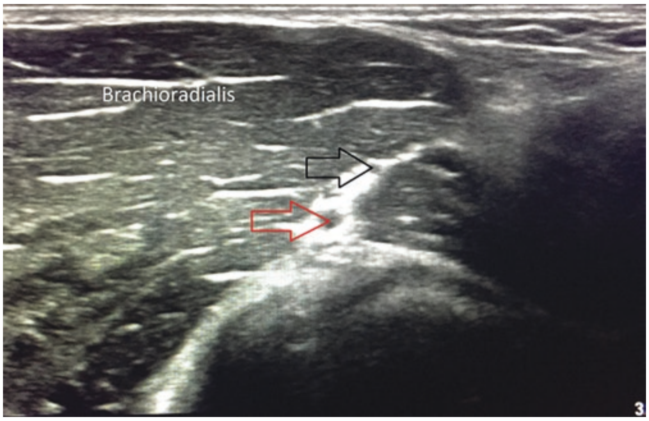

Fig. 11 Superficial (black open arrow) and deep (red open arrow) branches of the radial nerves

the radial head and lateral epicondyle (Fig. 10b). The common extensor tendon is seen attached to the lateral epicondyle. Just deep to the common extensor tendon is the radial collateral ligament attaching from the lateral epicondyle and integrating with the annular ligament to insert on the radial neck. The LUCL is the primary stabilizer against varus force. Imaging of the LUCL is difficult due to its curvilinear course and is best visualized by first locating the RCL and angle the transducer posteriorly toward the ulna [14, 16, 17]. Again, these structures should be evaluated both in the axial and sagittal planes.

The radial nerve is most easily located by first finding the superficial (sensory) and deep (motor) branches on the anterior view of the elbow joint [7]. They are situated in between the brachioradialis and brachialis muscles (Fig. 11) [14]. Then, follow these two nerves more proximally until they join to form the radial nerve.

2.4 Posterior Elbow

The triceps brachii muscle and tendon as well as the olecranon bursa are evaluated in the posterior elbow. The patient is positioned with the elbow flexed to 90 degrees (Fig. 12a) [14]. The transducer is placed in sagittal orientation over the posterior elbow. Several characteristic bony landmarks should be visualized (Fig. 12b). It is important to note that the olecranon fossa is normally filled with hyperechoic fat pad. This fat pad may be displaced by pathological process such as joint fluid, blood, or intra-articular loose bodies [18]. The olecranon bursa is located superficial to the triceps tendon and olecranon process.

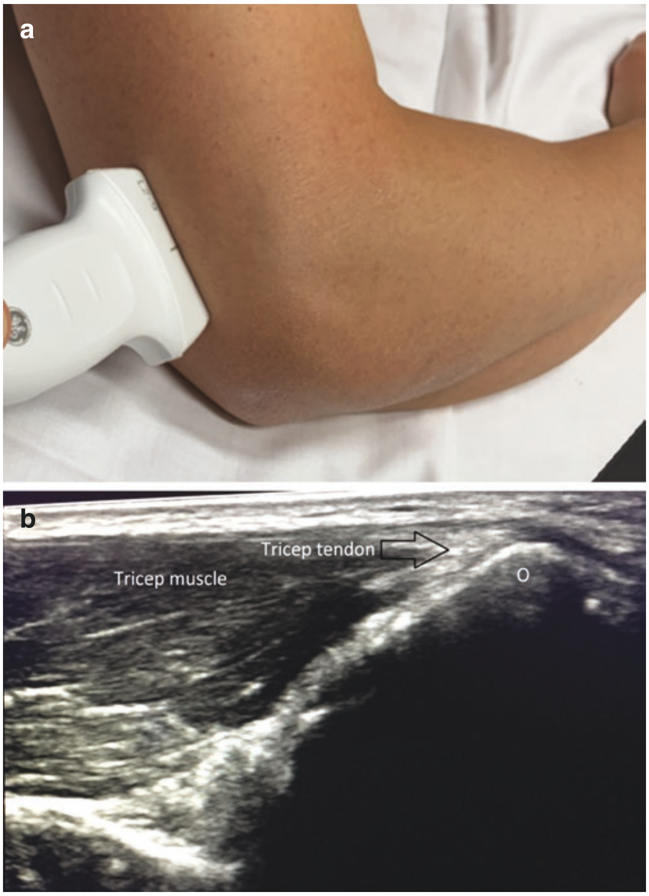

Fig. 12 (**a**) Arm positioning for evaluation of the posterior elbow. (**b**) Long axis view of the posterior elbow. O olecranon

3 Commonly Encountered Pathologies of the Elbow

3.1 Distal Bicep Tendon (DBT) Tear or Rupture

DBT injuries are typically seen in weight lifters [19, 20]. These patients often present with acute anterior elbow pain and report a 'popping' sensation during the process of lifting heavy weights. Physical examination reveals weakness in flexion and supination and a focal defect in the antecubital fossa [16]. US examination of complete ruptures will demonstrate anechoic or hypoechoic discontinuity at the expected insertion of the DBT on the radial tuberosity. Proximal retraction of the tendon may also be evident on US. Partial thickness tears will demonstrate focal defect of the tendon without complete break through.

3.2 Tennis Elbow (Lateral Epicondylitis) (Common Extensor Tendinosis)

Lateral epicondylitis is a misnomer for common extensor tendinosis as there is little inflammatory process involved. It is a painful condition presenting with pain at the lateral side of the elbow joint that increases during gripping, squeezing, and resisted wrist flexion. It is a self-limiting condition in most patients, with long duration of elbow complaints, concomitant neck pain, and severe pain at presentation are associated with poor outcomes at 12 months [21]. While tennis elbow is a clinical diagnosis, US imaging is a noninvasive tool that can be utilized for diagnostic confirmation. On US, lateral epicondylitis presents as thickened, heterogeneous echotexture of the common extensor tendon origin with increased color Doppler flow indicative of hyperemia. Intrasubstance calcifications may be seen in chronic cases [17, 22].

3.3 Golfers Elbow (Medial Epicondylitis) (Common Flexor Tendinosis)

Much like lateral epicondylitis, medial epicondylitis, or Golfer’s elbow, is tendinosis of the common flexor tendon as a result of chronic and repetitive wrist extension and forearm supination [23].This ultimately leads to degeneration of the tendon with irreparable fibrosis and calcification [24, 25]. US will demonstrate similar imaging appearances to that of lateral epicondylitis.

3.4 Ulnar Collateral Ligament Injury

The anterior band of the UCL is commonly injured secondary to chronic valgus force, as seen in many baseball pitchers [23, 26–28]. In the acute setting, these patients may report localized pain and a ‘popping’ sensation at the medial aspect of their elbow. They will often decrease their velocity or modify their pitching mechanism in order to compensate for the pain [27, 28]. On physical exam, patients will demonstrate significant valgus instability. On US, disruption of the UCL with widening of the ulnotrochlear joint suggests complete tear [16]. Partial thickness tears will demonstrate focal hypoechoic defects. Dynamic assessment of the UCL may be performed to evaluate for ligamentous laxity.

3.5 Lateral Collateral Ligament Complex Injury

The LUCL is the primary lateral stabilizer against varus stress. Injury to the LUCL is less common when compared with the contralateral UCL and is usually secondary to trauma in the setting of elbow dislocations [29]. Patients present with pain and swelling over the lateral elbow. Physical exam will reveals varus instability. US appearance is similar to that of UCL injury.

3.6 Olecranon Bursitis

The olecranon bursa is a fluid filled sac located superficial to the olecranon process posteriorly. Of all the elbow bursas, the olecranon bursa is the most commonly affected, and is usually secondary to repetitive overuse, trauma, or inflammation in the setting of rheumatoid, gout, or calcium pyrophosphate deposition disease (CPPD) [30]. Olecranon bursitis presents with localized pain, redness, and warmth in the posterior elbow region. On US, olecranon bursitis appears as increased fluid collection in the olecranon bursa and with associated hyperemia. Intra-bursal calcifications from triceps tendinitis may also be seen.

4 Interventional Procedures

All interventional procedures described below should be performed under sterile technique. The targeted area of injection should be carefully cleaned with antiseptic agents. Local anesthetic using 1% lidocaine can be used to create the skin wheel.

4.1 Needle Fenestration

Percutaneous ultrasound-guided needle fenestration, also known as dry needling, has been used with promising results in tendinopathy/tendinosis treatment. The technique involves repeatedly fenestrating the affected tendon under ultrasound guidance, primarily targeting the abnormal tendon to encourage localized bleeding and fibroblastic proliferation in order to promote ordered collagen formation and ultimately healing of the tendon [31–33]. The common extensor tendon of the elbow is one of the most common tendons treated with ultrasound-guided tendon needle fenestration [31–33]. To locate the common extensor tendon, the patient's arm is internally rotated, flexed to 90 degrees, and placed comfortably on a table. The characteristic bony landmark of the lateral epicondyle and overlying common extensor tendon should be visualized as described in the aforementioned section. An18G–20G needle can be inserted, in plane with the transducer, into the degenerated portions of the common extensor tendon [34]. While there are no consensus criteria on the number of punctures to be performed, several authors have suggested that punctures should be performed for approximately 15–20 passes, until the tendon is softened [35, 36]. Peritendinous injection of corticosteroids can be performed to reduce pain. Potential complications can arise from injections of joint and soft tissue, including, local infection, local reactions at the site (swelling, tenderness, warmth), self-limited post-injection pain flare, and tendon rupture. Patients are generally instructed to rest for 10–14 days and with no NSAID use during this period of time [36].

4.2 Epicondylitis Steroid Injection

Corticosteroid injections can be utilized to treat both medial and lateral epicondylitis that have failed conservative treatment. To begin the procedure, the common extensor tendon is first localized under ultrasound using the same technique in the aforementioned sections. Using sterile precautions, a 25G needle is inserted similarly as fenestration, and in plane with the transducer. Instead of puncturing the tendon as in fenestration, the needle target should be the tendon sheath or peritendinous soft tissues. A 2 ml combination of 1% lidocaine and methylprednisolone (40 mg/ml) can be injected. Complications are rare with infection being the most common [37].

4.3 Intra-articular Injection

Intra-articular injection of the elbow can be performed to alleviate a variety of conditions including osteoarthritis or inflammatory arthropathies such as gout or rheumatoid. The patient is positioned with his arm internally rotated and flexed to 90 degrees. The arm should be rested on a table comfortably. The transducer is placed over the elbow in long axis, paralleling the forearm. A similar technique is described previously for the evaluation of the lateral elbow. An 18-22G 1.5in needle can be inserted in plane with the transducer, aiming for the articular surface of the radial head [34]. When the needle makes contact with the radial head, then it is confidently intra-articular. Then the needle is slightly retracted to ensure that the bevel is free from the cartilage. A 1–2 ml injectate of methylprednisolone (40 mg/ml) and 2–3 ml of lidocaine 1% can be injected [34].

4.4 Olecranon Bursitis

The patient is positioned with the arm flexed at 90 degrees and resting on a table. Palpate for the area of greatest fluctuance and suspected bursitis. The transducer can be placed in either the long or short axis over the olecranon region depending on clinician preference. It is worth noting that the bursal fluid may contain heterogeneous debris and appear as echogenicities on US. A 16-20G 1in needle is inserted until the tip enters the bursa. When the bursa has been completely drained, a combination of 1 ml of methylprednisolone (40 mg/ml) and 1–2 ml of 1% lidocaine can be injected for relief.

5 Conclusion

US is a useful modality in both diagnosing and guiding therapeutic interventions of the elbow. The treating clinician should have a fundamental understanding of the normal anatomy, US techniques, common pathologies, and basic interventional procedures.

References

1. Yang NP, Chen HC, Phan DV, et al. Epidemiological survey of orthopedic joint dislocations based on nationwide insurance data in Taiwan, 2000-2005. BMC Musculoskelet Disord. 2011;12:253.
2. Bucknor MD, et al. Elbow imaging in sport: sports imaging series. Radiology. 2016;279(1):12–28. https://doi.org/10.1148/radiol.2016150501.
3. Stein JM, Cook TS, Simonson S, et al. Normal and variant anatomy of the elbow on magnetic resonance imaging. Magn Reson Imaging Clin N Am. 2011;19(3):609–19.
4. Teixeira PA, Omoumi P, Trudell DJ, et al. Ultrasound assessment of the lateral collateral ligamentous complex of the elbow: imaging aspects in cadavers and normal volunteers. Eur Radiol. 2011;21(7):1492–8.
5. Cutts S. Cubital tunnel syndrome. Postgrad Med J. 2007;83(975):28–31.
6. O'Driscoll SW, Horii E, Carmichael SW, et al. The cubital tunnel and ulnar neuropathy. J Bone Joint Surg Br. 1991;73(4):613–7.
7. Miller TT, Reinus WR. Nerve entrapment syndromes of the elbow, forearm, and wrist. AJR Am J Roentgenol. 2010;195(3):585–94.
8. Barco R, Antuña SA. Medial elbow pain. EFORT Open Rev. 2017;2:362–71.
9. Reilly D, Kamineni S. Olecranon bursitis. J Shoulder Elb Surg. 2016;25:158–67.
10. Middleton WD, Hertzberg BS. Ultrasound: the requisites. Philadpehia: Elsevier; 2016.
11. Beggs I, Bianchi S, Bueno A, et al. Musculoskeletal ultrasound technical guidelines. II. Elbow. Eur Soc Musculoskeletal Radiol, 2006.

12. Jacobson JA, Propeck T, Jamadar DA, Jebson PJ, Hayes CW. US of the anterior bundle of the ulnar collateral ligament: findings in five cadaver elbows with MR arthrographic and anatomic comparison—initial observations. Radiology. 2003;227(2):561–6.
13. Ward SI, Teefey SA, Paletta GA Jr, et al. Sonography of the medial collateral ligament of the elbow: a study of cadavers and healthy adult male volunteers. AJR Am J Roentgenol. 2003;180(2):389–94.
14. Jacobson JA. Fundamentals of Musculoskeletal Ultrasound. Philadelphia: Elsevier; 2018.
15. Bianchi S, Martinoli C. Elbow. In: Bianchi S, Martinoli C, editors. Ultrasound of the musculoskeletal system. New York: Springer; 2007. p. 349–408.
16. Konin GP, et al. US of the elbow: indications, technique, normal anatomy, and pathologic conditions. RadioGraphics. 2013;33(4):E125. https://doi.org/10.1148/rg.334125059.
17. Connell D, Burke F, Coombes P, et al. Sonographic examination of lateral epicondylitis. AJR Am J Roentgenol. 2001;176(3):777–82.
18. Brant WE, Helms CA. Fundamentals of diagnostic radiology. Philadelphia: Lippincott Williams & Wilkins; 2007.
19. Agins HJ, Chess JL, Hoekstra DV, Teitge RA. Rupture of the distal insertion of the biceps brachii tendon. Clin Orthop Relat Res. 1988;234(234):34–8.
20. Bourne MH, Morrey BF. Partial rupture of the distal biceps tendon. Clin Orthop Relat Res. 1991;271(271):143–8.
21. Smidt N, Lewis M, Van Der Windt DA, et al. Lateral epicondylitis in general practice: course and prognostic indicators of outcome. J Rheumatol. 2006;33:2053–9.
22. Levin D, Nazarian LN, Miller TT, et al. Lateral epicondylitis of the elbow: US findings. Radiology. 2005;237(1):230–4.
23. Ciccotti MC, Schwartz MA, Ciccotti MG. Diagnosis and treatment of medial epicondylitis of the elbow. Clin Sports Med. 2004;23(4):693–705.. xi
24. Laratta J, Caldwell JM, Lombardi J, et al. Evaluation of common elbow pathologies: a focus on physical examination. Phys Sportsmed. 2017;45:184–90.
25. Walz DM, Newman JS, Konin GP, Ross G. Epicondylitis: pathogenesis, imaging, and treatment. Radiographics. 2010;30(1):167–84.
26. Morrey BF, An KN. Articular and ligamentous contributions to the stability of the elbow joint. Am J Sports Med. 1983;11(5):315–9.
27. Schwab GH, Bennett JB, Woods GW, Tullos HS. Biomechanics of elbow instability: the role of the medial collateral ligament. Clin Orthop Relat Res. 1980;146(146):42–52.
28. Nazarian LN, McShane JM, Ciccotti MG, O'Kane PL, Harwood MI. Dynamic US of the anterior band of the ulnar collateral ligament of the elbow in asymptomatic major league baseball pitchers. Radiology. 2003;227(1):149–54.
29. Sheehan SE, et al. Traumatic elbow injuries: what the orthopedic surgeon wants to know. RadioGraphics. 2013;33(3):869–88. https://doi.org/10.1148/rg.333125176.
30. Blankstein A, Ganel A, Givon U, et al. Ultrasonographic findings in patients with olecranon bursitis. Ultraschall Med. 2006;27(6):568–71.
31. Burke CJ, Adler RS. Ultrasound-guided percutaneous tendon treatments. AJRAm J Roentgenol. 2016;207:495–506.
32. McShane JM, Nazarian LN, Harwood MI. Sonographically guided percutaneous needle tenotomy for treatment of common extensor tendinosis in the elbow. J Ultrasound Med. 2006;25:1281–9.
33. McShane JM, Shah VN, Nazarian LN. Sonographically guided percutaneous needle tenotomy for treatment of common extensor tendinosis in the elbow: is a corticosteroid necessary? J Ultrasound Med. 2008;27:1137–44.
34. Cardone DA, Tallia AF. Diagnostic and therapeutic injection of the elbow region. Am Fam Physician. 2002 Dec 1;66(11):2097–101.
35. Housner JA, et al. Sonographically guided percutaneous needle tenotomy for the treatment of chronic tendinosis. J Ultrasound Med. 2009;28(9):1187–92. https://doi.org/10.7863/jum.2009.28.9.1187.
36. Griffith JF. Diagnostic ultrasound: musculoskeletal. Philadelphia: Amirsys Publishing Inc./Elsevier; 2015.
37. Zayat AS, Buch M, Wakefield RJ. Arthrocentesis and injection of joints and soft tissues. In: Firestein GS, Budd RC, Gabriel SE, et al., editors. Kelley's Textbook of Rheumatology, vol. 1. 10th ed. Philadelphia: Elsevier; 2016. p. 802–16.

Wrist Joint Sonoanatomy and Ultrasound-Guided Wrist Joint Injection

Jason Kajbaf and George C. Chang Chien

1 Introduction

Ultrasound is a useful modality for the quick diagnosis of various hand and wrist pathologies. Given the superficial anatomy of the wrist, a high frequency linear probe can easily identify various wrist disorders, such as ligament tears or carpal tunnel syndrome. The wrist is a condyloid type synovial joint formed by the radius and articular disc proximally, and the proximal row of carpal bones distally (minus the pisiform). The ulna, although it does not articulate with the wrist joint, does form connections with the distal radius, as well as to the pisiform and triquetrum via the ulnar collateral ligament. Numerous additional ligaments and tendons help further stabilize the wrist. The following chapter will review sonographic wrist anatomy, and when applicable, injection techniques to perform with ultrasound guidance.

1.1 Osseous Structures

The wrist is a combination of three joints. It is, from proximal to distal, comprised of the distal radioulnar joint, radiocarpal joint, and midcarpal joints (Fig. 1). Of note, the carpal bones form the lateral and medial walls, as well as the floor of the carpal tunnel. The pisiform is the medial wall proximally, and the scaphoid is the lateral wall. Distally, the hook of hamate is the medial wall, and the tubercle of the trapezium is the lateral wall (Fig. 2). Although ultrasound is not the best method to evaluate trauma to bone, it is able to provide significant information on joints. For instance, articular cartilage degeneration, joint effusions, and osteophytes are all fairly easily seen. Furthermore, bones are important landmarks to be able to identify when attempting to locate various tendons, ligaments, and other soft tissue structures.

1.2 Flexor Compartment

On the anterior aspect of the wrist, the most superficial structure that will be visible will be the flexor retinaculum, the strong fibrous band that overlies the carpal tunnel. The flexor retinaculum attaches medially to the hook of hamate and pisiform bones, and laterally to the scaphoid and trapezium (Fig..3) [1]. Deep to this, there are three tendinous layers crossing the wrist. The most superficial layer consists of the flexor carpi radialis (FCR), palmaris longus (PL), and flexor carpi ulnaris (FCU) tendons. The intermediate layer consists of the flexor digitorum superficialis (FDS) tendons, and lastly, the deep layer consists of the flexor digitorum profundus (FDP) and flexor pollicis longus (FPL) tendons (Fig. 3) [2]. The intermediate and deep tendons course through the carpal tunnel along with the median nerve, which will be further described in a later section [3].

Again returning to the superficial most layer, the palmaris longus, an oft-missing accessory wrist flexor, passes anterior to flexor retinaculum and inserts itself into the palmar fascia. The FCR tendon, lateral to the PL, proceeds to attach partly to the scaphoid, then primarily to the base of the second metacarpal [3]. The FCU tendon, medial to the PL, similar to the other superficial layer tendons, crosses anterior to the flexor retinaculum, and then eventually ensues to attach to the hook of hamate and the base of the fifth metacarpal bone. Of note, the FCU tendon, along with the PL tendon, are the only wrist flexor tendons without any synovial sheath [3]. Proceeding to the intermediate layer, the tendons of the FDS pass through the carpal tunnel in pairs, with the third and fourth digit tendons crossing anteriorly to the second and fourth digit tendons [1]. The FDS continues anterior to the FDP tendons until the superficialis tendons split and dive deep to the FDP, attaching to the middle phalangeal bones. The FDP tendons continue and eventually attach themselves

J. Kajbaf (✉)
University of California, Los Angeles, Department of PM&R,
Los Angeles, CA, USA

G. C. Chang Chien
GCC Institute, Newport Beach, CA, USA

Ventura County Medical Center, Ventura, CA, USA

© Springer Nature Switzerland AG 2021

J. Li et al. (eds.), *Ultrasound Fundamentals*, https://doi.org/10.1007/978-3-030-46839-2_12

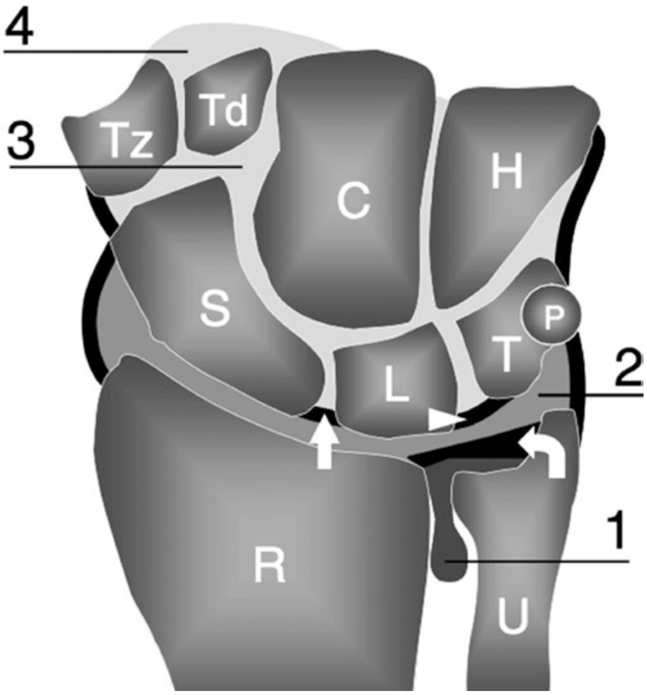

Fig. 1 Drawing of the wrist, demonstrating the Radius (R) and Ulna (U). The proximal carpal row from left to right: Scaphoid (S), Lunate (L), Triquetrum (T), and Pisiform (P). The distal carpal row from left to right: Trapezium (Tz), Trapezoid (Td), Capitate (C), and Hamate (H). The joints of the wrist are the labeled numbers: radioulnar joint (1), distal radiocarpal joint (2), midcarpal joints (3), and the carpometacarpal joints. Lastly, the straight arrow depicts the scapholunate joint/ligament, the arrowhead depicts the lunotriquetral joint/ligament, and the curved arrow depicts the triangular fibrocartilage

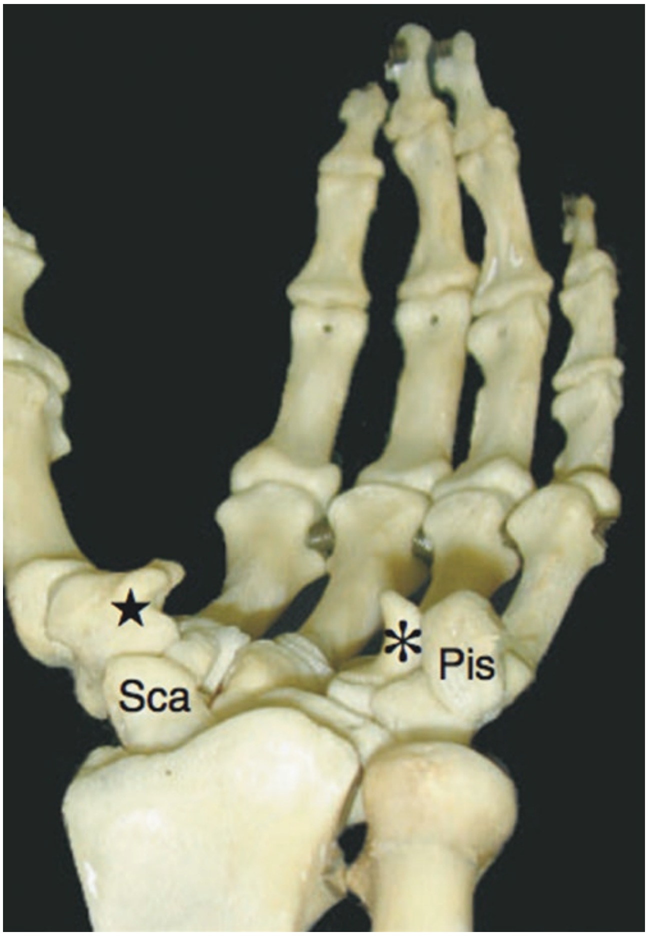

Fig. 2 The Scaphoid (Sca) and Pisiform (Pis) make the radial and ulnar borders of the proximal carpal row, respectively. The tubercle of the Trapezium (Star) and hook of Hamate (asterisk) make up the radial and ulnar borders of the distal carpal row, respectively. Attaching these structures, and forming the roof of the carpal tunnel, if depicted, would be the flexor retinaculum

to the anterior aspect of the distal phalangeal bones. As the FDS and FDP tendons cross the carpal tunnel, a common synovial sheath envelops them, whereas the FCR, the other tendon traversing the carpal tunnel, has its own separate synovial sheath [3].

1.3 Extensor Compartment

On the posterior, or dorsal aspect of the wrist, lie the extensor tendons of the wrist and digits. They all pass just deep to the extensor retinaculum, a 2 cm wide fibrous band that serves a similar purpose as the flexor retinaculum. However, unique to the extensor retinaculum is its vertically oriented bands that divide the extensor tendons into six compartments, labeled from radial to ulnar. Further adding space to these compartments are the depressions seen on the dorsal aspect of the radius and ulna (Fig. 4). Each compartment houses one or more tendons, as well as a common synovial sheath for that compartment [3].

The first and most radial dorsal compartment, affected in De Quervain's Tenosynovitis, is composed of the abductor pollicis longus (APL) and extensor pollicis brevis (EPB) (Fig. 5). Moving medially, the second compartment contains the extensor carpi radialis longus and brevis tendons (ECRL, ECRB) (Fig. 6). Then, separated from the second compartment by Lister's tubercle, the third compartment houses the extensor pollicis longus (EPL) (Fig. 7). Further medial lays the fourth compartment, which is comprised of the extensor digitorum (ED) tendons and extensor indices proprius (EIP) (Fig. 8). Between the radius and ulnar is the fifth compartment, which contains the extensor digiti quinti proprius (EDQ) (Fig. 9). Lastly, the ulnar most compartment (VI), holds the extensor carpi ulnaris tendon (ECU) (Fig. 10). One method to partially simplify the easily confused compartments is to recall that the tendons of the first three compartments alternate among longus and brevis tendons: APL, EPB, ECRL, ECRB, EPL [3].

The tendons of the first and third compartments together form the superior and inferior borders of the anatomic snuff-box (Fig. 11). This is of particular interest to delineate

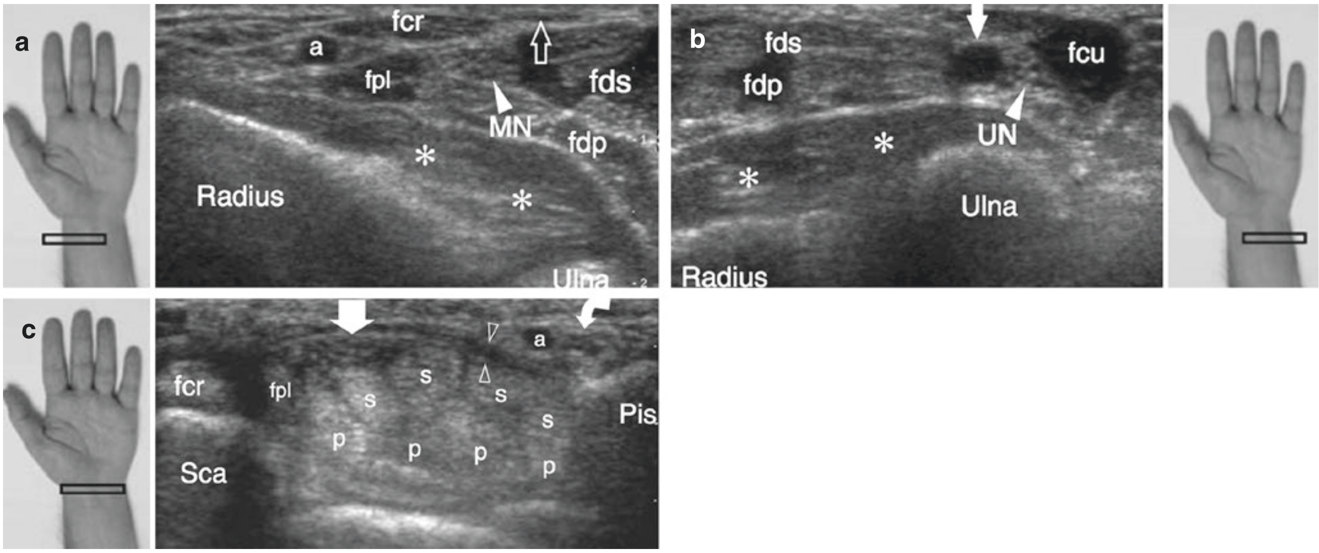

Fig. 3 (**a**) This cross-section demonstrates the radial side of the wrist, just proximal to the carpal tunnel. The radial artery (a), runs lateral to the flexor carpi radialis (fcr), which is just superior to the flexor pollicis longus (fpl). The median nerve (MN/arrowhead) is seen running between the fpl and flexor digitorum superficialis (fds). The flexor digitorum profundus (fdp) is seen just deep and medial to the median nerve. And lastly, the asterisks represent the pronator quadratus, which originates at the distal radius and inserts into the distal ulna (as seen in Fig. 3b). (**b**) The probe is moved medially to obtain the ulnar half of the proximal wrist. The same fds and fdp tendons are visible here, as is the insertion of the pronator quadratus on the distal ulna (asterisks). Further medial lie the ulnar artery (arrow), ulnar nerve (UN/arrowhead), and flexor carpi ulnaris (fcu). (**c**) This cross-section of the proximal carpal tunnel, scanned at the level of the proximal wrist crease, demonstrates the contents of the carpal tunnel, as well as the flexor carpi radialis (fcr), ulnar artery (a) and corresponding ulnar nerve (curved arrow). The scaphoid (sca) and pisiform (pis) form the radial and ulnar boundaries of the proximal portion of the carpal tunnel, which can be seen at this level. The arrowheads demonstrate the flexor retinaculum, or the "roof" of the carpal tunnel. Lastly, the contents of the proximal carpal tunnel from superficial to deep include the median nerve (arrow), flexor digitorum superficialis tendons (s), flexor pollicis longus tendon (fpl), and flexor digitorum profundus tendons

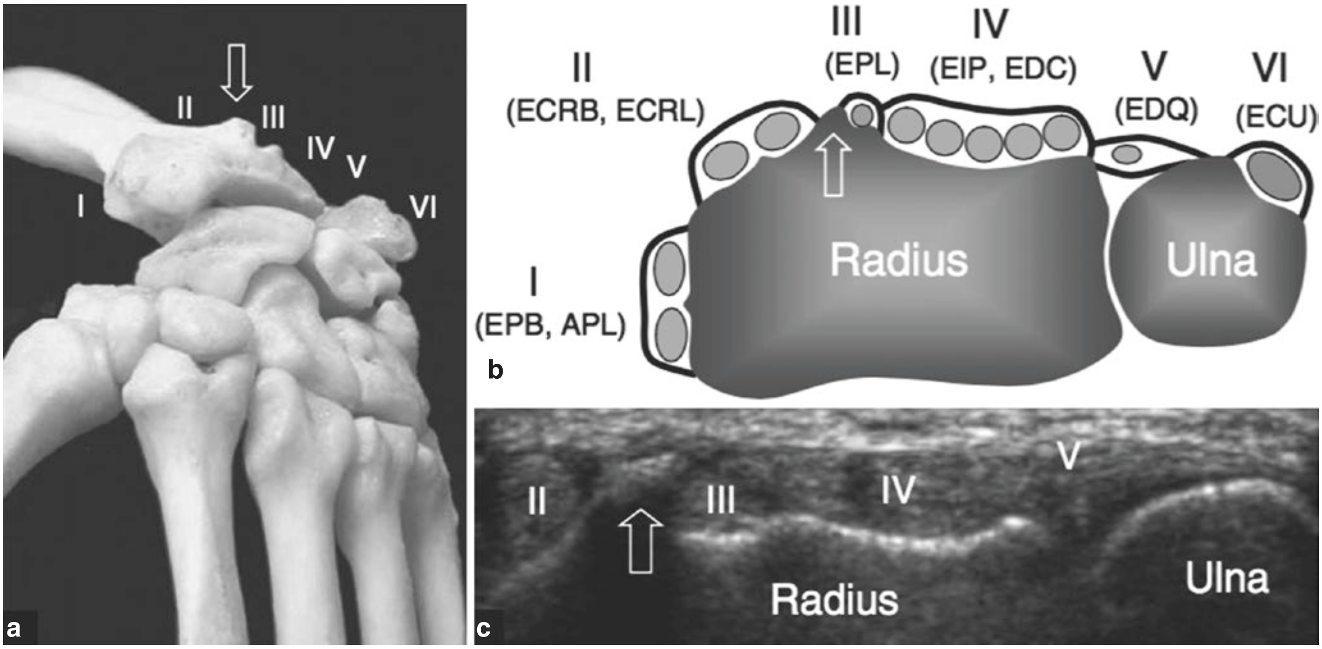

Fig. 4 (**a**) An osseous representation of the grooves that help form the six compartments of the dorsal wrist. (**b**) A simplified diagram showing the contents of the six compartments in a cross-sectional view. Note the hollow arrow, which represents Lister's tubercle, which separates the second and third compartments. (**c**) This sonographic image of the dorsal aspect of the wrist depicts the dorsal-most compartments. Again note the hollow arrow depicting the Lister's tubercle separating compartments two and three

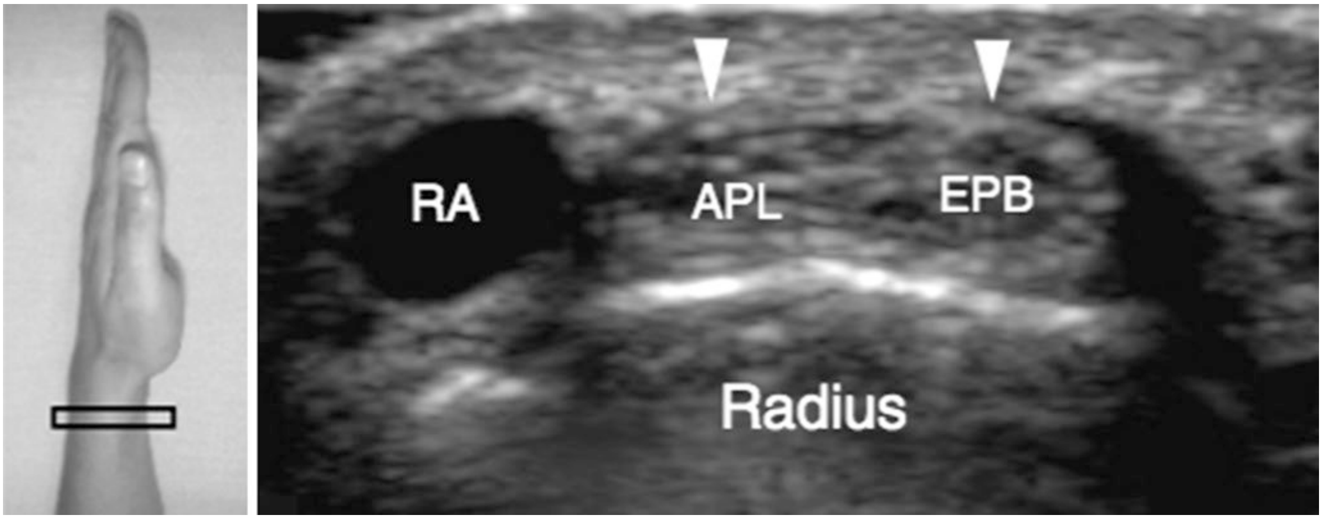

Fig. 5 First compartment. A short-axis view of the first compartment, which is composed of the abductor pollicis longus (APL) and extensor pollicis brevis (EPB) tendons. The arrowheads are pointing to the extensor retinaculum (the roof of all dorsal compartments). The radial artery (RA) runs just lateral to the first compartment

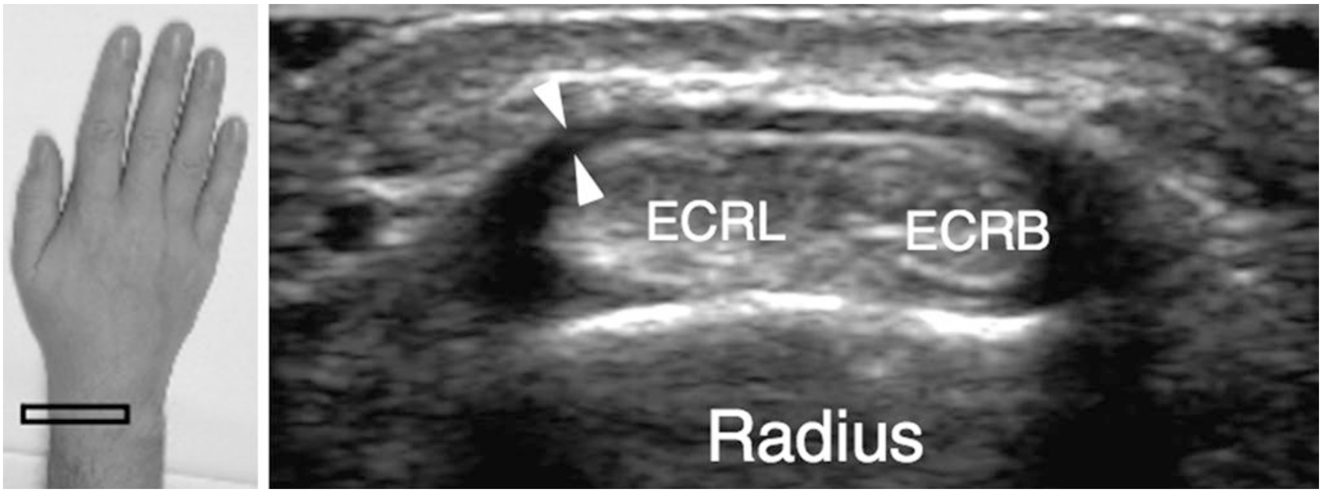

Fig. 6 Second compartment. A short-axis view of the second compartment, which is composed of the extensor carpi radialis longus and brevis (ECRL, ECRB) tendons. Again, covered by the extensor retinaculum dorsally (denoted by arrowheads)

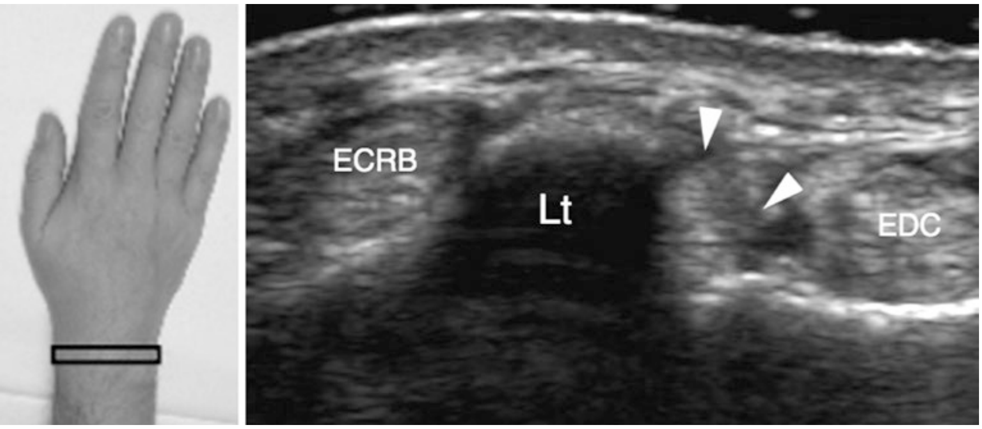

Fig. 7 Third compartment. A short-axis view of the third compartment, which is separated from the second compartment by Lister's tubercle (Lt). It composed of the extensor pollicis longus tendon (arrowheads). Extensor digitorum tendon (EDC) runs medial to the EPL, in the fourth compartment

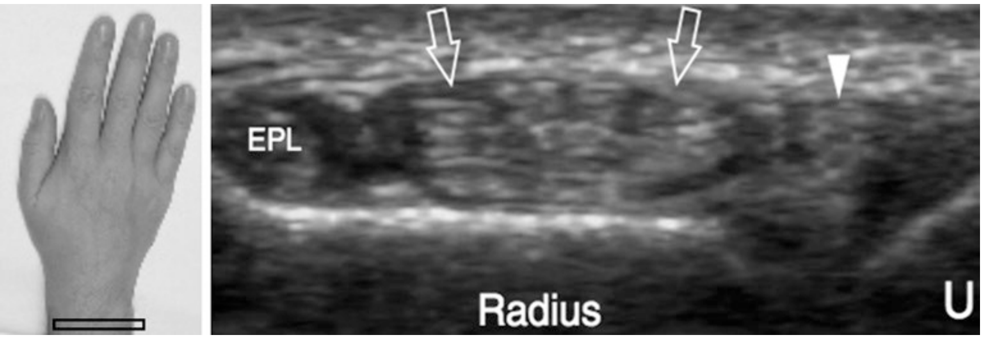

Fig. 8 Fourth compartment. A short-axis view of the fourth compartment, which is composed of the extensor indicis proprius and extensor digitorum tendons (arrows). The EPL, in the third compartment, runs medially. The extensor digiti quinti (arrowhead), in the fifth compartment, runs laterally

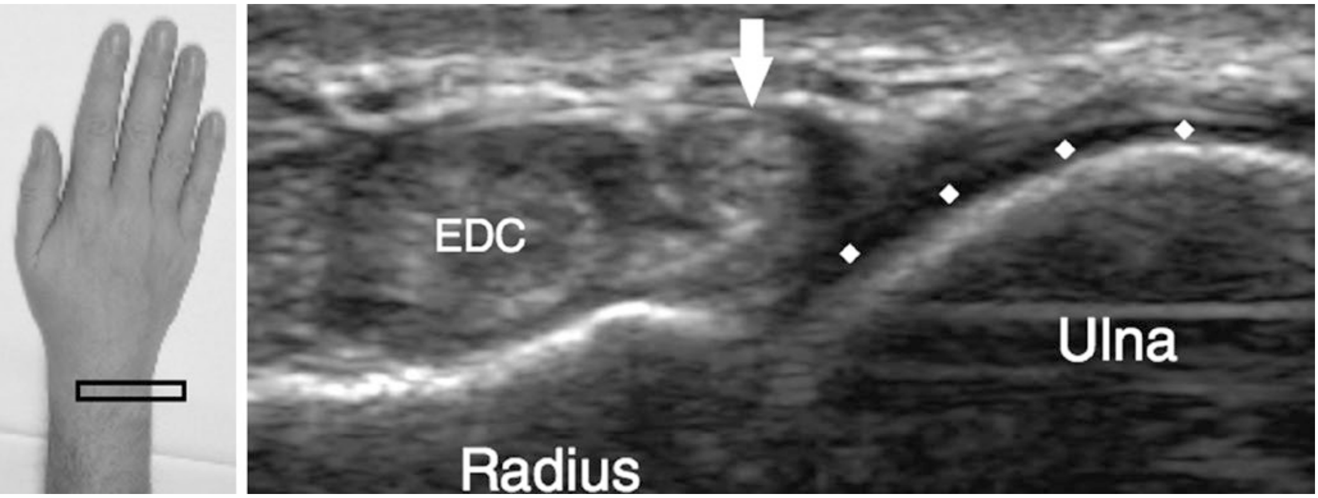

Fig. 9 Fifth compartment. A short-axis view of the fifth compartment, which is composed of the extensor digitorum tendon (arrow). The extensor digitorum tendons (EDC) are seen running medially, in the fourth compartment. The diamonds depict the articular cartilage of the distal ulnar head

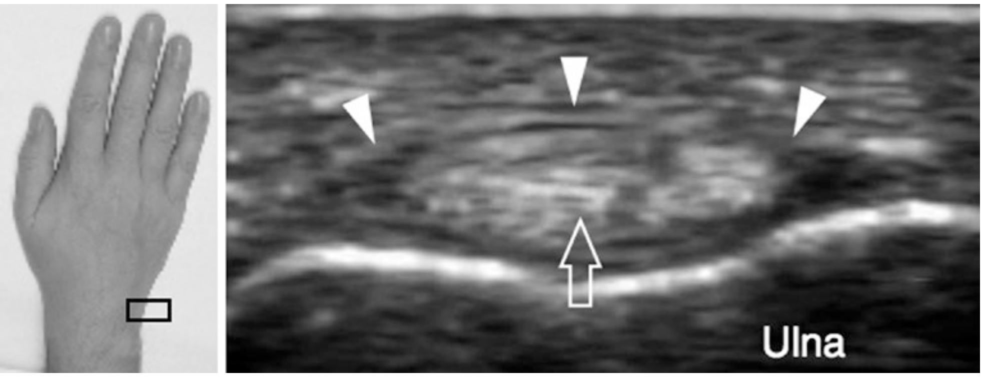

Fig. 10 Sixth compartment. A short-axis view of the sixth compartment, which is composed of the extensor carpi ulnaris tendon (arrow). The extensor retinaculum is seen overlying the tendon (arrowheads)

clinically, due to the fact that at the base of the snuff-box lies the scaphoid; tender palpation of this area may indicate either a fracture, or in the sub-acute to chronic setting, avascular necrosis of the scaphoid (Fig. 12). To a trained clinician, fractures may even be seen on ultrasound, which can be of high yield when examining a patient with pain in the snuff-box, but with negative x-rays. Ultrasound has been demonstrated to have up to 100% sensitivity to detect scaphoid fractures; however, there is variability among the level of training and comfort one has with using an ultrasound machine [4].

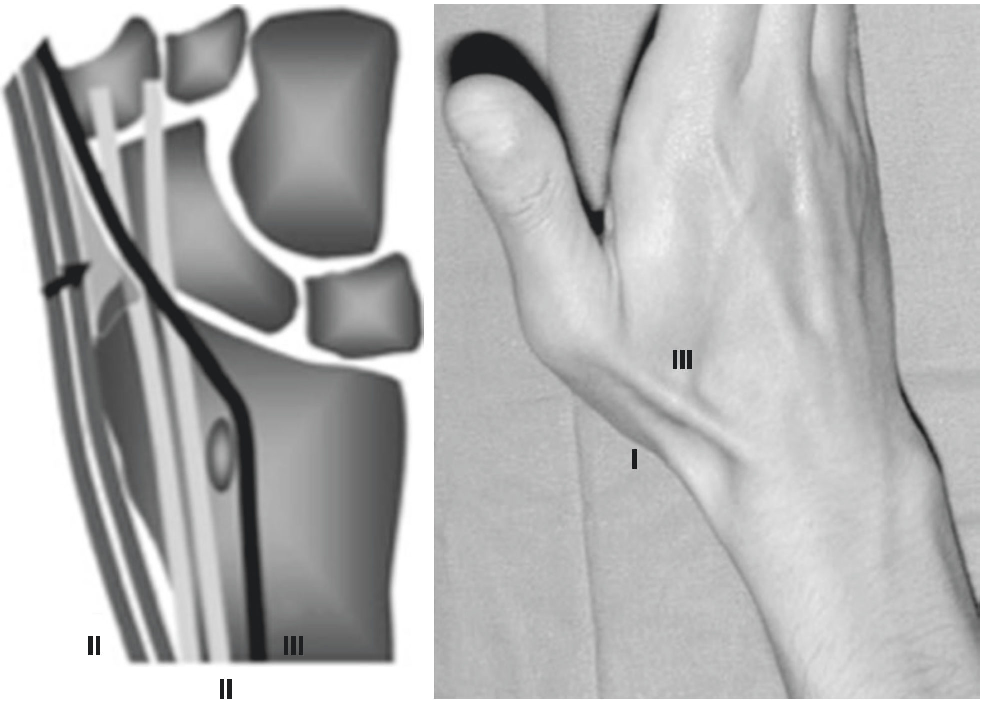

Fig. 11 The tendons of the first and third compartment (I &III) form the boundaries of the anatomic snuff box (arrow). The extensor pollicis longus of the third compartment crosses over the tendons of the second compartment (extensor carpi radialis longus and brevis)

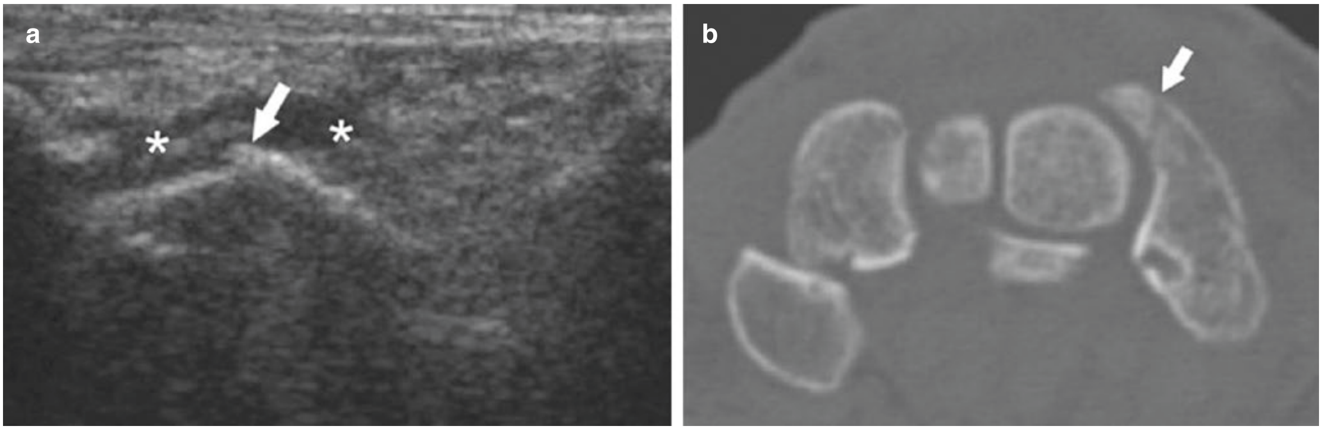

Fig. 12 (**a**, **b**) Figure (**a**) on the left demonstrates a scaphoid fracture that was not detected on x-ray. Fractures under ultrasound may be suspected when there is cortical irregularity (arrow), as well as overlying edema/hematoma formation (asterisks). Figure (**b**) on the right confirms the fracture with CT scan

1.4 Nerves

1.4.1 Median Nerve

The median nerve is the most commonly assessed nerve at the level of the wrist due to the profoundly common carpal tunnel syndrome. Proximal in the forearm, the median nerve can be found at the medial border of the cubital fossa; however, as it is tracked distally, it dives through the pronator teres, and courses between the FDS and FDP [5]. As the median nerve approaches the wrist, it begins to surface and enters the carpal tunnel superficial to the FDS and FPL tendons. At the proximal carpal tunnel (level of the pisiform) the median nerve is typically oval shaped, and at the distal carpal tunnel (level of the hook of hamate), the median nerve has taken a more flattened appearance (Fig. 13). It is important to recognize how nerve echogenicity differs from tendon echogenicity in order to be able to more easily differentiate and identify nerves, particularly when attempting various injections that are to be discussed in a later section. Nerves are sonographically a combination of hyper and hypoechoic structures, thus commonly referred to as a “honeycomb” appearance [3].

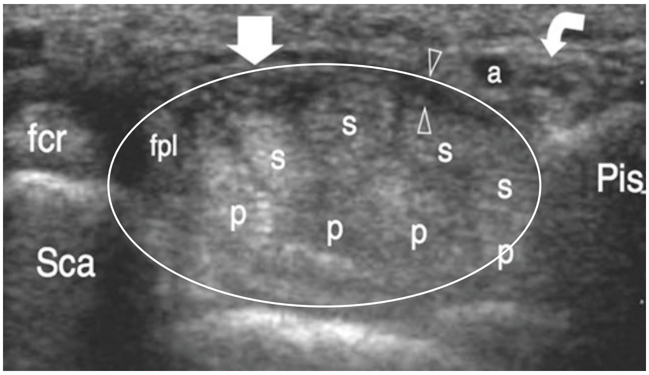

Fig. 13 Short-axis view of the median nerve (arrow) at the level of the proximal carpal tunnel. Tendons of the flexor digitorum superficialis (s) and profundis (p) run within the carpal tunnel with the median nerve. The scaphoid (Sca) and pisiform (Pis) form lateral and medial boundaries, respectively. The roof is formed by the flexor retinaculum (arrowheads). Lastly, also depicted in this cross-sectional image is the flexor carpi radialis (fcr) running outside of the carpal tunnel laterally. As well as the ulnar artery (a) and ulnar nerve (curved arrow) medially, again outside of the carpal tunnel

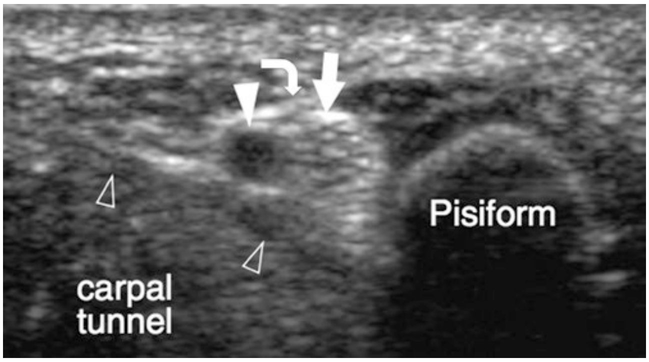

Fig. 14 A short-axis view of the ulnar nerve (arrow) and artery (arrowhead) as it travels through guyon's canal at the wrist. The flexor retinaculum (empty arrowheads) acts as the floor, the pisiform bone acts as the medial wall, and the palmar carpal ligament acts as the roof (curved arrow)

Most commonly, when a clinician is performing an ultrasound of the wrist, they are assessing for carpal tunnel syndrome, which although is a clinical diagnosis, also has several key sonographic markers to help make a more accurate diagnosis, as well as determine if a carpal tunnel injection has been effective. The cross-sectional area (CSA) of the median nerve at the level of the proximal carpal tunnel (level of the pisiform) has been shown to be suggestive of carpal tunnel syndrome when greater than 14cm [2, 6]. Furthermore, when the median nerve CSA at the proximal carpal tunnel is compared to the distal forearm (level of pronator quadratus), the wrist-to-forearm (WFA) ratio is obtained, and a ratio greater than 1.6 has been shown to be suggestive of carpal tunnel syndrome. These measurements can be of particular importance when considering a carpal tunnel steroid injection or surgical release of the flexor retinaculum. Improvements of CSA and WFA after intervention may be used to determine efficacy of the procedure [6].

1.4.2 Ulnar Nerve

The ulnar nerve can be injured in the wrist at Guyon's canal. Guyon's canal is formed by four boundaries, the pisiform medially, the hook of hamate laterally, the transverse carpal ligament serves as the floor, and the palmar carpal ligament serves as the roof (Fig. 14) [3]. The clinical importance of Guyon's canal lies in the anatomy of the ulnar nerve, which initially is a mixed motor and sensory serve; however, as it enters Guyon's canal, it sends off its sensory nerve fibers superficial to the canal via the dorsal cutaneous branch of the ulnar nerve. Thus leaving only motor nerve fibers in Guyon's canal, and thus would theoretically cause motor deficits if there is a compression of the ulnar nerve within this canal. Furthermore, compression of the ulnar nerve through this tunnel is commonly due mass lesions, such as ganglion cysts [5].

1.4.3 Radial Nerve

The Radial nerve is a purely sensory nerve at the level of the wrist and provides cutaneous innervation to the dorsum of the hand. Sonographically, the radial nerve can be found as it courses along the anatomic snuff-box, running over the tendons of the first extensor compartment [3].

1.5 Intrinsic Wrist Ligaments

Injury to any ligament of the wrist may result in severe pain; however, the following ligaments are more readily visible under ultrasound, and pathology can be more easily identified [1]. The scapholunate ligament plays a pivotal role in the stability of the proximal carpal row during wrist motion, primarily maintaining the scaphoid in its correct position [3]. Thus, any disruption or tear of this ligament commonly results in significant pain and discomfort, and may lead to SLAC (scapholunate advanced collapse) [7]. SLAC is a degenerative condition that has been described to have four stages. Stage one is the initial disruption of the scapholunate ligament in addition to mild degeneration of the radioscaphoid joint. Stage two involves more involved degeneration of the radioscaphoid joint, and stage three now involves degenerative changes of the midcarpal joint. Stage four is ultimately pan-radiocarpal osteoarthritis [8]. Furthermore, though less described as SLAC, disruption of the lunatotriquetral ligament also commonly results in pain, and may eventually lead to degeneration of various joints within the wrist [1].

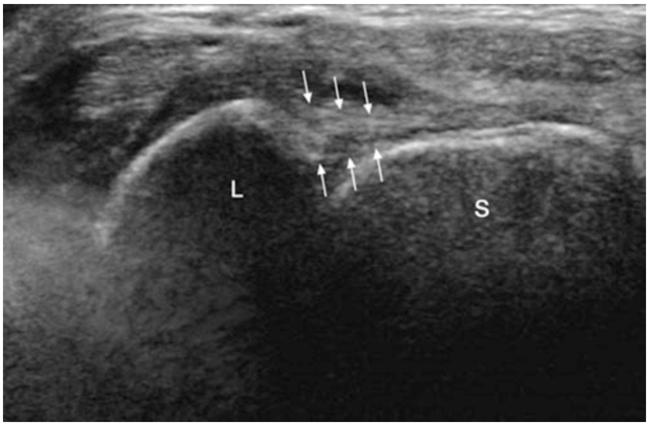

Fig. 15 A transverse view of the dorsal component of the scapholunate ligament (arrows) appearing as a fibrillar triangular structure running from the scaphoid (S) to lunate (L). Any irregularities of the fibular lines or increased fluid collection may indicate possible scapholunate disruption

In order to best visualize the scapholunate and lunatotriquetral ligaments, the wrist must be placed prone, and the ultrasound transducer should be placed just distal to Lister's tubercle. The scapholunate ligament in this position is seen as a triangular hyperechoic fibrillar structure connecting the scaphoid and lunate bones (Fig. 15). If the transducer is moved slightly more to the ulnar side of the dorsum of the wrist, the lunatotriquetral ligament may be found, connecting the lunate and triquetral bones.

The triangular fibrocartilage complex (TFCC) is a thick soft-tissue structure on the ulnar aspect of the wrist that is composed of multiple ligaments (articular disc, meniscus homologue, ulnocarpal ligament, dorsal & volar radioulnar ligament and extensor carpi ulnaris tendon sheathe) [9]. The TFCC primarily functions to absorb axial-loads on the wrist, increase the stability of the ulnar aspect of the wrist as well as the radio-ulnar joint. Clinically, disruptions of the TFCC may be suspected when a patient has pain on the ulnar aspect of the wrist that is further aggravated with ulnar deviation of the wrist during physical examination [9]. Subsequently, when TFCC tears are suspected, ultrasound may be used to attempt to visualize the disruption of the complex (Fig. 16) [3].

"Gamekeeper's thumb," or the disruption of the ulnar collateral ligament (a component of the TFCC described above), is commonly seen among skiers when stress is applied to the wrist when sustaining a fall while grasping ski poles. Tears of the ulnar collateral ligament are easily seen via small high frequency transducers, as in the hockey stick probes (Fig. 16) [5].

1.6 Rheumatoid Arthritis

Recently, with the improvements of ultrasound and the advent of power doppler, ultrasound has been found to have clinical application in rheumatologic diseases. Power doppler detects slow blood flow, which is apparent in synovial inflammation, whether it be due to an infection or other inflammatory processes [5]. Furthermore, when used in patients with rheumatoid arthritis, for instance, an increase in vascularity has been shown to correlate with subclinical disease, and thus may aid in the treatment of rheumatoid arthritis. A study by Fukae, et al. found that power doppler ultrasound (PDUS) may actually be used as a screening tool for rheumatoid arthritis, with a sensitivity of 92.3%, and specificity of 91.7% [10]. Furthermore, in addition to aiding in the diagnosis of rheumatoid arthritis, PDUS has also been shown to be effective in demonstrating response to treatment [11].

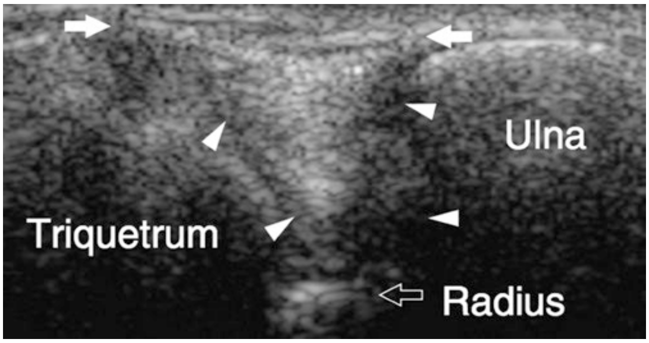

Fig. 16 A coronal view of the triangular fibrocartilage complex (arrowheads), which appears as a homogenously hyperechoic area. Note the intact ulnar collateral ligament just superficial to the TFCC

1.7 Carpal Tunnel Injection

As discussed earlier in this chapter, clinically suspected carpal tunnel syndrome can be diagnosed using ultrasound. Furthermore, it has also been demonstrated that the most effective ultrasound guided injection for carpal tunnel syndrome is the ulnar in-plane approach at the level of the proximal carpal tunnel (or proximal wrist crease) [12]. Using the pisiform bone as a landmark for the proximal carpal tunnel, a high frequency linear transducer is placed in the transverse plane (looking at the median nerve in short axis). Furthermore, in order to prevent piercing the ulnar artery that lays medial to the median nerve, the transducer should be moved out laterally enough so the ulnar artery is out of view, thus ensuring when the needle is introduced laterally to the ulnar artery [12, 13]. Once the needle is introduced, it should be advanced such that half of the injectate is introduced below the median nerve, and the other half just above, thereby making what is referred to as a "target sign." This hydro-dissection of the median nerve may further add to the clinical efficacy of a carpal tunnel steroid injection [13]. Table 1 further details studies comparing the ulnar in-plane approach to either palpation guided or ulnar out-of-plane injection techniques [13, 14].

Table 1 Summary of ultrasound guided carpal tunnel injection

Study	Study design	Population	Primary outcome measure	Results	Conclusions
Lee, et al. [14]	Prospective single-blind randomized clinical trial	N= 44 patients with mild to moderate CTS confirmed by nerve conduction study	Boston Carpal Tunnel Questionnaire (BCTQ)	Improved BCTQ and median nerve conduction parameters at 4 and 12 weeks using ultrasound guided ulnar in-plane approach compared with out-of-plane and blind approach ($p<0.05$)	US-guided local steroid injection using an in-plane ulnar approach in the CTS may be more effective than out-plane or blind injection.
	Injection of 40mg triamcinolone with 1ml of 1% lidocaine using:		Median nerve conduction study		
	Ultrasound guided ulnar in-plane approach				
	Ultrasound guided ulnar out-of-plane approach				
	Blind approach				
Ustun, et al. [15]	Prospective single-blind randomized clinical trial	N= 46	BCTQ at 6 and 12 weeks post injection	Improved BCTQ in both groups at 6 and 12 weeks.	Ultrasound guided ulnar-in plane carpal tunnel injections provide greater and more effective symptomatic relief when compared to landmark/palpation guided injections
	Injection of 40mg triamcinolone using:			Greater improvement at 12 weeks in ultrasound group ($p<0.05$)	
	Ultrasound guided ulnar in-plane approach			Quicker onset of symptom relief in ultrasound group ($p<0.05$)	
	Blind approach				

1.8 De Quervain's Tenosynovitis Injection

De Quervain's tenosynovitis, as described earlier, is the inflammation of the tendons in the first dorsal compartment of the wrist (EPL and APB). Ultrasound guided injections into the first dorsal compartment have been demonstrated to be an effective treatment option. A common approach is to place the arm in a neutral position, with the radial side up, then placing the transducer over the first dorsal compartment to obtain a short-axis view of the EPL and APB tendons. A dorsal-to-palmar injection path is taken, and the injectate is introduced into the compartment [15]. However, it is of particular interest to be wary of anatomic variations. Commonly, the first dorsal compartment may have sub-compartments, meaning the APB and EPL tendons are separated. Should this be the case, both compartments should be injected (Fig. 17) [16].

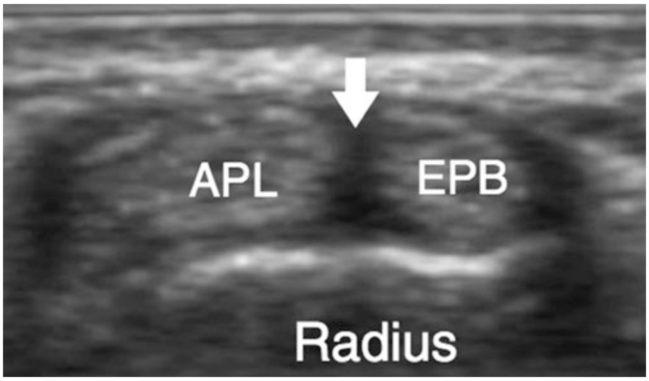

Fig. 17 Transverse view of the first dorsal compartment affected in De Quervain's tenosynovitis. This image depicts the common sub-compartmentalization of the first dorsal compartment. If this variation is present, and an injection is being considered, the clinician should first assess if there are inflammatory changes of either one or both tendons in the setting of De Quervain's tenosynovitis. If only one tendon is affected, then that sub-compartment should be injected. If both are affected, then both sub-compartments should be injected

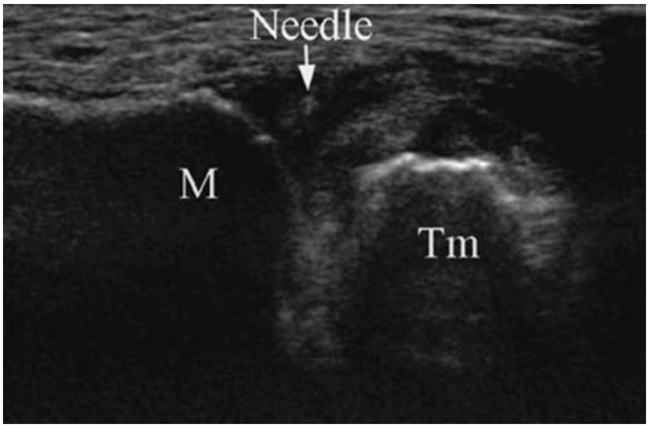

Fig. 18 A long axis view of the first carpometacarpal (CMC) joint (M First metacarpal; Tm Trapezium). With this view, the wrist is on a surface in a neutral position with the radial wrist positioned superiorly. An out-of-plane approach may then be taken, inserting the needle straight down into the joint

1.9 First Carpometacarpal (Trapeziometacarpal) Joint Injection

One of the most commonly affected joints in the hand, the first carpometacarpal (CMC) joint, is essential to normal thumb function [17]. Degenerative changes to this joint may lead to significant, functionally limiting pain. Conservative treatment measures typically involve a combination of wrist splints (thumb-spica), oral analgesics (i.e. NSAIDs), topical analgesics, and occupational therapy [18]. However, when these fail and the pain significantly limits daily function and use of the hand, a steroid injection may be considered for temporary pain relief.

The best way to visualize the first CMC joint is using a high frequency linear transducer, or hockey stick probe, positioned in the anatomic coronal plane over the first metacarpal. The transducer may then be gradually moved proximally until the joint is clearly identified [19]. Once visualized, osteoarthritis of the first CMC joint may be indentified sonographically when cortical irregularities, joint effusion, osteophyte formation, and/or articular space narrowing is seen (Fig. 18) [20]. With the ultrasound transducer properly positioned to best view the first CMC joint, a dorsal-to-palmar out of plane approach may then be used to introduce the needle into the joint space. For more severely degenerative joints, the thumb may be positioned in more adduction to further gap the joint [19].

1.10 Tendon Sheath Injection (Trigger Finger)

Chronic repetitive hand use commonly leads to inflammation of the A1 pulley and tendon swelling, and in turn resulting in constant triggering of the involved finger during flexion [21]. Trigger finger affects roughly 2 percent of the general population, and most commonly found in women, and in the fifth or sixth decade of life [22]. Prevalence is significantly greater in patients with diabetes mellitus and rheumatoid arthritis, as well as various other systemic illnesses [22]. Similar to the previously aforementioned diseases, trigger finger has been shown to respond well to steroid injections.

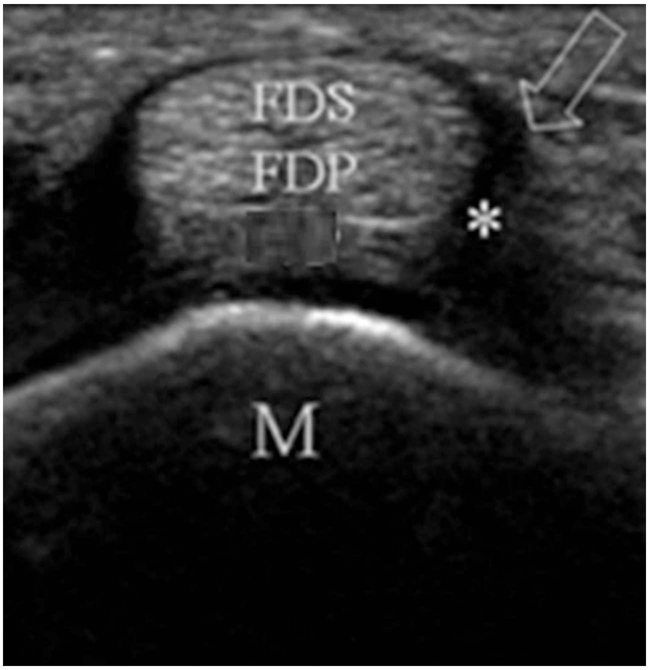

Fig. 19 A short axis view over a distal metacarpal (M) demonstrating the flexor digitorum superficialis (FDS) and flexor digitorum profundus (FDP) tendons overlying each other. The A1 pulley is seen as a hypoechoic structure (arrow; asterisk)

In order to perform this injection, the tendon sheath is best visualized in short axis, and the flexor digitorum superficialis and profundus tendons are seen lying on top of one another. Once visualized, a needle is then introduced out of plane aiming for the tendon sheath, and the injectate solution is introduced. Caution must be taken to not introduce the needle directly into the tendon (Fig. 19).

References

1. Lee JC, Healy JC. Normal sonographic anatomy of the wrist and hand. Radiographics. 2005;25(6):1577–90.
2. Gitto S, Draghi F. Normal sonographic anatomy of the wrist with emphasis on assessment of tendons, nerves, and ligaments. J Ultrasound Med. 2016;35(5):1081–94.
3. Bianchi S, Martinoli C. Wrist. In: Ultrasound of the Musculoskeletal System. Berlin: Springer; 2007. p. 425–94.
4. Kwee RM, Kwee TC. Ultrasound for diagnosing radiographically occult scaphoid fracture. Skeletal Radiol. 2018;47(9): 1205–12.

5. Sofka CM. Ultrasound of the hand and wrist. Ultrasound Q. 2014;30(3):184–92.
6. Lange J. Carpal tunnel syndrome diagnosed using ultrasound as a first-line exam by the surgeon. J Hand Surg Eur. 2013;38(6):627Y632.
7. Weiss KE, Rodner CM. Osteoarthritis of the wrist. J Hand Surg Am. 2007;32(05):725–46.
8. Watson HK, Ballet FL. The SLAC wrist: scapholunate advanced collapse pattern of degenerative arthritis. J Hand Surg Am. 1984;9(03):358–65.
9. Triangular Fibrocartilage Complex Injuries. In: Physiopedia. https://www.physio-pedia.com/Triangular_Fibrocartilage_Complex_Injuries. Accessed 18 Jul 2018.
10. Fukae J, Shimizu M, Kon Y, Tanimura K, Matsuhashi M, Kamishima T, et al. Screening for rheumatoid arthritis with finger joint power Doppler ultrasonography: quantification of conventional power Doppler ultrasonographic scoring. Mod Rheumatol. 2009;19(5):502–6.
11. Iagnocco A, Finucci A, Ceccarelli F, Perricone C, Iorgoveanu V, Valesini G. Power Doppler ultrasound monitoring of response to anti-tumour necrosis factor alpha treatment in patients with rheumatoid arthritis. Rheumatology. 2015;54(10):1890–6.
12. Chen P-C, Chuang C-H, Tu Y-K, Bai C-H, Chen C-F, Liaw M-Y. A Bayesian network meta-analysis: Comparing the clinical effectiveness of local corticosteroid injections using different treatment strategies for carpal tunnel syndrome. BMC Musculoskelet Disord. 2015;16(1):363.
13. Lee JY, Park Y, Park KD, Lee JK, Lim OK. Effectiveness of ultrasound-guided carpal tunnel injection using in-plane ulnar approach. Medicine. 2014;93(29):e350.
14. Üstün N, Tok F, Yagz AE, Kizil N, Korkmaz I, Karazincir S, et al. Ultrasound-guided vs. blind steroid injections in carpal tunnel syndrome. Am J Phys Med Rehabil. 2013;92(11):999–1004.
15. Bing J-H, Choi S-J, Jung S-M, Ryu D-S, Ahn J-H, Kang C-H, et al. Ultrasound-guided steroid injection for the treatment of de Quervain's disease: an anatomy-based approach. Skelet Radiol. 2018 May;47:1483–90.
16. Mcdermott JD, Ilyas AM, Nazarian LN, Leinberry CF. Ultrasound-guided Injections for de Quervain's Tenosynovitis. Clin Orthop Relat Res. 2012;470(7):1925–31.
17. Melville DM, Taljanovic MS, Scalcione LR, Eble JM, Gimber LH, Desilva GL, et al. Imaging and management of thumb carpometacarpal joint osteoarthritis. Skeletal Radiol. 2014;44(2):165–77.
18. Van Heest AE, Kallemeier P. Thumb carpal metacarpal arthritis. J Am Acad Orthop Surg. 2008;16(3):140–51.
19. Colio S, Smith J, Pourcho A. Ultrasound-guided interventional procedures of the wrist and hand anatomy, indications, and techniques. Phys Med Rehabil Clin North Am. 2016;27(3):589–605.
20. Jacobson J. Fundamentals of musculoskeletal ultrasound. 2nd ed. Philadelphia: Saunders; 2013.
21. Moore JS. Flexor tendon entrapment of the digits (trigger finger and trigger thumb). J Occup Environ Med. 2000;42:526–45.
22. Saldana MJ. Trigger digits: diagnosis and treatment. J Am Acad Orthop Surg. 2001;9:246–52.

Ultrasound Guided Brachial Plexus Block

Jinlei Li, Avijit Sharma, Ellesse Credaroli, Nalini Vadivelu, and Henry Liu

1 Anatomy

The brachial plexus is formed from the ventral rami of C4/5–T1 [1–3]. These nerve roots travel through the over the first rib into the axilla. Descending distally, the nerve roots become trunks, divisions, cords, and eventually the terminal peripheral nerve branches [4].

1. **Trunks**: The three trunks, superior (C5–C6), middle (C7), and inferior (C8, T1), emerge between the anterior and middle scalene muscles and lie on the floor of the posterior triangle of the neck [5]. The borders of the triangle are the posterior border of sternocleidomastoideus anteriorly, anterior border of trapezius posteriorly, and the middle third of the clavicle at the base. It is important to note that the subclavian artery also traverses the triangle. Several peripheral nerves take off before the divisions are formed, important ones include suprascapular nerve (C5–6), long thoracic nerve (C5–7), dorsal scapular nerve (C5), and nerve to subclavius (C5–6).
2. **Divisions**: As the plexus traverses posteriorly to mid clavicle, each trunk divides to form an anterior and posterior division. There are six divisions in total. Generally speaking, anterior divisions supply muscles of anterior compartments (flexors) and the posterior divisions supply muscles of the posterior compartments (extensors).
3. **Cords**: The six divisions then become three cords named in relation to the second part of the axillary artery [5]. The lateral cord is formed from the upper two anterior divisions at the lateral border of the first rib, the lower anterior division continues as the medial cord, and the posterior cord is comprised of the three posterior divisions. The prevertebral fascia of the neck ensheathes the axillary artery and cords. Local anesthetic is injected through this fascial layer when performing the brachial plexus block at this level.
4. **Peripheral nerves**: Distally, the cords become peripheral nerve branches of the brachial plexus [5]. Branches from the lateral cord include: lateral pectoral nerve (C5–C7), musculocutaneous nerve (C5–C7), lateral root of the median nerve (C5–C7). Branches from the medial cord are: medial pectoral nerve (C8, T1), medial cutaneous nerve of the arm (C8, T1), medial cutaneous nerve of the forearm (C8, T1), medial root of the median nerve (C8, T1), ulnar nerve (C8, T1). Branches from the posterior cord are: upper subscapular nerve (C5, C6), thoracodorsal nerve (C6–C8), lower subscapular nerve (C5, C6), radial nerve (C5–T1), axillary nerve (C5, C6) [5].

When performing peripheral nerve blocks, it is important to assess the patient's existing neurologic status, especially the upper extremity to be blocked prior to the procedure. The five main branches of the brachial plexus are: musculocutaneous nerve, axillary nerve, median nerve, radial nerve, and ulnar nerve [5].

1. The musculocutaneous nerve provides motor innervation to coracobrachialis, biceps, and brachialis. Strength can be tested with elbow flexion, humeral adduction, and flexion at the glenohumeral joint. The musculocutaneous nerve also provides cutaneous sensation to the lateral forearm [6], see Fig. 1.
2. The axillary nerve innervates the deltoid and teres minor muscles [7]. These muscles can be tested with shoulder abduction, and lateral rotation of the arm respectively. The nerve also provides sensation to the lateral shoulder. The median nerve innervates the flexor tendons of the wrist [8]. This includes flexor

---

J. Li (✉) · A. Sharma
Department of Anesthesiology, Yale University School of Medicine, New Haven, CT, USA
e-mail: Jinlei.Li@yale.edu; Avijit.sharma@yale.edu

E. Credaroli · N. Vadivelu
Department of Anesthesiology, Yale University, New Haven, CT, USA
e-mail: ellesse.credaroli@yale.edu; Nalini.vadivelu@yale.edu

H. Liu
Department of Anesthesiology & Perioperative Medicine, Hahnemann University Hospital Drexel University College of Medicine, Philadelphia, PA, USA

© Springer Nature Switzerland AG 2021

J. Li et al. (eds.), *Ultrasound Fundamentals*, https://doi.org/10.1007/978-3-030-46839-2_13

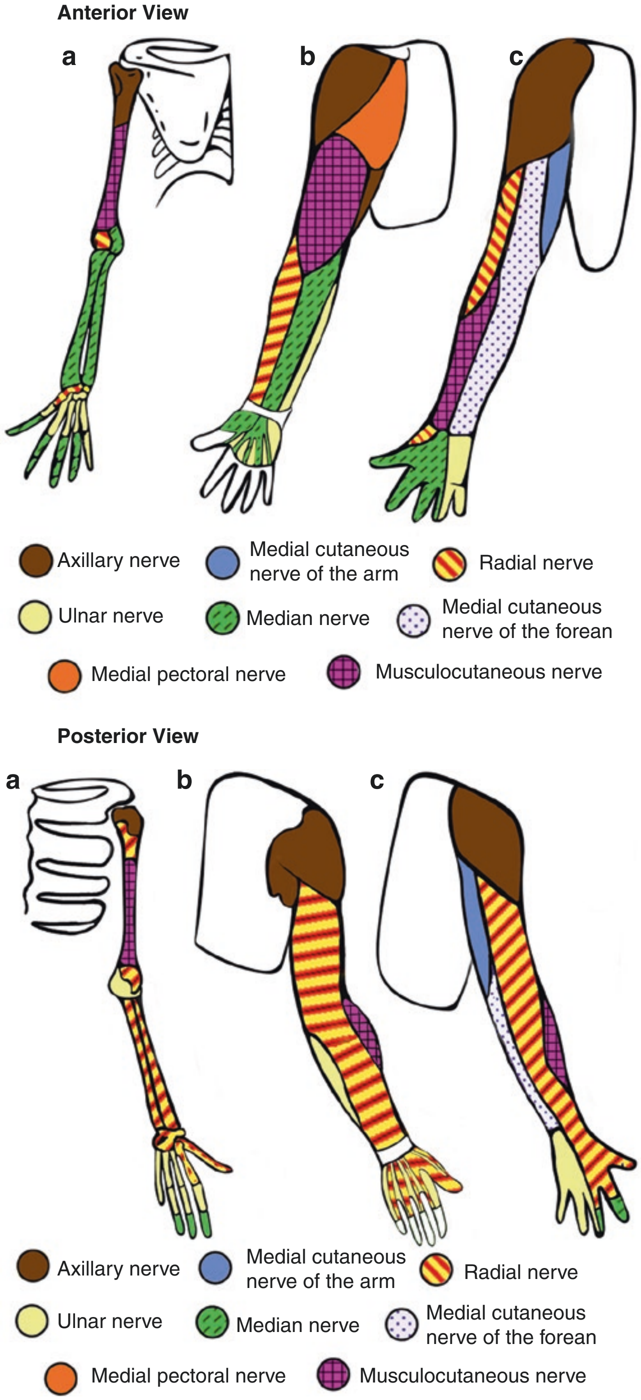
Anterior View
a
b
c
Axillary nerve
Medial cutaneous nerve of the arm
Radial nerve
Ulnar nerve
Median nerve
Medial cutaneous nerve of the forean
Medial pectoral nerve
Musculocutaneous nerve
Posterior View
a
b
c
Axillary nerve
Medial cutaneous nerve of the arm
Radial nerve
Ulnar nerve
Median nerve
Medial cutaneous nerve of the forean
Medial pectoral nerve
Musculocutaneous nerve

Fig. 1 Brachial plexus innervation of the upper extremity: Osteotome (**a**), myotome (**b**) and dermatome (**c**). (Original production with the help of Garrett Sendlewski)

carpi radialis, flexor carpi ulnaris, flexor digitorum superficialis, lateral half of flexor digitorum profundus, palmaris longus, flexor pollicis longus, pronator quadratus, pronator teres, opponens pollicis, abductor pollicis brevis, flexor pollicis brevis, and the first and second lumbricals [8]. Strength can be checked with wrist flexion, pronation of the forearm, abduction of the thumb, and flexion of the thumb at the first metacarpal joint, see Fig. 1.

3. The median nerve provides sensation to the thenar eminence as well as the first three digits anteriorly. Posteriorly, the median nerve innervates the second and third digit distal to the first proximal interphalangeal joint [8]. The fourth digit has dual innervation from median and ulnar nerve, see Fig. 1.
4. The radial nerve innervates the posterior compartment of the arm and forearm [9].These muscles include the triceps, anconeus, brachioradialis, extensor carpi radialis longus, extensor carpi radialis brevis, supinator, extensor digitorum, extensor digitorum minimi, extensor carpi ulnaris, extensor carpi radialis brevis, extensor carpi radialis longus, abductor pollicis longus, extensor pollicis brevis, extensor pollicis longus, extensor indicis. This can be tested by elbow and wrist extension. The radial nerve also provides sensation to the lateral part of the back of the hand as well as the webbed skin between thumb and index finger. It also provides sensory innervation to the posterior arm, elbow, and forearm [9], see Fig. 1.
5. The ulnar nerve innervates flexor carpi ulnaris and the medial half of flexor digitorum profundus [10]. Distally, the radial nerve also supplies palmaris brevis, abductor digiti minimi, flexor digiti minimi, opponens digiti minimi, third and fourth lumbricals, palmar and dorsal interossei muscles, adductor pollicis. The ulnar nerve can be tested abducting and adducting the digits. The ulnar nerve provides cutaneous innervation to both anterior and posterior medial one and a half fingers as well as the hypothenar eminence [10], see Fig. 1.

Although axons from multiple nerve roots go on to become peripheral nerves as the brachial plexus evolves, dermatomes representing a sensory distribution of a single spinal nerve can still be mapped out. In particular, there are certain characteristic points that always fall within each dermatome. For example, the C5 nerve root distribution is on the lateral side of the antecubital fossa proximal to the elbow [11]. C6 is the dorsal surface of the proximal phalanx of the thumb. C7 is the dorsal surface of the proximal phalanx of the middle finger. C8 dorsal surface of the proximal phalanx of the little finger and T1 is on the medial side of the antecubital fossa [11].

2 History

Brachial plexus blockade started with parathesia technique basing on anatomy/body surface landmark, followed by via nerve stimulator. Prior to the adoption of ultrasound, the success rate of brachial plexus blockade has been variable among different medical practitioners. The first documented ultrasound usage in regional anesthesia started with brachial plexus. In 1978 P. La Grange published the first case-series of Doppler ultrasound application for brachial plexus through supraclavicular approach and via visualization of subclavian Artery [12]. In 1989 P. Ting and V. Sivagnanaratnam demonstrated the anatomy of the axilla and observed the spread of local anesthetics during axillary brachial plexus block with B-mode ultrasonography [13]. By 1994 Steven Kapral and colleagues have systemically explored whole brachial plexus blockade using B-mode ultrasound [14]. In current anesthesia practice ultrasound guided brachial plexus blockade is increasingly being utilized for perioperative pain control as well as surgical anesthesia.

3 Indications

Brachial plexus blocks are indicated for any upper extremity procedures, including but not limited to shoulder, arm, elbow, wrist, hand procedures, see Table 1 below.

Table 1 Common upper extremity procedures and options of brachial plexus techniques

Common surgical procedures	Choice of PNBs	Potential adverse events	Clinical pearls
Clavicle	Interscalene brachial plexus block	Phrenic palsy	Addition of cervical plexus block is beneficial
Shoulder	Interscalene brachial plexus block	Phrenic palsy	Addition of Intercostal-brachial block or PEC II is beneficial if biceps tenodesis or rotator cuff repair when an axillary incision (T1–T2) is involved
Proximal Humerus	Interscalene brachial plexus block	Phrenic palsy	
Distal Humerus	Supraclavicular or infraclavicular or axillary brachial plexus block		
Elbow	Supraclavicular or infraclavicular or axillary brachial plexus block		Addition of Intercostal-brachial block or PEC II is beneficial when medial elbow is involved (T1–T2); if the surgeon needs neurological exam intraoperatively or postoperatively, block can be performed postoperatively after a satisfactory assessment of ulnar nerve, or place a catheter preoperatively without local anesthetics until a neurological exam is satisfactory.
Radius/ulna	Supraclavicular or infraclavicular or axillary brachial plexus block		
Wrist	Supraclavicular or infraclavicular or axillary brachial plexus block		
Hand	Supraclavicular or infraclavicular or axillary brachial plexus block		

PNB peripheral nerve block, *PEC II* pectoralis block II

4 Absolute/Relative Contraindications

1. Patient refusal
2. Local or systemic infection
3. Hemodynamic instability
4. Existing neuropathy in the surgical limb
5. Coagulopathy
6. Allergy to local anesthetics
7. The need for neurological exam perioperatively (block can be delayed until satisfactory assessments)
8. Concerns for compartment syndrome

5 Techniques

5.1 Distal Upper Extremity Blocks

Indicated for upper extremity procedures distal to the mid-humerus, commonly encountered are elbow, wrist and hand procedures. Approaches to brachial plexus blockade includes supraclavicular, infraclavicular and axillary brachial plexus blockade [15].

5.2 Supraclavicular Block

The supraclavicular block is a versatile block, also known as the spinal anesthesia for upper extremity. This block traditionally is performed at the divisions when the brachial plexus has the smallest surface area, it can also be performed at the level of the distal trunks/the origin of the divisions, commonly referred to as the high supraclavicular block. The three trunks and six divisions carry sensory and motor innervation for the upper extremity aside from the medial side of the arm which is supplied by T1/T2. This block results in anesthesia and analgesia of C5–T1. With this type of block, it is important to know the position of the pleura to reduce the risk of pneumothorax. The apex of the pleura is contained within the concavity of the first rib. It is also helpful to understand the lateral insertion of the sternocleidomastoid muscle on the medial third of the clavicle can be used as a landmark for the location of the first rib and the edge of the pleura.

To perform the block, the patient is placed in a semi-supine position with the head up at approximately 30° and turned to the contralateral side. Slight elevation of the head is preferred as this allows for increased venous drainage from the head, reducing vein engorgement in the neck. Once the field has been disinfected and sterility achieved, the ultrasound transducer is placed along the superior edge of the clavicle in line with the length of the bone. Place the linear probe along the clavicle as lateral as possible and then scan medially; the first artery encountered is the subclavian artery. The brachial plexus in the supraclavicular fossa sits lateral to the artery and superficial to the first rib (a bright/echogenic bone line with a shadow below) and the pleural (bright/echogenic line that moves with respiration, so called shimmering sign), see Fig. 2. The first needle path should be directed toward the “corner pocket” (i.e., the junction of the first rib and the subclavian artery, where divisions from the C8 and T1 are located). After a successful injection at the corner pocket, local anesthetics should lift the brachial plexus up from the first rib. The second injection can be given on top of the plexus.

A failed brachial plexus block via supraclavicular approach is commonly associated with ulnar nerve-sparing, which is nearly always due to the “corner pocket” failure when divisions from C8/T1 are not properly blocked. This can be prevented by the injection of local anesthetic above the first rib and lateral to the subclavian artery as stated above. Potential adverse events from this block include pneumothorax, hemothorax, Horner’s syndrome, and diaphragmatic paralysis. Risk of pneumothorax in the supraclavicular block is high with the blind technique in the past but has been significantly decreased with ultrasound guidance [1].

5.3 Infraclavicular Brachial Plexus Block

The infraclavicular block is performed at the level of the three cords, lateral cord, posterior cord and medial cord. The three cords carry sensory and motor innervation for the upper extremity aside from the medial side of the arm which is supplied by T1/T2. This block results in anesthesia and analgesia of C5–T1. With this type of block, it is important to know the position of axillary artery and vein as the three cords surround the axillary artery and the medial cord is located between the axillary artery and vein. On the other hand, pleural is far from the brachial plexus at this point, therefore pneumothorax is much less of a concern as compared to supraclavicular approach of the brachial plexus blockade.

To perform the block, the patient is placed in a semi-supine position, arm abducted at 90°, with the head up at approximately 30° and turned to the contralateral side. Once the field has been disinfected and sterility achieved, the ultrasound transducer is placed along the deltopectoral groove, the indentation in the muscular structure between the deltoid muscle and pectoralis major. The needle trajectory will be in a medial to lateral and cephalad to caudad direction to minimize the risks of pneumothorax, see Fig. 2. Deposition of local anesthetics around each cord provides the fastest onset of blockade effects. This block is the best location for brachial plexus catheter placement for distal upper extremity procedures as the pectoralis minor and major muscles help to secure the catheter in place. On the other hand, these muscles also make the brachial plexus in a deeper location and therefore this block technically speaking more challenging block as compared to other brachial plexus blockade techniques.

Potential adverse events from this block include vascular puncture, failed block, but less risk of diaphragmatic paralysis as compared to interscalene or supraclavicular blocks.

5.4 Axillary Brachial Plexus Block

The name comes from the approach of the brachial plexus block, therefore should be distinguished from the axillary nerve block, which targets the peripheral nerve that branches off the posterior cord proximally.

Fig. 2 Ultrasonographic presentations of brachial plexus. Panel (**a**) shows patient and probe positioning for interscalene block. Panel (**b**) shows positioning for supraclavicular block. Panel (**c**) is a sonographic image that corresponds to panels (**a**) and (**d**) corresponds to panel (**b**). SCM: sternocleidomastoid muscle, ASM: anterior scalene muscle, MSM: middle scalene muscle. The yellow arrows depict brachial plexus, the red arrow depicts subclavian artery, and the white arrow points towards the first rib, the orange arrow points at the pleural. Panel (**e**) shows patient and probe positioning for infraclavicular block while panel (**f**) shows positioning for axillary brachial plexus block. Panel (**g**) is a sonographic image that corresponds to panels (**e**) and (**h**) corresponds to panel (**f**). The red arrow points towards axillary artery. In panel (**g**), the cephalad most yellow arrow points towards the lateral cord while the inferior arrow points towards posterior cord. The caudal arrow points towards medial cord. In panel (**h**), the most medial arrow points at ulnar nerve while the inferior arrow points towards radial nerve. The superior arrow points at medial nerve. The lateral arrow points at musculocutaneous nerve. PMa: pectoralis major, PMI: pectoralis minor, CoBM: coracobrachialis muscle

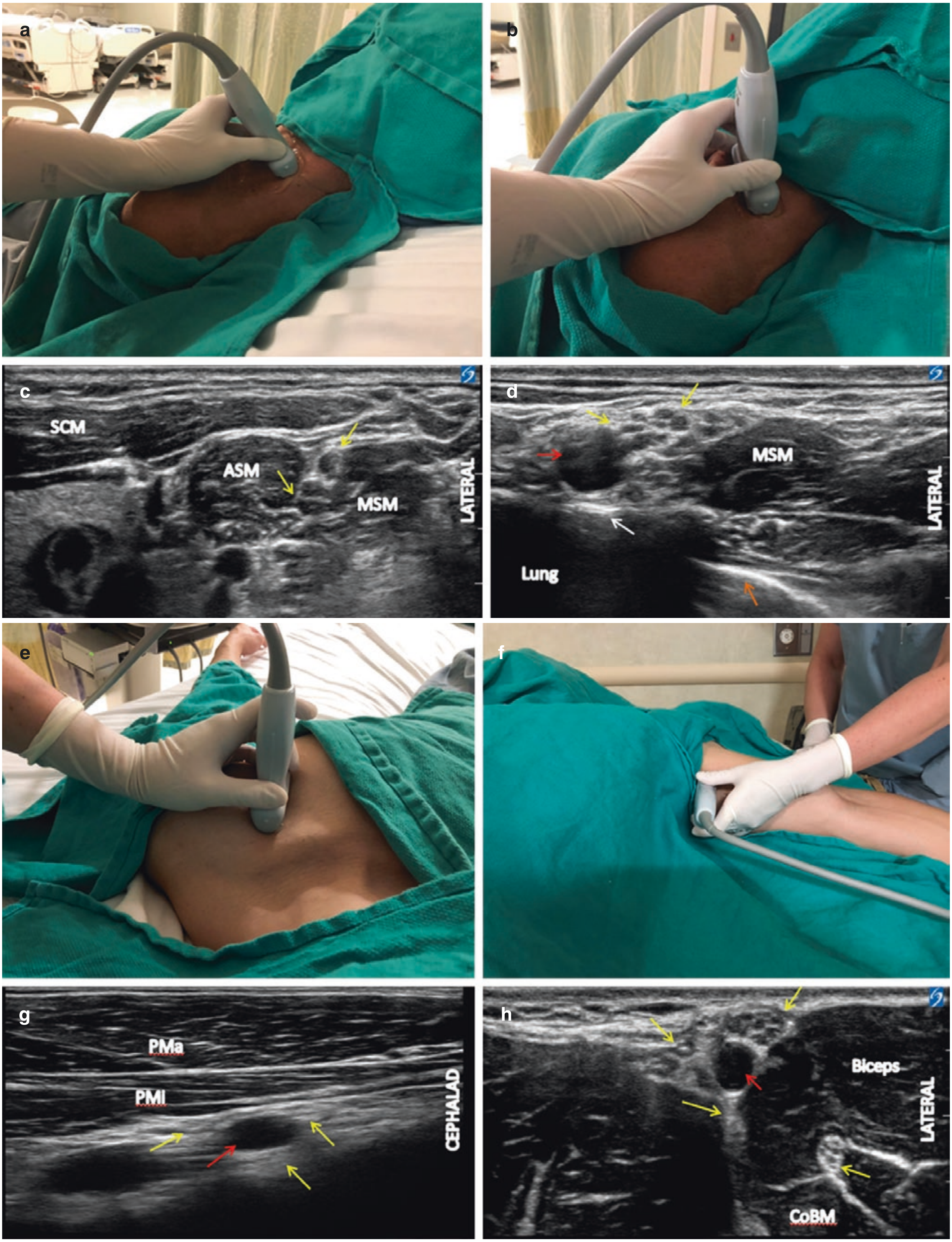
a
b
c
SCM
ASM
MSM
LATERAL
d
MSM
Lung
LATERAL
e
f
g
PMa
PMI
CEPHALAD
h
Biceps
LATERAL
CoBM

The main anatomical points of interest at this level of the brachial plexus are the median, ulnar, and radial nerves, as the axillary, musculocutaneous, and medial brachial cutaneous nerves have branched off the brachial plexus. Axillary brachial plexus block (when including the musculocutaneous nerve, which needs to be blocked separately) provides analgesia from the mid-arm down to the hand, making it an alternative approach to the supraclavicular or infraclavicular block for elbow, forearm, wrist, and hand surgery.

The musculocutaneous nerve is readily visualized and reliably anesthetized by a separate injection using ultrasound guidance, see Fig. 2. When required, the medial skin of the upper arm (T1/T2) can be blocked by an additional subcutaneous injection just distal to the axilla (intercostobrachial nerve), via ultrasound guided intercostal T2 nerve block, or through ultrasound guided Pectoral nerve block II (PEC II).

To perform the axillary brachial plexu block under ultrasound guidance, first position the patient supine, abduct the arm to 90° resting comfortably on a table, and rotate the head to the contralateral side. Using the short axis view of the linear transducer, the axillary artery, median, ulnar, and radial nerves can be identified. The axillary artery can be identified medially on the proximal arm. One or more axillary veins can be identified medially to the artery when avoiding excessive pressure with an ultrasound transducer. Further scanning laterally and cephalad will localize the musculocutaneous nerve, see Fig. 2.

When compared with interscalene and supraclavicular blocks, there may be lower risk of complications ie spinal cord and vertebral artery puncture (interscalene) or pneumothorax (supraclavicular). On the other hand, local anesthetic systemic toxicity seems to be more associated with this approach than others. The axillary brachial plexus block are typically utilized in clinical scenarios where access to the upper portions of the brachial plexus is limited (for example in patients with extensive ipsilateral neck dissection, head/neck radiation therapy due to head/neck cancer, morbid obesity). Under these circumstances, the brachial plexus blockade can be achieved with administering local anesthetic around the axillary artery. Multiple injections are usually required to reliably anesthetize the entire arm distal to the elbow. The radial branch of the brachial plexus is identified posterior and lateral or medial to the artery. The ulnar branch of the nerve is located superficial and lateral to the artery. The median branch is located superficially and laterally to the artery. These localizations can vary and the definitive nerve localization can be assisted with nerve stimulation techniques, though it is not absolutely necessary for the success of the block. The biceps (anterior and superficial), the coracobrachialis (anterior and deep) and the conjoined tendon of the teres major and latissimus dorsi (medial and posterior) surround the neurovascular bundle. The musculocutaneous nerve is located between the biceps and coracobrachialis muscles, but can also be located in either muscle, see Fig. 2.

The axilla is highly vascularized, small veins can be injured during needle placement resulting in an increased risk for uptake of local anesthetic and therefore local anesthetic systemic toxicity [1]. Catheter placement is not optimal with increased risk for infection and catheter dislodgement.

5.5 Proximal Upper Extremity Block

Indicated for any upper extremity procedure proximal to the mid-humerus, commonly encountered are the shoulder and proximal humerus procedures. Commonly utilized approach is interscalene brachial plexus block [15].

5.6 Interscalene Block

The interscalene block is indicated for shoulder and proximal humerus surgery. This is a block of the brachial plexus at the nerve roots/trunks level. This block is not recommended for hand surgery due to potential sparing of the inferior trunk and inadequate blockade of C8 and T1 nerve roots.

To perform the block, the patient is laid semi-supine with head up and turned contralaterally to the side of the block. Once the field has been disinfected and sterility achieved, the ultrasound transducer is placed in a transverse plane at the level of the cricoid cartilage (C6). After identifying the carotid artery, the probe is moved laterally to bring the anterior and middle scalene muscles into view. Between these structures is the brachial plexus. Alternatively, another technique to achieve interscalene view is to start from supraclavicular view and move probe upwards to achieve the classic traffic light sign of the three nerve roots between two muscles, anterior scalene muscle medially and middle scalene muscle laterally, see Fig. 2. After an adequate picture is obtained, a skin wheal is created with local anesthetic, after which the needle can be advanced in-plane and laterally to medially. A “pop” may be heard as the needle pierces through prevertebral fascia. Once the needle is adjacent to but not in the plexus, aspirate to ensure the needle is not in a blood vessel. Local anesthetic can then be injected lateral to the nerve roots and medial to the middle scalene muscle to complete the block. A known adverse event of this block is Horner’s syndrome which is the sympathectomy caused by blocking the sympathetic chain. This results in ipsilateral miosis, ptosis, and anhydrosis. This is self-resolved and should be mentioned to patients or family member during consenting process.

Interscalene block is associated with ones the highest risks of nerve injury in all peripheral nerve blocks with or without ultrasound guidance, including injury to dorsal scapular nerve, long thoracic nerve [16], and long term postoperative plexopathy [17]. Efforts should be made to avoid performing this block under general anesthesia and there is no need to inject into or between the nerve roots.

Summary of the commonly utilized brachial plexus blockade are listed in Table 2 below.

Table 2 Common approaches to brachial plexus blockade

Brachial plexus blocks	Block level	Clinical pearls
Interscalene brachial plexus block	Root/trunk (also called superior trunk approach [16])	Nearly 100% phrenic nerve involvement, but not all patients are clinically symptomatic. For procedures mid-humerus and above, missing C8–T1/ulnar nerve distribution
Supraclavicular brachial plexus block	Divisions	Less risk of phrenic palsy, suprascapular nerve frequently takes off earlier, one of the reasons that this block may not provide complete analgesia for shoulder procedure
Infraclavicular brachial plexus block	Cord	Much less risk of phrenic palsy, suprascapular nerve frequently takes off earlier, one of the reasons that this block may not provide complete analgesia for shoulder procedure
Axillary brachial plexus block	Several peripheral nerves	Minimum, if any, risk of phrenic palsy, muscular cutaneous nerve needs to be blocked separately

6 Conclusions

Brachial plexus is formed by C4–T1 and provides innervation to the upper extremity. Its location is relatively superficial and its blockade can mostly be achieved quickly and effectively by a liner probe using B-mode ultrasound. Various approaches of brachial plexus blockade offer clinicians the options of difference blocks serving different purpose, such as hand-sparing brachial plexus block for shoulder procedures using interscalene blocks, phrenic nerve sparing block in patients with severe pulmonary comorbidities by using axillary brachial plexus blocks. Brachial plexus blockade can be used alone by providing complete analgesia to the surgical upper extremity or as a complement to general anesthesia. An effective block helps with early recovery after surgery, opioid reduction, better pain control, PACU turn over as well as patient satisfaction [18].

For procedures proximal to mid-humerus, traditionally interscalene brachial plexus block is the choice of technique for efficacy. The inherent association of interscalene block with transit or persistent ipsilateral hemi-diaphragmatic paralysis should be put into consideration not necessarily in the healthy patients but definitely for those with existing respiratory conditions [19]. The search for alternative phrenic sparing blocks has never ceased. Alternative approaches of brachial plexus block such as the supraclavicular brachial plexus block [20], as well as upper trunk approach of interscalene block have been described with [21] or without [16] the addition of supraclavicular nerve from cervical plexus. Much attention has been focused on two peripheral nerve, the suprascapular nerve and axillary nerve. The suprascapular nerve block alone [19, 20], suprascapular block in conjunction with axillary nerve block [22], suprascapular block in combination with supraclavicular brachial plexus block [23], suprascapular block in combination with infraclavicular brachial plexus block [24], have all been investigated. It has also been shown that lateral pectoral nerve and subscapular nerve [25, 26] are also involved in shoulder pain. As of now, the effectiveness of these alternative blocks as compared to the gold standard interscalene brachial plexus block is evolving and the results are more mixed than definitive [27, 28], likely due to the complexed anatomy of glenohumeral joint innervation [25, 26].

Acknowledgement The authors would like to thank Mr. Garrett Sendlewski at Yale University Department of Anesthesiology for illustration.

References

1. Neal JM, Brull R, Chan VW, et al. The ASRA evidence-based medicine assessment of ultrasound-guided regional anesthesia and pain medicine: executive summary. Reg Anesth Pain Med. 2010;35(2 Suppl):S1–9.
2. Barrington MJ, Kluger R. Ultrasound guidance reduces the risk of local anesthetic systemic toxicity following peripheral nerve blockade. Reg Anesth Pain Med. 2013;38(4):289–99.
3. Wilbourn AJ. Iatrogenic nerve injuries. Neurol Clin. 1998;16(1):55–82.
4. Kim HJ, Park SH, Shin HY, Choi YS. Brachial plexus injury as a complication after nerve block or vessel puncture. Korean J Pain. 2014;27(3):210–8.
5. Limthongthang R, Bachoura A, Songcharoen P, Osterman AL. Adult brachial plexus injury: evaluation and management. Orthop Clin North Am. 2013;44(4):591–603.
6. Besleaga D, Castellano V, Lutz C, Feinberg JH. Musculocutaneous neuropathy: case report and discussion. HSS J. 2010;6(1):112–6.
7. McClelland D, Paxinos A. The anatomy of the quadrilateral space with reference to quadrilateral space syndrome. J Shoulder Elb Surg. 2008;17(1):162–4.
8. Isaacs J, Ugwu-Oju O. High median nerve injuries. Hand Clin. 2016;32(3):339–48.
9. Ljungquist KL, Martineau P, Allan C. Radial nerve injuries. J Hand Surg Am. 2015;40(1):166–72.
10. Woo A, Bakri K, Moran SL. Management of ulnar nerve injuries. J Hand Surg Am. 2015;40(1):173–81.
11. Kirshblum SC, Burns SP, Biering-Sorensen F, et al. International standards for neurological classification of spinal cord injury (revised 2011). J Spinal Cord Med. 2011;34(6):535–46.

12. la Grange P, Foster PA, Pretorius LK. Application of the Doppler ultrasound bloodflow detector in supraclavicular brachial plexus block. Br J Anaesth. 1978;50(9):965–7.
13. Ting PL, Sivagnanaratnam V. Ultrasonographic study of the spread of local anaesthetic during axillary brachial plexus block. Br J Anaesth. 1989;63(3):326–9.
14. Kapral S, Krafft P, Eibenberger K, Fitzgerald R, Gosch M, Weinstabl C. Ultrasound-guided supraclavicular approach for regional anesthesia of the brachial plexus. Anesth Analg. 1994;78(3):507–13.
15. Huang J, Li J, Wang H. The principles and procedures of ultrasound-guided anesthesia techniques. Cureus. 2018;10(7):e2980.
16. Burckett-St Laurent D, Chan V, Chin KJ. Refining the ultrasound-guided interscalene brachial plexus block: the superior trunk approach. Can J Anaesth. 2014;61(12):1098–102.
17. Sites BD, Taenzer AH, Herrick MD, et al. Incidence of local anesthetic systemic toxicity and postoperative neurologic symptoms associated with 12,668 ultrasound-guided nerve blocks: an analysis from a prospective clinical registry. Reg Anesth Pain Med. 2012;37(5):478–82.
18. Hadzic A, Williams BA, Karaca PE, et al. For outpatient rotator cuff surgery, nerve block anesthesia provides superior same-day recovery over general anesthesia. Anesthesiology. 2005;102(5):1001–7.
19. Kumara AB, Gogia AR, Bajaj JK, Agarwal N. Clinical evaluation of post-operative analgesia comparing suprascapular nerve block and interscalene brachial plexus block in patients undergoing shoulder arthroscopic surgery. J Clin Orthop Trauma. 2016;7(1):34–9.
20. Auyong DB, Yuan SC, Choi DS, Pahang JA, Slee AE, Hanson NA. A double-blind randomized comparison of continuous interscalene, supraclavicular, and suprascapular blocks for total shoulder arthroplasty. Reg Anesth Pain Med. 2017;42(3):302–9.
21. Lin JA, Chuang TY, Yao HY, Yang SF, Tai YT. Ultrasound standard of peripheral nerve block for shoulder arthroscopy: a single-penetration double-injection approach targeting the superior trunk and supraclavicular nerve in the lateral decubitus position. Br J Anaesth. 2015;115(6):932–4.
22. Dhir S, Sondekoppam RV, Sharma R, Ganapathy S, Athwal GS. A comparison of combined suprascapular and axillary nerve blocks to interscalene nerve block for analgesia in arthroscopic shoulder surgery: an equivalence study. Reg Anesth Pain Med. 2016;41(5):564–71.
23. Trabelsi W, Ben Gabsia A, Lebbi A, Sammoud W, Labbene I, Ferjani M. Suprascapular block associated with supraclavicular block: an alternative to isolated interscalene block for analgesia in shoulder instability surgery? Orthop Traumatol Surg Res. 2017;103(1):77–83.
24. Aliste J, Bravo D, Finlayson RJ, Tran DQ. A randomized comparison between interscalene and combined infraclavicular-suprascapular blocks for arthroscopic shoulder surgery. Can J Anaesth. 2018;65(3):280–7.
25. Eckmann MS, Bickelhaupt B, Fehl J, et al. Cadaveric study of the articular branches of the shoulder joint. Reg Anesth Pain Med. 2017;42(5):564–70.
26. Hebert-Blouin MN, Tubbs RS, Carmichael SW, Spinner RJ. Hilton's law revisited. Clin Anat. 2014;27(4):548–55.
27. Tran DQ, Elgueta MF, Aliste J, Finlayson RJ. Diaphragm-sparing nerve blocks for shoulder surgery. Reg Anesth Pain Med. 2017;42(1):32–8.
28. Bansal V, Shastri U, Canlas C, Gadsden JC. Diaphragm-sparing nerve blocks for shoulder surgery: an alternative approach. Reg Anesth Pain Med. 2017;42(4):544–5.

Hip Joint Sonoanatomy and Ultrasound-Guided Hip Joint Injection

Jason Kajbaf and George C. Chang Chien

Introduction

The hip, one of the most mobile joints, is amongst the most commonly injured regions in the human body. Furthermore, the hip is large and composed of numerous soft tissue and neurovascular structures, of which a large portion may be viewed with ultrasound imaging. The following will review the anatomy of the hip as seen with ultrasound, as well as review both diagnostic and interventional application of ultrasound with regard to the hip.

1 Anterior Hip Anatomy

The "hip" is a ball-and-socket synovial joint: the ball is the femoral head, and the socket is the acetabulum. The hip joint is the articulation of the pelvis with the femur, which connects the axial skeleton with the lower extremity. A smooth cushion of shiny white articular cartilage about 1/4 inch thick covers the femoral head and the acetabulum. Large ligaments, tendons, and muscles around the hip joint hold the bones (ball and socket) in place and keep it from dislocating. In order to help identify the structures of the anterior hip, this region may be divided into two layers, superficial and deep. The superficial layer consists of the Sartorius and Tensor Fascia Lata muscles, which originate from the anterior and lateral aspects of the anterior superior iliac spine, respectively (Fig. 1) [1]. Subsequently, the deep layer from lateral to medial is composed of the rectus femoris, iliopsoas, and pectineus muscles (Fig. 1). The rectus femoris, which is part of the quadriceps femoris muscle group, originates predominantly from the anterior inferior iliac spine; however, it also has originating fibers from the superior acetabular ridge and anterior capsule of the hip joint [1]. The iliopsoas muscle originates from two separate muscle bellies, the psoas muscle from the T12 to L5 vertebrae, and the iliacus, which primarily originates from the iliac fossa and iliac crest. These two muscles come together to form the iliopsoas as they pass through the anterior hip, and continue to travel and insert as a common tendon into the lesser trochanter of the femur [2]. The pectineus, which is part of the adductor muscle group, is seen in the anterior compartment under ultrasound, just deep to the femoral artery and vein, forming the floor of the femoral triangle [2]. Lastly, the neurovascular structures in the anterior hip are closely related to the iliopsoas muscle. The femoral nerve and lateral femoral cutaneous nerves run anteromedially and anterolaterally, respectively, to the iliopsoas as it courses beneath the inguinal ligament [2]. The femoral artery and vein, in turn, run medial to the iliopsoas muscle, just superficial to the pectineus muscle [2].

2 Anterior Hip Pathology

2.1 Hip Osteoarthritis Injection

Although ultrasound is not the best modality to diagnose osteoarthritis of the hip, it is an effective means to the treatment of such when it has been diagnosed. The ultrasound probe, commonly a low frequency curvilinear transducer, is placed in an oblique plane on the anterior hip parallel with the femoral neck. In this view, the anterior synovial recess, which is the inferior extension of the anterior joint capsule seen at the femoral head-neck junction (Fig. 2a) [3]. This synovial space is commonly widened in the setting of a joint effusion, which is commonly seen in the setting of osteoarthritis. In a normal hip joint, there is commonly less than 2 mm of fluid in this synovial space [4]. Furthermore, once this space is identified, the anterior acetabular labrum can be visualized as a triangular hyperechoic structure. Once the joint space is identified, the transducer should be rotated to

---

J. Kajbaf (✉)
University of California, Los Angeles, Department of PM&R, Los Angeles, CA, USA

G. C. Chang Chien
GCC Institute, Newport Beach, CA, USA

Ventura County Medical Center, Ventura, CA, USA

© Springer Nature Switzerland AG 2021
J. Li et al. (eds.), *Ultrasound Fundamentals*, https://doi.org/10.1007/978-3-030-46839-2_14

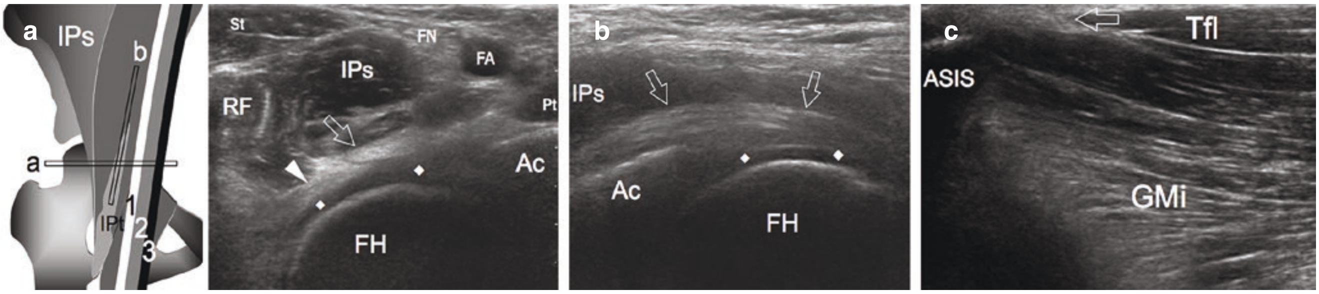

Fig. 1 (**a**) Transverse view of the anterior region of the hip just inferior to the anterior inferior iliac spine. Superficially, the Sartorius (St) is clearly visible. Slightly deeper, from lateral to medial, the rectus femorus (RF), Iliopsoas muscle (IPs), Femoral nerve (FN), and Femoral artery (FA), and Pectineus are seen. Deep structures including the anterior hip capsule (arrowhead), and the iliopsoas tendon (arrow) are visible, with the acetabulum (Ac) seen just medial to the femoral head (FH). (**b**) Longitudinal view of the anterior hip, again demonstrating the iliopsoas muscle (IPs) along with its deeper tendon (arrows). Just deep to the iliopsoas tendon, the anterior portion of the hip joint may be seen (diamonds), formed by the acetabulum (Ac) and femoral head (FH). (**c**) In order to get a view of the tensor fascia lata (Tfl) while in longitudinal plane, the transducer may be moved to the lateral portion of the anterior hip

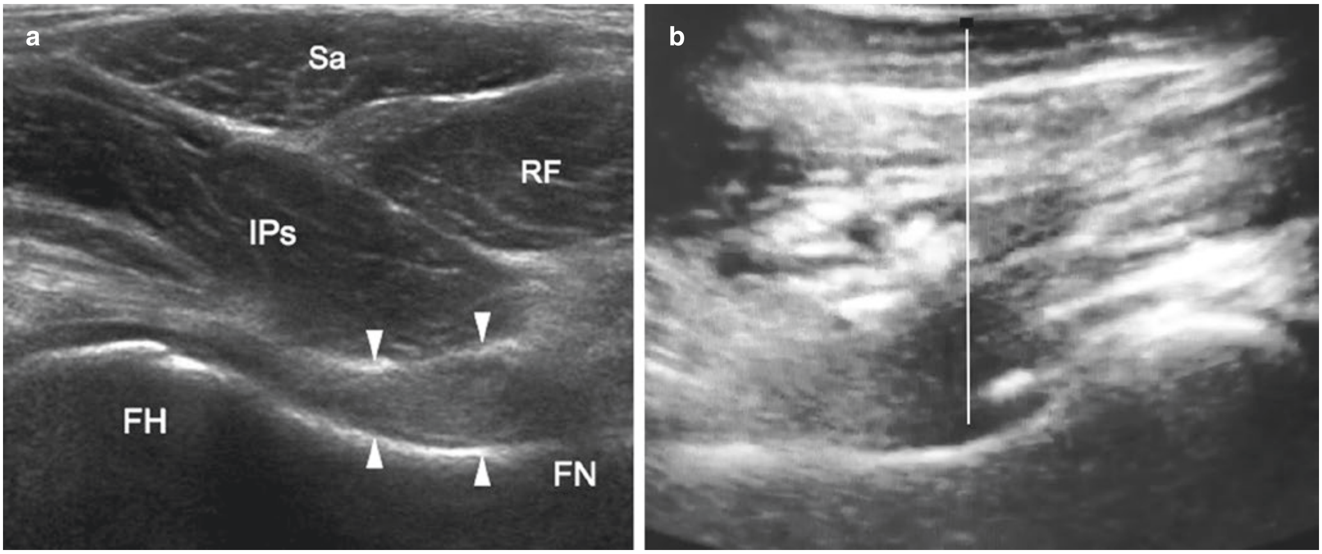

Fig. 2 (**a**) Transverse oblique view of the anterior hip at the level of the femoral head-neck junction (FH, FN) best demonstrates the anterior recess of the hip joint. This figure demonstrates an active joint effusion (arrowheads). This is the location where a needle may be introduced to perform an intra-articular hip injection under ultrasound. Superficial to the joint space lies the iliopsoas (IPs), rectus femoris (RF), and sartorius (Sa) muscles. (**b**) Transverse oblique view of the anterior hip at the level of the femoral head-neck junction. Here a needle can be introduced out of plane at the head-neck junction. As the solution is injected, it can be seen migrating throughout the joint capsule

the transverse plane and moved medially to identify the neurovascular bundle in order to ensure that these are avoided during the injection procedure. Once the neurovascular bundle has been identified, the transducer should then be rotated to the oblique view to again identify the joint space [4]. At this point, a needle can be safely inserted, in-plane or out-of plane to the target area, typically the head and neck junction of the femur. (Fig. 2b).

2.2 Snapping Hip Syndrome Diagnosis

Snapping hip syndrome is divided into two different etiologies, intra-articular or extra-articular. Intra-articular snapping hip syndrome is commonly due to labral tears, loose bodies, ligamentum teres tears, or even joint instability [5]. Extra-articular causes of snapping hip syndrome; however, can be further divided into two different categories: external or internal. External, the most common form of snapping hip syndrome, is attributed to the snapping of the posterior aspect of the iliotibial band or anterior aspect of the gluteus maximus tendon over the greater trochanter [5]. Internal is primarily due to snapping of the iliopsoas tendon over the iliopectineal eminence, or less commonly, the femoral head or lesser trochanter (Fig. 3). The snapping of the iliopsoas tendon over the iliopectineal eminence may be seen under dynamic ultrasound [5]. In order to perform dynamic ultrasound of snapping hip syndrome, the transducer should be placed transversely at the level of the ilium and the patient is then asked to flex, abduct, and externally rotate the hip [5].

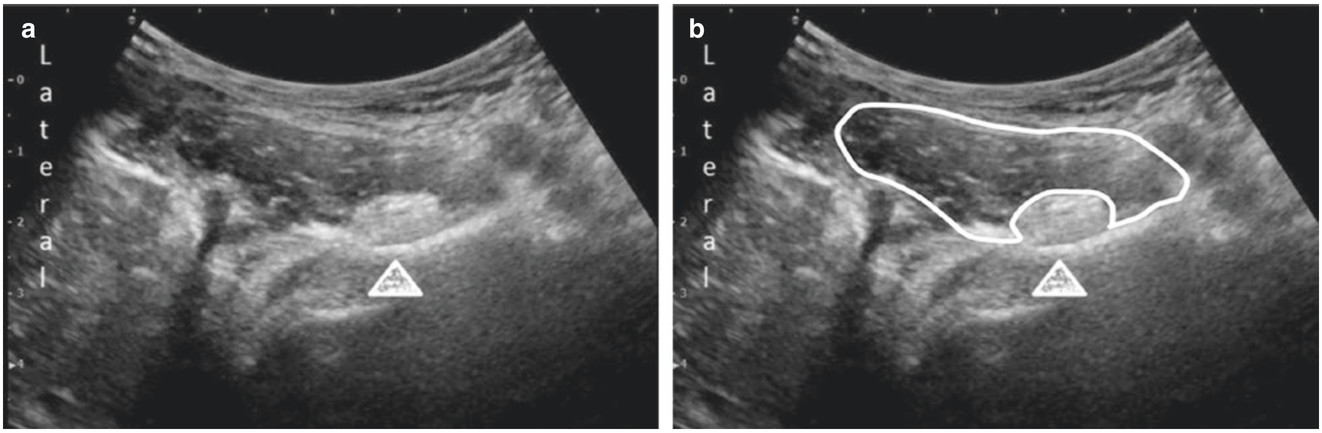

Fig. 3 Iliopsoas tendon at the level of the iliopectineal line. (**a**) Arrowhead pointing to the normal, hyperechoic psoas tendon. (**b**) The illiacus is the muscle that surrounds the psoas tendon at this level. They will fuse into the Iliopsoas tendon and insert at the lesser tubercle

2.3 Iliopsoas Tendinopathy/Bursitis Diagnosis and Injection

The psoas and iliacus muscles originate from the lumbar spine (transverse processes of T12 -L5) and pelvis (superior anterior iliac crest), which continue down the anterior hip merging into a single common tendon and inserting onto the lesser trochanter of the femur [6]. The iliopsoas muscle passes anterior to the pelvic brim and hip capsule in a groove between the anterior inferior iliac spine laterally and iliopectineal eminence medially. The musculotendinous junction is consistently found at the level of this groove. The iliopsoas bursa lies between the musculotendinous junction and the pelvic brim [7]. Overuse injury may occur in activities involving repeated hip flexion or external rotation of the thigh. Motions that call for repeated trunk flexion with hip flexion create a continuous shortening of the iliopsoas, which can exacerbate iliopsoas tendinopathy [8]. Younger athletes who engage in dynamic movements (jumpers, hurdlers) including forceful hip flexion are at higher risk. Reports of an audible snap or click in the hip or groin commonly are reported and associated with internal snapping hip syndrome as discussed earlier [9]. Repeated "snapping" can cause tendinopathy, and bursitis. Treatments options include physical therapy (stretching of hip flexors), acetaminophen and NSAIDs. Differential diagnosis includes hip OA, osteonecrosis of the femur and lumbosacral radiculopathy.

For an injection of the iliopsoas tendon, the patient is positioned in supine and the transducer is placed in a transverse oblique angle, parallel to the inguinal ligament, and superior to the femoral head, over the iliopectineal eminence (similar to viewing snapping hip syndrome). The bursa is at the interface between the bone and the tendon. The femoral neurovascular bundle, which lies medial to the femoral head, should be identified before proceeding with injection. Then, utilizing an in-plane approach from lateral to medial, a needle is advanced to the deep lateral region of the iliopsoas tendon, either between the tendon and iliopectineal ridge, or tendon and acetabular rim (Fig. 4) [4].

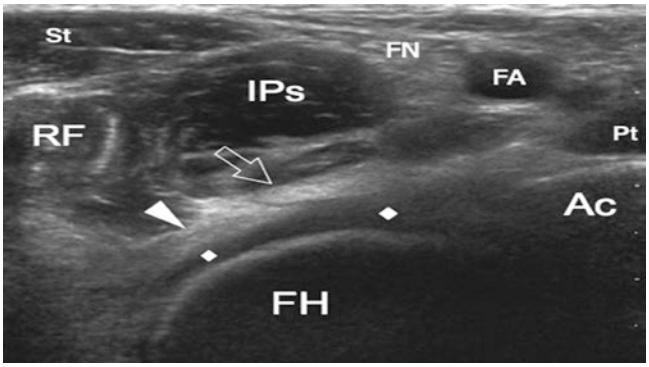

Fig. 4 Iliopsoas tendon in short axis. The triangle points to the hyperechoic tendon. The white line demonstrates the needle trajectory

2.4 Rectus Femoris Tear Diagnosis

The rectus femoris is the most commonly injured anterior thigh muscle; however, is much more prevalent at the distal attachment or within the central aponeurosis in the muscle belly, rather than proximally at the level of the hip [10]. These injuries, though, are most commonly seen among athletes, primarily soccer players. Proximal rectus tears, both partial or complete are readily visible with a high frequency transducer in both axial and longitudinal planes, beginning at the level of the anterior inferior iliac spine, and slowly moving inferiorly, medially and laterally (Fig. 5) [10].

3 Medial Hip Anatomy

The medial hip, from a musculoskeletal viewpoint, is not as complex or involved as the other parts of the hip. The medial hip is comprised of the adductor muscle group, and from

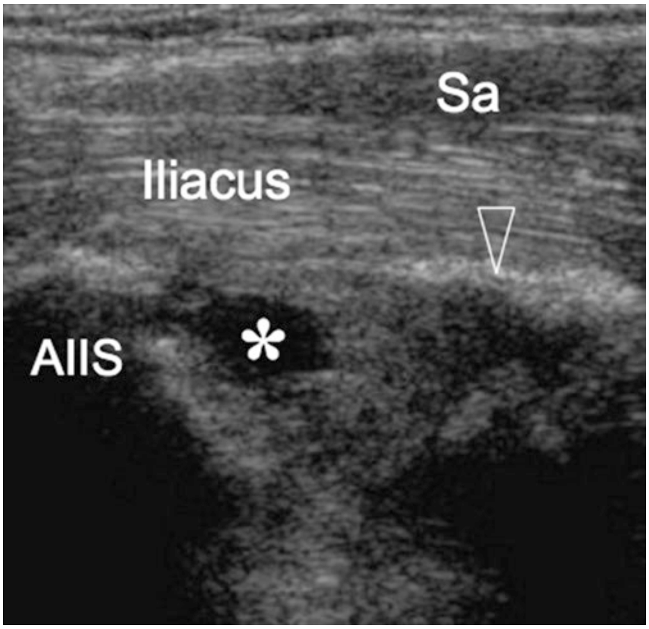

Fig. 5 Long axis view of the rectus femoris at its insertion point at the level of the anterior inferior iliac spine. The intact iliacus and Sartorius (Sa) are seen overlying the origin of the rectus femoris (arrowhead), which is retracted due to a tear. The hypoechoic area (asterisk) represents a hematoma formed due to the tear

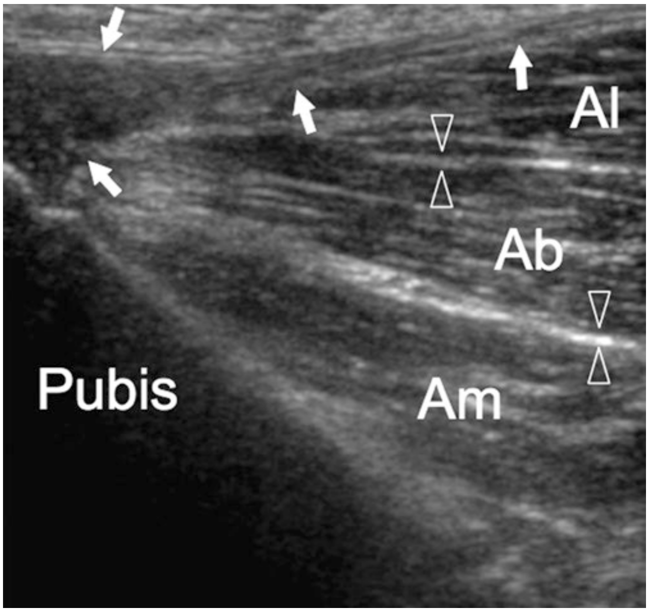

Fig. 6 Long-axis view of the medial hip. Superficially, the adductor longus muscle belly's (Al) tendons (arrows) converge proximally at pubis, the proximal attachment of the adductor longus. The adductor brevis (Ab), just deep to the adductor longus may be better differentiated via the intermuscular fascia (arrowheads). Again obviously distinct from the adductor brevis due to the intermuscular fascia, the adductor magnus (Am) lies deepest of all the adductor muscles

deep to superficial lie the adductor magnus (laterally) and gracilis (medially), followed by the adductor brevis and adductor longus muscles (Fig. 6) [1].

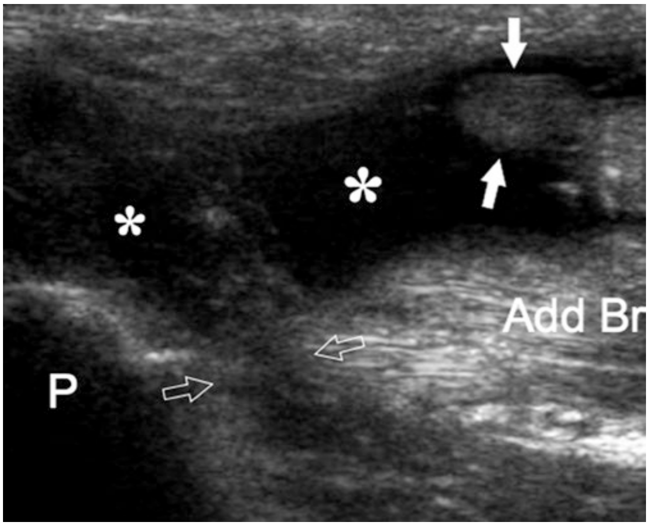

Fig. 7 Long-axis view of the medial hip demonstrating a combined tear of the adductor longus (white arrows), and the deeper adductor brevis muscle (empty arrows) at its insertion at the pubis (P). The areas of hypoechogenecity demonstrate hematomas due to the adjacent tears

4 Medial Hip Pathology

4.1 Adductor Tear

Adductor tears are not commonly encountered in the general population, and are typically more associated with athletes (soccer) after an injury with hip hyper-abduction [11]. The adductor longus and gracilis muscles are the most commonly affected adductor muscles [12]. When presented with a patient with acute groin pain and an adductor tear is suspected, ultrasound may be used to visualize possible pathology. Partial tears may be evident by irregularities among the tendon fibers, with areas of hypoechogenicity. However, full tears of the adductor longus or gracilis would demonstrate complete separation of the tendon from the pubis, with an area of hypoechogenicity between the pubis and torn tendon, representing hematoma formation (Fig. 7) [1].

5 Lateral Hip Anatomy

The lateral hip is a commonly seen injury in the general population. This area of the hip may be divided into a superficial and deep component. The anterior portion of the gluteus maximus and tensor fascia lata form the superficial group, and both of these muscles insert themselves into the iliotibial band, which continues down the lateral thigh and inserts into the lateral tibia [2]. The gluteus medius and minimus comprise the deeper component of the lateral hip (with the gluteus minimus lying just deep to the gluteus medius). Both of these muscles continue to across the hip and insert into the greater trochanter, thereby functioning as strong hip abductors (Fig. 8).

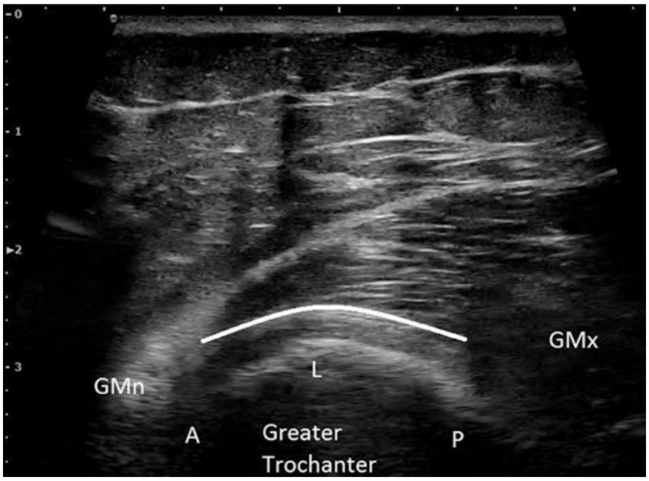

Fig. 8 Ultrasound appearance of a normal greater trochanter with (A) anterior facet where (GMn) gluteus minimus attaches, (L) lateral facet where gluteus medius attaches, and (P) posterior facet where (GMx) gluteus maximus overlies. The *white line* depicts the superior border of the gluteus medius tendon and the target of the greater trochanter bursa injection. Needle fenestration can be performed into the tendon in areas of pathology

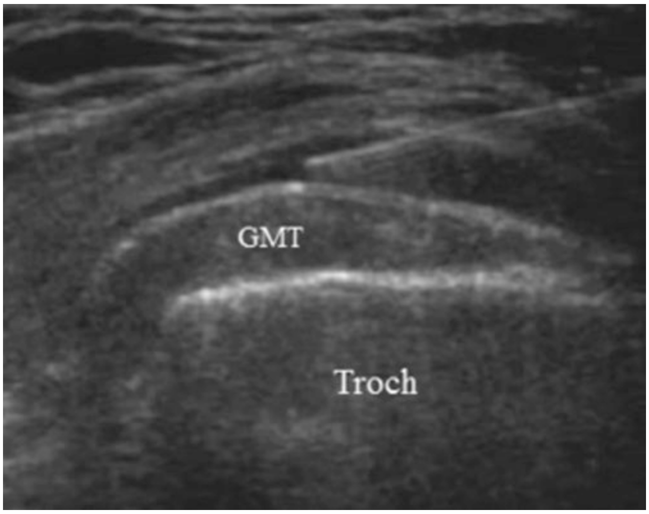

Fig. 9 Short-axis view of the gluteus medius tendon (GMT) at its attachment point on the lateral facet of the greater trochanter (Troch). The hyperechoic needle is seen here advancing into the trochanteric bursa between the gluteus maximus and medius, distending the bursa as the injectate is injected

6 Lateral Hip Pathology

6.1 Greater Trochanteric Pain Syndrome

Lateral hip pain is commonly simplified and diagnosed as trochanteric bursitis; however, this is a common misdiagnosis. Rather, the majority of lateral hip pain, or greater trochanteric pain syndrome, is due to tendinopathy of the gluteus medius, gluteus minimus, or tensor fascia lata, and only a minority of patients have inflammation of the greater trochanteric bursa [13]. Ultrasound may further help in the accurate diagnosis of underlying cause of greater trochanteric pain syndrome, which is essentially a catch-all diagnosis of lateral hip pain around the greater trochanter. A retrospective study by Long, et al. reviewed sonographic images of 877 patients diagnosed with greater trochanteric pain, and of the 877 only 20% had trochanteric bursitis, whereas 49.9% had gluteus tendinopathy and 28.5% had iliotibial thickening [13].

Sonographic examination of the lateral hip for greater trochanteric pain syndrome should begin by placing a high frequency linear transducer transversely over the greater trochanter. In this field, the insertion of the gluteus medius tendon on the lateral facet of the greater trochanter, and gluteus minimus tendon on the anterior facet of the greater trochanter are seen (Fig. 8). Between the gluteus maximus and gluteus medius tendon is the greater trochanteric bursa. Once visualized, an in-plane technique may be used to guide a needle into this bursa and deliver the desired injectate (Fig. 9).

7 Posterior Hip Anatomy

Finally, the posterior hip, which is also divided into deep and superficial component, with the gluteus maximus forming the superficial layer [2]. The deep layer, from superior to inferior, is comprised of the piriformis, superior gemellus, obturator internus, inferior gemellus, and quadratus femorus. All of these muscles continue laterally and typically insert to the trochanteric fossa, the region between the greater and lesser trochanters [1]. Inferomedial to these muscles is the origin of the long head of the biceps femoris and semitendinosus at the lateral border of the ischial tuberosity. Furthermore, the semimembranosus muscle originates from the inferior border of the ischial tuberosity (Fig. 10) [1].

8 Posterior Hip Pathology

8.1 Hamstrings Tendinopathy/Ischial Bursitis

The proximal attachment of the hamstrings tendons are commonly affected and inflamed with repetitive micro trauma or with acute trauma in situations with forced extension of the leg against resistance (commonly encountered in basketball or soccer) [14]. When proximal hamstring tendinopathy is suspected, the proximal attachment point may appear swollen and hypoechoic, and may also be associated with inflammation of the ischial bursa, or ischial bursitis (Fig. 11) [1]. Furthermore, while the hamstrings are collectively comprised of the biceps femoris (short and long heads), semitendinosus, and semimembranosus, the latter is less commonly affected [1]. Overall, given that the proximal hamstrings lie deep to a significant amount of soft tissue, clear visulization and accurate diagnosis can be challenging at times. Injection to treat hamstring tendinopathy may be performed by identifying the pathologic tendon(s) on ultrasound and injecting into the plane above them near the pathological site, avoiding direct injection into the tendon itself.

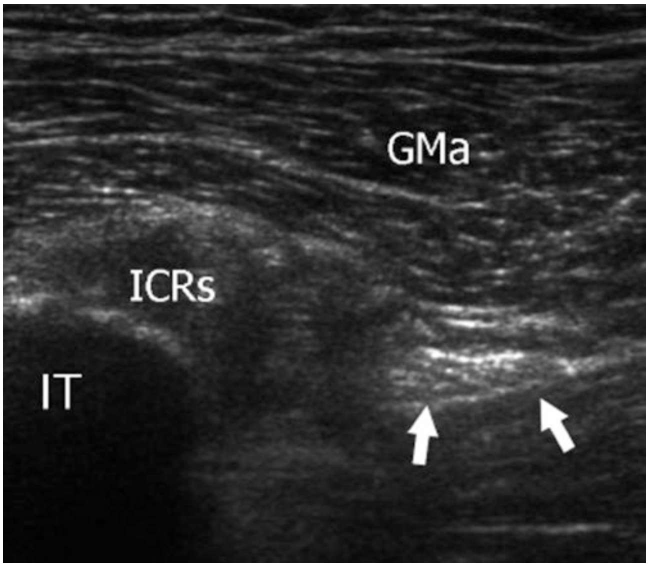

Fig. 10 Short-axis view of the posterior hip at the level of the ischial tuberosity (IT). The hamstring tendons at this level are indistinguishable, and are referred to here as the ischiocrural muscles (ICRs). The gluteus maximus is seen overlying the ischiocrural muscles, and the sciatic nerve (arrows) is running just deep to the gluteus maximus

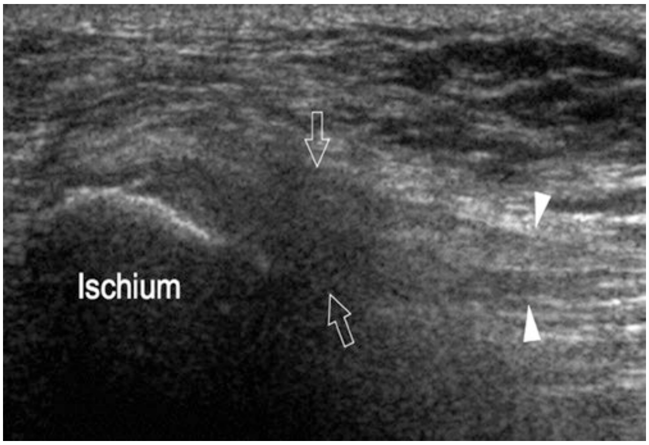

Fig. 11 Longitudinal view of the hamstrings (arrowheads) origin at the ischial tuberosity (Ischium). The area of edema and hypoechogenicity (empty arrows) represents local inflammation, or tendinopathy of the proximal hamstring muscles.

References

1. Bianchi S, Martinoli C. Wrist. In: Ultrasound of the musculoskeletal system, vol. 1. Berlin, Germany: Springer; 2007. p. 425–94.
2. Nestorova R, Vlad V, Petranova T, Porta F, Radunovic G, Mihu M, Iagnocco A. Ultrasonography of the hip. Med Ultrason. 2012;14:213–24.
3. Anderson E, Herring A, Bailey C, Mantuani D, Nagdev A. Ultrasound-guided Intraarticular hip injection for osteoarthritis pain in the emergency department. West J Emerg Med. 2013;14:505–8.
4. Payne JM. Ultrasound-guided hip procedures. Phys Med Rehabil Clin N Am. 2016;27(3):607–29.
5. Piechota M, Maczuch J, Skupiński J, Kukawska-Sysio K, Wawrzynek W. Internal snapping hip syndrome in dynamic ultrasonography. J Ultrason. 2016;16(66):296–303.
6. Balius R, Pedret C, Blasi M, Miguel M, Vallejo B, Margalet E, Bong DA, Martinoli C. Sonographic evaluation of the distal iliopsoas tendon using a new approach. J Ultrasound Med. 2014;33:2021–30.
7. Meaney J, Cassar-Pullicino V, Etherington R, Ritchie D, Mccall I, Whitehouse G. Ilio-psoas bursa enlargement. Clin Radiol. 1992;45:161–8.
8. Parziale JR, O'donnell CJ, Sandman DN. Iliopsoas bursitis. Am J Phys Med Rehabil. 2009;88:690–1.
9. Johnston CA, Wiley JP, Lindsay DM, Wiseman DA. Iliopsoas bursitis and tendinitis. Sports Med. 1998;25:271–83.
10. Pesquer L, Poussange N, Sonnery-Cottet B, Graveleau N, Meyer P, Dallaudiere B, Feldis M. Imaging of rectus femoris proximal tendinopathies. Skelet Radiol. 2016;45:889–97.
11. Rizio L, Salvo JP, Schürhoff MR, Uribe JW. Adductor Longus rupture in professional football players: acute repair with suture anchors. Am J Sports Med. 2004;32:243–5.
12. Robinson P, Barron DA, Parsons W, Grainger AJ, Schilders EMG, O'Connor PJ. Adductor related groin pain in athletes: correlation of MR imaging with clinical findings. Skelet Radiol. 2004;33:451–7.
13. Long SS, Surrey DE, Nazarian LN. Sonography of greater trochanteric pain syndrome and the rarity of primary bursitis. Am J Roentgenol. 2013;201:1083–6.
14. Blasier RB, Morawa LG. Complete rupture of the hamstring origin from a water skiing injury. Am J Sports Med. 1990;18:435–7.

Knee Joint Sonoanatomy and Ultrasound-Guided Knee Joint Injection

Jason Kajbaf and George C. Chang Chien

Introduction

Ranging from common degenerative processes such as osteoarthritis, to traumatic injuries such as ligament or tendon tears, the knee is amongst the most commonly damaged joints in both the young and elderly. Sonographic evaluation has proven to be a meaningful tool for the quick and accurate diagnosis of various knee pathologies. The knee is a hinge type synovial joint formed by the femur proximally, the tibia distally, and the patella superficially. The fibula, though does not articulate with the knee joint, does form connections with the femur via ligamentous structures laterally. A smooth cushion of shiny white articular cartilage about 1/4 inch thick covers the distal femur and proximal tibia. Large intra- and extra-articular ligaments, as well as surrounding muscles and tendons help stabilize the knee. The following will review sonographic knee anatomy, and when applicable, injection techniques to perform with ultrasound guidance.

1 Anterior Knee Anatomy

In order to reduce the amount of anisotropy, the anterior aspect of the knee is best viewed when placed in 20–30° of flexion, which can be obtained by placing a pillow under the knee [1]. By placing a high frequency linear ultrasound probe in a longitudinal plane just superior to the patella, the quadriceps tendon is seen superficially. Just deep to this lies the suprapatellar synovial recess and the suprapatellar fat pad (Fig. 1) [2]. As the probe is moved past the patella inferiorly, the patellar tendon can be seen superficially, inserting itself to the tibial tuberosity (Fig. 2) [3]. When evaluating the suprapatellar and infrapatellar bursae, it is important to realize that a small amount of pressure may displace the fluid and yield an unremarkable appearance.

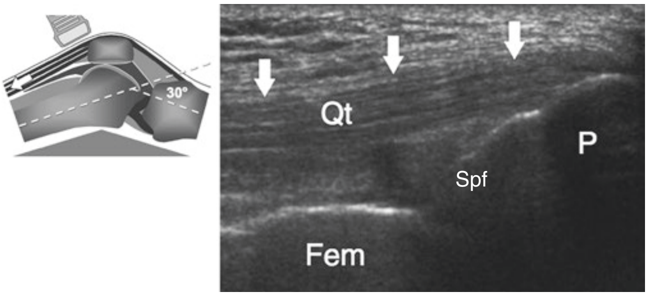

Fig. 1 Longitudinal view of the quadriceps tendon (arrows/Qt) at its insertion at the patella (P). This is best viewed with the knee partially flexed in order to make the quadriceps tendon taut and to minimize anisotropy. Just deep to the quadriceps tendon, the suprapatellar fat pad (Spf) can be seen, with the femur (Fem) seen as the deepest structure

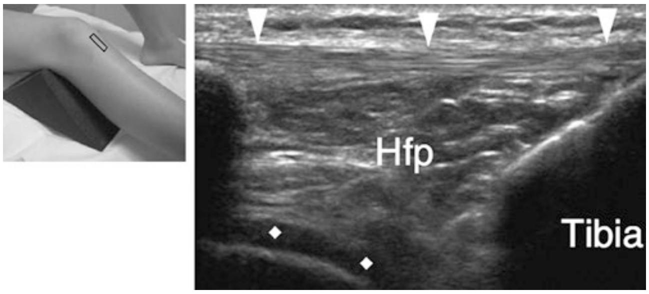

Fig. 2 Longitudinal view of the patellar tendon (white arrowheads) with the knee in slight flexion. Hoffa's fat pad (Hfp) is seen deep to the patellar tendon. The femoral articular cartilage can partially be seen in the image; however, a better view for the demonstration of the femoral articular cartilage for evaluation of knee osteoarthritis will be reviewed in a later image

---

J. Kajbaf (✉)
University of California, Los Angeles, Department of PM&R,
Los Angeles, CA, USA

G. C. Chang Chien
GCC Institute, Newport Beach, CA, USA

Ventura County Medical Center, Ventura, CA, USA

© Springer Nature Switzerland AG 2021
J. Li et al. (eds.), *Ultrasound Fundamentals*, https://doi.org/10.1007/978-3-030-46839-2_15

2 Anterior Knee Pathology

2.1 Knee Osteoarthritis

Knee osteoarthritis is an extremely common disorder, and can be quite debilitating [4]. Correlating the history and physical examination with radiographic findings commonly makes diagnosis; however, ultrasound has also been demonstrated to be a useful tool to help demonstrate osteoarthritic changes of the knee joint [5]. In order to evaluate for knee osteoarthritis (OA) via ultrasound, the knee should be placed in about 90° of flexion and the transducer is placed in a transverse plane just superior to the patella (Fig. 3a,b) [2]. In this view, the femoral articular cartilage is seen as a thin hypoechoic layer. Knee osteoarthritis can accurately be diagnosed with ultrasound if there is thinning of articular cartilage, increased echogenicity, or irregularities of the osseous surface [6]. Furthermore, if knee pain is suspected to be due to underlying knee osteoarthritis, an intra-articular injection with steroid, hyaluronic acid, and/or regenerative techniques including platelet rich plasma and stem cells have been demonstrated to provide varying levels of pain relief [7]. In order to perform an intra-articular knee injection under ultrasound, the knee should again be placed in mild flexion (20–30°) and the transducer is placed longitudinally over the distal quadriceps tendon. In cases of symptomatic knee OA, a knee effusion commonly ensues, which may be seen in the view described above in the suprapatellar synovial recess. Once the suprapatellar synovial recess is identified, the transducer may then be rotated to a transverse plane. With an in-plane approach in a lateral to medial direction, the needle is introduced into the suprapatellar synovial recess (Fig. 4). If there is a significant knee effusion, aspiration may be done prior to injecting the selected solution.

In situations where physical therapy, steroid injections, viscosupplementation, and even perhaps platelet rich plasma or stem cell injections have failed, and the patient wishes to further avoid a total knee replacement, another option exists with a genicular nerve block. The genicular nerves (superior-medial, inferior-medial, and superior-lateral) are the main innervating branches to the knee joint, and have been successfully blocked with local anesthetic and subsequent radiofrequency ablation under fluoroscopic guidance. Multiple studies; however, have demonstrated that the same procedure can be done with accuracy and safety using ultrasound guidance [8]. To identify the genicular nerves three basic landmarks may be utilized to place the ultrasound transducer, as described by Sarı, et al. in 2016. For the inferior-medial genicular nerve, the landmark is the medial border of the tibia, 1–1.5 cm from the lower medial border of the patella. The superior-medial genicular may be identified over the distal medial femur, 1–1.5 cm from the upper medial border of the patella. Lastly, the superior-lateral genicular nerve may be identified over the distal lateral femur, 1–1.5 cm from the upper lateral border of the patella (Fig. 5a,b) [9]. Over these respective landmarks, the Doppler function of

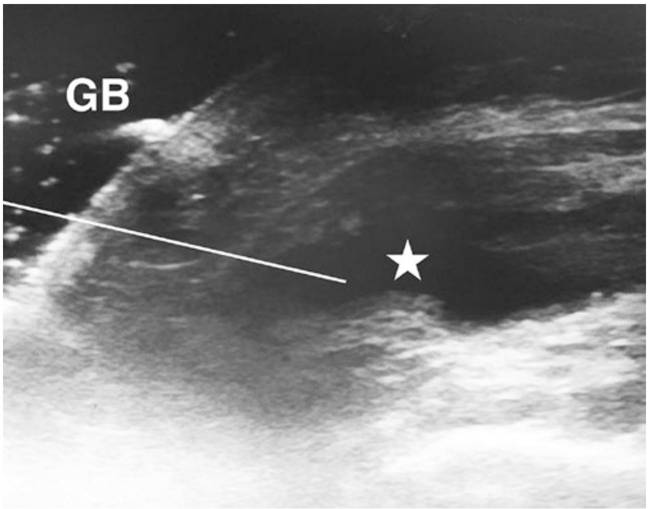

Fig. 4 With the knee fully extended or in slight flexion, a high frequency linear transducer placed over the distal quadriceps tendon in a longitudinal view, which demonstrates a knee effusion at the suprapatellar synovial recess. This space is continuous with the knee joint. When this is seen, the transducer may be rotated 90° to get a short-axis view of the lateral portion of the suprapatellar synovial recess (star). A needle can then be introduced using an in-plane approach to aspirate the effusion. Using this same technique, an intra-articular knee injection may be performed. This image shows this procedure done using a gel bridge (GB), which is commonly used for injections on curved or small surfaces, in order to improve the field of view

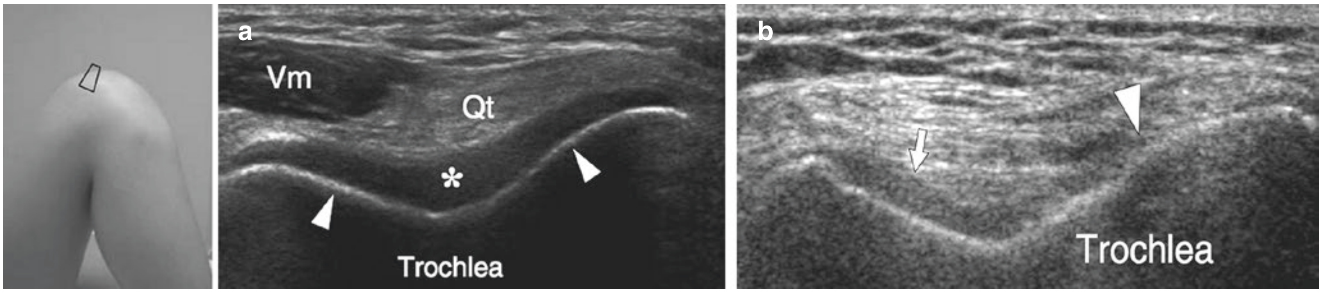

Fig. 3 (**a**,**b**) Evaluation for knee osteoarthritis. (**a**) With the knee in at least 90° of flexion, a high frequency linear transducer is placed just proximal to the patella. Here, the articular surface (arrowheads) of the femoral trochlea and its articular cartilage (asterisk) are visible in a healthy knee. The quadriceps tendon (Qt) and distal vastus medialis (Vm) may be seen superficially in this view. (**b**) In knee osteoarthritis, the layer of cartilage (arrow) may be thin or absent (arrowhead), and cortical disruption and/or bone spurs may be seen on the distal femur as hyperechoic irregularities

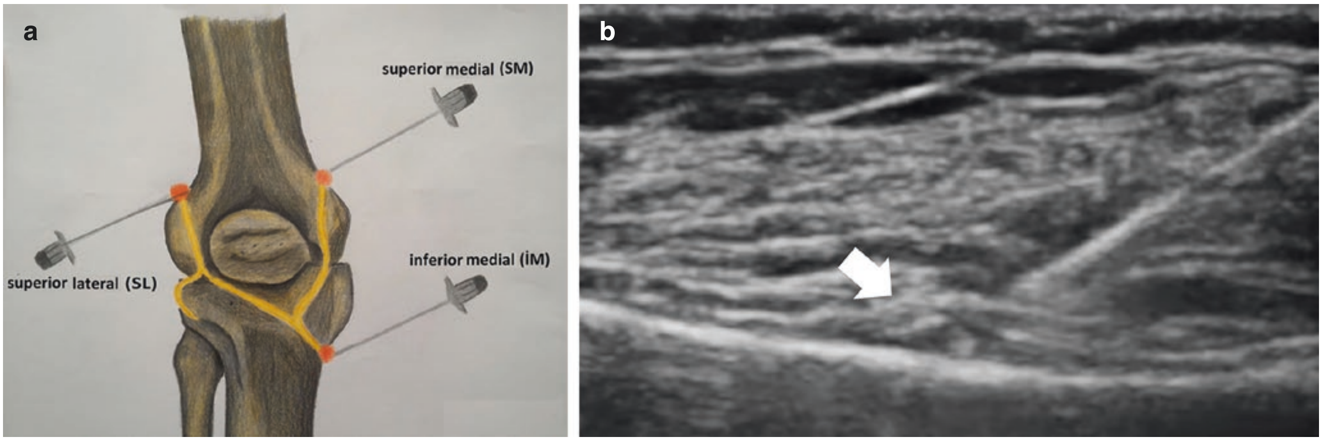

Fig. 5 (**a**) Pictorial depiction of the locations of the three targeted genicular nerves for a genicular nerve block/radiofrequency ablation. It is important to note that to the genicular artery, an easy to identify landmark under ultrasound, the genicular nerve is commonly located adjacent. (**b**) Ultrasound view of an inferomedial genicular nerve block using an in-plane technique. The genicular nerve is visible as a round hyperechoic structure (arrow). This same technique can be used for a genicular nerve radiofrequency ablation

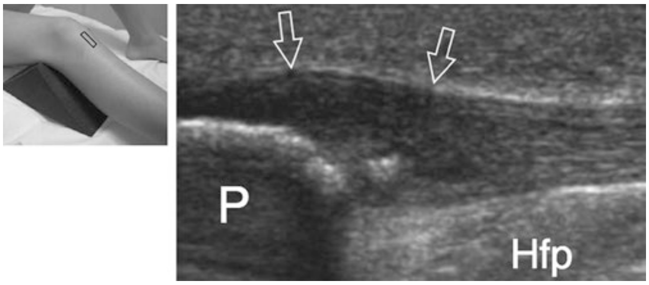

Fig. 6 Longitudinal view of an inflamed patellar tendon. Just near its proximal attachment at the patella (P), the patellar tendon is seen swollen (arrows), representing focal edema and inflammation of the patellar tendon. (Hfp- Hoffa's fat pad)

the ultrasound can be utilized to identify the genicular arteries, which are commonly found adjacent to the genicular nerves. Thus, once the nerve next to the artery is identified the needle for a block or electrode for radiofrequency ablation may be introduced with an in-plane technique under ultrasound and advanced to the genicular nerves [9].

2.2 Patellar Tendinopathy

Patellar tendinitis is an extremely common condition among jumping athletes, with some studies suggesting a prevalence of up to 45% in volleyball players and 32% in basketball players [10]. Patients commonly present with infrapatellar knee pain after activity; In severe cases the pain may be present at rest, and may be reproduced by palpation during physical examination [11]. Ultrasound evaluation of patellar tendinopathy may demonstrate an array of findings, ranging from a focal area of hypoechogenicity representing focal edema and inflammation, to diffuse tendon thickening and heteroechogenicity suggesting diffuse tendinopathy (Fig. 6) [12].

2.3 ACL Tear

The anterior cruciate ligament (ACL) is one of the most common injured ligament among athletes, and in the acute setting a patient typically presents with significant knee pain and edema following a "pop" sound. Once the initial edema has improved, instability and laxity of the knee is common with complete tears, and may be seen on physical examination either with lachman's maneuver or the anterior drawer test [13]. Furthermore, a recent study by Mahajan, et al. in 2015 demonstrated that patients with ACL tears had a significantly smaller ACL diameter at its insertion site on the tibia in contralateral limb, thereby suggesting that patient's with smaller ACLs may be prone to tears [13].

In order to evaluate for an ACL tear via ultrasound, the knee must be placed in full flexion with a high frequency linear probe placed longitudinally just distal to the patella. In this view, the distal ACL at its insertion on the tibia can be appreciated (Fig. 7). Ultimately though, ultrasound can only demonstrate the distal end of the ACL with accuracy, therefore MRI continues to remain the gold standard for the diagnosis of ACL injuries. However, a cadaver study by Smith, et al. demonstrated that ultrasound guided ACL injections are feasible and can be performed with accuracy, which may be useful in future studies researching the effectiveness of various regenerative procedures, such as stem cell and platelet rich plasma injections [14].

3 Posterior Knee Anatomy

In order to optimally assess the posterior knee, the patient is placed prone with the knee fully extended. Once positioned properly, it is best to start at the mid-calf with the transducer oriented in a transverse plane. At this level, the two heads of the gastrocnemius muscle can be identified, and the transducer is then moved to the medial aspect of the medial head of the

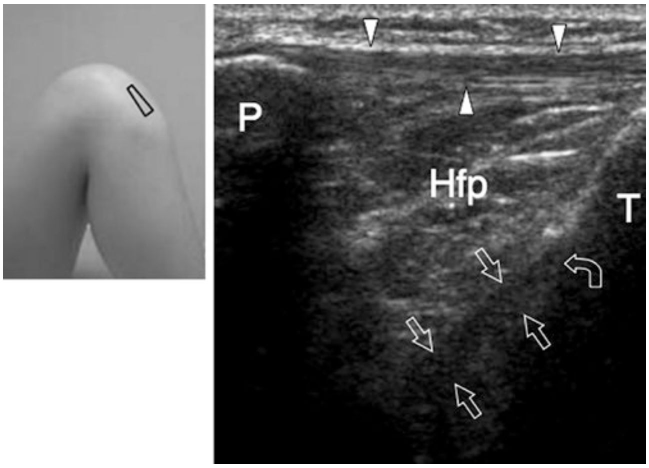

Fig. 7 With the knee fully flexed, the distal/tibial attachment of the ACL can be seen (arrows, curved arrow). From superficial to deep, the patellar tendon (arrowheads) is seen first just distal to the patella (P) followed by Hoffa's fat pad (Hfp) between the patellar tendon and ACL. Although the distal ACL can be visualized with some confidence, it remains difficult to view the entirety of the ACL, and thus ultrasound is not the modality of choice for the diagnosis of ACL tears. (T- Tibia)

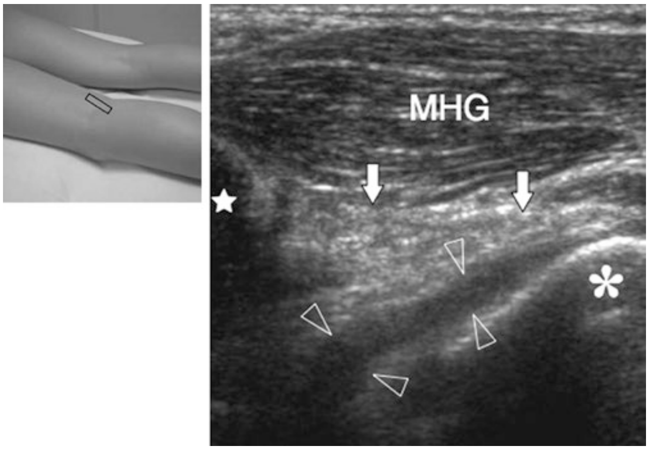

Fig. 8 Posterior view of the knee with a linear high frequency transducer. The medial head of the gastrocnemius (MHG) is seen superficially followed by a fat pad (arrows). The deepest structure seen is the intermediate and distal segments of the PCL (arrowheads) and its attachment to the tibia (asterisk). (Star- femur)

gastrocnemius. Subsequently, the transducer is then moved superiorly until the semimembranosis tendon is visible just lateral to the gastrocnemius [2]. Between these two muscles, if present, a baker's cyst can be seen [2]. Another key structure to identify posteriorly is the posterior cruciate ligament (PCL). The intermediate and distal portions of the PCL are be viewed by having the patient lay prone and the transducer placed in a sagittal oblique position over the middle of the popliteal fossa. The PCL is then seen deep to a triangular fat pad, as a linear hypoechoic cord-like structure (Fig. 8) [3].

4 Posterior Knee Pathology

4.1 Baker's Cyst

A Baker's cyst is a common finding among the general population, with some studies estimating a prevalence of up to 5%, and even higher in the elderly [15]. Furthermore, in patients with knee pain, a prevalence of up to 25.8% has been suggested [16]. Since a Baker's cyst communicates with the joint space, they are commonly associated with intra-articular pathology such as meniscal injuries and osteoarthritis [17]. Ultrasound-guided aspiration and injection with corticosteroid has been shown to provide significant resolution of symptoms [18]. This procedure can be performed with the same setup described earlier, with the patient lying prone with the ultrasound transducer over the medial head of the gastrocnemius and semimembranosus tendon (Fig. 9).

5 Medial Knee Anatomy

When examining the medial aspect of the knee, a high frequency linear transducer is placed longitudinally over the medial aspect of the knee joint, which can be palpated prior to placing the ultrasound probe. The first and most easily visible structure is the medial collateral ligament (MCL) (Fig. 10). The MCL appears as a thin hyperechoic linear structure, with superficial and deep layers. The deep layer is composed of the meniscofemoral and meniscotibial ligament, and is separated from the superficial layer by a thin hypoechoic line. Once the MCL is identified, the transducer should then be moved anteriorly in order to visualize the anterior horn of the medial meniscus [3]. If visualization of the medial meniscus, a valgus stress may be applied to the knee in order to increase the medial joint space. About 5-6 cm distal to the joint line, on the anteromedial aspect of the tibia is the attachment of the Sartorius, Gracilis, and Semitendinosus muscles via a common tendon [3].

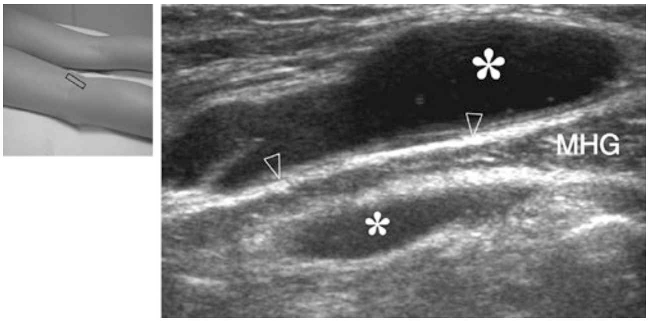

Fig. 9 Longitudinal view of the base and body of a Baker's cyst (asterisks) seen separated by the tendon (arrowheads) of the medial head of the gastrocnemius (MHG). Once Baker's cyst is identified, a needle can be inserted under ultrasound guidance for aspiration

6 Medial Knee Pathology

6.1 Medial Collateral Ligament Sprain

MCL sprains are extremely common injuries among athletes, particular in contact sports such a football and soccer. The MCL is typically injured when a valgus stress is applied to a mildly flexed knee with a firmly planted foot [18]. MCL sprains are graded from 1 to 3, with 1 being a stretch and no residual ligament laxity, 2 indicating a partial ligament tear and increased laxity, and 3 indicating a complete tear with significant laxity (Fig. 11) [19]. MCL sprains can ben seen on ultrasound as irregular hypoechoic areas within the ligament.

6.2 Pes Anserine Bursitis

Pes anserine bursitis is the inflammation of the bursa deep to the conjoined tendon of the Sartorius, Gracilis, and Semitendinosus muscles. Patients commonly have a history of obesity, knee osteoarthritis, or genu valgus, and present with pain along the medial aspect of the knee that may also be associated with edema [20]. As described earlier, placing the ultrasound transducer 5–6 cm distal to the medial joint line on the anteromedial aspect of the tibia, the pes anserine bursa can be readily visualized (Fig. 12). Once visualized, the bursa can be aspirated and subsequently injected with corticosteroid, which has been demonstrated to provide significant and immediate pain relief in patients with symptomatic pes anserine bursitis [21].

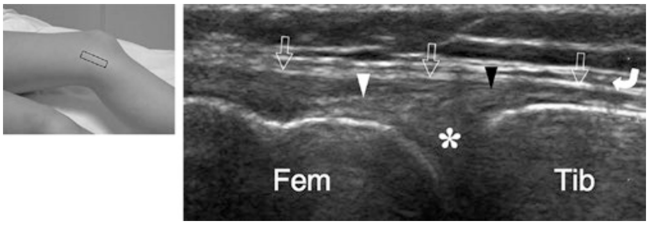

Fig. 10 Longitudinal view of the medial knee using a high frequency linear probe. A superficial fascia is seen overlying the entire medial knee is visualized (curved arrow). Just deep to this, the superficial layer of the MCL (arrows). The deep layer of the MCL is comprised of two parts, the meniscofemoral (white arrowhead) and menisctibial (black arrowhead), which are connected to the meniscus and fasten it to the femur (Fem) and tibia (Tib). This close relationship of the medial meniscus and MCL is why MCL injuries are commonly associated with medial meniscus injuries

6.3 Medial Meniscus Tear

Medial meniscus injuries are common among the general population, and even more so among athletes. The medial meniscus is typically injured with aggressive pivoting or turns, which forcefully twist the knee [22]. This is commonly seen in soccer, football, or basketball. In order to identify the medial meniscus, as described earlier, the ultrasound probe should be placed along the medial aspect of the knee, over

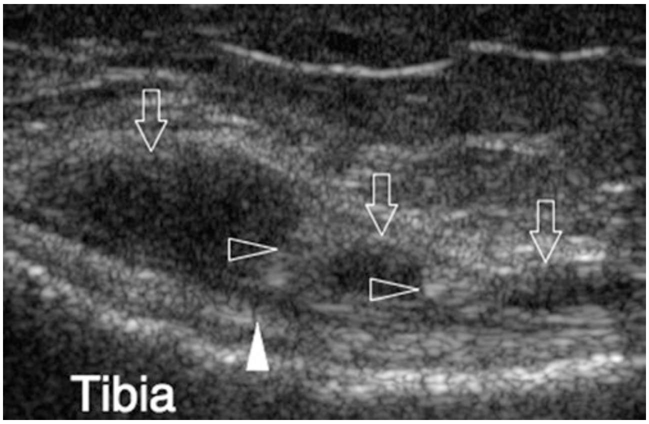

Fig. 12 Longitudinal view of the pes anserine complex near the distal attachment of the MCL (white arrowhead) using a high frequency linear probe. The pes anserine bursa is seen here distended (arrows), which accentuates its separation of the pes anserine tendons (empty arrowheads)

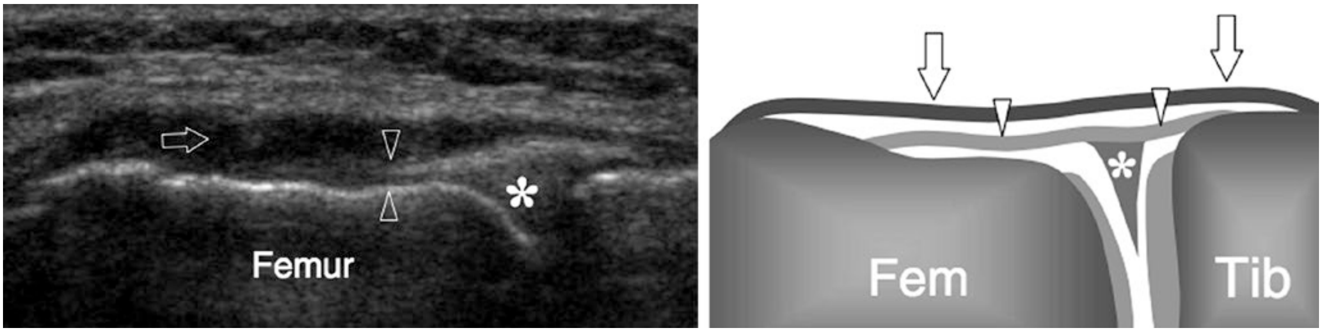

Fig. 11 Longitudinal view of the medial knee using a high frequency linear probe. The superficial layer of the MCL is seen disrupted and torn with associated local edema (arrow). The deep layer (arrowheads) associated with the meniscus (asterisk) remains intact. When the deep layer of the MCL is damaged, further evaluation of the medial meniscus should also be performed since an injury to one is commonly associated with an injury to the other

the MCL longitudinally, then moved slightly anterior and posterior to see the anterior and posterior horns of the medial meniscus, respectively (Fig. 13). Recently, a study by Alizadeh, et al. in 2012 showed that ultrasound could accurately diagnose a medial meniscus injury with similar sensitivity and specificity as MRI, particularly in the patients less than 30 years old [23]. Though many practitioners have been performing platelet rich plasma or stem cell injections to medial (and lateral) meniscus injuries, there have been no randomized clinical trials researching the effectiveness or efficacy of these regenerative medicine techniques.

7 Lateral Knee

The key structures to evaluate at the lateral knee include the lateral collateral ligament, lateral meniscus, and the distal iliotibial (IT) band at its insertion at Gerdy's tubercle. To begin, the patient may either lay lateral recumbent or prone with the leg internally rotated. In this position, a high frequency linear transducer should then be placed on the anterior to middle two thirds of the lateral aspect of the knee in long-axis [3]. The distal IT band can be ususally visualized; if there is difficulty in finding the IT band, palpation can aid to locate it as it courses over the lateral thigh and knee. When the diagnosis of IT band syndrome is in question, compression with the ultrasound probe will commonly illicit pain, thereby aiding in its diagnosis [3].

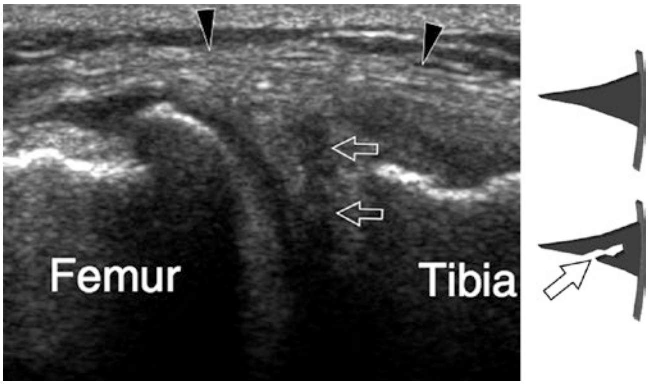

Fig. 13 Longitudinal view of the medial knee using a high frequency linear probe. An intact MCL is seen superficially (black arrowheads). However, just deep to this, a linear tear of the medial meniscus is seen as a linear hypoechoic area (arrows)

The lateral collateral ligament (LCL) starts at the lateral femoral condyle and inserts in to the fibular head. It appears as a thin (3–4 mm) cord-like fibrillar structure under ultrasound best visualized in long-axis (Fig. 14) [24]. The transducer can then be rotated 90° to obtain a transverse view and further observe for ligamentous pathology. Just deep to the LCL the proximal portion of the popliteal muscle can be seen, as well as the body and anterior horn of the lateral meniscus (Fig. 14) [2]. Lastly, the common peroneal nerve can also be seen, easier in the transverse plane, traversing over the fibular head and around the fibular neck (Fig. 15) [3].

8 Lateral Knee Pathology

8.1 Lateral Collateral Ligament Sprain

Lateral collateral ligament (LCL) sprains and tears are much less common than medial collateral ligament sprains due to the structure of the LCL [25]. However, when a partial or complete tear is suspected, more commonly in contact sports such as soccer or football, they can be visualized as a disruption of the fibrillations and hypoechoic, indicating a tear and local edema [3]. This appears sonographically similar to a MCL injury.

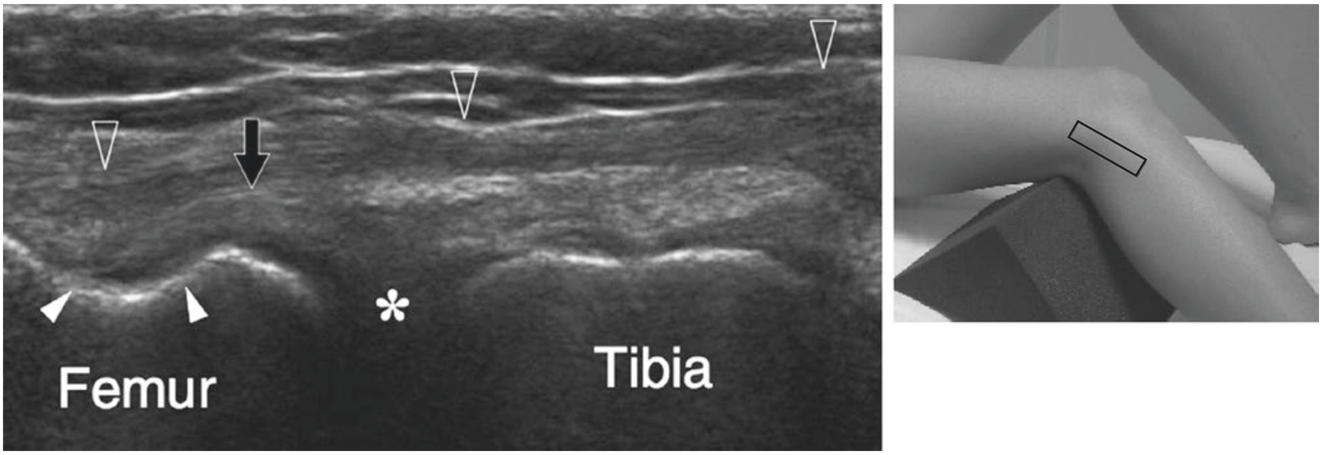

Fig. 14 Longitudinal view of the lateral knee using a high frequency linear transducer. Superficially, the lateral collateral ligament is easily seen (empty arrowheads). If the probe is moved slightly inferior, its distal attachment can be seen on the fibula. Furthermore, the origin of the popliteus tendon (black arrow) is seen on the lateral femur (white arrowheads). Lastly, similar to the medial meniscus, the lateral meniscus is seen as a triangular shaped structure (asterisk)

8.2 Lateral Meniscus Tear

Lateral meniscal tears, similar to other intra-articular soft tissue derangements typically encountered in athletes; however, is less commonly seen than medial meniscus injuries. A recent study by Sladjan, et al. demonstrated that ultrasound can accurately diagnose a chronic lateral meniscus tear, with sensitivities and specificities of 85% and 90%, resepectively [26]. Although platelet rich plasma and stem cell injections can be and are performed for lateral meniscus tears, there are currently no randomized clinical trials completed to confirm their efficacy and support their use. Sonographically, lateral meniscus tears appear similarly to medial meniscus injuries.

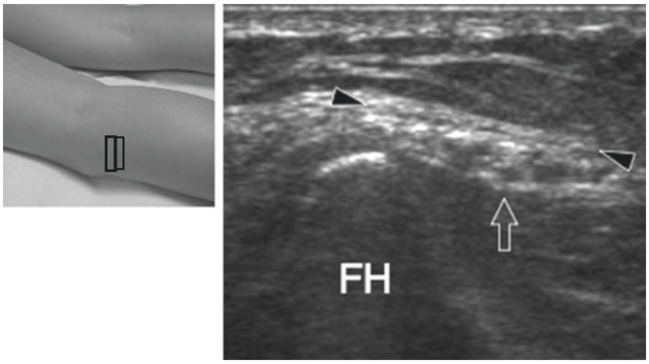

Fig. 15 Placing a high frequency linear transducer over the fibular head (FH), the common peroneal nerve is visible coursing superficial to it (arrow). (Black arrowheads- fascia layer covering the common peroneal nerve)

8.3 Common Peroneal Nerve Entrapment

The common peroneal nerve at the fibular head is a common area for entrapment neuropathy due to both its superficial location thereby making it easily compressible by body positioning, and due to the course it takes through a tight restricted space between bone and fascia [3]. These patients may present with paresthesias described in the distribution of the peroneal nerve initially, or weakness with dorsiflexion (foot drop) later in the disease course [27]. Ultrasound may help with diagnosis, etiology, and treatment of common peroneal nerve entrapment.

Nerve compression may be due to a ganglion cyst, which is one of the leading causes of peroneal nerve compression [3]. These cysts may be either intra- or extraneural, meaning located within or outside the nerve, respectively. They appear as hypoechoic cystic structures on ultrasound (Fig. 16a). Once identified, these ganglion cysts can be aspirated, using ultrasound for needle guidance. Lastly, when peroneal nerve entrapment with foot drop is suspected, ultrasound of muscles innervated by the peroneal nerve (i.e. tibialis anterior) may appear hyperechoic due to muscle atrophy and fatty infiltration (Fig. 16b) [3].

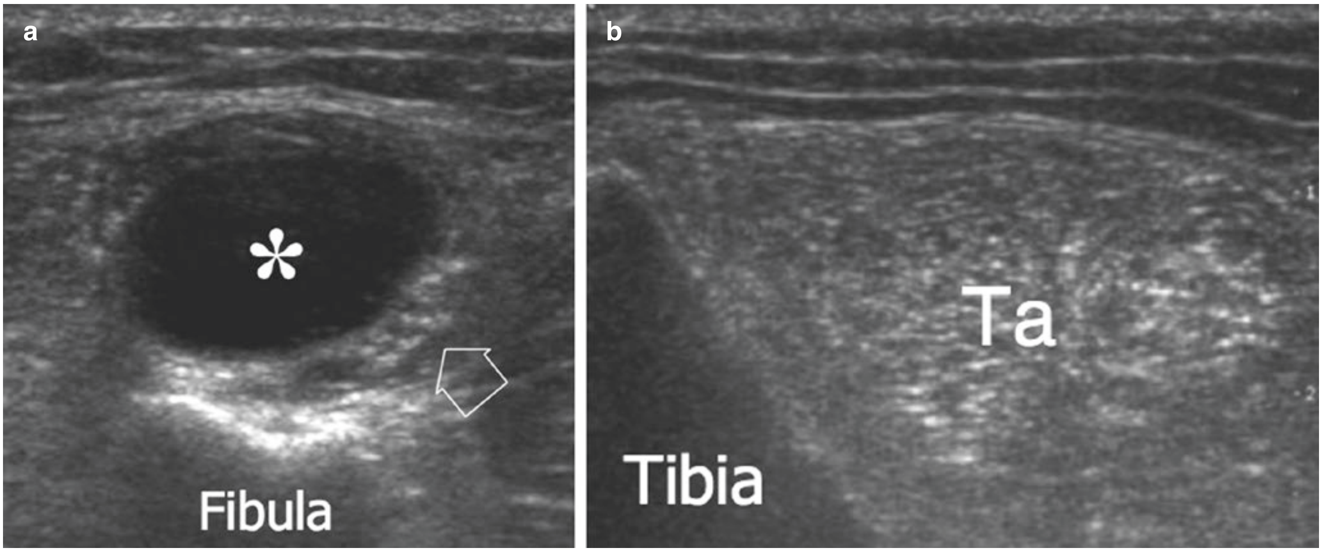

Fig. 16 (**a**) When peroneal nerve entrapment is suspected near the fibular head, a high frequency linear transducer can be placed just over it to identify any potential pathology. An extraneural ganglion cyst is seen here compressing the common peroneal nerve just deep to it (arrow). (**b**) Furthermore, another clue to a peroneal nerve neuropathy is the fatty atrophy (sonographically seen as hyperechoic changes) of distally innervated muscles of the peroneal nerve, such as the tibialis anterior (Ta)

References

1. Bianchi S, Zwass A, Abdelwahab IF, et al. Diagnosis of tears of the quadriceps tendon of the knee: value of sonography. AJR Am J Roentgenol. 1994;162:1137–40.
2. Jacobson JA. The knee. In: O'Neill JM, editor. Musculoskeletal ultrasound. New York: Springer; 2008.
3. Bianchi S, Martinoli C. Wrist. In: Ultrasound of the musculoskeletal system. Berlin: Springer; 2007. p. 425–94.
4. Elliott AL, Kraus VB, Luta G, Stabler T, Renner JB, Woodard J, Dragomir AD, Helmick CG, Hochberg MC, Jordan JM. Serum hyaluronan levels and radiographic knee and hip osteoarthritis in African Americans and Caucasians in the Johnston County Osteoarthritis Project. Arthritis Rheum. 2005;52:105–11.
5. Yanagisawa S, Ohsawa T, Saito K, Kobayashi T, Yamamoto A, Takagishi K. Morphological evaluation and diagnosis of medial type osteoarthritis of the knee using ultrasound. J Orthop Sci. 2014;19:270–4.
6. Riecke B, Christensen R, Torp-Pedersen S, Boesen M, Gudbergsen H, Bliddal H. An ultrasound score for knee osteoarthritis: a cross-sectional validation study. Osteoarthr Cartil. 2014;22:1675–91.
7. Richards MM, Maxwell JS, Weng L, Angelos MG, Golzarian J. Intra-articular treatment of knee osteoarthritis: from anti-inflammatories to products of regenerative medicine. Phys Sportsmed. 2016;44:101–8.
8. Yasar E, Kesikburun S, Kılıç C, Güzelküçük U, Yazar F, Kenan Tan A. Accuracy of ultrasound-guided genicular nerve block: a cadaveric study. Pain. 2015;19:899–904.
9. Sarı S, Aydın ON, Turan Y, Şen S, Özlülerden P, Ömürlü IK, Gulastı F. Which imaging method should be used for genicular nerve radio frequency thermocoagulation in chronic knee osteoarthritis? J Clin Monit Comput. 2016;31:797–803.
10. Hägglund M, Zwerver J, Ekstrand J. Epidemiology of patellar tendinopathy in elite male soccer players. Am J Sports Med. 2011;39:1906–11.
11. Figueroa D, Figueroa F, Calvo R. Patellar tendinopathy. J Am Acad Orthop Surg. 2016;24:e184–92. https://doi.org/10.5435/jaaos-d-15-00703.
12. Cook JL, Khan KM, Kiss ZS, et al. Patellar tendinopathy in junior basketball players: a controlled clinical and ultra- sonographic study of 268 patellar tendons in players aged 14-18 years. Scand J Med Sci Sports. 2000;10:216–20.
13. Mahajan PS, Chandra P, Negi VC, Jayaram AP, Hussein SA. Smaller anterior cruciate ligament diameter is a predictor of subjects prone to ligament injuries: an ultrasound study. Biomed Res Int. 2015;2015:1–8.
14. Smith J, Hackel JG, Khan U, Pawlina W, Sellon JL. Sonographically guided anterior cruciate ligament injection: technique and validation. Pm&r. 2015;7:736–45.
15. Kornaat PR, Bloem JL, Ceulemans RYT, Riyazi N, Rosendaal FR, Nelissen RG, Carter WO, Graverand M-PHL, Kloppenburg M. Osteoarthritis of the knee: association between clinical features and MR imaging findings. Radiology. 2006;239:811–7.
16. Picerno V, Filippou G, Bertoldi I, Adinolfi A, Sabatino VD, Galeazzi M, Frediani B. Prevalence of Baker's cyst in patients with knee pain: an ultrasonographic study. Reumatismo. 2014;65:264–70.
17. Fielding J, Franklin P, Kustan J. Popliteal cysts: a reassessment using magnetic resonance imaging. Skelet Radiol. 1991;20:433–5. https://doi.org/10.1007/bf00191086.
18. Köroğlu M, Çallıoğlu M, Eriş HN, et al. Ultrasound guided percutaneous treatment and follow-up of Bakers cyst in knee osteoarthritis. Eur J Radiol. 2012;81:3466–71.
19. MCL Tear Diagnosis. In: UCSF Medical Center. https://www.ucsfhealth.org/conditions/mcl_tear/diagnosis.html. Accessed 1 Sep 2018.
20. Uysal F, Akbal A, Gökmen F, Adam G, Reşorlu M. Prevalence of pes anserine bursitis in symptomatic osteoarthritis patients: an ultrasonographic prospective study. Clin Rheumatol. 2014;34:529–33.
21. Sarifakioglu B, Afsar SI, Yalbuzdag SA, Ustaömer K, Bayramoğlu M. Comparison of the efficacy of physical therapy and corticosteroid injection in the treatment of pes anserine tendino-bursitis. J Phys Ther Sci. 2016;28:1993–7.
22. Torn meniscus. In: Mayo Clinic. 2018. https://www.mayoclinic.org/diseasesconditions/torn-meniscus/symptoms-causes/syc-20354818. Accessed 1 Sep 2018.
23. Alizadeh A, Jandaghi AB, Zirak AK, Karimi A, Mardani-Kivi M, Rajabzadeh A. Knee sonography as a diagnostic test for medial meniscal tears in young patients. Eur J Orthop Surg Traumatol. 2012;23:927–31.
24. De Maeseneer M, Vanderdood K, Setal M. Sonog- raphy of the medial and lateral tendons and ligaments of the knee: the use of bony landmarks as an easy method for identification. AJR Am J Roentgenol. 2002;178:1437–44.
25. LCL Tear. In: UCSF Medical Center. https://www.ucsfhealth.org/conditions/lcl_tear/. Accessed 20 Aug 2018.
26. Sladjan T, Zoran V, Zoran B. Correlation of clinical examination, ultrasound sonography, and magnetic resonance imaging findings with arthroscopic findings in relation to acute and chronic lateral meniscus injuries. J Orthop Sci. 2014;19:71–6.
27. Iwamoto N, Isu T, Kim K, Morimoto D, Yamazaki K, Isobe M. Clinical feathers and treatment of peroneal nerve entrapment neuropathy. No Shinkei Geka. 2015;43:309–16.

Ankle Sonoanatomy and US Guided Joint Blocks

Soo Yeon Kim, Chaiyaporn Kulsakdinun, and Jung H. Kim

1 Introduction

The ankle joint is one of the most frequently injured joints in the lower extremity. Point of care ultrasound(US) examination has become increasingly popular in the assessment of abnormalities of tendons, ligaments, nerves and joints. It is clinically useful as most structures are superficial and well visualized with US. In this chapter, we will focus on commonly injured structures in the ankle (Fig. 1).

2 Ankle Sonoanatomy

2.1 Anterior Ankle

US examination of anterior ankle is performed with the patient in a supine position with the knee slightly flexed and foot flat on the table. The primary structures in anterior ankle are anterior ankle joint, tibialis anterior (TA), extensor hallucis longus(EHL), extensor digitorum longus,(EDL) and deep peroneal nerve (Table 1). The probe is placed in the sagittal plane with the foot in plantar flexion (Fig. 2). The anterior fat pad lies anterior to the tibiotalar joint. It is important to scan medial to lateral to examine the entire talar dome. In the case of an ankle joint effusion, the anterior fat pad gets displaced superiorly. Up to 3 mm of joint fluid is physiologic and is commonly seen [1].

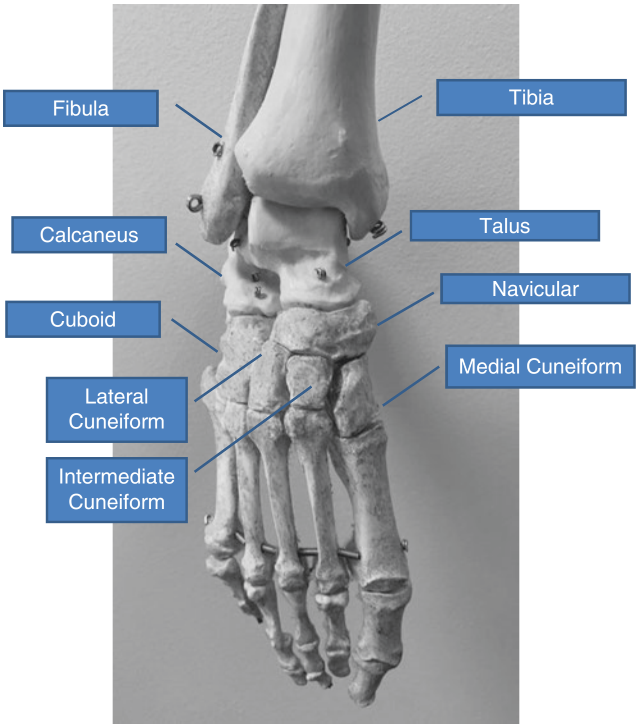

Fig. 1 Ankle joint bony anatomy

Table 1 Anterior ankle evaluation checklist

Anterior tibiotalar joint
Tibials anterior tendon
Extensor hallucis tendon
Extensor digitorum tendon
Deep peroneal nerve

Most of the anterior structures (Table 1) are easily identified in the transverse plane (Fig. 3). Most medially, the large oval shaped TA tendon can be found with its typical hyperechoic and fibrillar pattern. Tendons should be examined in full length from the myotendinous junction to its insertion at first cuneiform. The most common location of the tibialis anterior tendon tears is within 3.5 cm of the

---

S. Y. Kim
Department of Physical Medicine and Rehabilitation, Montefiore Medical Center, Bronx, NY, USA
e-mail: sookim@montefiore.org

C. Kulsakdinun (✉)
Department of Orthopedics, Montefiore Medical Center, Bronx, NY, USA
e-mail: ckulsakd@montefiore.org

J. H. Kim
Department of Anesthesiology, Perioperative, and Pain Medicine, Icahn School of Medicine at Mt. Sinai St. Luke's and Mt. Sinai West Hospitals, New York, NY, USA
e-mail: Jung.kim@mountsinai.org

© Springer Nature Switzerland AG 2021
J. Li et al. (eds.), *Ultrasound Fundamentals*, https://doi.org/10.1007/978-3-030-46839-2_16

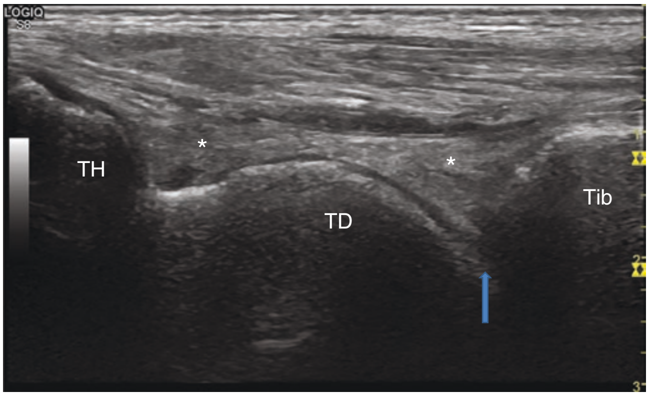

Fig. 2 Tibiotalar joint (Arrow). Sagittal imaging over the ankle joint shows hyperechoic anterior fat pad (∗), tibia(Tib), talar head (TH)

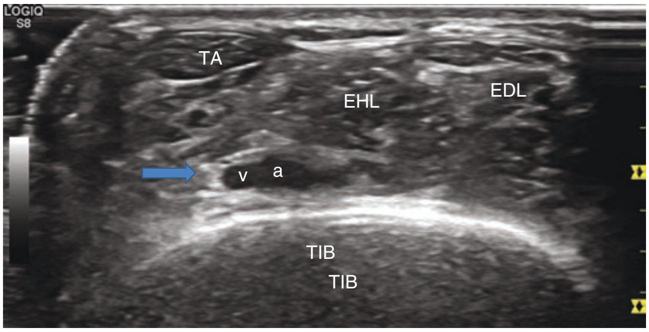

Fig. 3 Ankle US Transverse Plane: Tibials Anterior (TA), extensor halluces longus (EHL), tibia (TIB), dorsalis pedis artery (a), posterior tibial vein (v), deep peroneal nerve (arrow)

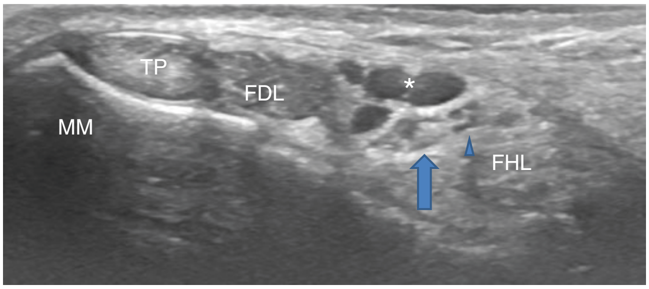

Fig. 4 Ankle US axial: Medial Malleolus (MM), Tibialis posterior (TP), flexor digitorum longus(FDL), posterior tibial artery and vein (∗), tibial nerve (arrow), medial calcaneal nerve (arrow head) and flexor halluxis longus (FHL)

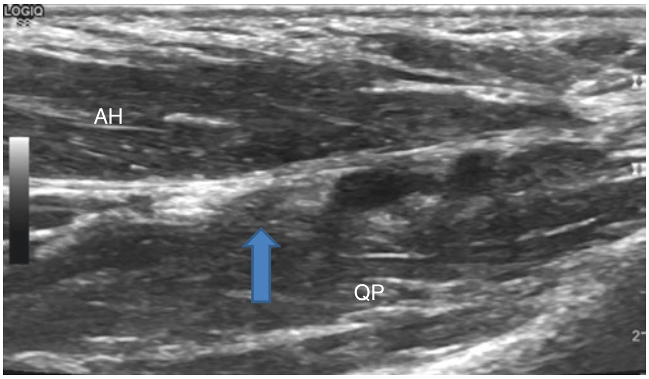

Fig. 5 Medial and lateral plantar nerve lie posterior to FDL and superficial to FHL, FBLPN(Arrow) lies between Abductor hallucis (AH) and Quadratus plantae (QP) [4]

Table 2 Medial ankle evaluation checklist

Tibialis posterior
Flexor digitorum longus
Tibial nerve and its branches
Flexor hallucis longus

insertion point [2]. Lateral to the TA tendon, the EHL and the EDL can be visualized. Proximally, the EDL looks like a single flattened tendon which eventually divides into 4 individual tendons for the second to fifth toes. Each tendon can be evaluated in long and short-axis views. The tibials anterior artery and deep peroneal nerve are seen just deep to the EHL and the EDL tendons, on the surface of Tibia.

2.2 Medial Ankle

For this evaluation, a "frog leg" position is preferred. A pillow is placed below the lateral ankle with slight pronation can be helpful. The structures that need to be evaluated in the medial ankle are listed in Table 2. In the axial plane (Fig. 4), all contents of tarsal tunnel can be easily identified. The tibialis posterior (TP) tendon lies in a shallow bony groove in the posterior aspect of the medial malleolus. The TP tendon can be followed down to its navicular insertion. The TP tendon is the most commonly injured tendon in the medial ankle. Up to 4 mm of fluid is considered physiologic [1]. A longitudinal split tear is also commonly seen near the medial malleolus. Posteriorly, the flexor digitorum longus (FDL), tibial neurovascular bundle, and flexor halluxis longus (FHL) can be visualized under the flexor retinaculum in this order from anterior to posterior. The entire course of tibial nerve and its medial calcaneal, medial and lateral plantar branches can be examined (Figs. 4 and 5). It is important to note that the medial calcaneal nerve or the first branch of lateral plantar nerve (FBLPN) entrapment can mimic more common conditions such as plantar fasciitis [3, 4].

2.3 Lateral Ankle

For lateral ankle evaluation (Table 3), the patient may be placed in lateral decubitus position. Posterior to the lateral malleolus is the retromalleolar groove, which contains peroneus longus (PL) and brevis (PB) tendons. At supramalleolar level, the PL tendon lies lateral to the PB muscle belly. Both of these structures arc around the malleolus as the PB becomes tendinous and sits superior to the PL tendon. At the inframalleolar region, the PB and PL tendons are separated by the peroneal tubercle of the calcaneus which allows the PB tendon to insert at the base of fifth metataral (Fig. 6). The short axis view may identify hypoechoic clefts or longitudinal split tears. If peroneus tendon subluxation is suspected, dynamic scanning should be performed from the neutral position to dorsiflexion and with eversion of the foot against resistance.

To evaluate the anterior talofibular ligament (ATFL), with the forefoot in slight inversion, the probe is placed parallel to the plantar surface at the lateral malleolus level (Fig. 7).

From the ATFL, keep the posterior edge of the probe on the lateral malleolus and rotate the anterior edge upwards towards the distal tibia. This maneuver will allow the visualization of anterior inferior tibiofibular ligament (Fig. 8).

To evaluate the calcaneofibular ligament, the probe is placed in an oblique coronal plane over the lateral malleolus and its inferior edge at 7 o'clock position with ankle in dorsiflexion (Fig. 9). The calcaneofibular ligament lies deep to the PL and PB tendons.

Table 3 Lateral ankle evaluation checklist

Peroneus longus and brevis
Anterior talofibular ligament
Anterior inferior tibiofibular ligament
Calcaneofibular ligament

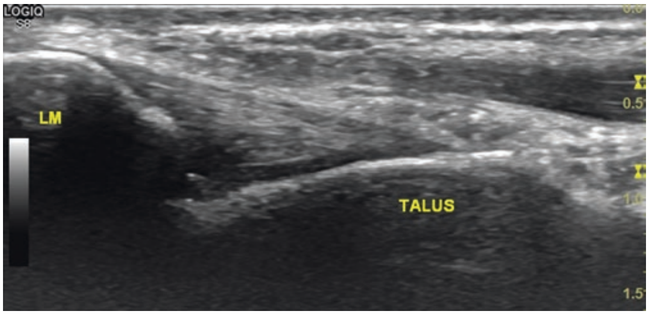

Fig. 7 Anterior talofibular ligament

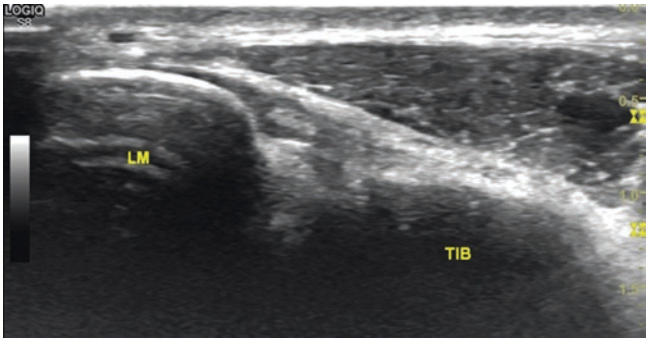

Fig. 8 Anterior tibiofibular ligament

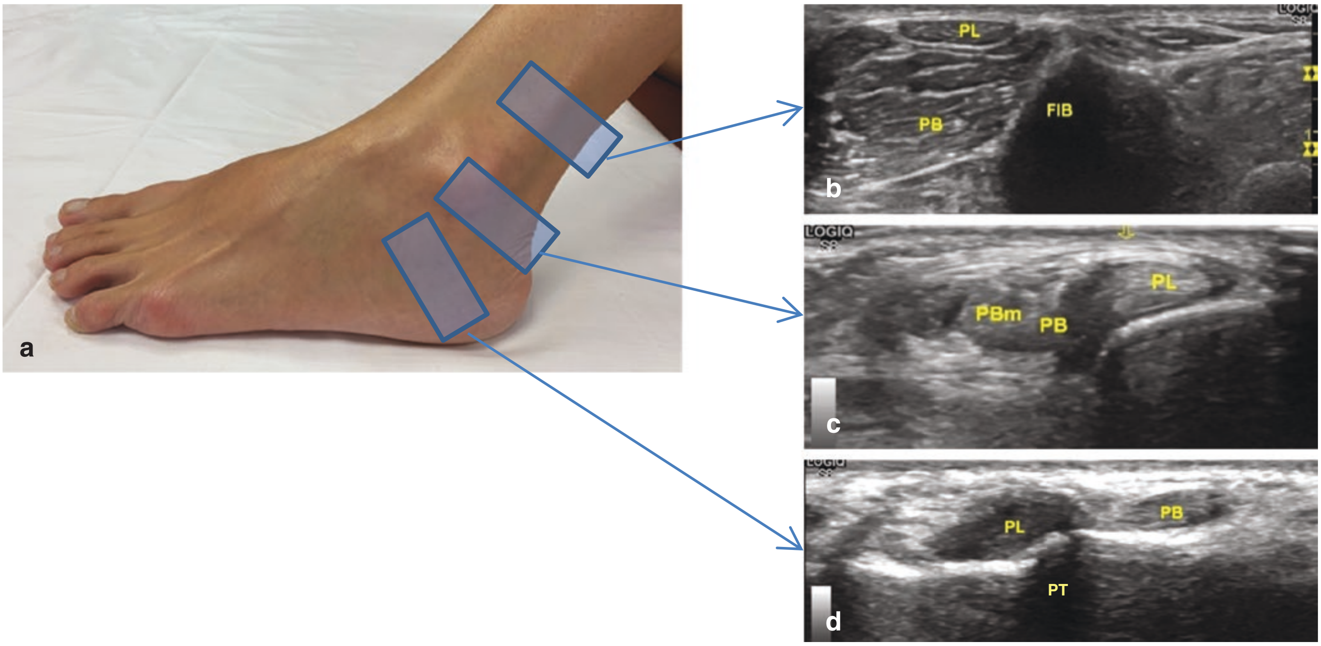

Fig. 6 Normal peroneal tendons. (**a**) Skeletal model showing the level of the probe position. (**b**) Peroneus brevis (PB) lies posterior to the longus. (**c**) In the retromalleolar groove, the tendons are restrained by the superior peroneal retinaculum (arrow) (**d**) PB and Peroneus longus (PL) in the inframalleolar area at the level of the peroneal tubercle (PT) of the calcaneus

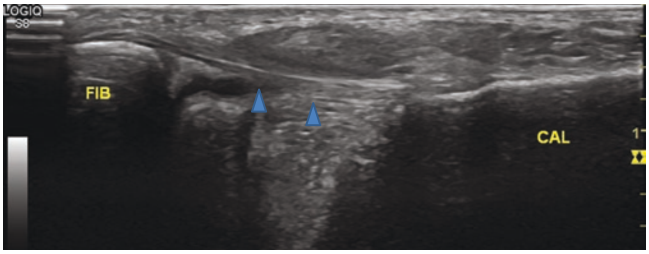

Fig. 9 Calcaneofibular ligament

Table 4 Posterior ankle evaluation checklist

Achilles tendon
Plantar fascia

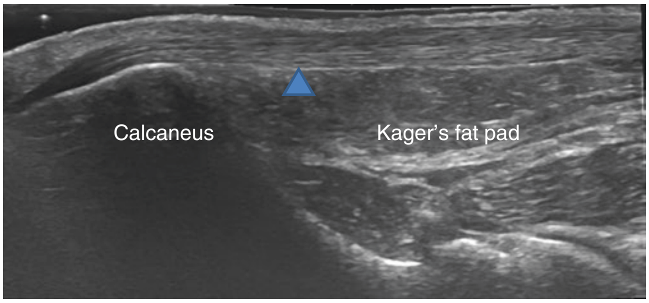

Fig. 10 Normal Achilles tendon

2.4 Posterior Ankle

For posterior ankle evaluation (Table 4), a patient is placed in a prone position with the foot hanging off the examination table. The Achilles tendon is a conjoined tendon of both soleus and gastrocnemius muscles and it is the largest weight-bearing tendon in the body. To evaluate the Achilles tendon, the foot should be dorsiflexed to reduce anisotropy. The Achilles tendon has uniform thickness and a fibrillar pattern. There is a fat pad anterior to the Achilles tendon is known as Kager's fat pad. Distally it may appear hypoechoic due to anisotropy because the fibers change their direction from horizontal to vertical to insert at the calcaneus. The average thickness of the Achilles tendon is approximately 5–6 mm [5]. The retrocalcaneal bursa can be seen distally (Fig. 10). The plantaris tendon can be seen medial to the Achilles tendon and may mimic residual fibers of the Achilles tendon in the case of a complete tear.

Moving the probe over the plantar aspect of the heel helps to evaluate the plantar aponeurosis at its calcaneal insertion. It should appear hyperechoic, uniform, and 4 mm or less in thickness [6] (Fig. 11).

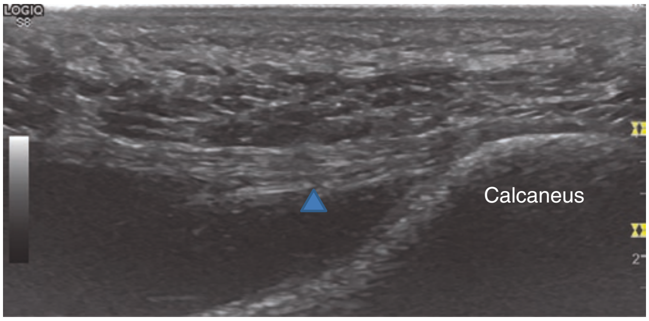

Fig. 11 Normal plantar fascia

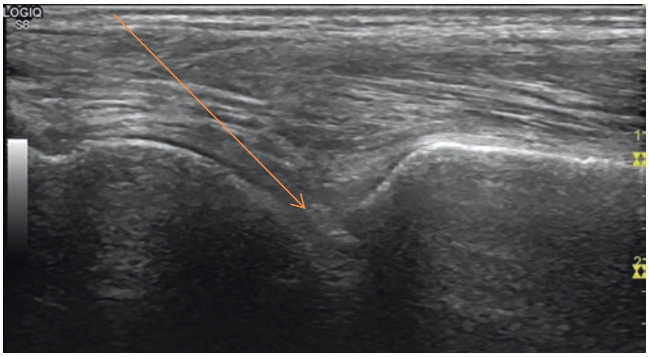

Fig. 12 Tibiotalar joint injection
Steps
1. Place the ultrasound probe along the long axis with respect to the tibialis anterior tendon and medial to it
2. Identify and avoid the dorsalis pedis artery
3. When the anterior recess of the joint is visualized, insert the needle using the in plane approach from distal to proximal
4. After negative aspiration, inject the medication

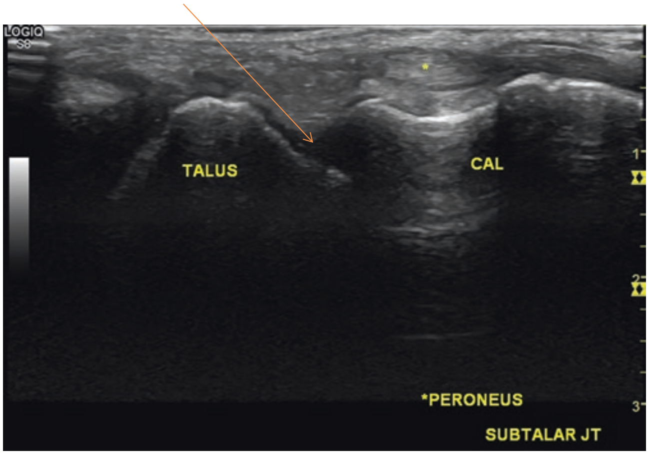

Fig. 13 Subtalar joint injection
Steps
1. Place the ultrasound probe in a coronal plane, along the calcaneofibular ligament anterior to the lateral malleolus
2. Using the out of pane technique, insert the needle toward the joint space
3. After negative aspiration, inject the medication

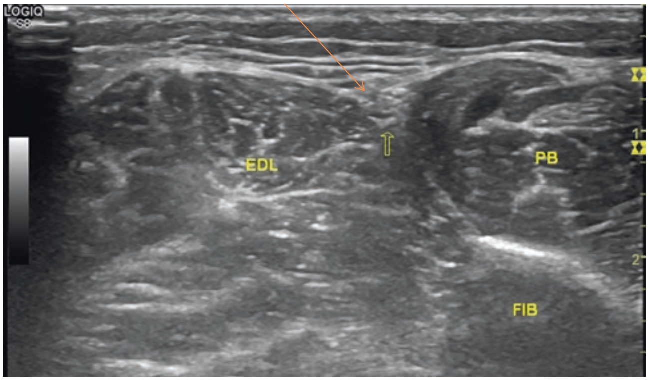

Fig. 14 Superficial peroneal nerve (SPN) block
Position: Lateral decubitus position with the injection site on top
Steps
1. Place the ultrasound probe in a sagittal plane, approximately 8–10 cm proximal to the ankle crease
2. The SPN is visualized between the peroneous brevis and extensor digitorum longus muscles
3. After negative aspiration, inject the medication

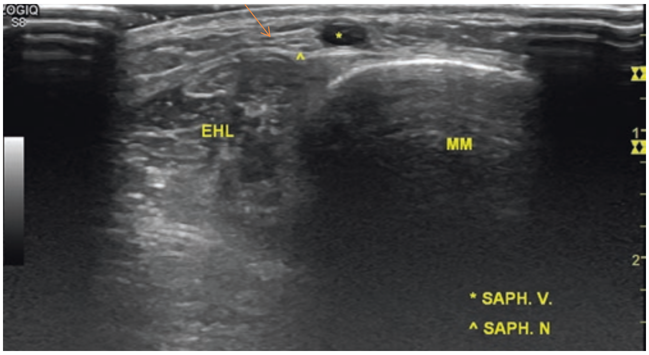

Fig. 15 Saphenous nerve (SN) block
Position: Supine
Steps
1. Place the ultrasound probe in a sagittal plane on the anteromedial aspect of ankle
2. The SN is visualized subcutaneously between the extensor hallucis longus tendon and the medial malleolus next to the great saphenous vein
3. After negative aspiration, inject the medication

3 Ultrasound Guided Ankle Injections and Nerve Blocks

3.1 Tibiotalar and Subtalar Joint Injection

Indications: Indications include pain arising from various arthritic conditions such as osteoarthritis, rheumatoid arthritis, crystalloid deposition disease, and synovitis.

Medications: 1 mL total containing 0.5 mL of local anesthesia (1% lidocaine or 0.25% bupivacaine) and 20 mg of triamcinolone or equivalent corticosteroid.

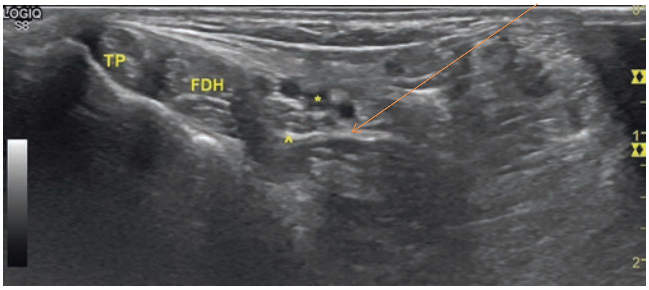

Fig. 16 Posterior tibial nerve (PTN) block
Position:
Supine: foot rolled outward and knee slightly bent
Prone: ankle elevated with a pillow on the anterior surface
Steps
1. Place the ultrasound probe in a coronal plane, towards the calcaneus posterior to the medial malleolus
2. The PTN is visualized at the level of the Achilles tendon and the medial malleolus posterior to the posterior tibial artery
3. After negative aspiration, inject the medication

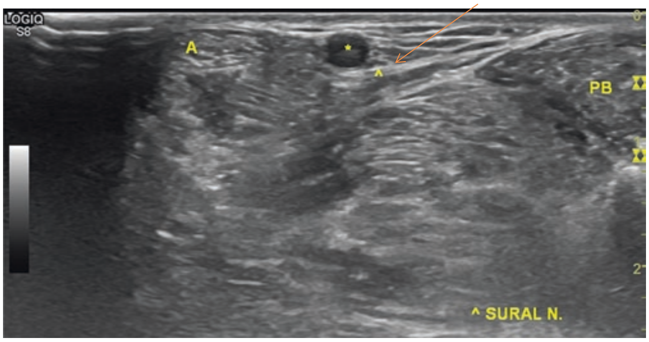

Fig. 17 Sural nerve (SN) block
Position: lateral decubitus with knee extended
Steps
1. Place the ultrasound probe in a coronal plane, towards the calcaneus posterior to the lateral malleolus
2. The SN is visualized between the Achilles tendon and the peroneous brevis
3. After negative aspiration, inject the medication

For all procedures we recommend strict sterile technique that includes cleaning the skin with an antiseptic solution, placing the transducer in a sterile cover, and using sterile, single use, ultrasound gel.

3.2 Ankle Blocks

Medications: 1 mL total containing 0.5 mL of local anesthesia (1% lidocaine or 0.25% bupivacaine) and 20 mg of triamcinolone or equivalent corticosteroid.

References

1. Nazarian LN, et al. Synovial fluid in the hindfoot and ankle: detection of amount and distribution with US. Radiology. 1995;197(1):275–8.
2. Mengiardi B, et al. Anterior tibial tendon abnormalities: MR imaging findings. Radiology. 2005;235(3):977–84.
3. Brown MN, Vanetti TK, Trescot AM, Karl HW. Medial calcaneal nerve entrapment. In: Trescot AM, editor. Peripheral nerve entrapments. Cham: Springer; 2016. p. 871–81.
4. Presley JC, et al. Sonographic visualization of the first branch of the lateral plantar nerve (Baxter nerve): technique and validation using perineural injections in a cadaveric model. J Ultrasound Med. 2013;32(9):1643–52.
5. van Dijk CN, et al. Diagnosis of ligament rupture of the ankle joint. Physical examination, arthrography, stress radiography and sonography compared in 160 patients after inversion trauma. Acta Orthop Scand. 1996;67(6):566–70.
6. Cardinal E, et al. Plantar fasciitis: sonographic evaluation. Radiology. 1996;201(1):257–9.

Ultrasound Guided Nerve Blocks for Lower Extremity

Christopher M. Harmon, Kelly S. Davidson, Erik Helander,
Matthew R. Eng, and Alan David Kaye

1 Fascia Iliaca Nerve Block

1.1 Introduction

The fascia iliaca overlies both the femoral and lateral femoral cutaneous nerves. The general idea is that by placing a large volume of local anesthetic beneath the fascia iliaca, there will be enough spread to reach both the femoral and lateral femoral cutaneous nerves. The technique was first described by Dalens et al. in which a landmark based approach was utilized to deposit local anesthetic in the fascia iliaca compartment in an attempt to anesthetize the femoral, lateral femoral cutaneous, and obturator nerves [1]. It was previously thought that the block would also spread to cover the lumbosacral plexus due to the presence of a fascial sheath tracking up towards it, but there has been a lack of evidence that this sheath exists [2]. The landmark based approach employs a loss of resistance technique with one pop when passing through the fascia lata and then a second with the fascia iliaca. This technique however is only about 38% effective in completely blocking the lumbar plexus nerve distribution [3]. The use of ultrasound guidance can significantly improve the sensory block to the medial thigh as well as femoral and obturator motor blocks [4].

1.2 Patient Positioning and Landmarks

For the ultrasound guided fascia iliaca block patients are typically in the supine position. To provide better access to the inguinal crease the bed should be flattened as much as can be tolerated by the patient. A good starting approach for ultrasound placement is to place the probe at the lateral third of a line drawn between the pubic tubercle and the anterior superior iliac spine and move medially until the femoral artery is visualized. This point at the lateral third of the imaginary line is the needle insertion point for the landmark-based technique.

1.3 Ultrasound Anatomy

Scan the inguinal crease until the femoral artery is identified. The iliopsoas muscle is located deep and lateral to the femoral artery and covered by a thin layer of fascia. The fascia iliaca overlies the iliacus muscle in the pelvis and merges with the layer of fascia above the psoas muscle more medially. The femoral nerve is located lateral to the femoral artery between the fascia iliaca and iliopsoas muscle. The fascia lata, which is a key component of the landmark-based technique, is more superficial in the subcutaneous layer. Following the fascia iliaca laterally will show it overlying the sartorius muscle [4].

1.4 Nerve Distribution

The area covered by the fascia iliaca block is dependent upon the amount of spread achieved and it's ability to reach the target nerves. The femoral nerve is responsible for motor function including the main hip flexors and knee extensors.

C. M. Harmon (✉)
Department of Anesthesiology, Thomas Jefferson University Hospital, Sidney Kimmel Medical College, Philadelphia, PA, USA

K. S. Davidson
Department of Anesthesiology, LSU-HSC, New Orleans, LA, USA
e-mail: kdav28@lsuhsc.edu; meng@lsuhsc.edu

E. Helander
Department of Anesthesiology, University of Florida-Gainesville, Gainesville, FL, USA

M. R. Eng
LSU-HSC New Orleans, Anesthesiology, New Orleans, LA, USA

A. D. Kaye
Departments of Anesthesiology and Pharmacology, Toxicology, and Neurosciences, Lousiana State University Health Sciences Center, Shreveport, LA, USA

Department of Anesthesiology, Department of Pharmacology Louisiana State University School of Medicine, Louisiana State University Health Sciences Center, New Orleans, LA, USA
e-mail: akaye@lsuhsc.edu

© Springer Nature Switzerland AG 2021
J. Li et al. (eds.), *Ultrasound Fundamentals*, https://doi.org/10.1007/978-3-030-46839-2_17

Its sensory distribution includes the anterior and medial thigh to the area of the knee, as well as the medial lower leg and ankle via the saphenous nerve. See the section on femoral nerve block for expanded details regarding the femoral nerve distribution. The lateral femoral cutaneous nerve covers sensation to the anterolateral thigh. As described above, coverage of the obturator nerve is inconsistent and details of its blockade and distribution are mentioned elsewhere in this chapter.

1.5 Technique

After properly disinfecting the skin and applying sterile gloves, the femoral artery is identified with the ultrasound transducer as described above. The fascia iliaca is located with the femoral artery between it and the iliopsoas muscle. Moving laterally will bring the sartorius muscle into view. Rotate the probe 90 degrees with the top marker now facing the umbilicus. Scan superiorly and laterally along the line between the pubic tubercle and anterior superior iliac spine to identify the “bowtie” where the internal oblique meets the sartorius. Before inserting the needle in-plane, a skin wheal is made to minimize patient discomfort. The needle can be visualized traversing the sartorius muscle and angled towards the bowtie between it and the internal oblique, with the fascia iliaca running beneath each muscle. A pop may be felt as the needle penetrates the fascia iliaca and a test of 1–2 mL of local anesthetic is given to ensure the correct space. With correct injection, the local anesthetic should be seen below the fascia iliaca and pushing the underlying iliacus muscle downwards. Once confident the correct space has been identified, a large volume (30 to 40 mL) of dilute local anesthetic is injected while advancing the needle carefully and continuing to dissect the muscle from the overlying fascia. Turning the probe back to its original orientation should show spread medially toward the femoral nerve and laterally beneath the sartorius muscle to ensure adequate blockade of both the femoral and lateral femoral cutanous nerves [4, 5]. As stated above, the blockade of the anterior branch of the obturator nerve may occur but is not reliable with this particular block.

2 Popliteal Nerve Block

2.1 Introduction

The goal of the popliteal nerve block is to localize the sciatic nerve in the region of the popliteal fossa just prior to its division into the tibial nerve (TN) and common peroneal nerve (CPN). It can provide anesthesia for foot and ankle surgeries, though needs to be combined with a saphenous or femoral block if the procedure is going to include the medial lower leg and ankle. By blocking the sciatic nerve more distal, it spares motor function for the thigh and hamstring muscles allowing knee movement and aiding in early ambulation. The use of ultrasound has increased the success and efficiency of these blocks given the variability in the location of the sciatic nerve split [6].

2.2 Patient Positioning and Landmarks

There is both a lateral and posterior approach to the popliteal nerve block. The posterior approach typically requires prone positioning, which can be difficult for many patients to tolerate. The lateral approach can be done either supine or lateral and has been shown to be equally as effective as the posterior approach [7]. If done supine, the foot needs to be placed on an elevated footrest or an assistant is needed to hold the foot in place on the bed with the knee bent. Placing the patient laterally allows them to lie comfortably with their knee maintained in a flexed position (Fig. 1).

2.3 Ultrasound Anatomy

With the ultrasound probe in the popliteal crease, the first step is to identify the popliteal artery. Other features that can be visualized at this level include the femur, popliteal vein, biceps femoris muscle, and the sciatic nerve or its branches. The popliteal fossa is bordered laterally by the biceps femoris muscle and medially by both the semimembranosus and semitendinosus muscles. Once the semitendinosus muscle and tendon are located, the popliteal artery should be visualized directly lateral. Moving further lateral from the artery will encounter the popliteal vein, followed by the tibial and common peroneal nerves. Though it can be highly variable depending on patient body habitus, these nerves are typically 2–5 cm deep at the level of the popliteal crease. Tracing the

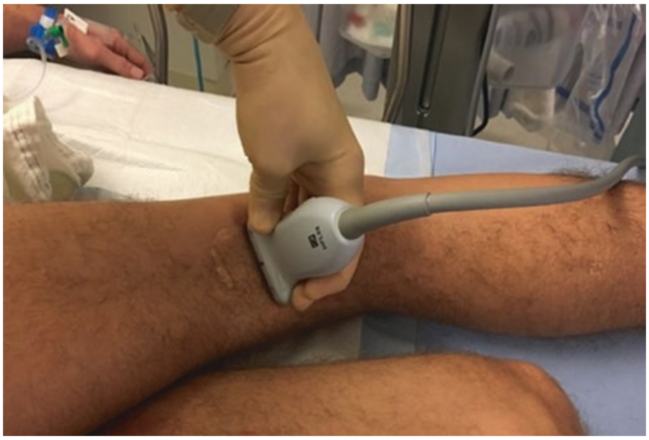

Fig. 1 Proper transducer positioning for lateral approach to popliteal nerve block

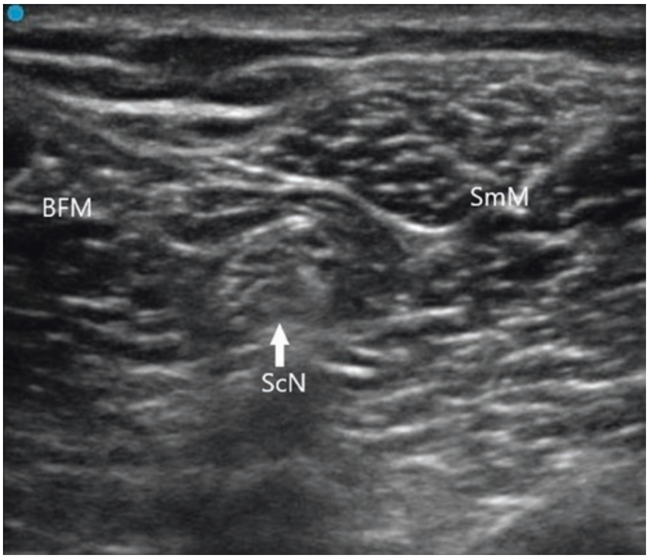

Fig. 2 Ultrasound anatomy for popliteal nerve block showing Sciatic nerve (ScN) prior to its division, Biceps femoris muscle (BFM), and Semimembrinosus muscle (SmM)

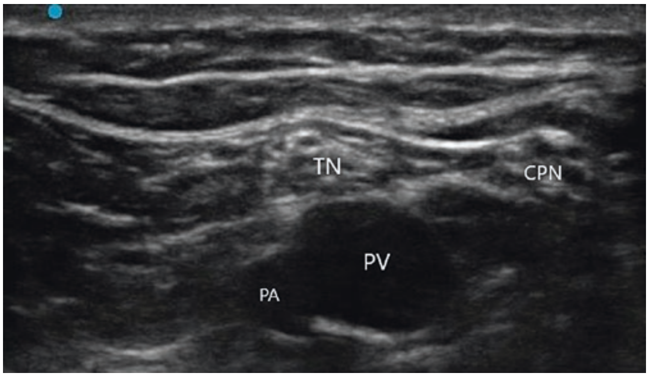

Fig. 3 Ultrasound anatomy for popliteal nerve block distal to the Sciatic Nerve split into the Tibial Nerve (TN) and Common Peroneal Nerve (CPN). Also shown are the Popliteal Artery (PA) and Popliteal Vein (PV)

nerves cephalad will show a convergence of the tibial and common peroneal nerves into the sciatic nerve (Figs. 2 and 3), which is highly variable and can occur anywhere from the popliteal fossa to more proximal in the thigh. At the level of the nerve bifurcation it may be difficult to still visualize the vascular structures, which dive deeper the more cephalad the ultrasound transducer is moved. Once the sciatic nerve is located, the transducer can be moved back caudad to trace the tibial and common peroneal nerves as they travel through the popliteal fossa and further into the lower leg. The common peroneal nerve will be lateral and slightly superficial to the tibial nerve and passes between the head and neck of the fibula below the popliteal fossa. Below the popliteal fossa, the tibial nerve can be followed as it dives deep to the gastrocnemius muscle [8, 9].

2.4 Nerve Distribution

Blocking the sciatic nerve at the level of its bifurcation allows for sparing of the hamstring muscles and therefore knee flexion. The tibial nerve gives off cutaneous sural nerve branches before terminating as the medial and lateral plantar nerves. The common peroneal nerve also gives off cutaneous sural branches prior to its termination as the superficial and deep peroneal nerves. If performed correctly, a popliteal nerve block should cover both motor and sensory to the lower extremity below the knee. As mentioned before, the saphenous nerve supplies the medial leg and foot and this will need to be blocked separately if the procedure is to involve these areas.

2.5 Technique

As described above, start by identifying the popliteal artery at or slightly above the popliteal crease with the ultrasound transducer in a transverse position. Once identified, the common peroneal and tibial nerves should be located slightly superficial and lateral to the popliteal artery. The transducer may need to be tilted or moved slowly more proximal in the thigh to bring the nerves into view. Once in view, they can be traced moving the transducer further cephalad until visualized coming together within the sciatic nerve sheath. The target for needle insertion should be right at the point where both nerves are visualized separately but still within the sciatic nerve sheath. For an out-of-plane approach, localize the area in the center and just directly below the transducer. Insert the block needle at a slightly cephalad angle to reach the sciatic nerves in the center of the ultrasound screen. For an in-plane approach, localize the area about 3 cm above the edge of the ultrasound transducer and then insert the block needle directly horizontal to the probe. The needle should be in clear view during any advancement to prevent inadvertent vascular or nerve injury. Once the needle pierces the sciatic nerve sheath, inject a small amount of local anesthetic to make sure it spreads to surround the individual components (common peroneal and tibial nerves) within the sheath. The needle may need to be adjusted in slightly different directions to ensure spread on all sides of the nerves. Scanning both cephalad and caudad while injecting should show local anesthetic spread within the sciatic and individual common peroneal/tibial nerve sheaths. If any significant resistance is met, stop injecting and withdraw the needle as this may signal an intraneural injection [6, 10–12].

3 Sciatic Nerve Block

3.1 Introduction

The sciatic nerve is the largest nerve in the body at its origin and is responsible for much of the motor and sensory function of the lower extremity. A sciatic nerve block is indicated for any foot and ankle surgery, below knee amputation, or knee surgery involving the posterior compartment. Many times it is necessary to combine the sciatic nerve block with a femoral nerve block in order to adequately cover the medial aspect of the lower leg and ankle. There are multiple approaches to the block that will be described separately below including anterior, transgluteal, and subgluteal. The sciatic nerve may also be blocked at the popliteal level for more distal lower extremity procedures and this technique is described elsewhere in this chapter. The choice of technique depends on the patient's ability to tolerate positioning, as well as the proceduralist's experience with any particular ultrasound guided approach.

3.2 Patient Positioning and Landmarks

Patient positioning for the sciatic nerve block is dependent on which approach is best for the patient and operator. For the anterior approach, the patient is supine with the hip slightly abducted. The hip and knee can be flexed to aid with exposure. The ultrasound transducer in initially placed at the level of the minor trochanter on the anteromedial aspect of the thigh [13] (Fig. 4). For the transgluteal and subgluteal approaches, the patient is in the lateral decubitus position with the hip and knee flexed. This may be uncomfortable or difficult depending on the particular patient and an anterior approach may be a better choice. For the transgluteal approach, the ischial tuberosity and greater trochanter are palpated and the transducer is initially placed between the two (Fig. 5). Given the depth, a curvilinear probe may be needed to adequately visualize the necessary structures. The subgluteal approach is done just below the gluteal crease where the nerve courses more superficial than at the transgluteal level [14] (Fig. 6).

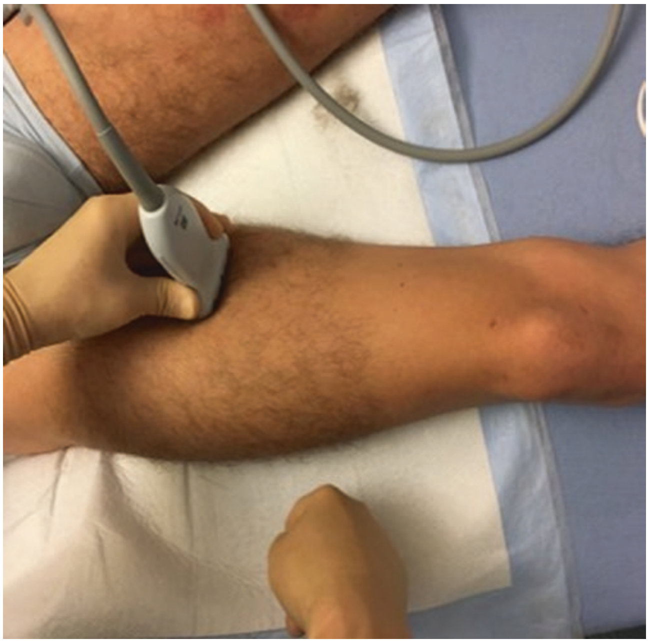

Fig. 4 Proper transducer positioning for anterior approach to sciatic nerve block

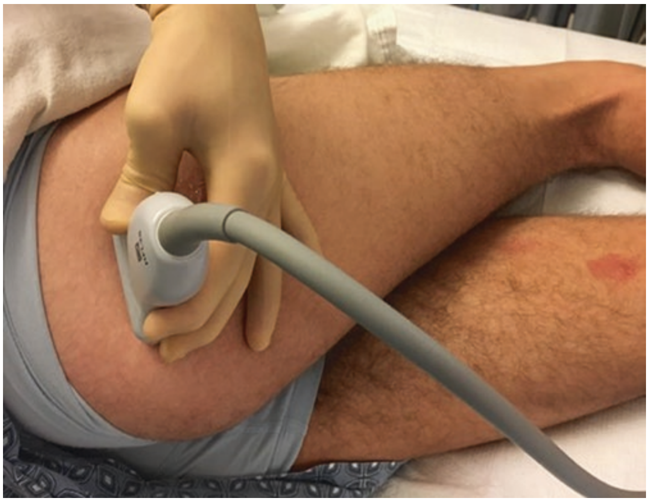

Fig. 5 Proper transducer positioning for transgluteal approach to sciatic nerve block

3.3 Ultrasound Anatomy

The sciatic nerve is the largest and only terminal branch of the sacral plexus. After exiting through the greater sciatic notch, it courses between the ischial tuberosity and the greater trochanter of the femur deep to the gluteus maximus muscle and superficial to the quadratus femoris muscle. This is the appropriate level for a transgluteal approach. In its proximal course, the sciatic nerve gives off articular branches to the posterior capsule of the hip. Occasionally these branches come off the sacral plexus directly. Following the nerve slightly further down the thigh will show it between the long head of the biceps femoris and the posterior surface of the adductor magnus muscle [15]. This is the appropriate level for a subgluteal approach (Fig. 7).

For an anterior approach, placing a curvilinear ultrasound transducer on the anteromedial aspect of the thigh at the level of the minor trochanter of the femur will show the femoral

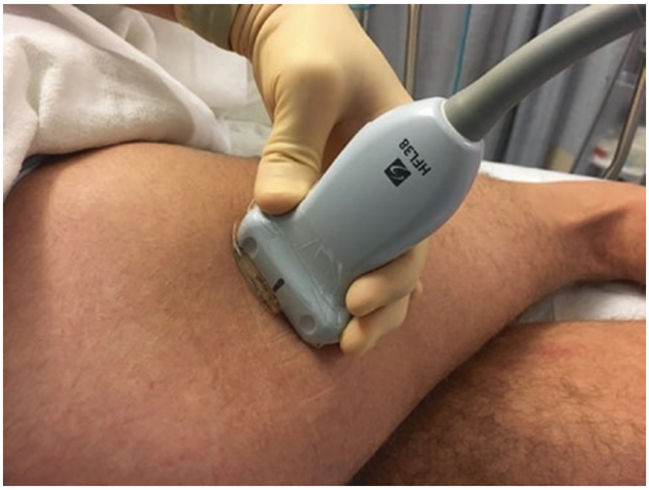

Fig. 6 Proper transducer positioning for subgluteal approach to sciatic nerve block

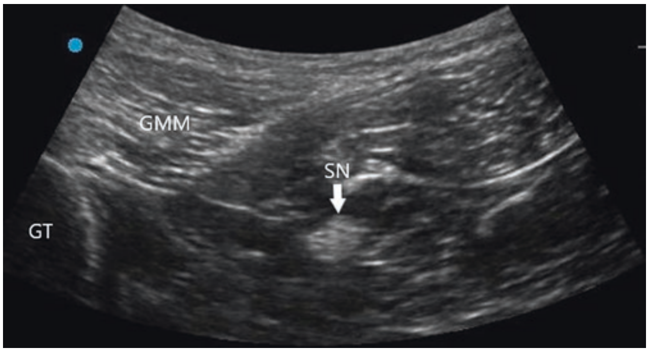

Fig. 7 Ultrasound anatomy for subgluteal approach to sciatic nerve block including Greater Trochanter of Femur (GT), Gluteus Maximus Muscle (GMM), and Sciatic Nerve (SN)

artery beneath the sartorius muscle. Deep to the femoral artery and directly below the vastus intermedius is the femur, which is hyperechoic with a dark shadow beneath it. The sciatic nerve can be seen as a hyperechoic structure medial to the femur and between the adductor magnus muscle and the deeper hamstring muscles (Fig. 8). The sciatic nerve continues its course down the posterior thigh to its bifurcation into the tibial and common peroneal nerves just above the popliteal crease [13, 14].

3.4 Nerve Distribution

The sciatic nerve block will cover the motor function of the hamstrings and biceps muscles, sensation to the posterior knee, and both motor and sensation to the entire leg below the knee with the exception of the medial aspect of the lower leg and ankle. If blocked high enough, it will also cover articular branches to the hip joint. The anterior approach is performed more distal along the nerve course and is therefore less reliable at blocking the articular branches to the hip and other more proximal sensory/motor branches. The posterior femorocutaneous nerve supplies the skin of the posterior aspect of the thigh and diverges from the sciatic nerve proximal to where the anterior approach is performed. This typically is of no significance unless the surgery is to involve the posterior thigh. It is generally blocked with the transgluteal and subgluteal approaches.

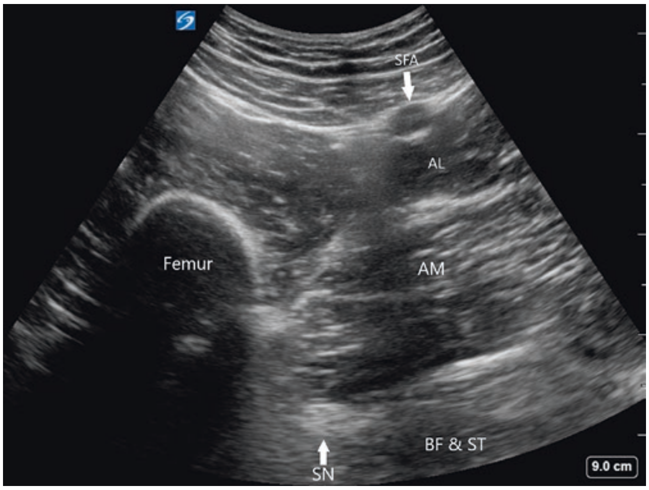

Fig. 8 Ultrasound anatomy for anterior approach to sciatic nerve block showing Superficial Femoral Artery (SFA), Adductor Longus Muscle (AL), Adductor Magnus Muscle (AM), Biceps Femoris Muscle (BF), Semitendinosus Muscle (ST), and Sciatic Nerve (SN)

3.5 Technique

For the anterior approach the patient is placed supine with the hip slightly abducted. Landmark based techniques were first described by Beck in 1963, followed by a newer technique in 1999 by Chelly and Delaunay [16, 17]. The subsequent introduction of ultrasound guided techniques allows for direct visualization of the nerve and its surrounding structures [18, 19]. Nerve stimulation is not required, though it may be helpful given the depth of the nerve and depending on the skill level of the operator. The curvilinear ultrasound transducer is placed at the level of the minor trochanter of the femur on the anteromedial aspect of the thigh just distal to the femoral crease. Scanning in this region will allow identification of the femoral artery first just beneath the sartorius muscle. The femur will be deep to the artery below the vastus intermedius muscle. Medial to the femur and just below the adductor magnus muscle is the hyperechoic sciatic nerve, typically at a depth of 8–10 cm. If having difficulty visualizing the nerve and the patient is in a cooperative state, having them dorsiflex or plantar flex the ankle may move the nerve within the fascial plane and make identification easier. Tilting the transducer slightly cephalad or caudad may also help clear up the image. Once the nerve is correctly identified, the block needle can be inserted in-plane or out-of-plane. The in-plane approach allows for continuous visualization of the entire needle, though may be difficult given the depth of the nerve in many patients and the steep angle necessary to reach it. For an in-plane approach, insert the block needle from the medial side of the transducer until it is successfully identified perineural. Inject a small amount of local anesthetic to confirm placement and assure that the needle is not intraneural, which would be felt as resistance to injection. Inject the remaining local anesthetic with constant visualization to ensure adequate spread around the sciatic nerve [13, 14, 17].

The transgluteal approach begins by placing the patient in the lateral decubitus position. Palpate the ischial tuberosity and greater trochanter and take note of the space between the two, as this will be where the transducer is initially. Directly after its exit from the pelvis through the greater sciatic notch, the sciatic nerve travels deep to the gluteus maximus muscle between the ischial tuberosity and greater trochanter of the femur. Under ultrasound guidance, identify the nerve at this level. Given the depth, a curvilinear ultrasound transducer may be necessary. Small movements may need to be made with the transducer either proximally or distally from the starting point in order to bring the nerve into a more clear view. Again, tilting the probe slightly in either direction may help with this as well. The block needle is inserted using an in-plane technique in a lateral to medial direction. Once the needle is directly adjacent to the nerve, inject a small amount of local anesthetic. The local anesthetic should shift the sciatic nerve away from the needle. Any significant resistance to injection is most likely indicative of an intraneural injection and the needle will need to be withdrawn slightly. After ensuring the needle is in the correct location, inject the remainder of the local anesthetic solution [13, 14].

The subgluteal approach is similar in initial positioning to the transgluteal approach, but it targets the sciatic nerve more distal in its course as it travels between the long head of the biceps femoris and the posterior surface of the adductor magnus muscle. This is typically more superficial than the transgluteal approach and the curvilinear transducer may not be necessary depending on patient body habitus. The ultrasound transducer is placed at the gluteal fold halfway between the greater trochanter and the ischial tuberosity. The sciatic nerve may be located closer to the ischial tuberosity, near the origin of the biceps femoris muscle. Following the nerve distally will show it coursing more superficial than in the transgluteal region. Once the nerve is correctly identified, the block needle is inserted in-plane in a lateral to medial direction. As with previous approaches, confirm successful needle placement with a small amount of local anesthetic before injecting the full volume [13, 20].

4 Obturator Nerve Block

4.1 Introduction

The obturator nerve block can be performed safely under ultrasound guidance and offers benefits for a number of different clinical situations and procedures. It can provide additional pain control for knee surgery, alone or in combination with a femoral and/or sciatic nerve block. It has been shown to be beneficial in anterior cruciate ligament (ACL) reconstruction by providing analgesia for the gracilis tendon harvest [21–23]. It is also used to aid with chronic hip pain or adductor spasticity that can accompany patients with hemiplegia, paraplegia, or a number of other neuromuscular disorders [24, 25]. Another proven benefit has been to prevent the obturator reflex during transurethral resection of bladder tumor (TURBT), which if left unblocked can cause a sudden thigh adduction jerk resulting in potential patient harm [26, 27]. There are a number of published approaches to the ultrasound guided obturator nerve block that can be split into the broader overall categories of either proximal or distal and these will be further discussed in the following sections.

4.2 Patient Positioning and Landmarks

For both proximal and distal approaches, the block can be done supine with the thigh abducted and externally rotated. There are multiple techniques described in the literature in regards to the proximal approach, one of which involves placing the patient in lithotomy or full hip flexion and external rotation, but only the supine positioning will be discussed in this chapter [28]. The initial transducer placement is either at the level of the inguinal crease with visualization of the femoral vascular structures or slightly inferior to the crease on the medial thigh in at attempt to visualize the obturator nerve branches themselves (Fig. 9).

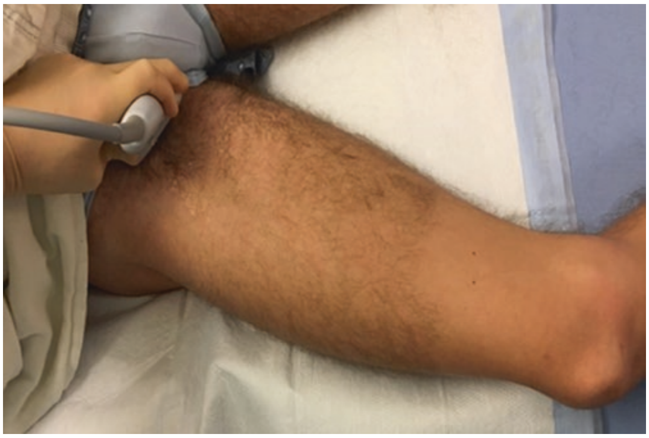

Fig. 9 Proper transducer positioning for both proximal and distal approaches to the obturator nerve block

4.3 Ultrasound Anatomy

Forming in the lumbar plexus from the anterior rami of L2-4, the obturator nerve then courses down into the pelvis medial to the psoas major muscle. It exits the pelvis through the obturator foramen and into the anteromedial thigh. At some point near its exit through the obturator foramen, the nerve bifurcates into an anterior and posterior branch. The actual position of this division is variable and one study showed that it occurred in the pelvis in 23% of cadaver subjects, at the level of the obturator foramen in 52%, and within the thigh in 25% [29]. Though separate, the anterior and posterior branches still course together between the pectineus and obturator externus muscles just past their exit from the obturator foramen (Fig. 10). Moving caudad to the level of the femoral crease will show the anterior branch of the obturator nerve between the fascial planes of the pectineus and adductor brevis muscles. As it courses further, it can be found between the adductor longus and adductor brevis muscles. The posterior branch of the obturator nerve is found between the fascial planes of the adductor brevis and adductor magnus muscles (Fig. 11). Further along its course, it may give off terminal articular branches to the medial aspect of the capsule of the knee joint. It may also supply articular branches to the hip, though these typically come off the common obturator nerve prior to its division [29].

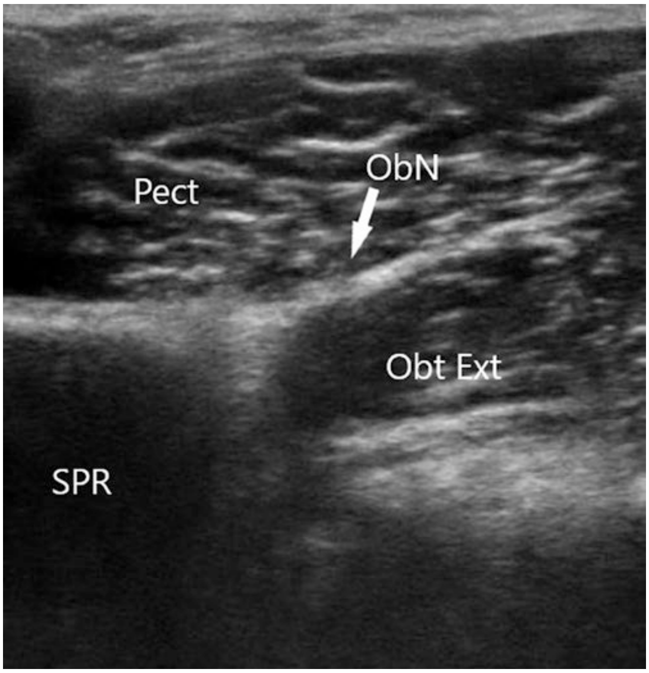

Fig. 10 Ultrasound anatomy for proximal approach to obturator nerve block including Pectineus Muscle (Pect), Obturator Nerve (ObN), Obturator Externus Muscle (Obt Ext), and Superior Pubic Ramus (SPR)

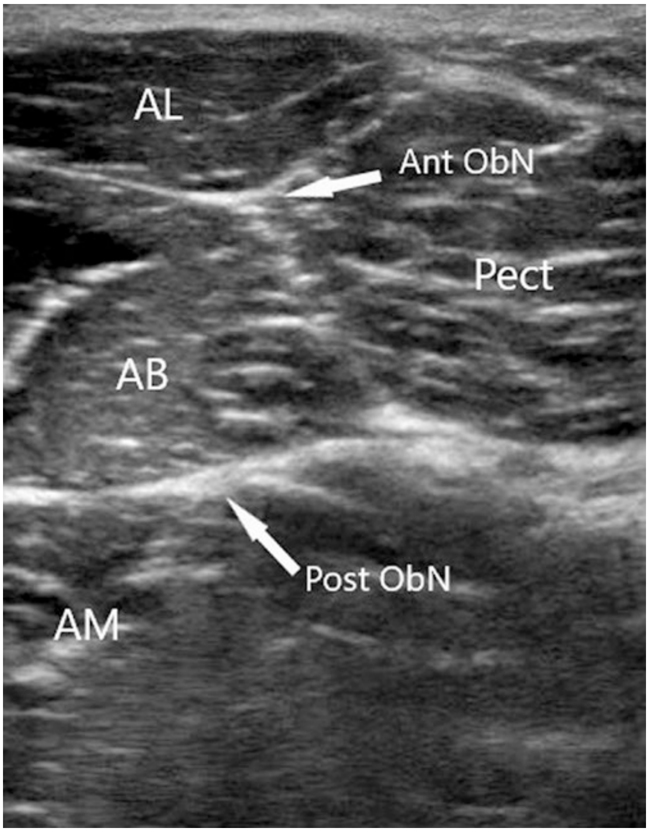

Fig. 11 Ultrasound anatomy for distal approach to obturator nerve block showing Anterior branch of Obturator Nerve (Ant ObN) between the Adductor Longus Muscle (AL) and Adductor Brevis Muscle (AB). Posterior branch of Obturator Nerve (Post ObN) between Adductor Brevis Muscle (AB) and Adductor Magnus Muscle (AM). Also show is the Pectineus Muscle (Pect)

4.4 Nerve Distribution

As mentioned previously, the common obturator typically gives off articular branches to the hip that may play an important role in chronic hip pain and spasticity. After its split, the anterior branch of the obturator nerve supplies motor branches to the adductor brevis, longus, and gracilis muscles. The anterior branch is also responsible for sensory branches to the medial thigh, though this is highly variable. The posterior branch supplies motor branches to the adductor magnus and brevis muscles. It has also been shown to supply the adductor longus and obturator externus muscles as well, though this too is variable. The posterior branch also gives cutaneous branches to the medial thigh and medial capsule of the knee from its articular branches. Overall, the cutaneous distribution of the obturator nerve is inconsistent and may have no sensory function in up to 50% of patients [30]. The obturator nerve is responsible for the majority of thigh adductor function, though there may be some co-innervation from either the sciatic or femoral nerves with their branches to the adductor magnus and pectineus muscles respectively

[31, 32]. In addition, about 10-30% of patients give off an accessory obturator nerve from the L3-4 roots that travels along with the femoral nerve and supply the pectineus muscle [29]. Due to this, successfully blocking the obturator nerve may not result in complete loss of adductor strength.

4.5 Technique

The distal approach to the obturator nerve block may be less technically challenging than the proximal approach, though the anterior and posterior branches need to be blocked separately and any articular branches to the hip that arise prior to the division will be missed. For the distal approach, the patient is placed supine with the thigh abducted and slightly rotated externally. The starting position for the ultrasound transducer is at the level of the inguinal crease to identify the femoral vessels. Moving medially along the crease will allow visualization of the individual adductor muscles, including the adductor longus, brevis, magnus, and pectineus muscles. Once the individual muscles are identified, a block needle is inserted in-plane and positioned between the fascia of the pectineus and adductor brevis muscles. Once it is confirmed that the needle is in the correct plane, half of the local anesthetic solution is injected to block the anterior branch of the obturator nerve. The needle will then need to be redirected at a steeper angle towards the plane between the deeper adductor brevis and adductor magnus muscles. The remaining local anesthetic is placed between these muscles in order to block the posterior branch of the obturator nerve. Another approach involves moving the transducer about 2-3 cm caudad along the medial thigh to block the anterior branch at its location between the adductor longus and adductor brevis muscles followed by the posterior branch between the adductor brevis and adductor magnus muscles [33]. It is important for both injections to make sure that the local anesthetic is spreading in the fascial plane and not being injected intramuscularly.

There are multiple proximal approaches described in the literature. The majority still begins with the patient supine with the thigh abducted and slightly externally rotated, but there are variations in probe placement and whether an in or out-of-plane technique in used. Regardless, the ultrasound transducer is initially placed in the inguinal crease medially at the same starting position as the distal approach. The transducer is then tilted about 50 degrees cranially until the pectineus muscle is seen with a hyperechoic structure deep and lateral to it. This structure is the inferior margin of the superior pubic ramus. The target for the block needle is the fascial plane between the pectineus and the deeper obturator externus muscle. Two published approaches describe inserting the needle out-of-plane, though this may be more difficult given the inability to visualize the needle completely during insertion [29, 34]. Another approach involves inserting the needle in-plane from lateral to medial [35]. Once the correct fascial plane is confirmed the local anesthetic solution is injected with careful attention to avoid intramuscular injection, as this will prevent adequate spread toward the obturator foramen.

5 Femoral Nerve Block

5.1 Introduction

Indications for femoral nerve block include surgery of the anterior thigh, femur, patella, quadriceps tendon, and knee. This block can also be used to provide analgesia for patients with acute hip fractures while awaiting operative intervention [36, 37]. Ultrasound-guided femoral nerve blockade allows the practitioner to visualize needle advancement while avoiding important structures that can be found in the vicinity of the femoral nerve. The femoral artery is typically located medial to the femoral nerve and the two structures are in close proximity to each other. Use of the ultrasound may reduce the incidence of arterial puncture compared with techniques that do not employ the use of this imaging modality. Ultrasound guidance also allows visualization of the spread of local anesthetic so that appropriate adjustments can be made if necessary. Secondary confirmation can be obtained using nerve stimulation, however, given the ability to visualize the needle and relevant anatomy, this is not required [37].

5.2 Patient Positioning and Landmarks

Ideally, the patient should be in the supine position. The table or bed should be flattened in order to optimize exposure to the inguinal area. Palpation of the femoral artery can provide a good starting point, however is not necessary. The transducer is placed transversely over the femoral pulse in the femoral crease. The transducer can be moved laterally to medially until the artery is identified [36] (Fig. 12).

5.3 Ultrasound Anatomy

The practitioner should first identify the pulsating femoral artery at the level of the inguinal crease. Sliding the transducer medially and laterally will allow the practitioner to visualize the vessel if its presence is not immediately apparent. The femoral nerve is located immediately lateral to the femoral artery in a sulcus in the iliopsoas muscle underneath

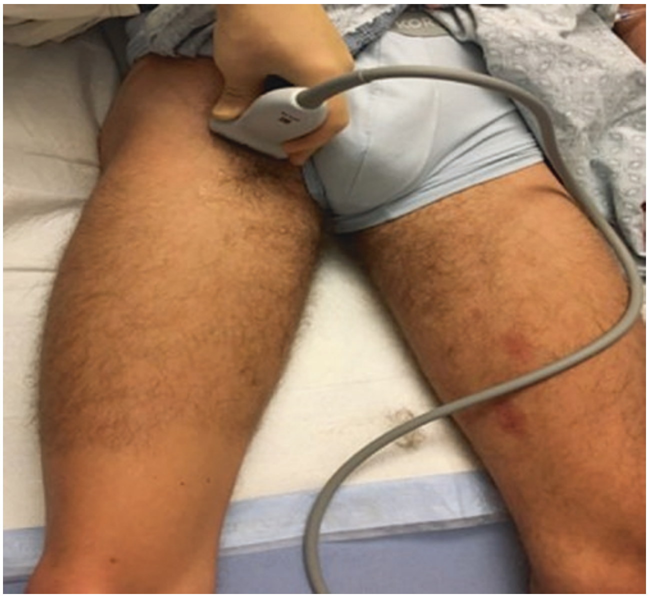

Fig. 12 Proper transducer placement for femoral nerve block

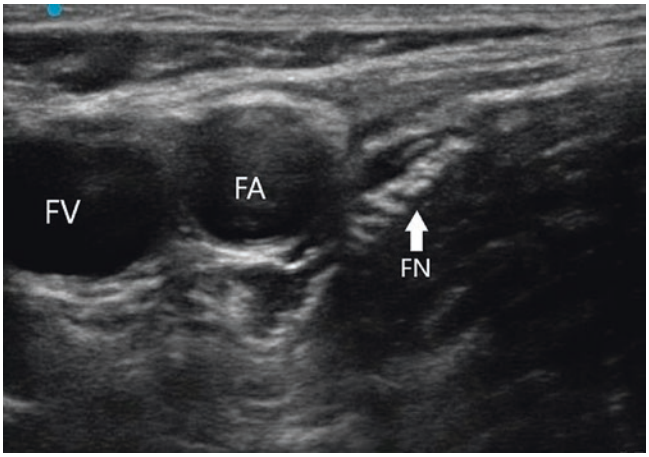

Fig. 13 Ultrasound anatomy for femoral nerve block showing Femoral Vein (FV), Femoral Artery (FA), and Femoral Nerve (FN)

the fascia iliaca. It will typically appear as a hyperechoic structure with a roughly triangular or oval shape. The femoral vein is located medial to the femoral artery and the fascia lata can sometimes be visualized on ultrasound in the subcutaneous layer. The typical depth of the femoral nerve is between 2 and 4 cm [37] (Fig. 13).

5.4 Nerve Distribution

The femoral nerve is derived from the ventral rami of L2 to L4 and is the largest branch of the lumbar plexus. This nerve provides motor innervation to the quadriceps muscle and supplies sensation to the anterior thigh and medial leg [38]. Due to the contribution to motor innervation of the quadriceps muscle, this block may not be favorable for patients undergoing surgery requiring early mobilization as it may increase the risk of falls postoperatively [39]. The femoral nerve gives off articular branches supplying the hip and anterior knee as well. It then gives rise to the saphenous nerve, which has terminal branches that innervate the medial side of the ankle joint [37].

5.5 Technique

With the patient supine, the skin over the femoral crease is prepped with disinfectant solution. The transducer is positioned transversely along the femoral crease and the femoral artery is identified. If the femoral nerve cannot be immediately visualized lateral to the artery, the transducer can be tilted proximally or distally which helps to distinguish the nerve from the iliopsoas muscle. The iliopsoas muscle and its fascia as well as the fascia lata should be identified in order to ensure delivery of local anesthetic to the desired plane. After identification of the femoral nerve, a skin wheal of local anesthetic is made approximately 1 cm away from the lateral edge of the transducer [37]. The needle is inserted in-plane and advanced from lateral to medial toward the lateral corner of the femoral nerve. Typically, two separate "pops" can be felt as the needle is advanced first through the fascia lata and then the fascia iliaca. Once the needle tip is under the fascia iliaca and adjacent to the femoral nerve, careful aspiration and then injection of 1–2 ml of local anesthetic is performed [37, 38]. If the needle is in the correct position, the practitioner will see the femoral nerve move away from the injection [36]. If the injection of local anesthetic does not appear to spread near the femoral nerve, repositioning of the needle and injection of additional local anesthetic may be required [37].

6 Saphenous Nerve Block

6.1 Introduction

The saphenous nerve is the terminal sensory branch of the femoral nerve and provides sensory innervation to the medial, anteromedial, and posteromedial aspects of the lower extremity from the distal thigh to the medial malleolus [40]. Indications for saphenous nerve block include saphenous vein harvesting or stripping or in conjunction with sciatic nerve block for foot and ankle procedures. It can also provide pain relief for patients having knee surgery as a part of a multi-modal pain regimen [41].

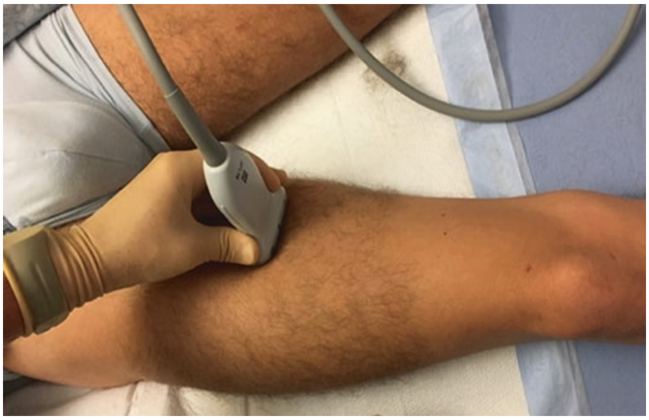

Fig. 14 Proper transducer placement for adductor canal block

6.2 Patient Positioning and Landmarks

6.2.1 Transsartorial Approach (Adductor Canal) to Saphenous Nerve Block

Typical patient positioning for the saphenous nerve block is supine with the patient's thigh externally rotated and abducted so that the practitioner has access to the medial thigh [41] (Fig. 14). The femoral artery travels with the femoral vein and branches of the femoral nerve, (including the saphenous nerve and the nerve to the vastus medialis) in the adductor canal. The adductor canal is an aponeurotic tunnel containing the aforementioned structures that courses between the anterior and medial compartment of the thigh [42].

6.2.2 Distal Saphenous Nerve Block

Below the knee, the saphenous nerve passes along the tibial side of the leg, adjacent to the great saphenous vein. Subcutaneous infiltration of the tissues in this region can provide adequate nerve blockade, however it is possible to perform under ultrasound guidance. At the ankle, a branch of the nerve is located medial to the subcutaneously positioned saphenous vein [41].

6.3 Ultrasound Anatomy

The sartorius muscle descends lateral to medial across the anterior thigh and forms a "roof" over the adductor canal. The muscle can be identified on ultrasound as an oval shape deep to a subcutaneous layer of adipose tissue. The canal is triangular in shape with the lateral border being is formed by the vastus medialis and medial border by the adductor longus proximally or magnus more distally. The saphenous nerve is often difficult to appreciate on the ultrasound image; however, it can appear as a small round hyperechoic structure medial to the artery. The femoral vein and artery accompany the saphenous nerve in the adductor canal and can typically be visualized 2–3 cm deep to the ultrasound probe. (Fig. 15) Above the knee, the saphenous nerve pierces the fascia lata between the tendons of the sartorius and gracilis muscles and then becomes a subcutaneous nerve [43].

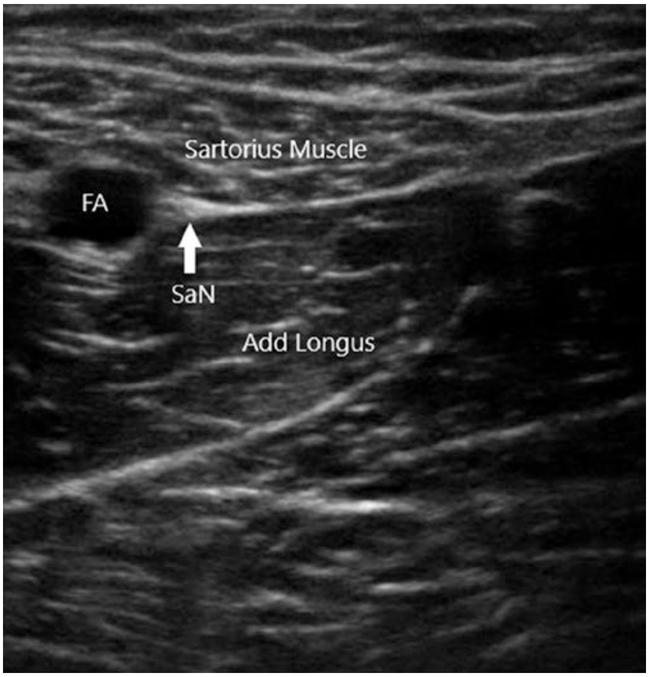

Fig. 15 Ultrasound anatomy for adductor canal nerve block including Sartorius Muscle, Femoral Artery (FA), Saphenous Nerve (SaN), and Adductor Longus Muscle (Add Longus)

6.4 Nerve Distribution

Saphenous nerve block results in anesthesia of a variable strip of skin on the medial leg and foot [43]. Although saphenous nerve block is strictly sensory, an injection of the local anesthetic in the adductor canal spread and cause partial motor block of the vastus medialis. Therefore, patients should be advised to use caution when attempting unsupported ambulation after proximal saphenous block to avoid increased risk of falls [39].

6.5 Technique

With the patient in the proper position, the skin is disinfected and the transducer is placed antero-medially, approximately mid thigh position or somewhat lower. If the artery is not immediately apparent, the use of color Doppler can be employed to identify the femoral artery and scan caudally from the inguinal crease [41]. To confirm identification of the sartorius muscle, scanning from its origin at the anterosuperior iliac spine down toward the medial knee is helpful [44]. Once the femoral artery is identified, the needle is inserted in-plane in a lateral-to-medial orientation, and advanced toward the femoral artery [45]. Once the needle tip is visualized medial to the artery and after careful aspiration, 1–2 mL of local anesthetic is injected to confirm the proper injection site. When injection of the local anesthetic does not appear to result in its spread beside the femoral artery, additional needle repositions and injections may be necessary [40]. The block can be achieved with as little as 5–10 mL of local anesthetic, with a maximum dose of 20 mL [45].

Saphenous nerve block can be achieved at more distal and superficial locations with simple subcutaneous infiltration of the tissues within the immediate vicinity of the nerve. This can be done under ultrasound guidance with the transducer placed below the knee at the level of the tibial tuberosity [45].

References

1. Dalens B, Tanguy A, Vanneuville G. Lumbar plexus blocks and lumbar plexus nerve blocks. Anesth Analg. 1989;69(6):852–4.
2. Xu Z, Ren Y, Tu L, et al. Anatomy of the femoral fascia sheath and its adjacent structures. Acta Anatom Sinic. 2013;44:364–7.
3. Capdevila X, Biboulet P, Bouregba M, Barthelet Y, Rubenovitch J, D'athis F. Comparison of the three-in-one and fascia Iliaca compartment blocks in adults. Anesth Analg. 1998;86:1039–41.
4. Dolan J, Williams A, Murney E, Smith M, Kenny G. Ultrasound guided fascia Iliaca block: a comparison with the loss of resistance technique. Reg Anesth Pain Med. 2008;33(6):526–31.
5. Haines L, Dickman E, Ayvazyan S, Pearl M, Wu S, Rosenblum D, Likourezos A. Ultrasound-guided fascia iliaca compartment block for hip fractures in the emergency department. J Emerg Med. 2012;43(4):692–7.
6. Chin K, Perlas A, Brull R, Chan V. Ultrasound guidance is advantageous in popliteal nerve blockade. Anesth Analg. 2008;107:2094–5.
7. Hadzic A, Vloka J. Popliteal nerve block through the lateral approach. A comparison with the posterior technique. Anesth Analg. 1998;88(6):1480–6.
8. Vloka J, Hadzic A, April E, Thys D. The division of the sciatic nerve in the popliteal fossa: anatomical implications for popliteal nerve blockade. Anesth Analg. 2001;92:215–7.
9. Manickam B, Perlas A, Chan V, Brull R. The role of a preprocedure systematic sonographic survey in ultrasound-guided regional anesthesia. Reg Anesth Pain Med. 2008;33(6):566–70.
10. Gray A, Huczko E, Schafhalter-Zoppoth I. Lateral popliteal nerve block with ultrasound guidance. Reg Anesth Pain Med. 2004;29:507–9.
11. Danelli G, Ghisi D, Ortu A. Ultrasound and regional anesthesia technique: are there really ultrasound guidance technical limits in sciatic nerve blocks? Reg Anesth Pain Med. 2008;33:281–2.
12. Perlas A, Brull R, Chan V, McCartney C, Nuica A, Abbas S. Ultrasound guidance improves the success of sciatic nerve block at the popliteal fossa. Reg Anesth Pain Med. 2008;33:259–65.
13. Ota J, Sakura S, Hara K, Saito Y. Ultrasound-guided anterior approach to sciatic nerve block: a comparison with the posterior approach. Anesth Analg. 2009;108:660–5.
14. Alsatli R. Comparison of ultrasound-guided anterior versus transgluteal sciatic nerve blockade for knee surgery. Anesth Essays Res. 2012;6(1):29–33.
15. Bruhn J, van Geffen G, Gielen M, Scheffer G. Visualization of the course of the sciatic nerve in adult volunteers by ultrasonography. Acta Anaesthesiol Scand. 2008;52:1298–302.
16. Beck G. Anterior approach to sciatic nerve block. Anesthesiology. 1963;24:222–4.
17. Chelly J, Delaunay L. A new anterior approach to the sciatic nerve block. Anesthesiology. 1999;91:1655–60.
18. Chan V, Nova H, Abbas S, McCartney C, Perlas A, Xu D. Ultrasound examination and localization of the sciatic nerve: a volunteer study. Anesthesiology. 2006;104:309–14.
19. Tsui B, Ozelsel T. Ultrasound-guided anterior sciatic nerve block using a longitudinal approach: expanding the view. Reg Anesth Pain Med. 2008;33:275–6.
20. Karmakar M, Kwok W, Hok A, Tsang K, Chui P, Gin T. Ultrasound-guided sciatic nerve block: description of a new approach at the subgluteal space. Br J Anesthesia. 2007;98(3):390–5.
21. McNamee D, Parks L, Milligan K. Post-operative analgesia following total knee replacement: an evaluation of the addition of an obturator nerve block to combined femoral and sciatic nerve block. Acta Anaesthesiol Scand. 2002;46(1):95–9.
22. Macalou D, Trueck S, Meuret P, et al. Postoperative analgesia after total knee replacement: the effect of an obturator nerve block added to the femoral 3-in-1 nerve block. Anesth Analg. 2004;99(1):251–4.
23. Sakura S, Hara K, Ota J, Tadenuma S. Ultrasound-guided peripheral nerve blocks for anterior cruciate ligament reconstruction: effect of obturator nerve block during and after surgery. J Anesth. 2010;24(3):411–7.
24. Heywang-Köbrunner S, Amaya B, Okoniewski M, Pickuth D, Spielmann R. CT-guided obturator nerve block for diagnosis and treatment of painful conditions of the hip. Eur Radiol. 2001;11(6):1047–53.
25. Lam K, Wong D, Tam C, et al. Ultrasound and electrical stimulator-guided obturator nerve block with phenol in the treatment of hip adductor spasticity in long-term care patients: a randomized, triple blind, placebo controlled study. J Am Med Dir Assoc. 2015;16(3):238–46.
26. Pladzyk K, Jureczko L, Łazowski T. Over 500 obturator nerve blocks in the lithotomy position during transurethral resection of bladder tumor. Cent Eur J Urol. 2012;65(2):67–70.
27. Bolat D, Aydogdu O, Tekgul Z, et al. Impact of nerve stimulator-guided obturator nerve block on the short-term outcomes and complications of transurethral resection of bladder tumour: a prospective randomized controlled study. Can Urol Assoc J. 2015; 9(11–12):E780–4.
28. Yoshida T, Onishi T, Furutani K, Baba H. A new ultrasound-guided pubic approach for proximal obturator nerve block: clinical study and cadaver evaluation. Anaesthesia. New York: McGraw Hill. 2016;71(3):291–7.
29. Anagnostopoulou S, Kostopanagiotou G, Paraskeuopoulos T, Chantzi C, Lolis E, Saranteas T. Anatomic variations of the obturator nerve in the inguinal region: implications in conventional and ultrasound regional anesthesia techniques. Reg Anesth Pain Med. 2009;34(1):33–9.
30. Bouaziz H, Vial F, Jochum D, et al. An evaluation of the cutaneous distribution after obturator nerve block. Anesth Analg. 2002;94(2):445–9.
31. Jochum D, Iohom G, Choquet O, et al. Adding a selective obturator nerve block to the parasacral sciatic nerve block: an evaluation. Anesth Analg. 2004;99(5):1544–9.
32. Woodburne R. The accessory obturator nerve and the innervation of the pectineus muscle. Anat Rec. 1960;136(3):367–9.
33. Soong J, Schafhalter-Zoppoth I, Gray A. Sonographic imaging of the obturator nerve for regional block. Reg Anesth Pain Med. 2007;32(2):146–51.

34. Taha A. Ultrasound-guided obturator nerve block: a proximal interfascial technique. Anesth Analg. 2012;114(1):236–9.
35. Lin J, Nakamoto T, Yeh S. Ultrasound standard for obturator nerve block: the modified Taha's approach. Br J Anaesth. 2015;114(2):337–9.
36. Atchabahianm A, Vandepitte I, Lopez, C. Ultrasound-Guided Femoral Nerve Block - NYSORA. 2018. Retrieved December 30, 2018, from https://www.nysora.com/techniques/lower-extremity/femoral/ultrasound-guided-femoral-nerve-block/.
37. Hadzic A. In: Carrera DXA, Clark T, Gadsden J, Karmakar M, Sala-Blanch X, Vandepitte C, editors. Chapter 35. Ultrasound-Guided Femoral Nerve Block | Hadzic's Peripheral Nerve Blocks and Anatomy for Ultrasound-Guided Regional Anesthesia, 2e | AccessAnesthesiology | New York: McGraw-Hill Medical. 2nd ed: McGraw-Hill; 2012. Retrieved from https://accessanesthesiology.mhmedical.com/content.aspx?bookid=518&sectionid=41534325.
38. Pardo M, Miller R. Basics of anesthesia. 6th ed. Philadelphia: Elsevier; 2011.
39. Ilfeld B. Single-injection and continuous femoral nerve blocks are associated with different risks of falling. Anesthesiology. 2014;121:668–9.
40. Horn J, Pitsch T, Salinas F, Benninger B. Anatomic basis to the ultrasound-guided approach for saphenous nerve blockade. Reg Anesth Pain Med. 2009;34(5):486–9.
41. Hadzic A. Chapter 38. Ultrasound-guided saphenous nerve block. Hadzic's peripheral nerve blocks and anatomy for ultrasound-guided regional anesthesia. 2nd ed. New York: McGraw-Hill; 2012. Retrieved from http://accessanesthesiology.mhmedical.com/content.aspx?bookid=518&sectionid=41534328
42. Saranteas T, Anagnostis G, Paraskeuopoulos T, Koulalis D, Kokkalis Z, Nakou M, Anagnostopoulou S, Kostopanagiotou G. Anatomy and clinical implications of the ultrasound-guided subsartorial saphenous nerve block. Reg Anesth Pain Med. 2011;36(4):399–402.
43. Sahin L, Sahin M, Istkay N. A different approach to an ultrasound-guided saphenous nerve block. Acta Anaesthesiol Scand. 2011;55(8):1030–1.
44. Hansen J. Chapter 6: lower limb. Netter's Clinical Anatomy, 4th ed. 2018.
45. Bendtsen T, Ana Clark T. Ultrasound-Guided Saphenous (Adductor Canal) Nerve Block – NYSORA. 2018. Retrieved December 30, 2018 from https://www.nysora.com/regional-anesthesia-for-specific-surgical-procedures/lower-extremity-regional-anesthesia-for-specific-surgical-procedures/foot-and-ankle/ultrasound-guided-saphenous-subsartorius-adductor-canal-nerve-block.

Part IV

Chest and Abdomen Ultrasound

The Role of Ultrasound in the Management of Cardiac Patients

Alan David Kaye, Cody M. Koress, O. Morgan Hall,
Mitchell C. Fuller, Matthew Brian Novitch, Jinlei Li,
and Henry Liu

1 Introduction

Cardiac care has evolved in recent years with regard to assessment and treatment strategies mainly related to ultrasound technology. Surgeries have also evolved and techniques for pain management of these surgeries have also developed. Thus, regional anesthesia techniques have been increasingly employed in cardiac surgical procedures to assist in acute pain management. At present, these regional techniques include chest wall blocks, sternal blocks, and neuraxial blocks. There is significant evidence that cardiac surgery patients benefit from utilization of these regional techniques.

Cardiovascular disease accounts for more than one-third of deaths globally [1] and more than $300 billion in costs in the United States [2]. Cardiovascular disease is the leading cause of mortality and morbidity for the aged population worldwide. Increases in the elderly population are expected to increase and therefore, it is projected that the volume of cardiovascular interventional procedures will increase [3, 4]. Minimally invasive cardiac procedures, including transcatheter aortic valve replacements (TAVR) are allowing for older and sicker patients to undergo interventional/surgical procedures. Despite decades of anesthetics powered by high dose opioids, at present multimodal analgesia have evolved, including in cardiovascular surgery Neuraxial and peripheral nerve blocks along with opioid sparing techniques have become essential components of these multimodal analgesic protocols [5, 6].

The use of regional anesthesia and neuraxial techniques in cardiac surgery date back to 1954 when one of the first heart surgeries was performed under thoracic epidural analgesia [7–9]. Advantages of thoracic epidural analgesia include decreased incidence of cardiovascular events (e.g., stroke, myocardial ischemia) [8, 10, 11], reduced respiratory complications, decreased renal failure, lower infection, shorter ICU stays, decreased cost of anesthesia, and earlier hospital discharge [11]. Along with efficacy, advantages of thoracic epidural analgesia include the ability to provide analgesia continuously throughout the perioperative period; while concerns include spinal and epidural hematomas [12, 13]. Additionally, the risk of post-cardiopulmonary bypass mediated coagulopathy may complicate the use of neuraxial techniques. Other concerns include the role of managing concurrent aspirin vis-à-vis use with systemic heparinization [14, 15]. High spinal has certain theoretical benefits but as well profound systemic effects [16, 17].

A. D. Kaye (✉)
Departments of Anesthesiology and Pharmacology, Toxicology, and Neurosciences, Lousiana State University Health Sciences Center, Shreveport, LA, USA

Department of Anesthesiology, Department of Pharmacology
Louisiana State University School of Medicine, Louisiana State University Health Sciences Center, New Orleans, LA, USA
e-mail: akaye@lsuhsc.edu

C. M. Koress
Department of Anesthesiology, LSU School of Medicine, Louisiana State University Health Sciences Center, New Orleans, LA, USA
e-mail: ckores@lsuhsc.edu

O. M. Hall
Department of Anesthesiology, LSU School of Medicine, New Orleans, LA, USA
e-mail: ohall2@lsuhsc.edu

M. C. Fuller
Medical College of Wisconsin, Wauwatosa, WI, USA

M. B. Novitch
University of Washington School of Medicine, Department of Anesthesiology, Seattle, WA, USA
e-mail: mnovitch@uw.edu

J. Li
Department of Anesthesiology, Yale University School of Medicine, New Haven, CT, USA

H. Liu
Department of Anesthesiology & Perioperative Medicine, Penn State Milton S. Hershey Medical Center, Hershey, PA, USA

© Springer Nature Switzerland AG 2021
J. Li et al. (eds.), *Ultrasound Fundamentals*, https://doi.org/10.1007/978-3-030-46839-2_18

The most commonly regional block of the paraxial nervous system is the paravertebral block (PVB) [18]. In recent years, the ultrasound-guided PVB has been shown to be a safe and effective analgesic technique compared with thoracic epidural analgesia [19, 20]. Common advantages from PVB include hemodynamic stability when compared to thoracic epidural analgesia [21] and reduced nausea, hypotension, and urinary retention [20].

Chest wall blocks are newer, simpler ultrasound guided techniques and include the pectoralis fascial blocks (PECS) in cardiac and other surgeries [21–26]. Another regional technique related to PECS is the serratus anterior plane (SAP) block that covers the hemithorax [27]. The SAP block can be effective in thoracic surgical procedures [28–30]. Recently, SAP, PECS II and intercostal nerve blocks (ICNB) were found to be equally efficacious in cardiac surgery in the pediatric population [31].

A recent addition to the evolving number of fascial blocks is the erector spinae block, which are easy to deliver via ultrasound and have few side effects (ESB) [32]. Based on a cadaveric and case reports, the ESB possesses an advantage for median sternotomy with efficacy and efficiency [33–37]. ESB has also been successfully used in transapical transcatheter aortic valve implantation [38]. Concerns include the potential for hematoma and related to lack of laterality, may require bilateral blocks for a standard sternotomy which can significantly increase risk of high local anesthetic plasma concentrations [39, 40].

2 Goal-Directed Echocardiography

Early identification of the mechanisms of shock in a critically ill patient is central to the practice of critical care medicine. Goal-directed echocardiography was developed to provide early, useful information for hemodynamic monitoring and determination of the type of shock (hypovolemic, obstructive, cardiogenic, or distributive) based on the assessment of left ventricular systolic dysfunction, left ventricular dilatation, right ventricular dilatation, pericardial effusion, cardiac tamponade, and pleural effusion (Table 1). The internationally standardized training and approach to goal-directed echocardiography is named basic critical care echocardiography (CCE) [41], which uses transthoracic ultrasound to answer basic clinical questions: Is the patient severely hypovolemic? Does the patient have marked left ventricular systolic dysfunction or high filling pressures? Does the patient have cor pulmonale? Is the patient in tamponade?

3 Intravenous Fluid Therapy Management

In regional anesthesia, identification of patients who are at risk of developing hypovolemia before administration of a neuraxial blockade can be useful for guiding therapy and to begin pre-emptive measures to reduce the risk of hypotension and the adverse outcomes associated with the condition. In this regard, fluid therapy guided by Inferior Vena Cava (IVC) ultrasound has been proven effective in the prevention of post-spinal anesthesia hypotension (PSAH) [43, 44]. Several methods of assessing patient fluid volume are effective in predicting risk of hypotension. In elderly patients undergoing spinal anesthetics, preoperative maximal diameter of IVC (dIVCmax) to IVC collapsibility index (IVCCI) ratio of less than 43 predicts spinal-induced hypotension [45]. To obtain this ratio, the IVC is measured at its maximum diameter at the end of expiration (dIVCmax) and IVCCI during spontaneous, quiet breathing calculated as [(IVC maximal diameter – IVC minimal diameter)/IVC maximal diameter] [45]. Additionally, IVCCI alone has good predictive value with sensitivity of 84%, specificity of 77%, and accuracy of 84%, as determined in a prospective study of 100 patient's volume status after spinal anesthesia by Salama et al. [44] Furthermore, this study also assessed the ratio of IVC to aorta diameter (IVC:Ao index) as a predictor of PSAH. It proved extremely effective in predicting the risk of hypotension with a sensitivity of 96%, specificity of 88%, and accuracy of 95% [44]. It is important to note in this study that age was another predictor of PSAH with elderly patients being more affected.

Table 1 Goal, pattern, and findings in cardiovascular pathogenesis

Goal	Pattern	Findings
Left ventricle	Left ventricular failure	Left ventricular hypokinesia, low aortic velocity-time integral
Right ventricle	Acute cor pulmonale	Right ventricular dilation, increased pulmonary artery pressures, tricuspid regurgitation via color-wave Doppler
Pericardium	Cardiac tamponade	Circumferential pericardial effusion with end-diastolic collapse of the right atrium
Fluid status	Severe hypovolemia	Small, hyperdynamic ventricles with IVC obliteration
	High filling pressure	High-velocity E wave (E/A >2) with short deceleration time using pulsed-wave Doppler

Adapted from Repessé et al. [42]

Assessment of IVC diameter via ultrasound allows for rapid, non-invasive approximation of central venous pressure, which avoids the need for a central venous catheter. IVC diameter correlates with intrapleural pressure and can be used to estimate the right atrial pressure (RAP). During spontaneous ventilation, an IVC measurement of less than 2.1 cm with an inspiratory collapse of greater than 50% during sniff correlates with a RAP of 0–5 mmHg, while an IVC measurement greater than 2.1 cm with less than 50% collapse during sniff correlate with a RAP of 10–20 mmHg [46]. Hypovolemia is indicated if the maximum IVC diameter is less than 1.0 cm. If a patient meets this condition, additional findings of a small, hyperdynamic LV with end systolic cavity obliteration are highly suggestive for hypovolemia.

Further investigation is warranted due to low systemic vascular resistance producing similar findings [46]. Other ultrasound techniques to approximate central venous pressure have been studied, including IVCCI and internal jugular vein aspect ratio, but these are less effective than maximal IVC diameter [47].

4 Cardiac Arrest

The use of point of care ultrasound (POCUS) in the management of cardiac arrest has the potential to improve patient outcomes by guiding treatment of the underlying conditions and by providing important prognostic information. In a prospective observational study, Gaspari et al. enrolled 793 cardiac arrest patients to better understand the prognostic value of POCUS [48]. The study evaluated patient outcome at three different levels – return of spontaneous circulation (ROSC), survival to hospital admission, and survival to hospital discharge. All patients received an ultrasound as part of initial assessment. Cardiac activity was detected in 263 of these patients. ROSC was achieved in 51% of patients with detectable cardiac activity while only 14% of patients without cardiac activity reached ROSC. Similar differences between the two groups were seen in survival to admission and survival to discharge [48]. Ultrasound guidance also allowed the physicians to deviate from standard Advanced Cardiac Life Support protocol by allowing diagnosis of the underlying condition. For example, 34 patients with pericardial effusion as the underlying condition for cardiac arrest were diagnosed, and their survival was greatly improved [48]. Other detectable underlying conditions of cardiac arrest include, cardiac tamponade, hypovolemia, and pulmonary embolism [49]. POCUS is also beneficial for monitoring the process of CPR, visualizing true vs. false asystole, and confirming cardiac rhythm [49, 50]. Potential exists for POCUS to monitor the efficacy of chest compressions during CPR, but further study is needed to validate POCUS in this setting [50].

Risks do exist when utilizing POCUS during cardiac arrest resuscitation. When using the ultrasound during CPR, there must be a break in chest compressions and resuscitation efforts [51]. It has been noted that these breaks often last longer than the recommended maximum pause of 10 seconds, which directly affects resuscitation effectiveness [52]. The benefits of the prognostic information collected via ultrasound use and guidance of treatment/patient management shown to improve patient outcomes within certain subgroups of cardiac arrest patients must be weighed with the risks of pausing resuscitation efforts. To date, there is still a lack of evidence for or against the use of POCUS managing these patients, so at present the decision should be on a case by case basis.

5 Emerging Roles of Ultrasound, Pulmonary Embolism

Transesophageal and transthoracic echocardiograms are a useful tool that anesthesiologists employ for early diagnostic examination of suspected pulmonary embolism (PE) in the perioperative setting. PE is a manifestation of venous thromboembolism that demands quick and accurate care to avoid hemodynamic catastrophe. Approximately 1 per 1000 adults each year present with symptomatic PE making it the most common cause of vascular death after myocardial infarction and stroke [53]. Moreover, major surgery has the highest odds ratio (18.95) of any independent risk factor for PE [54]. Therefore, it is imperative for anesthesiologists to be familiar with PE echocardiographic findings.

Acute massive PE is defined as a sustained systolic BP <90 mm Hg for at least 15 minutes in the setting of pulmonary vascular embolus [55]. Acute massive PE has a high mortality rate and is characterized by hemodynamic deterioration secondary to increased pulmonary vascular resistance in addition to the degree of obstruction of the embolic thrombus [56]. Subsequently, the blood pressure progressively builds in the right ventricle (RV) until systemic blood circulation plummets and cardiac arrest is achieved [57]. The parasternal long axis transthoracic view is a well validated approach to catch early sonographic changes of the RV before cardiac arrest occurs [58]. Specifically, this view detects the increase in RV diameter from 2/3 of the total LV size to larger than the LV. Additionally, there's a geometric RV change from an "egg shape" to a rounder "soccer ball shape". Such changes are also detectable on the apical four-chamber view. On the parasternal short axis view, high RV pressure drives the interventricular septum to flatten from the normal D-shape [58]. Transesophageal echo has also been well described in literature as a perioperative rescue procedure to help identify the underlying cause of hemodynamic instability, namely acute PE [59, 60]. Transesophageal views are obtained through esophageal and gastric windows totaling 16 views at four esophageal and transgastric levels, but a limited exam can be performed in emergent cases with 10 recommended views. This approach allows for estimation of systolic pulmonary arterial pressure and right ventricular systolic pressure through tricuspid regurgitation and right atrial pressure measurement [61]. The modified bicaval view is best suited to assess these parameters in the context of pulmonary hypertension and PE. Ultimately, both transesophageal and transthoracic ultrasonography approaches are ideal in the early detection of perioperative PE related to their accessibility and dynamic nature. They can be used alone or together by the modern anesthesiologist to best reduce morbidity and mortality.

6 Valvular Pathology

Patients with valvular heart disease (VHD) may present to the anesthesiologist for either cardiac or non-cardiac surgery. More than 10–13% of patients over the age of 75 may present with moderate to severe VHD [62, 63]. Approximately 30% of patients with severe, symptomatic VHD, usually with relevant comorbidities, do not undergo surgery [63]. Regardless of the cause, it is important to identify the lesion, quantify its severity, assess of the sequelae of value dysfunction on cardiac function, and assess possible concomitant ischemic heart disease. The pre-anesthesia assessment should include a history and physical to look for signs and symptoms of VHD and heart failure with typical comorbidities that include peripheral atherosclerosis, renal and hepatic dysfunction, and chronic obstructive pulmonary disease [64]. Typically, the evaluation of VHD lies with the cardiologist, though patients may present to the pre-operative clinic with undiagnosed disease. For the anesthesiologist, the most concern lies with undiagnosed, severe aortic stenosis, which can lead to hemodynamic collapse due to compromise of ventricular filling after administration of anesthesia. Operative mortality risk data is also available using the EuroSCORE and the STS scoring systems [65, 66].

Doppler echocardiography is the most common imaging modality used in the diagnosis of VHD, as it low-cost, non-invasive, and free from radiation, and is thus the gold standard according to multiple international societies [64, 67]. In patient with stenotic lesions, the severity of obstruction is assessed by changes in either flow velocities, pressure gradients, or valve orifice areas, which can be measured by ultrasound. In patients with regurgitate valve lesions, assessment should include several different quantitative measurements using Doppler imaging of the vena contracta and jet geometry, continuous wave Doppler recordings of the regurgitant flow, effective regurgitant orifice area, and pulsed wave Doppler measures of transvalvular blood flow. Diagnostic criteria are outlined in Tables 2 and 3.

Table 2 Diagnostic echocardiographic criteria for severe valve stenosis

	Aortic Stenosis	Mitral Stenosis	Tricuspid Stenosis
Valve area (cm^2)	<1.0	<1.0	–
Indexed valve area (cm^2/m^2 of BSA)	<0.6	–	–
Mean gradient	>40	>10	>5
Maximum jet velocity (m/s)	>4.0	–	–
Velocity ratio	<0.25	–	–

Adapted from Baumgartner et al. [68]

Table 3 Diagnostic echocardiographic criteria for severe valve regurgitation

	Aortic regurgitation	Mitral regurgitation		Tricuspid regurgitation
Qualitative				
Valve morphology	Aortic root enlargement, cusp defect or prolapse	Flail leaflet, ruptured papillary muscle		Abnormal/flail/large coaptation defect
Regurgitant jet flow color	Large in central jets, variable in eccentric jets	Very large central jet or eccentric jet adhering, swirling, and reaching the posterior wall of the left atrium		Very large central jet or eccentric wall impinging jet
Continuous wave signal of regurgitant jet	Dense	Dense/triangular		Dense/triangular with early peaking (peak <2 m/s in massive TR)
Other	Holodiastolic flow reversal in descending aorta (end-diastolic velocity >20 cm/s)	Large flow convergence zone		–
Semi-quantitative				
Vena contracta width (mm)	>6	≥7 (>8 for biplane)		>7
Upstream vein flow	–	Systolic pulmonary vein flow reversal		Systolic hepatic vein flow reversal
Inflow	–	E-wave dominant ≥1.5 m/s		E-wave dominant ≥1 m/s
Other	Pressure half-time <200 ms	Time-velocity integral (TVI)/TVI aortic >1.4		Proximal isovelocity surface area radius >9 mm^2
Quantitative		*Primary*	*Secondary*	
Effective regurgitant orifice area (mm^2)	≥30	≥40	≥20	≥40
Regurgitant volume (mL/beat)	≥60	≥60	≥30	≥45
Enlargement of cardiac chambers/vessels	Left ventricle diameters, volumes and ejection fraction	Left ventricle and left atrium		Right ventricle, right atrium, and inferior vena cava

Adapted from Lancellotti et al. [69]

7 Conclusion

In summary, ultrasound has an important evolving role in diagnostics and therapeutics in cardiac medicine. This is important as the world population ages and cardiac diseases remains one of the most common causes of morbidity and mortality. As techniques evolve into best practice strategies, cardiac patients with the use of ultrasound can expect reduced postoperative pain through regional nerve blocks. As well, the use of ultrasound in cardiac patients may ultimately result in more timely diagnosis and assessment, the potential for reduced opioid consumption, reduced morbidity and mortality, and shortened hospital stays.

References

1. WHO|Cardiovascular diseases (CVDs). WHO 2019.
2. Mozaffarian D, Benjamin EJ, Go AS, Arnett DK, Blaha MJ, Cushman M, Das SR, de Ferranti S, Després J-P, Fullerton HJ, Howard VJ, Huffman MD, Isasi CR, Jiménez MC, Judd SE, Kissela BM, Lichtman JH, Lisabeth LD, Liu S, Mackey RH, Magid DJ, McGuire DK, Mohler ER, Moy CS, Muntner P, Mussolino ME, Nasir K, Neumar RW, Nichol G, Palaniappan L, et al. Heart disease and stroke statistics—2016 update. Circulation. 2016;133:e38–360.
3. Bureau UC: older Americans 2017.
4. D'Agostino RS, Jacobs JP, Badhwar V, Fernandez FG, Paone G, Wormuth DW, Shahian DM. The Society of Thoracic Surgeons adult cardiac surgery database: 2018 update on outcomes and quality. Ann Thorac Surg. 2018;105:15–23.
5. Chakravarthy M. Regional analgesia in cardiothoracic surgery: a changing paradigm toward opioid-free anesthesia? Ann Card Anaesth. 2018;21:225.
6. Noss C, Prusinkiewicz C, Nelson G, Patel PA, Augoustides JG, Gregory AJ. Enhanced recovery for cardiac surgery. J Cardiothorac Vasc Anesth. 2018;32:2760–70.
7. Clowes GH, Neville WE, Hopkins A, Anzola J, Simeone FA. Factors contributing to success or failure in the use of a pump oxygenator for complete by-pass of the heart and lung, experimental and clinical. Surgery. 1954;36:557–79.
8. Chaney MA. Intrathecal and epidural anesthesia and analgesia for cardiac surgery. Anesth Analg. 2006;102:45–64.
9. Kowalewski RJ, MacAdams CL, Eagle CJ, Archer DP, Bharadwaj B. Anaesthesia for coronary artery bypass surgery supplemented with subarachnoid bupivacaine and morphine: a report of 18 cases. Can J Anaesth. 1994;41:1189–95.
10. Bignami E, Landoni G, Biondi-Zoccai GGL, Boroli F, Messina M, Dedola E, Nobile L, Buratti L, Sheiban I, Zangrillo A. Epidural analgesia improves outcome in cardiac surgery: a meta-analysis of randomized controlled trials. J Cardiothorac Vasc Anesth. 2010;24:586–97.
11. Chaney MA. Benefits of neuraxial anesthesia in patients undergoing cardiac surgery. J Cardiothorac Vasc Anesth. 1997;11:808–9.
12. Ho AM, Chung DC, Joynt GM. Neuraxial blockade and hematoma in cardiac surgery: estimating the risk of a rare adverse event that has not (yet) occurred. Chest. 2000;117:551–5.
13. Hemmerling T, Cyr S, Terrasini N. Epidural catheterization in cardiac surgery: the 2012 risk assessment. Ann Card Anaesth. 2013;16:169.
14. Horlocker TT, Wedel DJ, Rowlingson JC, Enneking FK, Kopp SL, Benzon HT, Brown DL, Heit JA, Mulroy MF, Rosenquist RW, Tryba M, Yuan C-S. Regional anesthesia in the patient receiving antithrombotic or thrombolytic therapy: American Society of Regional Anesthesia and Pain Medicine Evidence-Based Guidelines (Third Edition). Reg Anesth Pain Med. 2010;35:64–101.
15. Horlocker TT, Vandermeulen E, Kopp SL, Gogarten W, Leffert LR, Benzon HT. Regional anesthesia in the patient receiving antithrombotic or thrombolytic therapy. Reg Anesth Pain Med. 2018;43:263–309.
16. Lee TWR, Grocott HP, Schwinn D, Jacobsohn E. Winnipeg high-spinal anesthesia group: high spinal anesthesia for cardiac surgery: effects on beta-adrenergic receptor function, stress response, and hemodynamics. Anesthesiology. 2003;98:499–510.
17. Kowalewski R, Seal D, Tang T, Prusinkiewicz C, Ha D. Neuraxial anesthesia for cardiac surgery: thoracic epidural and high spinal anesthesia – why is it different? HSR Proc Intensive Care Cardiovasc Anesth. 2011;3:25–8.
18. D'Ercole F, Arora H, Kumar PA. Paravertebral block for thoracic surgery. J Cardiothorac Vasc Anesth. 2018;32:915–27.
19. Shora H, El Beleehy AA, Abdelwahab AA, Ali GA, Omran TE, Hassan EA, Arafat AA. Bilateral paravertebral block versus thoracic epidural analgesia for pain control post-cardiac surgery: a randomized controlled trial. Thorac Cardiovasc Surg. 2018; https://doi.org/10.1055/s-0038-1668496.
20. Scarfe AJ, Schuhmann-Hingel S, Duncan JK, Ma N, Atukorale YN, Cameron AL. Continuous paravertebral block for post-cardiothoracic surgery analgesia: a systematic review and meta-analysis. Eur J Cardio-Thoracic Surg. 2016;50:1010–8.
21. Pintaric TS, Potocnik I, Hadzic A, Stupnik T, Pintaric M, Novak Jankovic V. Comparison of continuous thoracic epidural with paravertebral block on perioperative analgesia and hemodynamic stability in patients having open lung surgery. Reg Anesth Pain Med. 2011;36:256–60.
22. Blanco R. The 'pecs block': a novel technique for providing analgesia after breast surgery. Anaesthesia. 2011;66:847–8.
23. Blanco R, Fajardo M, Parras Maldonado T. Ultrasound description of Pecs II (modified Pecs I): a novel approach to breast surgery. Rev Esp Anestesiol Reanim. 2012;59:470–5.
24. Kumar KN, Kalyane RN, Singh NG, Nagaraja PS, Krishna M, Babu B, Varadaraju R, Sathish N, Manjunatha N. Efficacy of bilateral pectoralis nerve block for ultrafast tracking and postoperative pain management in cardiac surgery. Ann Card Anaesth. 2018;21:333–8.
25. Fujiwara A, Komasawa N, Minami T. Pectoral nerves (PECS) and intercostal nerve block for cardiac resynchronization therapy device implantation. Springerplus. 2014;3:409.
26. Yalamuri S, Klinger RY, Bullock WM, Glower DD, Bottiger BA, Gadsden JC. Pectoral fascial (PECS) I and II blocks as rescue analgesia in a patient undergoing minimally invasive cardiac surgery. Reg Anesth Pain Med. 2017;42:764–6.
27. Blanco R, Parras T, McDonnell JG, Prats-Galino A. Serratus plane block: a novel ultrasound-guided thoracic wall nerve block. Anaesthesia. 2013;68:1107–13.
28. Khalil AE, Abdallah NM, Bashandy GM, Kaddah TA-H. Ultrasound-guided serratus anterior plane block versus thoracic epidural analgesia for thoracotomy pain. J Cardiothorac Vasc Anesth. 2017;31:152–8.
29. Hetta DF, Rezk KM. Pectoralis-serratus interfascial plane block vs thoracic paravertebral block for unilateral radical mastectomy with axillary evacuation. J Clin Anesth. 2016;34:91–7.
30. Moll V, Maffeo C, Mitchell M, Ward CT, Groff RF, Lee SC, Halkos ME, Jabaley CS, O'Reilly-Shah VN. Association of serratus anterior plane block for minimally invasive direct coronary artery bypass surgery with higher opioid consumption: a retrospective observational study. J Cardiothorac Vasc Anesth. 2018;32:2570–7.
31. Kaushal B, Chauhan S, Saini K, Bhoi D, Bisoi AK, Sangdup T, Khan MA. Comparison of the efficacy of ultrasound-guided serratus anterior plane block, pectoral nerves II block, and intercostal nerve block

for the management of postoperative thoracotomy pain after pediatric cardiac surgery. J Cardiothorac Vasc Anesth. 2019;33:418–25.
32. Forero M, Adhikary SD, Lopez H, Tsui C, Chin KJ. The erector spinae plane block: a novel analgesic technique in thoracic neuropathic pain. Reg Anesth Pain Med. 2016;41:621–7.
33. Adhikary SD, Bernard S, Lopez H, Chin KJ. Erector spinae plane block versus Retrolaminar block: a magnetic resonance imaging and anatomical study. Reg Anesth Pain Med. 2018;43:756–62.
34. Costache I, Pawa A, Abdallah FW. Paravertebral by proxy – time to redefine the paravertebral block. Anaesthesia. 2018;73:1185–8.
35. Krishna SN, Chauhan S, Bhoi D, Kaushal B, Hasija S, Sangdup T, Bisoi AK. Bilateral erector spinae plane block for acute post-surgical pain in adult cardiac surgical patients: a randomized controlled trial. J Cardiothorac Vasc Anesth. 2019;33:368–75.
36. Nagaraja PS, Ragavendran S, Singh NG, Asai O, Bhavya G, Manjunath N, Rajesh K. Comparison of continuous thoracic epidural analgesia with bilateral erector spinae plane block for perioperative pain management in cardiac surgery. Ann Card Anaesth. 2018;21:323–7.
37. Leyva FM, Mendiola WE, Bonilla AJ, Cubillos J, Moreno DA, Chin KJ. Continuous erector spinae plane (ESP) block for postoperative analgesia after minimally invasive mitral valve surgery. J Cardiothorac Vasc Anesth. 2018;32:2271–4.
38. Ueshima H, Hiroshi O. Transapical transcatheter aortic valve implantation performed with an erector spinae plane block. J Clin Anesth. 2018;46:84.
39. Ho AM-H, Karmakar MK, Ng SK, Wan S, Ng CSH, Wong RHL, Chan SKC, Joynt GM. Local anaesthetic toxicity after bilateral thoracic paravertebral block in patients undergoing coronary artery bypass surgery. Anaesth Intensive Care. 2016;44:615–9.
40. Ueshima H, Otake H. Ultrasound-guided pectoral nerves (PECS) block: complications observed in 498 consecutive cases. J Clin Anesth. 2017;42:46.
41. Mayo PH, Beaulieu Y, Doelken P, Feller-Kopman D, Harrod C, Kaplan A, Oropello J, Vieillard-Baron A, Axler O, Lichtenstein D, Maury E, Slama M, Vignon P. American College of Chest Physicians/La Société de Réanimation de langue Française statement on competence in critical care ultrasonography. Chest. 2009;135:1050–60.
42. Repessé X, Charron C, Vieillard-Baron A. Intensive care ultrasound: V. Goal-directed echocardiography. Ann Am Thorac Soc. 2014;11:122–8.
43. Ceruti S, Anselmi L, Minotti B, Franceschini D, Aguirre J, Borgeat A, Saporito A. Prevention of arterial hypotension after spinal anaesthesia using vena cava ultrasound to guide fluid management. Br J Anaesth. 2018;120:101–8.
44. Salama ER, Elkashlan M. Pre-operative ultrasonographic evaluation of inferior vena cava collapsibility index and caval aorta index as new predictors for hypotension after induction of spinal anaesthesia. Eur J Anaesthesiol. 2019;36:297–302.
45. Saranteas T, Spiliotaki H, Koliantzaki I, Koutsomanolis D, Kopanaki E, Papadimos T, Kostopanagiotou G. The utility of echocardiography for the prediction of spinal-induced hypotension in elderly patients: inferior vena cava assessment is a key player. J Cardiothorac Vasc Anesth. 2019;33(9):2421–7.
46. Porter TR, Shillcutt SK, Adams MS, Desjardins G, Glas KE, Olson JJ, Troughton RW. Guidelines for the use of echocardiography as a monitor for therapeutic intervention in adults: a report from the American Society of Echocardiography. J Am Soc Echocardiogr. 2015;28:40–56.
47. Prekker ME, Scott NL, Hart D, Sprenkle MD, Leatherman JW. Point-of-care ultrasound to estimate central venous pressure. Crit Care Med. 2013;41:833–41.
48. Gaspari R, Weekes A, Adhikari S, Noble VE, Nomura JT, Theodoro D, Woo M, Atkinson P, Blehar D, Brown SM, Caffery T, Douglass E, Fraser J, Haines C, Lam S, Lanspa M, Lewis M, Liebmann O, Limkakeng A, Lopez F, Platz E, Mendoza M, Minnigan H, Moore C, Novik J, Rang L, Scruggs W, Raio C. Emergency department point-of-care ultrasound in out-of-hospital and in-ED cardiac arrest. Resuscitation. 2016;109:33–9.
49. Miesemer B. Using ultrasound for cardiac arrest POCUS can improve detection and treatment of underlying pathologies. EMS World. 2017;46:40–2.
50. Blanco P, Martínez Buendía C. Point-of-care ultrasound in cardiopulmonary resuscitation: a concise review. J Ultrasound. 2017;20:193–8.
51. Clattenburg EJ, Wroe P, Brown S, Gardner K, Losonczy L, Singh A, Nagdev A. Point-of-care ultrasound use in patients with cardiac arrest is associated prolonged cardiopulmonary resuscitation pauses: a prospective cohort study. Resuscitation. 2018;122:65–8.
52. Berg KM. Finding a window: timing of cardiac ultrasound acquisition during cardiac arrest. Resuscitation. 2018;124:A11–2.
53. Tagalakis V, Patenaude V, Kahn SR, Suissa S. Incidence of and mortality from venous thromboembolism in a real-world population: the Q-VTE study cohort. Am J Med. 2013;126:832. e13–832. e21.
54. Heit JA, Spencer FA, White RH. The epidemiology of venous thromboembolism. J Thromb Thrombolysis. 2016;41:3–14.
55. Jaff MR, McMurtry MS, Archer SL, Cushman M, Goldenberg N, Goldhaber SZ, Jenkins JS, Kline JA, Michaels AD, Thistlethwaite P, Vedantham S, White RJ, Zierler BK. Management of massive and submassive pulmonary embolism, iliofemoral deep vein thrombosis, and chronic thromboembolic pulmonary hypertension. Circulation. 2011;123:1788–830.
56. Smulders YM. Pathophysiology and treatment of haemodynamic instability in acute pulmonary embolism: the pivotal role of pulmonary vasoconstriction. Cardiovasc Res. 2000;48:23–33.
57. Wood KE. Major pulmonary embolism: review of a pathophysiologic approach to the golden hour of hemodynamically significant pulmonary embolism. Chest. 2002;121:877–905.
58. Price S, Uddin S, Quinn T. Echocardiography in cardiac arrest. Curr Opin Crit Care. 2010;16:211–5.
59. Williams B, Sikorski R, Anders M, Galvagno S, Rock P, Mazzeffi M. Should we use perioperative transesophageal echocardiography more in non-cardiac surgery? J Cardiothorac Vasc Anesth. 2018;32:e71–3.
60. Shillcutt SK, Brakke TR, Thomas WR, Porter TR, Lisco SJ. The development of a perioperative echocardiography consult service: the nebraska experience. J Cardiothorac Vasc Anesth. 2015;29:777–84.
61. Yock PG, Popp RL. Noninvasive estimation of right ventricular systolic pressure by doppler ultrasound in patients with tricuspid regurgitation. Circulation. 1984;70:657–62.
62. Nkomo VT, Gardin JM, Skelton TN, Gottdiener JS, Scott CG, Enriquez-Sarano M. Burden of valvular heart diseases: a population-based study. Lancet. 2006;368:1005–11.
63. Iung B, Baron G, Butchart EG, Delahaye F, Gohlke-Bärwolf C, Levang OW, Tornos P, Vanoverschelde J-L, Vermeer F, Boersma E, Ravaud P, Vahanian A. A prospective survey of patients with valvular heart disease in Europe: the euro heart survey on valvular heart disease. Eur Heart J. 2003;24:1231–43.
64. Vahanian A, Alfieri O, Andreotti F, Antunes MJ, Barón-Esquivias G, Baumgartner H, Borger MA, Carrel TP, De BM, Evangelista A, Falk V, Iung B, Lancellotti P, Pierard L, Price S, Schäfers HJ, Schuler G, Stepinska J, Swedberg K, Takkenberg J, et al. The joint task force on the management of valvular heart disease of the European Society of cardiology (ESC) and the European Association for Cardio-Thoracic Surgery (EACTS). Eur J Cardio-thoracic Surg. 2012;42:S1–44.
65. Online STS risk calculator at http://riskcalc.sts.org/stswebriskcalc/calculate.
66. New EuroSCORE II (2011) at http://www.euroscore.org/calc.html.

67. Nishimura RA, Otto CM, Bonow RO, Carabello BA, Erwin JP, Guyton RA, O'Gara PT, Ruiz CE, Skubas NJ, Sorajja P, Sundt TM, Thomas JD. 2014 AHA/ACC guideline for the management of patients with valvular heart disease: executive summary. Circulation. 2014;129:2440–92.
68. Baumgartner H, Hung J, Bermejo J, Chambers JB, Evangelista A, Griffin BP, Iung B, Otto CM, Pellikka PA, Quiñones M. American Society of Echocardiography, European Association of Echocardiography: echocardiographic assessment of valve stenosis: EAE/ASE recommendations for clinical practice. J Am Soc Echocardiogr. 2009;22:1–23.
69. Lancellotti P, Tribouilloy C, Hagendorff A, Popescu BA, Edvardsen T, Pierard LA, Badano L, Zamorano JL. Recommendations for the echocardiographic assessment of native valvular regurgitation: an executive summary from the European Association of Cardiovascular Imaging. Eur Hear J Cardiovasc Imaging. 2013;14:611–44.

Ultrasound for Chest: Heart and TTE

Paula Trigo Blanco

1 Introduction

Echocardiography (cardiac ultrasonography) is a ubiquitous cardiac imaging technique used for the diagnosis and monitoring of cardiovascular diseases. There are two major techniques for echocardiography based on the location of the ultrasound transducer: Transthoracic echocardiography (TTE), which acquires images of the heart from chest wall and transesophageal echocardiography (TEE), which obtains images from a probe inserted into the esophagus.

TTE is a common bedside cardiac examination that can provide a high quality and comprehensive imaging study. Hemodynamics, left and right ventricular systolic performance and diastolic function can be objectively measured, and regional wall motion, valve function and the pericardium can be evaluated.

Clinical interpretation of an echocardiography study is highly dependent on image quality and the accuracy of acquisition. Hence, TTE images are obtained from standard transducer positions that visualize specific sectors of the heart. These standardized positions are the apical, subcostal, parasternal and suprasternal notch positions (see below).

1.1 Ultrasound Basics

An ultrasound (US) transducer contains a number of piezoelectric crystals which convert electrical energy into mechanical energy (vibrations) at the frequency of ultrasound (greater than 20,000 cycles per sec or 20KHz). Each individual crystal produces a beam of ultrasound which is known as a scan line. The scan lines can be fired off simultaneously, producing a rectangular image or at set delays, producing a fan shaped sector which can be electronically steered. When the ultrasound waves are transmitted into tissue, most are absorbed but some are reflected back by tissue interfaces towards the transducer. These returning ultrasound signals are converted back to electrical energy by the crystals and processed into visual images. For TTE, an electrocardiogram (ECG) is typically displayed with the image to assist with timing of events throughout the cardiac cycle [1].

There are different *US modes* [2]:

1. *Two-dimensional imaging (2D)*: 2D imaging is the most common US mode used clinically. Structures are viewed in a cross-section of the heart with high resolution [3]. It is used to evaluate anatomy and movement of cardiac structures. However, it cannot visualize blood flow in the heart and great vessels.
2. *M mode* (*Motion Mode*): A single scan line is displayed against time, providing a one-dimensional view. M-mode has the highest temporal resolution since there is no delay in building a sector from multiple scan lines. It is typically used for the timing of events throughout the cardiac cycle.
3. *Doppler imaging*: Doppler echocardiography provides information on blood flow in the heart and great vessels by processing the change in frequency and wavelength of the US echoes reflected from moving targets [4–6]. Doppler US allows quantitative assessment of the velocity (magnitude and direction) of blood flow and myocardial tissue. Doppler is used in several ways:
    - Pulsed-wave (PW) Doppler uses a single crystal to send and then receive a signal from a discrete location. It therefore measures localized velocity of typically laminar blood flow. Because the sampling is intermittent, the maximum Doppler shift is limited, and therefore the maximum velocity which can be measured is also limited (around 1.2 m/s). PW Doppler is most often used to measure left ventricular inflow and outflow as well as pulmonary and hepatic vein profiles.

P. Trigo Blanco (✉)
Southern New Hampshire Medical Center, Anesthesiology,
Nashua, NH, USA

© Springer Nature Switzerland AG 2021
J. Li et al. (eds.), *Ultrasound Fundamentals*, https://doi.org/10.1007/978-3-030-46839-2_19

- Continuous-wave (CW) Doppler uses two crystals simultaneously, one to send continuously and one to receive continuously. Velocities are measured along the entire length of the two US scan lines, not a specific depth as in PW. However, since there is continuous sampling, the velocities which can be measured are significantly higher. CW Doppler is used to estimate the severity of valve stenosis or regurgitation.
- Color-flow Doppler mapping (CFD or CFM) is a pulsed Doppler technique which color codes Doppler information and superimposes it over real time 2D imaging. Traditionally, flow towards the transducer is coded red, flow away from the transducer is blue and higher velocities are represented by brighter shades. To aid in detection of turbulent flow, there is a maximum (aliasing) velocity, beyond which the color code changes to the color representing the opposite direction. This leads to a "mosaic" pattern at the site of turbulent flow and enables sensitive screening for regurgitant flow. In some systems, variance from the mean velocity is coded as green.
- Tissue Doppler Echocardiography (TDE) [6] measures the velocity of the myocardium throughout the cardiac cycle. It is a pulsed Doppler technique which filters out the higher blood flow velocities and only measures the lower velocity of tissue movement (typically less than 0.2 m/s) US wave (Fig. 1).

1.2 Ultrasound Probes

The depth of penetration of an ultrasound wave varies inversely with the frequency of the transducer. Consequently, the frequency of a transducer is selected to achieve the desired depth of penetration. Also, transducers are constructed in different sizes and shapes for different purposes and image displays. There is usually a mark (dot or notch) on the probe to orient the user for image acquisition.

For TTE, a curved linear probe with a small "foot print" is utilized (Figs. 2a and 2b).

When performing a surface ultrasound such as TTE, there are 4 movements of the probe: translation, angulation (cephalad towards the patient's head or caudal towards the feet), rotation and tilt.

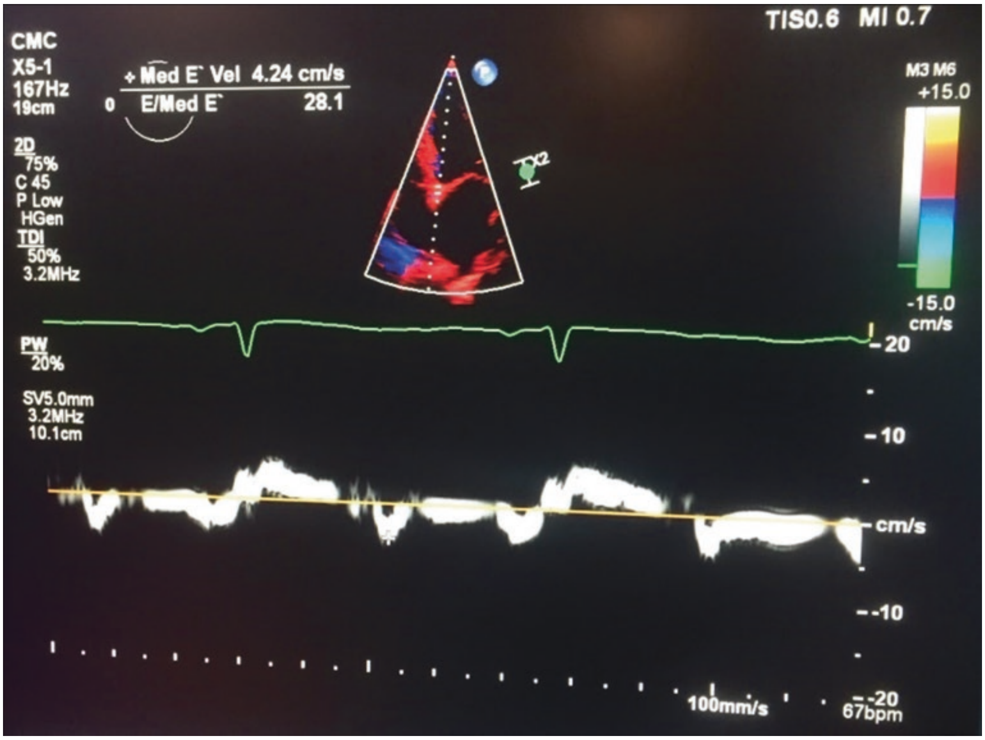

Fig. 1 Tissue Doppler echocardiography image

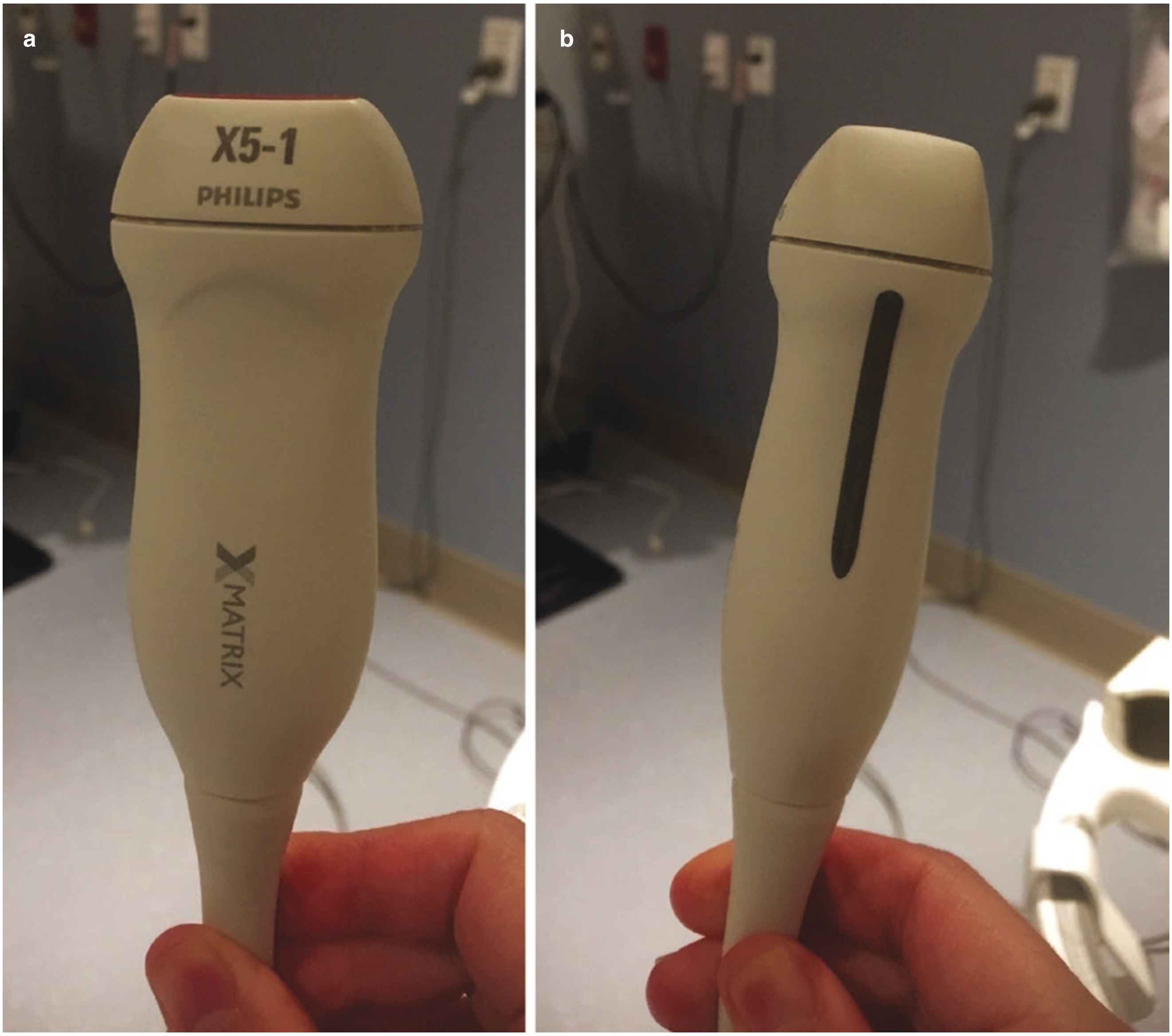

Fig. 2a and 2b Curved linear probe with a small "foot print" viewed anteriorly and laterally

2 TTE Anatomy and Windows

The term window refers to the physical location of the transducer on the chest wall. There are four standard acoustic windows used in a routine TTE examination: suprasternal, parasternal, apical, and subcostal. The image produced by a specific window is described by a corresponding view. The named view refers to the image plane as it relates to the axis of the heart using the left ventricle (LV) as the main reference point. For example, in a parasternal short-axis view the transducer is placed to the left of the sternum and rotated so that the image generated displays a short-axis view of the LV.

The *suprasternal window* is obtained with the patient in the supine position, the neck extended and the transducer placed in the suprasternal notch (orientation of probe, patient positioning for optimal viewing – extension/rotation – this would also be for any subsequent sections below). This window views the thoracic aortic arch and great vessels (brachiocephalic artery, left common carotid -LCCA-, and left subclavian artery -LSA-) (Figs. 3 and 4).

The *parasternal window* is obtained with the patient in the left lateral decubitus position. The transducer is placed on the left sternal edge in the third or fourth intercostal space. There are three views that can be acquired via the parasternal window: parasagittal long axis, right ventricular inflow-outflow, and short axis.

The *parasagittal long-axis view* provides images of the coronary sinus (CS), left atrium (LA), mitral valve (MV),

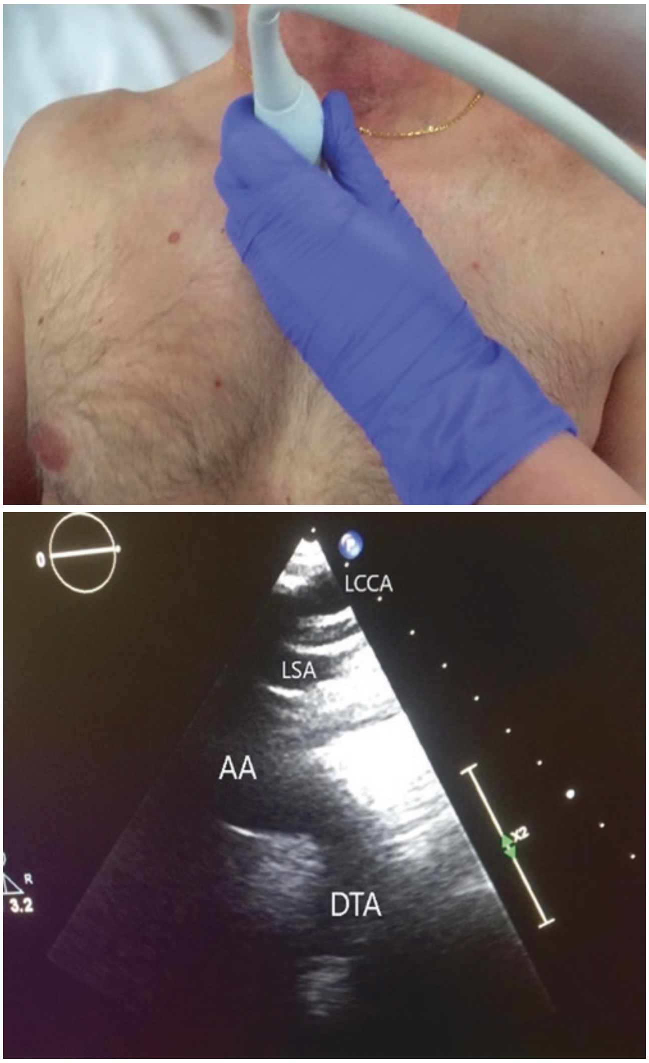

Figs. 3 and 4 Suprasternal window. LCCA (left common carotid artery), LSA (left subclavian artery), AA (aortic arch), DTA (descending thoracic aorta)

left ventricular septum and posterior wall, left ventricular outflow tract (LVOT), aortic root, sinuses of Valsalva (SOV), and descending thoracic aorta (DTA) (Figs. 5 and 6).

The *right ventricular inflow-outflow view* is obtained by angulating the probe medially and moving apically from the long-axis view. This view demonstrates the inferior vena cava (IVC), right atrium (RA), tricuspid valve (TV), right ventricle (RV) and the CS.

The *short-axis view* is obtained by rotating the probe approximately 90° and angulating it superior to inferior along the long axis of the LV. This view gives images of the interatrial septum, TV, pulmonic valve (PV), MV leaflets, LV papillary muscles, all of the LV wall segments except for the apex, and the aortic valve (AV) cusps (Figs. 7 and 8).

The *apical window* is obtained with the patient in the left lateral decubitus position. There are three routine views generated via the apical window: four-chamber view (it demonstrates the four cardiac chambers in plane), two-chamber view (useful to evaluate the LA, proximal LA appendage (LAA), MV, and anterior LV wall, and long-axis (or apical three-chamber) view. This is the best window to visualize the LV apex (Figs. 9 and 10).

The *subcostal window* is obtained with the patient supine and the transducer placed inferior to the sternum, angled slightly towards the patient's left. There are two views obtained via the subcostal window: *four-chamber view* (very useful to identify interatrial septal defects) and *inferior vena cava view* (used to estimate RA pressures by assessing for changes in size of the IVC during inspiration and expiration) (Figs. 11 and 12).

3 Applications. Clinical Indications

TTE should be performed in accordance with the guidelines and recommendations published by the American Society of Echocardiography (ASE) and the European Association of Cardiovascular Imaging [7, 8].

3.1 LV Systolic Function

One of the most common indications for TTE is the assessment of *LV systolic function.* Typically, this is reported as an ejection fraction [9] (EF, the percentage of the end diastolic volume ejected during systole) [9, 10]. The American Society of Echocardiography recommends the modified Simpson's method (biplane method of discs) to calculate LV volumes and EF. The ventricular endocardium is traced at end diastole and is divided along its long axis into a series of 'disks'. This is repeated in an orthogonal plane (at 90 degrees to the first) and the sum of the volume of each disc provides the LV end diastolic volume. The process is repeated at end systole and the EF can then be calculated. The software packages on most modern ultrasound platforms perform these calculations.

Fractional area change (FAC) of the LV can provide a simpler estimate systolic function which correlates well with EF [11]. The optimal view for calculating FAC is the LV short axis view from the mid transgastric acoustic window (Fig. 13).

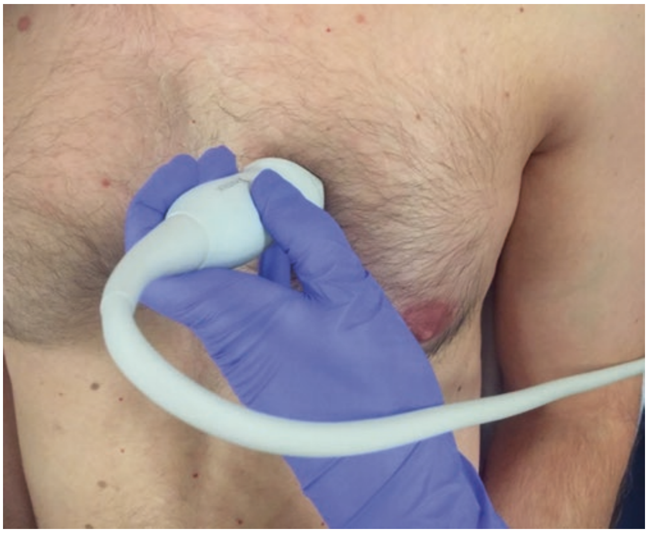

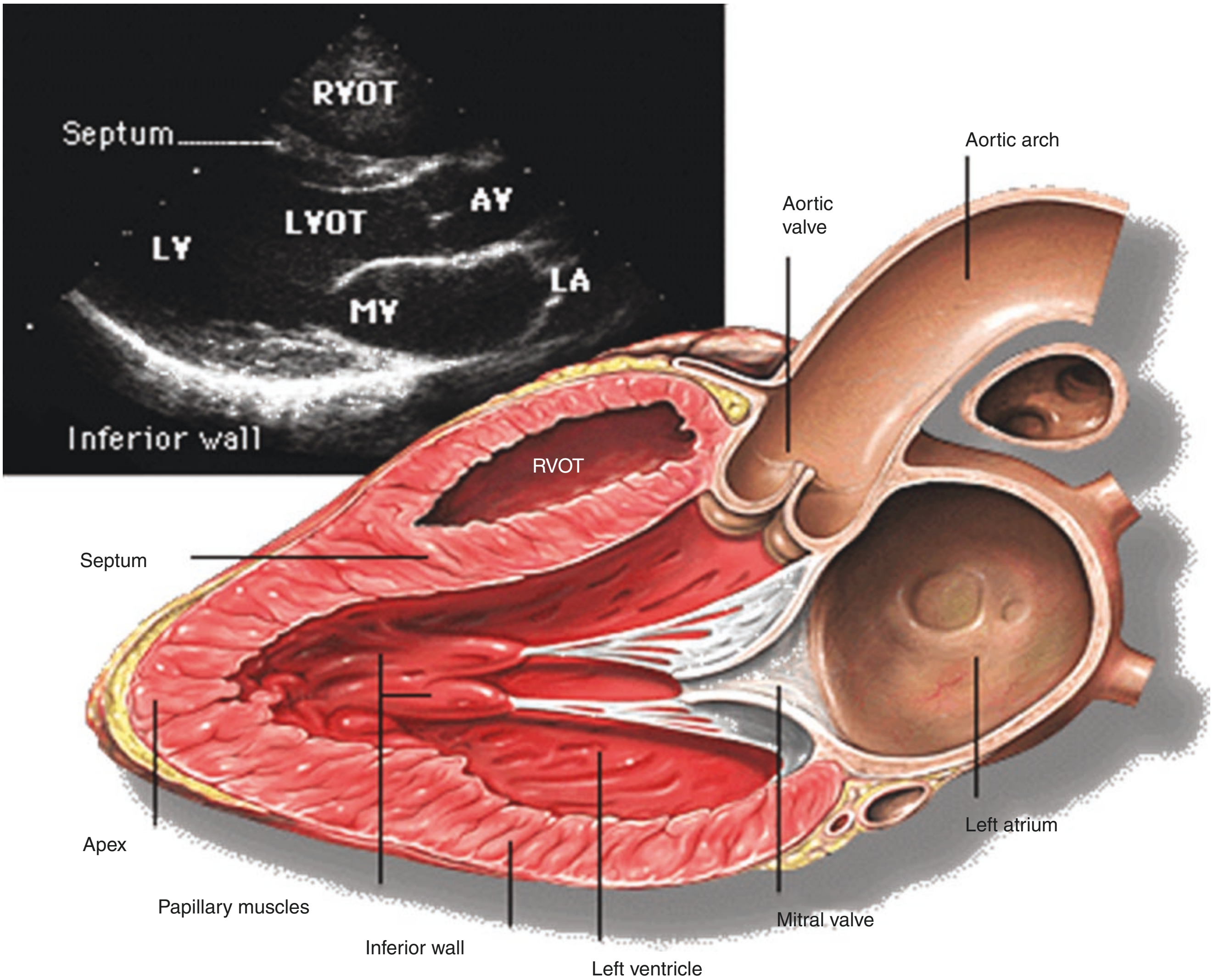
RVOT
Septum
LVOT
AV
LV
LA
MV
Inferior wall
Aortic arch
Aortic valve
RVOT
Septum
Apex
Papillary muscles
Inferior wall
Left ventricle
Mitral valve
Left atrium

Figs. 5 and 6 Parasternal window long-axis view. RVOT (Right ventricular outflow tract), LV (left ventricle), LVOT (left ventricular outflow tract), AV (aortic valve), MV (mitral valve), LA (left atrium). (Source: Ref. [26, 27])

Figs. 7 and 8 Parasternal window s*hort-axis view*. (Source: Ref. [26, 27])

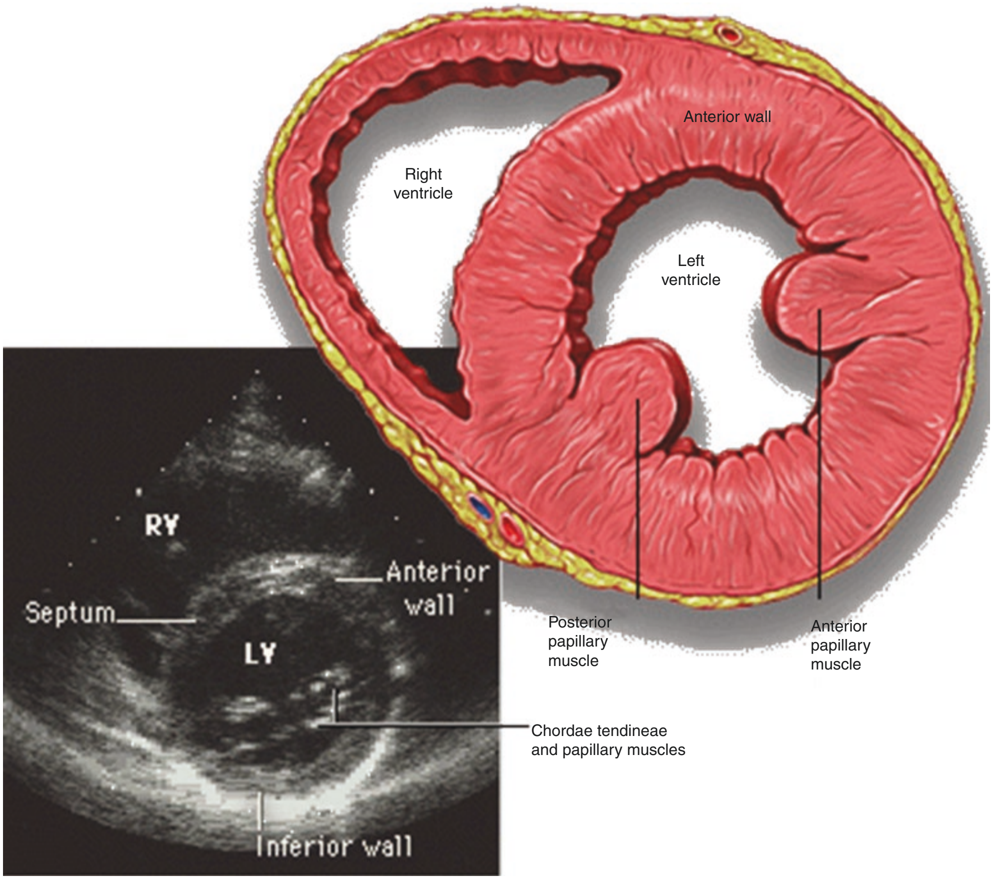
Anterior wall
Right ventricle
Left ventricle
Posterior papillary muscle
Anterior papillary muscle
RV
Anterior wall
Septum
LV
Chordae tendineae and papillary muscles
Inferior wall

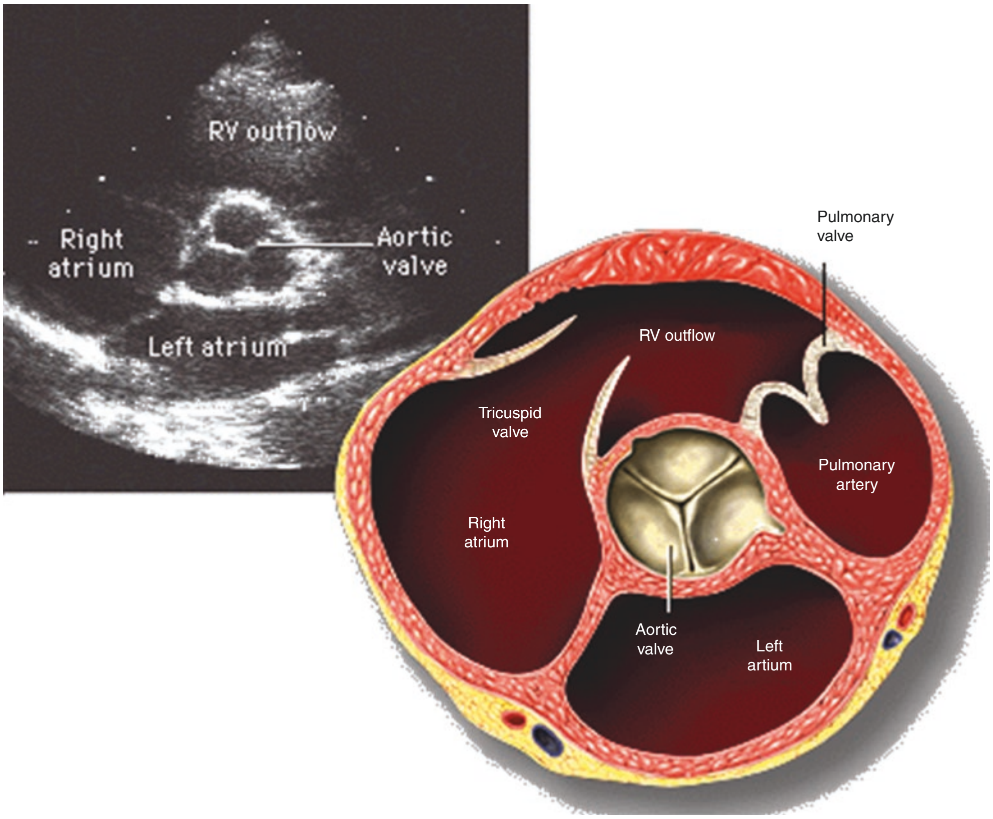
RV outflow
Right atrium
Aortic valve
Left atrium
Pulmonary valve
RV outflow
Tricuspid valve
Pulmonary artery
Right atrium
Aortic valve
Left artium

Figs. 9 and 10 Apical window four chambers view (it demonstrates the four cardiac chambers in plane). (Source: Ref. [26, 27])

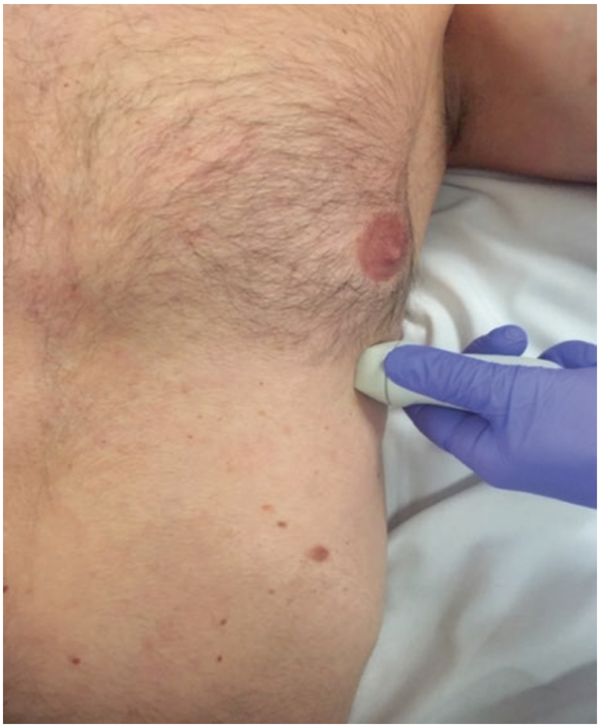

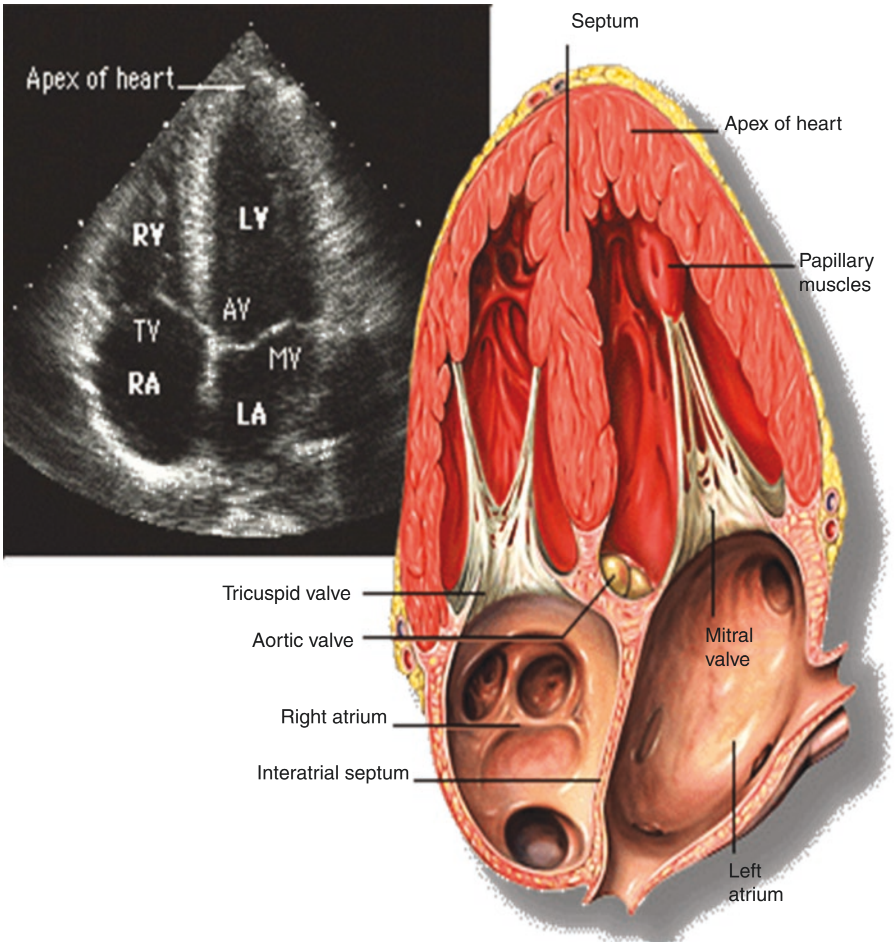
Apex of heart
RV
LV
AV
TV
MV
RA
LA
Septum
Apex of heart
Papillary muscles
Tricuspid valve
Aortic valve
Mitral valve
Right atrium
Interatrial septum
Left atrium

Figs. 11 and 12 Subcostal window *four-chamber view* (very useful to identify interatrial septal defects). (Source: Ref. [26, 27])

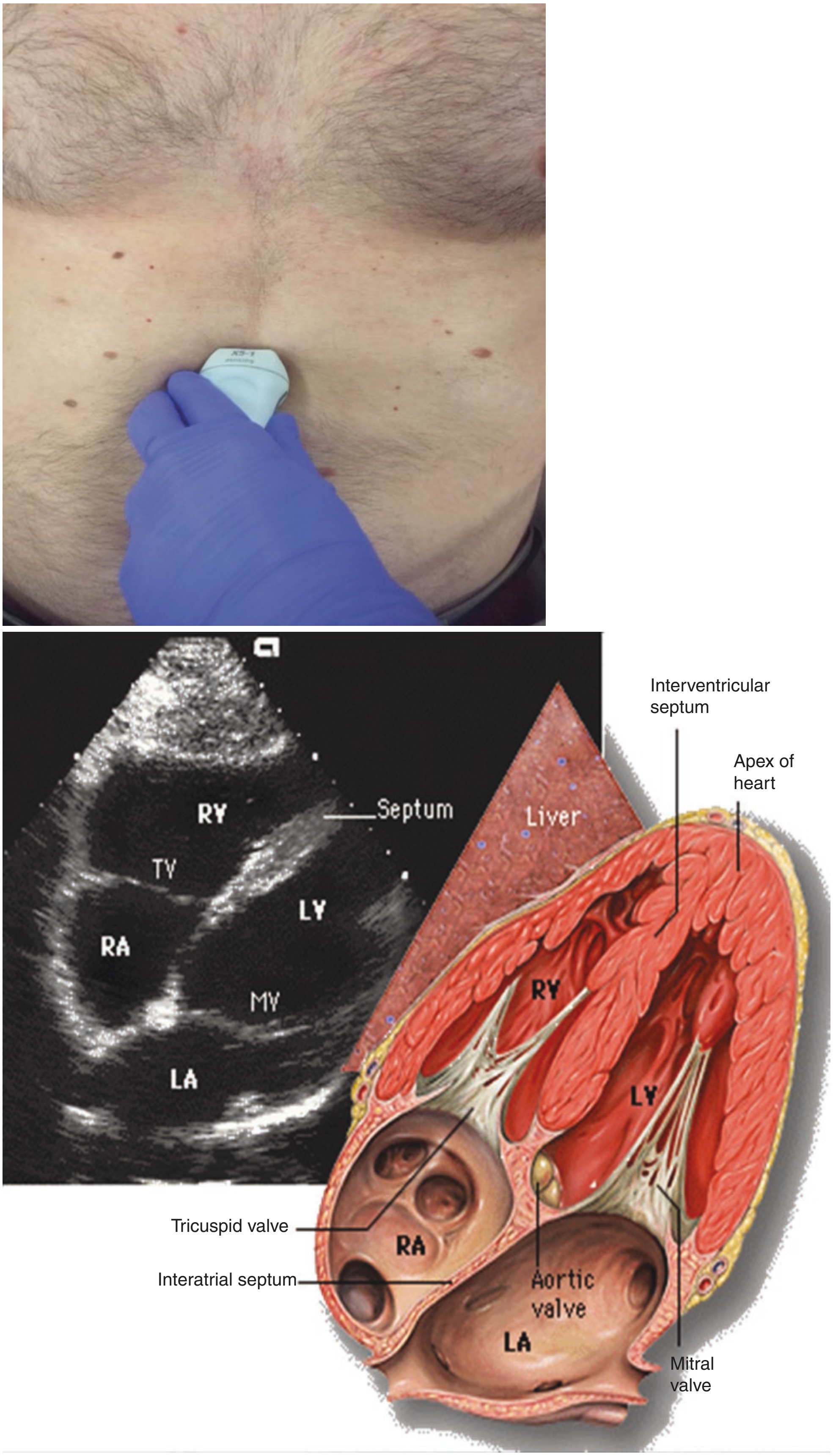
a
RV
Septum
TV
LV
RA
MV
LA
Liver
Interventricular septum
Apex of heart
RV
LV
RA
Tricuspid valve
Interatrial septum
Aortic valve
LA
Mitral valve

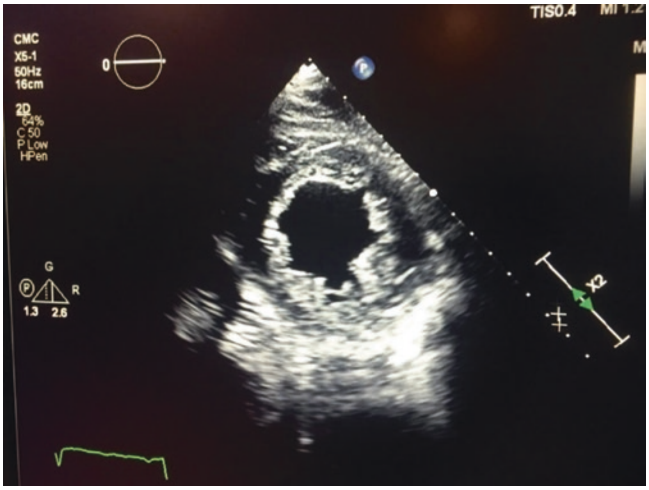

Fig. 13 LV short axis view from the mid transgastric acoustic window

The area of the LV cavity is traced in end-diastole (EDA) and end-systole (ESA). The difference between the two, divided by the EDA expressed as a percentage is the FAC. Note that FAC is based upon area, it does not take the apex into account and assumes that the LV contracts symmetrically. Thus, values of FAC will be smaller than the EF and are prone to error in an LV with regional wall abnormalities.

3.2 Diastolic Dysfunction

TTE can provide a comprehensive evaluation of diastolic filling of the ventricle, myocardial relaxation, and ventricular stiffness [12, 13].

When flow across the MV is assessed with PW Doppler, two waves are seen: an early [E] wave, (passive filling of the ventricle), and an atrial [A] wave (active filling during atrial systole). In a healthy heart, the E-wave velocity is slightly greater than that of the A wave (E > A) [14–16].

In cases with reduced LV compliance (elderly patients, chronic systemic hypertension, LV hypertrophy -LVH-, diastolic dysfunction), the A wave is greater than the E wave [17].

Another possible finding is an exaggeration of the E wave with a small or absent A wave. This indicates restrictive cardiomyopathy, constrictive pericarditis, or infiltrative cardiac disease (e.g. amyloidosis) [18, 19].

3.3 Wall Motion Abnormalities

Echocardiography is useful in detecting both stable coronary artery disease (stress echocardiogram [20]) and acute myocardial ischemia [21–23]. When ischemia occurs, contractile abnormalities of segments of the myocardium can be visualized by echocardiography prior to the appearance of electrocardiogram (ECG) changes or even clinical symptoms [24, 25] (Fig. 14).

3.4 Heart Valves Assessment

Echocardiography is the diagnostic test of choice for the assessment of valvular abnormalities: [28–31].

- Aortic stenosis (AS) and mitral stenosis (MS): TTE provides valuable information about the etiology of valve stenosis from 2D imaging as well as the severity of the stenosis using Doppler interrogation [32–35].
- Aortic regurgitation (AI) and mitral regurgitation (MR): CFM is the most useful technique to detect regurgitation [36, 37]. Quantification can be subjectively assessed by visual grading of the CFM images and more objectively by using a number of Doppler measurements.
- MV prolapse: diagnosis is made by visual inspection of the valve anatomy usually in the parasternal long axis view [38–42].
- Periprosthetic leak: echocardiography is a useful tool in the evaluation of prosthetic valve function. TEE is generally more sensitive than TTE [43].

3.5 Infective Endocarditis

Echocardiography is of paramount importance in the diagnosis of infective endocarditis. Although tissue diagnosis cannot be made by echocardiography, the demonstration of mobile masses attached to valve apparatus (2D) associated with regurgitation (CFM) is highly suggestive of vegetations. Again, TEE is more sensitive than TTE [44–46].

3.6 Embolic Sources

Echocardiography can detect cardiac sources of embolism, such as thrombi in the LAA [47], in an LV aneurysm or attached to an akinetic LV wall segment [48, 49]. Emboli from deep vein thrombosis may also be detected anywhere in the right side of the heart, the pulmonary artery and its proximal branches and less often in the left side of the heart via a patent foramen ovale or an atrial septal defect.

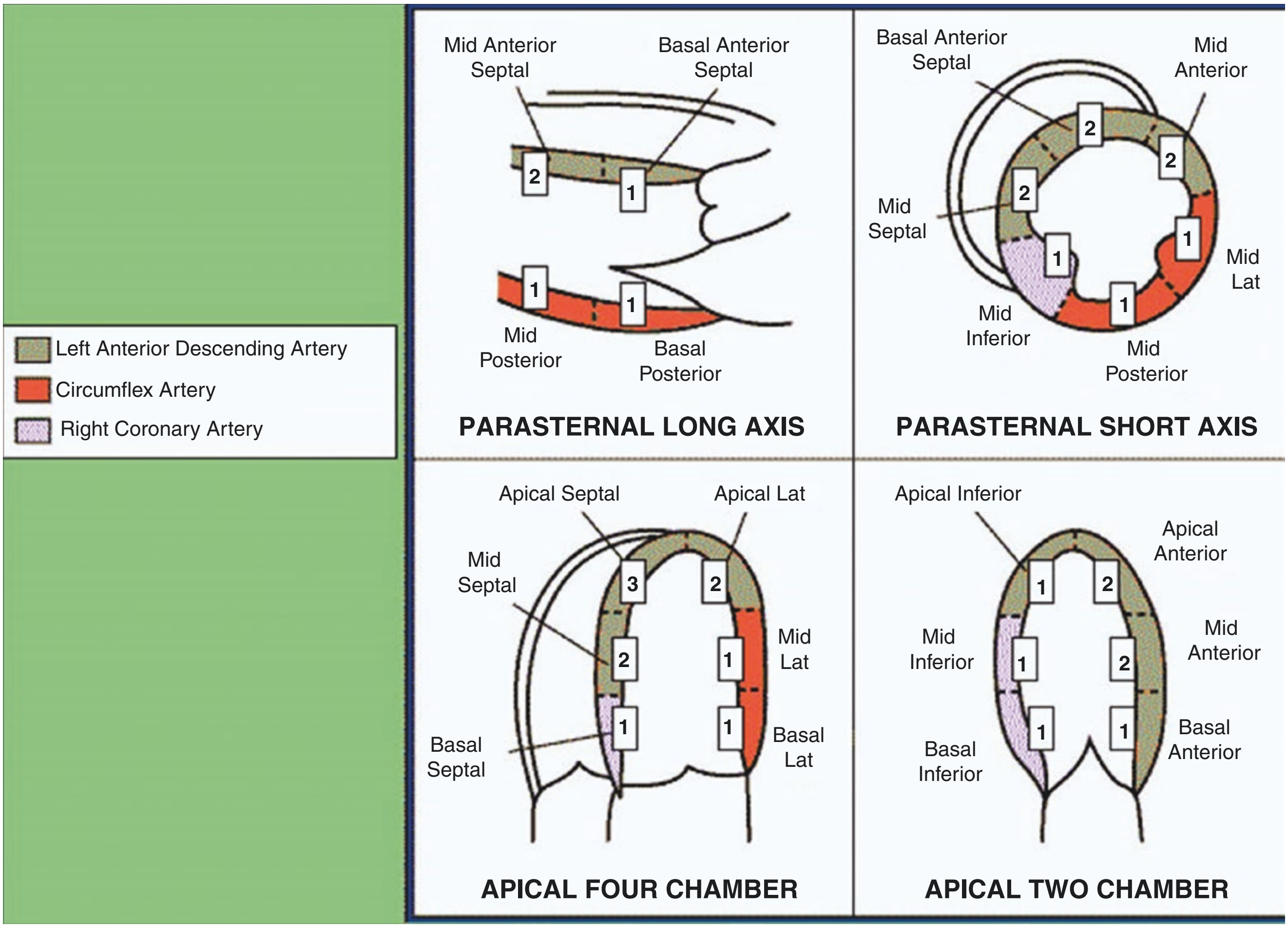
Left Anterior Descending Artery
Circumflex Artery
Right Coronary Artery
Mid Anterior Septal
Basal Anterior Septal
Mid Posterior
Basal Posterior
PARASTERNAL LONG AXIS
Basal Anterior Septal
Mid Anterior
Mid Septal
Mid Lat
Mid Inferior
Mid Posterior
PARASTERNAL SHORT AXIS
Apical Septal
Apical Lat
Mid Septal
Mid Lat
Basal Septal
Basal Lat
APICAL FOUR CHAMBER
Apical Inferior
Apical Anterior
Mid Inferior
Mid Anterior
Basal Inferior
Basal Anterior
APICAL TWO CHAMBER
1
2
3

Fig. 14 This image depicts the different coronary artery territories from different echocardiographic views. (Source: Ref. [26, 27])

3.7 Hypertrophic Cardiomyopathy

Hypertrophic cardiomyopathy may be concentric or asymmetric. In patients with hypertrophy of the interventricular septum, 2D imaging may reveal dynamic LVOT obstruction and systolic anterior motion of the MV with associated MR [50].

3.8 Volume Status

TTE is a non-invasive means of hemodynamic assessment that can be applied to critically ill patients, and is currently recommended as the first imaging technique in trauma patients as well as those with circulatory failure [51–53].

Mortality in trauma patients is greatest within the first 6 hours and may be preventable. Early detection of hypovolemia is critical [54]. The diameter of the IVC measured at the bedside with TTE provides a rapid and repeatable measure of intravascular volume status [55, 56] (Fig. 15).

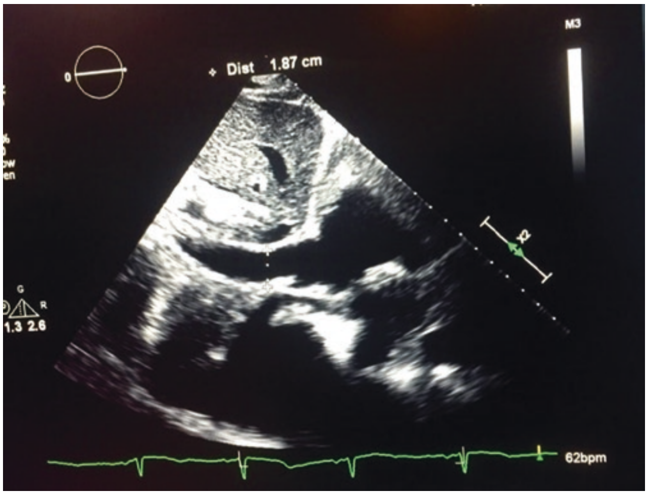
M3
Dist 1.87 cm
1.3 2.6
62bpm

Fig. 15 The subcostal window *inferior vena cava view* demonstrating the size of the IVC

Measurement of the IVC diameter has been found to be more accurate as a marker of early hypovolemic shock than other commonly used predictors of acute blood loss (blood pressure, heart rate, serum lactate level) [57–60].

3.9 Measurement of Cardiac Output (CO)

The earliest studies that calculated CO by using echocardiography (PW or CW Doppler techniques), measured the aortic blood flow in a suprasternal view of the ascending aorta [61].

Nowadays, the recommended method for calculating CO is obtained from a pulsed Doppler measurement of the AV annulus in the apical five-chamber view [62–64].

4 Echocardiography Advantages

TTE is a versatile, portable and safe cardiovascular imaging technique, able to provide real time views of cardiovascular structures with minimal patient discomfort.

5 Limitations and Pitfalls

TTE has technical limitations, such as suboptimal acoustic windows (obese patients, patients with chronic lung disease, or patients on mechanical ventilation).

Furthermore, the evaluation of ascending thoracic aortic dissections with TTE is difficult, and the frequent false-positive diagnosis is thought to be related to reverberation artifacts [65–67].

6 Conclusions

There is a growing trend of using ultrasound examination of the heart as a diagnostic tool for initial patient evaluation in acute settings.

Echocardiography is a valuable cardiac imaging technique. It often serves as one of the first-line imaging techniques in the assessment of cardiovascular disease due to its portability, low cost, lack of ionizing radiation and great ability to evaluate cardiovascular anatomy and function.

Echocardiographic images are evaluated in real time, which allows quick diagnostic interpretation. Two-dimensional, spectral and color-Doppler are pivotal techniques for cardiovascular evaluation. Newer techniques, such as tissue-Doppler imaging, myocardial deformation imaging, as well as three-dimensional echocardiography, may also have an important role.

References

1. Gramiak R, Waag RC, Simon W. Ciné ultrasound cardiography. Radiology. 1973;107(1):175–80.
2. Mohamed AA, Arifi AA, Omran A. The basics of echocardiography. J Saudi Heart Assoc. 2010;22(2):71–6.
3. Henry WL, DeMaria A, Gramiak R, et al. Report of the American Society of Echocardiography Committee on nomenclature and standards in two-dimensional echocardiography. Circulation. 1980;62(2):212–7.
4. Yoshida T, Mori M, Nimura Y, et al. Analysis of heart motion with ultrasonic Doppler method and its clinical application. Am Heart J. 1961;61:61–75.
5. McDicken WN, Sutherland GR, Moran CM, Gordon LN. Colour Doppler velocity imaging of the myocardium. Ultrasound Med Biol. 1992;18(6–7):651–4.
6. Mor-Avi V, Lang RM, Badano LP, et al. Current and evolving echocardiographic techniques for the quantitative evaluation of cardiac mechanics: ASE/EAE consensus statement on methodology and indications endorsed by the Japanese Society of Echocardiography. J Am Soc Echocardiogr. 2011;24(3):277–313.
7. Lang RM, Badano LP, Mor-Avi V, et al. Recommendations for cardiac chamber quantification by echocardiography in adults: an update from the American Society of Echocardiography and the European Association of Cardiovascular Imaging. Eur Heart J Cardiovasc Imaging. 2015;16(3):233–70.
8. Quiñones MA, Otto CM, Stoddard M, Waggoner A, Zoghbi WA, Doppler Quantification Task Force of the Nomenclature and Standards Committee of the American Society of Echocardiography. Recommendations for quantification of Doppler echocardiography: a report from the Doppler quantification task force of the nomenclature and standards committee of the American Society of Echocardiography. J Am Soc Echocardiogr. 2002;15(2):167–84.
9. Levy F, Dan Schouver E, Iacuzio L, et al. Performance of new automated transthoracic three-dimensional echocardiographic software for left ventricular volumes and function assessment in routine clinical practice: comparison with 3 Tesla cardiac magnetic resonance. Arch Cardiovasc Dis. 2017;110(11):580–9.
10. Tsang W, Salgo IS, Medvedofsky D, et al. Transthoracic 3D echocardiographic left heart chamber quantification using an automated adaptive analytics algorithm. JACC Cardiovasc Imaging. 2016;9(7):769–82.
11. Castiglioni L, Colazzo F, Fontana L, et al. Evaluation of left ventricle function by regional fractional area change (RFAC) in a mouse model of myocardial infarction secondary to valsartan treatment. PLoS One. 2015;10(8):e0135778.
12. Hoit BD. Left ventricular diastolic function. Crit Care Med. 2007;35(8 Suppl):S340–7.
13. Oh JK, Hatle L, Tajik AJ, Little WC. Diastolic heart failure can be diagnosed by comprehensive two-dimensional and Doppler echocardiography. J Am Coll Cardiol. 2006;47(3):500–6.
14. Galderisi M, Dini FL, Temporelli PL, Colonna P, de Simone G. Doppler echocardiography for the assessment of left ventricular diastolic function: methodology, clinical and prognostic value. Ital Heart J Suppl. 2004;5(2):86–97.
15. Faggiano P, Vizzardi E, Pulcini E, et al. The study of left ventricular diastolic function by Doppler echocardiography: the essential for the clinician. Heart Int. 2007;3(1):42.
16. Cohen GI, Pietrolungo JF, Thomas JD, Klein AL. A practical guide to assessment of ventricular diastolic function using Doppler echocardiography. J Am Coll Cardiol. 1996;27(7):1753–60.

17. Ghany R, Palacio A, Chen G, et al. A screening echocardiogram to identify diastolic dysfunction leads to better outcomes. Echocardiography. 2017;34(8):1152–8.
18. Hancock EW. Differential diagnosis of restrictive cardiomyopathy and constrictive pericarditis. Heart. 2001;86(3):343–9.
19. Zwas DR, Gotsman I, Admon D, Keren A. Advances in the differentiation of constrictive pericarditis and restrictive cardiomyopathy. Herz. 2012;37(6):664–73.
20. Zabalgoitia M, Ismaeil M. Diagnostic and prognostic use of stress echo in acute coronary syndromes including emergency department imaging. Echocardiography. 2000;17(5):479–93.
21. Esmaeilzadeh M, Parsaee M, Maleki M. The role of echocardiography in coronary artery disease and acute myocardial infarction. J Tehran Heart Cent. 2013;8(1):1–13.
22. Greaves SC. Role of echocardiography in acute coronary syndromes. Heart. 2002;88(4):419–25.
23. Romano S, Dagianti A, Penco M, Varveri A, Biffani E, Fedele F. Usefulness of echocardiography in the prognostic evaluation of non-Q-wave myocardial infarction. Am J Cardiol. 2000;86(4A):43G–5G.
24. Horowitz RS, Morganroth J, Parrotto C, Chen CC, Soffer J, Pauletto FJ. Immediate diagnosis of acute myocardial infarction by two-dimensional echocardiography. Circulation. 1982;65(2):323–9.
25. Smith JS, Cahalan MK, Benefiel DJ, et al. Intraoperative detection of myocardial ischemia in high-risk patients: electrocardiography versus two-dimensional transesophageal echocardiography. Circulation. 1985;72(5):1015–21.
26. https://en.wikipedia.org/wiki/Transthoracic_echocardiogram. Free to share and commercially use.
27. http://www.emcurious.com/blog-1/2014/10/30/ultrasound-leadership-academy-basic-cardiac. Ultrasound Leadership Academy: Basic Cardiac EM Curious. Licensed under a Creative Commons Attribution 4.0 International License. Free to share and commercially use.
28. Sordelli C, Severino S, Ascione L, Coppolino P, Caso P. Echocardiographic assessment of heart valve prostheses. J Cardiovasc Echogr. 2014;24(4):103–13.
29. Nishimura RA, Otto CM, Bonow RO, et al. 2014 AHA/ACC guideline for the management of patients with valvular heart disease: a report of the American College of Cardiology/American Heart Association Task Force on Practice Guidelines. J Am Coll Cardiol. 2014;63(22):e57–185.
30. Anwar AM, Nosir YF, Zainal-Abidin SK, Ajam A, Chamsi-Pasha H. Real-time three-dimensional transthoracic echocardiography in daily practice: initial experience. Cardiovasc Ultrasound. 2012;10:14.
31. Zamorano JL, Badano LP, Bruce C, et al. EAE/ASE recommendations for the use of echocardiography in new transcatheter interventions for valvular heart disease. Eur J Echocardiogr. 2011;12(8):557–84.
32. Burwash IG. Echocardiographic evaluation of aortic stenosis - normal flow and low flow scenarios. Eur Cardiol. 2014;9(2):92–9.
33. Baumgartner H, Hung J, Bermejo J, et al. Echocardiographic assessment of valve stenosis: EAE/ASE recommendations for clinical practice. J Am Soc Echocardiogr. 2009;22(1):1–23.. quiz 101-102
34. Michelena HI, Margaryan E, Miller FA, et al. Inconsistent echocardiographic grading of aortic stenosis: is the left ventricular outflow tract important? Heart. 2013;99(13):921–31.
35. Clavel MA, Ennezat PV, Maréchaux S, et al. Stress echocardiography to assess stenosis severity and predict outcome in patients with paradoxical low-flow, low-gradient aortic stenosis and preserved LVEF. JACC Cardiovasc Imaging. 2013;6(2):175–83.
36. Zoghbi WA, Enriquez-Sarano M, Foster E, et al. Recommendations for evaluation of the severity of native valvular regurgitation with two-dimensional and Doppler echocardiography. J Am Soc Echocardiogr. 2003;16(7):777–802.
37. Lancellotti P, Tribouilloy C, Hagendorff A, et al. European Association of Echocardiography recommendations for the assessment of valvular regurgitation. Part 1: aortic and pulmonary regurgitation (native valve disease). Eur J Echocardiogr. 2010;11(3):223–44.
38. Gripari P, Mapelli M, Bellacosa I, et al. Transthoracic echocardiography in patients undergoing mitral valve repair: comparison of new transthoracic 3D techniques to 2D transoesophageal echocardiography in the localization of mitral valve prolapse. Int J Cardiovasc Imaging. 2018;34(7):1099–107.
39. Pepi M, Tamborini G, Maltagliati A, et al. Head-to-head comparison of two- and three-dimensional transthoracic and transesophageal echocardiography in the localization of mitral valve prolapse. J Am Coll Cardiol. 2006;48(12):2524–30.
40. Patel V, Hsiung MC, Nanda NC, et al. Usefulness of live/real time three-dimensional transthoracic echocardiography in the identification of individual segment/scallop prolapse of the mitral valve. Echocardiography. 2006;23(6):513–8.
41. Sharma R, Mann J, Drummond L, Livesey SA, Simpson IA. The evaluation of real-time 3-dimensional transthoracic echocardiography for the preoperative functional assessment of patients with mitral valve prolapse: a comparison with 2-dimensional transesophageal echocardiography. J Am Soc Echocardiogr. 2007;20(8):934–40.
42. Tamborini G, Muratori M, Maltagliati A, et al. Pre-operative transthoracic real-time three-dimensional echocardiography in patients undergoing mitral valve repair: accuracy in cases with simple vs. complex prolapse lesions. Eur J Echocardiogr. 2010;11(9):778–85.
43. Teeter EG, Dakik C, Cooter M, et al. Assessment of paravalvular leak after transcatheter aortic valve replacement: transesophageal echocardiography compared with transthoracic echocardiography. J Cardiothorac Vasc Anesth. 2017;31(4):1278–84.
44. Afonso L, Kottam A, Reddy V, Penumetcha A. Echocardiography in infective endocarditis: state of the art. Curr Cardiol Rep. 2017;19(12):127.
45. Jassal DS, Aminbakhsh A, Fang T, et al. Diagnostic value of harmonic transthoracic echocardiography in native valve infective endocarditis: comparison with transesophageal echocardiography. Cardiovasc Ultrasound. 2007;5:20.
46. Chirillo F, Pedrocco A, De Leo A, et al. Impact of harmonic imaging on transthoracic echocardiographic identification of infective endocarditis and its complications. Heart. 2005;91(3):329–33.
47. Khan GN, Dairywala IT, Liu Z, Li P, Carroll J, Vannan MA. Three-dimensional echocardiography of left atrial appendage thrombus. Echocardiography. 2001;18(2):163–6.
48. Omran H, Jung W, Rabahieh R, et al. Imaging of thrombi and assessment of left atrial appendage function: a prospective study comparing transthoracic and transoesophageal echocardiography. Heart. 1999;81(2):192–8.
49. Doukky R, Khandelwal A, Garcia-Sayan E, Gage H. External validation of a novel transthoracic echocardiographic tool in predicting left atrial appendage thrombus formation in patients with nonvalvular atrial fibrillation. Eur Heart J Cardiovasc Imaging. 2013;14(9):876–81.
50. Varghese R, Itagaki S, Anyanwu AC, Trigo P, Fischer G, Adams DH. Predicting systolic anterior motion after mitral valve reconstruction: using intraoperative transoesophageal echocardiography to identify those at greatest risk. Eur J Cardiothorac Surg. 2014;45(1):132–7.. discussion 137-138

51. Mercado P, Maizel J, Beyls C, et al. Transthoracic echocardiography: an accurate and precise method for estimating cardiac output in the critically ill patient. Crit Care. 2017;21(1):136.
52. Jozwiak M, Monnet X, Teboul JL. Monitoring: from cardiac output monitoring to echocardiography. Curr Opin Crit Care. 2015;21(5):395–401.
53. Cecconi M, De Backer D, Antonelli M, et al. Consensus on circulatory shock and hemodynamic monitoring. Task force of the European Society of Intensive Care Medicine. Intensive Care Med. 2014;40(12):1795–815.
54. Drake SA, Wolf DA, Meininger JC, et al. Methodology to reliably measure preventable trauma death rate. Trauma Surg Acute Care Open. 2017;2(1):e000106.
55. Feissel M, Michard F, Faller JP, Teboul JL. The respiratory variation in inferior vena cava diameter as a guide to fluid therapy. Intensive Care Med. 2004;30(9):1834–7.
56. Nagdev AD, Merchant RC, Tirado-Gonzalez A, Sisson CA, Murphy MC. Emergency department bedside ultrasonographic measurement of the caval index for noninvasive determination of low central venous pressure. Ann Emerg Med. 2010;55(3):290–5.
57. Dipti A, Soucy Z, Surana A, Chandra S. Role of inferior vena cava diameter in assessment of volume status: a meta-analysis. Am J Emerg Med. 2012;30(8):1414–1419.e1411.
58. Fields JM, Lee PA, Jenq KY, Mark DG, Panebianco NL, Dean AJ. The interrater reliability of inferior vena cava ultrasound by bedside clinician sonographers in emergency department patients. Acad Emerg Med. 2011;18(1):98–101.
59. Sefidbakht S, Assadsangabi R, Abbasi HR, Nabavizadeh A. Sonographic measurement of the inferior vena cava as a predictor of shock in trauma patients. Emerg Radiol. 2007;14(3):181–5.
60. Akilli B, Bayir A, Kara F, Ak A, Cander B. Inferior vena cava diameter as a marker of early hemorrhagic shock: a comparative study. Ulus Travma Acil Cerrahi Derg. 2010;16(2):113–8.
61. Levy BI, Payen DM, Tedgui A, Xhaard M, McIlroy MB. Noninvasive ultrasonic cardiac output measurement in intensive care unit. Ultrasound Med Biol. 1985;11(6):841–9.
62. Tribouilloy C, Slama M, Shen WF, et al. Determination of left ventricular inflow by pulsed Doppler echocardiography: influence of mitral orifice area and blood velocity measurements. Eur Heart J. 1991;12(1):39–43.
63. Dericbourg C, Tribouilloy C, Kugener H, Avinee P, Rey JL, Lesbre JP. Noninvasive measurement of cardiac output by pulsed Doppler echocardiography. Correlation with thermodilution. Arch Mal Coeur Vaiss. 1990;83(2):237–44.
64. McLean AS, Needham A, Stewart D, Parkin R. Estimation of cardiac output by noninvasive echocardiographic techniques in the critically ill subject. Anaesth Intensive Care. 1997;25(3):250–4.
65. Malik SB, Chen N, Parker RA, Hsu JY. Transthoracic echocardiography: pitfalls and limitations as delineated at cardiac CT and MR imaging. Radiographics. 2017;37(2):383–406.
66. Kim MJ, Jung HO. Anatomic variants mimicking pathology on echocardiography: differential diagnosis. J Cardiovasc Ultrasound. 2013;21(3):103–12.
67. George A, Parameswaran A, Nekkanti R, Lurito K, Movahed A. Normal anatomic variants on transthoracic echocardiogram. Echocardiography. 2009;26(9):1109–17.

Ultrasound for Chest: Lung and Pleural Examination and Diagnosis

You Shang, Xiaojing Zou, and Hong Wang

1 Probe Types

Commonly used ultrasound probes can be divided into two major classes: High frequency linear and low frequency probes.A high frequency linear probe uses frequencies ranging from 9 to 12 MHz. This type of probe has the advantage of high resolution for shallow structures. It is suitable for examining the thoracic wall and pleura, and can display more detailed images of superficial structures, although the resolution decreases for deeper structures. Such probes are quite reliable and provide high specificity and sensitivity for ruling out pneumothorax.

A low frequency probe uses frequencies ranging from 1 to 5 MHz. Due to their reduced signal attenuation, they are suitable for examining deeper structures, such as the lung parenchyma. Typical low frequency probes include curvilinear, microconvex or phased array (Fig. 1).

2 Image Acquisition

Correct patient positioning, probe manipulation, and location of the examination points are essential for obtaining high quality ultrasound images.

2.1 Patient Positions

Correct positioning is necessary for obtaining high resolution ultrasound images. For lung examination, the patient can be in a supine, semi-recumbent, lateral, prone, or erect position. Certain positions will increase the sensitivity of detecting different pathology. For example, the semi-recumbent position is better than the supine position for ruling out apical pneumothorax, and the right lateral position is better than the supine position for ruling out right sided pleural effusion.

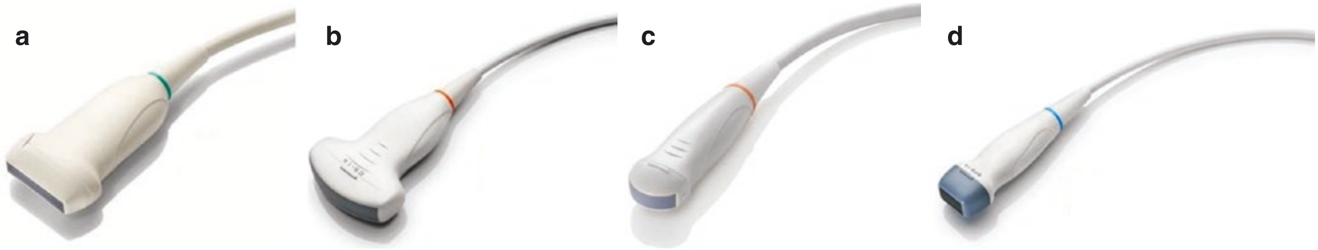

Fig. 1 Probes. (**a**) High frequency linear probe; (**b**) Low frequency curvilinear; (**c**) Microconvex; (**d**) Phased array (Courtesy of Mindray China)

Y. Shang · X. Zou
Institute of Anesthesiology and Critical Care Medicine, Union Hospital, Tongji Medical College, Huazhong University of Science and Technology, Wuhan, China

H. Wang (✉)
Department of Anesthesiology, West Virginia University, Morgantown, WV, USA
e-mail: Hong.wang1@wvumedicine.org

© Springer Nature Switzerland AG 2021

J. Li et al. (eds.), *Ultrasound Fundamentals*, https://doi.org/10.1007/978-3-030-46839-2_20

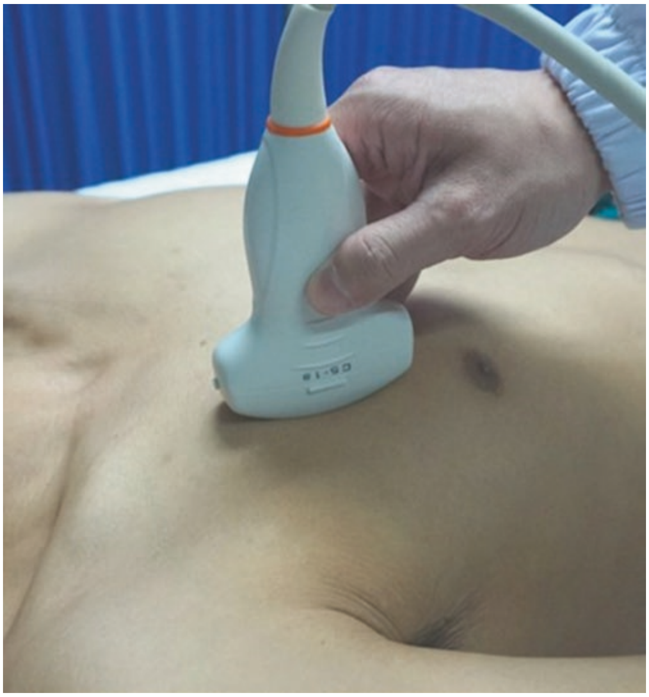

Fig. 2 Probe manipulations

2.2 Probe Manipulation

For steady and flexible handling, the probe should be held like a pen with the thumb and index finger. The remaining fingers spread out on the patient's skin to maintain stability. The center of the probe must be placed within rib interspaces and be oriented perpendicular to the chest wall (Fig. 2).

Every probe has a marker on one side that corresponds to the screen marker for orientation. The probe marker should be directed to the patient's head. In this view, the area to the left of the diaphragm indicates the thoracic cavity and the area to the right of the diaphragm represents the abdominal cavity.

2.3 Examination Points

There are several protocols of lung ultrasound examination. The BLUE protocol [1] includes a total of eight areas over the entire thorax. Following the BLUE protocol, an experienced ultrasound examiner can achieve a diagnostic accuracy of respiratory failure of over 90%.

The upper BLUE point (Fig. 3a) and lower BLUE point (Fig. 3b) are in the front of the chest, while the phrenic point (Fig. 3c) and the posterolateral alveolar pleural syndrome (PLAPS) point (Fig. 3d) are on the side of the chest. The PLAPS point is at the intersection of the posterior axillary line and the transverse phrenic line, and reveals over 90% of pleural effusions and alveolar consolidations [1]. To increase the sensitivity of diagnoses, examinations for pleural effusions should occur in the dependent areas such as the PLAPS point, while examinations for pneumothoraces should occur in the nondependent areas.

3 Normal Lines and Signs

Artifacts surrounding the pleural line provide important information during chest ultrasound examination.

3.1 Pleural Line

The pleural line is a horizontal hyperechoic line, appearing about 0.5 cm below the rib line (Fig. 4).

3.2 A-Line

A-lines are hyperechoic artifacts that are horizontal in orientation. A-lines repeat at regular intervals and are visible deeper to the pleural line (Fig. 4). During an ultrasound examination, the emitted ultrasound beam is reflected by the pleural membrane and bounced back to the transducer, which is then reflected again from the transducer back to the pleural membrane. These back-and-forth signals result in this regularly spaced artifact. The presence of A-lines can indicate normal lung tissue, chronic obstructive pulmonary disease (COPD), asthma, pulmonary emboli, or pneumothoraces.

3.3 Bat Sign

Identification of the bat sign is a basic step in any lung ultrasound, which is used to correctly locate the pleural line. The upper and lower ribs form the wings of the bat sign; and the pleural line forms the belly of the bat (Fig. 5). To ensure a clearly distinguishable bat sign, the transducer should be positioned perpendicular to the pleural surface [2].

3.4 Lung Sliding

Lung sliding is a visible dynamic movement of the pleural line observed in normal lungs. It arises from the pleural line and represents the free movement of the visceral pleura against the parietal pleura during respiratory cycles. Absence of lung sliding is caused by lung volume loss (e.g., pneumothorax, atelectasis, or pneumonectomy) or pleural adhesions (e.g., chemical pleurodesis, inflammation, or fibrotic lung diseases) [3].

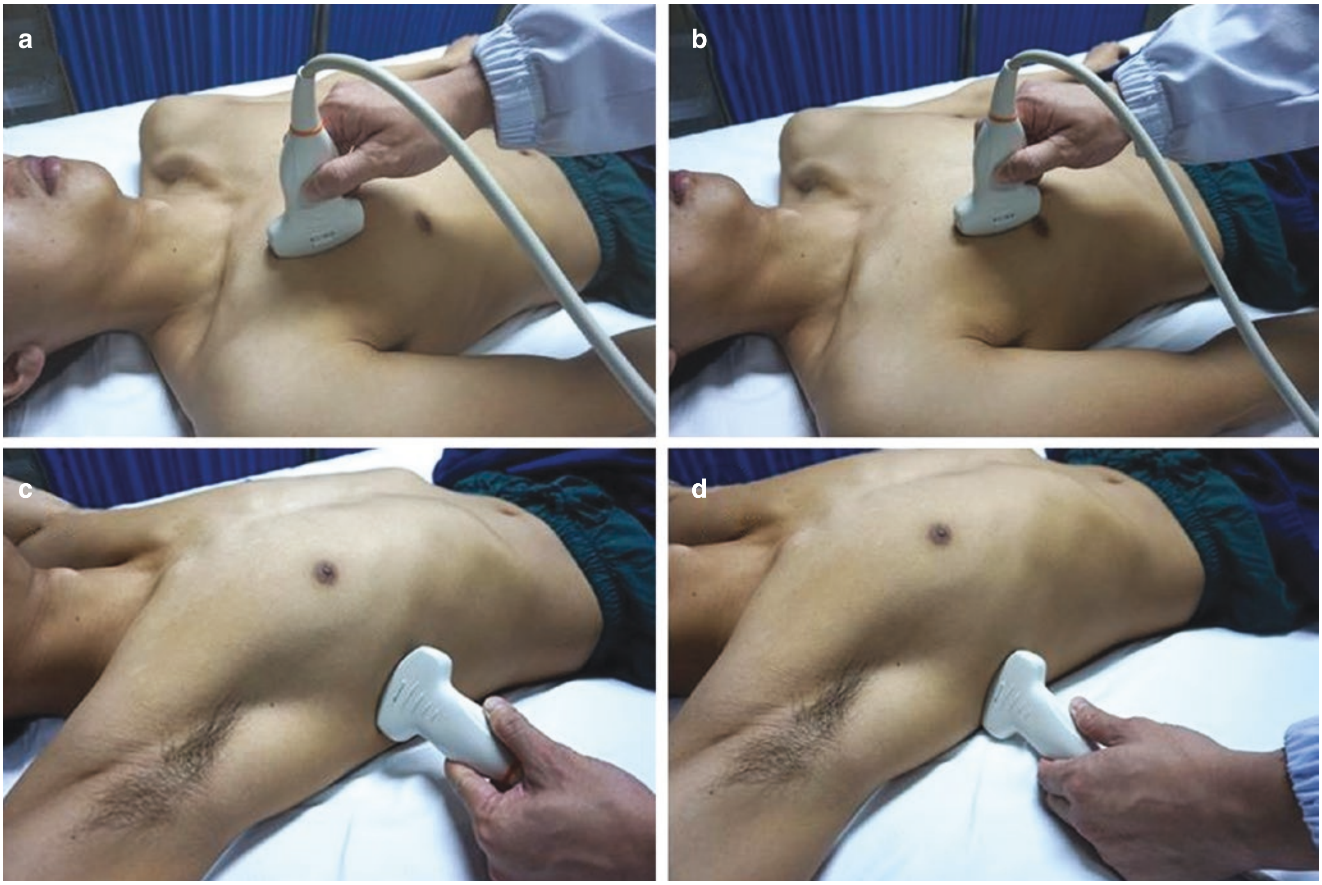

Fig. 3 Examination Points. (**a**) Upper blue point; (**b**) Lower blue point; (**c**) Phrenic point; (**d**) PLAPS point

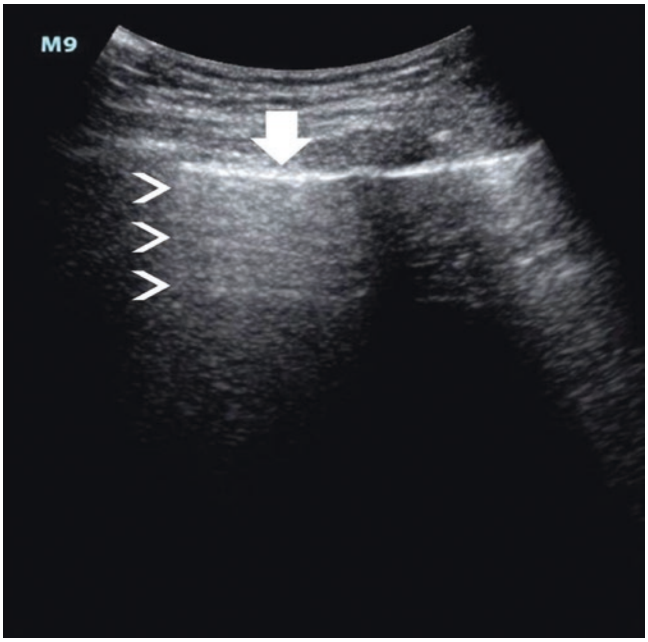

Fig. 4 Pleural line and A lines. White arrow indicates the pleural line; Arrowheads indicate A lines

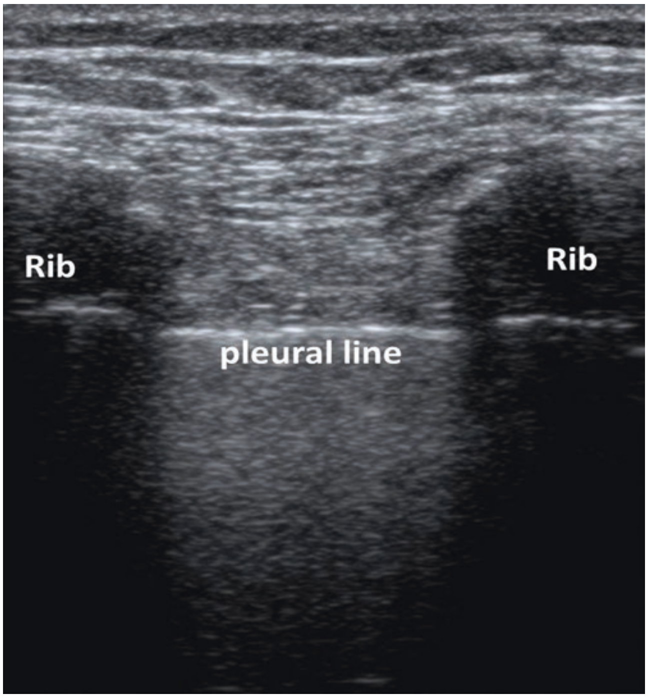

Fig. 5 Bat sign

3.5 Seashore Sign

Lung sliding in the M-mode will appear as a “seashore sign” (Figs. 6 and 8a). Over the pleural line, a “seashore sign” displays a stratified pattern and indicates a motionless chest wall. Below the pleural line, it is a homogeneous granular pattern indicating a normal aeration and motion of lung [4].

4 Pathological Lines and Signs

4.1 B-Line

B-lines arise at the pleural line. They are vertical and hyperechoic. They are also called comet-tail artifacts. B-lines move in concert with lung sliding and extend to the far field without fading. B-lines often erase A-lines (Fig. 7). Multiple B-lines (more than 3 in each field) appear when fluid begins to widen the interlobular septa. Diffuse B lines represent alveolar edema. The presence of B-lines can rule out pneumothorax completely [5]. In normal patients, B-lines can be seen only at the lower lung exam point (the PLAPS point) due to gravity dependent edema.

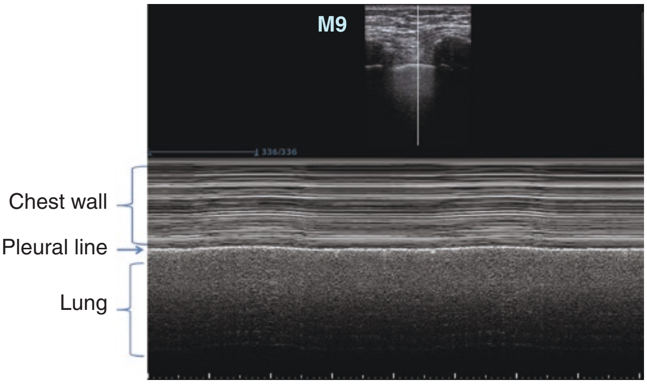

Fig. 6 Seashore sign

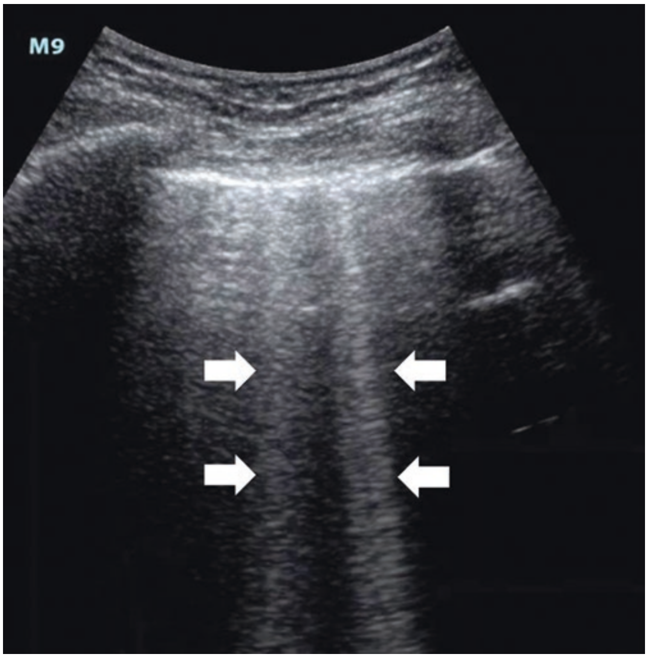

Fig. 7 B lines. Arrows indicate B lines

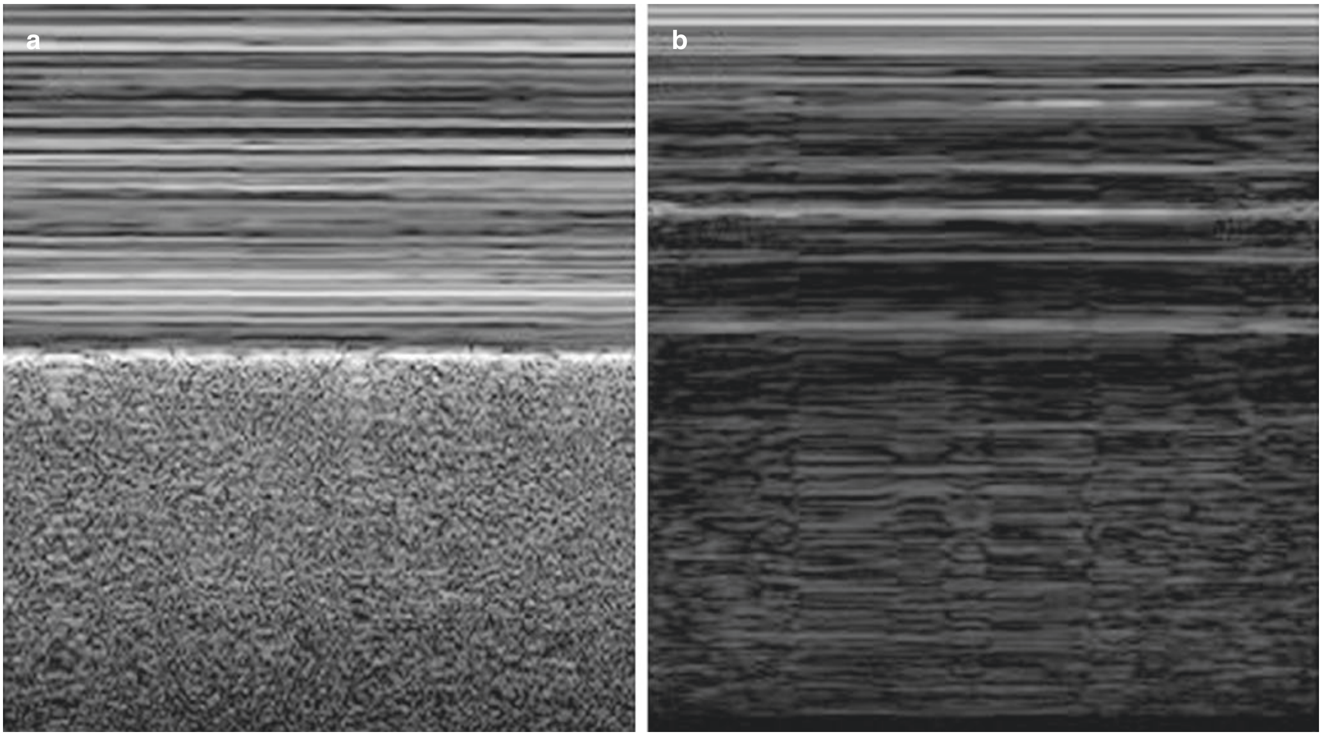

Fig. 8 Seashore sign (**a**) and Stratosphere sign (**b**)

4.2 Stratosphere Sign

The stratosphere sign is also called the "barcode sign". In the M-mode, the image shows parallel horizontal lines below and above the pleural line, indicating absence of lung sliding (Fig. 8b). Pneumothorax will show the stratosphere sign. Other conditions that impede normal lung movement can also cause the stratosphere sign. These include pneumonia, atelectasis, apnea, severe acute obstructive lung disease, and previous pleurodesis.

4.3 Pleural Effusion

Because sound waves can propagate through most fluids easily, the sonographic signs of a pleural effusion manifests as a dependent dark zone between the parietal and visceral pleura. This dark zone allows for visualization of the bright pleural lining around atelectatic lung tissue (Fig. 9) [6].

4.4 Quad and Sinusoid Sign

The quad sign consists of four borders: the pleural line (upper border), the lung line representing the visceral pleura (lower border), and two rib shadows. The quad sign indicated the presence of a pleural effusion (Fig. 10). In the M-mode, the appearance of visceral pleura movement is shown like a sinusoid waveform. This sign confirms free fluid collection [7].

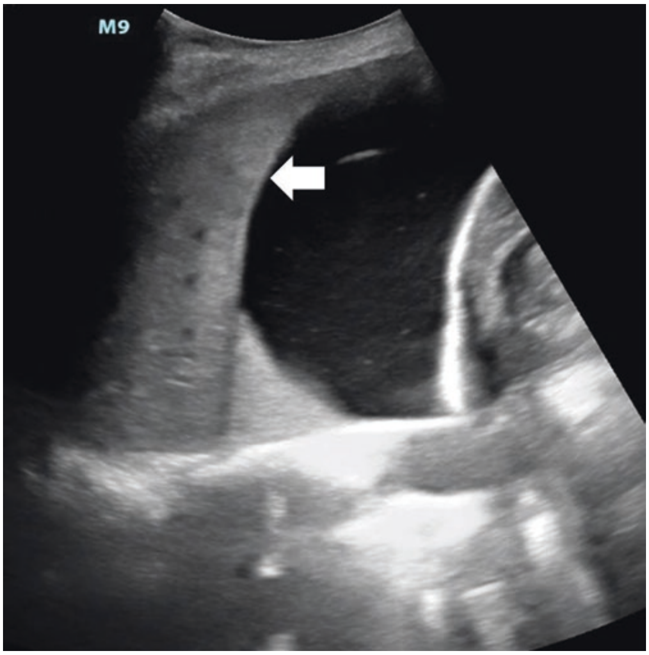

Fig. 9 Pleural Effusion with atelectatic lung tissue. Arrow indicates atelectatic lung tissue caused by pleural effusion

4.5 Lung Pulse

The lung pulse and lack of lung sliding indicate complete atelectasis. Lung pulse is due to the transmission of heartbeats to the adjacent lung. In the M-mode, ultrasound images demonstrate subtle pulses of the parietal pleura in concert with cardiac beats (Fig. 11). The lung pulse cannot be detected by ultrasound when visceral and parietal pleurae are separated by air (e.g., pneumothorax) or the lung is overinflated. The presence of a lung pulse can rule out a pneumothorax [8].

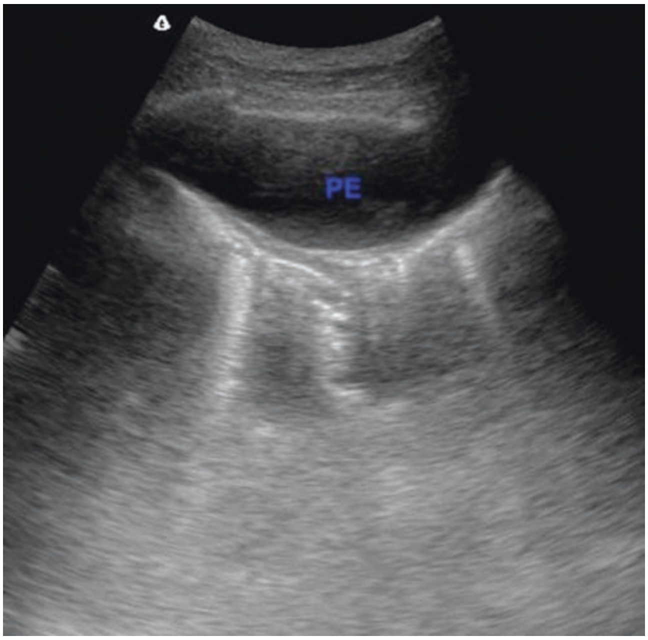

Fig. 10 Quad sign. PE indicates Pleural Effusion

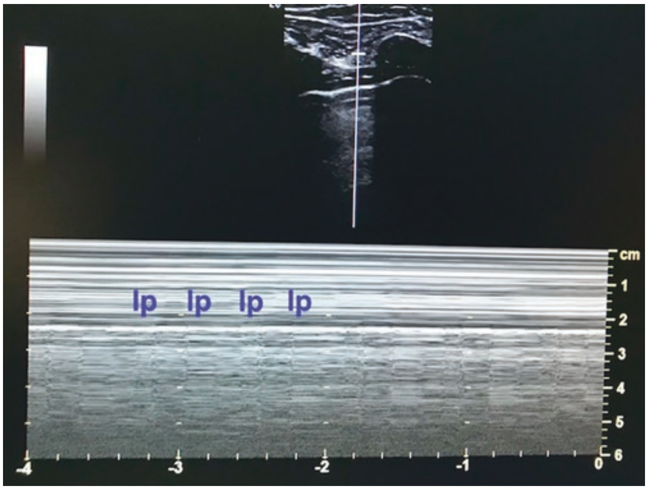

Fig. 11 Lung pulse. lp indicates lung pulse

5 Normal and Pathological Indicators

5.1 Normal Lung

A normal lung consists of lung sliding, A-lines and absence of pleural effusion. Lung sliding plus A-lines constitute the A-profile indicating a “dry” lung, which can promptly rule out pulmonary edema, pneumonia, and pneumothorax. However, the A-profile also appears in COPD, asthma, and the presence of a pulmonary embolism. In 30 percent of patients with normal lungs, isolated B-lines can be found in dependent lung regions.

5.2 Pneumothorax

In a patient with pneumothorax, air accumulates between visceral and parietal pleural layers. As a consequence, lung sliding signs and vertical B-lines are abolished. In the M-Mode, the stratosphere sign replaces the seashore sign. The presence of B-lines can rule out pneumothorax with 100% specificity [9, 10]. The absence of lung sliding, B-lines and lung pulse, as well as presence of lung point are signs of a pneumothorax.

Lung point is the transition point between the seashore and stratosphere signs on M mode, where lung sliding suddenly disappeared. Lung point indicates the border of the pneumothorax (Fig. 12). Lung point is 100% specific in diagnosing pneumothorax, but less common [11, 12]. Extensive pneumothorax can produce a lung point very posteriorly, or it may not produce one at all due to the compression of the majority of the lung.

Absence of lung sliding also appears in some other circumstances, such as pleural adherences, bullous emphysema, and chronic obstructive pulmonary disease.

5.3 Atelectasis

Atelectasis can result from a pleural effusion (Fig. 11), bronchial obstruction (resorptive atelectasis) or main stem intubation.

Sonographic findings of atelectasis reveal disappearance of lung sliding, and presence of lung pulse (transmission of heartbeat to the pleural line) [13].

Static air bronchograms, hyperechoic punctiform particles without any change during the respiratory cycle and air bubbles trapped and isolated from the whole respiratory cycle, can be seen with most resorptive atelectases and pneumonia [14].

Dynamic air bronchograms effectively rule out atelectasis with a sensitivity of 64.0% and specificity of 94.0%. They are a sign of pulmonary consolidation [15].

5.4 Alveolar-Interstitial Syndrome

Due to aggregation of extravascular water, diffuse alveolar edema and thickened interlobular septa can become visible during lung ultrasound. It manifests as multiple ‘B-lines’ or ‘comet tails’ arising from the pleural line, extending to the edge of the screen, and separated from each other by a distance of approximately 7 mm or less (Fig. 13) [16].

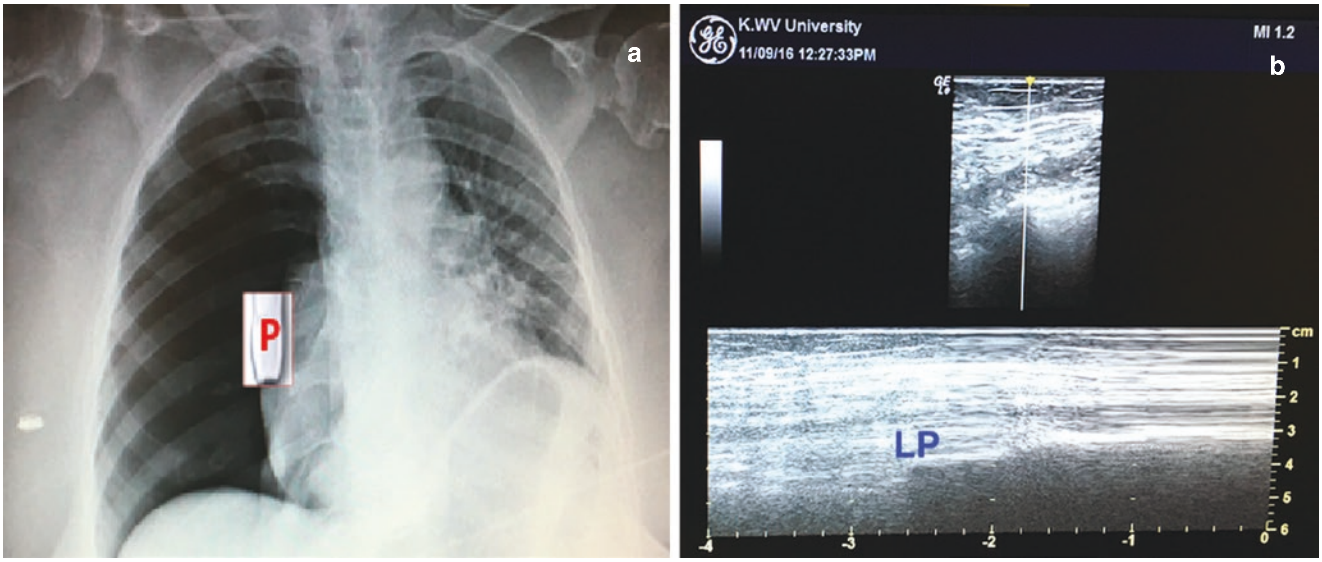

Fig. 12 Pneumothorax and Lung Point. P indicates probe position, LP indicates Lung Point

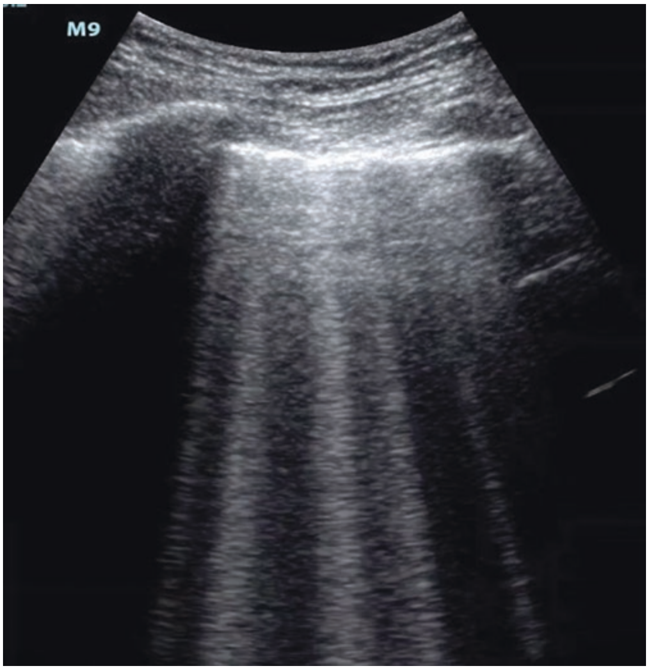

Fig. 13 Alveolar-interstitial syndrome

5.5 Pneumonia

Inflammation of the lung tissue can generate exudates. Exudates can enlarge the interstitial tissue, fill the alveoli, cross the visceral pleura, and invade the pleural cavity. Therefore, pneumonia can be classified as a fluid disorder. When interstitial fluid accumulates, multiple B-lines appear in the rib interspaces focally and asymmetrically, suggesting pneumonia [16]. The fluid-filled alveoli result in tissue-like patterns of lung consolidation without volume loss (Fig. 14). Consolidation is another marker of pneumonia can be found anywhere in the thoracic cavity. Consolidation of anterior chest due to bronchial dissemination is the most specific sign of pneumonia. Consolidation found at the PLAPS point is the most common sign. In some severe cases of pneumonia, the pleural surface is thickened and ragged.

Other sings of pneumonia include the shred sign (Fig. 15), dynamic air bronchograms, the absence of lung sliding and the presence of pleural effusions. The shred sign consists of a small juxtapleural consolidation that is visualized at the interface between poorly aerated alveoli and airless or fluid-filled alveoli [17].

Dynamic air bronchograms appear as mobile, hyper-echoic, punctiform areas corresponding to patent airways and air bubbles trapped within the bronchi that move with respirations. It is present in 90% of pneumonia [18, 19].

Lung sliding is impaired when exudate, acting as a biologic glue, adheres the lung to the chest wall. When the exudate is massive, there is often concomitant pleural effusion [20, 21].

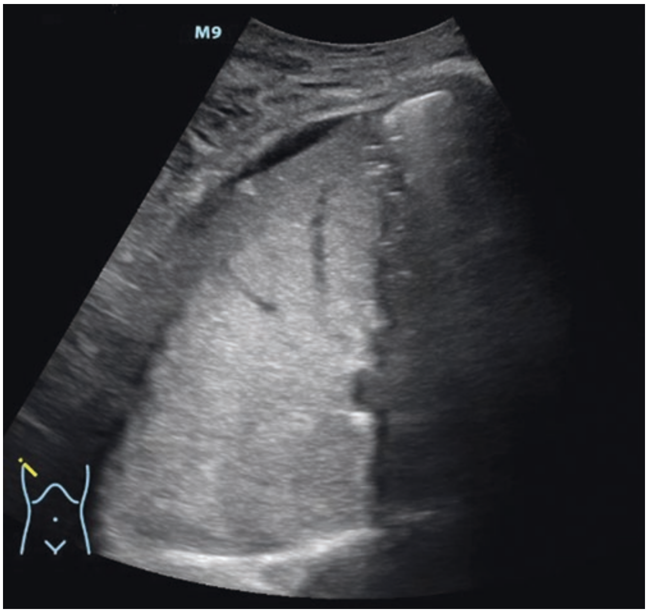

Fig. 14 Consolidation pattern without volume loss

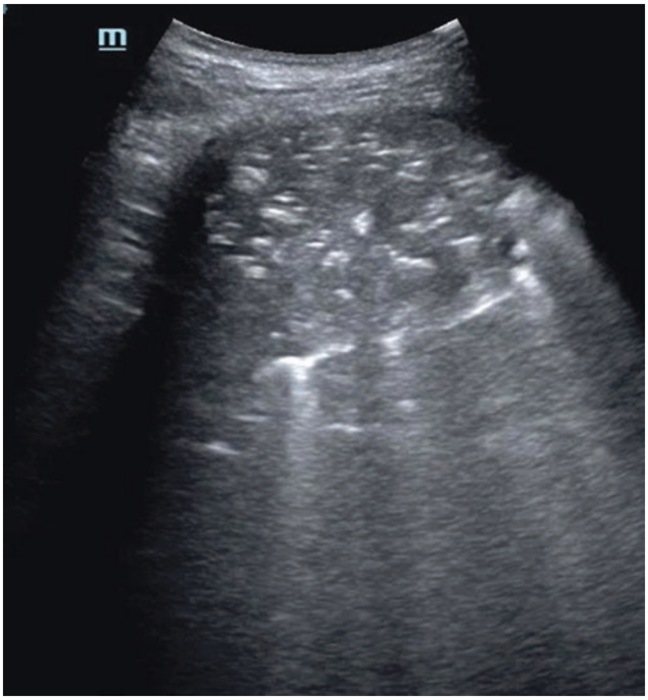

Fig. 15 The shred sign is suggestive of pneumonia

6 Conclusion

Lung ultrasound is a powerful bedside tool. It can help to timely diagnose various pulmonary pathologies. Due to its utility as a diagnostic tool, ease of use, and portability, lung ultrasound examination can be seamlessly integrated into the chest physical examination.

References

1. Lichtenstein DA, Mezière GA. Relevance of lung ultrasound in the diagnosis of acute respiratory failure: the BLUE protocol. Chest. 2008;134:117–25.
2. Lichtenstein DA, Lascols N, Mezière G, et al. Ultrasound diagnosis of alveolar consolidation in the critically ill. Intensive Care Med. 2004;30:276–81.
3. Volpicelli G, Elbarbary M, Blaivas M, et al. International liaison committee on lung ultrasound (ILC-LUS) for international consensus conference on lung ultrasound (ICC-LUS). International evidence-based recommendations for point-of-care lung ultrasound. Intensive Care Med. 2012;38(4):577–91.
4. Volpicelli G. Sonographic diagnosis of pneumothorax. Intensive Care Med. 2011;37:224–32.
5. Turner JP, Dankoff J. Thoracic ultrasound. Emerg Med Clin North Am. 2012;30:451–73.
6. Lichtenstein DA, Meziere G, Lascols N, et al. Ultrasound diagnosis of occult pneumothorax. Crit Care Med. 2005;33:1231–8.
7. Lichtenstein D. Lung ultrasound in the critically ill. Curr Opin Crit Care. 2014 Jun;20(3):315–22.
8. Prina E, Torres A, Carvalho CR. Lung ultrasound in the evaluation of pleural effusion. J Bras Pneumol. 2014;40(1):1–5.
9. Lichtenstein D, Hulot JS, Rabiller A, et al. Feasibility and safety of ultrasound-aided thoracentesis in mechanically ventilated patients. Intensive Care Med. 1999;25:955–8.
10. Lichtenstein DA, Lascols N, Prin S, et al. The “lung pulse”: an early ultrasound sign of complete atelectasis. Intensive Care Med. 2003;29(12):2187–92.
11. Espigares López MI, Meléndez Leal E, Pernia Romero A, Torres Morera LM. Pneumothorax: immediate ultrasound diagnosis in the critical patient. Rev Esp Anestesiol Reanim. 2018;65(9):541–2.
12. Lichtenstein DA, Meziere GA. Relevance of lung ultrasound in the diagnosis of acute respiratory failure: the BLUE protocol. Chest. 2008;134:117–25.
13. Lichtenstein D, Meziere G, Biderman P, et al. The “lung point”: an ultrasound sign specific to pneumothorax. Intensive Care Med. 2000;26:1434–40.
14. Parab SY, Solanki SL. Lung point and power slide signs help to improve the accuracy of lung ultrasound to diagnosepneumothorax. Saudi J Anaesth. 2017;11(1):121–2.
15. Lichtenstein D, Lascols N, Prin S, et al. The lung pulse, an early ultrasound sign of complete atelectasis. Intensive Care Med. 2003;29:2187–92.
16. Blaivas M. Lung ultrasound in evaluation of pneumonia. J Ultrasound Med. 2012;31(6):823–6.
17. Lichtenstein D, Meziere G, Seitz J. The dynamic air bronchogram. A lung ultrasound sign of alveolar consolidation ruling out atelectasis. Chest. 2009;135:1421–5.
18. Lichtenstein D, Goldstein I, Mourgeon E, et al. Lung ultrasound for critically ill patients. Am J Respir Crit Care Med. 2019;199(6):701–14.
19. Lichtenstein D, Goldstein I, Mourgeon E, Cluzel P, Grenier P, Rouby JJ. Comparative diagnostic performances of auscultation, chest radiography, and lung ultrasonography in acute respiratory distress syndrome. Anesthesiology. 2004;100:9–15.
20. Lichtenstein D, Mezière G, Seitz J. The dynamic air bronchogram. A lung ultrasound sign of alveolar consolidation ruling out atelectasis. Chest. 2009;135(6):1421–5.
21. Cortellaro F, Colombo S, Coen D, et al. Lung ultrasound is an accurate diagnostic tool for the diagnosis of pneumonia in the emergency department. Emerg Med J. 2012;29(1):19–23.

Ultrasound-Guided Nerve Blocks for Chest

Kaitlin Crane, Ibrahim N. Ibrahim, Elliott Thompson,
Monica W. Harbell, Elyse M. Cornett,
and Alan David Kaye

1 Introduction

The development of ultrasound-guided chest nerve blocks has involved a series of innovative techniques that aim to provide sufficient operative and postoperative analgesia with decreased risks and side effects for patients. Analgesia for chest wall procedures and surgeries has conventionally involved a multimodal approach including non-steroidal anti-inflammatory drugs (NSAIDS), opioids, ketamine, and acetaminophen, with or without local anesthetic infiltration. Many procedures such as intercostal drains placed following coronary artery bypass grafting or a thoracotomy can be excruciatingly painful and distressing for the patient. In most cases, multimodal approach has provided some, but not sufficient, pain relief for patients undergoing procedures involving the thorax and chest wall.

Pectoralis nerve (Pecs) and serratus plane blocks are the latest ultrasound-guided regional anesthesia techniques of the thorax and chest wall. These procedures utilize sonography to identify the various anatomical structures within the thoracic and axillary regions that act as landmarks for different compartments and nerve routes. The Pecs procedures were invented by the anesthesiologist Dr. Rafael Blanco, who described it in a 2011 letter to the editor. For the Pecs type I block, a linear array ultrasound probe is used to identify the pectoralis major and minor muscles before a long-acting local anesthetic is injected into the fascia between the two muscles. This nerve block involves the lateral pectoral nerve and the medial pectoral nerve. The Pecs type I block is effective for breast expander placement during reconstructive breast cancer surgery and subperctoral prosthesis, but does not provide analgesia for procedures that involve the axilla including axillary dissection and radical mastectomy [1]. The Pecs type II block divides the dose of local anesthetic in order to infiltrate two fascial compartments. One injection is placed between the pectoral major and minor muscles and the other is placed between the pectoralis minor and serratus anterior muscles. This technique provides anesthetic coverage to both the pectoral compartment including the pectoral nerves and to the axilla compartment including intercostal nerves. The serratus anterior plane block was later discovered as a more lateral approach than the Pecs I and II blocks. One of two methods is used to identify and inject the compartment between the serratus anterior and latissimus dorsi muscles which includes the intercostobrachialis nerves, long thoracic nerve, and thoracodorsal nerve [2].

In the past, thoracic epidural analgesia (TEA) or paravertebral blocks (PVB) have been used for extensive upper abdominal procedures [1]. TEA has long been considered to be the "gold standard" of providing acute pain management following thoracic and upper abdominal surgeries. However, it has been associated with many increased risks, including neurologic injury to the spinal cord from hemorrhagic and infectious etiologies. This technique usually involves catheter placement and infusion of a local anesthetic combined with epidural opioids using needle puncture guided by anatomic landmarks [3]. PVB is an

K. Crane · I. N. Ibrahim · E. Thompson · E. M. Cornett (✉)
Department of Anesthesiology, LSU Health Shreveport,
Shreveport, LA, USA
e-mail: kcran1@lsuhsc.edu; iibra1@lsuhsc.edu;
etho18@lsuhsc.edu; ecorne@lsuhsc.edu

M. W. Harbell
Department of Anesthesiology and Perioperative Medicine,
Mayo Clinic Arizona, Phoenix, AZ, USA
e-mail: harbell.monica@mayo.edu

A. D. Kaye
Departments of Anesthesiology and Pharmacology, Toxicology,
and Neurosciences, Lousiana State University Health Sciences
Center, Shreveport, LA, USA

Department of Anesthesiology, Department of Pharmacology
Louisiana State University School of Medicine, Louisiana State
University Health Sciences Center, New Orleans, LA, USA
e-mail: akaye@lsuhsc.edu

© Springer Nature Switzerland AG 2021
J. Li et al. (eds.), *Ultrasound Fundamentals*, https://doi.org/10.1007/978-3-030-46839-2_21

ultrasound-guided technique where the spinal nerves are blocked as they emerge from the intervertebral foramen by injecting anesthetic into the space adjacent to the vertebrae. This method has comparable pain relief to TEA while allowing for unilateral analgesia, often resulting in less adverse effects making it a popular alternative to TEA procedures [4]. What makes TEA and PVB techniques impractical for most chest wall surgeries, however, is the high number of complications that result in increased hospital stay for day surgery patients [5].

Overall, chest wall blocks have demonstrated more advantages and fewer disadvantages when compared to a multimodal approach, TEA, and PVBs, See Table 1. Chest wall blocks have provided an increased duration of analgesia, reduced postoperative morphine consumption, decreased side effects and complications, and increased patient satisfaction. These procedures have been innovative in allowing patients to be properly treated with analgesia for procedures and operations which only require a one-day stay in the hospital. They have few contraindications and little restrictions with regards to a patient's daily medications, including anticoagulants. Chest blocks have also essentially eliminated the risk of posterior midline anesthetic spread and subsequent hypotension. In this chapter, therefore, we discuss the details of chest wall blocks, anatomy or the pectoral and axillary regions, thoracic wall blocks, analgesic potential of pecs blocks and clinical applications of pecs block.

2 Anatomy of Pectoral and Axillary Regions

2.1 Skin

The skin over the chest wall consists of a thin outer layer (1—3 mm). The main anterior landmarks of the chest are the nipple and sternal notch [7]. Along the sternum marks the mid-sternal line which is located from the sternal notch down to the xiphoid process and extends through the linea alba to the umbilicus. The lateral sternal line can help identify the internal thoracic artery because it runs along the inside of the chest wall and is lateral to the lateral sternal line. The mid-clavicular line is drawn through the middle of the clavicle and this anatomic landmark runs medial to the nipple and areola [8]. See Fig. 1.

2.2 Subcutaneous Fat Forms

These structures are a lipid coat of varying thickness which line the entirety of the chest. In comparison to muscle, it is hypoechoic on ultrasound and is made of lobules separated by bands of connective tissue. These structures are highly malleability and very clearly visible when the tissues are compressed with a transducer [7].

Table 1 The primary uses, advantages, and disadvantages of various analgesic techniques for procedures involving the chest wall and thorax

Technique	Use	Advantages	Disadvantages
Multimodal approach	Acute pain control	No operative risks	High side effect profile (Nausea, vomitting, respiratory depression, urinary retention, constipation) Limited pain relief and patient satisfaction
TEA	Acute pain after thoracic surgery, abdominal surgery, and rib fractures	Superior perioperative analgesia compared to parental opioids	Bilateral analgesia only
		Less side effects than parental opioids	High side effect profile (Nausea, vomitting, respiratory depression, urinary retention, constipation)
		Single injection	Risks/Complications: unsuccessful catheter placement, dural puncture, postoperative radicular pain, peripheral nerve lesions, pleural puncture, pneumothorax, and rarely hemorrhagic and infectious complications
			Not appropriate/cost effective for day surgery operations
			Use of anatomical landmarks with no sonographic assistance
			Restrictions on the use on anticoagulants
PVB	Perioperative and postoperative analgesia for surgical procedures of chest wall, thorn, and abdomen	Comparable analgesia to TEA procedure	Not appropriate/cost effective for day surgery operations
		Ulilateral analgesia option	Risks/Complications: hypotension, epidural spread of local anesthetic, brachial plexus spread, pleural puncture, pneumothorax, vascular puncture, bleeding, infection, nerve injury
		Performed with use of anatomic landmarks or ultrasound guidance	Restrictions on the use on anticoagulants

Table 1 (continued)

Technique	Use	Advantages	Disadvantages
		Single or multiple one time injections	
		Less side effects than TEA	
		Fewer incidents of pneumothorax, total spinal anesthesia, and vascular injury	
Chest wall blocks:	Perioperative and postoperative analgesia for surgical procedures of chest wall and thorax:	Increased duration of analgesia	Absolute need for linear ultrasound probe
(A) Pecs I	(A) Breast surgeries, chest tubes, pacemaker implantation	Reduced postoperative morphine consumption	Risk of nerve injury, vascular injury, pleural puncture, pneumothorax, local anesthetic toxicity, upper limb fistula
(B) Pecs II	(B) Radical mastectomies, axillary clearance	Decreased side effects of nausea, vomiting, respiratory depression, urinary retention, and constipation	Relatively limited data reports on effectiveness/outcomes of chest wall blocks
(C) Serratus Anterior	(C) LD flaps, intercostal drains	Unilateral analgesia possible	
		Axillary region analgesia possible	
		Lower visual analog pain scores and increased patient satisfaction	
		Few complications reported in literature	
		Appropriate and cost effective for day care procedures	
		Eliminates risk of posterior midline spread and subsequent hypotension	
		Less restrictions on the use on anticoagulants	
		Few contraindications	

Adapted from Refs. [1, 3, 4, 6]

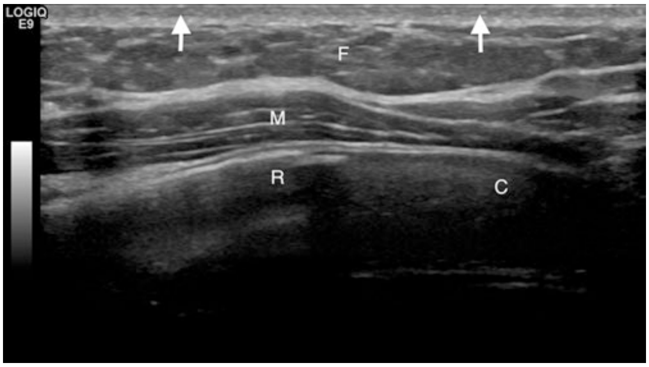

Fig. 1 Transverse section of the chest wall, showing its anatomy: F—subcutaneous fat, M – muscle, R—rib, C—cartilage, arrows—the skin

2.3 Muscle

The third layer of the chest is comprised of a complex set of muscles with variable features. The anatomy of these muscles does not differ in appearance of striated muscles in other anatomical regions. Some of the muscles have insertion in the form of a tendon [7]. The superficial muscles of the chest wall are the pectoralis major, the pectoralis minor, the subclavius and the serratus anterior. The pectoralis major muscle begins at the medial clavicle and lateral sternum and inserts on the humerus at the lateral lip of the bicipital groove. The major action of the pectoralis major is felxion, adduction, and medial rotation of the arm [9]. The pectorals minor begins near the costal cartilages at the third to fifth ribs and inserts on scapula at the medial border and superior surface of the coracoid process [9]. The serratus anterior runs along the anterolateral chest wall functioning to rotate the scapula [9]. The subclavius, latissimus dorsi, serratus posterior and abdominal wall muscles are muscles that also attach to the thoracic skeleton [9]. Each intercostal space contains three layers of muscle. The outermost external intercostal muscles are obliquely arranged in an anteroinferior direction functioning to elevate the ribs. The deeper internal intercostals are obliquely oriented in a posteroinferior direction functioning to depress the ribs. The innermost intercostals are a thin layer of muscle arranged similar to the internal intercostals. The transversus thoracis muscle located deep to the intercostal neurovascular bundles attaches to the inferior sternal body and to the posterior surface of the xiphoid process [8]. See Fig. 2.

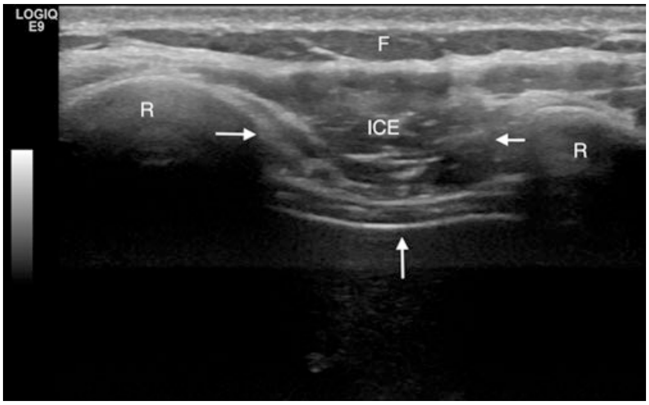

Fig. 2 Longitudinal section – intercostal space ("bat sign): F – subcutaneous fat. ICE – external intercostal muscle, R – ribs, horizontal arrows – internal intercostal muscle, upwards arrow – pleura

2.4 Cartilages and Bones

2.4.1 Ribs

There are 12 ribs noted in the thoracic wall. The first 7 ribs are known as "true ribs" because they connect directly to the sternum and manubrium. Ribs 8 to 10 are known as "false ribs" because they connect to the sternum via costal cartilages that connect together to form a single indirect connection. Ribs 11 and 12 are known as "floating ribs" because they have no attachment to the sternum. Their anterior extremity lies freely in the posterolateral abdominal wall sternum [8].

2.4.2 Sternum

The sternum is made up of 3 bones including, from superior to inferior, the manubrium, sternal body, and xiphoid process [8].

2.4.3 Sternoclavicular Joints

The sternoclavicular joint is the joint between the manubrium and the clavicle bone [8].

2.4.4 Scapula

The scapula is also known as the shoulder blade. It connects the humerus with the clavicle [8].

2.4.5 Vascular Network of Chest Wall

The thoracic wall is served by many arteries and veins. The first six anterior intercostal arteries stem directly from the internal thoracic artery. The remaining branch off the musculophrenic artery. The superior intercoastal artery branches into the two posterior intercostal arteries branch in the first two intercostal spaces and the remainder posterior intercostal arteries are branches of the descending thoracic aorta. The anterior intercostal veins return blood to the internal thoracic and musculophrenic veins. The posterior intercostal veins return blood to the azygos and hemiazygos veins [8]. See Fig. 3.

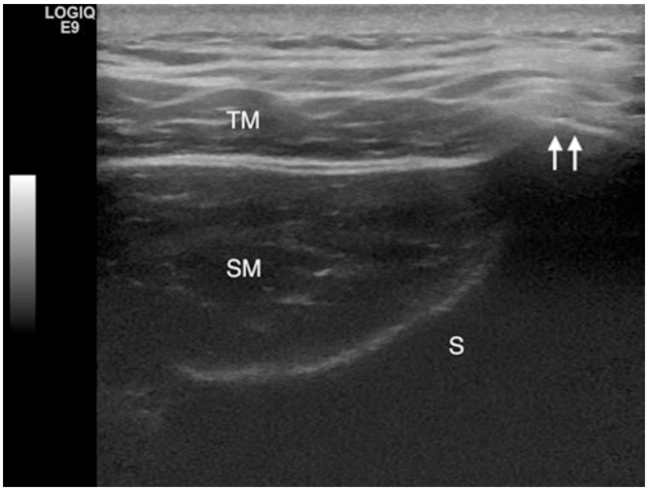

Fig. 3 Longitudinal section over the upper aspect of the scapula (S): TM—trapezius muscle, SM – supraspinatous muscle; spina of the scapula—arrows

2.4.6 Spinal Nerves of Thoracic Wall

The intercostal nerve originates at the ventral primary rami of spinal nerves T1–T11. Its branches include the lateral and anterior cutaneous branches. Motor innervation of intercostal nerves includes intercostal muscles, abdominal wall muscles (via T7 to T11), and muscles of the hand and forearm (via T1). Sensory innervation of the intercostal nerves includes the anterolateral skin of the chest and abdomen, as well as the skin of the upper limb on the medial side (via T1–T2). Intercostal nerves travel below the posterior intercostal artery in the costal groove.

Subcostal nerves originate at the ventral primary ramus of T12. They branch into lateral cutaneous branches and anterior cutaneous branches. Motor innervation of subcostal nerves includes muscles of the abdominal wall. Sensory innervation of subcostal nerves includes skin of the anterolateral abdominal wall. The subcostal nerve is equivalent to a posterior intercostal nerve found at higher thoracic levels [8].

2.4.7 Thoracic Lymph Nodes

Main lymph nodes of the thorax include the anterior mediastinal nodes which course along the brachiocephalic vessels and aorta. Axillary nodes are appropriately named as they are found in the axilla. Hilar nodes are found at the hilum of the lungs and supraclavicular nodes are found in and around carotid sheath below the level of the omohyoid muscle. Infraclavicular nodes are found along the cephalic vein in the deltopectoral groove. Intercostal nodes are found near the heads of the ribs, pectoral nodes are found in the lateral border of the pectoralis major along the path of the lateral thoracic vessels, and phrenic nodes on the thoracic surface of the respiratory diaphragm [8].

2.4.8 Endothoracic Fascia and Parietal Pleura

The border between the chest wall and the lungs is marked by the endothoracic fascia and the parietal pleura [7]. The endothoracic fascia is connective tissue lining the inner aspect of the chest wall. It is located between the parietal pleura and the muscles and bones of the thoracic wall. On ultrasound, in both normal and pathological conditions, it presents as a hyperechoic line with various artifacts visible deep to it [8].

3 Thoracic Wall Blocks

3.1 Pecs I and II Block

The PECS I block is a is aimed at blocking the medial and lateral pectoral nerves in the interfacial plane between pec minor and pec major. The ultrasound technique utilizes the sagittal plane below the lateral one third of the clavicle, transverse to the body axis. The approach is superomedial to inferolateral direction of the needle. Usually if a rib is seen, it is rib 2. The needle is advanced in plane and the local anesthetic is deposited between pec major and pec minor. For the PECS II block, a local anesthetic is injected between pec minor and serratus anterior at the level of the third rib, deeper than PECS I. The target nerves are the long thoracic nerve and intercostal nerves of the ribs. The ultrasound technique is much like PECS I with the probe being moved slightly caudal to visualize ribs 3 and 4. Once found the probe is rotated 90 degrees in a transverse plane and moved laterally keeping rib 3 in the middle of the view. The needle is introduced medially to laterally and local anesthetic is injected between pec minor and serratus anterior. About 10 cc local is used for PECS I while 20 cc local is used for PECS II. Complications are minimal to nonexistent. There is a risk of pneumothorax if the needle is introduced into the pleural cavity. Also, trauma to the intercostal vessels and thoracodorsal artery are of concern but minimal with the use of ultrasound guidance [10]. See Fig. 4.

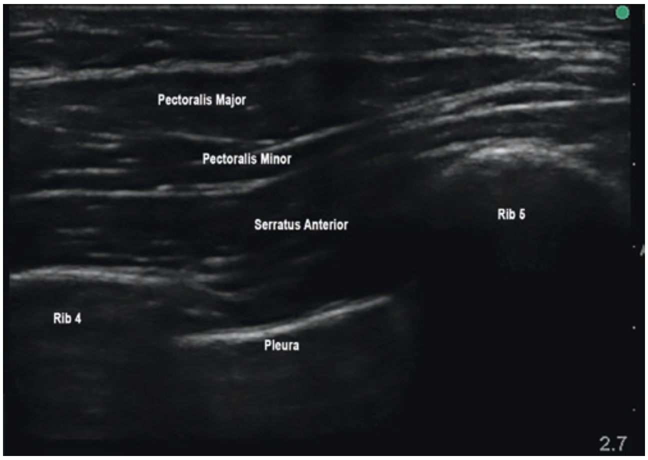

Fig. 4 Anatomical ultrasound image of the pectoralis major/serratus anterior

3.2 Serratus Anterior Block

The serratus anterior block is designed to block the intercostal nerves as well as the long thoracic nerve and thoracodorsal nerve in order to provide pain relief to the anterolateral and part of the posterior chest wall. Much like the PECS II block, except more caudal and posterior. There are two variants of the block either superficial or dep depending on the pain control goal. The ultrasound technique is much like PECS II. The probe is moved more caudal and lateral at the midaxillary line. The goal is to keep the fifth rib in the middle of the screen and the needle is introduced anteromedial to posterolateral. The injection is then placed superficial or deep with 20 cc of local anesthetic while aiming towards the rib. Much like the PECS II block, pneumothorax is a potential complication [10]. This block is utilized for thoracic and upper abdominal procedures especially in the case of flail chest and other chest trauma. One must be skilled in ultrasound visualization of the needle tip to prevent this complication.

3.3 Interpleural Block

An interpleural block is done when local anesthetic is injected into the pleural plane between the two layers of the pleura. The risk of pneumothorax is a little bit greater with this technique, even using ultrasound. In addition, adhesions and infection are also among the risks reported. The ultrasound technique is much like the other blocks described. The probe is placed in a transverse orientation at the midaxillary line at ribs 5 and 6. The pleura is viewed as a shiny white line below the intercostal membrane. A saline technique is used as the needle breaches the parietal pleura. Since the space has negative pressure, the saline will flow freely into the potential space of the parietal pleura, much like an epidural technique using a loss of resistance syringe. A catheter can be placed in this space as well for continuous infusion. This block can be utilized for upper abdominal procedures and chest procedures including breast surgery, thoracotomy, and renal surgery [10].

3.4 Intercostal Nerve Block

The intercostal nerves innervate the ribs and arise from the ventral rami of the thoracic nerve roots. The intercostal nerves contain both sensory and motor function and aid in respiration through innervation of the intercostal muscles. The nerve runs along the upper border of the rib below. The intercostal nerve block contains a band of pain control along the distribution of the nerve. The ultrasound technique is straightforward. The ribs are identified in a transverse plane with the ultrasound probe. The landmarks that are used are identifying either rib 2, 12, or the tip of the scapula at T7. The most ideal location to place the local anesthetic is about 6–7 cm lateral to the spinous process of the given side. The local can be placed wither in plane or out of plane by hydrodissection. Under ultrasound is it important to continue to see the pleura gliding with respiration to know that a pneumothorax has not been caused. About 3–5 cc of local anesthetic is enough.

3.5 Paravertebral Block

The paravertebral block is done on the posterior aspect of the patient at the midscapular line. The ultrasound probe is placed in the sagittal plane and moved medially until the paravertebral space is seen at the transverse process where the intercostal muscles disappear. The costotransverse ligament is seen between the transverse processes. The local is injected in plane or out of plane into the costotransverse ligament just before the pleura. The complications are like the other thoracic wall blocks, including pneumothorax and pleural puncture. The block is utilized for thoracic and breast surgery as well as multiple rib fractures [10]. There are many additives that can be utilized to prolong the duration of a regional nerve block. Magnesium is a novel additive that has been used successfully in PECS blocks to prolong the pain control aspects of the block [11].

4 Analgesic Potential of Pecs Blocks

4.1 Chest Wall Pain Syndrome

The mainstay of chest wall pain syndrome consists of singular or multiple localized areas of direct or referred chest pain as a direct result of injury or otherwise acute stress to the body. Specifically, it consists of a plethora of pathological etiologies that may or may not result in either acute or chronic pain, with estimates of total cost being approximately $8 billion per year surrounding 6 million people presenting to nation-wide Emergency Departments with chest pain [12]. Specific etiologies surrounding patients presenting with acute chest pain consist of cardiac, pulmonary, gastrointestinal, neurological, bone, muscular, dermatologic, psychiatric, and extrathoracic disorders, among these costochondritis, postherpetic neuralgia, postthoracotomay pain, neoplasia, intercostal neuralgia, and myofascial pain being the most common [12]. The most common treatment modalities, depending upon symptom-specific history, physical examination, and workup, involve initial application of NSAIDs/COX-2 Inhibitors, ice, and heat, with specific treatment algorithms dictating further treatment based upon recurrence or proper diagnostic workup [12]. Across a specific cohort study examining chest wall pain syndrome, *Verdon et al* found amongst 672 chest pain patient presentations, 300 cases ultimately were diagnosed with true chest wall pain syndrome, specifically being three times more frequent in etiology than true cardiac pathology [13]. Further, they describe the redundancy among diagnoses of costochondritis, anterior chest wall syndrome, atypical chest pain, and musculoskeletal chest pain syndrome, all of which are adequately described under a chest wall pain syndrome diagnosis. Among 24,620 primary care consultations, 44.6% had chest wall pain syndrome, 4% of thoracic pain being traumatic, 2.4% being diversified, 16% being cardiovascular disease, 11% being psychogenic pain, 10% being respiratory diseases, 8% being gastrointestinal disorders, and 4% having no specific diagnosis at 3-month follow up [13]. For the scope of this discussion, chest wall pain syndrome stemming specifically from intercostal neuralgia, traumatic rib injury, and post-operative thoracotomy pain modulation will be discussed in detail in addition to various analgesic techniques of which the Anesthetist may apply in a patient-specific and situationally appropriate manner.

4.2 Intercostal Neuralgia

Intercostal neuralgia simply describes pain which originates due to activation of the thoracic nerves based upon numerous etiologies and may be considered under the umbrella diagnosis of chest wall pain syndrome. It occurs most commonly post-thoracotomy, after rib trauma, during pregnancy, or after surgical stimulation of the intercostal nerves. Treatment involves a multidisciplinary approach involving both pharmacological and non-pharmacological interventions depending upon the etiological diagnosis. Non-pharmacological approaches involve behavior therapy, psychological counseling, transcutaneous electrical nerve stimulation (TENS), and various acupuncture techniques aimed at nerve desensitization and ultimately pain modulation. Initial pharmacological techniques involve anticonvulsants, such as Gabapentin 100–300 mg PO and Pregabalin 50 mg PO, coupled with or without Lidocaine topical agents. Second line treatments involve administration of Tricyclic antidepressants such as

Amitriptyline, Nortriptyline, Imipramine, or Desipramine 10–25 mg PO with increases of 25 mg every 2–4 weeks until adequate response is achieved. When neither non-pharmacological modalities nor pharmacological treatments achieve adequate pain control within this patient population, invasive treatment options may be pursued, consisting of an intercostal nerve block or paravertebral nerve block. If pain is still considered to be refractory, spinal cord stimulation, radiofrequency ablation, and surgical techniques may then be pursued [14].

Of specific use to the Anesthetist, thermal radiofrequency ablation (RFA) has been noted to be particularly useful amongst patients with intractable intercostal neuralgia. One specific case report noted that RFA completely resolved intercostal neuralgia in 2 specific patients post-lumpectomy and with concurrent esophageal carcinoma and non-small cell lung cancer. During image-guided RFA, medium frequency alternating current induces neural cell death via coagulation necrosis after initial nerve identification with local nerve block. The authors do note that this invasive technique is not without possible complications, of which include site infection, bleeding, possible pneumothorax via lung puncture, headaches, and neuroma formation. Within intercostal neuralgia, RFA techniques provide promising longer-term pain relief with avoidance of many adverse side effects involved in classic pharmacological treatments- renal damage, significant sedation, constipation, addictive potential, and gastrointestinal bleeding with overall decreases in respiratory complications, chronic postthoractomay pain (discussed further), and overall disability, all of which hold significant economic, medical, psychological, and financial effects [15].

4.3 Traumatic Rib Injury

Blunt force chest trauma resulting in rib fracture injuries is a significant cause of morbidity and mortality in the United States, with each subsequent rib fracture increasing the overall likelihood of complication development, the most concerning of which noted as "Flail Chest" development. Overall chest wall trauma focuses on surgical fixation where appropriate, chest physiotherapy, respiratory care, early mobilization, and combinations of effective analgesic techniques to ensure adequate respiration and pain modulation [16]. Within this patient group, epidural anesthetic administration in those with three or more rib fractures was found to have superior analgesic effects without decreases in respiratory function secondary to pain with overall reduction in mortality, due to pneumonia development or complications surrounding mechanical ventilation, versus IV narcotic PCA, lidocaine patch administration, or intercostal and paravertebral nerve blocks [16, 17]. Furthermore, overall respiratory factors such as tidal volume and minute expiratory volume parameters in addition to arterial oxygen pressure and arterial pH was found to be better in those patients receiving epidural administration [18]. It should be noted that intercostal nerve blocks showed more adequate pain control for initial rib fracture management versus conventional medications (IV narcotics/ PCA) with reduction in respiratory complications and overall mortality although overall pain modulation was found to decrease over time and thus additional pain control measures must be considered in comparison of these two modalities [19].

4.4 Post-Operative Thoracotomy

The pain associated with postoperative thoracotomy can be both debilitating and present unique difficulties in pain management. This stems from surgical stimulation resulting in peripheral sensitization, via A-delta and C nerve fibers, with subsequent central sensitization via changes in spinal dorsal horn neurons. Achieving intercostal nerve blockade is currently the primary component for effective nociceptive stimuli modulation versus an epidural approach [20].

The use of intercostal cryoanalgesic techniques in combination with IV PCA administration versus IV PCA pain modulation alone have been studied, specifically as it relates to respiratory function and subsequent patient morbidity. It was found that up until 2 months post-op, patients who received a combination treatment of both intercostal nerve cryoablation therapy in addition to IV PCA postoperatively had overall reductions in morphine consumption, optimized blood gas pH, increases in FEV1 and FVC values, as well as reduction in nausea, numbness, epigastric distention, and back pain incidence, and therefore should be considered as a highly effective treatment modality within this patient subgroup [21]. Of significant note, FEV1 values were restored at 2 months post-op to nearly preoperative values, a finding of which directly may impact patient recovery time and overall morbidity and mortality as a whole [21].

When examining various modalities to achieve intercostal nerve blockade in patients having undergone thoracotomy, specifically extrapleural vs interpleural continuous analgesic infusion, cryoanalgesia, or direct intercostal nerve blockade, it was found that while interpleural continuous infusion, cryoanesthesia, and direct intercostal blocks all play a significant role in pain modulation, extraplueral pocket creation with continuous infusion is superior in effective pain control versus systemic narcotics alone, additionally found to be at least as good as epidural approaches [20], the currently most common method of postthoracotomy analgesia. This primarily stems from extrapleural analgesia resulting in unilateral blockade, avoiding significant side effects of thoracic epidural administration such as urinary retention (42%), nausea

(22%), itching (22%), and hypotension via sympathetic tone reduction (3%) [20].

4.5 Analgesic Techniques and Approaches-Ultrasound-Guided and Video-Assisted Intercostal Nerve Cryoablation

Both ultrasound-guided and port video-assisted approaches have been described within the literature as applicable approaches in achieving thoracic nerve cryoablation, although currently noted to be an underutilized modality in intractable chest wall pain. Within the ultrasound-guided technique, the pleura can be easily identified, the patient can be monitored during inhalation throughout the procedure, and the safest approach for probe advancement can be achieved via visualization. Further, ultrasound allows for monitoring of acute events such as traumatic pneumothorax development. One noted downfall of this approach is the intercostal nerve cannot be visualized directly via ultrasound and thus probe placement just inferior to the intercostal groove with subsequent ice ball formation must be used to verify correct probe placement [22]. As it concerns a video-assisted approach in achieving intercostal nerve cryoablation, direct visualization of the cryoablation targets allow for the avoidance of repeated intercostal nerve blocks and epidurals, specifically circumventing potential pneumothorax, a plausible side effect classically associated with percutaneous blockade approaches. This approach allows for preservation of the pleura, a targeted and focused region to be ablated, and highly localized precision. This approach allows for a minimally invasive blockade to be achieved and avoids repetitive analgesic attempts in addition to reliance on long-term systemic pain pharmacotherapy [23].

5 Clinical Applications of Pecs Block

The use of Pecs blocks has been described for various procedures involving the anterior chest wall, see Table 2. The most common clinical application of Pecs block is to provide analgesia for breast surgery. Pecs blocks have also been utilized in other procedures, including cardiothoracic surgery, orthopedic surgery, rehabilitation, as well as chronic pain management.

Table 2 Clinical applications of pecs blocks

Breast surgery
Mastectomy
Lumpectomy
Breast augmentation
Tissue expander
Sentinel/axillary lymph node dissection
Cardiothoracic surgery
Pacemaker/defibrillator implantation
Trans-subclavian transcatheter aortic valve replacement
Sternotomy
Video-assisted thoracic surgery
Chronic post-thoracotomy pain
Other
Clavicle fracture
Acromioclavicular dislocation
Sentinel/axillary lymph node biopsy for malignant tumors of upper extremity
Port catheter placement or removal
Physical rehabilitation for pectoralis major muscle or latissimus dorsi muscle contracture
Post-herpetic neuralgia of anterior chest wall

5.1 Pecs Block for Breast Surgery

Multiple studies have shown that Pecs blocks can provide effective analgesia for breast surgery, including mastectomy, lumpectomy, breast augmentation, and sentinel and axillary lymph node dissection [24–29]. In several randomized studies, combined Pecs 1 and 2 blocks decreased postoperative opioid consumption, pain scores, and hospital length of stay, while improving patient satisfaction when compared to no block [24–28]. Interestingly, in a randomized study where intercostal and Pecs blocks were performed by the surgeon at the end of the surgery, there was no difference in pain, opioid consumption nor quality of recovery when compared to sham block. This may suggest a benefit to performing Pecs blocks prior to incision. Despite the lower opioid consumption associated with Pecs blocks, there is no consensus on its effect on postoperative nausea and vomiting (PONV), with a lower incidence of PONV in some studies [26, 28] and no effect in others [27, 30].

Pecs blocks can be combined with transversus abdominus plane blocks to provide pain relief after mastectomy with transverse rectus abdominus muscle flap surgery [31]. Although Pecs blocks are typically used for analgesia, there are case reports describing the use of Pecs blocks as surgical anesthesia for mastectomy in combination with dexmedetomidine sedation or additional local infiltration, thereby avoiding the need for general anesthesia [32, 33].

In one randomized study by Ekinci et al., the performance of Pecs 1 block compared to no block for subpectoral breast augmentation resulted in lower opioid consumption and pain scores [34]. However, in a randomized controlled trial by Cros et al. of Pecs 1 versus sham block, there were no differences in opioid consumption or pain scores [35]. In a subgroup analysis of patients undergoing major breast surgery, there was a statistical, but not clinically significant difference in pain scores of 3 [range:

0–4] in the Pecs group vs. 4 [2–5] in the control group (p = 0.04) [35]. In a direct comparison of Pecs 1 to Pecs 2 block in patients undergoing modified radical mastectomy, Pecs 2 block was found to provide superior analgesia compared to Pecs 1 block alone [36]. These studies suggest an analgesic limitation of performing Pec 1 block alone. This is not surprising since the Pecs 1 block only blocks medial and lateral pectoral nerves, which do not provide sensory innervation to the breast.

In a 2018 meta-analysis, Pecs blocks were found to be superior to paravertebral blocks in decreasing intraoperative opioid requirements [29]. However, paravertebral block was superior to Pecs block in reducing opioid consumption in the first 24 hours after surgery. Notably, paravertebral blocks were associated with a higher complication rate, with 2 cases of pneumothorax in the paravertebral studies compared to no complications in the Pecs block group. Although paravertebral block decreases the incidence of chronic post-mastectomy pain (CPMP) [37], Pecs block has not been shown to decrease CPMP [38, 39]. Pecs blocks may, however, have a role in the treatment of CPMP [40].

5.2 Pecs Block for Cardiothoracic Surgery

The use of Pecs blocks has also been described for several cardiothoracic surgeries. Kaushal and colleagues compared Pecs blocks, serratus anterior plane blocks, and intercostal nerve blocks for postoperative pain control in 108 pediatric patients undergoing cardiac surgery via thoracotomy [41]. In this prospective, randomized study, those who received Pecs blocks and serratus anterior blocks had lower pain scores and lower opioid consumption postoperatively than those who received intercostal nerve blocks. Pecs blocks and serratus anterior blocks provided equally effective analgesia in this patient population.

There are several case reports utilizing Pecs blocks for other cardiothoracic procedures. A Pecs 1 block combined with intercostal block was used for procedural anesthesia for pacemaker and defibrillator implantation [42]. Pecs 1 block with Pecs 2 block catheters provided effective postoperative pain relief after aortic valve replacement via median sternotomy [43]. In addition, Pecs 1 blocks can provide adequate anesthesia for trans-subclavian transcatheter aortic valve replacement when combined with dexmedetomidine sedation [44]. A combination of Pecs 1, Pecs 2, and serratus anterior plane block can provide surgical anesthesia for awake video-assisted thoracic surgery (VATS) thus preserving spontaneous ventilation [45]. Pecs 2 blocks with serratus anterior plane blocks have also been used in the treatment of chronic post-surgical pain after VATS [46] and open thoracotomy [47].

5.3 Other Clinical Applications of Pecs Blocks

There is a wide variety of other clinical applications of Pecs block, including orthopedic surgery, rehabilitation, as well as cancer and chronic pain management. Since the lateral pectoral nerve contributes to innervation of the lateral and anterior clavicle, Pecs blocks can provide analgesia for patients with middle third clavicle fractures or acromioclavicular dislocations [48]. In a patient with frozen shoulder and contraction of the pectoralis major muscle, the addition of a Pecs 1 blocks to an interscalene brachial plexus block was necessary to manipulate the shoulder, as the contraction of the pectoralis major muscle limited shoulder adduction [49]. The thoracodorsal nerve blockade achievable with Pecs blocks can facilitate physical rehabilitation of patients with latissimus dorsi muscle contraction, thus, enabling the patient to avoid surgical treatment [50].

Given the efficacy of Pecs blocks for axillary lymph node dissection in breast surgery, it is not surprising that Pecs blocks provide effective surgical anesthesia for sentinel and axillary lymph node biopsy for malignancy of the upper extremity [51]. Pecs blocks can also provide anesthesia for implantable central catheter port placement or removal [52]. Furthermore, Pecs 2 blocks have been used to treat acute zoster-associated pain and chronic post-herpetic neuralgia that affects the anterior chest wall [53, 54].

6 Summary and Conclusion

Various chest wall pathologies and necessary surgical procedures comprise the etiology of the modern-day diagnosis of chest wall pain syndrome, which subsequently results in increased healthcare costs, repeated and recurring procedures aimed at achieving analgesia, dependence on pain modulating pharmacotherapies, and increased morbidity and mortality of patients as a whole. Through various techniques of which have been discussed, achieving pectoralis nerve and serratus plane blocks provide promising results in reduction of thoracic chest wall pain, both initial and intractable. Specifically, through the use of these specific blockage techniques, the use of thoracic epidural, paravertebral, intercostal, and intrapleural blocks may be avoided when treating chest wall pain with various etiologies.

Through use of ultrasound-guided approaches, fascial layers may be specifically identified in order to perform interfascial analgesic injection for use over both the thoracic and abdominal walls. Chest wall local analgesic administration involves various approaches, all of which selected are patient specific, given history and likely etiology of the chest wall pain. As it specifically concerns ultrasound guidance, the Pecs I, Pecs II, and serratus anterior approaches are becoming increasingly accepted as alternatives to more invasive and timely pain management modalities. Specifically, the Pecs I block achieves hydrodissection of the fascial plane by separating the pectoralis major and minor muscles, with careful identification and localization of the thoracoacromial artery's pectoral branch, ultimately resulting in blockade of the lateral and medial pectoral nerves. The primary goal of the Pecs II approach to achieving blockade is to provide analgelsia by US-guided injection to both the pectoral nerves and under the pectoralis minor muscle via infiltration of two fascial compartments. Of importance during local anesthetic administration, the pectoral nerves within the pectoral compartment and the intercostal branches of the axilla and chest should be ensured to have received adequate (both dose and localization) analgesia. During this approach the local anesthetic dose is equally divided between the fascial zones, thus requiring two injection sites. The serratus anterior plane block is achieved by localized analgesia injection within the anatomical compartment between the latissimus dorsi and serratus anterior muscles, within which sit the intercostobrachialis nerve, lateral cutaneous branches of intercostal nerves T3–T9, long thoracic nerve, and thoracodorsal nerve. During this approach, care is taken to localize and identify the thoracodorsal artery that runs within the fascial plane between the latissumus dorsi and the serratus anterior muscles. This assists in analgesic injection approach while avoiding any significant procedural side effects when using ultrasound imaging.

The use of ultrasound-guided pectoralis and serratus anterior nerve blockade serves as a less invasive technique with fewer associated side effects in controlling intractable chest wall pain, in addition to various applications within the perioperative period, versus those associated with thoracic epidurals, paravertebral, intercostal, and intrapleural blocks. Specifically, Pecs blocks via either approach were found to reduce morphine consumption within the first 24 hours postoperatively in addition to pain scores within the first 12 hours versus the use of paravertebral blocks among patients having undergone mastectomy. The increased usage of these ultrasound-guided techniques, specifically surrounding breast and lateral thoracic wall surgery, have demonstrated their superior analgesic potential as minimally invasive, cost-effective reducers in overall morbidity associated with postoperative recovery, as well as their possible potential across a multitude of chronic pain syndromes.

References

1. Nair AS, Sahoo RK, Ganapathy M, Mudunuri R. Ultrasound guided blocks for surgeries/ procedures involving chest wall (Pecs 1,2 and serratus plane block) [Internet]. Anaesthesia, Pain & Intensive Care. Available from: http://www.apicareonline.com/oldsite/ultrasoundguidedblocksforsurgeries-proceduresinvolvingchestwall-pecs-12andserratusplaneblock/.
2. NYSORA. Pectoralis and Serratus Plane Blocks [Internet]. NYSORA. 2019 [cited 2019 Mar 18]. Available from: https://www.nysora.com/regional-anesthesia-for-specific-surgical-procedures/thorax/pectoralis-serratus-plane-blocks/.
3. Manion SC, Brennan TJ. Thoracic epidural analgesia and acute pain management. Anesthesiology. 2011;115(1):181–8. Available from: http://anesthesiology.pubs.asahq.org/Article.aspx?doi=10.1097/ALN.0b013e318220847c
4. Raj N. Thoracic Paravertebral Block | European Society for Paediatric Anaesthesiology [Internet]. ESPA. 2019 [cited 2019 Mar 18]. Available from: http://www.euroespa.com/science-education/specialized-sections/espa-pain-committee/us-regional-anaesthesia/truncal-blocks/thoracic-paravertebral-block/.
5. Blanco R. The 'pecs block': a novel technique for providing analgesia after breast surgery. Anaesthesia. 2011;66(9):847–8. Available from: http://www.ncbi.nlm.nih.gov/pubmed/21831090
6. Gonzales J. PECS versus PVBS for perioperative analgesic Management in Breast Surgery – American Society of Regional Anesthesia and Pain Medicine [internet]. ASRA News. 16(3):41–4. Available from: https://www.asra.com/pain-resource/article/83/pecs-versus-pvbs-for-perioperative-analg
7. Smereczyński A, Kołaczyk K, Bernatowicz E. Chest wall – underappreciated structure in sonography. Part I: examination methodology and ultrasound anatomy. J Ultrason. 2017;17(70):197–205. Available from: http://www.ncbi.nlm.nih.gov/pubmed/29075525
8. Moore KL, Dalley AF. Thorax. In: Clinically oriented anatomy. 4th ed. Philadelphia: Lippincott Williams & Wilkins. p. 60–173.
9. Blanco R, Fajardo M, Parras Maldonado T. Ultrasound description of Pecs II (modified Pecs I): a novel approach to breast surgery. Rev Esp Anestesiol Reanim. 2012;59(9):470–5. Available from: http://www.ncbi.nlm.nih.gov/pubmed/22939099
10. Chakraborty A, Khemka R, Datta T. Ultrasound-guided truncal blocks: a new frontier in regional anaesthesia. Indian J Anaesth. 2016;60(10):703–11. https://doi.org/10.4103/0019-5049.191665.
11. Abdelaziz Ahmed A. Efficacy of pectoral nerve block using bupivacaine with or without magnesium sulfate. Anesth Essays Res. 2018;12(2):440–5. https://doi.org/10.4103/aer.AER_37_18.
12. Waldman SD, Oken JE, Dugan S. Chest Wall pain syndromes. Pain Manag. 2006;1:672–89.
13. Verdon F, Burnand B, Herzig L, Junod M, Pécoud A, Favrat B. Chest wall syndrome among primary care patients: a cohort study. BMC Fam Pract. 2007;8:1–7.
14. Dureja GP, Intercostal Neuralgia: A Review. J Neurol Transl Neurosci. 2017;5(1):1076. https://www.jscimedcentral.com/Neuroscience/neuroscience-5-1075.pdf.
15. Abd-Elsayed A, Lee S, Jackson M. Radiofrequency ablation for treating resistant intercostal neuralgia. Ochsner J. 2018;18(1):91–3.
16. Unsworth A, Curtis K, Asha EE. Treatments for blunt chest trauma and their impact on patient outcomes and health service delivery. Scand J Trauma Resusc Emerg Med. 2015;23(1):1–9.
17. Hietbrink F, Peek J, Houwert RM, Marsman M, Smeeing DPJ, de Jong MB. Comparison of analgesic interventions for traumatic rib fractures: a systematic review and meta-analysis. Eur J Trauma Emerg Surg. 2019;45(4):597–622. https://doi.org/10.1007/s00068-018-0918-7. Epub 2018 Feb 6.
18. Hashemzadeh S, Hashemzadeh K, Hosseinzadeh H, Aligholipour Maleki R, Golzari SEJ, Golzari S. Comparison thoracic epidural and intercostal block to improve ventilation parameters and reduce pain in patients with multiple rib fractures. J Cardiovasc Thorac Res. 2011;3(3):87–91.
19. Hwang EG, Lee Y. Effectiveness of intercostal nerve block for management of pain in rib fracture patients. J Exerc Rehabil. 2014;10(4):241–4.

20. Detterbeck FC. Efficacy of methods of intercostal nerve blockade for pain relief after thoracotomy. Ann Thorac Surg. 2005;80(4):1550–9.
21. Kakaris S, Misthos P, Toparlaki O, Voyagis G, Anagnostopulu M, Sepsas E. The role of intercostal cryoanalgesia in post-thoracotomy analgesia. Interact Cardiovasc Thorac Surg. 2013;16(6):814–8.
22. Byas-Smith MG, Gulati A. Ultrasound-guided intercostal nerve cryoablation. Anesth Analg. 2006;103(4):1033–5.
23. Hunt I, Eaton D, Maiwand O, Anikin V. Video-assisted intercostal nerve cryoablation in managing intractable chest wall pain. J Thorac Cardiovasc Surg. 2010;139(3):774–5.
24. Bashandy GMN, Abbas DN. Pectoral nerves I and II blocks in multimodal analgesia for breast Cancer surgery. Reg Anesth Pain Med. 2015;40(1):68–74.
25. Versyck B, van Geffen G-J, Van Houwe P. Prospective double blind randomized placebo-controlled clinical trial of the pectoral nerves (Pecs) block type II. J Clin Anesth. 2017;40:46–50.
26. Karaca O, Pınar HU, Arpacı E, Dogan R, Cok OY, Ahiskalioglu A. The efficacy of ultrasound-guided type-I and type-II pectoral nerve blocks for postoperative analgesia after breast augmentation: a prospective, randomised study. Anaesth Crit Care Pain Med. 2019;38(1):47–52.
27. Neethu M, Pandey RK, Sharma A, Darlong V, Punj J, Sinha R, et al. Pectoral nerve blocks to improve analgesia after breast cancer surgery: a prospective, randomized and controlled trial. J Clin Anesth. 2018;45:12–7.
28. Wang K, Zhang X, Zhang T, Yue H, Sun S, Zhao H, et al. The efficacy of ultrasound-guided type II pectoral nerve blocks in perioperative pain Management for Immediate Reconstruction after modified radical mastectomy. A prospective, randomized study. Clin J Pain. 2017;34(3):1.
29. Singh P, Borle A, Kaur M, Trikha A, Sinha A. Opioid-sparing effects of the thoracic interfascial plane blocks: a meta-analysis of randomized controlled trials. Saudi J Anaesth. 2018;12(1):103.
30. Lanier ST, Lewis KC, Kendall MC, Vieira BL, De Oliveira G, Nader A, et al. Intraoperative nerve blocks fail to improve quality of recovery after tissue expander breast reconstruction. Plast Reconstr Surg. 2018;141(3):590–7.
31. Patel SY, Evans RM, Garcia Getting RE, Suz P. Pectoral nerve and transverse abdominis plane block in a patient undergoing mastectomy with transverse rectus abdominis muscle flap: a case report. A A Case Rep. 2017;8(8):210–2.
32. Moon E-J, Kim S-B, Chung J-Y, Song J-Y, Yi J-W. Pectoral nerve block (Pecs block) with sedation for breast conserving surgery without general anesthesia. Ann Surg Treat Res. 2017;93(3):166–9.
33. Murata H, Ichinomiya T, Hara T. Pecs block for anesthesia in breast surgery of the elderly. J Anesth. 2015;29(4):644.
34. Ekinci M, Ciftci B, Celik EC, Karakaya MA, Demiraran Y. The efficacy of different volumes on ultrasound-guided type-I pectoral nerve block for postoperative analgesia after subpectoral breast augmentation: a prospective, randomized, controlled study. Aesthetic Plast Surg. 2019;43(2):297–304. https://doi.org/10.1007/s00266-019-01322-8. Epub 2019 Feb 12.
35. Cros J, Sengès P, Kaprelian S, Desroches J, Gagnon C, Labrunie A, et al. Pectoral I block does not improve postoperative analgesia after breast Cancer surgery: a randomized, double-blind, dual-centered controlled trial. Reg Anesth Pain Med. 2018;43(6):596–604.
36. Goswami S, Kundra P, Bhattacharyya J. Pectoral nerve block1 versus modified pectoral nerve block2 for postoperative pain relief in patients undergoing modified radical mastectomy: a randomized clinical trial. Br J Anaesth. 2017;119(4):830–5.
37. Terkawi AS, Tsang S, Sessler DI, Terkawi RS, Nunemaker MS, Durieux ME, et al. Improving analgesic efficacy and safety of thoracic paravertebral block for breast surgery: a mixed-effects meta-analysis. Pain Physician. 18(5):E757–80.
38. Besch G, Lagrave-Safranez C, Ecarnot F, De Larminat V, Gay C, Berthier F, et al. Pectoral nerve block and persistent pain following breast cancer surgery: an observational cohort study. Minerva Anestesiol. 2018;84(6):769–71.
39. Versyck B, Groen G, Kampen J, Van Houwe P. The effect of pectoral block type II on persistent pain. Eur J Anaesthesiol. 2019;36(1):75–7.
40. Wijayasinghe N, Andersen KG, Kehlet H. Analgesic and sensory effects of the pecs local anesthetic block in patients with persistent pain after breast cancer surgery: a pilot study. Pain Pract. 2017;17(2):185–91.
41. Kaushal B, Chauhan S, Saini K, Bhoi D, Bisoi AK, Sangdup T, et al. Comparison of the efficacy of ultrasound-guided serratus anterior plane block, pectoral nerves II block, and intercostal nerve block for the Management of Postoperative Thoracotomy Pain after Pediatric Cardiac Surgery. J Cardiothorac Vasc Anesth. 2019;33(2):418–25.
42. Fujiwara A, Komasawa N, Minami T. Pectoral nerves (PECS) and intercostal nerve block for cardiac resynchronization therapy device implantation. Springerplus. 2014;3(1):409.
43. Richard AM, Bain SE, Nikravan S, Lilley RR, Velamoor GR, Flaherty JM, et al. Continuous pectoral fascia blocks for postoperative analgesia after median Sternotomy. A A Pract. 2018;11(6):145–7.
44. Alexander B, Angaramo G, Walz JM, Kakouros N, Moiz Hafiz A, Walker J, et al. A novel approach to managing trans-subclavian transcatheter aortic valve replacement with regional anesthesia. J Cardiothorac Vasc Anesth. 2018;32(3):1391–3.
45. Corso RM, Maitan S, Russotto V, Gregoretti C. Type I and II pectoral nerve blocks with serratus plane block for awake video-assisted thoracic surgery. Anaesth Intensive Care. 2016;44(5):643–4.
46. Piraccini E, Calli M, Byrne H, Corso RM, Maitan S. Ultrasound-guided pectoral nerves and serratus plane block for post thoracotomy pain syndrome. Minerva Anestesiol. 2017;83(8):888–9.
47. Fujiwara S, Komasawa N, Minami T. Pectral nerve blocks and serratus-intercostal plane block for intractable postthoracotomy syndrome. J Clin Anesth. 2015;27(3):275–6.
48. Schuitemaker R. JB, Sala-Blanch X, Rodriguez-Pérez CL, Mayoral R. JT, López-Pantaleon LA, Sánchez-Cohen AP. Bloqueo PEC II como componente mayor analgésico para operaciones de clavícula: descripción de 7 casos y revisión de la literatura. Rev Esp Anestesiol Reanim. 2018;65(1):53–8.
49. Ueshima H, Otake H. Pectoral nerves 1 block is effective for silent manipulation of frozen shoulder. J Clin Anesth. 2018;44:47.
50. Ueshima H, Otake H. Pectoral nerves block for a contraction of the latissimus dorsi muscle. J Clin Anesth. 2016;31:200.
51. Yokota K, Matsumoto T, Murakami Y, Akiyama M. Pectoral nerve blocks are useful for axillary sentinel lymph node biopsy in malignant tumors on the upper extremities. Int J Dermatol. 2017;56(3):e64–5.
52. Piliego C, Longo F, Costa F, Martuscelli M, Claps F, Agrò FE. Are we doing all we can for procedural pain? Evaluation of the efficacy of pectoral nerve block for port catheter positioning. Minerva Anestesiol. 2019;85(5):560–1. https://doi.org/10.23736/S0375-9393.18.13308-6. Epub 2019 Jan 4.
53. Oh DS. Pecs II block for intractable postherpetic neuralgia. J Anesth. 2018;32(3):460.
54. Kim Y-D, Park S-J, Shim J, Kim H. Clinical usefulness of pectoral nerve block for the management of zoster-associated pain: case reports and technical description. J Anesth. 2016;30(6):1074–7.

Ultrasound Guided Nerve Blocks for Abdomen

Shilpa Patil, Anusha Kallurkar, Yury Rapoport,
Pankaj Thakur, Andrew P. Bourgeois, Elyse M. Cornett,
Matthew R. Eng, and Alan David Kaye

1 Introduction

Regional analgesia of the abdominal wall has evolved and gained popularity over epidural anesthesia with the increasing use of minimally invasive laparoscopic techniques. Additionally, the increase in ambulatory surgery, an aggressive postoperative anticoagulation regimen, multimodal approaches in pain management, and an emphasis on early ambulation have all been enhanced by the use of regional anesthesia. Abdominal wall blocks provide somatic analgesia by anesthetizing multiple small nerves or plexuses, rather than targeting specific nerve structures, and are best used as part of a multimodal analgesic regimen. Interestingly, these blocks depend more on volume than on concentration of local anesthetic. Commonly used techniques include the (trans abdominal plane) TAP block, ilioinguinal-iliohypogastric (II-IH) block, and the rectus sheath block.

Ultrasound guidance is now considered a gold standard for abdominal wall blocks, although landmark-guidance is still used by some physicians. For example, the TAP block aims to anesthetize some or all of the lower 6 thoracic spinal nerves (T7-T12) and II-IH (L1). The block can be performed either by using a landmark technique or with the aid of ultrasound. Landmark-guided TAP block is described as: the site of needle insertion is immediately anterior to latissimo iliac point (LIP) and just superior to the iliac crest, in the triangle of Petit. McDonnell et al. [3] recommend penetration of the oblique muscle fascia represented as, seeking a double-pop as the end point for needle insertion whereas Rafi [4], on the other hand, recommends passing the needle tip over external lip of the iliac crest until a single pop is obtained. Ultrasound guidance has made this block more appealing because it improves the performance of the practitioner and increases the rate of successful blocks.

Abdominal blocks are also attractive alternatives for epidural anesthesia when performed with ultrasound guidance, as they can be performed during general anesthesia and in the supine position. Abdominal blocks can also be used to relieve visceral pain in patients undergoing surgery. However, inter-individual variability in spread and efficacy of these blocks makes these blocks most useful as part of a multimodal analgesic regimen. The abdominal wall is anatomically complex and small anatomical differences in needle tip placement can result in clinically significant differences between what seem to be otherwise similar techniques. In this manuscript we will discuss information regarding abdomen wall blocks, their advantages, disadvantages, recent advances in techniques, anatomy, indications, and complications for each block.

2 Anatomy of Abdomen

2.1 Transversus Abdominis Plane (TAP)

The lateral part of anterior abdominal wall consists of three layers of muscles: Tranversus abdominis (TA, inner most layer), the internal oblique (IO, middle layer) and the external oblique muscle (EO, outermost layer) (Fig. 1). The plane between the transversus abdominis and internal oblique muscles is referred to as Transversus Abdominis Plane (TAP). The ventral rami of T7-T12 spinal thoracic nerves run in this plane, which are responsible for the segmental cutaneous nerve supply of abdominal wall and TAP block aims to anesthetize these

---

S. Patil · A. Kallurkar · Y. Rapoport · P. Thakur
E. M. Cornett (✉)
Department of Anesthesiology, LSU Health Shreveport,
Shreveport, LA, USA
e-mail: spati1@lsuhsc.edu; yrapop@lsuhsc.edu;
pthaku@lsuhsc.edu

A. P. Bourgeois · M. R. Eng
Department of Anesthesiology, LSU Health Sciences Center,
New Orleans, LA, USA
e-mail: abour7@lsuhsc.edu; meng@lsuhsc.edu

A. D. Kaye
Departments of Anesthesiology and Pharmacology, Toxicology,
and Neurosciences, Lousiana State University Health Sciences
Center, Shreveport, LA, USA

Department of Anesthesiology, Department of Pharmacology
Louisiana State University School of Medicine, Louisiana State
University Health Sciences Center, New Orleans, LA, USA
e-mail: akaye@lsuhsc.edu

© Springer Nature Switzerland AG 2021
J. Li et al. (eds.), *Ultrasound Fundamentals*, https://doi.org/10.1007/978-3-030-46839-2_22

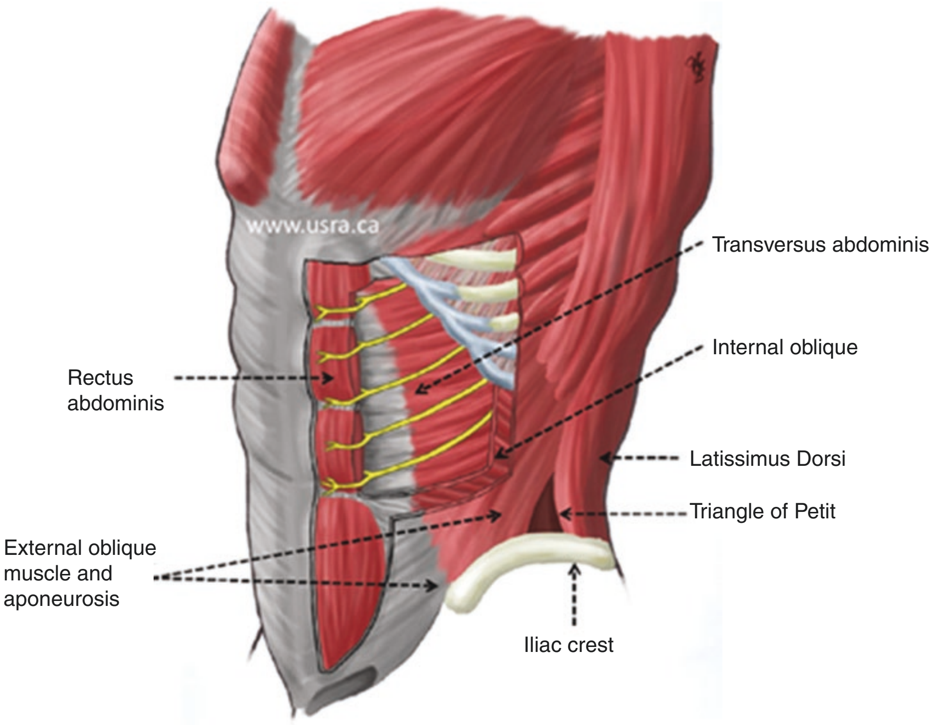

Fig. 1 muscular layers of anterior abdominal wall with spinal nerves in the plane between internal oblique muscle and transversus abdominis muscle. (Image courtesy- www.usra.ca)

anterior rami. TAP block was first introduced by A.N. Rafi [5] in 2001 and is increasingly becoming popular as an effective adjunct for analgesia in abdominal and inguinal surgeries.

2.2 Transversalis Fascia Plane (TFP)

A conventional TAP block needs a posterior approach to anesthetize the lateral cutaneous nerves of T7-T12 nerves. However, it is challenging to perform a nerve block of the lateral cutaneous branches of subcostal and iliohypogastric nerves, necessitating a different technique [17], and Transversalis Fascia Plane (TFP) block (Fig. 2) helps solve this problem.

Transversalis fascia (TF) is a thin aponeurotic membrane which is located between the inner surface of the transversus abdominis muscle (TA) and parietal peritoneum. In a TFP block, local anesthetic injected between the TA and TF will spread over the inner surface of the quadratus lumborum muscle (QL), blocking the proximal portions of the T12 and L1 nerves. This will produce a nerve block of both anterior and lateral branches of these nerves. TFP block targets the anatomical area between the lumbar plexus block and TAP block. During TFP block, similar to TAP block, the needle tip is directed just deep to the fascia of the TA, anterolateral to QL [18].

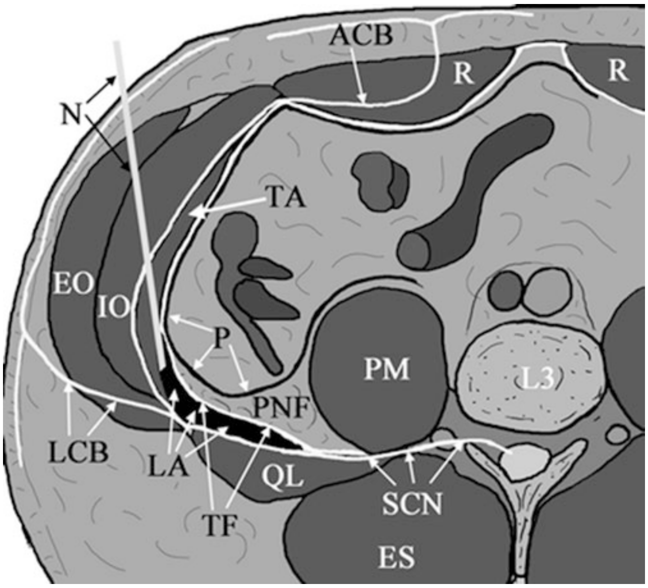

Fig. 2 Transverse diagram through the abdomen above the iliac crest. The location of the local anesthetic (LA) across the anterior surface of the quadratus lumborum (QL) and behind the transversalis fascia (TF) is shown. The following muscles are involved: rectus abdominis (R), erector spinae (ES), psoas (PM), transversus abdominis (TA), internal oblique (IO), and external oblique (EO). (Reprinted by permission from Springer, Hebbard et al. [17])

2.3 Structure of a Typical Thoracolumbar Spinal Nerve

Each spinal nerve divides into an anterior and a posterior primary ramus after they exit from the intervertebral foramen. The anterior ramus branches into lateral and anterior cutaneous nerves, while the posterior ramus travels backward. The anterolateral abdominal wall is primarily innervated by the anterior rami of the T6-L1 thoracolumbar spinal nerves, which become the intercostal (T6- T11), subcostal (T12), and ilioinguinal/iliohypogastric nerves (L1). These branches further communicate at multiple locations around the rectus sheath forming intercostal, upper TAP, lower TAP and rectus sheath plexus [19] (Fig. 3a, b).

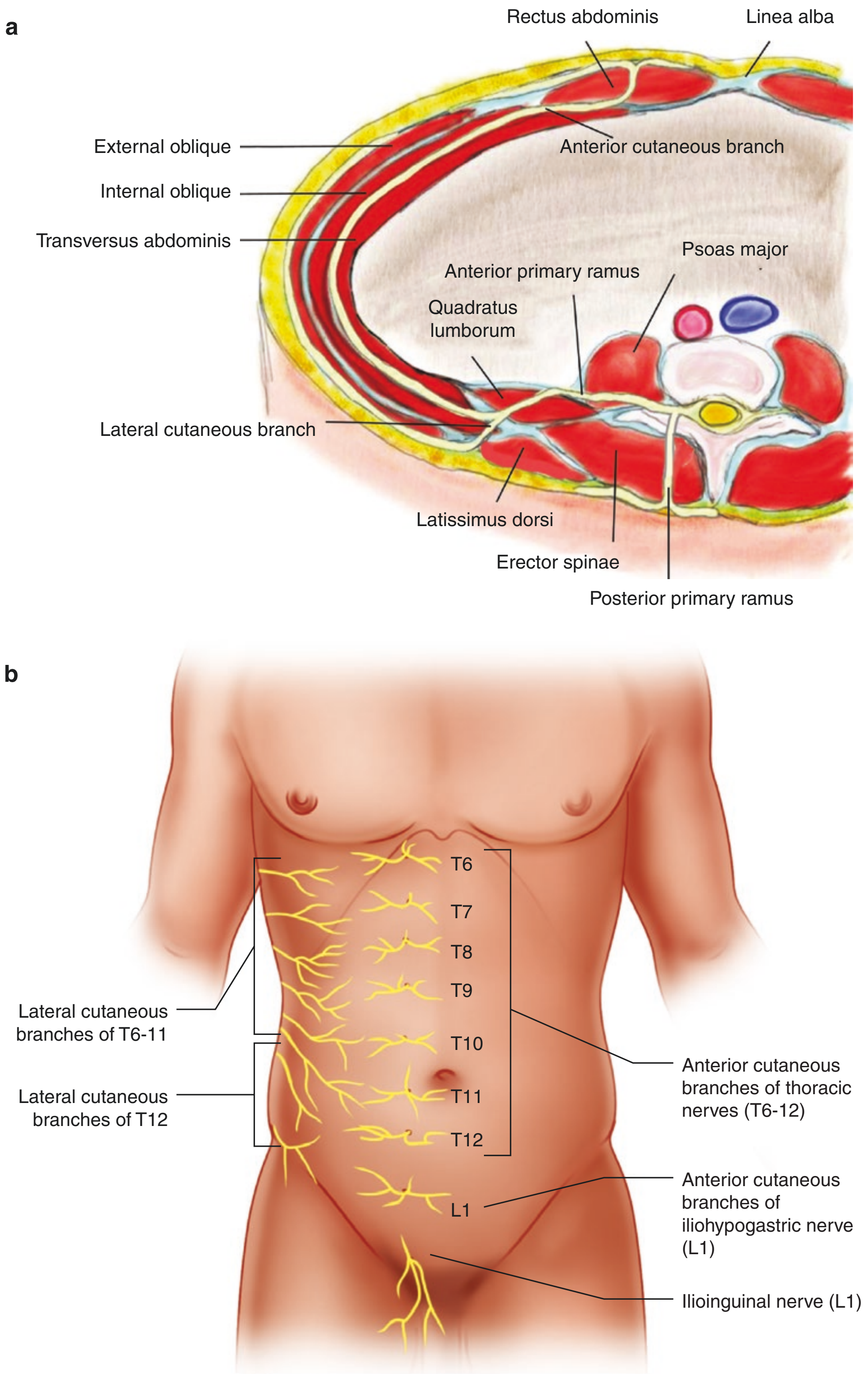
a
Rectus abdominis
Linea alba
External oblique
Anterior cutaneous branch
Internal oblique
Transversus abdominis
Psoas major
Anterior primary ramus
Quadratus lumborum
Lateral cutaneous branch
Latissimus dorsi
Erector spinae
Posterior primary ramus
b
T6
T7
T8
T9
T10
T11
T12
L1
Lateral cutaneous branches of T6-11
Lateral cutaneous branches of T12
Anterior cutaneous branches of thoracic nerves (T6-12)
Anterior cutaneous branches of iliohypogastric nerve (L1)
Ilioinguinal nerve (L1)

Fig. 3 (**a**) A representation of the pathway of the thoracolumbar spinal nerves (T12). This view of the left abdomen is cross-sectional. The anterolateral wall is supplied by the anterior ramus of the segmental nerves, which is further divided into anterior and lateral cutaneous branches. (**b**) The segmental distribution of cutaneous nerve on the anterolateral trunk. (Image courtesy-Hsiao-Chien Tsai et al. [31])

Anterior rami of T7-T12 nerves pass between internal oblique muscle (IO) and TA in TAP, piercing through rectus abdominis and form the anterior cutaneous branches which innervate the anterior abdominal wall from midline to midclavicular line. Anterior rami of T12 (subcostal nerve) crosses QL before entering TAP. While T6-T8 nerves supply the area below the xiphoid and parallel to the costal margin, T9-T12 nerves supply the periumbilical area and the lateral abdominal wall between the costal margin and iliac crest and L1 nerve supplies the anterior abdomen near the inguinal area and thigh [20]. The iliohypogastric (T12, L1) and ilioinguinal nerves (L1) are the terminal branches of lumbar plexus. These nerves emerge at lateral border of psoas major muscle and pass anterior to QL. They pierce lumbar fascia at the lateral border of QL and run in the plane between IO and TA. The iliohypogastric nerve further passes through IO and runs under external oblique muscle (EO), superior to the inguinal canal. Both these terminal branches innervate the skin of gluteal region, hypogastric region, upper medial part of thigh. They also innervate anterior scrotum in males and skin over mons pubis and labia majora in females.

The lateral cutaneous branches emerge near the angle of rib posteriorly. The lateral cutaneous branches of T7-T11 nerves then divide into anterior and posterior branches: the anterior branches supply the abdominal wall toward the lateral margin of rectus abdominis, and the posterior branches run posteriorly to supply the skin over latissimus dorsi. However, the lateral cutaneous branch of T12 nerve continues without any further bifurcation and supplies a part of the gluteal region. The subcostal and iliohypogastric nerves pass deep to the anterior surface of QL, which extends from 12th rib to iliac crest.

Since the lateral cutaneous branches of these thoracolumbar spinal nerves leave TAP posterior to the midaxillary line, a posterior approach may allow the TAP block to capture these nerves before entering the TAP where they undergo extensive branching and anastomoses. Most of the lateral cutaneous branches arise before the main spinal nerves enter TAP. This approach also has the potential to provide some degree of analgesia to lateral abdominal wall [11]. Other advantages of the posterior compared to the lateral technique include prolonged analgesia [21] and retrograde spread of the drug into paravertebral space [22].

L1 branches, which divide into ilioinguinal and iliohypogastric nerves, pass into TAP near the anterior part of the iliac crest. In pediatric cases, a direct ilioinguinal/iliohypogastric nerve block provides better analgesia for inguinal hernia surgeries than the TAP block [23].

2.4 Anatomy of Quadratus Lumborum Muscle (QL) and Thoracolumbar Fascia (TLF)

The quadratus lumborum muscle is a part of the posterior abdominal wall and is a continuation of transversus abdominis muscle. Quadratus lumborum muscle (QL) block is the extension of TAP block towards the dorsal region and involves an injection of a local anesthetic into the thoracolumbar fascia (TLF) (see Fig. 4). QL block in a single shot has the advantage of covering all the dermatomal segments from L2 to T4 segments as the drug is expected to travel from

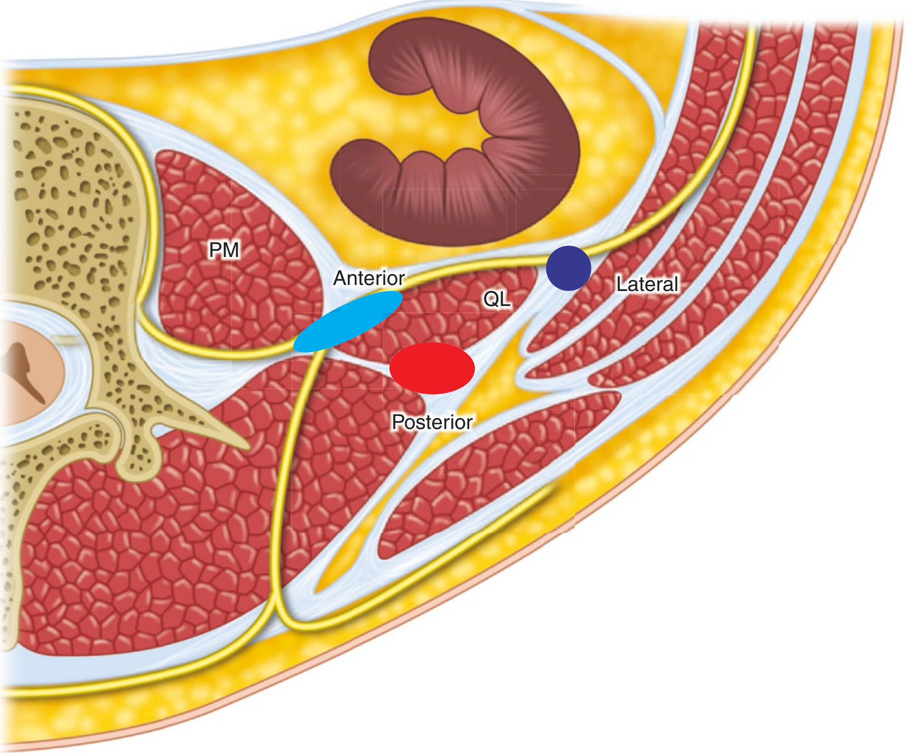

Fig. 4 Anatomic view of quadratus lumborum (QL) block (anterior, lateral, and posterior). The lateral QL block injects the local anesthetic at the lateral to the QL muscle. The posterior QL block injects the local anesthetic at the posterior to the QL muscle. The anterior QL block injected the local anesthetic between the PM muscle and the QL muscle. QL quadratus lumborum muscle, PM psoas major muscle, and gray line transversalis fascia. (Image and caption are used with permission, Hironobu Ueshima et al. [28])

the QL to higher paravertebral spaces. Many cadaver studies as well as imaging studies with dye have confirmed the spread of the anesthetic drug cranially up to lumbar nerve roots [24], paravertebral space [1], somatic nerves and thoracic sympathetic trunk in paravertebral spaces [25].

TLF is a sheet of fused aponeuroses and fascial layers that encases the muscles of the back extending from thoracic to lumbar spine. TLF is attached to the thoracic and lumbar vertebrae on its medial side, it continues with endothoracic fascia and fascia iliaca in the cephalic and caudal directions respectively. Local anesthetic drug spreads along the TLF and the endothoracic fascia into the paravertebral space, and is partly responsible for analgesia by the QL block [26]. Additionally, in the superficial layer of TLF, there is a thick network of sympathetic neurons and there are high-threshold and low-threshold mechanoreceptors and pain receptors sensitive to effects of the local anesthetics in TLF. These receptors may play a role in the development of both acute and chronic pain. QL block analgesia could at least partially be explained by the blockade of these receptors [27].

TLF is divided into 3 layers (anterior, middle, and posterior) around the muscles of the back. The anterior layer is anterior to QL, which also blends medially with the fascia of psoas major (PM) medially and with transversalis fascia laterally (see Fig. 5). Hence an anterior QL block includes injecting the drug between PM and QL muscles and the space between these muscles contain branches of lumbar plexus. Injection between the anterior layer of TLF and QL can reach the lower thoracic paravertebral space posterior to the endothoracic fascia [28]. The middle layer is located between QL and erector spinae muscles forming the site of injection for a posterior QL block, specifically into a space called lumbar interfascial triangle (LIFT), an area between middle fibers of TLF and paraspinal reticular sheath at the lateral border of erector spinae. The posterior layer of TLF encloses the erector spinae. Compared to TAP block, QL block carries an advantage of widespread coverage [14] and thereby leading to superior analgesia [29] for abdominal surgeries.

2.5 Lumbar Arteries

There are four paired lumbar arteries originating as posterolateral branches of the abdominal aorta on either side, at the level of L1-L4. These paired arteries course posterolateral to the vertebral bodies, then pass under the tendinous arches of PM and sympathetic trunks. After crossing QL, these arteries enter the space between the TA and IO muscles (see Fig. 6). Lumbar arteries form anastomoses with lower intercostal, subcostal, iliolumbar, deep circumflex iliac, inferior epigastric and contralateral lumbar arteries. A fifth pair of lumbar arteries may be occasionally present, typically smaller in caliber, arising from the median sacral artery [30]. See Fig. 7.

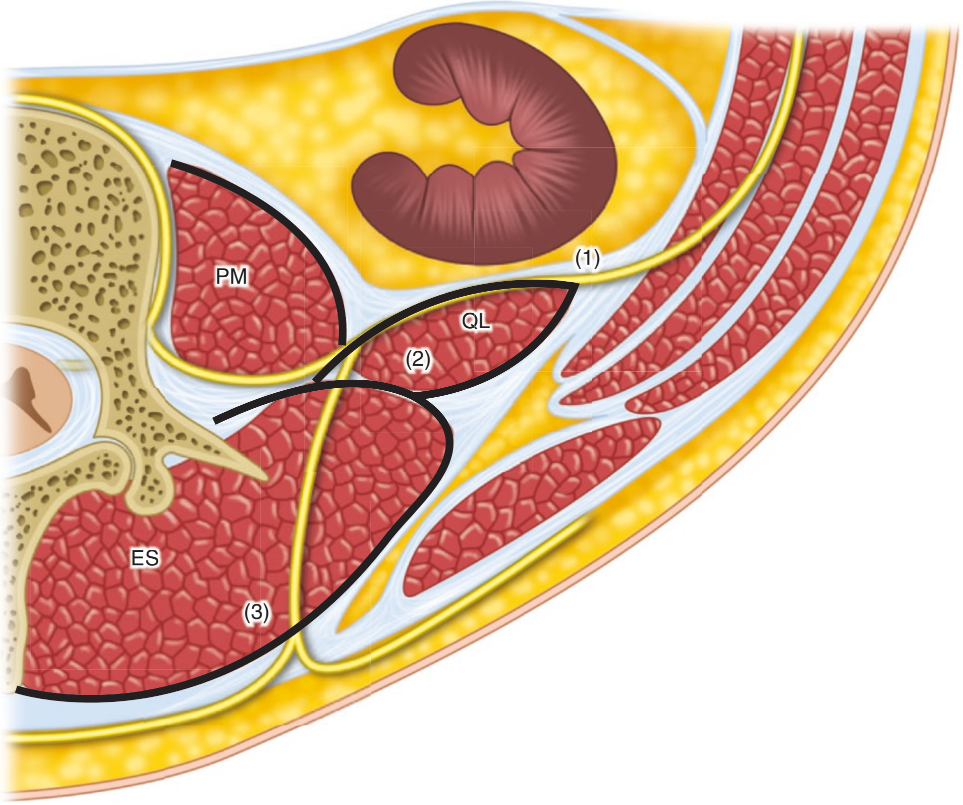

Fig. 5 Anatomic view of the thoracolumbar fascia (TLF) highlighted in black. The TLF is divided into 3 layers (anterior (1), middle (2), and posterior (3)). QL quadratus lumborum, ES erector spinae, and PM psoas major. (Image courtesy – Hironobu Ueshima et al. [28])

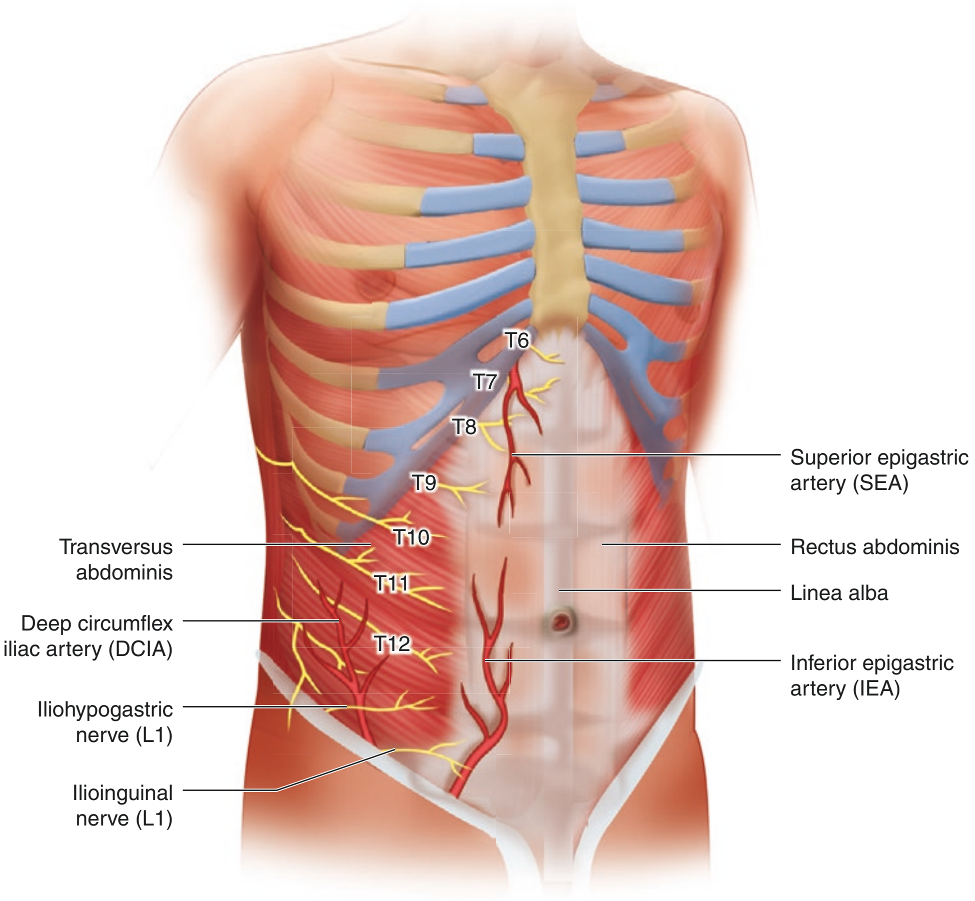
T6
T7
T8
T9
T10
T11
T12
Superior epigastric artery (SEA)
Transversus abdominis
Rectus abdominis
Linea alba
Deep circumflex iliac artery (DCIA)
Inferior epigastric artery (IEA)
Iliohypogastric nerve (L1)
Ilioinguinal nerve (L1)

Fig. 6 Distribution of neurovascular structure in the anterolateral abdominal wall. (Image courtesy- Hsiao-Chien Tsai et al. [31])

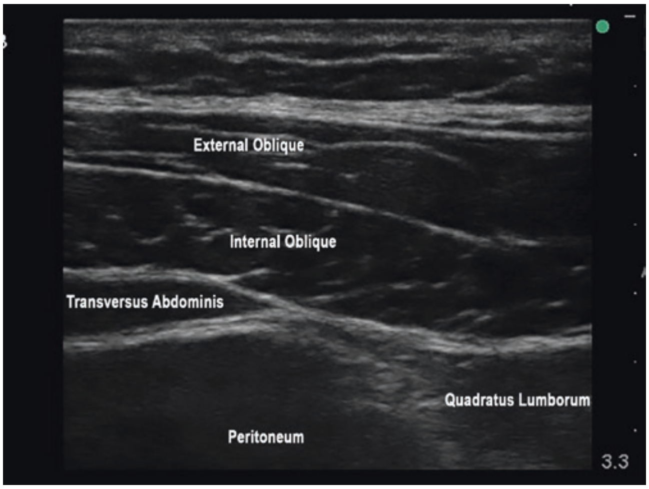
External Oblique
Internal Oblique
Transversus Abdominis
Quadratus Lumborum
Peritoneum
3.3

Fig. 7 Anatomical ultrasound of the Quadratus lumborum

3 Abdominal Wall Blocks

3.1 TAP Block

TAP block provides analgesia to the anterolateral abdominal wall. Classic TAP block technique, as was originally described by Rafi [5], implied injection of a local anesthetic preparation into a potential anatomical space between the internal oblique and transversus abdominis muscles in the area of the triangle of Petit, utilizing landmark technique.

Since the emergence of the method in 2001, it has proved its efficacy, safety, and evolved in many ways. Advancement in ultrasound technology allowed for more precise injection and spread of local anesthetic and lead to development of

Table 1 Variations of TAP blocks and corresponding nerve distribution area

Approach	Thoracolumbar nerves	Supplied area
Lateral	T10-T12	Infraumbilical part of anterior abdominal wall to midclavicular line
Posterior	T9-T12	As above + lateral abdominal wall
Subcostal	T6-T9	Upper abdominal wall above the umbilicus, parallel to the costal margin
Subcostal oblique	T6-L1	Entire abdominal wall

multitude of modifications in order to improve the distribution of the anesthesia and duration of pain relief. Currently, ultrasound –guided TAP block with "in-line" needle insertion is the gold standard of the procedure. A growing body of evidence supports the effectiveness of TAP block and its modifications for an array of abdominal surgeries both above and below the umbilicus including cesarean section, cholecystectomy, colectomy, prostatectomy, hernia repair and many others [6–8].

3.2 Nomenclature

Several TAP block modifications have emerged into practice in attempt to provide improved anesthetic coverage, however, well established and universally accepted nomenclature is still lacking. TAP block is a field block, thus the effect is mediated by wide spread of local anesthetic within the plane. Radiologic evaluation of the dye spread in several cadaveric studies revealed that there is more limited segmental nerve involvement than earlier though, when single approach is utilized [9, 10]. Thus, it is reasonable to categorize TAP block modifications based on the anatomical segments that are anesthetized. Subcostal (SCTAP) with its amended oblique subcostal version, posterior and lateral approaches are recognized (Fig. 1). Subcostal approach of the TAP block is believed to anesthetize the nerves around T6–T9. Lateral approach, with appropriate spread may block nerve roots of T10– T11 and cover the T12 distribution. Posterior TAP may extend the block to L1. (Table 1). All the above approaches can be used as a one single shot block, or combined consecutive blocks comprising of 2 or all 3.

3.3 Lateral TAP Block

With the patient supine, the ultrasound probe is placed in the midaxillary line just above the umbilicus, between the iliac crest and costal margin (Fig. 7). Three muscle layers are then identified. It may be necessary to scan the abdomen horizontally to identify rectus muscles first and then slide the probe laterally if the initial picture is not optimal and the structures are not easily visualized. Needle is then inserted at approximately 45-degree angle parallel to the long axis of the transducer on its medial side and advanced under constant visualization. Once needle reaches transversus abdominis muscle, it is then slowly withdrawn. When the tip of the needle is presumed to be in the plane between transversus and internal oblique muscles aspiration is performed. If aspiration is negative the plane is hydrodissected. One should see hypoechoic, elliptic spread of the injectate along with the separation of the fascial layers. Otherwise the needle should be repositioned.

3.4 Posterior TAP Block

Posterior approach is similar to lateral, with the difference that the probe is relocated immediately posterior to the midaxilary line so that one could see the transverse abdominis muscle tailing off and forming aponeurosis (Fig. 7). The injection is performed superficial to aponeurosis. It has been proposed and demonstrated in several studies that posterior approach provides better spread, more extensive posterior coverage of analgesia and longer duration compared to lateral alone [11].

3.5 Subcostal TAP Block

Since lateral and posterior TAP blocks provide analgesia only for abdominal surgeries below the umbilicus, subcostal approach (SCTAP) was developed in attempt to cover the upper abdomen for procedures extending supraumbilically. With patient supine, the probe is positioned close to the xiphoid process and parallel to the ipsilateral costal margin (Fig. 8a). Rectus muscle and transversus abdominis muscle are initially identified. Needle is then inserted in line with the probe pointing laterally and advanced until the tip reaches the fascia between 2 muscles, aiming to inject anesthetic medially to linea semilunaris.

Oblique subcostal block is a modification of the original single shot oblique approach. The block starts in a similar fashion as regular subcostal block, however after the plane between the muscles is hydrodissected and the pocket is created, the needle is slowly advanced laterally and down along the imaginary oblique subcostal line under direct ultrasounds guidance (Fig. 8b). Dynamic injection is performed while the needle is being advanced. Longer needle and more volume of local anesthetic is usually required. This allows for more extensive spread and broader coverage.

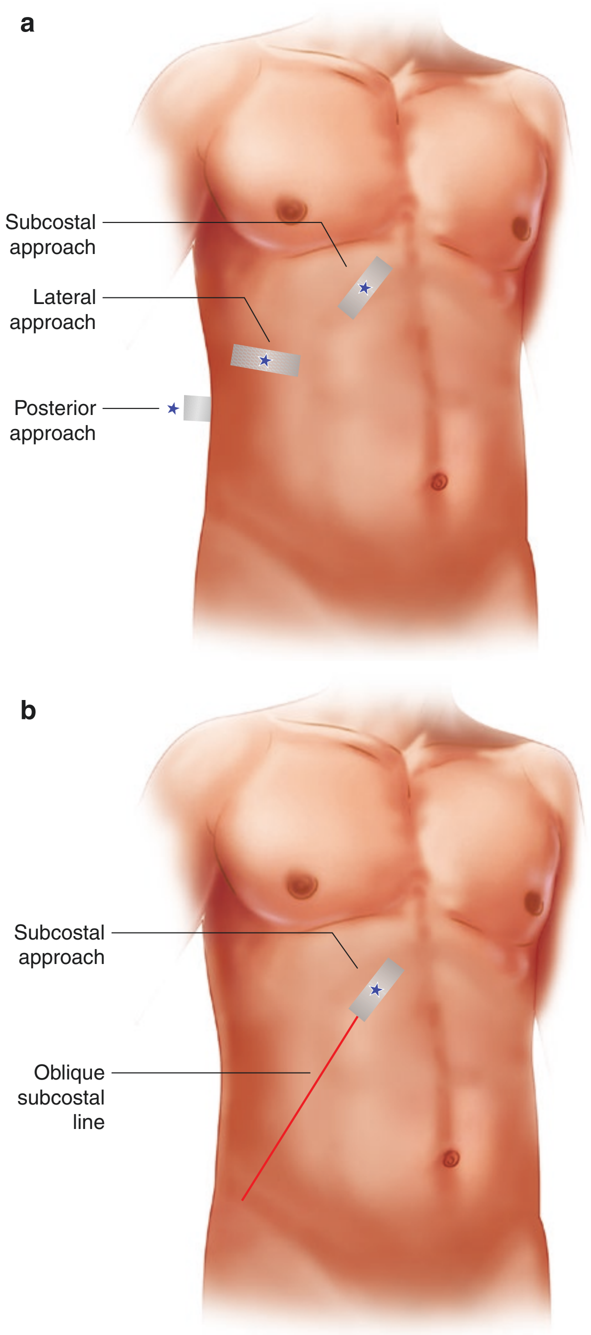

Fig. 8 (**a**) Three most common approaches of ultrasound guided Transversus abdominis plane blocks. (**b**) Probe position for Subcostal oblique block

The above-mentioned techniques can be combined and provide superior anesthesia for more extensive abdominal procedures involving both supraumbilical and infraumbilical territory (Table 1). So called dual TAP or four- quadrant TAP involves combination of SCTAP and Lateral/Posterior TAP unilaterally or bilaterally.

If prolonged anesthesia of the abdominal wall is required, continuous TAP block can be employed. This involves threading a perineural catheter into the TAP plane. More research is needed to fully validate this method.

3.6 Local Anesthetics and Complications

Amide-type anesthetics are widely utilized for TAP block with low concentration Bupivacaine (0.25%), Levobupivacaine or Ropivacaine (0.5%) being the most common options. Duration of action is typically 6–8 hrs. 15–20 ml of LA needs to be injected at one site to provide adequate spread. Adjuncts may be added to achieve longer duration. Epinephrine, opioids, dexamethasone, to name a few. Liposomal bupivacaine was approved for several field blocks including TAP blocks and some studies demonstrated duration of action up to 72 hours [12].

TAP block is considered a low risk procedure. One should avoid high injection pressure (above 15 psi) to reduce the risk of nerve damage. Ultrasound guidance significantly decreases risk of serious complications; cases of inadvertent peritoneal puncture have been reported. Local anesthetic toxicity is a possible complication, thus low concentration of anesthetics should be utilized given the large volume nature of the block, especially if several injections are performed. Patients should be monitored for signs of systemic local anesthetic toxicity and lipid emulsion needs to be readily available. Excessive spread to lower extremity compartments can lead to temporary femoral nerve paralysis, however, is usually self-limited.

3.7 Quadratum Lumborum Block

While TAP block was proven to effectively block somatic pain in the area of anterolateral abdominal wall, the need for more extensive and wider anesthetic coverage continued to persist. In 2007, a new approach came out and was initially described as extension of TAP which would provide analgesia to the posterior abdominal wall region along with anterior abdomen coverage [13]. Moreover, it was aimed to add visceral analgesic properties. The technique was later named Quadratum lumborum block (QLB) as quadratus lumborum muscle is the major ultrasound landmark for this procedure. Whereas thoracolumbar fascia is the cornerstone structure explaining the wide spread of the anesthetic, the exact mechanism of how the analgesia is produced is yet to be elucidated. It has been proposed that the effect is partially mediated through the spread of the anesthetic into the paravertebral space or even epidural space. This could explain visceral analgesia. However, this remains controversial. Another possible explanation lies in the light of anesthetic spread into intercostal space thus providing coverage for somatic nerves. Caudal spread may reach lumbar nerve roots, but this may vary and explains variations in the width of anesthesia reported by several authors. Most indications for QL block are overlapping with those for TAP block, including cesarean section, gynecologic procedures, abdominal surgery. Several reports of the block efficiency after percutaneous nephrolithotomy or nephrolithotripsy, nephrectomy, lumbar vertebrae surgery, femur surgery and vascular procedures involving femoral vessels exist, however very limited data is available [14, 15]. More studies are required to support these hypotheses. Block is performed under constant ultrasound guidance.

3.8 Types of QLB and Technical Aspects

The procedure can be accomplished with patient in the supine position and the table slightly tilted to the opposite side for optimal exposure. Alternatively, patient can be placed in lateral position. The transversally oriented ultrasound probe is placed between iliac crest and costal margin along the middle axillary line. After identification of the 3 abdominal muscles, the probe is slowly moved posteriorly until the muscles start fading and finally taper off into an aponeurosis. Quadratus lumborum muscle is then identified, just anterior to aponeurosis. Needle is inserted at 90-degree angle. After skin perforation, needle is then redirected in the selected direction based on the type of QL block being performed. After reaching the desired location and negative aspiration test, incremental injection is performed while looking for separation of muscle and fascia.

Four types of QLB blocks have been described. Similar to TAP blocks, universally accepted terminology is yet to be developed. Quadratum lumborum block 1or lateral block involves deposition of local anesthetic on the lateral side of QL muscle where it lies adjacent to transversalis fascia (Fig. 9). Quadratum lumborum block 2 or posterior block involves deposition of the anesthetic between the posterior side of the QL muscle and thoracolumbar fascia (Fig. 9). Quadratum lumborum block 3 or anterior block implies deposition of the anesthetic near the front aspect of the muscle at the level of its attachment to the L4 transversus process. Spread should be visualized between QL muscle and Psoas major muscle (Fig. 9). When performing Quadratum lumborum block 4 or intramuscular block, anesthetic is deposited directly into the QL muscle. Different approaches signify various spreads and thus all four can be combined. The optimal strategy remains subject of debate.

Another relatively new modality is the transversalis fascia plane block (TFP block), which was designed to produce block of the L1 nerve branches, the ilioinguinal and iliohypogastric nerves. This approach is very similar to QLB, however, they were developed independently. Local anesthetic is deposited between the transversalis fascia and the fascia of the transversus abdominis muscle. The block may provide pain relief following anterior iliac crest bone graft harvesting. More research is needed.

3.9 Local Anesthetics and Complications

Complications associated with abdominal wall blocks are relatively rare and can be divided into 3 main categories: needle or mechanical trauma, maldistribution of local anesthetic, and local anesthetic systemic toxicity (LAST) [2].

QL block, as well as TAP block, is a field or plane block. Therefore, a large volume of local anesthetic is required to achieve a desired effect. Total 20–30 mL of low concentration, diluted anesthetic is recommended to be administered unilaterally. The composition of the anesthetic preparation is similar to TAP block. Potential contributing factors for LAST in abdominal wall blocks include the use of relatively

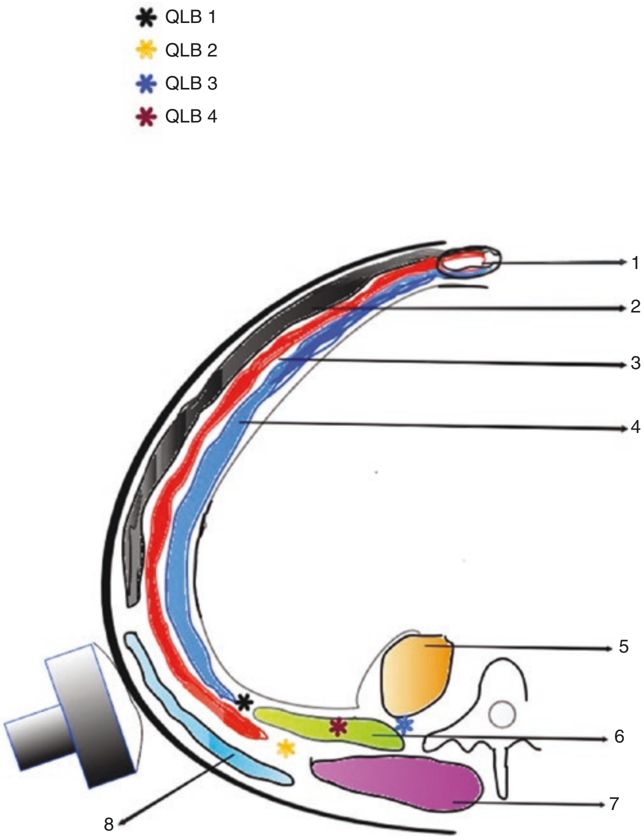

Fig. 9 Cross-section of the abdomen at the level of L5 vertebra with ultrasound probe. QLB 1—injection location for QLB 1, QLB 2—injection location for QLB 2, QLB 3— injection location for QLB 3, QLB 4— injection location for QLB 4. 1—rectus abdominis muscle, 2—external oblique muscle, 3—internal oblique muscle, 4 –transversus abdominis muscle, 5—psoas major muscle, 6—quadratus lumborum muscle, 7—erectores spinae muscle, 8—latissimus dorsi muscle

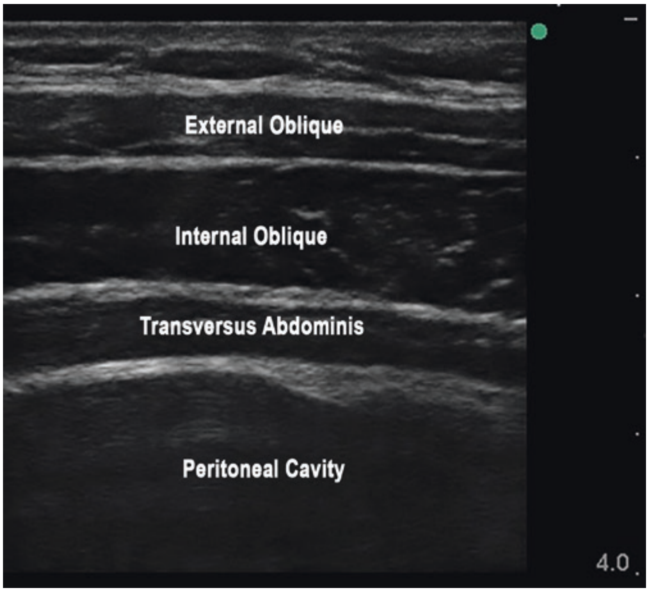

Fig. 10 TAP block anatomy without needle

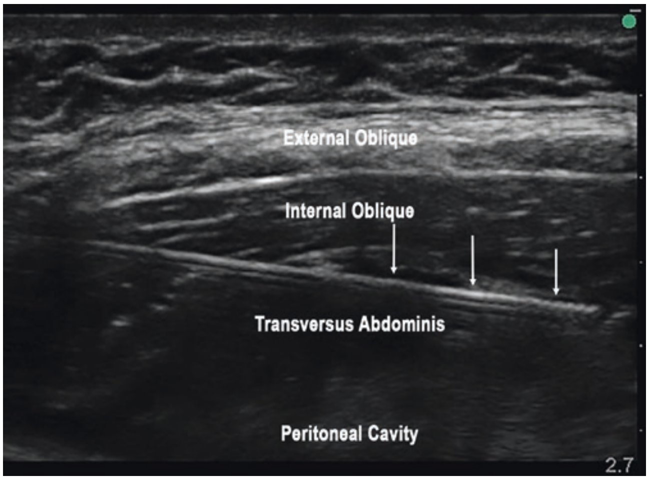

Fig. 11 TAP block anatomy with needle

large injection volumes to ensure adequate spread and bilateral blocks to cover midline incisions. While local anesthetic systemic toxicity is a concern, studies showed that end plasma concentration of the local anesthetic (ropivacaine) is significantly lower compared to that after TAP block, considering that equal amount of drug is given [16]. This signifies possible less vascular uptake compared to TAP block and theoretically lower risk of systemic toxicity.

There is a risk of needle trauma to the peritoneum and solid organs due to relative proximity to the kidney, liver, major blood vessels, thus adherence to constant needle visualization under ultrasound is strictly encouraged. No neurological complications have been reported as no large neural tissue is present in the immediate proximity to the QL planes. See Figs. 10 and 11.

3.10 Rectus Sheath Block

Rectus sheath block entails deposition of local anesthetic into potential space between the rectus abdominis muscles and the posterior fascial layer of rectus sheath. The block is performed above the umbilicus on both sides of the abdomen and is helpful in providing supplementary or primary postoperative analgesia after umbilical hernia repair or other procedures involving midline abdominal incision. Besides two rectus abdominis muscles and linea alba separating them, the inferior and superior epigastric vessels along with five inferior branches of intercostal and subcostal nerves are situated within the sheath. Block is performed under ultrasound guidance and large volume of local anesthetic is placed to achieve full anesthetic effect. Peritoneal and visceral perforation is possible thus tip of the needle should be constantly visualized. Few case reports demonstrating prolonged pain relief with continuous rectus sheath block involving catheter placement exist. However, limited data on the efficacy of the block is available.

A summary of type of block and corresponding dermatome can be found in Table 2.

4 Indications of Abdominal Wall Blocks

Selecting a prime candidate for abdominal wall blocks entails a thorough history and physical exam along with proper risk stratification of patients. The list below can be used to help physicians evaluate whether a patient is a good candidate for an abdominal block.

1. Patient's refusal for "spinal tap"
2. Surgeon's preference
3. Superficial skin site infection or sepsis for placement of neuroaxial anesthesia
4. Burn patients
5. Prerenal hypovolemic state that is contraindicated for neuroaxial anesthesia
6. Decompensated cardiac function (low EF, aortic stenosis)
7. Bleeding diathesis
8. Elevated Intracranial pressure, intracranial mass, traumatic head injury
9. Patients at a high risk for postoperative nausea and vomiting (PONV)
10. Obstructive sleep apnea patients at risk from increased opioid dosing. Patients with chronic pain and opioid tolerance
11. Patients with Muscular Dystrophy (Duchenne Muscular Dystrophy, Beckers Muscular Dystrophy)
12. Amyotrophic Lateral Sclerosis
13. Demyelinating disorders (Multiple Sclerosis)

Table 2 Surgery, dermatome and type of block used

Surgery	Dermatome	Type of block
Laparoscopic cholecystectomy	T7-L1	Rectus sheath block with right sided subcostal TAP block
Abdominoplasty	T7-L1	TAP block (triangle of Petit). Additional of subcostal TAP block will provide supra umbilical coverage and anesthetize entire abdominal wall [1].
Open/laparoscopy appendectomy	T10-L1	TAP block
Post cesarean section analgesia	T7-L1	TAP block
Total abdominal hysterectomy	L1 and blocks lateral and anterior cutaneous branches of the nerves; T10-L1	Bilateral ilioinguinal and iliohypogastric block, bilateral TAP block
Bowel resection	T7-L1	TAP block
Renal transplant	T7-L1	TAP block
Nephrectomy	Flank incision: T9-T11 Thoracoabdominal incision: T7-T12 Transabdominal incision: T6-T10	TAP block complemented with paravertebral block
Prostate bladder and ureteral surgeries	T7-L1	TAP block
Anterior iliac crest bone graft	T10-L1 T12-L1	TAP block Transversalis fascia block
Ileostomy, colostomy	T7-L1	Combination of ilioinguinal. Iliohypogastric, rectus sheath and TAP blocks.
Exploratory laparotomy	T7-L1	Bilateral rectus sheath and TAP block
Midline incision-bilateral block	T7-L1	Bilateral rectus sheath and bilateral TAP block
Inguinal hernia, hydrocele, orchidopexy	T12-L1	Ilioinguinal/iliohypogastric nerve block, TAP block
In children: midline incisions (umbilical hernia, pyloromyotomy, laparoscopic surgery, urachus cyst)	T7-T12	Rectus sheath block with right sided subcostal TAP block
Robot assisted prostatectomy	T12-L1	TAP block

14. Patients at risk for Malignant Hyperthermia with Volatile Anesthetics (Muscular Dystrophy)
15. Spinal deformities complicating placement of neuroaxial anesthesia

5 Summary and Conclusion

The 2016 ASA guidelines on ERAS and the American Society of Regional Anesthesia and Pain Medicine (ASRA) both state that the multimodal and interdisciplinary approach is recommended for control of acute pain and reducing nociceptive transmission. Regional anesthesia fulfills this role and has an immense impact in current practice of modern-day anesthesia, that can be applied for various abdominal surgeries without much alterations in hemodynamic status. Abdominal wall regional blocks generally do not provide analgesia beyond anterior axillary line but when combined with blocks like Quadratus lumborum block, they provide excellent somatic and visceral analgesia. Anesthesia for supra umbilical incisions can be accomplished with subcostal blocks, whereas laterally placed TAP blocks provide analgesia for T10-T12 dermatome. With the evolution of less invasive and improved postoperative monitoring, regional anesthesia provides the anesthesiologist with a choice other than neuraxial anesthesia, for control of acute pain and avoiding potential complications associated with general anesthesia. This, most certainly, not only reduces patients' systemic opioid requirements, decreasing side effects and FAST TRACKING patient in the post anesthetic care unit, but also avoid procedural complication from neuraxial anesthesia.

Recent advances in perioperative medicine and newer recommendations certainly support the use of safer multimodal anesthesia techniques. When presenting options for choice of anesthesia for abdominal wall surgeries, most patients consent and prefer regional anesthesia. These sophisticated techniques provide excellent surgical anesthesia and a delivery system for postoperative pain control. Using local anesthetics and opioid in synergy avoids the increased need of postoperative medication and the potential for systemic drug toxicity. Despite all the added advantages and procedure benefit as listed above, thorough risk stratifications must be practiced when considering abdominal wall blocks. Although small, these procedures still involve risk of local anesthetic toxicity if given large volume of local anesthetic involved (LAST); especially if bilateral blocks are needed in surgeries involving midline or transverse incisions. Other potential complications may include mechanical trauma from needle, inadvertent intra peritoneal or intravascular injection, visceral injury and injection site infection. With the use of ultrasound modality, inadvertent outcomes could be avoided. Patients understanding of the procedure and cooperation can be limiting factor for the procedure success. Some patients may even experience variable blocks or even block failure with need to convert to general anesthesia.

Absolute contraindications for regional anesthesia include, patient refusal and cooperation, signs of infection over the intended site of injection, coagulopathy and previous documented local anesthetics allergies. It may also be contraindicated to pursue regional anesthesia in uncooperative patients or pediatric patients, primarily in their inability to stay still while placing the block. Given the safety of evolving techniques that are now being employed in the abdominal wall surgeries along with knowledge of anatomy and procedural dexterity, these techniques are taking precedence over neuraxial anesthesia with excellent postoperative outcomes and improved patient satisfaction and earlier mobilization.

Nevertheless, the use of varied newer ultrasound imaging techniques in localizing fascial planes and nerve stimulation modalities, including providing direct visualization of the needle placement and anesthetic spread via hydrolocation have remarkably improved success and performances of the regional block. Thus, use of regional anesthesia techniques as compared to general anesthesia, also decreases incidence of postoperative nausea and vomiting and has less cognitive impairment. It not only improves the satisfaction of patients and earlier patient discharge; but is also cost effective, decreases the need for general or neuraxial anesthesia and their associated unwanted potential side effects.

References

1. Blanco R, Ansari T, Girgis E. Quadratus lumborum block for postoperative pain after caesarean section: a randomised controlled trial. Eur J Anaesthesiol. 2015;32(11):812–8.
2. Herring AA, Stone MB, Nagdev AD. Ultrasound-guided abdominal wall nerve blocks in the ED ☆. Am J Emerg Med. 2012;30(5):759–64.
3. Tuite D, Power C, Laffey JG, Sc B. Transversus abdominis plane block: a cadaveric and radiological evaluation. Reg Anesth Pain Med. 2007;32(5):399–404.
4. Confer- TAU. An audit of audit and continued educational and professional development. Article in Anaesthesia. 2001;56:1003–29.
5. Rafi AN. Abdominal field block: a new approach via the lumbar triangle. Anaesthesia, 2001;56(10):1024–6. https://doi.org/10.1046/j.1365-2044.2001.02279-40.x.
6. Brogi E, Kazan R, Cyr S, Giunta F, Hemmerling TM. Transversus abdominal plane block for postoperative analgesia: a systematic review and meta-analysis of randomized-controlled trials. Can J Anaesth, 2016;63(10):1184–96. https://doi.org/10.1007/s12630-016-0679-x. Epub 2016 Jun 15.
7. Champaneria R, Shah L, Geoghegan J, Gupta JK, Daniels JP. Analgesic effectiveness of transversus abdominis plane blocks after hysterectomy: a meta-analysis. Eur J Obstet Gynecol Reprod Biol, 2013;166(1):1–9. https://doi.org/10.1016/j.ejogrb.2012.09.012. Epub 2012 Oct 4.
8. Elkassabany N, Ahmed M, Malkowicz SB, Heitjan DF, Isserman JA, Ochroch EA. Comparison between the analgesic efficacy of transversus abdominis plane (TAP) block and placebo in open retropubic radical prostatectomy: a prospective, randomized, double-blinded study. J Clin Anesth, 2013;25(6):459–65. https://doi.org/10.1016/j.jclinane.2013.04.009. Epub 2013 Aug 17.
9. McDonnell JG, O'Donnell BD, Farrell T, Gough N, Tuite D, Power C, et al. Transversus abdominis plane block: a cadaveric and radiological evaluation. Reg Anesth Pain Med, 2007;32(5):399–404. https://doi.org/10.1016/j.rapm.2007.03.011.
10. Barrington MJ, Ivanusic JJ, Rozen WM, Hebbard P. Spread of injectate after ultrasound-guided subcostal transversus abdominis plane block: a cadaveric study. Anaesthesia, 2009;64(7):745–50. https://doi.org/10.1111/j.1365-2044.2009.05933.x.
11. Abdallah FW, Laffey JG, Halpern SH, Brull R. Duration of analgesic effectiveness after the posterior and lateral transversus abdominis plane block techniques for transverse lower abdominal incisions: a meta-analysis. Br J Anaesth, 2013;111(5):721–35. https://doi.org/10.1093/bja/aet214. Epub 2013 Jun 27.
12. Hutchins J, Delaney D, Vogel RI, Ghebre RG, Downs LS, Carson L, et al. Ultrasound guided subcostal transversus abdominis plane (TAP) infiltration with liposomal bupivacaine for patients undergoing robotic assisted hysterectomy: a prospective randomized controlled study. Gynecol Oncol, 2015;138(3):609–13.
13. Blanco R. Tap block under ultrasound guidance: the description of a "no pops" technique. Reg Anesth Pain Med. 2009 https://rapm.bmj.com/content/32/Suppl_1/130.2, http://dx.doi.org/10.1136/rapm-00115550-200709001-00249.
14. La Colla L, Uskova A, Ben-David B. Single-shot quadratus lumborum block for postoperative analgesia after minimally invasive hip arthroplasty a new alternative to continuous lumbar plexus block? Reg Anesth Pain Med, Jan/Feb 2017;42(1):125–126. https://doi.org/10.1097/AAP.0000000000000523.
15. Ueshima H, Hiroshi O. Lumbar vertebra surgery performed with a bilateral posterior quadratus lumborum block. J Clin Anesth, 2017;41:61. https://doi.org/10.1016/j.jclinane.2017.06.012. Epub 2017 Jul 3.
16. Murouchi T, Iwasaki S, Yamakage M. Quadratus lumborum block: analgesic effects and chronological ropivacaine concentrations after laparoscopic surgery. Reg Anesth Pain Med, Mar-Apr 2016;41(2):146–50. https://doi.org/10.1097/AAP.0000000000000349.
17. Hebbard PD. Transversalis fascia plane block, a novel ultrasound-guided abdominal wall nerve block. Can J Anaesth. 2009;56(8):618–20.
18. Chin KJ, Chan V, Hebbard P, Tan JS, Harris M, Factor D. Ultrasound-guided transversalis fascia plane block provides analgesia for anterior iliac crest bone graft harvesting. Can J Anesth Can d'anesthésie. 2012;59(1):122–3.
19. Rozen WM, Tran TMN, Ashton MW, Barrington MJ, Ivanusic JJ, Taylor GI. Refining the course of the thoracolumbar nerves: a new understanding of the innervation of the anterior abdominal wall. Clin Anat [Internet]. 2008 [cited 2016 Dec 21];21(4):325–33. Available from.: http://www.ncbi.nlm.nih.gov/pubmed/18428988.
20. Hebbard PD, Barrington MJ, Vasey C. Ultrasound-guided continuous oblique subcostal transversus abdominis plane blockade: description of anatomy and clinical technique. Reg Anesth Pain Med. 2010;35(5):436–41.
21. Yoshiyama S, Ueshima H, Sakai R, Otake H. A posterior TAP block provides more effective analgesia than a lateral TAP block in

patients undergoing laparoscopic gynecologic surgery: a retrospective Study. Anesthesiol Res Pract. 2016; 4598583. Published online 2016 Jan 28. https://doi.org/10.1155/2016/4598583.

22. Carney J, Finnerty O, Rauf J, Bergin D, Laffey JG, Mc Donnell JG. Studies on the spread of local anaesthetic solution in transversus abdominis plane blocks. Anaesthesia. 2011;66(11):1023–30.
23. Fredrickson MJ, Paine C, Hamill J. Improved analgesia with the ilioinguinal block compared to the transversus abdominis plane block after pediatric inguinal surgery: a prospective randomized trial. Paediatr Anaesth. 2010;20(11):1022–7.
24. Carline L, McLeod GA, Lamb C. A cadaver study comparing spread of dye and nerve involvement after three different quadratus lumborum blocks. Br J Anaesth. 2016;117(3):387–94.
25. Dam M, Moriggl B, Hansen CK, Hoermann R, Bendtsen TF, Børglum J. The pathway of injectate spread with the transmuscular quadratus lumborum block: a cadaver study. Anesth Analg. 2017;125(1):303–12.
26. Akerman M, Pejčić N, Veličković I. A review of the quadratus lumborum block and ERAS. Front Med. 2018;5.
27. Tesarz J, Hoheisel U, Wiedenhöfer B, Mense S. Sensory innervation of the thoracolumbar fascia in rats and humans. Neuroscience. 2011;194:302–8.
28. Ueshima H, Otake H, Lin J-A. Ultrasound-Guided Quadratus Lumborum Block: An Updated Review of Anatomy and Techniques. Biomed Res Int. 2017; 2752876., Published online 2017. https://doi.org/10.1155/2017/2752876.
29. La Colla MDL, Schroeder RMD. Quadratus lumborum block as sole, homeostatic-preserving anesthetic for a patient with multiple system atrophy undergoing open inguinal hernia repair: a case report. Case Rep Anesthesiol, 2018; 7161860. https://doi.org/10.1155/2018/7161860. eCollection 2018.
30. Standring S. Gray's anatomy, the anatomical basis of clinical practice, expert consult – online and print; 2008. p. 1576.
31. Tsai H-C, Yoshida T, Chaung T-Y, Yang S-F, Chang C-C, Yao H-Y, et al. Transversus Abdominis Plane Block: An Updated Review of Anatomy and Techniques. Biomed Res Int [Internet]. 2017 [cited 2020 May 26];8284363. Available from: https://www.ncbi.nlm.nih.gov/pmc/articles/PMC5684553/.

Part V

Ultrasound in Specialty Care

The Role of Ultrasound in the Critical Care Setting

Alan David Kaye, Cody M. Koress, Amir O. Elhassan,
Caroline Galliano, Nicholas S. Moore, Christina J. Pollock,
Matthew Brian Novitch, Krish D. Sekar,
and Amit Prabhakar

1 The Role of Ultrasound in Regional Anesthesia in the Intensive Care Setting: An Overview

The role of ultrasound in patient care has resulted in great improvements in the capacity to precisely deliver pain control techniques in an effective and relatively safe manner. Pain control in the critically ill population has specific challenges as many patients lack the ability to provide objective assessment of pain. Stress, related to many different disease states, can have significant physiological consequences. Thus, adequate pain control is important in reducing the stress response in critical illness. Untoward effects related to opioids include respiratory depression, altered mental status, and reduced bowel function. The use of ultrasound to effectively deliver regional anesthesia can significantly benefit patients in the critical care environment. Until ultrasound techniques became commonplace throughout the intensive care setting, the use of epidural analgesia was a critical component of multimodal therapy, although there was a lack of strong evidence-based studies demonstrating its significant benefits. One efficacious example was thoracic epidurals, mainly used in the ICU to treat patients undergoing thoracic, orthopedic, abdominal, and cardiovascular surgery, and for rib fractures [1–5].

The effect of epidural analgesia on mortality remains controversial. Certain studies have shown improved rates of mortality [6–10]. Other studies, including the MASTER (Multicentre Australian Study of Epidural Anesthesia) trial [11] and the Veteran Affairs study [12], reported no decrease in mortality rates in those patients with epidurals undergoing major abdominal surgery. A 2014 systemic review and meta-analysis performed by Popping et al. demonstrated a mortality benefit in patients receiving post-operative analgesia by an epidural. Strategies developed to aid in epidural placement in high risk patients include serum markers such as pro-calcitonin and C-reactive protein with suspected bacteremia [13] and the tunneling of epidural catheters to reduce infection [14].

2 Peripheral Nerve Blocks Utilizing Ultrasound

There are limited studies on the use of upper extremity blocks for patients in the critical care setting [15]. Use of peripheral nerve blocks and catheters has been demonstrated to decrease opioid consumption and pain scores, resulting in

---

A. D. Kaye (✉)
Departments of Anesthesiology and Pharmacology, Toxicology, and Neurosciences, Lousiana State University Health Sciences Center, Shreveport, LA, USA

Department of Anesthesiology, Department of Pharmacology Louisiana State University School of Medicine, Louisiana State University Health Sciences Center, New Orleans, LA, USA
e-mail: akaye@lsuhsc.edu

C. M. Koress
Department of Anesthesiology, LSU School of Medicine, Louisiana State University Health Sciences Center, New Orleans, LA, USA
e-mail: ckores@lsuhsc.edu

A. O. Elhassan
Ohio State University Health Sciences Center, Department of Anesthesiology, Columbus, OH, USA

C. Galliano · K. D. Sekar
Louisiana State University Health Sciences Center, Department of Anesthesiology, New Orleans, LA, USA
e-mail: kseka1@lsuhsc.edu

N. S. Moore
Harvard Medical School, Boston, MA, USA

C. J. Pollock
University of Arizona School of Medicine, Department of Anesthesiology, Tucson, AZ, USA

M. B. Novitch
University of Washington School of Medicine, Department of Anesthesiology, Seattle, WA, USA
e-mail: mnovitch@uw.edu

A. Prabhakar
Emory University School of Medicine, Department of Anesthesiology, Division of Critical Care, Atlanta, GA, USA
e-mail: amit.prabhakar@emory.edu

© Springer Nature Switzerland AG 2021
J. Li et al. (eds.), *Ultrasound Fundamentals*, https://doi.org/10.1007/978-3-030-46839-2_23

earlier mobilization and rehabilitation and higher patient satisfaction [16–18]. Trauma ICU patients potentially benefit from continuous nerve catheters related to sympathectomy-associated vasodilation and improved blood flow, such as in patients undergoing revascularization and re-implantation procedures [19].

Compartment syndrome can occur in patients with continuous upper extremity nerve catheters. Thus, it is important that the rate of infusion be as low as possible. Breakthrough pain in a patient receiving continuous upper extremity analgesia from a functional nerve catheter may indicate further clinical investigation into possible compartment syndrome [17, 20].

Neurological impairment and sedation can interfere with effective placement of one-shot nerve blocks and/or continuous upper extremity nerve catheters. Nerve stimulators and ultrasound have been demonstrated to decrease rates of injury to the nerves and neighboring structures [21]. Interscalene catheter placement can result in accidental phrenic nerve block and hemi diaphragm dysfunction, and require daily inspection. Weaning of ventilator support may result in respiratory compromise and requires close monitoring [15]. Reduced volumes of local anesthetic reduce the chance of phrenic nerve block [22, 23].

Continuous supraclavicular, infraclavicular, and axillary catheters can be used to provide post-operative analgesia and alternatively, brachial plexus blocks can now be performed with liposomal bupivicaine [15]. Liposomes are vesicular carriers composed of a lipid bilayer that encompasses an aqueous core. The lipid bilayer serves as a reservoir for lipid soluble drugs, whereas the aqueous interior is suitable for hydrophilic drugs such as local anesthetics and liposomal bupivacaine that has duration of 72–96 hours [15, 16].

3 Peripheral Nerve Blocks for the Lower Extremities

There are multiple blocks available for lower extremity analgesia, with multiple targets present from the lumbar plexus to the lower leg regions. Many of these patients require pain control related to trauma or crush injury and often require surgery with postoperative systemic support. Femoral catheters are used for anesthesia and analgesia in combination with other lower extremity blocks for various surgical procedures and analgesia [24]. Lumbar plexus blocks, also termed psoas block, can be combined with sciatic blocks with or without continuous catheters and can be employed for analgesia of the femoral, obturator, and lateral femoral cutaneous nerves [25]. The sciatic block can be combined with other blocks including femoral, lateral femoral cutaneous, obturator, etc. and it is rarely used alone [26]. It is utilized in ankle fractures and tibia fractures [26]. Ayling et al., in a large retrospective chart review, described adequate pain control with decreased opioid requirements in those patients undergoing lower limb amputation via continuous perineural infusions of local anesthetic [27].

4 Regional Analgesic Techniques in the Critical Care Setting

Many other regional injections and infusions are available in the ICU setting, each with the potential to reduce opioid requirements and enhance recovery. The transverse abdominal plane (TAP) block can be used for abdominal pain after abdominal or gynecological surgeries. Limitations of the TAP block involve sensation in the pelvic floor as well as visceral pain [28]. Other abdominal fascial plane blocks and thoracic fascial pain blocks can be used for a variety of surgeries in unstable trauma patients [28]. Celiac plexus blocks are useful to mitigate visceral cancer-related pain, including in the gastric and pancreatic areas [29], and can be combined with TAP or intercostal blocks in abdominal surgery. Intercostal blocks are commonly used for analgesia following upper abdominal surgery, thoracic surgery, and rib fractures, and frequently used during the placement of chest tubes and gastrostomy tubes [30]. Further, the paravertebral block and catheter infusions are excellent in unilateral chest trauma and procedures, including thoracotomies, nephrectomies, and breast surgery, and can be employed if an epidural catheter fails or if analgesia is inadequate [31].

Regarding morbidity and mortality of post-operative regional anesthesia, recent data is limited. Studies previously conducted by Moen and associates, as well as by Auroy and co-workers, have produced results consistent with low risk of permanent neurological damage or death [32].

5 Ultrasound for Cardiovascular/ Volume Status in the Intensive Care Setting

Intravenous resuscitation and assessment of volume status is vital to the care of the critically ill. Over-resuscitation, however, has been shown to increase mortality in the intensive care unit [33–36]. Clinical examination of volume status is difficult and, in many instances, inaccurate. This leads to the development of more objective means of assessment [5]. Several imaging modalities utilizing ultrasound have been developed, including visualization of inferior vena cava (IVC) diameter and respiratory variation, extravascular lung water, aortic blood velocity variation, and stroke volume variation.

Imaging of the IVC via point-of-care ultrasound has emerged as a non-invasive, rapid imaging modality popular with intensivists that ameliorates the need for invasive monitoring, expensive equipment, or expert echocardiographers. Data from multiple studies suggest that B-mode, sub-xyphoid transabdominal long axis imaging 2–3 cm caudal to the RA junction is the most reliable means of IVC assessment with inter-rater reliability [37–39]. A curvilinear probe in cardiac exam type should be placed in the sub-xyphoid position perpendicular to the skin. The IVC should be visualized in the center of the field by moving the probe to the right. To obtain the longitudinal plane, the probe is rotated 90°. Compared to the thick-walled, pulsatile aorta, the IVC is thin-walled and changes caliber with respiration. The IVC diameter is measured using time-motion mode throughout the respiratory cycle.

A positive linear relationship exists between the central venous pressure (CVP) and IVC diameter, thus CVP can be reasonably elucidated from IVC measurement [40–44]. Several indices, such as maximal IVC diameter, respiratory variations in IVC diameter, or a combination of both, can be used to evaluate CVP. Generally, in spontaneously breathing patients, a low IVC diameter and a high reduction in diameter with inspiration is associated with a low CVP, and a high IVC diameter with a low reduction in IVC diameter is associated with a high CVP. During positive pressure ventilation the changes in intrathoracic pressure are more predictable, however, the diameter of the IVC increases during insufflation compared to baseline [45]. There is controversy as to whether CVP can be used to accurately predict volume responsiveness, or rather predicts an increase in cardiac output in response to a fluid bolus. Data suggest that CVP is of little value in predicting volume status and fluid responsiveness [42, 46, 47]. These studies were unable to find a CVP above which would reliably predict patient fluid responsiveness and below which, would not. Other data suggest that maximal IVC diameter less than 15 mm will provide sufficient sensitivity and specificity in identifying fluid responsiveness in the proper clinical context [48].

In a systematic review and meta-analysis by Zhang et al. [49], respiratory variation in IVC diameter varying from 12% to 40% estimated fluid responsiveness with sensitivity of 78% and specificity of 86%. The diagnostic performance appeared to be better in mechanically ventilated patients who received colloids due to predictability in changes of intrathoracic pressure and the fact that crystalloids may not stay intravascular for very long in critically ill patients [50–52]. These data suggest the need for further studies evaluating the use of changes in IVC diameter to assess for fluid responsiveness and clinical endpoints. In practice, if the IVC diameter is small and collapses upon inspiration on initial assessment of a patient with undifferentiated shock, etiologies such as tension pneumothorax, pericardial tamponade, and massive pulmonary embolism can reliably be ruled out. These data are helpful in the assessment of a critically ill patient.

Lung ultrasound (LUS) has emerged as a rapid and accurate imaging modality in the assessment of pulmonary edema in patients that are over-resuscitated, signaling an important data point in the consideration of further volume resuscitation. Several studies have shown a correlation between mortality and extravascular lung water [53, 54]. The Fluid Administration Limited by Lung Sonography (FALLS) protocol, developed by Lichtenstein and Karakitsos [55], uses two distinct LUS signatures to assess the likelihood of interstitial edema. A-line is a horizontal artifact from a normal lung surface and its predominance indicates dry interlobular septa and low to normal left atrial pressure. B-line is described as a comet-tail artifact that most often indicates alveolar-interstitial syndrome consistent with pulmonary edema [56, 57]. In a patient with visualized A-line predominance, it is suggested that fluid administration will not immediately worsen or cause hydrostatic pulmonary edema. A-line predominance, however, is not an indication for additional fluid administration, as other clinical data must be taken into consideration. The FALLS protocol calls for ultrasonographic assessment at 2 standardized Bedside Lung Ultrasound in Emergency (BLUE) points on the anterior chest wall. A curvilinear probe is placed between the third and fourth ribs and between the sixth and seventh ribs between the parasternal and midclavicular line. Data from multiple trials suggest that LUS improves patient outcomes in the ICU and in other settings [58–63].

Though requiring more prerequisites and technical expertise, stroke volume respiratory variation and its surrogates throughout the left heart can predict fluid responsiveness in patients receiving mechanical ventilation without dysrhythmias or increased abdominal pressure [64]. The rise in intrapleural pressure associated with insufflation compresses the pulmonary vasculature and causes compression of the heart and venous inflow vessels. This reduces both right ventricular preload and left ventricular afterload, while at the same time increasing RV afterload and LV preload. It is thought that hypovolemia would accentuate these effects. For the purposes of measurement, left ventricular outflow tract dimensions do not change so changes in velocity-time integral (VTI) generated by Doppler must be used to evaluate variations in stroke volume. In small studies, respiratory variations in VTI predicted fluid responsiveness at a 20% threshold, while respiratory variations in aortic blood flow predict fluid responsiveness at a threshold of 12% [65, 66].

VTI can be measured using the apical five-chamber view by placing the probe first in the four-chamber view. The probe is then tilted ventrally to visualize the left ventricular outflow tract and aortic valve. The average of three measurements of respiratory variation should be measured over one respiratory cycle, beginning at inspiration. Evaluation of respiratory variation in aortic blood flow is simpler, as measurement can be obtained over several respiratory cycles [67].

6 Summary

A multimodal approach to pain control is recommended for the intensive care unit setting. The role of ultrasound has had a tremendous impact in terms of effective pain management and has had an evolving role in intensive care assessment and diagnostics. The use of ultrasound in regional analgesia can play a critical role and provides numerous definable benefits that epidurals in certain instances lack. Effective pain relief in the critical care setting can reduce physiologic and psychologic stress. In this regard, reduced use of opiate therapy decreases the risk for withdrawal syndrome, mental status impairment, delirium, nausea and vomiting, reduced gastrointestinal motility, and other opioid-mediated effects such as dose-dependent reduction in natural killer cell effects. Ultrasound in the intensive care setting is also emerging as a beneficial technology in multiple pathological processes. Even though many of the articles cited in this chapter are from small series and uncontrolled trials, future clinical research in this area should produce important best practice strategies for intensive care providers and the use of ultrasound.

References

1. Bulger EM, Edwards T, Klotz P, Jurkovich GJ. Epidural analgesia improves outcome after multiple rib fractures. Surgery. 2004;136(2):426–30.
2. Jensen CD, Stark JT, Jacobson LL, Powers JM, Joseph MF, Kinsella-Shaw JM, Denegar CR. Improved outcomes associated with the liberal use of thoracic epidural analgesia in patients with rib fractures. Pain Med. 2017;18(9):1787–94.
3. Galvagno SM Jr, Smith CE, Varon AJ, Hasenboehler EA, Sultan S, Shaefer G, To KB, Fox AD, Alley DE, Ditillo M, Joseph BA, Robinson BR, Haut ER. Pain management for blunt thoracic trauma: a joint practice management guideline from the Eastern Association for the Surgery of Trauma and Trauma Anesthesiology Society. J Trauma Acute Care Surg. 2016;81(5):936–51.
4. Carrier FM, Turgeon AF, Nicole PC, Trépanier CA, Fergusson DA, Thauvette D, Lessard MR. Effect of epidural analgesia in patients with traumatic rib fractures: a systematic review and meta-analysis of randomized controlled trials. Can J Anaesth. 2009;56(3):230–42. https://doi.org/10.1007/s12630-009-9052-7.
5. Monaco F, Biselli C, De Luca M, Landoni G, Lembo R, Zangrillo A. Thoracic epidural anesthesia in elderly patients undergoing cardiac surgery for mitral regurgitation feasibility study. Ann Card Anaesth. 2012;15(2):164–5. https://doi.org/10.4103/0971-9784.95085.
6. Maxwell C, Nicoara A. New developments in the treatment of acute pain after thoracic surgery. Curr Opin Anaesthesiol. 2014;27(1):6–11. https://doi.org/10.1097/ACO.0000000000000029.
7. Pöpping DM, Elia N, Marret E, Remy C, Tramèr MR. Protective effects of epidural analgesia on pulmonary complications after abdominal and thoracic surgery: a meta-analysis. Arch Surg. 2008;143(10):990–9; discussion 1000. https://doi.org/10.1001/archsurg.143.10.990.
8. Wijeysundera DN, Beattie WS, Austin PC, Hux JE, Laupacis A. Epidural anaesthesia and survival after intermediate-to-high risk non-cardiac surgery: a population-based cohort study. Lancet. 2008;372(9638):562–9. https://doi.org/10.1016/S0140-6736(08)61121-6.
9. Wu CL, Hurley RW, Anderson GF, Herbert R, Rowlingson AJ, Fleisher LA. Effect of postoperative epidural analgesia on morbidity and mortality following surgery in medicare patients. Reg Anesth Pain Med. 2004;29(6):525–33; discussion 515–9.
10. Park WY, Thompson JS, Lee KK. Effect of epidural anesthesia and analgesia on perioperative outcome: a randomized, controlled veterans affairs cooperative study. Ann Surg. 2001;234(4):560–9; discussion 569–71.
11. Rigg JR, Jamrozik K, Myles PS, Silbert BS, Peyton PJ, Parsons RW, Collins KS, MASTER Anaethesia Trial Study Group. Epidural anaesthesia and analgesia and outcome of major surgery: a randomised trial. Lancet. 2002;359(9314):1276–82.
12. Rodgers A, Walker N, Schug S, McKee A, Kehlet H, van Zundert A, Sage D, Futter M, Saville G, Clark T, MacMahon S. Reduction of postoperative mortality and morbidity with epidural or spinal anaesthesia: results from overview of randomised trials. BMJ. 2000;321(7275):1493.
13. Bell K, Wattie M, Byth K, Silvestrini R, Clark P, Stachowski E, Benson EM. Procalcitonin: a marker of bacteraemia in SIRS. Anaesth Intensive Care. 2003;31(6):629–36.
14. Bomberg H, Kubulus C. Tunnelling of thoracic epidural catheters is associated with fewer catheter-related infections: a retrospective registry analysis. Br J Anaesth. 2016;116(4):546–53. https://doi.org/10.1093/bja/aew026.
15. Schulz-Stubner S. Chapter 67: regional analgesia in the critically ill. In: Hadzic A, editor. Textbook of regional anesthesia and acute pain management. New York: McGraw-Hill; 2017.
16. Ehieli E, Yalamuri S, Brudney CS, Pyati S. Analgesia in the surgical intensive care unit. Postgrad Med J. 2017;93(1095):38–45.
17. Aguirre J, Del Moral A, Cobo I, et al. The role of continuous peripheral nerve blocks. Anesthesiol Res Pract. 2012;2012:560879. https://doi.org/10.1155/2012/560879.
18. Guedes L, Rebelo H, Oliveira R, et al. Regional analgesia in intensive care. Rev Bras Anestesiol. 2012;62:719–30. https://doi.org/10.1016/S0034-7094(12)70170-8.
19. Chelly JE, Ghisi D, Fanelli A. Continuous peripheral nerve blocks in acute pain management. Br J Anaesth. 2010;105(Suppl 1):i86–96. https://doi.org/10.1093/bja/aeq322.
20. Mar GJ, Barrington MJ, McGuirk BR. Acute compartment syndrome of the lower limb and the effect of postoperative analgesia on diagnosis. Br J Anaesth. 2009;102:3–11. https://doi.org/10.1093/bja/aen330.
21. Le-Wendling L, Enneking FK. Continuous peripheral nerve blockade for postoperative analgesia. Curr Opin Anaesthesiol. 2008;21(5):602–9. https://doi.org/10.1097/ACO.0b013e32830a4be6.
22. Nadeau MJ, Lévesque S, Dion N. Ultrasound-guided regional anesthesia for upper limb surgery. Can J Anaesth. 2013;60(3):304–20. https://doi.org/10.1007/s12630-012-9874-6.
23. Lee JH, Cho SH, Kim SH, Chae WS, Jin HC, Lee JS, Kim YI. Ropivacaine for ultrasound-guided interscalene block: 5 mL provides similar analgesia but less phrenic nerve paralysis than 10 mL. Can J Anaesth. 2011;58(11):1001–6. https://doi.org/10.1007/s12630-011-9568-5.
24. Farag E, Brown DL. Chapter 14 – femoral block. In: Brown's atlas of regional anesthesia. 5th ed. Philadelphia: Elsevier; 2017. p. 115–26.
25. Mounir-Soliman L, Brown DL. Chapter 12 – lumbar plexus block. In: Brown's atlas of regional anesthesia. Philadelphia: Elsevier; 2017. p. 97–102.
26. Farag E, Brown DL. Chapter 13 – sciatic block. In: Brown's atlas of regional anesthesia. Philadelphia: Elsevier; 2017. p. 103–13.
27. Ayling OG, et al. Continuous regional anaesthesia provides effective pain management and reduces opioid requirements following major lower limb amputation. Eur J Vasc Endovasc Surg. 2014;48(5):559–64.

28. Ehieli E, et al. Analgesia in the surgical intensive care unit. Postfrad Med J. 2017;93(1095):38–45.
29. Brown DL. Chapter 51 – celiac plexus block. In: Brown's atlas of regional anesthesia. Philadelphia: Elsevier; 2017. p. 321–8.
30. Brown DL. Chapter 35 – intercostal block. In: Brown's atlas of regional anesthesia. Philadelphia: Elsevier; 2017. p. 227–30.
31. Farag E. Chapter 39 – paravertebral block. In: Brown's atlas of regional anesthesia. Philadelphia: Elsevier; 2017. p. 245–8.
32. Schulz-stübner S, Boezaart A, Hata JS. Regional analgesia in the critically ill. Crit Care Med. 2005;33(6):1400–7.
33. Vincent J-L, Sakr Y, Sprung CL, et al. Sepsis in European intensive care units: results of the SOAP study. Crit Care Med. 2006;34(2):344–53.
34. Acheampong A, Vincent J-L. A positive fluid balance is an independent prognostic factor in patients with sepsis. Crit Care. 2015;19(1):251. https://doi.org/10.1186/s13054-015-0970-1.
35. Boyd JH, Forbes J, Nakada T, Walley KR, Russell JA. Fluid resuscitation in septic shock: a positive fluid balance and elevated central venous pressure are associated with increased mortality. Crit Care Med. 2011;39(2):259–65. https://doi.org/10.1097/CCM.0b013e3181feeb15.
36. Marik PE, Linde-Zwirble WT, Bittner EA, Sahatjian J, Hansell D. Fluid administration in severe sepsis and septic shock, patterns and outcomes: an analysis of a large national database. Intensive Care Med. 2017;43(5):625–32. https://doi.org/10.1007/s00134-016-4675-y.
37. Eisenberg PR, Jaffe AS, Schuster DP. Clinical evaluation compared to pulmonary artery catheterization in the hemodynamic assessment of critically ill patients. Crit Care Med. 1984;12(7):549–53.
38. Finnerty NM, Panchal AR, Boulger C, et al. Inferior vena cava measurement with ultrasound: what is the best view and best mode? West J Emerg Med. 2017;18(3):496–501. https://doi.org/10.5811/westjem.2016.12.32489.
39. Çelebi Yamanoğlu NG, Yamanoğlu A, Parlak İ, et al. The role of inferior vena cava diameter in volume status monitoring; the best sonographic measurement method? Am J Emerg Med. 2015;33(3):433–8. https://doi.org/10.1016/j.ajem.2014.12.014.
40. Akkaya A, Yesilaras M, Aksay E, Sever M, Atilla OD. The interrater reliability of ultrasound imaging of the inferior vena cava performed by emergency residents. Am J Emerg Med. 2013;31(10):1509–11. https://doi.org/10.1016/j.ajem.2013.07.006.
41. Feissel M, Michard F, Faller JP, Teboul JL. The respiratory variation in inferior vena cava diameter as a guide to fluid therapy. Intensive Care Med. 2004;30(9):1834–7. https://doi.org/10.1007/s00134-004-2233-5.
42. Kircher BJ, Himelman RB, Schiller NB. Noninvasive estimation of right atrial pressure from the inspiratory collapse of the inferior vena cava. Am J Cardiol. 1990;66(4):493–6.
43. Airapetian N, Maizel J, Alyamani O, et al. Does inferior vena cava respiratory variability predict fluid responsiveness in spontaneously breathing patients? Crit Care. 2015;19(1):400. https://doi.org/10.1186/s13054-015-1100-9.
44. Barbier C, Loubires Y, Schmit C, et al. Respiratory changes in inferior vena cava diameter are helpful in predicting fluid responsiveness in ventilated septic patients. Intensive Care Med. 2004;30(9):1740–6. https://doi.org/10.1007/s00134-004-2259-8.
45. Prekker ME, Scott NL, Hart D, Sprenkle MD, Leatherman JW. Point-of-care ultrasound to estimate central venous pressure: a comparison of three techniques. Crit Care Med. 2013;41(3):833–41. https://doi.org/10.1097/CCM.0b013e31827466b7.
46. Jardin F, Vieillard-Baron A. Ultrasonographic examination of the venae cavae. Intensive Care Med. 2006;32(2):203–6. https://doi.org/10.1007/s00134-005-0013-5.
47. Marik PE, Cavallazzi R. Does the central venous pressure predict fluid responsiveness? An updated meta-analysis and a plea for some common sense. Crit Care Med. 2013;41(7):1774–81. https://doi.org/10.1097/CCM.0b013e31828a25fd.
48. Eskesen TG, Wetterslev M, Perner A. Systematic review including re-analyses of 1148 individual data sets of central venous pressure as a predictor of fluid responsiveness. Intensive Care Med. 2016;42(3):324–32. https://doi.org/10.1007/s00134-015-4168-4.
49. Lee CWC, Kory PD, Arntfield RT. Development of a fluid resuscitation protocol using inferior vena cava and lung ultrasound. J Crit Care. 2016;31(1):96–100. https://doi.org/10.1016/j.jcrc.2015.09.016.
50. Zhang Z, Xu X, Ye S, Xu L. Ultrasonographic measurement of the respiratory variation in the inferior vena cava diameter is predictive of fluid responsiveness in critically ill patients: systematic review and meta-analysis. Ultrasound Med Biol. 2014;40(5):845–53. https://doi.org/10.1016/j.ultrasmedbio.2013.12.010.
51. Sánchez M, Jiménez-Lendínez M, Cidoncha M, et al. Comparison of fluid compartments and fluid responsiveness in septic and non-septic patients. Anaesth Intensive Care. 2011;39(6):1022–9. https://doi.org/10.1177/0310057X1103900607.
52. De Backer D, Cortés DO. Characteristics of fluids used for intravascular volume replacement. Best Pract Res Clin Anaesthesiol. 2012;26(4):441–51. https://doi.org/10.1016/j.bpa.2012.10.005.
53. Chung F-T, Lin S-M, Lin S-Y, Lin H-C. Impact of extravascular lung water index on outcomes of severe sepsis patients in a medical intensive care unit. Respir Med. 2008;102(7):956–61. https://doi.org/10.1016/J.RMED.2008.02.016.
54. Sakka SG, Klein M, Reinhart K, Meier-Hellmann A. Prognostic value of extravascular lung water in critically ill patients. Chest. 2002;122(6):2080–6. https://doi.org/10.1378/CHEST.122.6.2080.
55. Lichtenstein D, Karakitsos D. Integrating lung ultrasound in the hemodynamic evaluation of acute circulatory failure (the fluid administration limited by lung sonography protocol). J Crit Care. 2012;27(5):533. e11–533.e19. https://doi.org/10.1016/j.jcrc.2012.03.004.
56. Lichtenstein D, Mézière G, Biderman P, Gepner A, Barré O. The comet-tail artifact. Am J Respir Crit Care Med. 1997;156(5):1640–6. https://doi.org/10.1164/ajrccm.156.5.96-07096.
57. Lichtenstein DA, Mezière GA, Lagoueyte J-F, Biderman P, Goldstein I, Gepner A. A-lines and B-lines: lung ultrasound as a bedside tool for predicting pulmonary artery occlusion pressure in the critically ill. Chest. 2009;136(4):1014–20. https://doi.org/10.1378/CHEST.09-0001.
58. Covic A, Siriopol D, Voroneanu L. Use of lung ultrasound for the assessment of volume status in CKD. Am J Kidney Dis. 2018;71(3):412–22. https://doi.org/10.1053/j.ajkd.2017.10.009.
59. Donadio C, Bozzoli L, Colombini E, et al. Effective and timely evaluation of pulmonary congestion: qualitative comparison between lung ultrasound and thoracic bioelectrical impedance in maintenance hemodialysis patients. Medicine (Baltimore). 2015;94(6):e473. https://doi.org/10.1097/MD.0000000000000473.
60. Rusu D-M, Siriopol I, Grigoras I, et al. Lung ultrasound guided fluid management protocol for the critically ill patient: study protocol for a multi-centre randomized controlled trial. Trials. 2019;20(1):236. https://doi.org/10.1186/s13063-019-3345-0.
61. Platz E, Merz AA, Jhund PS, Vazir A, Campbell R, McMurray JJ. Dynamic changes and prognostic value of pulmonary congestion by lung ultrasound in acute and chronic heart failure: a systematic review. Eur J Heart Fail. 2017;19(9):1154–63. https://doi.org/10.1002/ejhf.839.
62. Anile A, Russo J, Castiglione G, Volpicelli G. A simplified lung ultrasound approach to detect increased extravascular lung water in critically ill patients. Crit Ultrasound J. 2017;9(1):13. https://doi.org/10.1186/s13089-017-0068-x.

63. Enghard P, Rademacher S, Nee J, et al. Simplified lung ultrasound protocol shows excellent prediction of extravascular lung water in ventilated intensive care patients. Crit Care. 2015;19(1):36. https://doi.org/10.1186/s13054-015-0756-5.
64. Marik PE, Cavallazzi R, Vasu T, Hirani A. Dynamic changes in arterial waveform derived variables and fluid responsiveness in mechanically ventilated patients: a systematic review of the literature. Crit Care Med. 2009;37(9):2642–7. https://doi.org/10.1097/CCM.0b013e3181a590da.
65. Feissel M, Michard F, Mangin I, Ruyer O, Faller JP, Teboul JL. Respiratory changes in aortic blood velocity as an indicator of fluid responsiveness in ventilated patients with septic shock. Chest. 2001;119(3):867–73. https://doi.org/10.1378/chest.119.3.867.
66. Charron C, Fessenmeyer C, Cosson C, et al. The influence of tidal volume on the dynamic variables of fluid responsiveness in critically ill patients. Anesth Analg. 2006;102(5):1511–7. https://doi.org/10.1213/01.ane.0000209015.21418.f4.
67. De Backer D, Fagnoul D. Intensive care ultrasound: VI. Fluid responsiveness and shock assessment. Ann Am Thorac Soc. 2014;11(1):129–36. https://doi.org/10.1513/annalsats.201309-320ot.

Clinical Utilization of Ultrasound in Vascular Disease

Matthew Brian Novitch, Anna J. Sudbury,
Mitchell C. Fuller, Jennifer J. Dennison, Cody M. Koress,
Amit Prabhakar, Vanessa Moll, Elyse M. Cornett,
and Alan David Kaye

1 Introduction

Atheromatous plaque formation in the cervical carotid arteries may lead to ipsilateral ischemic stroke or transient ischemic attack from embolization, thrombosis, or hemodynamic compromise. Visualization and assessment of the cervical carotid arteries can be achieved by carotid duplex ultrasonography. However, screening of asymptomatic patients is not recommended as the prevalence of symptomatic carotid stenosis is low and the risk of ipsilateral stroke in patients with asymptomatic carotid artery stenosis ≥50% is less than 1% annually [1–3]. However, in symptomatic and high-risk patients suspected of carotid stenosis, carotid duplex ultrasound is effective in detecting focal increases in peak systolic blood flow velocity indicative of ≥70% stenosis [4]. Newer modalities such as contrast enhanced, 3-dimensional, and compound B-mode ultrasound coupled with supplementary diagnostic information such as plaque morphology and collateral perfusion may offer advantages compared with traditional carotid duplex ultrasound.

An abdominal aortic aneurysm (AAA) is defined as segmental, full thickness dilation of the abdominal aorta to one and a half times the normal aortic diameter and is the most common arterial aneurysm in the human body [5]. It is an insidious condition that is largely asymptomatic with a 10–15% chance of survival after acute rupture. By the time patients are symptomatic, the AAA has likely ruptured lending to a clinical scenario in which secondary prevention via ultrasound screening ameliorates the morbidity and mortality of AAA. The United States Preventive Services Task Force (USPSTF) recommends a one-time screening for men ages 65–75 who have ever smoked (Grade B) and to selectively offer screening to men ages 65–75 who have never smoked (Grade C) [6]. There are approximately 1.1 million AAAs (prevalence, 1.4%) in the population aged 50–84 in the United States. USPSTF selection criteria (men with smoking history, aged 65–75) capture 29.5% of these AAAs with a cohort prevalence of 4.9% [7].

Renovascular disease is a significant cause of secondary hypertension, especially in patients presenting with an acute, severe or refractory increase in blood pressure. The prevalence of renovascular disease in the Medicare population is around 7% but is higher in patients that present with severe or malignant hypertension [8]. For diagnosis, renal artery duplex Doppler ultrasonography is a reasonable alternative to the more invasive gold-standard renal arteriography. In the hand of an experienced operator, the measurement of the resistive index ([peak systolic velocity – endo-diastolic

M. B. Novitch
University of Washington School of Medicine,
Department of Anesthesiology, Seattle, WA, USA
e-mail: mnovitch@uw.edu

A. J. Sudbury · M. C. Fuller · J. J. Dennison
Medical College of Wisconsin, Wauwatosa, WI, USA
e-mail: asudbury@mcw.edu; mfuller@mcw.edu;
jdennison@mcw.edu

C. M. Koress
Department of Anesthesiology, LSU School of Medicine,
Louisiana State University Health Sciences Center,
New Orleans, LA, USA
e-mail: ckores@lsuhsc.edu

A. Prabhakar
Emory University School of Medicine, Department of
Anesthesiology, Division of Critical Care, Atlanta, GA, USA

V. Moll
Emory University School of Medicine, Department of
Anesthesiology, Division of Critical Care Medicine,
Atlanta, GA, USA
e-mail: vanessa.moll@emory.edu

E. M. Cornett (✉)
Department of Anesthesiology, LSU Health Shreveport,
Shreveport, LA, USA
e-mail: ecorne@lsuhsc.edu

A. D. Kaye
Departments of Anesthesiology and Pharmacology, Toxicology,
and Neurosciences, Lousiana State University Health Sciences
Center, Shreveport, LA, USA

Department of Anesthesiology, Department of Pharmacology
Louisiana State University School of Medicine, Louisiana State
University Health Sciences Center, New Orleans, LA, USA
e-mail: akaye@lsuhsc.edu

© Springer Nature Switzerland AG 2021
J. Li et al. (eds.), *Ultrasound Fundamentals*, https://doi.org/10.1007/978-3-030-46839-2_24

velocity] divided by peak systolic velocity) may improve the diagnostic utility of renovascular ultrasonography in predicting outcome after revascularization.

In the extremities, ultrasonography is a relatively simple and inexpensive method to evaluate arterial and venous disease. Calculation of ankle-brachial index in the diagnosis and evaluation of peripheral vascular disease can be performed at the bedside using continuous-wave Doppler. The resting systolic pressure of the ankle is compared to the resting systolic pressure of the brachial artery with the ratio providing a measure of disease burden. The prevalence of peripheral arterial disease is approximately 20% in adults older than 55 years and is associated strongly with myocardial and cerebrovascular disease [9–11]. Deep vein thrombosis and pulmonary embolism, together known as venous thromboembolism, account for the third leading cause of vascular disease after acute myocardial infarction and stroke [12]. The annual economic burden of venous thromboembolism is estimated to be $7–10 billion each year for 375,000–425,000 newly diagnosed, medically treated incident cases [13]. The increasing incidence of clinical and environmental risk factors in an ageing population and the increased availability of effective imaging modalities is expected to increase this economic burden [14]. In patients with suspected deep vein thrombosis, compression ultrasonography is the diagnostic gold standard along with computerized tomography pulmonary angiography in suspected cases of pulmonary embolism.

2 ABI and Duplex Ultrasound for Vascular Disease

Several non-invasive measures of sub-clinical atherosclerosis, such as carotid artery intima-media thickness, carotid or aortic calcification and the ankle-brachial index (ABI) have been suggested as potential predictors of cardiovascular morbidity and mortality [15, 16]. Of these, the ABI (the ratio of systolic blood pressure in the ankle to that in the arm), has been most extensively described. It can easily be performed at the bedside but has in the recent past been predominantly deferred to the vascular laboratory setting. Initially, ABI was described for the noninvasive diagnosis of lower-extremity peripheral artery disease (PAD) and originally described in 1950 [17, 18]. ABI is also an indicator of atherosclerosis at other vascular sites and has been utilized as a predictive indicator for cardiovascular events and impairment of function, even when clinical symptoms of PAD are lacking [18, 19].

2.1 Relevant Anatomy and Physiology

As the blood pressure waveform travels distally from the heart it amplifies. This results in a progressive increase in systolic blood pressure (SBP) and a decrease in diastolic blood pressure (DBP). SBP amplification relies on retrograde wave reflection from resistant distal arterioles, which is additive to the antegrade wave [20]. However, this is not the sole explanation for the changes in pressure wave morphology [21]. As a result of increased intraluminal pressure, remodeling of vessel structure occurs in the lower extremities. This is characterized by increased wall thickening and unchanged inner radius [22]. The increase in wall thickness occurs during the second year of life when the hydrostatic pressure rises with walking. Contributors to SBP amplification are additive: reflected waves and changes in vessel wall thickness.

2.2 Body Position

Body position and knee or hip flexion can influence the ABI. The ABI averages 0.35 higher in the seated compared to the supine position. Patients should be supine for accurate ABI measurements, with the head and heels supported. Gornik et al. recommended a formula to correct the seated ABI in patients who cannot lie down [23]. However, no external validation of this formula has been described.

2.3 Cuff

Studies of brachial blood pressure measurement highlight the importance of an appropriate cuff size to avoid inaccurate measurements. Considerable overestimation can occur if the cuff is too small [24, 25]. The width of the cuff should be at least 40% of the circumferences of the limb.

2.4 Doppler

Doppler ultrasound uses waves reflecting off moving targets such as blood to measure aspects of flow. Christian Doppler first described the "Doppler shift": Blood velocity will increase where an artery is narrowed. This principle has served as the foundation for all vascular ultrasonography. For the ABI a handheld Doppler device with a 5–10 mHz probe can be used.

3 Measurement Protocol for the Ankle-Brachial Index with the Doppler Method

The ABI is performed by measuring the SBP from both brachial arteries and from both the dorsalis pedis and posterior tibial arteries. The SBP is recorded with a 5- or 10-MHz Doppler probe. Start with the right arm, then the right and left leg, and finally the left arm. During the exam the blood pressure may change and note that the two arm pressures taken at the start and end of the exam can serve as quality control. The first measurement (right arm in the above sequence) should be repeated at the end of the sequence and both results averaged to address a possible white coat effect of the first measurement. If the difference between the two measurements of the first arm exceeds 10 mmHg then the first measurement should be disregarded and only the second measurement considered. The maximum inflation is 300 mmHg. The patient should not smoke at least 2 hours before the ABI measurement [26]. Cuff inflation should be interrupted if pain is elicited. Caution is advised in 2 clinical situations: (1) Do not place the cuff over open wounds and ulcers. An impermeable dressing may be used, (2) Cuff inflation should be avoided over a recently placed bypass graft due to the potential risk of causing graft thrombosis.

3.1 Measuring the Brachial Pressure

The blood pressure cuff is placed on the arm, with the limb at the level of the heart. Position the transducer on the brachial artery (use ultrasound gel). The Doppler probe can be moved slightly to maximize the intensity of the signal. The blood pressure cuff is then inflated to about 20 mmHg above the expected systolic blood pressure of the patient. The Doppler signal should disappear. The cuff is slowly deflated. When the Doppler signal re-appears, the pressure is equal to the brachial systolic pressure. The brachial systolic pressure is recorded.

3.2 Measuring the Ankle Pressure

The blood pressure cuff is placed immediately proximal to the ankle. The DP signals are located using a Doppler probe (use ultrasound gel). Again, the Doppler probe is moved slightly until the strongest signal is heard. The cuff is first inflated until the signal disappears, then deflated until the Doppler signal re-appears. Record the measurement. Repeat the same measurement for the PT artery followed by the opposite leg.

3.3 Calculating the ABI

The ABI is calculated by taking the higher pressure of the two arteries at the ankle, divided by the brachial arterial systolic pressure (the higher of the two brachial systolic pressure measurements is used). In normal individuals, there should be less than 10 mmHg interarm systolic pressure gradient during a routine examination. A steady difference in pressure between the arms greater than 10 mmHg is suggestive of (and greater than 20 mmHg is diagnostic of) a subclavian or axillary arterial stenosis [27]. Left ABI = Highest Pressure in LEFT foot (PT or DP) Highest Average Arm Pressure (L or R), Right ABI = Highest Pressure in RIGHT foot (PT or DP) Highest Average Arm Pressure (L or R). See Table 1.

Table 1 Interpretation of the Ankle-Brachial Index (ABI) [28]

ABI value	Interpretation	Recommendation
Greater than 1.4	Calcification, vessel hardening	Refer to vascular specialist
1.0–1.4	Normal	None
0.9–1.0	Acceptable	None
0.8–0.9	Some arterial disease	Treat risk factors
0.5–0.8	Moderate arterial disease	Refer to vascular specialist
Less than 0.5	Severe arterial disease	Refer to vascular specialist

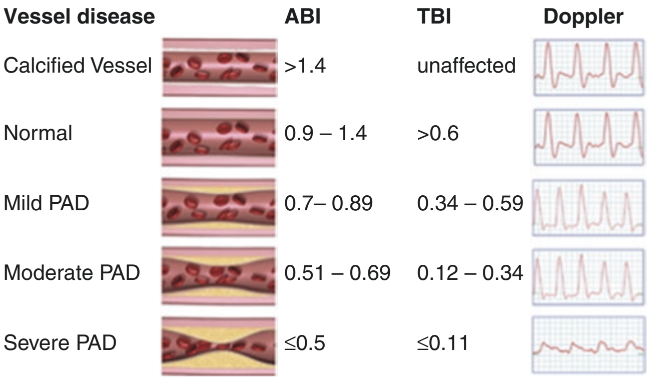

Vessel disease	ABI	TBI	Doppler
Calcified Vessel	>1.4	unaffected	
Normal	0.9 – 1.4	>0.6	
Mild PAD	0.7– 0.89	0.34 – 0.59	
Moderate PAD	0.51 – 0.69	0.12 – 0.34	
Severe PAD	≤0.5	≤0.11	

Fig. 1 Guidelines for interpreting ABI, TBI and Doppler waveforms in PAD. (Modified from Ref. [32]). PAD peripheral artery disease, ABI ankle-brachial index, TBI toe-brachial index

3.4 Sensitivity/Specificity

The actual sensitivity and specificity of the ABI have been estimated, respectively, at 79% and 96% [29]. The level of ABI also correlates with peripheral artery disease (PAD) severity, with a high risk of amputation when the ABI is less than 0.50. An ABI change of more than 0.15 is generally required to consider worsening of limb perfusion or improving after revascularization.

3.5 ABI Exercise

Measuring ABI after exercise enables the detection of additional patients with PAD, who have normal or borderline ABI at rest. The patient is asked to walk (commonly on a treadmill at 3.2 km/h at a 10–20% slope) until claudication pain occurs and impedes walking. Then the ABI is measured as described above. An ABI drop after exercise seems especially useful when a resting ABI is normal but there is clinical suspicion of PAD [30]. Alternative tests such as measurement of Duplex ultrasonography, Doppler waveforms, transcutaneous oxygen measurements, and Toe Brachial Index (TBI, toe systolic pressures used instead of DP or PT pressures) are also useful to unmask PAD [31]. A TBI less than 0.70 is usually considered diagnostic of PAD. See Fig. 1.

4 Duplex Ultrasound Examination

Duplex ultrasonography refers to the combination of both B-mode and pulsed Doppler analysis of the velocity of blood flowing in arteries and veins. High-frequency transducers are recommended to analyze vessels in the extremities as they provide excellent image resolution in superficial structures. Duplex ultrasound examination provides extensive information on both arterial anatomy and blood flow. It allows to localize occlusions and describe their morphologic features. Information concerning artery wall thickness, the degree of flow turbulence and changes in blood flow velocity can be provided. However, it depends greatly on the examiner's experience, and adequate qualification and training are mandatory.

4.1 Sensitivity and Specificity

The specificity of the duplex ultrasound is very high (92–98%) with a sensitivity of 77–83%. The sensitivity for assessing stenosis is variable and can depend on the anatomical location with a higher sensitivity in more proximal vessels [33]. Combined with the ABI, duplex ultrasound can provide information necessary for management decisions in the majority of patients with PAD, confirm the diagnosis, and provide information on lesion location and severity. PAD lesions are located by two-dimensional ultrasonography and color-Duplex mapping. Doppler waveform analysis, peak systolic velocities, and ratios can estimate the degree of vessel stenosis. Although noninvasive imaging studies are becoming more commonly used preoperatively, catheter-based angiography is still considered the gold standard. Duplex ultrasound is noninvasive, comprehensive, mobile, and well tolerated. Additionally, it does not expose the patient to nephrotoxic contrast, or radiation and can be performed on patients with implants. Disadvantages, however, are the high operator dependency which can lead to misinterpretation or delayed diagnosis. Limitations exist in the use in morbidly obese patients.

Duplex ultrasound is not only utilized in the detection and management of PAD but has been used in the diagnosis of deep venous thrombosis (DVT), venous insufficiency, and cerebrovascular, renal, mesenteric, and aortoiliac disease.

4.2 Clinical Pearls

While the ABI is an important diagnostic tool, it is also important to remember other signs of peripheral vascular disease. These include past medical history and exam findings, for example, pain when walking (claudication), paraesthesia (numbness), paralysis (weakness), pulselessness (of dorsalis pedis and posterior tibial pulses) and pallor of distal extremities. This is also known as the "5 Ps of ischemia". Paralysis and paraesthesia are often both seen in severe ischemia to the legs. Some patients have an ABI more than 1.40 that is related to stiff/calcified arteries, often observed in patients with diabetes, end-stage renal disease, and in the very elderly. A proportion of these patients actually do have occlusive artery disease [31]. Vascular polytetrafluoroethylene (PTFE) or polyester (Dacron) grafts contain air and hence duplex ultrasound scanning will not provide a clear evaluation of the grafts.

5 Evaluation for Deep Venous Thrombosis

For patients with the clinical suspicion of an acute deep venous thrombosis (DVT), venous ultrasound is the standard imaging test. There is variability and disagreement among societies regarding the necessary components of the test. The Society of Radiologists recommends a protocol involving a comprehensive duplex ultrasound from thigh to ankle with Doppler at certain sites, rather than a limited or complete compression-only examination [34]. Venous duplex ultrasound combines 2 components to assess for DVT: B-mode or gray-scale imaging with transducer compression maneuvers and Doppler evaluation consisting of color-flow Doppler imaging and spectral Doppler waveform analysis [35]. The diagnostic criteria for DVT include an evaluation of venous compressibility, intraluminal echoes, venous flow characteristics, and differential filling of the vessel in color Duplex. A common criterion for a DVT is the incompressibility of a vein. The vein can either appear dilated with echogenic thrombus present or dilated without a visible thrombus. Acute thrombosis can be isoechogenic and is visible in acute DVTs as low as 50% of the time [35]. See Tables 2 and 3.

5.1 Body Position

For a lower or upper rule out DVT, ultrasound patients can be in the supine, erect or reclined position. The examined leg should be supinated slightly at the hip. The calf veins are more easily viewed when the legs are lower, which allows for venous distension.

Table 2 Acuity of thrombus

Acuity	
Acute	Within the first 2 weeks after the thrombus forms
Subacute	>2 weeks and potentially up to 6 months after thrombus forms
Chronic	Usually >6 months old

Table 3 Ultrasound features of acute, subacute and chronic DVT. Features can be overlapping and are classified as indeterminate

Features	Acute	Subacute	Chronic
Attachment of thrombus to the vein wall	Loosely attached	Firmly attached	Firmly attached
Thrombus echogenicity	Hypoechoic or isoechoic	Variable (more echoic than acute DVT)	Hyperechoic (appears as a bright fibrous web or scar attached to the vein wall and protruding into the lumen)
Presence of free-floating or mobile thrombus tail	Possibly present	Usually absent	Absent
Vein wall appearance	Variable	Variable	Venous wall thickening and scarring. Calcium deposition may be perceived
Vein lumen	Distended	Will retract to normal size	Smaller than normal size (atrophic)
Compressibility	Slightly deformable, "spongy"	More compressible than acute	Partly non-compressible, likely partial recanalization

Modified from Ref. [36]

5.2 Limitations

The scanning quality in obese patients or those with severe edema might be limited. Acoustic windows might be limited in patients with open wounds or casts.

5.3 Equipment

Mid-frequency probe (5–8 Mhz), either linear or curvilinear can be used.

6 DVT Ultrasound Scanning

While a comprehensive duplex-ultrasound examination protocol is recommended by the Society of Radiology, the most commonly performed vascular ultrasound study is the "rule out DVT" compression study. The primary purpose of this examination is to determine if the patient has a thrombosis of the lower (or upper) extremity vessels. The procedure consists of compressing the popliteal, superficial femoral, and common femoral veins, ensuring that the vein is fully compressible and that it reforms normally with no evidence of obstructive clot. A normal respiratory movement within the vessel additionally points to patency of proximal veins. An examination protocol should always follow the same series of images. Figure 2.

6.1 Sensitivity and Specificity

The specificity of compression ultrasound for a calf DVT is 97.8% (97.0–98.4%). The sensitivity is 56.8% (95% confidence interval, 49–66.4%), which is less than that of duplex ultrasound for proximal DVT 96.5% (95% confidence interval, 95.1–97.6%) [37].

6.2 Lower Extremity

A comprehensive duplex ultrasound examination for lower extremity DVT involves interrogation from the thigh to the ankle [34], common femoral vein, saphenofemoral junction, proximal femoral vein, profunda femoris vein, midfemoral vein, distal femoral vein, popliteal vein, posterior tibial veins, and peroneal veins. At each position, the vein is analyzed for venous compressibility and the presence of echogenic thrombus with B-mode imaging. Additionally, venous flow characteristics are assessed to determine proximal occlusion. Each vein is interrogated with interval compression proximally and distally. Compression maneuvers are performed in the transverse view every 1–2 cm from the inguinal ligament to the calf. Proximal compression should interrupt the flow, while distal occlusion should augment flow. If augmentation is not demonstrated upon distal compression, a DVT should be suspected. The deep veins should be interrogated in both transverse and longitudinal views. In longitudinal views, both spectral Doppler images and color flow images are evaluated. Color flow is helpful in identifying partial vessel occlusion of acute echolucent thrombus or in areas in which compression is limited. Above the popliteal vein, normal venous flow is spontaneous and varies with respiration, augments with distal compression, and subsides with a Valsalva maneuver. Below the knee spontaneous flow may be absent but, flow should augment in the tibioperoneal veins distal compression. Continuous flow signals without respiratory variation, lack of augmentation with the release of proximal compression, and continuous flow during Valsalva maneuvers suggest proximal obstruction. Whereas distal obstruction might be suspected with diminished or absent augmentation with distal compression. Document the normal anatomy and any pathology. Include Doppler images demonstrating flow. See Fig. 3.

6.3 Clinical Pearls

The Femoral vein and artery usually run together. The popliteal vein lies superficial to the artery. The groin lymph nodes are well-circumscribed, non- compressible structures and can be mistakenly thought to be a non-compressible vein. Make sure you are looking at a vein, not a lymph node, by following the vein for a couple of centimeters. To completely

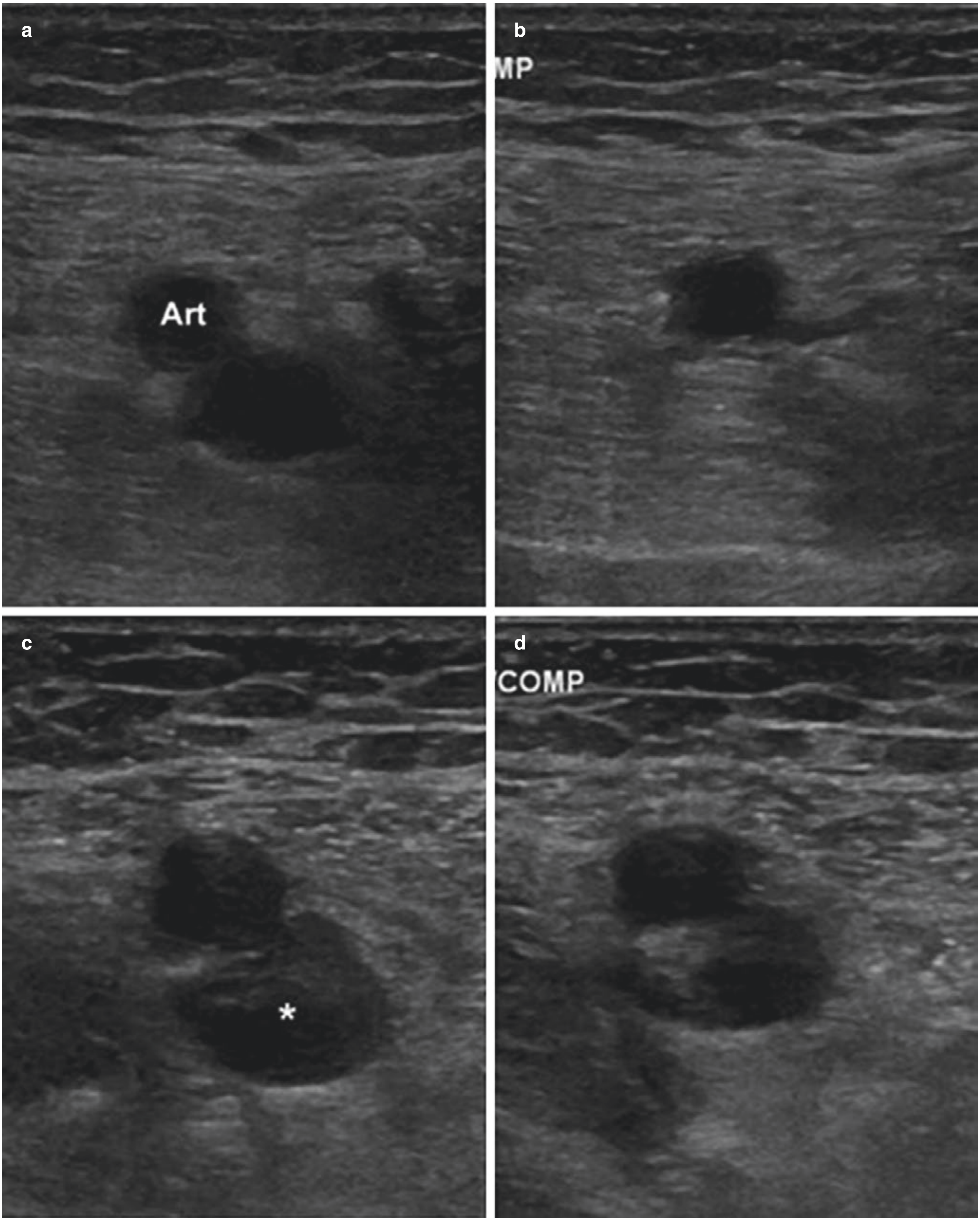

Fig. 2 Image of a normal femoral vein at baseline and acute DVT at 1-week follow-up. (**a**, **b**) Ultrasound images of a normal femoral vein without (**a**) and with (**b**) compression. The artery (Art) is anterior to the vein. After compression, the vein is completely collapsed, indicating normal compressibility. (**c**, **d**) Ultrasound images of acute femoral vein thrombus without (**c**) and with (**d**) compression after 1 week of follow-up. The acute DVT (∗ in **c**) is heterogeneous. It expands the vein. After compression (**d**), the vein does not collapse but has an oval shape indicating an acute DVT based on the non-compressible but deformable vein. DVT indicates deep venous thrombosis. (Taken with permission from Ref. [34])

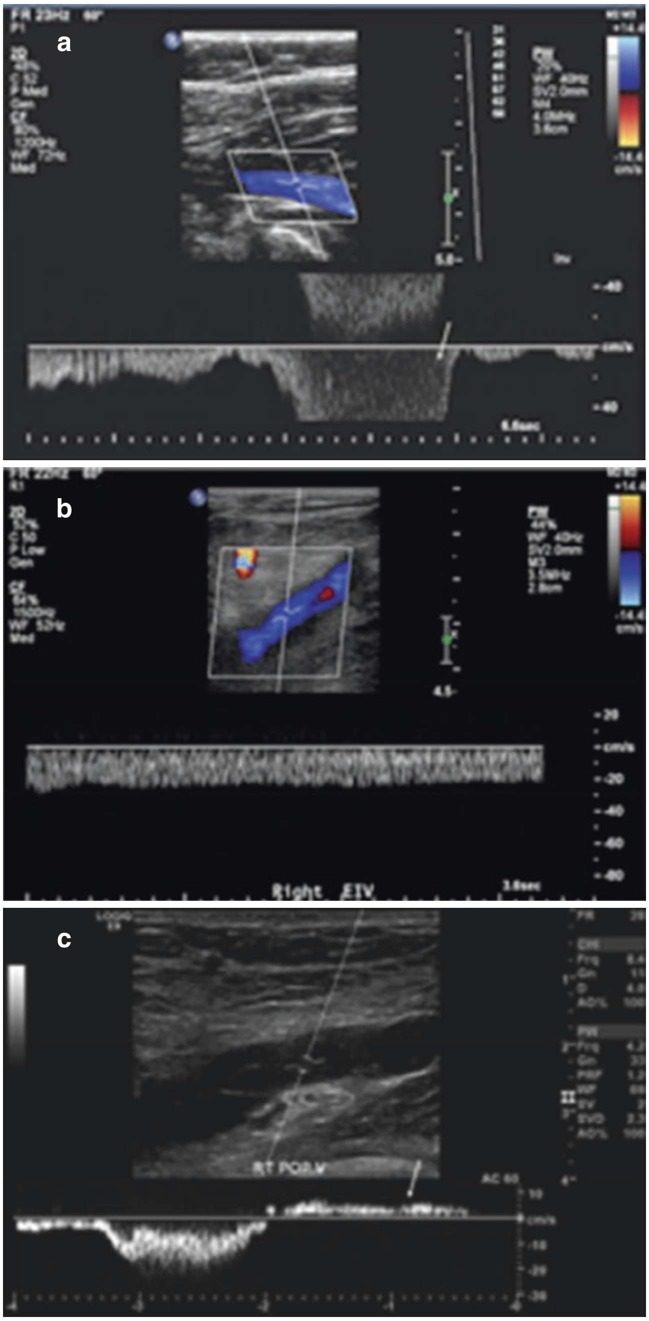

Fig. 3 Images of Spectral Doppler waveform analysis of the lower extremity veins. (**a**) Spontaneous and respirophasic flow with a normal response to an augmentation maneuver and aliasing of the pulsed Doppler signal (arrow). (**b**) Monophasic venous flow suggesting venous obstruction proximal to this segment. EIV indicates the external iliac vein. (**c**) Retrograde flow in the popliteal vein (POP V) after an augmentation maneuver (arrow), consistent with valvular incompetence in a patient with a history of deep venous thrombosis and the post-thrombotic syndrome. (Taken with permission from Ref. [36])

evaluate the femoral vein, also visualize the confluence of the greater saphenous and common femoral veins.

Poor compressibility might happen at the valve area and should not be confused with a DVT. Finally, common differentials include Bakers cyst in the medial popliteal fossa, superficial venous thrombosis of varices, tears in the calf muscle.

6.4 Upper Extremity

In the case of upper extremity DVTs, the compressibility of the vein is the main diagnostic criterion. The axillary, brachial, basilic and internal jugular veins are imaged with compression and color and spectral flow. Veins of the upper extremity are to a greater degree affected by cardiac and respiratory variations. Flow is severely limited during a Valsalva maneuver and the vein diameter increases. The subclavian vein is not easily compressible due to the overlying clavicle and is assessed using secondary signs including the absence of respiratory variability and cardiac pulsatility [38]. Thrombosis is diagnosed by direct visualization of thrombus, absent or incomplete color filling of the lumen, and an absent diameter response to rapid inspiration. The addition of Color Doppler to the duplex examination has increased the sensitivity and specificity of the examination and allowed for increased visualization of partial occlusions.

7 U/S Screening for Carotid Disease

Around 20–30% of all strokes are caused by extracranial carotid artery stenosis (CAS) [39], while intracranial CAS accounts for 5–10% of strokes [40]. Coronary Artery Disease (CAD) occurs secondary to atherosclerosis and the result of a build-up of atherosclerotic plaques rupturing, formation of a thrombus, and subsequent dislodging and blockage of branches of the carotid artery. Preventing strokes and adequately treating CAD before it progresses to stroke. Ultrasound technology, specifically via Doppler technology measuring flow velocities, has become vital in the assessment and treatment of CAD.

Proper, reproducible technique is vital for the accurate and valid testing of the degree of carotid artery stenosis. Ultrasonography can display the most proximal segment of the common carotid artery but cannot display the proximal segment of the left common carotid due to its rise from the aortic arch. Once the common carotid artery is identified, the internal carotid artery (ICA) should be differentiated from the external carotid artery (ECA). The ICA is located lateral and posterior to the ECA and is slightly larger.

7.1 Technique

For carotid ultrasonography, the recommended position is the overhead position, where the examiner sits above the patient's head and beside the end of the examination table so they are able to use two hands for the ultrasonography. In this position, the examiner should use their right hand for the right carotid artery and use their left hand for the left carotid artery. This position is beneficial because the examiner can use both hands and there are ample positions available for the ultrasonography probe. Finally, the ultrasound screen can be positioned immediately in front of the examiner to increase ease of measurement.

8 Color and Pulsed Wave Doppler Ultrasonography

Color Doppler is the main way to measure stenosis via color-encoded velocity information. To achieve a proper Doppler image, the sonic beam needs to be at a 30–60° angle to the skin, as opposed to a normal ultrasonographic image which is perfectly perpendicular. After identifying proper anatomical landmarks, one should adjust the velocity range. There is constant flow volume through the vessel, therefore the velocity of flow must change with the degree of stenosis. Therefore, the velocity of flow is fastest at the stenotic segment. The common carotid artery has a velocity of 30–40 cm/s [41]. If the upper limit of the color velocity scale is just below that of the flow velocity in the normal vessel, the increased flow velocity in the stenotic segment will be above the upper limit of the velocity scale and there will be an aliasing artifact [41]. The segment is stenoic if there is a segment presenting an aliasing artifact at the proper velocity scale setting. To measure exact flow velocity, pulsed wave Doppler is used. A small sample volume taken in the center of the artery is used to check the velocity of the segment, specifically the peak systolic and diastolic velocities are measured. Significant stenosis of the ICA is indicated by a peak systolic velocity of 125 cm/s or higher in the ICA, or twice as fast as that of the common carotid artery [42]. See Table 4.

Table 4 Proper interpretation of ICA stenosis based off of the proper measurements

	Peak systolic velocity	End diastolic velocity	ICA/CCA PSV ratio
Diameter stenosis %			
Normal	<125	<40	<2.0
<50	<125	<40	<2.0
50–69	125–230	40–100	2.0–4.0
≥70	>230	>100	>4.0
Near total occlusion	Variable	Variable	Variable
Total occlusion	Undetectable	Undetectable	Not applicable

Carotid Doppler and Pulse Wave Doppler Ultrasound is an invaluable tool for evaluation of carotid artery stenosis. It is able to detect atherosclerotic plaque including visualizing the intima-media thickness as a biomarker for atherosclerosis in addition to the classical carotid artery stenosis measurement. Anesthesiologists should be familiar with the physics and clinical findings of Doppler ultrasonography in performing Doppler ultrasonography studies of the carotid arteries and what it means for the overall health for their patient.

9 AAA Screening and Evaluation

Several randomized clinical trials have shown that ultrasound screening reduces aneurysm-related mortality with a reduced risk for rupture and emergency surgery [43–45]. The Society for Vascular Surgery recommends surveillance imaging at 3-year intervals for patients with an initial AAA diameter between 3.0 and 3.9 cm, an interval of 1 year for AAAs between 4.0 and 4.9 cm and 6 months for those between 5.0 and 5.4 cm. Aneurysm enlargement is significantly increased in smokers and in patients with a larger AAA diameter [46]. In hemodynamically stable patients with a symptomatic AAA, CT aortography is recommended. In this setting, ultrasound should be used to determine if an AAA is present. Once a AAA is diagnosed, a referral to a vascular surgeon should be placed.

Ninety-five percent of adults have an aortic diameter of ≤3.0 cm with the average diameter of the infrarenal aorta being approximately 2.0 cm. For the majority of patients, a segmental diameter of ≥3.0 cm is considered aneurysmal with an increase in diameter predicting worse clinical outcomes in men. In women, however, diameter is less predictive [46]. AAA most often affect the segment of the aorta between origins of the renal and inferior mesenteric arteries. Both the sensitivity and specificity are close to 100% making ultrasound the ideal test for screening. Some operators may have difficulty visualizing the aorta because of bowel gas or obesity.

The patient should lie supine, head-of-bed flat with the legs flat or knees slightly flexed. With a low frequency curvilinear transducer apply constant, firm pressure to the patient's abdomen, starting with images of the aorta in the transverse orientation at the level of the celiac artery takeoff with the vertebral body visible. The splenic and hepatic arteries should be visualized coming off the celiac trunk, sometimes looking akin to a seagull with the hepatic artery as the right wing and the splenic artery as the left wing. Next, moving inferiorly, the superior mesenteric artery (SMA) takeoff should be visualized coming off the aorta in a transverse orientation. Just superior to the umbilicus, the distal aorta at or just above the bifurcation should be visualized in a transverse orientation. Fanning the transducer inferiorly may be helpful. At all three sites, images with and without measurements in the AP and lateral directions should be saved.

Moving to images of the abdominal aorta in a sagittal orientation with the transducer oriented superiorly, the celiac trunk and SMA coming off the aorta should be visualized. The inferior mesenteric artery is usually no visible with ultrasound. Images with and without measurements of the widest segment visualized along with Doppler to confirm patency should be saved. All measurements should include the lumen plus intraluminal plaque, if present and should be "outer-layer to outer-layer" so as to not underestimate the vessel diameter.

10 U/S Screening in AKI Assessment: Resistive Index

Acute kidney injury (AKI) occurs in around 50% of intensive care patients with sepsis, cardiogenic shock or major surgery [47, 48]. Nearly 15% of ICU patients require renal replacement therapy, and AKI increases morbidity and mortality as a lone variable [47, 48]. Early detection and prevention are crucial for decreasing negative outcomes [49, 50]. An early manifestation of AKI is renal vasoconstriction, which can be measured by a variable called renal resistive index (RRI). This is a sonographic index that represents blood flow profiles of the intrarenal and interlobar arteries, specifically the relationship between the decline in flow velocity between the peak of systoly and the end of diastole in renal vessels [51, 52]. Elevated RRI is related to several different diseases such as atherosclerosis, diabetes, chronic kidney disease and histopathological outcomes (glomerular sclerosis, arteriolosclerosis, interstitial fibrosis), and is associated with elevated RRI [53–56]. One observational cohort study showed that RRI was a significant independent early predictor and discriminator for development of AKI stage 2 and 3 during the first week, but not for AKI stage, for ICU admission 1 [57]. The authors recommended measuring RRI as part of a broad ultrasound screening of vital organ function to contribute to the early detection of patients at risk of developing AKI.

10.1 Technique

Standardized, meticulous, and repeatable technique is vital to properly measure RRI in a clinical setting. A high resistance probe is optimal along with the use of color or power Doppler to help with vessel localization. Sampling for RRI should be done at the level of the arcuate or interlobar arteries, adjacent to medullary pyramids. Three reproducible waveforms should be produced, and an RRI is calculated by measuring the peak systolic velocity and the end systolic velocity and using the formula (peak systolic velocity – end diastolic velocity)/peak systolic velocity. The mean value of the three exams is used, and an RRI value 0.60 ± 0.01 (mean ± SD) is taken as normal with a value of 0.70 being considered the upper normal threshold by most physicians [58]. An increased RRI is regarded as an indicator of increased renal vascular resistance.

Below are summarized pearls for improving ultrasound views (Table 5).

In summary, ultrasound is important in assessing and treating vascular disease. Clinicians should appreciate the important information that can be obtained using ultrasound and its evolving importance in vascular disease.

Table 5 Pearls to optimize the ultrasound examination

Obese/edematous patients	A curvilinear probe can be utilized
Cannot compress the vein but a clot cannot be visualized	Assume that there is a DVT. Clots can be isoechoic and may not be well visualized.
Where is the popliteal vein?	Can be difficult to identify. Try maneuvers to distend the vessels (sitting up etc.). Alternatively, place the patient in the prone position and passively flexing the foot in the air. Color Doppler may also facilitate the finding of vessels.
The vein is not completely compressing	A normal vein will disappear when completely compressed. Make sure to center the vessel and compress transversely (not longitudinally).
How much pressure should be applied?	Appropriate pressure compresses the vein completely and dents the artery some.

References

1. Abbott AL. Medical (nonsurgical) intervention alone is now best for prevention of stroke associated with asymptomatic severe carotid stenosis: results of a systematic review and analysis. Stroke. 2009;40(10):e573–83.
2. Spence JD. Management of asymptomatic carotid stenosis. Neurol Clin. 2015;33(2):443–57.
3. Brott TG, et al. 2011 ASA/ACCF/AHA/AANN/AANS/ACR/ASNR/CNS/SAIP/ SCAI/SIR/SNIS/SVM/SVS guideline on the management of patients with extracranial carotid and vertebral artery disease: executive summary. Vasc Med. 2011;16(1):35–77.
4. AbuRahma AF, et al. Critical appraisal of the Carotid Duplex Consensus criteria in the diagnosis of carotid artery stenosis. J Vasc Surg. 2011;53(1):53–60.
5. Johnston KW, Rutherford RB, Tilson MD, Shah DM, Hollier L, Stanley JC. Suggested standards for reporting on arterial aneurysms. Subcommittee on Reporting Standards for Arterial Aneurysms, Ad Hoc Committee on Reporting Standards, Society for Vascular Surgery and North American Chapter, International Society for Cardiovascular. J Vasc Surg. 1991;13(3):452–8.
6. LeFevre ML. Screening for abdominal aortic aneurysm: U.S. Preventive Services Task Force recommendation statement. Ann Intern Med. 2014;161(4):281–90.
7. Kent KC, et al. Analysis of risk factors for abdominal aortic aneurysm in a cohort of more than 3 million individuals. J Vasc Surg. 2010;52(3):539–48.

8. Textor SC, Lerman L. Renovascular hypertension and ischemic nephropathy. Am J Hypertens. 2010;23(11):1159–69.
9. Hankey GJ, Norman PE, Eikelboom JW. Medical treatment of peripheral arterial disease. JAMA. 2006;295(5):547–53.
10. Parvar SL, Fitridge R, Dawson J, Nicholls SJ. Medical and lifestyle management of peripheral arterial disease. J Vasc Surg. 2018;68(5):1595–606.
11. Alahdab F, et al. A systematic review for the screening for peripheral arterial disease in asymptomatic patients. J Vasc Surg. 2015;61(3):42S–53S.
12. Raskob GE, et al. Thrombosis. Arterioscler Thromb Vasc Biol. 2014;34(11):2363–71.
13. Grosse SD, Nelson RE, Nyarko KA, Richardson LC, Raskob GE. The economic burden of incident venous thromboembolism in the United States: a review of estimated attributable healthcare costs. Thromb Res. 2016;137:3–10.
14. Di Nisio M, van Es N, Büller HR. Deep vein thrombosis and pulmonary embolism. Lancet. 2016;388(10063):3060–73.
15. Stein JH, et al. Use of carotid ultrasound to identify subclinical vascular disease and evaluate cardiovascular disease risk: a consensus statement from the American Society of Echocardiography Carotid Intima-Media Thickness Task Force. Endorsed by the Society for Vascular Medicine. J Am Soc Echocardiogr. 2008;21(2):93–111.
16. Greenland P, et al. Prevention conference V: beyond secondary prevention: identifying the high-risk patient for primary prevention: noninvasive tests of atherosclerotic burden: Writing Group III. Circulation. 2000;101(1):E16–22.
17. Carter SA. Indirect systolic pressures and pulse waves in arterial occlusive disease of the lower extremities. Circulation. 1968;37(4):624–37.
18. Ankle Brachial Index Collaboration, et al. Ankle brachial index combined with Framingham risk score to predict cardiovascular events and mortality. JAMA. 2008;300(2):197.
19. McDermott MM, et al. Associations of borderline and low normal ankle-brachial index values with functional decline at 5-year follow-up: the WALCS (Walking and Leg Circulation Study). J Am Coll Cardiol. 2009;53(12):1056–62.
20. Safar ME, Protogerou AD, Blacher J. Statins, central blood pressure, and blood pressure amplification. Circulation. 2009;119(1):9–12.
21. Hope SA, Tay DB, Meredith IT, Cameron JD. Waveform dispersion, not reflection, may be the major determinant of aortic pressure wave morphology. Am J Physiol Circ Physiol. 2005;289(6):H2497–502.
22. Humphrey JD. Mechanisms of arterial remodeling in hypertension: coupled roles of wall shear and intramural stress. Hypertens (Dallas, Tex. 1979). 2008;52(2):195–200.
23. Gornik HL, Garcia B, Wolski K, Jones DC, Macdonald KA, Fronek A. Validation of a method for determination of the ankle-brachial index in the seated position. J Vasc Surg. 2008;48(5):1204–10.
24. Manning DM, Kuchirka C, Kaminski J. Miscuffing: inappropriate blood pressure cuff application. Circulation. 1983;68(4):763–6.
25. Pickering TG, et al. Recommendations for blood pressure measurement in humans and experimental animals. Circulation. 2005;111(5):697–716.
26. Aboyans V, et al. Measurement and interpretation of the ankle-brachial index. Circulation. 2012;126(24):2890–909.
27. Conrad MC, Toole JF, Janeway R. Hemodynamics of the upper extremities in subclavian steal syndrome. Circulation. 1965;32(3):346–51.
28. Olin JW, et al. ACCF/AHA/ACR/SCAI/SIR/SVM/SVN/SVS 2010 performance measures for adults with peripheral artery disease. J Am Coll Cardiol. 2010;56(25):2147–81.
29. Lijmer JG, Hunink MG, van den Dungen JJ, Loonstra J, Smit AJ. ROC analysis of noninvasive tests for peripheral arterial disease. Ultrasound Med Biol. 1996;22(4):391–8.
30. Stein R, Hriljac I, Halperin JL, Gustavson SM, Teodorescu V, Olin JW. Limitation of the resting ankle-brachial index in symptomatic patients with peripheral arterial disease. Vasc Med. 2006;11(1):29–33.
31. Aboyans V, Ho E, Denenberg JO, Ho LA, Natarajan L, Criqui MH. The association between elevated ankle systolic pressures and peripheral occlusive arterial disease in diabetic and nondiabetic subjects. J Vasc Surg. 2008;48(5):1197–203.
32. Sibley RC, Reis SP, MacFarlane JJ, Reddick MA, Kalva SP, Sutphin PD. Noninvasive physiologic vascular studies: a guide to diagnosing peripheral arterial disease. Radiographics. 2017;37(1):346–57.
33. Hiatt WR, Jones DN. The role of hemodynamics and duplex ultrasound in the diagnosis of peripheral arterial disease. Curr Opin Cardiol. 1992;7(5):805–10.
34. Needleman L, et al. Ultrasound for lower extremity deep venous thrombosis. Circulation. 2018;137(14):1505–15.
35. Killewich LA, Bedford GR, Beach KW, Strandness DE. Diagnosis of deep venous thrombosis. A prospective study comparing duplex scanning to contrast venography. Circulation. 1989;79(4):810–4.
36. Gornik HL, Sharma AM. Duplex ultrasound in the diagnosis of lower-extremity deep venous thrombosis. Circulation. 2014;129(8):917–21.
37. Goodacre S, Sampson F, Thomas S, van Beek E, Sutton A. Systematic review and meta-analysis of the diagnostic accuracy of ultrasonography for deep vein thrombosis. BMC Med Imaging. 2005;5:6.
38. Giess CS, Thaler H, Bach AM, Hann LE. Clinical experience with upper extremity venous sonography in a high-risk cancer population. J Ultrasound Med. 2002;21(12):1365–70; quiz 1372–3.
39. Stroke in Childhood: Clinical Guidelines for Diagnosis, Management and Rehabilitation, By Paediatric Stroke Working Group · 2004, publisher: Clinical Effectiveness & Evaluation Unit, Royal College of Physicians.
40. Sacco RL. Extracranial carotid stenosis. N Engl J Med. 2001;345(15):1113–8.
41. Kim S, Lee S, Choi HS, Jung S, Ahn K, Kim B. Pseudostenosis at the origin of the vertebral artery on contrast-enhanced MRA: correlation with aortic motion on dynamic 3D time-resolved contrast-enhanced MRA. J Korean Soc Magn Reson Med. 2012;16(3):236–42.
42. Grant EG, et al. Carotid artery stenosis: gray-scale and Doppler US diagnosis—Society of Radiologists in Ultrasound consensus conference. Radiology. 2003;229(2):340–6.
43. Guirguis-Blake JM, Beil TL, Sun X, Senger CA, Whitlock EP. Primary care screening for abdominal aortic aneurysm. Rockville: Agency for Healthcare Research and Quality; 2014.
44. Ashton HA, et al. The Multicentre Aneurysm Screening Study (MASS) into the effect of abdominal aortic aneurysm screening on mortality in men: a randomised controlled trial. Lancet (London, England). 2002;360(9345):1531–9.
45. Scott RAP, Vardulaki KA, Walker NM, Day NE, Duffy SW, Ashton HA. The long-term benefits of a single scan for abdominal aortic aneurysm (AAA) at age 65. Eur J Vasc Endovasc Surg. 2001;21(6):535–40.
46. Chaikof EL, et al. The Society for Vascular Surgery practice guidelines on the care of patients with an abdominal aortic aneurysm. J Vasc Surg. 2018;67(1):2–77.e2.
47. Hoste EA, et al. RIFLE criteria for acute kidney injury are associated with hospital mortality in critically ill patients: a cohort analysis. Crit Care. 2006;10(3):R73.

48. Chertow GM, Burdick E, Honour M, Bonventre JV, Bates DW. Acute kidney injury, mortality, length of stay, and costs in hospitalized patients. J Am Soc Nephrol. 2005;16(11):3365–70.
49. Bagshaw SM, George C, Dinu I, Bellomo R. A multi-centre evaluation of the RIFLE criteria for early acute kidney injury in critically ill patients. Nephrol Dial Transplant. 2007;23(4):1203–10.
50. Hoste EAJ, et al. Epidemiology of acute kidney injury in critically ill patients: the multinational AKI-EPI study. Intensive Care Med. 2015;41(8):1411–23.
51. Spatola L, Andrulli S. Doppler ultrasound in kidney diseases: a key parameter in clinical long-term follow-up. J Ultrasound. 2016;19(4):243–50.
52. Ponte B, et al. Reference values and factors associated with renal resistive index in a family-based population study. Hypertension. 2014;63(1):136–42.
53. Bruno RM, et al. Dynamic evaluation of renal resistive index in normoalbuminuric patients with newly diagnosed hypertension or type 2 diabetes. Diabetologia. 2011;54(9):2430–9.
54. Masulli M, et al. Measurement of the intrarenal arterial resistance index for the identification and prediction of diabetic nephropathy. Nutr Metab Cardiovasc Dis. 2009;19(5):358–64.
55. Sugiura T, Wada A. Resistive index predicts renal prognosis in chronic kidney disease. Nephrol Dial Transplant. 2009;24(9):2780–5.
56. Calabia J, et al. The relationship between renal resistive index, arterial stiffness, and atherosclerotic burden: the link between macrocirculation and microcirculation. J Clin Hypertens. 2014;16(3):186–91.
57. Haitsma Mulier JLG, et al. Renal resistive index as an early predictor and discriminator of acute kidney injury in critically ill patients; a prospective observational cohort study. PLoS One. 2018;13(6):e0197967.
58. Tublin ME, Bude RO, Platt JF. The resistive index in renal Doppler sonography: where do we stand? Am J Roentgenol. 2003;180(4):885–92.

Pediatric Ultrasound

Allan Brook, Einat Blumfield, and Andrew Brook

1 Introduction

Cranial ultrasound is portable and easy to perform in sick term and preterm neonates, does not require sedation, and does not expose infants to ionizing radiation. Thanks to all of these aforementioned advantages, it is a commonly used modality in the Neonatal Intensive Care Unit (NICU) for screening in preterm neonates and for rapid diagnosis of abnormalities in term neonates at risk.

Preterm neonates who are <=32 weeks of gestation are at risk of suffering ischemic injuries to the brain that may present as periventricular leukomalacia or hemorrhagic lesions. The entity of hemorrhagic lesions consists of a spectrum of abnormalities ranging from germinal matrix hemorrhage to intraventricular hemorrhage, and periventricular hemorrhagic infarction.

In term neonates, the indications to perform a cranial sonogram may include hypoxic ischemic encephalopathy (HIE), seizures, multiple congenital abnormalities and genetic syndromes, as well as, intrauterine infections.

While MRI may be more accurate in detecting such abnormalities, it is not a suitable imaging modality for the critically ill patient. Ultrasound is performed at the bedside and may be repeated as required.

2 Cranial Ultrasound

2.1 Indications for Scanning

All premature infants who are <= 32 gestation weeks or weigh <=1500 g are screened with a cranial sonogram during the first week of their life.

Indications for scanning in term infants include, but are not limited to the following: HIE, seizures, coagulopathy, congenital malformations and evidence of intrauterine infection.

Infants with an open anterior fontanelle who are on extracorporeal membrane oxygenation (ECMO) are scanned daily with a cranial sonogram in search of an intracranial hemorrhage as they are anticoagulated.

In addition to all the above indications, which involve scanning in patients typically in the NICU or in the pediatric intensive care unit (PICU), infants with an open anterior fontanelle may be also scanned as out-patients with a cranial sonogram with the most common indication being macrocephaly. In these cases, the ventricular system is evaluated for hydrocephalus.

2.2 Technique of Imaging

The sonogram is performed with a small footprint sector 5–8 MHz transducer through the anterior fontanelle and may be supplemented with a linear 5–12 MHz transducer for high resolution images of the brain parenchyma and extra-axial spaces. Gray scale images are first obtained in the coronal plane and typically include at least 6–8 images beginning in the frontal lobes anterior to the frontal horns of the lateral ventricles, continuing with images through the frontal horns (Fig. 1), the bodies and atria (Fig. 2) of the lateral ventricles and ending in the occipital lobes posterior to the atria and occipital horns. Images in the sagittal plane then follow and include a mid-sagittal image (Fig. 3) demonstrating the corpus callosum supratentorially and the cerebellar vermis, fourth ventricle and the brainstem in the posterior fossa, followed by at least two parasagittal images from each side (Fig. 4); one that includes the lateral ventricle frontal horn, body and occipital horn and one that includes the temporal lobe and the temporal horn of each lateral ventricle. Additional scanning may be performed through the posterior fontanelle for improved visualization of the occipital lobes

A. Brook (✉)
Montefiore Medical Center, Radiology, Bronx, NY, USA

E. Blumfield
Children's Hospital of Montefiore, Albert Einstein College of Medicine, Radiology, Bronx, NY, USA

A. Brook
Albert Einstein College of Medicine class of 2024, Bronx, NY, USA

© Springer Nature Switzerland AG 2021
J. Li et al. (eds.), *Ultrasound Fundamentals*, https://doi.org/10.1007/978-3-030-46839-2_25

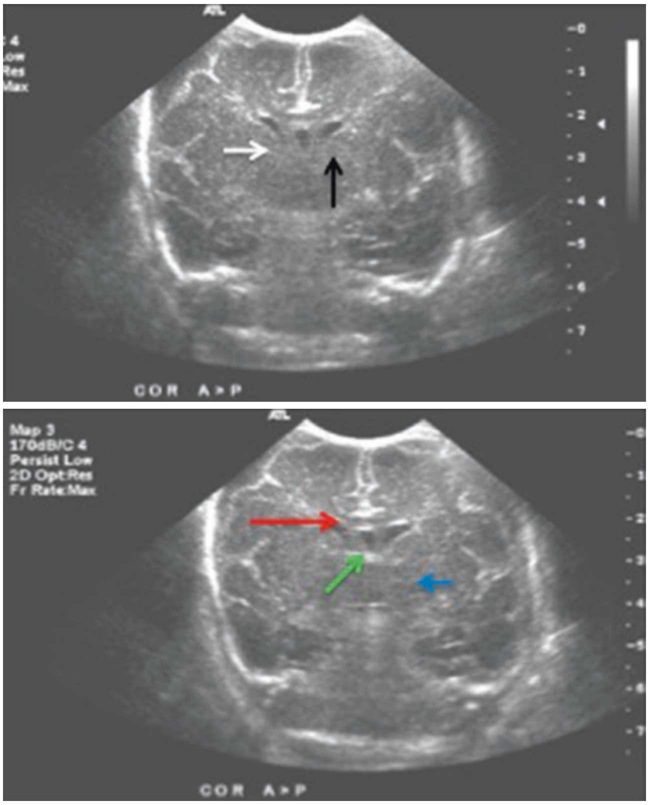

Fig. 1 Normal cranial sonogram in the coronal plane in a 27 week old premature newborn demonstrating the anterior body of the corpus callosum (red arrow). The cavum septum pellucidum is seen between the frontal horns of the lateral ventricles (green arrow). The left caudate nucleus head (black arrow), left thalamus (blue arrow) and the right caudothalamic groove (white arrow) are also marked on the image

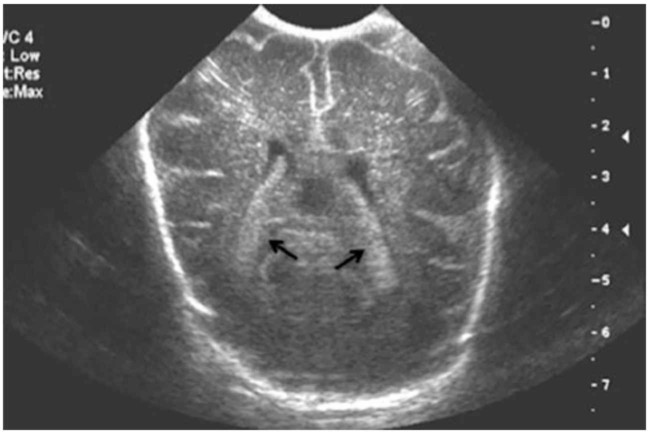

Fig. 2 Same patient as in Fig. 1 – Coronal image through the atria of the lateral ventricles demonstrate the normal choroid plexuses in the atria (arrows)

and the occipital horns of the lateral ventricles. Furthermore, images of the posterior fossa may be obtained through the mastoid windows (Fig. 5). This allows better depiction of posterior fossa hemorrhages and congenital abnormalities of the posterior fossa. Color and spectral wave Doppler scanning of the arterial and venous system may be added to the examination.

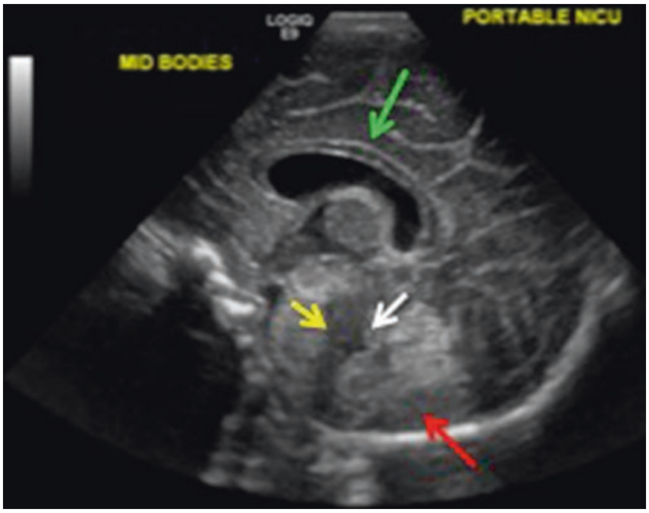

Fig. 3 Normal cranial sonogram in a 3 week old 34 week premature neonate- Mid-sagittal image demonstrates the normal corpus callosum (green arrow) supratentorially, and the normal cerebellar vermis (red arrow), the fourth ventricle (white arrow) and the brainstem (yellow arrow) in the posterior fossa

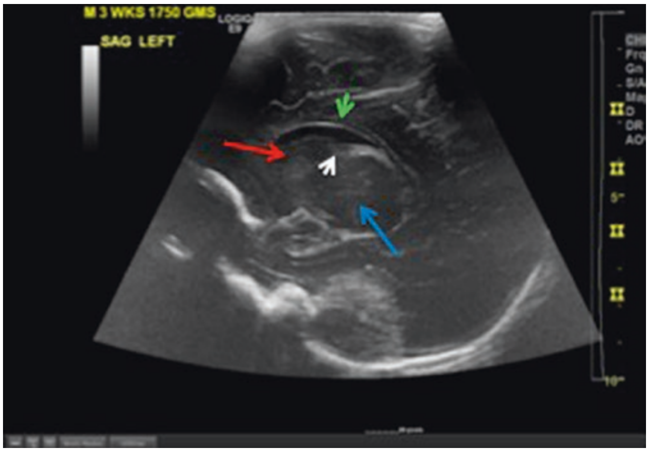

Fig. 4 Same patient as in Fig. 3. Left parasagittal image demonstrates the left lateral ventricle (green arrow), the left caudate nucleus head (red arrow), the left thalamus (blue arrow) and the left caudothalamic groove (white arrow)

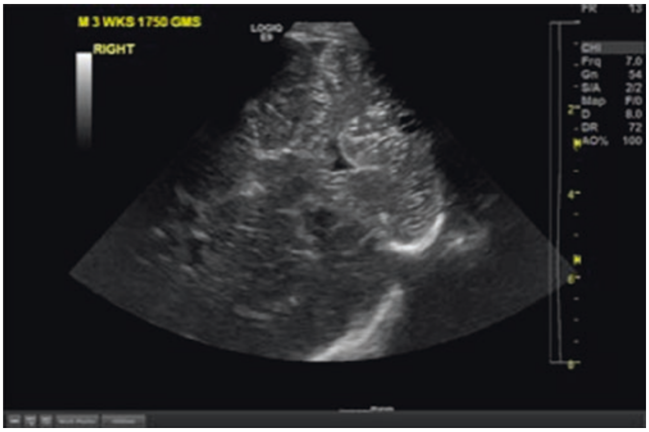

Fig. 5 Normal cerebellum seen via the mastoid window in a 24 days old, 35 week premature neonate

2.3 Findings in Preterm Infants

Hypoxic ischemic injury in preterm neonates may result in periventricular leukomalacia (Fig. 6). In these cases, ischemic injury to the periventricular white matter leads to cell necrosis, initially presenting with focal or diffuse areas of increased parenchymal echogenicity which later will progress to cystic changes. Eventually the cysts coalesce and there is loss of white matter with enlargement and irregular borders of the ventricles.

Another category of lesions in the premature brain are hemorrhagic lesions, which originate in the germinal matrix, located in the caudothalamic grooves. The germinal matrix is a hypervascular tissue, where deficient auto-regulation of cerebral blood flow may lead to germinal matrix hemorrhage. Germinal matrix hemorrhage may extend to the ventricles, and an intraventricular hemorrhage may be complicated with periventricular hemorrhagic infarct. These hemorrhagic lesions are classified as follows:

- Grade I - hemorrhage in the germinal matrix without extension to the ventricle - demonstrated as an echogenic area in the caudothalamic groove (Fig. 7)
- Grade II - Intraventricular hemorrhage with normal ventricular size - demonstrated as echogenic clots and hemorrhagic products within the ventricles which over time decrease in size and in echogenicity before they resolve.
- Grade III - intraventricular hemorrhage with ventricular enlargement - demonstrated similar to grade II but with ventriculomegaly.
- Grade IV - intraventricular hemorrhage and periventricular hemorrhagic infarct (Fig. 8) - demonstrated similar to grade III with echogenic foci in the periventricular white matter initially which later become cystic and eventually may lead to formation of porencephalic cysts.

Intraventricular hemorrhage may be complicated with hydrocephalus secondary to scarring in the pacchionian granulations or in the sylvius aqueduct hence further sono-

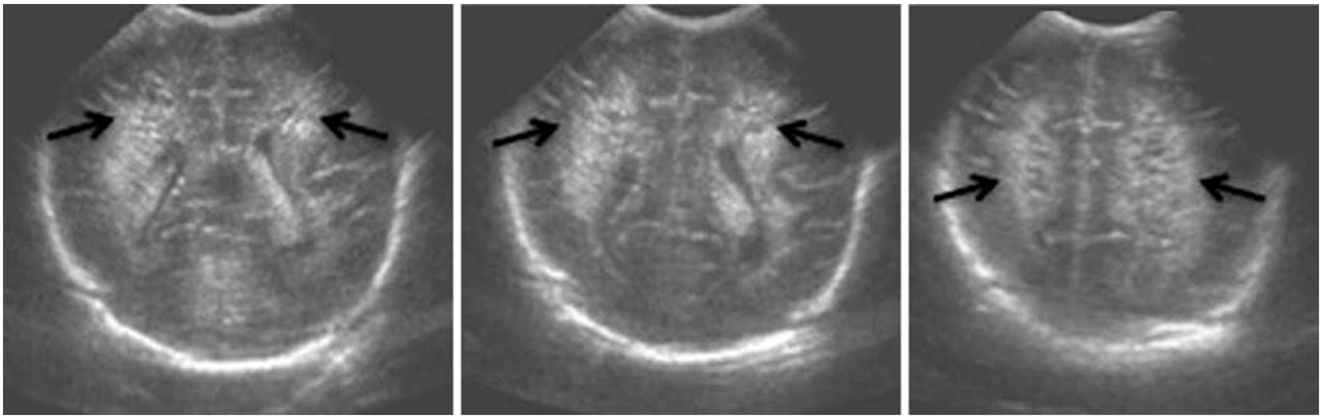

Fig. 6 Periventricular leukomalacia- Coronal images demonstrate increased echogenicity and microcystic changes in the periventricular white matter (arrows) in a 3 week old 25 week premature neonate

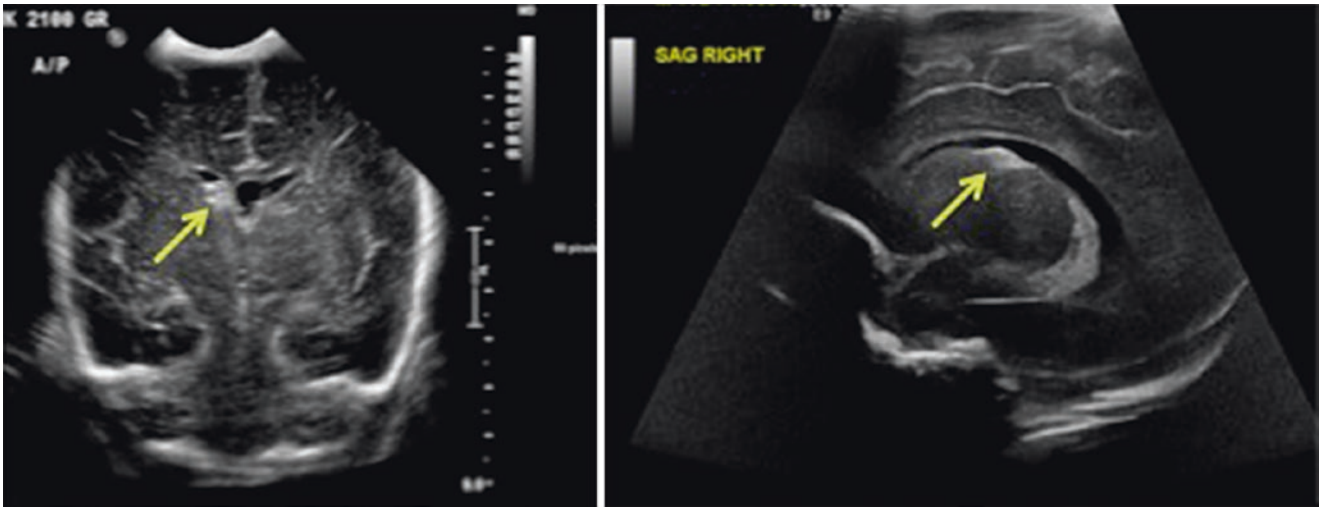

Fig. 7 Right germinal matrix (grade I) bleed - Images in the coronal and sagittal planes demonstrate an echogenic lesion in the right caudothalamic groove (arrow) in a 4 week old 31 week premature neonate

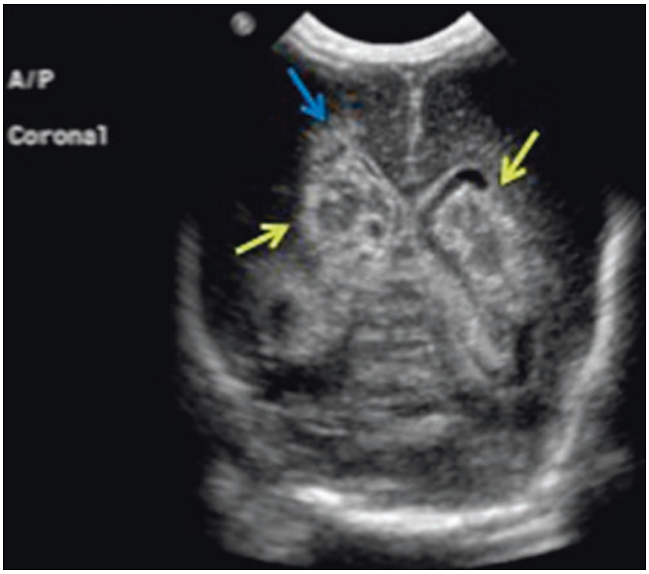

Fig. 8 Grade IV intraventricular hemorrhage - Coronal images demonstrate enlarged lateral ventricles, containing large, heterogeneous appearing blood clots (yellow arrows). In addition, there is a right frontal parenchymal periventricular hemorrhage (blue arrow), in a 12 days old, 23 week old premature neonate

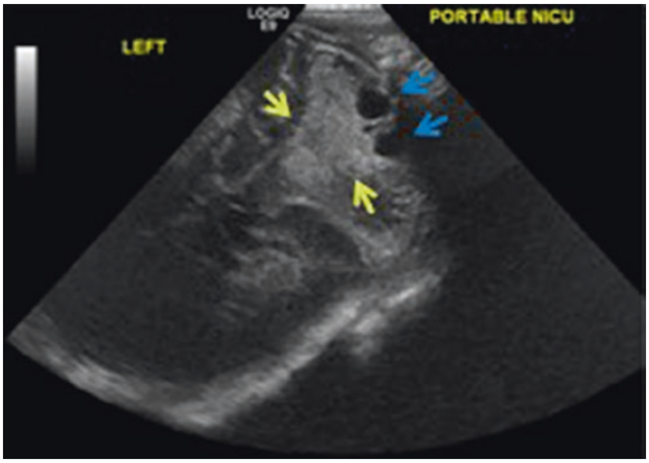

Fig. 9 Large sub-acute left cerebellar hemorrhage – Image via the left mastoid window demonstrates increased echogenicity in the left cerebellar hemisphere (yellow arrows) with cystic areas which represent encephalomalacia (blue arrows), in a 4 week old, 23 week premature neonate

graphic follow up is required when intraventricular hemorrhage is detected.

Cerebellar hemorrhages or infractions are being increasingly recognized in association with very low birth weight and are better depicted in the mastoid windows, they are most commonly unilateral, arising from the external granular layer and present as an echogenic lesion within the periphery of one of the cerebellar hemispheres, which later may progress to cystic encephalomalacia or focal atrophy (Fig. 9).

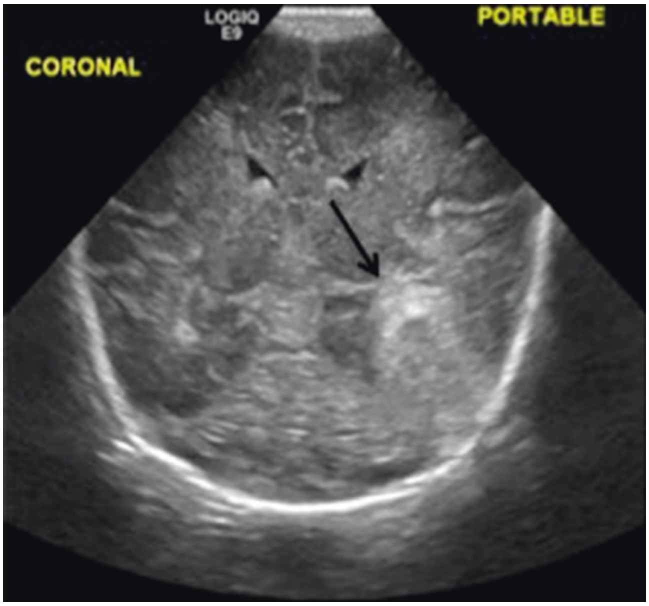

Fig. 10 Left occipital hematoma – coronal image demonstrates an echogenic area in the left occipital lobe consistent with a hematoma (arrow), in a 35 week newborn with intrauterine growth restriction and thrombocytopenia

2.4 Findings in Term Infants

Cerebral hemorrhages or infarcts may be detected in term infants in ultrasound, typically presenting as focal hyperechogenic areas (Fig. 10). Parenchymal calcifications may be detected in neonates with intrauterine infections, and congenital abnormalities such as agenesis of the corpus callosum (Fig. 11), absent cavum septum pellucidum, holoprosencephaly (Fig. 12) and dandy walker malformation may be detected as well. In these cases, MRI examination of the brain should be performed as well to assess for concomitant abnormalities.

2.5 Finding in Infants with Macrocephaly

While hydrocephalus may be detected with a cranial sonogram, the most common finding in asymptomatic infants with enlarged head circumference is benign enlargement of the subarachnoid spaces (BESS). This common entity usually presents in the first months of life with enlarged head circumference. A cranial sonogram typically demonstrates prominence of the subarachnoid spaces in the anterior and middle cranial fossae with mild enlargement of the ventricular system (Fig. 13). It is hypothesized that disequilibrium between formation and resorption of cerebrospinal fluid (CSF) is responsible for the enlargement of the subarachnoid spaces. The majority of patients are symptomatic and the enlargement of the subarachnoid spaces resolves by the age of 2 years.

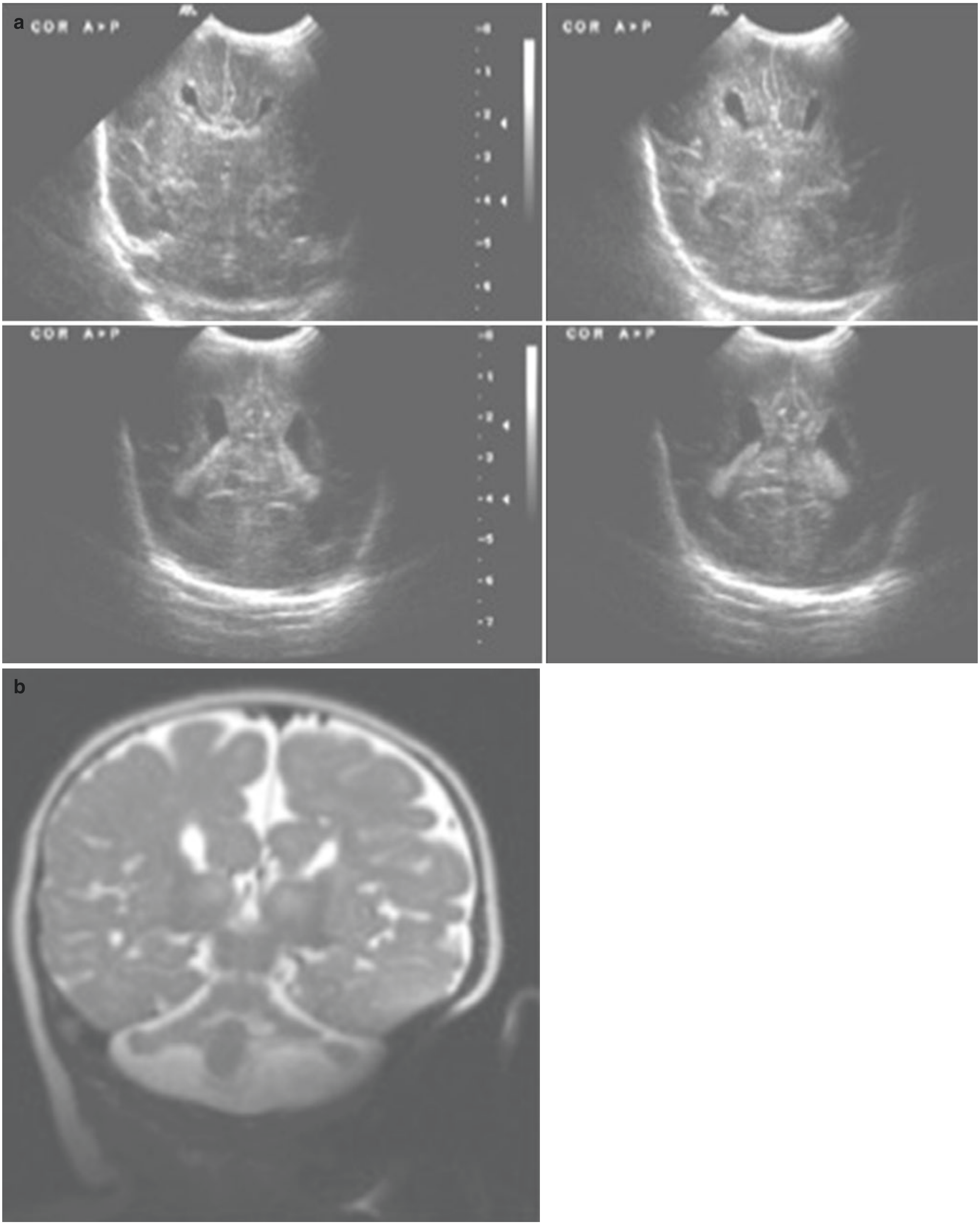

Fig. 11 Agenesis of the corpus callosum in a term newborn, diagnosed prenatally with ventriculomegally. (**a**) Sonographic images in the coronal plane demonstrate colpocephaly (the occipital horns, atria and the posterior bodies of the lateral ventricles are dilated, while the frontal horn are non-dilated). The normal corpus callosum is not identified. (**b**) Coronal T2 sequence from an MR examination shows agenesis of corpus callosum and a hypoplastic cerebellum

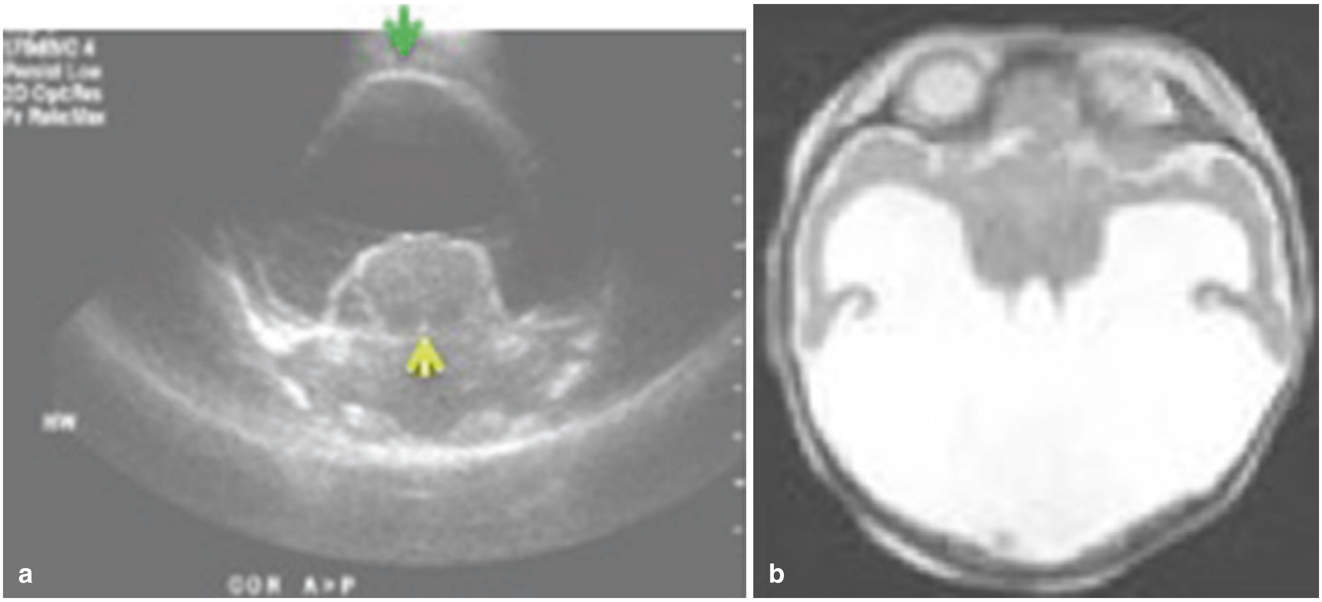

Fig. 12 Alobar holoprosencephaly in a term newborn. (**a**) Sonographic image in the coronal plane demonstrates a large mono-ventricle (green arrow) and fusion of the thalami (yellow arrow). (**b**) Axial T2 sequence from an MR examination demonstrates the same findings

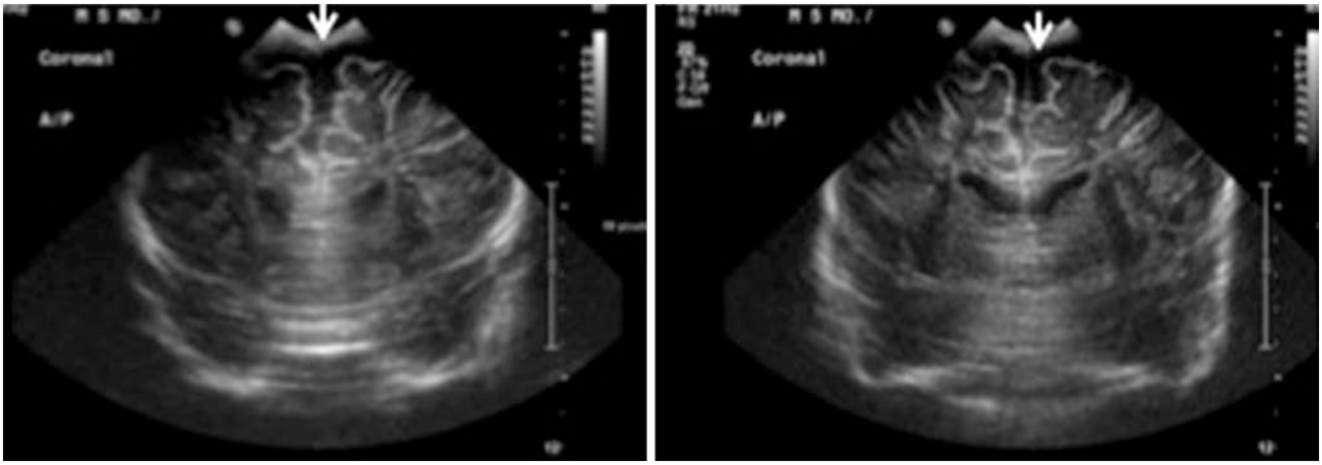

Fig. 13 Benign enlargement of the subarachnoid spaces in a 5 month old infant who presented with macrocephaly. Coronal images demonstrate prominence of the subarachnoid spaces in the vertex bilaterally (arrows)

Nevertheless, there are reports in the literature describing spontaneous subdural hematomas in infants with BESS, which may be secondary to stretching of bridging veins crossing through the subarachnoid and subdural spaces and secondary to increased motion of the brain within the skull.

3 Ultrasound of the spine

3.1 Ultrasound of the Spine

Sonographic imaging of the spine is obtained through the back, and is achievable while the posterior elements of the vertebrae are incompletely ossified. Therefore, it is most successful in the neonatal period and in early infancy and is significantly limited after the age of 6 months. Because of its clinical ease and the lack of need for sedation, ultrasound is considered the first modality of choice for imaging of the spinal canal during the neonatal period. In experienced hands, ultrasound has been shown to be highly accurate, hence MRI examinations are reserved for cases where ultrasound images were inadequate, inconclusive or when abnormalities are detected that require surgical planning.

Indications for a spinal sonogram include, but are not limited to the following:

- Lumbosacral stigmata that may be associated with spinal dysraphism or spinal cord tethering including a dimple, hair tuft, mass or a skin tag.

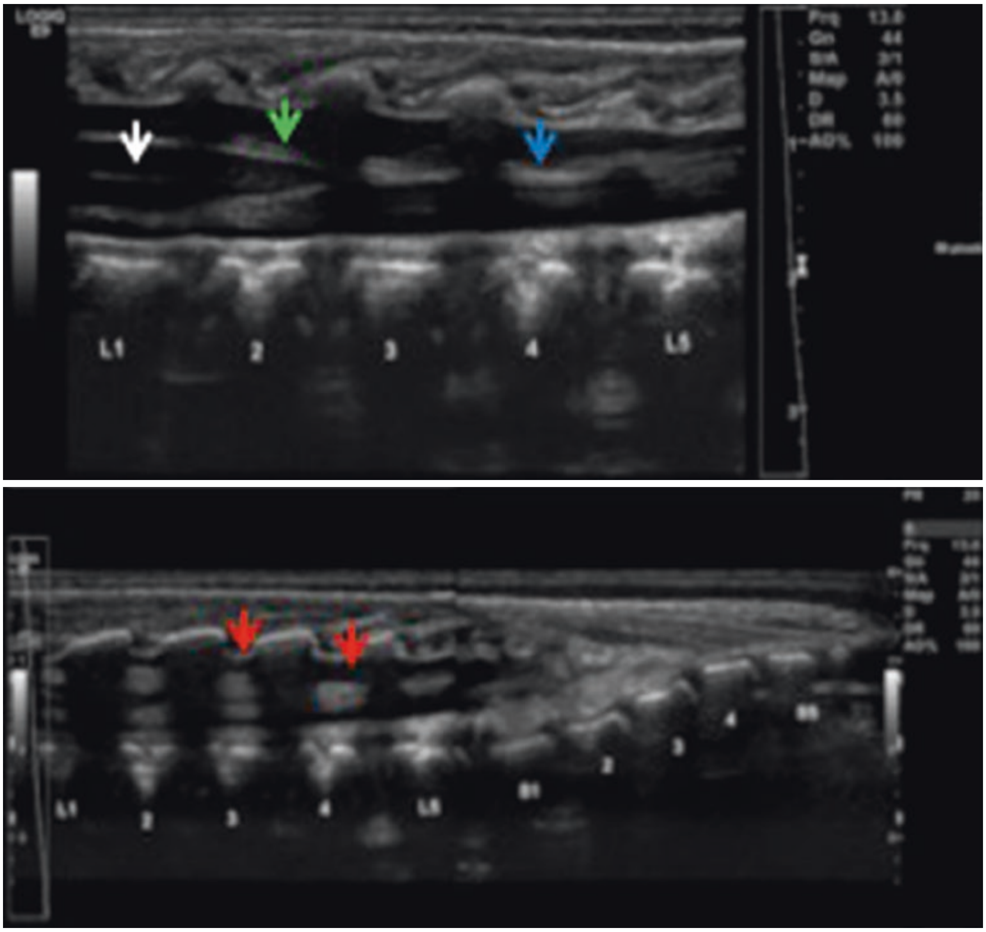

Fig. 14 Normal spinal sonogram. The conus medullaris is identified at the level of L2/3 (green arrow), the central canal within the spinal cord is identified as an echogenic line (white arrow), the filum terminale is a linear echogenic structure extending from the conus caudally (blue arrow). Cauda equina nerve roots are seen as well (red arrows)

- Sacral anomalies that may be associated with caudal regression syndrome.
- Anorectal malformations.
- Guidance for lumbar puncture in difficult cases.
- Evaluation for a hematoma following a lumbar puncture, from birth trauma or in infants with intracranial hemorrhage.

3.2 Technique and Normal Anatomy

Sonography of the infant spine should be performed using high-frequency linear array transducer, typically ranging from 9 to 12 MHz or higher. In larger babies, it may be necessary to utilize a lower-frequency transducers ranging from 5 to 9 MHz. A curvilinear transducer ranging from 3 to 9 MHz may be needed if a larger field of view is desired.

The examination is performed with the infant in prone position. A reverse Trendelenburg tilt may increase the amount of CSF in the spinal canal and improve visualization of its components.

The spinal canal is scanned in the transverse and sagittal planes. The entire spine including the cervical, thoracic and lumbosacral spine may be scanned; however, in the majority of cases a scan of the lumbosacral spine is sufficient to evaluate for spinal cord tethering or lumbosacral spinal dysraphism. Images are obtained through the spinal cord to assess for normal morphology and to determine the level of termination of the cord (Figs. 14 and 15). The cord is hypoechoic. The central canal within the cord is depicted as an echogenic line along the midline of the cord on the sagittal images and as an echogenic dot at the center of the cord in the transverse images. The cord terminates with the conus medullaris which is conical in shape and has a sharp tip. It is considered normal for the cord to terminate at or above the level of L2-3 and in preterm infants' termination at the level of the mid-body of L3 is considered the lowest limit of normal, but this should be followed with further sonograms to confirm that the cord reaches a normal level acceptable for a term infant. Vertebral body levels can be determined by one or more of the following methods:

- Identification of the Lumbosacral angle and hence L5 and S1 vertebrae (Fig. 14)
- Identifying the last rib and assuming the vertebra bearing this rib is T12 (Fig. 15)
- Identifying the tip of the thecal sac and assuming it is positioned at the level of S2 (Fig. 14)
- Counting from the first ossified coccyx segment (which may be variable and irreproducible).

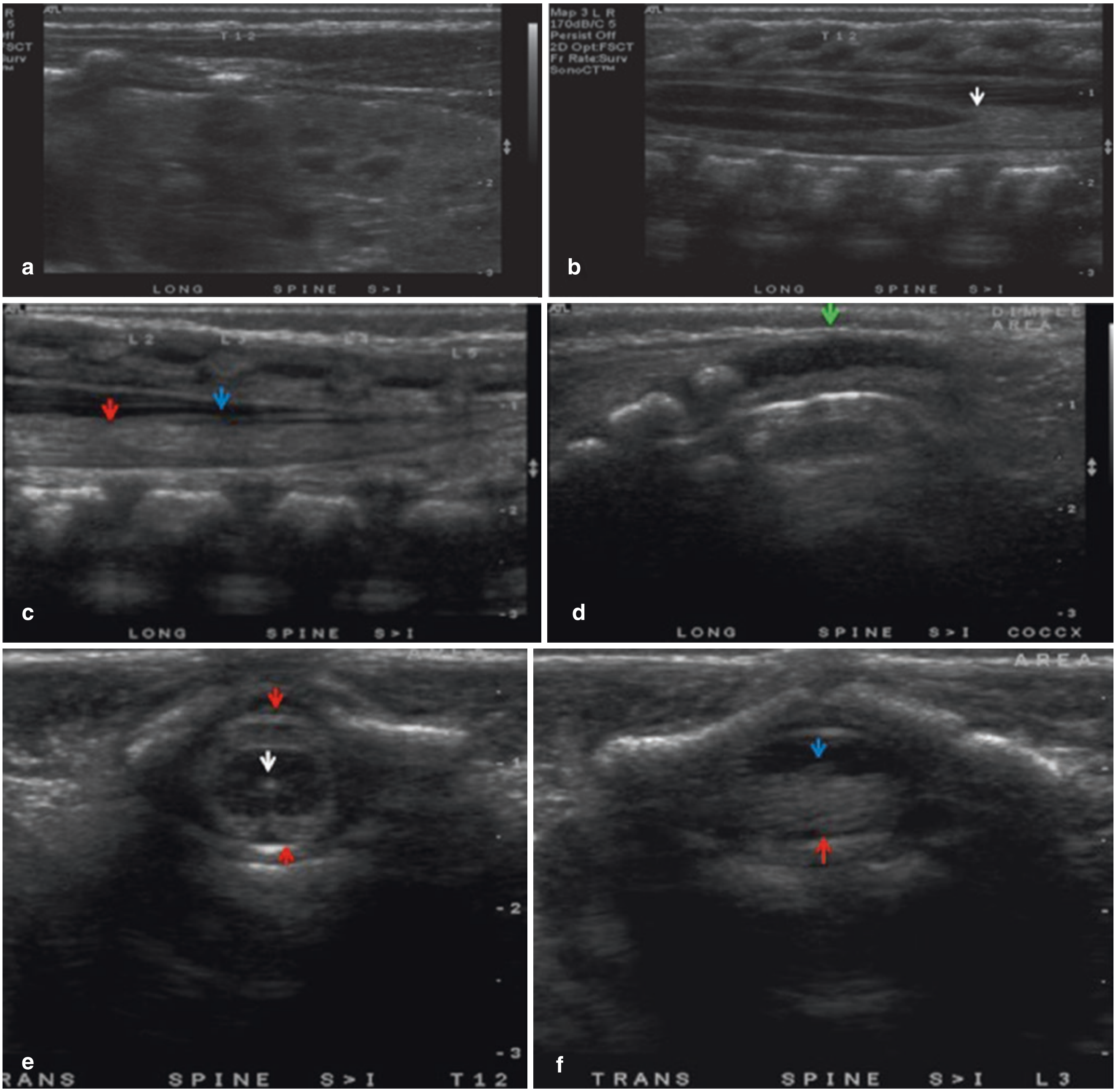
a
T12
LONG SPINE S>I
b
Map 3 L R
170dB/C 5
Persist Off
2D Opt:FSCT
Fr Rate:Surv
SonoCT™
T12
LONG SPINE S>I
c
L2
L3
L4
L5
LONG SPINE S>I
d
DIMPLE AREA
LONG SPINE S>I COCCX
e
RANS SPINE S>I T12
f
AREA
TRANS SPINE S>I L3

Fig. 15 Normal spinal ultrasound (**a**) Sagittal image lateral to the spine demonstrates the 12th rib marked as T12. (**b**) Mid-sagittal image demonstrating the tip of the conus medullaris at the level of L1/2 (white arrow). (**c**) Sagittal image below the level of the cord demonstrates the cauda equina nerve roots (red arrow) and the filum terminale (blue arrow). (**d**) Mid-sagittal image at the level of the coccyx demonstrates the hypoechoic un-ossified coccyx (green arrow). (**e**) Transverse image at the level of the spinal cord demonstrates the central canal as an echogenic dot at the center of the cord (white arrow), and the echogenic cauda equina nerve roots surrounding the cord (red arrows). (**f**) Transverse image below the level of the cord demonstrates the filum terminale (blue arrow) and the cauda equina nerve roots (red arrow)

If the vertebral body level cannot be determined using these methods, the position of the tip of the cord may be marked on the skin with a radiopaque marker under ultrasound and then a radiograph of the spine may be obtained. This will allow accurate determination of the vertebral body levels and most importantly will allow determination of the level of the spinal cord tip.

The level of the spinal cord tip is important when assessing for tethering, however it is also important to assess for motion of the cord and nerve roots with CSF pulsation, which is done with a CINE clip in the sagittal plane. It is also important to assess the position of the cord within the spinal canal, as the cord should be at the center of the canal. Posterior deviation of the cord within the canal, (Fig. 16)

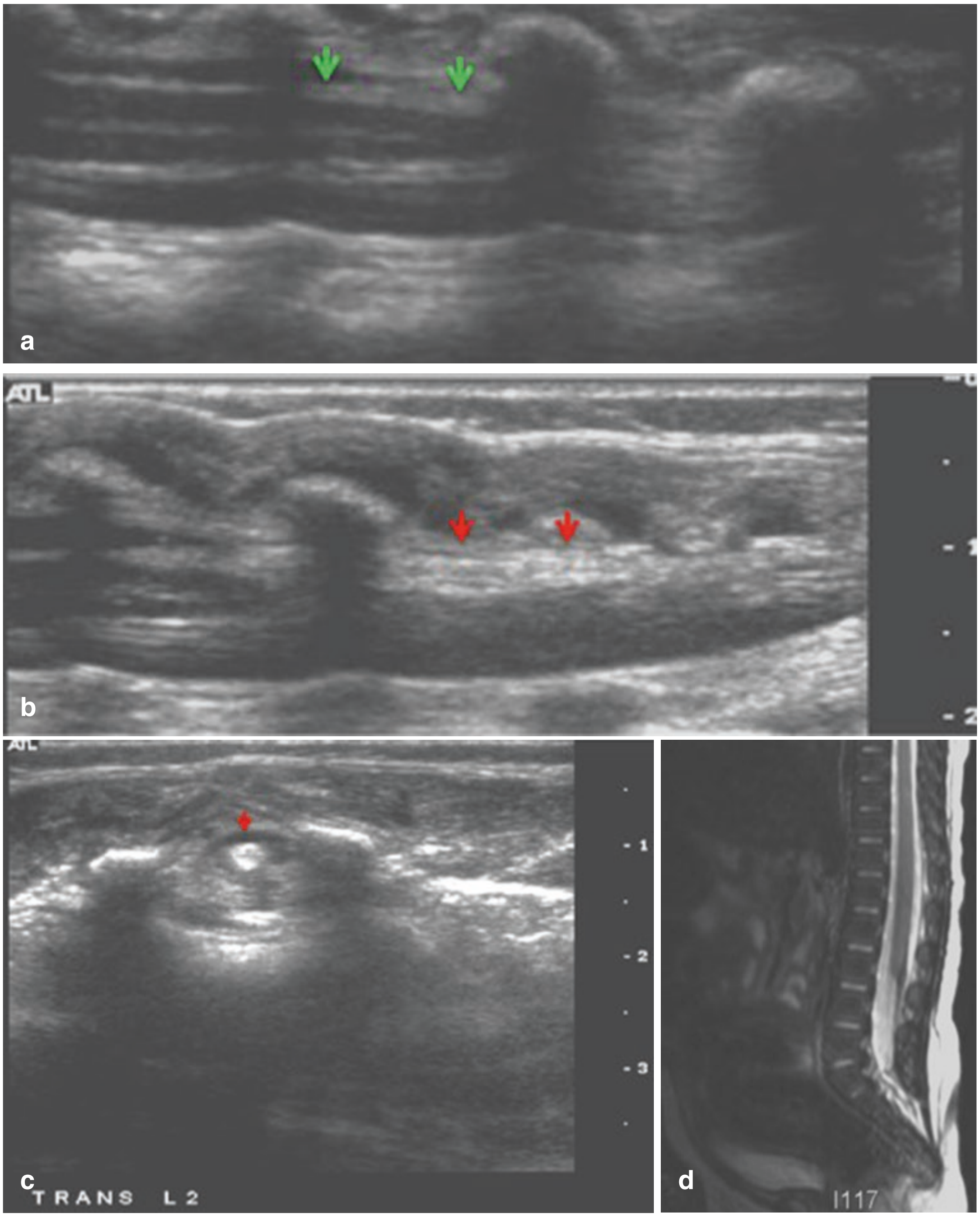

Fig. 16 Tight filum and tethered cord - (**a**) Sagittal image demonstrates the distal cord and the conus medullaris positioned at the posterior aspect of the spinal canal (green arrows). (**b**) Sagittal and (**c**) Axial images below the level of the cord demonstrate a thick and echogenic filum terminale (red arrows). (**d**) Sagittal T2 sequence from an MR examination demonstrates a tethered cord terminating at the level of L3/4 with a short fibrotic filum terminale

particularly with the infant in prone position, raises suspicion of tethering even if the cord terminates at a normal level.

Scans should extend below the level of the cord to demonstrate the filum terminale and the cauda equina nerve roots, as well as to evaluate for sinus tracts leading from the skin surface into the spinal canal. The normal filum terminale should measure up to 2 mm in thickness and should be mildly echogenic, similar to the cauda equina nerve roots (Fig. 15). The canal should be evaluated for a hematoma and for any abnormal loculations of fluid such an arachnoid cysts as well as for masses such as a lipoma.

3.3 Imaging Findings

There are several anatomical variants that may be detected incidentally on a spinal sonogram and do not cause any clinical symptoms. The most common is a filar cyst (Fig. 17), which is a cyst within the filum terminale and ventriculus terminalis. The ventriculus terminalis is a small, ependyma lined, oval, cystic structure positioned at the transition from the tip of the conus medullaris to the origin of the filum terminale. These findings usually regress after the first few weeks of life.

Congenital anomalies that may be detected on a spinal sonography include a sinus tract from the skin into the spinal canal (which is epithelial lined and is typically echogenic on the background of anechoic CSF), a tight filum (Fig. 16) (which presents as thickened echogenic filum due to fibrous and/or fatty changes with a low lying spinal cord positioned posteriorly within the spinal canal as it is tethered), a spinal lipoma (which appears as an echogenic mass attached to the cord), syringohydromyelia (demonstrated as a dilated, fluid filled central canal) (Fig. 18), as well as findings in the spectrum of caudal regression syndrome in which the spinal cord may terminate in a relatively high position with a truncated blunt ending rather a sharp conical shape of the conus medullaris. Other findings of spinal dysraphism such as meningocele and lipomyelocele (Fig. 19) may be detected as well with a spinal sonogram. However, in these cases MRI is frequently performed as the first modality of choice to better delineate the abnormalities and for surgical planning. Post-delivery or post-instrumentation hematomas may be also detected on a spinal sonogram.

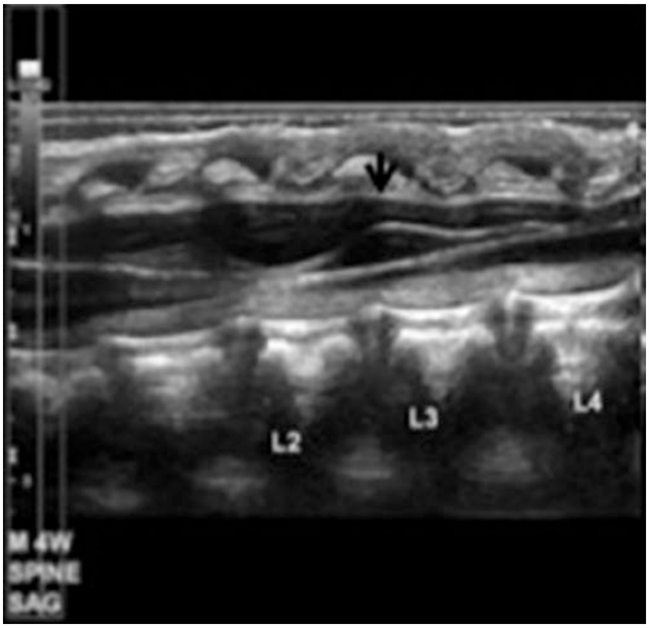

Fig. 17 Filar cyst. Ssagittal image demonstrates a cyst within the filum terminale (arrow)

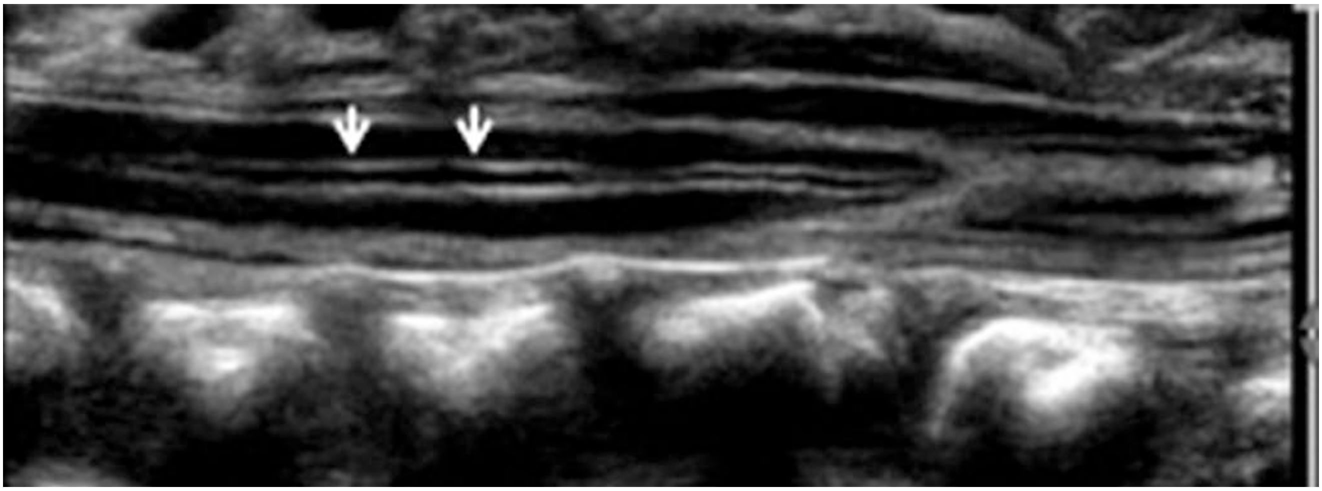

Fig. 18 Mild dilatation of the central canal in a newbrn with an anorectal malformation and vertebral segmentation anomalies. Sagittal image demonstrates the central canal within the cord to be mildly dilated with fluid (arrows)

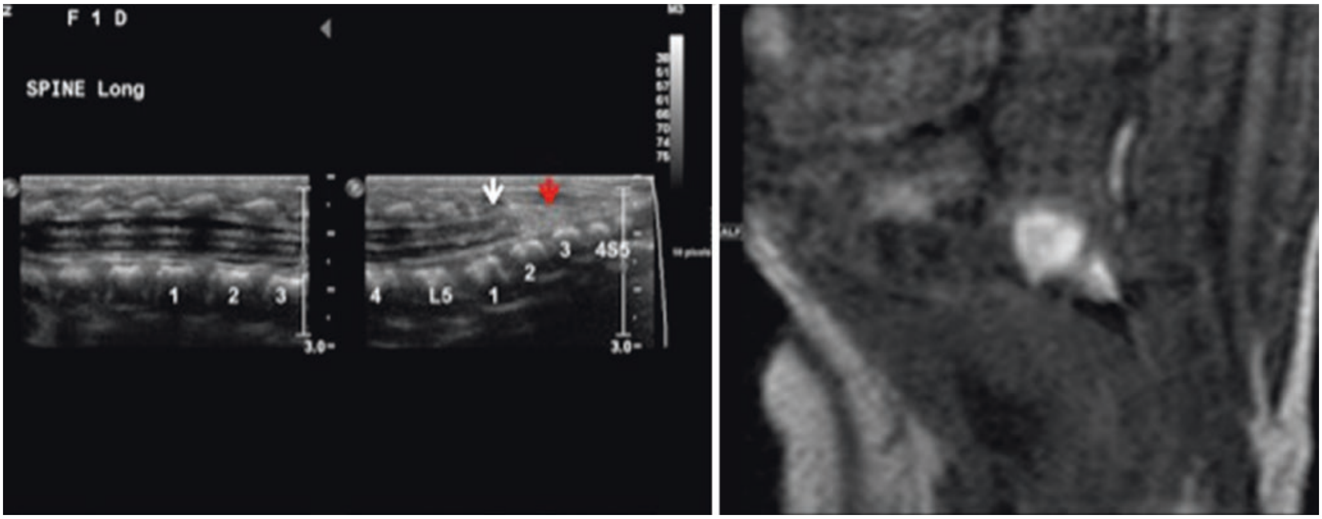

Fig. 19 Lipomyelocele in a NB with a sacral dimple. The mid-sagittal sonographic image on the left demonstrates a tethered cord terminating at the level of S2 (white arrow). The cord is attached to an echogenic mass which represents adipose tissue within the spinal canal (red arrow). The image on the left is a sagittal T1 sequence from an MR examination, demonstrating sacral dysraphism with fat in the spinal canal attached to the low lying spinal cord. The fat in the spinal canal communicates with subcutaneous fat via the sacral defect

Bibliography

1. AIUM Practice parameter for the performance of neurosonography in neonates and infants (2014) Website: https://www.aium.org/resources/guidelines/neurosonography.pdf.
2. Bowerman RA, Donn SM, Silver TM, Jaffe MH. Natural history of neonatal periventricular/intraventricular hemorrhage and its complications: sonographic observations. AJR Am J Roentgenol. 1984;143(5):1041–52. Review. PubMed PMID: 6385669.
3. Argyropoulou MI, Veyrac C. The rationale for routine cerebral ultrasound in premature infants. Pediatr Radiol. 2015;45(5):646–50. https://doi.org/10.1007/s00247-014-2985-1. Epub 2015 Apr 21. Review. PubMed PMID: 25896335.
4. Lowe LH, Bailey Z. State-of-the-art cranial sonography: Part 1, modern techniques and image interpretation. AJR Am J Roentgenol. 2011;196(5):1028–33. https://doi.org/10.2214/AJR.10.6160. Review. PubMed PMID: 21512067.
5. Di Salvo DN. A new view of the neonatal brain: clinical utility ofsupplemental neurologic US imaging windows. Radiographics. 2001;21(4):943–55. Review. PubMed PMID: 11452069.
6. Suara RO, Trouth AJ, Collins M. Benign subarachnoid space enlargement of infancy. J Natl Med Assoc. 2001;93(2):70–3. PubMed PMID: 12653385; PubMed Central PMCID: PMC2640637.
7. Kuruvilla LC. Benign enlargement of sub-arachnoid spaces in infancy. J Pediatr Neurosci. 2014;9(2):129–31.
8. AIUM practice parameter for the performance of ultrasound examination of the neonate and infant spine (2016) Website: https://www.aium.org/resources/guidelines/neonatalSpine.pdf.
9. Unsinn KM, Geley T, Freund MC, Gassner I. US of the spinal cord in newborns: spectrum of normal findings, variants, congenital anomalies, and acquired diseases. Radiographics. 2000;20(4):923–38. Review. PubMed PMID: 10903684.
10. Lowe LH, Johanek AJ, Moore CW. Sonography of the neonatal spine: part 1, Normal anatomy, imaging pitfalls, and variations that may simulate disorders. AJR Am J Roentgenol. 2007;188(3):733–8. Review. PubMed PMID: 17312061.
11. Lowe LH, Johanek AJ, Moore CW. Sonography of the neonatal spine: part 2, spinal disorders. AJR Am J Roentgenol. 2007;188(3):739–44. Review. PubMed PMID: 17312062

Fundamentals of Gynecologic Ultrasound

Barry Hallner, Nia Thompson, and Lisa Peacock

1 Use of Pelvic Ultrasonography

It is well understood that advancements in imaging technology with Computed tomography (CT), and Magnetic Resonance Imaging (MRI) provide invaluable and detailed imaging. These modalities provide useful information that guides both the management and treatment of patients. However, these imaging studies are expensive, require specific facilities for equipment, and often multiple operators or technicians. Additionally, these studies often require the use of dye or contrast which cannot be safely administered until laboratory studies have been reviewed and the absence of allergy to the agent has been confirmed. Patients with limited renal function may not be good candidates for imaging studies with dye or contrast due to delayed renal clearance. Additionally, patients with claustrophobia or large body habitus may be limited in their use of these modalities. While some of the studies can be obtained without dye or contrast, the majority of imaging related to the pelvis requires its use to obtain adequate results. The use of ultrasonography is safe, less expensive, and readily available [1]. Unlike other options for imaging, many forms of ultrasound are portable and can be mobilized to any patient or location. In resource limited environments, ultrasonography may be the only available option. Despite the evolution of technology, pelvic ultrasonography remains the preferred initial choice for imaging the female pelvis [2].

Indications for use of pelvic ultrasound include but are not limited to menstrual irregularities including amenorrhea, dysmenorrhea, abnormal uterine bleeding, delayed menses, polycystic ovarian syndrome; acute or chronic pelvic pain; suspected pelvic lesion or mass; infertility assessment and management; surveillance of previously detected abnormalities; evaluation of Mullerian and Congenital anomalies; identification and location of a foreign body; positioning of an intrauterine device; postoperative complications; localized guidance for invasive procedures; and as a part of the pre-operative gynecologic work up [3–5].

2 Examination Positioning and Techniques

In 2014 the American Institute of Ultrasound in Medicine (AIUM) published guidelines in regards to the safe and effective performance of pelvic ultrasound [4]. AIUM collaborates with the American College of Radiology (ACR), the American College of Obstetricians and Gynecologists (ACOG), the Society for Pediatric Radiology (SPR), and the Society of Radiologists in Ultrasound (SRU) to publish standardized guidelines useful for education, research and accreditation. Complete imaging of the female pelvis includes both trans-abdominal and trans-vaginal studies [4, 5]. Imaging of the female pelvis is unique in that it can involve the use of a special ultrasound probe placed transvaginally. The transvaginal probe is inserted through the vagina and images are obtained with higher clarity and accuracy than with the trans-abdominal approach.

2.1 Transvaginal Ultrasound Probes

A transvaginal probe is unique compared to an abdominal probe due to its use of a higher frequency at 5–10 MHz which allows for increased sensitivity [6]. In comparison to transabdominal imaging, the probe is physically closer to the object of interest, creating less attenuation and a clearer imaging [3, 5]. There are detailed specifications for disinfection and sterilization of the probes prior to each use. The transvaginal probe is inserted into a condom shaped cover

---

B. Hallner · N. Thompson
Female Pelvic Medicine and Reconstructive Surgery, Louisiana State University Health, New Orleans, LA, USA
e-mail: Bhalln@lsuhsc.edu; Nthom7@lsuhsc.edu

L. Peacock (✉)
Louisiana State University Health, Department of Obstetrics and Gynecology, New Orleans, LA, USA
e-mail: lpeac1@suhsc.edu

© Springer Nature Switzerland AG 2021

J. Li et al. (eds.), *Ultrasound Fundamentals*, https://doi.org/10.1007/978-3-030-46839-2_26

that is first filled with lubrication gel at the tip. The probe is then inserted all the way to the tip of the condom and secured at the base. Additional gel is then applied over the probe and then inserted into the vagina. Depending on the comfort level of the patient, the probe may be inserted by either the patient or technician. Facilities have varying guidelines for the presence of chaperones during the examination.

2.2 Patient Positioning

The patient is placed on an exam table in the dorsal lithotomy position. This allows for greater ease of access to both the lower abdomen and the vaginal area. Historically, it was required for the patient to have a full bladder prior to transabdominal imaging. The rationale being that the full bladder would push away bowel in the lower abdomen and reproductive organs towards the sacrum, allowing for better visualization during imaging [6]. Recent data has shown that a full bladder is not always necessary, and if a uterus cannot be optimally visualized trans-abdominally, it can be reassessed during the transvaginal portion of the exam [4, 5]. However, if a patient declines the vaginal portion of the exam or if due to structural reasons it cannot be performed, it is helpful to distend the bladder to improve the identification of adjacent structures. When performing a transvaginal ultrasound, the reverse is true as structures are best seen with an empty bladder [4]. There is also the option to perform the imaging transrectally in scenarios where near-point imaging data is crucial but the study cannot be performed transvaginally. Patient body habitus, and operator technique and skill are crucial to obtaining adequate and optimized images. All personnel including physicians who perform or interpret imaging, and technicians who obtained the images are required to maintain specialized certification [4].

3 Imaging of the Female Pelvis and Reproductive Tract

3.1 Transabdominal

Trans-abdominal images are obtained with a 3–8 MHz transducer [3, 5, 6]. Anatomically, the bladder is anterior to the uterus and usually is the first structure identified. If the bladder is full, it will appear as a large black fluid filled structure (Fig. 1). In the case that the bladder is not full, the technician may need to place more pressure on the abdominal wall to decrease the distance from the probe to the uterus allowing for adequate visualization. First, the uterus is imaged in both a transverse and longitudinal plane. After the uterus is visualized and measured in both planes, the technician will sweep gently to the right and left to identify the adnexa. The second structures identified are the right and left ovaries and the right and left fallopian tubes. It is often challenging to adequately identify and characterize the ovaries on trans-abdominal imaging. Because of this, assessment of the adnexal structures are best achieved on transvaginal imaging (Fig. 2). The close proximity of the ovaries to the major pelvic vasculature allows them to be used as adjunct landmarks for the identification of these structures. Lastly, the posterior cul-de-sac is examined for free fluid or masses in the pelvis. Patient body habitus, bowel, or gaseous distention may limit the quality of images obtained abdominally. In this case transvaginal images are more useful.

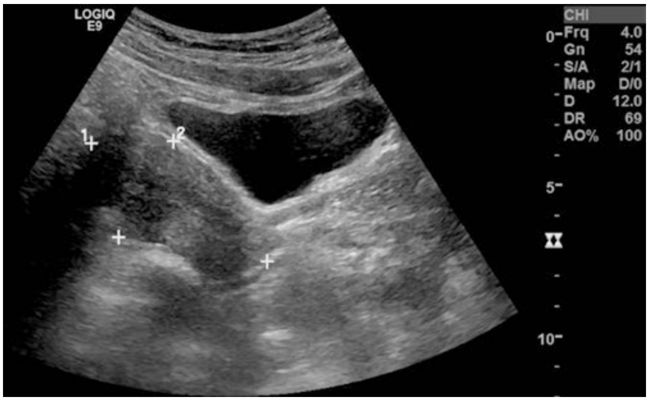

Fig. 1 Transabdominal image showing full bladder anterior to the uterus

3.2 Transvaginal

Initially, placing the patient in the lithotomy position or frog-leg position will allow for smooth transition to the vaginal portion of the exam. The patient is instructed to void as transvaginal images are best obtained with an empty bladder. For this portion of the exam, the probe is physically closer to the object of interest, therefore, the clarity and detail are better. It is important to ensure that the probe is completely inserted to image the deep structures of the pelvis. It is also possible to perform transperineal imaging when vaginal access is not always feasible, or when the object of interest is located low in the vagina. The structures in the pelvis are imaged in the same systematic fashion as they are trans-abdominally.

4 Uterus & Cervix

The cervix and endocervical canal are seen first. The cervix can then be followed to the fundus of the uterus. The appearance and consistency of the uterus should be assessed. Nabothian cysts are benign mucous filled cysts seen within the cervix on the surface (Fig. 3) [5]. The uterus is identified

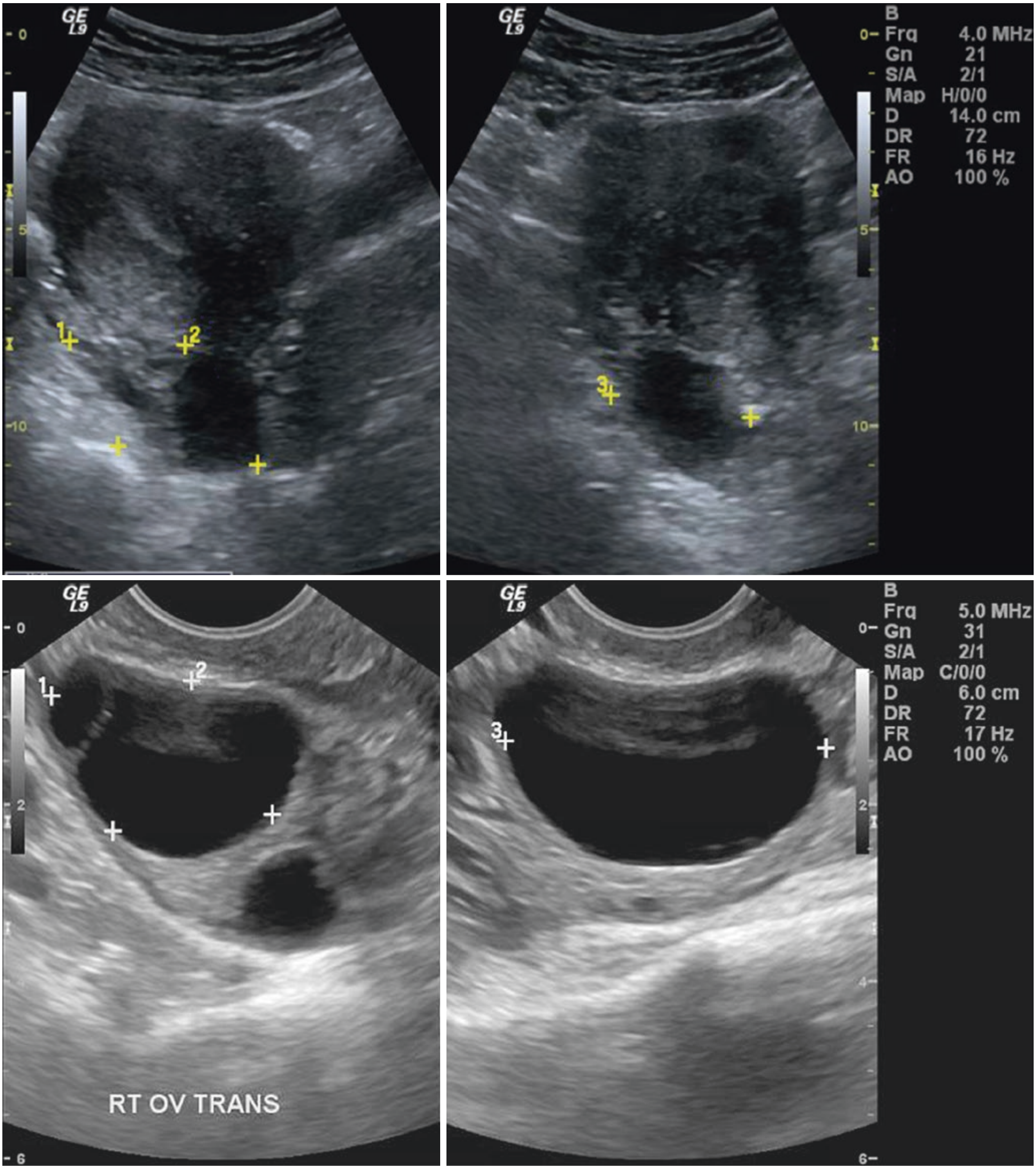
GE L9
1
2
3
B
Frq 4.0 MHz
Gn 21
S/A 2/1
Map H/0/0
D 14.0 cm
DR 72
FR 16 Hz
AO 100 %
0
5
10
B
Frq 5.0 MHz
Gn 31
S/A 2/1
Map C/0/0
D 6.0 cm
DR 72
FR 17 Hz
AO 100 %
2
4
6
RT OV TRANS

Fig. 2 Transabdominal images on the top identify an ovarian cyst. The exact same ovarian cyst is better characterized on the transvaginal images on the bottom

and imaged in the transverse and longitudinal (sagittal) planes. The depth of the uterus (anteroposterior) is obtained longitudinally. The width of the uterus is measured in the transverse view. The characteristics of the myometrium and endometrium, position of the uterus (anteverted, midposition, retroverted, anteflexed, retroflexed) and presence of any masses should be noted [4]. In this view, the posterior cul-de-sac can be assessed as well (Figs. 4 and 5).

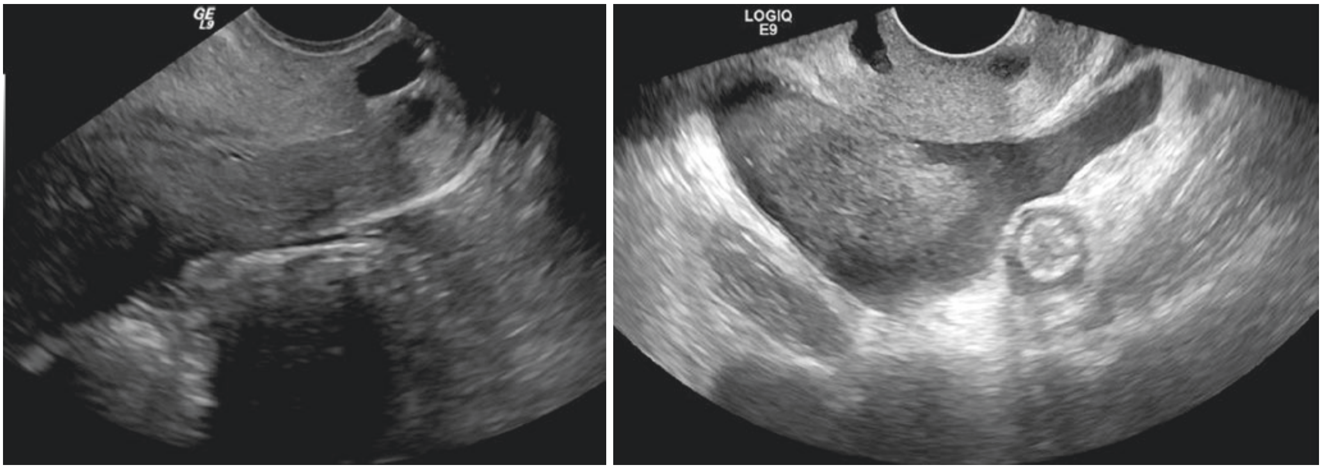

Fig. 3 Transvaginal images of Nabothian cysts in the cervix

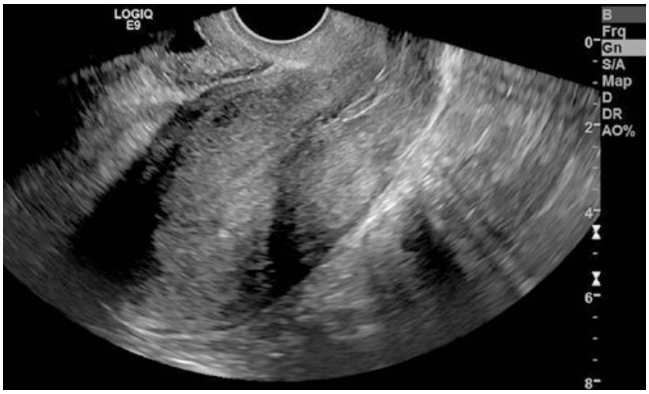

Fig. 4 Transvaginal longitudinal view of a normal cervix and uterus

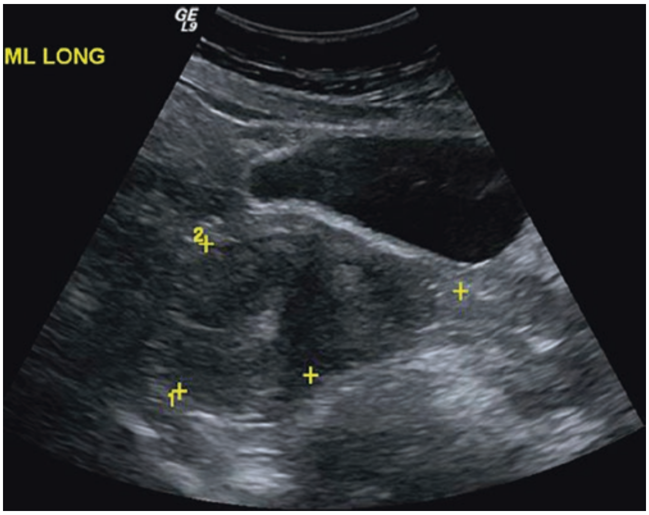

Fig. 5 Transabdominal view of a retroverted uterus with the fundus deviating posteriorly

The coronal view in combination with a longitudinal view is helpful to identify deviation in the anatomy such as congenital Mullerian anomalies, submucosal leiomyomas, as well as the location of intrauterine devices (Fig. 6). Additionally, 3-D imaging technology allows for the assessment of the uterus.

5 Endometrial Stripe

The width, texture, and consistency of the endometrium are assessed in both the longitudinal and transverse views. The endometrial stripe in postmenopausal women is typically thin and may be challenging to view. The stripe is easier to evaluate in premenopausal women who possess a thicker, more vascular endometrium. The endometrial canal down to the inner cervical os should be assessed for fluid, masses or focal abnormalities. The endometrial stripe should be measured in the anteroposterior fashion, excluding any fluid in the canal or adjacent myometrium (Fig. 7) [3, 7]. If a mass or lesion of the endometrium is identified, the characteristics of fluid around the mass should be detailed and doppler sonography should be utilized to further assess the vascularity of the mass or lesion [7]. Additionally, saline infusion sonography may also be helpful in better characterizing whether the lesion abuts or encompasses the endometrium. The appearance of the endometrium closely relates to the phases of the menstrual cycle. The endometrium will appear thin in the early proliferative phase, until it reaches the luteal phase where it appears thickened and homogenous just before menses [5]. Often, the trilaminar, or three-layer appearance of the endometrium is often discussed when detailing fertility issues and is often seen around the time of ovulation [6, 8].

Given that the appearance and size of the endometrium can change drastically during the menstrual cycle, the most reliable time to measure the endometrium is during the early proliferative phase when it is the thinnest. Measuring the endometrium in other phases of the cycle can lead to incor-

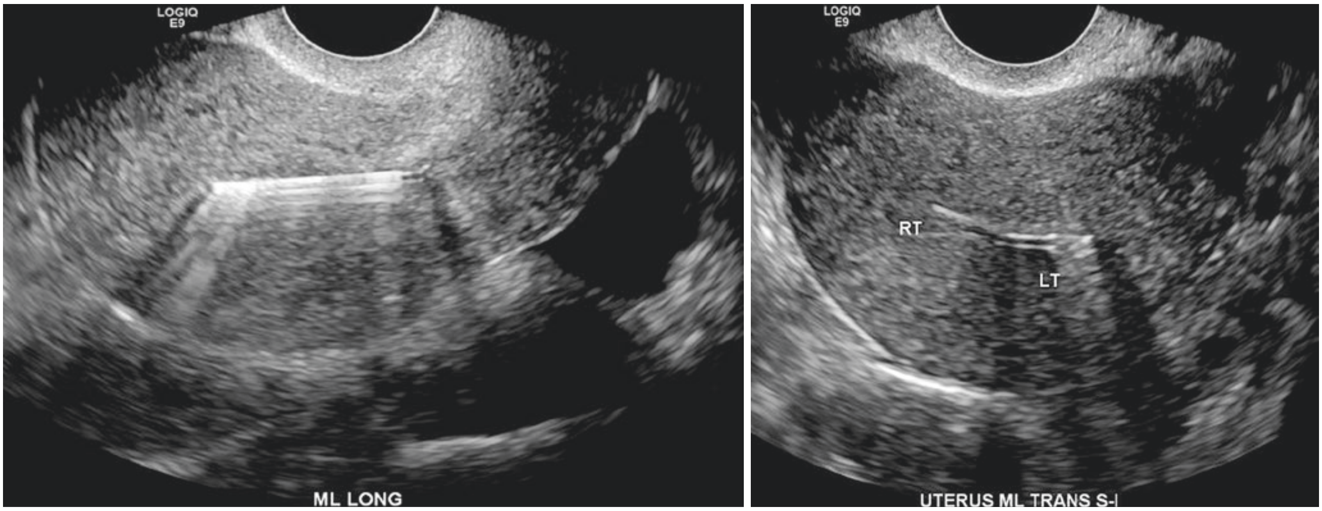

Fig. 6 Longitudinal (left) and Transverse (right) imaging of an Intrauterine device in correct position

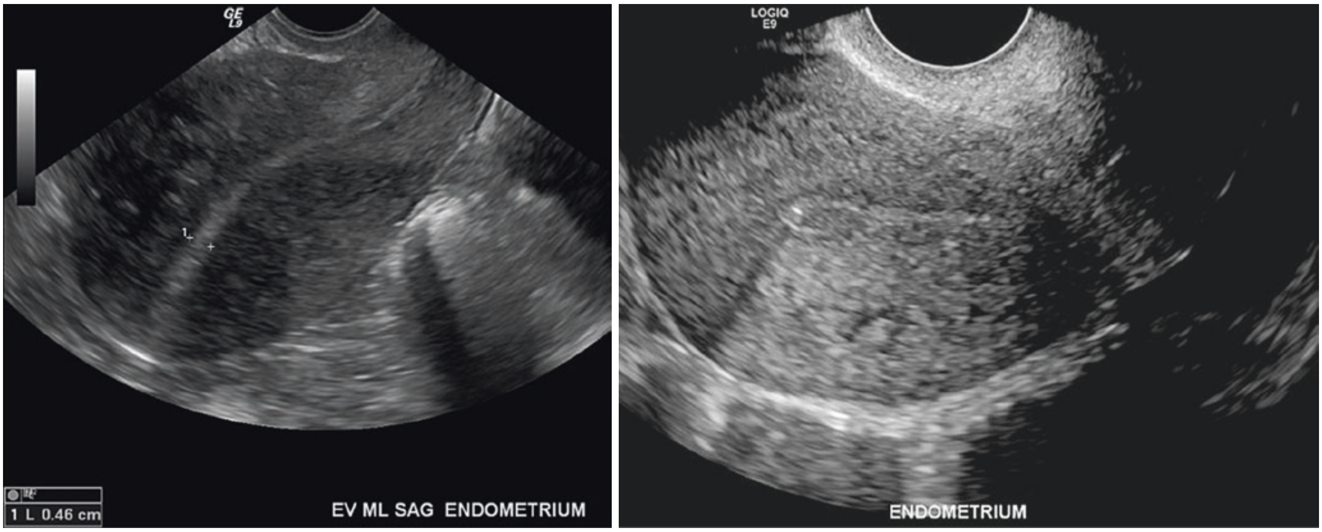

Fig. 7 Demonstrates measurement of the endometrial stripe in a premenopausal woman in the early proliferative phase of menstruation

rect diagnoses (Fig. 8). In postmenopausal patients, the endometrial stripe should measure less than 4 mm [5, 9]. A history of uterine surgery such as an endometrial ablation can make it challenging to identify a distinct endometrial stripe due to distortion and scarring [10].

6 Adnexal Structures: Fallopian Tubes and Ovaries

Identification of the adnexal structures can be challenging. In the transverse view at the level of the fundus and cornua, the tubo-ovarian ligament can be followed out laterally to the ovary and fallopian tube to assist with identification. Abnormal or unpredictable positioning of the adnexal structures is common in the presence of a large fibroid uterus, a history of pelvic surgery or hysterectomy, pelvic irradiation, malignancy, pelvic inflammatory disease, endometriosis, or inflammatory bowel disease. In postmenopausal women, the ovaries are often smaller and extremely challenging to identify due to the absence of characteristic follicles seen after the cessation of folliculogenesis [2]. The length, width, and depth of each ovary should be measured. Ovaries should appear smooth in contour, without internal echoes, and relatively internally avascular. Premenopausal menstruating women will have the presence of numerous follicles measuring no more than 3 cm in diameter [2, 6]. The ovary should appear full and round, in contrast to a thin smeared appearance of post-menopausal ovary (Fig. 9). In post-menopausal women large follicular cysts are abnormal, however, smaller 10 mm follicles are considered a benign variant [2, 6]. Fallopian tubes typically are not seen unless they are fluid filled, or if there's an associated lesion. Irregular borders, thick septations, nodules with blood flow, abundant vascularity, and solid tissue within the ovary may be indicative of malignancy [2, 5].

7 Cul-de-sac

The area posterior to the uterus is called the cul-de-sac or pouch of Douglas. This area is assessed for free fluid that can be visualized behind the cervix or uterus. Ultrasound has the capability to detect 10 mL or more of fluid in the cul-de-sac. Free fluid that appears echogenic with debris suggests hematoperitoneum, whereas fluid that appears anechoic is suggestive of an inflammatory or infectious process [5]. If the fluid does not ascend beyond the fundus it is considered minimal [11]. It is normal for the uterus to slide or mobilize over the anterior wall of the rectosigmoid, and lack of mobility can be suggestive of adhesive disease. During the transvaginal portion of the exam, the cervix should be gently pressed assessing the mobility of the uterus. If the uterus is fixed and non-mobile, there is concern for deep seeded endometriosis, or pelvic adhesive disease.

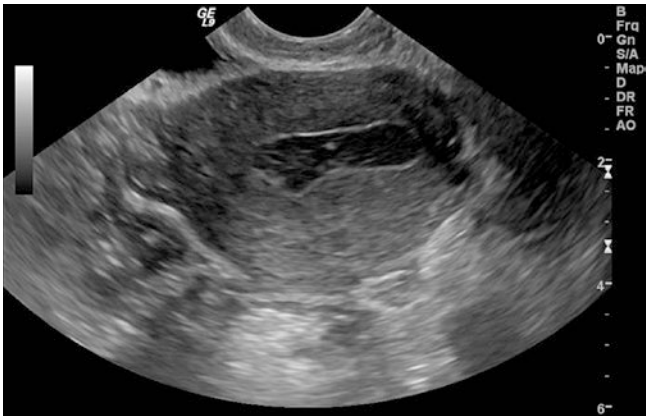

Fig. 8 Transvaginal imaging of the phases of menses is important to note. Clinically this patient was menstruating with menses noted in the endometrial canal

8 Doppler Studies

Both transbdominal and transvaginal imaging can be utilized to obtain doppler studies in the pelvis. Specifically, this technology is utilized to assess the vascular characteristics of structures by detecting blood flow to, through, or around an object of interest [2, 7, 12]. The velocity of red blood cells within arteries creates a wave form [13]. Color-coded doppler flow is superimposed over the gray-scale images. The color of the flow indicates the direction of the flow; red indicating that the blood is flowing towards the transducer and blue indicating flow away from the transducer. Additionally, the brightness of the color is proportional to the velocity of the flow [5, 14]. In particular, these studies are helpful when assessing for ovarian torsion, malignancy, and adnexal masses such as ovarian cysts (Fig. 10). For example, a mid-cycle study performed in a regularly menstruating woman can reveal a vascular circle around the periphery of a cystic appearing structure no larger than 3 cm consistent with a

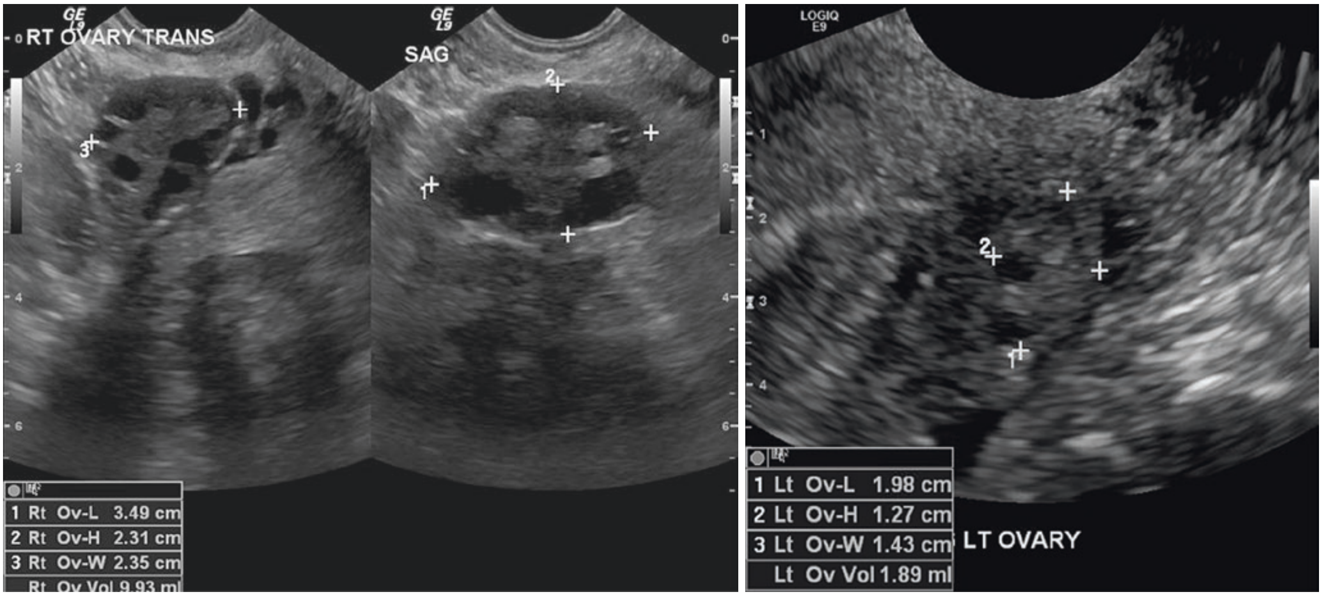

Fig. 9 Transvaginal, normal appearing ovaries with small cysts consistent with folliculogenesis in a premenopausal woman on the left. Post menopausal ovary on the right

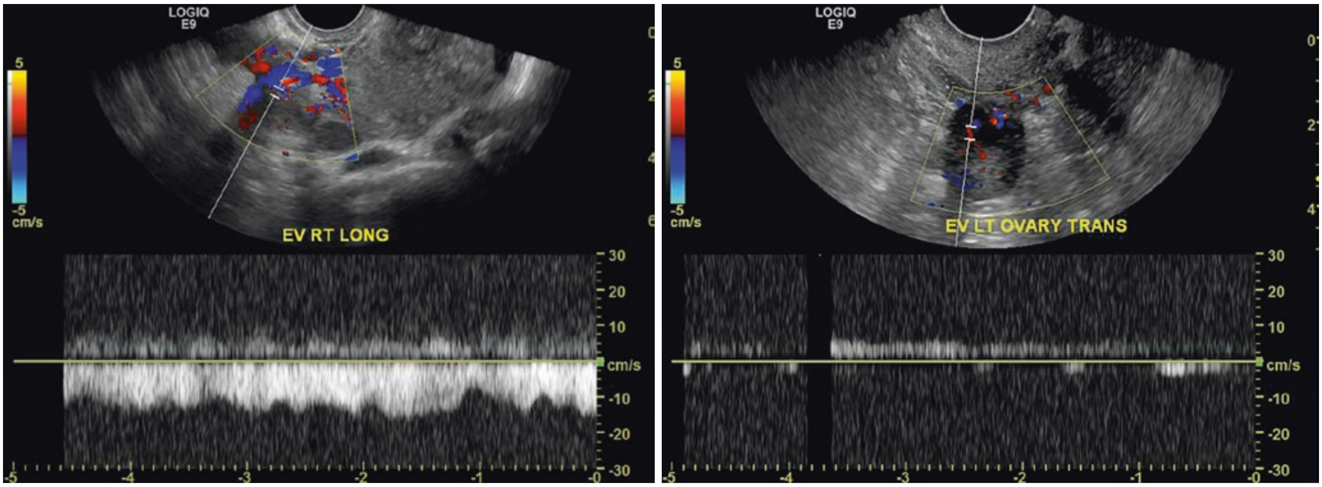

Fig. 10 Doppler imaging study assessing the vascular characteristics of a pelvic mass of unknown origin on the left and ovarian cyst on the right

benign corpus luteum cyst [2, 15, 16]. Due to the increased vascularity this could be mistaken for an ectopic pregnancy, however, any other abundance of vascular flow maybe concerning for the presence of a malignancy.

9 Saline Infusion Sonography (SIS)

In the late 1990s's practitioners began to use the technique of sonohysterography or saline infusion sonography (SIS) to better assess lesions within the endometrial cavity [17, 18]. SIS is useful when a focal lesion or mass is seen on transabdominal or transvaginal imaging that cannot be sufficiently characterized or in the presence of incongruent imaging and clinical symptomatology [19]. The first component of a SIS examination is a thorough transvaginal pelvic ultrasound. The probe is then removed, and a speculum is placed into the vagina. The cervix is visualized and cleansed with betadine or antiseptic solution. A 7 French Catheter is primed with sterile saline and then inserted into the cervix to just beyond the internal cervical os [5]. It is important to not advance the catheter much further beyond the inner os because this may disrupt the pathology within the uterus or cause a vasovagal response when advanced to the fundus. The speculum should be removed with close attention to not displacing the catheter and the transvaginal probe is then re-inserted. Slowly, approximately 20–40 mL can be injected to the uterus to distend the cavity [5]. During instillation of the sterile solution the technician should scan the uterus longitudinally and between both cornua for an adequate assessment of the cavity. This allows the technician to assess for a mobile lesion such as a polyp which should appear mobile and hyperechoic on imaging. In contrast, a submucosal fibroid would conform in a smooth contingent fashion along the endometrium and appear hypoechoic like the myometrium [20]. If there is concern for malignancy, SIS should not be a substitute for a pathologic tissue diagnosis [5]. SIS also be used to assess tubal patency. Air and fluid from the uterus should efflux into the tubes creating echogenic bubbles that should be seen traveling through each tube. In reproductive age women this exam should be performed in the setting of a negative pregnancy test and within 10 days of the last menstrual cycle when the endometrial lining is ideally the thinnest [17]. If an infection or pelvic inflammatory disease is suspected, then the SIS should not be performed due the lack of safety information in regards to the spread of pathogens into the upper genital tract [21]. Complications and side effects of the procedure are rare with only a 1% risk of infection [22].

10 Three-Dimensional Ultrasonography

Software now exists that allows the collection of data in order to project a 3-D image on a 2-D screen. Data is combined from many different planes, and can convey the volume of a structure [5, 23, 24]. This allows for detailed imaging and spatial orientation. In gynecology, there are many uses for this technology including, but not limited to the assessment of malignancy, complex adnexal masses, uterine cavities anomalies, Mullerian anomalies, and fertility related issues. It can then be used for surgical planning, monitoring the growth and size of leiomyomas after a uterine artery embolization, and characterization of endometrial and ovarian malignancies.

11 Pathology and Clinical Applications

With all imaging it is important to consider the clinical picture and symptomatology when creating a differential diagnosis.

11.1 Leiomyoma

Leiomyomas are the most common neoplasm found in the uterus and can either be asymptomatic or present with a variety of symptoms. The prevalence of affected women is estimated to be 20–40% [25, 26]. Based on their location within the myometrium, leiomyomas can be classified as submucosal, intramural, or subserosal [27]. Due to its high tissue contrast resolution, multiplanarity, and reproducibility, MRI represents the most accurate imaging modality for the evaluation of uterine leiomyomas. However, in comparison to ultrasound, MRI is time-consuming, expensive and limited to select cases. Indications for MRI, when uterine fibroids are suspected, include uncertainty of the anatomic location (e.g., uterine, adnexal, intestinal, etc.), histological origin of the mass (i.e. differentiating adenomyosis from malignant mesenchymal tumors), and accurate characterization of the fibroids secondary to uterine size (Fig. 11a, b) [28–30]. Moreover, MRI is indicated as a preoperative examination for uterine fibroid embolization and thermoablative procedures [31–33].

Uterine leiomyoma (fibroid) appear as solid, well-defined, round lesions within or attached to the myometrium. In general, they have an inhomogeneous "stripey" or "fasciculate" echostructure, characterized by radial shadowing. Echogenicity varies according to the different components: muscle cells, fibrous stroma, calcification, and lipomatous or hyaline degeneration. When fatty tissue is overrepresented, myomas may appear hyperechoic [34]. Calcification or a hyperechoic capsule caused by deposition of calcium salts is more frequently found in the uteri of postmenopausal women. Uterine fibroids are usually located in the corpus uteri (95%) and rarely in the cervix (5%) [35]. Intramural fibroids develop within the myometrial wall and are a more common location (50%) [36]. Intramural myomas are usually well demarcated due to the compression of the myometrium and subsequent formation of a pseudocapsule (Fig. 11a). When the growth of these masses involves another uterine layer, they may be classified as a subserous or a submucous myoma. Subserosal myomas are located beneath the peritoneal covering of the uterus and submucosal ones are located within the cavity of the uterus underlying the endometrium (Fig. 12a). A parasitic myoma is a rare type of pedunculated subserosal myoma that is partially or completely separated from the uterus and receives an alternative blood supply from other sources, such as the omentum and mesenteric vessels [37]. Broad ligament fibroids originate from hormonally sensitive smooth muscle elements, extend laterally from the uterus and are often confused with adnexal masses. In some cases, they can detach from the uterus and become mobile within the peritoneal cavity [38].

Submucosal myomas are located in close proximity to the endometrium (Fig. 12b). Submucosal myomas are thought to represent 5–10% of all leiomyomas, although this may be underestimated due to the difficulty in accurately diagnosing the location [39]. Submucosal myomas that extend into the uterine cavity while being attached to the myometrium by a pedicle are classified as pedunculated lesions. These myomas which extend into the uterine cavity are classified according to the depth of protrusion. The European Society of Hysteroscopy classifies submucosal myomas as follows [40]:

- Type 0: fibroid polyp (the mass is located entirely within the uterine cavity)
- Type I: >50% contained within the uterine cavity or <50% contained within the myometrium
- Type II: <50% contained within the uterine cavity or >50% contained within the myometrium

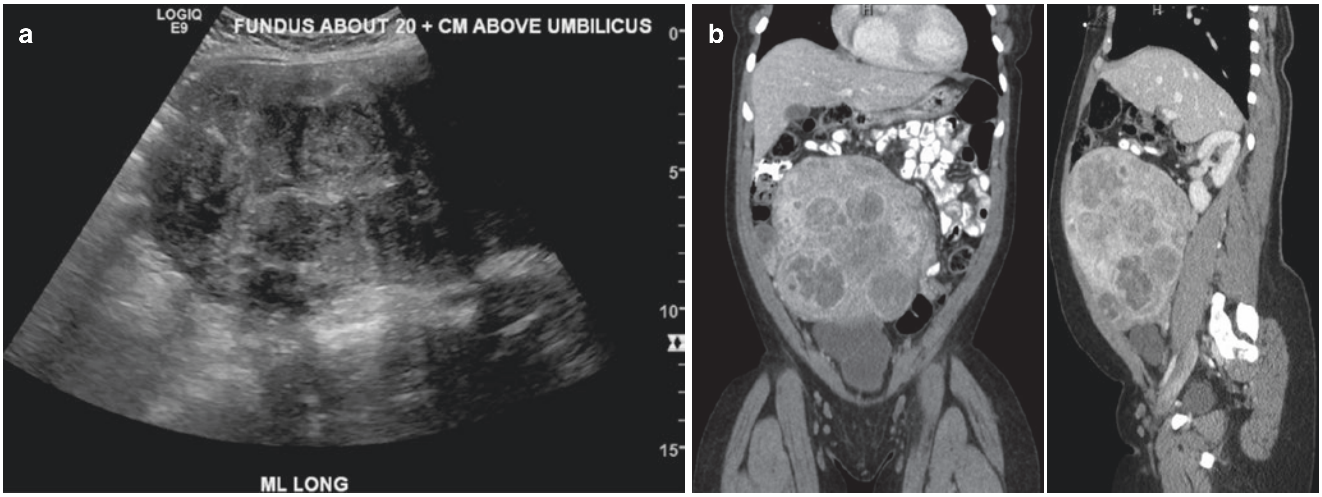

Fig. 11 (**a**) Transabdominal ultrasound images of a large fibroid uterus. You have limited ability to fully assess the extent of the fibroids secondary to overall uterine size. (**b**) CT imaging as seen on the right is a better imaging study for uteri of this size

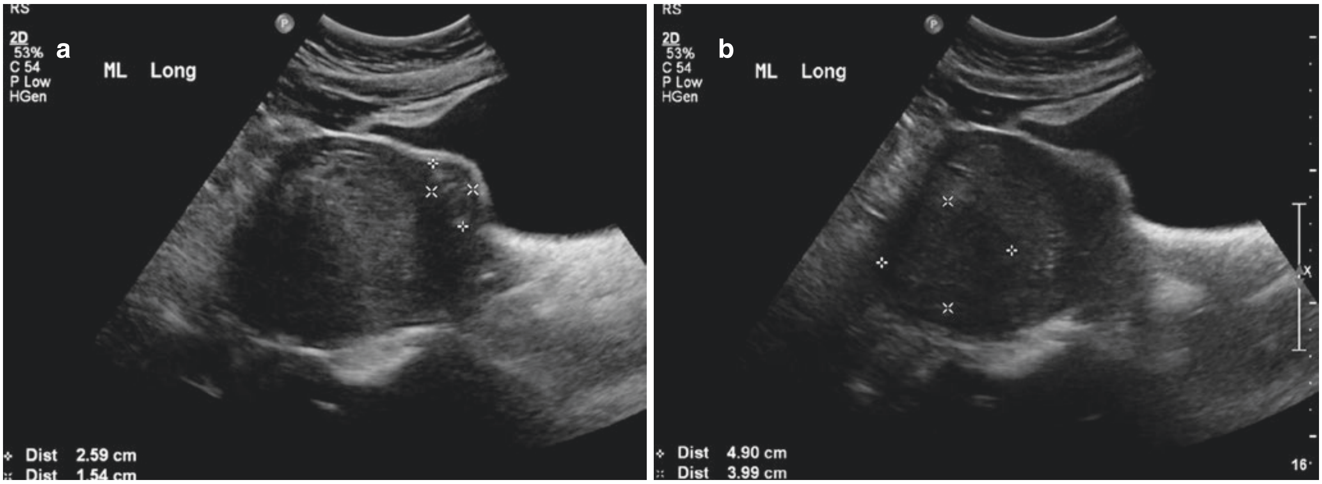

Fig. 12 Transvaginal images. (**a**) Small subserosal fibroid seen just under the serosa. (**b**) Larger submucosal fibroid seen abutting the endometrium on the right

Submucosal myomas can be easily studied by sonohysterography, a simple and well-tolerated procedure utilizing saline solution as the contrast medium. Published literature shows that this procedure provides equal accuracy to hysteroscopy in terms of location, breadth of attachment, and extent of protrusion into the uterine cavity of submucous myomas [36, 41].

Color or power Doppler imaging typically shows that myomas are devoid of rich vascularization. Circumferential flow around the lesion is often visible (perifibroid plexus), while central flow is poor. Centripetal branches reach the center of the tumor via peripheral arteries. The peripheral vascularity of fibroids is increased compared to that of both the normal myometrium and the center of the tumor [42]. Doppler ultrasound may facilitate distinguishing an endometrial polyp with a single feeding vessel from an intracavitary submucosal fibroid tumor or adenomyosis, where vascularization is characterized by diffusely spread vessels [43].

11.2 Leiomyosarcoma

Most benign uterine leiomyomas do not create a diagnostic challenge on imaging or microscopic examination because they have a classic appearance. However, variant subtypes and atypical features can serve as a source of misinterpretation and misdiagnosis when trying to identify leiomyosarcomas (LMS). Uterine leiomyosarcomas are rare aggressive tumors that can arise de novo or secondary to malignant degeneration of a leiomyoma [44, 45]. Leiomyosarcomas represent <0.13% of uterine smooth muscle tumors and have a reported prevalence of less than 1% in hysterectomy specimens [46, 47]. A recent large database evaluation suggested that unexpected uterine leiomyosarcomas were found in only 27 of 10,000 women undergoing hysterectomy with morcellation [48]. A Food and Drug Administration analysis in 2014 found a similar prevalence of unsuspected leiomyosarcoma in surgical specimens for presumed leiomyoma, with 1 in 498 specimens [49]. Imaging findings that may raise suspicion for uterine leiomyosarcomas include large irregular masses, heterogeneity, central necrosis, hemorrhage, and irregular margins [50].

11.3 Adenomyosis

Adenomyosis is defined as the presence of ectopic endometrial glands and stroma within the myometrium. It is a disease of the inner myometrium and results from infiltration of the basal endometrium into the underlying myometrium. Transvaginal ultrasonography (TVUS) and magnetic resonance imaging (MRI) are the main radiologic tools for the diagnosis of adenomyosis [51]. On ultrasound examination, adenomyosis appears as homogeneous tissue with an irregular ill-defined border that causes asymmetric thickening of the affected myometrium. A uterus affected by adenomyosis usually appears enlarged and globular with a regular external contour while a leiomyomatous one is enlarged with an irregular contour.

The characteristic findings of adenomyosis reflect the histopathologic changes of the disease process and can be broken down into three categories**:**

- Endometrial infiltration: echogenic striations and nodules, myometrial cysts, and “lollipop” diverticula (on HSG)
- Smooth muscle proliferation: focal or diffuse myometrial thickening with indistinct borders more commonly involving the posterior fundus and heterogenous echotexture manifesting as “venetian blind” appearance of thin linear shadows

- Vascularity: color Doppler demonstrating an increased number of tortuous vessels throughout the involved myometrium as opposed to leiomyomas which displace vessels

Adenomyosis affecting the junctional zone causes its thickening [36], which is detectable on 3D ultrasound examination in the coronal plane as an unclear demarcation of the endometrium/myometrium interface [36, 52]. The ready availability of ultrasound and the higher cost of MRI have led to ultrasound becoming the preferred modality for the initial evaluation, reserving MRI for equivocal cases [53].

11.4 Structural Abnormalities

The most common pelvic masses in neonates include hydrocolpos, hydrometrocolpos, and ovarian cysts. Hydrocolpos is characterized by distention of the vagina with fluid. Hydrometrocolpos is characterized by dilatation of both the uterus and vagina, with the vagina usually being distended to a greater extent [54]. The distending fluid can be serous, mucinous or possibly urinous if there is a urogenital sinus present. If the cavities are filled with blood, then the terms hematometrocolpos and hematocolpos would be applied. The endometrium is intrinsically normal, but the endometrial cavity is distended with fluid. Both hydrocolpos and hydrometrocolpos result from vaginal or cervical stenosis, hypoplasia, or agenesis which is often associated with other congenital anomalies of the uterus and kidneys [55]. On ultrasound there is a cystic midline mass. The presence of internal echoes can represent mucoid material and cellular debris. On the other hand, hematocolpos and hematometrocolpos in adolescent girls are more commonly associated with an imperforate hymen without an increase in associated congenital anomalies. Ultrasound in these cases typically demonstrate an echogenic, tubular, cystic midline mass with internal echoes representing fluid and debris [56].

11.5 Congenital Abnormalities

11.5.1 Müllerian Duct and Related Anomalies

The Müllerian (paramesonephric) ducts are the primordial components of the female reproductive tract. During embryogenesis, they differentiate into the fallopian tubes, uterus, cervix, and the upper two-thirds of the vagina. The distal third of the vagina develops from the urogenital sinus [57].

Various types of uterine anomalies can occur because of nondevelopment or failure of fusion of the distal segments of the Müllerian ducts. These include uterine hypoplasia or agenesis, unicornuate, didelphys, bicornuate, septate, and arcuate uterus. † In addition, There can be a peculiar anomaly of uterine morphology that is related to diethylstilbestrol referred to as a “T-shaped” uterus [58]. Due to the different embryologic origins of the upper two-thirds of the vagina, which originates from the Müllerian ducts, and the lower third, which originates from the urogenital sinus, vaginal anomalies such as hypoplasia, aplasia, duplication, or septa, may or may not coexist with uterine anomalies [59].

11.6 Endometrial Stripe

Endometrial abnormalities are common diagnostic challenges facing the radiologist and referring gynecologist. Ultrasound (US) is the primary imaging modality in this setting, but findings at sonohysterography and magnetic resonance (MR) imaging are often correlated with US findings. The endometrium demonstrates a wide spectrum of normal and pathologic appearances. Disease entities include hematometra and hematocolpos, and ovarian cysts; gestational trophoblastic disease; endometritis and retained products of conception; and bleeding caused by polyps, submucosal fibroids, endometrial hyperplasia, or endometrial adenocarcinoma. Accurate diagnosis requires the understanding of the fact that the appearance of the endometrium is related to multiple factors, including the patient’s age, stage in the menstrual cycle, and pregnancy status, as well as whether she is taking hormonal replacement therapy or tamoxifen therapy [60].

11.6.1 Endometrial Stripe Thickening

Endometrial hyperplasia is an abnormal proliferation of endometrial stroma and glands and represents a spectrum of endometrial changes ranging from glandular atypia to frank neoplasia. A definitive diagnosis can be made only with biopsy, and imaging cannot reliably allow differentiation between hyperplasia and carcinoma. Up to one-third of endometrial carcinomas are believed to be preceded by hyperplasia [61]. All types of endometrial hyperplasia (cystic, adenomatous, atypical) can cause diffusely smooth or, less commonly, focal hyperechoic endometrial thickening (Fig. 13). The US appearance of some lesions can simulate that of normal thickening during the secretory phase, e.g. sessile polyps, submucosal fibroids, cancer, and adherent blood clots, yielding potentially false-positive results [62]. Endometrial hyperplasia is considered whenever the endometrium appears to exceed 10 mm in thickness, especially in menopausal patients [63], although it can be reliably excluded in these patients only when the endometrium measures less than 5 mm. Endometrial hyperplasia may also cause asymmetric thickening with surface irregularity, an appearance that is suspicious for carcinoma. Because endometrial hyperplasia has a nonspecific appearance, any focal abnormality should lead to biopsy if there is clinical suspicion for malignancy (Fig. 14).

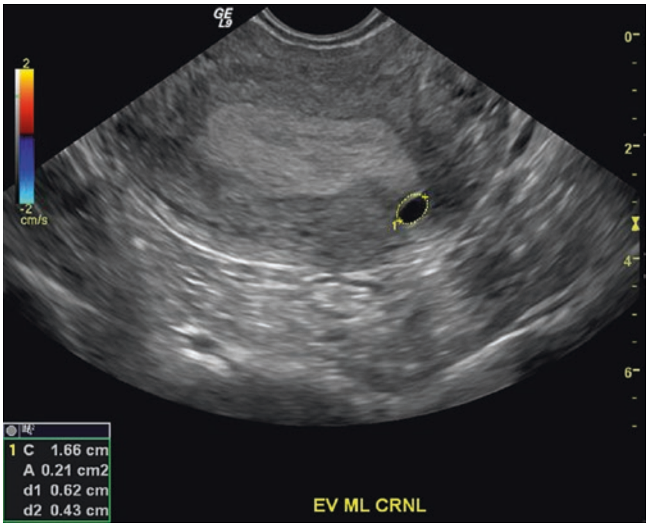

Fig. 13 Transvaginal. Presence of an Endometrial cyst in a normal thickness endometrial stripe in premenopausal woman

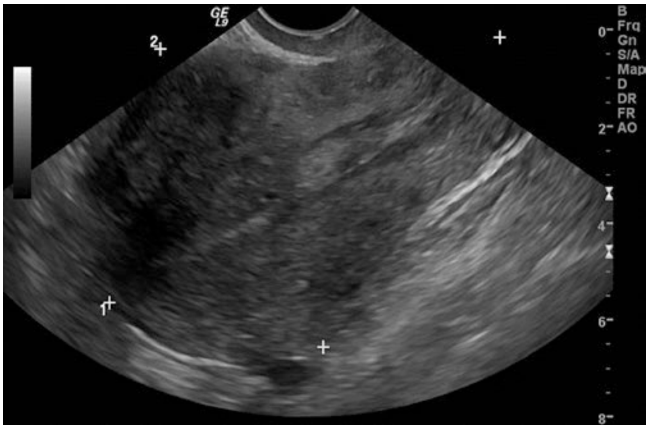

Fig. 14 Transvaginal. Thickened endometrial stripe in a postmenopausal women who was subsequently diagnosed with Endometrial adenocarcinoma

Abnormal endometrial stripe thickening is a concern in postmenopausal patients experiencing bleeding. The differential diagnosis can include endometrial atrophy (approximately 75% of cases), endometrial polyps, submucosal fibroids, endometrial hyperplasia, endometrial carcinoma (approximately 10%), and estrogen withdrawal [64]. Imaging should take place immediately after bleeding has stopped, when the endometrium is presumed to be thinnest and any disease entity will be most prominent. Endometrial thickness less than 5 mm at transvaginal US generally excludes cancer [65]. The atrophic postmenopausal endometrium may also be appreciated on MR imaging. Any thickness greater than 4 mm in the setting of postmenopausal bleeding or any endometrial heterogeneity or focal thickening seen during transvaginal US should be investigated further with sonohysterography, biopsy, or hysteroscopy.

Endometrial adenocarcinoma is a common invasive gynecologic malignancy. US signs of endometrial carcinoma include heterogeneity and irregular endometrial thickening. These signs are nonspecific and can be seen in endometrial hyperplasia as well as polyps, leading to biopsy of almost any irregularity in the setting of postmenopausal bleeding. However, polypoid tumors tend to cause more diffuse and irregular thickening than a polyp and more heterogeneity than endometrial hyperplasia [66]. A more specific US sign is irregularity of the endometrial-myometrial border, a finding that indicates invasive disease. A small amount of fluid in the endometrial canal is likely related to benign cervical stenosis and does not require further evaluation. However, an intrauterine fluid collection in a postmenopausal patient, although possibly related to cervical stenosis, should raise concern for endometrial (or cervical) carcinoma.

11.7 Endometrial Lesions

11.7.1 Endometrial Polyps

Endometrial polyps are a common cause of postmenopausal bleeding and are commonly seen in patients receiving tamoxifen. Although endometrial polyps may be visualized at transvaginal US as nonspecific endometrial thickening, they are frequently identified as focal masses within the endometrial canal. Polyps are best seen during sonohysterography and appear as echogenic, smooth, intracavitary masses outlined by fluid (Fig. 15) [67, 68].

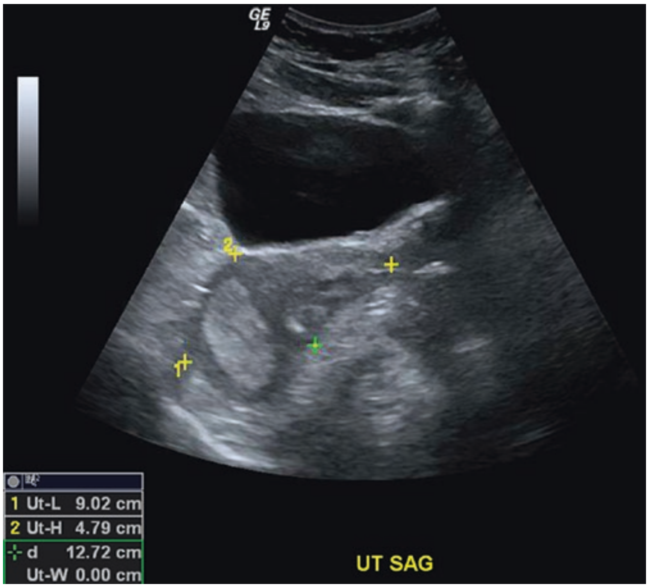

Fig. 15 Transvaginal. Endometrial polyp

Cystic spaces corresponding to dilated glands filled with proteinaceous fluid may be seen within the polyp [69]. The polyp may be broad-based and sessile or pedunculated. The point of attachment should not disrupt the endometrial lining [68]. Polyps may also be seen during hysterosalpingography as pedunculated filling defects within the uterine cavity or with T2-weighted MR imaging as low signal-intensity intracavitary masses surrounded by high-signal-intensity fluid and endometrium. Color Doppler US may be used to image vessels within the stalk. Fibroids or foci of endometrial hyperplasia or carcinoma can mimic a sessile polyp, and foci of atypical hyperplasia are sometimes found within polyps [62, 68].

11.8 The Cervix

The cervix is homogeneous in echotexture and similar in echogenicity to the uterine body, with a hypoechoic central canal. When imaging via CT, the cervix may not enhance like the remainder of the uterus, and the inner stromal layer typically enhances less than the outer stromal layer [70]. The endocervical canal, which can be identified by MR imaging, is indistinct on CT imaging. The lateral margins of the cervix can typically be differentiated from parametrial fat because of differences in density. However, CT is not sensitive for parametrial involvement in the setting of cervical cancer [71]. Nabothian cysts, which are formed by the retention of mucus within the endocervical glands, are commonly present in the cervix of parous women. They are multiple, translucent or opaque, and whitish to yellow on examination. Nabothian cysts usually occur at the transformation zone of the uterine cervix and are a few millimeters to 4 cm in diameter [72]. Although they are usually small and asymptomatic, large ones are rare and may be confused for benign or malignant tumors. They are commonly reported on ultrasound, but they are hyperintense on T2-weighted imaging and may have variable T1 signal, ranging from isointensity to hypointensity. Nabothian cysts typically have no solid enhancing components [72, 73].

11.9 Fallopian Tubes

11.9.1 Hydrosalpinx

Commonly, the fallopian tubes are not seen on imaging. However, when pathology is present, they are readily identified near the ovaries. The presence of a tubular shaped mass, cystic in appearance with or without projections, is indicative of a hydrosalpinx when seen on imaging. The folds of a fallopian tube may represent “beads on a string” [2, 74–76]. The tubular structure may often have incomplete projections or septations arising from the top and bottom part of the structure Also referred to as the waist sign [77]. Importantly, the structure should be independent of the ovary. The fluid within the structure should appear anechoic (Fig. 16).

11.9.2 Pyosalpinx

A sexually transmitted infection that starts at the vagina and endocervix and ascends up to The fallopian tubes and subsequently the pelvis is called pelvic inflammatory disease [21, 77]. Specifically, the fimbriae of the fallopian tube become obstructed due to the inflammatory reaction. The fallopian tubes become thickened, distended, and subsequently fill with pyogenic material [21]. Like a hydrosalpinx, ultrasound will show a distended tubular structure with debris, and echogenic fluid. On Doppler imaging, the fallopian tube walls may appear hypervascular (Fig. 16) [77].

11.10 Ovaries

Cystic structures less than 3 cm are considered within normal limits and physiologic in nature in reproductive age women [2]. However, structures larger than that are classified as pathologic ovarian cysts. All cystic structures in reproductive age women >3 cm should be investigated in detail on ultrasonography [2]. In postmenopausal women, cysts >1 cm should be detailed. Approximately 1% of the time, malignancy may be found in these lesions seen on ultrasonography [2]. The majority of ovarian cysts are of benign etiology and are classified as functional or benign neoplastic cysts [5].

11.10.1 Functional Cysts

In a reproductive age woman, a normal ovary has a variable appearances during the different stages of the menstrual cycle. Cysts that originate from ovarian follicles during folliculogensis are defined as functional cysts [5]. These cysts are either corpus luteal cysts, or follicular cysts and develop secondary to the collection of intrafollicular fluid, or hemorrhage in the case of a corpus luteal cyst. Functional cysts differ from other cysts because they are due to a collection of fluid as opposed to the proliferation of cells (Fig. 17). On imaging, follicular cysts are commonly referred to as simple cysts with regular borders, thin walls, and anechoic centers.

11.10.2 Hemorrhagic Cyst

Preceeding ovulation a dominant cyst on the ovary called a corpus luteum develops. Characteristically, the cyst has thick walls, no greater than 3 cm, and a peripheral ring of vascularity seen on color doppler [2]. Hemorrhage occurs within the walls of the corpus luteum. In the case that the hemorrhage expands, a hemorrhagic cyst will develop. On imaging they appear as cystic masses with a reticular (fishnet, cobwebs, lacy) pattern (Fig. 18). Hemorrhagic cysts occasionally are

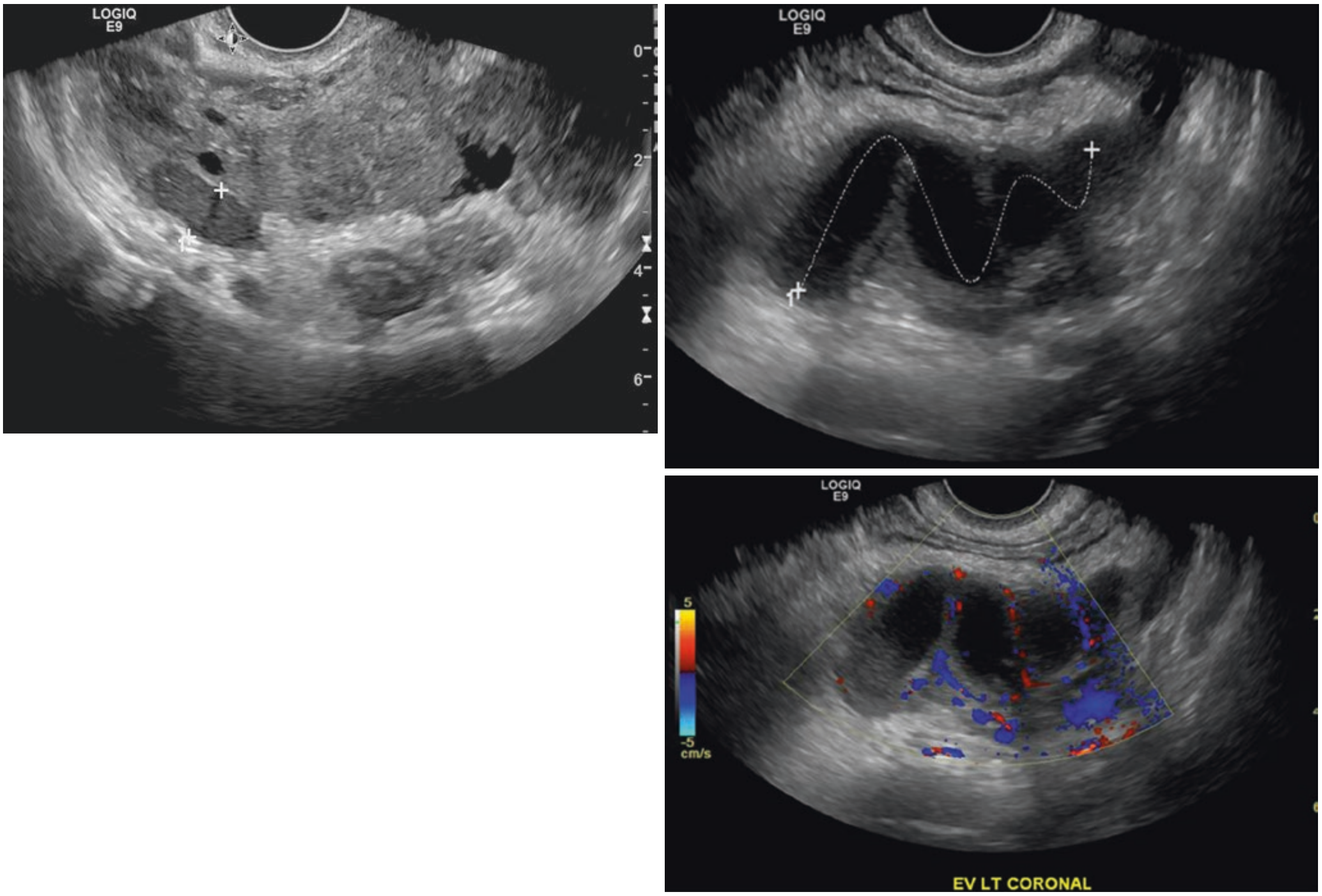
LOGIQ E9
0
2
4
6
LOGIQ E9
LOGIQ E9
5
-5 cm/s
EV LT CORONAL

Fig. 16 Transvaginal doppler study and 2-D imaging, Hydrosalpinx (right) compared to Pyosalpinx (left)

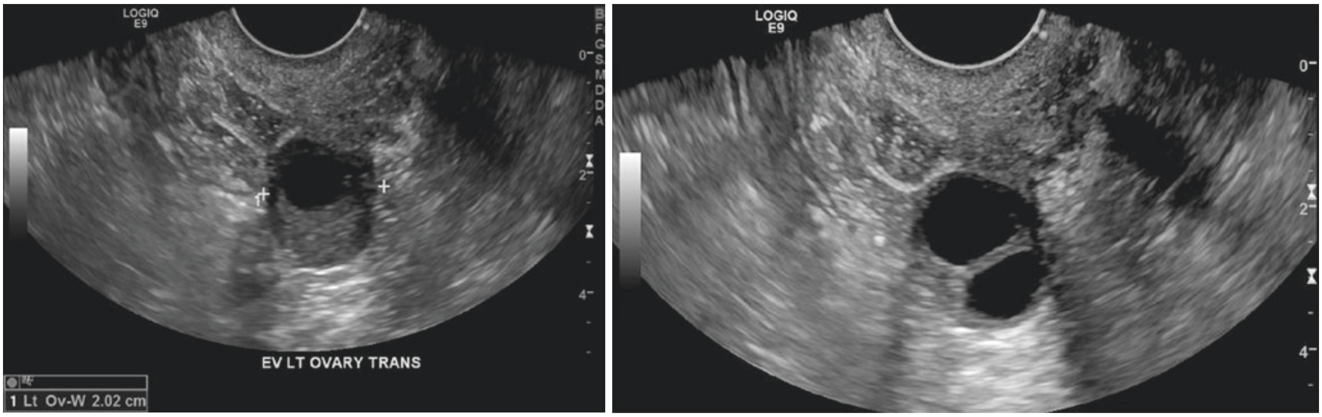
LOGIQ E9
0
2
4
EV LT OVARY TRANS
1 Lt Ov-W 2.02 cm
LOGIQ E9
0
2
4

Fig. 17 Transvaginal. Functional cysts of the ovary. Simple in appearance and <3 cm

solid appearing with concave areas and the absence of blood flow [2]. On average these cysts resolve in 8 weeks [2]. Any hemorrhagic cyst >5 cm should have repeat imaging to assess for resolution. Post-menopausal women do not ovulate; therefore, the presence of a hemorrhagic appearing cyst should be concerning for malignancy.

11.10.3 Benign Neoplastic Ovarian Cysts

Benign Serous and Mucinous Tumors. Surface epithelial cysts are classified as serous or mucinous and are lined with cells similar to those found within the fallopian tube. Approximately 20% of the time these cysts occur bilaterally [5]. On imaging these cysts appear oval in shape and have thin, smooth walls. These cysts do not have any solid components, septations, or vascularity. They are typically anechoic or appear as solid black on the ultrasound. Up to approximately 10 cm, most cysts are thought to be benign.

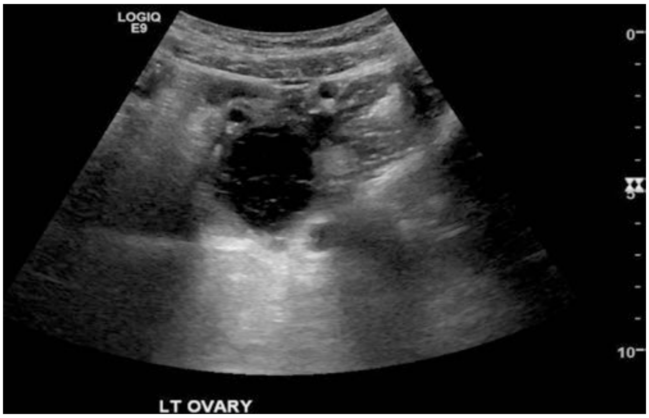

Fig. 18 Transabdominal. Three centimenter hemorrhagic cyst with the reticular pattern within the cyst

Mucinous cystadenoma and serous cystadenoma are the most common types of simple cysts on imaging; however, they require a pathologic diagnosis for confirmation. These cysts are most commonly benign and asymptomatic in most women (Fig. 19).

11.10.4 Endometriomas

Endometriosis occurs when endometrial glans and stroma are present outside of the uterus. The disease process is typically confined to the pelvis. Endometrial implants can be found on the uterosacral ligaments, periosteum, bowel, posterior cul-de-sac, and ovaries [5]. Implants found on the ovaries can develop into cystic lesions called endometriomas. There is a high sensitivity for the diagnosis of endometriomas on ultrasound when lesions measure greater than 20 mm [78]. On ultrasonography, endometriomas are cystic with a "ground glass" appearance, no solid components, and low-level internal echoes. They typically are unilocular and may have up to 4 mm thin septations [79]. Endometriomas are similar in appearance to corpus luteal cysts but have thicker walls and lack the vascular characteristics [80].

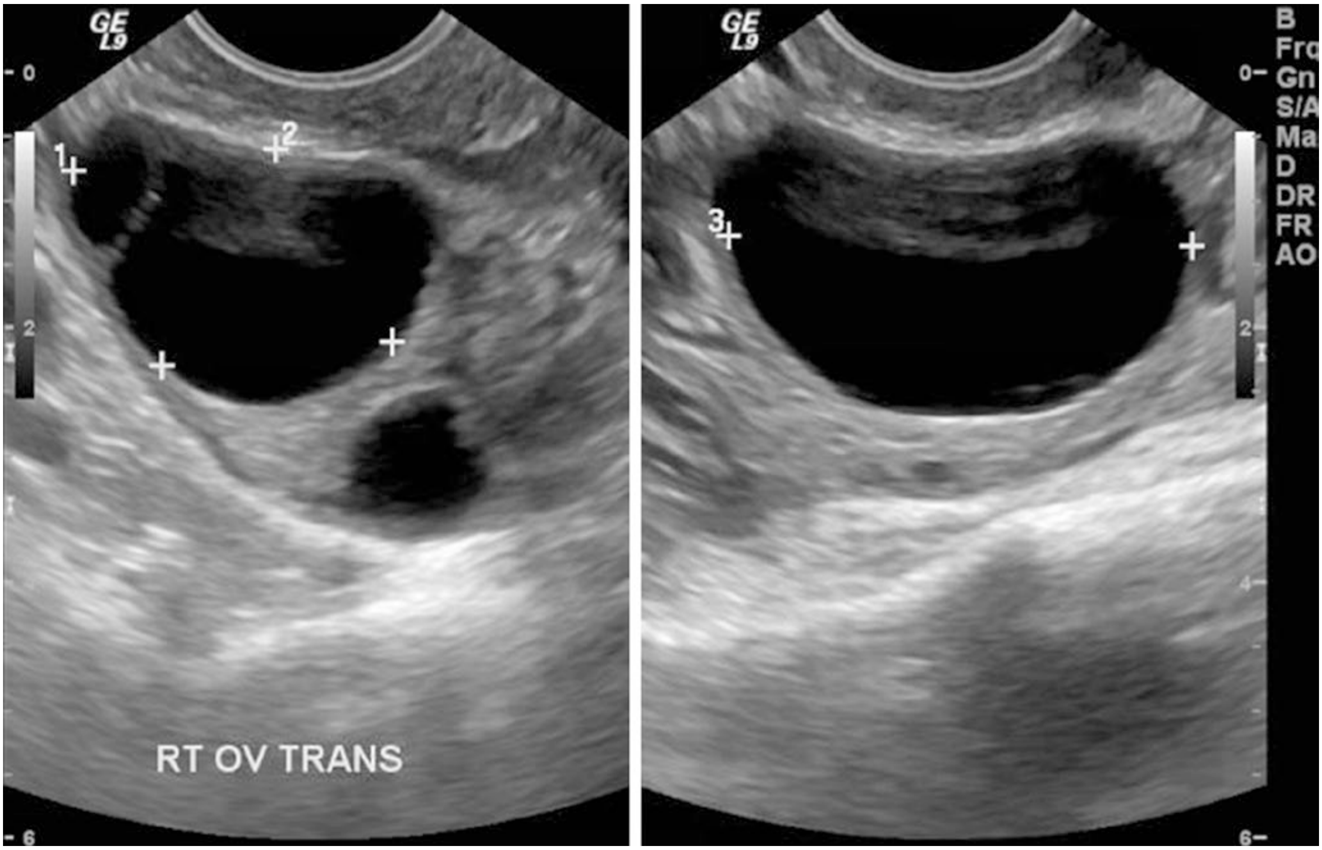

Fig. 19 Transvaginal. Mucinous vs serous cyst of the ovary

Endometriomas lack internal color flow on doppler imaging, and should not have wall nodules. Given that these cystic lesions can often imitate hemorrhagic cysts, repeat imaging in 6–12 weeks should be performed [2]. Resolution of the cysts would indicate that it was hemorrhagic in origin. A stable appearance of the cyst would confirm an endometrioma. The pathophysiologic mechanism in endometriosis is hormone dependent, therefore they are more common in reproductive age women. Occasionally, endometriomas that are multilocular in appearance can be seen in postmenopausal women. Approximately 1% of these cysts can transform into endometrioid or clear cell carcinoma [81].

11.10.5 Dermoid Cyst

Dermoid cysts are often referred to as ovarian teratomas. These cysts originate from the germ cell layers including ectoderm, mesoderm, and endoderm [5]. Dermoid cysts are classified into two different groups; mature or immature teratomas. Immature teratomas are classified as malignant lesions and arise from a combination of one or all of the three germ cell layers. Mature teratomas are classified as a benign lesion. There are three different types of mature teratomas; mature cystic teratoma, mature solid teratoma, and fetiform teratoma [5]. Among these the mature cystic teratomas are the most common. In general, the term “dermoid” most often refers to a mature cystic teratoma [2]. On average, these cysts are approximately 5–10 cm and are usually slow growing [82]. On ultrasonography, mature cystic teratomas have a distinct appearance. Given that the cyst contains all germ cell layers, they often are composed of hair, fat, bone, and sebaceous fluid. The presence of hair may create linear demarcations, lines, dots, and areas of acoustic shadowing [2, 5]. Rarely, floating spherical shaped structures can be seen within the cyst [83]. The Rokitansky protuberance is pathognomonic for the dermoid cyst and appears as rounded intramural nodules that are hyperechoic creating acute angles within the cell wall. Dermoid cysts should be followed by ultrasound every 6–12 months if they are not surgically removed. The risk of malignant transformation is less than 2% and most commonly occurs in women greater than 50 years of age [2, 84, 85].

11.11 Ovarian Torsion

Ovarian torsion is a gynecologic surgical emergency that can occur in women of all ages, with the highest prevalence in postmenarcheal, premenopausal women [86]. Symptoms of ovarian torsion are often nonspecific, making it difficult to differentiate from other causes of acute abdominal pain. The classic presentation includes sharp, localized right or left lower abdominal pain and tenderness with a palpable abdominal mass and peritoneal signs. Waves of nausea and vomiting as well as pyrexia have been observed [87–89]. In some cases, patients experience intermittent pain, making the diagnosis even more challenging [87]. The twisted ovary initially has compromised venous and lymphatic outflow, usually with sustained arterial inflow, resulting in edematous enlargement that stretches the ovarian capsule, causing pain [90].

Ultrasonography (US) is the primary imaging modality for evaluation of ovarian torsion. One series studying the effectiveness of US in diagnosing ovarian torsion yielded a positive predictive value of 87.5% and specificity of 93.3%, corroborating the potential for expeditiously making the diagnosis with this imaging modality [91]. US features of ovarian torsion include a unilaterally enlarged ovary, uniform peripheral cystic structures, a coexistent mass within the affected ovary, free pelvic fluid, lack of arterial or venous flow, and a twisted vascular pedicle [91, 92]. The most consistent finding in ovarian torsion is a large ovary [93].

This enlargement of the ovary is the hallmark of imaging findings in ovarian torsion; a morphologically normal-appearing ovary effectively excludes torsion as a diagnostic possibility [94, 95]. The presence of flow during color Doppler imaging does not allow exclusion of torsion, but instead suggests that the ovary may be viable, especially if flow is present centrally [90]. The classic color Doppler sonographic finding in ovarian torsion is the absence of arterial flow, but Doppler flow manifestations are highly variable due to the degree of vascular compromise. In one study involving patients with confirmed ovarian torsion, the absence of arterial flow was found in only 73% of cases [93]. In another study, 60% had normal color Doppler flow findings [93, 96].

Comparison of the gray-scale US appearance and flow of the contralateral ovary may aid significantly in diagnosis and is recommended to be performed at every examination. In addition, at transvaginal US, local tenderness of the affected ovary can be elicited in comparison with the fallopian tube, uterus, and neighboring structures. Local tenderness is exquisite in ovarian torsion and is not assessable with other imaging techniques [90].

11.12 Pelvic Inflammatory Disease

Pelvic inflammatory disease (PID) is a polymicrobial ascending infection that causes inflammation of the upper genital tract, including endometritis, salpingitis, pelvic peritonitis, and occasionally leading to tuboovarian abscess (TOA) formation [97]. The clinical presentation of pelvic inflamma-

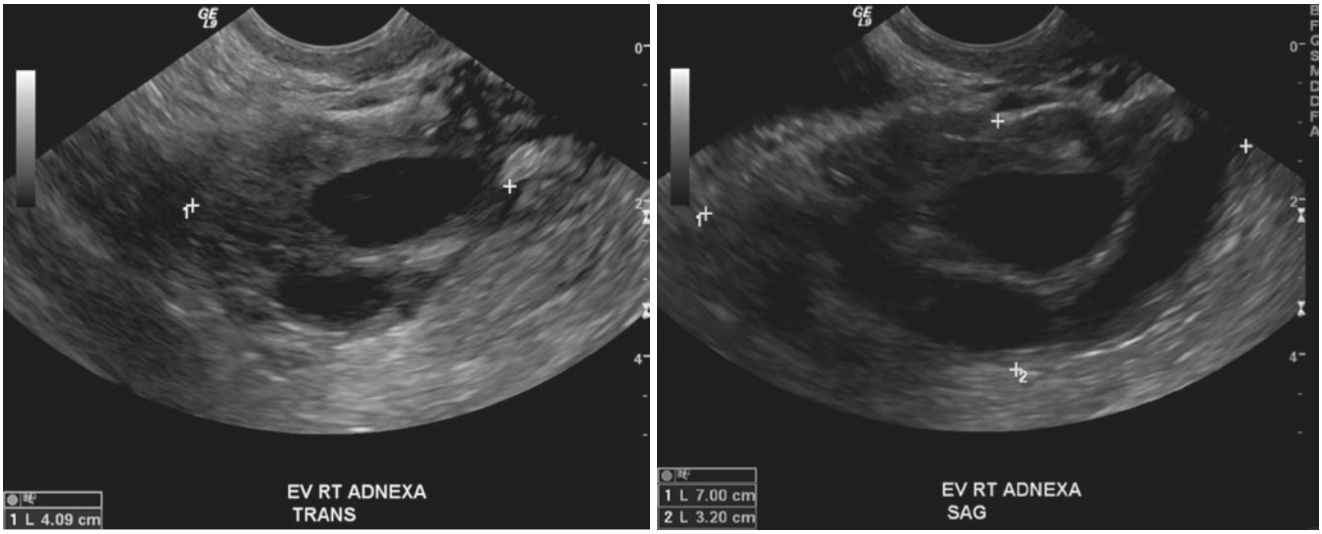

Fig. 20 Transvaginal. Pelvic inflammatory disease/tuboovarin abscess. Thickened walls indicating an inflammatory process and heterogenous fluid

tory disease (PID) is variable and can mimic other causes of acute pelvic pain. Systemic signs of infection, such as fever and an elevated white blood cell count, and pertinent physical examination findings, such as mucopurulent cervical discharge, leukorrhea, and cervical motion tenderness, can help to confirm the diagnosis of PID, but these features are not always present or reliable [98].

Pelvic ultrasound is not needed to make the diagnosis but is often used when the clinical diagnosis is uncertain. Although transvaginal ultrasound has limited ability to diagnose acute PID [99], the sonographic features of PID are important to recognize [100] and can lead to the development of tuboovarian abscess in some cases. The sonographic findings associated with the fallopian tubes are the most important features of PID that help to distinguish this condition from ovarian hemorrhage and ovarian torsion. As the tube and mesosalpinx become increasingly inflamed, they become edematous and hyperemic with thickening of the endosalpingeal folds. It produces an exudate that pours into the pelvis. This tubal and mesosalpingeal edema may initially be distinct from the ovary, and hyperemia seen with color Doppler imaging distinguishes this from a paraovarian clot that can be seen in some cases of ovarian hemorrhage with a leaking corpus luteum [86]. If the tube fills with exudate, it often has echoes, which can make the presence of the fluid subtle; when recognized, it often has a characteristic tubular configuration that may exhibit incomplete “septi” (thickened folds seen in the long axis) and the “cog wheel sign” (thickened folds in cross-section) [101].

With progression, the inflammation involves the ovary, such that the margin of the ovary is no longer distinguishable from the tube and mesosalpinx. At this stage, the sonographic findings become more confusing, indistinguishable on imaging from an ovarian malignancy, appearing as an adnexal mass with poorly identified margins, usually with locules of fluid containing echoes. The terminology for the adnexal inflammatory process is confusing [102–104]. Some reserve the term “tuboovarian abscess” for the case where an encapsulated collection of pus is evident, but others point out that these inflammatory collections are often multiloculated. In most cases, “tuboovarian phlegmon” would probably more accurately convey the heterogeneity of the composition of the inflamed tissue, but historically this term has not been used (Fig. 20) [86].

11.13 Peritoneal Inclusion Cysts

Cystic structures located in the pelvis that are non-ovarian in origin are defined as peritoneal inclusion cysts [105]. These cysts are also referred to as peritoneal pseudo cyst and inflammatory cyst of the pelvic peritoneum. Given the location and appearance they can easily be confused with adnexal masses.

Peritoneal adhesions caused by endometriosis, prior pelvic surgery, or pelvic inflammatory disease and an active ovary are necessary for the development of inclusion cysts. Current proposed theories are that absorption within the pelvis is delayed when there are many adhesions present. Due to steroidogenesis the ovary naturally secretes fluids [105]. The fluids are then trapped within these adhesions and lead to the development of peritoneal inclusion cysts [106, 107]. On imaging the ovaries are often seen lying adjacent to the mass or suspended within the mass [3, 108]. Since these cysts are isolated, they can follow the contour of surrounding organs and can be with or without the presence of septations (Fig. 21).

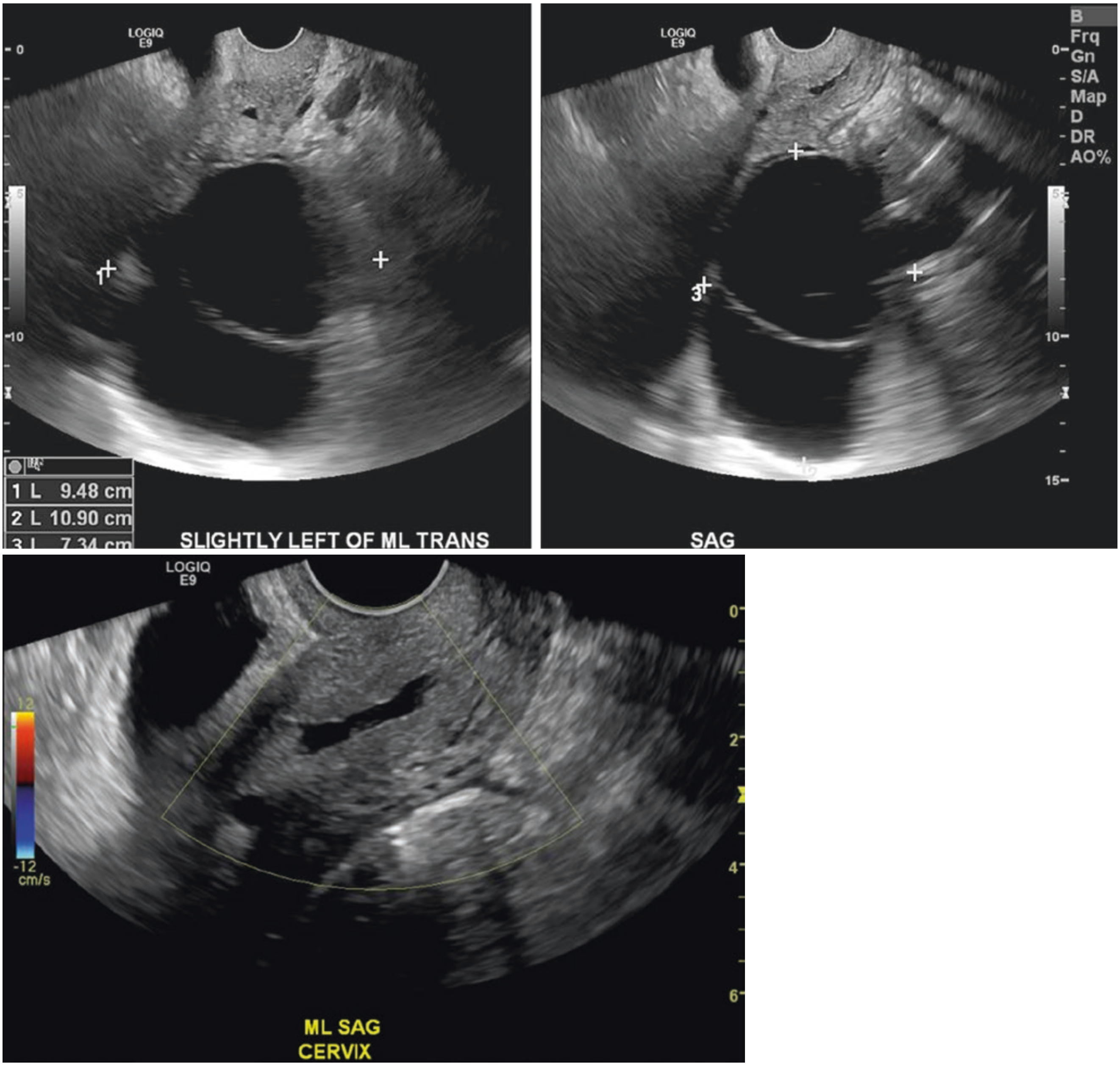

Fig. 21 Transvaginal, peritoneal inclusion cysts post-supracervical hysterectomy. Cervix seen on right

12 Conclusion

There are many different imaging appearances of the normal and abnormal uterus, tubes and ovaries. Ultrasound is usually the first modality utilized in the workup, but other modalities such as sonohysterography, hysterosalpingography, CT and MRI may aid in the diagnosis. For an accurate diagnosis, the patient's age, menstrual status, pregnancy status, and use hormonal replacement therapy should be taken into account.

References

1. Lizzi F, Mortimer A, Carstensen E, Kremkau F, Miller D, Miller M, Nyborg W, O'Brien W, Ziskin M. Bioeffects considerations for the safety of diagnostic ultrasound. J Ultrasound Med. 1988;7(9 Suppl):S1–38.
2. Levine D, et al. Management of asymptomatic ovarian and other adnexal cysts imaged at US Society of Radiologists in Ultrasound consensus conference statement. Ultrasound Q. 2010;26(3):121–31.
3. American Institute of Ultrasound in Medicine. AIUM practice guideline for the performance of pelvic ultrasound examinations. J Ultrasound Med. 2010;29(1):166–72.

4. American Institute of Ultrasound in Medicine. AIUM practice guideline for the performance of ultrasound of the female pelvis. J Ultrasound Med. 2014;33(6):1122–30.
5. Hoffman BL. Williams gynecology. 3rd ed. New York: McGraw-Hill Education; 2016. p. xxv, 1270.
6. Benacerraf BR, Goldstein SR, Groszmann YS. Gynecologic ultrasound: a problem-based approach: Elsevier Health Sciences; 2014. p. xix, 273.
7. American College of Obstetricians and Gynecologists. AIUM practice guideline for the performance of a focused reproductive endocrinology and infertility scan. J Ultrasound Med. 2012;31(11):1865–74.
8. Polat P, et al. Color Doppler US in the evaluation of uterine vascular abnormalities. Radiographics. 2002;22(1):47–53.
9. Committee on Gynecologic Practice. The American College of Obstetricians and Gynecologists Committee Opinion no. 631. Endometrial intraepithelial neoplasia. Obstet Gynecol. 2015;125(5):1272–8.
10. Chen L, ter Haar G, Hill CR. Influence of ablated tissue on the formation of high-intensity focused ultrasound lesions. Ultrasound Med Biol. 1997;23(6):921–31.
11. Khalife S, et al. Diagnostic accuracy of transvaginal ultrasound in detecting free pelvic fluid. J Reprod Med. 1998;43(9):795–8.
12. Funt SA, Hann LE. Detection and characterization of adnexal masses. Radiol Clin N Am. 2002;40(3):591–608.
13. Jaffe R, Warsof SL. Color doppler imaging in obstetrics and gynecology. New York: McGraw-Hill, Inc., Health Professions Division; 1992. p. xiii, 306.
14. Kurjak A, et al. The assessment of abnormal pelvic blood flow by transvaginal color and pulsed Doppler. Ultrasound Med Biol. 1990;16(5):437–42.
15. Baerwald AR, Adams GP, Pierson RA. Form and function of the corpus luteum during the human menstrual cycle. Ultrasound Obstet Gynecol. 2005;25(5):498–507.
16. Durfee SM, Frates MC. Sonographic spectrum of the corpus luteum in early pregnancy: gray-scale, color, and pulsed Doppler appearance. J Clin Ultrasound. 1999;27(2):55–9.
17. Hill R, et al. Ultrasound for the detection of foreign bodies in human tissue. Ann Emerg Med. 1997;29(3):353–6.
18. Isaacs JD Jr, Hines RS, Cowan BD. Sonohysterography: a unique technique for the evaluation of gynecologic disorders. J Miss State Med Assoc. 1997;38(12):447–9.
19. Lindheim SR, et al. Sonohysterography: a valuable tool in evaluating the female pelvis. Obstet Gynecol Surv. 2003;58(11):770–84.
20. Jorizzo JR, Chen MY, Riccio GJ. Endometrial polyps: sonohysterographic evaluation. AJR Am J Roentgenol. 2001;176(3):617–21.
21. Rock JA, Jones HW, Te Linde RW. Te Linde's operative gynecology. 10th ed. Philadelphia: Wolters Kluwer; 2015, 1467.
22. Bonnamy L, et al. Sonohysterography: a prospective survey of results and complications in 81 patients. Eur J Obstet Gynecol Reprod Biol. 2002;102(1):42–7.
23. Grigore M, et al. Comparative study of hysteroscopy and 3D ultrasound for diagnosing uterine cavity abnormalities. Rev Med Chir Soc Med Nat Iasi. 2016;120(4):866–73.
24. Al-Zinaty FMI, et al. Three-dimensional ultrasound versus hysteroscopy in uterine cavity assessment after failed intracytoplasmic sperm injection: a study for accuracy of a diagnostic test. Egypt J Hosp Med. 2018;72(5):4565–71.
25. Baird DD, Dunson DB, Hill MC, Cousins D, Schectman JM. High cumulative incidence of uterine leiomyoma in black and white women: ultrasound evidence. Am J Obstet Gynecol. 2003;188:100–7.
26. Robboy SJ, Bentley RC, Butnor K, Anderson MC. Pathology and pathophysiology of uterine smooth-muscle tumors. Environ Health Perspect. 2000;108(Suppl 5):779–84.
27. Munro MG, Critchley HO, Broder MS, Fraser IS. FIGO classification system (PALM-COEIN) for causes of abnormal uterine bleeding in nongravid women of reproductive age. Int J Gynaecol Obstet. 2011;113:3–13.
28. Bonneau C, Thomassin-Naggara I, Dechoux S, et al. Value of ultrasonography and magnetic resonance imaging for the characterization of uterine mesenchymal tumors. Acta Obstet Gynecol Scand. 2014;93(3):261e8.
29. Reiter MJ, Schwope RB, Lisanti CJ, et al. Can a T2 hyperintense rim sign differentiate uterine leiomyomas from other solid adnexal masses? Abdom Imaging. 2015;40(8):3182e90.
30. Yang Q, Zhang LH, Su J, et al. The utility of diffusion-weighted MR imaging in differentiation of uterine adenomyosis and leiomyoma. Eur J Radiol. 2011;79:e47–51.
31. Kirpalani A, Chong J, Yang N, et al. Diffusion-weighted imaging properties of uterine fibroids pre- and post-uterine fibroid embolization. Eur J Radiol. 2014;83:1620e5.
32. Mindjuk I, Trumm CG, Herzog P, et al. MRI predictors of clinical success in MR- guided focused ultrasound (MRgFUS) treatments of uterine fibroids: results from a single center. Eur Radiol. 2015;25:1317e28.
33. Deshmukh SP, Gonsalves CF, Guglielmo FF, et al. Role of MR imaging of uterine leiomyomas before and after embolization. Radiographics. 2012;32:E251–81.
34. Johari B, Koshy M, Sidek S. Lipoleiomyoma: a rare benign tumour of the uterus. BMJ Case Rep. 2014;2014:bcr2014205814.
35. Wallach EE, Vlahos NF. Uterine myomas: an overview of development, clinical features, and management. Obstet Gynecol. 2004;104(2):393–406.
36. McLucas B. Diagnosis, imaging and anatomical classification of uterine fibroids. Best Pract Res Clin Obstet Gynaecol. 2008;22(4):627–42.
37. Huang PS, Chang WC, Huang SC. Iatrogenic parasitic myoma: a case report and review of the literature. Taiwan J Obstet Gynecol. 2014;53(3):392–6.
38. Fasih N, Prasad Shanbhogue AK, Macdonald DB. Leiomyomas beyond the uterus: unusual locations, rare manifestations. Radiographics. 2008;28(7):1931–48.
39. Testa AC, Di Legge A, Bonatti M, Manfredi R, Scambia G. Imaging techniques for evaluation of uterine myomas. Best Pract Res Clin Obstet Gynaecol. 2016;34:37e53.
40. Wamsteker K, De Blok S, Gallinat A, et al. Fibroids. In: Lewis BV, Magos AL, editors. Endometrial ablation. Edinburgh: Churchill Livingstone; 1993. p. 161–81.
41. Leone FP, Lanzani C, Ferrazzi E. Use of strict sonohysterographic methods for preoperative assessment of submucous myomas. Fertil Steril. 2003;79(4):998e1002.
42. Exacoustos C, Romanini ME, Amadio A, et al. Can gray-scale and color Doppler sonography differentiate between uterine leiomyosarcoma and leiomyoma? J Clin Ultrasound. 2007;35(8):449e57.
43. Exacoustos C, Manganaro L, Zupi E. Imaging for the evaluation of endometriosis and adenomyosis. Best Pract Res Clin Obstet Gynaecol. 2014;28(5):655e81.
44. Geethamala K, Murthy VS, Vani BR, Rao S. Uterine leiomyomas: an ENIGMA. J Midlife Health. 2016;7:22–7.
45. Rha SE, Byun JY, Jung SE, et al. CT and MRI of uterine sarcomas and their mimickers. AJR Am J Roentgenol. 2003;181:1369–74.
46. Goto A, Takeuchi S, Sugimura K, Maruo T. Usefulness of Gd-DTPA contrast-enhanced dynamic MRI and serum determination of LDH and its isozymes in the differential diagnosis of leiomyosarcoma from degenerated leiomyoma of the uterus. Int J Gynecol Cancer. 2002;12:354–61.
47. Sato K, Yuasa N, Fujita M, Fukushima Y. Clinical application of diffusion-weighted imaging for preoperative differentiation between uterine leiomyoma and leiomyosarcoma. Am J Obstet Gynecol. 2014;210(368):e361–8.

48. Wright JD, Tergas AI, Burke WM, et al. Uterine pathology in women undergoing minimally invasive hysterectomy using morcellation. JAMA. 2014;312:1253–5.
49. Food and Drug Administration. Quantitative assessment of the prevalence of unsuspected uterine sarcoma in women undergoing treatment of uterine fibroids: summary and key findings. Silver Spring (MD): FDA; 2014. p. 2014.
50. Murase E, Siegelman ES, Outwater EK, Perez-Jaffe LA, Tureck RW. Uterine leiomyomas: histopathologic features, MR imaging findings, differential diagnosis, and treatment. Radiographics. 1999;19:1179–97.
51. Reinhold C, McCarthy S, Bret PM. Diffuse adenomyosis: comparison of endovaginal US and MR imaging with histopathologic correlation. Radiology. 1996;199:151–8.
52. Exacoustos C, Brienza L, Di Giovanni A, et al. Adenomyosis: three-dimensional sonographic findings of the junctional zone and correlation with histology. Ultrasound Obstet Gynecol. 2011;37(4):471e9.
53. Cunningham RK, Horrow MM, Smith RJ, Springer J. Adenomyosis: a sonographic diagnosis. Radiographics. 2018;38(5):1576–89.
54. Ali GM, Kordorff R, Franke D. Ultrasound volumetry in hematometrocolpos. J Clin Ultrasound. 1989;17:257–9.
55. Siegel MJ, Surratt JT. Pediatric gynecologic imaging. Obstet Gynecol Clin N Am. 1992;19:103–27.
56. Sailer JF. Hematometra and hematocolpos: ultrasound findings. AJR Am J Roentgenol. 1979;132:1010–1.
57. Sadler TW, Langman J. Langman's medical embryology. 8th ed. Philadelphia: Lippincot Williams & Wilkins; 2000.
58. The American Fertility Society. The American Fertility Society classifications of adnexal adhesions, distal tubal occlusion, tubal occlusion secondary to tubal ligation, tubal pregnancies, mullerian anomalies and intrauterine adhesions. Fertil Steril. 1988;49:944–55.
59. Edmonds DK. Congenital malformations of the genital tract and their management. Best Pract Res Clin Obstet Gynaecol. 2003;17:19–40.
60. Nalaboff K, Pellerito J, Ben-Levi E. Imaging the endometrium: disease and normal variants. Radiographics. 2001;21:1409–24.
61. Kurman RJ, Kaminski P. The behavior of endometrial hyperplasia: a long-term study of "untreated" hyperplasia in 170 patients. Cancer. 1985;56:403–12.
62. Sohaey R, Woodward P. Sonohysterography: technique, endometrial findings, and clinical applications. Semin Ultrasound CT MR. 1999;20:250–8.
63. Malpani A, Singer J, Wolverson MK, et al. Endometrial hyperplasia: value of endometrial thickness in ultrasonographic diagnosis and clinical significance. J Clin Ultrasound. 1990;18:173–7.
64. Fleischer AC. Sonographic assessment of endometrial disorders. Semin Ultrasound CT MR. 1999;20:259–66.
65. Ferrazzi E, Torri V, Trio D, et al. Sonographic endometrial thickness: a useful test to predict atrophy in patients with postmenopausal bleeding—an Italian multicenter study. Ultrasound Obstet Gynecol. 1996;7:315–21.
66. Fleischer AC. Transvaginal sonography of endometrial disorders: an overview. Radiographics. 1998;18:923–30.
67. Cullinan JA, Fleischer AC, Kepple DM, et al. Sonohysterography: a technique for endometrial evaluation. Radiographics. 1995;15:501–14.
68. Dubinsky TJ, Parvey HR, Gormaz G, et al. Transvaginal hysterosonography in the evaluation of small endoluminal masses. J Ultrasound Med. 1995;14:1–6.
69. Hulka CA, Hall DA, McCarthy K, et al. Endometrial polyps, hyperplasia, and carcinoma in postmenopausal women: differentiation with endovaginal sonography. Radiology. 1994;191:755–8.
70. Yitta S, Hecht E, Mausner E, et al. Normal or abnormal? Demystifying uterine and cervical contrast enhancement at multidetector CT. Radiographics. 2011;31:647.
71. Hricak H, Gatsonis C, Chi D, et al. Role of imaging in pretreatment evaluation of early invasive cervical cancer: results of the intergroup study American College of Radiology Imaging Network 6651–Gynecologic Oncology Group 183. J Clin Oncol. 2005;23(36):9329.
72. Okamoto Y, Tanaka YO, Nishida M, Tsunoda H, Yoshikawa H, Itai Y, et al. MR imaging of the uterine cervix: imaging-pathologic correlation. Radiographics. 2003;23:425–45.
73. Graef M, Karam R, Juhan V, et al. High signals in the uterine cervix on T2-weighted MRI sequences. Eur Radiol. 2003;13:118–26.
74. Patel MD, Acord DL, Young SW. Likelihood ratio of sonographic findings in discriminating hydrosalpinx from other adnexal masses. AJR Am J Roentgenol. 2006;186(4):1033–8.
75. Sokalska A, et al. Diagnostic accuracy of transvaginal ultrasound examination for assigning a specific diagnosis to adnexal masses. Ultrasound Obstet Gynecol. 2009;34(4):462–70.
76. Valentin L. Use of morphology to characterize and manage common adnexal masses. Best Pract Res Clin Obstet Gynaecol. 2004;18(1):71–89.
77. Rezvani M, Shaaban AM. Fallopian tube disease in the nonpregnant patient. Radiographics. 2011;31(2):527–48.
78. Moore J, et al. A systematic review of the accuracy of ultrasound in the diagnosis of endometriosis. Ultrasound Obstet Gynecol. 2002;20(6):630–4.
79. Van Holsbeke C, et al. Endometriomas: their ultrasound characteristics. Ultrasound Obstet Gynecol. 2010;35(6):730–40.
80. Bhatt S, Kocakoc E, Dogra VS. Endometriosis: sonographic spectrum. Ultrasound Q. 2006;22(4):273–80.
81. Kawaguchi R, et al. Clinicopathologic features of ovarian cancer in patients with ovarian endometrioma. J Obstet Gynaecol Res. 2008;34(5):872–7.
82. Comerci JT Jr, et al. Mature cystic teratoma: a clinicopathologic evaluation of 517 cases and review of the literature. Obstet Gynecol. 1994;84(1):22–8.
83. Umesaki N, et al. MR and ultrasound imaging of floating globules in mature ovarian cystic teratoma. Gynecol Obstet Invest. 2004;58(3):130–2.
84. Park JY, et al. Malignant transformation of mature cystic teratoma of the ovary: experience at a single institution. Eur J Obstet Gynecol Reprod Biol. 2008;141(2):173–8.
85. Hackethal A, et al. Squamous-cell carcinoma in mature cystic teratoma of the ovary: systematic review and analysis of published data. Lancet Oncol. 2008;9(12):1173–80.
86. Patel M, Young SW, Dahiya N. Ultrasound of pelvic pain in the nonpregnant woman. Radiol Clin N Am. 2019;57:601–16.
87. Warner MA, Fleischer AC, Edell SL, et al. Uterine adnexal torsion: sonographic findings. Radiology. 1985;154(3):773–5.
88. Farrell TP, Boal DK, Teele RL, Ballantine TV. Acute torsion of normal uterine adnexa in children: sonographic demonstration. AJR Am J Roentgenol. 1982;139(2):1223–5.
89. Anders JF, Powell EC. Urgency of evaluation and outcome of acute ovarian torsion in pediatric patients. Arch Pediatr Adolesc Med. 2005;159(6):532–5.
90. Chang HC, Bhatt S, Dogra VS. Pearls and pitfalls in diagnosis of ovarian torsion. Radiographics. 2008;28:1355–68.
91. Graif M, Itzchak Y. Sonographic evaluation of ovarian torsion in childhood and adolescence. AJR Am J Roentgenol. 1988;150(3):647–9.
92. Stark JE, Siegel MJ. Ovarian torsion in prepubertal and pubertal girls: sonographic findings. AJR Am J Roentgenol. 1994;163(6):1479–82.

93. Albayram F, Hamper UM. Ovarian and adnexal torsion: spectrum of sonographic findings with pathologic correlation. J Ultrasound Med. 2001;20(10):1083–9.
94. Bronstein ME, Pandya S, Snyder CW, et al. A meta-analysis of B-mode ultrasound, Doppler ultrasound, and computed tomography to diagnose pediatric ovarian torsion. Eur J Pediatr Surg. 2015;25:82–6.
95. Lam A, Nayyar M, Helmy M, et al. Assessing the clinical utility of color Doppler ultrasound for ovarian torsion in the setting of a negative contrast-enhanced CT scan of the abdomen and pelvis. Abdom Imaging. 2015;40:3206–13.
96. Pena JE, Ufberg D, Cooney N, Denis AL. Usefulness of Doppler sonography in the diagnosis of ovarian torsion. Fertil Steril. 2000;73(5):1047–50.
97. Workowski KA, Berman S. Sexually transmitted diseases treatment guidelines, 2010. MMWR Recomm Rep. 2010;59:1–110.
98. Mitchell C, Prabhu M. Pelvic inflammatory disease: current concepts in pathogenesis, diagnosis and treatment. Infect Dis Clin N Am. 2013;27(4):793–809.
99. Romosan G, Valentin L. The sensitivity and specificity of transvaginal ultrasound with regard to acute pelvic inflammatory disease: a review of the literature. Arch Gynecol Obstet. 2014;289(4):705–14.
100. Horrow MM. Ultrasound of pelvic inflammatory disease. Ultrasound Q. 2004;20(4):171–9.
101. Timor-Tritsch IE, Lerner JP, Monteagudo A, et al. Transvaginal sonographic markers of tubal inflammatory disease. Ultrasound Obstet Gynecol. 1998;12:56–66.
102. Amstey MS. Definition of pelvic abscess. Am J Obstet Gynecol. 1993;168:740–1.
103. Monif GR, Osborne NG. Tuboovarian complex versus tuboovarian abscesses. Am J Obstet Gynecol. 1993;169:751.
104. Nelson GH. Definition of pelvic abscess. Am J Obstet Gynecol. 1994;170:257.
105. Koninckx PR, Renaer M, Brosens IA. Origin of peritoneal fluid in women: an ovarian exudation product. BJOG Int J Obstet Gynaecol. 1980;87(3):177–83.
106. Kim JS, Lee HJ, Woo SK, Lee TS. Peritoneal inclusion cysts and their relationship to the ovaries: evaluation with sonography. Radiology. 1997;204:481–4.
107. Jain KA. Imaging of peritoneal inclusion cysts. AJR Am J Roentgenol. 2000;174(6):1559–63.
108. Guerriero S, et al. Role of transvaginal sonography in the diagnosis of peritoneal inclusion cysts. J Ultrasound Med. 2004;23(9):1193–200.

Ultrasound for Spine and Nerve Blocks

Chiedozie C. Uwandu, Emily Bouley, Timothy Montet,
Mark R. Jones, and Alan David Kaye

1 Introduction

Historically, anesthesiologists have relied on the palpation of anatomical landmarks for placement of neuraxial anesthesia. These landmarks include the iliac crests, spinous processes and interspaces. However, these are often challenging to identify due to patient variability and abnormal spine anatomy such as scoliosis. The increasing prevalence of obesity worldwide also contributes to the difficulty of relying on palpable landmarks for safe placement of neuraxial anesthesia. Problems with positioning, increased depth of ligamentum flavum, and inadequacy of equipment (such as the needle being too short) in obese patients also complicate the traditional landmark approach [1, 2].

The use of ultrasound guidance provides many advantages for the performance of neuraxial anesthesia. It can be used for real time guidance of the needle to the target and for visualization of the intervertebral space and the interlaminar window. It can estimate the depth to the ligamentum flavum in obese patients or patients with prior spine surgery, and, in patients with scoliosis, it can identify and quantify the rotation and curvature of the spine. It increases the safety profile of neuraxial anesthesia due to the ability to visualize critical structures such as blood vessels. Furthermore, it decreases the likelihood of multiple attempts at needle placement and the accompanying discomfort to patients [1–3].

2 Anatomy

Spinal vertebrae are composed of a body and a vertebral arch. The vertebral arch has a pedicle on each side that supports a lamina. The laminae support the spinous process posteriorly which is used as the primarily palpable landmark in neuraxial blockades. The spaces between pedicles of adjacent vertebrae comprise the intervertebral foramen (intervertebral spaces). Each vertebra has transverse processes that run horizontally and superior and inferior articular processes that form the facet joints with the articular processes of the adjacent vertebrae.

The thoracic spine is made up of 12 vertebrae (T1–T12). The spinous processes of the upper and middle thoracic vertebrae are angled very steeply. This renders certain ultrasound views quite challenging to obtain. However, the vertebrae of the lower thoracic vertebrae (T9–T12) are more similar to those of the lumbar vertebrae [14].

The lumbar spine is composed of five vertebrae (L1–L5) which are the largest segments of the spinal column and characteristically do not have transverse foramen in contrast to the cervical and thoracic levels. The spinous processes of the lumbar vertebrae are oriented such that the processes do not overlap the adjacent vertebrae. This orientation creates an interlaminar space between adjacent vertebrae where the contents of the spinal column can be easily accessed for neuraxial anesthesia. Posteriorly, three ligaments provide stability to the spinal column and cover the interlaminar space: the supraspinous ligament, the interspinous ligament, and the ligamentum flavum (superficial to deep) [4].

The caudal epidural space is entered via the sacral hiatus, which is formed from the lack of complete midline fusion of the laminae of S5, and in some instances S4, vertebrae. Basic anatomy of the sacral canal can be seen in Fig. 12. Generally, the dura extends down to the S2 level while the epidural

C. C. Uwandu (✉) · E. Bouley · M. R. Jones
Harvard Medical School, Beth Israel Deaconess Medical Center,
Department of Anesthesia, Critical Care, and Pain Medicine,
Boston, MA, USA
e-mail: cuwandu@bidmc.harvard.edu

T. Montet
Lousiana State University Health Science Center,
Department of Anesthesiology, New Orleans, LA, USA

A. D. Kaye
Departments of Anesthesiology and Pharmacology, Toxicology,
and Neurosciences, Lousiana State University Health Sciences
Center, Shreveport, LA, USA

Department of Anesthesiology, Department of Pharmacology
Louisiana State University School of Medicine, Louisiana State
University Health Sciences Center, New Orleans, LA, USA
e-mail: akaye@lsuhsc.edu

© Springer Nature Switzerland AG 2021

J. Li et al. (eds.), *Ultrasound Fundamentals*, https://doi.org/10.1007/978-3-030-46839-2_27

space extends down to the sacral hiatus, which is around S4 or S5 in the midline of the posterior sacrum. The sacral cornua mark the lateral borders of the sacral hiatus and can be palpated just lateral to midline of the distal sacrum [9].

3 Sonoanatomy of the Thoracic Spine

Due to the depth of neuraxial structures, a low frequency and curvilinear probe is typically used for imaging, although a linear high frequency probe can be used in lower BMI individuals. Although the bony components of the vertebral column can often deflect the ultrasound waves and obscure optimal image acquisition, recent improvements in ultrasound machine technology have improved the practicality of ultrasound use for neuraxial anesthesia.

The ease with which the thoracic neuraxial space may be viewed with ultrasound depends on the portion being examined. The four lower thoracic vertebrae (T9–12) are anatomically and sonographically similar to the lumbar vertebrae with broad, minimally angulated spinous processes. In the mid and upper thoracic vertebrae (T5–8), the tight interspaces and sharp angulation of the spinous processes lead to increased difficulty with visualization of the desired structures.

Using ultrasound, the vertebral canal is seen through the window created by the intervertebral and interlaminar spaces. The ligamentum flavum, the posterior dura mater, and the epidural space together generate a hyperechoic structure seen through these widows during the ultrasound. This hyperechoic structure is frequently called the posterior complex (PC) and lies anterior to the transverse process. Another similar structure is seen anteriorly which forms from the anterior dura mater and the posterior longitudinal ligament. This structure is frequently called the anterior complex (AC). The anterior and posterior complexes border the hypoechoic spinal cord [12].

The parasagittal oblique (PSO) view and the transverse interlaminar view are the most clinically significant during neuraxial blockades as the ultrasonic window created by the interlaminar and intervertebral spaces allows adequate visualization of the spinal column [12].

4 Position and Technique for Performing Parasagittal Oblique Scan in the Mid Thoracic Region

The patient is placed in either the lateral decubitus or, more commonly, the sitting position. The ultrasound machine is also placed on the opposite side of the bed from where the operator stands. The probe is moved cephalad to identify PSO views of the thoracic interlaminar spaces. The mid thoracic laminae appear as hyperechoic linear structures on ultrasound. They are separated by gaps which represent the interlaminar spaces. These spaces should be centered on the ultrasound screen and marked on the patient's skin as well. Thus, when attempting to obtain a transverse view, these marks help to confirm the location of the interlaminar spaces. The intervertebral levels can also be determined by identifying the sacrum and then counting from the L5-S1 junction upwards. The depth to the lamina should also be measured as an estimate of distance from the skin to the epidural space (Fig. 1).

5 Position and Technique for Performing Transverse Midline Scan in the Mid Thoracic Region

The transverse midline (TM) view of anterior and posterior complexes is limited in the mid thoracic region by the considerable overlap of the spinous processes. The structures that can be seen include transverse processes, spinous processes, lamina and ribs. Thus, the main use of the TM view is to identify the location of midline. (Fig. 2).

6 Indications for Thoracic Nerve Block

A thoracic epidural is typically placed for upper abdominal and thoracic operations. It is a crucial aspect of the perioperative pain management of patients undergoing what can typically be very painful surgeries. Thoracic epidurals can blunt the stress response to surgery, allow for early mobilization after surgery, and decrease the risk of postoperative complications such as atelectasis and pneumonia due to improved pain control. They have also been shown to decrease the rates of postoperative ileus by limiting the amount of opioid analgesics the patient requires. Although thoracic epidurals do not necessarily improve perioperative mortality, they do allow for surgeries to be successfully performed on high risk patients. Additionally, thoracic epidurals may reduce mortality in patients who have suffered multiple rib fractures [15].

7 Sonoanatomy of the Lumbar Spine

The anterior and posterior complexes depicted in the 'Sonoanatomy of the Thoracic Spine' section are important ultrasound landmarks during lumbar blockades. Similarly,

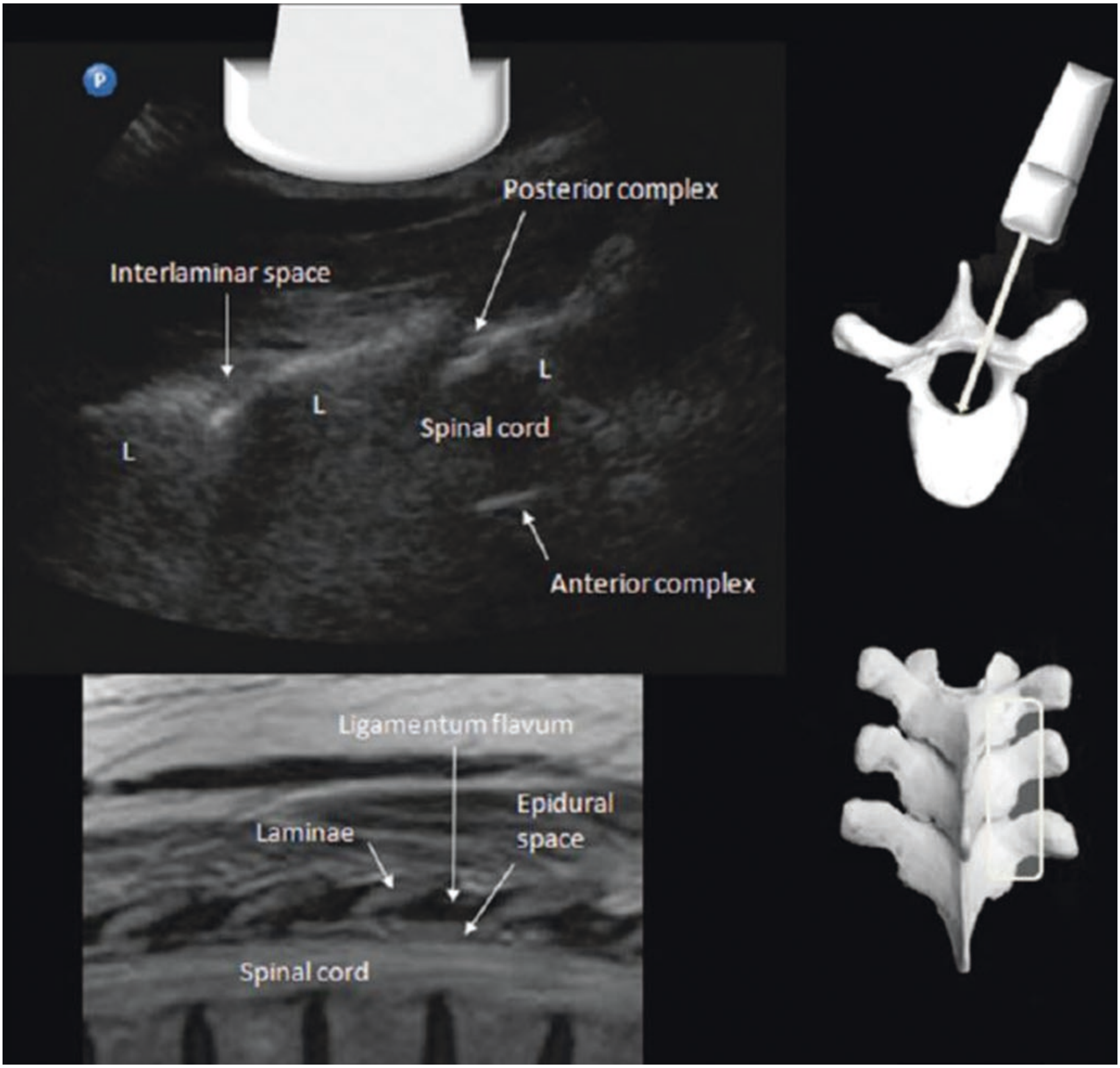

Fig. 1 Parasagittal oblique view of the mid-thoracic spine and corresponding magnetic resonance image. Despite the narrow interlaminar space, it is possible to visualize the posterior and anterior complex at one or more levels. At a minimum, the location of the interlaminar space can be determined by the dip or gap between successive laminae (L). Note that the spinal cord is hypoechoic and cannot be distinguished from the surrounding cerebrospinal fluid. (Reproduced from Jankovic and Chin [18])

the parasagittal oblique view and the transverse interlaminar view are the most clinically significant during lumbar blockades because the ultrasonic window created by the interlaminar and intervertebral spaces is used to visualize both the anterior and posterior complexes [12]. The posterior complex and corresponding epidural space are the ultimate target for epidural catheter placement.

There are five basic views when using ultrasound to visualize the lumbar spine:

(i) Parasagittal transverse process view
(ii) Parasagittal articular view
(iii) Parasagittal oblique view
(iv) Transverse spinous process view
(v) Transverse interlaminar view

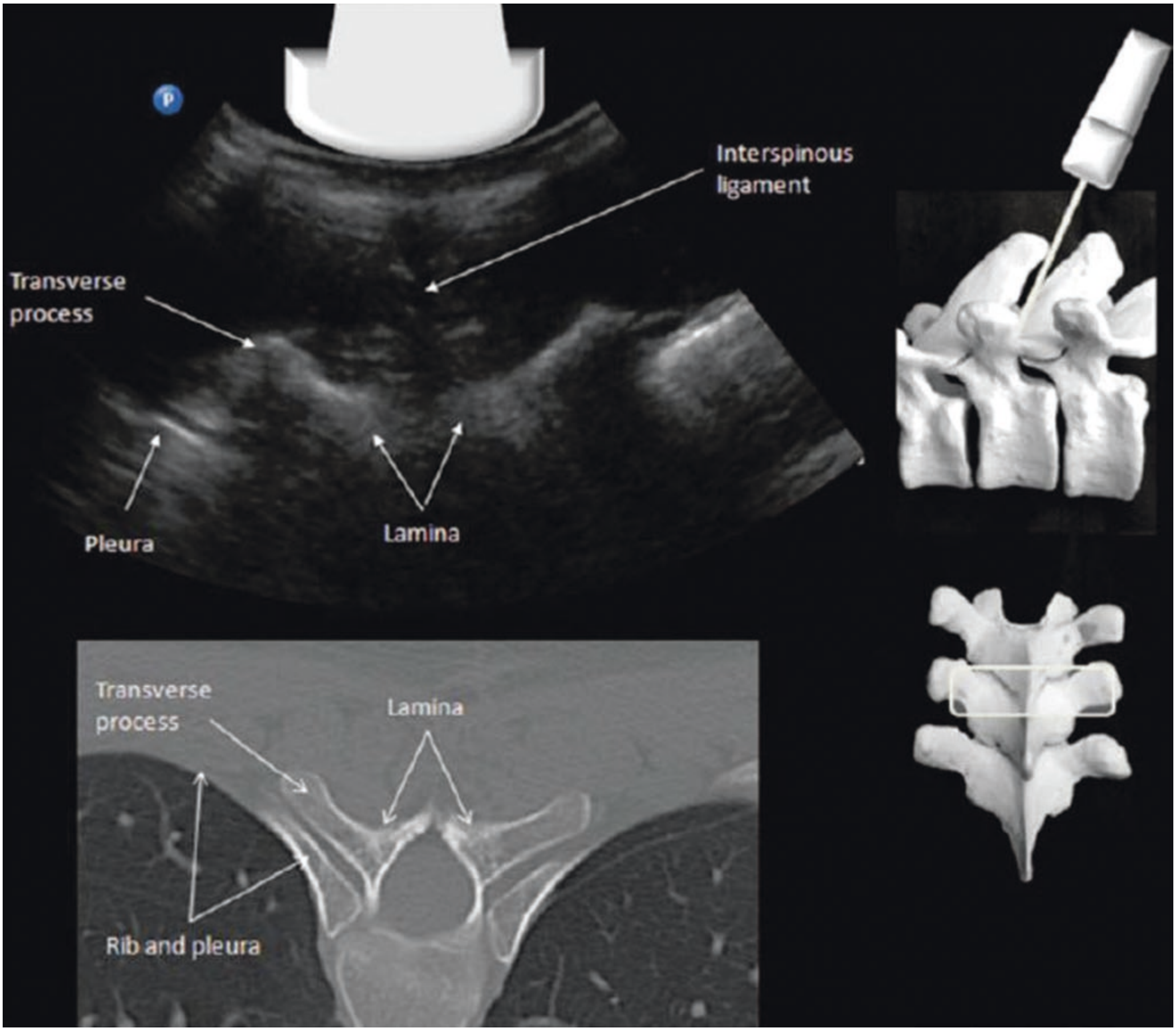

Fig. 2 Transverse view of the mid-thoracic spine and corresponding computed tomography image. An interlaminar view into the vertebral canal cannot be obtained because of the steeply sloping spinous processes and overlapping laminae. (Reproduced from Jankovic and Chin [18])

8 Position and Technique for Performing a Parasagittal Transverse Process (PST) Scan in the Lumbar Region

For this first view, the ultrasound probe is placed in sagittal orientation a few centimeters lateral to the midline of the lumbar spine. The transverse processes of the lumbar vertebrae appear as finger-like acoustic shadows known as the 'trident sign' [4]. It is important to note the depth of the transverse processes in relation to other structures to ensure correct identification. Superior to the finger-like shadows are the erector spinae muscles and inferior is the psoas major muscle (Fig. 3).

9 Position and Technique for Performing a Parasagittal Articular (PSA) Scan in the Lumbar Region

From the PST view, the probe is moved medially towards the spinous processes while maintaining a sagittal orientation. Hump-like acoustic shadows also known as the 'camel sign' are seen which are formed by the facet joints [4]. The facet joints are more superficial than the previously described transverse processes of the lumbar vertebrae (Fig. 4).

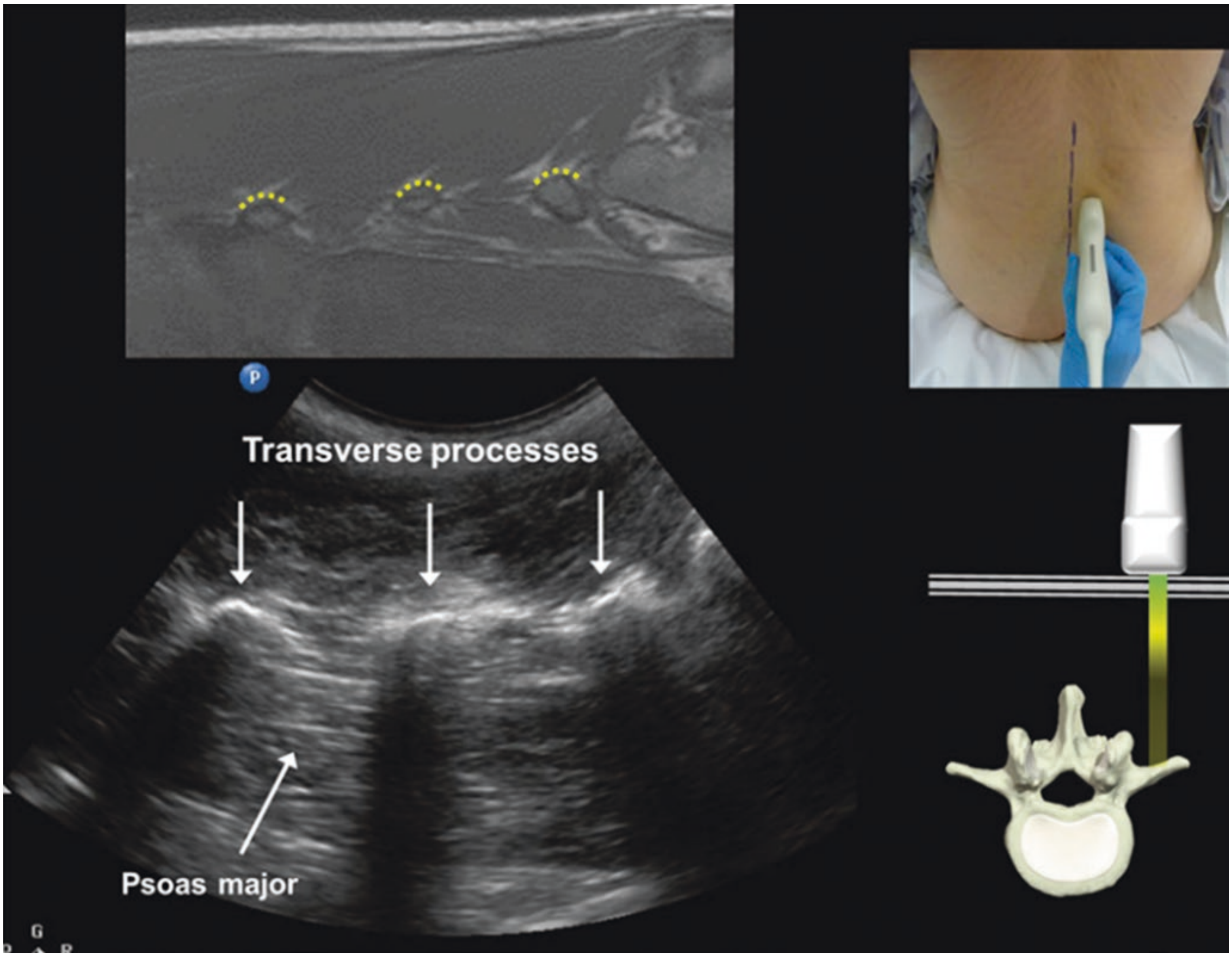

Fig. 3 Parasagittal transverse process (PST) view of the lumbar spine with corresponding computed tomography image and ultrasound probe orientation. The finger-like acoustic shadows of the transverse processes are shown. This is also known as the 'trident sign'. (Reproduced from Jankovic and Chin [18])

10 Position and Technique for Performing a Parasagittal Oblique (PSO) Scan in the Lumbar Region

The PSO view is attained by medially angulating the probe from the PSA view. The hump-like pattern transition to a 'sawtooth' pattern of acoustic shadows which are formed from the dense laminae and the interlaminar spaces [4]. In this view, the interlaminar space is utilized to visualize the contents of the vertebral column, including the posterior and anterior complexes which form two hyperechoic, parallel lines. While maintaining this orientation, the probe is slid caudally on the spine until the sacrum is identified by a long horizontal hyperechoic line. The junction of the 'sawtooth' pattern and the horizontal sacral line represents the L5-S1 vertebral interspace. While centering this junction on the ultrasound image, a mark is made on the patient at the midline of the probe's long side to identify the location of this interspace. The remaining interspaces of the lumbar region should also be identified this way by moving cephalad one vertebra and repeating the marking process. The interspace levels can also be identified in a descending order when the T12-L1 level is identified because of the characteristic articulation of the last rib with the T12 vertebra (Fig. 5).

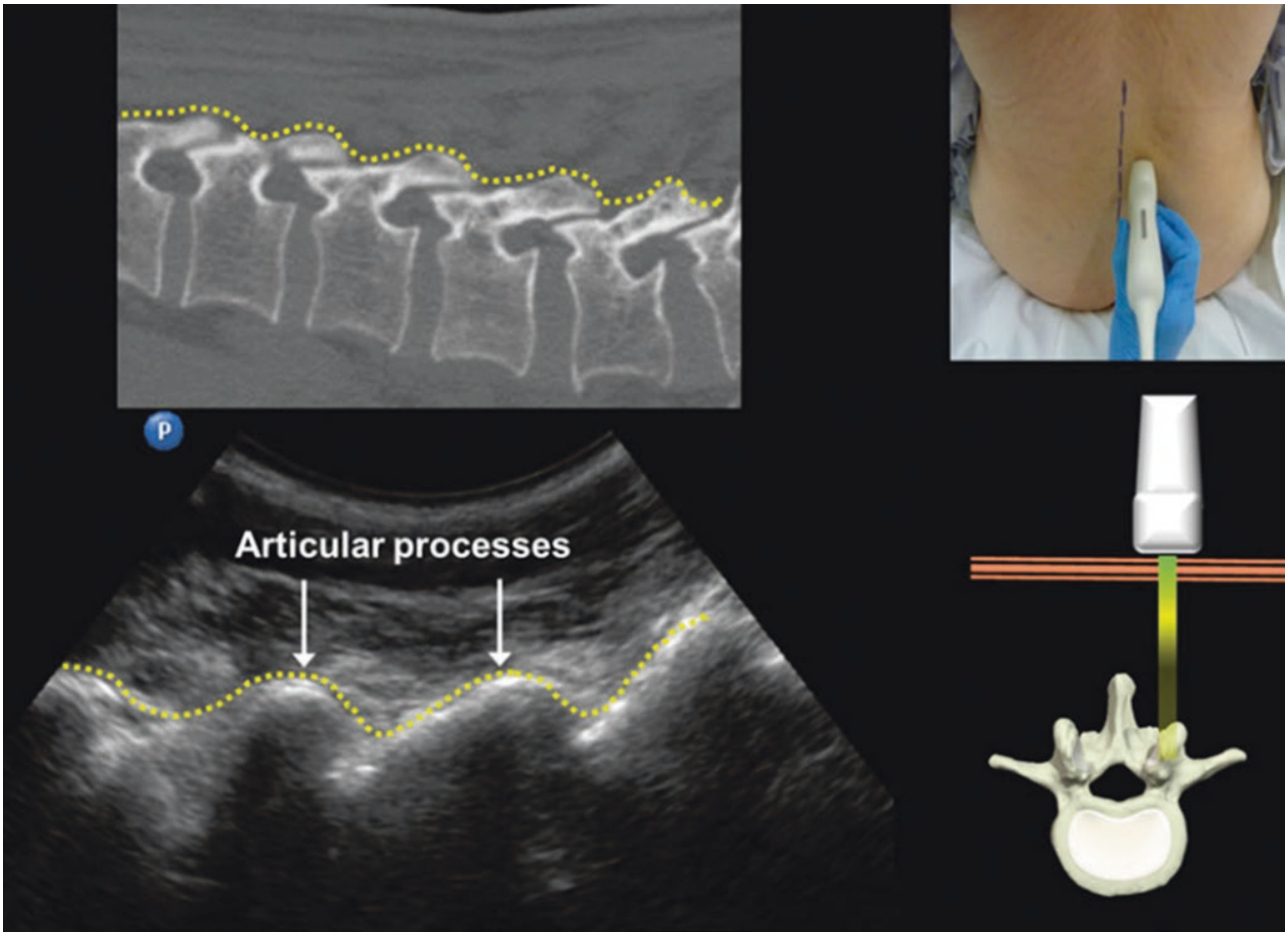

Fig. 4 Parasagittal auricular process (PSA) view of the lumbar spine with corresponding computed tomography image and ultrasound probe orientation. (Reproduced from Jankovic and Chin [18])

11 Position and Technique for Performing a Transverse Spinous Process Scan in the Lumbar Region

For this view, the probe is turned horizontally and placed on the midline directly transecting a palpable spinous process of the vertebrae. The spinous process can be identified by the acoustic shadow shaped like a spire which widens as the shadow projects from superficial to deep. The erector spinae muscles are superficial and lateral to the spinous process, and the lamina of the vertebral bodies are deep to the erector spinae muscles where the spinous process shadow begins to widen [4]. Although this view has little importance in identifying neuraxial structures, the orientation of the spinous process can be helpful in cases of scoliosis (Fig. 6).

12 Position and Technique for Performing a Transverse Interlaminar Scan in the Lumbar Region

By moving the probe slightly caudal or cephalad from the TSP view with a cephalad tilt to account for the curvature of the spinous process, the acoustic window of the interlaminar space is used to visualize the anterior and posterior complexes once again. The anterior and posterior complexes orient as a hyperechoic 'equals sign' that surround the spinal cord. The erector spinae muscles are superficial and lateral to the hypoechoic interspinous ligament. Once this view is obtained and centered, two marks are made on the patient corresponding to the midpoint of the probe's long and short

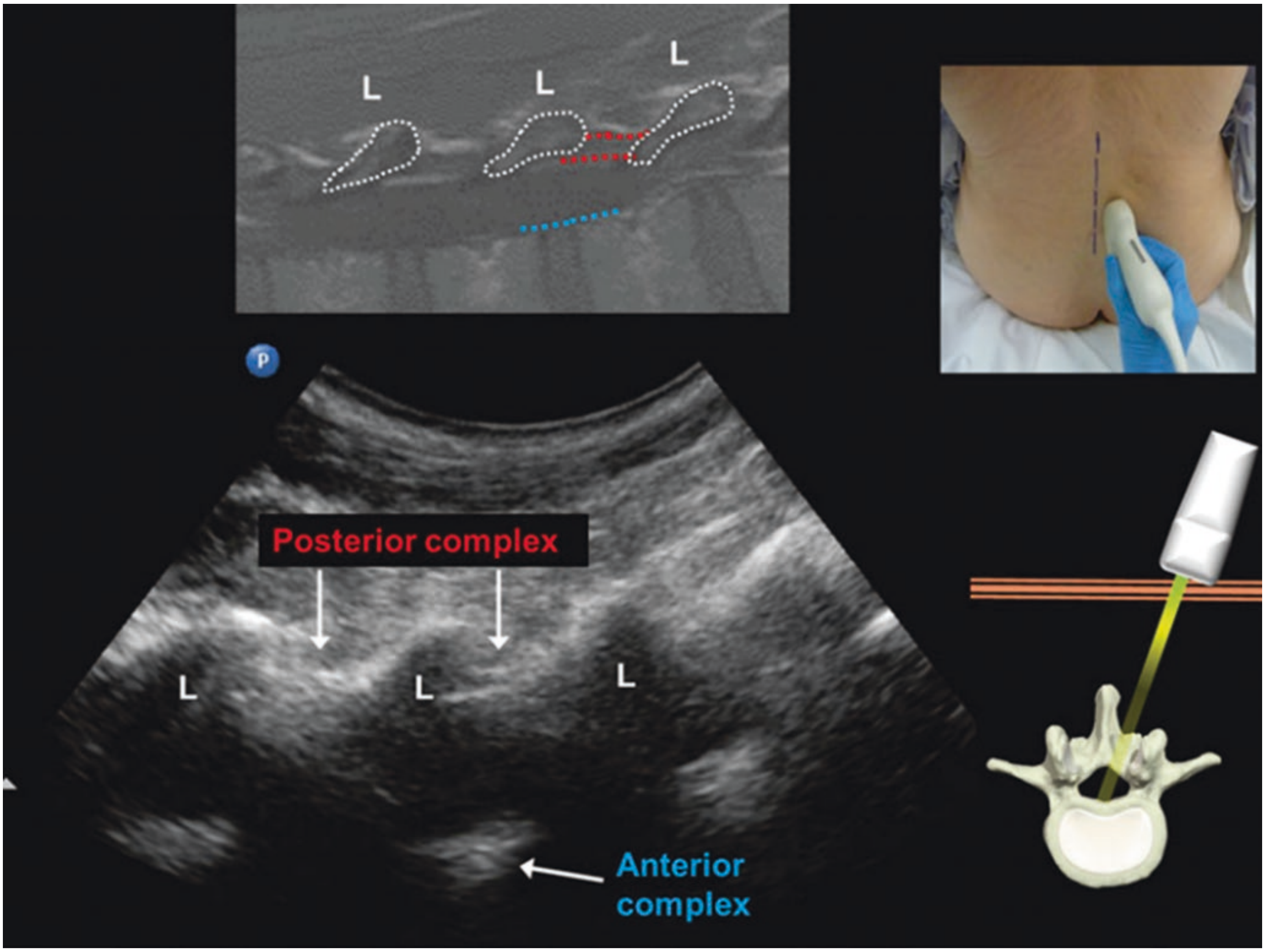

Fig. 5 Parasagittal oblique (PSO) view of the lumbar spine with corresponding computed tomography image and ultrasound probe orientation. This depicts the 'sawtooth' appearance of the laminae (L) and the alignment of the AC and PC. (Reproduced from Jankovic and Chin [18])

sides. The intersection of these marks designates the insertion site for the blockade. (Fig. 7) The angle of insertion is determined by the degree of cephalad tilt in the ultrasound probe needed to visualize this area (Fig. 8) [4].

13 Indications for Lumbar Nerve Blocks

A lumbar epidural is commonly placed for lower abdominal, pelvic, and lower extremity blocks. It is currently the gold standard for anesthesia during labor and delivery. It manages intrapartum pain and decreases the mother's sympathetic response to stress which may induce a decrease in blood flow to the placenta. The lumbar epidural catheter can also be used for epidural surgical anesthesia in the event of an emergent cesarean section or other obstetric complication. This allows both the mother and fetus to avoid the risks associated with general anesthesia [5]. Additionally, lumbar epidural injections with local anesthetic alone or in conjunction with steroids are shown to provide short- and long-term relief of low back pain and lower extremity pain in patients with central spinal stenosis and lumbar disc herniation [16, 17].

14 Ultrasound Guided Spinal

Spinal anesthesia involves a single injection of medication into cerebrospinal fluid located in the subarachnoid space. It has the advantages of quick onset, limited duration, and

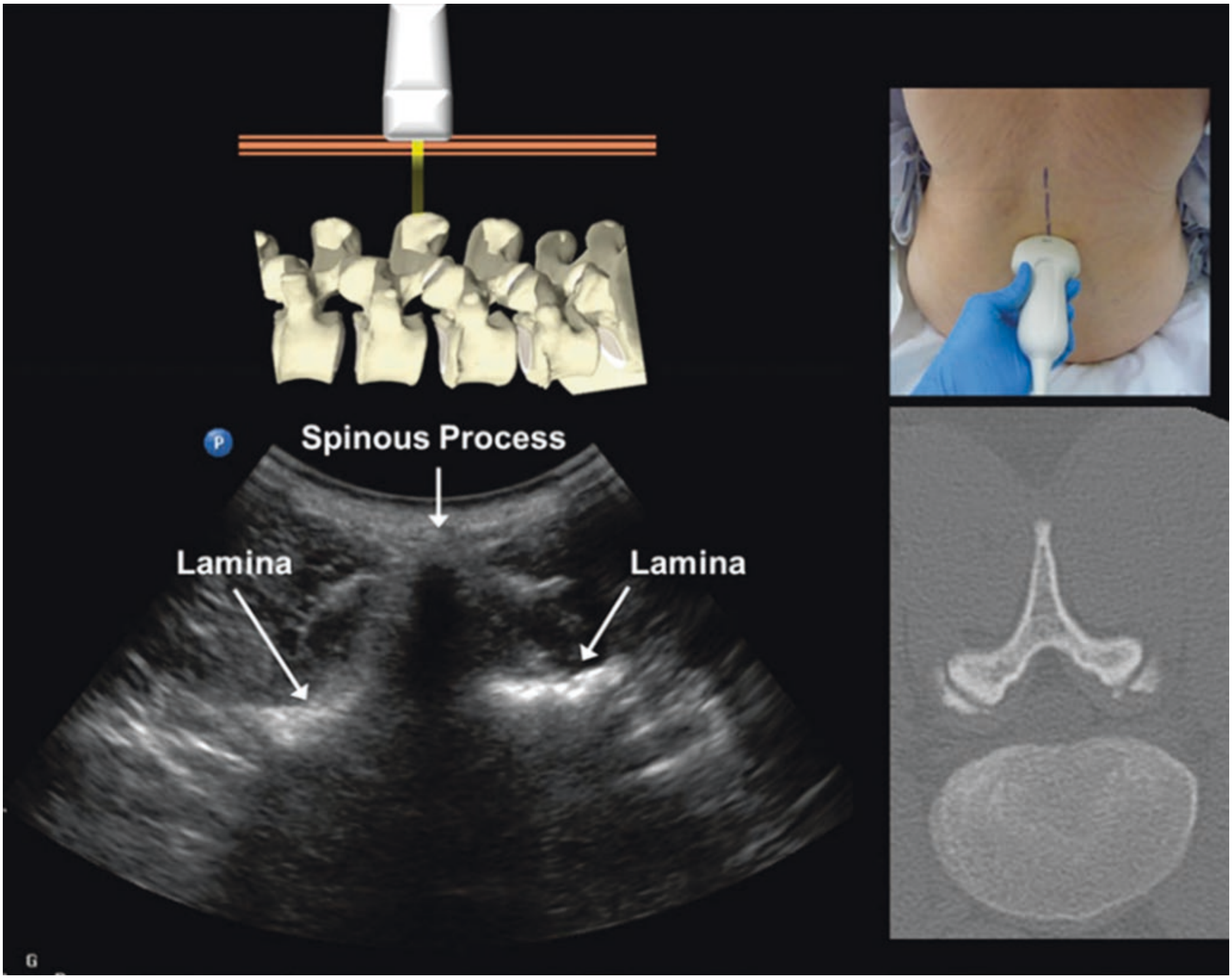

Fig. 6 Transverse spinous process (TSP) view of the lumbar spine with corresponding computed tomography image and ultrasound probe orientation. (Reproduced from Jankovic and Chin [18])

can avoid the need for general anesthesia in patients with multiple comorbidities. In comparison with general anesthesia, spinal anesthesia has been shown to lead to better outcomes, including reduction in cardiopulmonary adverse events, as well as less development of chronic pain and lower morbidity and mortality [11]. Spinal anesthesia can be used alone or combined with epidural anesthesia to treat the pain of labor in the obstetric population. It can also be used as a primary anesthetic or an adjunct for surgical procedures below the umbilicus. In the cancer pain population, neurolytic procedures involving the injection of alcohols are performed in those with advanced malignant disease to treat chronic cancer pain [10, 12]. Utilization of ultrasound for spinal anesthesia can be beneficial in populations where spine anatomy may be abnormal or post-surgical changes are present. Furthermore, in obese patients, ultrasound allows the provider to identify landmarks that are not otherwise palpable [3].

15 Basic Anatomy and Sonoanatomy

As seen below in Fig. 9, the arachnoid mater lies just deep to the dura mater. Deep to the arachnoid mater is the subarachnoid space within which cerebrospinal fluid is contained. In adults, the spinal cord ends in the conus medullaris around the level of the L2 vertebrae [12].

The sonographic anatomy for an ultrasound guided spinal procedure is the same as would be seen for a lumbar procedure, except that medication is deposited in the subarachnoid space rather than the epidural space. Please refer to lumbar ultrasound images in the previous section.

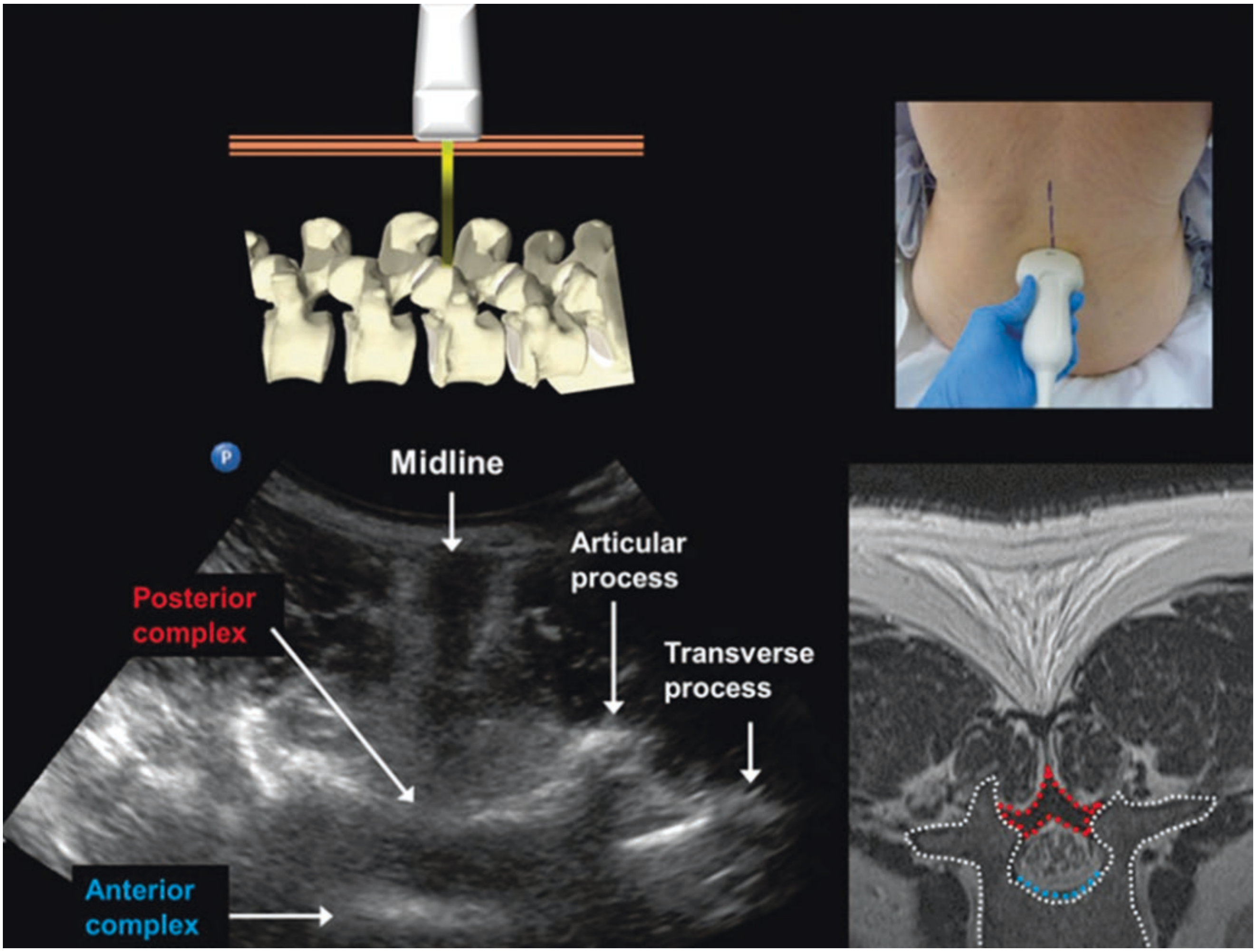

Fig. 7 Transverse interlaminar (TI) view of the lumbar spine with corresponding computed tomography image and ultrasound probe orientation. Note that a slight cephalad tilt may be needed to obtain this view. (Reproduced from Jankovic and Chin [18])

16 Positioning and Technique

This procedure can be done with the patient sitting, lateral decubitus, or in prone jackknife position in the case of the use of a hypobaric local anesthetic [12]. Typically the L2/L3 or L3/L4 interspace is the desired landmark and landmarks should be palpated where possible. Midline, paramedian, or Taylor's approach—a paramedian injection in the L5/S1 interspace—may be used [3]. The procedure itself is similar to a lumbar epidural, however an introducer needle is often used to engage in ligamentum flavum followed by a 25–27 gauge spinal needle with a pencil point tip, which is used to puncture the dura and enter the subarachnoid space while minimizing risk of post dural puncture headache. In the event a cutting needle is used, the bevel should be rotated vertically to align with dural fibers and minimize risk of tear. Elderly patients and those with stiffer tissues may warrant a 22 gauge cutting needle if accessing the subarachnoid space proves difficult [3].

17 Caudal Nerve Block

Caudal epidural injections can be performed as a single shot block or involve the threading of a catheter for continued analgesia. A caudal block will provide anesthesia to the lumbosacral region below the umbilicus and can be used in urogenital surgery or lower limb surgery [13]. A caudal epidural block can also be administered to provide pain control in the post-operative period, lessening the need for systemic opioids. Due to safety and efficacy of this procedure, it is a popular technique in the pediatric patient population. Though it can have similar applications in adult patients, the primary use of caudal epidural injection in this population is for those with chronic pain, particularly patients with radicular pain resulting from spinal stenosis or disc pathology and are especially useful in the context of post laminectomy syndrome, pain with sacral involvement, as well in patients whose pathology is bilateral or multilevel [6]. This procedure can

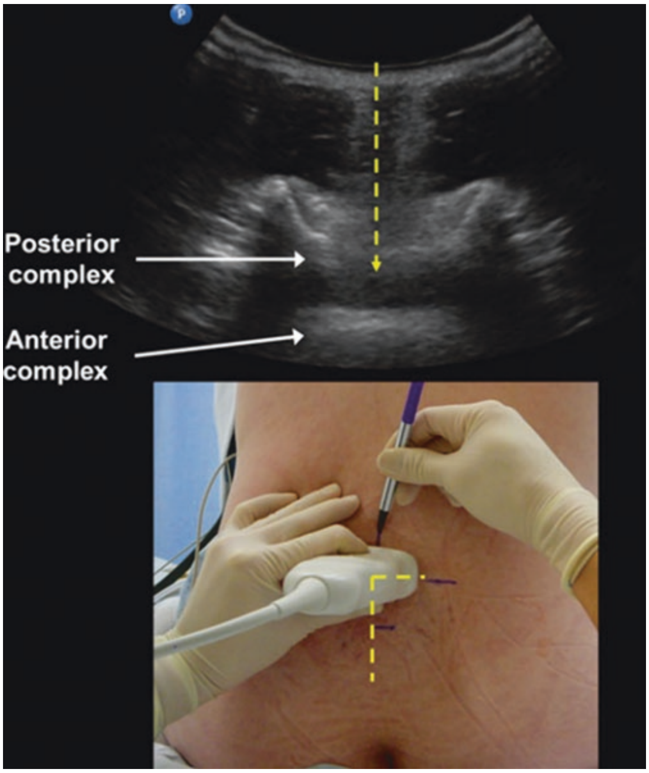

Fig. 8 In the transverse midline interlaminar view, the midline is centered on the ultrasound image, and marks are made at the midpoints of the probe's long and short sides. The intersection of these lines, shown by the yellow dashed line on the patient, denote an appropriate insertion site for a midline approach epidural at that level. (Reproduced from Jankovic and Chin [18])

also be beneficial in patients with peripheral neuropathy, phantom limb pain, CRPS, and cancer pain as well as pain of the pelvis, penis or testicles [7]. Some favor the caudal approach in patients with a history of spinal surgery because of ease of access to the epidural space. Compared to the lumbar epidural approach, the caudal technique also has a lower risk of inadvertent dural puncture [8]. Other patient characteristics that support this procedure include those who had decreased bone density, gas or feces in the rectum, or where fluoroscopy was contraindicated. Furthermore, modified positioning strategies can be used in obese patients who are unable to lie prone [6].

18 Sonoanatomy of the Caudal Epidural Space

The relevant sonoanatomy for a caudal epidural block is shown in Fig. 10.

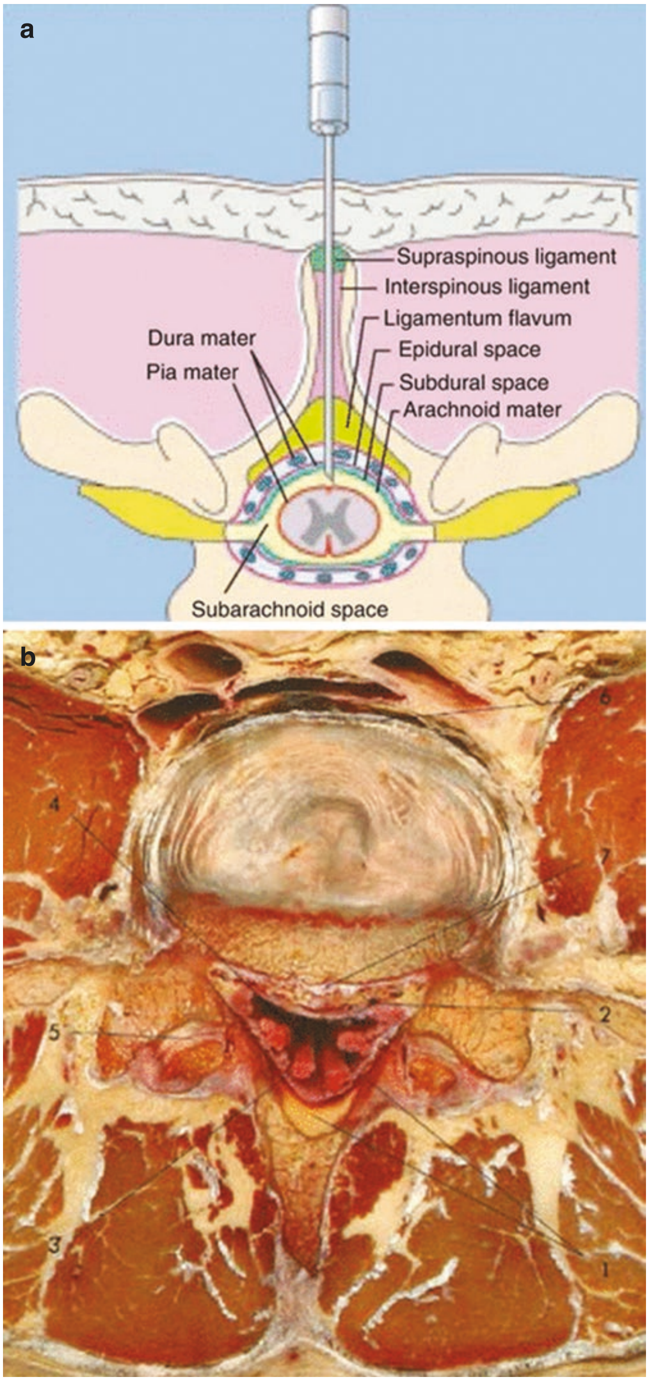

Fig. 9 (**a**) Subarachnoid position of the needle (**b**) Transverse dissection at the level of L4/L5. (1) Posterior epidural space with fat, (2) anterior epidural space with veins, (3) spinal dura mater, (4) subarachnoid space and cauda equina, (5) zygapophysial joint, (6) anterior longitudinal ligament, and (7) posterior longitudinal ligament. (Reproduced from Sehmbi and Chin [12])

As illustrated in Fig. 11, the proceduralist should scan caudally across the sacrum until two sacral cornua appear as inverted U's with the sacrococcygeal ligament between them seen as a hyperechoic line [8]. This has been referred to as the 'frog's eye sign' because the inverted U's appear similar to the bulging eyes of a frog. Rotation of the probe 90 degrees to a longitudinal and midline orientation will allow for optimal viewing of the sacral hiatus below the

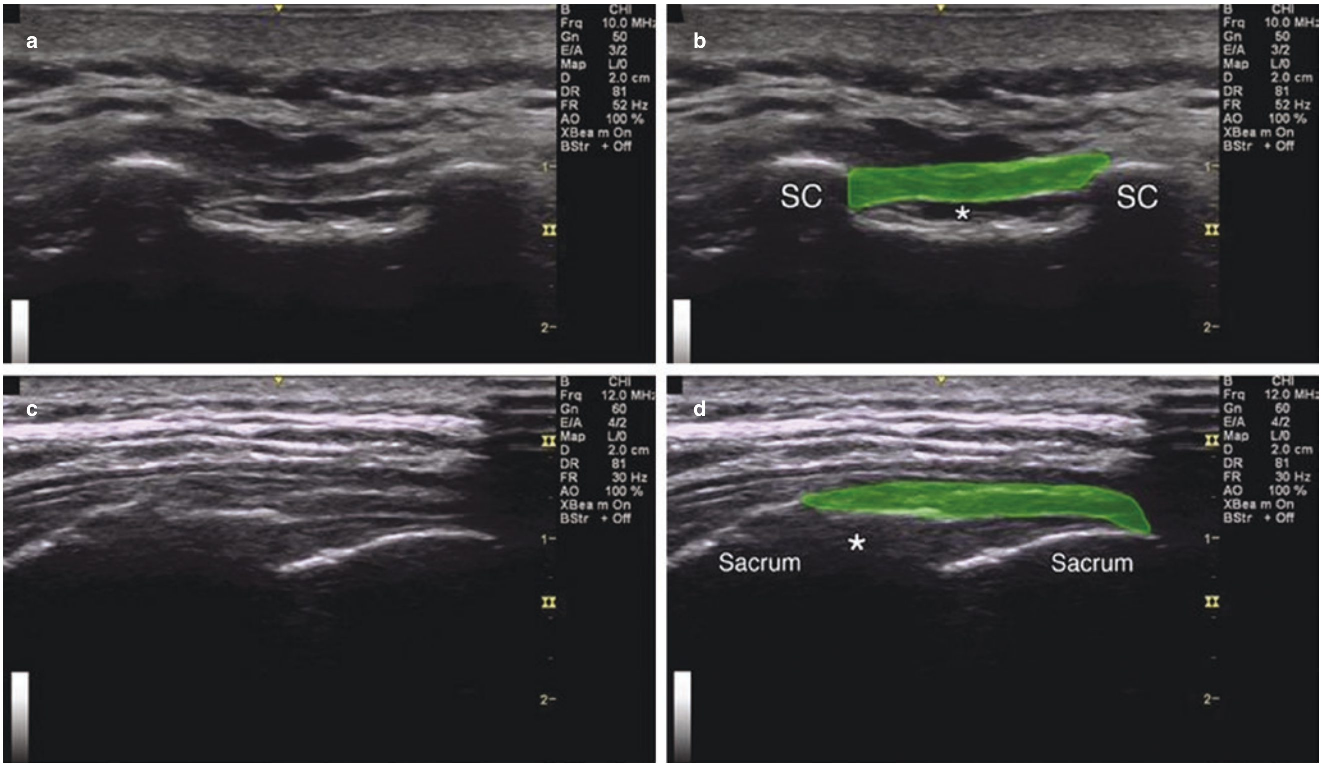

Fig. 10 (**a**) Axial view over sacral cornua. (**b**) Green indicates sacrococcygeal ligament, SC sacral cornua, asterisk indicates sacral hiatus. (**c**) Sagittal view of sacral hiatus. (**d**) Dorsal sacrum (left), green indicates sacrococcygeal ligament, asterisk indicates sacral hiatus. (Reproduced from Spinner [8])

sacrococcygeal ligament. The probe position can be marked with a surgical marker prior to prepping and draping the area to maintain orientation. Once the sacral hiatus is again identified, the skin and subcutaneous tissues are anesthetized along a trajectory towards the sacral hiatus in-plane from a caudal to cephalad direction, usually with the needle at about a 45 degree angle [7]. Ultrasound probe positioning on the patient for in-plane injection as well as sonographic image of in-plane injection can be seen in Fig. 12.

A 22 or 25 gauge spinal needle (or a Tuohy if a catheter is planned) is inserted along the same trajectory through the sacrococcygeal ligament, which is typically felt as a 'pop' as the needle traverses. Once through the sacrococcygeal ligament, aspiration should be performed to ensure no blood or cerebrospinal fluid is aspirated as the needle is advanced no more than 1 cm further [8]. It should be noted that one of the disadvantages to the use of ultrasound is that bony artifacts result in a poorly visualized needle tip upon entry into the sacral epidural space [6]. Upon completion of the procedure, the needle should be removed with a saline flush to clear the residual steroid.

19 Summary

In a busy clinical practice wherein landmark technique exhibits a high failure rate and use of fluoroscopy can be time consuming and impractical, ultrasound has increasing utility for neuraxial procedures. Ultrasound allows for improved visualization of anatomy in an era where landmarks cannot always be relied upon due to patient size or anatomical variations. Regional anesthesia procedures of the spine are increasing in popularity both as a primary anesthetic and an anesthetic adjuvant with concurrent increased use in the chronic pain population. With the increasing use of ultrasound, there is a breadth of imaging resources that can facilitate effective neuraxial anesthetic blocks.

Disclaimer There was no external funding in preparation of this manuscript.

Conflict of Interest Drs. Uwandu, Bouley, Jones, and Montet all have no conflicts of interest.

Dr. Kaye is a speaker for Depomed, Inc. and Merck, Inc.

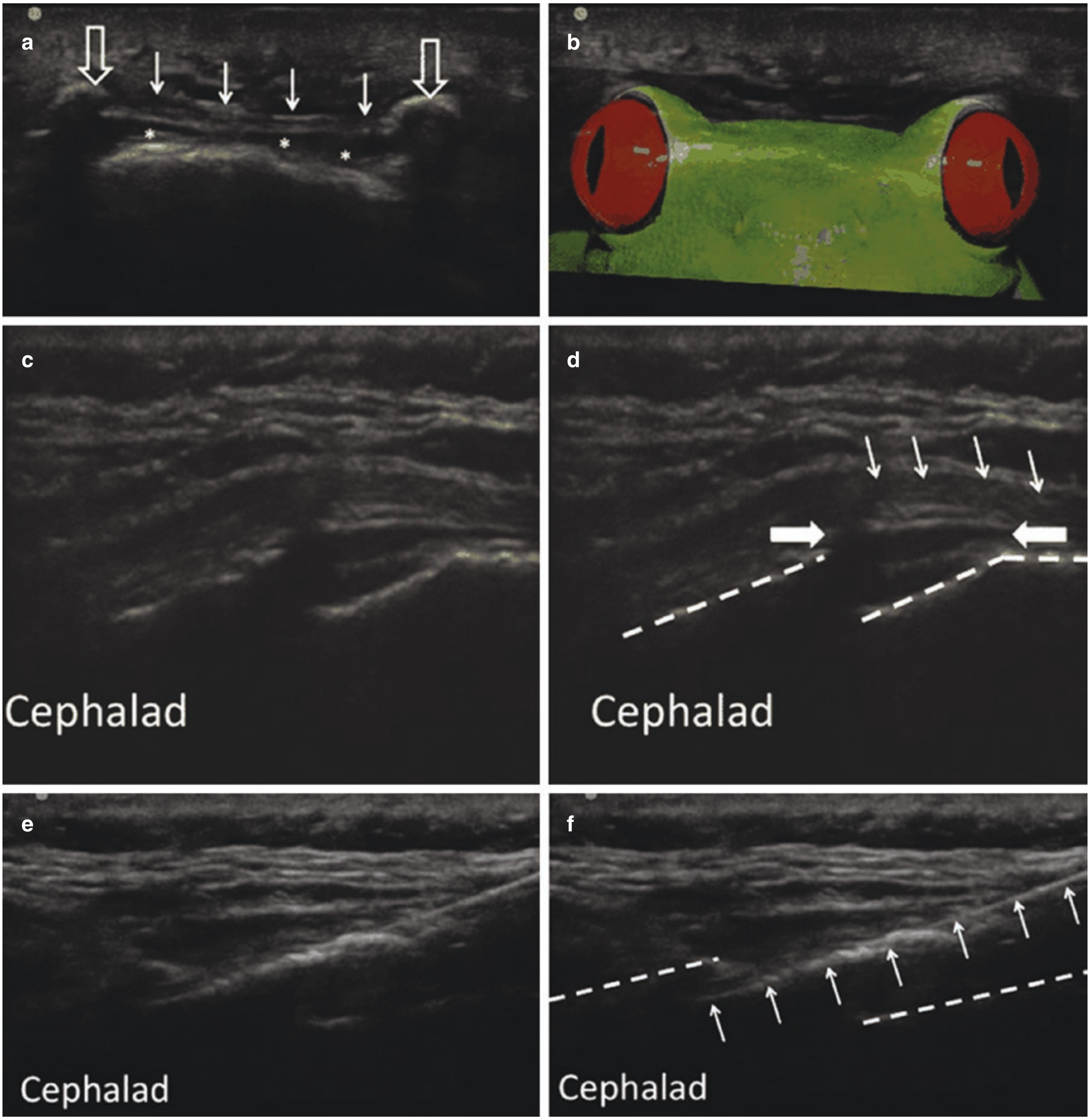

Fig. 11 Ultrasound images of the sacral canal (Reproduced with permission from Philip Peng Educational Series). (**a**) Short-axis scan of the sacrum at the level of the sacral hiatus, displaying the two sacral cornua (open arrows), and the hyperechoic sacrococcygeal ligament (line arrows) that extends between the two cornua and the sacral hiatus (asterisk) which is the hypoechoic space between the sacrococcygeal ligament and the posterior surface of the sacrum. (**b**) Figure same as **a** with frog eyes superimposed on the ultrasound image. (**c**) Long-axis view of the sacrum at the level of the sacral hiatus. (**d**) Same as **c** with the sacral hiatus outlined by bold arrows. The sacrococcygeal ligament (line arrows) is seen extending from the sacrum to the coccyx. More cephalad, the acoustic shadow of the dorsal sacrum bone completely obscures the ventral sacrum bone of the sacral canal (dashed lines). (**e**) Long-axis view of sacrum showing the needle insertion. (**f**) Same as **e** with line arrows to outline the needle which cannot be visualized deep in the sacral canal (dashed lines). The needle was inserted with in-plane technique. (Reproduced from Hanlon and Peng [6])

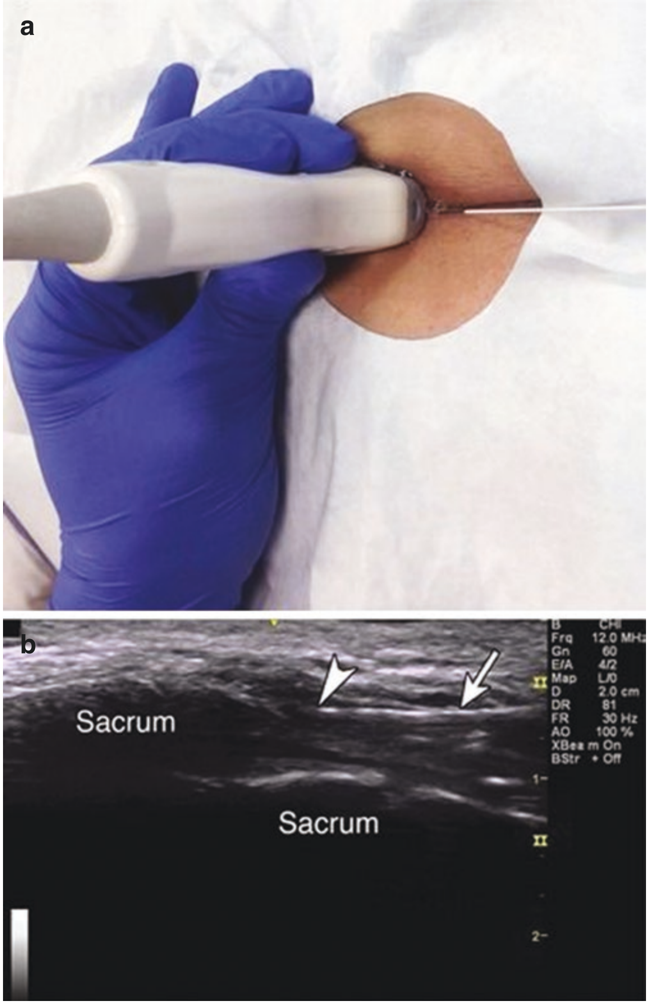

Fig. 12 (**a**) Example of sagittal probe position over sacrum with in-plane injection technique. (**b**) Arrowhead indicates needle tip traversing towards sacral hiatus, arrow indicates needle. (Reproduced from Spinner [8])

References

1. Chin KJ, Perlas A, Chan V, Brown-Shreves D, Koshkin A, Vaishnav V. Ultrasound imaging facilitates spinal anesthesia in adults with difficult surface anatomic landmarks. Surv Anesthesiol. 2012;56:143–4.
2. Vallejo M, Phelps A, Singh S, Orebaugh S, Sah N. Ultrasound decreases the failed labor epidural rate in resident trainees. Int J Obstet Anesth. 2010;19:373–8.
3. Perlas A, Chaparro LE, Chin KJ. Lumbar neuraxial ultrasound for spinal and epidural anesthesia: a systematic review and meta-analysis. Reg Anesth Pain Med. 2016;41(2):251–60.
4. Ghosh S, Madjdpour C, Chin K. Ultrasound-guided lumbar central neuraxial block. BJA Education. 2016;16:213–20.
5. Meng M-L, Smiley R. Modern neuraxial anesthesia for labor and delivery. F1000Research, 6. 2017:1211.
6. Hanlon JG, Peng PWH. Caudal epidural injections in adult patients. In: Jankovic D, Peng P, editors. Regional nerve blocks in anesthesia and pain therapy: traditional and ultrasound-guided techniques. Cham: Springer International Publishing; 2015. p. 585–96.
7. Abraham NR, et al. Epidural (cervical, thoracic, lumbar, caudal) block/injections. In: Deer TR, et al., editors. Treatment of chronic pain by interventional approaches: the american academy of pain medicine textbook on patient management; 2015. p. 149–57.
8. Spinner DA. Spine. In: Spinner D, Kirschner J, Herrera J, editors. Atlas of ultrasound guided musculoskeletal injections. Musculoskeletal medicine. New York: Springer; 2014. p. 123–37.
9. Hurdle M-F. Ultrasound guided spinal procedures for pain. PM&R Clinics of North America. 2016;27(3):673–86.
10. Narouze S, Peng PW. Ultrasound-guided interventional procedures in pain medicine: a review of anatomy, sonoanatomy and procedures. Reg Anesth Pain Med. 2010;35(4):386–96.
11. Kettner SC, Willschke H, Marhofer P. Does regional anaesthesia really improve outcome? Br J Anaesth. 2011;107(Suppl 1):i90–5.
12. Sehmbi H, Chin KJ. Neuraxial blocks: spinal and epidural anesthesia. In: Jankovic D, Peng P, editors. Regional nerve blocks in anesthesia and pain therapy: traditional and ultrasound-guided techniques. Cham: Springer International Publishing; 2015. p. 499–559.
13. Ting HYZ, Cheung SSK, Tsui BCH. Pediatric nerve blockade: trunk and neuraxial. In: Regional nerve blocks in anesthesia and pain therapy. Cham: Springer; 2015.
14. Reina, M.A., De Andres, J.A. (2015) Atlas of functional anatomy for regional anesthesia and pain medicine.
15. Manion SC, Brennan TJ. Thoracic epidural analgesia and acute pain management. Surv Anesthesiol. 2012;56(3):144–6.
16. Manchikanti L, Kaye AD, Manchikanti K, Boswell M, Pampati V, Hirsch J. Efficacy of Epidural Injections in the Treatment of Lumbar Central Spinal Stenosis; A Systematic Review. Anesthesiology and Pain Medicine; 2015.
17. Manchikanti L, Benyamin RM, Falco FJE, Kaye AD, Hirsch JA. Do epidural injections provide short- and long-term relief for lumbar disc herniation? A systematic review. Clin Orthop Relat Res. 2014;473:1940–56.
18. Jankovic D, Chin KJ. Neuraxial anatomy and sonoanatomy. In: Jankovic D, Peng P, editors. Regional nerve blocks in anesthesia and pain therapy: traditional and ultrasound-guided techniques. Cham: Springer International Publishing; 2015. p. 468–98.

Use of Ultrasound in Urology

Hemangini Thakkar, Patil Bhushan, Jamil S. Syed,
and Sujata Patwardhan

1 Introduction

Ultrasonography is a relatively inexpensive and fundamentally important urological assessment modality that can be used from antenatal care to adulthood. It is referred to as urologist's stethoscope as it provides valuable information that traditional physical examination cannot offer. Advantages of ultrasound include but are not limited to an avoidance of ionizing radiation, portability allowing use at the bed side, intensive care units, operative rooms and real-time functional evaluation of various organs.

2 Brief History of Ultrasound in Urology

In 1952 Wild and Reid attempted sonography of the prostate transrectally (TRUS); however, they did not succeed [1]. In 1963 Japanese urologists Takahashi and Ouchi also attempted prostate ultrasound, but image quality was not interpretable [2]. In 1971 Goldberg and Pollack performed sonography of kidneys in 150 patients and they could differentiate solid, cystic and complex renal masses with 96% accuracy [3]. From here on, ultrasound has grown leaps and bounds to its present state with various novel uses.

3 Basic Modes of Ultrasonography

3.1 Grey Scale B Mode Ultrasound

Grey scale is the primary mode of ultrasound used for the entire urinary tract. In spite of the development of multiple new ways and new modes of ultrasound, this remains the most important way to evaluate any organ in the body. Whether an ultrasound machine is considered being high end predominantly depends on its grey scale resolution. This uses pulse wave technology where ultrasound waves of broadband frequency are transmitted in pulses by a frequency transducer to the body and receives returning echoes from the body's tissues. These returning echoes produce real-time two-dimensional images in shades of grey. Each pixel's brightness is determined by the amplitude of the returning sound wave. Each frame is made up of multiple lines and each line is made up of multiple pixels. The set of data changes with time and it produces real-time image.

3.2 Doppler Sonography

Doppler sonography depends on the physical principle of frequency shift when an ultrasound beam strikes a moving object. When a sound wave of certain frequency strikes a moving object like blood, there is a change in frequency depending on the velocity of the moving object, the angle of isonation and the direction of the moving object. In colour Doppler, this change in frequency is measured and then colour coded and displayed on the screen. The colour code most commonly applied is blue indicating movement away from the transducer and red indicating movement towards the transducer. The greater the velocity of motion, the brighter the colour.

In power Doppler, the amplitude of frequency change is assigned to colour shade. It is less affected by backscatter wave and more sensitive for detecting blood flow. Hence the slowest velocity of a moving object can be detected by power

---

H. Thakkar (✉) · P. Bhushan · S. Patwardhan
Department of Urology, KEM Hospital, Mumbai, India

J. S. Syed
Department of Urology, Yale University School of Medicine,
New Haven, CT, USA

© Springer Nature Switzerland AG 2021
J. Li et al. (eds.), *Ultrasound Fundamentals*, https://doi.org/10.1007/978-3-030-46839-2_28

Doppler. It is less angle dependent than colour Doppler. However, it does not measure the velocity neither indicates the direction. This is mainly used in diagnosing conditions which requires the presence of minimal flow like in renal artery thrombosis, testicular torsion renal vein thrombosis (Fig. 1).

Spectral Doppler includes two types: continuous wave and pulsed wave. These analyse a spectrum of frequency; therefore, it is able to record blood flow velocities over time and displays the blood flow measurements graphically in a continuous waveform (Fig. 2). There have been major advances in Doppler sonography since it was discovered in early 1980. There are various parameters for measurement of flow, mainly peak systolic velocity (PSV), end diastolic velocity (EDV), resistive index (RI) and pulse index (PI). These parameters help practitioners identify and quantify vascular stenosis and vascularity of masses. It is also used in diagnosing arterial insufficiency in erectile dysfunction.

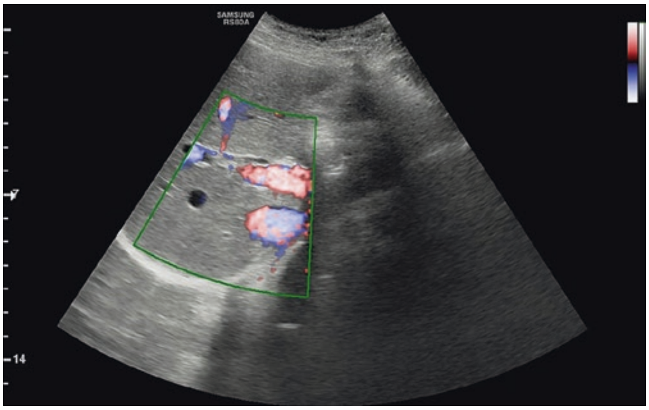

Fig. 1 Power Doppler of portal vein

3.3 Harmonic Scanning

When sound waves reach tissue, there are nonlinear propagations which generate fewer harmonics which are of higher amplitude. Because these harmonics are not subject to scattering at the frequency associated with the incident wave, there is less noise, artefact and better resolution (Fig. 3).

3.4 Spatial Compounding

Spatial compounding is a scanning mode where the direction of isonation is electronically altered and a composite image is generated. This reduces noise and artefact and improves the quality of image (Fig. 4).

There are various other modes of ultrasound which have specific applications. They are three-dimensional (3D) ultrasound, contrast-enhanced ultrasound (CEUS), sonoelastography, endoluminal sonography, high intensity focused ultrasonography (HIFU). Some of these are described later in this chapter.

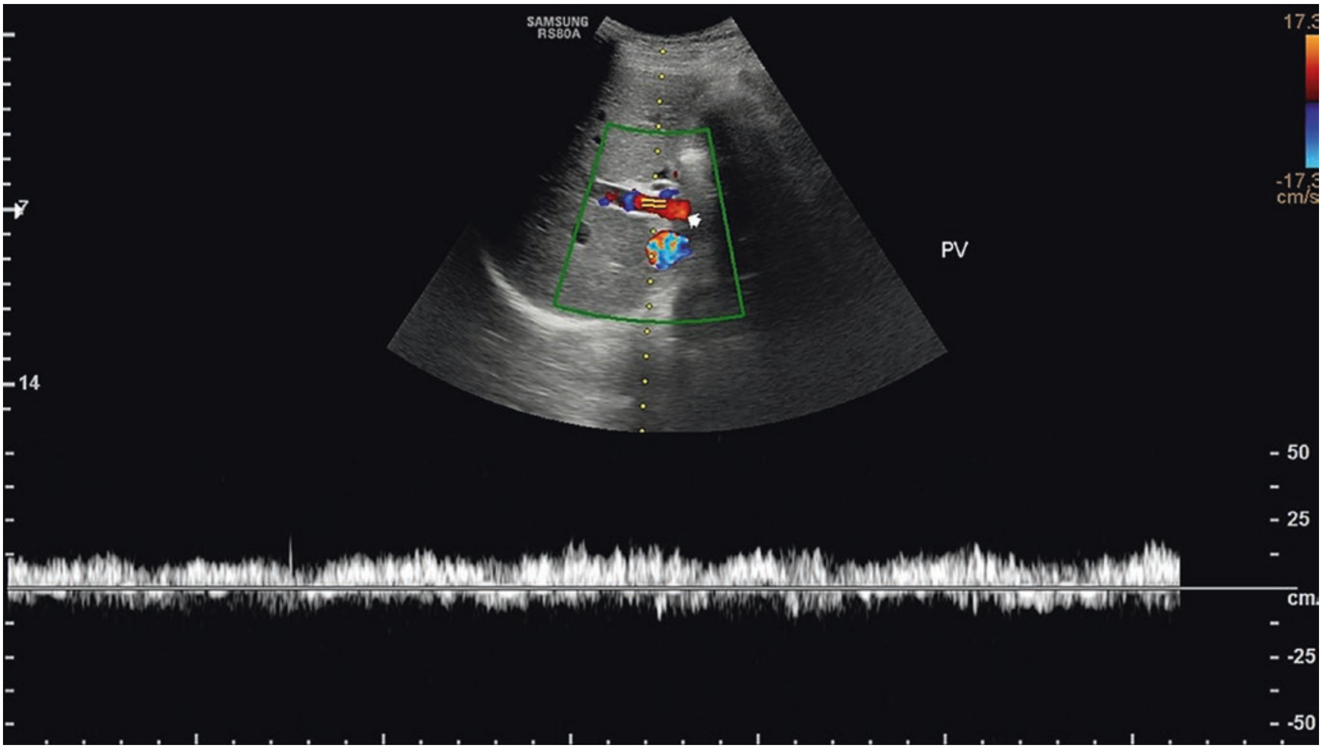

Fig. 2 Portal Vein Duplex Doppler showing flow within

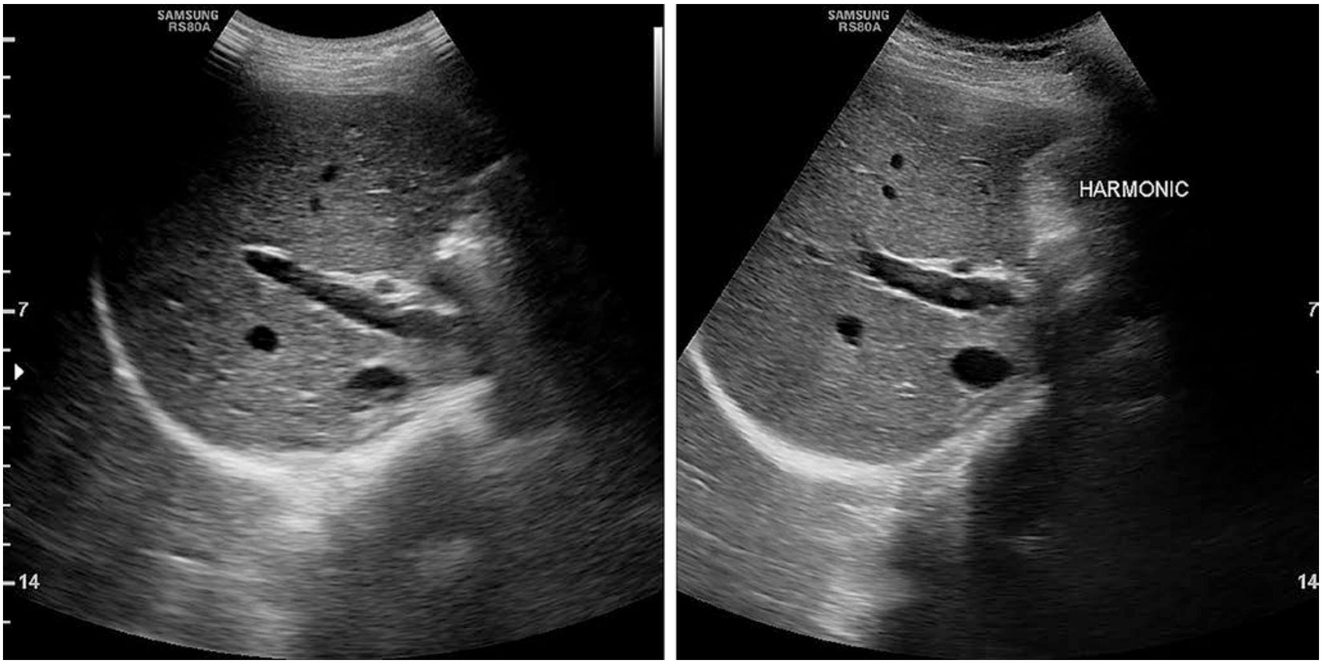
SAMSUNG RS80A
7
14
SAMSUNG RS80A
HARMONIC
7
14

Fig. 3 Harmonic scanning of liver showing greater details as compared to normal grey scale B mode scanning

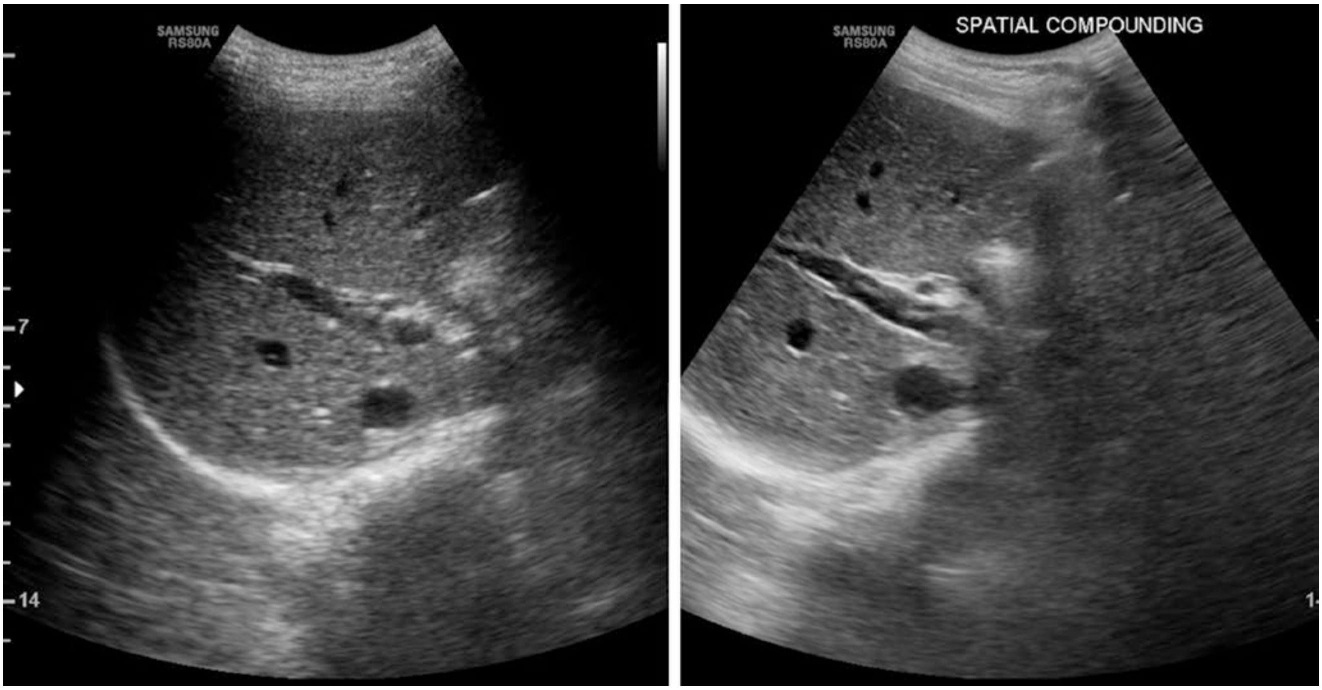
SAMSUNG RS80A
7
14
SAMSUNG RS80A
SPATIAL COMPOUNDING

Fig. 4 Spatial compounding scanning mode showing better details

4 Documentation, Reporting and Image Management System

Appropriate image storage with standard nomenclature should be properly maintained. Since each image may contain patient information, such as name, gender, age, medical record number and examination results, proper management of stored images should be strictly monitored per institutional policy.

5 Patient Safety

Diagnostic ultrasonography transmits energy to the patient that has potential to produce biologic effects. Two main biologic effects are mechanical and thermal effects. These effects are measured by two indices namely mechanical index (MI) and thermal index (TI). These indices are safety limits and are usually mentioned at the top of the image display.

When sound waves enter tissue, they produce a phenomenon called cavitation. Tiny gas-filled bubbles are formed which upon breaking releases energy and causes damage and in turn causes cavitation. Tissue containing air has high risk of cavitation as compared to solid organs. Risk of cavitation is low in solid urologic organs if the MI is kept below 0.7.

Thermal index (TI) indicates the probability of tissue temperature increasing by 1 °C within the sonographic field. Increases in tissue temperature depend on many factors like scanning frequency, time period of scanning, beam focusing, scanning mode and tissue density. Tissue temperature of up to 6 °C is not likely to cause much harm at scanning times less than 60 seconds; however, the exact mechanism of tissue heating is not well understood.

6 Renal Sonography

6.1 Antenatal Ultrasound Findings

Both the kidneys are seen in the foetus with a well differentiated cortex and medulla. Foetal kidney size is dependent on gestational age. Both kidneys are seen in the renal fossa at the paravertebral location once they have ascended by 11 weeks of life. Urine production begins by 13 weeks of gestation. With ultrasound, kidneys can be visualized at 16–18 weeks of life. Foetal kidneys show foetal lobulation and are more hypoechoic due to the sparsity of sinus fat and the abundance of fluid in tubules (Fig. 5).

Renal arteries are seen arising from the foetal aorta on either side in coronal view. Unlike the adult, antenatal renal arteries have a high resistance to flow with an RI of 0.67–0.88 in the third trimester (Figs. 6 and 7).

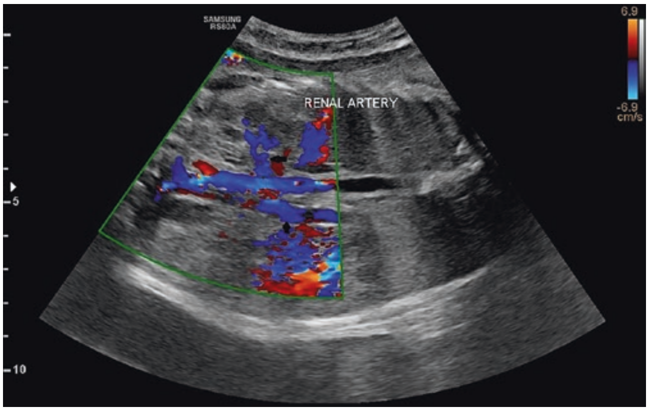

Fig. 6 Colour Doppler image of foetal kidneys, renal artery arising from aorta marked with black arrows

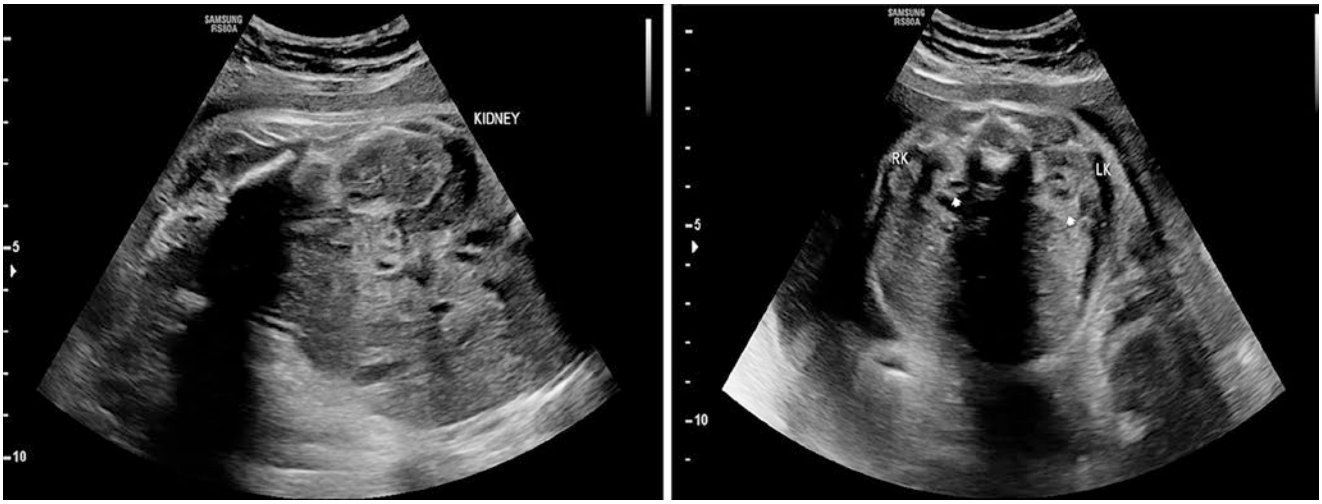

Fig. 5 Foetal kidneys in longitudinal and transverse scanning of foetal abdomen

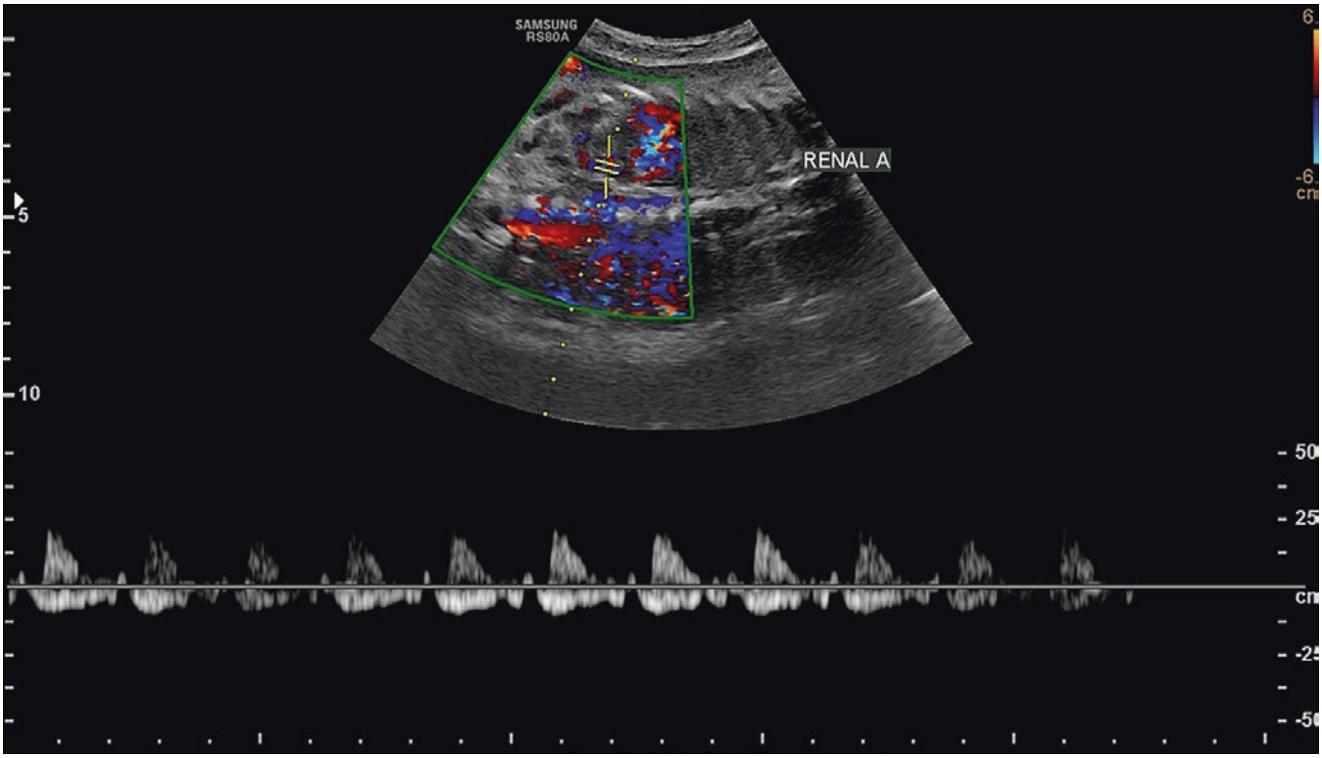

Fig. 7 Duplex Doppler of foetal renal artery showing high resistive index (RI)

Multiple congenital anomalies of the kidney can be detected on grey scale ultrasound, including the absence of a kidney, ectopic kidneys, crossed fused kidneys, ureteropelvic junction obstruction, ureteroceles and cystic diseases. Various associated anomalies, mainly VACTERAL anomalies, are also diagnosed on grey scale ultrasound. Foetal surgery such as a vesicoamniotic shunt is done under ultrasound guidance for posterior urethral valves.

6.2 Technique in Children and Adults

A curved array transducer frequency in the range of 1–7 MHz is frequently used in adult patients. For paediatric patients, a linear transducer frequency of 3–12 MHz is required. For intraoperative care, a 7–12 MHz high frequency transducer is commonly utilized.

Ultrasound of the right kidney is begun in the midclavicular line keeping the transducer longitudinal. The transducer is moved laterally until the entire kidney is visualized. After the longitudinal scan, the kidney is scanned transversely from the upper pole to the lower pole. The left kidney lies more cephalad than the right kidney and is better visualized with the patient positioned right side down and scanning from the anterior axillary line in longitudinal plane. Then the transducer is turned 90^0, and a transverse scan is done from left flank towards the anterior aspect.

6.3 Indications

1. Flank pain
2. Evaluation and monitoring of urolithiasis
3. Assessment of renal masses
4. Evaluation of perirenal structures
5. Evaluation of haematuria
6. Visualization of vesicoureteric reflux
7. postoperative evaluation
8. Ultrasound guidance to various intervention procedures like biopsies, cyst aspiration or as percutaneous access to collecting system
9. Evaluation of renal transplant
10. Renal trauma
11. Various congenital anomalies
12. Renal Doppler for renal artery stenosis

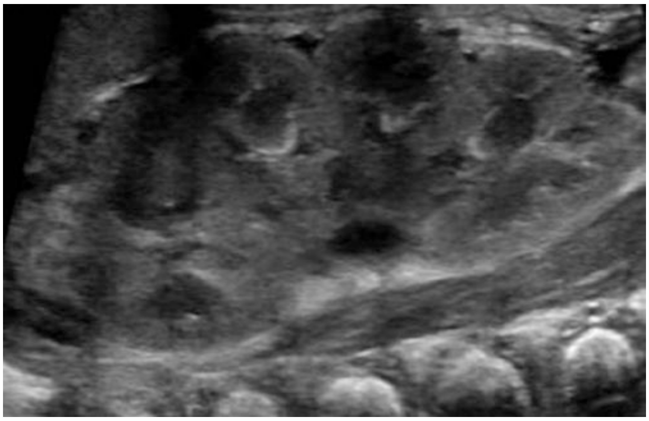

Fig. 8 Neonatal kidney showing prominent pyramids and scarcity of sinus echoes

6.4 Normal Ultrasound Findings

6.4.1 Neonate

Normal kidney size in the neonate is 3.5–4.5 cm in length and 2 cm in width. It gradually increases with age. The renal cortex is hyperechoic as compared with adult kidney due to the relative concentration and increased cellular volume of the glomeruli. Medullary pyramids appear more prominent as compared to the adult due to lower cortical size and its increased echogenicity. Also, there is sparsity of hyperechoic sinus echoes. As age increases, the hyperechogenicity of the sinus increases along with the size of the kidney. By 6 months of age, it assumes a normal adult pattern. The normal RI in a term neonate is <0.75 (Fig. 8).

6.4.2 Adult

The average adult kidney measures 10–12 cm in length and 4–5 cm in width. Measurements are done in the midsagittal plane where the maximum length is obtained. Each kidney shows a cortex which is hypoechoic as compared to the liver and further hypoechoic pyramids. Sinus echoes in the centre are hyperechoic. The thickness of parenchyma is the distance between the renal capsule and the central band of echoes. In the transverse plane, the renal hilum is seen with the renal vessels entering and exiting from it. The left renal hilum is visualized with the renal artery arising from aorta posterolaterally and the left renal vein anterior to it going across midline between the aorta and the superior mesenteric artery (SMA) to drain into the inferior vena cava (IVC). It is easier to visualize the right kidney as compared to the left kidney as bowel gas in the splenic flexure obscures the left kidney; however, the left renal origin is easier to visualize as the aorta lies on left side (Figs. 9, 10, 11, and 12).

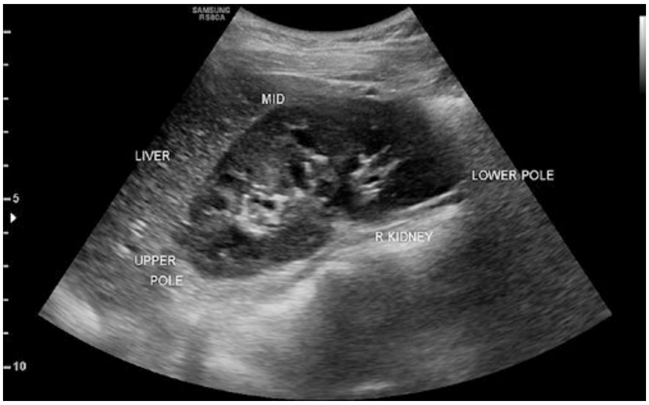

Fig. 9 Normal adult kidney

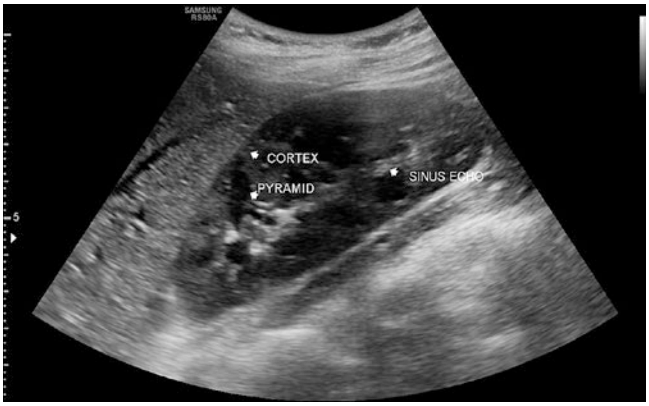

Fig. 10 Right kidney showing cortex, medulla and hyperechoic sinus echoes

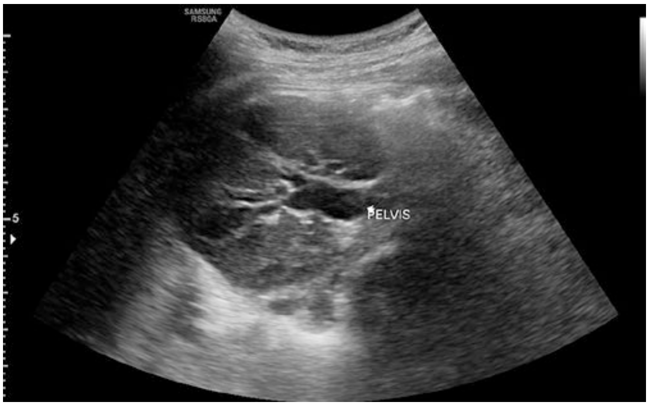

Fig. 11 Right kidney in transverse plane showing renal pelvis

6.4.3 Normal Doppler Waveform in Adult Renal Artery

Renal arteries on each side divide into segmental arteries. Segmental arteries are namely apical, upper, lower, middle and posterior. Each segmental artery divides into an interlobar artery which is present within the region of sinus echoes. These in turn divide into interlobular arteries present on either side of the pyramids. Interlobular arteries form arcades around the pyramids from which arise the arcuate arteries (Figs. 13 and 14). While evaluating for renal artery stenosis, the main renal artery at its origin, the trunk of the renal artery, the renal artery at the hilum and interlobar arteries at the upper mid and lower pole of the kidney are

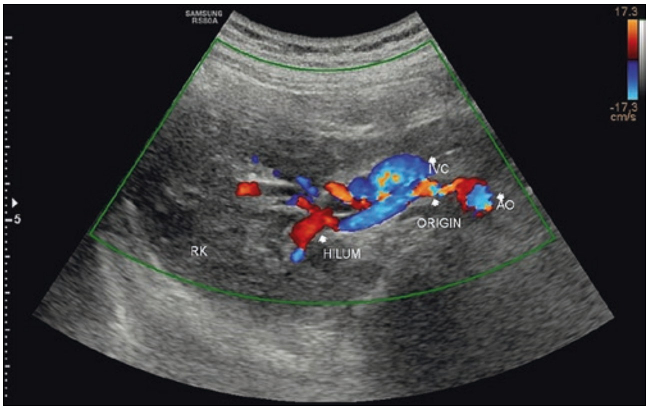

Fig. 12 Right renal artery arising from aorta entering into renal hilum

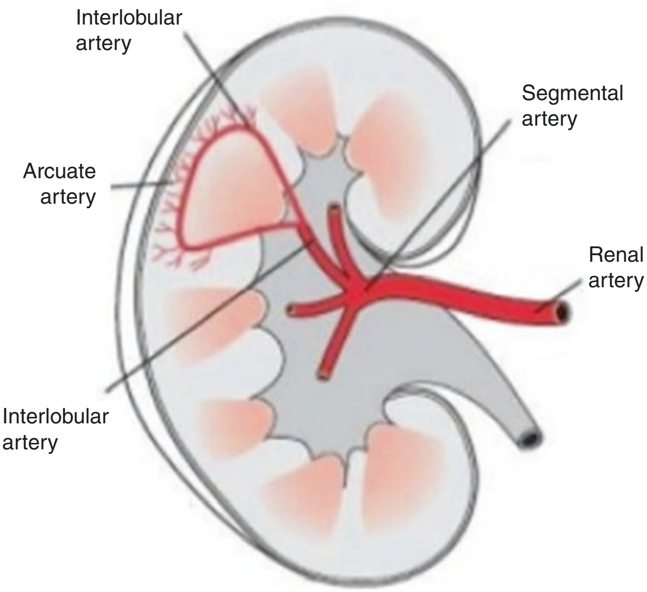

Fig. 13 Renal artery and its branches

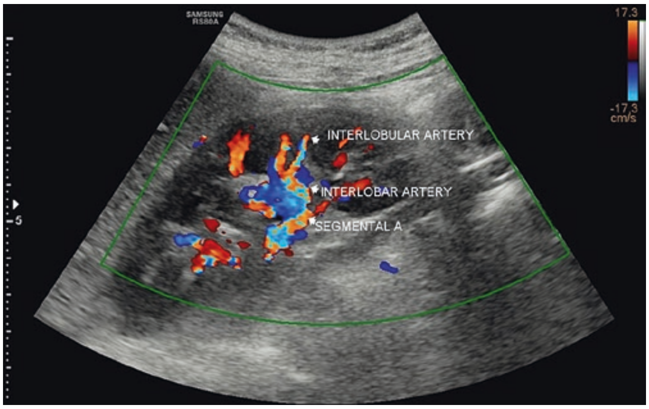

Fig. 14 Branches of intra-renal arteries

isonated. PSV, EDV and RI are measured at each artery. The normal renal artery has a sharp systolic upstroke, low resistance waveform and a continuous forward diastolic flow. The normal values of the renal artery at its origin are as follows: PSV <180 cm/s, renal aortic ratio of PSV (RAR) <3. At the level of the interlobar arteries RI <0.70, acceleration time (AT) <0.07 sec and acceleration index (AI) >3.5 m/s^2 (Fig. 15).

6.4.4 Renal Transplant

Grey scale, colour and spectral Doppler ultrasound are the prime modalities for renal transplant evaluation in the intra-operative period, immediate post-operative period and follow-up. Ultrasound is often performed with radionuclide imaging for medical and surgical evaluation [4].

6.4.5 Surgical Technique

Transplant kidneys, either cadaveric or from a living donor, are usually placed extraperitoneally in the right iliac fossa. It is placed in the left iliac fossa only if the right side is surgically contraindicated or a previous failed transplant is present.

In a cadaveric transplant, the main renal artery is harvested along with a cuff of cadaveric aorta and anastomosed usually end to end with recipient's internal iliac artery, or end to side with the external iliac artery. The renal vein of the donor is anastomosed end to side with recipient's external iliac vein. In a live donor, only the renal artery without an aortic cuff is anastomosed in the same way as in a cadaveric transplant. Urinary drainage is achieved with the donor ureter into the bladder dome. It can be also implanted into the native ureter or renal pelvis.

6.4.6 Normal Grey Scale Ultrasound Feathers of Transplant Kidney

Since the graft is placed extraperitoneal, it is superficial in location. With ultrasound, the transplanted kidney appears mildly hyperechoic due to its superficial location and can be scanned with standard curvilinear transducers and high frequency linear arrays. Normal collecting systems are mildly prominent in the immediate post-op period.

6.4.7 Doppler Features of Transplant Kidney

The origin or anastomotic site of the transplanted renal artery shows aliasing due to high velocity and mild narrowing at the anastomotic site. The normal parameters of a transplant renal artery are as follows: the PSV at the anastomotic site is <250 cm/s, the intrarenal RI is <0.5 and the AT is <0.07 sec (Figs. 16 and 17).

7 Ultrasound of Ureters

The ureters are paired muscular tubular structures that undergo peristaltic wave filling and emptying. In thin individuals, it is usually possible to visualize the ureters with a high frequency linear transducer (3–12 MHz) as the peristaltic wave fills and empties it. However, in obese individuals, a

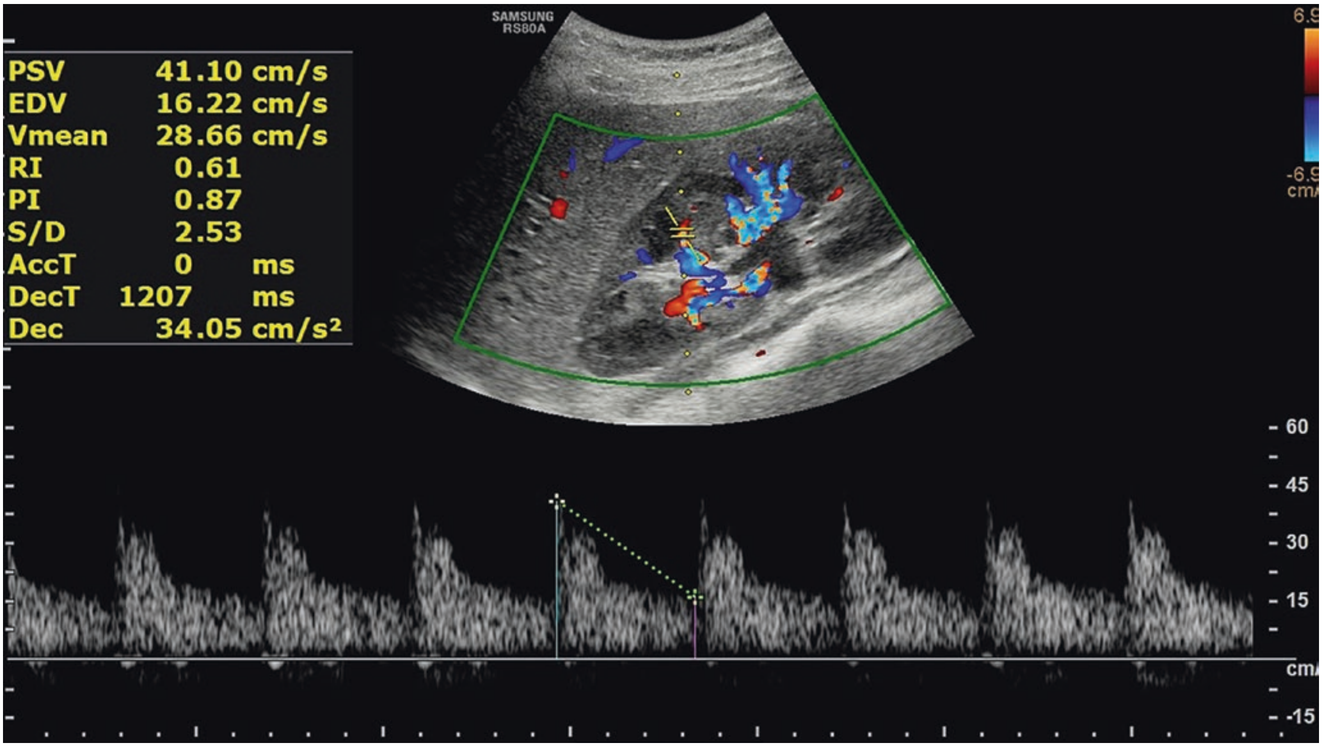

Fig. 15 Normal waveform pattern of renal artery

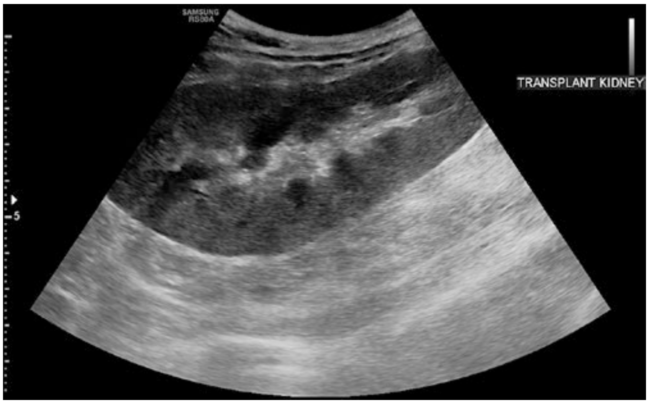

Fig. 16 Grey scale ultrasound of normal renal transplant kidney

curvilinear abdominal transducer is needed for visualization. In addition, dilated ureters are easier to be visualized with an abdominal transducer.

7.1 Technique

Gentle compression is applied at the ureteropelvic junction in a paramidline location close to the bladder. By using this method, it is possible to visualize the ureter by displacing bowel loops anteriorly. Usually it is possible to locate a ureteric calculus with grey scale ultrasound and can be correlated with radiographic imaging. The tinkling artefact of colour Doppler is useful for locating the site of a calculus. It is also possible to visualize the opening of the ureters within the bladder especially in those with vesicoureteral reflux.

8 Urinary Bladder

The urinary bladder is a muscular sac just above and behind the pubic bone. It is a triangular-shaped organ with a posterior base, anterior apex and an inferior neck with two inferolateral surfaces. It is lined by trabeculated transitional epithelium except at the trigone. It is an extraperitoneal structure located in the pelvis. Its main function is in the storage and release of urine.

8.1 Technique

Transabdominal pelvic sonography is done with a curved array transducer of 1–7 MHz frequency on a full bladder. In paediatric patients, a higher frequency transducer can be used. The patient is positioned supine and draped adequately. The scan is performed transversally from a cranial to caudal direction and then sagittal from right to left of the patient. Pre- and post-void bladder volumes are measured using the ellipse formula. Ureteric jets are observed on either side with

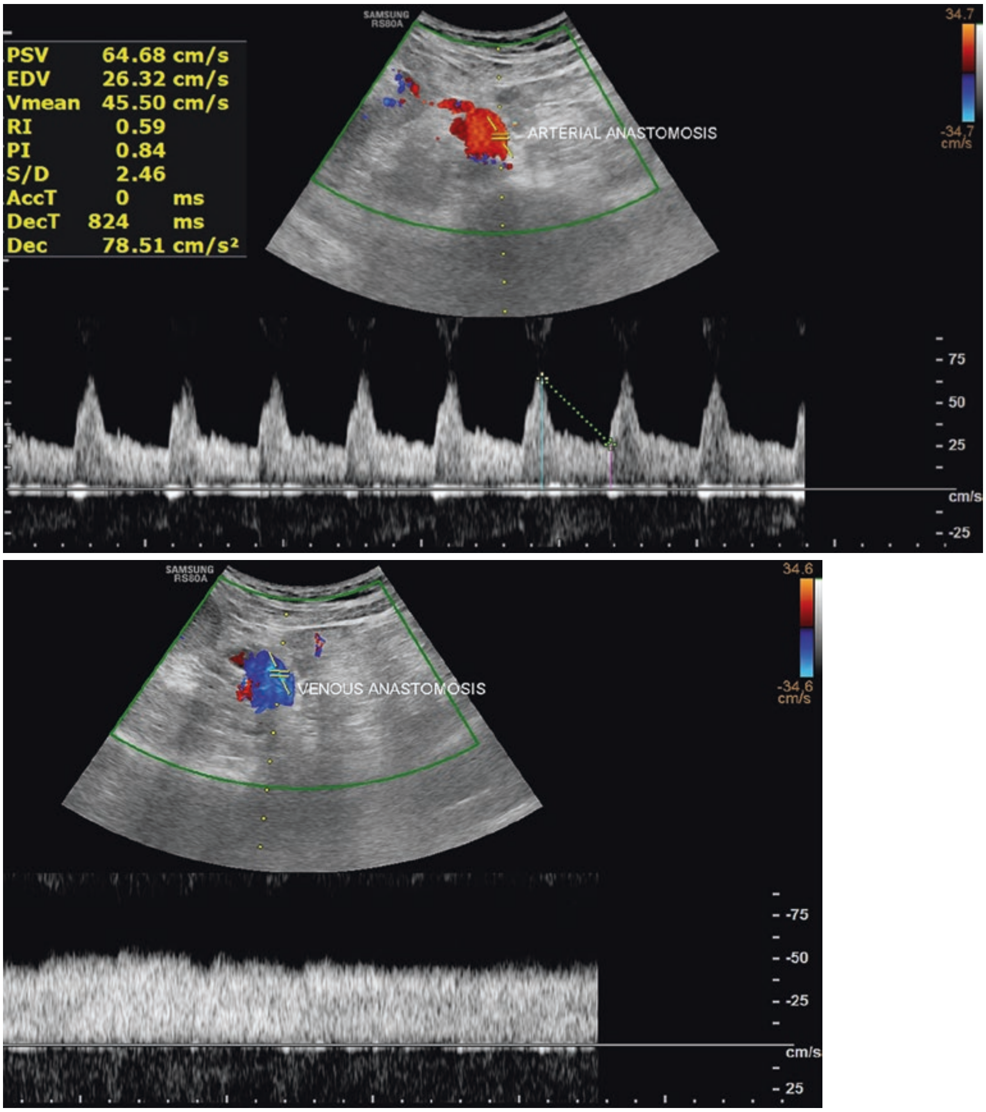

```
PSV     64.68 cm/s
EDV     26.32 cm/s
Vmean   45.50 cm/s
RI       0.59
PI       0.84
S/D      2.46
AccT     0     ms
DecT   824     ms
Dec     78.51 cm/s²
```

Fig. 17 Doppler features of transplant kidney

low PRF and low wall filter settings. In males the prostate is visualized, and its volume is measured. In females the uterus and ovaries can be seen. Vesicoureteral junctions are visualized at the trigone.

8.2 Indications

1. Measurement of pre and post void bladder volume
2. Assessment of prostate size and its morphology
3. Evaluation of haematuria
4. Evaluation of bladder outlet obstruction
5. Evaluation of bladder masses
6. Evaluation of lower ureters
7. Evaluation of lower urinary tract infection
8. For confirmation of catheter position and guide for removal of retained catheter

8.3 Normal Ultrasound Features

A full bladder volume can vary from 100 to 500 ml. Bladder volume is usually measured by the ellipse volume formula. The bladder wall thickness depends on bladder filling rather than on age. An empty bladder is 5 mm and a full bladder is 3 mm. A normal fluid filled bladder is anechoic with well-defined walls. As a rule of thumb, the bladder should empty at least approximately 10% of its pre-micturition volume. Ureteric jets can be visualized with the colour Doppler mode. The presence of a ureteric jet in a normal non-obstructed kidney means that the kidney is functioning adequately, and in the kidney with a calculus, it means the calculus is not fully obstructive. Transvaginal or transrectal scans can also be performed for the evaluation of the bladder. The posterior urethra is also evaluated in children with possible posterior urethral valves (Figs. 18 and 19).

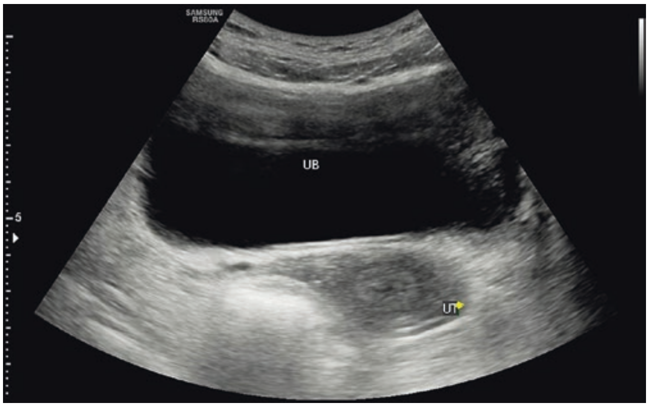

Fig. 18 Urinary bladder in transverse plane in a female patient showing uterus posterior to bladder

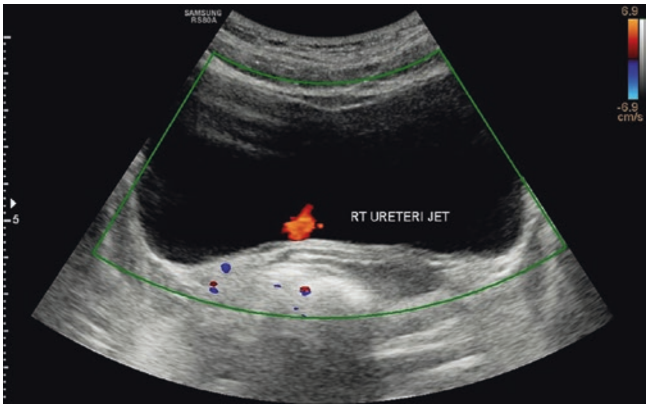

Fig. 19 Normal right ureteric jet

9 Ultrasonography of the Scrotum

The scrotum contains the testicles, epididymis and part of the spermatic cord. Because the scrotum and its contents are superficial in location, they are best evaluated by high frequency linear array transducers with frequencies in the range of 3–18 MHz. Grey scale ultrasound, colour and spectral Doppler are used to differentiate many acute and chronic pathologies involving the testicles and epididymis in addition to detailed anatomic evaluation.

9.1 Technique

The examination is carried out in a quiet and warm room which is comfortable to the patient. The patient is lying supine with the scrotum supported on a towel. Gentle contact is made after applying conducting gel. Both testicles are examined from the upper to lower pole in a transverse scanning pattern and then from medial to lateral in a sagittal scanning pattern. After scanning of the testes, the epididymis is seen in its entire extent starting with head, body and its tail. Examination is extended over the inguinal canal for the cord and its contents. After completing a grey scale examination, colour and spectral Doppler, examination is done and the vascularity of the testes and epididymis are evaluated.

9.2 Indications

1. Acute scrotal pain in children and adult
2. Evaluation of scrotal trauma
3. Assessment of scrotal swelling and masses
4. Evaluation of infertility
5. Postoperative scrotal evaluation

9.3 Normal Ultrasound of Tests

Both testes are oval structures in the scrotal sac with medium echogenicity, measuring approximately $4*3*2$ cm in the adult. In the centre of each testicle, there is an echogenic linear septum which is called the mediastinum testes. Around the mediastinum testes, a hypoechoic area, rete testis, is seen, which drains into the epididymis through 10–15 efferent ductules. The peripheral echogenic line seen around the testicle is the tunica albuginea. The tunica vaginalis is a continuation of the peritoneum. A normal testicular appendix is a hypoechoic oval structure between the testicle and the head of the epididymis about 1–7 mm in size.

The vascular supply of the testes is from the testicular artery, a direct branch of the aorta. It enters into the inguinal canal as a supratesticular artery along with other cord structures. At the posterosuperior aspect of the testes, it divides into branches and pierces the tunica albuginea and forms the capsular artery around the testes. This in turn gives rise to centripetal branches which go up to the mediastinum testes. The supratesticular artery, the capsular artery and intratesticular centripetal arteries all show low impedance to flow with an RI in the range of 0.48–0.78.

9.4 Normal Ultrasound of Epididymis

The epididymis is a hypoechoic structure with nearly the same echogenicity as the testes situated posterolateral to it. It has a triangular-shaped head situated at the upper pole of the testicle, a linear body and tail at the lower pole of the testes. The appendix epididymis is a small oval structure attached to the head of the epididymis. Vascular supply is

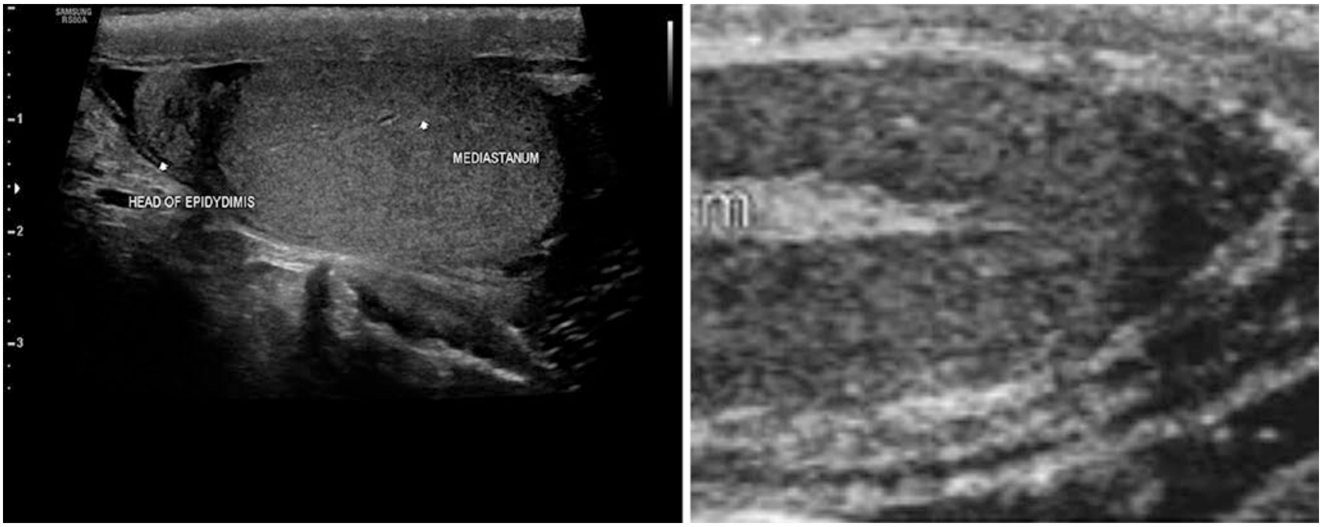
SAMSUNG RS80A
-1
-2
-3
HEAD OF EPIDYDIMIS
MEDIASTANUM

Fig. 20 Normal testicle with mediastinum of testis

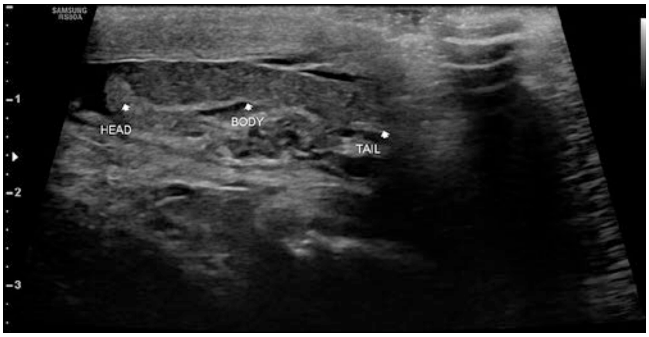
SAMSUNG RS80A
-1
-2
-3
HEAD
BODY
TAIL

Fig. 21 Grey scale ultrasound of normal epididymis showing head, body and tail

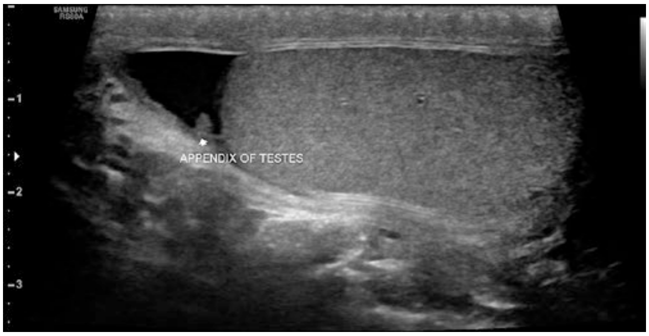
SAMSUNG RS80A
-1
-2
-3
APPENDIX OF TESTES

Fig. 22 Appendix of testicle

from the deferential artery, branches of the superior vesicle artery and from the testicular artery with a resistive index nearly identical to the testicular artery (Figs. 20, 21, 22, 23, 24, and 25).

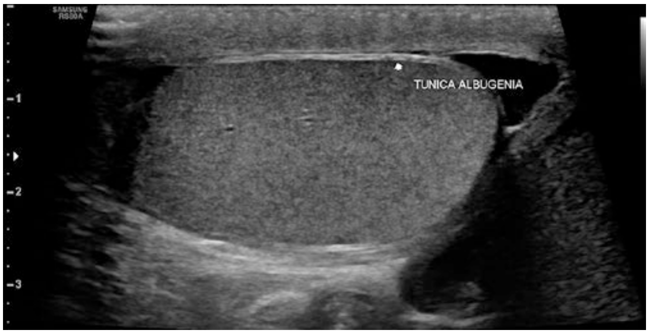
SAMSUNG RS80A
-1
-2
-3
TUNICA ALBUGENIA

Fig. 23 Tunica albuginea around testicles

10 Ultrasonography of Prostate Seminal Vesicles and Vas Deference

The prostate is situated behind the urinary bladder and can be evaluated transabdominally and transrectally (TRUS). Along with prostate evaluation, the seminal vesicles and vas deferens evaluations are carried out which are situated behind prostate.

10.1 Technique

10.1.1 Transabdominal Scan

It is performed with a curvilinear transducer of 1–7 MHz frequency. The patient is asked to come with a full bladder or near full bladder. He is positioned supine and the transducer is kept transversely, longitudinally and angulated caudally till the prostate is visualized.

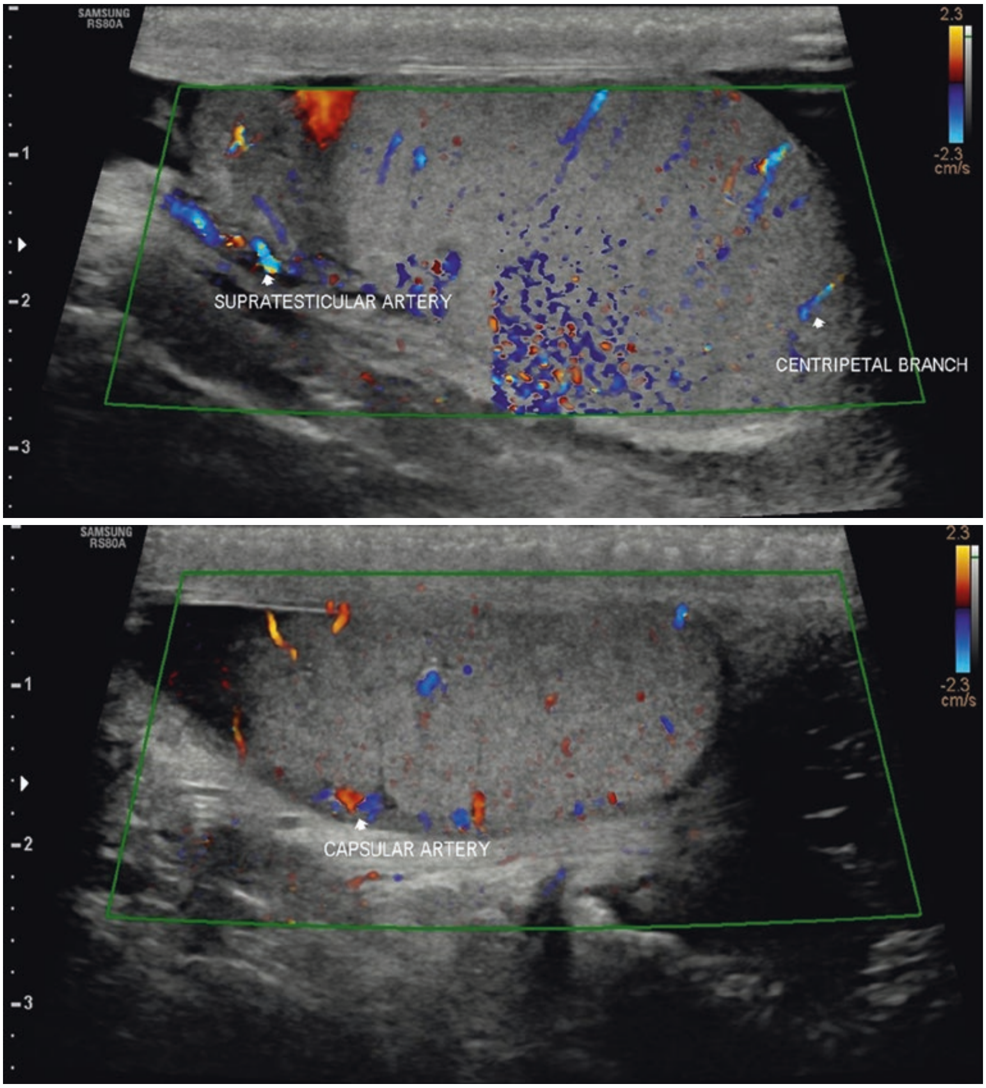

Fig. 24 Vascular supply of testicle showing supra testicular artery, capsular artery and centripetal arteries

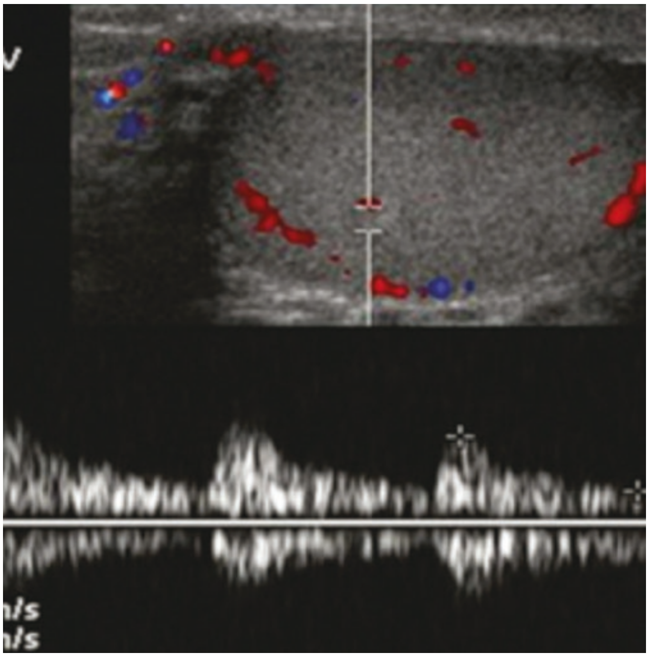

Fig. 25 Normal Doppler of the testicular arteries

10.1.2 Transrectal Ultrasound (TRUS)

TRUS is performed with an intracavitary end firing or side firing transducer of 4–9 MHz. It must have colour and spectral Doppler capability, with facility for 3D scanning if required. Before starting the examination, the patient is asked to go through a bowel preparation followed by a simple bowel enema. The patient is asked to empty their bladder before starting the examination. The patient is asked to lie in the lateral decubitus position with one knee extended and one knee flexed towards the chest. It is essential to perform digital rectal examination before inserting the ultrasound transducer. If the patient has local pain, or has a stricture, haemorrhoids, or a rectal mass that is picked up during digital exam, TRUS examination is relatively contraindicated. The transducer is covered with a plastic sheath with gel inside. Once covered with a plastic sheath, a generous amount of local anaesthetic gel is applied over the sheath before inserting the transducer in the anus. Introduce the transducer gently using mild pressure directed posteriorly. Once the anal sphincter resistance is overcome, the transducer is angulated anteriorly as the prostate is situated anterior to the rectum. One should avoid applying too much pressure as it can be very uncomfortable and the peripheral zone of prostate (where most cancers are found) may get obscured. In transverse and sagittal planes, the prostate examination is carried out from right to left. Gradually the transducer is moved posteriorly for seminal vesicle and vas deferens evaluation. Again, the transducer is adjusted to visualize the periprostatic tissue as far laterally as possible. Once these organs are evaluated, the rectal wall is seen as much as possible for any focal mass or circumferential growth of the rectum. After carrying out grey scale examination, colour and spectral Doppler examination of the prostate is performed with adjusting the machine parameters to low scale and high colour gain.

10.2 Indications

1. Measurement of prostatic volume in benign enlargement of prostate
2. Focal lesion palpable on digital rectal examination
3. Symptoms of lower urinary tract infection including prostatitis, prostatic abscess
4. Abnormal transabdominal examination of prostate
5. Suspected congenital abnormality
6. Haematospermia
7. Male infertility evaluation
8. For carrying out various intervention procedures

10.3 Normal Ultrasound Features of Prostate, Seminal Vesicles and Vas Deference

10.3.1 Prostate Gland

Both lobes of the prostate gland are of similar echogenicity with a medium level of echogenicity. The gland is described based on zonal architecture. These divisions consist of the anterior fibromuscular stroma which is devoid of glandular tissue, a periurethral zone around the urethra, a predominantly anterior and cranially situated transition zone, a posterior and cranially situated central zone through which the ejaculatory duct passes and an anterior and posteriorly situated peripheral zone. The prominence of the urethra is due to the hypoechoic urethral muscles. The neurovascular bundle is situated bilaterally along the posterolateral aspect of the prostate in between the prostate and seminal vesicle. Normal adult prostatic volume is approximately 30 cc. About 70% of prostatic carcinoma is situated in the peripheral zone, 20% in the transition zone and 10% in the central zone. Benign prostatic hyperplasia (BPH) is a nodular hyperplasia of fibrous, muscular and glandular tissue within the periurethral zone and transition zone. In younger men, zonal anatomy is not well depicted with the peripheral zone appearing hyperechoic compared to central and transition zone. The peripheral zone is well differentiated from the transitional zone in the older male (Figs. 26, 27, 28, and 29).

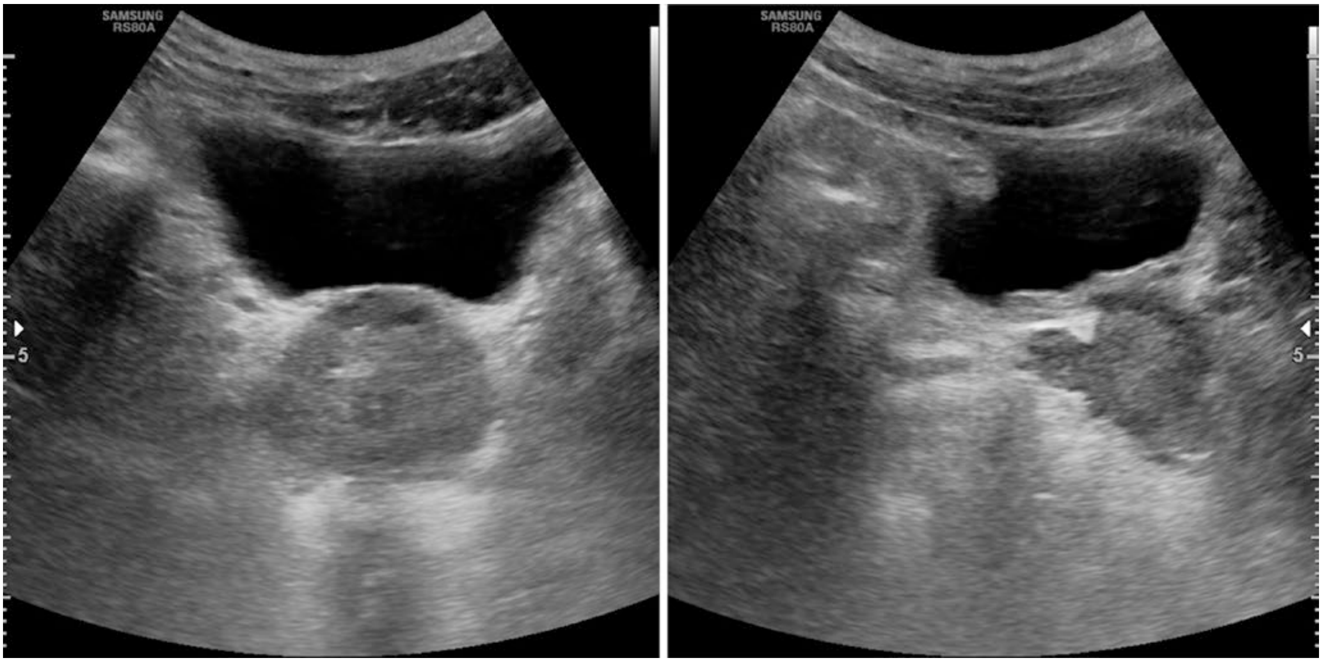

Fig. 26 Transabdominal scan of prostate gland, longitudinal and transverse scan

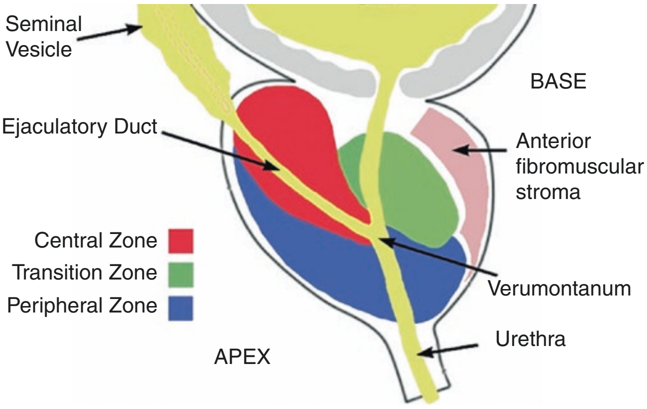
Seminal Vesicle
Ejaculatory Duct
Central Zone 🟥
Transition Zone 🟩
Peripheral Zone 🟦
APEX
BASE
Anterior fibromuscular stroma
Verumontanum
Urethra

Fig. 27 Schematic diagram of zones of prostate gland

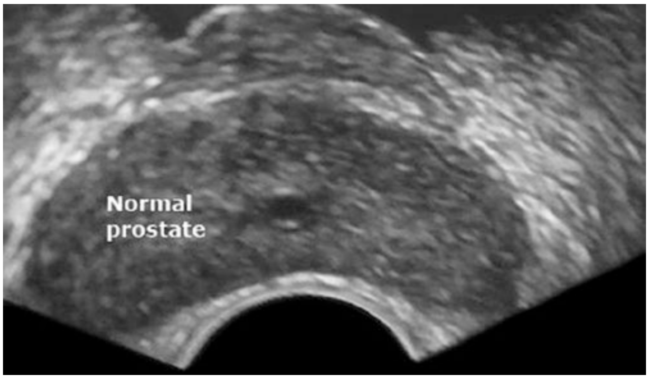
Normal prostate

Fig. 28 TRUS showing prostate gland

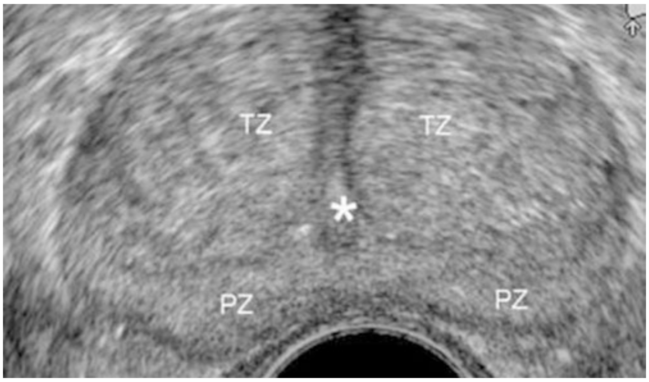

Fig. 29 TRUS of prostate gland showing zonal anatomy

10.3.2 Seminal Vesicle and Vas Deference

The seminal vesicles are situated posterior to the bladder and caudal to the distal ureters. It joins the distal ductus deferens to form the ejaculatory duct on either side to drain into the prostatic urethra at the verumontanum. They are elongated ovoid cystic septated structures measuring about 3–4 cm in length and 1.5–2 cm in width. It shrinks in size with very advanced age. Asymmetry is a common finding. The vas deferens continues from the tail of the epididymis, runs in the spermatic cord in the inguinal canal. Once it enters into the abdomen, it runs posteriorly into the lateral pelvis and inferiorly behind the bladder to the seminal vesicles and medial to the distal ureter to join the duct of SV to form the ejaculatory duct. The distal portion of the VD is mildly dilated and here it measures approximately 0.5 cm in width (Figs. 30 and 31). The ejaculatory duct is approximately 5–8 mm in size seen on oblique scan on TRUS as a joining of the SV and VD going to the verumontanum.

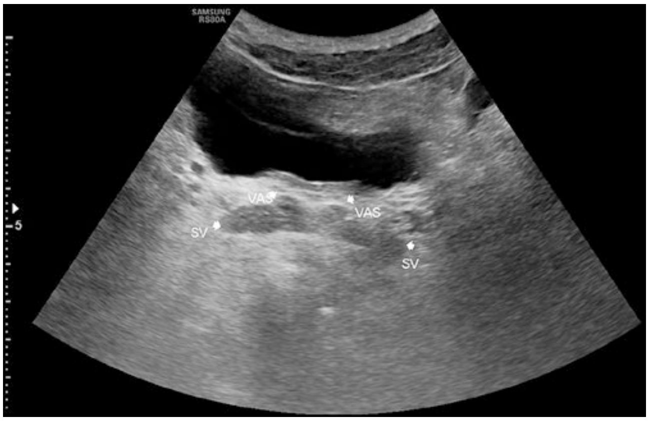
SAMSUNG RS80A
VAS
VAS
SV
SV
-5

Fig. 30 Transabdominal scan showing seminal vesicle and vas deference in transverse scan

11 Ultrasound of Penis

Ultrasound with colour and spectral Doppler is an excellent way to evaluate the penis and erectile function. Since the penis is a superficial structure, it is best evaluated with a high frequency linear transducer.

11.1 Indications

1. Evaluation of erectile dysfunction
2. Penile trauma or pain
3. Penile curvature
4. Priapism
5. Evaluation of fibrosis of corpora cavernosa
6. Evaluation of urethral stricture

11.2 Technique

The examination is carried out in quiet room with dim light and the patient lying in supine position.

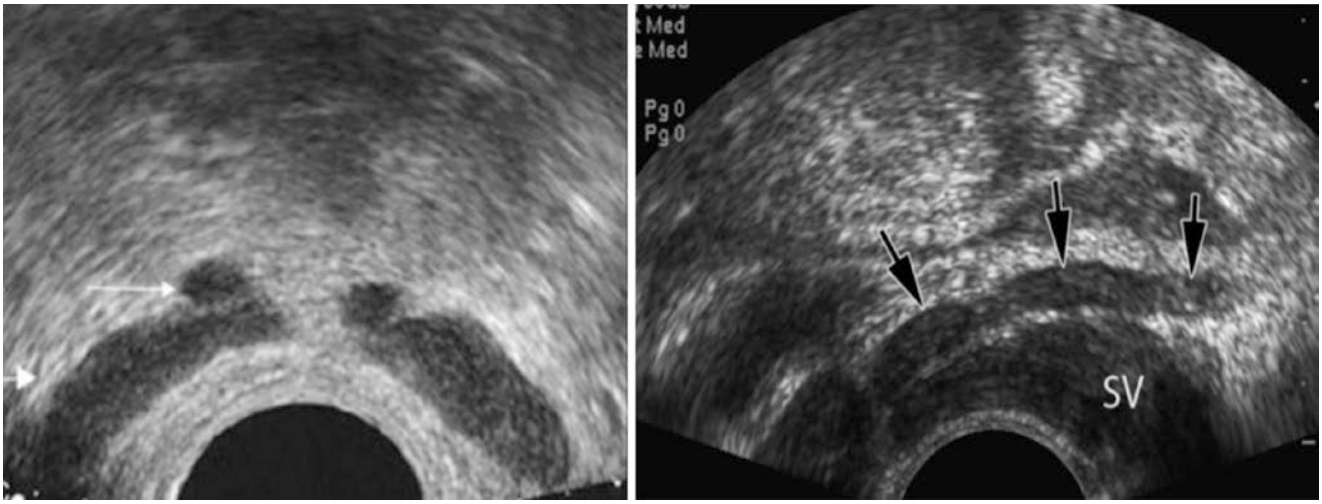

Fig. 31 TRUS showing seminal vesicle and vas deference in transverse and longitudinal scan

11.3 Grey Scale Ultrasound

The penis is placed in its anatomical position over the abdomen and evaluated in transverse and longitudinal directions with a high frequency transducer of 5–12 MHz. The transducer is moved from distal to proximal with the penis in a flaccid state.

11.4 Colour and Spectral Doppler Examination

For the evaluation of erectile dysfunction, a vasoactive drug is injected in the corpora cavernosa with a 26G needle in the corpora cavernosa unilaterally. Initially 1 ml of vasoactive drug is injected, and the dose can be repeated. Colour and spectral Doppler examination are carried out every 5 min for 20–25 min with each injection. Peak systolic velocity (PSV), end diastolic velocity (EDV) and resistive index (RI) are measured with each 5-min interval in both cavernosal arteries.

12 Ultrasound Anatomy of Penis

The corpora cavernosa are iso- to hypoechoic cylindrical structures covered by the tunica albuginea. It has a central cavernosal artery. The corpus spongiosum is a midline ventral cylindrical structure with a central urethra. It is more echogenic as compared to the corpora cavernosa, and it is also covered by tunica albuginea. Buck's Fascia covers the tunica albuginea circumferentially. The vascular supply to each cavernosa is through the cavenosal artery in its centre. The internal pudendal artery, a branch of the internal iliac artery, gives a branch to the bulb as the bulbourethral artery. After giving rise to this branch, it gives a branch to two dorsal arteries and two cavernosal arteries on the right as well as the left side. The bulbar and spongiosal veins along with the cavernosal vein drain into the internal pudendal vein. Also, venous drainage occurs through the superficial dorsal vein on either side and the deep dorsal vein in the centre (Figs. 32 and 33).

12.1 Normal Features on Colour and Spectral Doppler Evaluation

In the flaccid state, the normal cavernosal arteries show monophasic flow with a maximum PSV of 10–15 cm/s (Fig. 34). After injection of a vasoactive drug, the PSV as well as EDV increases. As the vein occlusion begins, PSV increases and diastolic flow EDV starts to decrease. At about 10–15 min after injection, PSV reaches a maximum of 40–60 cm/s and EDV becomes zero and then becomes reversed. This remains for another 5–10 min and then it returns to its initial flaccid state.

12.2 Sonourethrography

Urethral strictures or diverticulums can be evaluated by sonourethrography by injecting local anaesthetic gel into the urethra in a retrograde fashion. Gel distends the urethra as well as anaesthetizes its distal portion and delineates its pathology (Fig. 35).

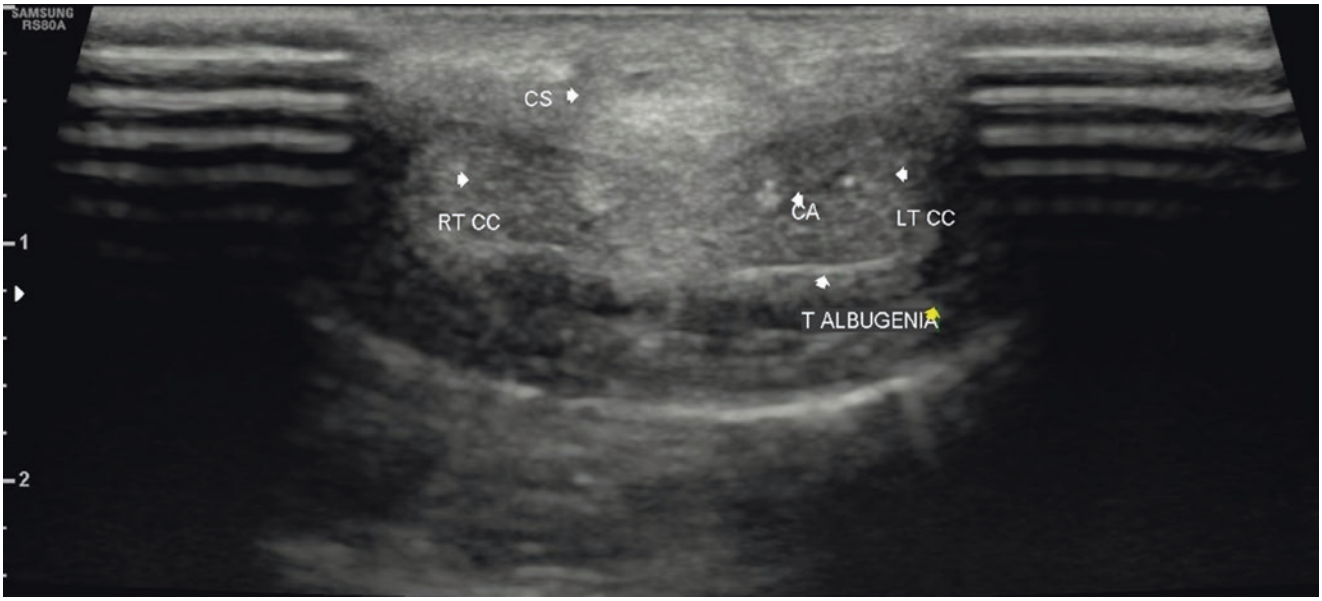

Fig. 32 Transverse scan of corpora cavernosa and spongiosa of penis

13 Ultrasound in Urological Intervention

13.1 Ultrasound Guided Per Cutaneous Renal Access

In older days, fluoroscopy was commonly used for any percutaneous renal access. Now with better ultrasound machines, ultrasound guided renal access is recommended.

13.1.1 Indications

- Obstructive nephropathy secondary to stone disease, malignancy, strictures requiring urgent decompression
- Renal access in PCNL procedure [5]
- Infected hydronephrosis or pyonephrosis
- Renal mass biopsy [6]
- Renal transplant biopsy when serum creatinine rises significantly or oliguria
- Renal cyst aspirations for cytology or sclerosis in symptomatic patients [7, 8]
- Renal or perirenal abscess or collection aspirations or drainage with pigtailing [9, 10]
- Pigtail drainage in psoas abscess

13.1.2 Prerequisites

- Prothrombin time or INR
- Serum evaluation for Hepatitis B, Hepatitis C or HIV virus
- Site confirmation
- Consent
- 10 ml 2% Lignocaine
- No. 11 Surgical blade
- Spinal needle 18 G/22 cm long for PCN or aspirations or 18G biopsy gun or coaxial gun for biopsy, pigtail catheter 10F for adult
- Sclerosant agent like tetracycline or absolute alcohol (95%)
- 0.035 Or 0.038 inch Straight tip or J tip guide wire
- Facial dilator no. 8, 9, 10
- Suture material

13.1.3 Procedures

All renal interventions can be done under local anaesthesia except PCNL surgery which requires general anaesthesia or spinal anaesthesia. Renal access can be achieved in supine, prone or lateral position. We at our institute prefer prone or lateral position for percutaneous renal access with scanning starting from a medial paraspinal area and gradually taken laterally. Transplant kidney biopsy is done in supine position. Once we decide the desired calyx, the entry site is marked with the needle hub. Local anaesthetic agent is injected. A small incision is made about 0.5 cm in length with an 11 blade. Haemostasis is achieved. An ultrasonography probe should be fixed at the site of entry point. For PCN an 18 G 15–22-cm-long needle is advanced under ultrasound guidance till it enters into the desired calyx. Entry into the desired calyx is confirmed with free flow of urine from the needle or aspiration of urine from the needle. After that a

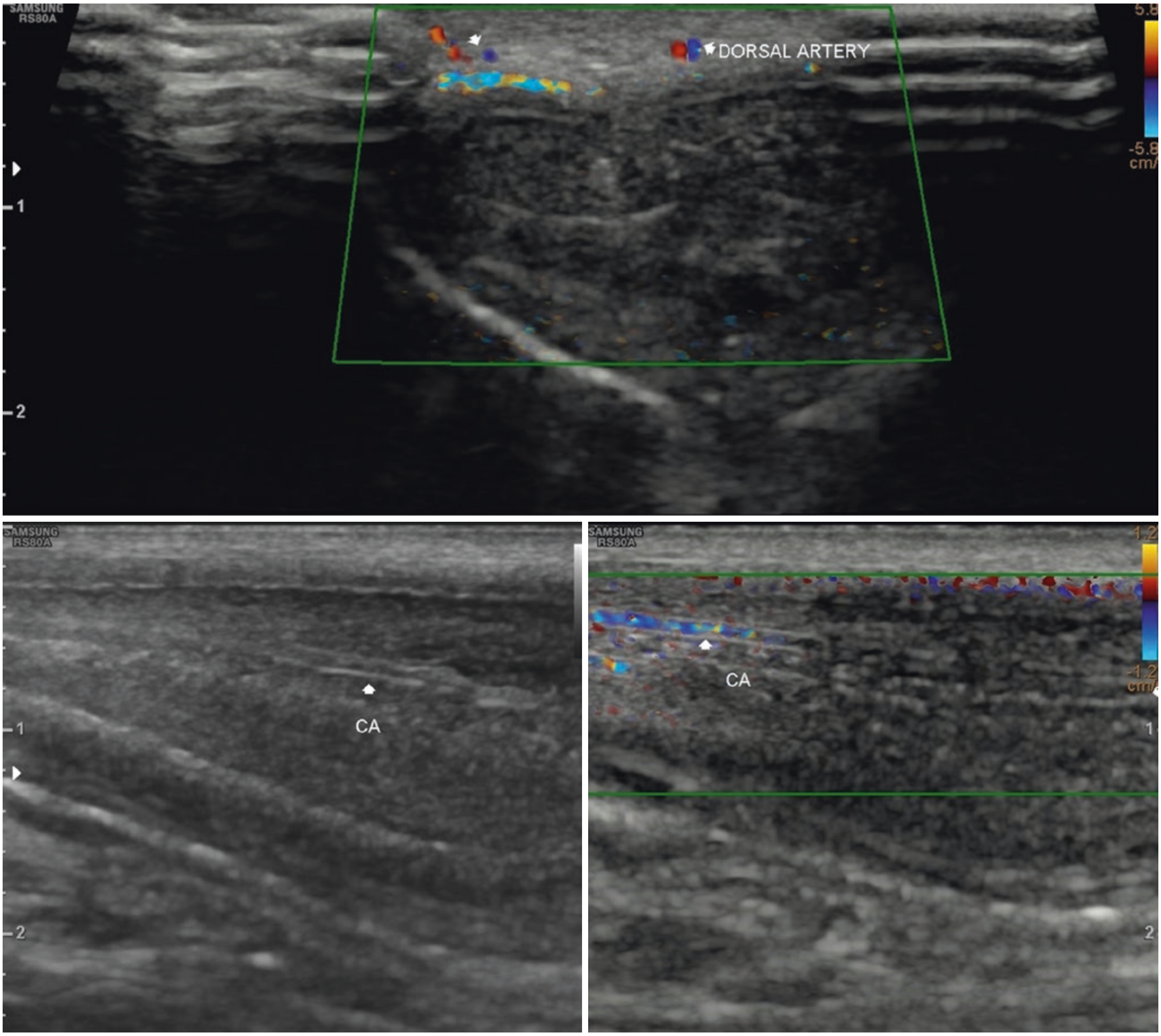

Fig. 33 Dorsal artery of penis and longitudinal scan of cavernosal artery

0.035-inch straight tip guide wire is introduced through needle into the pelvic collecting systems. Now we can serially dilate the tract under sonographic control. The ideal tract should be short, straight and avoid major vessels.

For biopsy, after making an incision either a core biopsy needle or coaxial biopsy gun is advanced into the target. Samples are taken and collected in a formalin jar [11–16].

For pigtail catheter placement, after dilating the tract sequentially with 8, 9 and 10 number dilators, a 10F pigtail catheter is introduced. Once inside the pelvicalyceal system, the catheter forms a curve and is left in place, it is sutured to skin and left to gravity.

For sclerosing a cyst, after aspirating cyst fluid, one fourth of the volume aspirated is irrigated in the form of a sclerosing agent. It is mixed thoroughly with residual fluid in the cyst and left in situ. Follow-up scan after 1 week and 4 weeks is done. If it has refilled, a second or third session may be required to achieve a desirable result [17–20].

13.1.4 Advantages of Ultrasound Over Fluoroscopic Guidance

- No radiation hazards.
- Real time monitoring of the needle
- With use of Doppler ultrasound, we can prevent injury to major vessels and prevent injury to the other organs.

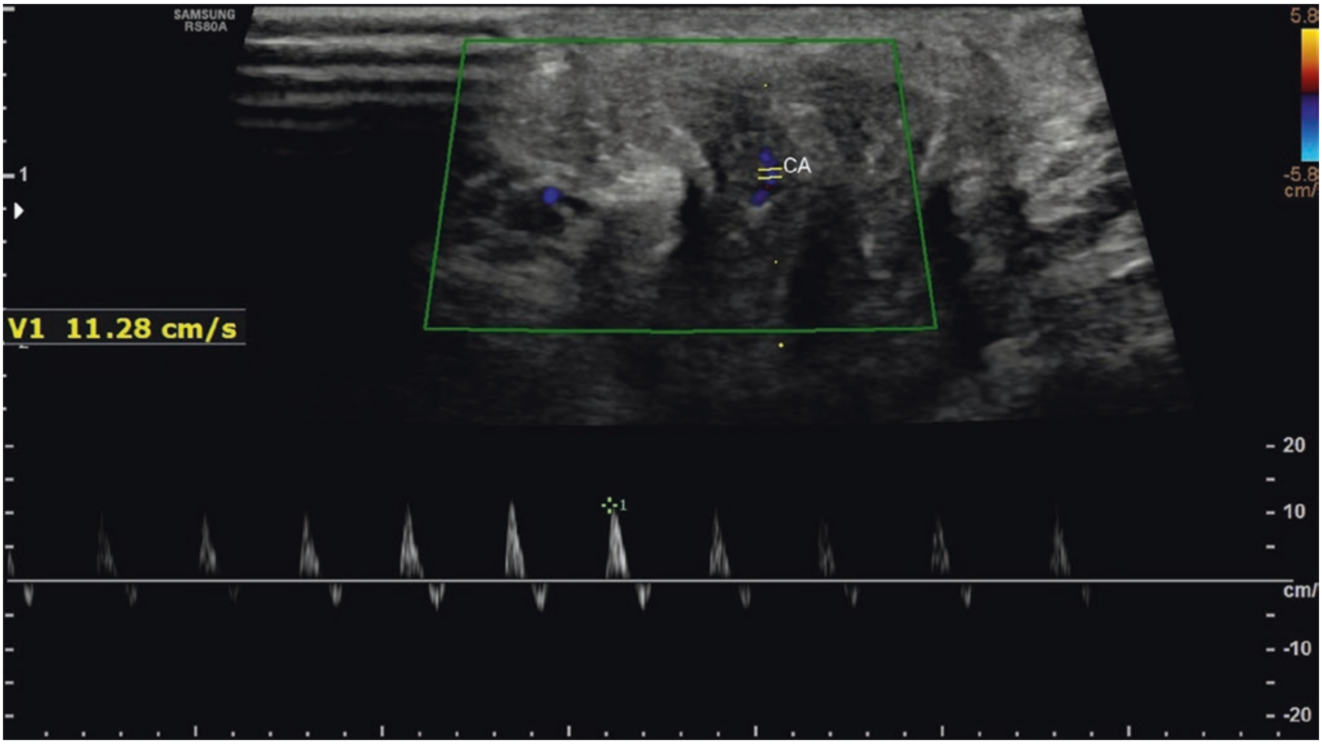

Fig. 34 Normal Doppler of corpora cavernosal artery in a flaccid state

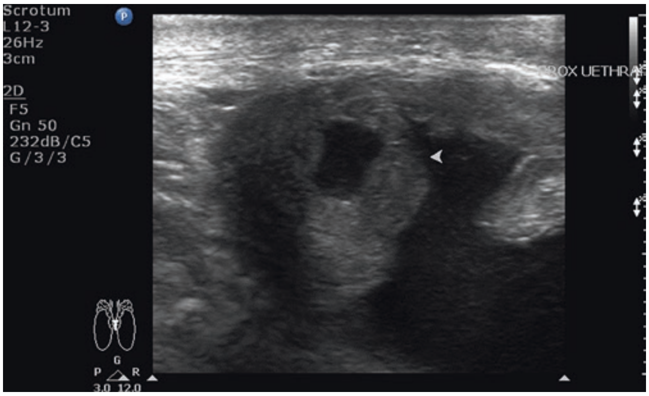

Fig. 35 Sonourethrography

14 TRUS Guided Prostate Biopsy

14.1 Indications

High PSA
Abnormal DRE

14.2 Contraindications

Coagulopathy
Acute prostatitis
Immunocompromised patients

14.3 Prerequisites

- Stop antiplatelet agents for 5–7 days before biopsy TRUS prostate biopsy can be safely performed in patients who are continuing aspirin without increasing the risk of significant bleeding.
- Use unfractionated heparin or low molecular weight heparin in patients with warfarin therapy. Ideally the INR must be less than 1.5.
- Antibiotic prophylaxis should be considered, and the choice of antibiotics depends upon local antibiotic policy. We routinely prescribe Ciprofloxacin 500 mg two doses. First dose around 2 hours before procedure and second dose 10 hours after procedure.
  All patients with prosthesis like joint prosthesis heart valves, pacemakers should receive antibiotics to prevent endocarditis or prosthesis infection as per standard guidelines
- Anaesthesia: Most urologists do TRUS biopsy under topical anaesthesia with 2% lignocaine jelly. We use topical anaesthesia with infiltration anaesthesia for biopsy. 22gauge 20cms Chiba needle is used for infiltration anaesthesia.

14.4 Procedure

Insert endorectal transducer with biopsy needle guide in rectum. After complete screening of the prostate for any pathol-

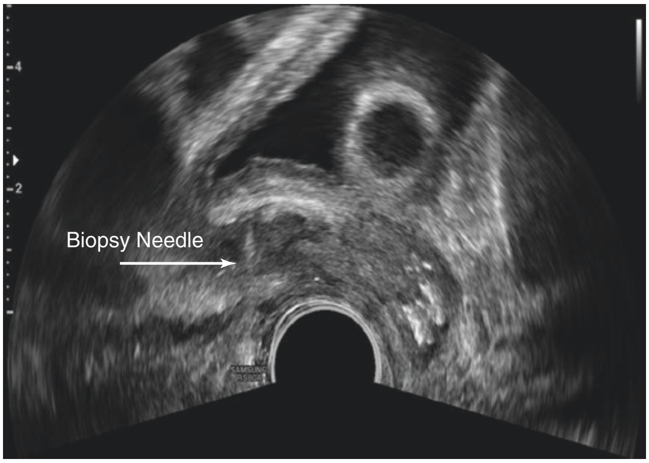

Fig. 36 TRUS biopsy with needle tip in right lobe

ogy, inject 5 ml lidocaine 2% on each side in the fat plane between the prostate base and SV.

For prostatic biopsy, various spring-driven biopsy guns are available. An 18 gz 22 cm biopsy gun is ideal for prostate biopsy.

The length of tissue sampled with these guns is 1.5 cm

Extended 12 core biopsy, six from each lobe, predominantly in the peripheral zone is targeted. If a focal lesion is seen, then a few more cores are obtained through that (Fig. 36) [21, 22].

14.5 Complications [23]

- Haematospermia – This is a common complication (35–40%). Most patients do not require any treatment, pre-procedure counselling and reassurance usually helps.
- Haematuria – This is the second most common complication (10–15%). Less than 1% patient require hospitalization for significant haematuria for which catheterization is required.
- Rectal bleeding
- Prostatitis, fever and epididymitis
- Urinary retention

15 Intra-operative Urologic Ultrasound

Use of intra-operative ultrasound is increasing over the last few years. It is routinely used in open surgeries and also in advanced laparoscopic and robotic surgeries.

15.1 Indications

- Tumour localization during partial nephrectomy
- Focal ablative therapy for SRMs
- Identification and confirmation of tumour thrombus in IVC during radical nephrectomy
- Renal transplantation and auto-transplantation to confirm normal flow in renal vasculature
- During testicular sparing surgery for testicular lesions
- To confirm viability of testes in torsion or testicular injuries
- For percutaneous access of pelvic calyceal system
- Failed urethral catheterization US guided suprapubic drainage of bladder

15.2 Transducers

Various transducers are available for intraoperative use. A curved or linear high frequency transducer is typically used.

Laparoscopic ultrasound transducers can be easily passed through 10–12 mm laparoscopic port. The diameter of the transducer is usually less than 10 mm and the length is usually 35–50 cm.

These are side firing transducers. LUS transducer screens the target organ by directly placing the probe with a frequency of 6–10 hz.

Most transducers can be sterilized by low temperature plasma sterilization. One should follow the instructions from manufacturers for sterilization of transducers for intraoperative use.

16 Sonoelastography

Sonoelastography is an ultrasound imaging technique where low-amplitude, low-frequency shear waves (less than 0.1 mm displacement and less than 1 kHz frequency) are propagated through internal organs, while real-time Doppler techniques are used to image the resulting vibration pattern. When a discrete hard inhomogeneity, such as a tumour, is present within a region of soft tissue, a decrease in the vibration amplitude will occur at its location. This forms the basis for tumour detection using sonoelastography. Sonoelastography is superior to colour Doppler imaging in identification of malignant areas in prostate, but at present it is not a replacement for standard random biopsies.

17 Endoluminal Ultrasonography

In this imaging technique, flexible catheters with high frequency transducers are inserted into a tubular structure such as the ureter, urethra, with the help of endoscopy. This high frequency transducer uses a frequency of 12.5–20 MHz. Endoscopy enables direct visualization of the lumen of the ureter, urethra and bladder, but it does not provide any information about submucosal tissues. With the help of high frequency endoluminal transducers, submucosal tissues can be imaged for various pathologies such as strictures and neoplasms, to name a few. It is also helpful in detection of crossing vessels and high insertion of the ureter [24, 25].

18 Contrast-Enhanced Ultrasound (CEUS)

Micrometre-sized, encapsulated, gas-filled microbubbles are used in contrast-enhanced ultrasonography (CEUS). These microbubbles help to enhance the ultrasonic signals. One of the characteristics of malignancy is neoangiogenesis. CEUS is helpful in imaging malignancies like kidney and prostate as intravascular microbubbles helps to identify altered perfusion pattern in areas of neoangiogenesis. At present its role in biopsy of prostate and kidney is under evaluation [26, 27] (Fig. 37).

CEUS in paediatric VUR

Ultrasound equipment with contrast-specific software is required

Before start of procedure, ask the patient to empty the bladder. Catheterize the patient with a 5–8 French catheter and empty the residual urine.

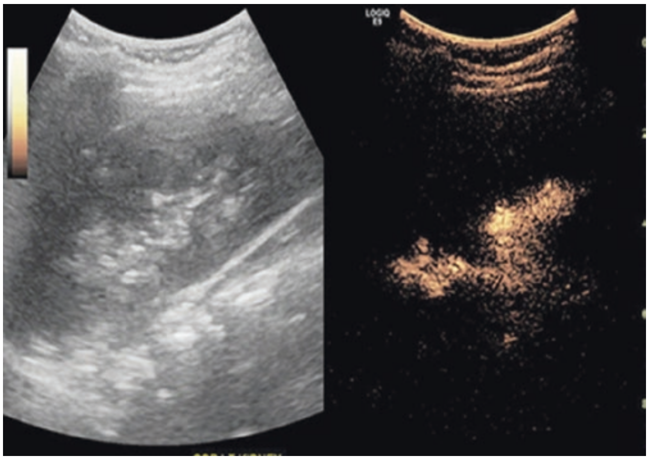

Fig. 37 CEUS showing grade 3 VUR

Fill the bladder with contrast in one of two methods

1. 1 ml of contrast is injected in 500 ml of saline. Connect the intravenous tubing to catheter and slowly fill the bladder till capacity.
   The bladder, ureter and kidneys are scanned while filling to identify passive reflux and during voiding to identify active reflux.
2. Fill the bladder with saline till capacity and then directly inject the contrast through catheter into the bladder.

Advantages No radiation

Disadvantage Difficult to identify grade 1 reflux

CEUS has also become a powerful additional tool for imaging renal lesions. With its lack of nephrotoxicity, the absence of ionizing radiation and the ability to evaluate the enhancement pattern of renal lesions quickly and in real-time, CEUS has unique advantages over traditional modes. Established applications are differentiation between solid tumours, pseudolesions and complex cysts; characterization of complex cysts with different malignant potential; and evaluation of tumour ablation [28].

References

1. Wild JJ, Reid JM. Application of echo-ranging techniques to the determination of structure of biological tissues. Science. 1952;115(2983):226–30.
2. Takahashi H, Ouchi T. The ultrasonic diagnosis in the field of urology. Proc JPN Soc Ultrasonics Med. 1963;3:7.
3. Goldberg BB, Pollack HM. Differentiation of renal masses using A-mode ultrasound. J Urol. 1971;105(6):765–71.
4. Kolofousi C, Stefanidis K, Cokkinos DD, Karakitsos D, Antypa E, Piperopoulos P. Ultrasonographic features of kidney transplants and their complications: an imaging review. ISRN Radiol. 2012;2013:480862. https://doi.org/10.5402/2013/480862. Published 2012 Dec 2.
5. Chu C, Masic S, Usawachintachit M, Hu W, Yang W, Stoller M, Li J, Chi T. Ultrasound-guided renal access for percutaneous nephrolithotomy: a description of here novel ultrasound-guided needletechniques. J Endourol. 2016;30(2):153–8.
6. Bosniak MA. The small (less than or equal to 3.0 cm) renal parenchymaltumor: detection, diagnosis, and controversies. Radiology. 1991;179(2):307.
7. Hanna RM, Dahniya MH. Aspiration and sclerotherapy of symptomatic simple renal cysts: value of two injections of a sclerosing agent. AJR Am J Roentgenol. 1996;167:781–3.
8. Skolarikos A, Laguna MP, de la Rosette JJMCH. Conservative and radiological management of simple renal cysts: a comprehensive review. BJU Int. 2012;110(2):170–8.
9. Shu T, Green JM, Orihuela E. Renal and perirenal abscesses in patients with otherwise anatomically normal urinary tracts. J Urol. 2004;172(1):148–50.

10. Lee SH, Jung HJ, Mah SY, Chung BH. Renal abscesses measuring 5 cm or less: outcome of medical treatment without therapeutic drainage. Yonsei Med J. 2010;51(4):569–73. Lang EK. Renal, perirenal, and pararenal abscesses: percutaneous drainage. Radiology. 1990;174(1).
11. Marconi L, Dabestani S, Lam TB, Hofmann F, Stewart F, Norrie J, Bex A, Bensalah K, Canfield SE, Hora M, Kuczyk MA, Merseburger AS, Mulders PFA, Powles T, Staehler M, Ljungberg B, Volpe A. Systematic review and meta-analysis of diagnostic accuracy of percutaneous renal tumour biopsy. Eur Urol. 2016;69:660–73.
12. Lane BR, Samplaski MK, Herts BR, et al. Renal mass biopsy–a renaissance? J Urol. 2008;179:20–7. https://doi.org/10.1016/j.juro.2007.08.124.
13. Jeon HG, Seo SI, Jeong BC, et al. Percutaneous kidney biopsy for a small renal mass: a critical appraisal of results. J Urol. 2016;195:568–73. https://doi.org/10.1016/j.juro.2015.09.073.
14. Torres Muñoz A, Valdez-Ortiz R, González-Parra C, Espinoza-Dávila E, Morales-Buenrostro LE, CorreaRotter R. Percutaneous renal biopsy of native kidneys: efficiency, safety and risk factors associated with major complications. Arch Med Sci. 2011;7:823–31.
15. Fergany AF, Hafez KS, Novick AC. Long-term results of nephron sparing surgery for localized renal cell carcinoma: 10-year followup and 82 to 92 percent for large>4 cms renal masses. J Urol. 2000;163:442–5.
16. Hoare D, Evans H, Richards H, Samji R. Evaluating the role for renal biopsy in T1 and T2 renal masses: a single-centre study. Can Urol Assoc J. 2018;2(5):E226–E23; Yang CS, Choi E, Idrees MT, Chen S, Wu HH. Percutaneous biopsy of the renal mass: FNA or core needle biopsy? Cancer Cytopathol. 2017;125:407–15.
17. Lin YH, Pan HB, Liang HL, et al. Single session alcohol-retention sclerotherapy for simple renal cysts: comparison of 2-and 4-h retention techniques. AJR Am J Roentgenol. 2005;185:860–6.
18. Okeke AA, Mitchelmore AE, Keeley FX Jr, et al. A comparison of aspiration and sclerotherapy with laparoscopic de-roofing in the management of symptomatic simple renal cysts. BJU Int. 2003;92:610–3.
19. Yang CF, Liang HL, Pan HB, et al. Single-session prolonged alcohol-retention sclerotherapy for large hepatic cysts. AJR Am J Roentgenol. 2006;187:940–3.
20. Mohsen T, Gomha MA. Treatment of symptomatic simple renal cysts by percutaneous aspiration and ethanol sclerotherapy. BJU Int. 2005;96:1369–72.
21. von Knobloch R, et al. Bilateral fine-needle administered local anaesthetic nerve block for pain control during TRUS-guided multi-core prostate biopsy: a prospective randomised trial. Eur Urol. 2002;41:508.
22. EAU – ESTRO –ESUR SIOG guidelines on prostate cancer. European Association of Urology 2018.
23. AUA/SUNA white paper on the incidence, prevention and treatment of complications related to prostate needle biopsy. American Urological Association Web site. http://www.auanet.org/common/pdf/practices-resources/quality/patient_safety/Prostate-Needle-Biopsy-White-Paper.pdf. Accessed February 22, 2013.
24. Goldberg BB, Liu JB. Endoluminal urologic ultrasound. Scand J Urol Nephrol. 1991;137(suppl):147–54.
25. Lin L, Bagley DH, Liu J-B. Role of endoluminal sonography in evaluation of obstruction of the ureteropelvic junction. Am J Roentgenol. 2008;191:1250–4.
26. Duran C, Beltrán VP, González A, Gómez C, Riego JD. Contrast-enhanced voiding urosonography for vesicoureteral reflux diagnosis in children. Radiographics. 2017;37(6):1854e69. https://doi.org/10.1148/rg.2017170024.
27. Chua ME, Kim JK, Mendoza JS, Fernandez N, Ming JM, Marson A, Lorenzo AJ, Lopes RI, Takahashi MS. The evaluation of vesicoureteral reflux among children using contrast-enhanced ultrasound: a literature review. J Pediatr Urol. 2019;15:12e17.
28. Bertolotto M, Bucci S, Valentino M, Currò F, Sachs C, Cova MA. Contrast-enhanced ultrasound for characterizing renal masses. Eur J Radiol. 2018;105:41–8. https://doi.org/10.1016/j.ejrad.2018.05.015. Epub 2018 May 16.

Ultrasound Guided Interventions

Junaid Raja, Igor Latich, and Mahan Mathur

1 Introduction

The use of ultrasound (US) in order to guide interventions provides several advantages over other imaging modalities and is an essential skill for any proceduralist. Ultrasound offers the ability to image in real-time and can dynamically characterize the location and contour of structures with high spatial resolution by near direct visualization [1]. In addition, US is relatively inexpensive and is more readily available and portable than other imaging modalities [2]. Moreover, the ability to guide intervention without the use of ionizing radiation provides critical advantages particularly in pediatric, pregnant and younger patients [1].

Magnetic resonance imaging (MRI) guided interventions, in addition to requiring costly and specially made tools, requires an interventionalist to frequently enter and exit the procedure room and a patient to be moved in and out of the gantry during procedures thus resulting in near time rather than real time imaging. Computerized tomography (CT) is also similarly limited by physical limitations of entering and exiting the procedure suite and sliding the patient on the gantry. While CT fluoroscopy shortens the time between intervention and imaging, real time acquisition is still not achieved and intra-procedural radiation exposure is increased to the interventionalist. Fluoroscopic imaging allows for real time imaging, although anatomic contours can only be identified transiently and after administration of contrast media. In addition, fluoroscopy is associated with escalating doses of radiation, though less than what is seen in CT guided procedures. In contrast, ultrasound (US) allows real time imaging of dynamic anatomy without ionizing radiation and with the use of equipment that does not require any additional specifications beyond sterility and utility.

The mechanism of image acquisition also favorably distinguishes sonography from other imaging modalities. The use of high frequency sound waves carries a significantly lower risk of short- and long-term adverse effects on patients than ionizing radiation. There is a negligible risk of inadvertent acoustic cavitation (the creation of damaging shear waves), from diagnostic sonography as well as a near negligible possibility of thermal injury from energy transfer from the high frequency sonographic waves [1]. In contrast, with ionizing radiation, metrics measuring ionizing radiation exposure such as total cumulative patient dose, dose area product and skin dose must be monitored. In the short-term, radiation burns can occur from excess exposure during fluoroscopic or CT procedures, with a theoretical long-term risk for neoplasia from repeated or high dose exposures. Magnetic resonance imaging also portends risks of periprocedural thermal burns and hearing damage that are obviated in sonographic procedures.

2 Tools

There are three major categories of equipment required to perform sonographically guided interventional procedures: an US machine, sterile drapes, and procedure specific instruments.

I. Ultrasound machine

The US machine consists of hardware and software components, both of which are imperative to understand before performing the intervention. The hardware consists of a piezoelectric crystal embedded within a probe that serves as an emitter and receiver of sonographic waves, as well as a monitor. The probe can vary both in regard to its physical shape (e.g. linear, curved, etc.) and frequency. Probe selection is critical in acquiring satisfactory images for interventions and is predominantly dependent on the body surface contour as well as the desired depth for imaging focus or intervention. Given the small caliber of instruments used in interventional

---

J. Raja (✉) · I. Latich · M. Mathur
Department of Radiology and Biomedical Imaging,
Yale School of Medicine, New Haven, CT, USA
e-mail: Junaid.Raja@yale.edu; Igor.Latich@yale.edu;
Mahan.Mathur@yale.edu

© Springer Nature Switzerland AG 2021
J. Li et al. (eds.), *Ultrasound Fundamentals*, https://doi.org/10.1007/978-3-030-46839-2_29

radiology procedures (typically sub-millimeter in diameter) and the superior spatial resolution of high frequency sonography, it is generally preferred to use the highest frequency probe possible to image the target of intervention. The software components can be used to further refine the images during the procedure. This includes zooming to limit the field of view to the relevant anatomy, contrast to enhance the distinction between the targeted tissue and its surroundings, color Doppler to assess for target and surrounding vascularity, and focus to allow further delineation of the target relative to the surrounding tissue.

II. Sterility

The issue of sterility is paramount in US guided interventions. Special probe and machine covers exist to ensure that the proceduralist is able to use image guidance and make any requisite image processing modifications without increasing the risk of infection. Certain operators opt to disinfect the US probe prior to the start of each procedure in lieu of employing plastic covers. This approach is less common and generally deemed disadvantageous in preserving the longevity of equipment. Standard pre-procedural precautions are always performed, including cleaning and disinfecting the skin as well as draping adjacent anatomy to protect the integrity of the sterile field. The sterile field must be broad enough so that if there is respiratory artifact, patient motion, or the initial site of intervention is inadequate, a nearby site may be used without having to create another sterile field.

III. Instrumentation

The instrumentation used for each procedure may vary slightly. In interventional radiology (IR), the three major categories of equipment used include sharps, wires, and catheters [3].

(i) Sharps:

Sharps generally include hollowed bored metal such as needles and trocars, and solid metal probes as used in thermal ablations (Fig. 1). The tips of the needle system can differ slightly: single wall, biopsy, Chiba, and spinal needles are beveled which allows for steering towards or away from structures, while trocars have a three-sided contour that does not allow for steering. In addition, the Chiba, spinal, and trocar systems differ from a single wall needle as they contain a stylet to occlude the hollow bore lumen until satisfactory positioning is obtained. Biopsy needle systems have a unique stylet/needle mechanism in that the stylet tip is a solid beveled needle with a carriage along its distal aspect. When extended, this allows a tissue core to fill the carriage and when the spring-loaded mechanism is deployed, the cutting action of the needle sheath covers the "stylet" and acquires a tissue sample. Chiba and spinal needles differ primarily in length and tensile strength. Ablation probes also vary in shape based

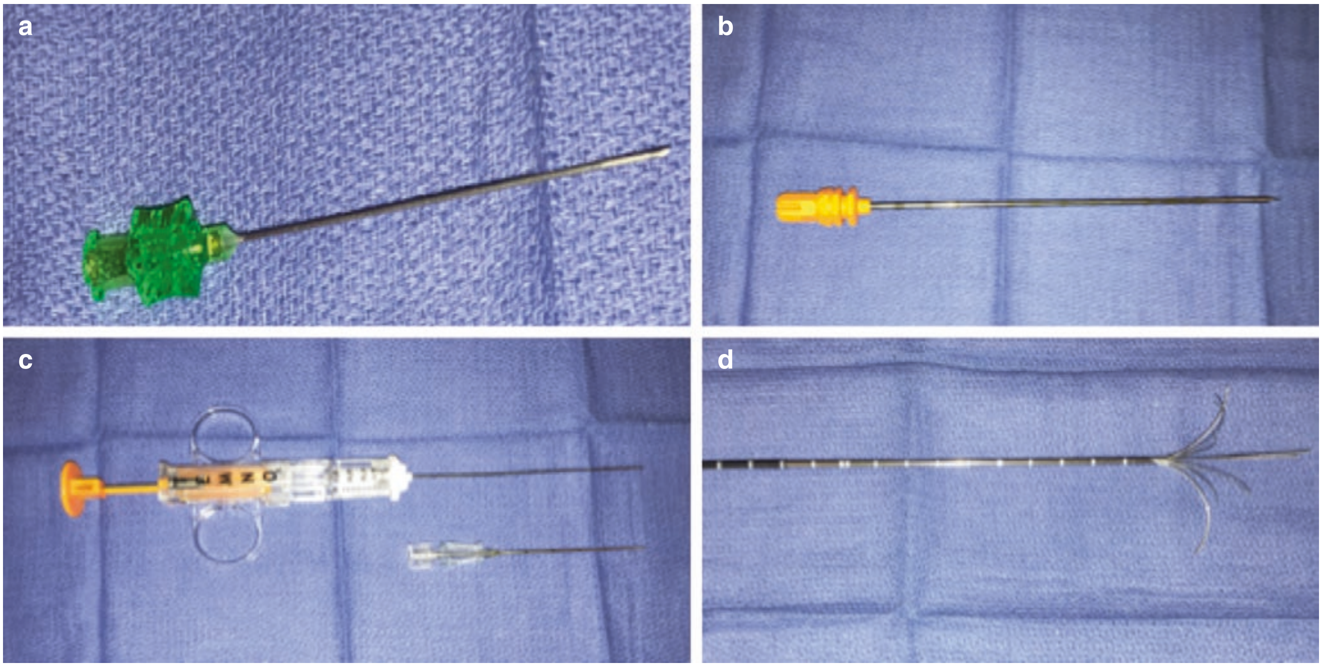

Fig. 1 Needles and ablation probes. Figure (**a**) demonstrates a 21 gauge needle as part of a micropuncture access set. Figure (**b**) demonstrates a 17 gauge trocar needle. Figure (**c**) demonstrates an adjustable Coaxial Temno™ Biopsy Device (Top – 18 gauge biopsy needle; bottom – 17 gauge guiding cannula). Figure (**d**) demonstrates a radiofrequency ablation probe

on the platform and manufacturer. The diameter of needles used for most interventional procedures generally ranges from 24 G to 16 G (0.02–0.05 inches) with choice of size dependent primarily on the clinical indication, size, and contour of the target as well as proximity to high risk structures. The diameter of probes used for ablative procedures is typically dependent on the ablation technique intended (e.g. cryotherapy, microwave ablation, radiofrequency ablation) but is also generally of a similar caliber (20 G to 16 G; 0.03–0.05 inches).

(ii) Wires:

The use of wires in US guided procedures is critical as they provide a general guide and roadmap for the procedure and are used as the intermediary between sharp hollow metal (the needles) and flexible hollow plastic (the catheters). Wires can be hydrophilic ("water loving") or hydrophobic ("water fearing"), have a stiff or floppy tip, have a straight, angled, or curved distal contour, and can vary in their length and caliber (generally 0.018 inches or 0.035 inches) (Fig. 2). Stiff guidewires are frequently used to provide support for catheter placement and perform balloon dilatation, while hydrophilic wires are used to cross stenotic lesions or traverse tortuous structures (e.g. placement of a nephroureteral or biliary tube/stent). Determination of whether to use straight, angled, or curved tipped wire is dependent on the contour of the structure in which the wire is being placed. Lastly, the determination of wire size and caliber also depends on the size and amount of anatomy to be traversed, the caliber of the needle system used and intended catheter to be used.

(iii) Catheters:

Catheters in US guided procedures serve as conduits between the skin and a targeted cavity. In general, there are two types of catheters: guiding catheters that are used to gain access into a structure and drainage catheters. Guiding catheters are seldom navigated under ultrasound guidance and are thus outside the scope of this chapter. A drainage catheter is a hollow plastic tube, which can vary in stiffness, shape of the distal end (pigtail, straight, star), and size (Fig. 3). Choice of catheter is predicated upon the clinical indication, structure or organ to be accesses, density of fluid to be drained, patient comfort considerations, and many others.

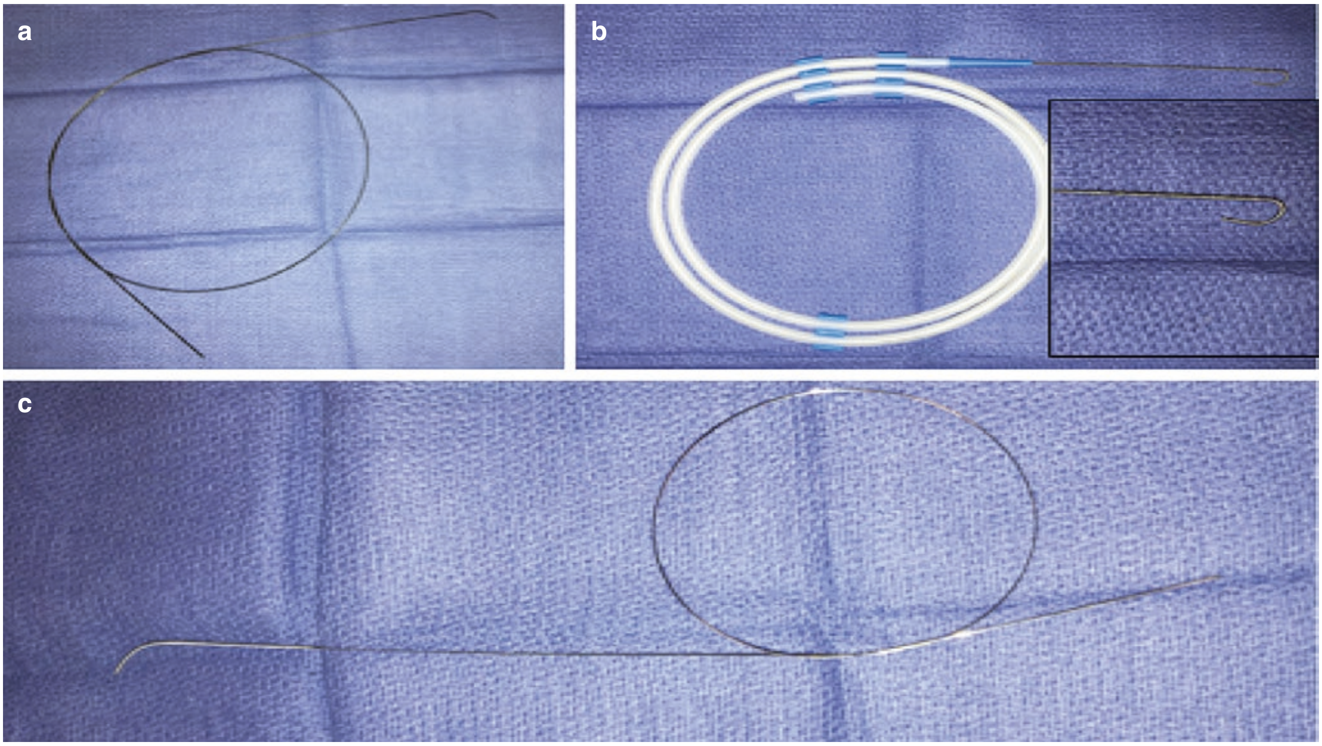

Fig. 2 Wires. Figure (**a**) demonstrates a 0.035 inch Glidewire. Figure (**b**) demonstrates a 0.035 inch J-tipped Glidewire (with inset showcasing the distal "J" shaped tip). Figure (**c**) demonstrates a 0.018 inch wire

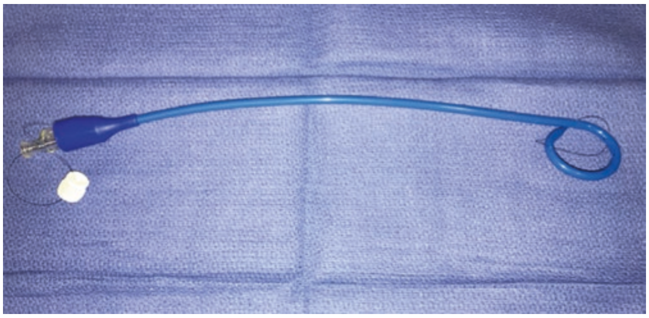

Fig. 3 Example of a drainage catheter. A drainage catheter is a hollow plastic tube, which can vary in stiffness, shape of the distal end and size. The following figure demonstrates an 8 Fr locking loop ("pigtail") drainage catheter

3 Tasks

The specific interventional procedures that may be performed under sonographic guidance are broad in scope and are continuously increasing and evolving. Common procedures include biopsies, drainages, sclerotherapy, nerve blocks, musculoskeletal interventions, ablations, and high intensity focused ultrasound, among many others. To optimize an ultrasound-guided procedure, one has to consider distance to the lesion, availability of an appropriate acoustic window and presence of any critical intervening structures. Patient cooperation is important in many interventional procedures This is particularly in the case of ultrasonography where optimal imaging windows may require that patients follow directions, such as breath-holding, which allows for improved visualization of structures whose real time position may be subject to motion (liver, kidneys) Body habitus may limit some US guided interventions. Presence of gas within or superficial to a target may also make it difficult to resolve the structure adequately, which in turn may necessitate CT guidance.

(i) Biopsy

Biopsies are amongst the most commonly performed US-guided interventional procedures and consist of tissue sampling for pathologic analysis. With the exception of lung, bone, and brain biopsies, US is the first line modality of choice for biopsy when feasible. Common indications include masses or dystrophic calcifications within the breast, thyroid, liver, or kidney, or enlarged lymph nodes (Fig. 4). If the target structure contains liquid or is viscous, aspiration is generally performed in which a small caliber single wall sheathed Chiba needle is introduced percutaneously under sonographic observation and a sample is aspirated via a syringe. There are two main approaches to obtaining a core needle biopsy: coaxial and non-coaxial A coaxial system is frequently preferred with larger targets such as the breast, liver, and kidney where multiple samples are required. In this setting, a hollow bore guiding needle is placed under US guidance into the target. Thereafter a biopsy needle replaces the stylet within the guiding needle and is deployed under sonographic observation to ensure the needle tip remains within the target for both adequacy of sampling and safety. An advantage of the coaxial system is that the guiding needle is kept just proximal to or within the lesion while the biopsy needle is used to make multiple passes to acquire the required number of samples. This minimizes potential laceration to intervening tissues and can significantly decrease procedure time.

In a non-coaxial system, the biopsy needle is passed directly ("bareback") into the target. This may be desirable when a lesion is superficial and there is insufficient tissue to anchor a guiding needle. An alternative to core needle biopsy is fine needle aspiration. Passes may be performed with a single wall needle under image guidance directly into the structure of interest. The to and fro manipulation of the needle allows the hollow bevel to collect the target tissue. This approach is frequently seen with thyroid nodules and lymph nodes that may be too small for targeting by a core needle system [4]. In general, the acquired tissue within the biopsy needle is then handed off to a cytopathologist who ensures adequacy of the collected sample prior to terminating the procedure. A limitation of the aspiration technique is that it disrupts tissue architecture and so frequently a core biopsy technique is preferred. Additional US biopsy techniques used in conjunction with direct scope visualization also exist (e.g. endovascular, endobronchial, endoscopic, and hysteroscopic), but are beyond the scope of this chapter.

(ii) Drainage:

Drainage is another common US guided intervention, which, as the name implies, consists of percutaneous evacuation of a (usually liquid containing) cavity. For collections containing simple fluid (seroma, for instance), a simple aspiration may be sufficient. For evacuation of larger collections or those containing viscous or frankly infected fluid drainage may be performed with the aid of a catheter. In this approach, sonographic guidance is used to advance a needle for the Seldinger technique by which a satisfactorily sized needle (single wall, Chiba, sheathed or trocar) into the collection (Fig. 5). A wire is passed through the needle into the collection with continuous sonographic imaging. In general, a stiff wire with a floppy tip is used and

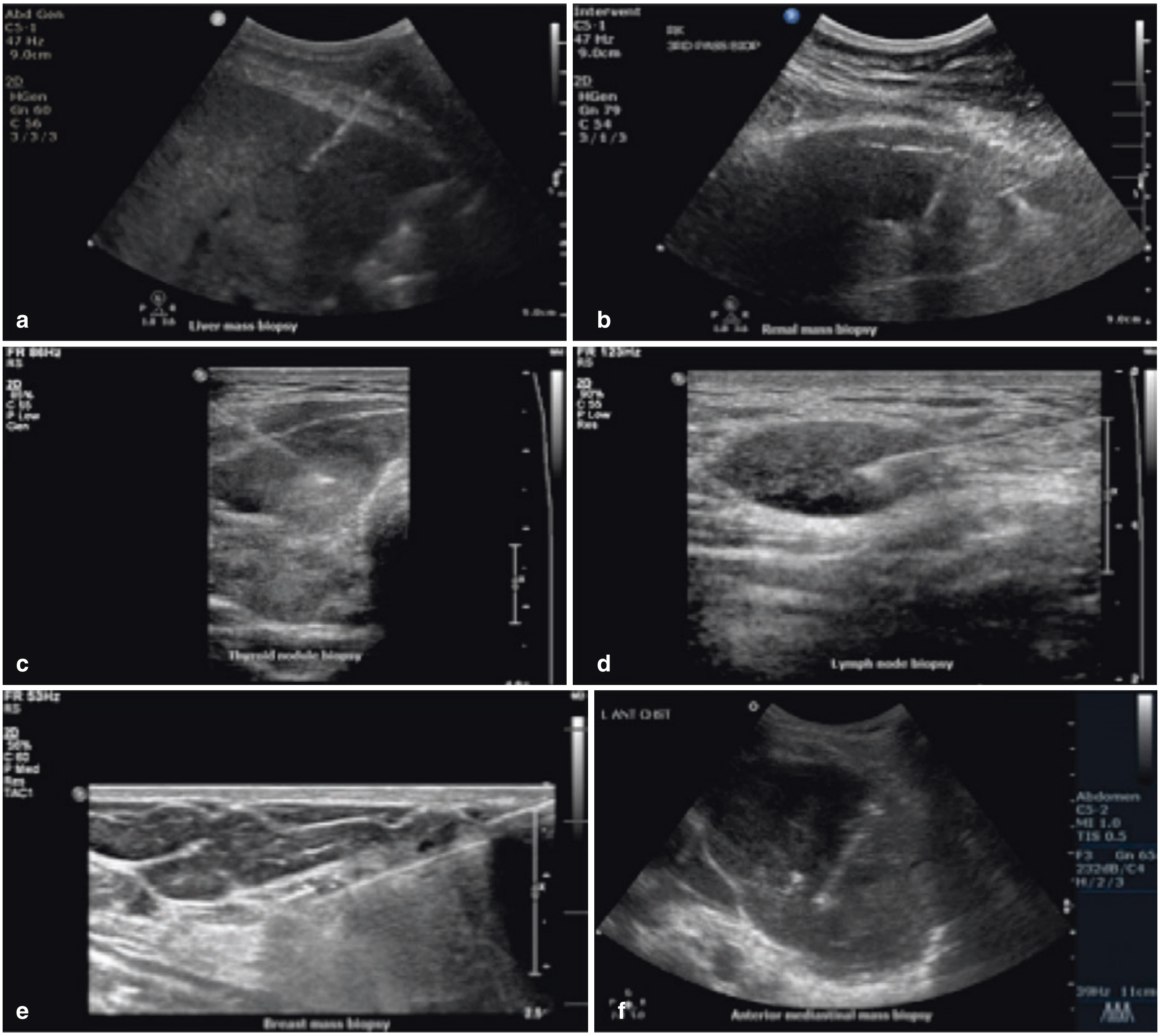
a
Liver mass biopsy
b
Renal mass biopsy
c
Thyroid nodule biopsy
d
Lymph node biopsy
e
Breast mass biopsy
L ANT CHEST
f
Anterior mediastinal mass biopsy

Fig. 4 Needle biopsy. Multiple gray-scale images demonstrate needle biopsy of several organ systems including liver (**a**), kidney (**b**) thyroid nodule (**c**), lymph node (**d**) breast mass (**e**) and anterior mediastinal mass (**f**)

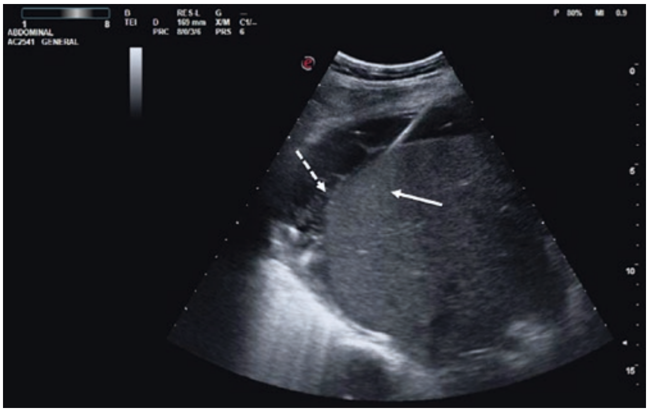

Fig. 5 Drainage. Gray-scale image of the right upper quadrant demonstrates the presence of a needle tip (solid arrow) within a complex hypoechoic perihepatic collection which contains multiple internal septations (dashed arrow)

enough wire looped within the cavity to decrease the risk of inadvertent dislodgement during subsequent manipulation. Next, a dermatotomy is made at the needle entry site and the needle is exchanged over the wire for a rigid dilator to create a subcutaneous tract. The desired catheter then replaces the dilator and is advanced to ensure all side holes on the catheter are within the collection. The wire is then removed and the distal tip of the catheter is generally secured by use of a loop forming mechanism to ensure that the catheter remains in position. Finally, catheter placement and function is confirmed both by aspiration through the catheter as well as by sonography. The more proximal portion of the catheter is then tethered to the skin via a suture and covered with a sterile dressing usually consisting of gauze and an adhesive film or tape.

(iii) Sclerotherapy

Sclerotherapy is another procedure that may be performed with sonographic guidance. The concept of sclerotherapy consists of thermally or chemically obliterating a fluid containing cavity, dilated vein, or vascular malformation. Common indications include acceleration resolution of a fluid-filled cavity causing discomfort or at risk for infection (e.g. a post surgical seroma), preventing dermal complications of vascular stasis in superficial vessels (e.g. venous varicosities), and treating painful malformations and cosmesis [5, 6]. In contrast to simple drainage, a small quantity of a sclerosant such as sodium tetradecol sulfate, polidocanol, hypertonic saline, or ethanol is injected to chemically induce the serosal lining to irreversibly bind to itself and obliterate the cavity (Fig. 6). In vascular sclerotherapy, sonographic imaging is used to place a Chiba or single wall needle into the targeted vessel of interest. Once adequate placement is confirmed a dilute sclerosant is instilled to gradually induce apposition and fusion of the vessel walls. A portion of the injected sclerosant is carried antegrade through the venous system; however, given the valvular incompetence that underlies venous varicosities, a portion remains static or near static in the targeted vessel area of the blood pool [7]. This approach can also be used in the treatment of lymphangitic and vascular malformations [8]. Additionally, thrombin injections to treat large, enlarging or painful pseudoaneurysms can also be performed sonographically. This involves instilling small aliquots of thrombin in the pseudoaneurysm under continuous US guidance (usually color Doppler) to promote clotting of the defect [9].

(iv) Thrombectomy

Thrombectomy is a newer but important procedure that can be performed with sonographic guidance. Real-time sonography provides an essential role in diagnosing an occlusion and ensuring adequacy of the procedure with restoration of flow afterwards. This procedure is most frequently performed in patients on dialysis with clotted fistulas or grafts or in patients with a deep venous thrombosis [10, 11]. Following sterilization and local anesthesia, US guidance is used to cannulate the thrombosed vessel usually from either the antegrade or retrograde approach depending operator preference [12, 13]. Thereafter, if mechanical thrombectomy is desired, a wire or catheter exchange is then performed and advanced under ultrasound visualization. Serial passes are performed to retract the clot and optimize patency of the target vessel. If pharmacologic thrombolysis is preferred, a wire exchange is performed and an appropriately sized catheter is positioned with US confirmation in close proximity to the thrombus. Subsequently, a thrombolysis agent such as tissue plasminogen activator (tPA), urokinase, or streptokinase is slowly infused with periodic or continuous sonographic observation as the thrombus slowly disintegrates [14, 15]. Once color and spectral Doppler imaging confirms adequate flow within the newly patent vessel, the infusion catheter is removed and the site is cleaned and dressed.

(v) Nerve blocks

Nerve blocks are another procedure that can be performed under US guidance. Following sterilization and local anesthesia, a Chiba or spinal needle is advanced under real time sonographic imaging in close proximity to a nerve or plexus (intercostal, brachial plexus, femoral, etc.) or into the epidural space as clinically indicated (Fig. 7). Once placement is confirmed either by sonography or flow of cerebrospinal fluid on removal of the stylet, instillation of an anes-

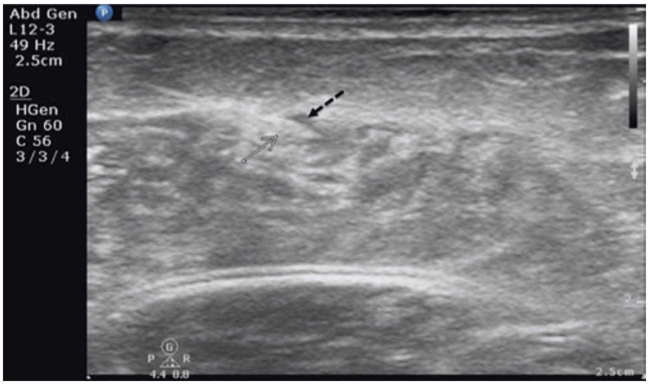

Fig. 6 Sclerotherapy. Gray-scale image of the right lower extremity demonstrates the presence of a sclerotherapy needle (solid arrow) within a venous varicosity (dashed arrow)

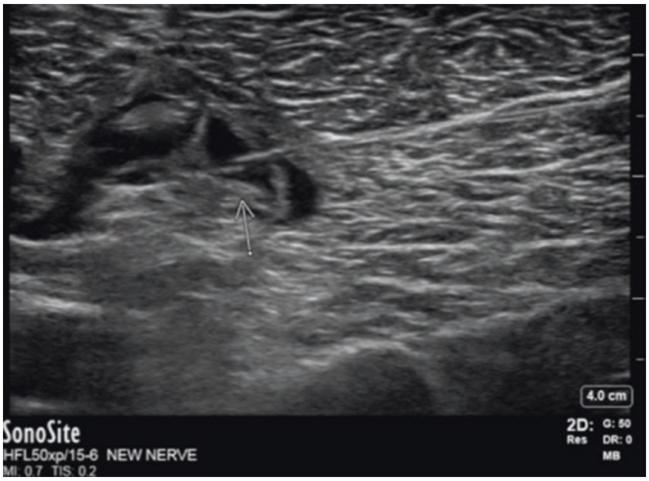

Fig. 7 Nerve block. Gray-scale image of the left lower extremity demonstrates the distal tip of a needle (arrow) within the saphenous nerve

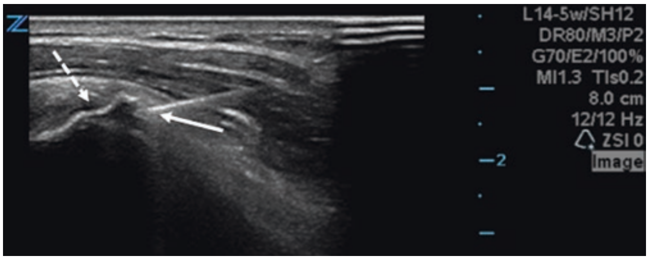

Fig. 8 Musculoskeletal intervention (steroid injection): Gray-scale image of the right upper extremity demonstrates the presence of the needle tip (solid arrow) in the biceps tendon sheath, with an adjacent calcification (dashed arrow)

thetic is then performed. In the case of a local nerve block, real-time ultrasonography can also visually demonstrate the volume of anesthetic instilled by showcasing the adjacent tissue displacement [16].

(vi) Musculoskeletal interventions

Various musculoskeletal interventions also use sonographic guidance. These include arthrocentesis and joint injections that essentially use the technique of fine needle aspiration to access an anatomic fluid filled cavity (that is, the joint space). Once the joint is accessed, a joint injection procedure would require instillation of steroids or other anesthetics. Similarly, sonographic guidance can be used for injecting tendinous pathology, such as tenosynovitis and de Quervin's tendonitis, with steroids using principles similar to nerve blocks into the peri-tendinous soft tissue (Fig. 8) [17, 18].

(vii) Oncotherapy

One of the most rapidly evolving areas in interventional radiology is oncotherapy. Thermal, chemical and electric ablation procedures can use sonography for guidance of the probe into the target as well as real-time monitoring of the procedure and to exclude related post procedural complications. Ablation techniques include cryoablation, in which profound hypothermia is induced via helium argon gas to "freeze" a mass, microwave and radiofrequency ablation, in which electromagnetic radiation is converted to thermal energy to induce necrosis and "burn" a mass, ethanol ablation, in which an appropriate amount of 98% ethanol is injected under US guidance directly into a lesion and irreversible electroporation, in which an electric current is used to induce apoptosis [19, 20]. In each of these procedures, the overlying skin is sterilized and anesthetized and a small dermatotomy is made before the probe tip is guided under US visualization to the target area (Fig. 9). Real time US observation can be performed during the course of the ablation procedure to monitor the change of surrounding tissue characteristics in the ablation zone.

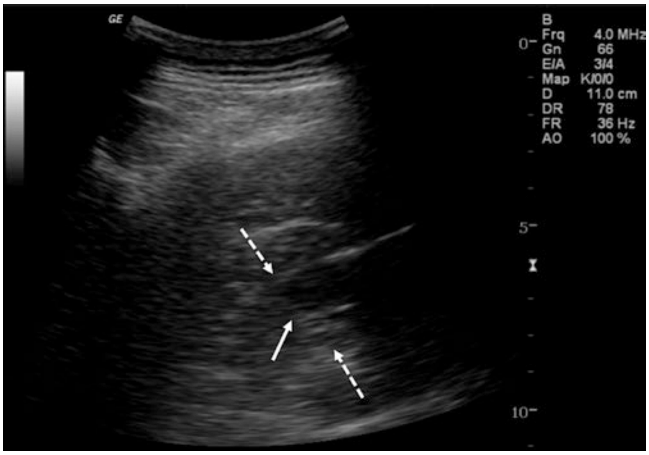

Fig. 9 Oncotherapy (radiofrequency ablation): Gray-scale image of the right kidney demonstrates the presence of a radiofrequency ablation probe (arrow) within a hypoechoic interpolar right renal mass (dashed arrows)

(viii) High intensity focused ultrasound

Lastly, US itself can be used as an interventional technique. High intensity focused ultrasound (HIFU) is a technique in which alternating high frequency is transmitted to induce acoustic cavitation for the purpose of destroying a target lesion or mass [21, 22]. This technique involves using conventional diagnostic US to localize the target tissue and then using a high intensity sonographic probe to deliver therapeutic waves to the target [23].

4 Pearls and Pitfalls

The use of sonography for interventional procedures requires understanding of several technical factors. These include optimization of sound waves for imaging, effects of pressure on tissue displacement, and the role of coupling agents to improve contact and transmission of sonographic waves. The use of color and spectral Doppler imaging can help distinguish blood vessels from nonvascular structures, differentiate fluid from solid masses, and can discriminate arterial and venous flow (Fig. 10). This principle can be useful, particularly when accessing biliary ducts or urinary structures percutaneously [24–26]. In addition, color Doppler, by use of twinkle artifact, can help identify calculi and can facilitate the identification of a needle or probe tip [27].

An essential technique for US guided intervention, both to improve safety and efficacy, is imaging within the long axis plane for the needle or probe (Fig. 11). When imaging along the long axis, both the needle tip and the immediate trajectory can be visualized. Projecting the trajectory allows the proceduralist to adjust needle position and minimize the risk of injury to nearby structures such as adjacent vasculature, nerve, pleura, or bowel.

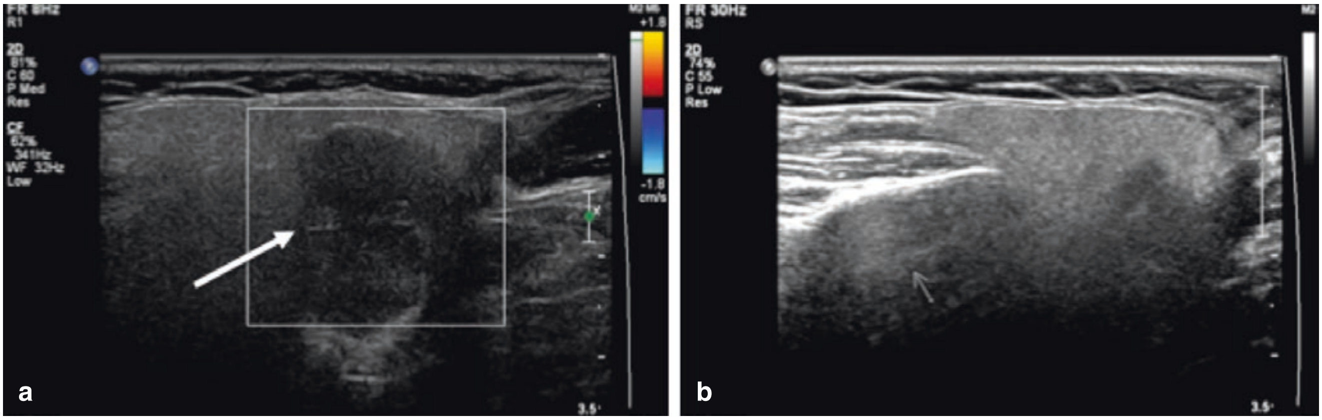

Fig. 10 Use of color Doppler imaging in interventional procedures. Pre-procedural color Doppler image (**a**) demonstrates the presence of a hypoechoic mass (arrow) without internal vascularity in the right parotid gland. The lack of detectable color flow suggests that the mass contains fluid. Gray-scale image performed during aspiration (**b**) demonstrates needle tip within the collection (arrow) with cytology revealing the presence of an abscess

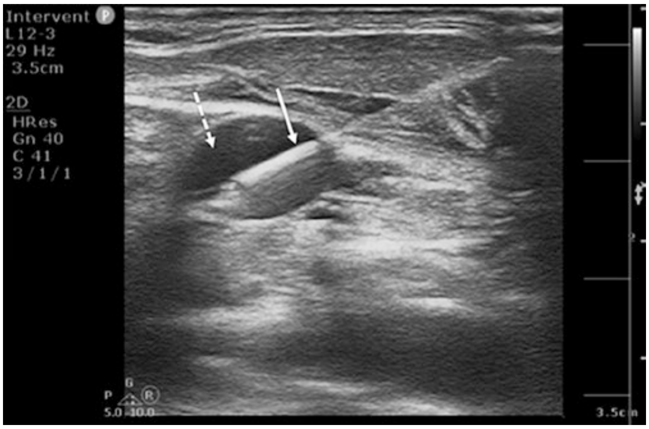

Fig. 11 Gray-scale image demonstrates the long axis view of a needle (solid arrow) used to obtain access for a central venous catheter (dashed arrow)

Limiting the introduction of air into the field of imaging is integral for safely and effectively performing sonographically guided procedures, which can happen particularly during coaxial biopsies. Air is usually introduced during exchanges of the guiding needle stylet for the biopsy needle and vice versa. If air is introduced into the target, definitive visualization of the needle tip is obscured which can compromise safety, and the likelihood of obtaining an adequate tissue sample may be diminished (e.g. if the trajectory is not altered to obtain additional tissue). One strategy to minimize this effect is to drip a small quantity of saline into the guiding needle hub and form a water seal within the guiding needle to prevent entry of air.

Naturally, just as there are techniques for optimizing imaging, there are also pitfalls to avoid during US guided interventions, the largest category of which includes artifacts. Although some artifacts can be helpful (e.g. twinkle artifact), others can lead to misinterpretation of the visualized tissue. These artifacts are more comprehensively described elsewhere in this book and can include tissue vibration and blooming artifacts that can overestimate vascularity, beam width and slide lobe artifacts that can either misinterpret non-focal zone echoes or echoes from outside of the main beam as within the structure of interest, and refraction, multipath, and speed displacement artifacts that can lead to the misinterpretation of the geospatial position and/or depth of a target of interest.

Finally, one of the biggest pitfalls in sonographic-guided interventions is the limitations of sonography itself. For example, US is best utilized for superficial to intermediate depth imaging with diminished image quality at greater depths. Consequently, US guided pelvic abscess drainage may be feasible in a pediatric patient with a small body size and habitus, whereas a similar procedure in an obese adult may be technically infeasible due to lack of contrast resolution at the targeted depth of intervention. Ultrasound is also limited in procedures that involve gas-containing structures. The most typical interventions in which this becomes a prohibitive concern generally involve intra-abdominal procedures for which gas filled loops of bowel may be interposed with the anatomy or pathology of interest preventing localization of depth or span by sonography. This can also become an issue in the setting of necrotic or gangrenous masses, which does not inherently exclude the ability to perform sonographic guided interventions, though does limit the confidence and comfort with which adequacy of the intervention performed is achieved.

5 Future Directions

Sonographically guided interventions, like many other aspects of US, are more widely utilized in European and other international healthcare settings than in the United States, however, these trends are changing. The benefit of improved US technology and resolution in performing real-time interventions without ionizing radiation, in a relatively portable setting, and at a cheaper cost to other cross-sectional guided interventions is leading to more widespread adoption of sonographic-guided interventional procedures. Moreover, there is tremendous interest in expanding the horizon for the types of procedures that can be performed with US guidance and optimization for effective interventions.

An area in which research is already in progress includes contrast-enhanced US biopsies. The benefit of contrast enhancement includes improving the resolution for poorly visualized or isoechoic masses in order to target structures that were not previously visible (e.g. isoechoic hepatocellular carcinoma) or to more sharply define therapeutic margins (e.g. demarcating ablation zone in treating malignancies) [28–30]. Multi-dimensional reconstructions are another potentially revolutionary technique in which there is evolving research, allowing the proceduralist to image and negotiate a needle or probe beyond a single plane [31]. Ultrasound directed percutaneous arteriovenous dialysis fistula formation is another exciting cutting edge sonographic procedure on the horizon.

6 Conclusion

There is an ever expansive and evolving role for sonography in image guided procedures. The ability to perform real-time, ionizing radiation free, inexpensive, and high-resolution imaging facilitates the safe and effective performance of a diverse multitude of procedures as has been described. Moreover, renewed interest for innovation to refine current techniques and to create new applications accentuates the flexibility and agility of sonography. It is imperative that proceduralists are able to confidently use US imaging to guide their procedures as multiple disciplines including interventional radiology, critical care, anesthesiology, emergency medicine, cardiology, and vascular surgery now routinely use US for image guided procedures in both hospital and outpatient settings.

References

1. Holm HH, Skjoldbye B. Interventional ultrasound. Ultrasound Med Biol. 1996;22(7):773–89.
2. Nicolaou S, et al. Ultrasound-guided interventional radiology in critical care. Crit Care Med. 2007;35(5):S186–97.
3. Northcutt BG, et al. Wires, catheters, and more: a primer for residents and fellows entering interventional radiology. Radiographics: a review publication of the Radiological Society of North America, Inc. 2015;35(5):1621–2.
4. CARMECI C, et al. Ultrasound-guided fine-needle aspiration biopsy of thyroid masses. Thyroid. 1998;8(4):283–9.
5. Darvall KAL, et al. Recovery after ultrasound-guided foam sclerotherapy compared with conventional surgery for varicose veins. BJS. 2009;96(11):1262–7.
6. Zuckerman D, Yeager T. Percutaneous ethanol sclerotherapy of postoperative lymphoceles. AJR Am J Roentgenol. 1997;169(2):433–7.
7. Smith PC. Chronic venous disease treated by ultrasound guided foam sclerotherapy. Eur J Vasc Endovasc Surg. 2006;32(5):577–83.
8. Blaise S, et al. Treatment of low-flow vascular malformations by ultrasound-guided sclerotherapy with polidocanol foam: 24 cases and literature review. Eur J Vasc Endovasc Surg. 2011;41(3):412–7.
9. Sackett WR, et al. Ultrasound-guided thrombin injection of iatrogenic femoral pseudoaneurysms: a prospective analysis. Am Surg. 2000;66(10):937.
10. Ascher E, Hingorani A, Marks N. Duplex-guided balloon angioplasty of failing or nonmaturing arterio-venous fistulae for hemodialysis: a new office-based procedure. J Vasc Surg. 2009;50(3):594–9.
11. Shenoy S, Darcy M. Ultrasound as a tool for preoperative planning, monitoring, and interventions in dialysis arteriovenous access. Am J Roentgenol. 2013;201(4):W539–43.
12. Egan G, et al. Ultrasound guidance for difficult peripheral venous access: systematic review and meta-analysis. Emerg Med J. 2013;30(7):521–6.
13. Lu M, et al. Ultrasound-guided pharmacomechanical thrombolysis and angioplasty for treatment of acute thrombotic prosthetic arteriovenous access: 5-year experience with 154 procedures in a single center. Ultrasound Med Biol. 2018;44(11):2314–22.
14. García-Medina J. Value of duplex ultrasound assistance for thromboaspiration and dilation of thrombosed native arterio-venous fistulae. Cardiovasc Intervent Radiol. 2013;36(6):1658–63.
15. Huang H-L, et al. Combination of duplex ultrasound-guided manual declotting and percutaneous transluminal angioplasty in thrombosed native dialysis fistulas. Ren Fail. 2005;27(6):713–9.
16. Liu SS, Ngeow JE, YaDeau JT. Ultrasound-guided regional anesthesia and analgesia: a qualitative systematic review. Reg Anesth Pain Med. 2009;34(1):47–59.
17. Kumbhare D, et al. Ultrasound-guided interventional procedures: myofascial trigger points with structured literature review. Reg Anesth Pain Med. 2017;42(3):407–12.
18. Louis LJ. Musculoskeletal ultrasound intervention: principles and advances. Radiol Clin N Am. 2008;46(3):515–33.
19. Lanza E, et al. Percutaneous image-guided cryoablation of breast cancer: a systematic review. J Vasc Interv Radiol. 2015;26(11):1652–1657. e1.
20. Rossi S, Fornari F, Buscarini L. Percutaneous ultrasound-guided radiofrequency electrocautery for the treatment of small hepatocellular carcinoma. J Interven Radiol. 1993;8(3):97–103.
21. Chaussy CG, Thüroff S. High-intensity focused ultrasound for the treatment of prostate cancer: a review. J Endourol. 2017;31(S1):S-30–7.
22. Wu F, et al. Extracorporeal focused ultrasound surgery for treatment of human solid carcinomas: early Chinese clinical experience. Ultrasound Med Biol. 2004;30(2):245–60.
23. Evans KD, Weiss B, Knopp M. High-Intensity Focused Ultrasound (HIFU) for specific therapeutic treatments: a literature review. J Diagn Med Sonograph. 2007;23(6):319–27.
24. Park BK. Ultrasound-guided genitourinary interventions: principles and techniques. Ultrasonography. 2017;36(4):336.
25. Stables DP, Ginsberg NJ, Johnson ML. Percutaneous nephrostomy: a series and review of the literature. Am J Roentgenol. 1978;130(1):75–82.
26. Teplick SK, et al. Percutaneous interventional gallbladder procedures: personal experience and literature review. Gastrointest Radiol. 1990;15(1):133–6.
27. Longo JM, et al. Percutaneous vascular and nonvascular puncture under US guidance: role of color Doppler imaging. Radiographics. 1994;14(5):959–72.

28. Gérard M, et al. Visualization of hepatic arteries with 3D ultrasound during intra-arterial therapies. In: Medical imaging 2016: image-guided procedures, robotic interventions, and modeling: International Society for Optics and Photonics; 2016.
29. Gummadi S, Eisenbrey JR, Lyshchik A. Contrast-enhanced ultrasonography in interventional oncology. Abdom Radiol. 2018;43(11):3166–75.
30. Nolsøe CP, et al. Use of ultrasound contrast agents in relation to percutaneous interventional procedures: a systematic review and pictorial essay. J Ultrasound Med. 2018;37(6):1305–24.
31. Arif M, Moelker A, van Walsum T. Needle tip visibility in 3D ultrasound images. Cardiovasc Intervent Radiol. 2018; 41(1):145–52.

Ultrasound Application in Dermatologic Conditions

Chang Ye Wang, Kavita Darji, Felipe Aluja Jaramillo,
Ximena Wortsman, and A. Mary Guo

1 Introduction

The diagnosis of dermatologic disorders can often be made with the unaided eye; however, the clinical examination does not provide reliable visualization of deeper cutaneous structures. In cases where the diagnosis cannot be ascertained from visual inspection, a skin biopsy is traditionally performed to provide *ex vivo* histologic clues. More recently, polarized dermoscopy has become a common bedside aid for the visualization of skin structures below the 0.06–0.10 mm depth required for photon depolarization [1]. Nevertheless, depth is an important measure that cannot be readily perceived on direct visualization or dermoscopy.

On the other hand, ultrasonography (U/S) easily captures depth and often penetrates much deeper. With a high-frequency U/S probe working at 50 MHz, *in vivo* tissues located up to 8–9 mm depth can be visualized with an axial resolution of 0.05 mm [2]; at 18 MHz, the penetration depth increases to 60 mm. Lower frequency probes can reach even deeper depths at the cost of resolution. Most modern U/S machines are equipped with variable frequency probes, and the operator can choose from a pre-defined range of frequencies to optimize the trade-off between penetration depth and resolution. Furthermore, U/S can visualize blood flow in real-time without the need of intravenous contrast. Due to its great portability and safety profile, U/S has broad clinical utility, and is widely available in both inpatient and outpatient settings to help with the diagnosis and management of dermatologic conditions [3].

With regards to its limitations, U/S cannot detect pigments such as melanin and has difficulty visualizing very small or epidermal-only lesions [3, 4]. Lesions smaller than 0.10 mm cannot be accurately discerned at 15–24 MHz, and lesions smaller than 0.05 mm cannot be accurately discerned at ≥50 MHz. For adequate diagnostic power, a high frequency probe ≥15 MHz and a trained operator are required, but this is no different from any other imaging modality. The literature on the use of ultrasonography in dermatology is growing, and peer-reviewed guidelines have recently become available [3]. American Institute of Ultrasound in Medicine (www.aium.org) and European Federation of Societies in Ultrasound in Medicine and Biology (www.efsumb.org) provide lectures and training courses during their annual meetings and throughout the year.

Other modern techniques such as confocal laser microscopy (CLM) and optical coherence tomography (OCT) may offer greater resolution but are often limited by their depth of penetration. CML is useful for the diagnosis of superficial pigmented lesions, but has poor penetration beyond 0.2 mm [5–7]. OCT is primarily useful for epithelial skin tumors with thickness ≤1.5 mm, such as actinic keratosis and superficial basal cell carcinoma [5, 8].

2 The Basics

2.1 Tools

For dermatologic conditions, a multichannel color Doppler U/S machine with variable-frequency transducer ≥15 MHz is recommended [9]. All U/S examinations should be performed in the following sequences in at least two perpendicular axes: initially in grayscale, then with color Doppler, and lastly with a spectral curve analysis of the regional vessels [9]. Lesional to perilesional comparisons may be helpful, and 3-D reconstruction is optional

C. Y. Wang · K. Darji · A. M. Guo (✉)
Department of Dermatology, Saint Louis University School of Medicine, St. Louis, MO, USA
e-mail: change.wang@health.slu.edu; kavita.darji@health.slu.edu; amary.guo@health.slu.edu

F. A. Jaramillo
Department of Radiology, Fundación Universitaria Sanitas, Country Scan, Bogotá, Colombia

X. Wortsman
Department of Dermatology, University of Chile and Pontifical Catholic University of Chile, Santiago, Chile

© Springer Nature Switzerland AG 2021
J. Li et al. (eds.), *Ultrasound Fundamentals*, https://doi.org/10.1007/978-3-030-46839-2_30

[10]. A copious amount of gel is recommended to allow easier adjustment of focal point and optimal visualization. The probe is positioned over the gel without compressing the skin. The fifth finger is often used to stabilize the hand and minimize the "floating" of the hand directly above the gel (Fig. 1).

2.2 Ultrasonography of the Normal Skin

The epidermis most often appears as a highly hyperechoic monolaminar layer due to its high keratin content, but on palmoplantar skin, it takes on a bilaminar appearance [9]. Below the very thin epidermis, the dermis appears as a thick moderately hyperechoic band due to its rich collagen content. In photoaged skin, echogenicity of the upper dermis is decreased due to glycosaminoglycan deposition [9]. Below the dermis, the hypodermis, also known as the subcutaneous tissue or the subcutis, contains hypoechoic fat lobules and hyperechoic fibrous septae (Fig. 2).

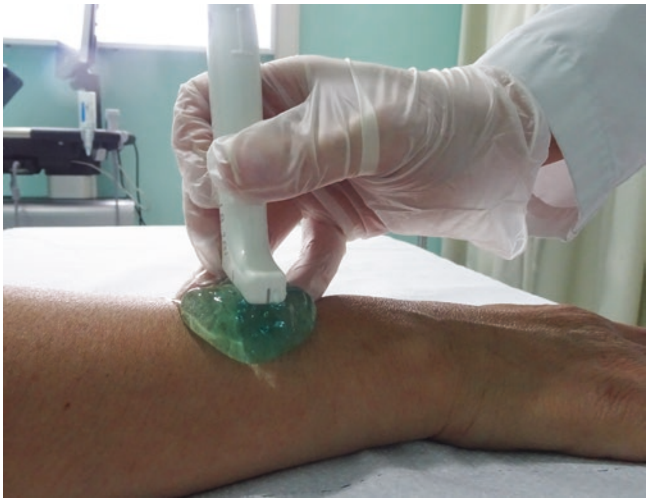

Fig. 1 Dermatologic ultrasound technique. Notice the copious amount of gel on top of the skin and the position of the little finger to stabilize the hand

Fig. 2 Normal skin at the dorsum of the forearm (transverse views). (**a**) Greyscale (color filter) and (**b**) Color Doppler

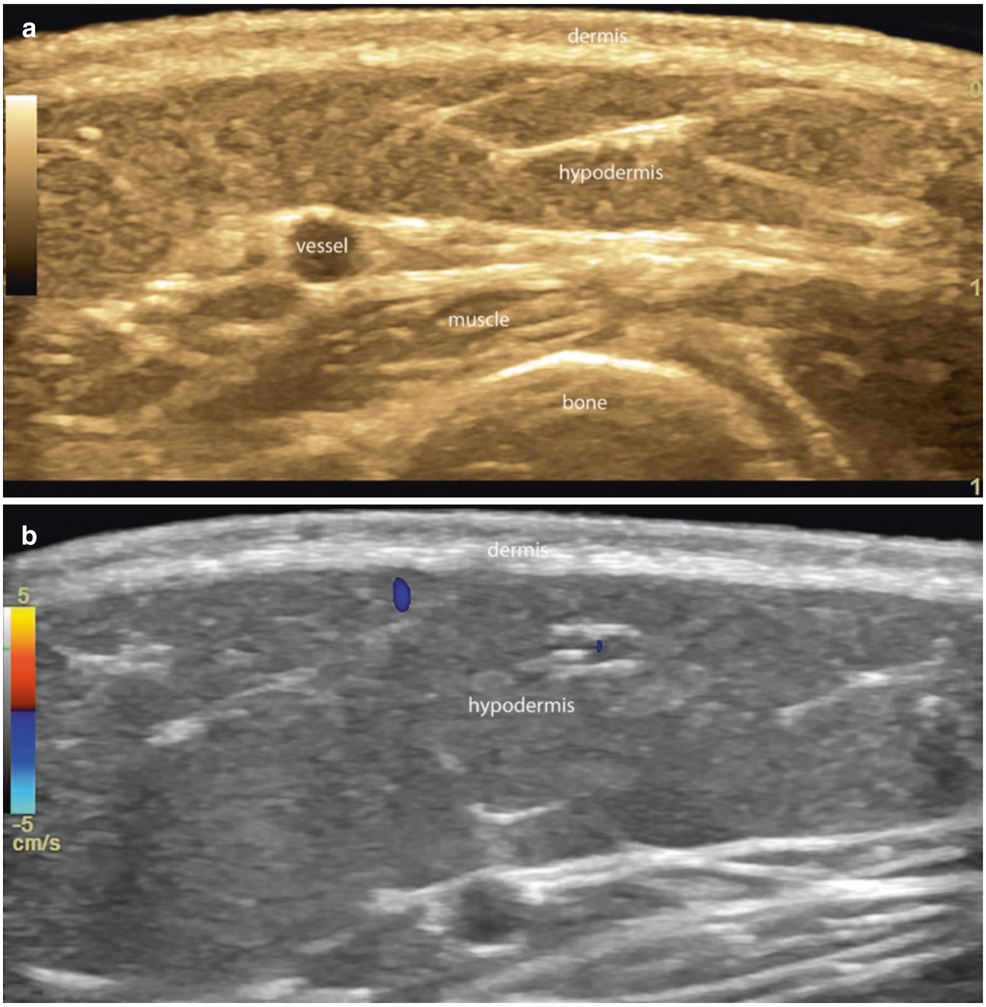

2.3 Ultrasonography of the Nail

The nail plate, the nail bed that contains the nail matrix, the hyponychium, and the nail folds compose the nail unit [11]. The nail plate appears as a 0.30–0.65 mm thick bilaminar structure [12], with two parallel hyperechoic lines representing the dorsal (external) and ventral (internal) plate [9]. The nail bed is a hypoechoic layer that extends from the ventral plate to the distal phalanx, which appears as a hyperechoic line [11]. In the nail bed, there are multiple low-flow arterial and venous vessels near the distal phalanx [13]. The nail matrix region is located in the proximal part of the nail bed [12]. The lateral and proximal nail folds lack any hypodermal adipose tissue (Fig. 3) [13].

3 Malignant Cutaneous Neoplasms

Ultrasonography can discriminate primary skin malignancies from normal skin based on their different echogenicity and blood flow patterns. Additionally, it is also a potent tool for locoregional staging of the malignancy. Contrast-enhanced ultrasound (CEUS) has shown early promise in distinguishing malignant neoplasms from benign lesions by evaluating their vascular kinetics [14]. In some series, malignant neoplasms may appear more rigid than benign neoplasms on ultrasound elastography, possibly due to different cellular characteristics and extracellular matrix composition [15, 16].

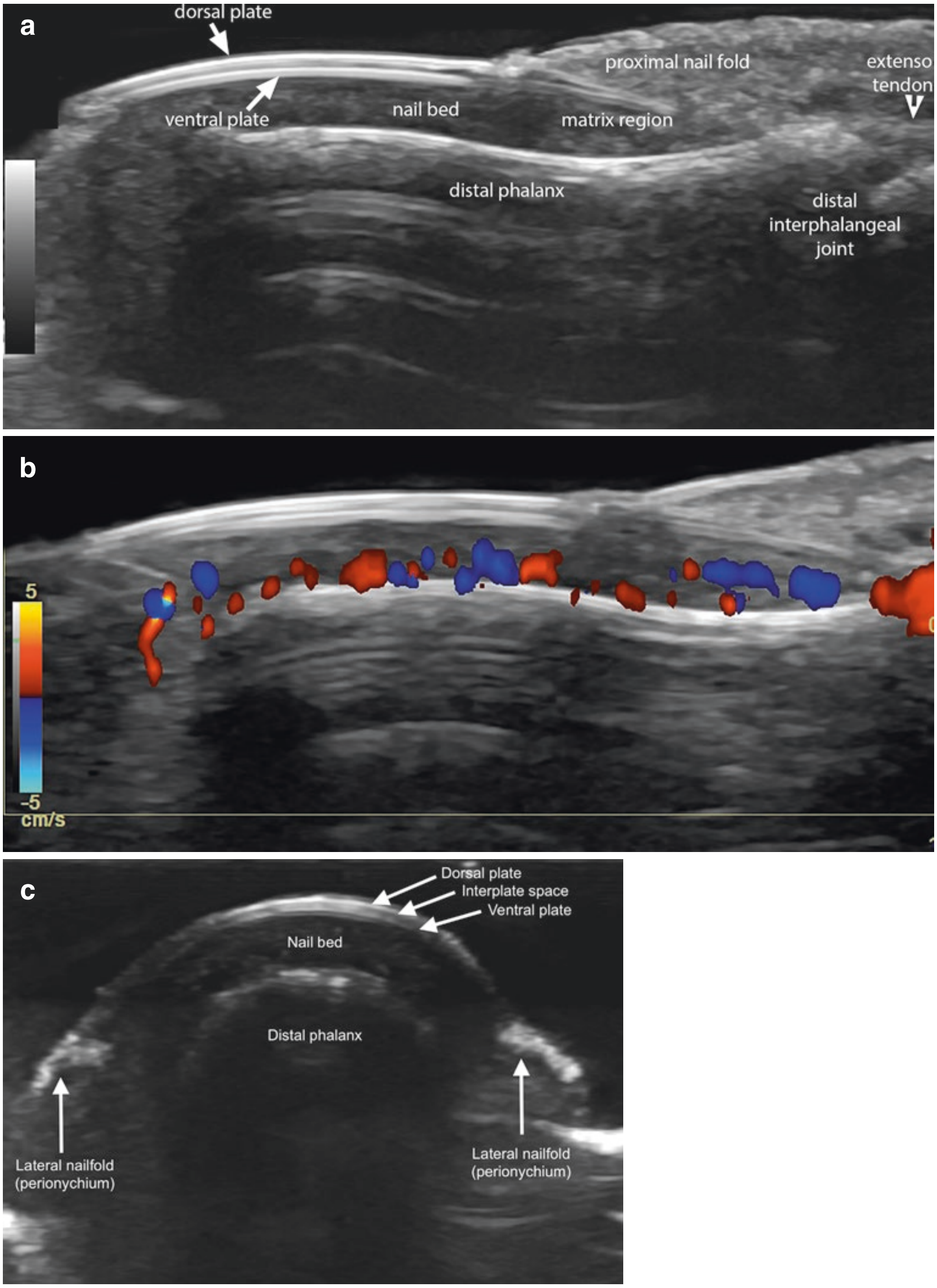
a
dorsal plate
proximal nail fold
extenso
tendon
ventral plate
nail bed
matrix region
distal phalanx
distal
interphalangeal
joint
b
5
-5
cm/s
c
Dorsal plate
Interplate space
Ventral plate
Nail bed
Distal phalanx
Lateral nailfold
(perionychium)
Lateral nailfold
(perionychium)

Fig. 3 Normal nail. (**a**, **b**) Longitudinal view, right index finger. (**a**) Greyscale and (**b**) Color Doppler. Notice that the blood flow (in colors) is closer to the bony margin of the distal phalanx and does not touch the ventral plate. (**c**) Anatomic components of the nail unit and periungual zone (transverse view)

3.1 Malignant Melanoma

Malignant melanoma is responsible for the majority of skin cancer-related death [17]. On U/S, it appears as a well-defined oval-to-fusiform hypoechoic lesion with prominent vascularity [10]. The main utility of ultrasonography for melanoma is its ability to measure tumor depth, which can help guide biopsy technique and surgical planning (Fig. 4) [18]. U/S-measured tumor depth has been shown to closely correlate with the histologic Breslow depth (BD) [19], which is the most important prognosticator for melanoma [20]. Although U/S may sometimes overestimate tumor depth due to underlying lymphocytic infiltration or nevus remnant [21], multiple studies have shown that high frequency U/S probes can reliably identify deep melanomas >1 mm BD [19, 21, 22].

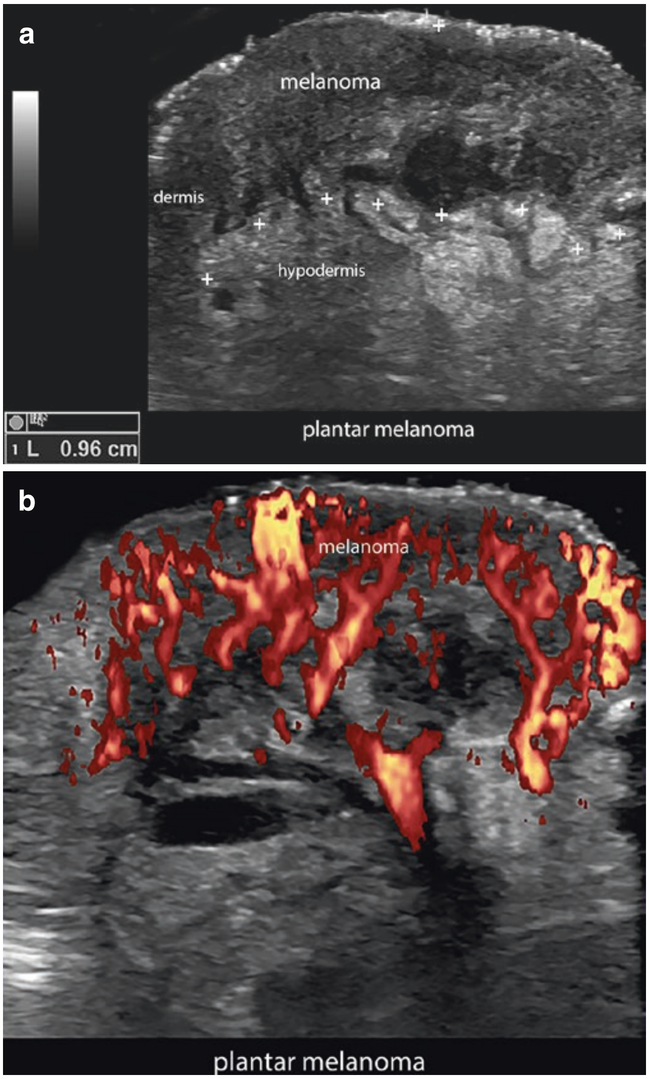

Fig. 4 Melanoma in the plantar region. (**a**) Greyscale and (**b**) Power Doppler demonstrate ill-defined hypoechoic dermal and hypodermal mass (9.6 mm depth) with increased echogenicity of the hypodermis due to edema. On power Doppler, there is prominent blood flow (in color) within the mass

Moreover, U/S allows for early detection of local satellites (<2 cm from the primary lesions), in-transit metastases (≥2 cm from the primary lesion), and nodal metastases [23]. Local satellites and in-transit metastases appear as subcutaneous hypoechoic oval structures with large anechoic areas, which may resemble fluid collections or abscesses but correspond to hypercellular regions [24, 25]. These sonographic features are superior to clinical exam and dermoscopy for distinguishing MM satellites or metastases from blue nevi, which tend to be dermal fusiform homogeneous lesions. Signs of nodal metastases include hypoechogenicity of the medulla, presence of cortical hypoechoic nodules, a rounded shape, and cortical hypervascularity [26].

3.2 Squamous Cell Carcinoma (SCC)

Unlikely primary SCC of other organs, SCC of the skin usually carries a favorable prognosis; however, cutaneous SCC can occasionally act aggressively and metastasize [27]. On U/S, cutaneous SCC appears as an irregularly shaped hypoechoic and heterogeneous lesion with increased vascular flow (Fig. 5) [10, 28, 29]. More recent data has identified tumor thickness as an important prognosticator of disease progression [30], and has shown that U/S can provide reliable depth measurement for surgical intervention [31]. This is especially important for cutaneous SCC of the scalp, where there is little resistance against tumor spread below the galeal plane [32]. Furthermore, U/S can also help detect the presence of local and nodal metastases in SCC, which is especially important for head and neck tumors [33, 34].

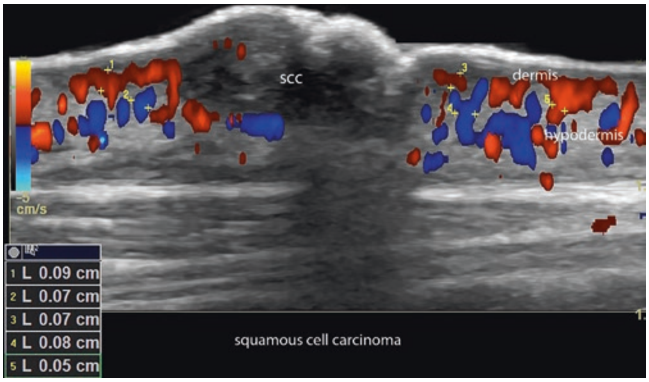

Fig. 5 Squamous cell carcinoma (SCC) in the anterior aspect of the right leg. Color Doppler (longitudinal view) shows slightly lobulated hypoechoic dermal and hypodermal mass that displaces the epidermis upward. Notice the thickening of the epidermis and the presence of some vessels within the mass and the increased vascularity (in colors) in the periphery of the tumor. The markers are measuring the thickness of the regional vessels

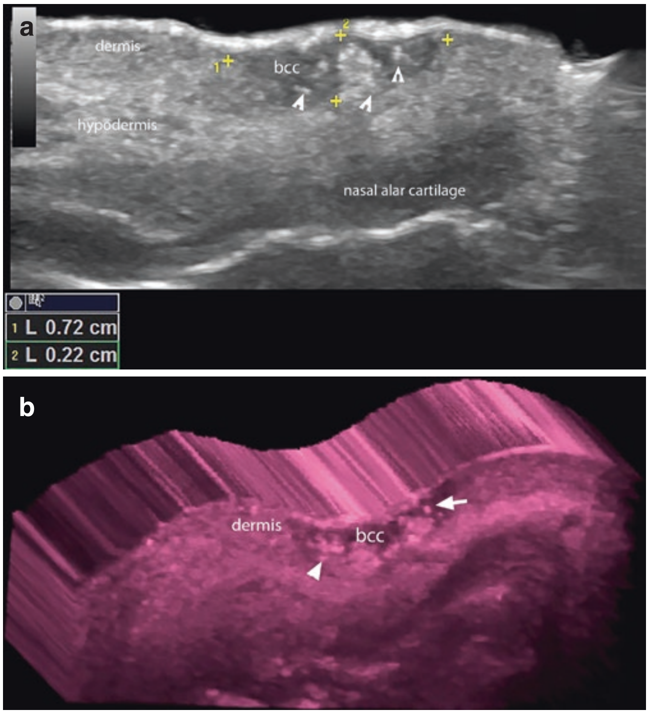

Fig. 6 Basal cell carcinoma in the tip of the nose (right side; transverse view). (**a**) Greyscale and (**b**) 3D reconstruction presents an oval-shaped, hypoechoic dermal lesion with hyperechoic spots (arrows). These spots have been interpreted as an artifact produced by the tumoral nests and are not seen in melanoma or squamous cell carcinoma

3.3 Basal Cell Carcinoma (BCC)

BCC is the most common and least aggressive cutaneous malignancy [35]. On U/S, BCC appears as a hypoechoic lesion with scattered hyperechoic spots within the lesion (Fig. 6) [10, 36]. Commonly, BCC demonstrates low-flow vascularity within or at its periphery. Interestingly, the hyperechoic spots are almost pathognomonic of BCC, and can even be used to predict the tumor subtype and risk of recurrence [4, 37]. Along with U/S-measured tumor dimensions, this information can be very helpful for choosing an optimal method of tumor destruction.

4 Benign Vascular Neoplasm

4.1 Infantile Hemangioma

Hemangiomas are the most common type of benign tumors in infancy. They classically have a proliferative phase during the first few months of life, and then slowly regress and often resolve over the next few years [35]. On ultrasound, a proliferating hemangioma appears as a poorly-defined hypoechoic mass that is highly vascular with arterial and venous flow and sometimes arteriovenous shunts (Fig. 7) [10]. As it regresses, a hemangioma loses vascularity and gains echogenicity, and eventually becomes a hypovascular hyperechoic lesion in its complete regression phase [26]. An ulcerated hemangioma demonstrates abrupt loss of the hyperechoic epidermis and disruption of the dermis and hypodermis [9]. A recent study suggests that the use of U/S-measured hemangioma depth can facilitate selection of the optimal treatment modality and improve patient outcome [38].

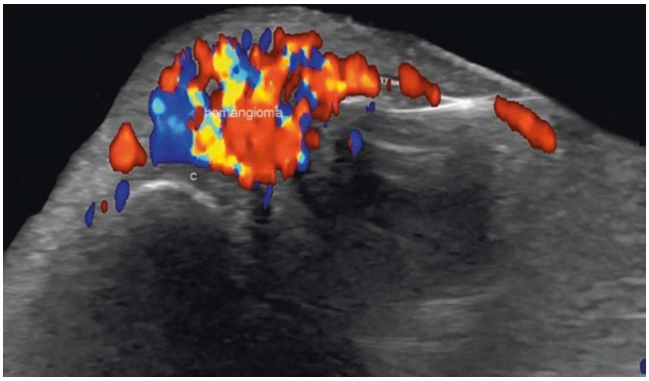

Fig. 7 Infantile hemangioma in the tip of the nose. Color Doppler (transverse view) shows hypervascular dermal and hypodermal mass that involves the left alar nasal cartilage (the right alar nasal cartilages is unremarkable)

4.2 Vascular Malformations

Vascular malformations are derived from abnormal embryonic morphogenesis of capillary, venous, arterial, or lymphatic channels [35], and are often classified accordingly [39]. Alternatively, they can be classified based on their vascular flow velocity on Doppler: arterial and arteriovenous malformations demonstrate high velocity with prominent color, while venous, capillary, and lymphatic malformations demonstrate low velocity that may not be detected if less than 2 cm/s (Fig. 8) [40]. On plain U/S, each lesion presents as a collection of anechoic tubules (arterial or venous), pseudocystic spaces (venous or lymphatic), or hyperechoic areas (capillary) [26]. In low-flow lesions, thrombi appear as non-compressible hypoechoic lacunae, whereas phleboliths appear as tiny hyperechoic spots [10]. In contrast with hemangiomas, vascular malformations typically do not have a mass-like appearance. Furthermore, U/S can be used to help with surgical planning and to monitor treatment progress [41].

5 Benign Solid and Cystic Neoplasm

5.1 Epidermal and Trichilemmal Cyst

Derived from the follicular infundibulum [35], an intact epidermal cyst contains loosely packed keratin and appears as a circumscribed hypoechoic-to-anechoic oval structure

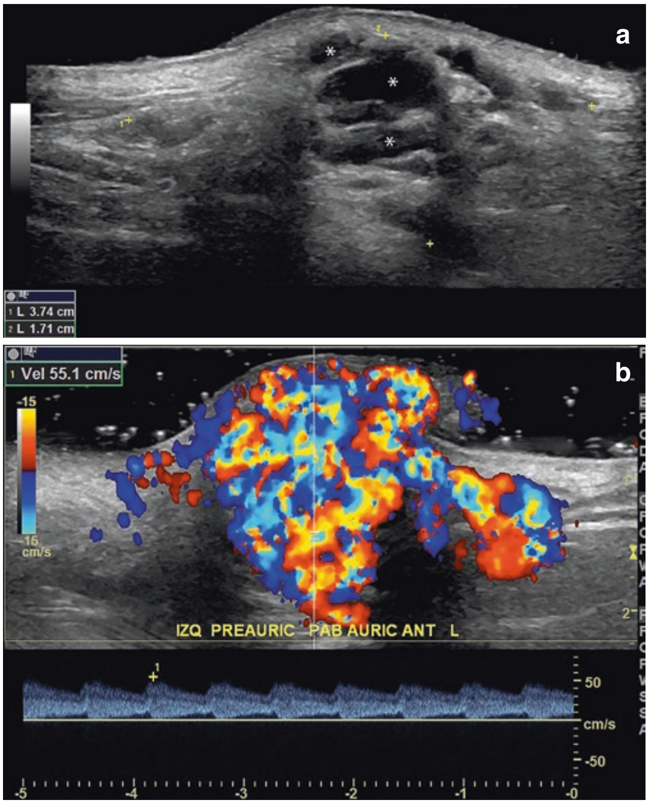

Fig. 8 Arterio-venous vascular malformation in the preauricular region. (**a**) Grey scale (longitudinal view) shows multiple anechoic tubular and lacunar dermal and hypodermal spaces (∗). Measurements of the area occupied by these structures among markers (3.74 cm long × 1.71 thickness). (**b**) Color Doppler spectral curve analysis presents turbulent arterialized venous flow with high velocity up to 55.1 cm/s (reference of a normal carotid artery: 60–120 cm/s)

extending from the dermis to the hypodermis (Fig. 9) [9]. Sometimes the punctum connecting the cyst to the skin surface may be visualized. Due to the hypoechoic nature of the cyst, there is often notable posterior acoustic enhancement underneath the cyst. With Doppler, increased vascular flow can be observed in the periphery of the cyst. Upon rupture, the cyst becomes a more ill-defined or lobulated hypoechoic-to-heterogeneous structure (Fig. 10) [42]. Around the ruptured cyst, there is often robust ill-defined hypoechoic foreign body reaction along with increased hypodermal echogenicity [42].

A trichilemmal cyst is often found on the scalp and its cyst wall lacks a granular layer [35]. On US, it appears similar to an epidermal cyst, but often lacks the punctum and sometimes has a hyperechoic center due to calcification or compact hair tracts [26]. If inflamed, increased vascularity may be seen at its periphery [32].

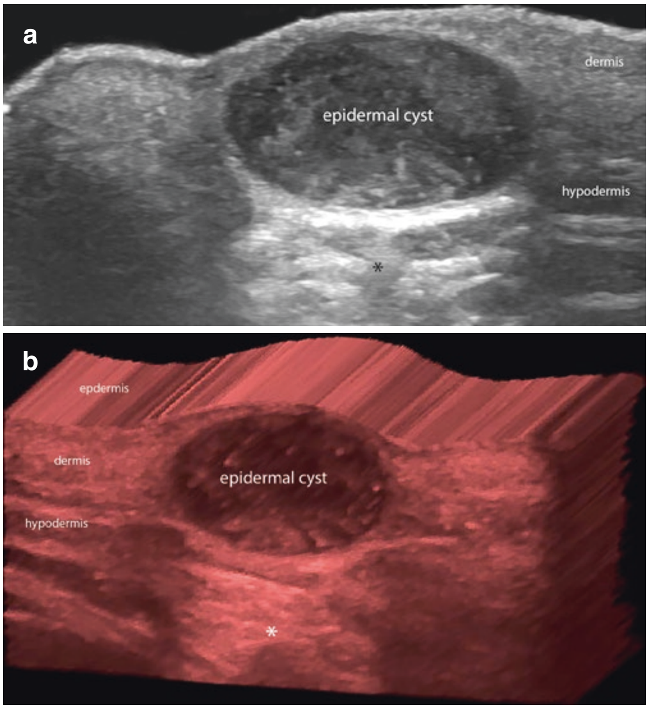

Fig. 9 Intact epidermal cyst. (**a**) Greyscale and (**b**) 3D reconstruction demonstrate well-defined, oval-shaped hypoechoic dermal and hypodermal structure that produces posterior acoustic reinforcement artifact (∗)

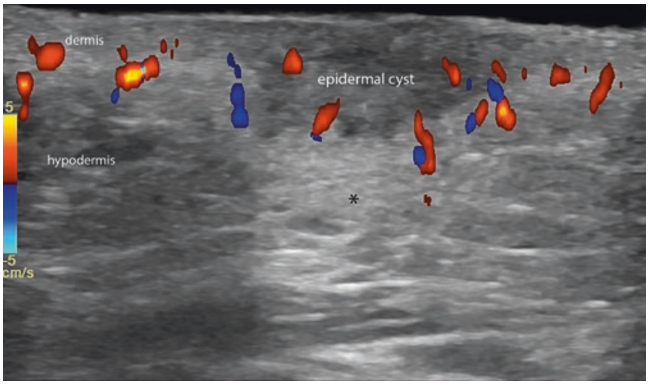

Fig. 10 Remnant of a ruptured epidermal cyst. Color Doppler shows ill-defined hypoechoic dermal and hypodermal structure that generates posterior acoustic reinforcement artifact (∗). There is increased dermal and hypodermal vascularity in the periphery of the remnant cyst

5.2 Pilomatrixoma

A pilomatrixoma is a hair matrix-derived benign subcutaneous neoplasm often found on the head and upper trunk of children [35]. On sonography, its appearance may vary, but most commonly presents as a "targetoid nodule" with central calcified hyperechoic debris surrounded by a hypoechoic rim (Fig. 11) [43]. On color Doppler, its degree of vascularity is highly variable, ranging from a hypovascular nodule to a hemangioma-like hypervascular lesion [26].

5.3 Neurofibroma

A neurofibroma is a benign tumor of the peripheral nerve sheath classically associated with Neurofibromatosis 1 and 2 [44]. It may present as a cutaneous, subcutaneous, or plexi-

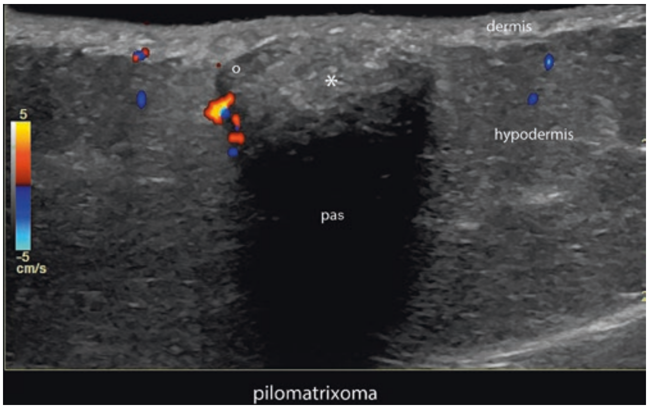

Fig. 11 Pilomatrixoma. Color Doppler (transverse view; right cheek) demonstrates well-defined, oval-shaped dermal and hypodermal structure with hypoechoic rim (o) and hyperechoic calcified center (*). There is posterior acoustic shadowing (pas) artifact due to the presence of calcifications

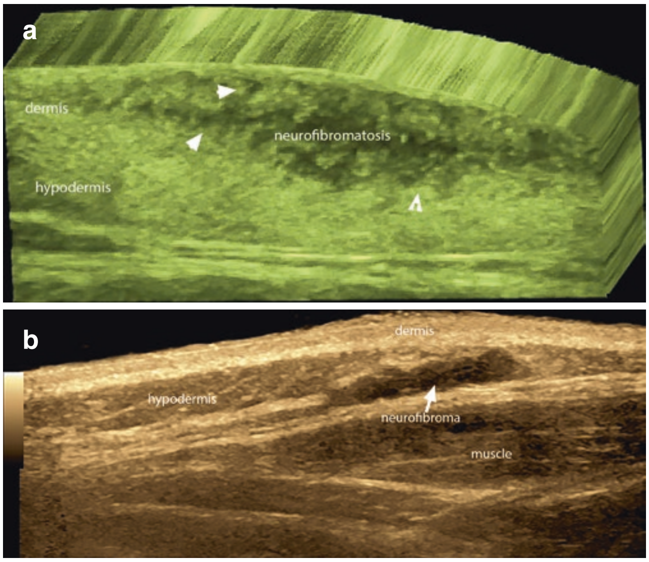

Fig. 12 (**a**) Cutaneous plexiform neurofibromatosis. 3D gray scale ultrasound reconstruction (transverse view) presents multiple and tortuous hypoechoic dermal and hypodermal neural tracts that displace the epidermis upward. (**b**) Nodular form of neurofibromatosis. Greyscale ultrasound (color filter; transverse view) shows lobulated, oval-shaped, hypoechoic hypodermal structure (arrow)

form tumor. On US, a non-plexiform neurofibroma presents as an avascular hypoechoic-to-heterogenous focal pseudonodular or nodular area involving the dermis and sometimes the hypodermis, whereas a plexiform neurofibroma presents as a collection of multiple hypovascular hypoechoic tracts that follow the tortuous paths of nerves (Fig. 12) [45]. In some nodular neurofibromas, it is possible to detect the afferent and efferent neural branches.

5.4 Wart

In warts, human papillomavirus induces epidermal hyperplasia and cutaneous neovascularization [35]. On ultrasound, they present as hypoechoic fusiform lesions involving the epidermis and dermis (Fig. 13) [9]. Color Doppler reveals increased vascular flow in the underlying dermis. Plantar bursitis can often be observed underneath a plantar wart [46].

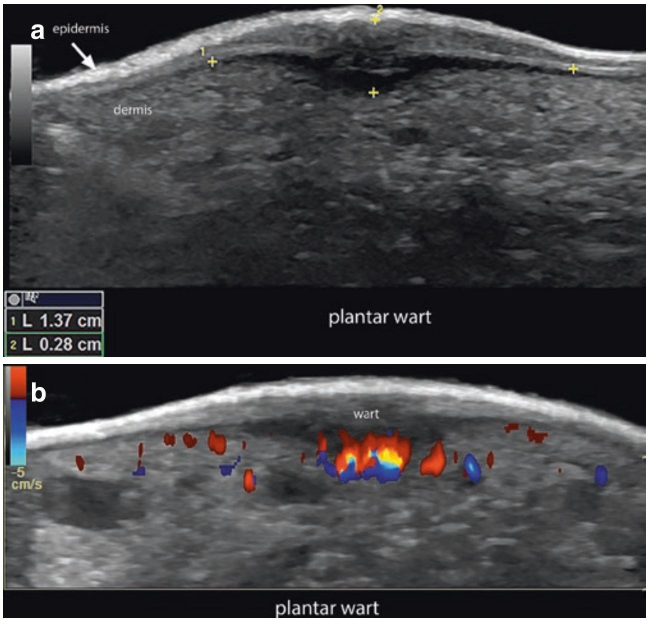

Fig. 13 Plantar wart. (**a**) Greyscale and (**b**) Color Doppler demonstrate fusiform shaped, hypoechoic, epidermal and dermal structure (1.37 cm transverse × 0.28 cm thickness). Notice the bilaminar appearance of the epidermis due to the plantar location. There is increased dermal vascularity within the dermal part of the lesion

6 Benign Neoplasms Involving the Nail

6.1 Periungual Wart

Warts can involve the nail folds and may subsequently extend to the nail matrix and nail bed. Similar to other warts, periungual warts present as eccentric hypoechoic fusiform lesions on U/S, but often appear hypovascular [11]. Periungual warts may affect the nail matrix and lead to onychodystrophy, which on U/S appears as thickening of both nail plates and increased space between them [47] (Fig. 14).

6.2 Subungual and Periungual Pyogenic Granulomas

Pyogenic granulomas (PGs) are also known as lobular capillary hemangiomas. They are reactive lesions that have a predilection for the nail fold and can be associated with trauma or systemic drugs [35]. Composed of inflamed proliferating granulation tissue, PGs appear clinically as friable red papules that may bleed profusely [26, 35]. On U/S, periungual PGs often appear as round to oval hypoechoic dermal papules, while subungual PGs appear as poorly defined subtly thickened hypoechoic areas in the proximal nail bed or matrix [26].

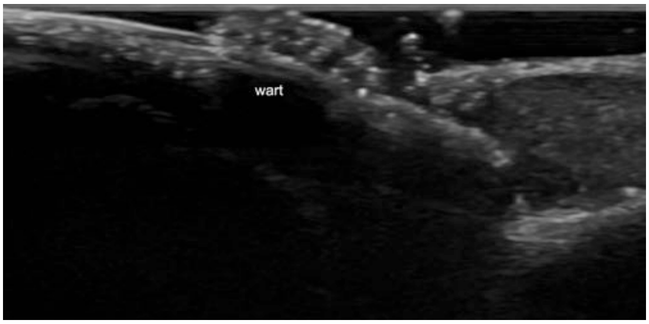

Fig. 14 Subungual/periungual warts. Ultrasound in longitudinal view. There is a hypoechoic fusiform eccentric hypovascular lesion, with an exophytic hyperechoic component located in the proximal nail fold. This lesion is associated with thickening of the adjacent portions of the nail plates

The vascularity of PGs may vary, except for the telangiectatic variant, which is often hypervascular [26]. Upward displacement and thickening of the nail plates can be seen, but the bony margin of the distal phalanx is usually spared [26].

6.3 Glomus Tumor

A glomus tumor is a benign but painful hamartoma derived from the neuromyoarterial glomus cells responsible for thermoregulation at the arteriovenous anastomosis [35, 48]. Clinically, it often appears as a subtle red-blue macule, and has a predilection for the nail bed [35]. On ultrasound, it appears as a well-defined oval hypoechoic mass with increased vascularity (Fig. 15) [11]. Scalloping of the distal phalanx may be observed in the setting of a longstanding glomus tumor [48].

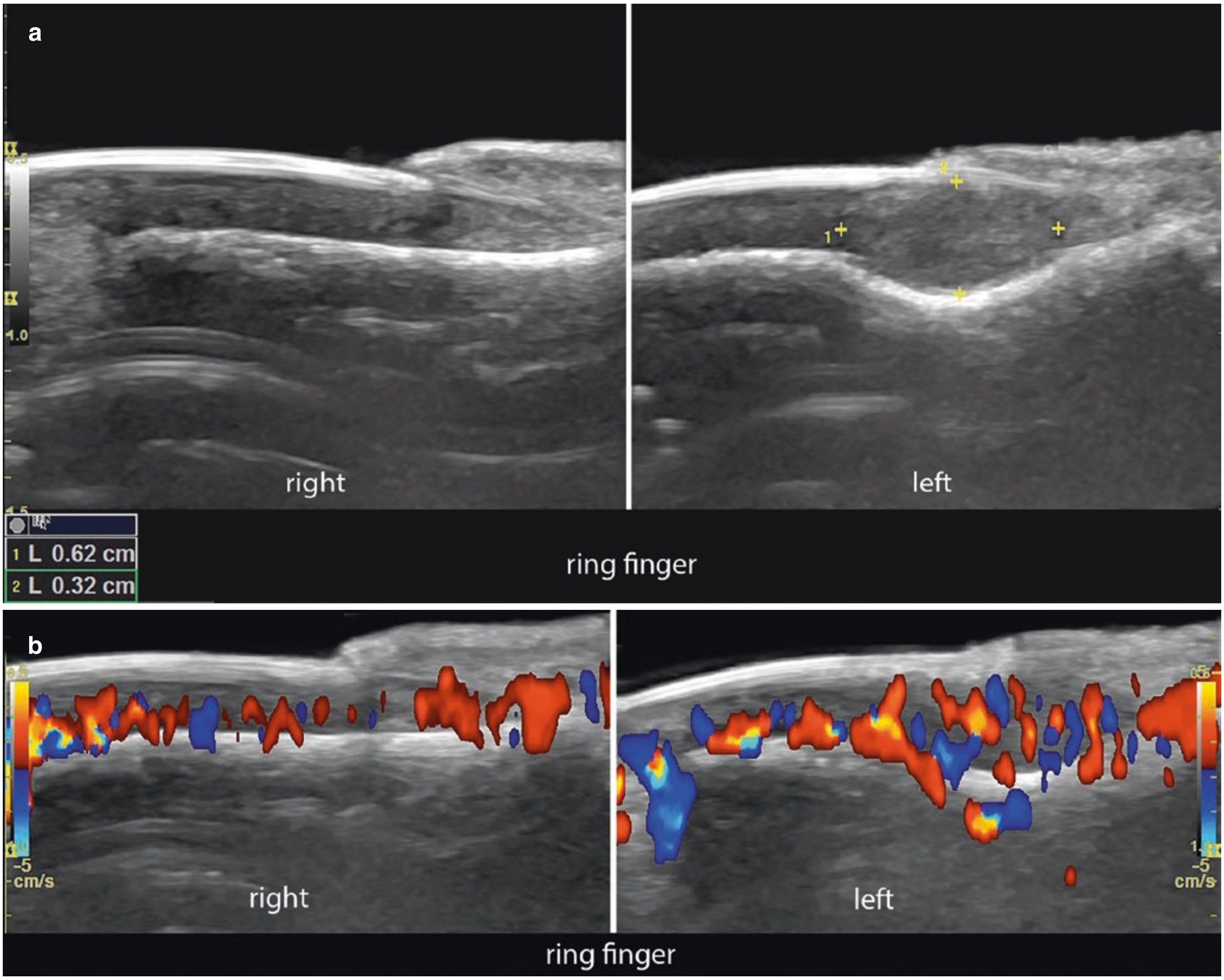

Fig. 15 Glomus tumor. (**a**) (Greyscale) and (**b**) (Color Doppler) comparison side-by-side ultrasound images (right and left ring fingers) present a well defined, oval-shaped, hypoechoic nodule (6.2 mm long × 3.2 mm thickness) in the proximal part of the nail bed of the left ring finger that affects the matrix region. Notice the upward displacement of the nail plate and the scalloping of the bony margin in (**a**), as well as, the hypervascularity of the mass in (**b**)

6.4 Periungual Fibroma

A periungual fibroma often originates from the proximal nail fold and appears as a pink papule of various shapes [35]. While a single tumor is often serendipitous, multiple lesions on the same patient can be associated with tuberous sclerosis and may be referred to as Koenen's tumors [35]. On U/S, they appear as shallow hypoechoic tumors that may be round, oval, fusiform, or polypoid (Fig. 16) [11]. On color Doppler, they are often hypovascular, except the angiofibroma subtype that is hypervascular [49]. Over time, these tumors may compress the nail matrix and contribute to onychodystrophy and deep longitudinal grooves in the nail plate.

6.5 Digital Myxoid, Synovial, and Mucoid Cyst

Digital myxoid or synovial cysts are common benign periungual structures derived from mucoid degeneration of connective tissues between the proximal nail fold and the distal interphalangeal joint (DIJ) [48]; these cysts are often connected to the DIJ with protrusion of intra-articular content into the skin. On the other hand, the term "digital mucoid cyst" may specifically refer to the less common subungual lesions, which are caused by subungual collagen degeneration and classically do not connect to the DIJ. On U/S, a myxoid or synovial cyst appears as a periungual round or oval avascular anechoic cystic structure with a tortuous anechoic tract connecting to the DIJ (Fig. 17) [26]. A subungual mucoid cyst has a similar appearance but typically lacks the connecting tract. Focal internal echoes within the cyst may be seen due to mucinous debris [11], and osteophytes are common in DIJ connected to synovial cysts [49]. Involvement or compression of the nail matrix region may cause onychodystrophy.

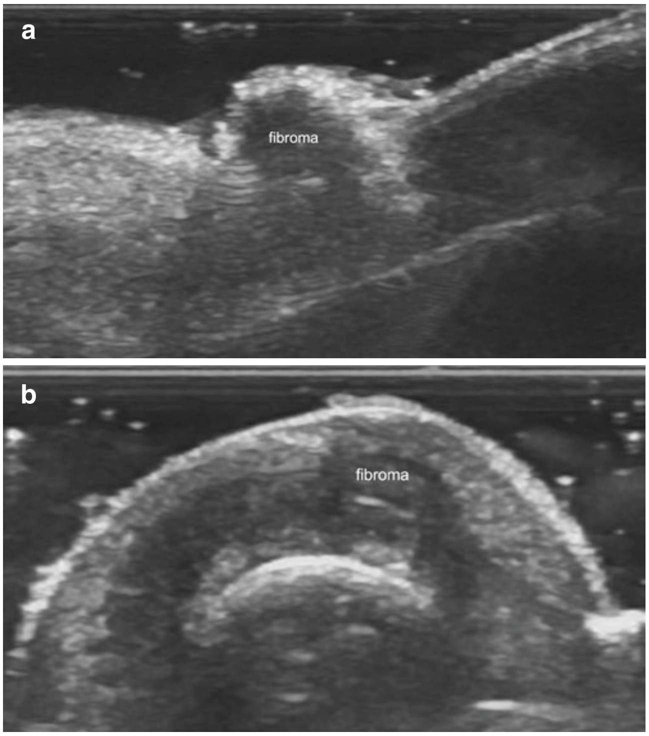

Fig. 16 Periungual fibroma, fibrokeratoma or Koenen's fibroma. Ultrasound (**a**) longitudinal and (**b**) transverse views. There is a hypoechoic, rounded, eccentric, lesion in the proximal third of the nail bed with extension to the nail matrix. There is an exophytic component seen as a polypoid, hypoechoic and hypovascular lesion involving the proximal nail fold

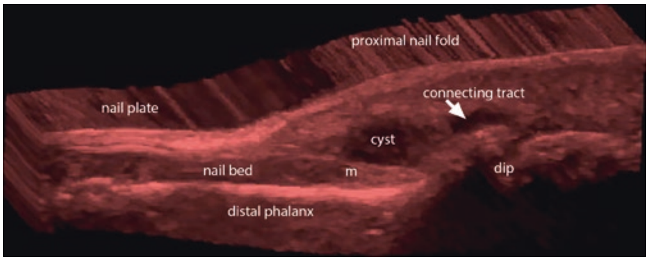

Fig. 17 Periungual synovial cyst. 3D greyscale ultrasound reconstruction of the ungual region shows an oval-shaped, anechoic dermal structure located in the proximal nail fold that connects to the distal interphalangeal joint (arrow). Abbreviations: dip, distal interphalangeal joint; m, matrix region

6.6 Subungual Exostosis

Subungual exostosis is a benign bony overgrowth of the distal phalanx, often associated with trauma or chronic local irritation [11]. It is most often seen on the great toes of young patients as a hard tender subungual nodule that elevates the nail plate [35]. On U/S, it appears as an eccentric hyperechoic band connected to the bony margin (Fig. 18). A cartilaginous hypoechoic cap may overlie the hyperechoic bony outgrowth [11]. On Doppler, the lesion itself demonstrates minimal vascularity [50], but there is often increased vascular flow in the surrounding thickened hypoechoic nail bed due to inflammation [26]. The diagnosis should be confirmed with X-ray [35].

6.7 Nail Findings of Systemic Autoimmune Diseases

Interestingly, changes in the nail bed vasculature are often observed in the setting of connective tissue diseases. Patients with systemic scleroderma often demonstrate decreased vascularity and echogenicity of the nail bed along with nail plate dystrophy, whereas patients with rheumatoid arthritis have a thickened hypervascular nail bed and proximal nail fold with increased echogenicity [11]. Patients with systemic lupus may have a hypovascular nail bed due to repetitive small thromboembolic events.

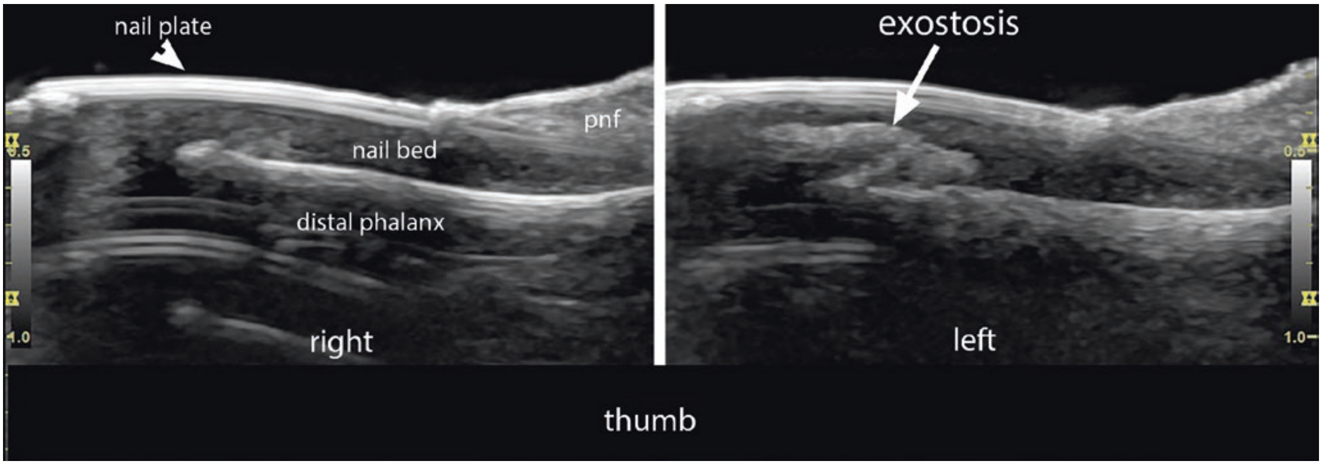

Fig. 18 Subungual exostosis. Greyscale (side-by-side comparison; right and left thumbs) shows hyperechoic band emerging from the bony margin of the distal phalanx that protrudes into the nail bed

7 Cutaneous Inflammatory Processes

7.1 Hidradenitis Suppurativa, Pilonidal Cyst, Acne Conglobata, and Dissecting Cellulitis of the Scalp

These four diseases are often collectively referred to as the follicular occlusion tetrad due to their similar pathophysiology [35]. They mainly affect apocrine gland-bearing skin and are thought to be caused by occlusion and rupture of the pilosebaceous units, leading to vigorous inflammation [51]. Clinically, there often present with boggy tender nodulocystic lesions and draining fistulous tracts. However, the fluid collection in these lesions is usually sterile, and surgical drainage is usually not effective. Therefore, it is important to distinguish them from cutaneous abscesses. On U/S, there are subcutaneous hypoechoic-to-anechoic cystic structures and fistulous tracts connecting to dilated hair follicles (Fig. 19) [9]. Within these spaces, there are often tiny linear hyperechoic hair fragments that are not seen in abscesses [9, 52]. On color Doppler, there is increased vascularity in the surrounding tissue due to inflammation [10]. Local lymph nodes are not enlarged, but may show cortical thickening and decreased echogenicity [53].

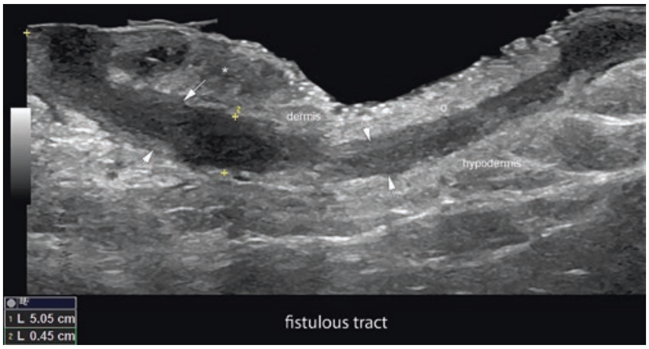

Fig. 19 Hidradenitis suppurativa. Greyscale ultrasound (longitudinal view, right perineal region). Hypoechoic fistulous tract (5.05 cm long × 0.45 cm thickness; between markers) running in the dermis and hypodermis with hypoechoic laminar bands (arrows) in the periphery suggestive of fibrosis. There is an increased echogenicity of the underlying hypodermis due to edema. Notice the thickening and decreased echogenicity of the dermis (*) adjacent to the fistulous tract in the left side of the image and the apparently "normal" appearance of the dermis (o) in the right side of the image

7.2 Psoriasis

Psoriasis is a chronic immune-mediated multi-organ disease [35]. On U/S, psoriatic plaques show a thickened undulating epidermis and a hypoechoic hypervascular upper dermis. The nail plates lose their definition and become thickened and undulating, while the nail bed becomes thickened and hypervascular with decreased echogenicity [26]. Psoriatic arthritis (PsA) demonstrates prominent hypoechoic synovium, anechoic fluid, increased vascularity, and periarticular erosions [26, 54]. Compared to onychomycosis, which typically show loss of interplate space proximally and decreased plate-DIJ distance on US, psoriatic nails often show preserved interplate space but are frequently associated with PsA changes in the DIJ (Fig. 20) [55]. Other than the above three locations, psoriasis can also affect the enthesis and bony margins, which may also be examined using ultrasonography.

7.3 Scleroderma and Morphea

Scleroderma is an autoimmune connective tissue disease of unknown etiology [35]. The ultrasonography features vary

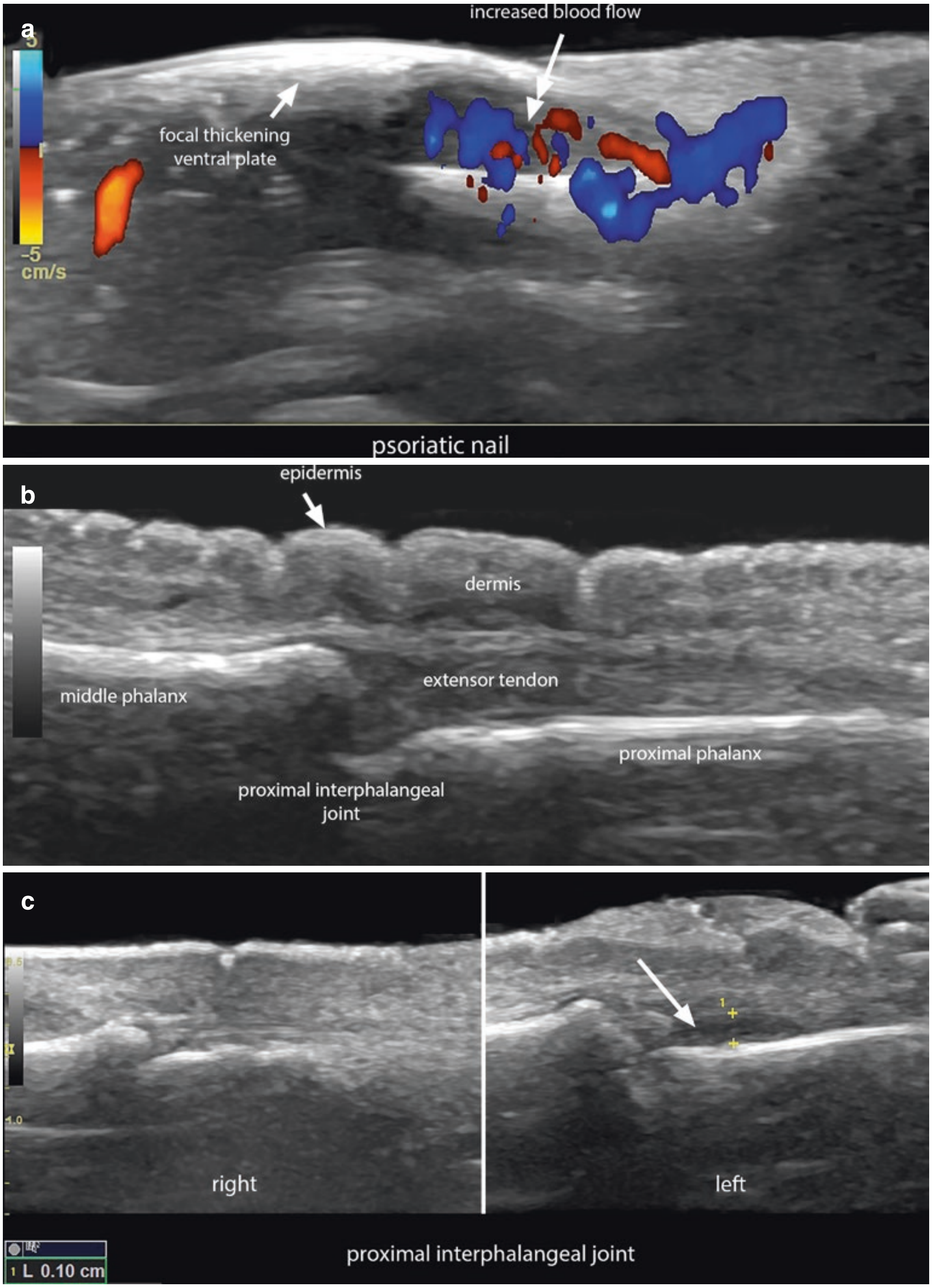
a
increased blood flow
5
focal thickening
ventral plate
-5
cm/s
psoriatic nail
b
epidermis
dermis
extensor tendon
middle phalanx
proximal phalanx
proximal interphalangeal
joint
c
right
left
1 L 0.10 cm
proximal interphalangeal joint

Fig. 20 Psoriasis. (**a**) Nail psoriasis. Color Doppler (longitudinal view) shows an increased thickness of the nail bed, hyperechoic focal thickening of the ventral plate and increased vascularity in the proximal nail bed. (**b**) Cutaneous and extensor tendon involvement. Greyscale ultrasound (middle finger; longitudinal view) demonstrates thickening and decreased echogenicity of the dermis with thickening and undulation of the epidermis (arrow). There is decreased echogenicity of the insertion of the central band of the extensor tendon in the base of the middle phalanx. (**c**) Joint involvement. Greyscale ultrasound (side-by-side comparison; right and left index fingers) shows a mild distention with fluid (arrow and markers) in the proximal interphalangeal joint of the left index finger

between different phases of scleroderma and can be helpful in monitoring disease progression, especially for deep lesions [56]. During the active phase, the dermis becomes thickened and hypoechoic, while the hypodermis becomes hyperechoic [10]. During the late phase, there is marked thinning of the dermis and loss of subcutaneous fat [26]. Increased cutaneous blood flow and increased hypodermal echogenicity are highly sensitive and specific markers of active disease (Fig. 21) [10]. More recently, there have been suggestions that ultrasound elastography may be useful in assessing the extent of subtle skin involvement in systemic sclerosis [57].

7.4 Other Inflammatory Diseases

The ultrasound can identify subperichondrial serous effusion in relapsing polychondritis and differentiate it from repetitive

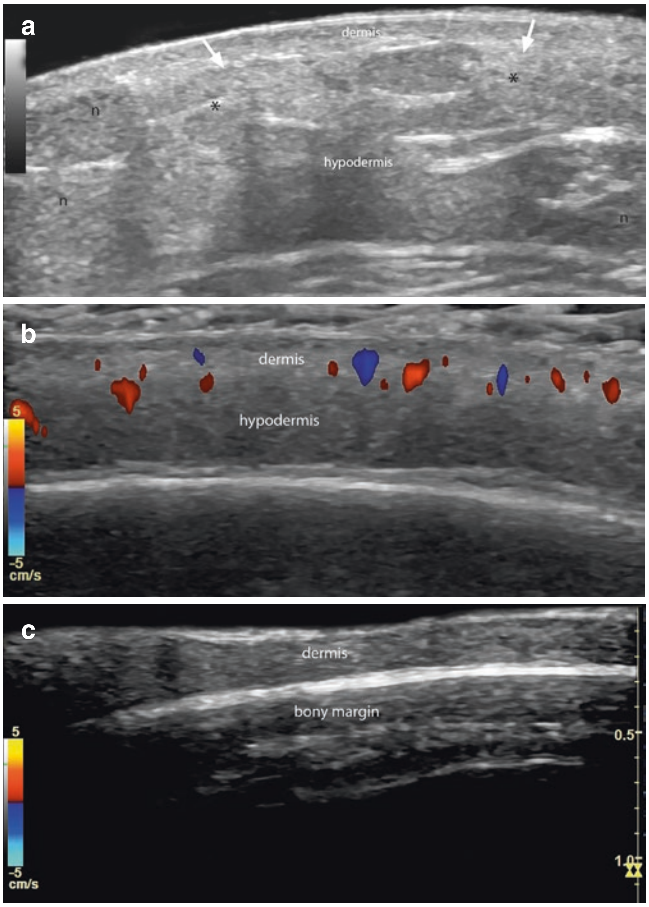

Fig. 21 Morphea. Active morphea (**a**, **b**). (**a**) Greyscale (anterior aspect of the right thigh) and (**b**) Color Doppler ultrasound(scalp). (**a**) Areas with increased echogenicity of the hypodermis (∗) and loss of the border (arrows) between the dermis and hypodermis are seen in (**a**). Notice the areas with normal (n) echogenicity of the hypodermis in the periphery. In (**b**), there is increased dermal and upper hypodermal blood flow. (**c**) Inactive and atrophic morphea. Color Doppler ultrasound (scalp) presents a morphea with atrophy of the dermis and hypodermis. There is a lack of fatty hypodermal tissue and no signs of regional hypervascularity

traumatic damage [58, 59]. It is also useful for monitoring disease activity and screening of extra-auricular cartilage involvement in relapsing polychondritis [60, 61]. In dermatomyositis, ultrasound is one of the three accepted imaging modalities for confirmation of muscular involvement, as it can identify increased interstitial echogenicity in skeletal muscle [62]. In nodular fasciitis, the characteristic sonography finding involves poorly defined hypoechoic 1.8–3.5 cm lobulated masses adjacent to the fascia [63].

7.5 Panniculitis

Panniculitis refers to inflammation of the adipose tissue, and may involve the fat lobules or septa [35]. U/S is a non-invasive modality that can help define the predominant pattern of inflammation [9]. In both septal and lobular panniculitis, the hypodermis becomes hyperechoic due to edema (Fig. 22). In a predominantly septal panniculitis such as erythema nodosum, other than hyperechogenicity of the hypodermal fat, the fibrous septa become markedly thickened and hypoechoic [9]. In the case of fat necrosis, anechoic hypodermal pseudocysts may also be detected due to liquefaction of the fat [9]. Rarely, hyperechoic hypodermal calcium deposits with associated posterior acoustic shadows may be seen in infant fat necrosis [64, 65]. On color Doppler, all panniculitides tend to demonstrate increased hypodermal vascularity.

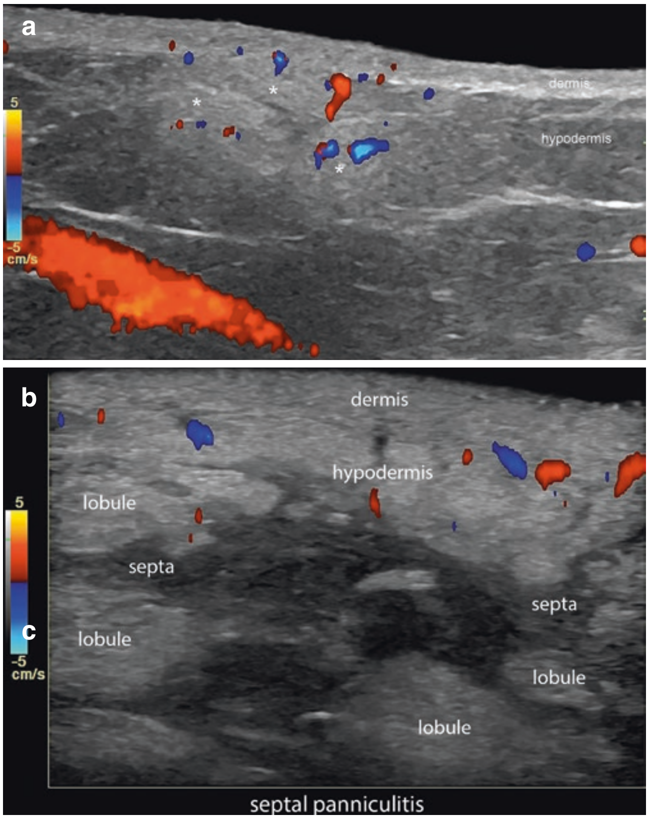

Fig. 22 Panniculitis. (**a**) Predominantly lobular and (**b**) Predominantly septal. Color Doppler ultrasounds (**a**, anterior aspect of the right arm (longitudinal view); **b**, abdominal wall). (**a**) Lupus panniculitis. A diffuse increase of the hypodermal echogenicity (∗). (**b**) Granulomatous panniculitis. Heterogeneous echogenicity of the hypodermis with hyperechoic fatty lobules and hypoechoic tissue in the septae. In both types, there is a loss of definition of the borders between the dermis and hypodermis and regional hypodermal hypervascularity

7.6 Mycetoma

Mycetomas arise as the result of chronic granulomatous infections due to bacteria or fungi [35]. They are more common in tropical rural regions and commonly affect the lower limbs [66].

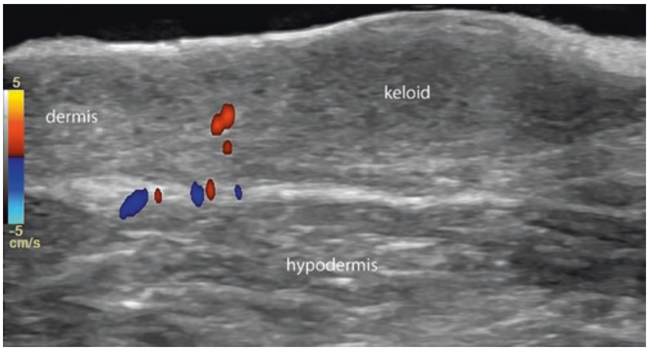

Fig. 23 Active keloid. Color Doppler ultrasound (longitudinal view; left foot).Thickening and decreased echogenicity of the dermis with a laminar pattern and upward displacement of the epidermis. Slightly increased vascularity (in colors) within and adjacent to the keloid region

On U/S, mycetomas demonstrate hypoechoic communicating tracts and the classic “dot-in-circle” sign with a single hyperechoic dot within a round hypoechoic structure [9]. On Doppler, there is often increased vascularity surrounding the lesion.

7.7 Keloid

On ultrasound, a keloid appears as a hypoechoic or heterogeneous thickening of the dermis, commonly with a laminar pattern and an upward displacement of the epidermis (Fig. 23) [57]. Because the lower threshold for blood flow detection on U/S is about 2 cm/s, dermal blood flow in normal skin is usually undetected. Therefore, U/S detection of blood flow within a keloid is often indicative of active growth stimulated by underlying inflammation and angiogenesis that is often seen on histology. This U/S finding can be very helpful for keloids undergoing treatment, especially considering that biopsies of keloids are often contraindicated.

8 Miscellaneous Skin Conditions

8.1 Other Subcutaneous Nodules: Gouty Tophus, Rheumatoid Nodule, Xanthoma

On U/S, gouty tophi appear as poorly-defined heterogenous hyperechoic masses with interspersed hypoechoic areas, acoustic shadowing, and adjacent bone erosion [67]. Rheumatoid nodules may also often appear close to the bone, but are rarely erosive; they appear as homogeneous hypoechoic masses with a sometimes less echoic center likely due to necrosis [67]. Xanthomas appear as well-defined homogenous hypoechoic nodules sometimes associated with large tendons [68].

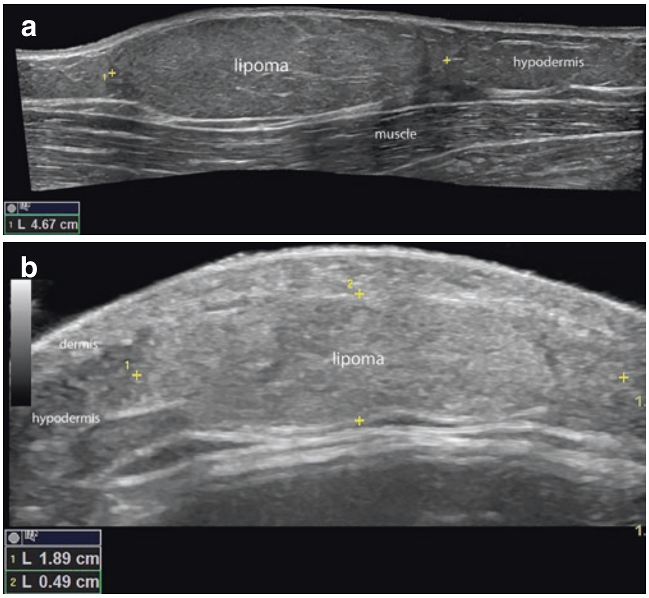

Fig. 24 Lipomas (greyscale ultrasounds). (**a**) Fibrolipoma (longitudinal view; ventral right forearm). Well-defined, oval-shaped hypoechoic hypodermal mass (4.67 cm long; between markers), almost isoechoic with the adjacent hypodermal fatty tissue. (**b**) Angiolipoma (transverse view; dorsal right arm). Oval shaped, hyperechoic hypodermal mass (1.89 cm transverse × 0.49 cm thickness)

8.2 Lipoma

Lipoma is the most common soft tissue benign tumor and often presents as an oval to round mass that is parallel to the axis of skin layers [67]. The echogenicity of lipomas varies according to the tissue attached to the fat. Thus, fibrolipomas tend to be hypoechoic, and angiolipomas tend to be hyperechoic (Fig. 24). On color Doppler, lipomas tend to demonstrate low vascularity. Suspicious ultrasonographic signs of malignancy include: size ≥ 5 cm, heterogeneous echogenicity, and hypervascularity within the mass.

8.3 Foreign Bodies

Foreign bodies are sometimes inoculated into the skin, and patients may be aware of only the cutaneous symptoms and not the underlying inoculation [69]. On ultrasound, solid foreign objects often appear as hyperechoic geometric structures surrounded by hypoechoic hypervascular granulomatous inflammation (Fig. 25) [10]. Synthetic material such as metal or glass often produces posterior acoustic reverberation artifact [49]. Ultrasound can also be used to rule out deep hematomas and abscesses sometimes associated with foreign objects [10]. A wide area of examination is strongly recommended, as the object may lie far away from the primary skin lesion. Furthermore, sterile gel is recommended for open skin [10]. When there is soft tissue emphysema, a lateral approach or water bath for distal limbs can be helpful [70].

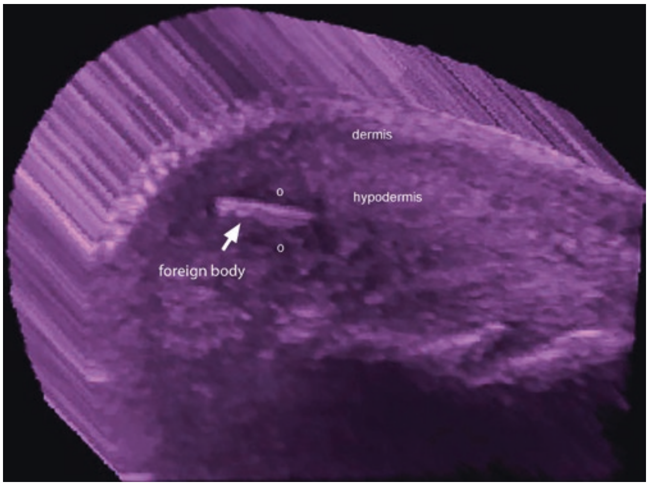

Fig. 25 Foreign body. 3D reconstruction (greyscale with a color filter; longitudinal view). In the pulp of the index finger, there is a bilaminar hyperechoic hypodermal structure (arrow; a splinter of wood). A thin band of hypoechoic inflammatory tissue (o) surrounds the foreign body

8.4 Cosmetic Fillers

Other than the danger of rare acute vascular occlusion, fillers may also cause subacute-to-chronic edema, nodules, granulomas, and morphea-like reactions [71]. Sometimes, there is a lack of clear clinical history from the patient. In these cases, ultrasonography can provide helpful clues. On U/S, fillers are usually located in the hypodermis. The most commonly used hyaluronic acid (HA) filler produces anechoic pseudocysts, while HA-lidocaine mixtures and high-density HA create additional echoes within the pseudocysts (Fig. 26a) [71]. Polyacrylamide gel also produces anechoic pseudocysts, but the pseudocysts are often associated with hyperechogenicity of the underlying hypodermis [71]. For non-degradable fillers, polymethylmethacrylate appears as hyperechoic dots with a comet-tail artifact, and calcium hydroxyapatite appears as hyperechoic bands with posterior acoustic shadowing artifacts [72]. Pure silicone appears as an anechoic deposit, while silicone oil can be seen as hyperechoic deposits with posterior reverberation artifacts, thereby creating a “snowstorm” pattern (Fig. 26b) [72]. Although most filler-induced vascular occlusion involves smaller dermal vessels, a thorough color Doppler examination of related facial arteries should be performed after more immediate measures [10].

8.5 Live Organisms

Particularly in tropical regions, non-microbial parasites such as larvae or worms may infiltrate the skin. On US, these parasites may be identified as well-defined objects with spontaneous movement and inherent bloodflow [9, 73]. For myiasis and filariasis, U/S may be used to visualize the spontaneous movements of larvae or worms inside cavities and lymphatic channels [74].

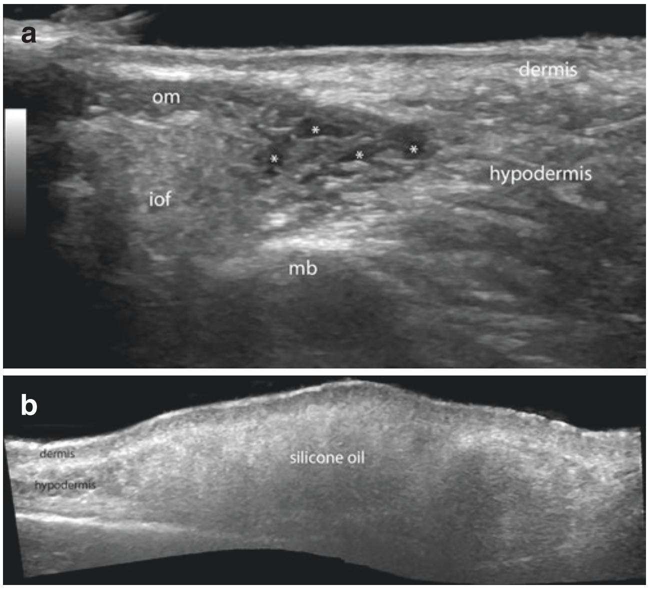

Fig. 26 Cosmetic fillers (greyscale ultrasounds; longitudinal views). (**a**) Hyaluronic acid. Oval and round shaped anechoic pseudocystic deposits in the inferior and medial part of the orbicularis muscle of the right lower eyelid and the adjacent hypodermis of the upper part of the cheek. (**b**) Silicone oil. Hyperechoic hypodermal deposits with diffuse reverberance artifact (“snow storm” appearance) in the glabellar region. Abbreviations: om, orbicularis muscle; iof, intraorbital extraconal fat pad; mb, bony margin of the maxilla, hyperechoic calcified center (*)

9 Other Uses of Ultrasound in Dermatology

Many skin conditions can be caused by underlying vascular abnormalities, and color Doppler U/S is a cost-effective and minimally invasive tool that can provide both anatomic and physiologic information about the vasculature [75]. For leg ulcers, U/S can be used to assess arterial and venous insufficiency, and may even uncover occult soft-tissue and bone infections [35]. It is also frequently used to rule out deep venous thrombosis [76] and to conduct comprehensive deep venous system evaluation for diseases such as Klippel-Trenaunay Syndrome [77]. For arterial diseases such as temporal arteritis, U/S may help diagnose and identify the optimal biopsy site, thereby avoiding risky sites and unnecessary biopsies [78].

U/S is also an essential tool for office-based vein procedures. Before leg vein phlebectomy, reflux from the deep venous system as well as the saphenofemoral and saphenopopliteal junctions must be ruled out or corrected, often under the guidance of duplex ultrasound [79]. Subsequently, duplex U/S is often used confirm the target vein segment. Duplex U/S can also help to visualize the flow of foamed agents during sclerotherapy to avoid inadvertent arterial injection [35]. After the procedure, it can be further used to confirm successful treatment.

Furthermore, U/S can also be used as a primary treatment modality to promote skin healing in lipodermatosclerosis [80] and recalcitrant wounds [81]. HIFU (high intensity focused ultrasound) is a therapeutic modality that directs highly concentrated soundwaves to a precise target in deep tissue. Its frequency can be manipulated to produce heat, cavitation, or shock waves [82]. In principle, this modality can be used to destroy tumors, fat, or deep-tissue deposits such as calcium stones [35]. Due to its ability to generate heat, HIFU can also be used for treatment of rhytids. Lastly, via cavitation of the stratum corneum [83] and heating of deep tissues [84], U/S can also be used to enhance transdermal delivery of drugs such as anti-inflammatories and topical lidocaine [85].

References

1. Pan Y, Gareau DS, Scope A, Rajadhyaksha M, Mullani NA, Marghoob AA. Polarized and nonpolarized dermoscopy: the explanation for the observed differences. Arch Dermatol. 2008;144(6):828–9.
2. Shung KK. High frequency ultrasonic imaging. J Med Ultrasound. 2009;17(1):25–30.
3. Wortsman X, Alfageme F, Roustan G, Arias-Santiago S, Martorell A, Catalano O, et al. Guidelines for performing dermatologic ultrasound examinations by the DERMUS group. J Ultrasound Med. 2016;35(3):577–80.
4. Wortsman X, Vergara P, Castro A, Saavedra D, Bobadilla F, Sazunic I, et al. Ultrasound as predictor of histologic subtypes linked to recurrence in basal cell carcinoma of the skin. J Eur Acad Dermatol Venereol. 2015;29(4):702–7.
5. Welzel J, Schuh S. Noninvasive diagnosis in dermatology. J Dtsch Dermatol Ges. 2017;15(10):999–1016.
6. Xiong YD, Ma S, Li X, Zhong X, Duan C, Chen Q. A meta-analysis of reflectance confocal microscopy for the diagnosis of malignant skin tumours. J Eur Acad Dermatol Venereol. 2016;30(8):1295–302.
7. Borsari S, Pampena R, Lallas A, Kyrgidis A, Moscarella E, Benati E, et al. Clinical indications for use of reflectance confocal microscopy for skin cancer diagnosis. JAMA Dermatol. 2016;152(10):1093–8.
8. Schuh S, Kaestle R, Sattler EC, Welzel J. Optical coherence tomography of actinic keratoses and basal cell carcinomas – differentiation by quantification of signal intensity and layer thickness. J Eur Acad Dermatol Venereol. 2016;30(8):1321–6.
9. Wortsman X. Sonography of dermatologic emergencies. J Ultrasound Med. 2017;36(9):1905–14.
10. Wortsman X. Common applications of dermatologic sonography. J Ultrasound Med. 2012;31(1):97–111.
11. Aluja Jaramillo F, Quiasua Mejia DC, Martinez Orduz HM, Gonzalez Ardila C. Nail unit ultrasound: a complete guide of the nail diseases. J Ultrasound. 2017;20(3):181–92.
12. Cecchini A, Montella A, Ena P, Meloni GB, Mazzarello V. Ultrasound anatomy of normal nails unit with 18 Mhz linear transducer. Ital J Anat Embryol. 2009;114(4):137–44.
13. Wortsman X, Jemec GBE. Ultrasound imaging of nails. Dermatol Clin. 2006;24(3):323–8.
14. Stramare R, Gazzola M, Coran A, Sommavilla M, Beltrame V, Gerardi M, et al. Contrast-enhanced ultrasound findings in soft-tissue lesions: preliminary results. J Ultrasound. 2013;16(1):21–7.
15. Botar-Jid CM, Cosgarea R, Bolboaca SD, Senila SC, Lenghel LM, Rogojan L, et al. Assessment of cutaneous melanoma by use of very- high-frequency ultrasound and real-time elastography. AJR Am J Roentgenol. 2016;206(4):699–704.
16. Dasgeb B, Morris MA, Mehregan D, Siegel EL. Quantified ultrasound elastography in the assessment of cutaneous carcinoma. Br J Radiol. 2015;88(1054):20150344.
17. Ekwueme DU, Guy GP Jr, Li C, Rim SH, Parelkar P, Chen SC. The health burden and economic costs of cutaneous melanoma mortality by race/ethnicity-United States, 2000 to 2006. J Am Acad Dermatol. 2011;65(5 Suppl 1):S133–43.
18. Machet L, Belot V, Naouri M, Boka M, Mourtada Y, Giraudeau B, et al. Preoperative measurement of thickness of cutaneous melanoma using high-resolution 20 MHz ultrasound imaging: a monocenter prospective study and systematic review of the literature. Ultrasound Med Biol. 2009;35(9):1411–20.
19. Maj M, Warszawik-Hendzel O, Szymanska E, Walecka I, Rakowska A, Antczak-Marczak M, et al. High frequency ultrasonography: a complementary diagnostic method in evaluation of primary cutaneous melanoma. G Ital Dermatol Venereol. 2015;150(5):595–601.
20. Shaikh WR, Dusza SW, Weinstock MA, Oliveria SA, Geller AC, Halpern AC. Melanoma thickness and survival trends in the United States, 1989 to 2009. J Natl Cancer Inst. 2015;108(1):djv294.
21. Fernandez Canedo I, de Troya Martin M, Funez Liebana R, Rivas Ruiz F, Blanco Eguren G, Blazquez Sanchez N. Preoperative 15-MHz ultrasound assessment of tumor thickness in malignant melanoma. Actas Dermosifiliogr. 2013;104(3):227–31.
22. Guitera P, Li LX, Crotty K, Fitzgerald P, Mellenbergh R, Pellacani G, et al. Melanoma histological Breslow thickness predicted by 75-MHz ultrasonography. Br J Dermatol. 2008;159(2):364–9.
23. Blum A, Schlagenhauff B, Stroebel W, Breuninger H, Rassner G, Garbe C. Ultrasound examination of regional lymph nodes significantly improves early detection of locoregional metastases during the follow-up of patients with cutaneous melanoma. Cancer. 2000;88(11):2534–9.
24. Catalano O, Caraco C, Mozzillo N, Siani A. Locoregional spread of cutaneous melanoma: sonography findings. AJR Am J Roentgenol. 2010;194(3):735–45.
25. Catalano O, Siani A. Cutaneous melanoma: role of ultrasound in the assessment of locoregional spread. Curr Probl Diagn Radiol. 2010;39(1):30–6.
26. Wortsman X. Ultrasound in dermatology: why, how, and when? Semin Ultrasound CT MR. 2013;34(3):177–95.
27. Que SKT, Zwald FO, Schmults CD. Cutaneous squamous cell carcinoma: management of advanced and high-stage tumors. J Am Acad Dermatol. 2018;78(2):249–61.
28. Mandava A, Ravuri PR, Konathan R. High-resolution ultrasound imaging of cutaneous lesions. Indian J Radiol Imaging. 2013;23(3):269–77.
29. Pertik B, Yıldız H. Differentiation of benign and malignant skin lesions with color and power Doppler ultrasonography. J Clin Anal Med. 2013;4:107–11.
30. Thompson AK, Kelley BF, Prokop LJ, Murad MH, Baum CL. Risk factors for cutaneous squamous cell carcinoma recurrence, metastasis, and disease-specific death: a systematic review and meta-analysis. JAMA Dermatol. 2016;152(4):419–28.
31. Song WJ, Choi HJ, Lee YM, Tark MS, Nam DH, Han JK, et al. Clinical analysis of an ultrasound system in the evaluation of skin cancers: correlation with histology. Ann Plast Surg. 2014;73(4):427–33.
32. Wortsman X, Wortsman J, Matsuoka L, Saavedra T, Mardones F, Saavedra D, et al. Sonography in pathologies of scalp and hair. Br J Radiol. 2012;85(1013):647–55.
33. Aoyagi S, Izumi K, Hata H, Kawasaki H, Shimizu H. Usefulness of real-time tissue elastography for detecting lymph-node metastases in squamous cell carcinoma. Clin Exp Dermatol. 2009;34(8):e744–7.

34. Dudau C, Hameed S, Gibson D, Muthu S, Sandison A, Eckersley RJ, et al. Can contrast-enhanced ultrasound distinguish malignant from reactive lymph nodes in patients with head and neck cancers? Ultrasound Med Biol. 2014;40(4):747–54.
35. Bolognia J, Schaffer JV, Cerroni L. Dermatology: Philadelphia. Elsevier; 2018.
36. Jasaitiene D, Valiukeviciene S, Linkeviciute G, Raisutis R, Jasiuniene E, Kazys R. Principles of high-frequency ultrasonography for investigation of skin pathology. J Eur Acad Dermatol Venereol. 2011;25(4):375–82.
37. Vega N, Wortsman X, Navarrete N, Sazunic I. Color Doppler ultrasound supports early diagnosis of mixed high and low risk of recurrence subtypes in the same basal cell carcinoma lesion. Dermatol Surg. 2018;44(5):741–3.
38. Li M, Liu J, Valeska M, Luo D, Zhou B. Clinical evaluation of color Doppler ultrasound in selecting the optimal treatment modality for infantile hemangioma. Chin Med Sci J. 2017;32(2):100–6.
39. Steinklein JM, Shatzkes DR. Imaging of vascular lesions of the head and neck. Otolaryngol Clin N Am. 2018;51(1):55–76.
40. Mulligan PR, Prajapati HJS, Martin LG, Patel TH. Vascular anomalies: classification, imaging characteristics and implications for interventional radiology treatment approaches. Br J Radiol. 2014;87(1035):20130392.
41. Dubois J, Soulez G, Oliva VL, Berthiaume MJ, Lapierre C, Therasse E. Soft-tissue venous malformations in adult patients: imaging and therapeutic issues. Radiographics. 2001;21(6):1519–31.
42. Yuan WH, Hsu HC, Lai YC, Chou YH, Li AF. Differences in sonographic features of ruptured and unruptured epidermal cysts. J Ultrasound Med. 2012;31(2):265–72.
43. Hwang JY, Lee SW, Lee SM. The common ultrasonographic features of pilomatricoma. J Ultrasound Med. 2005;24(10):1397–402.
44. Ferner RE. Neurofibromatosis 1 and neurofibromatosis 2: a twenty first century perspective. Lancet Neurol. 2007;6(4):340–51.
45. Zarchi K, Wortsman X, Jemec GBE. Ultrasound as a diagnostic aid in identifying neurofibromas. Pediatr Dermatol. 2014;31(4):535–7.
46. Wortsman X, Jemec GB, Sazunic I. Anatomical detection of inflammatory changes associated with plantar warts by ultrasound. Dermatology. 2010;220(3):213–7.
47. Wortsman X, Jemec GBE. Dermatologic ultrasound with clinical and histologic correlations. New York: Springer; 2013.
48. Baek HJ, Lee SJ, Cho KH, Choo HJ, Lee SM, Lee YH, et al. Subungual tumors: clinicopathologic correlation with US and MR imaging findings. Radiographics. 2010;30(6):1621–36.
49. Wortsman X. Sonography of the nail. In: Wortsman X, editor. Dermatologic ultrasound with clinical and histologic correlations. New York: Springer; 2013. p. 419–76.
50. Chiou H-J, Chou Y-H, Chiou S-Y, Wang H-K. High-resolution ultrasonography in superficial soft tissue tumors. J Med Ultrasound. 2007;15(3):152–74.
51. Napolitano M, Megna M, Timoshchuk EA, Patruno C, Balato N, Fabbrocini G, et al. Hidradenitis suppurativa: from pathogenesis to diagnosis and treatment. Clin Cosmet Investig Dermatol. 2017;10:105–15.
52. Cataldo-Cerda K, Wortsman X. Dissecting cellulitis of the scalp early diagnosed by color Doppler ultrasound. Int J Trichology. 2017;9(4):147–8.
53. Haeusermann P, Kump E, Rovo A, Tichelli A, Itin P, Gratwohl A, et al. Partial reconstitution of cutaneous microvessels in long-term survivors after allogeneic bone marrow transplantation. Dermatology. 2009;219(1):32–41.
54. Gutierrez M, Filippucci E, De Angelis R, Filosa G, Kane D, Grassi W. A sonographic spectrum of psoriatic arthritis: “the five targets”. Clin Rheumatol. 2010;29(2):133–42.
55. Ally Essayed SM, al-Shatouri MA, Nasr Allah YS, Atwa MA. Ultrasonographic characterization of the nails in patients with psoriasis and onychomycosis. Egypt J Radiol Nucl Med. 2015;46(3):733–9.
56. Goldsmith LA, Katz SI, Gilchrest BA, Paller A, Leffell DJ, Wolff K. Fitzpatrick’s dermatology in general medicine. 8th ed., 2 volume set. New York: McGraw-Hill Education; 2012.
57. DeJong HM, Abbott S, Zelesco M, Kennedy BF, Ziman MR, Wood FM. The validity and reliability of using ultrasound elastography to measure cutaneous stiffness, a systematic review. Int J Burns Trauma. 2017;7(7):124–41.
58. Wortsman X, Jemec GB. Sonography of the ear pinna. J Ultrasound Med. 2008;27(5):761–70.
59. Taniguchi Y, Nishikawa H, Nakayama S, Amano E, Terada Y. Clinical implications of ultrasonography in monitoring disease activity of relapsing polychondritis. Rheumatology. 2016;55(7):1250.
60. Inotani S, Taniguchi Y, Nishikawa H, Amano E, Nakayama S, Terada Y. AB1157 Clinical implications of ultrasonography (US) in monitoring disease activity of relapsing polychondritis (RP) and comparative investigation by us between auricle of rp, repeated trauma and healthy subject. Ann Rheum Dis. 2018;77(Suppl 2):1682.
61. Eksombatchai D, Boonsarngsuk V, Amornputtisathaporn N, Suwatanapongched T, Kurimoto N. Tracheobronchial involvement in relapsing polychondritis diagnosed on endobronchial ultrasound. Intern Med. 2013;52(7):801–5.
62. Stonecipher MR, Jorizzo JL, Monu J, Walker F, Sutej PG. Dermatomyositis with normal muscle enzyme concentrations: a single-blind study of the diagnostic value of magnetic resonance imaging and ultrasound. Arch Dermatol. 1994;130(10):1294–9.
63. Khuu A, Yablon CM, Jacobson JA, Inyang A, Lucas DR, Biermann JS. Nodular fasciitis: characteristic imaging features on sonography and magnetic resonance imaging. J Ultrasound Med. 2014;33(4):565–73.
64. Tognetti L, Filippou G, Bertrando S, Picerno V, Buonocore G, Frediani B, et al. Subcutaneous fat necrosis in a newborn after brief therapeutic hypothermia: ultrasonographic examination. Pediatr Dermatol. 2015;32(3):427–9.
65. Vasireddy S, Long SD, Sacheti B, Mayforth RD. MRI and US findings of subcutaneous fat necrosis of the newborn. Pediatr Radiol. 2009;39(1):73–6.
66. Gooptu S, Ali I, Singh G, Mishra RN. Mycetoma foot. J Fam Community Med. 2013;20(2):136–8.
67. Nalbant S, Corominas H, Hsu B, Chen LX, Schumacher HR, Kitumnuaypong T. Ultrasonography for assessment of subcutaneous nodules. J Rheumatol. 2003;30(6):1191–5.
68. Bude RO, Adler RS, Bassett DR. Diagnosis of Achilles tendon xanthoma in patients with heterozygous familial hypercholesterolemia: MR vs sonography. Am J Roentgenol. 1994;162(4):913–7.
69. Halaas GW. Management of foreign bodies in the skin. Am Fam Physician. 2007;76(5):683–8.
70. Bianchi S, Baert AL, Abdelwahab IF, Derchi LE, Martinoli C, Rizzatto G, et al. Skin and subcutaneous tissue. In: Ultrasound of the musculoskeletal system. Berlin, Heidelberg: Springer; 2007.
71. Wortsman X. Identification and complications of cosmetic fillers: sonography first. J Ultrasound Med. 2015;34(7):1163–72.
72. Wortsman X, Wortsman J, Orlandi C, Cardenas G, Sazunic I, Jemec GB. Ultrasound detection and identification of cosmetic fillers in the skin. J Eur Acad Dermatol Venereol. 2012;26(3):292–301.
73. Bowry R, Cottingham RL. Use of ultrasound to aid management of late presentation of Dermatobia hominis larva infestation. J Accid Emerg Med. 1997;14(3):177–8.
74. Rocha A, Braga C, Belem M, Carrera A, Aguiar-Santos A, Oliveira P, et al. Comparison of tests for the detection of circulating filarial antigen (Og4C3-ELISA and AD12-ICT) and ultrasound in diagnosis of lymphatic filariasis in individuals with microfilariae. Mem Inst Oswaldo Cruz. 2009;104(4):621–5.

75. Thibault PK. Duplex examination. Dermatol Surg. 1995;21(1):77–82.
76. Quere I, Leizorovicz A, Galanaud JP, Presles E, Barrellier MT, Becker F, et al. Superficial venous thrombosis and compression ultrasound imaging. J Vasc Surg. 2012;56(4):1032–8.e1.
77. Qi HT, Wang XM, Zhang XD, Zhang MH, Li CM, Bao SG, et al. The role of colour Doppler sonography in the diagnosis of lower limb Klippel-Trenaunay syndrome. Clin Radiol. 2013;68(7): 716–20.
78. Ball EL, Walsh SR, Tang TY, Gohil R, Clarke JM. Role of ultrasonography in the diagnosis of temporal arteritis. Br J Surg. 2010;97(12):1765–71.
79. Georgiev M, Ricci S, Carbone D, Antignani P, Moliterno C. Stab avulsion of the short saphenous vein technique and duplex evaluation. J Dermatol Surg Oncol. 1993;19(5):456–64.
80. Damian DL, Yiasemides E, Gupta S, Armour K. Ultrasound therapy for lipodermatosclerosis. Arch Dermatol. 2009;145(3):330–2.
81. Caswell D, McNulty BM. Low-frequency, therapeutic ultrasound treatment for congenital ectodermal dysplasia in toddlers. Ostomy Wound Manage. 2008;54(10):58–61.
82. Ziskin MC. Fundamental physics of ultrasound and its propagation in tissue. Radiographics. 1993;13(3):705–9.
83. Polat BE, Hart D, Langer R, Blankschtein D. Ultrasound-mediated transdermal drug delivery: mechanisms, scope, and emerging trends. J Control Release. 2011;152(3):330–48.
84. Machet L, Boucaud A. Phonophoresis: efficiency, mechanisms and skin tolerance. Int J Pharm. 2002;243(1–2):1–15.
85. Oberli MA, Schoellhammer CM, Langer R, Blankschtein D. Ultrasound-enhanced transdermal delivery: recent advances and future challenges. Ther Deliv. 2014;5(7):843–57.

Part VI

Emergency Ultrasound

Fundamentals of Point of Care Ultrasound Applications in Perioperative Settings

Sonya Bohaczuk and Yan Lai

1 Introduction

Ultrasound has had tremendous and timeless impacts on many medical professions but there are few specialties that utilize ultrasound as both a diagnostic and interventional or procedural tool. Some of these medical subspecialties have led practical developments and published a prolific body of evidence that deepened our contemporary understanding of ultrasound applications. These include radiology, cardiology, emergency medicine, critical care medicine, pain management, and anesthesiology. Collaborations between experts of these fields have translated valuable ultrasound technology into relevant clinical settings that improved patient care as well as care delivery. One such example is the evolution of transesophageal echocardiogram (TEE) as a diagnostic tool in cardiology into its use in cardiac anesthesiology as both a diagnostic and therapeutic tool.

The surgical and perioperative periods are unique settings because they demand the use of a combination of diagnostic strategies and therapeutic interventions in a dynamic and rapidly changing clinical environment. Timely diagnosis and treatment of iatrogenic trauma or medically induced disturbances in patient conditions that may have catastrophic consequences can greatly impact on patient outcomes. Many experts have published on and employed the I-AIM framework in their approach to POCUS [2]. I-AIM stands for **I**ndication, **A**cquisition, **I**nterpretation, and **M**edical decision making. It focuses on a specific clinical indication or problem in order to drive utilizing a particular technique to arrive at a decision and executing an intervention [2]. Common examples of focused indications include full stomach, pneumothorax, hypovolemia, difficult airway, and internal hemorrhage. The identification or recognition of these indications drives specific ultrasound applications such as gastric, lung, cardiac, airway, or trauma. The next steps in I-AIM is to learn the skills to acquire ultrasound images and interpret the findings in a focused manner that only responds to the original indications and ultimately determines decision making. To illustrate the practicality of this framework, a clinical scenario can bring into question whether a patient is full stomach or not and whether they would be a candidate for safe and elective surgery (i.e. indication). Gastric ultrasound images are acquired and interpreted as the patient having full stomach (i.e. acquisition and interpretation). Finally, surgery is postponed or anesthetic techniques are modified based on the provider's interpretation (i.e. medical decision making). This same framework can be applied to other well described clinical contexts that have specific indications that are matched with a particular ultrasound technique that in turn would yield a change in decision making. This change in decision making can potentially impact on patient safety and outcomes. Some other well described indications include pulmonary edema, diaphragmatic paresis, cardiac tamponade, pulmonary embolism, dysfunctions or pathologies of various cardiac valves, and impaired cardiac contractility. When applied in the appropriate clinical settings (a patient with severe history of diabetic gastroparesis who has received large amount of opioids before surgery, a patient who is dyspneic after a brachial plexus block, severe hypotension intraoperatively, difficulty troubleshooting ventilator settings to improve oxygenation in a patient with pulmonary disease, a trauma patient, etc…), POCUS has the potential to change perioperative management considerably.

However, it is also important to note that POCUS is an emerging field that is currently undergoing development in technique and evidence. Some aspects of POCUS such as airway or gastric ultrasound have not been subjected to the same degree of academic evaluation compared to cardiac or lung ultrasound techniques that have enjoyed much more fertile contributions from cardiology, critical care, and emergency medicine fields. For instance, there has been less pub-

---

S. Bohaczuk · Y. Lai (✉)
Mount Sinai West and St. Luke's Hospitals, Department of Anesthesiology, Perioperative, and Pain Medicine, Icahn School of Medicine at Mount Sinai Medical Center, New York, NY, USA
e-mail: yan.lai@mountsinai.org

© Springer Nature Switzerland AG 2021

J. Li et al. (eds.), *Ultrasound Fundamentals*, https://doi.org/10.1007/978-3-030-46839-2_31

lished knowledge on how airway ultrasound can accurately diagnose esophageal intubations or how gastric ultrasound can apply to other surgical population such as pediatric and obstetric patients. Experts are still refining certain novel techniques while increasing our general knowledge and applicability of others. We must acknowledge that while ultrasound has proven useful in answering focus clinical questions or providing more depth of insights to derangements in patient conditions, there are still limitations and gaps in our understanding. While the concept of performing preoperative lung or cardiac ultrasound exams in a hip fracture patient exhibiting symptoms is fascinating and potentially impactful, to date there are no population studies that definitively illustrate that these specific ultrasound interventions are efficacious and cost effective in terms of patient outcomes and safety.

Despite these current shortcomings, POCUS promises great potential in the areas of education and implementation. Anesthesiologists are already extremely familiar with many of the procedural aspects of ultrasound as well as the practical use of ultrasound equipment. The ubiquitous nature of ultrasound in all types of anesthesiology practices makes it easy to expand POCUS. Practitioners might not be familiar with the various POCUS terminologies or the subtle skills to acquire complex images, but the basic understanding of ultrasound knobs and the manual dexterity with acquiring images for peripheral blocks or vascular access makes POCUS relatively easy to teach and simple to master. Many national anesthesiology societies and ultrasound organizations are brainstorming guidelines and standards for ultrasound applications in the perioperative settings. Regulatory bodies and board certification institutions are incorporating elements of POCUS for resident training and continuing medical education. It would not be a surprise to foresee the implementation of POCUS into clinical pathways and perioperative surgical homes for local healthcare institutions, its applications and documentation of results serving as benchmarks for governing establishments or insurance companies to dictate future reimbursement models, as well as POCUS transitioning into perioperative standards or routine practice. Similar to how the stethoscope has characterized advances in medicine in the 19th and 20th century, the modern point of care ultrasound in the perioperative setting will share the potential and capability in changing the application, interpretation, and medical decision making for our patients. As physicians, it is essential to master the fundamental aspects of POCUS in the 21th century.

2 Gastric Ultrasound

2.1 Indications

The American Society of Anesthesiologists (ASA) offers pre-operative fasting guidelines to reduce risk of pulmonary aspiration of gastric contents in healthy patients [3]. However, a number of patient factors may contribute to variations and delay in gastric emptying, including diabetic gastroparesis, critical or end-stage illness, high dose opioids, anatomic anomalies, neuromuscular disease, and pregnancy [2, 4, 5]. On the other hand, more urgent procedures might require additional information to accurately analyze the benefits and risks of proceeding with surgery with less fasting time for selected patients. Finally, concerns regarding poor historians or patients unable to provide a history make an objective technique to ascertain gastric contents desirable [6]. All of these scenarios have potential to change medical decisions on proceeding with surgery preoperatively, alterations in anesthetic techniques and airway management intraoperatively, as well as decisions to provide mechanical ventilation or starting oral intake postoperatively.

2.2 Acquisition of Image and Sonoanatomy

A low-frequency curvilinear transducer is required to achieve adequate depth of ultrasound penetration in typical adult patients. Gastric ultrasound can be performed with the patient in supine or in right lateral decubitus (RLD) positions. Visualization of fluid in the supine position suggests higher gastric volume since fluid is more evenly distributed in the stomach when the patient is supine [7, 8]. The RLD is more sensitive to smaller amount of fluid since fluid tends to migrate with gravity towards dependent portions of the stomach. In fact, most literature has focused on patients in the RLD position, where the dependent region is the antrum of the stomach. This portion of the stomach just proximal to the pylorus is a region well visualized by ultrasound with easily recognizable anatomic landmarks [7].

The ultrasound transducer is oriented sagittally (Fig. 1), beginning subxiphoid and scanning left or right until the descending aorta or IVC appear in long axis view as a deep structure. The liver will be seen superficially below the muscles of the abdominal wall, and the antrum of the stomach will be the hollow viscous that is just deep to the caudal edge of the liver, superficial to the pancreas (Fig. 2).

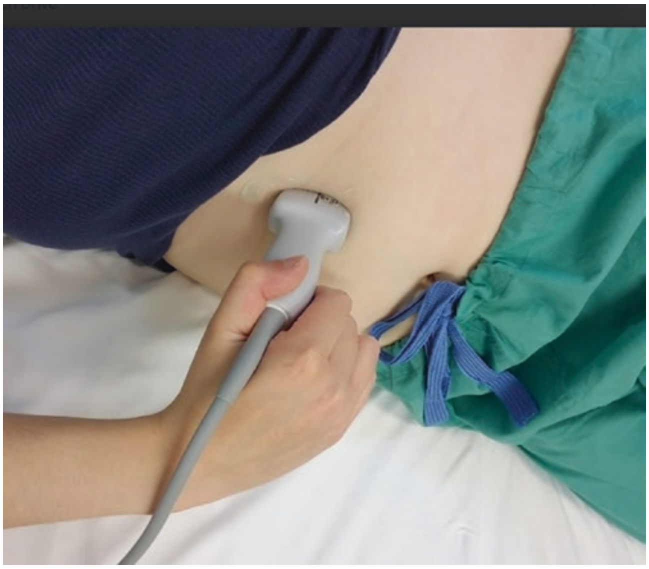

Fig. 1 Sagittal probe looking for gastric antrum

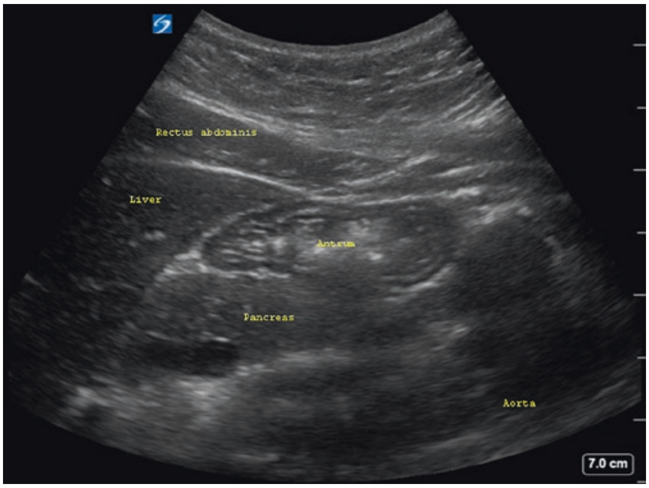

Fig. 2 Empty stomach with labeled surrounding structures

2.3 Clinical or Pathological Interpretation and Medical Decision Making

The empty stomach appears as an ovoid, “target” shaped structure due to the relative echogenicity of the 5 gastric wall layers (Fig. 2) [9]. The stomach containing clear liquid appears similarly, but with a larger anechoic central region (Fig. 3). Small amount of clear fluid may be present in the fasting stomach due to normal gastric secretions. Larger volumes of recently consumed clears may be mixed with air, yielding a “starry” appearance (Fig. 4) [7].

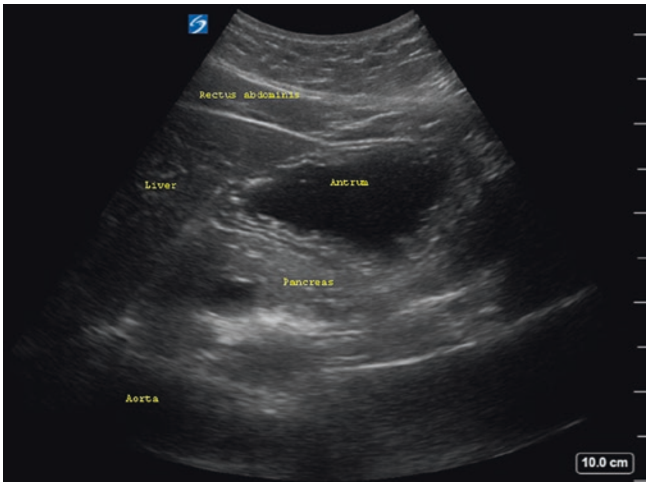

Fig. 3 Stomach with liquid

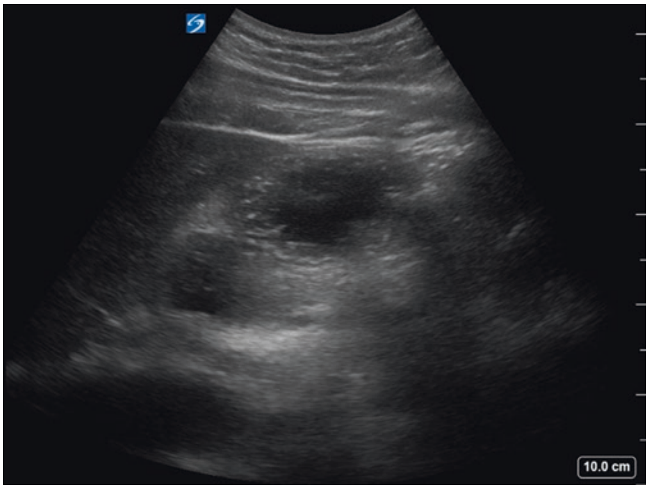

Fig. 4 Stomach with liquid and air

Though the volume that constitutes aspiration risk is not well defined or validated, the volume of secretions in fasting patients has been well studied, and is quantified as less than 1.5 mL/kg [7]. There is a well-validated, linear relationship between the cross-sectional area of the antrum (measured via caliper trace around the outermost serosal layer of the stomach on ultrasound) and the associated gastric volume, described by Perlas et al. [10] as:

$$\text{Gastric volume}\left(\text{mL}\right) = 27 + 14.6\left(\text{cross sectional area of antrum in right lateral decubitus}\right) - 1.28\left(\text{age}\right)$$

This formula, along with published version of an applied nomogram, can be used to calculate the volume of the stomach (Fig. 5). A stomach with a volume above 100 mL, which represents approx. 1.5 ml/kg in the average 70 kg person, is consistent with a higher than normal fasting stomach content and may favor a change in anesthetic plan. Experts also propose a simpler semi-quantitative approach, whereby a "grade 0 antrum" has no appreciable content, a "grade 1 antrum" has liquid content that can be seen in RLD but not supine, and a "grade 2 antrum" has clear fluid visible in both positions [8].

Solid gastric contents appear as "frosted," heterogeneous and hyperechoic, potentially with pockets of air that may reflect ultrasound beams and obscure deeper structures (Fig. 6) [7]. The finding of solid stomach contents present an elevated risk for aspiration and may favor a change in anesthetic plan, whether rapid sequence induction, delay of elective procedure, or alternative technique.

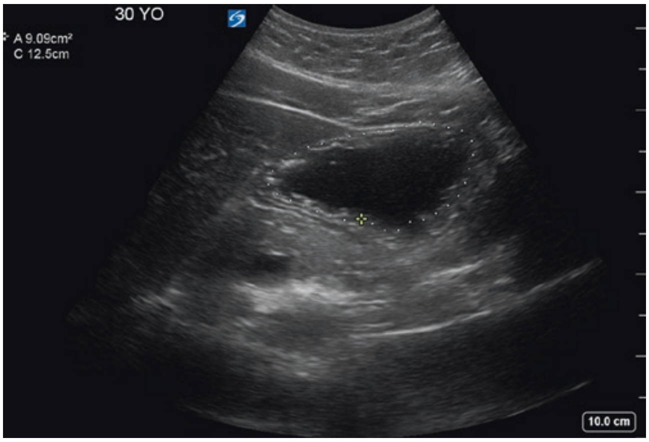

Fig. 5 Figure 3 with CSA caliper measurement to determine fluid volume. Using the equation, volume = 27.0 + (14.6∗9.09) − (1.28∗30) = 121 mL, which is >1.5 mL/kg in this 70 kg, 30 year old patient

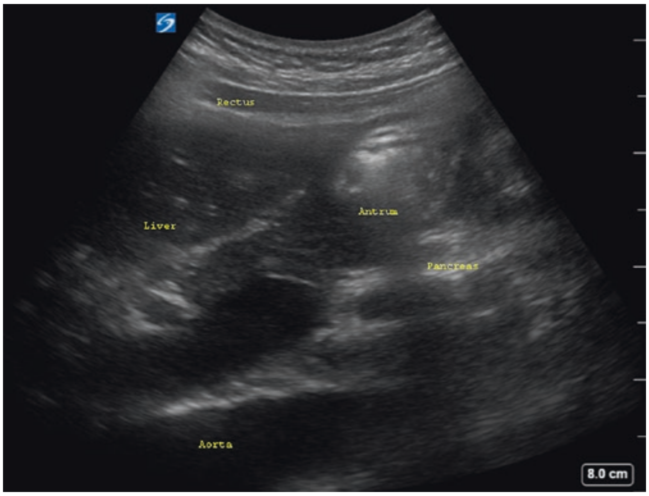

Fig. 6 Stomach with food

3 Lung Ultrasound

3.1 Indications

Point of care lung ultrasound has been widely adopted within emergency medicine, trauma surgery, and critical care [11]. Within the field of anesthesiology, lung ultrasound offers the information to quickly distinguish between multiple etiologies of respiratory distress and hypoxia, including those caused directly by recent clinical intervention. With a rapid bedside scan, pneumothorax, pleural effusion, and diaphragmatic paresis (which may have occurred during block placement or central line insertion) may be assessed and distinguished from interstitial or alveolar processes, such as pulmonary edema or pneumonia [12]. Of note, for the most part, the lung itself is not being assessed during this exam; rather, the *artifacts* generated by the interface of lung, pleural membranes, and surrounding structures are interpreted [13].

3.2 Acquisition of Image and Sonoanatomy

Linear, curvilinear, and phased array ultrasound transducers can all be employed to assess pathologies, and the order of exam may vary depending on level of suspicion for a particular pathology [11].

Pneumothorax is commonly assessed in the supine position along the apical portion of the lung fields with a high frequency linear transducer, allowing air to rise to the anterior chest where it is most easily imaged. The probe is placed in the second through fourth intercostal space in a parasagittal plane along the midclavicular line (Fig. 7). When a patient

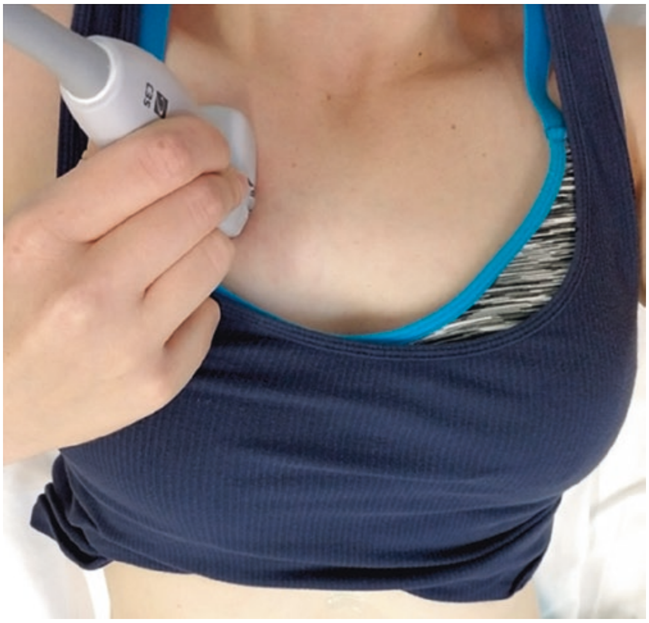

Fig. 7 Parasagittal lung ultrasound

is breathing, the visceral and parietal pleural slide against each other, generating a "curtain closing" or "ants marching" appearance, referred to as "lung sliding." "Lung pulse" occurs in the apneic patient or between breaths, when the two layers of pleura move along each other due to pulsatile cardiac motion. "B lines" are laser-like vertical reverberation artifacts generated between aerated lung and interstitial fluid at the deepest edge of the ultrasound screen (Fig. 8). These appear as "comet-tails" or "rockets" that extend from the visceral pleura to lung parenchyma, and appear to move in-sync with lung sliding. The presence of lung sliding, B lines, or lung pulse effectively rule out pneumothorax [11–13]. In M-mode (motion mode), which focuses on a single ultrasound beam over time, the "seashore" sign is generated where the less mobile chest wall appears in the shallow field and the lung appears deep, with a bright line in the center generated by the pleura (Fig. 9).

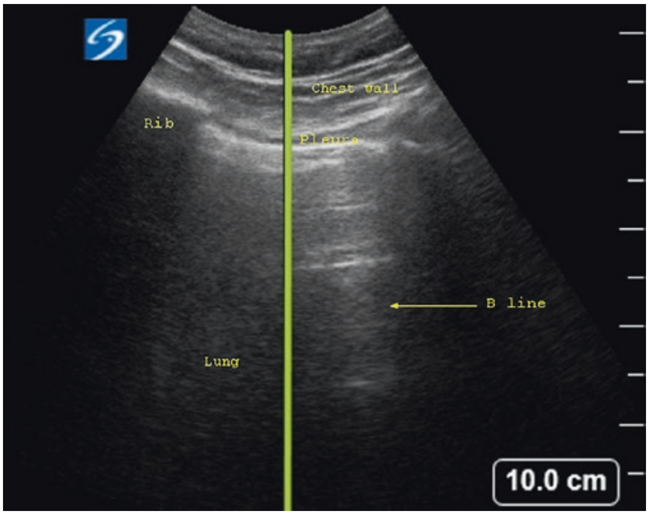

Fig. 8 Parasagittal anterior chest, B lines labeled

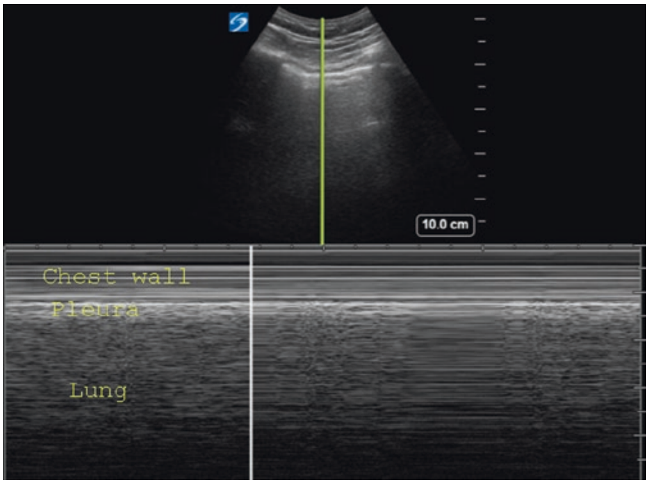

Fig. 9 Seashore sign

Pleural effusion is assessed in the sitting or supine position, with probe placed along the axillary or posterior axillary line to locate the most dependent region where fluid will pool (Fig. 10). A low frequency curvilinear transducer is typically chosen for adequate penetration. The diaphragm is identified by scanning along the base of the chest wall, and will appear as a hyperechoic line along the more inferior solid organ upon which it abuts (spleen on left, liver on right). In normal lung, the aerated lung will also appear adherent to the diaphragm, with no appreciable gap (Fig. 11).

Ultrasound can also be used to assess diaphragmatic excursion, such as in the setting of respiratory distress after brachial plexus block (most commonly the interscalene block). The diaphragm can be assessed either by imaging through the spleen and liver, or by imaging between intercostal spaces. When imaging through the spleen and liver, a low frequency probe is placed subcostal and aimed cranially, medially, and dorsally, as perpendicular to the diaphragm as possible, using the solid organ as an acoustic window to the diaphragm [14]. When imaging between intercostal spaces, a high frequency probe is oriented sagittal, placed at approximately the 8th to 10th intercostal space in the anterior axillary line, and moved inferiorly until diaphragmatic movement is seen [15]. In either case, the patient is typically supine.

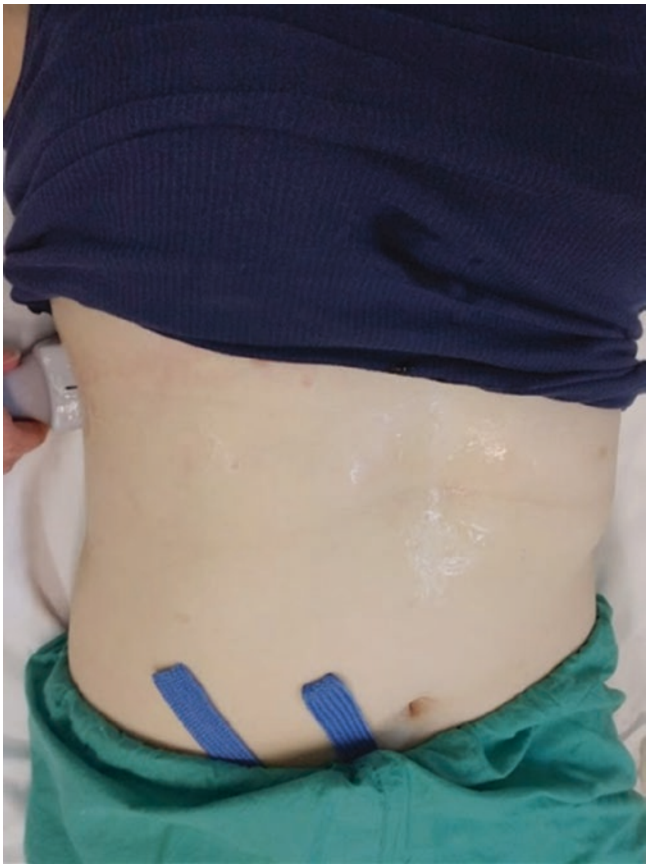

Fig. 10 Posterior axillary line probe

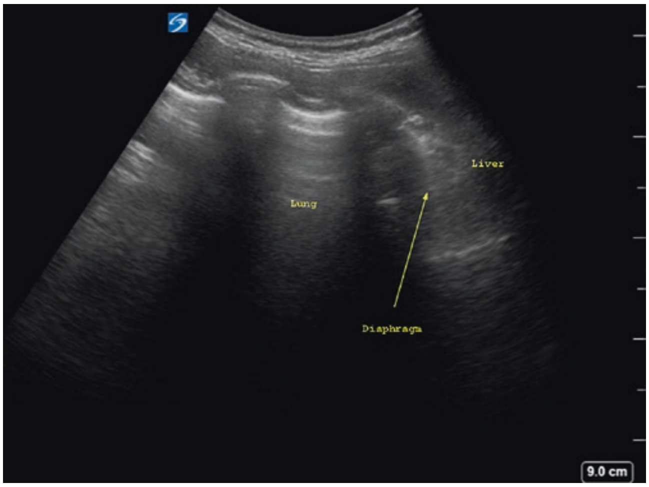

Fig. 11 Posterior axillary line, no effusion

3.3 Clinical or Pathological Interpretation and Medical Decision Making

If there is air sitting between the visceral and parietal pleura, as occurs during a pneumothorax, the pleural layers will not slide against each other. If there is air overlying the visceral pleura, B-lines will not be generated at this interface. In M-mode, the seashore sign will be replaced by the "barcode sign" or "stratosphere sign" where the deep portions of the screen (lung) appear similar to the shallow fields (chest wall) due to loss of the pleural interface (Fig. 12). Pneumothorax is confirmed with localization of the "lung point," which is 100% specific to pneumothorax, but not always visible [13, 16]. The lung point occurs at the transition point, where in one screen it is possible to see normal visceral and parietal pleural interface alongside the obliterated interface, moving as breathing occurs. The lung point is localized by scanning laterally and posteriorly until normal lung interface is identified. Three or fewer B lines in a field are consistent with normal lung, while more than three B lines within a single intercostal field are associated with interstitial edema [12]. If multiple B lines are seen, scanning the anterior, lateral, and posterior lung fields can help to distinguish localized processes, such as pneumonia, from diffuse processes, such as congestive heart failure or ARDS. Typically, an eight-region anterior lung scan is performed at minimum to assess for interstitial pathology [11].

Pleural effusion is more likely to be detected with ultrasound than chest radiograph, and will appear as an anechoic layer between the diaphragm and the lung [17]. Depending on the blood or protein content of the fluid, it may appear anechoic throughout or may have echogenic strands or clots. Movement of the lung through the anechoic fluid will may also be appreciated in M-mode ("sinusoid sign") [11].

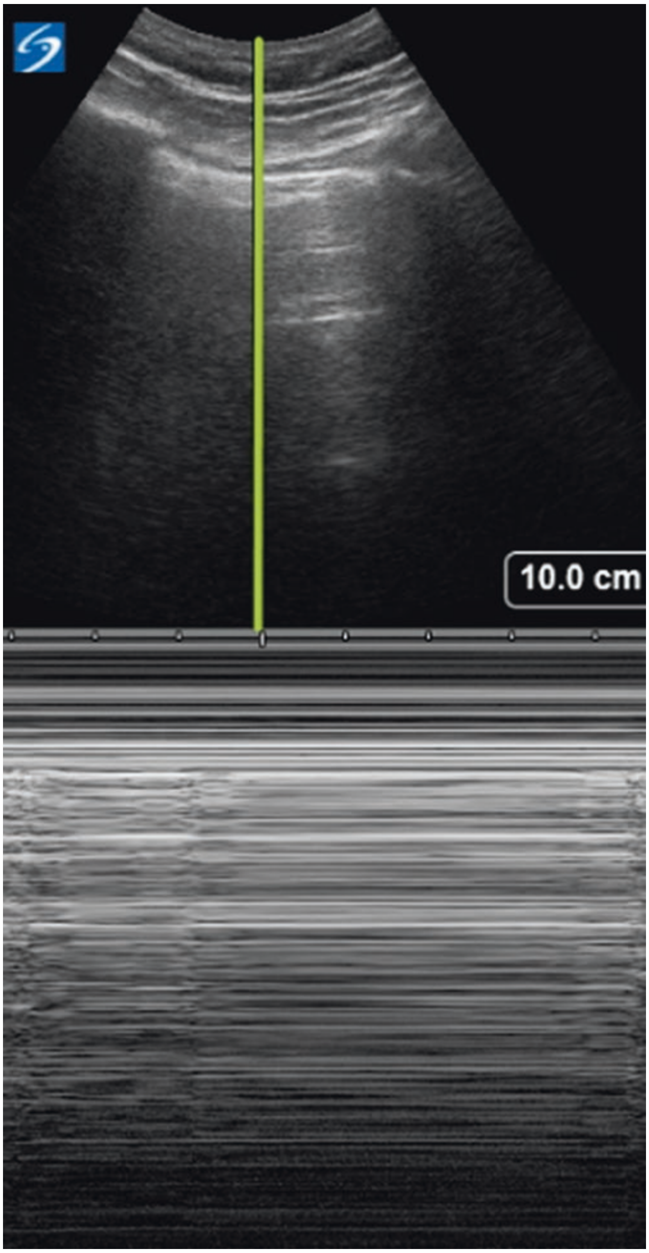

Fig. 12 Barcode sign (breath hold)

In the subcostal technique, diagphragmatic excursion is measured by asking the patient to sniff and measuring the inflection (Fig. 13). Normal excursion is 2.8 ± 0.6 cm, measured in M-mode during sniff, with slightly higher values seen in men than women [14, 18]. The diaphragm thickening fraction can also be calculated (change in thickness at inspiration vs expiration/thickness at expiration), with an average reported change of 54% [14]. In the intercostal technique, the diaphragm thickening fraction can also be measured [15].

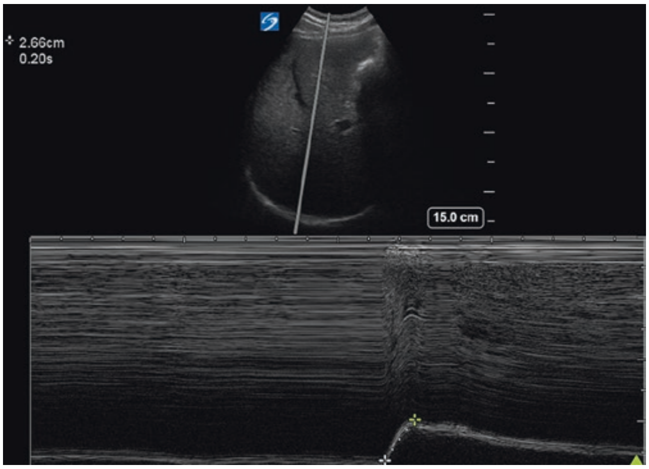

Fig. 13 Diaphragmatic excursion w/sniff, 2.66 cm by caliper measurement in this patient

4 Cardiac Ultrasound

4.1 Indications

FATE (**F**ocused **A**ssessed **T**ransthoracic **E**chocardiography) allows for immediate qualitative assessment of volume status, cardiac chamber characteristics such as dimension, contractility and wall motion; and gross valvular function [19, 20]. This can become important perioperatively to determine appropriate anesthetic technique or to troubleshoot major disturbances in hemodynamic instability. Real-time and dynamic FATE exam can guide decision to proceed or postpone surgery in an unstable patient with signs and symptoms of hypotension with multiple competing etiologies or ambiguous causes. Point of care cardiac ultrasound can also dictate needs for additional and other formal testing (TTE performed by cardiologist, detailed assessment of valvular function, stress testing) or the placement of invasive lines before surgery.

4.2 Acquisition of Image and Sonoanatomy

The phased-array probe is preferred for cardiac ultrasound [19]. Its small size makes it easy to navigate between bony structures of the anterior chest, while maintaining the wide imaging area and the depth of penetration necessary to obtain an adequate exam. For subcostal views, the patient is supine with knees flexed. While parasternal and apical views may also be obtained with a supine patient, left lateral decubitus position displaces structures of interest anteriorly, producing a higher quality image.

4.3 Clinical or Pathological Interpretation and Medical Decision Making

Cardiac Ultrasound Interpretation [19–22]:

View	Probe Placement	Ultrasound View	Notable structures and key features	Potential pathology to note	Further assessment
Subcostal 4 chamber view	Subxiphoid, marker aimed to left shoulder Fig. 14	Fig. 15	All 4 cardiac chambers, mitral and tricuspid valves	Hypertrophic or dilated chambers, contractility, wall motion abnormalities, valvular lesions, pericardial effusion or tamponade	Massive PE may show bowing of intraventricular septum into LV during systole [23]
Subcostal IVC view	R subcostal, slightly off medial, marker aimed cephalad Fig. 16	Fig. 17	IVC in long axis, as it meets the right atrium	Widely dilated IVC or collapsed IVC, indicating volume status	M-mode assessment of IVC collapsibility during inspiration [24]: Normal IVC diameter is <1.5 cm, with >50% collapse on inspiration. Complete collapse suggests hypovolemia, while diameter >3 cm without change during inspiration suggests hypervolemia.
Parasternal long axis (PLAX) view	L sternal border, roughly 3rd intercostal, marker aimed to right shoulder Fig. 18	Fig. 19	Right ventricle, intraventricular septum, left ventricle, left ventricle inflow and outflow, aortic and mitral valves	Hypertrophic or dilated ventricles, LV or RV wall motion abnormality, contractility, mitral or aortic valvular lesions, ascending aorta dilation, dilated left atrium, pericardial effusion or tamponade	Aortic stenosis can be qualitatively assessed in terms of cusp mobility and thickness.
Parasternal short axis (PSAX) view	L sternal border, roughly 3rd intercostal, marker aimed to left shoulder Fig. 20	Fig. 21	Right ventricle, intraventricular septum, left ventricle	Hypertrophic or dilated ventricles, LV or RV wall motion abnormality, contractility, pericardial effusion or tamponade, hypovolemia	Hypovolemia will present with a hyperdynamic LV with walls appearing to touch during systole Massive PE may show collapsed LV compared to RV (D-shaped LV)
Apical 4 chamber view	Point of maximum impulse, marker aimed to left axilla Fig. 22	Fig. 23	All 4 cardiac chambers, mitral and tricuspid valves	Hypertrophic or dilated chambers, wall motion abnormalities, contractility, valvular lesions, pericardial effusion or tamponade	Best view to assess RV size (should appear less than 2/3 size of LV) [23]

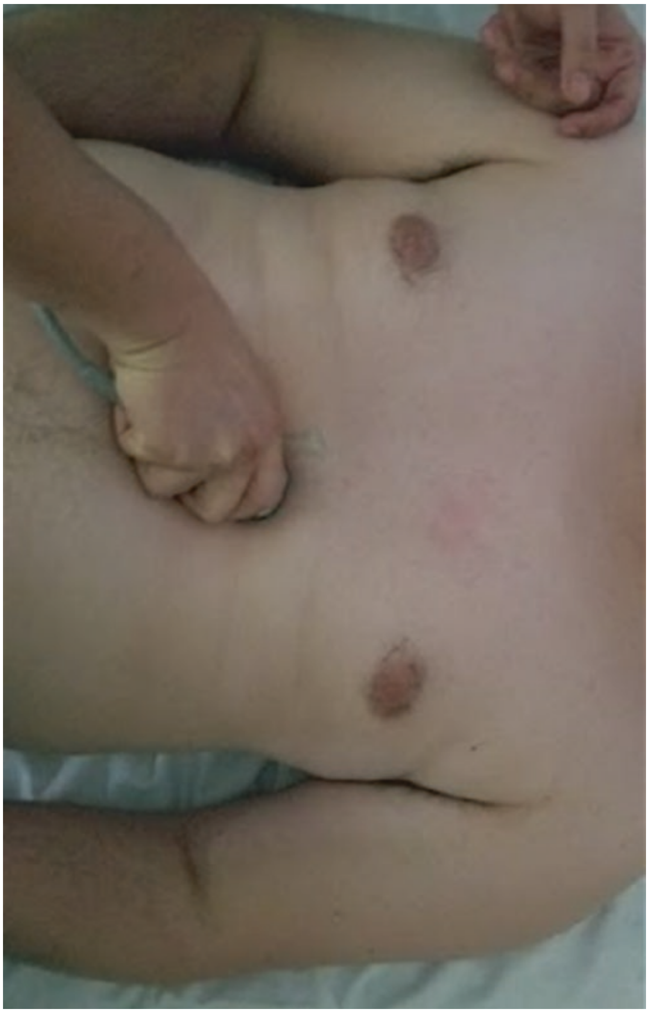

Fig. 14 SUBCOSTAL 4C probe position

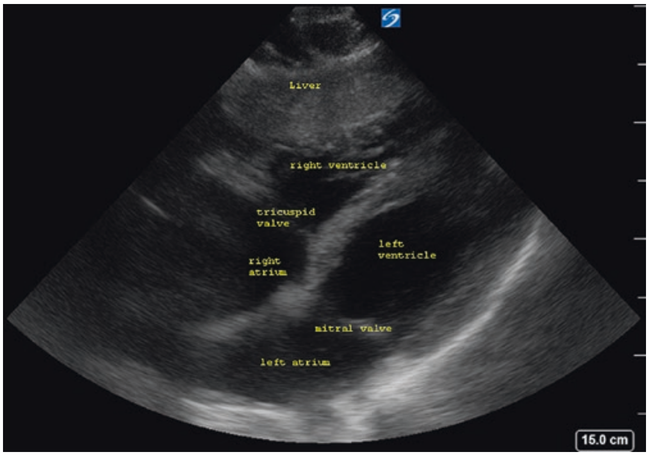
Liver
right ventricle
tricuspid valve
right atrium
left ventricle
mitral valve
left atrium
15.0 cm

Fig. 15 SUBCOSTAL 4C ultrasound view

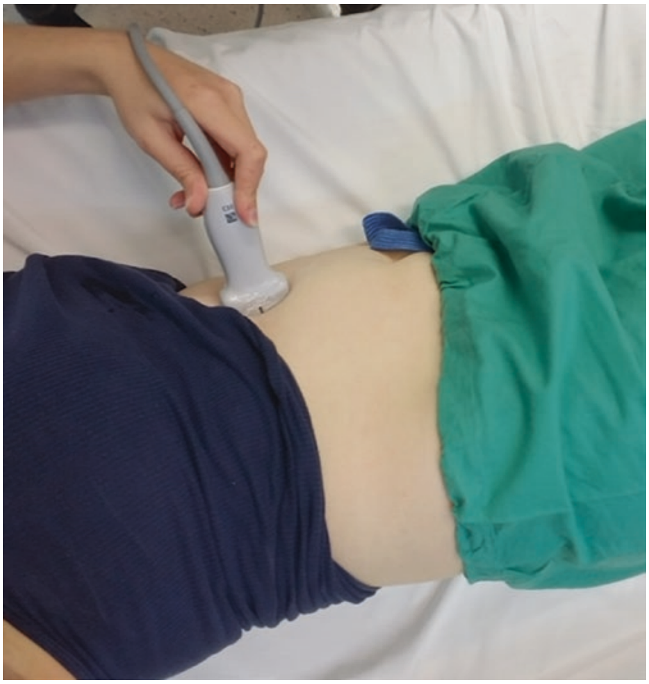

Fig. 16 SUBCOSTAL IVC probe position

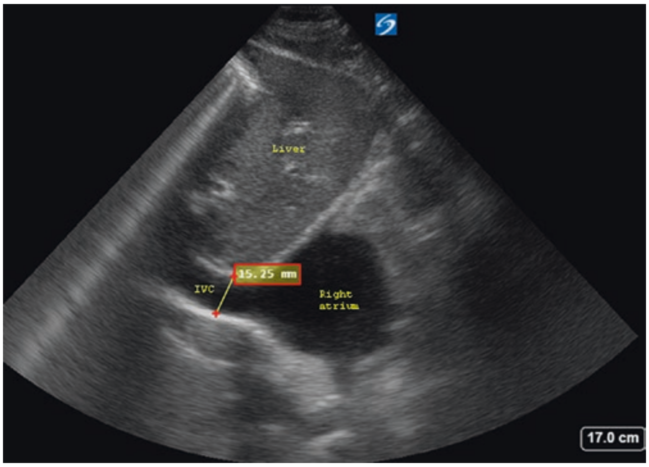
Liver
15.25 mm
IVC
Right atrium
17.0 cm

Fig. 17 SUBCOSTAL IVC ultrasound view

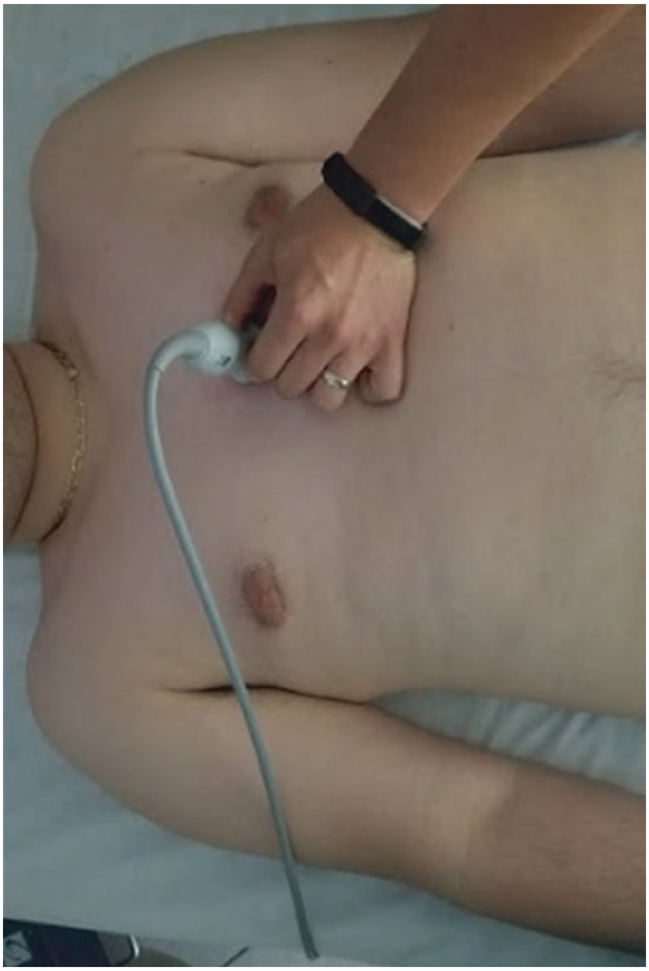

Fig. 18 PLAX probe position

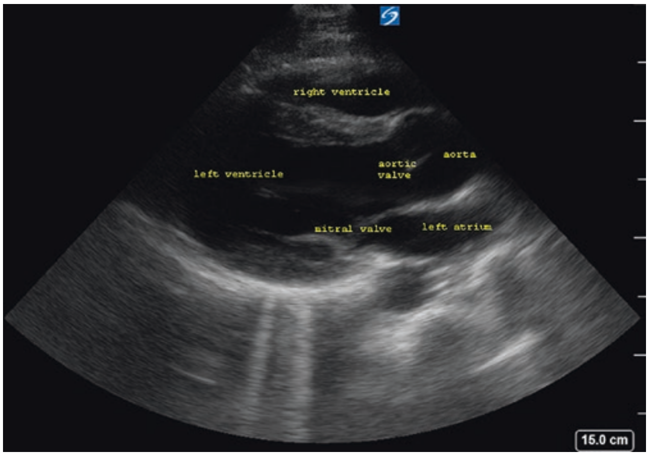
right ventricle
aorta
aortic valve
left ventricle
mitral valve
left atrium
15.0 cm

Fig. 19 PLAX ultrasound view

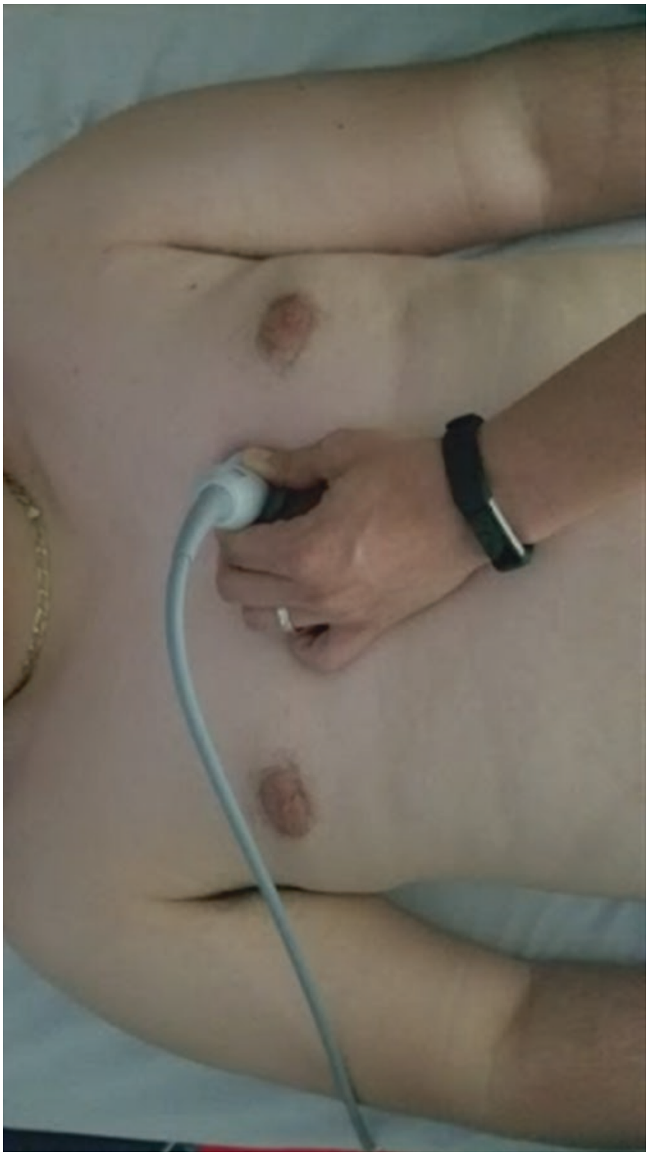

Fig. 20 PSAX Probe position

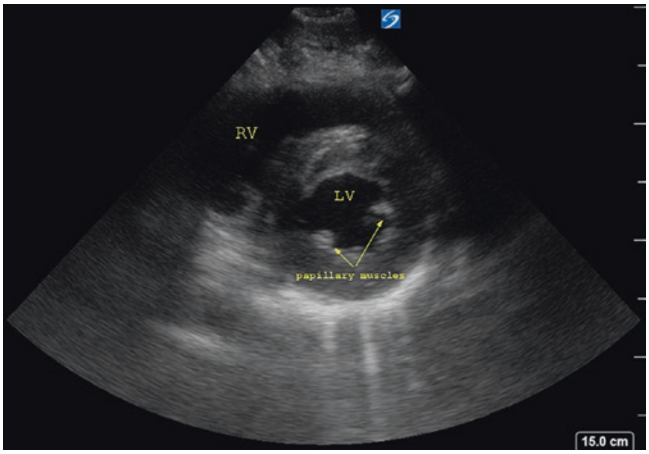
RV
LV
papillary muscles
15.0 cm

Fig. 21 PSAX Ultrasound View

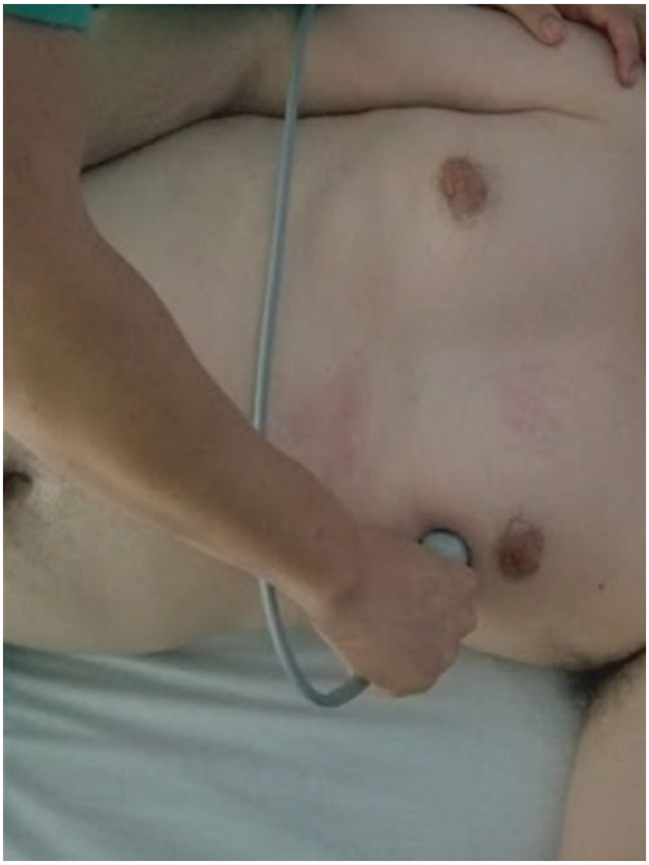

Fig. 22 A4C Probe position

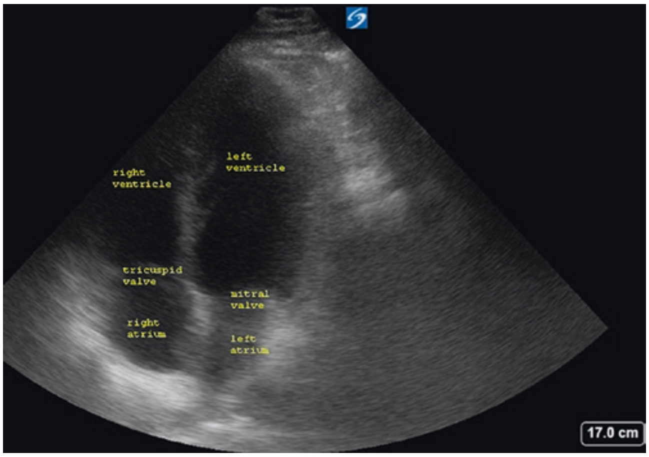

Fig. 23 A4C Ultrasound View

5 Additional Point of Care Techniques: Airway Ultrasound and FAST Exams

5.1 Indications

Airway ultrasound and FAST (**F**ocused **A**ssessment with **S**onography for **T**rauma) exams are highlighted here briefly as additional techniques. Airway ultrasound has limited use as a diagnostic tool compared to its other POCUS counterparts. FAST exam is traditionally performed in emergency settings for trauma and the majority of its elements (looking for pericardial fluid and occult fluid in abdominal recesses) have been incorporated in cardiac/FATE exams in POCUS. Also, FAST exam is described in detail in other chapters and repetitive elements of FAST will not be mentioned here.

Point of care airway ultrasound can be used to assess landmarks on the anterior neck in patients who have challenging anatomy (morbid obesity, congenital anatomical changes, and acquired anatomical changes due to head and neck malignancy, surgery or radiation to the neck). Airway ultrasound assesses for sonoanatomy landmarks such as tracheal cartilages, cricoid cartilage, thyroid cartilage, membranes and ligaments between cartilages, air interfaces, thyroid glands; muscles of the neck, relevant anatomy of laryngeal inlet, vocal cords, esophagus, vessels, and thyroid gland. Airway ultrasound can be useful to localize cricothyroid membrane and hyoid bone for airway blocks (recurrent laryngeal nerve and trans-tracheal nerve blocks) used during awake fiberoptic intubations as well as cricothyrodotomy; localize tracheal rings for dilatational tracheostomy; detection of esophageal intubations, and to evaluate for vocal cord function.

5.2 Acquisition of Image and Sonoanatomy

Place a high frequency linear transducer in a transverse orientation on the neck and scan in a consistent manner either from cephalad to caudad or in reverse (Fig. 24). From caudad to cephalad, visualize the tracheal rings and cartilages to localize potential tracheostomy sites. At this level, the esophagus and the thyroid gland can also be visualized (Fig. 25) Insufflating or desufflating the endotracheal tube pilot balloon can detect movement in either the tracheal or esophageal lumen to evaluate the location of the endotracheal tube. As the transducer ascends more cephalad, cricoid cartilage and subsequently the thyroid cartilage can be visualized. Between the cricoid cartilage and the thyroid cartilage is the cricothyroid membrane, a landmark for both the trans-tracheal block and cricothyroidotomy. Slightly more superior to this plane are the vocal cords and the laryngeal inlet (Fig. 26). Vocal cord abnormalities (unilateral or complete paralysis of vocal folds) can be detected if the patient is asked to phonate. As the transducer is moved to the lower mandibular recess, the hyoid bone and its cornua can be visualized on both sides. The cornu of the hyoid bone is the landmark for the superior laryngeal block. The transducer can also be placed in a parasagittal view (Fig. 27) to visualize all the tracheal, cricoid, and thyroid cartilages as well as the cricothyroid membrane and the hyoid bone in the same view (Fig. 28).

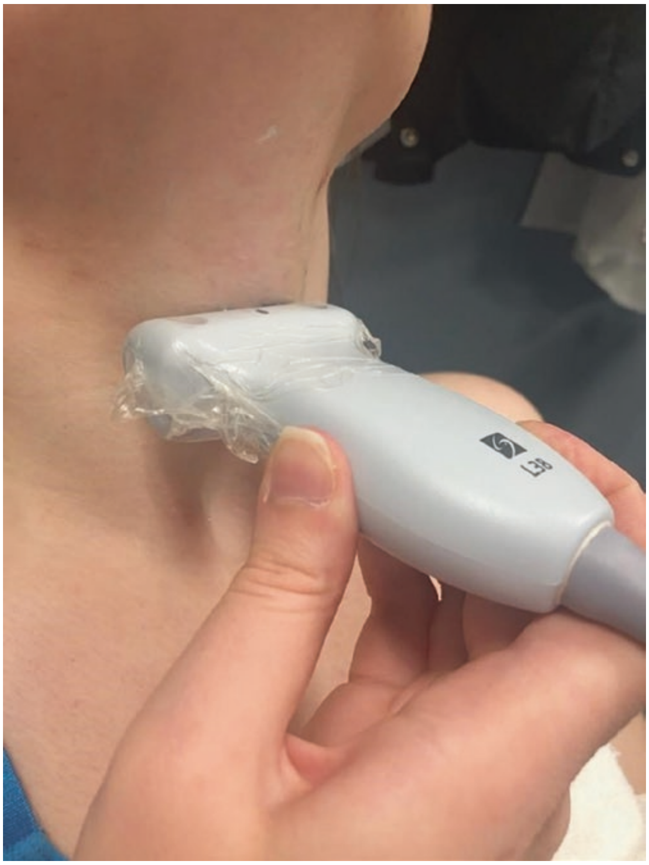

Fig. 24 Transverse scan of neck

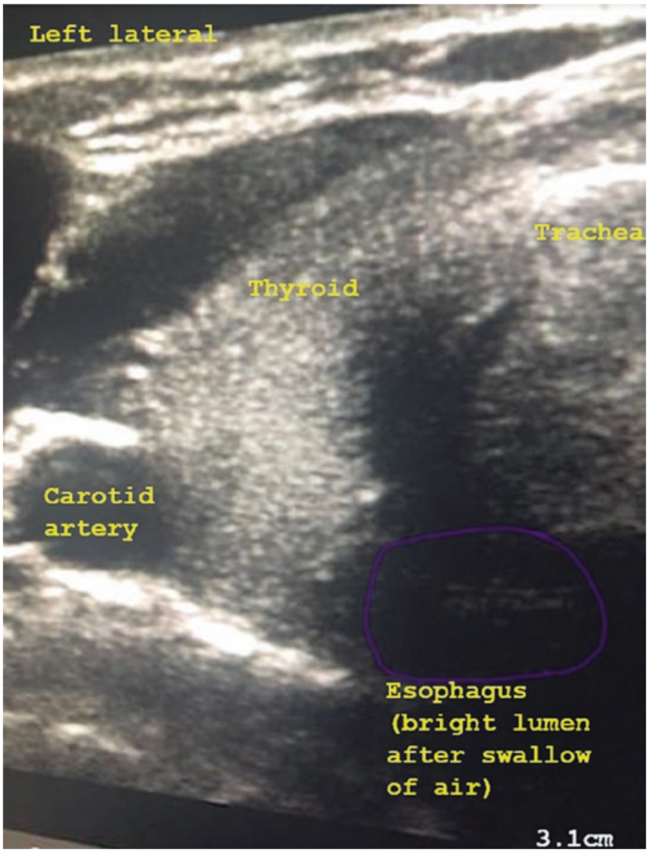
Left lateral
Trachea
Thyroid
Carotid artery
Esophagus (bright lumen after swallow of air)
3.1cm

Fig. 25 Transverse view of left of midline: esophagus (purple circle), trachea, and thyroid

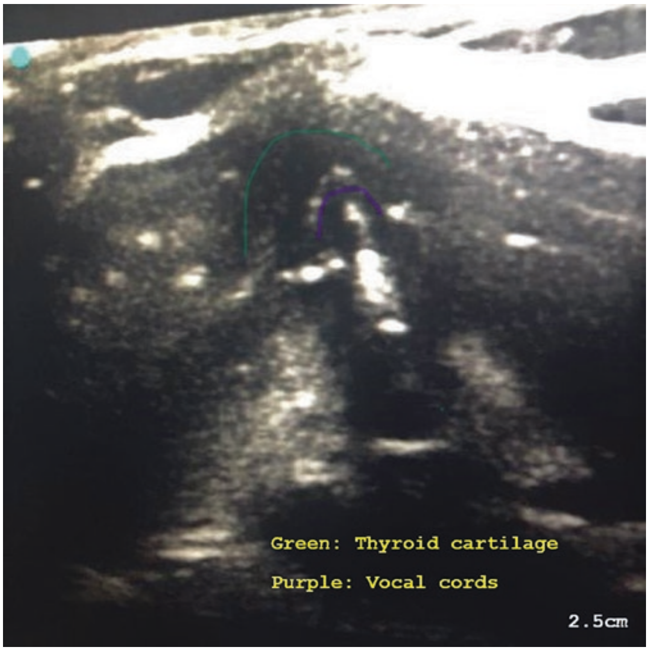
Green: Thyroid cartilage
Purple: Vocal cords
2.5cm

Fig. 26 Vocal cords

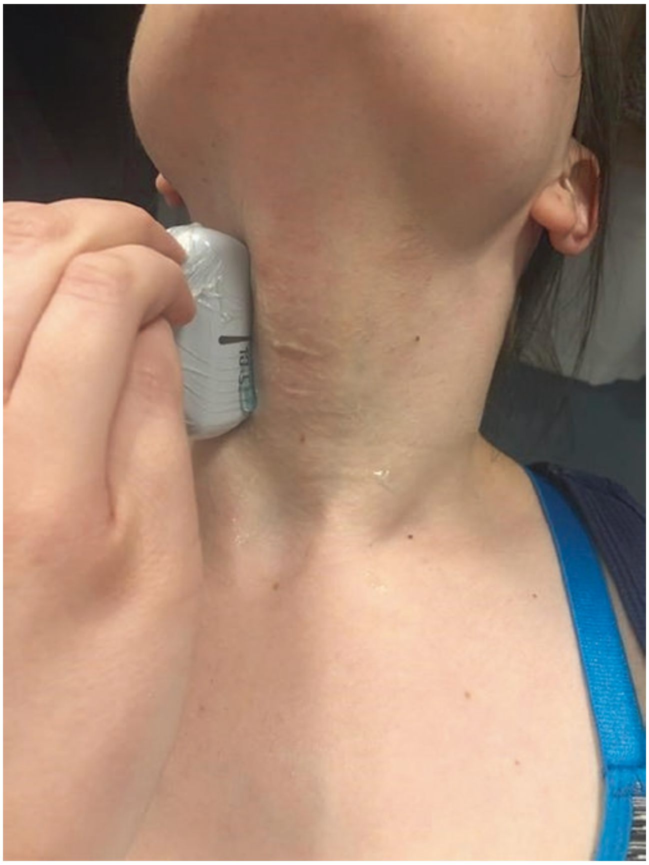

Fig. 27 Parasagittal scan of neck

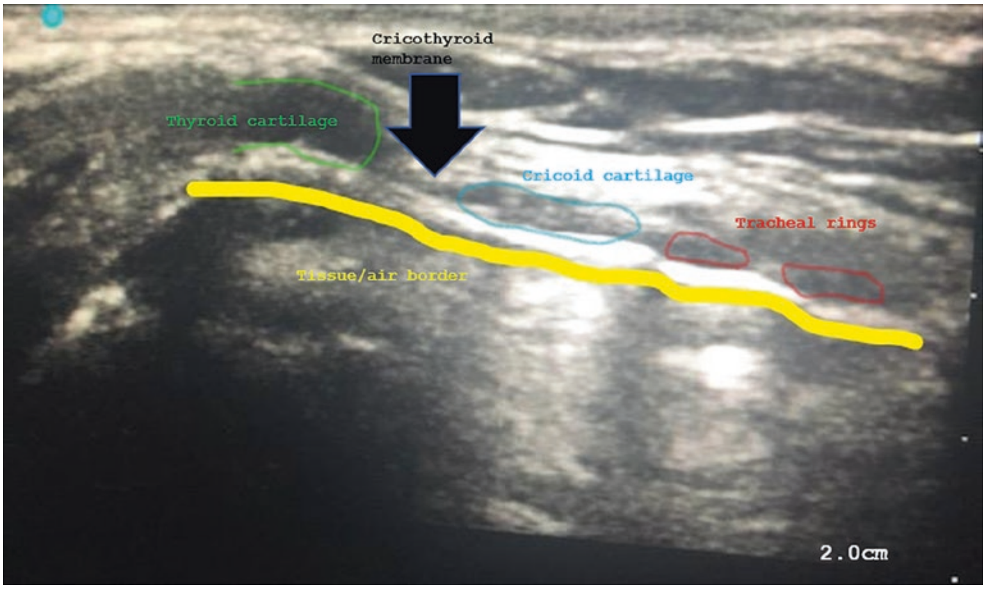

Fig. 28 Parasagittal ultrasound view

5.3 Clinical or Pathological Interpretation and Medical Decision Making

Airway ultrasound may potentially be useful to detect esophageal placement of endotracheal tube although better and faster methods should be employed (capnography, compliance, condensation of clear endotracheal tube, and peak airway pressures). Airway ultrasound could assist in identifying cricothyroid membranes, inter-tracheal membranes, or hyoid bone and could contribute to the current difficult airway algorithm. Lastly, airway ultrasound can potentially assist in identifying vocal cord dysfunction or paralysis caused by injury to recurrent laryngeal nerve if fiberoptic guidance or topicalization techniques are not available.

References

1. Gillman LM, Kirkpatrick AW. Portable bedside ultrasound: the visual stethoscope of the 21st centrury. Scand J Trauma Resusc Emerg Med. 2012;20:18.
2. Haskins S, Kruisellbrink R, Boublik J, et al. Gastric ultrasound for the regional anesthesiologist and pain specialist. Reg Anesth Pain Med. 2018;43:689–98.
3. Practice guidelines for preoperative fasting and the use of pharmacologic agents to reduce the risk of pulmonary aspiration: application to healthy patients undergoing elective procedures; an updated report by the American Society of Anesthesiologists Task Force on preoperative fasting and the use of pharmacologic agents to reduce the risk of pulmonary aspiration. Anesthesiology. 2017;126:376–93.
4. Dupont G, Gavory J, Lampert P, et al. Ultrasonographic gastric volume before unplanned surgery. Anaesthesia. 2017;72:1112–6.
5. Van de Putte P, Vernieuwe L, Jerjir A, et al. When fasted is not empty: a retrospective cohort study of gastric content in fasted surgical patients. Br J Anaesth. 2017;118:363–71.
6. Van de Putte P, van Hoonacker J, Perlas A. Gastric ultrasound to guide anesthetic management in elective surgical patients non-compliant with fasting instructions: a retrospective cohort study. Minerva Anesthesiol. 2018;84:787–95.
7. Van de Putte P, Perlas A. Ultrasound assessment of gastric content and volume. Br J Anaesth. 2014;113:12–22.
8. Perlas A, Davis L, Khan M, et al. Gastric sonography in the fasted surgical patient: a prospective descriptive study. Anesth Analg. 2011;113:93–7.
9. Sijbrandij L. Op den Orth J. Transabdominal ultrasound of the stomach: a pictorial essay. Eur J Radiol. 1991;13:81–7.
10. Perlas A, Mitsakakis N, Liu L, et al. Validation of a mathematical model for ultrasound assessment of gastric volume by gastroscopic examination. Anesth Analg. 2013;116:357–63.
11. Volpicelli G, Elbarbary M, Blaivas M, et al. International evidence-based recommendations for point-of-care lung ultrasound. Intensive Care Med. 2012;38:377–591.
12. Haskins S, Tsui B, Nejim J, et al. Lung ultrasound for the regional anesthesiologist and acute pain specialist. Reg Anesth Pain Med. 2017;42:289–98.
13. Volpicelli G. Sonographic diagnosis of pneumothorax. Intensive Care Med. 2011;37:224–32.
14. Matamis D, Soilemezi E, Tsagourias M, et al. Sonographic evaluation of the diaphragm in critically ill patients: technique and clinical applications. Intensive Care Med. 2013;39:801–10.
15. Tsui JJ, Tsui BC. A novel systemic ABC approach to diaphragmatic evaluation (ABCDE). Can J Anaesth. 2016;63:636–7.
16. Liechtenstein D, Meziere G, Biderman P, et al. The "lung point:" an ultrasound sign specific to pneumothorax. Intensive Care Med. 2000;26:1434–40.
17. Liechtenstein D, Goldstein I, Mourgeon E, et al. Comparative diagnostic performances of auscultation, chest radiography, and lung ultrasonography in acute respiratory distress syndrome. Anesthesiology. 2004;100:9–15.
18. Boussuges A, Gole Y, Blane P. Diaphragmatic motion studied by m-mode ultrasonography: methods, reproducibility, and normal values. Chest. 2009;135:391–400.
19. Via G, Hussain A, Wells M, et al. International evidence-based recommendations for focused cardiac ultrasound. J Am Soc Echocardiogr. 2014;27:683.el–683.c33.
20. Spencer K, Kimura B, Korcarz C, et al. Focused cardiac ultrasound: recommendations from the American Society of Echocardiography. J Am Soc Echocardiogr. 2013;26:567–81.
21. Haskins S, Tanaka C, Boublik J, et al. Focused cardiac ultrasound for the regional anesthesiologist and pain specialist. Reg Anesth Pain Med. 2017;42:632–44.

22. Holm J, Frederiksen C, Juhl-Olsen P, et al. Perioperative use of focus assessed thoracic echocardiography (FATE). Anesth Analg. 2012;115:1029–32.
23. Rudski L, Lai W, Afilalo J, et al. Guidelines for the echocardiographic assessment of the right heart in adults: a report from the American Society of Echocardiography. J Am Soc Echocardiogr. 2010;23:685–713.
24. Seif J, Mailhot T, Perera P, et al. Caval sonography in shock: a noninvasive method for evaluating intravascular volume in critically ill patients. J Ultrasound Med. 2012;31:1885–90.

Ultrasound for Abdomen and FAST: Evaluation and Diagnosis

Christopher L. Moore, Jacob Avila, and John W. Combs

1 Introduction

Non-traumatic abdominal pain accounts for 7–10% of all emergency department (ED) patients [1]. However, this does not mean that traumatic abdominal pain is insignificant in the emergency setting. In fact, there are an estimated 38 million ED visits for trauma, and it is the leading cause of death in persons younger than 45 years of age [2]. As common presentations of abdominal pathology range from benign to life-threatening, point-of-care ultrasound (POCUS) is an invaluable tool in the initial evaluation of both traumatic and non-traumatic abdominal pain. In this chapter, we seek to outline some of the major pathologies that ultrasound is effective in detecting in both non-traumatic and traumatic abdominal pain.

2 Sonographic Evaluation of the Aorta

2.1 Aortic Aneurysm

An aortic aneurysm (AA) is defined as an abnormal dilation of the three layers of the aorta [3]. The symptoms, presentation, and treatments vary depending on the location and size of the aneurysm [3]. In the United States, there are approximately 11,000 cases of ruptured aortic aneurysms per year, with an overall mortality of 80%–95%. Earlier diagnosis has been associated with a dramatic decrease in the mortality rate [4]. The most commonly used gold standard for diagnosis is a Computed Tomography (CT) angiogram, but it has its limitations [5]. Namely, it is not a bedside test that can be performed in hemodynamically unstable patients, it requires intravenous (IV) access, and exposure to IV contrast and radiation. The patient's history can be unreliable, with some studies indicating that only 5% of patients with AA's will have symptoms prior to when a complication occurs, such as aortic rupture [6]. The physical exam is notoriously unreliable as well. The classic triad of hypotension, abdominal pain, and a pulsatile abdominal mass is present in less than 50% of patients with a ruptured AA [7]. The sensitivity of the physical exam for the detection of unruptured AA is only 50–65% [4]. Ultrasound does not have the limitations of a CT angiogram and has been found to be an accurate bedside modality for the diagnosis of AA.

2.2 Ultrasound Diagnosis of Aortic Aneurysm

Thoracic AA's can be identified using bedside echo. While abdominal AA's are more common in the infrarenal location, the entire abdominal aorta should be evaluated from the subxiphoid area down to its division into the iliac arteries [8]. In order to perform this examination, the curvilinear probe is preferred, but the phased array transducer can also be used. The probe should initially be placed in the subxiphoid area in a transverse cut with the probe marker facing towards the patients right. The aorta is identified superficial to and slightly left of the vertebral body (Fig. 1). An abdominal AA is defined as an aorta with a diameter from outer wall to outer wall greater than 3 cm (Fig. 2) [9]. Care must be taken to measure the entire abdominal aorta in short axis in order to avoid missing a saccular aneurysm, which is present in approximately 25% of all abdominal AA's [6]. In a meta-analysis of 11 studies that included 944 patients, bedside ultrasound was found to have a

---

C. L. Moore (✉)
Yale School of Medicine, Department of Emergency Medicine,
New Haven, CT, USA
e-mail: chris.moore@yale.edu

J. Avila
University of Kentucky, Emergency Medicine,
Lexington, KY, USA
e-mail: jacob.avila@uky.edu

J. W. Combs
Jackson Memorial Hospital, Emergency Medicine,
Miami, FL, USA
e-mail: john.combs@jhsmiami.org

© Springer Nature Switzerland AG 2021
J. Li et al. (eds.), *Ultrasound Fundamentals*, https://doi.org/10.1007/978-3-030-46839-2_32

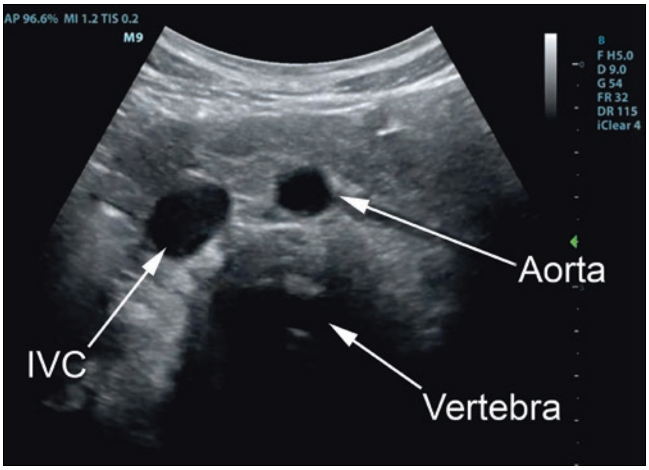
AP 96.6% MI 1.2 TIS 0.2
M9
B
F H5.0
D 9.0
G 54
FR 32
DR 115
iClear 4
Aorta
IVC
Vertebra

Fig. 1 This is a transverse view of the abdominal aorta. The vertebral body is deep to the aorta and the IVC is to the patient's right

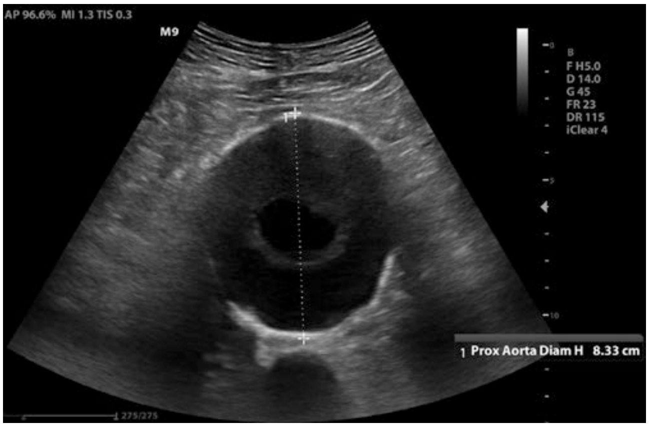
AP 96.6% MI 1.3 TIS 0.3
M9
B
F H5.0
D 14.0
G 45
FR 23
DR 115
iClear 4
1 Prox Aorta Diam H 8.33 cm

Fig. 2 An image of an abdominal aortic aneurysm. Note that the sonographer measures the diameter from outer wall to outer wall, and does not measure the much smaller intraluminal diameter

pooled sensitivity of 97.5% and a pooled specificity of 98.9% for abdominal AA [7].

2.3 Aortic Dissection

Aortic dissection (AD) is a disease with a poor prognosis. Around 40% of patients with acute AD die immediately, and have been reported to have a 1% per hour increased mortality rate if they survive the initial insult [3]. While most patients with this disease will present with a sudden onset of severe pain in the chest, abdomen, flank or back, these symptoms can be non-specific [3]. Additionally, 8–15% of patients with AD will present without any pain [10]. Physical exam derangements are seen in <50% of patients with Acute AD [11]. CT angiogram is considered the gold standard, but has the same limitations as previously discussed. The findings on chest x-ray (CXR) are non-specific, and may be normal in 12–18% of patients with AD [12].

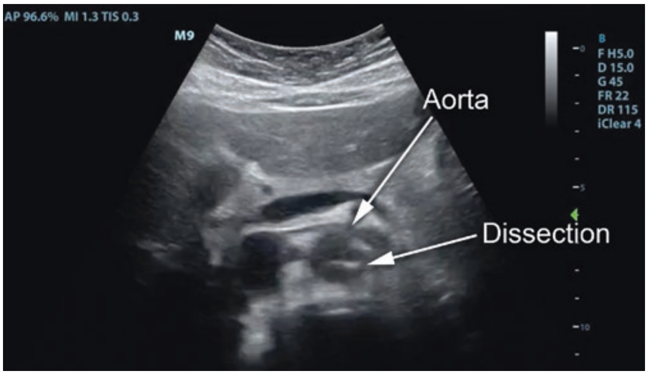
AP 96.6% MI 1.3 TIS 0.3
M9
B
F H5.0
D 15.0
G 45
FR 22
DR 115
iClear 4
Aorta
Dissection

Fig. 3 A transverse image of an abdominal aortic dissection at the level of the splenic vein. Note the echogenic intraluminal flap which is diagnostic of dissection

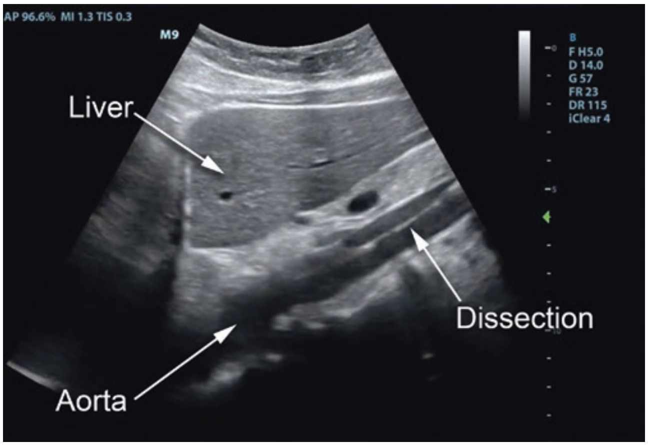
AP 96.6% MI 1.3 TIS 0.3
M9
B
F H5.0
D 14.0
G 57
FR 23
DR 115
iClear 4
Liver
Dissection
Aorta

Fig. 4 A longitudinal image of an abdominal aortic dissection, the intraluminal flap is prominently shown here

2.4 Ultrasound Diagnosis of Aortic Dissection

The same windows that can be used for the identification of an abdominal AA should be used for an abdominal AD. Care must be taken to evaluate for a mobile flap within the lumen of the aorta, which would diagnose a dissection. (Figs. 3 and 4). Transabdominal bedside ultrasound has been found to have a sensitivity of 70%–80% and a specificity of 100% [6].

2.5 Conclusion

Bedside ultrasound is an invaluable tool when evaluating your patient for aortic emergencies. One must keep in mind that the utility of ultrasound lies in the ability to adequately identify the aorta. Multiple studies have evaluated the frequency of obtaining adequate views of the aorta, and the rate of inadequate views of the aorta range from 0% to 52% of the time [13, 14].

3 Sonographic Evaluation of the Gallbldder

3.1 Using Ultrasound to Evaluate Gallbladder Disease

Abdominal pain is a common complaint among patients in the ED [1]. Gallbladder disease affects over 20 million Americans per year and accounts for 3–11% of all hospital admissions [15, 16]. Both right upper quadrant (RUQ) pain and epigastric pain are indications to perform a point-of-care ultrasound (POCUS) to evaluate the gallbladder and biliary system. When evaluating the gallbladder, the clinician should seek to identify gallstones, signs of cholecystitis, and the presence of biliary obstruction. Any of these findings warrants further investigation; the correct treatment can often be determined by the initial ultrasound. A quick bedside ultrasound can be used to help diagnose cholelithiasis, cholecystitis, choledocholithiasis, and cholangitis, particularly when taking into account the clinical presentation of the patient.

Whereas the curvilinear transducer is the ideal probe to image the gallbladder and biliary system, the phased array transducer may be used as well. These low-frequency probes can image structures at the depth necessary to visualize the gallbladder. Though the gallbladder may be positioned anteriorly it is often located beneath fatty tissue in the abdomen, making a low-frequency probe optimal. With the patient in the supine position, the clinician places the ultrasound probe in the RUQ to image the gallbladder. Several strategies can be used to find the gallbladder; success with any of these strategies can vary based on patient anatomy. A normal gallbladder will have a thin hyperechoic wall, will appear near the caudal tip of the liver, and will be filled with simple anechoic fluid (Fig. 5).

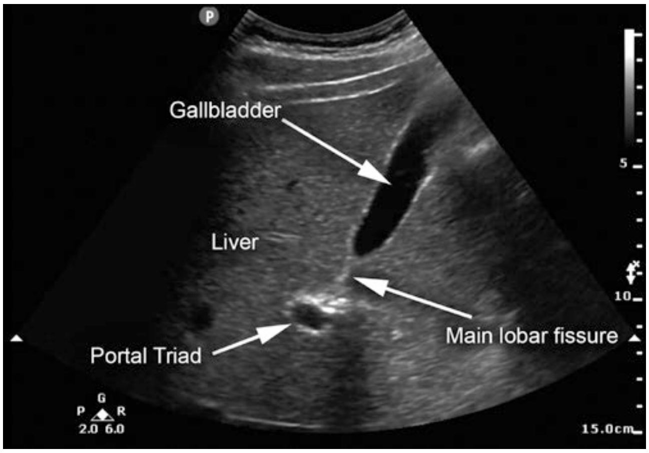

Fig. 5 An image of a normal gallbladder. This image is known as the "exclamation point" sign—with the portal triad making the point of the exclamation mark

3.2 Technique for Gallbladder POCUS

In the *subcostal* approach, the clinician places the probe in a transverse orientation just beneath the rib margin on the right side. Alternatively, the probe can be placed in the coronal plane, similar to performing a RUQ view on an E-FAST. With the probe in the coronal orientation, a quick fanning motion will often reveal the gallbladder (as well as the IVC). A clinician may also try the *"X-7"* approach, the name of which references the placement of the probe 7 centimeters to the right of the patient's xiphoid process. This location will be between two ribs. Thus, a twisting or rotating motion to aim the plane of the ultrasound between these ribs is often helpful. If finding the gallbladder still proves to be difficult, it may be helpful to have the patient lay in the left lateral decubitus position. Another maneuver is to have the patient take a deep breath and hold it for as long as possible. Both of these techniques help to bring the gallbladder out from underneath the ribcage. Since the liver is highly vascular, a clinician may make use of color Doppler to differentiate the gallbladder from a blood vessel. If blood flow is seen after placing the color Doppler window over the anechoic structure of interest, then that structure is likely to be a blood vessel (Fig. 6).

3.3 Ultrasound Diagnosis of Biliary Pathology

There are many pathophysiologic processes that may alter the normal anatomy of the gallbladder or biliary tree. These can be found and interpreted with a POCUS of the biliary system. There is evidence that an initial POCUS of the gallbladder has a 96% sensitivity for identifying the presence of gallstones [17]. Another study found that initial POCUS has a high sensitivity (88%) as well as a high specificity (87%) for finding the presence of gallstones [18]. In fact, one study demonstrated that patients who had their gallbladder evaluated by POCUS and did not receive follow up imaging had a shorter LOS by over 2 hours [16]. Other studies have also shown decreases in patient LOS in the ED when emergency physicians make use of POCUS [19]. The evidence supporting the use of advanced imaging as a follow up after initial gallbladder POCUS is lacking. CT has been shown to provide no further diagnostic information about the pathology of the biliary system after initial gallbladder POCUS [20]. In

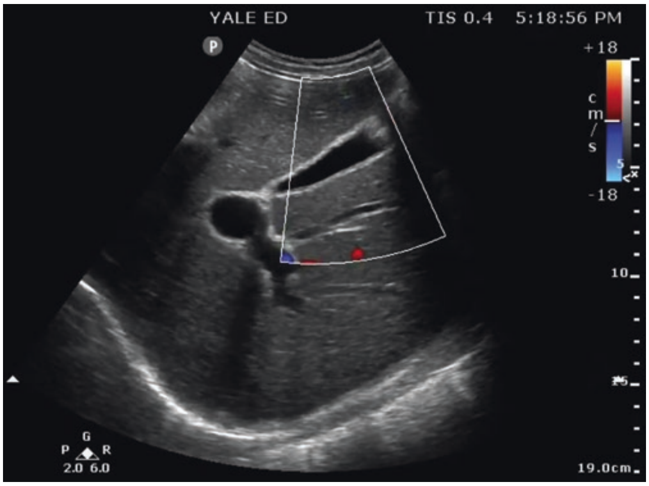

Fig. 6 An image of a normal gallbladder. Note the lack of flow on color Doppler. The bile duct is seen deep to the gallbladder, the bile duct also has a lack of flow on color Doppler

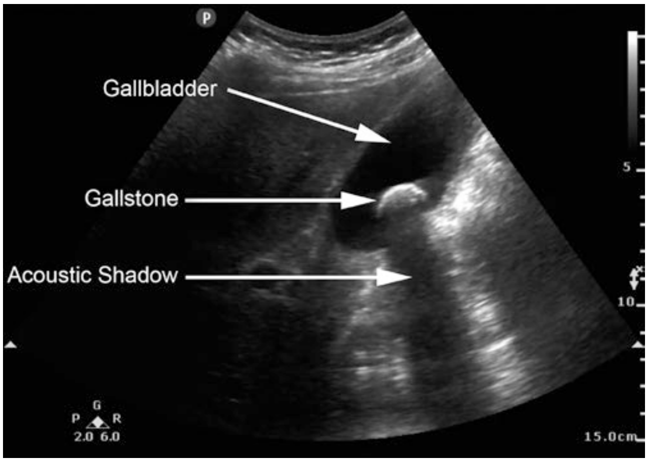

Fig. 7 An image of a gallbladder with a prominent intraluminal gallstone with posterior acoustic shadowing

fact, an initial screening POCUS may be optimal for all patients who may possibly have gallstones, as up to 39% of patients who present to the ED with isolated acute nontraumatic epigastric pain and tenderness are found to have a symptomatic gallstone on POCUS [21].

Cholelithiasis may be identified by the presence of a hyperechoic rim within the gallbladder with posterior acoustic shadowing deep to it. A gallstone is a highly absorptive surface for sound waves, and thus the anterior surface of the gallstones will be visible, but deep to the stones there will be an acoustic "shadow". This shadow represents complete loss of signal distal to the surface of the gallstones as sound waves cannot penetrate through the stone (Fig. 7) [22]. A wall-echo-shadow (WES) sign may occur when a gallbladder is completely contracted against gallstones (Fig. 8). Sometimes, biliary sludge may be seen within the gallbladder as well. This appears as an echogenic layer within the gallbladder lumen without shadowing. Biliary sludge often occurs in critically ill patients and may be a precursor to gallstones (Fig. 9).

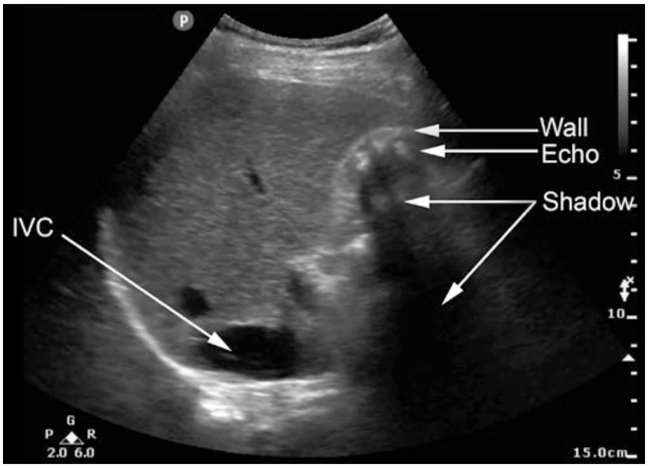

Fig. 8 A gallbladder with a gallstone occupying the entire lumen, showing a classic Wall-Echo-Shadow (WES) sign. Note the IVC deep to these structures

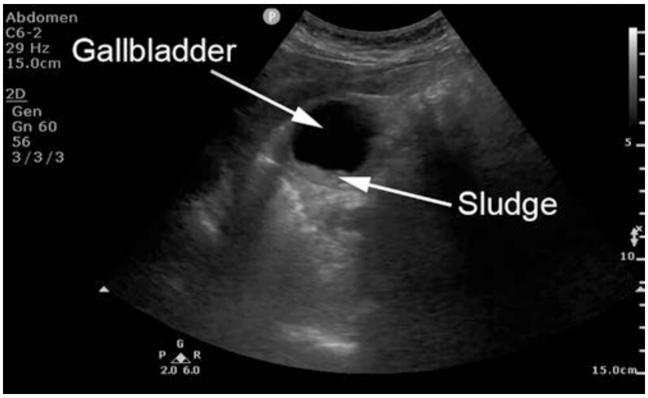

Fig. 9 A gallbladder showing sludge layering in the dependent portion of the lumen

Cholecystitis may also be seen using POCUS. There are several sonographic findings that are associated with the diagnosis of cholecystitis (Fig. 10). Classically, a patient will have sonographic Murphy's sign, which is abdominal tenderness when the sonographer visualizes the gallbladder and presses on the abdominal wall at that location [23]. Another finding is the presence of gallbladder wall thickening, as an edematous gallbladder wall may indicate inflammation. The measurement is taken across the anterior edge of the gallbladder in the transverse plane. A normal measurement is 3 mm or less, while a measurement of greater than 3 mm suggests the presence of gallbladder wall edema (and in the correct clinical setting, cholecystitis). Pericholecystic fluid can be seen as a hypoechoic rim of fluid surrounding the gallbladder representing edema of the gallbladder as well as

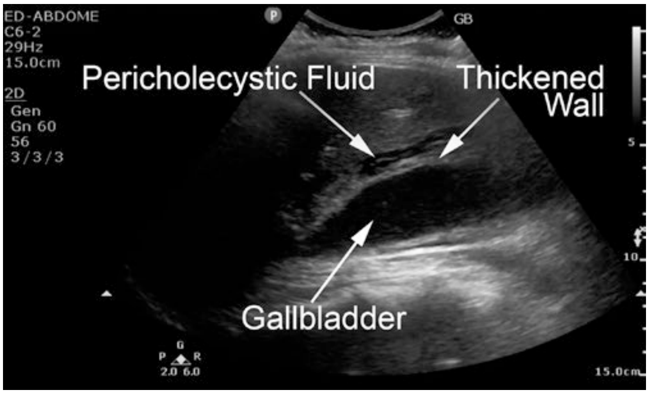

Fig. 10 A gallbladder with a thickened wall and with pericholecystic fluid, these findings are associated with cholecystitis

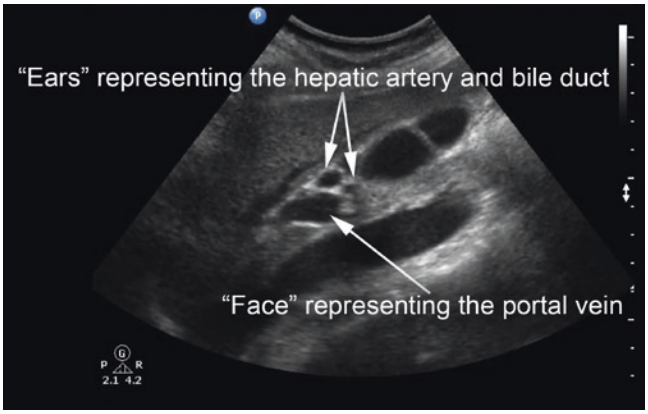
"Ears" representing the hepatic artery and bile duct
"Face" representing the portal vein
2.1 4.2

Fig. 11 An image of the "Mickey Mouse" sign, which shows the three components of the portal triad—the portal vein, the common hepatic artery, and the common bile duct. The gallbladder is seen more superficial to the portal triad in this image

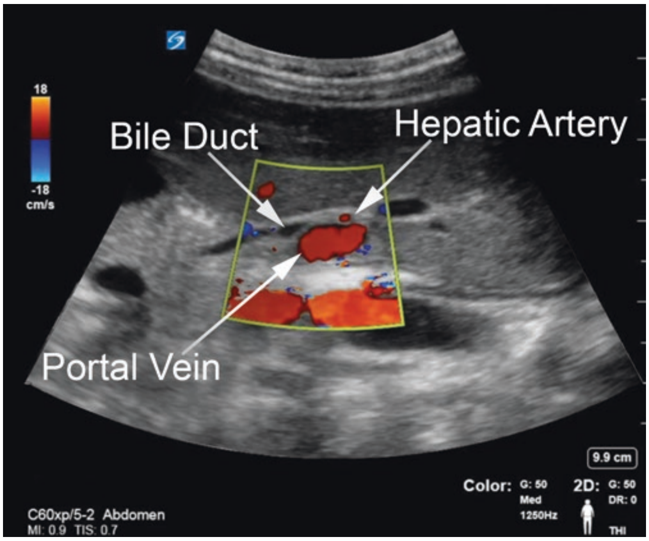

Fig. 12 An image of the portal triad utilizing color Doppler. Note that the common bile duct does not demonstrate flow on color Doppler

the fossa in which it lies; this finding is suggestive of the presence of cholecystitis. Emphysematous cholecystitis will have similar findings as above, but will also display hyperechoic foci of air with "dirty shadowing" or comet tail artifact created by the presence of gas within the wall of the gallbladder.

There are other findings associated with biliary pathology as well. The common bile duct (CBD) should be measured to investigate the possibility of choledocholithiasis. A stone within the CBD causes an obstruction of flow, and thus the CBD more proximal to the obstruction will dilate. The CBD can be found in the transverse or longitudinal axis. In the transverse axis, the CBD will be found as a part of the portal triad, which contains the CBD, portal vein, as well as the hepatic artery. These 3 structures appear circular in the transverse plane, and are often referred to as the "Mickey Mouse sign" (Fig. 11). By utilizing color Doppler, the CBD may be distinguished from the 2 blood vessels as it is the only structure without measurable Doppler flow. In the longitudinal plane, the CBD will appear to run right next to the portal vein (Fig. 12). The CBD may be measured in either of these orientations perpendicularly from inner wall to inner wall, and should be less than 2–3 mm in a young patient. In a patient who has had a cholecystectomy, a measurement of up to 1 cm may be normal. The CBD is traditionally thought to dilate with age, adding about a millimeter per decade over the age of 40, but recent evidence does not reliably demonstrate this phenomenon [24].

3.4 Pitfalls in Sonographic Evaluation of Gallbladder Disease

A common pitfall for novice sonographers is misidentifying the duodenum as the gallbladder. The duodenum is a partially retroperitoneal organ that lies near the liver, and can be seen as a round structure in a similar location to the gallbladder. Fortunately, the appearance of the duodenum is significantly different than the gallbladder, and with training, a sonographer can easily avoid becoming confused. The duodenum displays peristalsis, has a hypoechoic outer wall, and does not attach to the main lobar fissure (MLF) or sonographic cystic pedicle (SCP) (Fig. 5).

4 Sonographic Evaluation of the Kidneys

4.1 Kidney Stone Disease

There are more than one million ED visits every year due to kidney stone disease in the United States and the prevalence of kidney stones in the general population has been increasing since the early 1990’s [25, 26]. An initial point-of-care ultrasound (POCUS) assessment of the kidneys is associated with quicker disposition times and decreased radiation exposure when compared to initial CT, but is not associated with an increased risk of adverse patient outcomes [27, 28]. In fact, there is evidence that when ultrasound is used as the initial imaging study in suspected ureterolithiasis, follow up imaging studies (such as CT) are only performed in 20% of cases [29]. These factors make a POCUS the ideal first-line method to evaluate patients with a suspected kidney stone.

When indicated, the clinician performs a POCUS of the kidneys to look for hydronephrosis to confirm the presence of ureteral obstruction, not necessarily to find the stone itself [30]. The most common indications for performing a POCUS of the kidneys are flank pain and hematuria. On some occasions a stone may be seen in the ureter, but this is not required to make the diagnosis of ureterolithiasis in the correct clinical setting. POCUS of the kidneys performed by an emergency clinician has been shown to have a sensitivity of 72.6% and specificity of 73.3% when assessing for hydronephrosis (when hydronephrosis is confirmed by CT scan) [31]. This sensitivity improves to 92.7% when the POCUS is performed by an ultrasound fellowship trained emergency physician. Using POCUS may add diagnostic value to a clinical prediction rule that does not incorporate ultrasound, in particular in patients with a moderate probability of kidney stone [32].

4.2 Technique for POCUS of Kidneys

To perform a POCUS assessment of the kidneys, a curvilinear or phased array transducer is recommended, as the kidneys are retroperitoneal structures and best imaged with a lower frequency probe. With the patient in the supine position, the clinician should place the ultrasound probe on the patient’s mid to posterior-axillary line with the probe indicator directed towards the patient’s head to obtain a coronal image of the right upper quadrant (RUQ), in the same location one would place the probe to evaluate the RUQ in an E-FAST. The renal architecture should come in to view. A normal kidney is surrounded by the hyperechoic Gerota’s fascia, has a hypoechoic cortex, and has a hyperechoic internal renal pelvis (Fig. 13). The ureter is not visible in a normal kidney but may be visible in the presence of hydroureter. The clinician should ideally fan through the kidney in this plane as well as the transverse plane to see the whole architecture of the kidney in three dimensions although a single plane may be adequate. The kidney on the left side should be evaluated in a similar fashion; it is pertinent to remember that the left kidney is generally more superior and posterior than the right. If rib shadows are blocking the view of the kidney, a twisting motion forward (like the handle of a motorcycle) will aim the imaging plane of the ultrasound between the ribs.

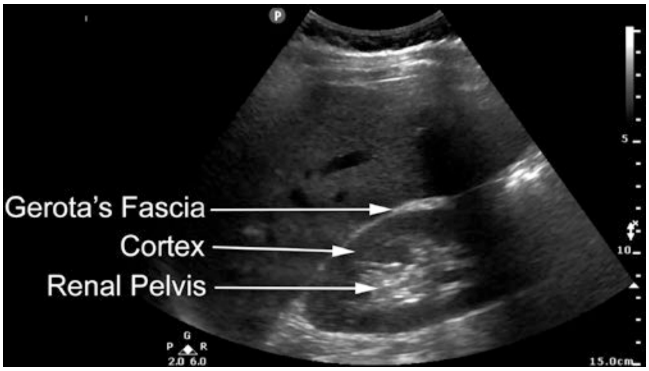

Fig. 13 The normal appearance of the kidney in the RUQ. Note the echogenic renal pelvis inside of the renal cortex

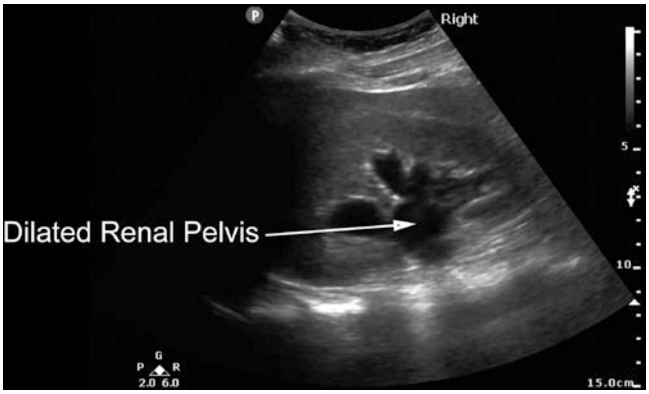

Fig. 14 An image of moderate hydronephrosis with a dilated renal pelvis

4.3 Using Ultrasound to Evaluate Kidney Stone Disease

Hydronephrosis occurs when the outflow to the ureter is blocked, causing the urine to back up into the renal calyces and pelvis. Although ureterolithiasis is a common cause of hydronephrosis, other processes can cause obstruction of urinary outflow, such as extrinsic compression of the urinary tract by a tumor [33]. Hydronephrosis is a dynamic process and may develop and resolve relatively quickly (on the order of minutes to hours) [34]. Hydronephrosis is diagnosed by seeing the presence of anechoic fluid within the renal collecting system. This will form a characteristic pattern of dilated calyces draining into a dilated renal pelvis (Fig. 14) [35]. As mentioned, hydronephrosis is an indirect sign of ureteral blockage, typically from a kidney stone, and it may be difficult to see a stone if it is in the retroperitoneum and obscured

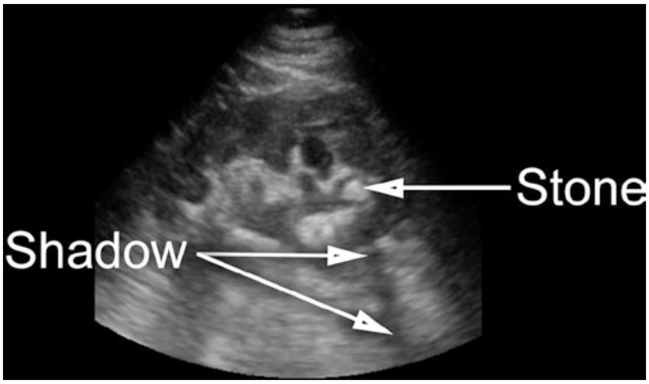

Fig. 15 Example of a stone within the renal collecting system. Note the acoustic shadowing posterior to the stone. This image also demonstrates mild hydronephrosis

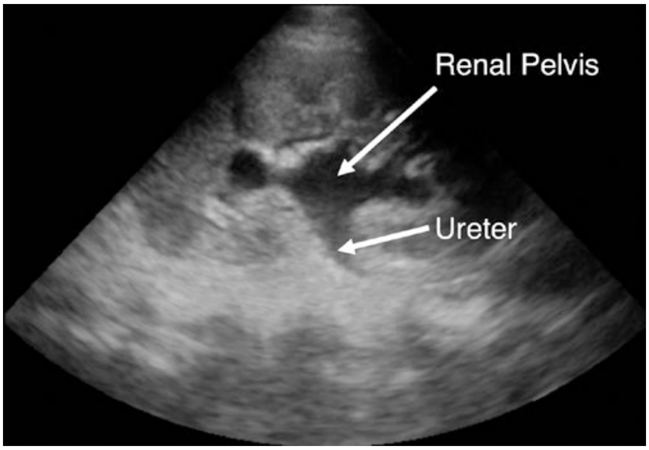

Fig. 16 Mild hydronephrosis. Note the mild dilation of the ureter and renal pelvis

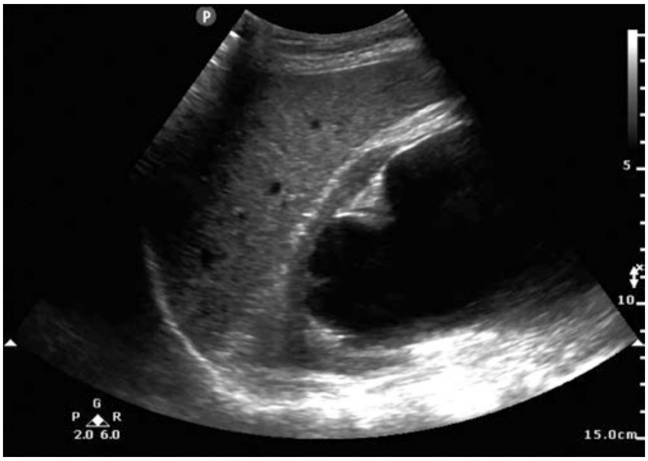

Fig. 17 Severe hydronephrosis. Note the complete obliteration of the renal architecture

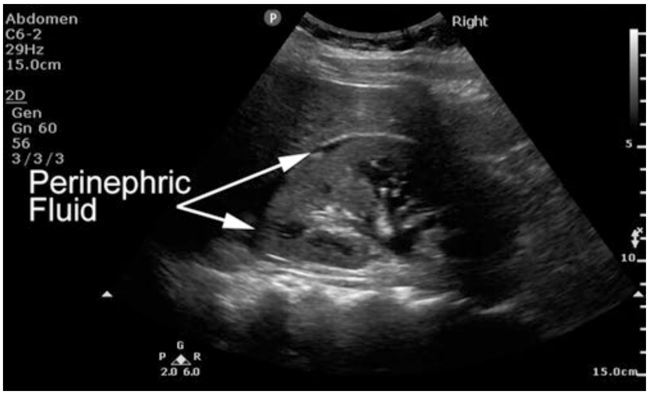

Fig. 18 An image of hydronephrosis with calyceal rupture. Note the free fluid contained within Gerota's Fascia

by bowel, though in some cases the stone may be visualized (Fig. 15) [30]. If the ureter is visible, it may be tracked inferiorly to try to identify a stone. The stone will be hyperechoic and will typically project a shadow artifact behind it. In addition, 2D and color Doppler of the bladder may be performed to support the diagnosis of kidney stone. A stone may be visible at the ureterovesicular junction (UVJ) in 2D imaging. When performing color Doppler of the bladder, a ureter that is obstructed would have reduced or no flow of urine into the bladder compared to a ureter that is not.

Hydronephrosis is typically measured qualitatively into 3 broad categories: mild, moderate, and severe. Mild hydronephrosis involves only the renal pelvis (Fig. 16), whereas moderate hydronephrosis involves dilated renal calyces as well (Fig. 14). Severe hydronephrosis causes distortion of the renal architecture with parenchymal thinning of the cortex (Fig. 17). Moderate or severe hydro are fairly easily identified by clinicians with basic training in POCUS, while correctly identifying mild hydro and differentiating from renal vasculature can sometimes be challenging [36]. Color Doppler may be used to identify vasculature as opposed to the collecting system which should not show flow [35].

There are many different findings that may be associated with a kidney stone other than hydronephrosis. Complications such as calyceal rupture may be seen as perinephric fluid on POCUS, but will not track into Morison's pouch (Fig. 18). A stone at the UVJ may be seen using color Doppler demonstrating a characteristic "twinkle artifact" (Fig. 19) [32].

4.4 Pitfalls in Sonographic Evaluation of Kidney Stone Disease

A pitfall that novice sonographers can make is to mistakenly misidentify renal cysts as hydronephrosis [37]. This pitfall can be avoided by only considering the anechoic fluid within the renal pelvis that tracks into the calyces as a true representation of hydronephrosis. A renal cyst should be circular and encapsulated with a thin rim. (Fig. 20).

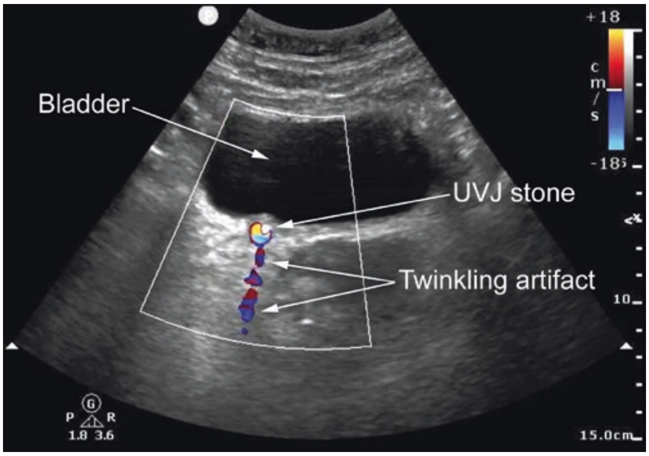

Fig. 19 A kidney stone seen at the UVJ just posterior to the bladder. This color Doppler signal is known as the twinkle artifact

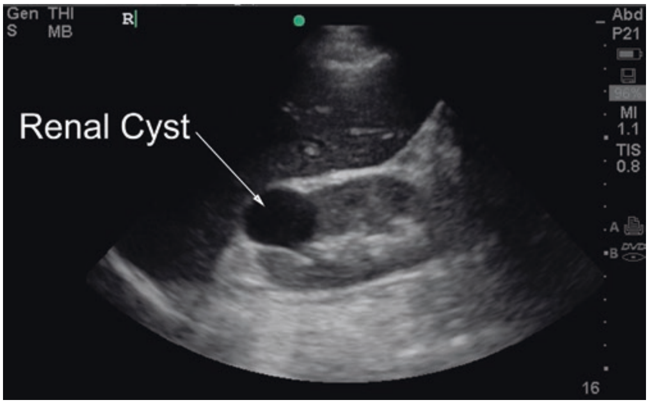

Fig. 20 A simple renal cyst, not to be confused with hydronephrosis

When correctly used, POCUS of the kidney can help correctly identify renal colic, potentially expediting care and decreasing inappropriate CT use.

5 The Fast Exam

5.1 Background

Traumatic injuries are common and range from minor to life-threatening. Determining which ones need surgical intervention is of utmost importance since the time to the operating room (OR) has been correlated with patient outcomes [38]. Earlier in the twentieth century diagnostic peritoneal lavage (DPL) was used to relatively rapidly determine if there was intraperitoneal hemorrhage [39]. DPL has fallen out of favor due to its invasiveness and lack of specificity. Computed tomography (CT), with its increased speed and accuracy, has become a key diagnostic test in trauma. However, CT has its limitations in an acute trauma setting, particularly in an unstable patient. As a rapid, non-invasive, repeatable bedside study without ionizing radiation, ultrasound represents the best *initial imaging modality* in the trauma patient.

The sonographic assessment of patients with trauma was first introduced in the 1970's and a standardized assessment, the Focused Assessment of Sonography in Trauma, or the FAST exam, was first coined in 1995 [40, 41]. This exam included the evaluation of the peritoneum for hemorrhage and the heart for hemopericardium. The Extended FAST exam, or EFAST, was subsequently coined and includes the evaluation for a pneumothorax and hemothorax [42]. Many studies have been published that evaluate the accuracy of the EFAST exam, and in 2018 a Cochrane review was published that included 34 studies with 8635 adult and pediatric patients and reported a pooled specificity of 96%, and a pooled sensitivity of 74% [43].

The EFAST examination seeks to identify four different traumatic pathologies: pneumothorax, hemothorax, hemopericardium and hemoperitoneum. This fact is important to keep in mind, since the accuracy for ultrasound for each of the separate disease entities varies.

5.2 Ultrasound Accuracy in Hemoperitoneum

While it is still more accurate than any other current bedside test, the disease in which ultrasound has the lowest accuracy is in the evaluation of hemoperitoneum [43]. This is likely due to two factors, the first of which is a common limitation with any ultrasound application: user experience. Novice bedside sonographers are not as accurate as experienced sonographers [44]. The number of abdominal FAST examinations suggested to reach competence generally ranges from 30–50 scans [44–46]. The second factor is that there is a certain amount of fluid that must accumulate before the ultrasound can reliably identify it. If the patient receives a bedside ultrasound in the hyper-acute phase of trauma, it is possible that not enough fluid has yet accumulated to identify it on ultrasound. The minimum amount of hemorrhage that must be present in the peritoneum before ultrasound can reliably pick it up varies from 50–650 cc's [47–52]. This value depends on where the fluid will accumulate first (pelvis vs right upper quadrant vs left upper quadrant), how the patient is positioned (Trendelenburg vs reverse Trendelenburg), and operator training.

5.3 Ultrasound Accuracy in Hemopericardium

The incidence of hemopericardium due to blunt trauma is rare [53]. Press et al. did a chart review at a single institution over an 8.5 year period that included 29,236 blunt trauma patients and found the prevalence of clinically significant hemopericardium was 0.06% [54]. However, when detected, ultrasound has very favorable test characteristics for its diagnosis. When hemopericardium is present, especially in penetrating trauma, its sensitivity and specificity have been reported to be as high as 100% [55–57]. Additionally, its use in penetrating cardiac trauma has been shown to increase survival from 57.1% to 100% [57].

5.4 Ultrasound Accuracy in Pneumothorax

Traditionally, auscultation and chest x-ray (CXR) have been the preferred bedside modalities for diagnosing and excluding pneumothorax (PTX). However, their diagnostic performance is not ideal. For example, auscultation sensitivity for a PTX ranges from 50–58% [59, 60]. While CXR does have acceptable specificity, its sensitivity is woefully inadequate, with a reported pooled sensitivity of 46% [61]. The sonographic evaluation for a PTX has been demonstrated to have equivalent specificities, but much improved sensitivities compared to CXR, with a pooled sensitivity of 87% [61].

5.5 Ultrasound Accuracy in Hemothorax

As is the case for pneumothorax, auscultation and CXR are often considered the preferred bedside tests for the diagnosis or exclusion of a hemothorax. However, when trauma patients are being evaluated, they often are in the supine position, which is the position least amenable to correct diagnosis by CXR [62]. A meta-analysis of 12 studies evaluating for hemothorax found CXR to have a pooled sensitivity of 54%, while ultrasound had a pooled sensitivity of 67% [63]. Although not as impressive as the numbers seen in the sonographic assessment of pneumothorax and hemothorax, ultrasound has been shown to be highly accurate in the detection of hemothorax [63]. The same limitation that we see in the evaluation of hemoperitoneum exists when using ultrasound to detect hemothorax. Namely, that there is a certain amount of fluid that must accumulate before it can be consistently identified on ultrasound.

5.6 EFAST Exam for Penetrating vs Blunt Thoracoabdominal Trauma

While most of the data pertaining to the EFAST exam includes blunt trauma patients, there is ample data that shows similar results and implications for penetrating trauma [2, 58, 64, 65].

5.7 How to Perform the EFAST Exam

5.7.1 Evaluation of Hemoperitoneum

The curvilinear transducer is the preferred transducer in the evaluation for hemoperitoneum due to its higher resolution and large window. If a curvilinear transducer is not available, a phased-array transducer may be used. The abdominal assessment includes 3 windows: the right upper quadrant (RUQ), pelvis, and the left upper quadrant (LUQ). With regards to where to begin, the identification of hemoperitoneum may be considered to be a binary exam. This means there are two options: either there is free fluid or there isn't free fluid. In order to most efficiently and quickly identify the presence of free fluid, one should consider starting in the area in which abdominal free fluid is mostly likely to accumulate, followed by the second most likely place fluid would accumulate, etc. The most common location for an EFAST exam to be positive is in the RUQ, so this would be the most advantageous place to start [66]. The next most common place is in the pelvis, and the least common place to pick up isolated free fluid is the LUQ [66].

5.7.2 RUQ Evaluation

The transducer should be placed in the mid to anterior axillary line near the T4-T6 area with the probe marker facing in the cephalad position in a coronal plane. The ultrasound is a 2-D imaging modality that is examining a 3-D structure, so full sweeps of the area should be performed. Free fluid will appear hypoechoic on ultrasound and typically accumulates in specific areas. The most common place for fluid to first accumulate is the interface between the caudal tip of the liver and the inferior pole of the kidney (Fig. 21). The next most common locations for fluid to accumulate are the interface

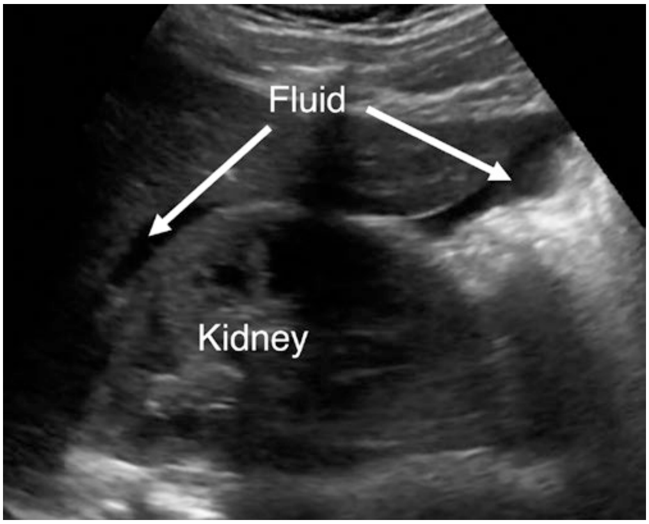

Fig. 21 An image of free fluid at the caudal tip of the liver, near the inferior pole of the kidney

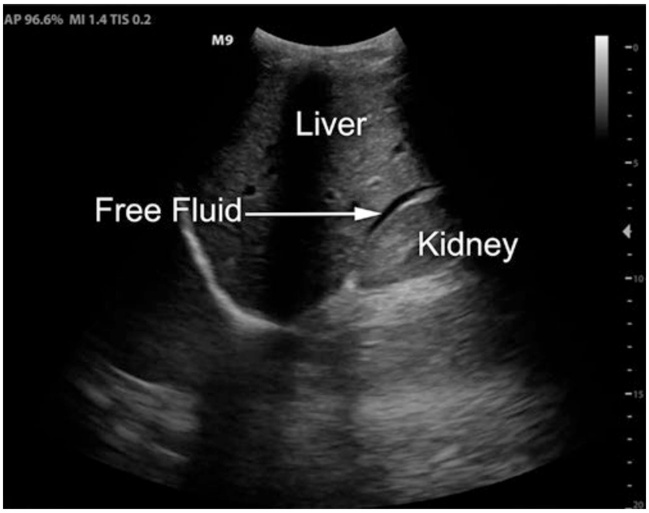

Fig. 22 Free fluid within Morrison's pouch

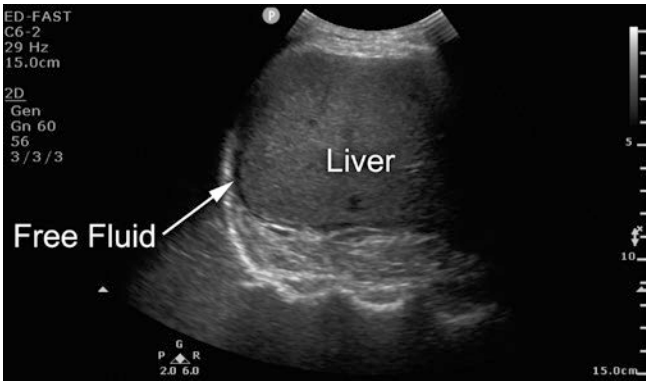

Fig. 23 Free fluid in the suprahepatic region

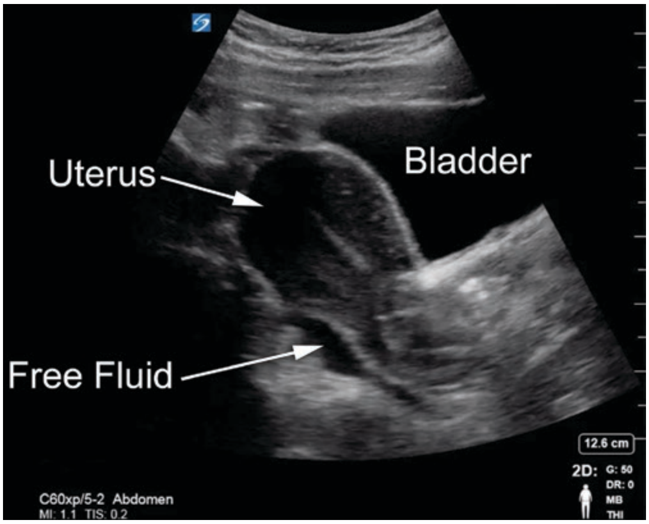

Fig. 24 Free fluid seen just posterior to the uterus in the pouch of Douglas (female)

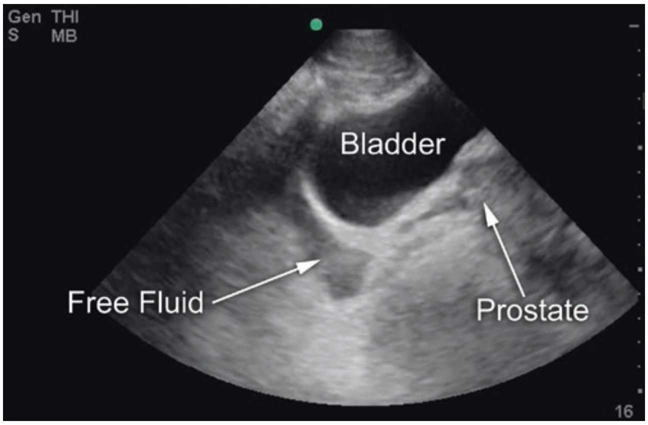

Fig. 25 Free fluid seen in the rectovesicular pouch. The presence of a prostate indicates this patient is a male

between the kidney and the liver (Morrison's pouch) (Fig. 22), followed by the suprahepatic region [66], (Fig. 23).

5.7.3 Pelvic Evaluation

The transducer should be placed in the suprapubic region just cephalad to the pubic symphysis, with the probe marker facing cephalad and in a sagittal orientation. Free fluid will accumulate just superior and posterior to the bladder in males, and between the uterus and bladder or posterior to the uterus in females, depending on the presence of either an anteverted or retroverted uterus (Figs. 24 and 25) [66]. A diligent and full sweep from one side of the pelvis to the other is necessary and if desired, a transverse view can also be obtained of the same area. Of note, a full bladder is necessary for the most accurate evaluation of the pelvis as the bladder functions as an acoustic window for the sonographic beams to reach the most dependent portions of the peritoneum. A decompressed bladder allows the intestines to fill the area, causing the air in them to inhibit the sound waves from reaching the area to be evaluated.

5.7.4 LUQ Evaluation

The LUQ is not a mirror image of the RUQ and as such, fluid has a propensity to accumulate in different areas. In most patients, the spleen is a smaller organ than the liver, so the window that can be used is often smaller in the LUQ. The probe should be placed in a similar orientation and location as the RUQ, save for the fact that it should be placed more towards the posterior axillary line and often a rib space or two higher than the typical location on the RUQ. The most common location for fluid to accumulate in the LUQ is the suprasplenic region (Fig. 26), followed by the spleno-renal interface (Fig. 27), followed by the interface between the caudal edge of the liver and the superior right paracolic gutter [66].

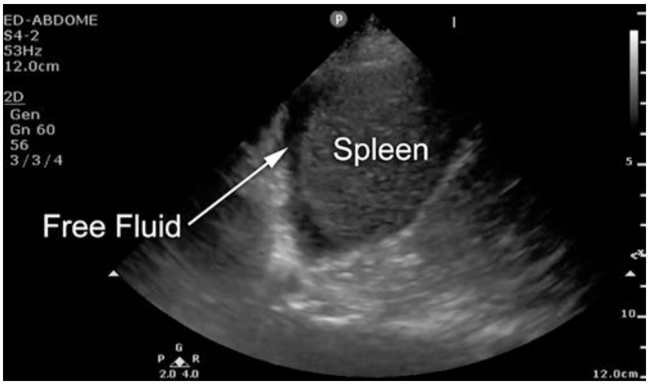

Fig. 26 Free fluid in the suprasplenic region

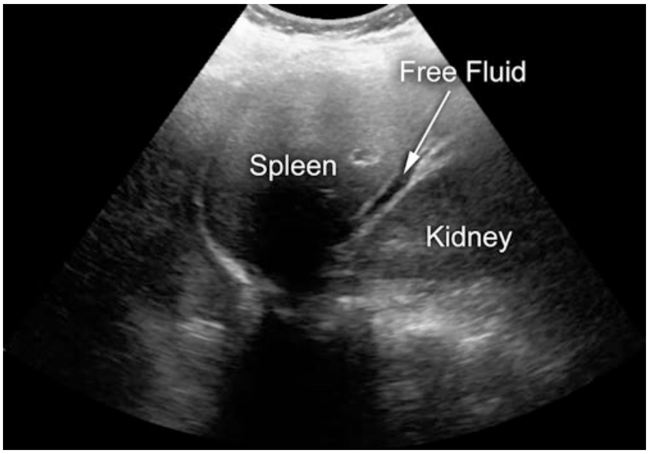

Fig. 27 Free fluid in the splenorenal interface

5.7.5 Hemopericardium Assessment

The curvilinear transducer, while the preferred transducer for evaluation of hemoperitoneum, may not be the best in the evaluation of hemopericardium. The phased-array transducer is often the preferred transducer for echocardiography. The most common view used to evaluate the pericardium is the subxiphoid view. The phased-array transducer should be placed in the subxiphoid area with the probe marker facing towards the patients left. Care must be taken to make sure that the transducer is placed underneath the xiphoid in order for the sound beam to reach the pericardium. Hemopericardium is visualized as a rim of hypoechoic fluid surrounding the heart (Fig. 28). Fluid preferentially accumulates around the right side of the heart due to the lower pressure of that side of the heart [67]. Echocardiographic tamponade can be identified by visualizing diastolic chamber collapse in the setting of a pericardial effusion. The first chamber to demonstrate diastolic chamber collapse is the right atrium (RA), followed by the right ventricle (RV), followed by the left side of the heart [68]. If the patient is in shock and a pericardial effusion is visualized, the IVC should also be evaluated. The IVC is a surrogate marker of the CVP, which if elevated, can help solidify the diagnosis of traumatic tamponade [69]. If a subxiphoid view of the heart is unable to be visualized, a parasternal or apical view can also be used.

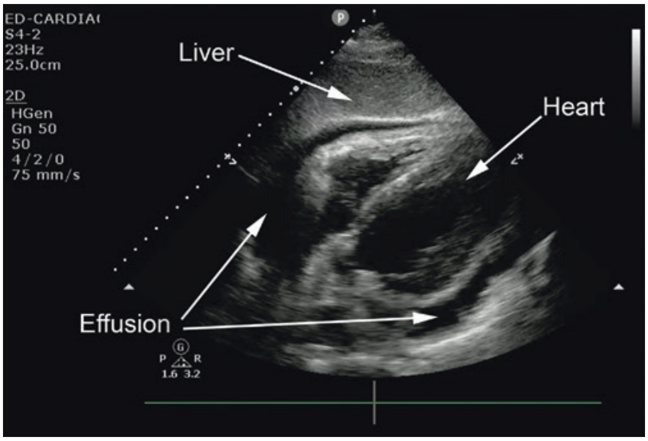

Fig. 28 This subxiphoid image of the heart shows a pericardial effusion

5.7.6 Hemothorax Assessment

The evaluation of the hemothorax is performed in a very similar location to the RUQ and LUQ windows of the peritoneum. However, instead of focusing on the area below the diaphragm, focus should be placed above the diaphragm. The probe should be placed in the mid to posterior axillary line in a coronal plane with the probe marker facing cephalad, usually centered around the T4 area. Under normal circumstances there are two artifacts that one should be aware of to rule out a hemothorax: The spine and mirror signs. The mirror sign occurs when a fluid filled structure (i.e., the liver) is in contact with an air filled structure (i.e., the lungs) [22]. When this interface occurs, a mirror artifact of the fluid filled structure is created where the air-filled structure is located. In the setting of an air-filled thorax, there will be a mirror image artifact of the liver or spleen seen *above* the diaphragm. This helps exclude a hemothorax. The next sign one should evaluate is the presence or absence of a spine sign. The spine can easily be seen when the liver or spleen is used as an acoustic window. Air blocks sounds waves, and when there is no pleural effusion, the sound waves cannot reach the vertebral bodies superior to the liver/spleen and posterior to the lung. This causes the spine to disappear once the diaphragm starts. (Fig. 29). A negative spine sign and a positive mirror sign rule out a pleural effusion, while a positive spine sign and a negative mirror sign rule one in (Fig. 30).

5.7.7 Pneumothorax Assessment

The preferred transducer for the sonographic assessment of a pneumothorax is the linear transducer due to its superior

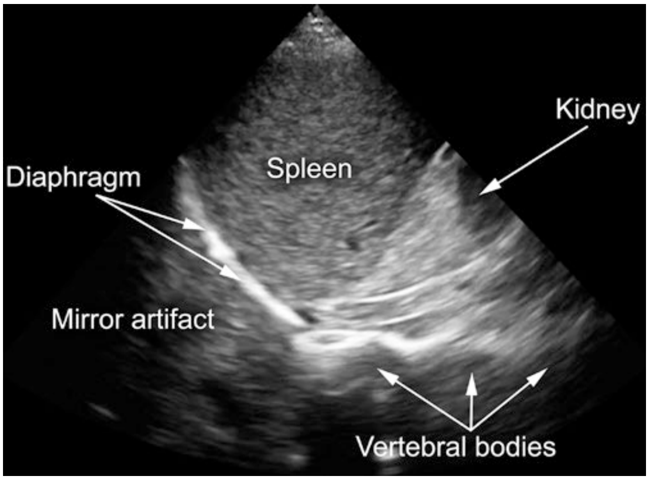

Fig. 29 A normal LUQ view showing mirror image artifact superior to the diaphragm

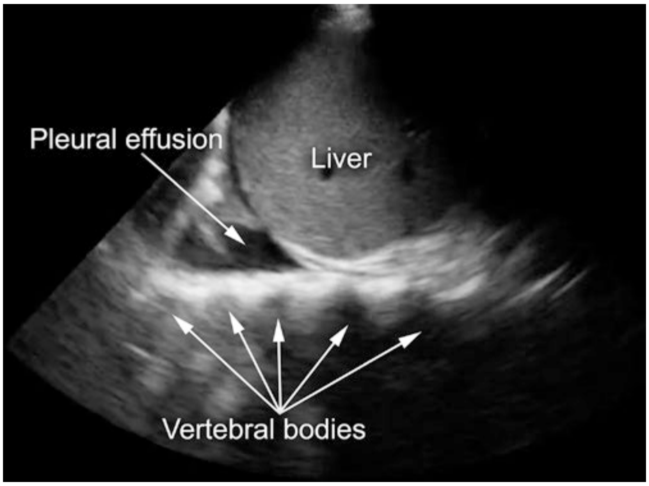

Fig. 30 The spine sign seen superior to the diaphragm, in conjunction with the lack of mirror image artifact, indicate that there is free fluid in the right hemithorax

resolution of superficial structures. However, the curvilinear transducer can also be used if the depth is shallow and the image is under-gained. The transducer should be placed in the sagittal orientation on the anterior chest wall along the mid-clavicular line in the location that is most anterior on the patient. In a supine patient, this location is often rib spaces 6–8, while in a semi-recumbent patient, that location may be right under the clavicle, at rib spaces 2–3 [70]. The pleural line is seen as a hyperechoic line just underneath the ribs, which are themselves seen in the transverse orientation. (Fig. 31). The area that must be diligently observed in real-time is the pleural line. The hyperechoic pleural line is always visible irrespective if there is a pneumothorax or not. In the evaluation of a pneumothorax one must identify *sliding* of that pleural line with respiration. Lung sliding is the sonographic visualization of the visceral pleura moving relative to the parietal pleura. If sliding is visualized, a pneumothorax can be excluded in that area. In the right clinical setting the absence of lung sliding could rule-in a pneumothorax [71]. The reason why lung sliding is not always diagnostic of a pneumothorax is because there are other situations where lung sliding can be lost, such as a severe exacerbation obstructive airways disease, apnea and pleurodesis, among others [72]. If the absence of lung sliding is seen, an attempt should be made to look for a lung point, which is the place on the chest wall where the pneumothorax begins [71]. This finding is thought to be highly specific for a PTX [73].

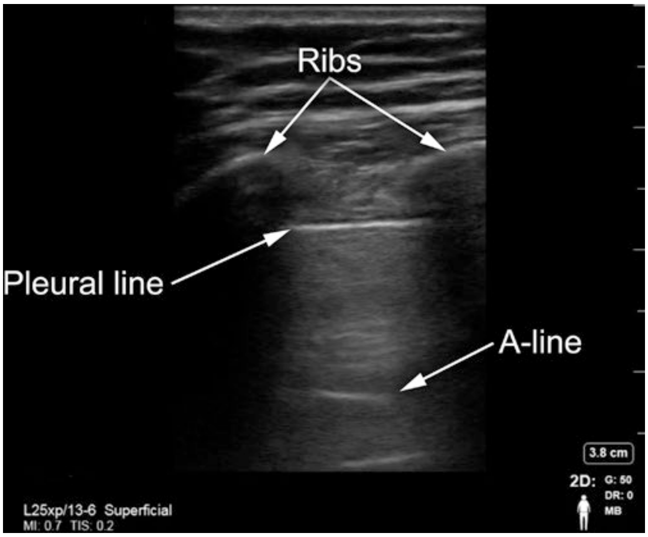

Fig. 31 A normal image of the pleural line. Note the A-line which is a normal artifact seen in air-filled lungs

6 Summary

The EFAST exam is an exam that looks for hemoperitoneum, hemothorax, PTX and the presence of a pericardial effusion. Most of the data is obtained with blunt trauma patients, but there is abundant literature supporting its use in penetrating truncal trauma as well [74].

References

1. Cervellin G, Mora R, Ticinesi A, Meschi T, Cornelli I, Catena F, Lippi G. Epidemiology and outcomes of acute abdominal pain in a large urban Emergency Department: retrospective analysis of 5,340 cases. Ann Translat Med. 2016;4(19):362.
2. Melniker LA, Leibner E, McKenney MG, Lopez P, Briggs WM, Mancuso CA. Randomized controlled clinical trial of point-of-care, limited ultrasonography for trauma in the emergency department: the first sonography outcomes assessment program trial. Ann Emerg Med. 2006;48(3):227–35.

3. Hiratzka LF, Bakris GL, Beckman JA. ACCF/AHA/AATS/ACR/ASA/SCA/SCAI/SIR/STS/SVM guidelines for the diagnosis and management of patients with Thoracic Aortic Disease: a report of the American College of Cardiology Foundation/American Heart Association Task Force on Practice Guidelines, American Association for Thoracic Surgery, American College of Radiology, American Stroke Association, Society of Cardiovascular Anesthesiologists, Society for Cardiovascular Angiography and Interventions, Society of Interventional Radiology, Society of Thoracic Surgeons, and Society for Vascular Medicine. Circulation. 2010;121(13):e266–369.
4. Costantino TG, Bruno EC, Handly N, Dean AJ. Accuracy of emergency medicine ultrasound in the evaluation of abdominal aortic aneurysm. J Emerg Med. 2005;29(4):455–60.
5. Manning BJ, Kristmundsson T, Sonesson B, Resch T. Abdominal aortic aneurysm diameter: a comparison of ultrasound measurements with those from standard and three-dimensional computed tomography reconstruction. J Vasc Surg. 2009;50(2):263–8.
6. Lech C, Swaminathan A. Abdominal aortic emergencies. Emerg Med Clin North Am. 2017;35(4):847–67.
7. Concannon E, McHugh S, Healy DA. Diagnostic accuracy of non-radiologist performed ultrasound for abdominal aortic aneurysm: systematic review and meta-analysis. Int J Clin Pract. 2014;68(9):1122–9.
8. Hertzer NR. A primer on infrarenal abdominal aortic aneurysms. F1000Res. 2017;6:1549.
9. Taheri MS, Haghighatkhah H, Pourghorban R, Hosseini A. Multidetector computed tomography findings of abdominal aortic aneurysm and its complications: a pictorial review. Emerg Radiol. 2013;20(5):443–51.
10. Fojtik JP, Costantino TG, Dean AJ. The diagnosis of aortic dissection by emergency medicine ultrasound. J Emerg Med. 2007;32(2):191–6.
11. Pape LA, Tsai TT, Isselbacher EM. Aortic diameter >or = 5.5 cm is not a good predictor of type a aortic dissection: observations from the International Registry of Acute Aortic Dissection (IRAD). Circulation. 2007;116(10):1120–7.
12. Williams J, Heiner JD, Perreault MD, McArthur TJ. Aortic dissection diagnosed by ultrasound. West J Emerg Med. 2010;11(1):98–9.
13. Heegaard W, Hildebrandt D, Spear D, Chason K, Nelson B, Ho J. Prehospital ultrasound by paramedics: results of field trial. Acad Emerg Med Off J Soc Acad Emerg Med. 2010;17(6):624–30.
14. Studer M, Hempel D, Rouhani S, Dubsky H, Pivetta E, Kimberly HH. Addition of a lateral view improves adequate visualization of the abdominal aorta during clinician performed ultrasound. Am J Emerg Med. 2014;32(3):256–9.
15. Everhart JE, Khare M, Hill M, Maurer KR. Prevalence and ethnic differences in gallbladder disease in the United States. Gastroenterology. 1999;117(3):632–9.
16. Hilsden R, Leeper R, Koichopolos J, Vandelinde JD, Parry N, Thompson D, Myslik F. Point-of-care biliary ultrasound in the emergency department (BUSED): implications for surgical referral and emergency department wait times. Trauma Surg Acute Care Open. 2018;3(1):e000164.
17. Kendall JL, Shimp RJ. Performance and interpretation of focused right upper quadrant ultrasound by emergency physicians. J Emerg Med. 2001;21(1):7–13.
18. Scruggs W, Fox JC, Potts B, Zlidenny A, McDonough J, Anderson CL, Larson J, Barajas G, Langdorf MI. Accuracy of ED bedside ultrasound for identification of gallstones: retrospective analysis of 575 studies. West J Emerg Med. 2008;9(1):1–5.
19. Blaivas M, Hardood RA, Lambert MJ. Decreasing length of stay with emergency ultrasound examination of the gallbladder. Aca Emerg Med. 1999;6(10):1020–3.
20. Harvey RT, Miller WT Jr. Acute biliary disease: initial CT and follow-up US versus initial US and follow-up CT. Radiology. 1999;213(3):831–6.
21. Adhikari S, Morrison D, Lyon M, Zeger W, Krueger A. Utility of point-of-care biliary ultrasound in the evaluation of emergency patients with isolated acute non-traumatic epigastric pain. Intern Emerg Med. 2014;9(5):583–7.
22. Feldman MK, Katyal S, Blackwood MS. US artifacts. Radiographics. 2009;29(4):1179–89.
23. Bree RL. Further observations on the usefulness of the sonographic Murphey sign in the evaluation of suspected acute cholecystitis. J Clin Ultrasound. 1995;23(3):169–72.
24. McArthur TA, Planz V, Fineberg NS, Tessler FN, Robbin ML, Lockhart ME. The common duct dilates after cholecystectomy and with advancing age: reality or myth? J Ultrasound Med. 2013;32(8):1385–91.
25. Scales CD, Smith AC, Hanley JM. Saigal CS; urologic diseases in America project. Prevalence of kidney stones in the United States. Eur Urol. 2012;62(1):160–5.
26. Foster G, Stocks C, Borofsky MS. Emergency department visits and hospital admissions for kidney stone diease, 2009: statistical brief #139. Healthcare Cost and Utilization Project (HCUP). Agency for Healthcare Research and Quality. 2006–2012.
27. Smith-Bindman R, Aubin C, Bailitz J, Bengiamin RN, Camargo CA Jr, Corbo J, Dean AJ, Goldstein RB, Griffey RT, Jay GD, Kang TL, Kriesel DR, Ma OJ, Mallin M, Manson M, Manson W, Melnikow J, Miglioretti DL, Miller SK, Mills LD, Miner JR, Moghadassi M, Noble VE, Press GM, Stoller ML, Valencia VE, Wang J, Wang RC, Cummings SR. Ultrasonography versus computed tomography for suspected nephrolithiasis. N Engl J Med. 2014;371(12):1100–10.
28. Park YH, Jung RB, Lee YG, Hong CK, Ahn JH, Shin TY, Kim YS, Ha YR. Does the use of bedside ultrasonography reduce emergency department length of stay for patients with renal colic?: a pilot study. Clin Exp Emerg Med. 2016;3(4):197–203.
29. Sternberg KM, Littenberg B. Trends in imaging use for the evaluation and follow up of kidney stone disease: a single center experience. J Urol. 2017;198(2):383–8.
30. Dalziel PJ, Noble VE. Bedside ultrasound and the assessment of renal colic: a review. Emerg Med J. 2013;30(1):3–8.
31. Daniels B, Gross CP, Molinaro A, Singh D, Luty S, Jessey R, Moore CL. Stone plus: evaluation of emergency department patients with suspected renal colic, using a clinical prediction tool combine with point-of-care limited ultrasonography. Ann Emerg Med. 2016;67(4):439–48.
32. Sutijono, et al. Twinkle twinkle little stone: utilizing color Doppler in emergency ultrasound diagnosis of a ureterovesicular stone. Crit Ultrasound J. 2010;2(2):77–9. [Online ISSN 2036-7902]
33. Rotariu P, Yohannes P, Alexianu M. Management of malignant extrinsic compression of the ureter by simultaneous placement of two ipsilateral ureteral stents. J Endourol. 2001;15(10):979–83.
34. Perry KJ, Ko P, Mariana P, Ciaccio AJ. Time course resolution of hydronephrosis with spontaneous ureteral stone passage. West J Emerg Med. 2010;11(1):105.
35. O'Neill WC. Renal relevant radiology: use of ultrasound in kidney disease and nephrology procedures. Clin J Am Soc Nephrol. 2014;9(2):373–81.
36. Herbst MK, Rosenberg G, Daniels B, Gross CP, Singh D, Molinaro AM, Luty S, Moore CL. Effect of provider experience on clinician-performed ultrasonography for hydronephrosis in patients with suspected renal colic. Ann Emerg Med. 2014;64(3):269–76.
37. Tarzamni MK, Sobhani N, Nezami N, Ghiasi F. Bilateral parapelvic cysts that mimic hydronephrosis in two imaging modalities: a case report. Cases J. 2008;1(1):161.
38. Medrano NW, Villarreal CL, Price MA. Multi-institutional multidisciplinary injury mortality investigation in the civilian pre-hospital environment (MIMIC): a methodology for reliably measuring pre-

hospital time and distance to definitive care. Trauma Surg Acute Care Open. 2019;4(1):e000309.

39. Nishijima DK, Simel DL, Wisner DH, Holmes JF. Does this adult patient have a blunt intra-abdominal injury? J Am Med Assoc. 2012;307(14):1517–27.
40. Rippey JC, Royse AG. Ultrasound in trauma. Best practice & research. Clin Anaesthesiol. 2009;23(3):343–62.
41. Rozycki GS, Ochsner MG, Schmidt JA. A prospective study of surgeon-performed ultrasound as the primary adjuvant modality for injured patient assessment. J Trauma. 1995;39(3):492–8; discussion 498–500
42. Kirkpatrick AW, Sirois M, Laupland KB. Hand-held thoracic sonography for detecting post-traumatic pneumothoraces: the extended focused assessment with sonography for trauma (EFAST). J Trauma. 2004;57(2):288–95.
43. Stengel D, Leisterer J, Ferrada P, Ekkernkamp A, Mutze S, Hoenning A. Point-of-care ultrasonography for diagnosing thoracoabdominal injuries in patients with blunt trauma. Cochrane Database Syst Rev. 2018;12:CD012669.
44. Thomas B, Falcone RE, Vasquez D. Ultrasound evaluation of blunt abdominal trauma: program implementation, initial experience, and learning curve. J Trauma. 1997;42(3):384–8; discussion 388-90
45. Gracias VH, Frankel HL, Gupta R. Defining the learning curve for the focused abdominal sonogram for trauma (FAST) examination: implications for credentialing. Am Surg. 2001;67(4):364–8.
46. Ma OJ, Gaddis G, Norvell JG, Subramanian S. How fast is the focused assessment with sonography for trauma examination learning curve? Emerg Med Australas. 2008;20(1):32–7.
47. Branney SW, Wolfe RE, Moore EE. Quantitative sensitivity of ultrasound in detecting free intraperitoneal fluid. J Trauma. 1995;39(2):375–80.
48. Paajanen H, Lahti P, Nordback I. Sensitivity of transabdominal ultrasonography in detection of intraperitoneal fluid in humans. Eur Radiol. 1999;9(7):1423–5.
49. Rose JS. Ultrasound in abdominal trauma. Emerg Med Clin North Am. 2004;22(3):581–99.. vii
50. Abrams BJ, Sukumvanich P, Seibel R, Moscati R, Jehle D. Ultrasound for the detection of intraperitoneal fluid: the role of Trendelenburg positioning. Am J Emerg Med. 1999;17(2):117–20.
51. Miller MT, Pasquale MD, Bromberg WJ, Wasser TE, Cox J. Not so FAST. J Trauma. 2003;54(1):52–9.. discussion 59–60
52. Von Kuenssberg Jehle D, Stiller G, Wagner D. Sensitivity in detecting free intraperitoneal fluid with the pelvic views of the FAST exam. Am J Emerg Med. 2003;21(6):476–8.
53. Fitzgerald M, Spencer J, Johnson F, Marasco S, Atkin C, Kossmann T. Definitive management of acute cardiac tamponade secondary to blunt trauma. Emerg Med Australasia. 2005;17(5–6):494–9.
54. Press GM, Miller S. Utility of the cardiac component of FAST in blunt trauma. J Emerg Med. 2013;44(1):9–16.
55. Rozycki GS, Feliciano DV, Ochsner MG. The role of ultrasound in patients with possible penetrating cardiac wounds: a prospective multicenter study. J Trauma. 1999;46(4):543–51; discussion 551–2.
56. Rozycki GS, Ballard RB, Feliciano DV, Schmidt JA, Pennington SD. Surgeon-performed ultrasound for the assessment of truncal injuries: lessons learned from 1540 patients. Ann Surg. 1998;228(4):557–67.
57. Rozycki GS, Feliciano DV, Schmidt JA. The role of surgeon-performed ultrasound in patients with possible cardiac wounds. Ann Surg. 1996;223(6):737–44.. discussion 744–6
58. Plummer D, Brunette D, Asinger R, Ruiz E. Emergency department echocardiography improves outcome in penetrating cardiac injury. Ann Emerg Med. 1992;21(6):709–12.
59. Chen SC, Markmann JF, Kauder DR, Schwab CW. Hemopneumothorax missed by auscultation in penetrating chest injury. J Trauma. 1997;42(1):86–9.
60. Bokhari F, Brakenridge S, Nagy K. Prospective evaluation of the sensitivity of physical examination in chest trauma. J Trauma. 2002;53(6):1135–8.
61. Ebrahimi A, Yousefifard M, Mohammad KH. Diagnostic accuracy of chest ultrasonography versus chest radiography for identification of pneumothorax: a systematic review and meta-analysis. Tanaffos. 2014;13(4):29–40.
62. Atkinson P, Milne J, Loubani O, Verheul G. The V-line: a sonographic aid for the confirmation of pleural fluid. Crit Ultrasound J. 2012;4(1):19.
63. Rahimi-Movaghar V, Yousefifard M, Ghelichkhani P. Application of ultrasonography and radiography in detection of hemothorax; a systematic review and meta-analysis. Emerg. 2016;4(3):116–26.
64. Hall MK, Omer T, Moore CL, Taylor RA. Cost-effectiveness of the cardiac component of the focused assessment of sonography in trauma examination in blunt trauma. Acad Emerg Med Off J Soc Acad Emerg Med. 2016;23(4):415–23.
65. Mayron R, Gaudio FE, Plummer D, Asinger R, Elsperger J. Echocardiography performed by emergency physicians: impact on diagnosis and therapy. Ann Emerg Med. 1988;17(2):150–4.
66. Lobo V, Hunter-Behrend M, Cullnan E. Caudal edge of the liver in the Right Upper Quadrant (RUQ) view is the most sensitive area for free fluid on the FAST exam. West J Emerg Med. 2017;18(2):270–80.
67. Goodman A, Perera P, Mailhot T, Mandavia D. The role of bedside ultrasound in the diagnosis of pericardial effusion and cardiac tamponade. J Emerg Trauma Shock. 2012;5(1):72–5.
68. Pepi M, Muratori M. Echocardiography in the diagnosis and management of pericardial disease. J Cardiovasc Med (Hagerstown). 2006;7(7):533–44.
69. Himelman RB, Kircher B, Rockey DC, Schiller NB. Inferior vena cava plethora with blunted respiratory response: a sensitive echocardiographic sign of cardiac tamponade. J Am Coll Cardiol. 1988;12(6):1470–7.
70. Mennicke M, Gulati K, Oliva I, et al. Anatomical distribution of traumatic pneumothoraces on chest computed tomography: implications for ultrasound screening in the ED. Am J Emerg Med. 2012;30(7):1025–31.
71. Volpicelli G, Elbarbary M, Blaivas M. International evidence-based recommendations for point-of-care lung ultrasound. Intensive Care Med. 2012;38(4):577–91.
72. Ziapour B, Haji HS. Anterior convergent chest probing in rapid ultrasound transducer positioning versus formal chest ultrasonography to detect pneumothorax during the primary survey of hospital trauma patients: a diagnostic accuracy study. J Trauma Manag Outcomes. 2015;9:9.
73. Lichtenstein DA, Mezière GA. Relevance of lung ultrasound in the diagnosis of acute respiratory failure: the BLUE protocol. Chest. 2008;134(1):117–25.
74. Quinn AC, Sinert R. What is the utility of the Focused Assessment with Sonography in Trauma (FAST) exam in penetrating torso trauma? Injury. 2011;42(5):482–7.

Practicality of Ultrasound in Emergency Medicine

Jason Arthur, Scott Bomann, and Christopher L. Moore

1 Introduction

> *Emergency, clinical point-of-care ultrasound performed, interpreted, and integrated into clinical care by emergency physicians is a fundamental skill in the practice of emergency medicine*. [1]

1.1 History

Ray Mayron was practicing emergency medicine (EM) in the mid-1980's when he learned that the department of cardiology at his hospital was discarding their aging ultrasound machine. His midwestern practicality led him to adopt the cast-off machine and repurpose it to diagnose cardiac tamponade in the emergency department (ED). In 1988 he published a case series on the topic and in doing so described one of the first uses of point-of-care ultrasound and the birth of emergency ultrasound (EUS) [2].

EM organizations quickly realized that ultrasound was a powerful tool when placed in the hands of the treating physician. In 1990 the American College of Emergency Physicians (ACEP) publicly endorsed physician-performed ultrasound. They were joined soon thereafter by the Society of Academic Emergency Medicine (SAEM) and together recommended incorporation into EM Graduate Medical Education [3]. By 1991 ACEP had begun including ultrasound in its list of core content for EM training. In 1994 they had created ultrasound competency guidelines [4]. However by the late 90s and despite a decade worth of encouragement, few emergency physicians (EPs) had access to point-of-care ultrasound [5, 6]. A major change occurred in May of 2001 when the Council of Emergency Medicine Residency Directors (CORD) issued a mandate: EM training programs must teach ultrasound and resident physicians must demonstrate ultrasound proficiency. The policy was necessary to overcome the political and financial arguments which had kept EUS from thriving [7, 8]. That same year, ACEP published the first guidelines on Emergency Ultrasound to provide a guide for training and administering Emergency Ultrasound programs. While there is still wide variability in the expertise, comfort, and use of ultrasound by EPs, this tool is now firmly entrenched in the training and scope of practice of EM.

1.2 Differentiating the Undifferentiated

Undifferentiated patients present to the ED acutely and may be unable to provide a meaningful history. EPs are taught to have a worst-first mentality to ensure critical diagnoses are not missed. EPs may not have the luxury of the patient stability typically seen in a clinic setting. In fact, nowhere else in medicine is it necessary to diagnose, provide treatment, and disposition unfamiliar patients of all acuity levels within such a short time frame. Point-of-care ultrasound is, by its very nature, a pragmatic and practical tool. It is designed to offer immediate diagnostic, procedural, and therapeutic guidance and is an indispensable instrument in the practice of emergency medicine.

EUS is focused imaging performed by the EP to answer a specific clinical question. It is a focused diagnostic test that is distinct from the physical exam. In properly trained hands it has been shown to far exceed the diagnostic accuracy of many physical exam findings such as free fluid in the abdomen, valvular heart disease, central venous pressure, cardiac failure, pleural effusions, pericardial effusions, pneumonia, pneumothorax, pulmonary edema, deep vein thrombosis (DVT), symptomatic biliary stones, abscesses, urinary retention, and

---

J. Arthur
University of Arkansas for Medical Sciences, Department of Emergency Medicine, Little Rock, AR, USA

S. Bomann
Wellington Regional Hospital, Department of Emergency Medicine, Wellington, New Zealand

C. L. Moore (✉)
Yale School of Medicine, Department of Emergency Medicine, New Haven, CT, USA
e-mail: chris.moore@yale.edu

© Springer Nature Switzerland AG 2021
J. Li et al. (eds.), *Ultrasound Fundamentals*, https://doi.org/10.1007/978-3-030-46839-2_33

retinal detachment among many others [1, 9, 10]. When patient present in extremis or with an ambiguous clinical picture, EUS often reveals the diagnosis and guides management decisions.

2 Equipment

Selecting equipment for an ED or other site where point-of-care ultrasound is performed requires an understanding of the needs and resources available. There is no single ultrasound device which works for every environment or meets every budget. When evaluating equipment, it is important not to start with evaluation of specific machines but rather the specific needs, uses, and budget of the facility. These will help tailor the search to devices relevant for the facility. Facilities which use ultrasound solely for vascular access have different equipment needs than those which routinely perform more advanced echocardiography.

Most EDs opt for a minimum of a phased array and linear probe. Phased array probes typically have a lower frequency which allows them to adequately image deeper structures and makes them suitable for a variety of exams such as echocardiography, obstetrical, abdominal, and thoracic ultrasonography. Linear probes typically have higher frequency ranges which allow for higher resolution imaging but limit the depth which they can adequately image. Linear probes are routinely used for vascular access and nerve blocks as well as soft tissue, musculoskeletal, ocular, vascular, testicular, and thoracic ultrasound. Facilities may also use the curvilinear, micro curvilinear, endocavitary, ultra-high frequency linear, and/or transesophageal probes depending on their clinical needs. Manufacturers typically offer a variety of software options for a given ultrasound model and this can affect the price and function of the machine widely. Some facilities have additional constraints, such as space, which create significant limitations on which devices can be used. In contrast to the machines used in radiology and cardiology, ED devices generally run on battery power, have a smaller footprint and use more limited software packages. Understanding the facility's goals for ultrasound over the next 5–10 years will help focus selection efforts to achieving those goals.

Evaluation of specific equipment often starts with prior experience, discussion with colleagues in similar environments, or exposure to equipment which is typically available for display at national meetings or in ultrasound courses. After a short list of devices has been compiled, discussion with manufacturer representatives to evaluate these in person is routine. Vendors typically bring devices and technical experts to the facility considering their products.. These are opportunities to familiarize yourself, your colleagues, and others within your facility with these devices. Prices are provided as part of a quote from the manufacturer. Quotes are routinely confidential and expire after a certain time frame, typically 30–90 days. Most manufacturers include a warranty in the purchase price. While warranties vary among manufacturers, 5 years is a fairly standard. Warranties may be extended beyond the initial period, though these extensions may be less cost effective than buying a new machine. While many devices continue to be useful beyond five-years, most have extensive wear-and-tear and lack the novel features of the newer machines.

Cost is an important factor faced by every facility when selecting ultrasound devices. The most expensive device is not necessarily the best device for a facility. However, purchasing a device which meets current, but not future, goals of a facility may result in premature replacement of equipment with increased total costs in the long term. Manufacturers often will provide discounts for trading in old units and many include discounts for purchasing multiple devices. Refurbished devices are also available, typically from third party sellers rather than from equipment manufacturers.

3 Administrative Issues

3.1 Training & Credentialing

Ultrasound training varies by medical specialty and evolves with time. EM organizations have provided guidelines for EUS training since 2001 [11] which are regularly updated to reflect contemporary research as well as new techniques and studies. EUS is considered a procedure or focused diagnostic test. The EP uses ultrasound technology to acquire images, interpret the findings in the context of the patient, and integrate those findings into the clinical management of acute or critical medical conditions [12, 13].

Ultrasound technology and clinical guidelines have evolved rapidly over a relatively short period of time. As such, there is a spectrum of ultrasound practice and with prior formal training among ABEM certified EPs. Some have advanced skills, utilizing a broad range of ultrasound applications, while others have a more limited skillset. Regardless of the breadth of ultrasound usage, four key elements of competency must be ensured: an understanding of the indications and limitations of EUS, a knowledge of ultrasound physics and the ability to incorporate those principles into image acquisition, an understanding of and ability to interpret normal anatomy and pathology, and the ability to effectively integrate this information into the clinical care of the patient [12].

There are two pathways to obtaining training in EUS. The more common track is through completion of an Accreditation Council for Graduate Medical Education (ACGME) approved EM program and Board Certification in Emergency

Medicine by the American Board of Emergency Medicine (ABEM) [12]. EM as a specialty first published ultrasound competency guidelines in 1994 (Mateer) and training guidelines in 1997. Since 2001, demonstration of ultrasound proficiency has been a mandatory requirement for residency completion.

The second pathway is practice based and geared towards those EPs who completed their residency prior to the mandate for EUS education. This pathway typically requires introductory training with both lecture and practical sessions followed by ongoing education focused on training in one or two clinical applications until the EP attains competency in the core applications of EUS [13]. Some facilities with well-developed EUS education programs offer preceptorships to help facilitate this process [12]. As with all training, ongoing education through continued medical education, quality assurance, and timely feedback ensure that competency is maintained and skills are honed [12]. Fellowship Training in EUS is not required for the clinical use of EUS. EUS fellowships are designed to develop and apply advanced studies, provide education on program management, mentor those pursuing ultrasound research, and develop the fellow as an ultrasound educator [12].

Credentialing of a physician and granting privileges for procedures is required by the Joint Commission which accredits hospitals. In historical terms, it is the hospital's agreement that a physician is competent to provide a given service or perform a given procedure [13]. Commonly there are underlying political controversies between specialties and within a hospital. Often the specialty which first utilizes a technology asserts ownership of that technology. Traditional imaging specialties can create hurdles to credentialing in point-of-care ultrasound (POCUS), ultimately hindering attempts to provide high quality patient care [13]. Anticipating pitfalls is critical to pursuing privileging. Identifying allies within other departments who use POCUS such as surgery, critical care, anesthesia, obstetrics, and cardiology allows for cohesiveness and political strength. The collective wisdom from the shared experiences of these colleagues will only enhance patient care. Likewise, identifying members of the organization who are unsupportive of POCUS presents a valuable opportunity to anticipate and circumvent pitfalls. However, privileging in point-of-care ultrasound is assisted by multiple policy documents. The American Medical Association (AMA) House of Delegates passed HR 802 in 1999 which stipulated that ultrasound is within the scope of practice for properly trained physicians and that specialty-specific guidelines should be followed [13]. These have been reaffirmed multiple times by the AMA, most recently in 2010 with the passage of H-230.960 [14]. Likewise, this is supported by the ACEP Ultrasound Guidelines [12] which have been recognized by the American Institute of Ultrasound in Medicine [15]. Accreditation of point-of-care ultrasound is not currently required but may be linked to reimbursement in the future. The 2008 Medicare Improvements for Patients and Providers Act of 2008 requires advanced imaging services to be accredited but this excludes ultrasound. Despite this, some payers require accreditation. For this reason, ACEP created the Clinical Ultrasound Accreditation Program (CUAP) as a mechanism for EDs to provide assurance that their programs meet the current guidelines for EUS [13].

3.2 Quality Assurance

Quality assurance (QA) mechanisms are often a requirement of privileging as they are necessary to provide Ongoing Professional Practice Evaluation (OPPE). More importantly, timely QA ensures that providers are technically competent and maintain consistently accurate interpretations to provide the best clinical care of patients. All QA mechanisms should evaluate the technical aspects of the study as well as the clinical decision process. This requires that the physician record images and clips of the study and document their findings for later review [13]. While methods of retaining and reporting imaging results vary, many facilities utilize electronic databases which allow quality assurance mechanisms to interface with the electronic medical record. ACEP publishes Emergency Ultrasound Standard Reporting Guidelines which provide suggested reporting elements and example documents for this purpose [16]. Sufficient mechanisms to call back the patient should also be available to the reviewer to mitigate the risk of diagnostic error [12]. In general, until providers are credentialed, all images should be reviewed, while those who have attained full privileging in point-of-care ultrasound should have adequate review to ensure ongoing competency [12]. In systems with the adequate resources, providing QA on all studies is ideal.

3.3 Billing & Reimbursement

Ultrasound adds value to healthcare by improving patient safety, increasing patient satisfaction, decreasing utilization of more costly or limited resources, and improving clinical decision making [12]. In countries such as the United States, where reimbursement for services ensures the ability of healthcare organizations to provide ongoing care, recognition of and reimbursement for the value of ultrasound is critical. Physicians who are trained and credentialed to perform point-of-care ultrasound may bill for ultrasound. In order to bill for ultrasound services there must be a clinical indication for the study, an order must be placed, images must be permanently recorded, a written report must be generated [13]. In the united states, Current Procedural Terminology (CPT) codes are assigned to specific ultrasound studies. While a complete discussion of billing is beyond the scope of this chapter, it is important to note that complete and limited ultrasounds may be performed. Completed ultrasounds have specifically listed anatomic structures in a given area. EPs may bill for completed studies, provided that they fulfill the required components of the study. Most, however, will bill only limited studies, which answer clinical questions or guide procedures [12, 13].

4 Applications of Ultrasound

Since 2001, the American College of Emergency Physicians (ACEP) has published guidelines on Emergency Ultrasound. These guidelines are regularly updated and outline the basic and advanced applications of Emergency Ultrasound [17].

4.1 Core Applications of Ultrasound

ACEP recommends that trainees in EUS have a multifaceted ultrasound education. While they encourage the use of free, open-access medical education (FOAMed) and simulation, they still consider small group hands-on training and supervised performance with quality review to be the cornerstone of training in EUS [18]. Like all procedures, there is a continuum from basic to advanced.

ACEP requires completion of core studies for graduation from an EM Residency. Core studies include the Focused Assessment with Sonography in Trauma (FAST), focused echocardiography, basic thoracic, obstetrical, aortic, renal, biliary, soft tissue, ocular, and deep vein thrombosis (DVT) ultrasounds. Additionally, completion of training in the following ultrasound guided procedures are also considered core: central venous access, peripheral venous access, pericardiocentesis, thoracentesis, paracentesis, and abscess incision and drainage [19]. The FAST exam has evolved into the Extended Focused Assessment with Sonography in Trauma (E-FAST) which includes thoracic views to assess for hemothorax and pneumothorax. This adaptation builds upon the FAST and serves as a gateway to other core applications of ultrasound. ACEP recommends that trainees in EUS complete a minimum of 25–50 quality-reviewed exams for each application and a minimum of 150–300 across all applications depending on how many applications are used [18].

4.2 Advanced Applications of Emergency Ultrasound

EUS is growing in both scope. As more physicians utilize ultrasound, new applications are discovered. As personal skill with ultrasound develops, new doors are opened to perform more advanced studies. Because advanced applications continue to adapt, it is difficult to provide an all-inclusive list of studies. However, the ACEP has recognized certain topics as advanced or fellowship level. These serve as a guideline for many EUS fellowships to ensure a well-rounded education. Advanced applications of core studies, such as advanced thoracic, cardiac, ocular, abdominal organ, and vascular assessment, are a cornerstone of Fellow level education. Additional advanced applications are organ specific, such as airway, ENT, uterus and adnexal, testicular, bowel, appendix, intussusception, pyloric stenosis, fracture, tendon and muscle, and joint ultrasound. Additionally, more advanced ultrasound guided procedures, such as ultrasound guided nerve blocks, lumbar punctures, gastrostomy, jejunostomy, and suprapubic tube placements are also taught at the fellowship level [19].

A relatively new application of Emergency Ultrasound has been the use of Resuscitative Transesophageal Echocardiography (TEE). Traditionally TEE has been the purview of cardiology and cardiac anesthesia. EPs have long recognized the usefulness of echocardiography in cardiac arrest and patients with profound shock and have been early adopters of transthoracic echocardiography (TTE). However transthoracic echocardiography can be extremely limited by patient habitus, underlying medical conditions, real estate within a resuscitation bay, and/or ongoing cardiopulmonary resuscitation. Resuscitative TEE is an attempt to overcome these barriers and answer questions that TTE cannot. Resuscitative TEE centers on four key views: the mid-esophageal four chamber view, the mid-esophageal long axis, the bicaval view, and the trans-gastric short axis. The first case series of ED use of resuscitative TEE was published in 2008 [20]. Multiple studies since that time have demonstrated that simulation-based training in Resuscitative TEE is effective and sustained over time [21, 22]. Several facilities have launched Resuscitative TEE programs with many, if not all, involved in ongoing research. One study found that Resuscitative TEE had a diagnostic impact in 78% of cases and influenced therapeutic choices in 67% of cases where it was used [23]. Another demonstrated that Resuscitative TEE had a diagnostic, therapeutic, or prognostic impact in 97% of cases [24]. The progression from TTE to Resuscitative TEE has promulgated in the establishment of a clinical policy by the American College of Emergency Physicians supporting the performance of resuscitative TEE. That policy defines the training standards, technique, quality assurance, and cleaning procedures which should be used for EP performed studies [25].

There is an application specific continuum of skill from basic to advanced EUS upon which all EPs fall. Some may possess advanced cardiac ultrasonography skills but only basic or even absent skill with testicular, appendix, or pyloric ultrasound. For this reason, while the scope of EUS continues to grow, the importance of ongoing education grows along with it.

4.3 Future Directions

4.3.1 Pocket Carried Devices

Advancement of ultrasound technology has allowed image quality to improve with decreasing device size and cost. Portable hand-carried ultrasound devices emerged in the late 1990s and true pocket carried devices in the late 2000s [26]. Since that time there has been an explosion of devices available on the market. Today, portable and ultra-portable ultrasound units are offered by a variety of companies, including Sonosite, General Electric, Philips, Clarius, and Butterfly. Devices such as the Butterfly IQ cost as little as $2000 and allow the EP to quite literally carry the machine in their pocket.

Handheld and pocket-carried devices currently range in price from approximately $2000–10,000, and some are even available to lease. The lower direct cost presents the opportunity for those organizations unable to afford traditional devices to implement ultrasound. This reduced cost may allow developing nations, rural and critical access facilities, and non-profit healthcare organizations to provide advanced care otherwise unattainable. Likewise, many educators use handheld ultrasound devices for medical education. The size of these devices also presents the opportunity to increase diagnostic accuracy in environments where size and weight restrict the use of other diagnostic modalities. Portable ultrasounds are used with increasing frequency on aeromedical transport and are beginning to be used by ground-based EMS units. For the military, hand held ultrasound devices represent one of the most weight and size efficient pieces of diagnostic equipment. They provide an opportunity to advance the care provided by Hospital Corpsmen and Medics provided at the site of injury. For special operations units, who often operate with a limited footprint and with little resources, the devices can supplement the humanitarian mission which is often a cornerstone of developing indigenous forces in addition to providing advanced care within their units.

Handheld devices present a great opportunity but also a great responsibility. As with traditional ultrasound machines, these devices should be used only by qualified health professionals and be approved by the facility. Often devices require use of a tablet or phone, and in these cases the facility should approve of both the probe and tablet or phone [26]. While many may be enthusiastic to obtain and use their own personal handheld ultrasound, care should be taken to ensure that governmental and institutional requirements are met prior to clinical use. Many facilities require the devices to be inspected by biomedical engineers, have cleaning protocols developed with infection control officers, and ensure that images are retained for documentation in the medical record, billing, and quality assurance.

Vertical, Horizontal, & Longitudinal Integration

EM has championed the use of point-of-care ultrasound, however ultrasound is utilized by a multitude of specialties. It is used by EMS and on the battlefield, in clinics by a variety of specialties from internal medicine to dermatology, and throughout the hospital. Despite this, relatively few outside of EM have significant breadth of experience with ultrasound. As a specialty, EM has formalized ultrasound education, quality assurance, and documentation standards. This expertise was recognized and utilized by the University of South Carolina School of Medicine in helping to create the first vertical, four-year, ultrasound curriculum in undergraduate medical education.(cite hoppman) The explosion of point-of-care ultrasound along with variation in training and quality assurance means that the future will require a multidisciplinary approach to integration of ultrasound across medicine.

There is a spectrum of ultrasound user and administrator within every organization. Some physicians or departments may have no experience or limited experience with poorly developed systems. Others within the same facility will have expertise and well developed archival, quality assurance, billing, and documentation mechanisms. Departments such as EM, anesthesiology, and cardiology often have well developed systems to administer point-of-care ultrasound services. Vertical integration of these systems, from the ED throughout the hospital allows the entire facility to benefit from the experience of these departments. Vertical integration can occur as loosely as inviting guest lectures from outside departments or scanning with members of another department. This is low hanging fruit for facilities with graduate medical education, as most resident physicians will have prearranged rotations outside of their department. These rotations are an opportunity to share knowledge between the departments. Alternatively, more formal integration can occur by appointing a director of point-of-care ultrasound or “chief ultrasound officer”. This person can help with educational efforts of various departments as well as establish protocols for quality reporting, quality assurance, and billing throughout the facility.

As the use of ultrasound expands, it will be important for well networked facilities to integrate their ultrasound operations horizontally. For organizations with multiple sites this may be as simple as using a common image archival system whereby studies performed at one site can be reviewed if a patient is transferred. This is especially useful for those who have one large hospital, often colloquially known as the mothership, surrounded by multiple satellite facilities. In these systems, transfers from the satellite facilities to the mothership are common. Integration of ultrasound between these sites allows for efficient use of resources. For instance, critical ultrasound findings may trigger rapid transfer and those ultrasounds may be reviewed prior to arrival by the receiving physician. One can imagine where a patient with a large abdominal aortic aneurysm, positive FAST exam, or ectopic pregnancy could initiate an ED-to-ED transfer and have both the receiving EP and specialist review the images while the patient is enroute to mobilize resources and expedite care. As systems such as this are developed, unrelated facilities may also benefit from similar arrangement. Many states operate image repositories as part of the state trauma systems. These repositories currently allow imaging from multiple facilities to be uploaded and sent to the receiving facility for review, preventing both redundant imaging and delay while waiting for images to be uploaded from a disc upon arrival of the patient. It's not difficult to imagine a similar system evolving for the use of point-of-care ultrasound. While creating these systems is challenging, the efficiency of the end product is worth the effort. A simpler method of integrating is shared didactics and QA. Methods such as this can be as basic as inviting outlying facilities, related or unrelated, to ultrasound rounds and providing feedback on cases where ultrasound was utilized.

Longitudinal integration of ultrasound has been developing for years, however the pace has greatly accelerated with the advent of hand-held ultrasound devices. While ultrasound has long been part of graduate medical education, its introduction into undergraduate medical education is a relatively new phenomenon. Many medical schools are now including mandatory ultrasound education within the clinical and preclinical years. Additionally, some have advocated for inclusion of clinically focused ultrasound education in premedical education. Some are even including ultrasound education as part of Science, Technology, Engineering, and Mathematics (STEM) programs in secondary education. Longitudinal integration will likely provide one of the next great leaps in ultrasound by creating a generation of physicians who are primed with knowledge and skills before entering their medical careers. As a result, they will master basic studies sooner, progress more quickly to advanced studies, and potentially even pioneer new techniques that will to continue to improve patient care.

References

Introduction

1. Ultrasound guidelines: emergency, point-of-care and clinical ultrasound guidelines in medicine. Ann Emerg Med. 2017;69(5) https://doi.org/10.1016/j.annemergmed.2016.08.457.
2. Mayron R, Gaudio FE, Plummer D, Asinger R, Elsperger J. Echocardiography performed by emergency physicians: Impact on diagnosis and therapy. Ann Emerg Med. 1988;17(2):150–4. https://doi.org/10.1016/s0196-0644(88)80301-9.
3. Marin JR, Lewiss RE. Point-of-care ultrasonography by pediatric emergency medicine physicians. Pediatr Emerg Care. 2015;31(7):525. https://doi.org/10.1097/pec.0000000000000492.
4. Use of ultrasound imaging by emergency physicians. Ann Emerg Med. 1997;30(3):364–5. https://doi.org/10.1016/s0196-0644(97)70185-9.
5. Cook T, Roepke T. Prevalence and structure of ultrasound curricula in emergency medicine residencies. J Emerg Med. 1998;16(4):655–7. https://doi.org/10.1016/s0736-4679(98)00064-x.
6. Witting M, Euerle B, Kenneth H, Butler K. A comparison of emergency medicine ultrasound training with guidelines of the society for academic emergency medicine. Ann Emerg Med. 1999;34(4) https://doi.org/10.1016/s0196-0644(99)80171-1.
7. Heller MB. Residency training in emergency ultrasound: fulfilling the mandate. Acad Emerg Med. 2002;9(8):835–9. https://doi.org/10.1197/aemj.9.8.835.
8. Counselman FL. The status of bedside ultrasonography training in emergency medicine residency programs. Acad Emerg Med. 2003;10(1):37–42. https://doi.org/10.1197/aemj.10.1.37.
9. Simel DL, Rennie D, Keitz SA. *The rational clinical examination: Evidence-based clinical diagnosis*. New York: McGraw-Hill; 2009.
10. Gottlieb M, Holladay D, Peksa GD. Point-of-care ocular ultrasound for the diagnosis of retinal detachment: a systematic review and meta-analysis. Acad Emerg Med. 2019; https://doi.org/10.1111/acem.13682.

Administrative Issues

11. Marin JR, Lewiss RE. Point-of-care ultrasonography by pediatric emergency medicine physicians. Pediatr Emerg Care. 2015;31(7):525. https://doi.org/10.1097/pec.0000000000000492.
12. Ultrasound guidelines: emergency, point-of-care and clinical ultrasound guidelines in medicine. Ann Emerg Med. 2017;69(5) https://doi.org/10.1016/j.annemergmed.2016.08.457.
13. Tayal VS, Blaivas M, Foster TR. Ultrasound Program management: a comprehensive resource for administrating point-of-care, emergency, and clinical ultrasound. Cham: Springer; 2018.
14. Privileging for Ultrasound Imaging H-230.960. AMA. https://policysearch.ama-assn.org/policyfinder/detail/Ultrasound?uri=/AMADoc/HOD.xml-0-1591.xml. Accessed 14 May 2019.
15. Recognition of American College of Emergency Physicians Policy Statement "Ultrasound guidelines: emergency, point-of-care, and clinical ultrasound guidelines in medicine." Official Statement. https://www.aium.org/officialStatements/45. Accessed 14 May 2019.
16. Emergency ultrasound standard reporting guidelines. https://www.acep.org/globalassets/uploads/uploaded-files/acep/by-medical-focus/ultrasound/eus_srgs_111511_edited0116.pdf. Published October 2011.

Applications of Ultrasound

17. Marin JR, Lewiss RE. Point-of-care ultrasonography by pediatric emergency medicine physicians. Pediatr Emerg Care. 2015;31(7):525. https://doi.org/10.1097/pec.0000000000000492.
18. Ultrasound guidelines: emergency, point-of-care and clinical ultrasound guidelines in medicine. Ann Emerg Med. 2017;69(5) https://doi.org/10.1016/j.annemergmed.2016.08.457.
19. Nomura J, Shipley D, Moore C. Appendix The core content of clinical ultrasonography fellowship training. https://www.acep.org/globalassets/uploads/uploaded-files/acep/by-medical-focus/ultrasound/core_content_clin_us_fellow_trng_030514.pdf.
20. Blaivas M. Transesophageal echocardiography during cardiopulmonary arrest in the emergency department.

Resuscitation. 2008;78(2):135–40. https://doi.org/10.1016/j.resuscitation.2008.02.021.

21. Byars D, Tozer J, Joyce J, Vitto M, Taylor L, Kayagil T, Jones M, Bishop M, Knapp B, Evans D. Emergency physician-performed transesophageal echocardiography in simulated cardiac arrest. West J Emerg Med. 2017;18(5):830–4. https://doi.org/10.5811/westjem.2017.5.33543.
22. Arntfield R, Pace J, Mcleod S, Granton J, Hegazy A, Lingard L. Focused transesophageal echocardiography for emergency physicians—description and results from simulation training of a structured four-view examination. Crit Ultrasound J. 2015;7(1) https://doi.org/10.1186/s13089-015-0027-3.
23. Arntfield R, Pace J, Hewak M, Thompson D. Focused transesophageal echocardiography by emergency physicians is feasible and clinically influential: observational results from a Novel Ultrasound Program. J Emerg Med. 2016;50(2):286–94. https://doi.org/10.1016/j.jemermed.2015.09.018.
24. Teran F, Dean AJ, Centeno C, Panebianco NL, Zeidan AJ, Chan W, Abella BS. Evaluation of out-of-hospital cardiac arrest using transesophageal echocardiography in the emergency department. Resuscitation. 2019;137:140–7. https://doi.org/10.1016/j.resuscitation.2019.02.013.
25. Guidelines for the use of Transesophageal Echocardiography (TEE) in the ED for cardiac arrest. Ann Emerg Med. 2017;70(3):442–5. https://doi.org/10.1016/j.annemergmed.2017.06.033.
26. Appropriate use criteria for handheld/pocket ultrasound devices. Ann Emerg Med. 2018;72(4) https://doi.org/10.1016/j.annemergmed.2018.07.042.

Index

A
A 7 French Catheter, 257
Abdominal aortic aneurysm (AAA)
  definition, 227
  prevalence, 227
  screening and evaluation, 234, 235
Abdominal wall blocks
  epidural anesthesia, 205
  indications, 214, 215
  lumbar arteries, 209, 210
  QLB
    definition, 212
    local anesthetics and complications, 213, 214
    types, 213
  quadratus lumborum, 208, 209
  rectus sheath block, 214, 215
  regional anesthesia, 205
  TAP block
    external oblique muscle, 205, 206
    internal oblique, 205, 206
    lateral block, 211
    local anesthetics and complications, 212
    modifications, 211
    nomenclature, 211
    posterior block, 211
    subcostal block, 211, 212
    tranversus abdominis, 205, 206
  TFP, 206
  thoracolumbar spinal nerve, 207, 208
  TLF, 208, 209
Abductor pollicis longus (APL), 110, 112
Accreditation Council for Graduate Medical Education (ACGME), 366
Acromioclavicular (AC) joint, 91, 94
Acute kidney injury (AKI), 235
Acute massive PE, 165
Adductor tears, 132
Adenomyosis, 259
Airway management
  airway anatomy, 61
  confirmation of, 62
  emergency situations, 62
  prediction of difficult, 61, 62
  regional anesthesia, 62
  usage, 61
Alobar holoprosencephaly, 242, 244
American College of Emergency Physicians (ACEP), 365, 368
American Institute of Ultrasound in Medicine (AIUM), 251
American Medical Association (AMA) House of Delegates, 367
American Medical Society for Sports Medicine (AMSSM), 80
American Society of Anesthesiologists (ASA), 338
American Society of Echocardiography (ASE), 29
Anisotropy, 14
Ankle
  anatomy, 143
  anterior ankle, 143, 144
  lateral ankle
    anterior tibiofibular ligament, 145
    ATFL, 145
    calcaneofibular ligament, 145, 146
    evaluation, 144, 145
    peroneus longus and brevis, 145
  medial ankle, 144
  posterior ankle, 146
  PTN, 147
  saphenous nerve, 147
  SPN, 147
  subtalar joint injection, 146, 147
  sural nerve, 147
  tibiotalar joint injection, 146
Ankle-brachial index (ABI)
  anatomy, 228
  body position, 228
  cuff size, 228
  Doppler method, 229
  Doppler ultrasound, 228
  physiology, 228
Anterior cruciate ligament (ACL), 137, 138
Anterior inferior tibiofibular ligament, 145
Anterior talofibular ligament(ATFL), 145
Axillary brachial plexus block, 124, 126

B
Baker’s cyst, 138, 233
Barcode sign, 342
Barlow maneuver, 83
Basal cell carcinoma (BCC), 321
Bedside Lung Ultrasound in Emergency (BLUE), 223
Bedside ultrasound
  applications, 17
  knobology, 19, 20
  needle visualization, 23, 24
  probe manipulation, 21, 22
  probe selection, 17–19
  scanning terminology, 20, 21
  structure visualization and needle orientation, 21, 23
Benign enlargement of the subarachnoid spaces (BESS), 242
Benign neoplastic ovarian cysts, 263, 264
Benign prostatic hyperplasia (BPH), 297
Benign serous and mucinous tumors, 263, 264
Bicep tendonitis, 82
Bicipital groove, 89

© Springer Nature Switzerland AG 2021
J. Li et al. (eds.), *Ultrasound Fundamentals*, https://doi.org/10.1007/978-3-030-46839-2

Brachial plexus
  absolute/relative contraindications, 123
  anatomy
    axillary nerve, 121, 122
    cords, 121
    divisions, 121
    median nerve, 122
    musculocutaneous nerve, 121
    peripheral nerve, 121
    radial nerve, 122
    trunks, 121
    ulnar nerve, 122
  axillary block, 124, 126
  distal upper extremity blocks, 123
  history, 122, 123
  indications, 123
  infraclavicular block, 124
  interscalene block, 126, 127
  proximal block, 126
  supraclavicular block, 123, 124
Brachial plexus blocks, 71
Brachial systolic pressure, 229
Butterfly IQ, 369

C
Calcaneofibular ligament, 145, 146
Calcific tendinosis, 93, 95
Calcific tendonitis, 82
Capnography, 62
Cardiac arrest, 165
Cardiac disease
  acute massive PE, 165
  cardiac arrest, 165
  diagnostic echocardiographic criteria, 166
  goal-directed echocardiography, 164
  intravenous fluid therapy management, 164, 165
  mortality and morbidity, 163
  paravertebral block, 164
  pectoralis fascial blocks, 164
  thoracic epidural analgesia, 163
  valvular heart disease, 166
Carotid artery stenosis (CAS), 233
Carotid Doppler, 234
Carotid ultrasonography, 233, 234
Carpal tunnel syndrome, 116
Carpometacarpal (CMC) joint, 118
Caudal nerve block
  anesthesia, 279
  modified positioning strategies, 280
  safety and efficacy, 279
  sonoanatomy, 280–283
Caudothalamic grooves, 241
Cavum septum pellucidum, 240
Celiac plexus blocks, 222
Central venous pressure (CVP), 223
Cerebellar hemorrhage, 242
Christian Doppler, 228
Clinical Ultrasound Accreditation Program (CUAP), 367
Color Doppler ultrasonography, 10, 234
Compartment syndrome, 222
Contrast-enhanced ultrasonography (CEUS), 286, 304
Coronary artery disease (CAD), 233
Corpora cavernosa, 299
Corpus luteum, 262
Council of Emergency Medicine Residency Directors (CORD), 365
Cranial ultrasound
  anterior coronal neonatal brain, 49
  imaging techniques, 239
    cavum septum pellucidum, 240
    cerebellum via mastoid window, 240
    corpus callosum, 239, 240
    normal choroid plexuses in atria, 239, 240
  indications for scanning, 239
  infants
    alobar holoprosencephaly, 242, 244
    corpus callosum, 242, 243
    macrocephaly, 242, 244
    occipital hematoma, 242
  neonatal ultrasound, 48
  normal coronal view of cranium, 48
  normal parasagittal view at the lateral ventricles, 50
  normal posterior coronal view, 50
  normal sagittal view of cranium, 48, 49
  preterm infants
    caudothalamic groove, 241
    cerebellar hemorrhage, 242
    grade IV intraventricular hemorrhage, 241, 242
    periventricular leukomalacia, 241
  role in preterm neonates, 239
  spinal sonogram
    benefits, 244
    filar cyst, 247, 248
    indications, 244
    lipomyelocele, 248, 249
    mild dilatation of central canal, 248
    normal anatomy, 245
    technique, 245, 246
    tight filum and tethered cord, 247
  step-wise technique, 47
  transabdominal and transperineal ultrasound, 48
  transcranial Doppler ultrasound, 49, 51
  transcranial ultrasonography, 51, 52
  Zika virus, 51
Cricothyrotomy, 62
Critical care echocardiography (CCE), 164
Critical care management, *see* Intensive care setting
Cul-de-sac, 256
Current Procedural Terminology (CPT) codes, 367
Curvilinear transducer, 6
Cutaneous inflammatory process
  acne conglobata, 326
  dissecting cellulitis of the scalp, 326
  hidradenitis suppurativa, 326
  inflammatory diseases, 327, 328
  keloid, 329
  morphea, 326, 328
  mycetomas, 328
  panniculitis, 328
  pilonidal cyst, 326
  psoriasis, 326, 327
  scleroderma, 326, 328

D
Deep venous thrombosis (DVT), 230
  clinical aspects, 231, 233
  femoral vein, 231, 232
  lower extremity, 231
  sensitivity and specificity, 231
  upper extremity, 233
De Quervain's tenosynovitis, 117, 118
De Quervin's tendonitis, 313
Dermatology

  benign neoplasms
    digital myxoid, synovial, and mucoid cyst, 325
    glomus tumor, 324
    periungual fibroma, 325
    periungual warts, 323, 324
    subungual and periungual pyogenic granulomas, 323, 324
    subungual exostosis, 325, 326
    systemic autoimmune diseases, 325
  benign solid and cystic neoplasm
    epidermal and trichilemmal cyst, 321, 322
    neurofibroma, 322, 323
    pilomatrixoma, 322, 323
    warts, 323
  benign vascular neoplasm
    infantile hemangiomas, 321
    vascular malformations, 321, 322
  color Doppler US, 330
  cosmetic fillers, 330
  cutaneous inflammatory process
    acne conglobata, 326
    dissecting cellulitis of the scalp, 326
    hidradenitis suppurativa, 326
    inflammatory diseases, 327, 328
    keloid, 329
    morphea, 326, 328
    mycetomas, 328
    panniculitis, 328
    pilonidal cyst, 326
    psoriasis, 326, 327
    scleroderma, 326, 328
  deep venous system, 330
  diagnosis, 317
  foreign bodies, 329, 330
  gouty tophus, rheumatoid nodule, xanthoma, 329
  high intensity focused ultrasound, 331
  lipoma, 329
  live organisms, 330
  malignant cutaneous neoplasms
    BCC, 321
    malignant melanoma, 320
    SCC, 320
  nail, 319
  normal skin, 318
  tools, 317, 318
Dermoid cysts, 265
Developmental dysplasia of the hip (DDH), 83
Diameter of IVC (dIVCmax), 164
Diastolic blood pressure (DBP), 228
Digital myxoid, 325
Distal bicep tendon (DBT), 104
Distal upper extremity blocks, 123
Doppler echocardiography, valvular heart disease, 166
Doppler shift, 228
Double tract/double lumen signs, 62
Duplex Doppler Sonography, 10
Duplex ultrasonography, 230
  body position, 230
  deep venous thrombosis, 230
  equipment, 231
  5 Ps of ischemia, 230
  limitations, 231
  specificity and sensitivity, 230

E
Ejaculatory duct, 298
Elbow
  acute and chronic injuries, 99
  anterior elbow, 101–103
  articulations, 99, 100
  brachialis muscle and tendon, 99, 101
  bursa, 100
  checklist, 100, 102
  CT and MRI, 99
  DBT, 104
  epicondylitis steroid injection, 106
  Golfer's elbow, 105
  intra-articular injection, 106
  lateral elbow, 103, 104
  LUCL, 99, 100, 105
  medial elbow, 101, 103
  medial epicondyle, 99
  needle fenestration, 105, 106
  olecranon bursitis, 105, 106
  posterior elbow, 104
  tennis elbow, 105
  UCL, 99, 100, 105
Emergency medicine (EM)
  advanced applications of, 368
  billing and reimbursement, 367, 368
  core applications of ultrasound, 368
  credentialing, 367
  equipments for, 366
  history, 365
  horizontal integration, 369
  indifferentiated patients, 365, 366
  longitudinal integration, 370
  pocket carried devices, 369
  quality assurance, 367
  training, 366, 367
  vertical integration, 369
Emergency Ultrasound Standard Reporting Guidelines, 367
End diastolic velocity (EDV), 286
Endocavitary transducers, 6, 8
Endoluminal sonography, 286
Endoluminal ultrasonography, 304
Endometrial abnormalities, 260
Endometrial adenocarcinoma, 261
Endometrial hyperplasia, 260–262
Endometrial polyps, 261, 262
Endometrial stripe thickening, 260, 261
Endometriomas, 264, 265
Endometriosis, 264
Epicondylitis steroid injection, 106
Epidermal cyst, 322
Epididymis, 294, 295
Epidural analgesia, 221
Erectile dysfunction, 286, 298
European Society of Hysteroscopy, 258
EuroSCORE, 166
Extended Focused Assessment with Sonography in Trauma (E-FAST), 368
Extensor carpi radialis brevis (ECRB), 110, 112
Extensor carpi radialis longus (ECRL), 110, 112
Extensor carpi ulnaris tendon (ECU), 110, 113
Extensor compartment, 110
  anatomic snuff-box, 110, 114
  APL and EPB, 110, 112
  ECU, 110, 113
  ED and EIP, 110, 113
  EDQ, 110, 113
  EPL, 110, 112
  extensor carpi radialis longus and brevis, 110, 112
  scaphoid fracture, 113, 114
Extensor digiti quinti proprius (EDQ), 110, 113
Extensor digitorum (ED) tendons, 110, 113

Extensor indices proprius (EIP), 110, 113
Extensor pollicis brevis (EPB), 110, 112
Extensor pollicis longus (EPL), 110, 112
Extracorporeal membrane oxygenation (ECMO), 239

F
Fascia iliaca nerve block
  compartment, 149
  nerve distribution, 149, 150
  patient positioning and landmarks, 149
  technique, 150
  ultrasound anatomy, 149
Femoral nerve block
  nerve distribution, 157
  patient positioning and landmarks, 156
  surgery, 156
  technique, 157
  ultrasound anatomy, 156, 157
Fibrocartilaginous structures, 80
Filar cyst, 247
5 Ps of ischemia, 230
Flexor carpi radialis (FCR), 109
Flexor carpi ulnaris (FCU), 109
Flexor compartment, 109–111
Flexor digitorum profundus (FDP), 109
Flexor digitorum superficialis (FDS), 109
Flexor pollicis longus (FPL), 109
Fluid Administration Limited by Lung Sonography (FALLS) protocol, 223
Focused Assessed Transthoracic Echocardiography (FATE), 343
Focused Assessment with Sonography in Trauma (FAST), 368
Free, open-access medical education (FOAMed), 368

G
Ganglion cyst, 82
Gastric antrum, 339
Germinal matrix hemorrhage, 241
Glenohumeral joint, 94, 96
Glomus tumor, 324
Goal-directed echocardiography, 164
Golfer's elbow, 105
Grade 0 antrum, 340
Grade IV- intraventricular hemorrhage, 241
Graf method, 83
Greater occipital nerve block, 67–69
Greater trochanteric pain syndrome, 133
Grey scale B Mode ultrasound, 285
Gynacolgic ultrasound, 251
  See also Pelvic ultrasonography

H
Hamstrings tendinopathy/ischial bursitis, 133, 134
Handheld devices, 369
Harcke method, 83
Harmonic scanning, 286
Head and neck blocks
  brachial plexus blocks, 71
  greater occipital nerve block, 67–69
  infraorbital nerve block, 66, 67
  interscalene nerve block, 71, 72
  lesser occipital nerve block, 68, 69
  mental nerve block, 67
  regional anesthesia, 65
  stellate ganglion blocks, 73–75
  superficial cervical plexus block, 69–71
  supraclavicular nerve block, 72, 73
  supraorbital nerve block, 65, 66
  trigeminal nerve block, 65, 66
Hematooperitoneum, 256
Hematospermia, 303
Hematuria, 303
Hemorrhagic cyst, 262, 263
Hidradenitis suppurativa, 326
High intensity focused ultrasound (HIFU), 313
Hip
  anterior hip
    anatomy, 129, 130
    iliopsoas tendinopathy/bursitis diagnosis, 131
    osteoarthritis injection, 129, 130
    rectus femoris tear, 131
    snapping hip syndrome, 130, 131
  lateral hip
    anatomy, 132, 133
    pathology, 133
  medial hip
    anatomy, 131, 132
    pathology, 132
  posterior hip
    anatomy, 133, 134
    pathology, 133, 134
Hip dysplasia, 83
Hydrocolpos, 260
Hydrometrocolpos, 260
Hyoid bone, 61, 62
Hyomental distance ratio, 62
Hypoechoic urethral muscles, 297
Hypopharynx, 61
Hypoxic ischemic injury, 241

I
Iliohypogastric nerve, 208
Ilioinguinal nerves, 208
Iliopsoas bursa, 131
Infantile hemangiomas, 321
Inferior vena cava (IVC), 164, 222
Infraclavicular brachial plexus block, 124
Infraorbital nerve block, 66, 67
Infraspinatus muscle, 89, 92
Infraspinatus tendon, 87, 90, 93
Intensive care setting
  peripheral nerve blocks, 221, 222
  regional analgesic techniques, 222
  regional anesthesia, ultrasound role, 221
  volume status, 222
    central venous pressure, 223
    IVC imaging, 222, 223
    lung ultrasound, 223
    velocity-time integral, 223
Intercostal nerve blocks (ICNB), 164
Internal carotid artery (ICA), 233, 234
Interscalene block, 126, 127
Interscalene nerve block, 71, 72
Intra-articular injection, 106
Intravenous fluid therapy management, 164, 165
Intraventricular hemorrhage, 241, 242
IVC collapsibility index (IVCCI) ratio, 164

K
Keloid, 329
Klippel-Trenaunay Syndrome, 330
Knee
    anterior knee
        ACL tear, 137, 138
        anatomy, 135
        osteoarthritis, 136, 137
        patellar tendinitis, 137
    lateral knee
        anatomy, 140, 141
        lateral meniscal tears, 141
        LCL sprains, 140
        peroneal nerve entrapment, 141
    medial knee
        anatomy, 138, 139
        MCL sprains, 139
        medial meniscus tear, 139, 140
        pes anserine bursitis, 139
    posterior knee
        anatomy, 137, 138
        pathology, 138
Knobology, 19, 20

L
Laryngomalacia, 56
Larynx, 61
Lateral collateral ligament (LCL) sprains, 140
Lateral epicondylitis, 105
Lateral meniscal tears, 141
Lateral ulnar collateral ligament (LUCL), 99, 100, 104, 105
Leiomyoma, 258, 259
Leiomyosarcomas (LMS), 259
Lesser occipital nerve block, 68, 69
Linear array transducers, 6, 7
Lipomyelocele, 248, 249
Long head bicep tendon, 87, 89, 90, 92, 95
Lower extremity
    fascia iliaca block
        compartment, 149
        nerve distribution, 149, 150
        patient positioning and landmarks, 149
        technique, 150
        ultrasound anatomy, 149
    femoral nerve block
        nerve distribution, 157
        patient positioning and landmarks, 156
        surgery, 156
        technique, 157
        ultrasound anatomy, 156, 157
    obturator nerve block
        nerve distribution, 155, 156
        pain control, 154
        patient positioning and landmarks, 154
        technique, 156
        ultrasound anatomy, 155
    popliteal nerve block
        goal, 150
        nerve distribution, 151
        patient positioning and landmarks, 150
        technique, 151
        ultrasound anatomy, 150, 151
    saphenous nerve block
        distal, 158
        nerve distribution, 158
        technique, 158, 159
        transsartorial approach, 158
        ultrasound anatomy, 158
    sciatic nerve block
        anterior approach, 153, 154
        definition, 152
        nerve distribution, 153
        patient positioning and landmarks, 152
        subgluteal approach, 154
        transgluteal approach, 154
        ultrasound anatomy, 152, 153
Lung and pleural examination and diagnosis
    image acquisition
        BLUE protocol, 186
        patient positioning, 185
        PLAPS point, 186, 187
        probe manipulation, 186
    probe types, 185
Lung point, 342
Lung sliding, 341
Lung ultrasound (LUS), 223

M
Macrocephaly, 244
Malignant cutaneous neoplasms
    BCC, 321
    malignant melanoma, 320
    SCC, 320
Malignant melanoma, 320
Mallampati score, 61
Mechanical index (MI), 288
Medial collateral ligament (MCL) sprain, 139
Medial epicondylitis, 105
Medial meniscus injuries, 139, 140
Meningocele, 248
Mental nerve block, 67
Morphea, 326, 328
Mothership, 369
Mucoid cyst, 325
Müllerian (paramesonephric) ducts, 260
Multicentre Australian Study of Epidural Anesthesia (MASTER) trial, 221
Musculoskeletal ultrasound
    Achilles tendon, 81
    advantages, 79
    disadvantages, 80
    fluid collection, 80
    foreign body, 82
    ganglion cyst, 82
    hand-held US, 79
    injections, 83, 84
    medial ankle structures, 80
    nerve entrapment, 82
    pediatric developmental dysplasia of hip, 83
    peroneal tendon instability, 83
    peroneus brevis tendon split tear, 83
    rotator cuff tears, 82
    shoulder pathology, 82
    soft tissue masses, 80
    spring (deltoid) ligament tear, 81
    technical considerations, 80
    ultrasound palpation test, 81
Mycetomas, 328

N
Neck ultrasound
  cricoid cartilage and cricothyroid membrane, 57
  hyoid bone, 55
  larynx, 56
  thyroid gland
    anatomy, 57
    pathology, 58
    sonoanatomy, 58
  trachea
    anatomy, 58
    clinical applications, 58, 59
    pathology, 58
    sonoanatomy, 58
  vocal cords
    anatomy, 56
    pathology, 56, 57
    sonoanatomy, 56
Needling techniques
  body ergonomics, 27, 28
  in-plane vs. out-of-plane approach, 25, 26
  needle selection, 27
  needle-beam angle, 26
  proper needle handling, 26, 27
Nerve entrapment, 82
Neuraxial blockades
  lumbar spine
    indications, 277
    parasagittal articular scan, 274, 276
    parasagittal oblique scan, 275, 277
    parasagittal transverse process scan, 274, 275
    sonoanatomy, 272, 273
    transverse interlaminar scan, 276, 277, 279, 280
    transverse spinous process scan, 276, 278
  parasagittal oblique scan, 272, 273
  sonoanatomy, 272
  spinal vertebrae anatomy, 271, 272
  thoracic nerve block, 272
  transverse midline scan, 272, 274
  ultrasound guidance, 271
Neurofibroma, 322, 323

O
Obstructive sleep apnea (OSA), 55
Obturator nerve block
  nerve distribution, 155, 156
  pain control, 154
  patient positioning and landmarks, 154
  technique, 156
  ultrasound anatomy, 155
Occipital hematoma, 242
Olecranon bursitis, 105, 106
Oncotherapy, 313
Ongoing Professional Practice Evaluation (OPPE), 367
Oropharynx, 61
Orthopaedics, ultrasound in, *see* Musculoskeletal ultrasound
Ortolani maneuver, 83
Ovarian torsion, 265

P
Paravertebral block (PVB), 164
Patellar tendinitis, 137
Peak systolic velocity (PSV), 286
Pectoralis fascial blocks (PECS), 164
Pediatric developmental dysplasia of the hip (DDH), 83
Pediatric intensive care unit (PICU), 239
Pelvic inflammatory disease (PID), 265, 266
Pelvic ultrasonography
  adenomyosis, 259, 260
  cervix, 252–254, 262
  endometrial polyps, 261, 262
  endometrial stripe, 254, 255, 260, 261
  fallopian tubes
    Cul-de-sac, 256
    doppler studies, 256, 257
    hydrosalpinx, 262
    ovaries, 262
    premenopausal menstruating women, 255
    pyosalpinx, 262
    saline infusion sonography, 257
  functional cysts
    benign neoplastic ovarian cysts, 263, 264
    dermoid cysts, 265
    endometriosis, 264, 265
    hemorrhagic cyst, 262–263
  leiomyoma, 258, 259
  leiomyosarcomas, 259
  Müllerian ducts, 260
  ovaries
    Cul-de-sac, 256
    doppler studies, 256, 257
    premenopausal menstruating women, 255
    saline infusion sonography, 257
    torsion, 265
  patient positioning, 252
  pelvic inflammatory disease, 265, 266
  peritoneal inclusion cysts, 266
  structural abnormalities, 260
  three-dimensional ultrasonography, 257
  trans-abdominal images, 252
  transvaginal images, 252
  transvaginal ultrasound probes, 251, 252
  uses, 251
  uterus, 252, 253
Penis ultrasound
  clinical indications, 298
  color and spectral Doppler examination, 299
  grey scale ultrasound, 299
  sonourethrography, 299
  technique, 298
  ultrasound anatomy, 299
Perioperative ultrasound
  airway ultrasound and FAST exams
    clinical/pathological interpretation, 348
    esophagus, trachea and thyroid, 347
    image acquisition and sonoanatomy, 346
    indications, 346
    medical decision making, 348
    parasagittal scan of neck, 347
    parasagittal ultrasound view, 348
    transverse scan of neck, 347
    vocal cords, 347
  cardiac ultrasound
    A4C probe position, 346
    A4C ultrasound view, 346
    clinical/pathological interpretation, 343
    image acquisition and sonoanatomy, 343
    indications, 343
    medical decision making, 343
    PLAX probe position, 345

        PLAX ultrasound view, 345
        PSAX probe position, 345
        PSAX ultrasound view, 345
        subcostal 4C probe position, 344
        subcostal 4C ultrasound view, 344
        subcostal IVC probe position, 344
        subcostal IVC ultrasound view, 344
    gastric ultrasound
        clinical/pathological interpretation, 339
        empty stomach, 339
        fluid volume measurement, 340
        gastric antrum, 339
        image acquisition and sonoanatomy, 338
        indications, 338
        medical decision making, 339, 340
        stomach with food, 340
        stomach with liquid and air, 339
    I-AIM framework, 337
    lung ultrasound
        barcode sign, 342
        B lines, 341
        clinical/pathological interpretation, 342
        image acquisition and sonoanatomy, 340, 341
        indications, 340
        medical decision making, 342
        posterior axillary line, no effusion, 342
        seashore sign, 341
Peritoneal inclusion cysts, 266
Periungual fibroma, 325
Periungual warts, 323, 324
Periventricular leukomalacia, 241
Peroneal tendon instability, 83
Peroneus brevis (PB), 145
    muscles, 83
    tendon split tear, 83
Peroneus longus (PL), 83, 144–145
Pes anserine bursitis, 139
Phased array transducers, 6, 7
Pilomatrixoma, 322, 323
Plastic polyetheretherketone (PEEK), 82
Pleural effusion, 341, 342
Pneumothorax, 340, 342
Pocket carried devices, 369
Point-of-care ultrasound (POCUS), 165, 337, 338, 346, 367
Polyester (Dacron) grafts, 230
Polyps, 261, 262
Popliteal nerve block
    goal, 150
    nerve distribution, 151
    patient positioning and landmarks, 150
    technique, 151
    ultrasound anatomy, 150, 151
Portable ultrasounds, 369
Posterior tibial nerve (PTN), 147
Post-menopausal women, 255
Post-spinal anesthesia hypotension (PSAH), 164
Pouch of Douglas, *see* Cul-de-sac
Premenopausal menstruating women, 255
Prostate gland, 297
Prostate seminal vesicles and vas deference
    indications, 297
    transabdominal scan, 295
    transrectal ultrasound, 296, 297
    ultrasound features, 298
Proximal brachial plexus block, 126
Psoriasis, 326, 327
Pulmonary embolism (PE), 165
Pulsatility index (PI), 286
Pulse wave technology, 285
Pulsed wave doppler, 8, 10
Pulsed wave Doppler ultrasonography, 234
Pyogenic granulomas (PGs), 323, 324
Pyosalpinx, 262

Q
Quadratum lumborum block (QLB)
    definition, 212
    local anesthetics and complications, 213, 214
    types, 213
Quadratus lumborum muscle (QL), 206, 208, 209

R
Rectus femoris tear, 131
Rectus sheath block, 214, 215
Regional anesthesia, 62
Renal resistive index (RRI), 235
Renal sonography
    antenatal ultrasound findings, 288, 289
    in children and adults, 289
    clinical indications, 289
    Doppler waveform in adult renal artery, 290, 291
    kidney transplant, 291
    normal ultrasound findings, 290
    renal transplant, 291
    surgical technique, 291
Renovascular disease, 227
Resuscitative Transesophageal Echocardiography (TEE), 368
Return of spontaneous circulation (ROSC), 165
Rheumatoid arthritis (RA), 116
Right atrial pressure (RAP), 164
Right lateral decubitus (RLD), 338
Rotator cuff tear, 82, 87, 92, 93, 95

S
Saline infusion sonography (SIS), 257
Saphenous nerve (SN), 147
Saphenous nerve block
    distal, 158
    nerve distribution, 158
    technique, 158, 159
    transsartorial approach, 158
    ultrasound anatomy, 158
Scapholunate advanced collapse (SLAC), 115
Sciatic nerve block
    anterior approach, 153, 154
    definition, 152
    nerve distribution, 153
    patient positioning and landmarks, 152
    subgluteal approach, 154
    transgluteal approach, 154
    ultrasound anatomy, 152, 153
Science, Technology, Engineering, and Mathematics (STEM) programs, 370
Scleroderma, 326, 328
Sclerotherapy, 312
Scrotum ultrasound
    anatomy, 294
    epidydimis, 294, 295
    indications, 294
    technique, 294
    testes, 294

Seashore sign, 341, 342
Serratus anterior plane (SAP) block, 164
Severe valve regurgitation, 166
Severe valve stenosis, 166
Shoulder
  interventional techniques, 96
  pathology
    acromioclavicular joint, 94
    calcific tendinosis, 93, 95
    glenohumeral joint osteoarthritis, 94
    long head bicep tendon subluxation/dislocation, 92, 95
    rotator cuff tear, 92, 93, 95
    SASD, 96
    subacromial impingement, 95, 96
    tendinosis, 91
  patient positioning and anatomy, 94
    acromioclavicular joint, 88, 91, 94
    glenoid, proximal humeral head and distal clavicle, 88
    infraspinatus, 89–93
    long head bicep tendon, 87, 89, 90
    glenoid, proximal humeral head and distal clavicle, 87
    infraspinatus, 87
    supraspinatus muscle, 87
    teres minor, 87
    SASD, 91, 94, 95
    subscapularis, 87, 89, 90
    supraspinatus muscle, 89–92
    teres minor, 89–93
    tuberosity facet anatomy, 87, 89
Shoulder pathology, 82
Snapping hip syndrome, 130, 131
Society of Academic Emergency Medicine (SAEM), 365
Society of Cardiovascular Anesthesiologists (SCA), 29
Soft tissue masses, 80
Sonoelastography, 286, 303
Spatial compounding, 286
Spectral Doppler, 286
Squamous cell carcinoma (SCC), 320
Static Graf method, 83
Stellate ganglion blocks, 73–75
Stratosphere sign, 342
STS scoring systems, 166
Subacromial bursitis, 82
Subacromial impingement, 95, 96
Subacromial subdeltoid (SASD) bursa, 91, 94–96
Subglottic stenosis, 62
Submucosal myomas, 258, 259
Subscapularis muscle, 87, 89, 90
Subserosal myomas, 258
Subtalar joint injection, 146, 147
Subungual exostosis, 325, 326
Superficial cervical plexus block, 69–71
Superficial peroneal nerve (SPN), 147
Superior mesenteric artery (SMA), 234
Supraclavicular block, 123, 124
Supraclavicular nerve block, 72, 73
Supraorbital nerve block, 65, 66
Supraspinatus muscle, 87, 89–92
Sural nerve (SN), 147
Synovial cysts, 325
Syringohydromyelia, 248
Systolic blood pressure (SBP), 228

T
Tendon fenestration, 96
Tendon sheath injection, 118
Tennis elbow, 105
Tenosynovitis, 313
Teres minor, 87, 89, 90, 92, 93
Testes, 294
Thermal index (TI), 288
Thoracic epidural analgesia, 163
Thoracolumbar fascia (TLF), 208, 209
Thoracolumbar spinal nerve, 207, 208
Thrombectomy, 312
Tibialis posterior (TP) tendon, 144
Tibiotalar joint injection, 146
Tracheostomy, 62
Trans abdominal plane (TAP) block, *see* Abdominal wall blocks
Transabdominally as well as transrectally (TRUS), 295
Transcatheter aortic valve replacements (TAVR), 163
Transcranial Doppler ultrasound (TCD), 49, 51
Transcranial ultrasonography (TCS)
  brain parenchyma, 51, 52
  post-operative localization of brain implants, 51
Transesophageal echocardiogram (TEE), 337
Transthoracic echocardiography (TTE)
  apical window, 174
  clinical indications
    cardiac output measurement, 181
    diastolic dysfunction, 179
    embolic sources, 179
    heart valves assessment, 179
    hypertrophic cardiomyopathy, 180
    infective endocarditis, 179
    LV systolic function, 174, 179
    volume status, 180
    wall motion abnormalities, 179
  echocardiography advantages, 181
  limitations, 181
  parasternal window, 173, 174
  subcostal window, 174
  suprasternal window, 173
Transvaginal/transrectal scan, 293
Transversalis fascia plane (TFP), 206
Transverse abdominal plane (TAP) block, 222
Triangular fibrocartilage complex (TFCC), 116
Trichilemmal cyst, 322
Trigeminal nerve block, 65
Tuboovarian abscess, 266
Tuboovarian phlegmon, 266
Tunica albuginea, 294
Tunica vaginalis, 294

U
Ulnar collateral ligament (UCL), 99–101, 103, 105
Ultrasound
  aliasing, 14
  anisotropy, 14
  comet tail artifact, 13, 14
  definition, 3
  Doppler sonography
    blood flow velocity, 8
    color Doppler ultrasound, 10
    description, 8
    power Doppler, 11
    pulsed wave doppler, 8, 10
  frequency, 3
  image generation
    amplitude-mode, 5
    brightness-mode, 5
    intrinsic features, 4, 5

    motion-mode, 5
  mirror images, 12, 13
  posterior acoustic enhancement, 11, 13
  resolution, 6
  reverberation artifact, 12, 13
  ring down, 13
  shadowing, 11, 12
  side-lobes, 13
  strength of wave, 3
  tissue vibration, 15
  transducer piezoelectric crystal failure, 14
  transducers
    curvilinear transducers, 6
    endocavitary transducers, 6, 8
    linear array transducers, 6, 7
    phased array transducers, 6, 7
    piezoelectric crystals, 6
    piezoelectric elements, 6
    position, 6, 9, 10
  twinkle artifact, 15
  wavelength, 3
Ultrasound (US) basics
  Doppler echocardiography, 171, 172
  M mode, 171
  2D imaging, 171
  ultrasound probes, 172
Ultrasound guided interventions
  advantages, 313
  biopsy, 310
  disadvantages, 314
  drainage, 310, 311
  future aspects, 314, 315
  high intensity focused ultrasound, 313
  ionizing radiation, 307
  musculoskeletal interventions, 313
  nerve blocks, 312, 313
  oncotherapy, 313
  sclerotherapy, 312
  thrombectomy, 312
  tools
    catheters, 309
    sharps, 308, 309
    sterility, 308
    ultrasound machine, 307, 308
    wires, 309
Ultrasound guided spinal
  basic anatomy and sonoanatomy, 278, 280
  neurolytic procedures, 278
  positioning and technique, 279
  spinal anesthesia, 277
Ultrasound Palpation Test, 81
Upper extremity, *see* Brachial plexus
Ureters, ultrasound, 291
Urethral stricture, 299
Urinary bladder ultrasound
  anatomy, 292
  indications, 293
  scrotum, 294
  transabdominal pelvic sonography, 292
  ultrasound features, 293
Urology, ultrasound in
  contrast-enhanced ultrasonography, 304
  Doppler sonography, 285, 286
  endoluminal ultrasonography, 304
  grey scale B mode ultrasound, 285
  harmonic scanning, 286
  history, 285
  intra operative ultrasound, 303
  patient safety, 288
  penis (*see* Penis ultrasound)
  prostate (*see* Prostate seminal vesicles and vas deference)
  renal (*see* Renal sonography)
  sonoelastography, 303
  spatial compounding, 286
  TRUS guided prostate biopsy
    complications, 303
    contraindications, 302
    indications, 302
    pre-requisites, 302
    procedure, 302, 303
  ultrasound guided per cutaneous renal access
    clinical indications, 300
    vs. fluoroscopic guidance, 301
    prerequisites, 300
    procedure, 300, 301
  ureters, 291, 292
  urinary bladder
    anatomy, 292
    indications, 293
    technique, 292, 293
    ultrasound features, 293
US guided vascular access
  artery cannulation, 40, 41
  ASE and SCA guidelines, 29
  catheter/needle assembly, 31
  complications, 29
  femoral vein cannulation, 40
  guidewire advancement, 42
  internal jugular vein cannulation
    pre-procedure checklist, 35
    screening, 35, 36
    step-by-step approach, 36–39
  landmark techniques, 29
  long axis in-plane approach, 34, 35
  needle puncture and cannulation, 30
  oblique in-plane approach, 35
  patient hemodynamics monitoring, 29
  peripheral venous cannulation, 41, 42
  probe selection, 29
  real time guidance, 30
  short axis technique, 34
  static imaging, 30
  sterile gel application, 30
  sterile technique, 29, 30
  subclavian vein cannulation, 39, 40
  US imaging, 29
  vessel abnormality diagnosis, 32, 34
  vessel identification, 31
Uterine leiomyoma (fibroid), 258

V
Valvular heart disease (VHD), 166
Vascular disease
  abdominal aortic aneurysm, 234, 235
  ABI (*see* Ankle-brachial index (ABI))
  AKI assessment, U/S screening in, 235
  carotid disease, U/S screening for, 233, 234
  color Doppler ultrasonography, 234
  Duplex ultrasonography (*see* Duplex ultrasonography)
  DVT ultrasound scanning (*see* Deep venous thrombosis (DVT))
  pulsed wave Doppler ultrasonography, 234

Vascular malformations, 321, 322
Vascular polytetrafluoroethylene (PTFE), 230
Velocity-time integral (VTI), 223
Vesico-amniotic shunt, 289
Vesicoureteral junctions, 293
Vesicouureteral reflux (VUR), 304
Vocal cords, 347

W

Wrist
  carpal tunnel syndrome, 116
  carpometacarpal joint, 118
  De Quervain’s tenosynovitis, 117
  extensor compartment, 110
    anatomic snuff-box, 110, 114
    APL and EPB, 110, 112
    ECU, 110, 113
    ED and EIP, 110, 113
    EDQ, 110, 113
    EPL, 110, 112
    extensor carpi radialis longus and brevis, 110, 112
    scaphoid fracture, 113, 114
  flexor compartment, 109–111
  intrinsic wrist ligaments, 115, 116
  median nerve, 114, 115
  osseous structures, 109, 110
  radial nerve, 115
  rheumatoid arthritis, 116
  tendon sheath injection, 118
  ulnar nerve, 115

Z

Zika virus, 53